Progress in Landslide Research and Technology

Irasema Alcántara-Ayala
Željko Arbanas
David Huntley
Kazuo Konagai
Matjaž Mikoš
Kyoji Sassa
Shinji Sassa
Huiming Tang
Binod Tiwari *Editors*

Progress in Landslide Research and Technology, Volume 1 Issue 2, 2022

OPEN ACCESS

Springer

Progress in Landslide Research and Technology

The Open Access book series of the International Consortium on Landslides (ICL) aims to be the common platform for the publication of recent progress in landslide research and technology for practical applications and the benefit of society contributing to the Kyoto Landslide Commitment 2020, which is expected to continue up to 2030 and even beyond for the global promotion of understanding and reducing landslide disaster risk as well as the 2030 Agenda Sustainable Development Goals. The contributions include original and review articles, case studies, activity reports and teaching tools for the promotion of understanding and reducing landslide disaster risks.

Irasema Alcántara-Ayala •
Željko Arbanas • David Huntley •
Kazuo Konagai • Matjaž Mikoš •
Kyoji Sassa • Shinji Sassa •
Huiming Tang • Binod Tiwari
Editors

Progress in Landslide Research and Technology, Volume 1 Issue 2, 2022

Springer

Editors
Irasema Alcántara-Ayala
Institute of Geography
National Autonomous University of Mexico
Mexico City, Mexico

David Huntley
Geological Survey of Canada
Vancouver, BC, Canada

Matjaž Mikoš
Faculty of Civil and Geodetic Engineering
University of Ljubljana
Ljubljana, Slovenia

Shinji Sassa
National Institute of Maritime,
Port and Aviation Technology
Port and Airport Research Institute
Yokosuka, Japan

Binod Tiwari
Department of Civil and Environmental
Engineering
California State University, Fullerton
Fullerton, CA, USA

Željko Arbanas
Faculty of Civil Engineering
University of Rijeka
Rijeka, Croatia

Kazuo Konagai
International Consortium on Landslides
Kyoto, Japan

Kyoji Sassa
International Consortium on Landslides
Kyoto, Japan

Huiming Tang
China University of Geosciences
Wuhan, China

This work contains media enhancements, which are displayed with a "play" icon. Material in the print book can be viewed on a mobile device by downloading the Springer Nature "More Media" app available in the major app stores. The media enhancements in the online version of the work can be accessed directly by authorized users.

ISSN 2731-3794 ISSN 2731-3808 (electronic)
Progress in Landslide Research and Technology
ISBN 978-3-031-18470-3 ISBN 978-3-031-18471-0 (eBook)
https://doi.org/10.1007/978-3-031-18471-0

Cover illustration: A large-scale rapid landslide was induced by the mainshock of the 2016 Kumamoto Earthquake. The landslide hit the Aso-Ohashi Bridge on the national road (center on the bottom) and it disappeared. (Photograph provided by the Kyushu Regional Development Bureau, Ministry of Land, Infrastructure, Transport and Tourism, Japan)

This Springer imprint is published by the registered company Springer Nature Switzerland AG
The registered company address is: Gewerbestrasse 11, 6330 Cham, Switzerland

Springer Nature More Media App

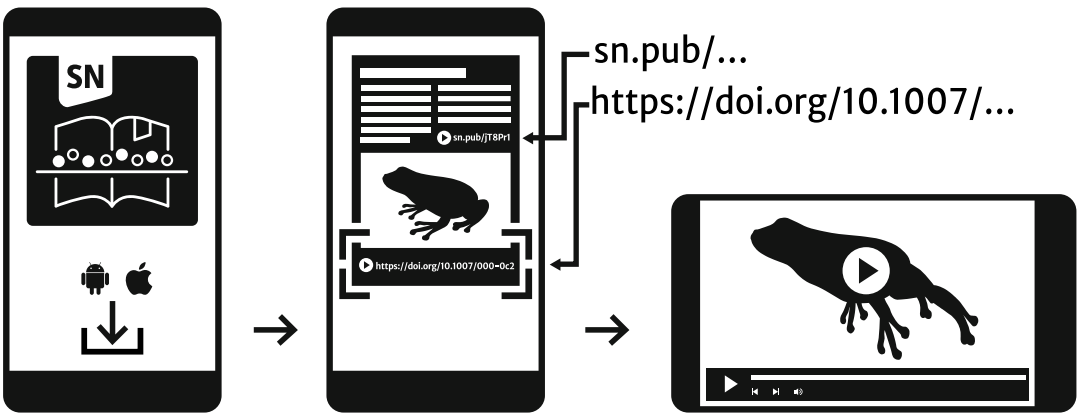

Support: customerservice@springernature.com

Editorial Board of the Book Series

KLC2020 Managing Committee

Kyoji Sassa (Chairman), Secretary General, Secretariat of the Kyoto Landslide Commitment 2020
Kaoru Takara, Managing Director, Secretariat of the Kyoto Landslide Commitment 2020
Matjaž Mikoš, Chair of the Global Promotion Committee of the International Programme on Landslides and Kyoto Landslide Commitment 2020
Qunli Han, Co-chair of the Global Promotion Committee of the International Programme on Landslides and Kyoto Landslide Commitment 2020
Nicola Casagli, President of the International Consortium on Landslides
Peter Bobrowsky, Immediate past President of the International Consortium on Landslides

Advisory Members for KLC2020

Abou Amani, Director, Division of Water Sciences, Secretary, Intergovernmental Hydrological Programme (IHP), UNESCO
Soichiro Yasukawa, Programme specialist, Coordinator for Disaster Risk Reduction and Resilience, UNESCO
Daniel Lebel, Director General, Geological Survey of Canada, Natural Resources Canada, Canada
John Ludden, President of the International Union of Geological Sciences (IUGS)
John LaBrecque, Chair of IUGG GeoRisk Commission, Center for Space Research, University of Texas at Austin, USA
Rafig Azzam, President of the International Association for the Engineering Geology and the Environment (IAEG)
Paolo Canuti, past President of the International Consortium on Landslides (ICL), Italy
Sàlvano Briceño, First chair of the Global Promotion Committee of the International Programme on Landslides
Badaoui Rouhban, Chair of the KLC2020 Launching Session and Moderator of ISDR-ICL Sendai Landslide Partnerships 2015–2025 Session of 3rd WCDRR in 2015

KLC2020 Official Promoters

Host Organization

International Consortium on Landslides (ICL)/Nicola Casagli

Public Sectors: KLC2020 Official Promoters-Public

International Unions/Associations, Governmental Organizations, Universities and Research Institutes

The International Union of Geological Sciences (IUGS)/John Ludden
The International Union of Geodesy and Geophysics (IUGG)/Kathy Whaler
The International Association for the Engineering Geology and the Environment/Rafig Azzam
International Geosynthetics Society (IGS)/John Kraus
Geological Survey of Canada, Natural Resources Canada, Canada/Daniel Lebel
Faculty of Civil and Geodetic Engineering, University of Ljubljana, Slovenia/Matjaž Mikoš

Private Sectors: KLC2020 Official Promoters-Private

Companies and Corporation

Standing Editors for KLC2020 Book Series

Editorial Office

Secretariat of the Kyoto Landslide Commitment 2020
International Consortium on Landslides (ICL)
138-1 Tanaka-Asukai cho, Sakyo-ku, Kyoto 606-8226, Japan
E-mail: klc2020@iclhq.org

Global Promotion Committee of the International Programme on Landslides and Kyoto Landslide Commitment 2020

A Commitment to the Sendai Framework and the Sustainable Development Goals

Chair

Matjaž Mikoš (Faculty of Civil and Geodetic Engineering, University of Ljubljana)

Co-chairs

Qunli Han (Integrated Research on Disaster Risk, IRDR)
Soichiro Yasukawa (Programme Specialist on Disaster Risk Reduction, UNESCO, Paris)
Hiroshi Kitazato (Treasurer of IUGS)
John LaBrecque (Chair of IUGG GeoRisk Commission)

Secretary

Kyoji Sassa (IPL World Centre, Director)

Members of the IPL-KLC Global Promotion Committee

ICL Full Members

Geotechnical Engineering Office, Hong Kong, China; UNESCO Chair for the Prevention and the Sustainable Management of Geo-hydrological Hazards—University of Florence, Italy: Korea Institute of Geoscience and Mineral Resources (KIGAM), Korea; Faculty of Civil and Geodetic Engineering, University of Ljubljana (ULFGG), Slovenia; and other members (total 59 members from 29 countries/regions).

ICL Supporting Organizations

UNESCO, UNDRR, WMO, FAO, UNU, ISC, WFEO, IUGS, IUGG, Government of Japan (CAO, MEXT, MAFF, MLIT)

KLC2020 Official Promoters

Host Organization

International Consortium on Landslides (ICL)/Nicola Casagli

Public Sectors: KLC2020 Official Promoters—Public

- The International Union of Geological Sciences (IUGS)/John Ludden
- The International Union of Geodesy and Geophysics (IUGG)/Kathy Whaler
- The International Association for the Engineering Geology and the Environment (IAEG)/Rafig Azzam

- International Geosynthetics Society (IGS)/John Kraus
- Geological Survey of Canada, Natural Resources Canada, Canada/Daniel Lebel
- Faculty of Civil and Geodetic Engineering, University of Ljubljana, Slovenia/Matjaž Mikoš
- China University of Geosciences, Wuhan, China/Huiming Tang
- Department of Civil Engineering, National Taiwan University, Chinese Taipei/Shang-Hsien Hsien
- Institute of Rock Structure and Mechanics, the Czech Academy of Sciences/Josef Stemberk
- Institute of Cold Regions Science and Engineering, Northeast Forestry University, China/Wei Shan

Private Sectors: KLC2020 Official Promoters—Private

- Marui & Co. Ltd, Japan
- Nippon Koei Co., Ltd, Japan
- Ellegi srl, Italy
- IDS GeoRadar s.r.l., Italy
- Chuo Kaihatsu Corporation, Japan
- Godai Corporation, Japan
- Kiso-Jiban Consultants Co., Ltd, Japan
- Kokusai Kogyo Co., Ltd., Japan
- OSASI Technos, Inc., Japan

IPL World Centre

IPL World Centre (IWC) was established in 2006 by the Tokyo Action Plan to serve, as it does, as the secretariat of IPL,GPC/IPL as well as of UNITWIN UNESCO-KU-ICL Programme. IWC also serves as the secretariat of KLC2020. IWC is a part of the legal body (NPO-ICL registered in Kyoto, Japan) of ICL. The Council of the IWC consists of advisors from Ministry of Education, Sports, Science and Technology, Ministry of Agriculture, Forestry and Fisheries, Ministry of Land, Infrastructure and Tourism of the Government of Japan, UNESCO, and of members from ICL Headquarters, chairs of GPC/IPL-KLC, presidents and officers of ICL.

Secretariat of GPC/IPL-KLC

Secretary

Kyoji Sassa
International Consortium on Landslides
138-1 Tanaka-Asukai cho, Sakyo-ku, Kyoto 606-8226, Japan
Tel: +81 (75) 723 0640
Fax: +81 (75) 950 0910
E-mail: klc2020@iclhq.org
URL: https://www.landslides.org/; https://www.landslides.org/ipl-info/
UNITWIN UNESCO-KU-ICL Programme
UNITWIN Headquarters Building
Kyoto University Uji Campus
Uji, Kyoto 611-0011, Japan
E-mail: unitwin@iclhq.org

Contents

Editorial of the New Open Access Book Series "Progress in Landslide Research and Technology"

Kyoji Sassa

Abstract

The Kyoto Landslide Commitment 2020—A Commitment to the ISDR-ICL Sendai Partnerships 2015–2025, the Sendai Framework for Disaster Risk Reduction 2015–2030, the 2030 United Nations Agenda Sustainable Development Goals, the New Urban Agenda, and the Paris Climate Agreement was established with signatures by 90 partner organizations in November 2020 (Sassa in Landslides 18:5–20, 2021). To secure and provide a global and stable platform for the Kyoto Landslide Commitment 2020 to be continued until 2030 and beyond, an open access book series was proposed by the KLC2020 Secretariat in 2022. The high-level panel discussion during the Fifth World Landslide Forum examined the proposal, and all panelists and participants accepted the proposal. Then, the Launching Declaration of the ICL Open Access Book Series "Progress in Landslide Research and Technology" for the Kyoto Landslide Commitment 2020 was adopted by all panelists and the onsite and online participants of WLF5 on 3 November 2021 (Sassa in Landslides 19:1–5, 2022). This article is a progress report of the founding two issues of "Progress in Landslide Research and Technology" in 2022 for all authors, potential readers of this book series as well as KLC2020 signatory partners, KLC2020 official promoters, and ICL members.

Keywords

Open access book series • Kyoto Landslide Commitment 2020 • ICL journal landslides • ICL book series P-LRT

1 Introduction

A new open access book series "Progress in Landslide Research and Technology (P-LRT)" has been launched in 2022 as the core platform for the prometon of Kyoto Landslide Commitment 2020—A Commitment to the ISDR-ICL Sendai Partnerships 2015–2025, the Sendai Framework for Disaster Risk Reduction 2015–2030, the 2030 United Nations Agenda Sustainable Development Goals, the New Urban Agenda and the Paris Climate Agreement.

The International Consortium on Landslides launched the ICL official journal, ***Landslides***: Journal of the International Consortium on Landslides. It was the first international journal on landslides, aiming to integrate landslide research in many fields of science as a scientific field studying landslide phenomena, namely landslide science. Vol. 1 in 2004 was comprised of 80 pages/issue × 4 issues, namely 323 pages/year. This journal was well received by many scientists studying landslides. This journal's total number of pages increased to 3977 pages/year in 2021 over the last 19 years. It is now a good platform for landslide science.

In order to promote the Kyoto Landslide Commitment 2020, practical application of the recent progress in landslide research and technology for landslide disaster risk reduction must be sought for practice and society. To pursue this aim, a new open access book series, "Progress in Landslide Research and Technology" was founded. The target readers of the open access book series are practitioners and other stakeholders who apply in practice the most advanced knowledge of science and technology for landslide disaster risk reduction. Articles must be written in a simplified way that is easily understandable by these practitioners and stakeholders.

K. Sassa (✉)
The International Consortium on Landslides and KLC2020 Secretariat, Kyoto, Japan
e-mail: secretariat@iclhq.org

I. Alcántara-Ayala et al. (eds.), *Progress in Landslide Research and Technology, Volume 1 Issue 2, 2022*, Progress in Landslide Research and Technology,
https://doi.org/10.1007/978-3-031-18471-0_1

2 Categories of P-LRT

1. **Original articles reporting the progress of landslide research and technology (minimum 8 pages)**

Articles must be written user-friendly for practice. An author is requested to write an easy-to-understand article, allowing readers to apply it for practice without searching for references in other publications, with a substantial number of figures, photos, elaborate explanations, and videos when necessary. Thus, P-LRT limits the minimum page number for each category. The maximum limit of pages is not pre-decided. The followings are eight regular categories of P-LRT.

2. **Review articles (minimum 8 pages)**

Review of landslide research and technology in a thematic area of landslides. A review article integrating a series of research and technology of the author or its group is also welcome.

An active researcher and active research group have published a specific topic or finding as short articles in many journals. For practical purposes, a long article integrating all related findings is effective to understand the whole concept and apply it to practices.

3. **ICL landslide lessons (minimum 20 pages)**

Lessons by global and emerging experts with distinguished achievements in one of the specific aspects in understanding and reducing landslide disaster risk.

This category is a new category. Then, no article was published in Vol. 1, No. 1, and Vol. 1, No. 2.

More than 20 pages of landslide lessons are expected in Vol. 2 in 2023 which is useful for landslide risk reduction activities.

4. **IPL/WCoE/Kyoto Commitment activities (minimum 8 pages)**

Progress or achievements of the projects of the International Programme on Landslides (IPL) and the World Centres of Excellence on Landslide Risk Reduction (WCoEs), and the Kyoto Landslide Commitment.

This category was included in "Journal Landslides" until 2021. However, this category in "Journal Landslides" was terminated and moved to P-LRT. IPL ad WCOE and Kyoto Landslide Commitment are activities for landslide risk reduction.

5. **Teaching tools with online extras (minimum 8 pages)**

User-friendly teaching tools with extras (i.e., photos, illustrations, videos, guidelines & manuals) online to fill the gap between the available level of science and technologies and their practical use in society. This category cannot be included in any journal. Very necessary and useful for mastering some technologies. Vol. 1, No. 1 includes LS-RAPID landslide simulation manuals 58 pages) for the whole process from stable ground to initial local failure, progressive failure, creating a landslide body, rapid landslide motion, and termination with 17 video tutorials. Vol. 1, No. 2 includes "Teaching tools "Undrained dynamic loading ring shear testing with video" (35 pages) with 16 video tutorials. Vol. 1, No. 2 includes another teaching tool "How to Teach Remotely the Vegetation Works to Protect Slopes against Mass Wasting: A Case of Using Video Materials in Bhutan."

6. **Technical notes & Case studies (minimum 4 pages)**

Technical note and case studies on landslides and landslide disaster risk reduction practice. Each issue of Vol. 1, No. 1 and No. 2 includes one technical notes and case studies.

7. **World Landslide Reports**

Landslide reports from landslide-prone developing countries and urbanizing areas of the developed countries from around the world. No book processing charge, but limited to approximately 40–50 pages (around 10% of the total page) per issue. These categories are planned to accommodate Landslide reports mainly from landslide-prone developing countries. 3 reports were submitted from Bangladesh, Vietnam, and Iran to Vol. 1, No. 2.

8. **Introduction of KLC2020 Official Promoters (1–3 pages)**

KLC2020 Official Promoters are eligible for this category. The introduction of the official promoters is published in all issues throughout the year.

Remarks for categories

"Editorial" is an article written or invited by the Editorial Board. This is one of categories of this book series which will be published in front of regular categories of articles. Editorials are not open-call categories. But proposals for Editorial are welcome. Please contact the Secretariat of the Kyoto Landslide Commitment 2020, <E-mail: klc2020@iclhq.org>.

3 Photo/Illustration on the Front Cover of P-LRT

The front cover of each issue includes a photo or an illustration published in the issue. The editorial board examined the cover photo/illustration of Vol. 1, No. 1 and selected one photo from "Early warning system against rainfall-induced landslide in Sri Lanka by Konagai et al." The final design of the cover will be made by Springer Nature. The selected cover photo is shown in Fig. 1. Photo/Illustration on the Front cover of Vol. 1, No. 2 is not yet decided at the time of writing this article.

4 Contents of Vol. 1, No. 1

The founding issue is very special. Three forewords from the ICL, the International Union of Geological Sciences, the International Union Geodesy and Geophysics, and three greetings of the 5th World Landslide Forum from United Nations Organizations which support the International Consortium on Landslides, the International Programme on Landslides, and the Kyoto Landslide Commitment 2020 are published before the table of contents.

After the table of contents before regular categories, three articles are presented prior to articles in regular categories; (1) Preface for aim and outline of this book series, (2) History of the International Consortium on Landslides as the proposer of the Kyoto Landslide Commitment 2020, and (3) Programme of the ICL "International Programme on Landslides."

Forewords

- President Nicola Casagli of the ICL (with video)
- President John Ludden of the International Union of Geological Sciences (IUGS) (with video)
- President Kathy Whaler of the International Union Geodesy and Geophysics (IUGG) (with video).

Greetings of the 5th World Landslide Forum

- Mami Mizutori, Special Representative of UN Secretary-General for Disaster Risk Reduction/Head of UN Office for Disaster Reduction
- David Malone, UN Under-Secretary-General/Rector of United Nations University (with video)
- Shamila Nair-Bedouelle, Assistant Director-General for Natural Sciences of UNESCO (with video).

Fig. 1 Cover photo of Vol. 1, No. 1 Aranayaka landslide in Kegalle District, Sri Lanka occurred in May 2016, after a long rainfall and killing 127 persons and destroying 75 houses (Technical Cooperation for Landslide Mitigation Project by JICA. All rights reserved)

Preface

Aim and Outline of the Book Series "Progress in Landslide Research and Technology" (9 pages) by Kyoji Sassa and Matjaž Mikoš.

Introduction of ICL and IPL

- International Consortium on Landslides: from IDNDR, IGCP, UNITWIN, WCDRR 2 & 3 to Kyoto Landslide Commitment 2020 (35 pages) by Kyoji Sassa, Paolo Canuti, Peter Bobrowsky, and Nicola Casagli.

This article describes the history of ICL starting from IDNDR (International Decade for Natural Disaster Reduction) and the UNESCO-IUGS Joint programme IGCP-425: Landslide Hazard Assessment and Cultural Heritage (1998–2003) to Kyoto Commitment 2020.

- International Programme on Landslides—A Short Overview of its Historical Development (19 pages) by Matjaž Mikoš, Kyoji Sassa, Qunli Han.

This article describes the initial foundation of the International Programme on Landslides—IPL at UNESCO in 2002. The current second stage of IPL was defined and established by the 2006 Tokyo Action Plan "Strengthening Research and Learning on Landslides and Related Earth System Disasters for Global Risk Preparedness." The ICL exchanged a Memorandum of Understandings to promote IPL with each of the ICL supporting organizations: five UN organizations and 2 global stakeholders on science and engineering. All IPL activities in the past were overviewed.

Review of the Founding Issue of P-LRT for all regular articles other than the above of Vol. 1, No. 1 was made by Sassa S (2022).

5 Authors and Articles in Vol. 1, No. 1 and No. 2

On the day of writing this article, both issues have not yet been published. Vol. 1, No. 1 is now being processed for publication in Springer Nature. It will be published in December 2022. All accepted articles of Vol. 1, No. 2 have been sent to Springer Nature. It will be published in December 2022.

Two initial issues are reviewed to share the information of the founding issues of the open access book series with readers, authors/editors/official promoters, and other people involved in understanding and reducing landslide disaster risk.

Figure 2 presents the authors of articles in the main six categories (Editorial, Original articles, Review articles, IPL/WCOE/KLC activities, Teaching Tools, Technical Notes and Case studies) excluding six forwards/greetings and introduction of 16 official promoters in Vol. 1, No. 1. The total number of authors is 120 persons from 24 countries, UNESCO and the International Geosynthetics Society. The largest number of authors are from Japan and Italy, both are 20. More than 5 authors are from Canada (8), Slovenia (7), Indonesia (6), Thailand (6) and USA (6), Czech (5), France (5), Sri Lanka (5), and UK (5).

Figure 3 presents the authors of articles in the main seven categories (Editorial, Original articles, Review articles, IPL/WCOE/KLC activities, Teaching Tools, Technical Notes and Case studies, and World Landslide Reports) in Vol. 1, No. 2.

The total number of authors is 102 persons from 18 countries/regions. The largest number of authors is 31 from Japan. More than 5 authors are 14 from Vietnam, 9 from Canada and Croatia, 7 from India, 6 from China and Ukraine, and 5 from Chinese Taipei.

6 Title and Contents of the Open Access Book Series

At the launching of this book series, the ICL terminated all other book publications and proceedings such as books for the triennial World Landslide Forum and proceedings for the annual IPL Symposium in 2022. Therefore, ICL publication is the following one journal and one book series.

Landslides: Journal of the International Consortium on Landslides

Progress in Landslide Research and Technology: Book Series of the International Consortium on Landslides

Different from most other book series, each issue title of this book series is the book series title + Volume Number-Issue number + publication year as below.

Book Series Title: Progress in Landslide Research and Technology

Issue Title for Vol. 1, No. 1: Progress in Landslide Research and Technology, Volume 1 issue 1, 2022
Issue Title for Vol. 1, No.2: Progress in Landslide Research and Technology, Volume 1 issue 2, 2022

Table 1 presents the total pages and the breakdown of Vol. 1, No. 1, and Vol. 1, No. 2 of P-LRT. The total number of pages is 426 pages for Vol. 1, No. 1, and 413 pages for Vol. 1, No. 2.

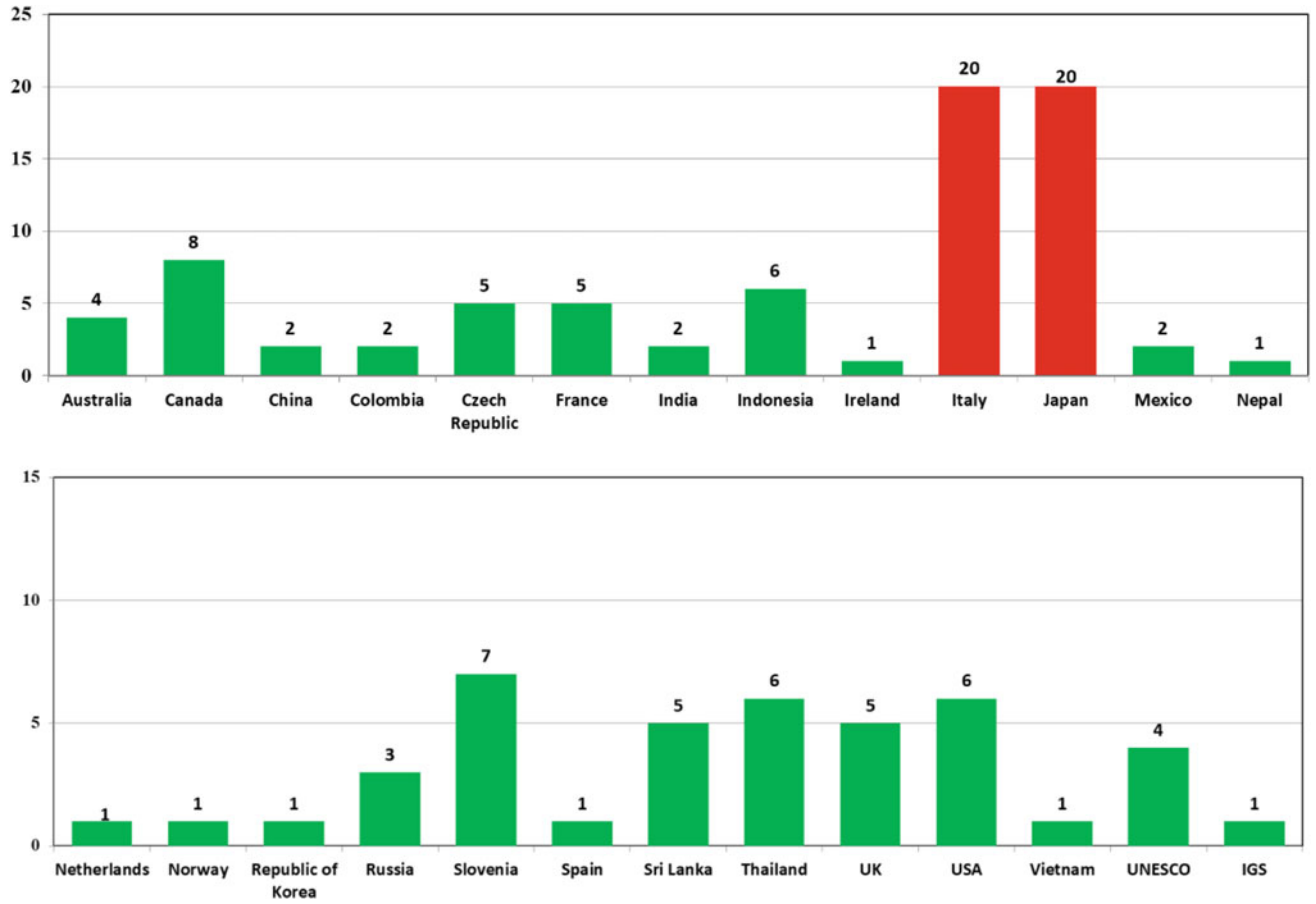

Fig. 2 The number of authors from each country, United Nations organization, and international organization in the six categories of articles published in Vol. 1, No. 1

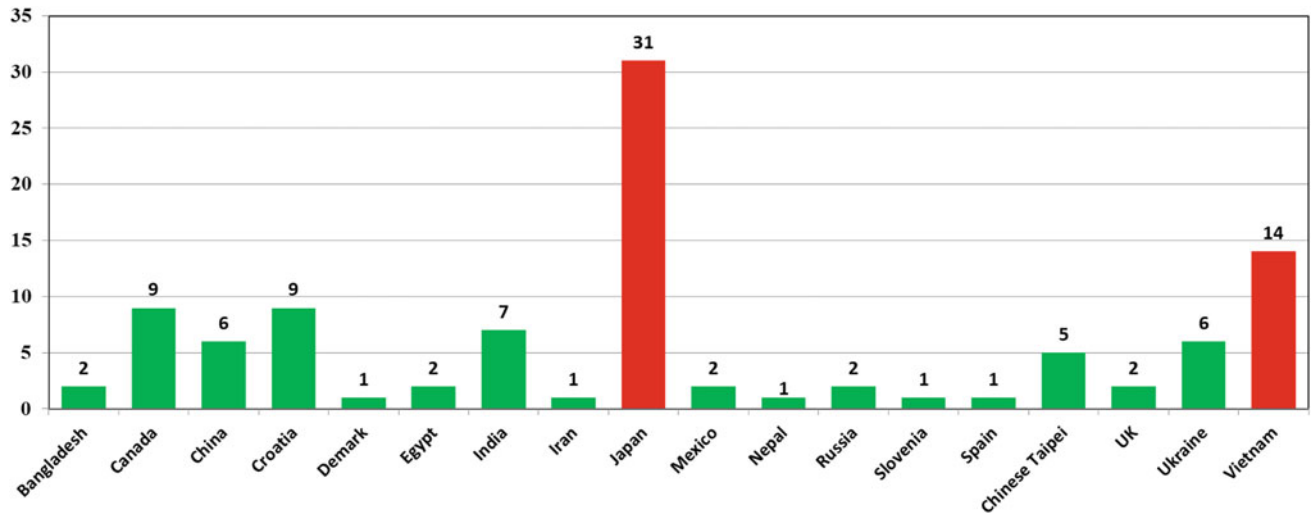

Fig. 3 The number of authors from each country/region in the seven categories of articles published in Vol. 1, No. 2

Table 1 Total pages and breakdown of Vol. 1–1 and Vol. 1–2

Vol. 1, No. 1			Vol. 1, No. 2		
Breakdown	Number of articles	Number of pages	Breakdown	Number of articles	Number of pages
Front matters	3	7	Front matters	3	7
Forewords/greeting	6	12	Forewords	0	0
Table of contents	1	4	Table of contents	1	5
Editorial (ICL history and IPL overview)	3	63	Editorial	1	7
Original articles	11	123	Original articles	13	150
Review articles	1	5	Review articles	6	73
IPL/WCOE/KLC activities	10	116	IPL/WCOE/KLC activities	4	58
Teaching tools	1	58	Teaching Tools	2	42
Technical notes and case studies	1	8	Technical notes and case studies	1	7
World landslide reports	0	0	World landslide reports	3	34
Official promoters	16	28	Official promoters	16	28
Back matters	1	2	Back matters	1	2
Total	54	426	Total	51	413

The Vol. 1, No. 1 issue contains 27 articles (total 373 pages) with DOI numbers, and the Vol. 1, No. 2 issue contains 30 articles (total 371 pages) with DOI numbers. The category of original articles constitutes the largest number of articles (11) and the largest number of pages (123 pages) for Vol. 1, No. 1, and those numbers are 13 articles and 150 pages respectively for Vol. 1, No. 2.

The category of the IPL/WCOE/KLC activities includes 10 articles with 116 pages in Vol. 1, No. 1, and 4 articles and 58 pages in Vol. 1, No. 2. The category of Teaching tools with video tutorials includes 1 article in Vol. 1, No.1, 2 articles in Vol. 1, No. 2. Teaching tools with video tutorials will be very effective in the technical transfer for the landslide risk reduction. The new category of articles in Vol. 1, No. 2 is the World Landslide Reports from developing countries. The book processing fee is free for this category. The KLC2020 official promoters are introduced at the last of each issue.

7 Rate (%) of the Numbers of Articles and Pages of Each Category

We analyzed the rate of the number of articles and pages of each category and the difference between the No. 1 and No. 2 issues in the four pie charts of Figs. 4 and 5.

Figure 4 presents Rate (%) of six categories (Editorial, Original articles, Review articles, IPL/WCOE/KLC, Teaching Tools, Technical notes and Case studies) in Vol. 1, No. 1.

The largest category both in the article number and the page number is the original article, and 40.74 and 32.98 respectively. The next category both in the article number and the page number is IPL/WCOE/KLC activities.

IPL/WCOE/KLC activities were included in Landslides: Journal of International Consortium on Landslides until the year 2021. But this category in the Journal was terminated and moved to this book series. The maximum number of pages of this category in the Journal was 6 pages. The maximum number of pages is not specified in this book series, but the minimum number of pages is specified as 8 pages. A Report of Word Centre of Excellence (WCoE) from India in Vol. 1, No. 2 is 29 pages. Other reports are 19 pages from Japan, 17 pages from Canada, and others. Those reports of activities of WCoEs, IPL (International Programme on Landslides) projects, and other KLC2020 activities are very important for Kyoto Landslide Commitment. Those long articles shall promote the understanding and reducing landslide disaster risk in other countries and regions.

Figure 5 presents Rate (%) of seven categories (Editorial, Original articles, Review articles, IPL/WCOE/KLC activities, Teaching Tools, Technical Notes and Case studies, and World Landslide Reports) in Vol. 1, No. 2.

The largest category both in the article number and the page number is original article, and 43.33 and 40.43 respectively. Both rates are greater than those in Vol. 1, No. 1 (40.74 and 32.98).

The next category both in the article number and the page number is Review articles, and 20.00 and 19.68 respectively.

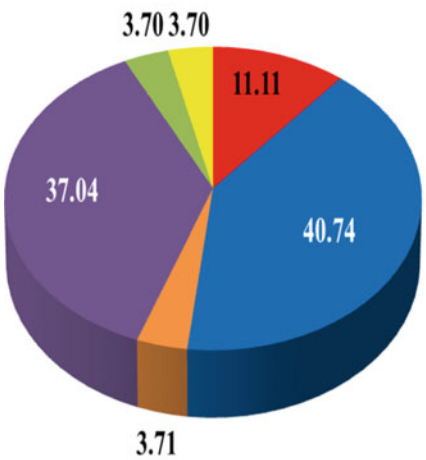

A: Rate (%) of six categories in article number
Total number: 27 articles

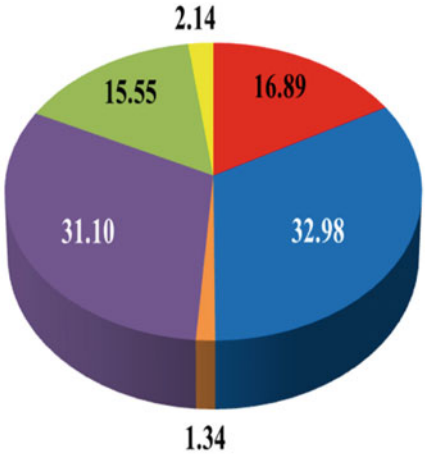

B: Rate (%) of six categories in page number
Total number: 373 pages

Editorial	Original articles	Review articles	IPL/WCOE/KLC activities	Teaching Tools.	Technical Note and Case studies

Fig. 4 Rate (%) of six categories (Editorial, Original articles, Review article, IPL/WCOE/KLC, Teaching Tools, Technical Notes) in Vol. 1, No. 1

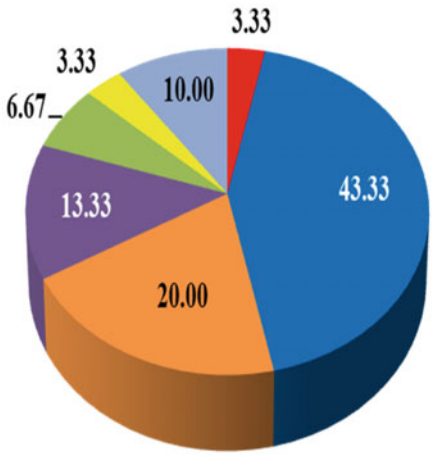

A: Rate (%) of seven categories in article number
Total number: 30 articles

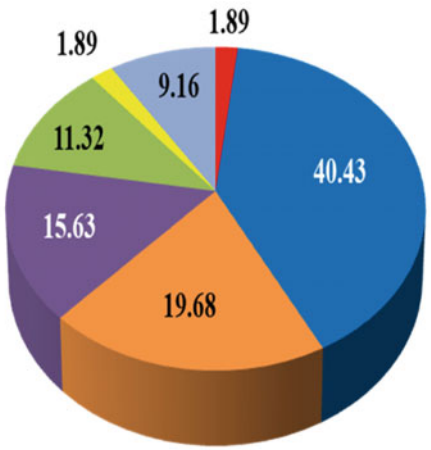

B: Rate (%) of seven categories in page number
Total number: 371 pages

Editorial	Original articles	Review articles	IPL/WCOE/KLC	Teaching Tools.	Technical Notes	World Landslide Reports

Fig. 5 Rate (%) of seven categories (Editorial, Original articles, Review articles, IPL/WCOE/KLC, Teaching Tools, Technical Notes and World Landslide Reports) in Vol. 1, No. 2

This is different from those in Vol. 1, No. 1. The upper limit of page number is not specified in all categories. However, the rate of the number of articles and number of pages are close both in No. 1 and No. 2.

The number of articles for Technical notes and Case studies is very small.

The definition of original articles in the Journal "Landslides" is original scientific research and investigation.

The definition of original articles in P-LRT is original articles reporting the progress of landslide research and technology.

Namely original articles in Journal "Landslides" requires originality in scientific research and technology. Many papers undergo changes in categories from original articles to Technical Notes and Case studies during the review process of the Journal Landslides. During the further progress of the publication of P-LRT, we will examine what is the best edition of the book series for the technical and scientific knowledge transfer to promote landslide disaster risk reduction.

Acknowledgements On behalf of the Kyoto Landslide Commitment 2020 and the International Consortium on Landslides, I extend my sincere thanks to all of 120 authors for Vol. 1, No. 1 and 102 authors for Vol. 1, No. 2 of the founding issues of the new book series "Progress in Landslide Research and Technology."I appreciate all editors working for Vol. 1, No. 1 and Vol. 2, No. 2. The KLC2020 Secretariat as well as the ICL thank for the KLC2020 official promoters who promote the Kyoto Landslide Commitment 2020 and provide financial support for the implementation of the KLC2020 activities.The founding issue of this book acknowledged three forewords from ICL President, IUGS President, IUGG President, and three greetings from the Special Representative of UN Secretary General for Disaster Risk Reduction, UN Under-Secretary General/Rector of United Nations University, and Assistant Director-General for Natural Sciences of UNESCO. Those supports have encouraged all people contributing to this book series.

References

Sassa K (2021) The Kyoto Landslide Commitment 2020: launched. Landslides 18:5–20. https://doi.org/10.1007/s10346-020-01575-4

Sassa K (2022) The Fifth World Landslide Forum and progress of the open access book series for Kyoto Landslide Commitment 2020. Landslides 19:1–5. https://doi.org/10.1007/s10346-021-01820-4

Sassa S (2022) Review of the founding issue of P-LRT: progress in landslide research and technology. Prog Landslide Res Technol 1(2) (in this issue)

Original Articles

Key Techniques of Prevention and Control for Reservoir Landslides Based on Evolutionary Process

Huiming Tang, Liangqing Wang, Changdong Li, and Zongxing Zou

Abstract

The essence of reservoir landslide treatment is to change its evolution process. It is hard to guarantee the effectiveness and safety of the landslide prevention and control technology that ignores the evolution processes. Guided by the thought of evolution, this study introduced some key techniques of reservoir landslide prevention and control. Seven evolution modes are summarized for rock slides and the optimal control measures suitable for each evolution mode and different evolution stages are suggested. The dynamic stability evaluation method is proposed considering the evolution process of the slip zone soil strength. This study introduces the methods for determining optimal pile positions for step-shaped sliding surfaces, the optimal plane arrangement of stabilizing piles, and their reasonable embedded lengths. Finally, two demonstration bases for comprehensive prevention and control of large reservoir landslides that were established in the Three Gorges Reservoir area (TGRA) were introduced, which is of great scientific and application value to the improvement of reservoir landslide prevention and control techniques.

Keywords

Reservoir landslide • Landslide prevention and control • Evolution process • Demonstration base

1 Introduction

Landslide, one of the world's major geohazards, are often accompanied by huge social and economic losses and poses a great threat to human lives as well as sustainable development. Water is one of the main driving factors of landslide evolution, especially for those located in reservoir areas (Zhang et al. 2021). The hydrogeological conditions have undergone significant and continuous changes under the impact of the long-term fluctuation of reservoir water level and seasonal rainfall, which increased the difficulty of reservoir landslide prevention and control. For instance, since the first impoundment in 2003, a total of 4256 large-scale landslides have been identified in the world-renowned Three Gorges Reservoir area (TGRA), costing the government up to 100 billion RMB in the treatment, yet many challenges remained (Tang et al. 2019). Reservoir landslide has become an important factor threatening the safety of waterborne transport and engineering construction in reservoir areas, and it is urgent to carry out in-depth research on its prevention and control.

Deficiencies still exist in the current research on reservoir landslide prevention and control. On the one hand, reservoir landslides have the basic characteristic of evolution, which is accompanied by different evolution modes and evolution stages that are highly related to the landslide's structural development, deformation failure patterns, and deterioration law of physical and mechanical parameters. The design of reservoir landslide control measures that ignore these factors fails to fully consider the synergistic effect of the landslide-control-structure system, which makes it difficult to guarantee its control effect and long-term stability of

H. Tang (✉) · L. Wang
Faculty of Engineering, China University of Geosciences, Wuhan, 430074, Hubei, China
e-mail: tanghm@cug.edu.cn

L. Wang
e-mail: wangliangqing@cug.edu.cn

C. Li · Z. Zou
Badong National Observation and Research Station of Geohazards, China University of Geosciences, Wuhan, 430074, China
e-mail: lichangdong@cug.edu.cn

Z. Zou
e-mail: zouzongxing@cug.edu.cn

I. Alcántara-Ayala et al. (eds.), *Progress in Landslide Research and Technology, Volume 1 Issue 2, 2022*, Progress in Landslide Research and Technology,
https://doi.org/10.1007/978-3-031-18471-0_2

landslide. On the other hand, although institutions worldwide have attached great importance to the role of large in-situ test bases in geohazard research, few relevant demonstration bases have been built in the field of reservoir landslide prevention and control. Therefore, it is essential to carry out the study on reservoir landslide prevention and control techniques based on evolutionary processes and construct relevant demonstration bases.

2 Evolution Modes of Reservoir Landslide

By analyzing the geological structure, development pattern, evolutionary characteristics, and evolutionary process of reservoir landslides, seven types of rock landslide evolution modes are summarized as shown in Fig. 1. Seven evolution mode include progressive slip along gentle-dip layer I, progressive slip along gentle-dip layer II, bucking failure along steep-dip layer, creep slip along deep layer, plastic flow slip of weak interlayer, breakthrough abrupt slip in inclined cross-cutting layer and toppling failure in steep anti-dip layer. Each of the above evolution modes is divided into three evolutionary stages, and the corresponding evolutionary features of each evolutionary stages are described as follows.

For the mode of progressive slip along gentle-dip layer I (Fig. 1a), vertical tension cracks appear on the surface of the slope's frontal part under the manual excavation or river cutting in its stage I, named the leading edge unloading rebound stage. Then, in the crack extension stage (stage II), surface water seeps in along these cracks and accelerate the process of erosion or dissolution, so the cracks continue to expand in depth, which causes a new unloading effect on the rock mass behind the cracks, forming multiple sets of parallel tension cracks. Eventually, in the sliding surface penetration damage stage (stage III), the sliding mass keeps creeping until the mechanical properties of the slip zone are weakened to fail to balance the sliding force.

Different from the previous mode, progressive slip along gentle-dip layer II's cracks develop from the trailing edge to the leading edge of the landslide (Fig. 1b). In stage I, also called the trailing edge tension fracture formation stage, the crack is formed under the joint effect of the tensile stress and surface water at the trailing edge of the landslide. In stage II, (crack extension stage), the cracks develop from the surface to the deep until the underlying weak interlayer of the landslide is cut. In stage III (sliding surface penetration damage stage), the weak layer or sliding zone of the landslide is further softened and cracks expand into the trenches under the continuous effect of rainfall and gravity. When heavy rainfall continues in the landslide area, the sliding surface gradually penetrates, and the trailing edge fissure water provides lateral gradient force. Once the sliding force of the upper rock mass exceeds the resistance force providing by the sliding surface, the landslide occurs.

In stage I of bucking failure along steep-dip layer mode (Fig. 1c), also called the slight bending and deformation stage, the buoyancy between rock layers gradually increases and the shear strength of weak layer gradually decreases under the effect of rainfall and groundwater. Affected by this, the stratum of the landslide's shallow surface of the upper part began to creep, and the lower part is squeezed under gravity. In the creeping and squeezing, the trailing edge rock starts cracking and bending at the slope toe. During this process, the landslide comes to stage II (bending bulge loosening stage), and the interlaminar dislocation of the landslide shallow stratum gets increasingly intense. It led to the formation of a tension collapse zone at the trailing edge and a bending shape with a tension fracture zone at the toe of the landslide. Finally, with the gradual penetration of the tension fracture zone and the gradual enlargement of the tension collapse zone, the leading edge of the landslide slides out along the tension fracture zone and the rock stratum at the trailing edge slides along the sliding surface, that is, collapse slip stage (stage III).

The creep slip along deep layer mode includes three stages: deep slip zone formation stage (stage I), creep-slip stage (stage II), and start-slip destabilization stage (stage III) (Fig. 1d). During stage I, various factors such as gravity, tectonic movement, river undercutting and rainfall make the deep shear stresses of unstable slopes develop and concentrate, and then the creep shearing occurs locally. Further, in the stage II, some shear creeping surface are gradually penetrated from the local to the whole affected by gravity, rainfall, and other external loads. Finally, affected by the river erosion and water level fluctuation, deformation and failure occur in the location of steep terrain with groundwater retention, and even overall sliding failure.

As shown in Fig. 1e, the evolution stages of plastic flow slip of weak interlayer mode differ significantly. In the trailing edge crack formation stage (stage I), the deep weak layer flows to the free face affected by various external factors, causing tensile stress in the middle and rear part of the landslide. Cracks begin to appear under tensile stress and gradually increase and deepen with the continuous plastic flow of the landslide. In the subsequent crack extension stage (stage II), the sliding mass moves along the weak structural plane as a whole with the tension cracks developed. The sliding mass disintegrates under differentiated plastic flow developed in the uneven weak layer. Finally, the sliding zone expends laterally driven by the finest path of shear stress elimination. The expending process is terminated by its slipping-off separation in the overall slip disintegration stage (stage III).

At the beginning of breakthrough abrupt slip in inclined cross-cutting layer mode, affected by tectonic stress and

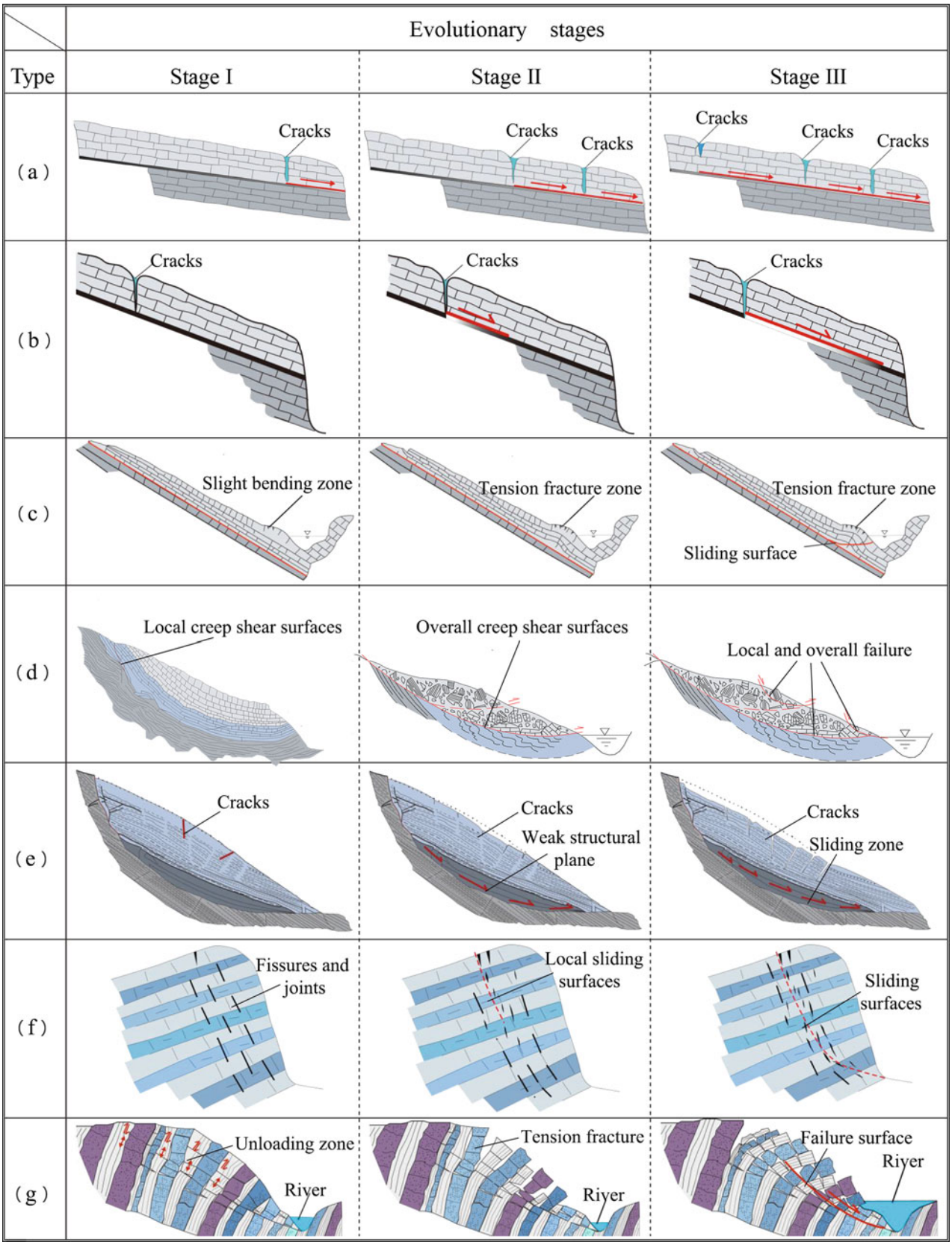

Fig. 1 Seven evolution types and stages of reservoir rock landslide

unloading rebound effect, initial fissures and joints develop in the shallow surface layer parallel to the slope surface, which is summarized as the intra-layer tensile fracture formation stage (stage I) (Fig. 1f). Under internal and external effects, the strength of the rock mass continues to decrease. Therefore, the tension fracture continues to expand and the local sliding surfaces start connecting, which is called the tension fracture development stage (stage II). With the continuous expansion of tension fracture, the sliding surface continues to develop towards the slope toe. When the sliding surface is totally formed, the whole rock mass falls, which is the cut layer fracture penetration stage (stage III).

For the toppling failure in steep anti-dip layer mode (Fig. 1g), initial toppling is its stage I, where, the rock mass undergoes interlayer shear movement due to a strong unloading rebound. Then, a certain depth of unloading zone is formed near the surface of the landslide, where the tension fracture is developed. The rock stratum begins to bend extensively towards the free surface and the tension fracture or tension deformation developed along the existing transverse joints, results in further segmentation of the rock column. Subsequently, the intact rock column is divided into several short rock columns by the new tension fracture and the existing transverse joints. The slope enters the self-stabilizing creep stage (stage II), in which the rock mass deforms at a low rate. With the rise of water level, a unified tension shear fracture surface is formed in the front part of the slope and shear slip occurs. The steep failure surface develops in depth and finally intersects with this tension shear fracture surface in front of the slope. Then, an interconnected shear surface is formed and results in an overall slicing slip, that is, the formation of unified shear surface and failure stage (stage III).

3 Suitability of Reservoir Landslide Control Measures Based on the Evolution Process

The evolution mechanism is an important aspect in the study of reservoir landslides. Most of the reservoir landslides are nurtured by tectonic dynamics and river valley dynamics, then evolve due to human engineering construction, and finally occur under the action of disaster-causing factors such as earthquakes, rainfall and reservoir water. During the evolution process, the landslide constantly undergoes structural changes and parameter deterioration, resulting in different forms of deformation and failure. The essence of reservoir landslide control is to change its evolution process. The effectiveness and long-term safety of reservoir landslide control measures that ignore this process are hard to guarantee. According to the division of seven reservoir landslide evolution modes and corresponding evolution stages, the specific control measures suitable for reservoir landslides in different evolution stages are suggested in Table 1. These measures have been successfully employed in the landslide management of the TGRA and have achieved satisfactory results.

Hongshibao landslide is a typical landslide management demonstration project in the TGRA that considered the landslide evolution process (Tang et al. 2019). Hongshibao landslide area is about 600 m long from north to south, higher in the south and lower in the north, with an elevation of 270–70 m and a width of about 500 m from east to west. Due to the characteristics of landslide evolution, various engineering countermeasures were used to reinforce the slope, including slope reduction and load shedding for the suitable slope position, setting retaining walls to improve the shallow stability and the arranging stabilizing piles in the slope. As shown in Fig. 2, the most effective protective measures are cantilever piles and anchor piles. Two rows of anti-slip piles were arranged to solve the problem of deep and shallow anti-slip stability of the site slope, and also to solve the slope stability problem caused by the reservoir water level changes sharply between 175 and 145 m. Based on the monitoring and observations reported, the above control measures have an effective and obvious control effect on the Hongshibao landslide.

4 Evaluation of Reservoir Landslide Dynamic Stability

With the evolution of landslides, the stability of landslides constantly evolves and develops, which is a dynamic process. Therefore, dynamic stability evaluation is required to evaluate the stability state of landslides.

Dynamic Stability Evaluation Method

In the evaluation of landslide stability, a dynamic stability evaluation method is proposed considering the evolution process of the slip zone soil strength. Firstly, the constitutive model and shear strength evolution model are developed for describing the relation between shear stress and shear displacement, and the relation between shear strength and shear displacement, respectively.

The strength properties are evolving during the process of the deformation and failure of slip zone soil, and the process is of continuous damage (Yan et al. 2022). From the aspect of damage theory, soil damage is regarded as a process of accumulation of plastic deformation in the soil and weakening of soil strength. Consequently, soil can be divided into two parts Fig. 3a: a damaged part and an undamaged part (or intact part). So, based on the Lemaitre strain equivalence hypothesis, the shear strength of slip zone soil can be formulated by,

Table 1 Recommended reservoir landslide control measures based on evolution process

Type	Evolution mode	Structural characteristics	Evolution stages		Recommended control measures
(a)	Progressive slip along gentle-dip layer I	① Gentle dip angle bedding rock structure; ② Medium to thick hard rocks; ③ Horizontal bedding plane	Stage I	Leading edge unloading rebound	Surface drainage
			Stage II	Crack extension	Surface drainage and the certain support measures in leading edge
			Stage III	Sliding surface penetration damage	Anchor cable support can be set when the slope is steep, and stabilizing piles combined with corresponding drainage measures can be set when the slope is gentle
(b)	Progressive slip along gentle-dip layer II	① Gentle dip angle bedding rock structure; ② Medium to thick hard rocks; ③ Horizontal bedding plane	Stage I	Trailing edge tension fracture formation	Surface and underground drainage
			Stage II	Crack extension	Surface and underground drainage, slope excavation and load shedding in the rear part
			Stage III	Sliding surface penetration damage	The combination of slope excavation and load shedding and prestressed anchor cables setting, supplemented by corresponding drainage measures
(c)	Bucking failure along steep-dip layer	① Steep dip angle bedding rock structure; ② Thin to medium bedding rock stratum; ③ Horizontal bedding plane	Stage I	Slight bending and deformation	Surface drainage
			Stage II	Bending bulge loosening	Surface and underground drainage, and slope toe pressed and backfilled if necessary
			Stage III	Collapse slip	Slope excavation and load shedding in the rear part, stabilizing pile set in the front part and supplemented by corresponding drainage measures
(d)	Creep slip along deep layer	① Steep dip angle in the upper part and gentle dip angle in the lower part bedding rock structure; ② Concave bending bedding plane	Stage I	Formation of deep sliding zone	Surface and underground drainage
			Stage II	Creep-slip	Underground drainage and supplemented by real-time monitoring of slope surface and deep slope displacement
			Stage III	Start-slip destabilization	Relocate residents if landslide is very large
(e)	Plastic flow slip of weak interlayer	① Bedding rock structure or quasi-homogeneous rock mass; ② Soft plastic belt under sliding mass	Stage I	Trailing edge crack formation	Surface and underground drainage
			Stage II	Crack extension	Drainage is the main concern, and anti-slip piles should be set at the front edge of the slope
			Stage III	Overall slip disintegration	Drainage and front support protection. Relocate residents if landslide is very large
(f)	Breakthrough abrupt slip in inclined cross-cutting layer	① Steep anti-dip bedding rock structure; ② Thin to medium bedding rock stratum; ③ Slight toppling bedding plane	Stage I	Intra-layer tensile fracture formation	Surface drainage
			Stage II	Tension fracture development	Surface and underground drainage, the front part is supplemented by certain support measures
			Stage III	Cut layer fracture penetration	Anchor cable support
(g)	Toppling failure in steep anti-dip layer	① Steep anti-dip bedding rock structure; ② Thin to medium bedding rock stratum; ③ Toppling bedding plane	Stage I	Initial toppling	Surface drainage
			Stage II	Self-stabilizing creep	Drainage, real-time monitoring of landslide
			Stage III	Formation of unified shear surface and failure	Prestressed anchor cable support, and backfill pressure monitoring in the leading edge

$$\tau = K_s u(1-D) + \tau_r D \tag{1}$$

where τ represents the shear stress in the microelement; u is the shear displacement; the damage degree D is a physical value reflecting the evolution process, which varies with the shear deformation of the soil, ranging from 0 to 1. K_s as the shear stiffness with a unit of kPa/mm, the slope of linear deformation stage in Fig. 3b. τ_r is the residual strength of the damage part, see in Fig. 3c.

The damage degree directly reflects the evolution of shear stress in the slip zone soil, and it can be solved from the perspective of statistical damage theory. So, it is assumed that the microelement strength of the slip zone soil obeys Weibull probability distribution in the process of shear damage:

$$p(x) = \frac{m}{u_0}\left(\frac{x}{u_0}\right)^{m-1} exp\left[-\left(\frac{x}{u_0}\right)^m\right] \tag{2}$$

Thus, the shear stress evolution equation of the slip soil is obtained as follows:

$$\tau = \begin{cases} K_s u, \ (u < u_y) \\ K_s u\left\{exp\left[-\left(\frac{u-u_y}{u_0}\right)^m\right]\right\} \\ +\tau_r\left\{1 - exp\left[-\left(\frac{u-u_y}{u_0}\right)^m\right]\right\}, (u \geq u_y) \end{cases} \tag{3}$$

where the parameters K_s, u_y and τ_r can be obtained by shear stress-shear displacement curve. The parameters u_0 and m in the model can also be further determined based on the properties of the curve. When the soil shear deformation is before the yield point, only elastic deformation occurs, that is $u < u_y$; when the soil deformation exceeds the yield point, the damage occurs in the soil, that is $u \geq u_y$.

Meanwhile, by adopting the property of peak point of τ–u curve, the model parameter u_0 and m can be solved as,

$$m = \frac{K_s(u_p - u_y)}{(K_s u_p - \tau_r) ln\left(\frac{K_s u_p - \tau_r}{\tau_p - \tau_r}\right)}, \ u_0 = \frac{u_p - u_y}{\sqrt[m]{ln\left(\frac{K_s u_p - \tau_r}{\tau_p - \tau_r}\right)}} \tag{4}$$

where u_p and τ_p are the shear displacement and shear stress corresponding to the peak point of the τ–u curve, respectively, in this peak point, it requires $\frac{\partial \tau}{\partial u}\big|_{u=u_p} = 0, \tau|_{u=u_p} = \tau_p$.

Based on the shear constative model and the linear relation between the model parameters and the normal stress, the evolution model of shear strength τ_s with the shear placements is expressed as (Fig. 4),

$$\tau_s = \begin{cases} \tau_p, \ (u < u_p) \\ K_s u\left\{exp\left[-\left(\frac{u-u_y}{u_0}\right)^m\right]\right\} \\ +\tau_r\left\{1 - exp\left[-\left(\frac{u-u_y}{u_0}\right)^m\right]\right\}, (u \geq u_p) \end{cases} \tag{5}$$

The shear strength of the slip zone soil evolves with the displacement, which leads to the stability factor of landslide evolves with the displacement. According to the force balance condition of the landslide slice along the sliding surface direction (Fig. 5), the residual thrust P_i of slice i based on the strength reduction method is as follows:

$$P_i = P_{i-1}\cos(\alpha_{i-1} - \alpha_i) + T_i - R_i/F_r \tag{6}$$

where P_{i-1} represents the residual thrust of slice $i-1$; α_{i-1} and α_i are the inclination angles of the sliding surface at slice $i-1$ and slice i, respectively, for the anti-warping part of the landslide, the value is negative; T_i represents the sliding component of the gravity of the slice i, $T_i = W_i \sin\alpha_i$; R_i is the anti-sliding force of slice i,$R_i = \tau_i l_i$; τ_i represents the shear strength provided by the slip zone at the slice i, which can be calculated by the shear constitutive model; F_r is the overall strength reduction factor.

Based on the equilibrium analysis of forces at the slice i in the direction perpendicular to the sliding surface, the normal stress σ_{ni} is formulated by,

$$\sigma_{ni} = \frac{P_{i-1}\ sin(\alpha_{i-1} - \alpha_i) + W_i'\ cos\,\alpha_i}{l_i} \tag{7}$$

where W_i' is the effective gravity of slice i, $W_i' = W_{1i}' + W_{2i}'$, and W_{2i}' is the effective gravity of the part of slice i below the groundwater level, that is, the effective gravity of the soil below the water level is used to calculate the anti-sliding force regardless of whether there is a stable seepage field or not.

Then, under the condition of the preset strength reduction factor F_r, calculate the residual thrust P_n by one from the first slice at the rear edge of the landslide by Eq. 6. When the landslide is in a critical state, that is limit equilibrium state, the strength reduction factor F_r in this state is defined as the stability factor F_s of the landslide. Since the Eq. 6 for solving the residual thrust contains the shear strength τ_i, which is an exponential function obtained from the shear constitutive model (Eq. 5). In the shear constitutive model, all parameters are related to the normal stress σ_{ni}, so the evolution of shear strength τ_i with displacement u is related to the normal stress σ_{ni}, and each landslide slice has different normal stress. Therefore, the solution of landslide stability factor is a highly nonlinear problem with an analytical expression of stability factor, which can only be calculated by an iterative method. The detailed flow of the landslide dynamic stability evaluation method is shown in Fig. 6.

The Case Study of Outang Landslide

The Outang landslide, a typical large deep bedding bedrock landslide in TGRA, is located in Anping Town, Fengjie

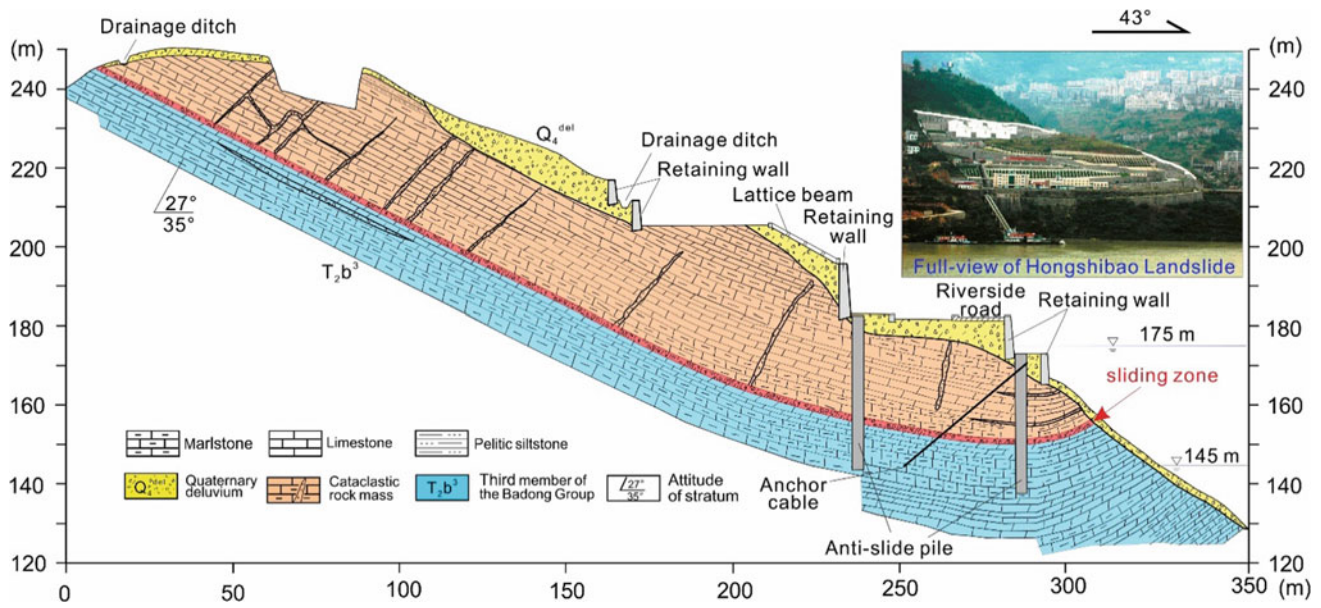

Fig. 2 Cross section of the Hongshibao landslide, whose toe is affected by fluctuations of the TGR level. Drainage ditches, retaining walls, lattice beams and stabilizing piles were constructed to stabilize this actively creeping landslide (Tang et al. 2019)

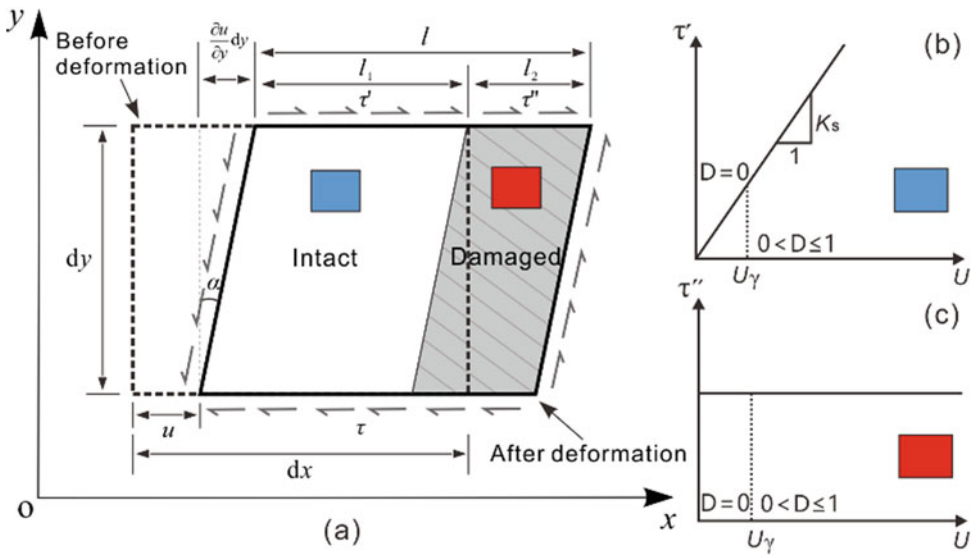

Fig. 3 The microelement damage mechanics model of the slip soil during shear process (Yan et al. 2022)

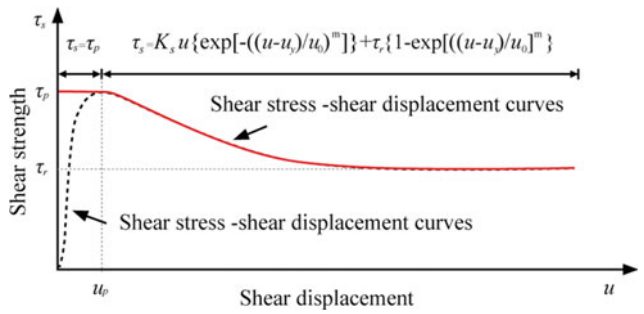

Fig. 4 The τ–u and τ_r–u curves of slip zone soil (Yan et al. 2022)

County, Chongqing City. The landslide is 1990 m long in the N–S longitudinal direction and 899 m wide in the E–W transverse direction, with a total area of 1.769 million m^2 and a total volume of 89.5 million m^3. The landslide is composed of Slide 1, Slide 2 and Slide 3 (Fig. 7a and b), the front elevation of the landslide is 90–102 m, and the rear elevation is 705 m. The slip zone soil is mainly the argillization product of carbonaceous claystone and carbonaceous shale, which is black and gray black, with high clay content, luster and good toughness (Fig. 7c and d).

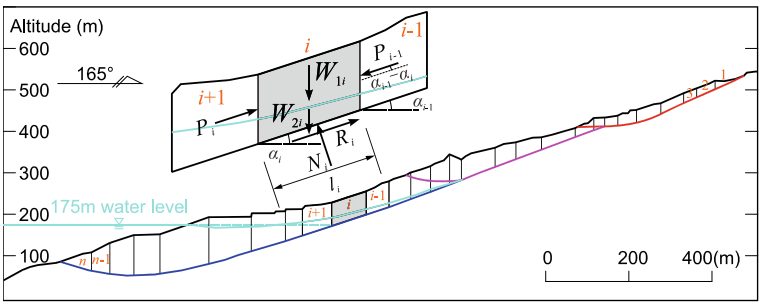

Fig. 5 Force analysis of the slices of a landslide (Yan et al. 2022)

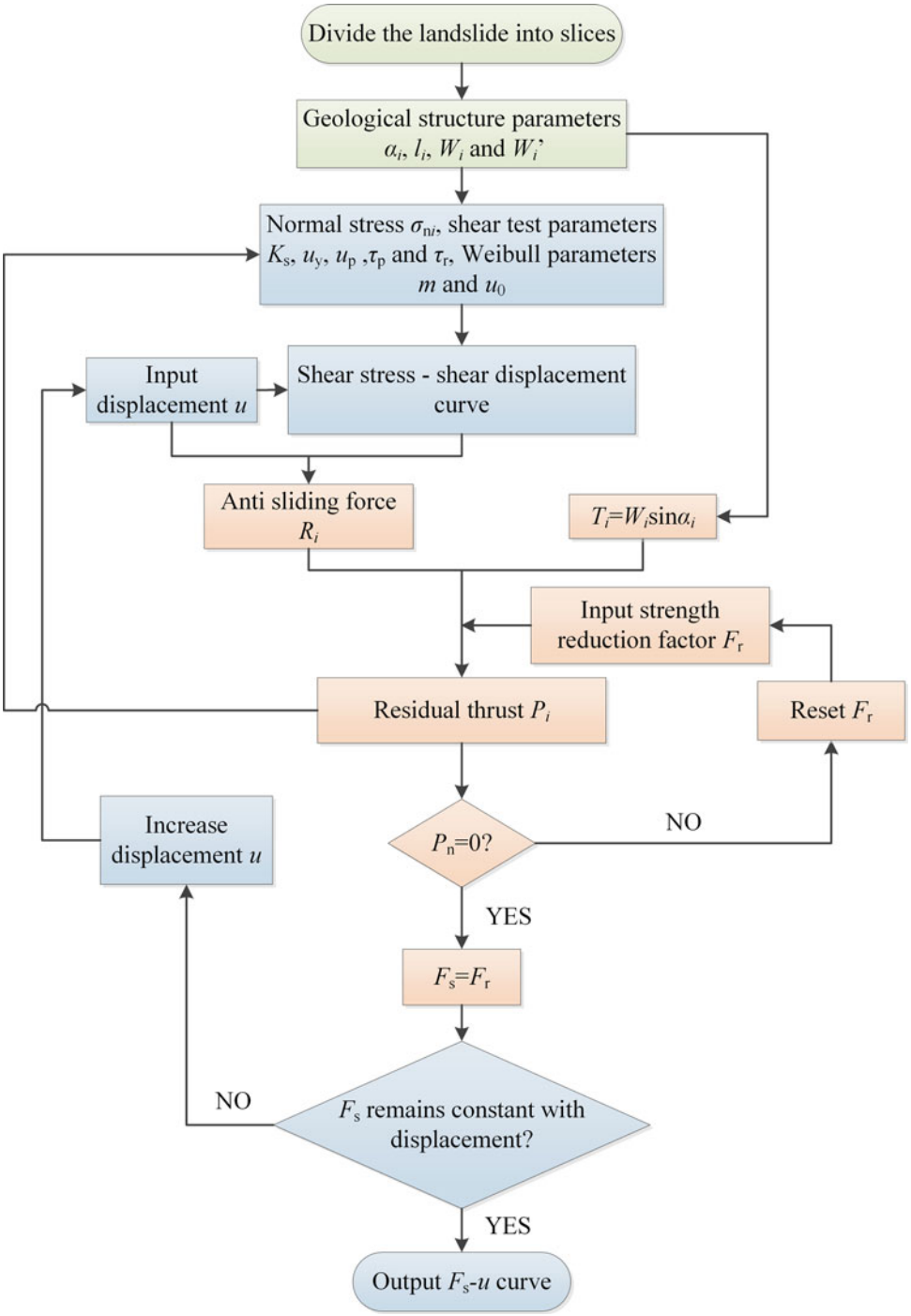

Fig. 6 Flow of landslide dynamic stability evaluation method (Yan et al. 2022)

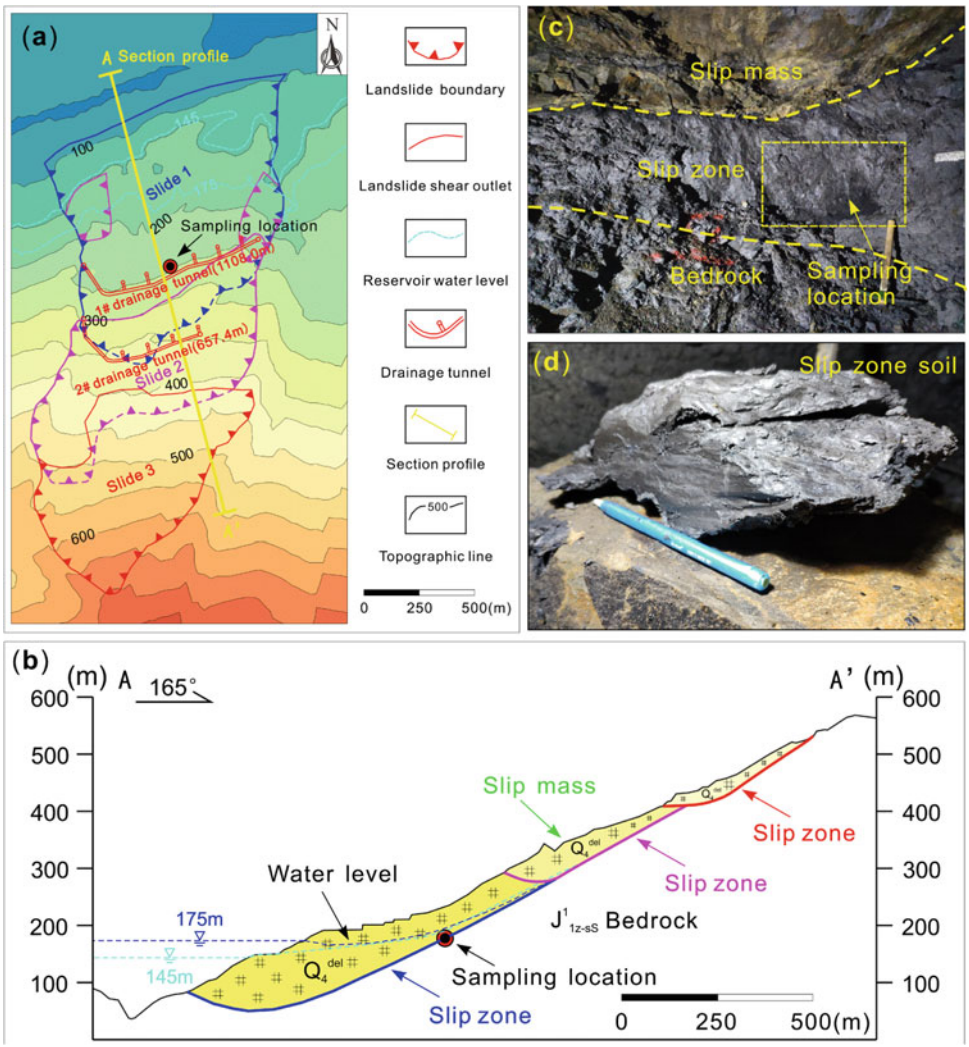

Fig. 7 **a** the plain view of the landslide; **b** the main section of the landslide; **c** the overall view of the landslide; **d** the slip zone of the landslide (Yan et al. 2022)

The stability evolution of Outang landslide without considering groundwater condition and 175 m water level condition is analyzed respectively. From Fig. 8, it shows that with the increase of landslide displacement, the landslide stability factor decreases at a gradually decreasing attenuation rate, and the stability factor tends to a constant value under large displacement, which is consistent with the strain softening phenomenon of the slip zone soil: the shear strength gradually decreases with displacement and tends to be constant until reaching the residual strength stage. It also shows that the displacement required for a constant stability factor is greater than the displacement required for the slip zone soil to reach the residual strength stage. It is attributed to that the Outang landslide is a deep giant landslide, and the normal stress of the slip zone is high stress, up to 2000 kPa, the strain softening phenomenon of the sip zone soil is less obvious under large normal stress, and the displacement required to decay from peak strength to residual strength increases.

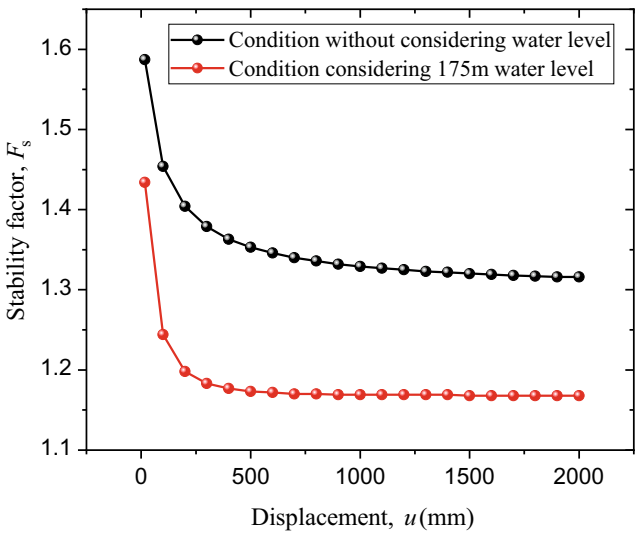

Fig. 8 Stability evolution characteristics of Outang landslide (Yan et al. 2022)

Without considering the reservoir water level, the stability factor of Outang landslide gradually decreases from 1.587 to 1.316 and remains constant, indicating that the landslide deformation has a significant impact on the stability of the landslide. Under the condition of 175 m reservoir water level, the landslide stability factor gradually evolves from 1.434 to 1.168, and then remains constant. Comparing the stability of the landslide with or without considering the reservoir water, it is concluded that the reservoir water has a significant impact on the stability of Outang landslide, and the attenuation amplitude of the peak stability factor with the water level ΔF_{s-w} is 0.153, and the attenuation amplitude of residual stability factor with the water level ΔF_{s-w} is 0.148. The main reason for the effect of reservoir water on landslide stability is that the reservoir water causes the reduction of the effective gravity of the anti-sliding section of the landslide. The front part of the Outang landslide has a small inclination angle and even an inverted section, which is the main anti-sliding section. Affected by the reservoir water, the effective gravity of the anti-sliding section decreases, resulting in the reduction of the effective normal stress and anti-sliding force of the landslide, which leads to the reduction in the landslide stability factor. Therefore, the drainage engineering is a feasible measure for preventing and controlling large-scale landslides.

5 Key Techniques of Reservoir Landslide Prevention and Control

Determination of Optimal Pile Position for Landslide with Step-shaped Sliding Surface

Previous determinations of the optimal stabilizing pile location have generally been based on the idealized assumption of arc-shaped sliding surfaces. This assumption, however, may involve considerable error especially for the identified numerous colluvial landslides located in the TGRA of China that have step-shaped sliding surfaces. To address the problem, a strategy, termed the local safety partitioning (LSP) methodology, for accurately determining optimal pile locations for step-shaped configurations. Instead of assuming the sliding surface to be arc-shaped, this strategy considers the actual sliding shapes.

The LSP methodology contains a framework of several implantation steps, in which the Swedish slice method is initially employed to calculate the local safety factors of each soil slice above the sliding surface; then, several landslide mass partitions are identified as high-safety partitions and low-safety partitions, and finally the stabilizing pile is placed between high-safety masses and low-safety masses, as schematized in Fig. 9.

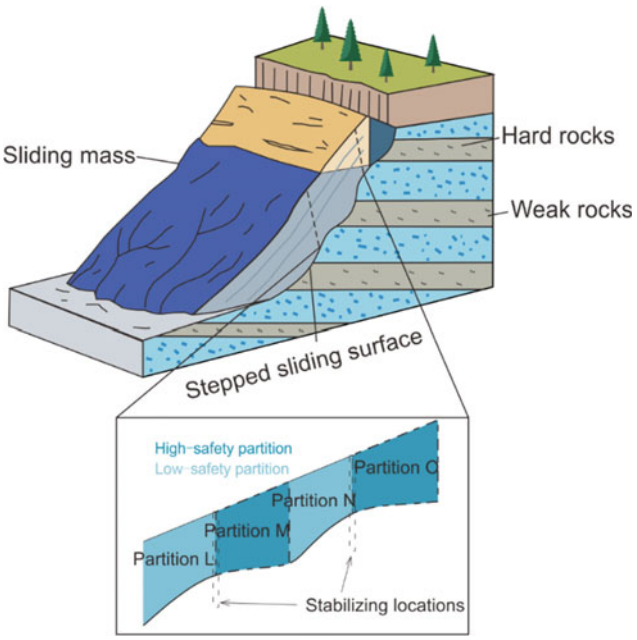

Fig. 9 Schematic diagram for the landslide with stepped sliding surface and local partitions of high and low safety (Tan et al. 2018)

The LSP methodology basically contains four sequential calculation steps:

(i) Divide the landslide mass into slices, designated I in Fig. 10. For each slice we generally require the bottom brim to be a straight line, thus a careful slicing should be conducted. This is in line with the Swedish slice method.

(ii) Acquire the K_{Li} of every individual slice, then draw the local safety-slice number curve to find out the mutational points on the curve. Procedures for identifying the mutational points would be executed including: first calculate out the slopes of every adjacent two K_{Li} values, next make subtraction of two adjacent slopes and acquire the slope subtraction values, then identify the biggest value of slope subtraction. Thus, the mutational point corresponds to the mid slice of the three subsequent slices. For example, slices 5, 6 and slices 6, 7 in Fig. 10 have the biggest slope subtraction, then slice 6 corresponds to the mutational point on the curve. Further, when the K_{Li}—slice number curve has more than one inflection, the procedure should be repeated around each inflection until all the mutational points are identified.

(iii) Identify partitions by mutational slices (slices covering mutational points) as denoted by III in Fig. 10, then calculate the local safety factor (K_L) of each

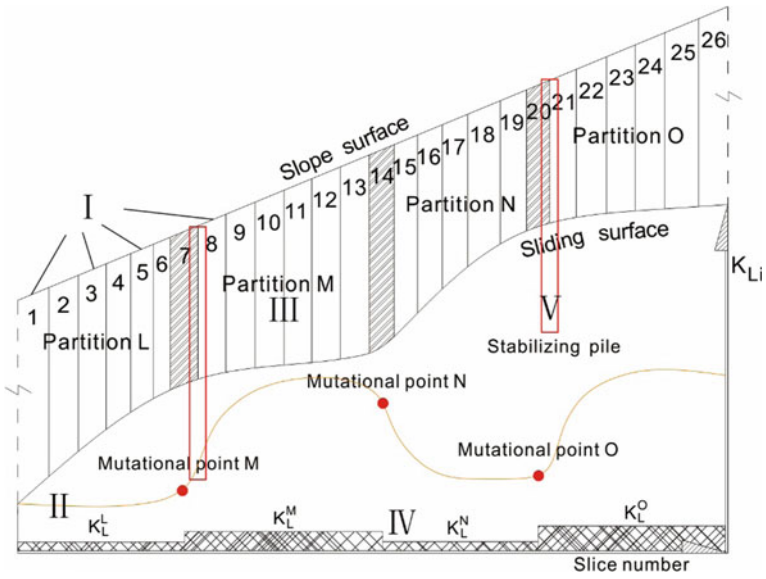

Fig. 10 Schematic diagram for the implementation of the LSP methodology. It is introduced to explain step (i) to (iv) for an explicit demonstration (Tan et al. 2018)

partition (IV in Fig. 10). For this step, adjacent two mutational slices would be identified as the two boundaries of the local partition. As illustrated in Fig. 10, the K_{Li}—slice number curve has three mutational points, denoting the mutational slice No. 7, 14 and 20. Then, four partitions were identified by the three slices, characterized by discriminating high and low K_L.

(iv) Put the stabilizing pile in between two partitions, where behind the pile (opposite to the sliding direction) contacts the partition with high K_L and in front the pile contacts the partition with low K_L.

The performance of the presented methodology is illustrated using the Jinle No. 2 landslide case for well-rounded demonstration and using the Yancun landslide case for additional validation. The results indicate that analysis of a reinforced landslide employing the LSP methodology acquires the largest factor of safety and smallest deflection, shear force and bending moment on the pile body compared with any other case from a series of positions which incorporating traditional positions for arc-shaped sliding surfaces. The presented methodology provides a simple but accurate determination of the optimal stabilizing pile location for stepped sliding surfaces, although it may involve errors and unexpected limitations when applied to arc shapes and peculiar scenarios.

Optimal Plane Arrangement Method of Stabilizing Piles

Among the current reinforcement structures, it is preferable to use the stabilizing piles to ensure safety of landslides, especially the large-scale colluvial landslides. Many colluvial landslides with pile improvement encouraged engineers to pay more attention on the design and effectiveness of stabilizing piles. With further studies on the landslides and stabilizing piles, more and more researchers have realized that landslide is a three-dimensional object rather than a two-dimensional profile, the conventional uniformly distributed driving force acting on the stabilizing piles should be replaced with the three-dimensional spatial distributed driving force in plane. Therefore, the engineers have to reconsider the corresponding issues related to the design of stabilizing piles, especially in the aspects of the pile spacing, stability of landslide and plane arrangement of piles. Though there are still several literatures that involve the soil arching effect, three-dimensional distribution characteristics of driving force and the concept of plane arrangement of stabilizing piles for colluvial landslides; unfortunately, only few of them can perform the quantitative studies on the whole optimal plane arrangement of stabilizing piles based on soil arching effect and the three-dimensional distributed driving force.

A novel optimal plane arrangement of stabilizing piles in terms of the provided half simplified flattened ellipsoid model, which can be used to describe the three-dimensional characteristics of sliding mass for colluvial landslides has been presented (see Fig. 11). By studying the friction soil arching effect between the adjacent stabilizing piles, a reasonable pile spacing model for stabilizing piles was deduced in consideration of the driving force and shear strength of sliding mass as well as the dimension of pile cross-section. Furthermore, the concept of stability limit was put forward to confine the rational arrangement region for stabilizing piles; consequently, the region beyond the rational arrangement region is not necessary to set piles anymore (see Fig. 12).

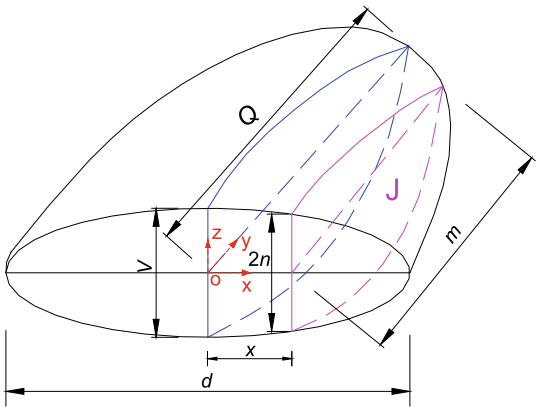

Fig. 11 Sketch of half flattened ellipsoid model for describing the spatial morphology of sliding mass for colluvial landslides. (V is the maximum depth of sliding mass, Q is the maximum horizontal distance from the pile to the crest, d is the width of landslide in the section along the pile-row, section J is the longitudinal profile with x distance to the major slip profile, $2n$ is the depth of sliding mass in section J, m is the distance along the oy axis direction in section J) (Li et al. 2015)

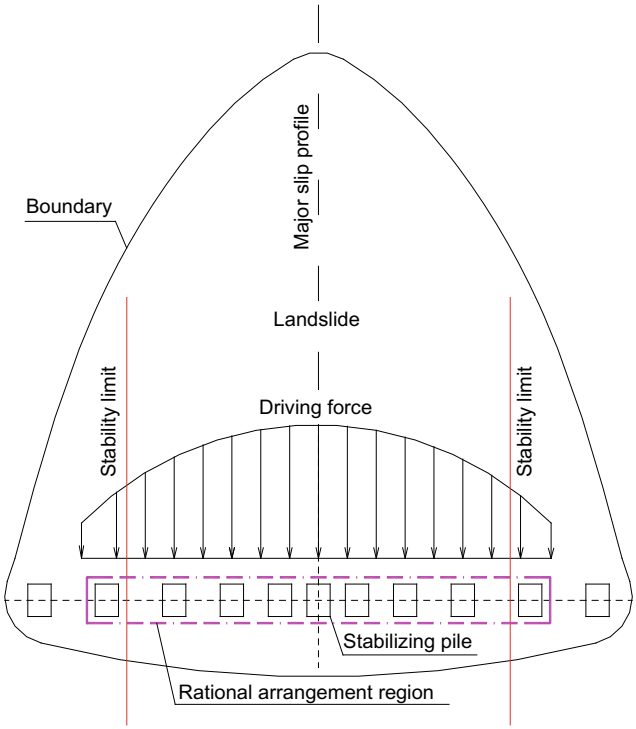

Fig. 12 Sketch of stability limit and rational arrangement region for stabilizing piles in a colluvial landslide (Li et al. 2015)

The friction soil arching effect was used to obtain the reasonable range of pile spacing. The corresponding calculation model can be utilized to determine the upper limit of the pile spacing because of the consideration merely on the effect of the friction soil arching. The solution of the reasonable net pile spacing S based on the friction soil arching can be obtained as (Li et al. 2015):

$$S = \frac{c \cdot a \cdot (2H + 1)}{q \cdot (1 - \tan\varphi) - \gamma \cdot H \cdot (\cos\theta \cdot \tan\varphi - \sin\theta)} \tag{8}$$

As stated above, the calculation model for net pile spacing (S) depends on the effect of the friction soil arching. Consequently, the pile spacing presented by Eq. 8 should be the maximum pile spacing. It is assumed that the total number of needed stabilizing piles is N, and any maximum net pile spacing S_i can be written as (Li et al. 2015):

$$S_i = \frac{c \cdot a \cdot (2H + 1)}{q_i \cdot (1 - \tan\varphi) - \gamma \cdot H \cdot (\cos \cdot \tan\varphi - \sin\theta)} \tag{9}$$

where q_i is the driving force intensity of the number i stabilizing pile along the ox direction, $i = 1, 2, \ldots, N$.

Erliban landslide located in Yichang City, China, was taken as an example to exhibit the optimal plane arrangement of stabilizing piles for colluvial landslides. Erliban landslide is a typical colluvial landslide located on the left bank of the Xiangxi River in Yichang City, China (Li et al. 2013). In view of the technical regulation of geological investigation and engineering design for landslide control in reservoir region of Three Gorges in Hubei Province (The head office for prevention and control of geohazards in the Three Gorge Reservoir Region of Hubei Province, 2003), the safety factor (F_s) of Erliban landslide should be 1.15, i.e., F_s = 1.15.

In the light of the definition of scale factor and the geometrical relationship, the position of stability limit of Erliban landslide can be obtained as X = 57.8 m in the XOY coordinate system presented in Fig. 14. Therefore, the stability coefficient of landslide is 1.02 in the major slip profile and is 1.15 at the stability limit section of X = 57.8 m (see Fig. 13). The blue curve with red dots shows the change trend of the stability coefficient of landslide from the major slip profile to the stability limit section.

Based on the confinement of rational arrangement region by the stability limit, the corresponding rational arrangement region for Erliban landslide can be determined by the bold magenta dash dot line in Fig. 13. Considering the impact of the pile length above the slip surface on pile spacing, an improved optimal non-uniformly spaced arrangement model was put forward. In view of the comparison between the conventional uniformly spaced arrangement and the improved optimal non-uniformly spaced arrangement, the improved optimal non-uniformly spaced arrangement method only requires 25 stabilizing piles rather than the 31 stabilizing piles in the conventional scheme, with an obtainable saving of 19.4% in the number of stabilizing piles (Li et al. 2015).

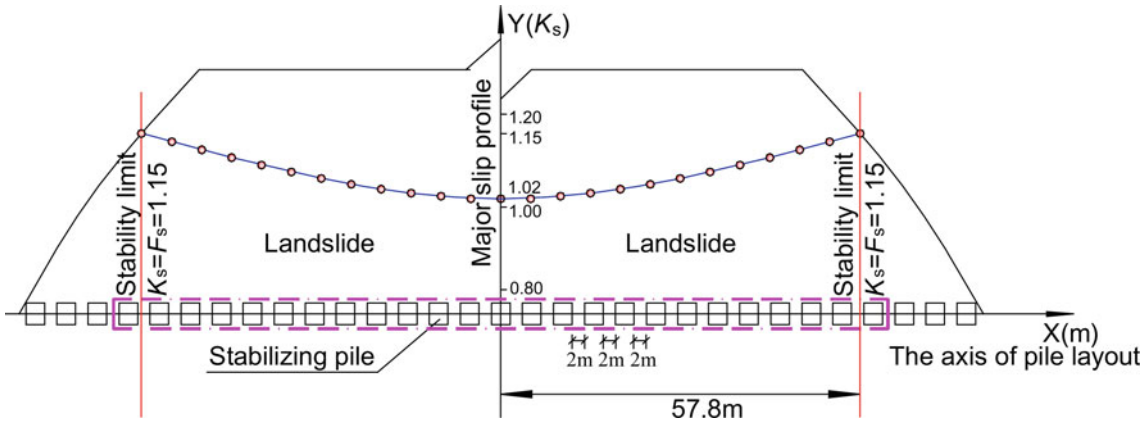

Fig. 13 Determination of the location of stability limit and rational arrangement region for Erliban landslide (Li et al. 2015)

Reasonable Embedded Length Determination Method of Stabilizing Piles

The reinforcement effect of landslides is influenced by the design parameters of stabilizing piles, especially the embedded depth has a great influence on the effect of stabilizing piles. For instance, the Jurassic strata are characterized by hard and weak interbedded rocks. Determining a reasonable embedded length is crucial to the design of piles that stabilize landslides. However, the presence of upper hard and lower weak bedrock presents a challenge when attempting to determine the reasonable embedded length of stabilizing piles. It is generally accepted that stabilizing piles can be set to stabilize a landslide. In engineering practice, strength design is always used to design stabilizing piles by focusing on bending moments and shear forces. However, pile deformation is rarely considered, especially when complex layered bedrock is present. Therefore, it is necessary to determine the reasonable embedded length of piles in bedrock with upper hard rock and lower weak rock based on the deformation control requirements set by industrial standards.

There is typically a negative power function relationship between the embedded ratio (ω) of a pile and the horizontal displacement of the pile head (xh) (Li et al. 2019), so the reasonable embedded ratio can be obtained if the allowable horizontal displacement of the pile head is known.

To better describe the embedded condition of the pile, an embedded pile ratio (ω) can be defined as the ratio between the embedded pile length and the total pile length. According to industrial standards (TB 10,025/J127; Standardization Administration of China 2006), the allowable degree of pile deformation ($x$hp) should be less than 1/100 of the pile length above the slip surface (h1), and it should also not exceed 10 cm. As pile head deflection is mainly dependent on the embedded length ratio of the pile (ω), the thickness of the upper hard rock layer in the bedrock (Th), the coefficient of subgrade reaction of the hard rock (Kh), the coefficient of subgrade reaction of the weak rock (Kw) (see Fig. 14), and the driving force per unit width behind the landslide (P), the horizontal displacement of the pile can be expressed as follows (Li et al. 2019):

$$\begin{cases} x_h = f(\omega,\ T_h,\ K_h,\ K_w,\ P) \\ x_{ha} \le 0.01 h_1 \\ x_{ha} \le 10\ cm \end{cases} \tag{10}$$

Here, $x$ha is an upper limit on the horizontal displacement of the pile head. For a given landslide, h1, Th, Kh, Kw, and P can be determined. Consequently, due to the negative power function relationship between the embedded ratio and horizontal displacement (see Fig. 15), the reasonable embedded ratio (ωr) for piles can be expressed as below (Li et al. 2019):

$$\begin{cases} \omega_r = a x_{ha}^b \\ x_{ha} \le 0.01 h_1 \\ x_{ha} \le 10\ cm \end{cases} \tag{11}$$

where a and b are undetermined constants that can be obtained from the completed work (Li et al. 2019).

The No.1 Majiagou landslide is approximately 540 m long and 200 m wide, approximately 9.7 km^2 in area and 1.3 million m^3 in volume, and has an average thickness of 12.7 m (Qinghai Province No. 906 Engineering Investigation and Design Institute 2006). The pile spacing (L) is 7.0 m. The total length of the stabilizing pile ($\boldsymbol{h}$) is 22 m with a cantilever section length ($\boldsymbol{h}_1$) of 14 m and an embedded section length ($\boldsymbol{h}_2$) of 8 m. The current horizontal displacement of the pile head in the No. 1 landslide is roughly 15.0 cm. Assuming the presence of a lower weak rock layer, it is necessary to obtain the reasonable embedded length of the stabilizing pile to control pile deformation. In the original design scheme, the embedded length of pile ($\boldsymbol{h}_2$) is 8 m. According to industrial standards (TB 10,025/J127,

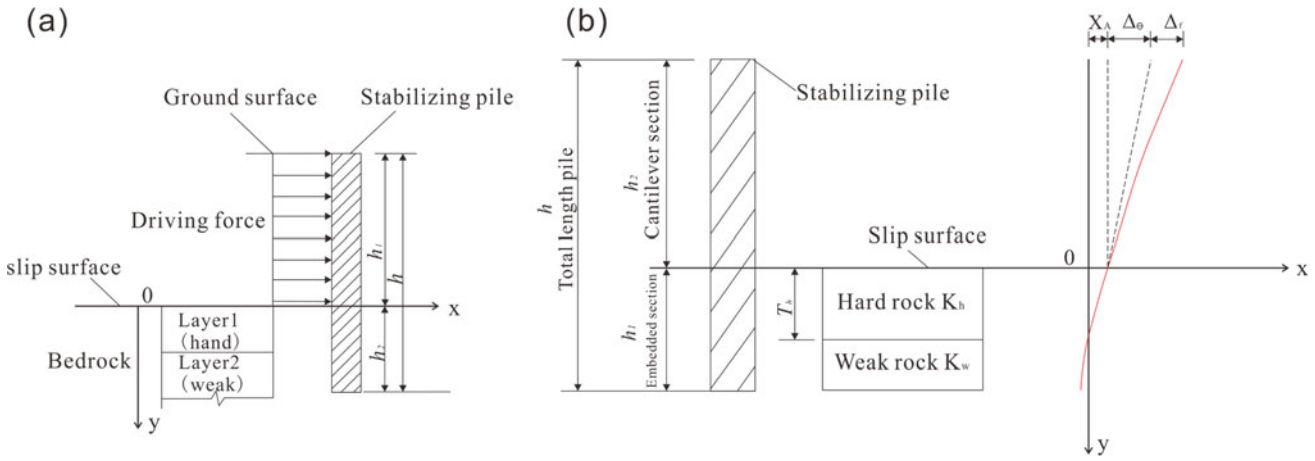

Fig. 14 Deformation calculation model of stabilizing pile in upper hard and lower weak bedrock; **a** sketch of a laterally loaded pile; **b** sketch of the deformation of a stabilizing pile subjected to the driving force of landslide (modified from Li et al. 2019)

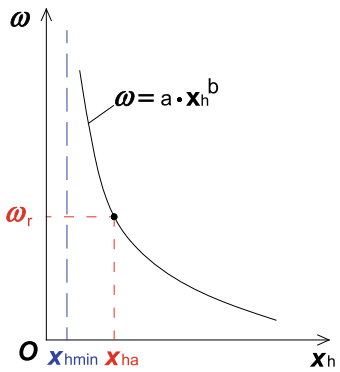

Fig. 15 Approach for determining the reasonable embedded ratio of a pile (Li et al. 2019)

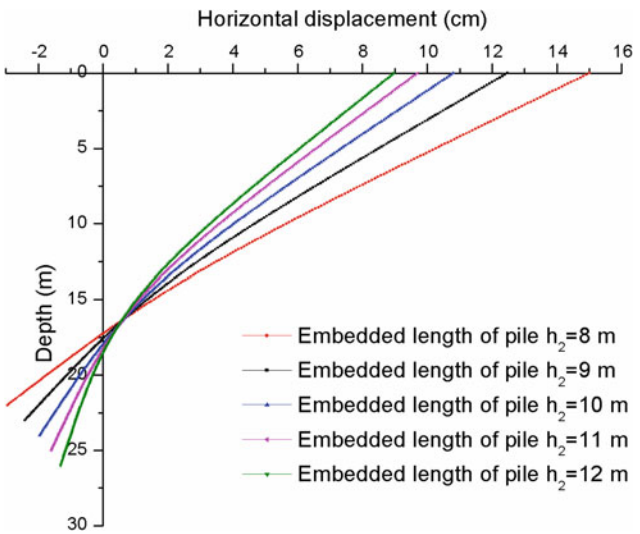

Fig. 16 Calculation results for pile deformations based on different embedded lengths (Li et al. 2019)

2006) and the second surveying and designing institute of the National Department of China Railway (1983), the recommended common embedded ratio of stabilizing piles ranges from 1/3 to 1/2. Consequently, to limit pile deformation, we consider embedded pile lengths (h_2) of 9, 10, 11, and 12 m. The calculated pile deformation levels found for these conditions are shown in Fig. 16 (Li et al. 2019).

Based on the assumption of an upper hard rock layer and a lower weak rock layer, the reasonable embedded length of piles for the Majiagou No. 1 landslide can be investigated in detail. By calculation by the above-mentioned model, it can be obtained that the reasonable embedded ratio (ω_r) of the piles is 0.435. Therefore, the corresponding reasonable embedded length (h_{2r}) of a pile is 10.8 m, i.e., the embedded length (h_{2r}) of a pile is at least 10.8 m to maintain pile head deformation within 10 cm as an industrial standard. According to the embedded ratios of stabilizing piles, the embedded ratio (ω) should increase from the current value of 0.364–0.435 to meet industrial standards. Therefore, the embedded ratio of stabilizing piles should be carefully considered during piles design due to its crucial influence on pile behavior (Li et al. 2019).

6 Demonstration Bases for Reservoir Landslides Prevention and Control

Huangtupo Landslide Demonstration Base

The Badong Huangtupo landslide demonstration base is located in the Huangtupo landslide area, which is the largest reservoir landslide by volume in TGRA (Tang et al. 2015a, b) (Fig. 17). This demonstration base is the largest underground landslide monitoring and testing facility in the world built to foster research, teaching, academic exchange on TGRA

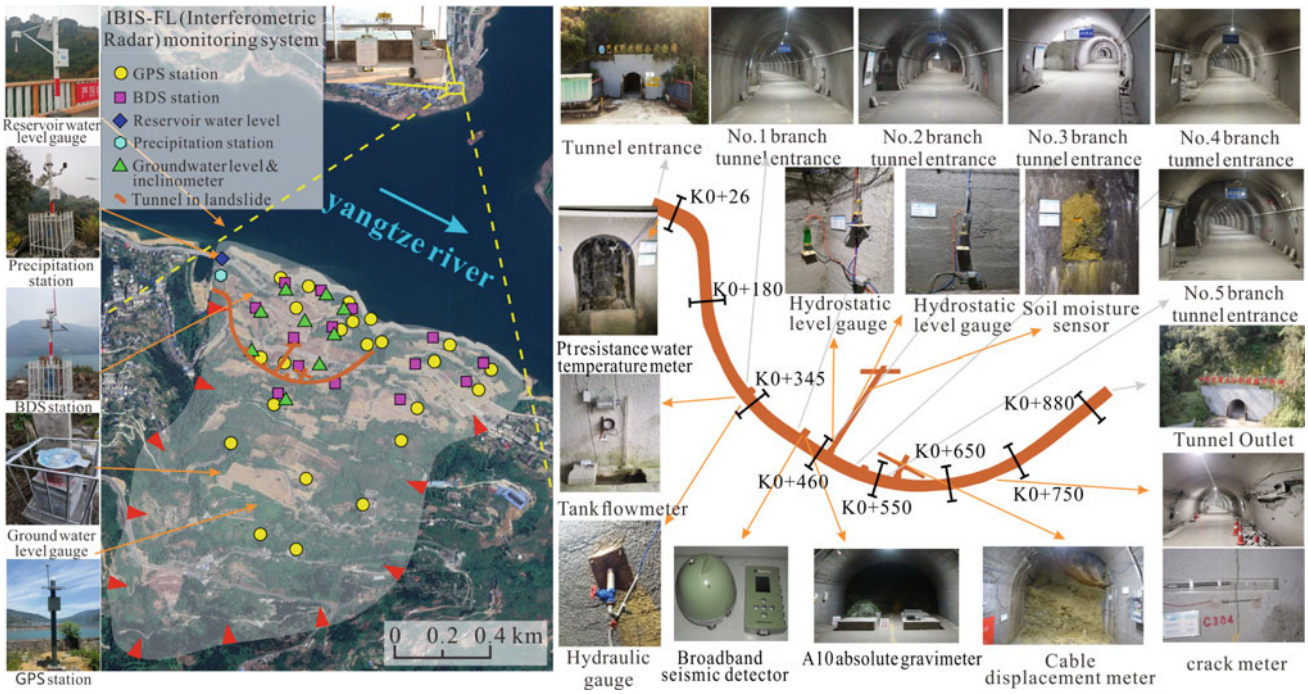

Fig. 17 Huangtupo landslide demonstration base (modified from Juang 2021)

geohazards. The station was designed and constructed and has been operated, by the China University of Geosciences since 2012. Over 10,000 people with a variety of geology-related backgrounds from >20 countries have visited this demonstration base.

The Huangtupo landslide demonstration base consists of a tunnel complex and a series of monitoring systems (Fig. 17). The tunnel complex, built in the Huangtupo riverside sliding mass #1, consists of a main tunnel with a length of 908 m and a width of 5 m, five branch tunnels (5–145 m long, 3.5 m wide), two test tunnels, and 35 observation windows. The test tunnels exposed the sliding zones of the landslide, facilitating their direct observation and the execution of scientific experiments, such as large-scale in-situ mechanical tests and deep deformation monitoring. The monitoring systems measure deformation as well as hydrologic, meteorological and hydro-chemical variables. The deformation system is composed of a slope surface displacement measurement unit and an underground displacement measurement unit. The slope surface displacement unit includes a number of GPS (Global Positioning System) and BDS (BeiDou Navigation Satellite System) measurement points, as well as an IBIS-FL (Interferometric Radar) monitoring system (Fig. 17). The underground displacement unit includes nine deep inclinometer boreholes, a number of crack meters installed on the ground and the walls of tunnels, and many hydrostatic level gauges that measure the settlement of the tunnels in the sliding mass. The hydrologic system includes a number of devices that allow for observation of the water level of the Yangtze River, the groundwater level, and water discharge of the tunnels (Fig. 17). A small meteorological station is located on the landslide and provides rainfall data. All these monitoring devices, except the inclinometers, have recently been updated with real-time acquisition and automatic transmission features (Tang et al. 2019).

In addition to the aforementioned monitoring system, the 3D deformation monitoring network techniques were also applied in the Huangtupo landslide demonstration base, including the flexible inclinometer (Zhang et al. 2018) and the pipeline trajectory inertial measurement instrument (Zhang et al. 2020).

The flexible inclinometer consists of a controller and a flexible inclinometer probe, of which, the length of the flexible inclinometer probe and the interval of the units can be customized depending on the specific application conditions before encapsulation (Fig. 18a). Encapsulated by silicone, the flexural rigidity of the flexible inclinometer probe can be ignored relative to the landslide mass, with displacement coupling well to the landside mass. With the advantages of good deformation coupling, large deformation capacity, and automatic measurement, the flexible inclinometer is suitable for continuous real-time monitoring of landslide deep displacement that undergoes multi evolutionary stages.

The pipeline trajectory inertial measurement instrument based on deformation-coupled pipeline trajectory measurement is deployed to fill the deficiencies of traditional

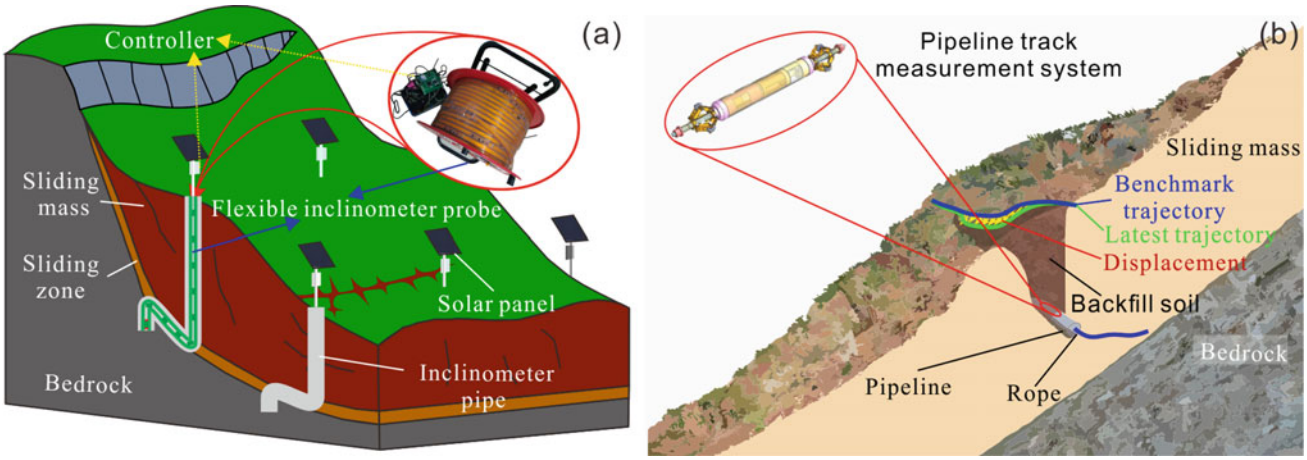

Fig. 18 3D deformation monitoring network techniques **a** the flexible inclinometer; **b** the pipeline trajectory inertial measurement instrument

instrumentation for measuring landslide displacement distributed along lateral direction (Fig. 18b). The developed instrument, primarily comprised of a single shaft gyro, two-axis accelerometers, and an external roller encoder, is designed to expediently calculate a pipeline trajectory with an Eulerian transformation when obtaining several basic physical variables, e.g., the axial linear velocity, pitch angle, roll angle, and azimuth angle. The pipeline trajectory inertial measurement instrument combined with pipeline and rope can be see as a pipeline track measurement system. With the pipeline trajectory measured at different times and compared with the benchmark trajectory, the pipeline track measurement system possesses the ability to reflect the displacement evolution feature of landslides. The results of prototype simulation tests imply a single measurement accuracy of a 12 cm/100 m span and a singly periodic multiple (more than five times) measurement accuracy of a 3 cm/100 m span, which meets medium-precision displacement measurement requirements for a landslide.

Majiagou Landslide Demonstration Base

The Majiagou landslide demonstration base is located in the Majiagou landslide in Zigui of TGRA. This demonstration base provides a platform to study the landslide stability during the reservoir operation, the interaction mechanism between the landslide and stabilizing structures, and the optimization design of stabilizing structures (Hu et al. 2017). An integrated, in-situ multi-parameter monitoring system was designed and installed during the test pile construction. The system included surface displacement and borehole monitoring, as well as experimental pile monitoring (Fig. 19). The surface deformation monitoring relied on five GPS stations and two fiber-sensing cables. The borehole monitoring system includes 15 boreholes, distributed along the main sliding direction, with different types of sensors installed to measure the deep displacement of the Majiagou landslide. The monitoring of the experimental piles (40 m long) relied on earth pressure gauges, stress gauges, strain gauges and fiber sensors. The earth pressure gauges were positioned on the surface of the piles to measure the lateral earth pressure. The stress gauges, strain gauges and strain-sensing fibers were installed in the stabilizing piles to measure the axial stress and the deflection of the piles. In each test pile, 26 stress gauges and strain gauges were installed to measure the longitudinal pile stress and strain. The thermo-sensing fibers were distributed along the experimental piles to monitor the change of temperature within the landslide.

7 Conclusions

This study introduced the recent advances in key techniques for reservoir landslide prevention and control based on evolutionary process.

The reservoir rock landslides can be divided into seven types based on the evolution modes, namely, progressive slip along gentle-dip layer I, progressive slip along gentle-dip layer II, bucking failure along steep-dip layer, creep slip along deep layer, plastic flow slip of weak interlayer, breakthrough abrupt slip in inclined cross-cutting layer and toppling failure in steep anti-dip layer, respectively. Then, according to the classification of the seven reservoir landslide evolution modes and corresponding evolution stages, the specific control measures suitable for reservoir landslides in different evolution stages are suggested and successfully employed in the management of Hongshibao landslide located in the TGRA.

A dynamic stability evaluation method is proposed considering the evolution process of the slip zone soil strength for the evaluation of landslide stability. This method is a

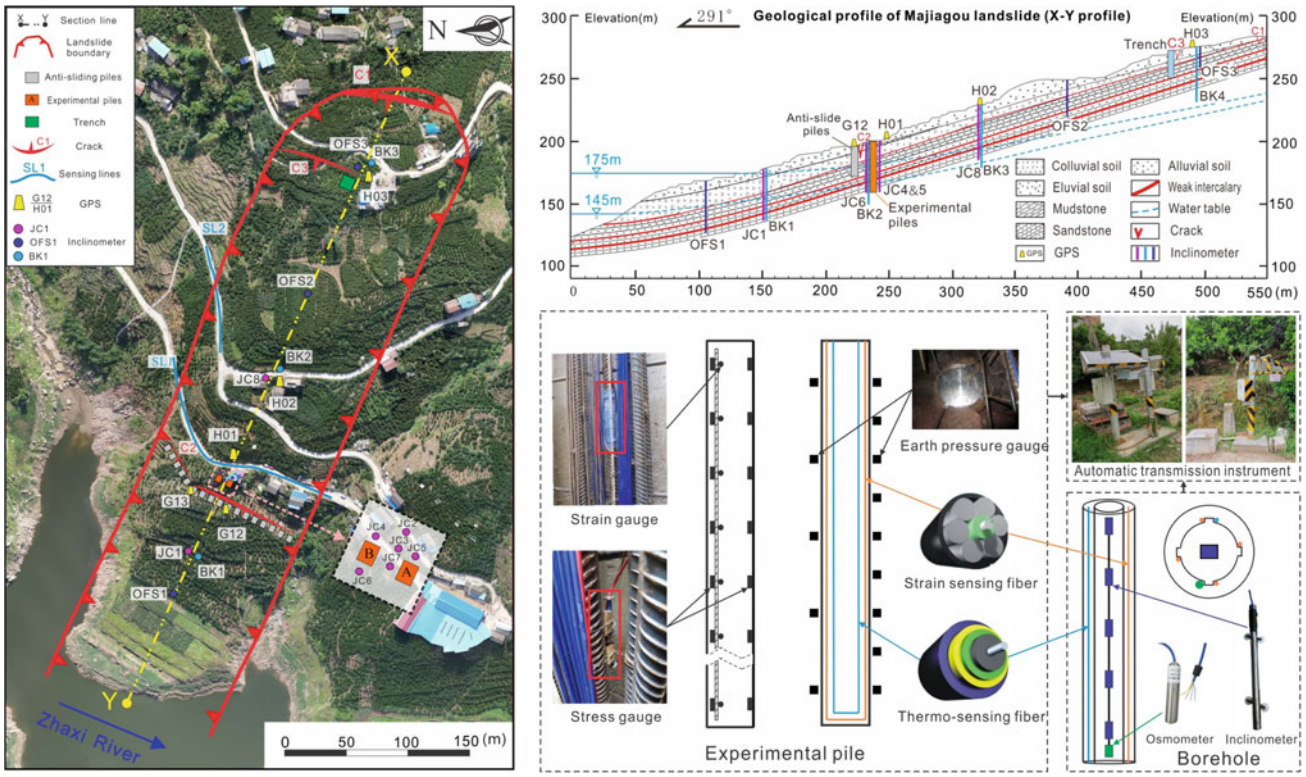

Fig. 19 Majiagou landslide demonstration base (Tang et al. 2019)

two-step regime: the constitutive model and shear strength evolution model for describing the relation between shear stress and shear displacement, and that between shear strength and shear displacement, respectively; and calculation of the stability factor as a function of the shear strength determined from the shear displacement of the slip zone soil. Then, we introduce three key techniques of reservoir landslide prevention and control: (1) determination of optimal pile position for step-shaped sliding surface, (2) the optimal plane arrangement method of stabilizing piles and (3) a reasonable embedded length determination method of stabilizing piles. In the first technique, we mainly address the actual sliding shapes rather than assuming an arc-shaped sliding surface, by adopting the so-called local safety partitioning (LSP) methodology. The second technique aims at solving the problem of unevenly distributed driving force that has not been properly addressed in conventional two-dimensional treatment. Further, the third technique gives the reasonable embedded length of piles in bedrock by incorporating the pile deformation into the supporting structure, which is important especially when complex layered bedrock is present.

Last, two demonstration bases for reservoir landslides prevention and control are introduced. The two demonstration bases with comprehensive monitoring system realize excellent applications of the new prevention and control techniques based on landslide evolution process, which can provide technical support for the landslide control of the same kind.

Acknowledgements The authors would like to express their sincere gratitude to the Ministry of Science and Technology of China and the National Natural Science Foundation of China (Nos: 42077268) for supporting this work.

References

Hu X, Tan F, Tang H, Zhang G, Su A, Xu C, Zhang Y, Xiong C (2017) In-situ monitoring platform and preliminary analysis of monitoring data of Majiagou landslide with stabilizing piles. Eng Geol 228:323–336

Juang CH (2021) BFTS-Engineering geologists' field station to study reservoir landslides. Eng Geol 284:106038

Li CD, Tang HM, Hu XL, Wang LQ (2013) Numerical modelling study of the load sharing law of anti-sliding piles based on the soil arching effect for Erliban landslide, China. KSCE J Civil Eng 17 (6):1251–1262

Li C, Wu J, Tang H, Wang J, Chen F, Liang D (2015) A novel optimal plane arrangement of stabilizing piles based on soil arching effect and stability limit for 3D colluvial landslides. Eng Geol 195:236–247

Li C, Yan J, Wu J, Lei G, Wang L, Zhang Y (2019) Determination of the embedded length of stabilizing piles in colluvial landslides with upper hard and lower weak bedrock based on the deformation control principle. Bull Eng Geol Env 78(2):1189–1208

Tan Q, Tang H, Huang L, Li C, Kou T (2018) LSP methodology for determining the optimal stabilizing pile location for step-shaped soil sliding. Eng Geol 232:56–67

Tang H, Li C, Hu X, Su A, Wang L, Wu Y, Criss R, Xiong C, Li Y (2015a) Evolution characteristics of the Huangtupo landslide based on in situ tunneling and monitoring. Landslides 12(3):511–521

Tang H, Li C, Hu X, Wang L, Criss R, Su A, Wu Y, Xiong C (2015b) Deformation response of the Huangtupo landslide to rainfall and the changing levels of the Three Gorges Reservoir. Bull Eng Geol Environ 74(3):933–942

Tang H, Wasowski J, Juang CH (2019) Geohazards in the three Gorges Reservoir Area, China—lessons learned from decades of research. Eng Geol 105267

Yan J, Zou Z, Mu R, Hu X, Zhang J, Zhang W, Su A, Wang J, Luo T (2022) Evaluating the stability of Outang landslide in the Three Gorges Reservoir area considering the mechanical behavior with large deformation of the slip zone. Nat Hazards

Zhang Y, Tang H, Li C, Lu G, Cai Y, Zhang J, Tan F (2018) Design and testing of a flexible inclinometer probe for model tests of landslide deep displacement measurement. Sensors 18(1):224

Zhang Y, Tang H, Lu G, Wang Y, Li C, Zhang J, An P, Sheng P (2020) Design and testing of inertial system for landslide displacement distribution measurement. Sensors 20(24):7154

Zhang J, Tang H, Tannant DD, Lin C, Xia D, Liu X, Zhang Y, Ma J (2021) Combined forecasting model with CEEMD-LCSS reconstruction and the ABC-SVR method for landslide displacement prediction. J Clean Prod 293:126205

Landslide Research and Technology in Patent Documents

Matjaž Mikoš

Abstract

Science, Technology, and Innovation play a crucial role in the Sendai Framework for Disaster Risk Reduction 2015–2030 (SF DRR). The International Consortium on Landslides (ICL) initiated the Sendai Landslide Partnerships 2015–2025 as a voluntary commitment to SF DRR. In 2020, the ICL launched the Kyoto 2020 Commitment for Global Promotion of Understanding and Reducing Landslide Disaster Risk (KLC 2020) as a follow-up of the Sendai Landslide Partnerships 2015–2025. Closely related to the above-mentioned Innovation are patents as a form of intellectual property rights and are often used as an innovation assessment parameter. This article reports on a study conducted to look at the patent documents that are available in open-access databases in order to evaluate how well they relate to the field of landslide research and technology. Landslide-related patent documents were extracted using different search terms in the patent document titles, abstracts, claims and/or their general text from the Google Patents, using the Espacenet tools from the European Patent Office, and the Derwent Patent Index inside the Web of Science offered by Clarivate Analytics, respectively. The extracted patent documents were analyzed with regard to the applicant respectively inventor affiliation (academic, non-academic, country of affiliation) and to the technical field of a patent using well-known patent classifications. The most active countries claiming landslide-related patents were recognized. Furthermore, review and research articles in SpringerLink and SCOPUS databases were searched to study how often scientific articles are citing landslide-related patents. The results of the study can be summarized as follow: (i) in the Google Patents database there are 15,000 + landslide-related patent documents, and in the Espacenet and the Derwent Innovation index database 5000+, respectively. In the patents titles, abstracts, and claims, processes are more often used to describe the patent than the technology; (ii) the number of technological (non-science) based patents is higher than that of academic (science-based) patents, with some specific field of applications, where the situation is the opposite; (iii) with regard to the different areas of technology to which landslide-related patent documents pertain, the categories "G-Physics" and "E-Fixed constructions" are clearly prevailing: "G" for debris flows and landslides, and "E" for fallings rocks and mudflows; (iv) the majority of landslide-related patents are filled and/or granted in China, followed by Japan and South Korea, USA and EU member countries—five major emerging economies (called BRICS) are outperforming developed countries, with a very prevailing Chinese contribution; (v) only a fraction of the order of a few one-in-thousands of landslide-related patents documents are cited in journal review and research articles.

Keywords

Citations • Innovation • Intellectual property • Landslides • Patents • Technology transfer

1 Introduction

Technological learning and innovation are essential for economic growth and development, and are major determinants of long-term improvements in income and living standards. While in the more advanced economies technological progress involves the generation of new knowledge that can be applied to productive activity, for developing countries technological progress is strongly influenced by their ability to access, adapt and diffuse technological knowledge that has been generated abroad (UNCTAD

M. Mikoš (✉)
University of Ljubljana, UNESCO Chair on Water-related Disaster Risk Reduction, c/o UL FGG, Jamova c. 2, SI-1000 Ljubljana, Slovenia
e-mail: matjaz.mikos@fgg.uni-lj.si

I. Alcántara-Ayala et al. (eds.), *Progress in Landslide Research and Technology, Volume 1 Issue 2, 2022*, Progress in Landslide Research and Technology,
https://doi.org/10.1007/978-3-031-18471-0_3

2014). Strengthening the technological capabilities of developing countries will be critical for the achievement of the 2030 Agenda for Sustainable Development (UNCTAD 2019). The status and trends of innovation can be assessed through patent analysis, as was done for India by Abraham and Moitra (2001), or e.g. technological development of a selected technology such as UAV (Unmanned Aerial Vehicle) can be reviewed through patent analysis of its hardware and software as done by Chen et al. (2016).

But technological progress is not only important for economic growth and development, but also plays a role in increasing society resilience against natural disasters. Callaghan (2016) claims that disasters decreasing the number of factors of production would stimulate innovations that will reduce the use of them—technological innovation is therefore of great importance in mitigating climate disasters, including natural disasters.

Science, Technology and Innovation thus play a crucial role in the Sendai Framework for Disaster Risk Reduction 2015–2030 (UNISDR 2015). This is more clearly visible in the Science and Technology Roadmap to Support the Implementation of the Sendai Framework for Disaster Risk Reduction 2015–2030 (UNISDR 2019). Cui et al. (2021) studied scientific challenges of research on natural hazards and disaster risk, with the emphasis on China. As one of the short-termed goals (2021–2025) for China, technology platform construction was named, including policy communication in science and technology innovation. Closely related to innovation are intellectual property rights, among them also patents. Hu et al. (2018) studied the innovative response to climate disasters in modern and historical China. In modern China (investigated period 2005–2013), past climate disasters have led to an increase in the number of disaster-mitigating patents that boost also innovations in other fields. In historical China (investigated period 11 to 1910) climate disaster only spurred innovations in disaster mitigation fields and not in others. They concluded that it is important for policymakers, including governments, to increase investment into research and technological development sectors after climate disaster.

As a widely known example, we may name the Reinforced Earth®, originally invented in 1963 as a method of using composite earth as a supporting structure—until nowadays claiming numerous patent families, trademark and design rights as forms of intellectual property (RECo 2022).

An inventor receives a patent, if (i) the invention is new, (ii) an "inventive" step is recognizable, and (iii) the idea has to be industrially applicable or useful (Ullberg 2020). The patent system grants and enforces temporal exclusive, transferrable, and licensable private rights on inventions—that provide solutions to (mostly) technical problems in the area of products and processes (Ullberg 2020). Patents are an important result of progress in science and technology and related innovation activities—but not all patents are science-based, they can also be non-science-based (Wang and Li 2018). University-owned patents are more related to scientific questions while corporate-owned patents are more connected with direct commercial goals (Sterzi 2013).

Bae et al. (2014) analyzed existing patents related to real-time monitoring and detection technology for landslides on natural terrain. The purpose of patent analysis was to understand landslide hazard technology trends and to develop new advanced technology. The study searched patent data using key words related to landslide monitoring and detection in Korea, the USA, Japan, China (Hong Kong), Europe, and Taiwan. The patents were divided into five main categories and five to seven subcategories in each main category and analyzed by year, country, and applicants. The results were utilized to derive a portfolio of promising technologies for each country.

Jelić (2018) presented systematic overview of patented inventions created in twenty-first century by Serbian scientists and inventors in the field of seismic safety of structures and landslide remediation, as well as examples of their specific application.

The International Consortium on Landslides (ICL) initially launched a book series entitled "ICL Contribution to Landslide Disaster Risk Reduction" (CLDRR; Springer 2022b) to publish integrated research on all aspects of landslides. As decided by the Kyoto 2020 Commitment for Global Promotion of Understanding and Reducing Landslide Disaster Risk (KLC 2020), this book series was in 2022 replaced by an open-access book series entitled "Progress in Landslide Research and Technology" (P-LRT), published by Springer Nature (Sassa 2021b). The book series is one of the ICL main contributions to the KLC 2020 Landslide Commitment. Many signatories of the KLC 2020 Landslide Commitment are active in technology development and technology transfer (Konagai 2021a; 2021b; 2021c; 2021d). This article is well aligned with the title and aims of the new ICL book series, as well as it is a contribution to the KLC 2020 Landslide Commitment activities (Sassa 2021a).

In this study, the focus was given to the field of progress in landslide research and technology as can be evaluated by the wealth of landslide-related patents in freely accessible databases of patent documents, using the basics of patent searching (Clarke 2018).

The following research questions were defined when working for this study:

- what is the number of landslide-related patent documents in diverse databases;
- what is the share of landslide-related patent documents coming from academic institutions, research institutions, ministries or other public bodies, and industry;

- in which technical fields landslide-related inventions are claimed;
- which countries are leaders in patenting landslide technologies;
- how often scientific journals cite landslide-related patent documents?

2 Materials and Methods

2.1 Meaning of the Term "Patent"

When searching in databases or on the web for information related to patents, we should bare in mind that the English word "patent" has several meanings (Lexico 2022):

- patent as noun with synonyms such as copyright, licence, legal protection, right, … or adjective with synonyms such as patented, licensed, protected, … (this meaning is of relevance for this study);
- patent as adjective with synonyms such as obvious, clear, evident, apparent, … (and this is not relevant for this study).

and results of a search must be checked for this difference (for more definitions on the term "patent" you may see (Collins 2022)). Furthermore, some publishers (e.g. Springer Nature) demand that all the authors of a manuscript reveal their potential competing interests among them also whether they held any patents related to the content of published articles. This fact complicates any search for patents in their database (i.e. SpringerLink).

2.2 Patent Documents Databases

There are different search engines available to search for patent documents, among others:

- Espacenet is a free-of-charge patent search engine offered by the European Patent Office (EPO 2022a) that includes 130 + million patent documents from around the world (EPO 2022b).
- Google Patents is a patent search engine created by Google that includes 120 + million patent publications from 100 + patent offices around the world (Google 2022).
- Derwent Innovations Index is a research tool within Web of Science (Clarivate 2022a) with patent information on more than 30 million inventions detailed in over 65 million patent documents from over 50 patent issuing authorities, including information on patent citations.
- Innography PatentScout™ is a private web-based platform (Clarivate 2022c).

The Espacenet database of inventions and technical developments covers the period from 1782 to today. The following definitions are helpful to understand the elements of patent documents (EPO 2022b):

- *Applicant*: A person (i. e. natural person) or an organization (i. e. legal entity) that has filed a patent application. There may be more than one applicant per application.
- *Claims:* Part of a patent application or specification. Defines the technical features for which protection is sought. There are dependent and independent claims. Independent claims contain the main features of the invention. Any independent claim can be followed by one or more dependent claims.
- *Classification:* Patent classification is a system of sorting inventions and their documents into technical fields covering all areas of technology. Espacenet shows the International Patent Classification (IPC, established in 1971; IPC 2022) and the Cooperative Patent Classification (CPC 2022), where available. Every patent document, regardless of whether it is an application or a granted patent, is given one or more classification symbols by an examiner indicating that it is allocated to a specific area of technology.
- *Country codes:* consist of two letters indicating the country or organization where the patent application was filed or granted.
- *Description*: Part of a patent application or specification. Discloses the invention as claimed, specifies the technical field to which the invention relates and indicates any prior art the applicant is aware of.
- *Inventor:* A person designated as an inventor in a patent application. An inventor can also be an applicant. An inventor is always a natural person. There may be more than one inventor per application.
- *Patent family*: Set of interrelated patent applications filed in one or more countries to protect the same or a similar invention by a common inventor and linked by a common priority (or priorities).

In the Google Patents database one can search among patent titles, abstracts, claims, or in all three of them.

In the Derwent Innovations Index one can search among patent titles ("Title"), patent titles and abstracts ("Topic"), inventor names ("Inventor"), patent assignee names ("Assignee") and patent numbers ("Patent Number").

2.3 Patent Classifications

Patent offices worldwide use the International Patent Classification (IPC 2022). There are approximately 70 000 different IPC codes for different technical areas, grouped to

classes A to H: A-Human necessities, B-Performing operations; transporting, C-Chemistry; metallurgy, D-Textiles; paper, E-Fixed constructions, F-Mechanical engineering; lighting; heating; weapons; blasting engines or pumps, G-Physics, H-Electricity.

The Cooperative Patent Classification (CPC 2022) is an extension of the IPC and is jointly management by the European Patent Office (EPO) and the US Patent and Trademark Office (USPTO 2022). It is divided into nine sections, A-H (as in IPC) and Y, and there are approximately 250,000 classifications entries (CPC 2022). Not being part of the IPC, the Class Y is for general tagging of new technological developments and cross-sectional technologies. There is available a statistical mapping of the IPC to CPC classification, if needed.

2.4 Patent Documents Citations

Looking at patent documents, a research question whether and to which extent these documents are cited in scientific literature, specifically in the indexed journals that are available in diverse databases. We used SpringerLink and SCOPUS to look at the total number of landslide-related patents cited. To look at the individual review and original research articles citing landslide-related patent documents, we have selected Web of Science (Clarivate 2022b) as a global citation database with almost 1.9 billion cited references from over 171 million records.

3 Results and Discussion

3.1 The Number of Landslide-related Patent Documents

We used a set of over 30 search terms in the three databases (Espacenet, Google Patents, and Derwenta Innovations Index) and the results are shown in Tables 1, 2 and 3. We tried to cover the variety of landslide forms (Hungr et al. 2014), without going into too much detailed description of different forms—mainly the terms "earth", "debris", "falling rock/stone", "landslide", "mudflow", "rock avalanche", and "rockfall" were used. We intentionally did not want to add some typical technological solutions (structural measures), such as "retaining wall" or "drainage", since they have very high number of patent documents (e.g. "retaining wall(s)" with over 100,000 patent documents having this term in their description).

Typically, the largest number of landslide-related patent documents were found when searching in all text fields or description (Espacenet), and less when looking only in the Title or Abstract. For the Google Patents database, the best option was to look at the "Title, Abstract, and Claims"—only Abstracts or Claims can yield too high numbers (i.e. 135,828). For the Derwenta Innovation Index, only Title and Topic was searchable, yielding comparable number of patent documents. Comparing all three databases, the most patent documents are related to "Retaining walls" followed by "Landslide(s)", "Debris flow(s)", "Mudflow(s)", "Rock fall (s)", and "Falling rock(s)". It is clear that more general terms describing processes rather than technology are prevailing—overlooking the search term "Retaining walls" as a geotechnical technique not applicable only in landslide disaster risk reduction. In total, a rough estimation is that in the Google Patents database there is 15,000 + landslide-related patent documents, and in the Espacenet and the Derwent Innovation index database 5000+, respectively.

3.2 Patent Documents, Inventors and Applicants

For the analysis of science and non-science-based landslide-related patents we used only the Espacenet database and the selected 18 search terms in "Claims" (Table 4). The Inventors respectively Applicants were grouped into Academic institutions and Research institutions for science-based patents, and to Ministries and Industry for non-science-based patents (for search terms see the legend at the end of Table 4). General conclusion can be that the number of technological (non-science) based patents is higher than that of academic (science-based) patents, with some specific field of applications, where the situation is the opposite (e.g. "Debris flow(s)", "Landslide displacement", "Landslide monitoring").

3.3 Patent Documents and Technical Field

We have classified the landslide-related patent documents from two databases: (i) the Espacenet using 4 search terms (Debris flow(s), Falling rock(s), Landslide(s), Mud flow(s)) in Title, and (ii) Derwent innovation Index using the same 4 search terms in Topic. We applied the International Patent Classification (IPC 2022), and the results are given in Tables 5 and 6. The total number of patent documents in Tables 5 and 6 can vary as patents documents can be attributed to more than just one category. The Derwent Innovation Index database yields more landslide-related patent documents than the Espacenet database.

In both databases, the prevailing patent documents are found by searching the term "Landslide(s)", followed by the term "Debris flow(s)", "Falling rock(s)" and "Mud flow(s)". With regard to the different areas of technology to which landslide-related patent documents pertain, the categories

Table 1 Results of landslide-related patent documents found in the Espacenet database (EPO 2022b)

Search term	Part of the patent document					
	Title	Abstract	Claims	Title, abstract or claims	Description	All text fields
Earth flow(s) = Earth-flow(s)	14	68	93	162	580	691
Earth slide(s) = Earth-slide(s)	10	39	17	60	135	188
Debris flow(s)	1141	1742	2170	2787	11,315	11,754
Debris flow early warning	33	47	58	79	124	140
Debris flow monitoring	56	84	113	141	273	286
Deep seated landslide(s) = Deep-seated landslide(s)	1	4	2	6	8	12
Earthquake landslide(s)	10	39	25	48	276	291
Earthquake induced landslide(s) = Earthquake-induced landslide(s)	3	4	2	4	45	47
Falling rock(s) = Falling-rock(s)	385	976	1166	2008	9765	10,111
Falling stone(s)	212	635	430	1090	3195	3718
Landslide(s)	3383	7028	8520	11,985	50,733	52,423
Landslide activity	2	3	5	6	88	88
Landslide dam break	1	3	3	5	7	9
Landslide deformation	36	94	108	154	490	503
Landslide depth	4	8	9	15	46	52
Landslide detection	48	68	117	144	373	390
Landslide disaster(s)	110	309	301	472	2446	2484
Landslide displacement	79	131	172	205	466	478
Landslide drainage	5	10	12	16	39	42
Landslide early warning	83	155	72	173	208	281
Landslide early warning method	27	29	21	36	24	40
Landslide early warning system	20	24	22	35	38	48
Landslide emergency	13	27	18	34	93	101
Landslide hazard	42	63	163	191	621	651
Landslide mitigation	0	0	1	1	11	12
Landslide monitoring	285	448	439	579	1442	1504
Landslide observation	2	4	10	11	58	58
Landslide reinforcement	8	11	21	28	103	106
Landslide retaining	13	13	19	32	52	63
Landslide risk	39	121	116	182	408	454
Landslide safety	12	29	32	48	87	96
Landslide stability	18	64	61	96	274	288
Landslide susceptibility	20	22	36	41	91	94
Landslide velocity	0	1	8	8	16	16
Landslide vulnerability	0	2	4	4	20	20
Mudflow(s)	82	130	234	382	1309	1542
Mud flow(s) = Mud-flow(s)	103	700	2162	2661	12,615	13,213
Preventing landslide(s)	73	108	143	238	888	988
Rainfall-induced landslide(s)	12	18	18	27	104	109
Rock avalanche(s)	1	5	13	18	97	103
Rock fall(s) = Rock-fall(s)	171	380	722	1026	4855	5235
Shallow landslide(s)	15	30	30	44	286	293
Submarine landslide(s)	43	52	62	68	359	398

Table 2 Results of landslide-related patent documents found in the Google Patents database (Google 2022)

Search term	Part of the patent document			
	Title	Abstract	Claims	Title, abstract and claims
Earth flow(s)	518	38,674	135,828	254
Earth slide(s)	279	56,539	135,828	87
Debris flow(s)	6781	135,828	135,828	3845
Debris flow early warning	123	604	6064	108
Debris flow monitoring	215	8914	46,251	158
Deep seated landslide(s)	0	19	42	0
Earthquake landslide(s)	65	409	453	54
Earthquake induced landslide(s)	14	82	103	10
Falling rock(s)	1075	9431	12,913	490
Falling stone(s)	470	9015	17,808	129
Landslide(s)	4694	10,354	10,813	3872
Landslide activity	3	109	304	3
Landslide dam break	12	72	113	10
Landslide deformation	121	1152	1338	105
Landslide depth	106	728	1535	98
Landslide detection	252	1304	2192	204
Landslide disaster(s)	262	1672	1316	224
Landslide displacement	201	1155	1664	197
Landslide drainage	67	785	950	46
Landslide early warning	322	863	1183	299
Landslide early warning method	134	418	610	119
Landslide early warning system	147	491	862	134
Landslide emergency	44	261	297	39
Landslide hazard	147	1163	1065	121
Landslide mitigation	243	817	999	133
Landslide monitoring	845	2304	2534	788
Landslide observation	825	2390	2719	759
Landslide reinforcement	116	1178	1243	99
Landslide retaining	62	629	756	48
Landslide risk	118	659	727	98
Landslide safety	37	1507	912	34
Landslide stability	67	1650	1170	49
Landslide susceptibility	24	43	71	21
Landslide velocity	33	529	1,313	32
Landslide vulnerability	69	450	535	60
Mudflow(s)	4614	10,961	13,784	3756
Mud flow(s)	2211	52,130	124,229	1334
Preventing landslide(s)	477	3109	2450	304
Rainfall-induced landslide(s)	35	153	199	29
Rock avalanche(s)	164	13,586	15,558	66
Rock fall(s)	2288	29,891	37,681	1455
Shallow landslide(s)	32	128	148	26
Submarine landslide(s)	57	154	413	50

Table 3 Results of landslide-related patent documents found in the Derwent Innovation Index database (Clarivate 2022a)

Search term	Part of the patent document	
	Title	Topic
Earth flow(s) = Earth-flow(s)	5	22
Earth slide(s) = Earth-slide(s)	2	13
Debris flow(s)	1082	1854
Debris flow early warning	35	67
Debris flow monitoring	49	73
Deep seated landslide(s) = Deep-seated landslide(s)	1	1
Earthquake landslide(s)	23	95
Earthquake induced landslide(s) = Earthquake-induced landslide(s)	1	1
Falling rock(s) = Falling-rock(s)	140	496
Falling stone(s)	342	1011
Landslide(s)	3273	6553
Landslide activity	0	2
Landslide dam break	0	1
Landslide deformation	63	127
Landslide depth	4	12
Landslide detection	39	62
Landslide disaster(s)	211	444
Landslide displacement	101	159
Landslide drainage	4	5
Landslide early warning	81	136
Landslide early warning method	21	25
Landslide early warning system	24	33
Landslide emergency	13	20
Landslide hazard	24	61
Landslide mitigation	0	1
Landslide monitoring	316	454
Landslide observation	1	6
Landslide reinforcement	3	8
Landslide retaining	4	6
Landslide risk	43	118
Landslide safety	12	26
Landslide stability	23	46
Landslide susceptibility	9	12
Landslide velocity	0	0
Landslide vulnerability	3	4
Mudflow(s)	48	146
Mud flow(s) = Mud-flow(s)	112	497
Preventing landslide(s)	58	225
Rainfall-induced landslide(s)	11	15
Rock avalanche(s)	7	11
Rock fall(s) = Rock-fall(s)	210	662
Shallow landslide(s)	14	24
Submarine landslide(s)	34	49

Legend Topic = Title and Abstract

Table 4 Landslide-related patent documents with at least 100 claims found in the Espacenet database (EPO 2022b), with respect to inventors and applicants' category

Landslide-related patent documents		Inventors and applicants from			
Search term	No. of Claims	Academic institutions	Research institutions	Ministries	Industry
Debris flow(s)	2170	605	480	48	705
Debris flow monitoring	113	30	21	5	51
Falling rock(s) = Falling-rock(s)	1166	183	105	14	525
Falling stone(s) = Falling-stone(s)	430	76	64	3	190
Landslide(s)	8520	1988	935	110	3659
Landslide deformation	108	56	19	2	28
Landslide detection	117	25	17	2	47
Landslide disaster(s)	301	106	55	8	91
Landslide displacement	172	91	15	2	49
Landslide hazard	163	83	28	11	44
Landslide monitoring	439	173	51	3	170
Landslide risk	116	46	32	3	28
Mudflow(s)	234	24	39	3	31
Mud flow(s) = Mud-flow(s)	2162	176	170	13	773
Preventing landslide(s)	143	13	13	1	50
Rock fall(s) = Rock-fall(s)	722	55	45	6	264

Legend abbreviations used for Academic institutions (College, University, Univ), Research Institutions (Institute, Research, Res, Inst), Ministries (Ministry, Min), Industry (Co, Comp, Eng, Ltd, Plc)

Table 5 International Patent Classification (IPC 2022) used for classification of patents and utility models according to the different areas of technology to which they pertain. Selected landslide-related patent documents from the Espacenet database (EPO 2022b), with respect to the field of IPC

		Search term in title			
	Category of IPC	Debris flow(s)	Falling rock(s)	Land-slide(s)	Mud flow(s)
A	Human necessities	14	5	70	2
A01	*Agriculture; Forestry; Animal husbandry; Hunting; Trapping; Fishing*	*11*	*2*	*58*	*2*
B	Performing operations; Transporting	25	14	84	3
C	Chemistry; Metallurgy	9	2	22	1
D	Textiles; Paper	0	4	1	0
E	Fixed constructions	512	309	1276	75
E01	*Constructions of roads, railways, or bridges*	*115*	*283*	*126*	*3*
E02	*Hydraulic engineering; Foundations; Soil-shifting*	*419*	*55*	*1115*	*21*
E03	*Water supply; Sewerage*	*22*	*0*	*68*	*0*
E21	*Earth or rock drilling; Mining*	*22*	*18*	*107*	*53*
F	Mechanical engineering; Lightning; Heating; Weapons; Blasting	21	24	67	6
G	Physics	660	52	2125	42
G01	*Measuring; Testing*	*295*	*35*	*1235*	*30*
G06	*Computing; Calculating or counting*	*210*	*15*	*512*	*5*
G08	*Signalling*	*233*	*20*	*700*	*12*
G09	Educating; Cryptography; Display; Advertising; Seals	*34*	*2*	*112*	*0*
H	Electricity	33	8	158	1
H02	*Generation, conversion, or distribution of electric power*	*9*	*3*	*56*	*0*
H04	*Electric communication technique*	*21*	*2*	*94*	*1*
A-H	Total patent documents	1141	385	3383	103

Legend Categories A to H are taken from the IPC

Table 6 International Patent Classification (IPC 2022) used for classification of patents and utility models according to the different areas of technology to which they pertain. Selected landslide-related patent documents from the Derwent Innovation Index database (Clarivate 2022a), with respect to the field of IPC

		Search term in topic			
	Category of IPC	Debris flow(s)	Falling rock(s)	Land-slide(s)	Mud flow(s)
A	Human necessities	89	22	566	32
A01	*Agriculture; Forestry; Animal husbandry; Hunting; Trapping; Fishing*	*47*	*7*	*419*	*25*
B	Performing operations; Transporting	224	90	683	102
B65	*Conveying; Packing; Storing; Handling thin or filamentary material*	8	8	*123*	5
C	Chemistry; Metallurgy	40	11	163	88
D	Textiles; Paper	3	5	17	1
E	Fixed constructions	734	336	2525	268
E01	*Constructions of roads, railways, or bridges*	*142*	*178*	*276*	*15*
E02	*Hydraulic engineering; Foundations; Soil-shifting*	*530*	*89*	*2059*	*51*
E03	*Water supply; Sewerage*	*58*	*0*	*219*	*4*
E21	*Earth or rock drilling; Mining*	*68*	*105*	*249*	*199*
F	Mechanical engineering; Lightning; Heating; Weapons; Blasting	83	45	214	49
G	Physics	872	78	3186	80
G01	*Measuring; Testing*	*375*	*43*	*1791*	*48*
G06	*Computing; Calculating or counting*	*256*	*22*	*856*	*16*
G08	*Signalling*	*326*	*26*	*1029*	*15*
G09	Educating; Cryptography; Display; Advertising; Seals	*34*	*7*	*130*	*2*
H	Electricity	78	20	420	14
H02	*Generation, conversion, or distribution of electric power*	*23*	*4*	*129*	*6*
H04	*Electric communication technique*	*47*	*10*	*249*	*8*
A-H	Total patent documents	1854	496	6553	497

Legend Categories A to H are taken from the IPC

"G-Physics" and "E-Fixed constructions" are clearly prevailing: "G" for debris flows and landslides, and "E" for fallings rocks and mudflows. Other IPC categories are much less present—in the order of a few percentages.

Within the category "E-Fixed constructions", the most abundant is category "E02-Hydraulic engineering; Foundations; Soil-shifting" (roughly one third of all landslide-related patent documents). Within the category "G-Physics", the most abundant is category "G1- Measuring; Testing" followed by "G08-Signalling".

3.4 Patent Families, Country of Publication

For the analysis of landslide-related patent documents with regard to the country of publication we used patent family distribution in the Espacenet, the Google Patents, and the Derwent Innovation Index databases for 4 search terms in titles of patent documents ("Debris flow(s)", "Falling rock (s)", "Landslide(s)", "Mud flow(s)"). In all three databases, the most abundant category of patents was related to "Landslide(s)", followed by "Debris flow(s)". For country codes we used the two-letter abbreviations from the Espacenet. The search string for the Espacenet database was limited to the Title. The search string for the Google Patents database was limited to Title, Abstract, and Claim: e.g. (TI = (debris flow)) (AB = (debris flow)) (CL = (debris flow)) country:EP. The search in the Derwent Innovation Index was performed for Topics, covering patent titles and abstracts, and country of publication was searched in the Patent Number. The results are given in Tables 7, 8 and 9.

The majority of all landslide-related patents are filled and/or granted in China (abbr. CN). This is a bit less so pronounced for patents related for falling rock(s) and mud flow(s). Due to China contribution, the five major emerging economies: Brazil, Russia, India, China, and South Africa, are outperforming the rest of the world, also major developed countries: USA, European Union, Japan and Republic of Korea. The majority of landslide-related patents are issued by national patent offices in single countries, and thus the contribution of the World Intellectual Property Organization (WIPO) and the European Patent Office (EPO) jointly is only

Table 7 The number of patent families of landslide-related patent documents from the Espacenet database (EPO 2022b), with respect to the country of patent publications

		Search term in title			
Code	Country of patent publication	Debris flow(s)	Falling rock(s)	Landslide(s)	Mud flow(s)
AT	Austria	1	9	5	1
AU	Australia	3	4	10	7
BR	Brazil	1	4	2	4
CA	Canada	2	3	6	10
CH	Switzerland	3	11	6	1
CN	China	1052	128	2802	38
DE	Germany	0	8	11	6
EP	European Patent Office (EPO)	3	16	14	6
FR	France	0	3	6	5
GB	United Kingdom	2	0	3	7
IN	India	0	0	0	0
IT	Italy	1	4	7	0
JP	Japan	32	67	311	6
KR	Republic of Korea	58	181	112	0
RU (SU)	Russian Federation (Soviet Union)	0 (0)	2 (2)	81 (48)	9 (11)
TW	China Taipei	8	5	21	5
US	United States of America	17	11	27	30
WO	World Intellectual Property Organization (WIPO)	20	8	36	10
ZA	South Africa	4	2	3	3
	Total patent documents	1157	386	3460	104

Legend Country codes are taken from the Espacenet

a few percentages, in all three databases. This is in line with the general picture of the world patent applications.

Cheng and Drahos (2018) studied China Patent Office and concluded that in 2011 the Chinese patent office overtake U.S. in terms of patent applications and became the biggest patent office in the world. From 2010 to 2020, the proportion of international patents granted to inventors from high-income countries fell from 78 to 48% (NSB & NSF 2022). The U.S. share of international patents declined from 15 to 10%. The same share declined from 35 to 15% for Japan and 12% to 8% for the EU-27. In contrast, China's share of international patents increased from 16% in 2010 to 49% in 2020.

WIPO (2021) reports that in 2020 in total 45.7% of all patent applications worldwide was filled in China (1,497,159 out of 3,276,700 applications). With regards to patent applications, China was followed by USA, Japan, Republic of Korea, Germany, France, UK, Switzerland, India, and the Netherlands—considering resident and non-resident patent applicants. In the field of landslide-related patents, India and the Netherlands are much less active, and also USA are behind Japan and Republic of Korea, but in front of EU member countries.

Following the undisputed China as number one, the next strongest countries in patent applications are: USA and Republic of Korea for debris flow(s), Republic of Korea and Japan for falling rock(s) and for landslide(s), and USA for mud flow(s).

3.5 Patent Documents Citations

The annual number of patent applications in the world can be taken from the World Bank data (World Bank 2022a, b), the data for 1990, 2000, 2019 and 2020 are presented in Table 10. Worldwide, there is a steady growth of patent applications, from less than 1 million in 1990 to over 3 million in 2020. Residents of countries where patent applications were filled, are generally outnumbering non-residents for many countries, but not in Australia, Brazil, Canada, India, South Africa, and USA.

Looking at the World Bank data (data.worldbank.org), since 2000 the ratio between the number of scientific and technical journal articles published in the World to the number of patent applications in the World is roughly 1:1, in favor of the patent applications for a few 10%—in 2000:

Table 8 Selected landslide-related patent documents from the Google Patent database (Google 2022), with respect to the country of patent publication

		Search term in title, abstract, and claim			
Code	Country of patent publication	Debris flow(s)	Falling rock(s)	Landslide(s)	Mud flow(s)
AT	Austria	2	0	0	0
AU	Australia	9	3	3	3
BR	Brazil	10	1	1	1
CA	Canada	22	1	2	14
CH	Switzerland	5	0	1	0
CN	China	3142	284	3508	1059
DE	Germany	120	1	5	27
EP	European Patent Office (EPO)	37	5	6	18
FR	France	17	0	0	0
GB	United Kingdom	9	0	0	5
IN	India	0	0	0	0
IT	Italy	0	0	0	0
JP	Japan	78	143	145	11
KR	Republic of Korea	90	54	66	9
RU (SU)	Russian Federation (Soviet Union)	14 (0)	0 (0)	82 (20)	22 (22)
TW	China Taipei	14	2	3	2
US	United States of America	114	4	19	52
WO	World Intellectual Property Organization (WIPO)	75	6	23	30
ZA	South Africa	0	0	0	0
	Total patent documents	3880	494	3937	1341

Legend Country codes are taken from the Espacenet

1,377,500 patent applications to 1,066,335 articles; in 2018: 3,325,500 patent applications to 2,554,319 articles. Both categories are growing, but the ratio remains approximately stable. The annual productivity of scientific articles can also be estimated using Scimago data (SJR 2022) that gives the productivity in 2021 in the world close to 5 million citable documents (articles, reviews, and conference papers). This estimate is higher than the of the World Bank, since also conference papers are taken into account.

For the analysis on patent document citations in scientific articles, we have selected two databases, SpringerLink and SCOPUS. The search string for SpringerLink was done within Articles "patent AND (landslides OR "debris flow" OR "falling rock" OR mudflow)", and the search string for SCOPUS database was: ALL ("debris flow" OR "falling rock" OR landslide OR "mud flow") AND patent AND (LIMIT-TO (DOCTYPE, "AR")) AND (LIMIT-TO (SUBJAREA, "EQART") OR LIMIT-TO (SUBJAREA, "ENGI")) AND (LIMIT-TO (SRCTYPE, "j"))—the search was for landslide-related and patent-related articles published in journals limited to two subject areas of "Earth and Planetary Science" and "Engineering", respectively, for the period between 2012 and 2021. The results of this search are given in Table 11. Even though SCOPUS was limited to only two subject areas, the number of citing landslide-related patent documents was comparable to SpringerLink. The absolute number of citations is extremely low (a few tens of citations per year only), having in mind the total number of landslide-related patent documents (Tables 7, 8 and 9). Only a fraction of the order of a few one-in-thousands of landslide-related patents documents are cited annually in journal review and research articles. This situation does not change, if we add mentions of patent documents to their citations.

Finally, we have selected 10 landslide-related journals from the Web of Science database that regularly publish scientific articles and technical papers on landslide science and technology. Half of them were as such already recognized by Mikoš (2017), who studied top publications in geological engineering and engineering geology. We searched for those published articles in these ten journals that are citing patent documents and are to some extent related to landslide risk reduction. Table 12 shows all those 45 landslide-related articles that cite a patent document as a reference (14 articles) or at least mention patents in the text (31 articles). This analysis is another proof that landslide-related patent documents are extremely rarely cited in scientific literature if measured by journal articles.

Table 9 Selected landslide-related patent documents from the Derwent Innovation Index database (Clarivate 2022a), with respect to the country of patent publications searched in the Patent Number

		Search term in topic			
Code	Country of patent publication	Debris flow(s)	Falling rock(s)	Landslide(s)	Mud flow(s)
AT	Austria	1	2	0	0
AU	Australia	12	5	21	11
BR	Brazil	2	3	20	10
CA	Canada	9	7	17	34
CH	Switzerland	2	4	7	1
CN	China	1739	232	5659	337
DE	Germany	4	52	15	1
EP	European Patent Office (EPO)	21	22	49	36
FR	France	1	10	13	0
GB	United Kingdom	2	4	4	14
IN	India	5	6	46	4
IT	Italy	0	4	16	2
JP	Japan	25	16	400	24
KR	Republic of Korea	39	162	235	9
RU (SU)	Russian Federation (Soviet Union)	3 (0)	7 (0)	77 (0)	18 (0)
TW	China Taipei	5	1	32	6
US	United States of America	71	26	140	118
WO	World Intellectual Property Organization (WIPO)	48	28	141	66
ZA	South Africa	1	2	3	1
	Total patent documents	1887	484	6553	514

Legend Country codes are taken from the Espacenet

Table 10 Patent applications in the World Bank database (i.e. World Development Indicators), given for selected countries where patents were filled, and separately for residents and non-residents (World Bank 2022a, b)

		Residents				Non-residents		
Country	1990	2000	2019	2020	1990	2000	2019	2020
Australia	–	1928	2637	2368	–	20,073	27,121	26,926
Austria	2025	1961	2066	2124	670	340	208	173
Brazil	2389	3179	5464	5280	5148	14,104	19,932	19,058
Canada	2549	4187	4238	4452	24,375	35,435	32,250	30,113
China	5853	25,397	1,243,914	1,345,243	5,365	34,804	173,317	173,538
France	12,378	13,870	14,103	12,771	4260	3483	1766	1542
Germany	30,724	51,736	46,632	41,260	8605	10,406	20,802	19,845
India	1147	2206	19,454	23,141	2673	6332	34,173	33,630
Italy	–	7877	9229	10,061	–	1396	898	947
Japan	333,230	387,364	245,372	227,348	34,360	49,501	62,597	61,124
Korea, Republic of	9082	72,831	171,603	180,477	16,738	29,179	47,372	46,282
Russian Federation	–	23,377	23,337	23,759	–	8960	12,174	11,225
South Africa	1093	895	567	542	4943	2400	6347	6146
Switzerland	2987	2083	1369	1384	1081	468	348	301
United Kingdom	19,310	22,050	12,061	11,990	8928	10,697	7189	8659
United States of America	90,643	164,795	285,113	269,586	80,520	131,100	336,340	327,586
World	687,700	874,800	2,231,800	2,304,400	309,800	502,700	994,300	972,300

Table 11 Number of journal review and research articles in SpringerLink and SCOPUS citing landslide-related patent documents (Elsevier 2022; Springer Nature 2022a)

	SpringerLink			SCOPUS		
Year	Patent-related articles	Citing patent documents	Mentioning patents	Patent-related articles	Citing patent documents	Mentioning patents
2021	27	3	2	37	1	–
2020	19	4	–	22	–	2
2019	11	2	–	10	–	-
2018	13	–	–	16	–	2
2017	18	4	5	20	1	-
2016	10	1	–	13	2	2
2015	23	1	2	21	–	2
2014	11	1	2	6	–	–
2013	6	1	1	11	–	1
2012	7	1	–	4	–	–
In total						

Table 12 Cited landslide-related patent documents in the ten selected landslide-related journals from the Web of Science database (Clarivate 2022b)

Journal (period under study)	Articles citing a patent (WoS citations)	Citation from the text	As a references
Acta Geotechnica (2006–2022)	Wu et al. (2021) (1 citation)	A patented additive was developed to be added to the air injection to accelerate consolidation of soft ground so that the fractures remain stable for longer time	Wu (2015)
	Di Prisco and Pisanò (2014) (5 citations)	A recently patented device (tensioned elements TFEG®—Guided Extrusion Force Transfer) has been taken as a reference for numerical analyses, trying to keep the geometrical configuration as simple as possible, but sufficiently accurate to reproduce the most relevant structural details	No
Bulletin of Engineering Geology and the Environment (2015–2022)	Kahraman et al. (2022) (no citations)	Patented hard rock Tunnel Boring Machine (TBM) cutterhead equipped with microwave generating mechanism Patented microwave assisted rock cutting method	Feng et al. (2019) Lindroth et al. (1991)
	Ying et al. (2021) (1 citation)	A casing and grouting method for micropiles, small-diameter drilled piles	Groneck and Amour (2000)
	Wang et al. (2021b) (no citations)	The research team of the author developed patented triaxial apparatus for unsaturated soil that can control the suction in soil	No
	Xue et al. (2021) (no citations)	A patented soil matric potential sensor was used in the study (Patent No.: DE10164018B4)	No
	Wang et al. (2021a) (7 citations)	Patented rock straight shear rheometer	No
	Zhou et al. (2021) (1 citation)	A patented electrically conductive wick drain and a specially designed automated power supply to carry out field electroosmosis tests on a sludge landfill site	No
	Wei et al. (2020) (4 citations)	Patented SH agent made of modified PVA and water is a nontoxic liquid and a soluble polymer, has 6% solid matter and generates a film and a silk-like web in soil after drying, and the film is insoluble in water	No

(continued)

Table 12 (continued)

Journal (period under study)	Articles citing a patent (WoS citations)	Citation from the text	As a references
	Jiang et al. (2020) (no citations)	Patent pending floating ball method (FBM) is a groundwater level monitoring technique for vacuum preloading	No
	Cui et al. (2019) (13 citations)	A patented non-disturbance sampling technique for rock cores under high in situ stress relaxation during the coring procedure	No
	Mastrorocco et al. (2018) (12 citations)	Patent pending Leica™ TruView is a plug-in that allows visualization of 3D Virtual Reality (VR)	No
	Li et al. (2017) (6 citations)	A patented device for estimating joint roughness coefficient (JRC) and peak shear strength of rock joints by the National Patent Office of China	No
	Fan et al. (2017) (6 citations)	Deep dislocation displacement monitoring of the slip surface is typically obtained from the advised method in the patented "device about measuring the depth of slip surface and deep dislocation displacement"	Meng et al. (2007)
	Ghobadi et al. (2015) (7 citations)	Patented method Hydroxylating Conversion Treatment (HCT)] has been used to protect carbonate stones such as marble, limestone and travertine	US (2001)
Computers and Geotechnics (1985–2022)	Li et al. (2020) (2 citations)	A new design with non-uniform thickness geotextile mats, where the height of geotextile mats varies, i.e. shorter mats were used close to the bottom while relatively higher mats were used for the top layers, was proposed and patented to enhance the stability of dike	No
	Cai et al. (2019) (26 citations)	The artificial ground freezing technique was patented by German mining engineer F. H. Poetsch in 1883	No
	Vitel et al. (2015) (74 citations)	Patented by Poetsch in Germany in 1883, the artificial ground freezing technique (AGF) appeared 150 years ago in coal mines in South Wales	No
	Park et al. (2011) (5 citations)	The electric discharge occurs through the Electro-power impact cell (Korea patent 10–2009-0,113,602)	No
	Fan and Hsieh (2011) (13 citations)	A series of connecting elements are used to incorporate reinforced earth embankments with soil nails. The connecting element, improved from a patented connecting method (Chou and Fan 2004), consists of a series of stainless steel wire ropes and stainless steel pipes	Chou and Fan (2004)
	Cividini et al. (2011) (1 citation)	A key point of the technology used in this study is represented by a valve, internationally patented by Visconti Fondazioni (Milan, Italy), that seals the bottom section of the casing	No
	Chupin et al. (2009) (18 citations)	A sleeved grout pipe and a double packer are used to inject grout into sand. A patented cement-based grout, similar to those manufactured for fieldworks, is utilized	No
Engineering Geology (1965–2022)	Comina et al. (2021) (no citations)	In this study, the application an innovative (patent pending) soil improving system by injections of a sand/gravel mixture was evaluated	No
	Li et al. (2021) (2 citations)	The B–P shear test system consists of a YSD-200 two-dimensional fracture tester for rock and soil with a special fixture, which was developed and patented	No

(continued)

Table 12 (continued)

Journal (period under study)	Articles citing a patent (WoS citations)	Citation from the text	As a references
	Tan et al. (2020) (2 citations)	A patented door-opening system is utilised to assist the door opening process for initiating debris flows uniformly and quickly	No
	Massimi et al. (2016) (2 citations)	Twisting Theory (TWT) and Twisting Algorithm (TWA) were developed by M. Buscema in 2010 at Semeion Research Center of Sciences of Communication in Rome and are protected (Buscema 2014)	Buscema (2014)
Geomorphology (1987–2022)	Vayssière et al. (2019) (5 citations)	The automatic resistivity profiling (ARP) uses a patented multi-electrode device that is connected to wheel-based electrodes that roll over the ground surface	No
	Chambers et al. (2011) (109 citations)	Mobile resistivity mapping was undertaken using the automated resistivity profiling (ARP) technique, which uses a patented multi-electrode device (Geocarta SA, France) in order to make direct current (DC) measurements of subsurface electrical resistivity along profiles with the aim of producing horizontal property maps	No
	Prior and Hooper (1999) (30 citations)	The Enhanced Surface Rendering (ESR) is a patented method used for high-quality data acquired in water depths greater than 250 m, to display data as an artificially illuminated surface depicting bottom morphology and/or acoustic amplitude	No
	Florinsky (1996) (26 citations)	Digital elevation models (DEMs) and DEM analysis methods are used for fault recognition as about 90% of fault geomorphic indices can be defined quantitatively—also the patented technique of thalweg revealing	Eliason and Eliason (1987)
Geotextiles and Geomembranes (1984–2022)	Koerner and Koerner (2018) (36 citations)	In 1966, H. Vidal of France wrote the first of several papers on "reinforced earth", a technique he initiated, developed, patented and promoted (Vidal 1969)	Vidal (1969)
	Hou et al. (2017) (25 citations)	Zhang (2005) proposed a patented horizontal-vertical (H-V) reinforcement that attached several small inclusions vertically to the horizontal reinforcement	Zhang (2005)
	Koerner and Koerner (2013) (85 citations)	In 1966, H. Vidal of France wrote the first paper on reinforced earth, a technique he initiated, developed, patented and promoted (Vidal 1969)	Vidal (1969)
	Liu et al. (2009) (8 citations)	The second method is to embed two shielded thin copper wires in the Prefabricated vertical drain (PVD),—this method has been patented (Ren 2004)	(Ren, 2004)
	Koerner and Koerner (2006) (86 citations)	Flexible sand-filled tubes were made as early as 1957, but they were not very successful. Eventually in 1967, a patent was granted to a Danish firm	No
	Hazarika (2006) (68 citations)	Geofoam usage dates as far back as the 1960s, when a patent for using geofoam as pavement insulation was granted in the USA	No
	Koerner and Koerner (1996) (6 citations)	Efforts to form flexible sand-filled tubes were made as early as 1957, but were not very successful. Eventually, in 1967, a patent was granted The process of joining two sheets of geotextiles to form erosion control mattresses was developed in 1965, and numerous patented systems are available	No

(continued)

Table 12 (continued)

Journal (period under study)	Articles citing a patent (WoS citations)	Citation from the text	As a references
Journal of Geotechnical and Geoenvironmental Engineering (2000–2022)	Holtz (2017)	Some years ago, French architect Henri Vidal invented a system he called Terre Armée (Reinforced Earth) for construction of retaining walls. Reinforced Earth has three primary components: select granular backfill, galvanized steel strips for reinforcement, and precast concrete facing panel elements. Worldwide patents were granted in 1966, and by the early 1970s the technology was well established in France and several other countries	No
Landslides (2004–2022)	Rossi et al. (2018) (96 citations)	Innovative circular-shaped airframe fully supporting flight dynamics of a multicopter drone, patented in Italy and patent pending in EU and USA	No
	Xiao et al. (2017) (17 citations)	Soil mixture to promote vegetation for slope protection and landslide prevention (patented in 1980's)	No
	Lu et al. (2014) (77 citations)	Patented PSInSAR™ technique	No
Natural Hazards (1989–2022)	Du et al. (2020) (no citations)	A transparent experimental device to study the migration mechanism of fine particles in aquifers during water injection was patented	No
	Kazeev and Postoev (2017) (4 citations)	Institute of Environmental Geosciences of Russian Academy of Sciences (IEG RAS) has developed the criteria for limit state of the soil mass, and the methodology of the limit-state calculations, and these numerical simulations received three patents. Based on the patented methodology for limit-state analysis, a new practical method to increase slope resistance has been developed and patented. It involves construction of artificial cuts similar to erosional downcuts of natural gully or ravine	No
Rock Mechanics and Rock Engineering (2000–2022)	Castanon-Jano et al. (2017) (27 citations)	Since 1975, numerous devices have been invented to improve the dynamic behavior of falling rock protection barriers. In total, 174 patent families (inventions) have been found describing a new energy dissipating device or a new barrier in which these devices play an important role. The 174 patent families represent 120 different assignees, Fatzer (a company of the Brugg group) and Pfeifer Isofer being the most significant in both numbers of applications and granted IPR (intellectual property rights)	Thomel (1998) Von Allmen (2004) Moreillon (2006)
	Ishida et al. (2017) (66 citations)	Acoustic emission (AE) monitoring due to the stress memory effect has been applied to stress measurement in rocks, the application was patented by Kanagawa and Nakasa (1978)	Kanagawa and Nakasa (1978)

4 Conclusions and Further Work

The analysis of landslide-related patent documents, using three patent databases (Escapenet, Google Patents, Derwent Innovation Index) was performed to assess to which extent landslide science and technology is mirrored in patent applications, and what is the share of academic versus non-academic institutions. In the second part of the analysis, technical fields of patent applications were studied and countries that are the most productive ones with regard to landslide-related patent applications were searched for. The study finished by patent citation analysis in published scientific literature. The results of this study can be summarized as follow:

(i) In the Google Patents database there is 15,000 + landslide-related patent documents, and in the Espacenet and the Derwent Innovation Index database 5000+, respectively. In the patents' titles, abstracts

and claims, processes are more often used to describe the patent than the technology.

(ii) The number of technological (non-science) based patents is higher than that of academic (science-based) patents, with some specific field of applications, where the situation is the opposite.

(iii) With regard to the different areas of technology to which landslide-related patent documents pertain, the categories "G-Physics" and "E-Fixed constructions" are clearly prevailing: "G" for debris flows and landslides, and "E" for fallings rocks and mudflows.

(iv) The majority of landslide-related patents are filled and/or granted in China, followed by Japan and South Korea, USA and EU member countries—five major emerging economies (called BRICS) are outperforming developed countries, with a very prevailing Chinese contribution.

(v) Only a fraction of the order of a few one-in-thousands of landslide-related patents documents are cited in journal review and research articles.

Further analyses of landslide-related patent documents may be done with regard to other scientific information sources such as conference proceedings, or also to social media such as Twitter or Researchgate. Nevertheless, it is quite obvious that landslide-related patent documents are not studied by landslide scientists and researchers, hopefully this important category of intellectual property finds much more application in real word solutions when planning and executing landslide disaster risk reduction.

Acknowledgements The author would like to acknowledge the financial support of Slovenian Research Agency by core funding P2-0180, and of the University of Ljubljana from the Development Fund for the activities of the UNESCO Chair on Water-related Disaster Risk Reduction (WRDRR). The article was also prepared under the umbrella of the World Centre of Excellence on Landslide Risk Reduction (2020–2023), recognized by the International Programme on Landslides (IPL).

References

Abraham BP, Moitra SD (2001) Innovation assessment through patent analysis. Technovation 21(4):245–252. https://doi.org/10.1016/S0166-4972(00)00040-7

Bae KS, Sawng Y-W, Chae B-G, Choi J, Son JK (2014) Strategy of technology development for landslide hazards by patent analysis. J Eng Geol 24(4):615–629 (in Korean with English abstract). https://doi.org/10.9720/kseg.2014.4.615

Buscema M (2014) Twisting theory (TWT): a new theory and a new class of algorithms able to model the global deformations of the space, considering the trajectories of only a little sample of points along the time flow. Number: US8666707 B2

Cai H, Li S, Liang Y, Yao Z, Cheng H (2019) Model test and numerical simulation of frost heave during twin-tunnel construction using artificial ground-freezing technique. Comput Geotech 115:103155. https://doi.org/10.1016/j.compgeo.2019.103155

Callaghan CW (2016) Disaster management, crowdsourced R&D and probabilistic innovation theory: toward real time disaster response capability. Int J Disaster Risk Reduction 17:238–250. https://doi.org/10.1016/j.ijdrr.2016.05.004

Castanon-Jano L, Blanco-Fernandez E, Castro-Fresno D, Ballester-Muñoz F (2017) Energy dissipating devices in falling rock protection barriers. Rock Mech Rock Eng 50:603–619.https://doi.org/10.1007/s00603-016-1130-x

Chambers JE, Wilkinson PB, Kuras O, Ford JR, Gunn DA, Meldrum PI, Pennington CVL, Weller AL, Hobbs PRN, Ogilvy RD (2011) Three-dimensional geophysical anatomy of an active landslide in Lias Group mudrocks, Cleveland Basin UK. Geomorphology 125(4):472–484. https://doi.org/10.1016/j.geomorph.2010.09.017

Chen S, Laefer DF, Mangina E (2016) State of technology review of Civilian UAVs. Recent Patents Eng 10(3):160–174. https://doi.org/10.2174/1872212110666160712230039

Cheng W, Drahos P (2018) How China built the World's Biggest Patent Office—the pressure driving mechanism. Int Rev Intellect Property Competition Law 49(1):5–40. https://doi.org/10.1007/s40319-017-0655-1

Chou NNS, Fan CC (2004) Structure for fastening soil nails to reinforced soil retaining walls. US patent no. US6742967B1

Chupin O, Saiyouri N, Hicher P-Y (2009) Modeling of a semi-real injection test in sand. Comput Geotecgnics 36(6):1039–1048. https://doi.org/10.1016/j.compgeo.2009.03.014

Cividini A, Locatelli L, Contini A, Gioda G (2011) A numerical interpretation of load tests on vibro-piles. Comput Geotech 38(2):287–297. https://doi.org/10.1016/j.compgeo.2010.11.009

Clarivate (2022a) Dervent innovations index basic search. Philadelphia, USA: Clarivate Analytics. https://www.webofscience.com/wos/diidw/basic-search. Last accessed 23 Apr 2022

Clarivate (2022b) Web of science core collection cited references search. Philadelphia, USA: Clarivate Analytics. https://www.webofscience.com/wos/woscc/cited-reference-search. Last accessed 23 Apr 2022

Clarivate (2022c) Patent intelligence software patentscout. Philadelphia, USA: Clarivate Analytics. https://clarivate.com/products/ip-intelligence/patent-intelligence-software/patentscout/. Last accessed 23 Apr 2022

Clarke NS (2018) The basics of patent searching. World Patent Inf 54:S4–S10. https://doi.org/10.1016/j.wpi.2017.02.006

Collins (2022) Collins English dictionary. Harpers Collins Publisher, Glasgow, Scotland. https://www.collinsdictionary.com/dictionary/english/patent. Last accessed 11 May 2022

Comina C, Mandrone G, Arato A, Chicco J, Duo E, Vacha D (2021) Preliminary analyses of an innovative soil improving system by sand/gravel injections—geotechnical and geophysical characterization of a first test site. Eng Geol 293:106278. https://doi.org/10.1016/j.enggeo.2021.106278

CPC (2022) Cooperative patent classification (CPC). European Patent Office & United States Patent and Trademark Office. Available at: https://www.cooperativepatentclassification.org/home. Last accessed 19 Apr 2022

Cui P, Peng J, Shi P, Tang H, Ouyang C, Zou Q, Kiu L, Li C, Lei Y (2021) Scientific challenges of research on natural hazards and disaster risk. Geogr Sustain 2:216–223. https://doi.org/10.1016/j.geosus.2021.09.001

Cui Z, Sheng Q, Leng X, Ma Y (2019) Investigation of the long-term strength of Jinping marble rocks with experimental and numerical approaches. Bull Eng Geol Environ 78(2):877–882. https://doi.org/10.1007/s10064-017-1132-2

di Prisco C, Pisanò F (2014) Numerical modeling and mechanical analysis of an innovative soil anchoring system. Acta Geotech 9 (6):1013–1028. https://doi.org/10.1007/s11440-013-0250-7

Du M, Gong B, Xu Y, Zhao Z, Zhang L (2020) Migration mechanism of fine particles in aquifer during water injection. Nat Hazards 102 (3):1095–1116. https://doi.org/10.1007/s11069-020-03947-4

Eliason JR, Eliason VLC (1987) Process for structural geologic analysis of topography and point data. US Patent No. 4698759, International Classification G01V 3/18, US Classification 364/420, 107 pp

Elsevier (2022) SCOPUS. Elsevier, Amsterdam, The Netherlands. https://www.scopus.com/. Last accessed 8 May 2022

EPO (2022a) European Patent Office. https://www.epo.org/. Last accessed 23 Apr 2022

EPO (2022b) Espacenet patent search. European Patent Office. Available at: https://www.epo.org/searching-for-patents/technical/espacenet.html. Last accessed 22 May 2022

Fan YB, Yang SW, Xu LK, Li SH, Feng C, Liang BF (2017) Real-time monitoring instrument designed for the deformation and sliding period of colluvial landslides. Bull Eng Geol Environ 76(3):829–838. https://doi.org/10.1007/s10064-016-0848-8

Feng XT, Lu GM, Li YH, Zhang XW (2019) Cutter head for microwave presplitting type hard-rock tunnel boring machine. United States Patent No. 10,428,654 B2. https://patents.google.com/patent/US10428654B2/en. Last accessed 18 Apr 2022

Ghobadi MH, Torabi-Kaveh M, Miri M, Mahdiabadi N (2015) An introduction to the karst geomorphology of the Bisetun-Taqe Bostan historical region (northeast Kermanshah, Iran) with special emphasis on karst development as a serious threat for the UNESCO World Heritage Site. Bull Eng Geol Environ 74(3):1071–1086. https://doi.org/10.1007/s10064-014-0662-0

Google (2022) Google Patents. https://patents.google.com/. Last accessed 22 May 2022

Groneck PB, Amour TA (2000) U.S. Patent No. 6,012,874. Washington, DC: U.S. Patent and Trademark Office

Hazarika H (2006) Stress–strain modeling of EPS geofoam for large-strain applications. Geotext Geomembr 24(2):79–90. https://doi.org/10.1016/j.geotexmem.2005.11.003

Holtz RD (2017) 46th Terzaghi lecture: geosynthetic reinforced soil: from the experimental to the familiar. J Geotech Geoenvironmental Eng 143(9):03117001. https://doi.org/10.1061/(ASCE)GT.1943-5606.0001674

Hou J, Zhang M, Dai Z, Li J, Zeng F (2017) Bearing capacity of strip foundations in horizontal-vertical reinforced soils. Geotext Geomembr 45(1):29–34. https://doi.org/10.1016/j.geotexmem.2016.07.001

Hu H, Lei T, Hu J, Zhang S, Kavan P (2018) Disaster-mitigating and general innovative responses to climate disasters: evidence from modern and historical China. Int J Disaster Risk Reduction 28:664–673. https://doi.org/10.1016/j.ijdrr.2018.01.022

Hungr O, Leroueil S, Picarelli L (2014) The Varnes classification of landslide types, an update. Landslides 11(2):167–194. https://doi.org/10.1007/s10346-013-0436-y

IPC (2022) International Patent Classification. World Intellectual Property Organization, Geneva, Switzerland. https://ipcpub.wipo.int/. Last accessed 18 Apr 2022

Ishida T, Labuz JF, Manthei G, Meredith PG, Nasseri MHB, Shin K, Yokoyama T, Zang A (2017) ISRM suggested method for laboratory acoustic emission monitoring. Rock Mech Rock Eng 50(3):665–674. https://doi.org/10.1007/s00603-016-1165-z

Jelić M (2018) Patented inventions of Serbian scientists in the field of seismic reliability of structures and landslide remediation with application. Procedia Structural Integrity 13:391–397. https://doi.org/10.1016/j.prostr.2018.12.065

Jiang Y, He N, Zhou Y, Xu B, Zhan X, Ding Y (2020) Investigation on in situ test and measurement technique of groundwater level in vacuum preloading. Bull Eng Geol Environ 79(3):1209–1223. https://doi.org/10.1007/s10064-019-01633-9

Kanagawa T, Nakasa H (1978) Method of estimating ground pressure. US Patent No. 4107981

Kazeev A, Postoev G (2017) Landslide investigations in Russia and the former USSR. Nat Hazards 88(Suppl. 1):81–101. https://doi.org/10.1007/s11069-016-2688-z

Konagai K (2021a) More than just technology for landslide disaster mitigation: signatories to The Kyoto Landslide Commitment 2020—No. 1. Landslides 18(1):513–520. https://doi.org/10.1007/s10346-020-01588-z

Konagai K (2021b) More than just technology for landslide disaster mitigation: signatories to The Kyoto Landslide Commitment 2020—No. 2. Landslides 18(2):799–805. https://doi.org/10.1007/s10346-021-01620-w

Konagai K (2021c) More than just technology for landslide disaster mitigation: signatories to The Kyoto Landslide Commitment 2020—No. 3. Landslides. 18(5):1951–1957. https://doi.org/10.1007/s10346-021-01634-4

Konagai K (2021d) More than just technology for landslide disaster mitigation: signatories to The Kyoto Landslide Commitment 2020—No. 4. Landslides 18(6):2335–2340. https://doi.org/10.1007/s10346-021-01653-1

Koerner RM, Koerner GR (2018) An extended data base and recommendations regarding 320 failed geosynthetic reinforced mechanically stabilized earth (MSE) walls. Geotext Geomembr 46 (6):904–912. https://doi.org/10.1016/j.geotexmem.2018.07.013

Koerner RM, Koerner GR (2013) A data base, statistics and recommendations regarding 171 failed geosynthetic reinforced mechanically stabilized earth (MSE) walls. Geotext Geomembr 40:20–27. https://doi.org/10.1016/j.geotexmem.2013.06.001

Koerner GR, Koerner RM (2006) Geotextile tube assessment using a hanging bag test. Geotext Geomembr 24(2):129–137. https://doi.org/10.1016/j.geotexmem.2005.02.006

Koerner RM, Koerner GR (1996) Geotextiles used as flexible forms. Geotext Geomembr 14(5–6):301–311. https://doi.org/10.1016/0266-1144(96)00018-0

Lexico (2022) Oxford English Dictionary—Synonyms. https://www.lexico.com/synonyms/patent. Last accessed 8 May 2022

Li Y, Xu Q, Aydin A (2017) Uncertainties in estimating the roughness coefficient of rock fracture surfaces. Bull Eng Geol Environ 76 (3):1153–1165. https://doi.org/10.1007/s10064-016-0994-z

Li A, Zhou M, Tian Y, Yang S (2020) Effect of rockfill berm on the stability of large geotextile mat dikes on soft clay. Comput Geotech 128:103839. https://doi.org/10.1016/j.compgeo.2020.103839

Li M, Zhang C, Fang H, Du M, Su Z, Wang F (2021) Effects of water content on shear properties of bentonite–polymer composite structure. Eng Geol 287:106098. https://doi.org/10.1016/j.enggeo.2021.106098

Lindroth DP, Morrell RJ, Blair JR (1991) Microwave assisted hard rock cutting. United States Patent No. 5,003,144. https://patents.google.com/patent/US5003144A/en. Last accessed 18 Apr 2022

Liu H-L, Chu J, Ren Z (2009) New methods for measuring the installation depth of prefabricated vertical drains. Geotext Geomembr 27:493–496. https://doi.org/10.1016/j.geotexmem.2009.05.001

Lu P, Catani F, Tofani V, Casagli N (2014) Quantitative hazard and risk assessment for slow-moving landslides from Persistent Scatterer Interferometry. Landslides 11(4):685–696. https://doi.org/10.1007/s10346-013-0432-2

Massimi V, Asadi-Zeydabady M, Buscema M, Dominicini D, Lodwick W, Simeoni L (2016) The contribution of artificial adaptive system to limit the influence of systematic errors in the definition of the kinematic behavior of an extremely-slow landslide. Eng Geol 203:30–44. https://doi.org/10.1016/j.enggeo.2015.12.022

Mastrorocco G, Salvini R, Vanneschi C (2018) Fracture mapping in challenging environment: a 3D virtual reality approach combining terrestrial LiDAR and high definition images. Bull Eng Geol Environ 77(2):691–707. https://doi.org/10.1007/s10064-017-1030-7

Meng XY, Li SH, Wang XK (2007) The device about measuring the depth of slip surface and deep dislocation displacement. Patent Publication Number: CN2854507 Y

Mikoš M (2017) Landslides: a top international journal in geological engineering and engineering geology? Landslides 14(5):1827–1838. https://doi.org/10.1007/s10346-017-0869-9

Moreillon A (2006) European Patent No. 1 156 158 B1. Lausanne. Switzerland

NSB & NSF (2022) Science and Engineering Indicators 2022: The State of U.S. Science and Engineering. NSB-2022–1. National Science Board, National Science Foundation, Alexandria, VA, USA. https://ncses.nsf.gov/pubs/nsb20221. Last accessed 23 May 2022

Park H, Lee S-R, Kim T-H, Kim N-K (2011) Numerical modeling of ground borehole expansion induced by application of pulse discharge technology. Comput Geotech 38(4):532–545. https://doi.org/10.1016/j.compgeo.2011.03.002

Prior DB, Hooper JR (1999) Sea floor engineering geomorphology: recent achievements and future directions. Geomorphology 31(1–4):411–439. https://doi.org/10.1016/S0169-555X(99)00090-2

RECo (2022) Reinforced Earth Company. https://www.reinforcedearth.co.uk/about-reinforced-earth/. Last accessed 3 May 2022

Ren ZY (2004) A prefabricated vertical drain with capability for penetration depth measurement. China Patent No. 0119469.0

Rossi G, Tanteri L, Tofani V, Vannocci P, Moretti S, Casagli N (2018) Multitemporal UAV surveys for landslide mapping and characterization. Landslides 15(5):1045–1052. https://doi.org/10.1007/s10346-018-0978-0

Sassa K (2021a) The Kyoto Landslide Commitment 2020: launched. Landslides 18(1):5–20. https://doi.org/10.1007/s10346-020-01575-4

Sassa K (2021b) New open access book series "progress in landslide research and technology." Landslides 18(11):3509–3512. https://doi.org/10.1007/s10346-021-01759-6

SJR (2022) Scimago Journal & Country Rank. Scimago Lab. https://www.scimagojr.com/. Last accessed 23 May 2022

Springer Nature (2022a) Springer Link. Springer Nature, Heidelberg, Germany. https://link.springer.com/. Last accessed 8 May 2022

Springer Nature (2022b) Book Series ICL Contribution to Landslide Disaster Risk Reduction. Springer Nature, Heidelberg, Germany. https://www.springer.com/series/16332. Last accessed 14 May 2022

Sterzi V (2013) Patent quality and ownership: an analysis of UK faculty patenting. Res Policy 42:564–576. https://doi.org/10.1016/j.respol.2012.07.010

Tan D-Y, Yin J-H, Feng W-Q, Qin J-Q, Zhu Z-H (2020) New simple method for measuring impact force on a flexible barrier from rockfall and debris flow based on large-scale flume tests. Eng Geol 279:105881. https://doi.org/10.1016/j.enggeo.2020.105881

Thomel L (1998) European Patent No. 0 877 1 22 A1. Juan les Pins. France

Ullberg E (2020) Patent System. In: Carayannis EG (Ed) Encyclopedia of creativity, invention, innovation and entrepreneurship. Springer, Cham, pp 1820–1821. https://doi.org/10.1007/978-3-319-15347-6_506

UNCTAD (2014) Transfer of technology and knowledge sharing for development—science, technology and innovation issues for developing countries. UNCTAD Current Studies on Science, Technology and Innovation, No. 8. United Nations Conference on Trade and Development. Geneva, Switzerland. 63p. https://unctad.org/system/files/official-document/dtlstict2013d8_en.pdf. Last accessed 30 Apr 2022

UNCTAD (2019) A framework for science, technology and innovation policy reviews—harnessing innovation for sustainable development. United Nations Conference on Trade and Development. Geneva, Switzerland. 43p. https://unctad.org/system/files/official-document/dtlstict2019d4_en.pdf. Last accessed 30 Apr 2022

UNISDR (2015) Sendai framework for disaster risk reduction 2015–2030. Geneva, Switzerland: United Nations Office for Disaster Risk Reduction. 36p. https://www.preventionweb.net/files/43291_sendaiframeworkfordrren.pdf. Last accessed 23 Apr 2022

UNISDR (2019) The science and technology roadmap to support the implementation of Sendai framework for disaster risk reduction 2015–2030. Geneva, Switzerland: United Nations Office for Disaster Risk Reduction. 5p. https://www.preventionweb.net/files/65131_file.pdf. Last accessed 23 Apr 2022

USPTO (2022) United States Patent and Trademark Office. https://www.uspto.gov/. Last accessed: 23 Apr 2022

Vayssière A, Rue M, Recq C, Gardère P, Thamó-Bozsó E, Castanet C, Virmoux C, Gautier E (2019) Lateglacial changes in river morphologies of northwestern Europe: an example of a smooth response to climate forcing (Cher River, France). Geomorphology 342:20–36. https://doi.org/10.1016/j.geomorph.2019.05.019

Vidal H (1969) United States Patent No. 3, vol. 421, 326, 14 Jan 1969

Vitel M, Rouabhi A, Tijani M, Guérin F (2015) Modeling heat transfer between a freeze pipe and the surrounding ground during artificial ground freezing activities. Comput Geotech 63:99–111. https://doi.org/10.1016/j.compgeo.2014.08.004

Von Allmen HP (2004) European Patent No. 1 469 130 A1. Tafers. Switzerland

Wang L, Li Z (2018) Knowledge transfer from science to technology—the case of Nano medical device technologies. Front Res Metrics Analytics 3:11. https://doi.org/10.3389/frma.2018.00011

Wang D, Chen G, Jian D, Zhu J, Lin Z (2021a) Shear creep behavior of red sandstone after freeze-thaw cycles considering different temperature ranges. Bull Eng Geol Environ 80(3):2349–2366. https://doi.org/10.1007/s10064-020-02046-9

Wang S, Zhan Q, Wang L, Guo F, Liu T, Pan Y (2021b) Unsaturated creep behaviors and creep model of slip-surface soil of a landslide in Three Gorges Reservoir area China. Bull Eng Geol Environ. 80(7):5423–5435. https://doi.org/10.1007/s10064-021-02303-5

Wei L, Chai S, Guo Q, Wang P, Li F (2020) Mechanical properties and stabilizing mechanism of stabilized saline soils with four stabilizers. Bull Eng Geol Environ 79(10):5341–5354. https://doi.org/10.1007/s10064-020-01885-w

WIPO (2021) World Intellectual Property Indicators 2021. World Intellectual Property Organization, Geneva, Switzerland. 230 p. https://doi.org/10.34667/tind.44461, https://www.wipo.int/edocs/pubdocs/en/wipo_pub_941_2021.pdf. Last accessed 8 May 2022

World Bank (2022a) Data Bank. World Development Indicators. Patent Applications, Nonresidents. https://databank.worldbank.org/data/reports.aspx?dsid=2&series=IP.PAT.NRES. Last accessed 23 May 2022

World Bank (2022b) Data Bank. World Development Indicators. Patent Applications, Residents. The World Bank (2022a) Data Bank. World Development Indicators. Patent Applications, Residents. https://databank.worldbank.org/reports.aspx?dsid=2&series=IP.PAT.RESD. Last accessed 23 May 2022

Wu H (2015) A soft soil foundation treatment method with different depth disturbance and drainage consolidation. China. Patent No. 201510301241.4

Wu H-M, Ma N, Ma Q-K, Lin X-F, Song C (2021) Accelerating consolidation of soft ground by aerosol injection technique: a field study. Acta Geotech 16(9):2997–3004. https://doi.org/10.1007/s11440-021-01185-x

Xiao H, Huang J, Ma Q, Wan J, Li L, Peng Q, Rezaeimalek S (2017) Experimental study on the soil mixture to promote vegetation for slope protection and landslide prevention. Landslides 14(1):287–297. https://doi.org/10.1007/s10346-015-0634-x

Xue K, Wen Z, Zhu Z, Wang D, Luo F, Zhang M (2021) An experimental study of the relationship between the matric potential, unfrozen water, and segregated ice of saturated freezing soil. Bull Eng Geol Environ 80(3):2535–2544. https://doi.org/10.1007/s10064-020-02052-x

Ying C, Hu X, Siddiqua S, Hossam Makeen GM, Xia P, Xu C, Wang Q (2021) Model tests for observing the deformation characteristics of micropile boreholes during drilling in a soil-limestone mixture. Bull Eng Geol Environ 80(8):6373–6393. https://doi.org/10.1007/s10064-021-02319-x

Zhang MX (2005) Three-dimensional (3D) reinforcing elements. State Intellectual Property Office, China, Patent NO. zl 2005100028241.8

Zhou H, Fang Y, Chen M, Li W (2021) Experimental analysis of the effect of mineral composition and water content of clay soil on electroosmotic efficiency. Bull Eng Geol Environ 80(1):705–715. https://doi.org/10.1007/s10064-020-01945-1

Scalable Platform for UAV Flight Operations, Data Capture, Cloud Processing and Image Rendering of Landslide Hazards and Surface Change Detection for Disaster-Risk Reduction

David Huntley, Drew Rotheram-Clarke, Roger MacLeod, Robert Cocking, Philip LeSueur, Bill Lakeland, and Alec Wilson

Abstract

This International Programme on Landslide (IPL) Project 202 paper presents a scalable remote piloted aircraft system (RPAS) platform that streamlines unoccupied aerial vehicle (UAV) flight operations for data capture, cloud processing and image rendering to inventory and monitor slow-moving landslides along the national railway transportation corridor in southwestern British Columbia, Canada. Merging UAV photogrammetry, ground-based real-time kinematic global navigation satellite system (RTK-GNSS) measurements, and satellite synthetic aperture radar interferometry (InSAR) datasets best characterizes the distribution, morphology and activity of landslides over time. Our study shows that epochal UAV photogrammetry, benchmarked with periodic ground-based RTK-GNSS measurements and satellite InSAR platforms with repeat visit times of weeks (e.g., RADARSAT-2 and SENTINEL-1) to days (e.g. RADARSAT Constellation Mission) provides rapid landslide monitoring capability with cm-scale precision and accuracy.

Keywords

Landslides • Remote piloted aircraft system • Unoccupied aerial vehicle • Photogrammetric change-detection • Satellite synthetic aperture radar interferometry • Real-time kinematic global navigation satellite systems

D. Huntley (✉) · D. Rotheram-Clarke · R. Cocking · P. LeSueur
Geological Survey of Canada, 1500-605 Robson Street, Vancouver, BC V6B 5J3, Canada
e-mail: david.huntley@nrcan-rncan.gc.ca

D. Rotheram-Clarke
e-mail: drew.rotheram-clarke@nrcan-rncan.gc.ca

R. Cocking
e-mail: robert.cocking@nrcan-rncan.gc.ca

P. LeSueur
e-mail: philip.lesueur@nrcan-rncan.gc.ca

R. MacLeod
Geological Survey of Canada, 9860 West Saanich Road, Sidney, BC V8L 4B2, Canada
e-mail: roger.macleod@nrcan-rncan.gc.ca

B. Lakeland · A. Wilson
Spexi Geospatial Inc, 700-510 Seymour Street, Vancouver, BC V6B 3J5, Canada
e-mail: bill@spexigeo.com

A. Wilson
e-mail: alec@spexigeo.com

1 Introduction

Unoccupied aerial vehicle (UAV) photogrammetry is increasingly incorporated into local, regional and national geohazard monitoring protocols for vulnerable economic infrastructure and communities (Casagli et al. 2017; Turner et al. 2015; Rossi et al. 2018; Sestras et al. 2021). Optical UAV imagery and light detection and ranging (LiDAR) data captured during field surveys are desktop-processed to generate point cloud digital surface models (DSMs) and digital elevation models (DEMs). UAV photogrammetry, when benchmarked with satellite synthetic aperture radar interferometry (InSAR) and ground-based real-time kinematic (RTK) global navigation satellite system (GNSS) measurements, provides cm-scale resolution geospatial data for geohazard mapping and landscape change-detection monitoring (Booth et al. 2013; Handwerger et al. 2021; Huntley et al. 2021a, b, c a, b).

1.1 Monitoring for Landslide Hazards, Change-Detection, Disaster-Risk Reduction

From environmental, logistical and transportation safety perspectives, rapidly deployable UAVs offer a low-carbon footprint alternative to geological mapping using fixed-wing

I. Alcántara-Ayala et al. (eds.), *Progress in Landslide Research and Technology, Volume 1 Issue 2, 2022*, Progress in Landslide Research and Technology,
https://doi.org/10.1007/978-3-031-18471-0_4

aircraft and helicopters, particularly along linear transportation routes and around remote northern communities. In Canada, high-resolution photogrammetry and change-detection monitoring (cf. Huntley et al. 2021a, b) requires a UAV with an optical sensor payload in excess of 250 g, subscription-based commercial software for flight plans and data acquisition, along with trained and certified operators and observers following strict Transport Canada (TC) regulations for operating remote piloted aircraft systems (RPAS). The number of UAVs and appropriately trained field operatives available limits the duration and spatial coverage of surveys, and generic utility as a geohazard monitoring tool.

In this paper, we apply an easily scalable RPAS platform, developed by Spexi Geospatial Inc. (www.fly.spexigeo.com [URL 2022]), to landslide inventory mapping and change-detection monitoring in western Canada. This RPAS streamlines UAV flight operations for data capture, cloud processing and image rendering to aid in the inventory and monitoring of slow-moving landslides along a strategically important section of the national railway network traversing the Thompson River valley in south-central British Columbia (BC) (Fig. 1a). Combining field-based landslide investigation with multi-year geospatial and *in-situ* time-series monitoring leads to a more resilient railway national transportation network able to meet Canada's future socioeconomic needs, while ensuring protection of the environment and resource-based communities from landslides related to extreme weather events and climate change.

1.2 Study Area

Landslides along a ten-kilometre stretch of the Thompson River valley between Ashcroft and Spences Bridge (Fig. 1b) have negatively impacted critical railway infrastructure, arable land, fisheries, and other natural resources since the 1880s (Fig. 1b). In the late nineteenth century, prehistoric mass movements reactivated as sudden onset, rapid retrogressive flow-slides during the fall and winter months at a time when terraces were intensively irrigated for agricultural land use, and toe slopes were incised and over-steepened during railway construction (Stanton 1898; Clague and Evans 2003).

Field-based geological and geophysical mapping, combined with InSAR analyses (Fig. 1c), and in situ semi-continuous monitoring, provide insight into landslide activity, deformation mechanisms, and potential acceleration triggers along this critical section of the national railway transportation corridor (Bunce and Chadwick 2012; Journault et al. 2018; Huntley et al. 2019a, b; Holmes et al. 2020). Each of these techniques record increased landslide activity in winter, when river and groundwater levels are lowest (Macciotta et al. 2014; Hendry et al. 2015; Schafer et al. 2015; Journault et al. 2018). Permanent GNSS monuments on Ripley Landslide record cumulative annual displacement on the order of 10 cm year^{-1} to 20 cm year^{-1}, peaking in winter (Bunce and Chadwick 2012; Macciotta et al. 2014; Hendry et al. 2015; Huntley et al. 2021a).

RADARSAT-2 and SENTINEL-1 InSAR results from 2013 to 2020 indicate similar magnitudes and spatial–temporal patterns of displacement (Journault et al. 2018; Huntley et al. 2021b, c). From south to north along the railway transportation corridor, these include the following landslides of concern with an average 1D line-of-sight (LoS) displacement greater than 3 cm year^{-1}: Ripley Landslide, Red Hill Slide, South Slide, North Slide, and Goddard Slide (Fig. 1c). Regions of highest landslide activity intersecting with railway infrastructure correlate with cutbank erosion and channel bed scour on the outside bends of the river.

The economic importance of this transportation corridor, along with the need to understand and manage the safety risk related to the landslides that threaten the route, mandate the Thompson River valley a research priority for NRCAN and the GSC. As part of the International Consortium on Landslides (ICL) International Programme on Landslides (IPL) Project 202, landslides in the Thompson River valley serve as field laboratories to test and compare the reliability and effectiveness of different static, dynamic, and real-time monitoring technologies (e.g., Huntley et al. 2017; Huntley et al. 2019a, b).

Multiple landslides were surveyed each day, depending on areal extent of the flight plans, weather conditions, and time of day (Fig. 2). Flights were undertaken on October 20 (Nepa Slide, Ripley Landslide, South Slide) and November 01 2021 (Red Hill Slide, North Slide). For each survey, UAV RTK base stations were established over stable GCPs (e.g., NP-02, Fig. 3). Geo-referenced image files captured during flights were stored on UAV memory cards, and then downloaded to cloud storage for later desktop processing.

2 Method of Investigation

2.1 Remote Piloted Aircraft System Monitoring

Accurate and precise elevation models derived from UAV datasets serve as baseline references for rigorous landslide change-detection monitoring (Casagli et al. 2017; Rossi et al. 2018; Sestras et al. 2021). Repeat UAV surveys aim to capture changes in morphology of landslides in proximity to at-risk railway infrastructure (Fig. 2). To improve the understanding of landslide geomorphology and kinematics, and to benchmark UAV, we incorporated ground-based RTK-GNSS surveys and satellite InSAR displacement rates into the monitoring strategy for the Thompson River valley (Huntley et al. 2021a, b, c). Under ideal conditions, each

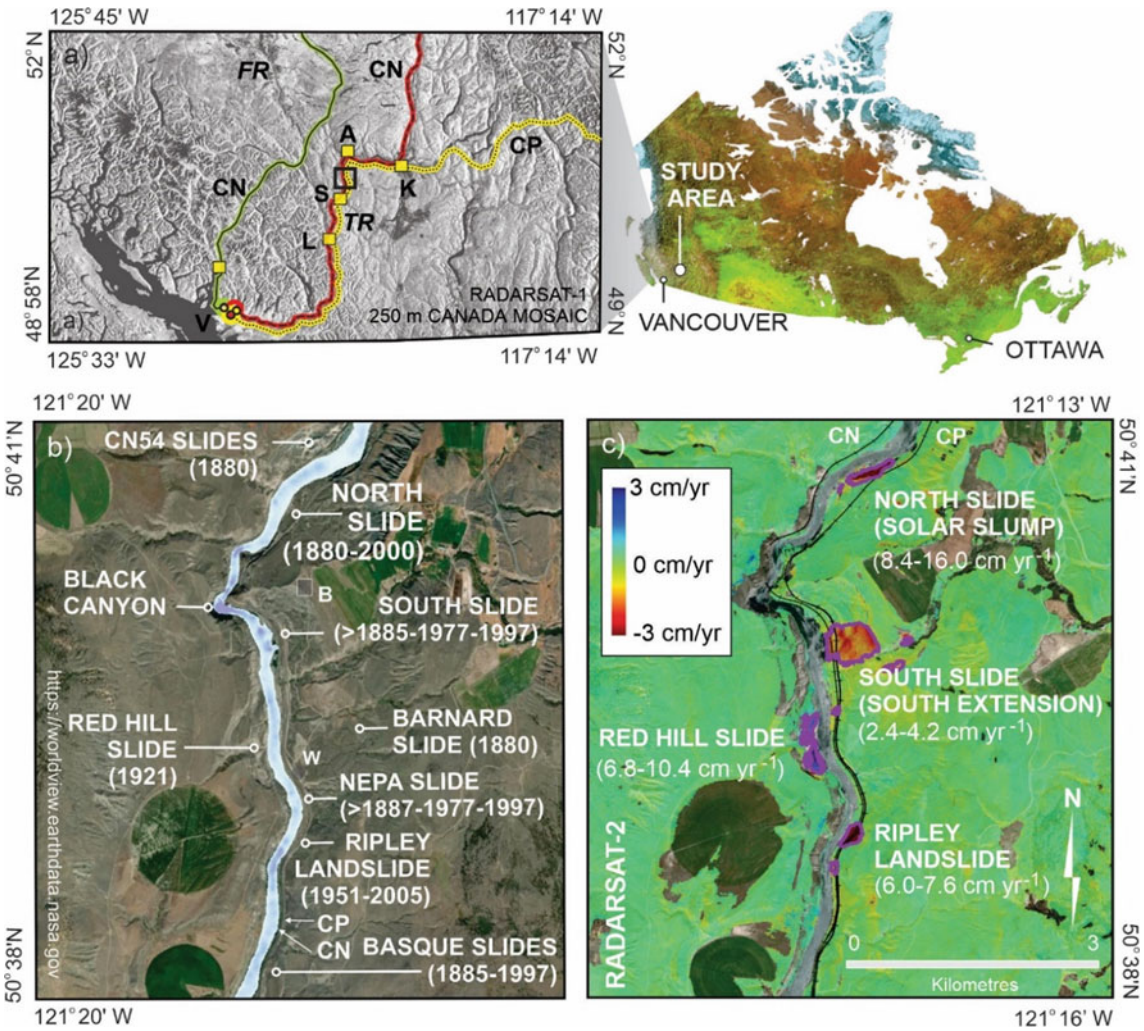

Fig. 1 Study area, showing landslides in relation to national railway infrastructure: **a** southwestern British Columbia showing major transportation corridors. **b** Historical activity of slow-moving landslides of the Thompson with potential to negatively impact national railway infrastructure, operational services, the environment, local communities, and national economy (after Clague and Evans 2003). **c** *Landslides of concern* determined from InSAR results for the Thompson River valley, showing CN and CP tracks (solid black lines); RADARSAT-2 average linear displacement rate rastered at 3 cm year^{-1}, with purple polygons delimiting 4-sigma confidence levels (modified from Huntley et al. 2021c). CN—Canadian National Railways; CP—Canadian Pacific Railways; *TR*—Thompson River; *FR*—Fraser River

year, monthly change-detection flights could be flown to catch seasonal changes in landslide displacement. In practice, poor weather conditions, limited human resources, and other unforeseen challenges result in less consistent UAV time-series datasets.

2.2 RPAS Landslide Inventory and Change-Detection

The GSC operated a DJI Phantom 4 between 2016 and 2021 (Huntley et al. 2021a). Although the 24-megapixel camera required flight altitudes < 30 m above ground level, longer flight times and more batteries, and generated a large number of images per flight plan, this UAV allowed flexible, inexpensive acquisition of aerial imagery. UAV surveys took between one day (Ripley Landslide and North Slide) to two days (South Slide and Nepa Slide) to execute, depending on areal extent of the flight plan, weather conditions, and time of day. Survey flight planning was conducted using Map Pilot (2016–2020), while Pix4D Mapper structure-from-motion (SfM) photogrammetric software enabled production of 2 cm-resolution DSMs from orthomosaiced aerial images. These DSMs were benchmarked with multi-year RTK-GNSS datasets (Fig. 3; Huntley et al. 2021a, b). This standardized process was time-consuming and data-intensive, requiring weeks to months of desktop processing to yield meaningful outputs.

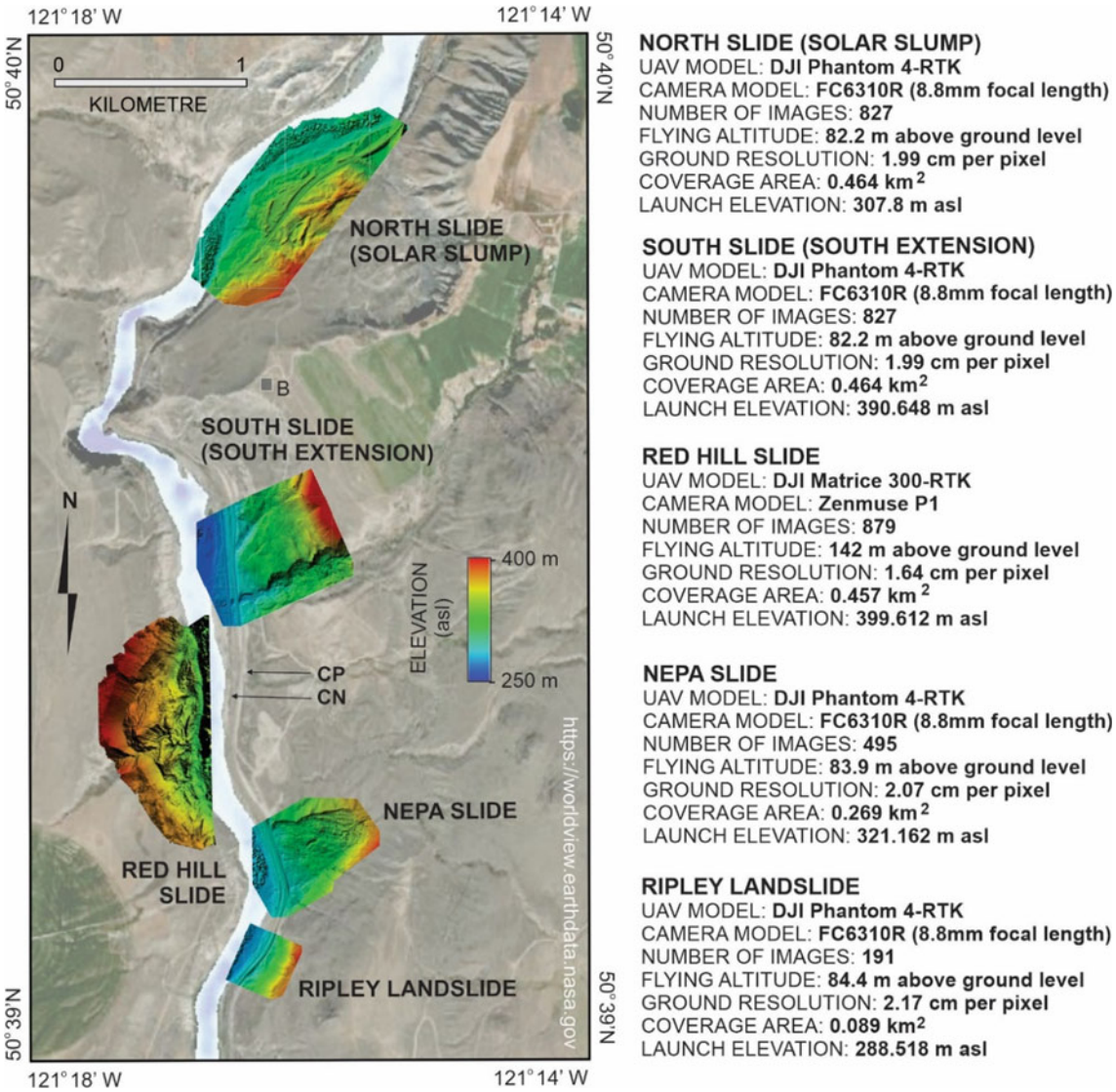

Fig. 2 Landslide of concern along the Thompson River valley railway corridor: flight plan footprints and DEMs generated from point clouds for the 2021 UAV surveys. Flight statistics generated using the Spexi Geospatial platform. Orthomosaic DSMs are shown in Fig. 3

Spexi Geospatial Inc. has developed a flight operations platform for autonomous UAV flight and data capture and back-end cloud processing, analytics, and rapid sharing capabilities that rivals the computing capabilities of commercial software, but is more cost-effective and intuitive to operate (www.fly.spexigeo.com [URL 2022]). Enabling automated data acquisition, processing, and rapid sharing capabilities through a standardized process meant faster response and faster results. The RPAS ensured that platform technology did not require hardware installations, and that cloud-hosted software was accessible on most desktop and mobile devices connected to the internet.

In 2021, the GSC began operating a DJI Phantom 4 Pro V2 with a 48-megapixel optical payload, and a DJI Matrice 300 with 35 mm lens; both with RTK capabilities. These upgrades allowed flight altitudes > 70 m above ground level, shorter flight times and fewer battery changes, and a smaller number of images and file sizes per flight plan. Flight plans for Ripley Landslide, South Slide, North Slide and Nepa Slide (Fig. 2) were set up using Spexi Geospatial and DJI platforms prior to fieldwork. Flight and photogrammetry variables included: altitude above ground level (72 m = 2 cm per pixel resolution); front and side overlaps for photograms (80% and 70%, respectively); flight direction (0–180°); speed (8 m s^{-1}); and gimbal pitch (-90° for planform photograms). Contour maps (50 cm intervals), DEMs, DSMs, and orthomosaic photograms were readily generated from selected imagery and point clouds using the Spexi Geospatial platform (Figs. 2; and 3b–e), and exported into Global Mapper and ArcGIS software for further

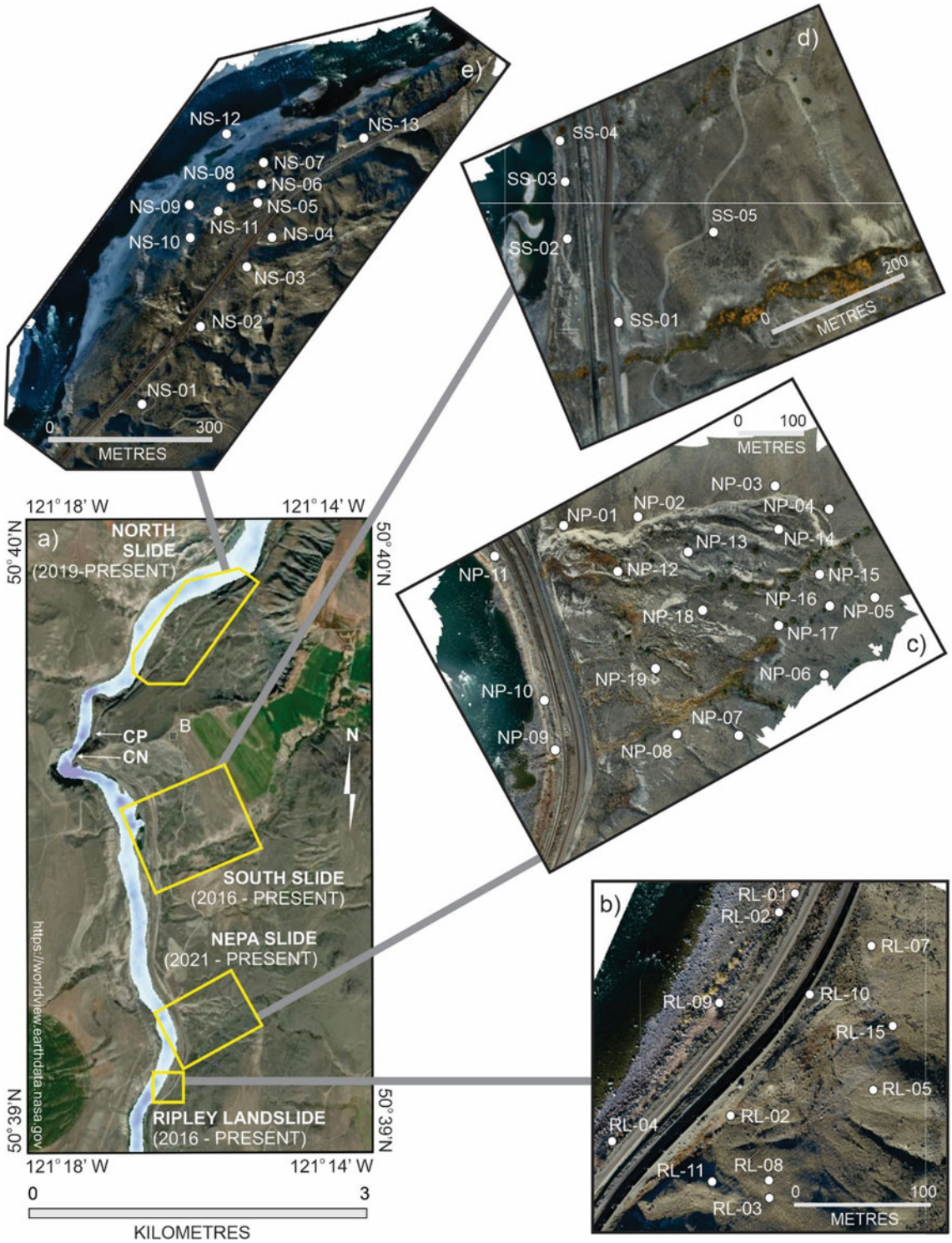

Fig. 3 Landslides of concern in the Thompson River valley with GCPs and UAV digital surface mosaics. **a** Location of RTK-GNSS surveyed landslides along the railway corridor. **b** Ripley Landslide, 15 GCPs established in 2016 (GCP-06 and GCP-12 are beyond the southern limit of landslide captured in photogram). **c** Nepa Slide, 19 GCPs established in 2021. **d** South Slide, 11 GCPs established in 2016 (GCP-06 to GCP-11 are beyond the northern limit of landslide captured in photogram); **e** North Slide, 13 GCPs established in 2019–2021

processing and change-detection monitoring. Useful platform review products included metadata reports on survey parameters, UAV and camera properties, camera locations with X, Y, and Z error estimates, point cloud parameters, and coordinate systems.

Change-detection monitoring focused on the most active landslides identified during inventory: Ripley Landslide (2016–2018) and North Slide (2019–2021). For Ripley Landslide, planimetric displacement was first mapped using co-relation processing (cf. Lucieer et al. 2014; Turner et al. 2015; Türk 2018) on hill-shaded UAV DSMs with 1.5 times exaggeration, and the sun at azimuth 310 and 45° altitude. Areas of vegetation and recent track ballast work on hill-shaded images were masked prior to processing to reduce the areas with substantial change not related to slide movement. Two images were created for E/W (X) and N/S (Y) displacement, while elevation changes (Z) were derived from the 2016 and 2018 DSMs. These values were added and squared to produce a single raster containing positive 3D displacement values, with larger values representing more displacement (Fig. 4; Huntley et al. 2021a).

For the North Slide, a more sophisticated, but less personnel time-consuming approach was possible with recent advances in cloud-based data storage and processing. Following the methodology of Gojcic et al. (2021), we employed a fully automated deformation analysis workflow that estimated 3D displacement vectors from point cloud data. Dense 3D displacement vector fields were estimated by searching for corresponding cloud points across DSM epochs at September 2019 and September 2021. The displacement patterns and magnitudes derived from UAV photogrammetry were evaluated with RTK-GNSS measurements of GCPs collected on the same days as the UAV surveys, and high-temporal resolution differential InSAR results from a RADARSAT Constellation Mission (RCM) time-series spanning August 2020 to September 2021.

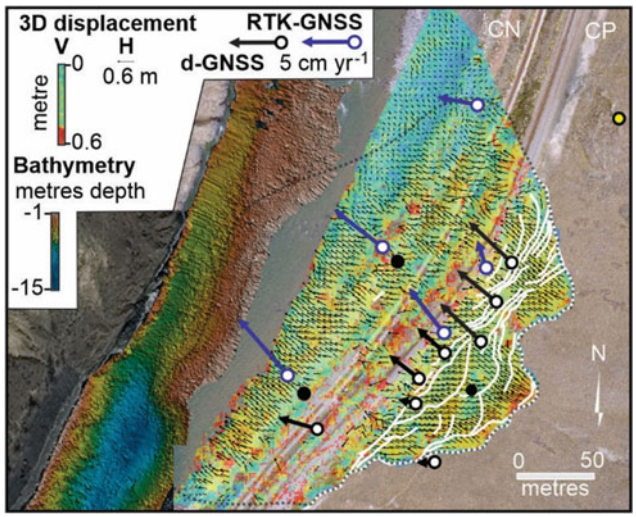

Fig. 4 Ripley Landslide surface displacement data derived from UAV overflights in 2016 and 2018 and multi-beam bathymetry data collected in 2018; plotted with RTK-GNSS (average annual rate for 2017, 2018 and 2019) and d-GNSS displacement data (November 2018 to June 2019, expressed as cm year^{-1}). Stable d-GNSS unit—yellow dot; active d-GNSS unit—black and white dot; inactive d-GNSS—black dot. Active GCP—blue dot (modified from Huntley et al. 2021a)

2.3 RPAS Landslide Benchmarking

UAV photogrammetry provides cm-scale resolution geospatial data for geohazard mapping and landscape change-detection monitoring when benchmarked with RTK-GNSS measurements that provide the three-dimensional coordinates of moving points on landslides (e.g., Turner et al. 2015; Rossi et al. 2018). Prior to UAV surveys, a prime ground control point (GCP) was established on a stable post-glacial terrace near Black Canyon (Fig. 1b). The absolute position of this base station (WGS84 + NAD83 UTM Zone 10 E5614082.268 N619963.25, 390.648 m asl) was determined from a post-processed RINEX file using the Canadian Spatial Reference System Precise Point Positioning tool after a nine-hour occupation. The reported absolute positional accuracy was 0.8 cm horizontally and 1.3 cm vertically (95% Σ).

All RTK-GNSS surveys used the 2016 prime GCP coordinate values as the stable reference (Fig. 1b). Additional GCPs were established on, and adjacent to landslides of concern (Fig. 3a) using distinctively painted stable boulders and anthropogenic features. RTK-GNSS rover measurements at GCPs occupied for a minimum of two minutes at 1 Hz were reported with horizontal precisions of better than 2 cm and vertical precisions of 3 cm. All RTK-GNSS positioning data were reviewed, corrected for antenna laybacks, heights and edited for erroneous data points (Huntley et al. 2017, 2021a).

At each GCP station, ground observations were made of slope gradient, surficial materials, material texture, material thickness, slope morphology, moisture conditions, ongoing geomorphic processes, land cover, and nearby anthropogenic activities. These observations corroborated terrain and landslide classifications determined from optical satellite imagery and UAV photogrammetry.

2.4 RCM Landslide Benchmarking

RCM SAR datasets were examined to further refine the spatial and temporal distribution of landslide activity (Fig. 5a). Twelve RCM scenes from the end of August to early December, 2020, and twenty scenes from January to September 2021 were acquired during descending orbit passes (west-ranging) at a nominal ground resolution of 3 m,

with an ideal revisit frequency of 4 days (Huntley et al. 2021b, c). RCM data was processed using GAMMA software following the methodology of Samsonov et al. and Dudley et al. SAR images were precisely aligned with a chosen master using normalized cross-correlation to yield SAR data cubes that could be analyzed spatially, or in time (Fig. 5b, step 1).

InSAR processing and landslide change-detection benefited from an accurate high-resolution DEM to simulate and remove the topographic effects from the interferograms (Barret et al. 2012; Hu et al. 2019). Co-registered RCM stacks were benchmark geocoded with a 1 m-pixel resolution airborne LiDAR dataset, 1 arc-second resolution Advanced Land Observation Satellite (ALOS) World DEM

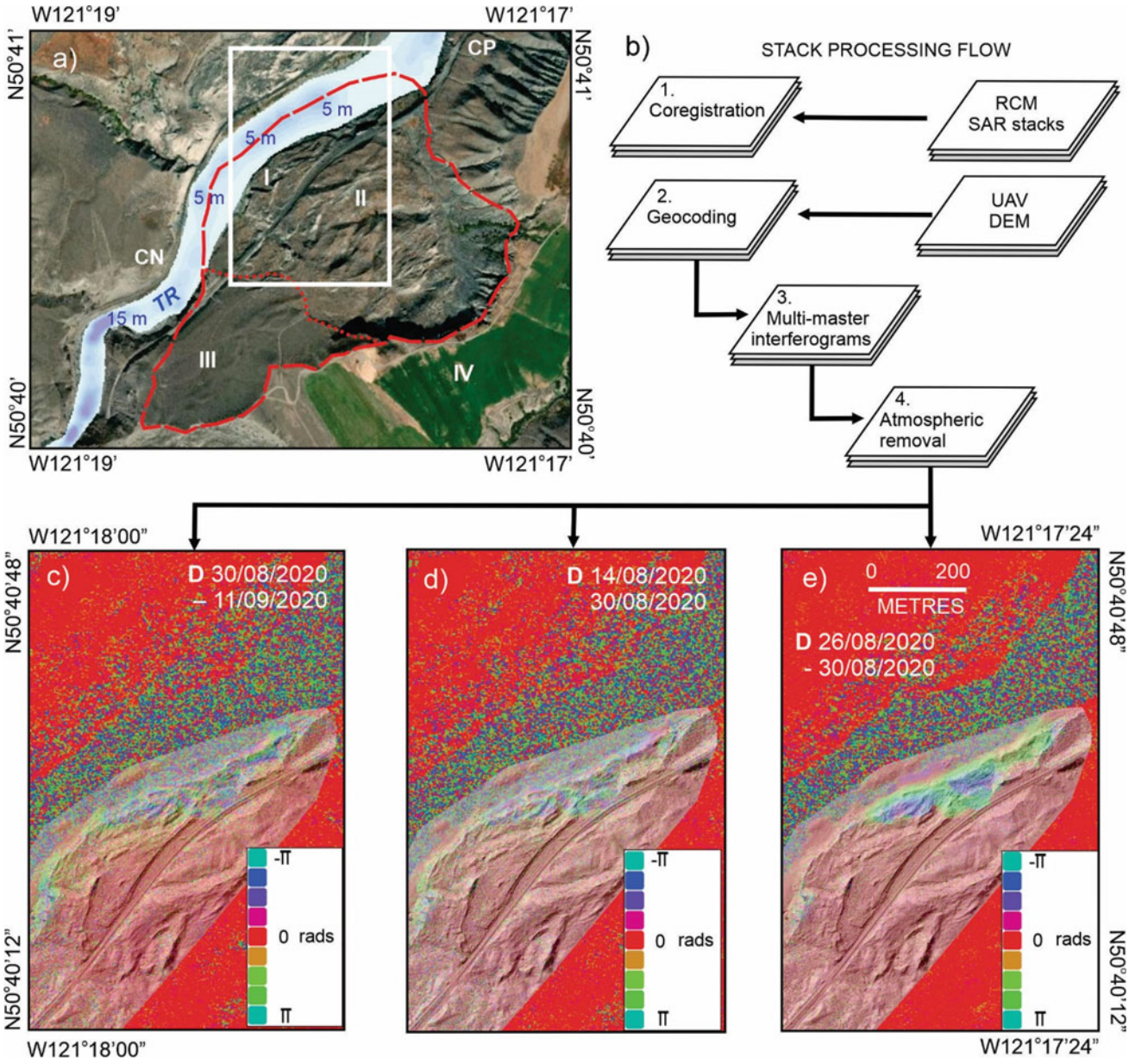

Fig. 5 Differential InSAR analysis of RCM time-series results. **a** Extent of North Slide: (I) active slide toe (0.08 km^2) with tension cracks, sparse vegetation and steep scarp faces (post 2000); (II) inactive slide main body and head scarp (0.55 km^2) with sparse vegetation, and subdued scarp faces and slide blocks (ca. 1880); (III) inactive slide body (0.37 km^2) with established vegetation ground cover, and subdued surface morphology (ancient, i.e., > 300 years before present); (IV) stable postglacial slopes and terraces supporting irrigated crops and cattle pasture. **b** Generalized InSAR processing steps followed in this paper (modified from Huntley et al. 2021b). **c** RCM interferogram, 2020/08/30–2020/09/11 (28 days). **d** RCM interferogram, 2020/08/14–2020/08/30 (16 days). **e** RCM interferogram, 2020/08/26–2020/08/30 (4 days). UAV-derived SFM-DSM overlain at 50% transparency for topographic context (modified from Huntley et al. 2021b, c)

data, UAV photogrammetry (2 cm pixel-resolution), and ground-based RTK-GNSS measurements (x, y, z ± 3 cm) (Fig. 5b, step 2; Fig. 6). DEMs were resampled and aligned with the multi-master interferograms to provide a height value for each SAR pixel. This helped to remove topographic signals in interferograms (Fig. 5b, steps 3 and 4), corrected orbit information as needed, and provided the relationship between SAR and map data used later for projecting results back into map space (Huntley et al. 2021b, c). Additional RCM processing created a robust time-series for LoS displacement of GCPs in 2021. RTK-GNSS measurement from 2019–2020 are shown for comparison (Fig. 6a).

3 Results and Discussion

3.1 Ripley Landslide

At 0.089 km^2, Ripley Landslide has the smallest flight plan footprint and areal extent (0.026 km^2) (Fig. 2). Orthomosaic images and DSMs from 2016 to 2021 capture the active floodplain of Thompson River at *ca.* 260 m asl, and railway infrastructure crossing a gentle to steep slope (<12 to > 35°) with subdued translational-rotational slide blocks, tension cracks, closed depressions, and prominent head and side scarps. A glacial outwash terrace, with a surface elevation of 360 m asl, lies upslope and east of the active landslide. Fifteen permanent GCPs were established on stable boulders and anthropogenic features in 2016 (Fig. 3b). Nine earth material units are recognized from ground observations in the vicinity of GCPs, and on UAV imagery from 2016 to 2021 (Figs. 2 and 3b; Huntley et al. 2020). GCPs along the CN and CP tracks (RL-01, RL-04, RL-09 and RL-10) are established on cobble and boulder ballast up to 3 m thick. This anthropogenic layer overlies up to 25 m of glaciolacustrine clay and silt, and glacial boulder-rich diamicton (basal till) with shear surfaces 10–15 m below surface, resting on fractured andesite (Huntley et al. 2019a, b; Huntley et al. 2020).

Upslope of the tracks, unconsolidated sediment thickness decreases in the main slide body, with GCPs established on silt and sand-rich alluvial outwash, colluviated till and glaciofluvial gravels. Beneath RL-02, -08 and -11, this veneer covers up to 5 m of glaciolacustrine clay and silt draped on fractured andesite and rhyolite. Above the head scarp, GCPs are established shallow deposits (< 2 m thick) of colluvium and glaciofluvial outwash resting on igneous bedrock (RL-03, RL-05, RL-07, RL-15).

Change-detection monitoring

Repeat UAV surveys of Ripley Landslide in 2016 and 2018 characterized the spatial extent, magnitude and direction of landslide movement (Fig. 4). UAV photogrammetry reveals that over much of the slide body, movement is to the NW, except along the northern and southern flanks, where displacement is W. In contrast, channel scour along the slide toe and submerged bedrock bounding the landslide drives the body mass generally to the W.

Co-relation results from 2016–2018 show > 50 cm NW displacement of blocks along steep-dipping, retrogressive backscarps to the main slide body. This high value is consistent with the InSAR and GNSS monument data that captured significant displacement in 2017 (Bunce and Chadwick 2012; Huntley et al. 2021a). Displacement along the tracks reflects subsidence of the slide body (also expressed in deformation of the lock-block retaining wall), and the addition of ballast during routine safety maintenance. A zone of high displacement at the south flank of the slide foot is likely the consequence of toe-slope erosion as evidenced by the 15 m-deep scour pool mapped by the bathymetric surveys (Fig. 4). Across much of the foot slope however, 3D displacement values are lower, reflecting translational movement of the slide mass over sub-horizontal failure planes beneath the tracks and river.

Between 2017 and 2019, five GCPs recorded significant horizontal displacement on the landslide; RTK-GNSS measurement precision and accuracy discounted GCPs showing 3 cm or less movement. Upslope of the train tracks, on the main slide body, RL-10 recorded 8.7 cm of movement to the NNW. Disturbance during track maintenance accounted for the anomalous vector for RL-10 and slower displacement rate. Downslope of the tracks, across the slide toe, 11.3 cm of WNW displacement was measured at RL-02; RL-04 displaced 16.4 cm NW; and RL-09 moved 18.3 cm NW over the three-year observation period. The remaining GCPs were on stable portions of the slope, and adjacent to the landslide (Huntley et al. 2021a).

A new UAV and RTK-GNSS change-detection program was initiated in 2022 following significant slope modification during a stakeholder geotechnical investigation in 2020–2021 (Huntley et al. 2021c). The DEM and DSM captured in October 2021 (Figs. 2 and 3) will serve as the baseline for further RPAS change-detection monitoring at Ripley Landslide.

3.2 Nepa Slide

The flight plan footprint for Nepa Slide is 0.254 km^2, with the disturbed land covering 0.136 km^2. The 2021 orthomosaic image and DSM capturing the active floodplain of Thompson River at *ca.* 265 m asl, and railway infrastructure crossing a gentle toe slope (< 12°). The main translational slide body consists of sparsely vegetated hummocky blocks and closed depressions, flanked by prominent head and side

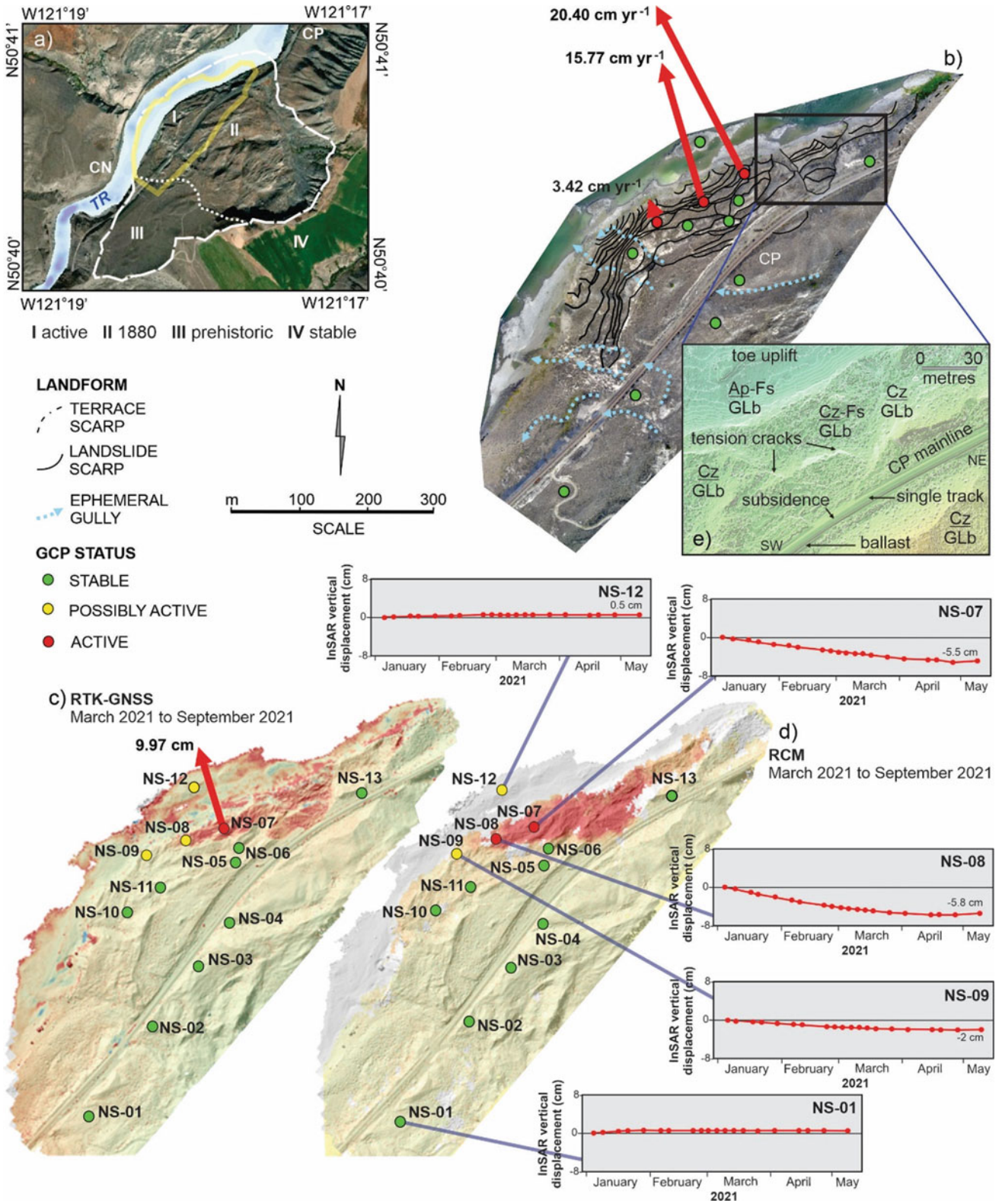

Fig. 6 Geomorphology, change-detection monitoring, and at-risk railway infrastructure. **a** Extent of North Slide and footprint of UAV flight plans (2019, 2020, and 2021)—yellow line. **b** Plan view orthomosaic image of the "Solar Slump" showing distribution of terrace and landslide scarps, ephemeral gullies, and GCPs across the slide toe; with RTK-GNSS displacement vectors shown for NS-07, -08 and -09. **c** March to September 2021 UAV change detection results using cloud-processing solution M3C2 (after Gojcic et al. 2021), showing stable (green dots), possibly active (yellow dots), and active GCPs (red dots). **d** RCM change-detection results for January to September 2021, showing LoS vertical displacement of active GCPs. **e** Surficial geology and geomorphology in vicinity of subsidence and tension cracks encroaching on railway infrastructure: Ap-Fs—alluvial plain, disturbed by slow-moving slide; Cz-Fs—active colluvium, disturbed by slow-moving slide; GLb—glaciolacustrine blanket deposit (underlying Ap and Cz)

scarps. A dendritic network of ephemeral channels, infilled with saturated silt and sand-rich alluvial outwash and organic sediments, and fed by springs and irrigation runoff, incises these blocks. A glacial outwash terrace with a, surface elevation of 390 m asl, lies upslope and east of the active landslide (Fig. 2).

Nineteen GCPs were installed on Nepa Slide in 2021 (Fig. 3c) to establish whether portions of the main body are reactivating. Below the CN and CP tracks, NP-09, -10 and -11 rest on cobble and boulder ballast up to 3 m thick. Like Ripley Landslide, this anthropogenic layer overlies > 10 m of fine-grained glaciolacustrine deposits and boulder-rich till with shear surfaces extending under Thompson River. GCPs on stable terrain north of the slide body (NP-01, NP-02, NP-03 and NP-04) sit on a wind-reworked alluvial silt and sand veneer draping boulder-rich till (< 3 m thick). These coarser surface units overlie glaciolacustrine silt and clay > 20 m in thickness. Along the southern flank, boulder-rich till (2–5 m thick), resting on fractured andesite and rhyolite, underlies NP-05, NP-06, NP-07 and NP-08. Across the main slide body and upslope of the tracks, GCPs (NP-12 to NP-19) sit on slide blocks comprising colluviated till and glaciofluvial sand and gravel (<5 m thick), overlying glaciolacustrine clay and silt beds (>10–15 m thick).

Change-detection monitoring

As part of the new UAV and RTK-GNSS change-detection program initiated in 2022, the orthophoto mosaic, DEM and DSM of Nepa Slide captured in October 2021 (Figs. 2; and 3) will serve as the baseline for further RPAS and InSAR change-detection monitoring.

3.3 Red Hill Slide

The Red Hill Slide flight plan footprint is 0.457 km^2, with the 2021 orthomosaic image and DSM capturing a 0.298 km^2 rotational-translational landslide with moderate to steep slopes between > 12° and < 37° and 145 m of relief (Fig. 2). Vegetation-free slide blocks with back scarps 5–20 m high are incised by a steep-sided ephemeral gully channeling irrigation and hillslope runoff. The stratigraphy exposed above the active river floodplain (*ca.* 265 m asl) comprises glaciolacustrine silt and clays, truncated and overlain till diamicton, sand and gravel outwash, and wind-reworked silt-rich alluvial terrace formed at 410 m asl.

Change-detection monitoring

The DEM and DSM of Red Hill Slide captured in November 2021 (Figs. 2; and 3) will serve as the baseline for further RPAS and InSAR change-detection monitoring.

3.4 South Slide (South Extension)

At 0.464 km^2, the South Slide (South Extension) shares the largest flight plan footprint with the North Slide (Solar Slump) (Fig. 2). The "South Extension" has an approximate area of 0.144 km^2. The October 2021 orthomosaic image and DSMs captures the active floodplain of Thompson River and tributary alluvial fan at *ca.* 265 m asl. Railway infrastructure crosses the slide toe with slopes ranging from > 12 to < 27°. The slide body consists of a northern portion with eroded slide blocks and closed depressions, relatively free of vegetation cover; and a southern extension showing no surficial evidence of movement (e.g., tension cracks, slide scarps). A glacial outwash terrace with a surface elevation of 400 m asl lies upslope and east of the active landslide.

Eleven GCPs were positioned across the headwall, toe slope and south extension of South Slide in 2016 (Fig. 3d). GCPs along the CN and CP tracks (SS-01, SS-02, SS-03, SS-04, and SS-09) are established on thick (>15 m) glaciolacustrine clay, silt and glacial boulder-rich diamicton (basal till). The toe slope is excavated to accommodate the CN and CP tracks, and draped in a cobble and boulder ballast up to 5 m thick. Upslope of the tracks, unconsolidated sediment thickness increases in the main slide body, with SS-05 to SS-11 established on silt and sand-rich alluvial outwash, overlying glaciolacustrine and till units > 25 m in thickness.

Change-detection monitoring

Although InSAR analysis delimits an extensive area of displacement between SS-01 and SS-05 (Fig. 1c), repeat RTK-GNSS surveys have not taken place since installation. The South Slide (South Extension) orthophoto mosaic, DEM and DSM, captured in October 2021 (Figs. 2, 3 and 6a), will serve as the baseline for further RPAS and InSAR change-detection monitoring.

3.5 North Slide (Solar Slump)

The merged mosaics and DSMs (Figs. 2, 3e and 6b) capture the baseline surface condition of the North Slide, long with the extent of bare earth and vegetation growth (e.g., grasses, shrubs, and trees). Metre-scale anthropogenic features (e.g., train tracks, signals bungalow, solar panel array) are resolvable in the orthophoto mosaic and DSM. Geomorphic features visible include: terraces graded to 340 m and 300 m asl, with steep river-cut scarps; ephemeral gullies draining the inactive nineteenth century slide surface; active slide blocks, scarps and tension cracks across the "Solar Slump"; and the toe bulge in the active floodplain of Thompson River (Figs. 2 and 3e).

In 2019, eleven permanent GCPs were installed across the North Slide toe slope; another station was added in 2020 on the floodplain toe slope bulge; and a thirteenth installed at the NW limit of the active toe slope in 2021 (Fig. 2d). On the Thompson River floodplain (*ca.* 270 m asl), a boulder veneer drapes back-tilted clay and silt beds beneath NS-12. Bedrock does not outcrop in the survey area. Inactive and active slide blocks with GCPs are incised by ephemeral gullies and by cut-bank erosion during high river stages (during summer months).

Over the slide toe, GCPs are established boulders resting on boulder-rich diamicton (basal till) and glaciofluvial sand and gravel outwash (5–10 m thick) overlying > 20 m of glaciolacustrine clay and silt. Landslide scarps across the "Solar Slump" form subparallel to the orientation of the river channel. In the northwest, cutbank erosion along a 200 m section of Thompson River has exposed and triggered a series of slumps in terraced glaciolacustrine and till deposits below 280 m asl. These small slumps ($\leq$ 50 m^2) are directly impacting railway infrastructure (Fig. 6b, e) and contributing to slope unloading. Landslide scarps follow the arc of relict back-rotated slide blocks (GCPs NS-05, NS-06, NS-10 and NS-11), and increase in size and activity toward the river (GCPs NS-07, NS-08 and NS-09). Tension cracks are extrapolated beneath railway ballast close to the solar panel array and signals bungalow (between GCPs NS-04, NS-05 and NS-13).

Southeast and upslope of the CP tracks, retrogressive translational back-rotated slide blocks and scarps from the 1880 landslide are now subdued features due to 140 years of wind deflation, soil creep, and surface runoff. Slopes $\geq$ 12° are draped in a veneer of colluviated till, glaciofluvial outwash and glaciolacustrine sediments. The historical landslide and active "Solar Slump" are gullied by ephemeral streams that drain to a coarse alluvial fan prograding into Thompson River along the western margin of the toe slope (Fig. 6b).

Change-detection monitoring

RTK-GNSS measurement precision and accuracy discounts points showing 3 cm or less movement (NS-01, NS-02, NS-03, NS-04, NS-05, N-06, N-10 and NS-11). Those GCPs with annual differences of > 3 cm were considered robust measurements. Between 2019 and 2020, NS-07, NS-08 and NS-09 all showed displacement vectors to the NNW (Fig. 6 b). Maximum annual displacement values of 15.77 cm year^{-1} (NS-08) and 20.40 cm year^{-1} (NS-07). Significantly, the displacement vectors indicate movement toward the scour pools lying adjacent to the "Solar Slump" (Figs. 2 and 5a).

Aligning the GCPs and manually picking tie points to improve point cloud registration between the two surveys significantly enhanced the quality of the M3C2 point cloud comparison results (Fig. 6c). A qualitative assessment of preliminary results of point cloud-based change-detection monitoring for the North Slide is presented here. An area of 436 m^2 with displacement values > 5 cm between September 2019 and September 2021 lies NW of the CP track (NS-07, NS-08 and NS-13), extending onto the Thompson River floodplain (NS-12). Individual slide block surfaces are resolved, with RTK-GNSS measurement at NS-07 recording 10 cm of NW displacement between March and September 2021. Localized displacement SW of NS-10 records the formation of colluvial cones by a small debris fall along the river embankment. Significantly, UAV change-detection photogrammetry shows the extent of encroachment by the active portion of the landslide on railway infrastructure (ballast and tracks; Fig. 6e).

The 2020 RCM InSAR results reveal severe deformation at the North Slide "Solar Slump" from the end of August to middle September (Fig. 5c–e). Several fringes indicate movement of approximately 2–5 cm over 28-day (Fig. 5c) and 16-day periods (Fig. 5d), indicating a rapid and complex deformation pattern in the most affected zones. The 4-day interferogram (Fig. 5e) shows nearly a full fringe cycle, indicating a rapid and complex deformation pattern on shorter time scales. Maximum deformation over this 4-day period is estimated to be $\sim$ 2 cm.

We are currently developing a robust multi-year RCM time-series. The January to May 2021 interval is briefly discussed here, but the aim is to extend coverage on either side of this time-series (Rotheram-Clarke et al. *In prep.*). The spatial extent captured by RCM showing the cumulative deformation from January 5, 2021 to May 9, 2021 (Fig. 6d) is very similar to that seen with the UAV imagery. The colour stretch is $\pm$ 5 cm, indicating measurement of approximately 5–6 cm of line-of sight deformation at NS-07 and NS-08. There is also uplift between NS-07 and NS-12, which is where back-tilted clay-silt beds are exposed in the active floodplain (Huntley et al. 2021b). Research efforts are now directed at comparing the two time-series and converting satellite LoS displacements to correspond with movement vectors derived from UAV and RTK-GNSS datasets.

4 Conclusions and Evaluation

Proactive landslide disaster-risk management requires knowledge of the timing and magnitude of ground displacement events. NRCAN-GSC, through IPL Project 202, provides foundational geospatial information on landslides and other geohazards threatening natural resources, national socioeconomic infrastructure, communities and public safety.

This paper demonstrates the investigative capacity of a RPAS for landslide monitoring along the Canada's national railway transportation corridor. UAV photogrammetric techniques allow the representation of large surfaces with dense spatial sampling. Orthomosaic 3D time-series offer clear

advantages with respect to InSAR time-series analysis providing only LoS displacement measurements over large areas, and RTK-GNSS surveys of GCPs which provide data that are spatially accurate, but necessarily limited to a small number of control points. UAV photogrammetry and RTK-GNSS surveys show landslides have a significant motion that is only partly captured by satellite InSAR monitoring. This is a clear demonstration of a limitation in east–west-up-down sensitive InSAR, since failing slopes are largely moving NW or SE, so a significant amount of movement is likely not recognized by satellite monitoring alone.

The RPAS presented in this paper generates high spatial resolution epochal geo-coded imagery suitable for landslide disaster-risk management. UAV photogrammetry, when benchmarked with RTK-GNSS, satellite InSAR, and other geospatial and temporal datasets will help stakeholders develop a more resilient railway national transportation network able to meet Canada's future socioeconomic needs, while ensuring protection of the environment and resource-based communities from natural disasters related to extreme weather events and climate change.

4.1 RPAS Evaluation

We demonstrate the Spexi Geospatial RPAS allows trained UAV pilots to quickly and easily capture imagery, and transfer processed data to stakeholders (e.g., government agencies, railway industry, remote communities) in a timely manner. The time elapsed from flight request to data delivery is comparable to commercial SfM applications. The RPAS is capable of simultaneous deployment on multiple landslides > 3 km^2 allowing for more productive fieldwork. Geospatial datasets (orthophoto mosaics, DEMs and DSMs) have processed X, Y, Z accuracies of 3 to 5 cm: comparable to RTK-GNSS and InSAR measurements. Resulting datasets from the collected and processed imagery with a pixel resolution of 2.5 cm can easily resolve small surface features (e.g., GCPs, railway ties, bedrock fractures and tension cracks). Orthophoto mosaics, DEMs and DSMs captured in 2021 (Figs. 2 and 3) will serve as the baseline for further RPAS landslide change-detection monitoring along the national railway corridor in the Thompson River valley, and elsewhere across Canada.

Across NRCAN (and other Federal Agencies), there are numerous applications for UAV photogrammetry (Fig. 7). In addition to monitoring landslides along the national railway corridors, the RPAS presented in this paper has applications for modelling tsunami run-up in coastal communities, mapping active faults, monitoring volcanic hazards, recognizing geohazards along pipelines and power transmission right-of-ways, delineating permafrost deterioration in northern regions, and for deployment during bedrock mapping traverses.

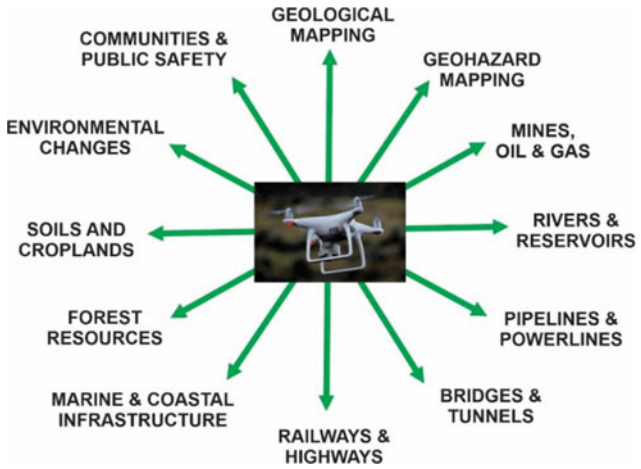

Fig. 7 UAV applications broadly relevant to mandates of NRCAN and other government departments (e.g., Department of National Defence; Environment and Climate Change Canada; Innovation, Science and Economic Development Canada; National Research Council Canada; Parks Canada; Public Safety Canada; Royal Canadian Mounted Police; Transportation Safety Board; Fisheries and Oceans Canada; Infrastructure Canada; Canadian Coast Guard; Canadian Police College; and Canadian Transportation Agency)

Acknowledgements The Government of Canada, through the Ministry of Transport and Ministry of Natural Resources, is funding field-based landslide research in the Thompson River valley, BC, and elsewhere across Canada. The authors wish to acknowledge the support of Danny Wong (Canadian Pacific Railways, Calgary, Alberta) and Trevor Evans (Canadian National Railways, Kamloops, British Columbia). Anonymous reviewers improved an early version of the manuscript.

References

Barrett B, Whelan P, Dwyer N (2012) The use of C- and L-band Repeat-Pass Interferometric SAR coherence for soil moisture change detection in vegetated areas. Open Remote Sens J 5:37–53. https://doi.org/10.2174/1875413901205010037

Booth A, Lamb M, Avouac J-P, Delacourt C (2013) Landslide velocity, thickness, and rheology from remote sensing: La Clapière landslide, France. Geophys Res Lett 40:4299–4304. https://doi.org/10.1002/grl.50828

Bunce C, Chadwick I (2012) GPS monitoring of a landslide for railways. In: Landslides and engineered slopes—protecting society through improved understanding, pp 1373–1379

Casagli N, Frodella W, Morelli S, Tofani V, Ciampalini A, Intrieri E, Raspini F, Rossi G, Tanteri L, Lu P (2017) Spaceborne, UAV and ground-based remote sensing techniques for landslide mapping, monitoring and early warning. Geoenvironmental Disasters 4(9):23. https://doi.org/10.1186/s40677-017-0073-1

Clague J, Evans S (2003) Geologic framework for large historic landslides in Thompson River valley, British Columbia. Environ Eng Geosci 9:201–212

Gojcic Z, Schmid L, Wieser A (2021) Dense 3D displacement vector fields for point could-based landslide monitoring. Landslides 18:3821–3832. https://doi.org/10.1007/s10346-021-01761-y

Handwerger A, Booth A, Huang M, Fielding E (2021) J Geophys Research, Earth Surf 126:21. https://doi.org/10.1029/2020JF005898

Hendry M, Macciotta R, Martin D (2015) Effect of Thompson River elevation on velocity and instability of Ripley Slide. Can Geotech J 52(3):257–267

Holmes J, Chambers J, Meldrum P, Wilkinson B, Williamson P, Huntley D, Sattler K, Elwood D, Sivakumar V, Reeves H, Donohue S (2020) 4-Dimensional electrical resistivity tomography for continuous, near-real time monitoring of a landslide affecting transport infrastructure in British Columbia, Canada. Near Surface Geophys 15. https://doi.org/10.1002/nsg.12102

Hu X, Bürgmann R, Lu Z, Handwerger A, Wang T, Miao R (2019) Mobility, thickness, and hydraulic diffusivity of the slow-moving Monroe Landslide in California revealed by L-band satellite radar interferometry. J Geophys Res Solid Earth 124:7504–7518. https://doi.org/10.1029/2019JB017560

Huntley D, Bobrowsky P, Zhang Q, Zhang X, Lv Z (2017) Fibre bragg grating and brillouin optical time domain reflectometry monitoring manual for the Ripley landslide, near Ashcroft, British Columbia. GSC Open File 8258:66

Huntley D, Bobrowsky P, Hendry M, Macciotta R, Best M (2019a) Multi-technique geophysical investigation of a very slow-moving landslide near Ashcroft, British Columbia, Canada. J Environ Eng Geophys 24(1):85–108. https://doi.org/10.2113/JEEG24.1.87

Huntley D, Bobrowsky P, Hendry M, Macciotta R, Elwood D, Sattler K, Chambers J, Meldrum P (2019b) Application of multi-dimensional electrical resistivity tomography datasets to investigate a very slow-moving landslide near Ashcroft, British Columbia, Canada. Landslides 16:1033–1042. https://doi.org/10.1007/s10346-019-01147-1

Huntley D, Holmes J, Bobrowsky P, Chambers J, Meldrum P, Wilkinson P, Elwood D, Sattler K, Hendry M, Macciotta R (2020) Hydrogeological and geophysical properties of the very slow-moving Ripley Landslide, Thompson River valley, British Columbia. Can J Earth Sci 21. https://doi.org/10.1139/cjes-2019-0187

Huntley D, Bobrowsky P, MacLeod R, Cocking R, Joseph J, Rotheram-Clarke D (2021a) Ensuring resilient socio-economic infrastructure: field testing innovative differential GNSS-InSAR-UAV monitoring technologies in mountainous terrain near Ashcroft, British Columbia, Canada. J Mountain Sci 18(1):1–20. https://doi.org/10.1007/s11629-020-6552-y

Huntley D, Rotheram-Clarke D, Pon A, Tomaszewicz A, Leighton J, Cocking R, Joseph J (2021b) Benchmarked RADARSAT-2, SENTINEL-1 and RADARSAT CONSTELLATION MISSION change detection monitoring at North Slide, Thompson River valley, British Columbia: implications for a landslide-resilient national railway network. Can J Remote Sens. https://doi.org/10.1080/07038992.2021.1937968

Huntley D, Rotheram-Clarke D, Cocking R, Joseph J, Bobrowsky, P (2021c) Understanding Plateau and Prairie Landslides: annual report on landslide research in the Thompson River valley, British Columbia, and the Assiniboine River valley, Manitoba-Saskatchewan (2020–2021c to 2021c–2022); Geological Survey of Canada, Open File 8838, 73 pages

Journault J, Macciotta R, Hendry M, Charbonneau F, Huntley D, Bobrowsky P (2018) Measuring displacements of the Thompson River valley landslides, south of Ashcroft, B.C., Canada, using satellite InSAR. Landslides 15(4):621–636. https://doi.org/10.1007/s10346-017-0900-1

Lucieer A, de Jong S, Turner D (2014) Mapping landslide displacements using structure from Motion (SfM) and image correlation of multi-temporal UAV photography. Prog Phys Geogr 38(1):97–116

Macciotta, R, Hendry, M, Martin, D, Elwood, D, Lan, H, Huntley, D, Bobrowsky, P, Sladen, W, Bunce C, Choi, E and Edwards, T (2014) Monitoring of the Ripley Slide in the Thompson River Valley, B.C. Geohazards 6 Symposium, Proceedings Volume, Kingston, Ontario, Canada

Rossi G, Tanteri L, Tofani V, Vannocci P, Moretti S, Casagli N (2018) Multitemporal UAV surveys for landslide mapping and characterization. Landslides 15:1045–1052. https://doi.org/10.1007/s10346-018-0978-0

Schafer M, Macciotta R, Hendry M, Martin D, Bobrowsky P, Huntley D, Bunce C, Edwards T (2015) Instrumenting and monitoring a slow moving landslide. GeoQuebec 2015 Paper, 7 p

Sestras P, Bilaşco S, Roşca S, Dudic B, Hyas A, Spalević V (2021) Geodetic and UAV monitoring in the sustainable management of shallow landslides and erosion of a susceptible. Remote Sens 13:28. 10.3390

Stanton R (1898) The great land-slides on the Canadian Pacific Railway in British Columbia. Proc Civil Eng 132:1–48

Türk T (2018) Determination of mass movements in slow-moving landslides by the Cosi-Corr method. Geomatics, Natural Hazards, Risk 9(1):325–336. https://doi.org/10.1080/19475705.2018.1435564

Turner D, Lucieer A, de Jong S (2015) Time series analysis of landslide dynamics using an unmanned aerial vehicle (UAV). Remote Sens 7:1736–1757. https://doi.org/10.3390/rs70201736

Ongoing Persistent Slope Failures at the Toe of a Giant Submarine Slide in the Ryukyu Trench that Generated the AD 1771 Meiwa Tsunami

Kiichiro Kawamura, Kazumasa Oguri, Mutsuo Inoue, Kan-Hsi Hsiung, Taishi Kudaka, and Ken Takai

Abstract

This study investigates sedimentation processes and associated submarine sliding on the floor of the Ryukyu Trench. Three dive surveys were conducted using the manned submersible *Shinkai 6500* (hereafter 6K) in the trench. The AD 1771 Meiwa tsunami was generated by a giant submarine slide on the landward trench slope in this region. Dive survey site 6K#1469 was located on a mouth of the submarine canyon in the forearc basin. Dive survey site 6K#1468 was located on the uppermost part of the submarine slide, where steps and fissures were observed. Dive survey site 6K#1467 was located at the toe of the submarine slide, which is covered by a muddy sediment layer. Core sample 6K#1467 measured 36.3 cm long and comprised muddy sediments interlayered with silt and/or sand laminations. The paleocurrent direction of the laminated sediments is mostly from north to south, indicating that they were not transported along with the trench but were from the landward slope, probably via repeated small submarine slides. The sedimentation rate for sample 6K#1467 was estimated at 2.42 mm/year using a depth profile of $^{210}Pb_{ex}$ concentration within 10 cm deep and a date for the sediment of ~ 50 year ago. Based on the sedimentation rate and the number of laminae, the typical recurrence interval of the silt/sand layers is calculated to be ~ 6 year. We interpret these results as indicating that repeated small submarine slides have occurred persistently (recurrence interval of ~ 6 year) at the toe of the investigated giant submarine slide in the Ryukyu Trench over the last 50 year.

Keywords

Submarine slide • *Shinkai 6500* • ITRAX • ^{210}Pb • Paleocurrent • Ryukyu Trench

K. Kawamura (✉)
Graduate School of Science and Technology for Innovation, Yamaguchi University, 1677-1 Yoshida, Yamaguchi-City, Yamaguchi, 753-8512, Japan
e-mail: kiichiro@yamaguchi-u.ac.jp

K. Oguri
HADAL and Nordcee, Department of Biology, University of Southern Denmark, Campusvej 55, 5230 Odense M, Denmark
e-mail: ogurik@biology.sdu.dk

K. Oguri
Research Institute for Global Change (RIGC), JAMSTEC, 2-15 Natsushima-cho, Yokosuka-City, Kanagawa, 237-0061, Japan

M. Inoue
Low Level Radioactivity Laboratory, Institute of Nature and Environmental Technology, Kanazawa University, Nomi, Ishikawa, 923-1224, Japan
e-mail: i247811@staff.kanazawa-u.ac.jp

K.-H. Hsiung
Research Institute for Marine Geodynamics (IMG), JAMSTEC, 2-15 Natsushima-cho, Yokosuka-City, Kanagawa, 237-0061, Japan
e-mail: hsiung@jamstec.go.jp

T. Kudaka
Faculty of Science, Yamaguchi University, 1677-1 Yoshida, Yamaguchi-City, Yamaguchi, 753-8512, Japan

K. Takai
Institute for Extra-Cutting-Edge Science and Technology Avant-Garde Research (X-Star), JAMSTEC, 2-15 Natsushima-cho, Yokosuka-City, Kanagawa, 237-0061, Japan
e-mail: kent@jamstec.go.jp

1 Introduction

Numerous coralline and reef boulders are considered to have been deposited by paleo-tsunamis on the Sakishima Islands at the southeastern end of Japan (Goto et al., 2010; Hisamitsu et al. 2014). Araoka et al. (2013) reported that eight tsunamis have struck the Sakishima Islands during the last ~ 2400 year (250 ± 100 BC, AD 200 ± 100, AD 550 ± 100, AD 800 ± 100, AD 1100 ± 100, AD 1400 ± 100, AD 1600 ± 100, and AD 1800 ± 100), as inferred from radiocarbon dating of 92 *Porites* boulders. The latter two events are consistent with historically recorded

I. Alcántara-Ayala et al. (eds.), *Progress in Landslide Research and Technology, Volume 1 Issue 2, 2022*, Progress in Landslide Research and Technology,
https://doi.org/10.1007/978-3-031-18471-0_5

events that occurred in 1625 and 1771, respectively (Araoka et al. 2013; Hisamitsu et al. 2014).

The giant 1771 Yaeyama tsunami (or 1771 Meiwa tsunami) resulted in runups of up to 30 m and 12,000 deaths on the Sakishima Islands in the southwestern Ryukyu Arc (Nakamura et al. 2009; Okamura et al. 2018). Nakamura et al. (2009) proposed that this tsunami was caused by an earthquake of moment magnitude (Mw) 8.0 that occurred in subducted sediments beneath the accretionary wedge. However, Okamura et al. (2018) reported that a submarine slide on the accretionary prism is a plausible source of the 1771 tsunami, based on a simple simulation and seismic survey results.

Most such submarine slides occur on the hanging wall of active thrust faults (Kawamura et al. 2009; Yamada et al. 2009), whereby the hanging wall is thrust upward during fault motion which subsequently collapses to initiate a submarine slide. A submarine slide results from slope instability caused by steepening of the hanging wall through cumulative thrust motion. The thrust events might be recorded in downslope basins as submarine slide deposits.

In this study, we investigate the sedimentation processes of turbidite layers in the Ryukyu Trench floor. Our results show that these layers have resulted from repeated small submarine slides originating from the landward trench slope that are caused by small collapse of the hanging wall of the frontal thrust. The recurrence interval of the slides is calculated roughly at $\sim$ 6 year. We conclude that the hanging wall of the frontal thrust has collapsed by repeated retrogressive submarine slides for at least $\sim$ 50 year ago.

2 Tsunamigenic Submarine Slides

Submarine slides are generally formed by source area, main track and depositional area (Fig. 1). The source and depositional areas are formed by extensional and compressional deformations, so that these are characterized by subsidence and uplifting, respectively. These seabed vertical motions could generate a tsunami. The size of the tsunami wave would not only be controlled by its geological architecture, but also by deformation speed, physical and mechanical properties of seabed materials and water depth of the submarine slides (Kawamura et al. 2017).

There are many historical accounts of tsunamigenic submarine slides. We briefly introduce the representative recent historical examples except for the 1777 Meiwa tsunami mostly following Kawamura et al. (2014).

The Lisbon earthquake of around Mw 8.5 occurred on November 1, 1755 on the Sao Vincentre Fault, off the coast of Portugal. Large tsunamis devastated Lisbon and other North Atlantic coasts both in Europe and Africa. Gracia et al. (2003) showed the probability for tsunamis genesis partly by submarine slides on the hanging wall of the thrust fault.

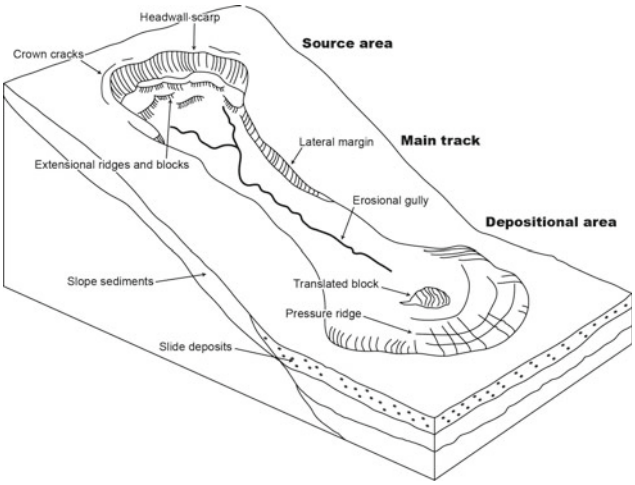

Fig. 1 General topography and internal structure of submarine slides (After Kawamura 2020)

On March 27, 1964, a moment magnitude Mw 9.2 earthquake generated large tsunamis of tsunami magnitude (Mt) 9.1 in Alaska (Abe 1979). Plafker and Mayo (1965) described localized tsunami waves excited by submarine slides that occurred in river deltas, terminal moraines, and so on. The tsunamis were approximately 3.0–4.5 m high and hit many bay areas about 19–20 min after the earthquake.

On June 15, 1896, the Meiji Sanriku earthquake generated devastating tsunamis with a maximum run-up of 37 m, and caused the worst tsunami disaster in Japanese history, despite having a surface wave magnitude (Ms) of only 7.2 and a low seismic intensity (Tanioka and Satake 1996). Abe (1979) showed that in spite of the low Ms, the Mt of this event was up to 8.6. To explain the discrepancy between Ms and Mt, the 1896 Sanriku earthquake has been variously attributed to slow rupture along the fault (Kanamori 1972), submarine slides (Kanamori and Kikuchi 1993), and additional rapid uplift of a sediment wedge (Tanioka and Seno 2001). Kawamura et al. (2012; 2014) supported the submarine slide scenario on the basis of topographic analysis and the geologic architecture.

On 1 April, 1946, Ms 7.1 earthquake occurred and generated large tsunamis (Mt = 9.3) along the Alaskan coastline that killed 167 people. Fryer et al. (2004) suggested that these tsunamis resulted from submarine slides (the Ugamak Slide), with head scars at water depths of approximately 200 m in the coastal area.

On 17 July, 1998, tsunamis with maximum wave heights of 15 m inundated Sissano in Papua New Guinea following Mw 7.1 earthquake (Kawata et al. 1999). Based on detailed seafloor mapping data, Tappin et al. (2001, 2008) concluded that the large tsunami was caused by a submarine slide

located offshore from the lagoon. This tsunami was rapidly excited by the earthquake (Newman and Okal 1988), but it was generated by subsequent submarine slides (2008).

On 12 January, 2010, the Haiti earthquake (Mw = 7.0) exhibited a primarily strike–slip motion, it nevertheless generated a tsunami (Hornbach et al. 2010). The earthquake caused liquefaction in several river deltas, which prograded rapidly and were prone to failure. It was concluded that the earthquake initiated a slide-generated tsunami along the shoreline.

Similar tsunamis occurred at Bay of Palu, induced by an earthquake in Sulawesi Island of Indonesia on 28 September, 2018 (Mw = 7.5) (Sassa and Takagawa 2019). These were excited by submarine slides along the bay due to liquefaction of coastal regions (Sassa and Takagawa 2019). Maximum run-up height was 11.3 m and average inundation distance was ∼ 200 m (Sassa and Takagawa 2019). The number of casualties was 2000 and the number of missing persons exceeds 5000.

In summary, all of these historical examples of tsunamis induced by submarine slides and/or presumable ones were excited by earthquake activity. These examples strongly suggested that the preconditioning factors on submarine slopes play an important role in excitation of the tsunamigenic submarine landslides. Therefore, understanding the preconditioning factors, not only using monitoring systems, but also using topographic analyses are significant to reduce the loss of the lives by tsunamis. Size and frequency of small submarine landslides could demonstrate the state of the slope stability.

3 Detailed Bathymetry and Dive Surveys

The landward trench slope of the southwestern Ryukyu Arc is composed of a steep upper slope, forearc basin, and accretionary prism from north to south (Okamura et al. 2018; Fig. 2). These forearc structures west of 122° 40′ E have been disrupted owing to tectonic movements related to arc–continent collision at Taiwan, back-arc rifting of the Okinawa Trough, and the high subduction obliquity of the Philippine Sea Plate (PSP), which contains ridges and seamounts (Okamura et al. 2018) and is converging with the Amur plate at a rate of 62–72 mm/year (Seno et al. 2005). At the Amur plate, the prism has been sliding to the west, relative to the arc, along dextral strike-slip faults that are clearly imaged by bathymetric mapping along the landward prism margin (Okamura et al. 2018; Fig. 2). The fault motion is interpreted to have been caused by slip-partitioning of the oblique subduction of the PSP (Okamura et al. 2018).

We conducted three dive surveys using the manned submersible *Shinkai 6500* (hereafter 6K) in the Ryukyu Trench region during cruise YK16-11 by the vessel

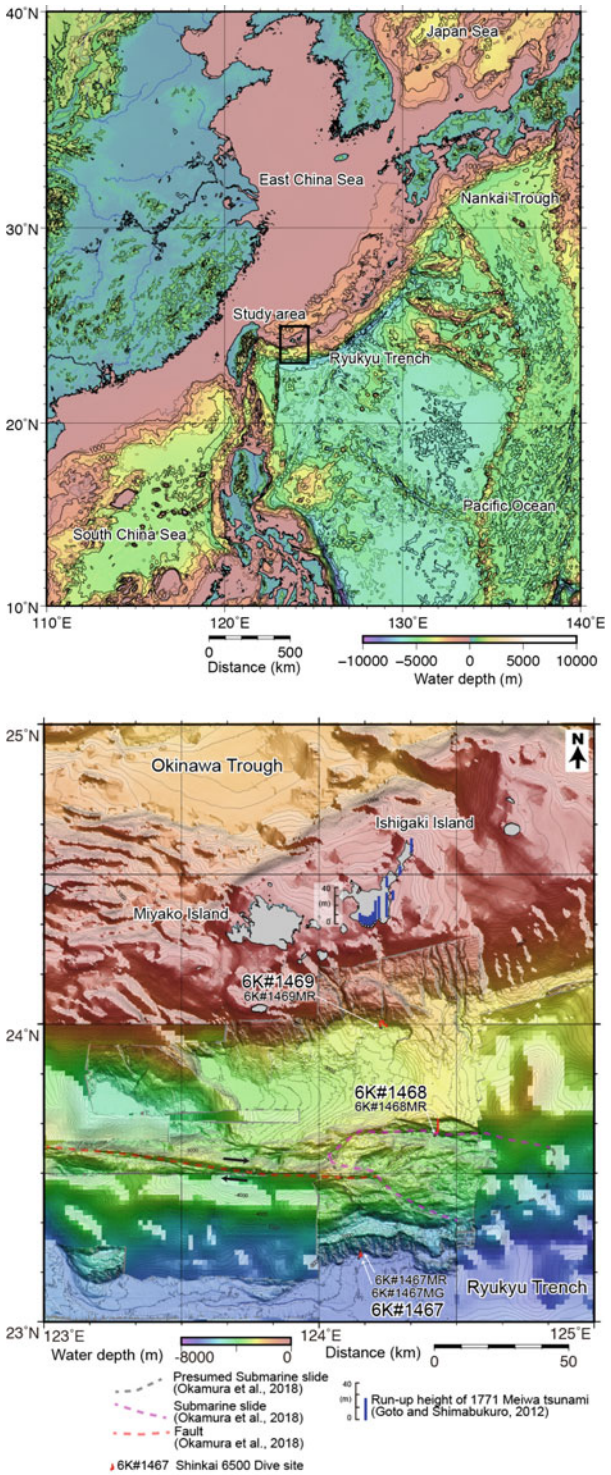

Fig. 2 Detailed topography and bathymetry in the study area. Upper shows location of the study area (black square) using ETOPO1, and lower shows dive locations using bathymetric survey data. Red lines indicate the dive routes followed during surveys from the *Shinkai 6500* vessel: 6K#1467, 6K#1468, and 6K#1469. Blue bars around Ishigaki Island show the run-up height of the AD 1771 Meiwa Tsunami (after Goto and Shimabukuro 2012). Broken lines demarcate the outline of the presumed submarine slide (gray), the submarine slide (pink), and the fault (red) identified by seismic surveys

Yokosuka. The dive surveys are referred as 6K#1467, 6K#1468, and 6K#1469 (Figs. 2 and 3). Survey 6K#1467 was performed on 1 September 2016 on the Ryukyu Trench floor at the foot of the landward trench slope. On the lower slope at a water depth of 6350 m, we collected a sediment core sample from the flat seafloor (sample 6K#1467MG)

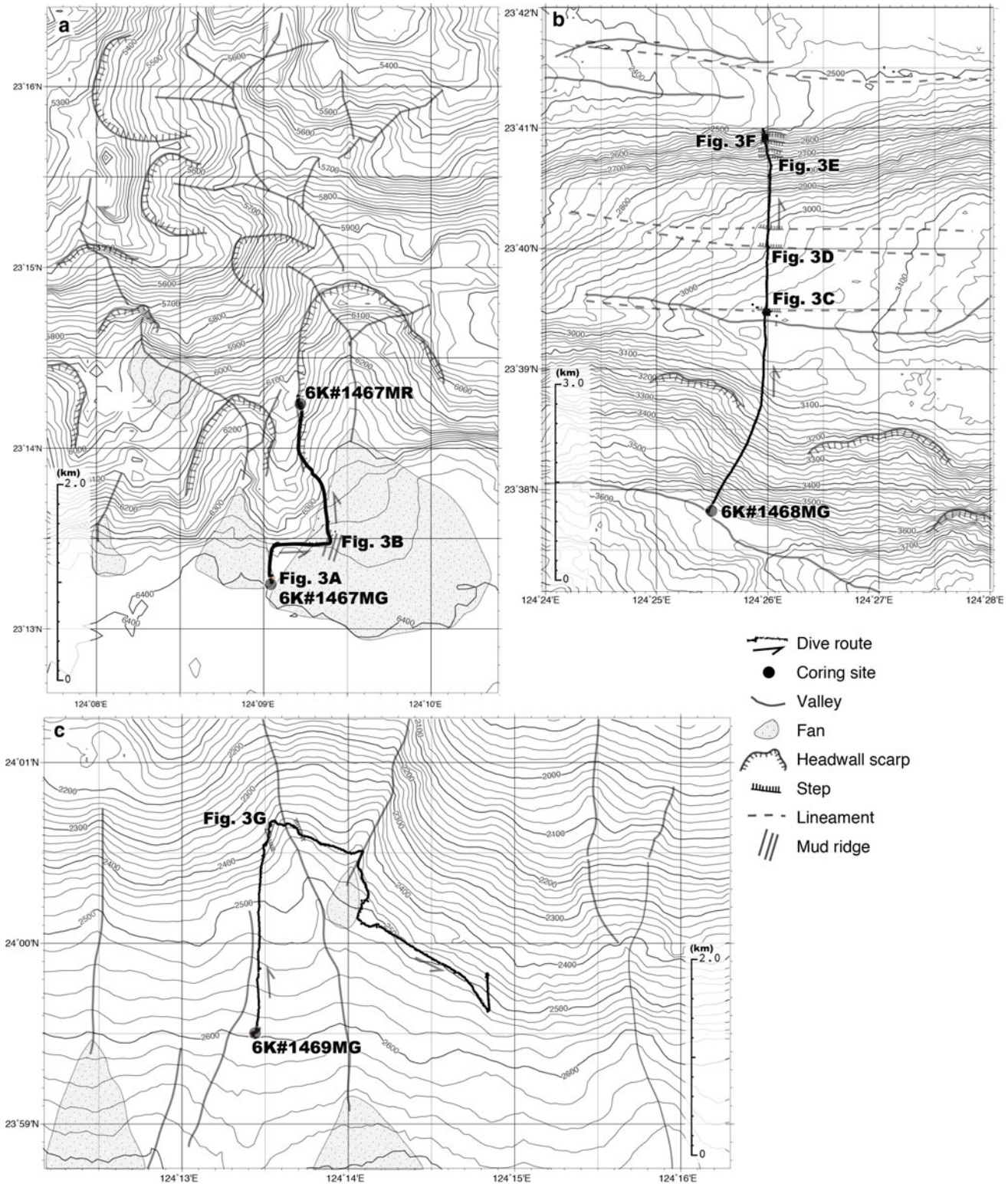

Fig. 3 Detailed bathymetry in the dive survey areas: **a** 6K#1467, **b** 6K#1468, and **c** 6K#1469

using the Monterey Bay and Aquarium Research Institute (MBARI) type corer. At 6160 m water depth, we discovered an outcrop comprising of three horizontal brown sediment layers each of which measured ∼ 20 cm in thickness. At 6115 m water depth, we collected a sediment core sample from the landward trench slope (sample 6 K#1467MR) using an MBARI corer, following which we left the seafloor at 6093 m water depth (Figs. 3 and 4).

Survey 6K#1468 was conducted on 2 September 2016. We landed on the seafloor at a depth of 3653 m at a site located at the foot of a cliff that might represent a lateral wall of submarine channel and/or headwall scar of the submarine slide that generated the 1771 Meiwa tsunami (Okamura et al. 2018). The slope extends over a distance of ∼ 1.8 km from ∼ 3600 to ∼ 3100 m water depth. The entire slope is covered with thick sediment, with no apparent faults, microbial mats, or colonies of chemosynthetic organisms. On the gentle slope extending from ∼ 3100 to 2900 m water depth, we observed several fault-related cliffs oriented mostly E–W and small outcrops of layered sedimentary rocks. The slope from ∼ 2900 to 2500 m water depth was not covered by fresh soft sediment, but instead comprised of partially hardened mud rocks at the seafloor (Figs. 3 and 4).

Survey 6K#1469 was performed on 3 September 2016. We landed at a water depth of about 2600 m, where the seafloor was flat and gray-colored, with several small dunes. We observed a step oriented NNE–SSW, which might represent the western wall of a shallow channel. The step has a relief of ∼ 1.0–1.5 m and exposes two units of strata. Farther eastward, we observed the western wall of the channel (Figs. 3 and 4).

4 Descriptions of Core Samples

Core sample 6K#1467MG was 35.5 cm long and was collected at 23°13.3014′N, 124°9.0358′E in 6371 m of water depth (Fig. 3). This core is composed of dark-olive-gray (2.5Y3/1) ashy silty clay throughout. The clay contains interbeds of fine- to medium-grained sand at 4, 8.4, 12, 14, 22, and 27 cm in core depth. A dark-olive-black (7.5Y2/2) silty clay layer was observed at 5–6 cm, and a yellowish-olive-black (10Y3/2) clay at 13.0–13.5 cm (Fig. 5).

Core sample 6K#1467MR was a length of 37 cm and was collected from a gentle slope with a thick cover of soft mud at 23°14.2477′ N, 124° 9.2242′ E in 6115 m of water depth (Fig. 3). This core is composed of olive-black (7.5Y3/1) ashy clayey silt throughout. The clayey silt is massive above 16 cm and is interbedded with darker-colored laminae below 16 cm. An olive-black (5Y3/1) clay layer (2 mm thick) occurs at 20 cm (Fig. 5). The bedding planes in this core have a dip of 5–10°, as discovered during vertical penetration by the corer.

Core sample 6K#1468MG was 38 cm long and was collected at 23° 37.8476′ N, 124° 25.4856′ E in 3653 m of water depth (Fig. 3). The sampling site is characterized by mud on a flat seafloor with small mounds of about 20 km in diameter. The core sample is yellowish gray (2.5Y4/1) at 0–6 cm, gradually becoming darker at 6–12 cm, dark grayish yellow (2.5Y4/2) at 12–35 cm, and brownish black (2.5Y3/2) at 35–38 cm (Fig. 5).

Core sample 6 K#1469MR was 26 cm long and was collected at 23° 59.5252′ N, 124° 13.4547′ E in 2583 m of water depth (Fig. 3). The seafloor at the sampling site is characterized by a flat floor with small white mounds (10–15 cm in diameter). The core sample is composed of bioturbated calcareous ooze, with numerous planktonic foraminifers and calcareous nannofossils throughout. The core color changes gradually with depth, being dark olive (5Y4/3) at 0–24 cm as a brownish surface oxidized layer, and dark olive gray (2.5Y3/1) at 24–39 cm as a grayish anoxic layer. The color at the boundary between these two layers is lighter than the grayish layer at 18–22 cm and is pale gray at 24–30 cm (Fig. 5).

5 Methods

5.1 Natural Gamma Radiation and Gamma-Ray Densitometry

In order to detect chemical characteristics of lamina, Natural gamma radiation (NGR) and gamma-ray attenuation (GRA) bulk densities were measured over 2 cm intervals using a multisensor core logger (MSCL). Here, we briefly explain these measurement methods, details of which can be found in Blum (1997).

Potassium (^{40}K), thorium (^{232}Th), and uranium (^{238}U) are radioisotopes that have a sufficiently long decay life to produce an appreciable amount of gamma rays. Minerals that fix K, U, and Th, such as clay minerals, are the principal source of NGR. Other sources include arkosic silts and sandstones, potassium salts, bituminous and alunitic schists, phosphates, certain carbonates, some coals, and felsic or mafic igneous rocks.

The bulk density of sediments and rocks is estimated from the measurement of GRA. GRA data can provide a precise and densely sampled record of bulk density, which is an indicator of changes in lithology and porosity. GRA records are frequently used for core-to-core correlation. Another important application of GRA measurements is the calculation of acoustic impedance and the construction of synthetic seismograms.

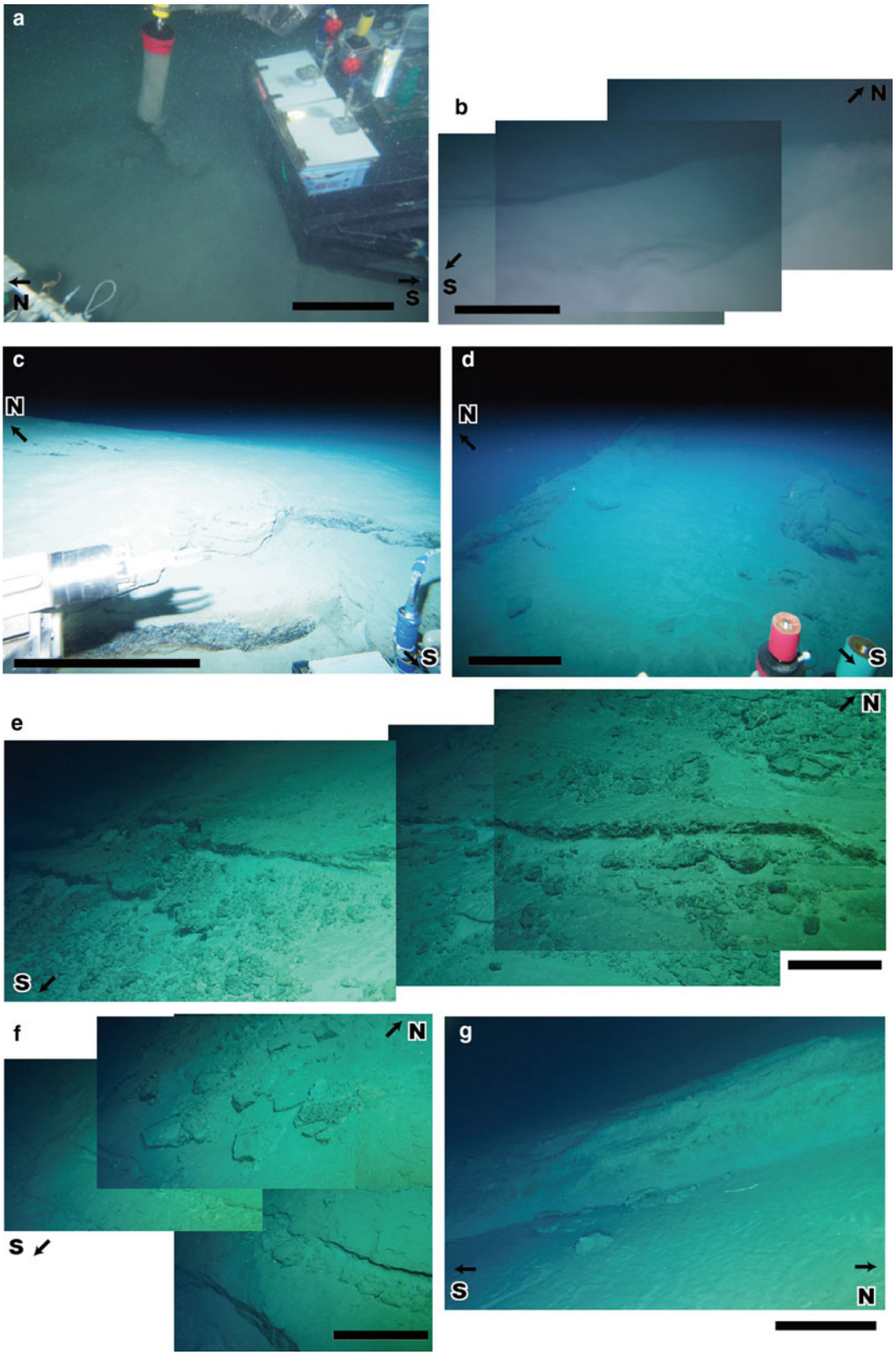

Fig. 4 Photographs taken during the dive surveys. The locations of the photographs are shown in Fig. 3. A: Sediment core collected from muddy seafloor in the Ryukyu Trench, 6K#1467. B: Parting lineations on a deep-sea fan in the Ryukyu Trench, 6K#1467. C: An E–W step with a height of ~ 1 m, 6K#1468. D: An E–W step with a height of ~ 0.5 m, 6K#1468. E: An E–W headwall scarp with a height of ~ 0.5 m and mudstone blocks measuring several centimeters in diameter, 6K#1468. F: An E–W headwall scarp with a height of ~ 0.5 m high and mudstone blocks measuring several centimeters in diameter, 6K#1468 and G: Lateral wall with a height of ~ 1 m high along a valley, 6K#1469

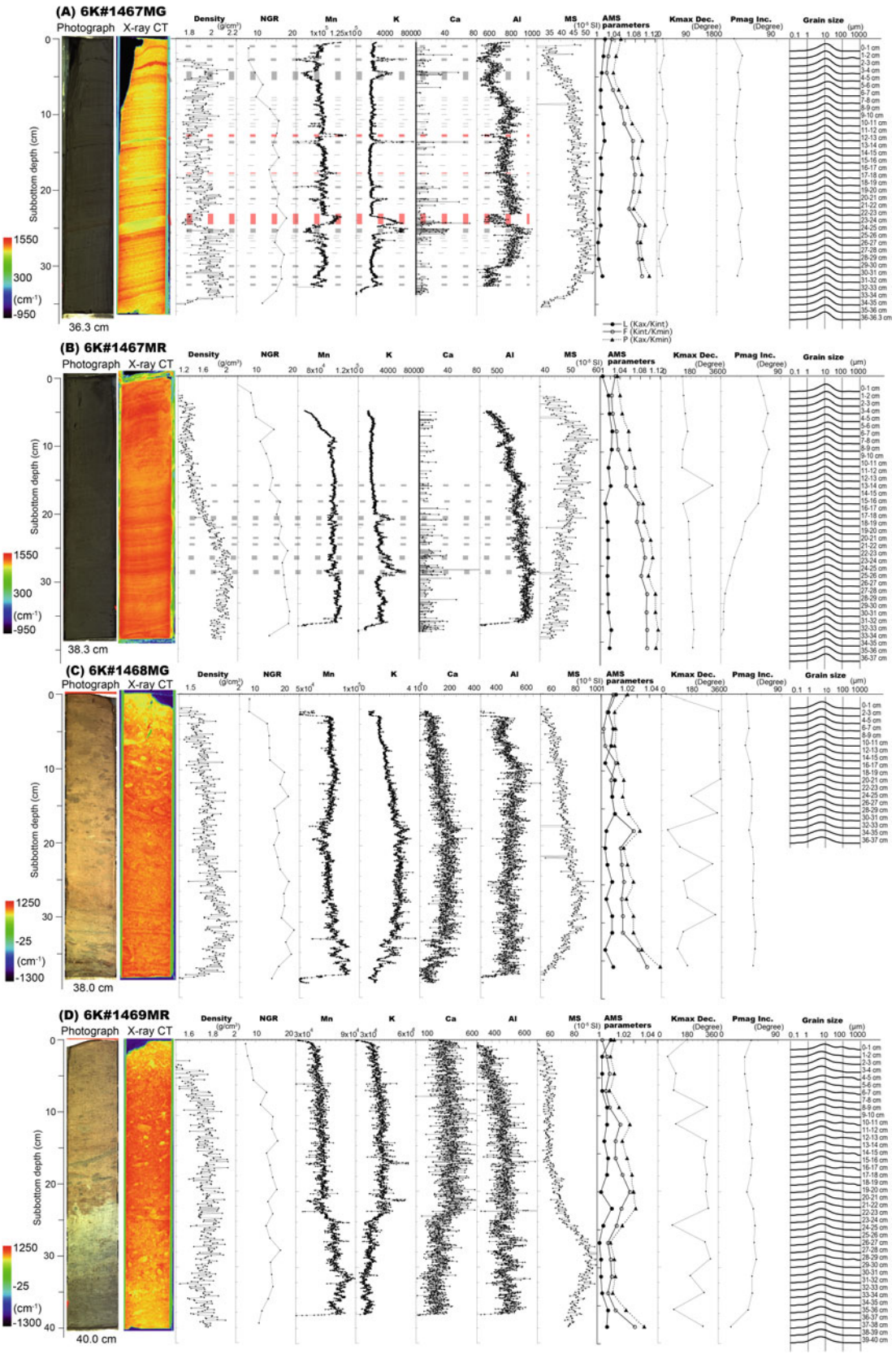

Fig. 5 Core samples profiles: **a** 6K#1467MG, **b** 6K#1467MR, **c** 6K#1468MG, and **d** 6K#1469MR. Columns (from left to right) are core photograph, X-ray CT image, density measured by gamma-ray attenuation (GRA), natural gamma ray (NGR), representative ITRAX element profiles (Mn, K, Ca, and Al), magnetic susceptibility (MS), AMS parameters (P, F, and L), K_{max} declination (K_{max} Dec.), paleomagnetic inclination (Pmag Inc.), and grain size distribution

5.2 Grain Size Determinations

Grain size distributions were determined using a Mastersizer laser diffraction grain size analyzer (Sysmex Co. Ltd.). Approximately 0.1 g of wet sediment sampled at a 1 cm interval (2 cm interval for 6K#1468MG) was disaggregated in boiling water in a glass beaker and then left for 24 h. Each sample was further disaggregated by ultrasonic treatment for 30–60 s just before measurement.

5.3 Analysis of Element Contents

Element profiles were measured on the split face of the core samples using an ITRAX XRF core scanner (Cox Analytical Systems). First, a flat surface was made on each core sample, following which element contents were measured at 0.2 mm intervals, for 10 s at each point. The analytical conditions of the scanner were 30 kV and 55 mA.

5.4 $^{210}Pb_{ex}$ measurements

^{210}Pb is a natural radionuclide of the uranium decay series and has a half-life of 22.3 year. In sediments, ^{210}Pb originates from (1) the decay reaction of ^{226}Ra within the mineral matrix (supported fraction), and (2) the adsorption of ^{210}Pb atoms onto the surfaces of particles, derived from the decay of ^{222}Rn in the water column or from the atmosphere (unsupported fraction) (Koide et al. 1972). Unsupported ^{210}Pb, also termed excess ^{210}Pb or $^{210}Pb_{ex}$, can be used to determine mass accumulation rates over a time scale of about 100 year (e.g., Nittrouer et al. 1979). ^{137}Cs (half-life of 30 year) is an artificial radionuclide dispersed into the natural environment mainly by nuclear bomb tests after 1953. The maximum ^{137}Cs fallout was recorded in 1963, with fallout levels decreasing after the cessation of atmospheric nuclear bomb tests. In the marine environment, ^{137}Cs has been supplied both by atmospheric fallout and by sediments discharged by rivers (Smith and Ellis 1982; Ritchie and McHenry 1990). Since ^{137}Cs is used as a chronological tracer, ^{137}Cs profiles in sediment are commonly used in conjunction with $^{210}Pb_{ex}$ profiles to determine sediment accumulation rates (e.g., Baskaran and Naidu 1995; Kato et al. 2003).

5.5 Magnetic Fabric Analyses

To obtain an indication of the sedimentary fabric, we measured the anisotropy of magnetic susceptibility (AMS) using an AGICO KLY-4S anisotropy magnetic susceptometer. Test specimens were encased in plastic cubes with a volume of 7 cm^3. The resultant measurement interval through the cores was therefore $\sim$ 1.9 cm. The obtained AMS values are represented by magnetic ellipsoids, of which the maximum, intermediate, and minimum axes are denoted by K_{max}, K_{int}, K_{min}, respectively. In general, the magnetic ellipsoid indicates the degree of alignment of magnetic particles in sediments (i.e., the magnetic fabric; Tarling and Hrouda, 1993). In this study, we used the following parameters: P (degree of anisotropy) = K_{max}/K_{min}, F (degree of foliation) = K_{int}/K_{min}, and L (degree of lineation) = K_{max}/K_{int}.

Paleomagnetism was measured on the same AMS plastic cube samples and using a superconductive magnetometer (2G-Enterprises, CA, US). We conducted step-wise alternating-field demagnetization during measurements of paleomagnetism. Since declination data are gradually shifted downward due to twisting to twisting during coring, magnetic north was corrected accordingly using the least-square method to reconstruct the in situ north direction of the core.

6 Results

6.1 Physical Properties and Grain Size Distribution

Core-sample density values based on the GRA measurements range from 1.2 to 2.0 g/cm^3 (Fig. 5). In the uppermost 4–5 cm, density values are mostly 1.5–1.6 g/cm^3, reflecting a high water content. Density values increase gradually with burial depth, reflecting burial consolidation. NGR counts increase with burial depth because of the increase in radioactive nuclei in a given sample volume with increasing burial consolidation.

Grain size distributions show a peak at $\sim$ 10 μm diameter in cores 6K#1467MG and 6K#1467MR. Due to the presence of laminae, sand-sized particles are found in several horizons in the core sediments. Grain size distributions show mostly silty clay with peaks at $\sim$ 5–10 μm diameter in cores 6 K#1468MG and 6K#1469MR. In these cores, the grain size of sediment in the shallow horizons ($<\sim$ 5 cm deep) is larger than that in the deeper horizons ($>\sim$ 20 cm deep).

6.2 Element Profiles

We measured 56 elements, of which four representative element (Mn, K, Ca, and Al) profiles are presented in Fig. 5. These profiles enabled two types of parallel bands to be identified in cores 6K#1467MG and 6K#1467MR. One type is low-Computed Tomography (CT)-value bands, which are

characterized by high Mn and K, and low Ca and Al values, as depicted by broken red lines (three lines for sample 6 K#1467MG) in Fig. 5a. The other type is high-CT-value bands, which are characterized by low Mn, high K, relatively high Ca, and moderate Al values, as shown by broken gray lines (28 lines for sample 6K#1467MG and 8 lines for 6K#1467MR) in Fig. 5a, b.

6.3 $^{210}Pb_{ex}$ Measurements

$^{210}Pb_{ex}$ concentrations measured in the sediments and a depth for sample 6K#1467MG were presented in Fig. 6 and Table 1. The $^{210}Pb_{ex}$ concentration was ~ 666 Bq/kg at 0–1 cm depth and gradually decreased with increasing burial depth to ~ 200 Bq/kg at 7–8 cm depth. The trend in $^{210}Pb_{ex}$ concentration showed a constant exponential decline with burial depth without any vertical mixing related to bioturbation. The absence of significant sediment mixing was also supported by X-ray CT images (Fig. 5b).

6.4 Magnetic Fabrics

Most of the magnetic susceptibility values in the studied cores lie between 0.1×10^{-3} and 1.5×10^{-3} SI units. There are sharp peaks in the range of ~ $2.0–3.0 \times 10^{-3}$ SI units in silt layers (Fig. 5).

Paleomagnetic directions in all of the core samples were mostly stable from 50 to 800 G during the stepwise alteration of field demagnetization. In this study, we used declination and inclination data under 200 G conditions. Paleomagnetic inclinations are mostly 40–50° downward for the Brunhes chron, but those of 6K#1467MR vary from 70 to 5° downward.

The magnetic susceptibility of the samples is $4–9 \times 10^{-4}$ SI throughout the cores (Fig. 5). This range reflects differences in the content, type, and/or amount of magnetic mineral grains. Following Tarling and Hrouda (1993), the magnetic minerals contributing to the magnetic susceptibility and its anisotropy in our samples were assumed to be ferrimagnetic and paramagnetic mineral grains.

Values of P, F, and L for samples 6K#1468MG and 6K#1469MR are mostly 1.02 throughout the cores (Fig. 5). These values indicate that the magnetic mineral grains are arranged with a low degree of preferred orientation (almost random) in the sediment, most likely as a result of intense bioturbation. In contrast, values of P and F in 6K#1467MG and 6K#1467MR change from 1.03 to 1.10 downward, but L values are low throughout the cores (Fig. 5). This pattern of values shows that the magnetic mineral grains are arranged with a strong preferred orientation, most likely as a result of the parallel laminae in the core sediments.

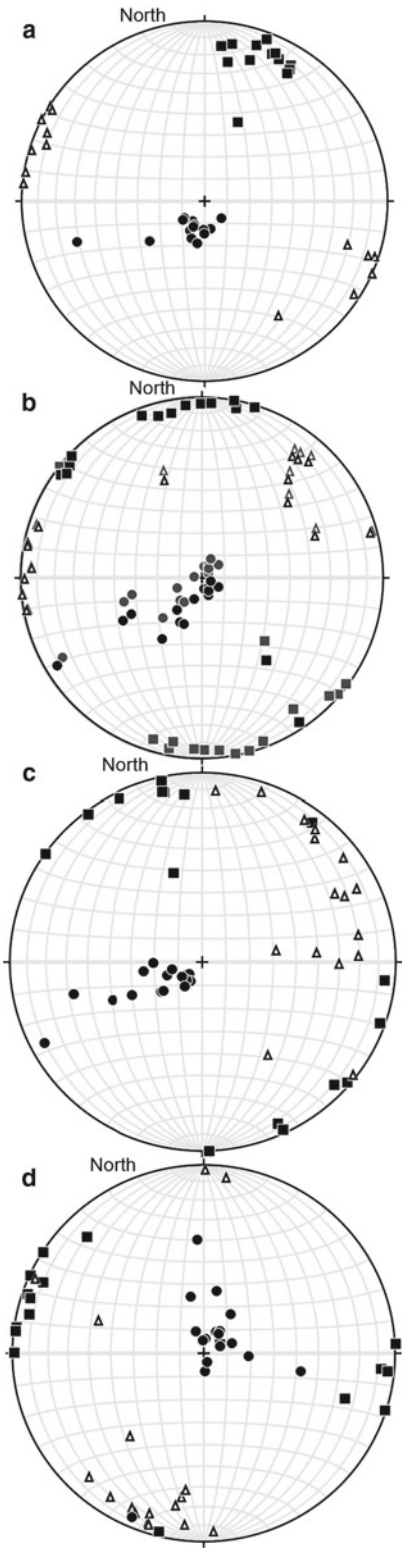

Fig. 6 Lower-hemisphere stereoplots of K_{max} (solid squares), K_{int} (open triangles), and K_{min} (solid circles) for core samples **a** 6K#1467MG, **b** 6K#1467MR, **c** 6K#1468MG, and **d** 6 K#1469MR. In (**b**), gray points indicate original data, and black points depict data that were rotated mostly parallel to a slope of about 10° tilted southward

Table 1 $^{210}Pb_{ex}$ profile data for sample 6K#1467MG

Depth (cm)	excessPb (Bq/kg)
0–1	666.1 ± 11.2
1–2	555.9 ± 8.5
2–3	388.8 ± 5.6
4–5	296.6±5.0
7–8	204.2±3.9

7 Discussion

As mentioned above, core samples 6K#1467MG and 6K#1467MR are characterized by two types of sediment bands. One is three low-CT value bands of clay layers, and the other is high-CT-value of sandy and silty laminae. The total number of laminae can be counted 28 sandy and silty laminae using element profiles as shown in Fig. 5. The sedimentary grains in the thick laminae could be supplied from a shallower slope than the carbonate compensate depth, because these consist of relative high Ca at 5, 15, 22, and 25 cm deep. In contrast to these thick laminae, thin laminae without high Ca might be formed by sedimentary grains supplied from a slope area directly above the trench floor.

7.1 Paleocurrent Analysis of the Core Samples

We used paleomagnetic north directions in each core under 200 G AF demagnetization conditions because these measurements are stable. We corrected the K_{max} directions of the AMS using paleomagnetic north in each core following the method of Kawamura et al. (2002). The corrected data, magnetic susceptibilities, and AMS data for each core are illustrated in Fig. 6 with respect to present-day north as a reference frame.

The corrected K_{max} directions show some consistency (Fig. 6). K_{max} directions are concentrated along NW–SW for 6K#1468MR and WNW–ESE for 6K#1469MR, and are sub-parallel to the slope direction, whereas those for 6K#1467MG dip to the south at $\leq$ 10°, suggesting imbrication of the sedimentary grains.

In contrast, K_{max} directions for sample 6K#1467MR dip south at $\sim$ 5° and paleomagnetic inclinations are 40–50° downward, whereas the inclinations of sample 6K#1467MR are shallower with increasing burial depth owing to the downslope gradient of the bedding plane. Therefore, we tilted the dataset of 6K#1467MR by 10° southward to adjust for the downslope gradient. As a result, the post-rotation plots are similar to those for 6K#1467MG (Fig. 6b).

According to Kawamura et al. (2002), the paleocurrent directions for 6K#1467MG and 6K#1467MR can be interpreted as indicating flow from north to south.

7.2 Mass Accumulation Rates on the Trench Floor

Figure 7 presents a $^{210}Pb_{ex}$ profile for sample 6K#1467MG. The cumulative mass for $^{210}Pb_{ex}$ was calculated as:

$$W = \int \rho r dD$$

where W is the cumulative mass of sediment (g/cm^2), ρ is the dry bulk density of the sediment (g/cm^3), and D is the depth from the top of the core (cm).

Mass accumulation rates were calculated from the $^{210}Pb_{ex}$ profile (Fig. 7). To consider compaction of the sediment buried, the mass accumulation rate was expressed in g/cm^2/year using $^{210}Pb_{ex}$ concentration and cumulative mass (g/cm^2). For sample 6 K#1467MG, exponential mass accumulation curves were fitted (Koide et al. 1972). The calculated mass accumulation rate was 2.42 g/cm^2/year.

7.3 Submarine Sliding at the Toe of the Ryukyu Accretionary Prism

The paleocurrent direction of the laminated sediments is estimated to have been from north to south, indicating that

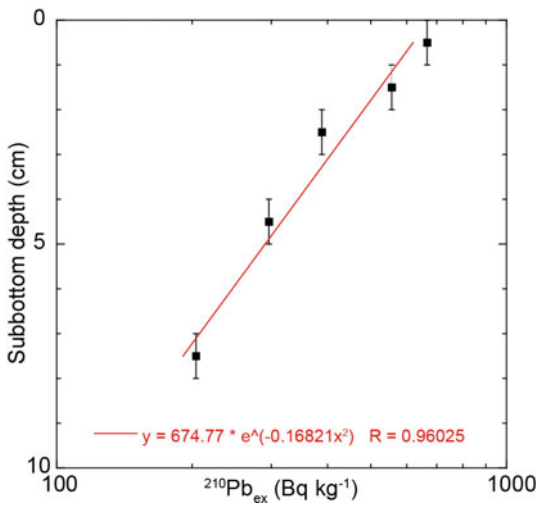

Fig. 7 $^{210}Pb_{ex}$ profile for sample 6K#1467MG

the sediments were not transported along the trench but rather from the landward slope, probably from repeated submarine slides. The mean sedimentation rate for 6K#1467MG was calculated at 2.42 mm/year using $^{210}Pb_{ex}$ concentration measurements and an age for the 10 cm horizon of roughly 50 year ago. Using the estimated sedimentation rate and the total number of laminae detected using element profiles within 10 cm deep (8 laminae as shown in Fig. 5), we simply calculated that the recurrence interval of the silt/sand layers is typically ~ 6 year for sample 6K#1467MG. These results indicate that repeated ~ 6-year-interval submarine slides have occurred continuously at the toe of the landward trench slope in the Ryukyu Trench over the last ~ 50 year, suggesting that the toe of the accretionary wedge is in a continually unstable state with respect to the triggering of submarine slides.

8 Summary

(1) We performed three dive surveys using the 6K manned submersible in the Ryukyu Trench. These dive sites were near a large submarine slide that generated the AD 1771 Meiwa tsunami.
(2) Dive site 6K#1468 was on the uppermost part of the submarine slide, where recent steps and fissures were observed. Dive site 6K#1467 was located at the toe of the submarine slide, which was covered by a muddy sediment layer. No chemosynthetic biocommunities were observed. Core sample 6K#1467MG comprised muddy sediments interlayered with silt and/or sand laminations.
(3) The paleocurrent direction of the laminated sediments was from north to south, indicating that the sediments were not transported along the trench but rather from the landward slope, probably as a result of the occurrence of repeated small submarine slides.
(4) The sedimentation rate for core sample 6K#1467MG was calculated as 2.42 mm/year by $^{210}Pb_{ex}$ measurements through the core and an age for the 10 cm horizon of ~ 50 year ago.
(5) We infer that small submarine slides repeated at an interval of ~ 6 year have occurred persistently at the toe of the landward trench slope in the Ryukyu Trench during the last ~ 50 year.

Acknowledgements We thank the captains, crew, shipboard scientists, and operation teams of the *Shinkai 6500* submersible during the YK16-11 cruise. The authors gratefully acknowledge Y. Yamamoto (Kochi University) for help with the measurement of magnetic properties, and M. Murayama, G. Uramoto, and T. Matsuzaki (Kochi University) for grain-size analyses. This study was performed under the cooperative research programs of the Institute of Nature and Environmental Technology, Kanazawa University (Acceptance No. 18026) and the Center for Advanced Marine Core Research (CMCR), Kochi University (17B062).

References

Abe K (1979) Size of great earthquakes of 1837–1974 inferred from tsunami data. J Geophys Res 84:1561–1568. https://doi.org/10.1029/JB084iB04p01561

Araoka D, Yokoyama Y, Suzuki A, Goto K, Miyagi K, Miyazawa K, Matsuzaki H, Kawahata H (2013) Tsunami recurrence revealed by *Porites* coral boulders in the southern Ryukyu Islands, Japan. Geology 41:919–922. https://doi.org/10.1130/G34415.1

Baskaran M, Naidu AS (1995) ^{210}Pb-derived chronology and the fluxes of ^{210}Pb and ^{137}Cs isotopes into continental shelf sediments, East Chukchi Sea Alaskan Arctic. Geochimica et Cosmochimica Acta 59(21):4435–4448. https://doi.org/10.1016/0016-7037(95)00248-X

Blum P (1997) Physical properties handbook: a guide to the shipboard measurement of physical properties of deep-sea cores. ODP Tech Note 26.https://doi.org/10.2973/odp.tn.26.1997

Fryer GJ, Watts P, Pratson LF (2004) Source of the great tsunami of 1 April 1946: a landslide in the upper Aleutian forearc. Mar Geol 203:201–218. https://doi.org/10.1016/S0025-3227(03)00305-0

Goto K, Kawana T, Imamura F (2010) Historical and geological evidence of boulders deposited by tsunamis, southern Ryukyu Islands, Japan. Earth-Sci Rev 102:77–99. https://doi.org/10.1016/j.earscirev.2010.06.005

Goto K, Shimabukuro A (2012) The 1771 Meiwa tsunami revealing by multidisciplinary researches. Kagaku, 82, 208–214 (in Japanese)

Gracia E, Danobeitia J, Verges J, PARSIFAL Team (2003) Mapping active faults offshore Portugal (36°N–38°N): Implications for seismic hazard assessment along the southwest Iberian margin. Geology 31(1):83–86.https://doi.org/10.1130/0091-7613(2003)031<0083:MAFOPN>2.0.CO;2

Hisamitsu A, Goto K, Imamura F (2014) Local paleo-tsunami size evaluation using numerical modeling for boulder transport at Ishigaki Island Japan. Episodes 37(4):265–276. https://doi.org/10.18814/epiiugs/2014/v37i4/006

Hornbach MJ, Braudy N, Briggs RW, Cormier M-H, Davis MB, Diebold JB, Dieudonne N, Douilly R, Frohlich C, Gulick SPS, Johnson HE III, Mann P, McHugh C, Ryan-Mishkin K, Symithe SJ, Taylor FW, Templeton J (2010) High tsunami frequency as a result of combined strike-slip faulting and coastal landslides. Nat Geosci 3:783–788. https://doi.org/10.1038/ngeo975

Kanamori H (1972) Mechanism of tsunami earthquakes. Phys Earth Planet Inter 6:346–359. https://doi.org/10.1016/0031-9201(72)90058-1

Kanamori H, Kikuchi M (1993) The 1992 Nicaragua earthquake: a slow tsunami earthquake associated with subducted sediments. Nature 361:714–716. https://doi.org/10.1038/361714a0

Kato Y, Kitazato H, Shimanaga M, Nakatsuka T, Shirayama Y, Masuzawa T (2003) ^{210}Pb and ^{137}Cs in sediments from Sagami Bay, Japan: sedimentation rates and inventories. Prog Oceanogr 57:77–95. https://doi.org/10.1016/S0079-6611(03)00052-1

Kawamura K (2020) Submarine slides and tsunamis 1. Introduction for the lectures. Geotech Eng Mag 68(4):29–30 (in Japanese)

Kawamura K, Kanamatsu T, Yamada Y (2017) Submarine slides and marine geohazards: the study results so far and current problems. J Geol Soc Jpn 123(12):999–1014 (Japanese with English abstract). https://doi.org/10.5575/geosoc.2017.0031

Kawamura K, Laberg JS, Kanamatsu T (2014) Potential tsunamigenic submarine landslides in active margins. Mar Geol 356:44–49. https://doi.org/10.1016/j.margeo.2014.03.007

Kawamura K, Ogawa Y, Anma R, Yokoyama S, Kawakami S, Dilek Y, Moore GF, Hirano S, Yamaguchi A, Sasaki T, YK05-08 Leg 2, YK06-02 Shipboard Scientific Parties (2009) Structural architecture and active deformation of the Nankai accretionary prism, Japan: submersible survey results from the Tenryu submarine canyon. Geol Soc Am Bull 121:1629–1646.https://doi.org/10.1130/B26219.1

Kawamura K, Sasaki T, Kanamatsu T, Sakaguchi A, Ogawa Y (2012) Large submarine landslides in the Japan Trench: a new scenario for additional tsunami generation. Geophys Res Lett 39:L05308. https://doi.org/10.1029/2011GL050661

Kawata Y, Benson BC, Borrero JL, Davies HL, deLange WP, Imamura F, Letz H, Nott J, Synolakis C (1999) Tsunami in Papua New Guinea was as intense as first thought. Eos Transaction AGU 80(9):101–112. https://doi.org/10.1029/99EO00065

Kawamura K, Ikehara K, Kanamatsu T, Fujioka K (2002) Paleocurrent analysis of turbidites in Parece vela Basin using anisotropy of magnetic susceptibility. Journal of the Geological Society of Japan 108(4):207–218. https://doi.org/10.5575/geosoc.108.207

Koide M, Soutar A, Goldberg ED (1972) Marine geochemistry with ^{210}Pb. Earth Planet Sci Lett 14:442–446. https://doi.org/10.1016/0012-821X(72)90146-X

Nakamura M (2009) Fault model of the 1771 Yaeyama earthquake along the Ryukyu Trench estimated from the devastating tsunami. Geophys Res Lett 36:L19307. https://doi.org/10.1029/2009GL039730

Newman AV, Okal EA (1998) Sandaun earthquake as studied by teleseismic energy. Eos Transaction AGU 79(45):F564

Nittrouer CA, Sternberg RW, Carpenter R, Bennett JT (1979) The use of Pb-210 geochronology as a sedimentological tool: application to the Washington continental shelf. Mar Geol 31(3/4):297–316. https://doi.org/10.1016/0025-3227(79)90039-2

Okamura Y, Nishizawa A, Fujii Y, Yanagisawa H (2018) Accretionary prism collapse: a new hypothesis on the source of the 1771 giant tsunami in the Ryukyu Arc SW Japan. Sci Rep 8:13620. https://doi.org/10.1038/s41598-018-31956-8

Plafker G, Mayo LR (1965) Tectonic deformation, subaqueous slides and destructive waves associated with the Alaskan March 27, 1964 earthquake; an interim geologic evaluation. United States Department of the Interior Geological Survey Open-file report, USGS, 19p. https://doi.org/10.3133/ofr65124

Ritchie JC, McHenry JR (1990) Application of radioactive fallout cesium-137 for measuring soil erosion and sediment accumulation rates and patterns: a review. J Environ Qual 19(2):215–233. https://doi.org/10.2134/jeq1990.00472425001900020006x

Sassa S, Takagawa T (2019) Liquefied gravity flow-induced tsunami; first evidence and comparison from the 2018 Indonesia Sulawesi earthquake and tsunami disasters. Landslides 16:195–200. https://doi.org/10.1007/s10346-018-1114-x

Seno T (2005) Plate motions in the world. J Geogr 114(3):350–366 (in Japanese with English abstract). https://doi.org/10.5026/jgeography.114.3_350

Smith JN, Ellis KM (1982) Transport mechanism for Pb-210, Cs-137 and Pu fallout radionuclides through fluvial–marine systems. Geochim Cosmochim Acta 46:941–954. https://doi.org/10.1016/0016-7037(82)90050-3

Tanioka Y, Satake K (1996) Tsunami generation by horizontal displacement of ocean bottom. Geophys Res Lett 23:861–864. https://doi.org/10.1029/96GL00736

Tanioka Y, Seno T (2001) Sediment effect on tsunami generation of the 1896 Sanriku tsunami earthquake. Geophys Res Lett 28:3389–3392. https://doi.org/10.1029/2001GL013149

Tappin DR, Watts P, McMurtry GM, Lafoy Y, Matsumoto T (2001) The Sissano, Papua New Guinea tsunami of July 1998—offshore evidence on the source mechanism. Mar Geol 175:1–23. https://doi.org/10.1016/S0025-3227(01)00131-1

Tappin DR, Watts P, Grilli ST (2008) The Papua New Guinea tsunami of 17 July 1998: anatomy of a catastrophic event. Nat Hazard 8:243–266. https://doi.org/10.5194/nhess-8-243-2008

Experimental Simulation of Landslide Creep in Ring Shear Machine

Netra Prakash Bhandary

Abstract

Soil material undergoes a volumetric change when deformed, and the change continues until the material reaches its critical state. In granular soils, the critical state is one that exhibits the least frictional resistance, but in clayey materials, the frictional resistance decreases further upon shearing due to particle reorientation in the plane of failure, and the material volume attains a stable or steady state only after a large amount of shear deformation, which depending on the material type varies from a few to tens of centimeters. This state of shear deformation is generally known as the residual state. This article focuses on residual-state creep shear tests on common clayey materials for the purpose of experimentally simulating the landslide creep and understanding the displacement behavior of large-scale creeping landslides. As a general understanding, the deep-seated creeping landslides displace as a result of residual-state shearing of clayey material in the slip surface. So, a modified bishop-type torsional ring shear machine was developed for studying the residual-state shear creep behavior of clayey soils. In the ring shear tests, the material is first sheared under a strain-controlled pattern, and after the sample reaches its residual state of shear, different sets of constant shear loads are applied until the sample fails again and again. The test results reveal that at the residual state of shear, the creep behavior is exhibited only after a load equivalent to the residual frictional resistance of the material is applied. Moreover, it was understood that the displacement required for the beginning of the tertiary stage of creep of particular soil material, i.e., the early stage of creep failure is the same for all sets of creep loads.

Keywords

Landslide creep • Ring shear machine • Residual-state shear

1 Introduction

Large-scale creeping landslides often refer to massive mass movements that slide down the mountain slopes at a creeping rate of displacement, ranging from a few to tens of centimeters a year. Depending on the geohydrological conditions, the displacement rate fluctuates, but in many cases, it is found to be only a few centimeters a year. Such a slow rate of land sliding is often also referred to as creeping displacement, and the soil material in the slip surface of such landslides is often found to be clayey, which is generally found and considered to be in its residual state of shear due to continuous landslide displacement for a long time.

Even when the geohydrological conditions do not change, the landslide activity continues under the influence of gravitational force-produced shear component along the shear surface that can be considered almost equal to the amount of shear resistance produced along the shear surface, i.e., a condition of limit state failure. However, Patton (1984) describes that such landslides keep moving even when the slip surface shear resistance is slightly greater than the driving shear forces. If we consider that the stress conditions on the slip surface material do not change for a certain duration but the landslide is in constant downslope movement, we can compare this situation with creep phenomenon, which basically is time-dependent rise in strain under a constant applied stress. So, it is considered that the large-scale landslide displacement behavior can be understood through shear creep tests on clayey materials. However, due to already occurred large shear deformation (or displacement), the shear resistance along the slip surface cannot be treated as that of an only slightly sheared soil

N. P. Bhandary (✉)
Department of Environmental Design (Faculty of CRI), Ehime University, Matsuyama, 790-8577, Japan
e-mail: netra@ehime-u.ac.jp

I. Alcántara-Ayala et al. (eds.), *Progress in Landslide Research and Technology, Volume 1 Issue 2, 2022*, Progress in Landslide Research and Technology,
https://doi.org/10.1007/978-3-031-18471-0_6

material. So, use of a ring shear machine has been in practice for the last several decades, especially when evaluating landslides and large deformation ground problems. The ring shear machine can shear an annular soil specimen for nearly infinite amount of shear deformation and helps to measure peak and residual shear resistances of a clayey soil material.

In general, the shear strength of a soil is defined as its maximum resistance to applied shear force (Skempton 1964; 1985; Bishop et al. 1971; Lupini et al. 1981, Giba and Egashira 1992; Gibo 1994; Nakamura et al. 2010). When a soil is sheared, the developed shear resistance first reaches a peak value at a comparatively short time or less deformation. During this process, the soil material undergoes volume change due to vertical movement of soil particles and depending on the outward (known as dilation) or inward (known as contraction) movement of the particles, the developed peak shear resistance is high or low. The peak shear resistance, especially for overconsolidated or dense materials, is attained when the rate of outward vertical movement (i.e., dilation) of soil particles is maximum. Immediately after the peak value, upon further shearing, the shear resistance drops gradually until fully softened shear resistance is achieved, which is generally known as critical state (refer to Fig. 1). Shearing beyond the critical state may result in slight volume change (normally contraction), which is basically due to reorientation of clayey particles in the shear zone, but after the reorientation process is over, no further volume change is theoretically supposed to take place, and the frictional resistance exhibited remains constant. This very state is referred to as residual state of shear for clayey soil materials (Skempton 1964, 1985; Lupini et al. 1981).

So far, most creep tests on soil materials have employed a triaxial compression cell or an oedometer (such as Ter-Stepanian 1963; Yen 1969; Waker 1969; Campanella and Vaid 1974; Nelson and Thompson 1977; Patton 1984; Feda 1989; Picarelli et al. 2001; Picarelli et al. 2004; Augustesen et al. 2004; Leoni et al. 2008; Yin et al. 2010; Brandes and Nakayama 2010, etc.), but these methods largely differ from the state of shear explained above, i.e., creep shear behavior of the slip surface material or the landslide creep, which may be ideally defined as a time-dependent slow displacement under no change in driving forces or stresses and can be represented by creep displacement curves shown in Fig. 2.

At residual state of shear, a clay material is supposed to have zero to negligible cohesion and no effect of dilation or contraction. What helps the slip surface material at this state develop shear resistance is the true inter-particle frictional force generated amongst the soil particles. So, the existing creep test methods do not truly help understand the mechanism of creeping landslide displacement. So, for this study, an existing torsional ring shear machine was modified to make it also capable of measuring residual-state creep displacement under any amount of applied constant shear stresses. A special care was taken not to let the residual-state slip surface material undergo strength recovery due to period of shear stagnation while changing from ordinary shear to creep shear. So, in this article, the focus mainly goes onto introducing the residual-state creep shear test method for the experimental simulation of landslide creep, understanding the residual-state creep displacement behavior of different types of clayey materials, and linking the findings of this

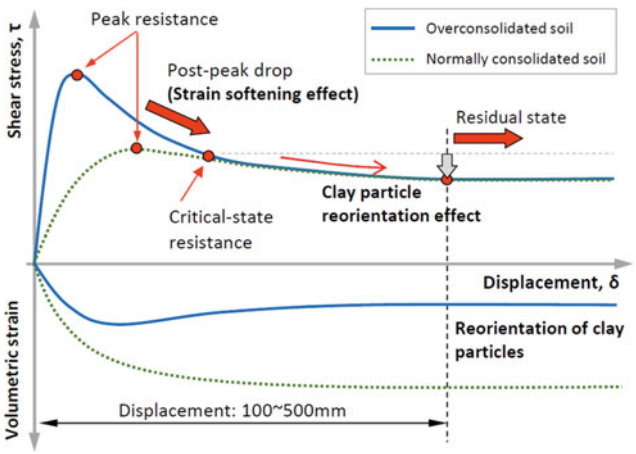

Fig. 1 General trend of pre- and post-peak shear resistance and shear deformations in ring shear tests (based on Skempton 1985)

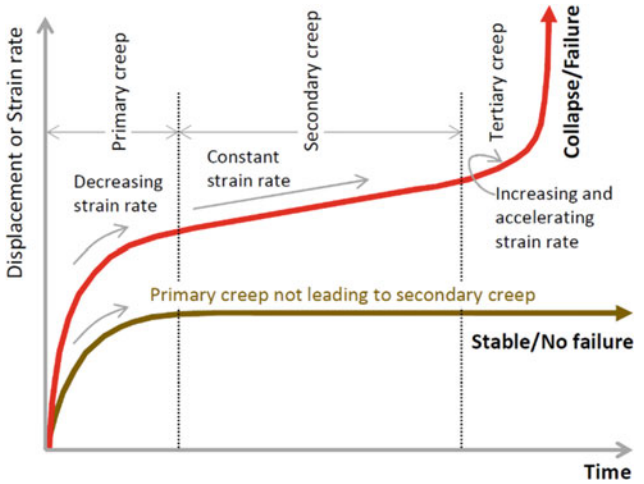

Fig. 2 Ideal creep displacement curves showing primary, secondary, and tertiary states of shear creep and primary creep not leading to secondary creep

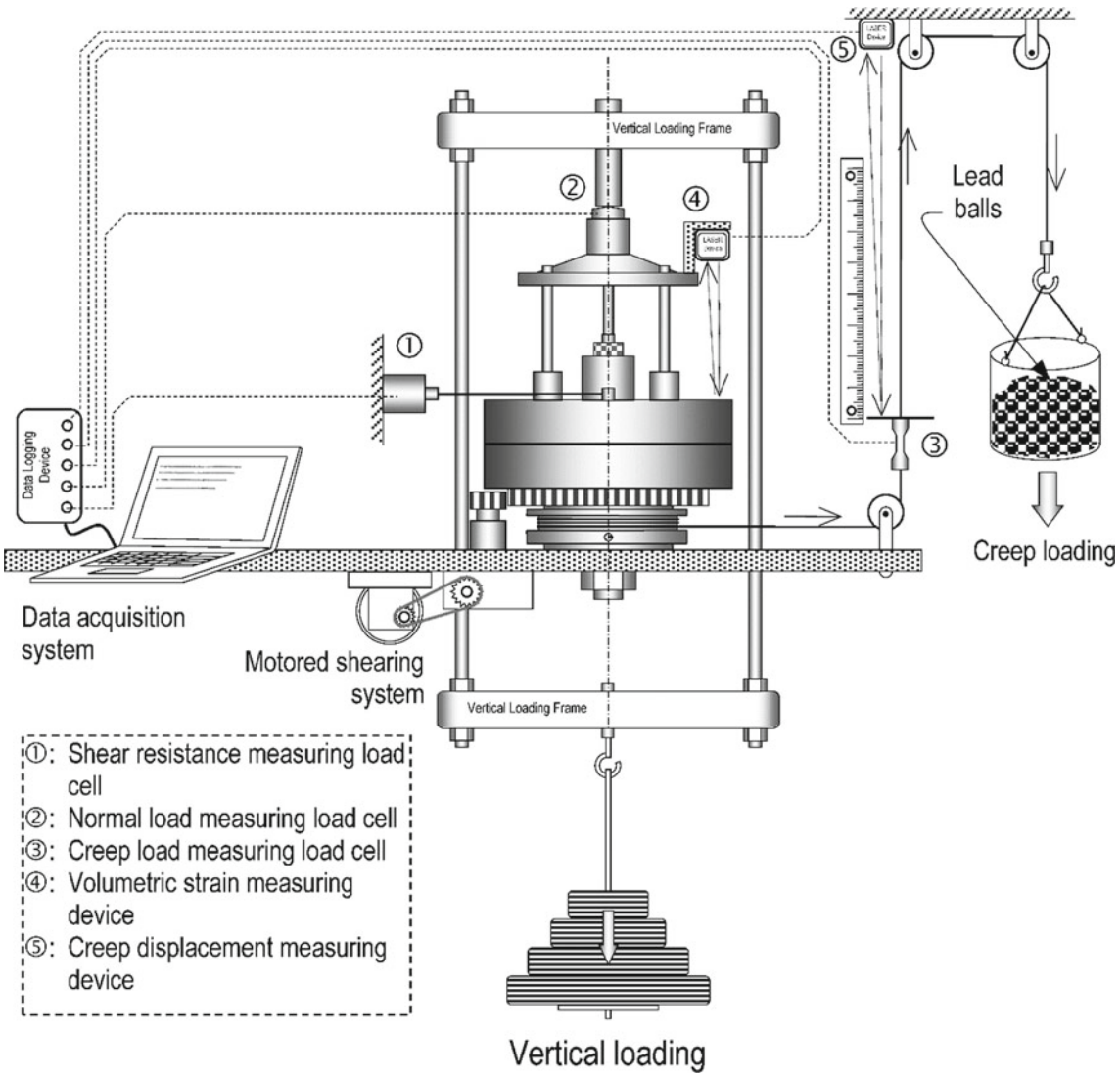

Fig. 3 Modified ring shear machine and experimental setup for the residual-state creep tests

experimental study with the creeping type landslide displacement behavior.

2 Material and Method

2.1 Modified Ring Shear Machine

A torsional ring shear machine (Bishop et al. 1971) was used in this study after a few special modifications. The annular specimen container of the ring shear machine measures 8 cm inner diameter and 12 cm outer diameter with a total depth of 3.2 cm. To perform the residual-state creep tests, the ring shear machine was modified based on the transitional change of the strain-controlled motor-driven shear into creep load shearing without completely releasing the applied shear stress, which is capable of measuring the creep displacement with respect to time under the application of a constant creep load, as shown in Fig. 3. The lower part of the ring shear machine has been designed to allow the applied creep load to act directly on the slip surface of the test specimen, and the displacement or deformation due to the creep load can be recorded in the displacement recorder unit. The deformation of the specimen with respect to time and the corresponding changes in the volume of the specimen, if any, during the creep tests can be recorded automatically. The testing process involves strained-controlled shearing, confirmation of residual state, application of various creep shear stresses (or stress-controlled shearing) and recording of time-displacement histories.

2.2 Test Materials

Landslide slip surface materials generally are clayey soils composed of common clay minerals such as smectite, chlorite, and illite. These minerals generally have very high specific surface area, higher cation exchange capacity, and greater affinity to water. For this reason, large-scale creeping landslides have been extensively studied from clay mineralogical perspective and are often interpreted as a long-term geomorphological process influenced significantly by mineralogical changes (e.g., Yatabe et al. 1991; 2007, Torii et al. 2006). So, in this study, all tests were conducted using commercially available kaolin clay, Toyoura sand powder finer than 75 μm, and their mixtures with commercially available Na-bentonite powder (with about 50% smectite content) in different desired proportions. The mix proportion of Na-bentonite in kaolin and the sand powder was 5, 10, 15, 20, and 25% by weight. The main purpose of increasing the amount of Na-bentonite in the test samples was to achieve decreasing residual strength or residual friction angle (ϕ_r) of the test samples. The physical properties and ring shear results of the tested mix samples are presented in Table 1. In the 'sample name' column, SP refers to sand powder, K refers to kaolin powder, B refers to bentonite powder, and the figures after these notation letters refer to the percentage of the material mixed in that test sample. For example, SP100 refers to 100% sand powder, K100 refers to 100% kaolin while SP95+B5 refers to 95% sand powder and 5% bentonite, K75+B25 refers to 75% kaolin and 25% bentonite.

2.3 Experimental Program

In the residual-state shear creep tests, two main steps were followed: (1) ordinary ring shear tests and (2) residual-state shear creep tests. The ordinary ring shear tests were conducted to achieve the soil materials residual state of shear. This state was confirmed when the shearing had reached a state of constant values for the load-cell reading and dial gauge reading after about 10 cm of shear displacement. In the residual-state shear creep tests, the first creep load was calculated on the basis that the applied shear stress was 90% of the residual-state shear resistance, which is referred in this study as 'Residual-state Creep Stress Ratio' and is denoted by R_{RCS}. A 90% residual-state creep stress ratio is denoted by $R_{RCS} = 0.9$. Then, the material specimen was left under creep loading for several hours and displacement was recorded with the passage of time. After one set of creep test was considered or observed to have been over, the creep load was increased in subsequent steps and time-displacement histories were recorded. The overall experimental flow of the residual-state shear creep tests is shown in Fig. 4. The applied R_{RCS} values in case of all tested samples varied from 0.9000 to 1.0300 in a step of 0.005.

All material samples were prepared for the tests by first uniformly mixing them with appropriate amount of distilled water and then deairing for complete saturation. The deaired liquid samples were then poured into the specimen maker and consolidated under a pressure of 98.1 kN/m^2 until the primary consolidation was confirmed to be over. Then, the

Table 1 Physical properties and ring shear results of the clayey soils

Sample name	Solid Density, Gs (g/cm^3)	Liquid Limit, LL (%)	Plastic Limit, PL (%)	Plasticity index, PI (%)	Grain size distribution (%)			Residual friction angle, φr (°)
					< 2 μm	2–75 μm	75–425 μm	
SP100	2.623	–	–	–	14.5	85.5	0	29.46
K100	2.609	47.5	27.1	20.3	67.0	33.0	0	26.28
SP95+B5	2.627	35.8	15.6	20.2	19.0	81.0	0	25.62
K95+B5	2.618	52.5	20.3	32.3	63.0	37.0	0	24.95
SP90 +B10	2.634	52.8	18.6	34.2	24.9	75.1	0	23.44
K90+B10	2.636	66.2	21.9	44.4	61.0	39.0	0	22.36
SP85+B15	2.653	71.8	19.2	52.6	27.0	73.0	0	21.09
SP80+B20	2.660	94.0	19.9	74.1	32.0	68.0	0	19.58
K85+B15	2.653	83.8	21.8	62.0	51.0	49.0	0	18.91
SP75+B25	2.678	108.8	24.8	84.0	34.2	65.8	0	16.96
K80+B20	2.673	98.6	20.8	77.8	49.0	51.0	0	15.19
K75+B25	2.692	122.8	28.8	94.1	46.4	53.8	0	11.03

SP Sand powder; *K* Kaolin powder, *B* Bentonite powder

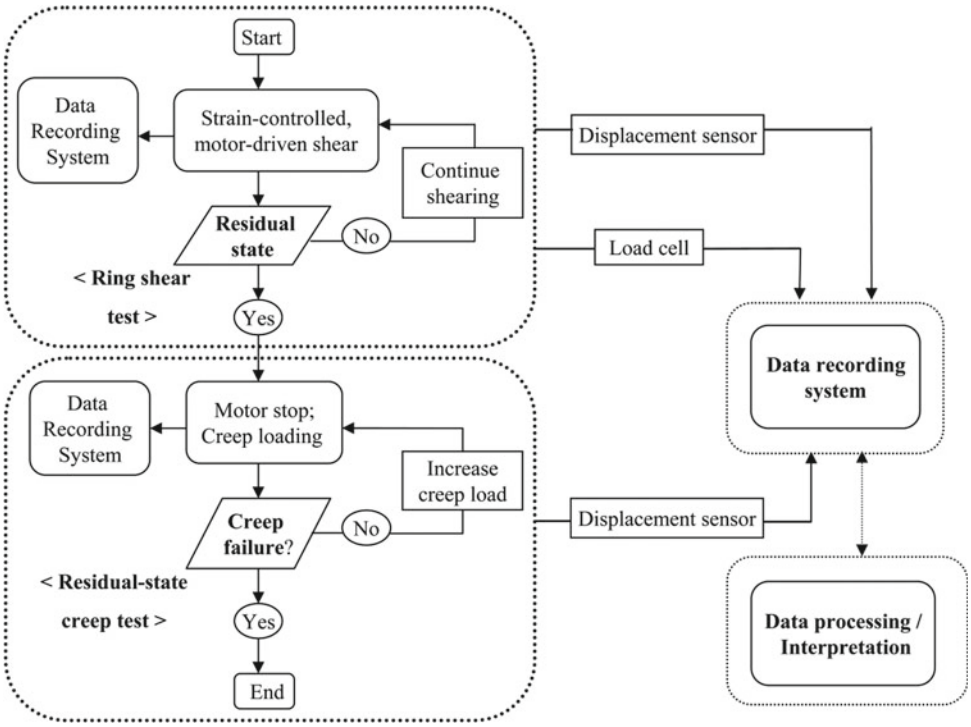

Fig. 4 Overall experimental flow of residual-state creep test

specimen was transferred into the ring shear machine's sample container and consolidated again under a pressure of 196.2 kN/m^2. However, to avoid unwanted machine friction due to high normal pressure, all shear tests were conducted under a normal pressure of 98.1 kN/m^2 (with an overconsolidation ratio of 2.0). The shearing condition was confirmed to be fully drained by allowing sufficient time to dissipate excess pore water pressure, for which the average rate of displacement through the slip surface was set at 0.15 mm/min. At first, strain-controlled shearing was conducted until the residual state of shearing was achieved and residual strength was obtained. Then, the strain-controlled shearing was stopped for about 10 min, and preparations for the creep test were made.

To avoid confusions and discrepancies due to unknown parameters, some important assumptions were made in this study, which are as follows:

- At the residual-state of shear, there is no influence of further displacement on the shear resistance of the slip surface soil.
- The amount of recovered shear strength, if any, due to reduction in the rate of shear (e.g., Bhat and Yatabe 2015; Scaringi et al. 2018) or due to the state of no shear is negligible.
- The effect on the shear resistance due to lack of uniformity in sample preparation, if any, effective stress application accuracy, etc. is negligible.
- The change in the shear behavior due to changes in the value of the R_{RCS}, if any, is negligible.
- There is no influence of any amount of displacement in the amount of shear resistance if the sheared material has already reached its residual state

3 Results and Discussion

Creep deformation in soil materials is often explained in three stages, as also illustrated in Fig. 2. In the beginning, the deformation increases rapidly but slows down to a certain value; this stage is known as primary creep. Then, the rate of deformation becomes constant; this is known as secondary creep. Finally, the deformation rate starts to increase exponentially leading to complete failure; this stage is known as tertiary creep. So, in this study, the test results are basically summarized in three stages of creep.

Of the residual-state shear creep test results of total 12 clayey material samples (refer to Table 1), four representative test results for the K100, SP100, K75+B25, and SP75 +B25 samples are presented respectively in Figs. 5, 6, 7 and 8, and the basic parameters obtained from the test results in Figs. are summarized respectively in Tables 2, 3, 4 and 5. Owing to the space constraint, the test results for the other eight samples are not presented but all those results are used in interpreting the residual-state creep failure behavior in

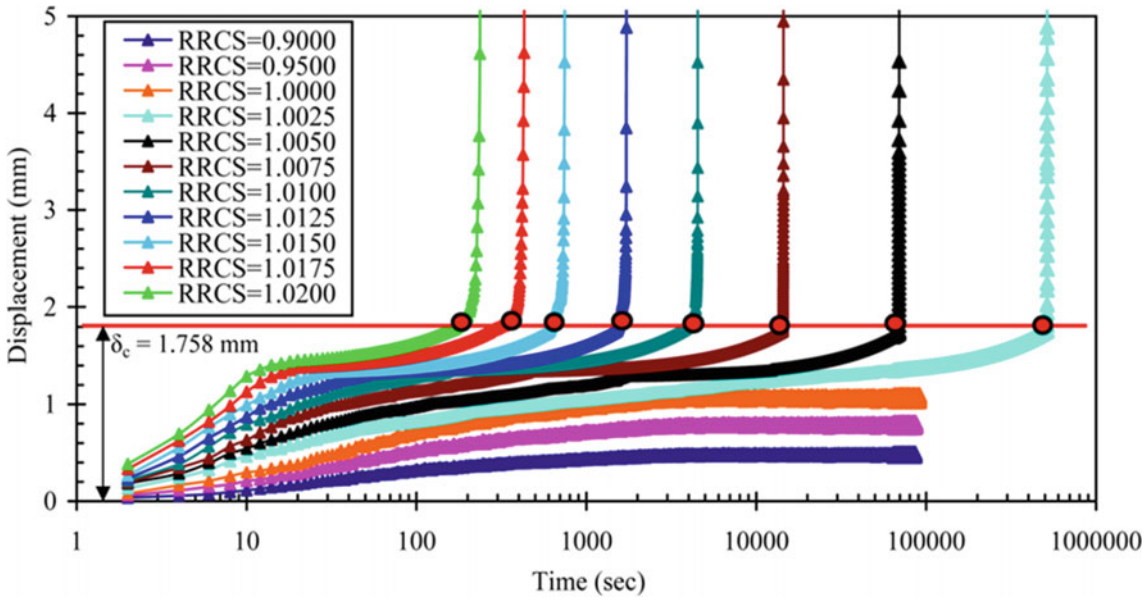

Fig. 5 A typical set of residual-state shear creep test results of the K100 sample (i.e., 100% kaolin powder)

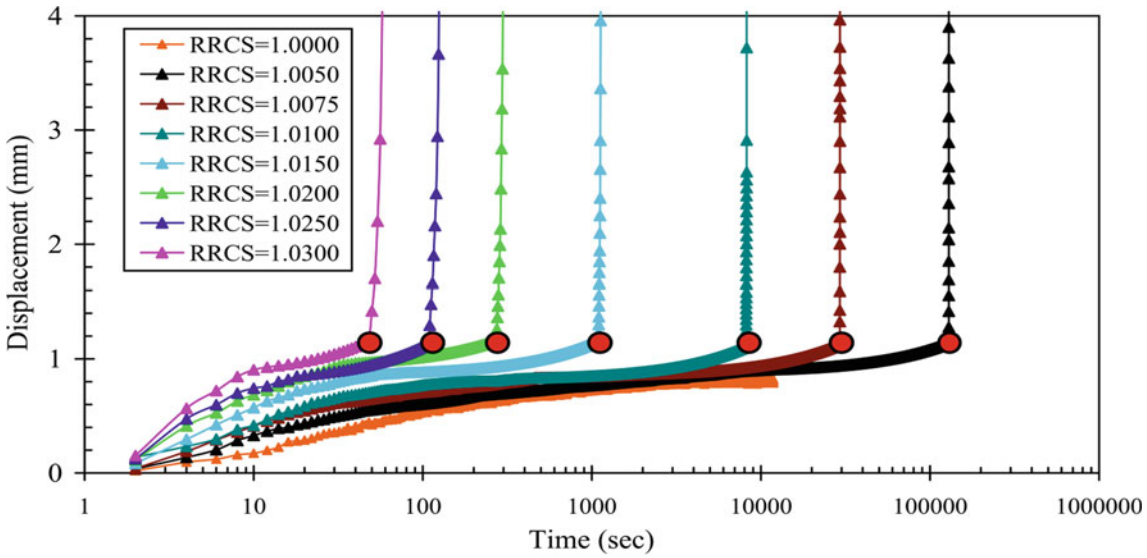

Fig. 6 A typical set of residual-state shear creep test results of the SP100 sample (i.e., 100% sand powder)

subsequent discussion. As indicated in the above figures and tables, t_1 refers to the elapsed time up to the end of primary creep (or beginning of the secondary creep), δ_1 refers to the amount of displacement corresponding to t_1, t_f refers to the time when secondary creep ends and tertiary creep begins (i.e., final stage of creep failure), and δ_c refers to the amount of displacement corresponding to t_f.

Particularly in the figures above, it is evident that for all cases of R_{RCS}, the amounts of displacement at the time of failure, i.e., at the beginning of the tertiary creep, are more or less the same (also refer to Tables 2, 3, 4 and 5). It indicates that regardless of the amount of applied creep stress, the soil material in its residual state of shear fails only after a certain amount of displacement is achieved. So, in this study, this typical amount of displacement is named as 'critical displacement' and is denoted by δ_c. In case of the K100 sample (Fig. 5), an averaged critical displacement is around 1.758 mm. Likewise, it is 1.414 mm for SP100 sample (Fig. 6), 4.014 mm for K75+B25 sample (Fig. 7), and 2.89 mm for SP75+B25 sample (Fig. 8).

Although the test results of other eight samples are not presented, the critical displacements for the SP95 +B5, K95 +B5, SP90+B10, K90+B10, SP85+ B15, SP80+B20, K85 + B15, and K80 +B20 samples were estimated to be

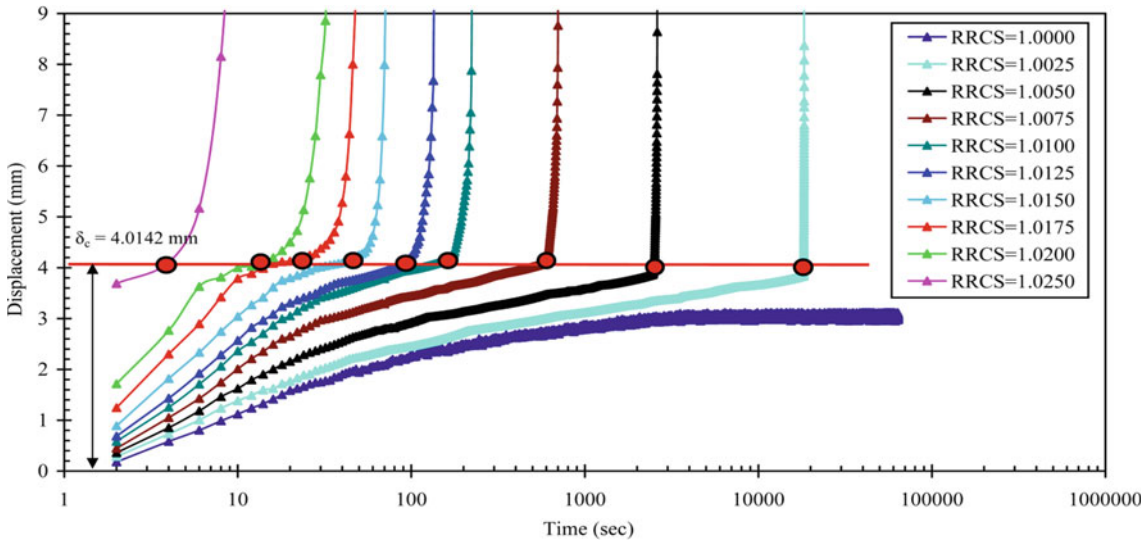

Fig. 7 A typical set of residual-state shear creep test results of the K75+B25 sample (i.e., 75% kaolin powder and 25% bentonite powder)

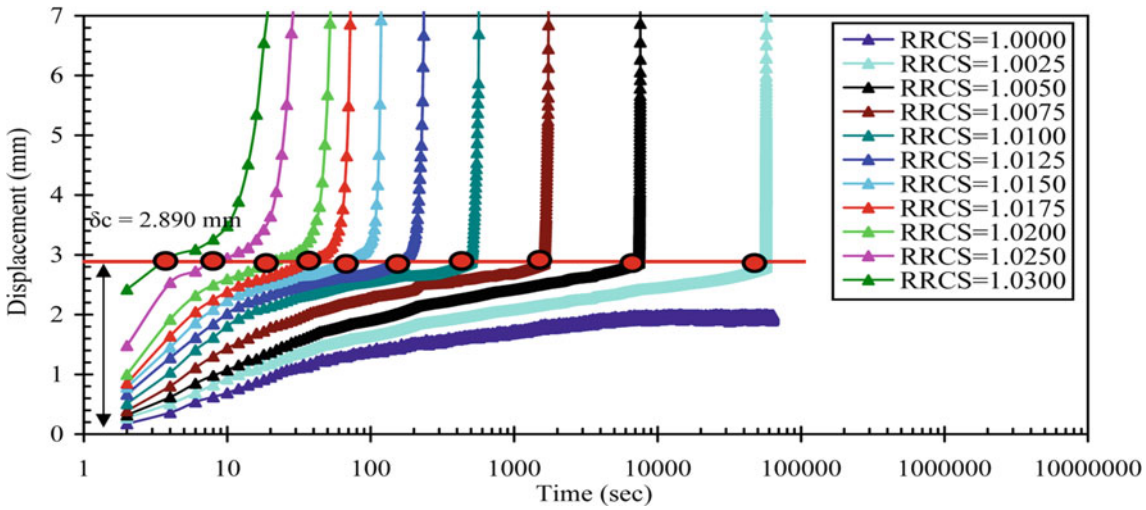

Fig. 8 A typical set of residual-state shear creep test results of the SP75+B25 sample (i.e., 75% sand powder and 25% bentonite powder)

1.925 mm, 1.974 mm, 2.104 mm, 2.250 mm, 2.363 mm, 2.653 mm, 2.783 mm, and 3.136 mm, respectively. All these values of critical displacement are plotted against the values of angle of residual friction (ϕ_r) (as presented in Table 1) in Fig. 9. Except for a few points, the trend of decrease in critical displacement with increased angle of residual friction is quite linear. This trend clearly reveals that the critical displacement is inversely proportional to residual friction characteristic of a clay material.

The concept of critical displacement may be understood further through coefficient of friction. Basically, any material exhibits two types of frictional behaviors as governed by coefficient of static friction μ_s (i.e., frictional resistance in rest) and coefficient of kinematic friction μ_k (i.e., frictional resistance while in motion). The coefficient of static friction is usually greater than the coefficient of kinematic friction, which means a stationary object always needs a greater force to move than to keep it in motion. In a soil material too, the initial force required shear it is always greater than the force required to keep it shearing. So, in this case too, in the beginning the coefficient of static friction (μ_s) governs the displacement, e.g., in primary and secondary stages of creep, but as soon as the displacement reaches its critical value, the coefficient of kinematic friction (μ_k) comes into scene to govern the frictional behavior, which leads to accelerated displacement and thereby to complete failure. So, the amount of displacement required for transitional change of μ_s to μ_k is understood as critical displacement in this study.

The test results also reveal that creep deformation for R_{RCS} values equal to or below 1.0 does not progress to secondary

Table 2 Summary of the residual-state creep tests on the K100 sample (refer to Fig. 5)

Test No	R_{RCS}	t_1 (sec)	δ_1 (mm)	t_f (sec)	δ_c (mm)	Remarks
1–11	1.0200	18	1.401	152	1.751	Failure
1–10	1.0175	20	1.392	268	1.749	Failure
1–9	1.0150	28	1.340	606	1.750	Failure
1–8	1.0125	62	1.358	1502	1.760	Failure
1–7	1.0100	136	1.375	3846	1.782	Failure
1–6	1.0075	558	1.380	14,370	1.755	Failure
1–5	1.0050	1688	1.391	69,220	1.758	Failure
1–4	1.0025	19,632	1.591	515,252	1.761	Failure
1–3	1.0000	4222	1.072	–	–	No failure
1–2	0.9500	3916	0.784	–	–	No failure
1–1	0.9000	3544	0.483	–	–	No failure

Table 3 Summary of the residual-state creep tests on the SP100 sample (refer to Fig. 6)

Test No	R_{RCS}	t_1 (s)	δ_1 (mm)	t_f (s)	δ_c (mm)	Remarks
1–8	1.0300	10	0.9144	48	1.1580	Failure
1–7	1.0250	18	0.8493	108	1.1321	Failure
1–6	1.0200	36	0.9648	272	1.1621	Failure
1–5	1.0150	94	0.8824	1094	1.1604	Failure
1–4	1.0100	420	0.8294	8182	1.1074	Failure
1–3	1.0075	1850	0.8612	29,294	1.1284	Failure
1–2	1.0050	10,770	0.9026	129,170	1.1412	Failure
1–1	1.0000	5074	0.8099	–	–	No failure

Table 4 Summary of the residual-state creep tests on the K75 + B25 sample (refer to Fig. 7)

Test No	R_{RCS}	t_1 (s)	δ_1 (mm)	t_f (s)	δ_c (mm)	Remarks
1–10	1.0250	3	3.6904	4	4.1049	Failure
1–9	1.0200	6	3.6306	10	3.9984	Failure
1–8	1.0175	10	3.7883	16	4.0843	Failure
1–7	1.0150	18	3.7513	28	3.9941	Failure
1–6	1.0125	38	3.7064	64	3.9554	Failure
1–5	1.0100	106	3.9788	172	4.1854	Failure
1–4	1.0075	338	3.8878	602	4.1014	Failure
1–3	1.0050	1324	3.6644	2468	3.8657	Failure
1–2	1.0025	10,292	3.6680	18,264	3.8382	Failure
1–1	1.0000	3806	2.9752	–	–	No failure

and tertiary stages (e.g., first three test cases in Fig. 5), which means regardless of the length of time, the clay material does not fail in creep. However, as soon as the R_{RCS} value gets greater than 1.0, the creep failure does take place, and the trend is greater the R_{RCS} value, shorter the time up to failure. Moreover, amongst the tested samples, $R_{RCS} = 1.03$ was found to be the upper limiting value revealing any greater value would result in instantaneous failure. This more or less indicates that creep failure in residual state of shear of clayey materials is exhibited from a shear loading equivalent to residual shear resistance to an increase in shear loading by 3% of the residual shear resistance.

Furthermore, variation of failure time (t_f) with residual-state creep stress ratio (R_{RCS}) for all tested samples

Table 5 Summary of the residual-state creep tests on the SP75+B25 sample (refer to Fig. 8)

Test No	R_{RCS}	t_1 (s)	δ_1 (mm)	t_f (s)	δ_c (mm)	Remarks
1–11	1.0300	2	2.4643	4	2.9556	Failure
1–10	1.0250	4	2.5363	8	2.9187	Failure
1–9	1.0200	10	2.5953	20	2.9247	Failure
1–8	1.0175	20	2.6451	36	2.8942	Failure
1–7	1.0150	38	2.6635	76	2.9312	Failure
1–6	1.0125	92	2.6756	168	2.8945	Failure
1–5	1.0100	276	2.6764	504	2.8757	Failure
1–4	1.0075	918	2.6753	1622	2.8545	Failure
1–3	1.0050	3826	2.6766	7428	2.8624	Failure
1–2	1.0025	20,294	2.5452	56,892	2.7925	Failure
1–1	1.0000	6460	1.9825	–	–	No failure

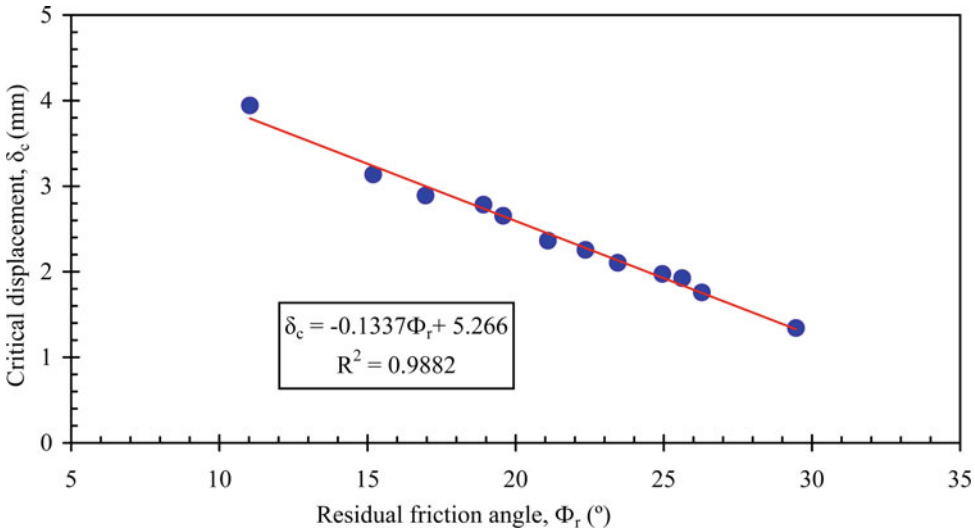

Fig. 9 Relation between critical displacement (δc) and residual friction angle (φr) of the clayey soils

is shown in Fig. 10. It is more than clear from this figure that the failure time (t_f) is a function of residual-state creep stress ratio (R_{RCS}) and residual friction angle (ϕ_r). For a particular sample, there is a fine trend of curvilinear decrease in logarithmic time of failure (i.e., $\log(t_f)$) with the increase in residual-state creep stress ratio (R_{RCS}), while t_f is seen to get longer with a greater angle of residual friction (ϕ_r). This tri-parametric relationship between failure time (t_f), residual-state creep stress ratio (R_{RCS}), and angle of residual friction (ϕ_r) can be well considered an important basis for predicting residual-state creep failure of clayey materials. Moreover, establishment of a numerical relationship between these three parameters is considered to help predict creeping landslide displacements. For example, if a landslide can be precisely assessed to give representative angle of residual friction of the slip layer clay and state of shear stress application, the time required up to complete sliding can be very well estimated.

4 Concluding Remarks

Application of creep deformation theory in predicting deep-seated landslide failures has been a topic of interest to landslide researchers for a long time. However, most of the work done so far is focused on understanding creep failure behavior of soil materials within the range from strain hardening to strain softening, which does not adequately explain the creep failure mechanism of clayey materials that have already reached a state of residual friction, such as in large-scale creeping landslides. In this study, a modified ring shear machine was used to conduct ordinary ring shear tests and residual-state creep shear tests. Altogether 12 lab-prepared clay samples were used in the test sets, and the recorded time-displacement data series were interpreted to understand the residual-state creep deformation behavior of clayey materials. One of the most important understandings

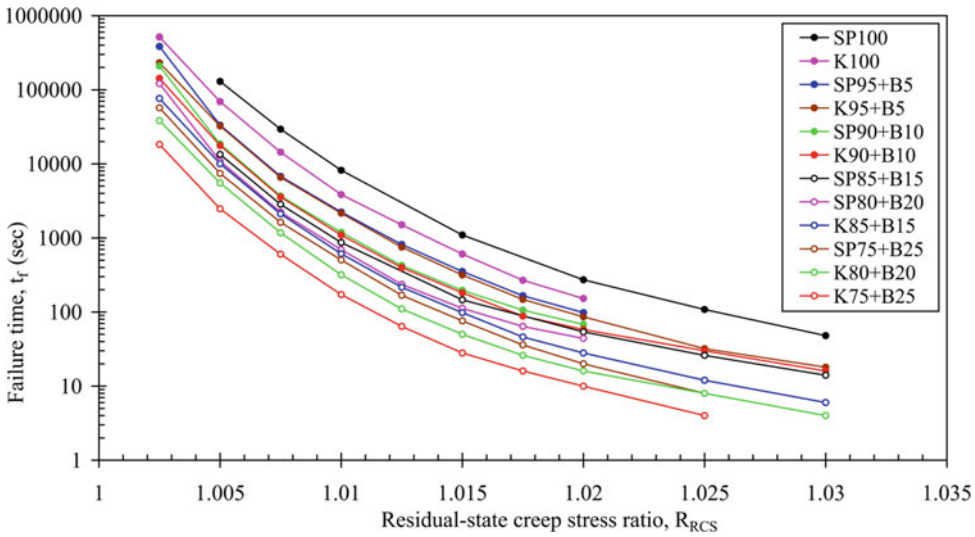

Fig. 10 Variation of failure time (t_f) with residual-state creep stress ratio (R_{RCS})

is when $R_{RCS} \leq 1.0$, no clay material exhibits creep failure in the state of residual shear, but it takes place only when $R_{RCS} > 1$. In addition, the amount of displacement required for tertiary creep to begin in a particular clay material was found to be the same regardless of the amount of creep load applied. This amount of displacement (i.e., critical displacement) is inversely related with the residual shear strength (or the angle of residual friction) of clay materials. Furthermore, the time until complete failure or the failure time (t_f) is a function of residual-state creep stress ratio (R_{RCS}) and angle of residual friction (ϕ_r). Finally, a numerical relationship between these three parameters needs to be established for predicting landslide creep displacement and failure.

Acknowledgements Majority of the experimental data used in this article are extracted from the undergraduate and graduate theses of the students that worked with me in their graduation research. As the lead researcher on this topic, I would like to acknowledge the primary data obtained from tremendous set of laboratory experiments conducted by Deepak Raj Bhat, who obtained his Doctor of Engineering degree from Ehime University in 2014 and Yuka Okamoto, who obtained her master's degree in 2013. Prof. Ryuichi Yatabe, who supervised my doctoral dissertation research in 2000–2003 and also critically commented on the significance of these experimental data in understanding the real landslide creep behavior, is the main motivation for the idea that led to modifying an existing torsional ring shear machine and conduct residual-state shear creep tests. Moreover, the financial assistance of JSPS Grant-in-aid for scientific research (Kaken-hi, Kiban-C, 2012–2014) helped develop the modified ring shear machine employed in this study.

References

Augustesen A, Liingaard M, Lade PV (2004) Evaluation of Time-Dependent Behavior of Soils. Int J Geomech ASCE 30 (3):137–156

Bhat DR, Yatabe R (2015) Effect of shearing rate on residual strength of landslide soils. In: Lollino G et al (Eds) Engineering geology for society and territory 2. Springer, Cham, pp 1211–1215. https://doi.org/10.1007/978-3-319-09057-3_212

Bishop AW, Green E, Garge VK, Andresen A, Brown JD (1971) A new ring shear apparatus and its application to the measurement of residual strength. Geotechnique 21(4):273–328

Brandes HG, Nakayama DD (2010) Creep, strength and other characteristics of Hawaiian volcanic soils. Geotechnique 60 (4):235–245

Campanella RG, Vaid YP (1974) Triaxial and plane strain creep rupture of an undisturbed clay. Can Geotech J 11(1):1–10

Feda J (1989) Interpretation of creep of soil by rate process theory. Geotechnique 39(4):667–677

Gibo S, Egashira K (1992) Relation between reorientation of clay particles and the residual strength of mudstone of the Shimajiri group. Trans Jpn Soc Irrig Drain Reclam Eng 161:19–24 (in Japanese with English abstract)

Gibo S (1994) Ring shear apparatus in measuring residual strength and its measurement accuracy. J Jpn Landslide Soc 31(3):24–30 (in Japanese with English abstract)

Leoni M, Karstunen M, Vermeer PA (2008) Anisotropic creep model for soft soils. Geotechnique 58(3):215–226

Lupini JF, Skinner AE, Vaughan PR (1981) The drained residual strength of cohesive soils. Geotechnique 31(2):181–213

Nakamura S, Gibo S, Egashira K, Kimura S (2010) Platy layer silicate minerals for controlling residual strength in landslide soils of different origins and geology. Geology 38(8):743–746

Nelson JD, Thompson EG (1977) A theory of creep failure in over consolidated clay. J Geotech Eng Proc Am Soc Civil Eng 103:1281–1293

Patton FD (1984) Groundwater pressure and stability analyses of landslides. In: Proceedings of IV international symposium on landslides, vol 3, pp 43–60

Picarelli L, Urciuoli G, Russo C (2001) Effect of groundwater regime on the behavior of clayey slopes. Can Geotech J 41:1995–2004

Picarelli L, Urciuoli G, Russo C (2004) Effect of groundwater regime on the behaviour of clayey slopes. Can Geotech J 41(3):467–484

Scaringi G, Hu W, Xu Q, Huang R (2018) Shear-rate-dependent behavior of clayey bimaterial interfaces at landslide stress levels. Geophys Res Lett 45:766–777. https://doi.org/10.1002/2017GL076214

Skempton AW (1964) Long-term stability of clay slopes. Geotechnique 14(2):75–101

Skempton AW (1985) Residual strength of clays in landslides, folded strata and the laboratory. Geotechnique 35(1):3–18

Ter-Stepanian G (1963) On the long term stability of slopes. Nor Geotech Inst 52:1–14

Torii T, Kitagawa R (2006) Mineralogical characteristics of smectite formed in the toyooka tuff formation of the kobe group-special attention to the occurrence of landslide in this region. Clay Sci Soc Jpn 45(4):238–249 (in Japanese with English abstract)

Waker LK (1969) Undrained creep in sensitive clay. Geotechnique 19 (4):515–529

Yatabe R, Yagi N, Enoki M, Nakamori K (1991) Strength characteristics of landslide clay. J Jpn Landslide Soc 28(1):9–16 (in Japanese with English abstract)

Yen BC (1969) Stability of slopes undergoing creep deformation. Soil Mech Found Div SM 4:1075–1096

Yin ZY, Chang CS, Karstunen M, Hicher PY (2010) an anisotropic elastic-viscoplastic model for soft clays. Int J of Sol and Struc 47:665–677

Assessment of the Effects of Rainfall Frequency on Landslide Susceptibility Mapping Using AHP Method: A Case Study for a Mountainous Region in Central Vietnam

Chi Cong Nguyen, Phuoc Vo, Viet Long Doan, Quang Binh Nguyen, Tien Cuong Nguyen, and Quoc Dinh Nguyen

Abstract

Vietnam's mountainous regions often encounter landslides, frequently resulting in fatalities, infrastructure damage, and landscape destruction. A landslide susceptibility map is an effective tool for mitigating disaster impacts on hazard-prone areas. This study investigates the applicability of the Analytic Hierarchy Process to produce a landslide susceptibility index. Eight major impact factors are analyzed using SAGA, a GIS-based toolkit, including slopes, aspect, land use, soil type, elevation, distance to road, distance to stream, and antecedent rainfall. Four landslide susceptibility maps are produced corresponding to frequency scenarios of 3-day antecedent rainfall data which is taken from Regional Frequency Analysis (RFA). We assess the modeling performances using Area Under the Curve (AUC) index and the results show that the AHP model has good performance. The findings demonstrate a significant influence of rainfall antecedent conditions on the susceptibility map of landslides in this study area.

Keywords

Landslide susceptibility • Analytic hierarchy process • Regional frequency analysis • Area under the Curve • Landslide density index

1 Introduction

Landslide is one of the most regular natural catastrophes in mountainous areas. The term landslide refers to the movement of a mass of rock, debris, or earth down a slope under the influence of gravity (Cruden and Varnes 1996). In places that are impacted by landslides, it is common to have significant damage to numerous houses, as well as infrastructure and agriculture. Landslides are governed by many causative factors, namely geological, hydrological, land cover, morphological, and other factors (Reichenbach et al. 2018). Understanding the influences and mechanisms of these factors on landslides would be significant for the prevention and mitigation of damage from the landslides.

The landslide susceptibility map is considered an effective way to prepare and react in advance to avoid disasters. The map would highlight potential areas for landslides that are likely to occur in a specific area under the influences of causative factors (Brabb 1985). Many approaches have been applied for developing susceptibility maps and can be categorized into five classes (i) geomorphological mapping, (ii) analysis of landslide inventories, (iii) heuristic approaches, (iv) process-based methods, and (v) statistically based modeling methods (Khan et al. 2019).

The above methods can be grouped into quantitative and qualitative techniques. Quantitative techniques tend to develop susceptibility maps based on evaluating relationships between landslides inventory and governing factors for

Supplementary Information
The online version contains supplementary material available at https://doi.org/10.1007/978-3-031-18471-0_7.

C. C. Nguyen · P. Vo (✉) · V. L. Doan · Q. B. Nguyen
The University of Danang, University of Science and Technology, Danang, Vietnam
e-mail: vnducphuoc@dut.udn.vn

C. C. Nguyen
e-mail: nccong@dut.udn.vn

V. L. Doan
e-mail: dvlong@dut.udn.vn

Q. B. Nguyen
e-mail: nqbinh@dut.udn.vn

T. C. Nguyen
Phenikaa University, Hanoi, 12116, Vietnam
e-mail: cuong.nguyentien@phenikaa-uni.edu.vn

Q. D. Nguyen
Vietnam Institute of Geosciences and Mineral Resources, Da Dong, Vietnam

I. Alcántara-Ayala et al. (eds.), *Progress in Landslide Research and Technology, Volume 1 Issue 2, 2022*, Progress in Landslide Research and Technology,
https://doi.org/10.1007/978-3-031-18471-0_7

projecting probabilities of landslides (Guzzetti et al. 1999; Khan et al. 2019; Reichenbach et al. 2018). On the other hand, qualitative techniques estimate landslide sites according to the use of landslide inventory subjectively and traditionally (Khan et al. 2019; Guzzetti et al. 1999). On the one hand, quantitative techniques are likely to give more appropriate susceptibility zonation for high-quality monitoring data. On the other hand, qualitative techniques are more suitable for large areas but often provide low-quality data.

One of the qualitative techniques- the Analytic Hierarchy Process (AHP) method (Saaty 1987; Saaty and Vargas 1991) can be a practical approach to solve data quality problems. This approach is widely used in landslide susceptibility analysis (Pradhan and Althuwaynee, Reichenbach et al. 2018; Pourghasemi et al. 2012). The method is especially suitable to provide zonation at provincial and regional scales. AHP would rank and weigh the contribution of factors based on the expert judgments (Hansen 1984). Each causative factor have been analysed attentively for figuring out its impacts on landslide susceptibility analysis. The assessment can be called semi-quantitative (Reis et al. 2012; Van et al. 2016). It can be used efficiently to predict landslide susceptibility over large areas (Kanungo et al. 2012).

The results of a landslide susceptibility zonation strongly relies on landslide monitoring data; however, the quality of monitoring data in Vietnam is poor and limited to access (Chuang and Shiu 2018). In addition, data collection from many regions in Vietnam is mainly based on reports from local people and local committees. However, these reports may contain some spatial and temporal misleading for mapping and identifying landslide mechanisms (Hung 2011). Some datasets are provided by different authorities, such as transportation sectors and flood and storm committees, leading to many complications in collecting data for research projects.

Selecting appropriate rainfall data for landslide analysis is one of the concerning problems. Many pieces of landslides susceptibility research have been carried out using annual rainfall data instead of antecedent rainfall (Hung 2011). Meanwhile, antecedent rainfall is a significant trigger corresponding to most landslide incidents in the region (Naidu et al. 2018; Pradhan et al. 2017). In this research region, most of the landslides are strongly correlated to 3-days antecedent rainfall caused by tropical storms and monsoon (Phuoc et al. 2019). Therefore, the analysis of the landslide susceptibility index based on yearly rainfall is still questionable, affecting the accuracy of the maps. This gap can be covered by selecting appropriate antecedent rainfall periods of data for estimating the susceptibility index of landslides.

The projection of the susceptibility index offers a scientific foundation for predicting the occurrence of landslides. Nevertheless, these pieces of research are still limited in the study area. As mentioned before, research on landslides often relies on yearly rainfall and may fail to include the frequency terms (Pradhan et al. 2017; Phuoc et al. 2019). Additionally, the quality of the findings might be significantly impacted by short and insufficient monitoring periods and low-density monitoring stations of precipitation data (Naidu et al. 2018). To enhance the predictability of landslide susceptibility, the Regional Frequency Analysis (RFA), which is used to calculate rainfall frequency, is added into the modeling of landslide susceptibility (Hosking and Wallis 1997, 2005; Phuoc et al. 2019).

The RFA algorithm provides likelihood spatial distribution maps of different antecedent periods and various frequencies of rainfall (Nguyen and Nguyen 2017). These maps are useful for investigating terrain instability based on GIS analysis (Pradhan and Althuwaynee, Pradhan et al. 2017, Hansen 1984). The application of this method can overcome the limitation of current spatial and temporal data which can make important contributions to increasing the certainty of landslide susceptibility calculating.

Therefore, this research aims to investigate the impact of rainfall frequencies on landslide susceptibilities using RFA and AHP methods. The RFA approach evaluates and provides the spatial distribution of antecedent rainfall in various frequencies. A GIS-based AHP analysis would be practical to generate landslide susceptibility zoning in large areas. The landslide susceptibility map, represented according to rainfall return periods, would be critical for preventing and mitigating landslide hazards in the research region.

2 Case Study

The study focuses on evaluating landslide susceptibility for three mountainous districts of the Quang Ngai province (Fig. 1). This study area covers an area of 1.352 km^2. The highest altitude of the study area is 1694 m and is in the west, near the Central Highland provinces and the Truong Son Mountain range. Quang Ngai Province's lowland area is east of the study area.

This region is very susceptible to landslides and has lately had several occurrences. Landslides often occur in this region between September and December, which is also a time of heavy rainfall (more than 70% of the region's annual 2500 mm rainfall is accounted for by rainfall from tropical storms and tropical monsoons). According to reports from local natural disaster management authorities, extreme antecedent rainfall is the principal trigger of landslides in the region.

The natural condition of the mountainous area has increasing the risk of landslides. Firstly, the steep slope terrain is a major cause for the instability of shallow landslides. A considerable proportion of natural forests are replaced by forest plantations, agriculture, or bush which enhances the erosion and instability of land, leading to soil mass

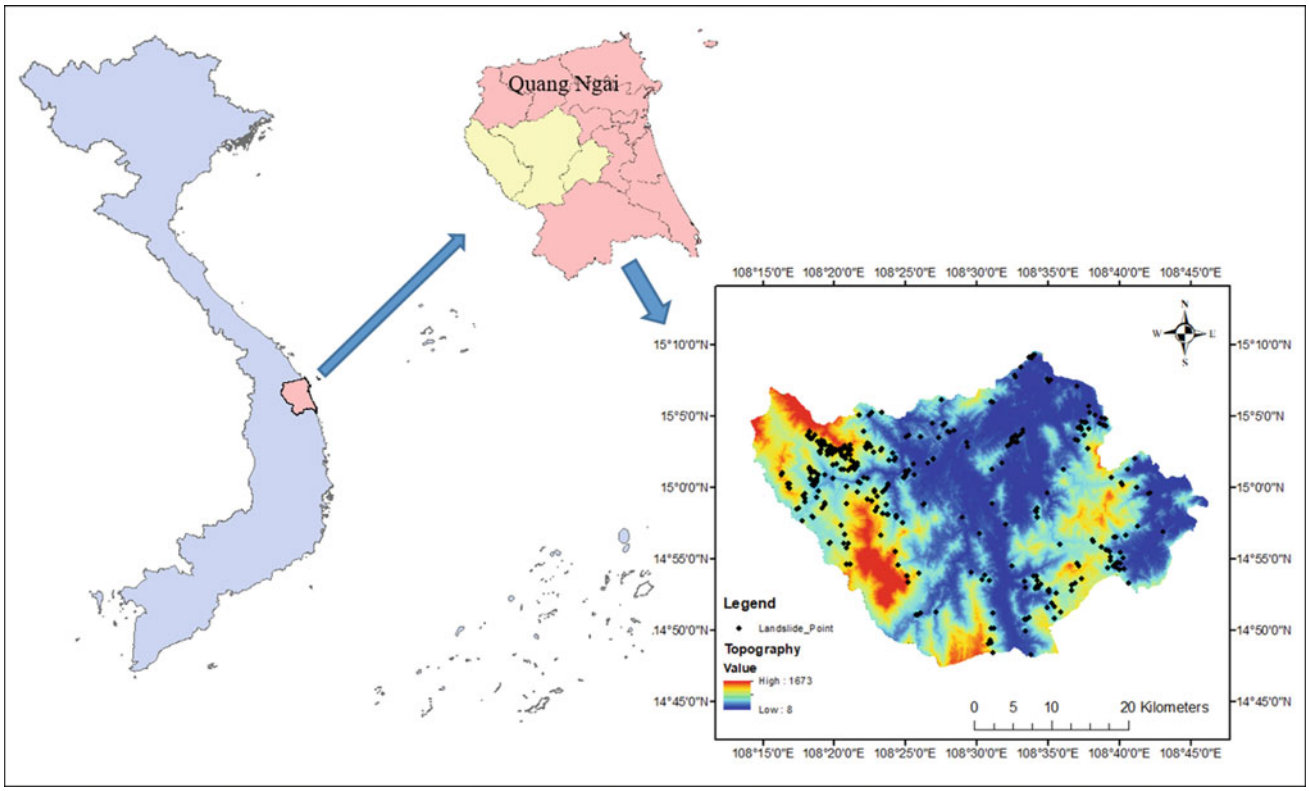

Fig. 1 Location of the study area and the landslide inventory map

movement on the shallow surface. Another problem is the high density of streams together with high antecedent rainfalls making it a significant contribution to the high risk of landslides in the region. Finally, rapid investment in road infrastructure, resulting in changing terrain in road buffering, increases slope instability along these roads.

3 Materials and Methods

A GIS-based multi-criterion analysis is used for developing landslide susceptibility maps. Seven landslide causative factors, including slopes, aspects, elevation, soil types, land use, distance to road, and distance to stream, were used to spatially investigate the landslide susceptibility of the region (Khan et al. 2019; Reichenbach et al. 2018; Pourghasemi et al. 2012). The method also utilized the advantages of spatial analysis to highlight the probability of landslides based on an analysis of geographical, topographical, and meteorological data and landslide events (Khan et al. 2019; Chuang and Shiu 2018). To ensure the projection of susceptibility, high-quality geographical distribution data of influencing factors are collected and analyzed (Hansen et al. 1995; Feizizadeh et al. 2014; Pham et al. 2017). The whole procedure is carried out on QGIS 3.12. and on the SAGA toolkit. Maps are also generated by using QGIS 3.12.

A database of 339 landslides that occurred between 2010 and 2018 was used in this study to construct the susceptibility assessment and validation. The database was compiled using data from landslide inventories based on Landsat satellite images and yearly reports from the flood and storm committee. The landslide locations were then split into two groups using spatial randomization, with 237 locations as a training dataset and the remaining 102 locations as a testing dataset.

To develop landslide susceptibility and lessen uncertainty in the outcomes, we prepare and collect high-resolution geographical and temporal data on the causative factors. In addition, rainfall data was taken from RFA for 3-day antecedent rainfall following two common frequencies of P50% and P20% and two extreme frequencies of 2% and 1% instead of using annual rainfall data. The diagram of the entire process is represented in Fig. 2.

An AHP processing pair-wise comparison matrix is suggested after consulting with experts and literature reviewing. Contribution weights of environment factors (slopes, aspects, elevation, land used, soil types, and distance to rivers) and human activities factors (distance to roads) are analyzed according to the training dataset. These causative elements, coupled with four maps of 3-day antecedent rainfall according to four frequencies (P50, P25, P2, P1%), are utilized to construct landslide susceptibility indices after reclassifying geographical distribution following contribution weights.

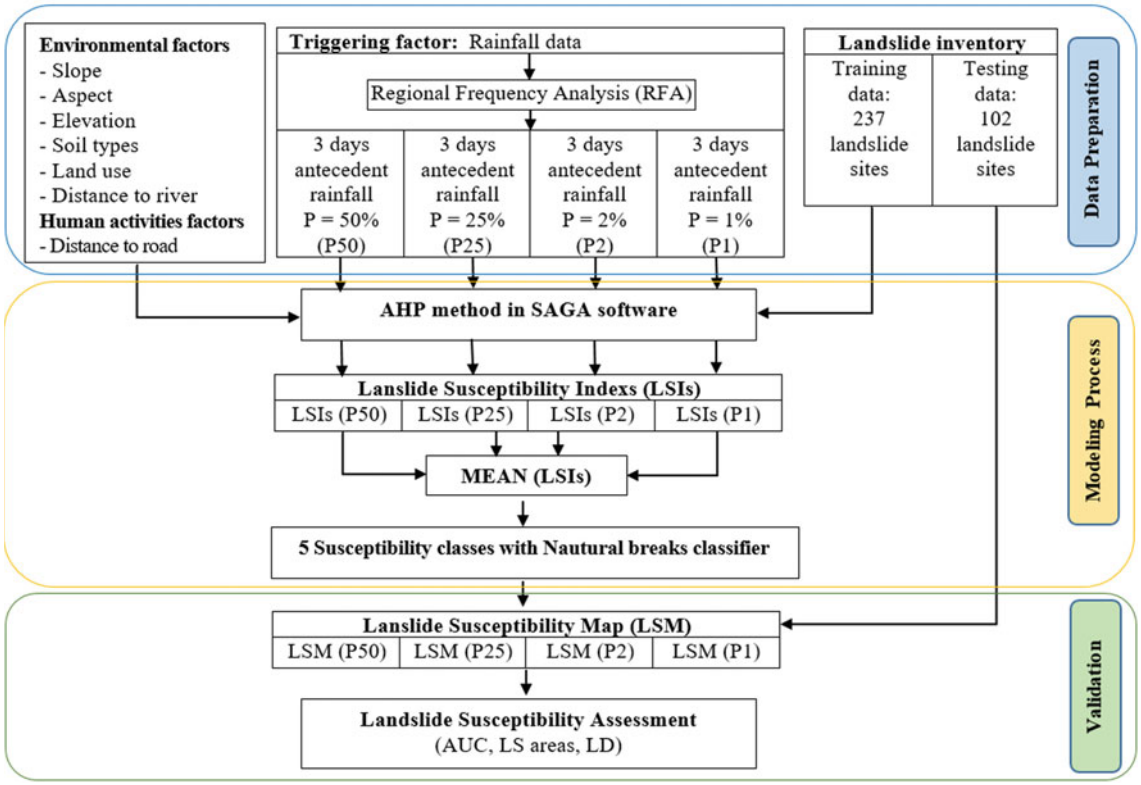

Fig. 2 Diagram of landslide susceptibility project using AHP and RFA methods corresponding to four frequencies scenarios of rainfall

These maps are utilized for generating a landslide susceptibility map with five classifications (very high, high, medium, low, and very low) using the Natural Break classifier. These susceptibility thresholds were then manipulated to build the landslide susceptibility maps for the research area corresponding to each rainfall frequency. The quality of projection results is validated using Area Under the Curve (AUC) index and Landslide Density (LD) using the testing dataset.

3.1 Landslide Causative Factors

This research produces a landslide susceptibility index based on the relative importance of eight influencing factors: rainfall, slope, elevation, aspect, distance to streams, distance to roads, land use, and soil type.

- Rainfall: Phuoc et al. (2019) indicated that 3-day antecedent rainfall is the most significant trigger of landslides. The inventory also highlights that landslides happened in the region annually and more incidents were recorded corresponding to extreme rainfall events. Thus, we examine the impacts of precipitation triggers for two groups of 3-day antecedent scenarios: (i) regular rainfall scenarios correspond to frequency p = 50% (P50) and 25% (P25); (ii) extreme rainfall scenario group with frequency p = 2% (P2) and 1% (P1). Maps of the distribution of rainfall are produced for each rainfall scenario. These maps represent better temporal and spatial resolution than other interpolation methods (Nguyen and Nguyen 2017). This research used RFA-based rainfall data observed for many years from 75 rain gauge stations for the interpolation. The spatial distribution of 3-day antecedent rainfall for the research area is shown in Fig. 3.
- Terrain slope: Terrain slope is the most significant variation in landslide causatives. The review from Reichenbach et al. (2018), and Naidu et al. (2018) have accentuated the critical role of the factors in the instabilities of the interested area. The terrain slope in the research area was prepared from the SRTM DEM (30 × 30 m) using the QGIS 3.12. The obtained results are subsequently classified into different classes based on correlation with landslide occurrence and ranging from 10 to 70° with 10° steps.
- Terrain aspect: The terrain aspect has a strong interrelationship with land cover, soil strength, and moisture, which directly influence landslide initiation (Khan et al. 2019). Therefore, assessing the influences of terrain directions on landslides would contribute to the projection of landslide susceptibility. The aspect layer for the research is also generated from the collected DEM.
- Soil type: Due to differences in shear strength and hydraulic conductivity, soil types respond differently to

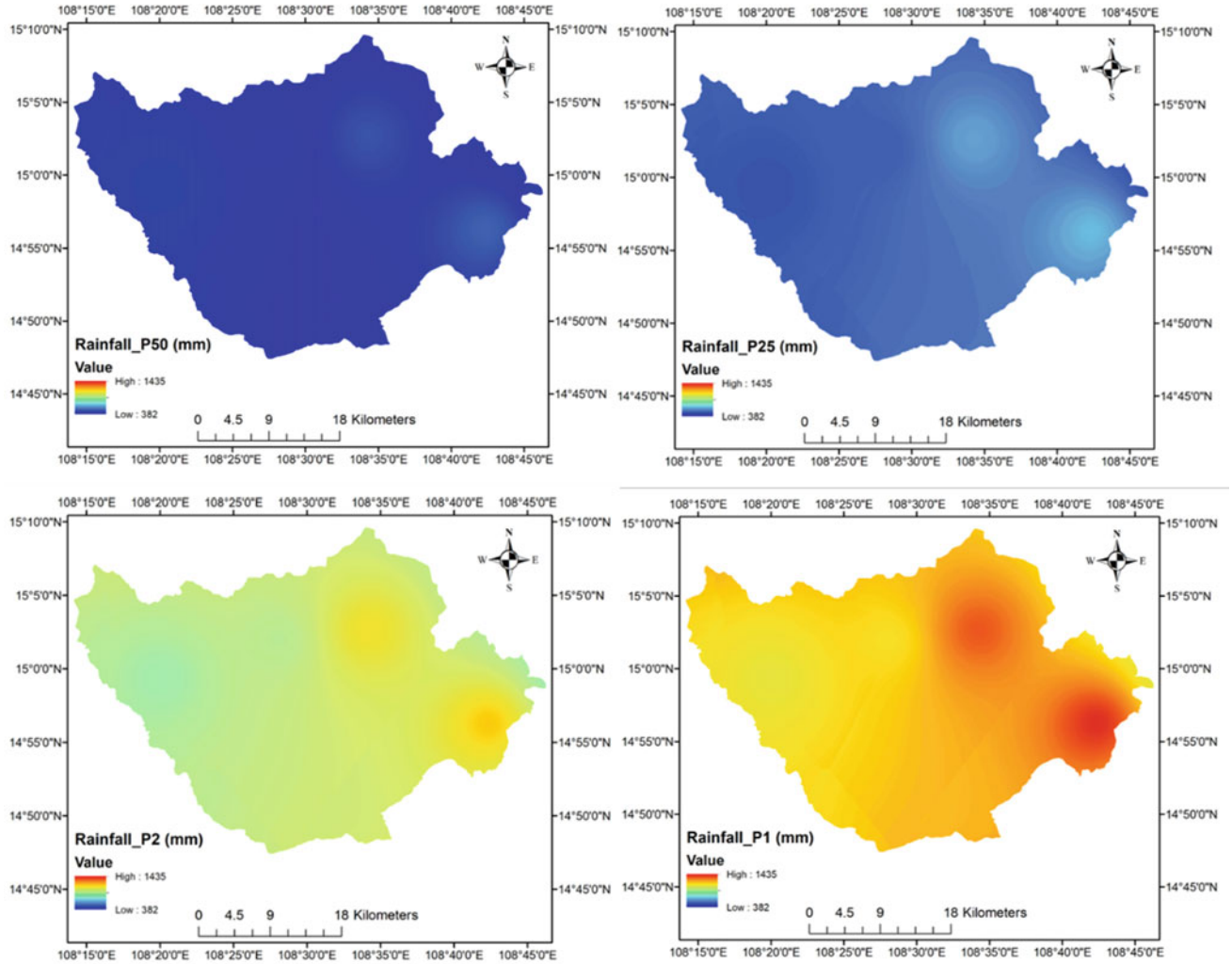

Fig. 3 Spatial distribution of 3-day antecedent rainfall corresponding to four frequencies P50%, P25%, P2%, and P1%

rainfall (Chuang and Shiu 2018). Consequently, reaching a saturated situation, which is an important trigger to landslides, is more likely to be a unique value associated with each soil type. Integrating the relationship between spatial distribution of soil types and occurred incidents would enhance certainty for landslide susceptibility assessment. Spatial distribution soil types data in the research area is provided by local management agencies and processes in ESRI ArcGIS.

- Land-cover: According to Khan et al. (2019), land cover is the main influential parameter of slope stability. A good vegetation cover would work effectively in retaining water, reducing erosion, and improving the stability in the area (Reichenbach et al. 2018). The research has used a land-use map in the year 2010 for slope instability investigation for the province.
- Distance to roads: In mountainous areas, the development of transportation may lead to a reduction in the stability of the slope and eventually landslides. Therefore, distances from the road become a significant trigger to landslide occurrences. In the research, a database of the transportation system is collected from local authorities and processed to use in landslide susceptibility analysis.
- Distance to stream: Many studies have commonly used the factor—distances to streams—to analyze landslides susceptibility (Khan et al. 2019). The contribution of spatial distributions of the rivers and springs in landslides is evaluated in a GIS environment using data from authorities.
- Elevation: is the height of the terrain surface that affects landslide occurrences (Varnes 1984). Rocks appearing at higher elevations are less weathered due to geo-environmental factors. Therefore, landslides often have less frequency in very high elevation areas (Pham et al. 2019). In this study area, the inventory data shows that the most susceptible to landslide incidence is with in elevation range of 720–900 m.

3.2 Analytic Hierarchy Process Method

The AHP method has been used widely to develop an appropriate landslides susceptibility map. A pair-wise comparison matrix provides an estimation of landslide causative factors' contribution. A range with numerical values from 1 to 9 was recommended for comparing criteria by Saaty (1987). Each of these numbers shows the degree of importance in a way that 1 shows equal importance and 9 show the extremely strong importance of a criterion compared to another quantitative criterion (Saaty 1987).

The greatest weight in the AHP method represents a layer having the most significant impact on determinations of the objective. In other words, the criteria for weighing each information unit are also based on the greatest effect played by that factor in the layer. A range with numerical values ranging from 1 to 9 was proposed to compare the criteria. In addition, Consistency Ratio (CR) and Consistency Index (CI) would be calculated to estimate the consistency of the AHP process (Saaty 1987). Note that the CR value must be less than 0.1. If not, the pair-wise table is considered inconsistent (Saaty 1987).

$$CI = \frac{\lambda_{\max} - n}{n - 1} \tag{1}$$

$$CR = \frac{CI}{RI} \tag{2}$$

where: λ_{max} represents the largest Eigenvector of the matrix and n represents the total causative factors (order of the matrix) used in the projection. CR (Consistency Ratio) and CI (Consistency Index), RI (random index) is the average value of CI for a randomly generated pairwise matrix.

To estimate the contribution and correlation of each causative factors to the phenomena, a frequency analysis was established for landslide events. 102 landslides were used to figure out the relationship between landslides and rainfall characteristics in the research area. Another 237 landslides were utilized in spatial analysis, and 102 landslides were used to validate the result.

3.3 Regional Frequency Analysis Method

The regional frequency analysis method was first proposed by Hosking and Wallis in 1997. The method can be used with any kind of data (Hosking and Wallis 1997). In this work, it is regional rainfall. In the regional rainfall frequency method, the index rainfall is computed as the average of the local series (Hosking and Wallis 1997), based on an L-moment procedure (Ngongondo et al. 2011). However, in this study, we used a likelihood of observed sample-based Bayesian Markov chain Monte Carlo (MCMC) procedure as suggested by Gaume et al. (2010). Because it uses the full likelihood function, which is aneffective and flexible way to represent information for a site, whether it is count, interval, or magnitude.

Following Dalrymple (1960), the quantile of non-exceedance probability F at site i may be written:

$$X_i(F) = \mu_i x(F) \tag{3}$$

where x(F) is the regional quantile of non-exceedance probability F, the index rainfall μi is the average value of the sample for site i.

A Bayesian MCMC procedure is now relatively common for hydrological applications (Gaume et al. 2010; Nguyen et al. 2014). Following the Bayes' theorem, the likelihood of the sample given the parameters of the statistical model $L(D|\theta)$ can be related to the likelihood or density of probability of the parameters given the sample $p(\theta|D)$.

$$p(\theta|D) = \frac{L(D|\theta)p(\theta)}{p(D)} \tag{4}$$

where $p(\theta)$ is the prior distribution of θ, p(D) is the probability of sample D, which is unknown.

The inference approach applied herein is directly derived from Gaume et al. (2010). It is based on the likelihood of the available data sets and a Bayesian MCMC algorithm for estimating the growth curve parameters and their posterior distribution according to the observed data set. The likelihood of the observed sample (D) is calculated as follows:

$$L(D|\theta) = \prod_{i=1}^{S} \left[\prod_{j=1}^{n_i} f_\theta \left(\frac{x_{ij}}{\mu_i} \right) \right] \tag{5}$$

where f_θ is the probability density function of the selected statistical distribution for the regional growth curve, and θ corresponds to the vector of parameters of the distribution selection to be estimated.

The study will only briefly present this procedure. The details of the algorithm are included in the R software library nsRFA. This method has been applied to the Central and Central Highlands regions of Vietnam (Nguyen and Nguyen 2017).

4 Result and Discussion

4.1 Analytic Hierarchy Process

Based on the contribution from experts and literature reviews, a pair-wise comparison matrix has been introduced for AHP for landslide susceptibility maps production (See Table 1). With CI = 0.1005 and CR = 0.072 < 01, the matrix is adequate for further analysis.

The analysis of the recorded landslides shows a strong correlation between distance from stream and distance from roads to landslide zonation. While spatial distribution of landslides is strongly correlated to the distance to transportation systems and stream system, the highest proportion of landslide events falls into the closest area to the stream with a 200 m buffer distance. It is also marked that the influence of road on the phenomena is more likely limited in areas lower than 600 m buffer zone, while the impacts of distance from stream tend to continue and reduce steadily until over the distance of 1000 m.

Investigating the impact of soil types also highlights that those landslides are more likely to happen in areas with Epi Lithi Ferralic Acrisols as the most instability soil and Epi

Table 1 AHP pair-wise comparison matrix for landslide susceptibility analysis

	Slope	Rainfall	Land use	Road	Aspect	Soil map	River	Elevation	Weight
Slope	1	3	3	5	5	3	7	9	0.318
Rainfall	0.333	1	0.333	3	3	0.333	5	7	0.122
Land use	0.333	3	1	5	3	3	5	9	0.217
Road	0.2	0.333	0.2	1	0.333	0.333	3	5	0.058
Aspect	0.2	0.333	0.333	3	1	0.333	3	5	0.078
Soil map	0.333	3	0.333	3	3	1	5	7	0.155
River	0.143	0.2	0.2	0.333	0.333	0.2	1	3	0.034
Elevation	0.111	0.143	0.111	0.2	0.2	0.143	0.333	1	0.018

Table 2 Landslide causative factors classes weight

Causatives factors	Classes	Rating	Causatives Factors	Classes	Rating
Slope (°)	0 - 10	1	Rainfall (mm)	380–499	1
	10–20	3		499–616	2
	20–30	5		616–733	3
	30–40	7		733–850	4
	40–50	9		850–967	5
	50–60	7		967–1084	6
	> 60	1		1084–1201	7
Aspect	Noth	3		1201–1318	8
	Northeast	3		1318–1435	9
	East	5	Elevation (m)	< 145	1
	Southwest	9		145–175	9
	South	5		175–415	3
	Southwest	3		415–565	5
	West	1		565–720	7
	Northwest	1		720–900	9
Soil type	Epi Lithi Ferralic Acrisols	9		900–1135	5
	Epi Lithi Humic Acrisols	7		> 1135	1
	Hapli Ferralic Acrisols	5	Distance to road (m)	0–200	7
	Hapli Humic Acrisols	3		200–400	5
	Others	1		400–600	3
Land use	Forest	5		> 600	1
	Residental area	1	Distance to stream (m)	0–200	7
	Timber	9		200–400	5
	Agriculture	3		400–600	3
	Bush	7		> 600	1

Lithi Humic Acrisols as the second. So, these soil types are respectively assigned with points of 9 and 7 in contribution factors. From 2010 to 2018, forest production and bust accounted for the highest landslide frequencies in terms of land cover (Table 2).

4.2 Landslides Susceptibility

Implementation GIS-based AHP analysis with RFA rainfall data and other seven causative factors on SAGA toolkit generated four landslides susceptibility maps. These maps are then used to calculate a mean of landslide susceptibility map as a basis for classifying based on Landslide Susceptibility Indexes (LSIs) following the natural break approach. There are five levels of susceptibility for this phenomenon represented in Table 3 and Fig. 4: very low, low, medium, high, and extremely high. Spatial distributions of landslide susceptibility find a strong correlation with slopes map, which is the most contributing factor. Most of the high and very high risk of landslides fall into 40–50° terrain slopes.

Table 3 Susceptibility level

Level	Landslide susceptibility index
Very low	LSI < 3.29
Low	3.29 < LSI < 4.02
Medium	4.02 < LSI < 4.68
High	4.68 < LSI < 5.41
Very high	LSI > 5.41

However, spatial distributions of slides also indicate the contribution of other factors to landslide susceptibility. Figure 4 represents the statistical index of the mean of landslide susceptibility. Susceptibility is in a range from 1.7 to 7.7. Whereas the value in the range of 10% percentile and 90% percentile are 3.3 and 6.2, respectively. The deviation of the result represents the consistency of the projection, with the mean value being 4.2 and the standard deviation being 0.87.

Figures 5 and 6 highlight the impacts of rainfall on the landslide susceptibility index in the area. Four landslide susceptibility maps were produced using AHP according to different 3-day antecedent rainfall frequencies—50, 25 2, and 1%. There is a significant increase of landslides in high-risk areas according to the increasing rainfall frequencies. The proportion of high and very high increases doubled compared from P25 to P2%. There was a significant increase in very high landslide susceptibility following the rising of rainfall frequencies from P50% to P1%. In contrast, the proportion of low susceptibility areas reduced from 25% in P50% to over 5.2% in P1%. The figure for medium susceptibility is more likely to remain the same in comparison to these frequencies, which account for a quarter of the research area.

Landslide susceptibility shown in Fig. 5 would be useful for natural disaster prevention sectors in the development plan in this research region. Undoubtedly, it would highlight locations at considerable risk of landslide based on real-time precipitation and then make decisions for evacuation and prevention. Consequently, the damage to properties, infrastructure, and human life in the area is reduced.

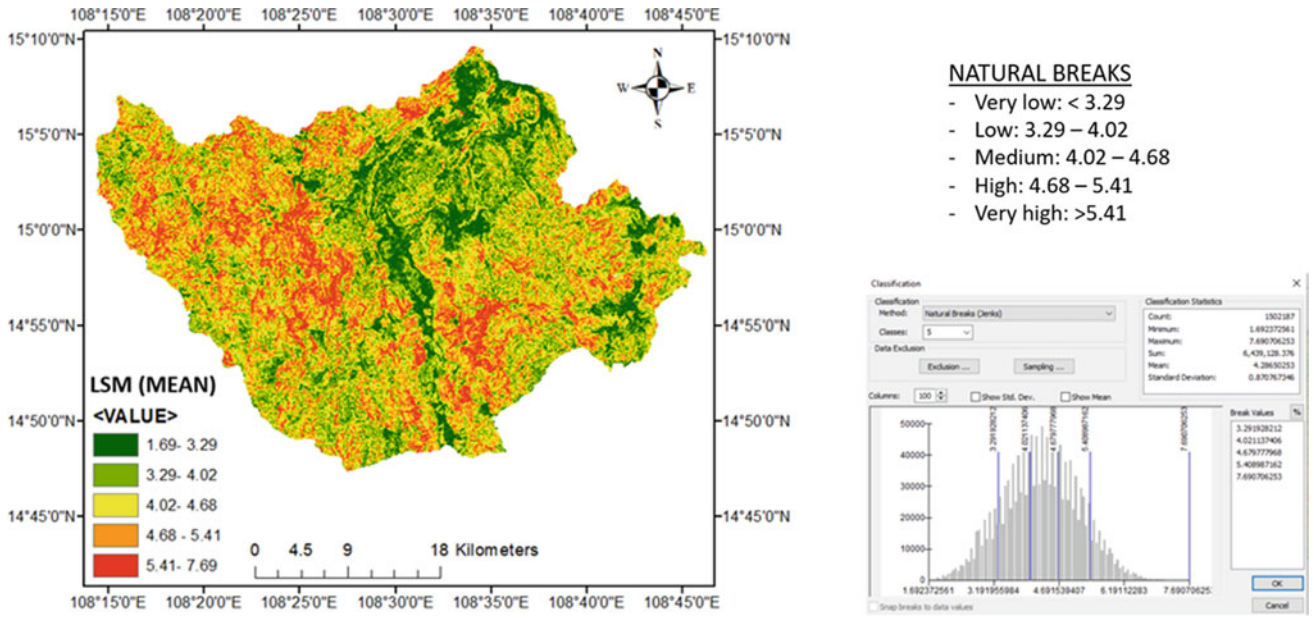

Fig. 4 Map of mean of landslide susceptibility based on 3-day antecedent rainfall

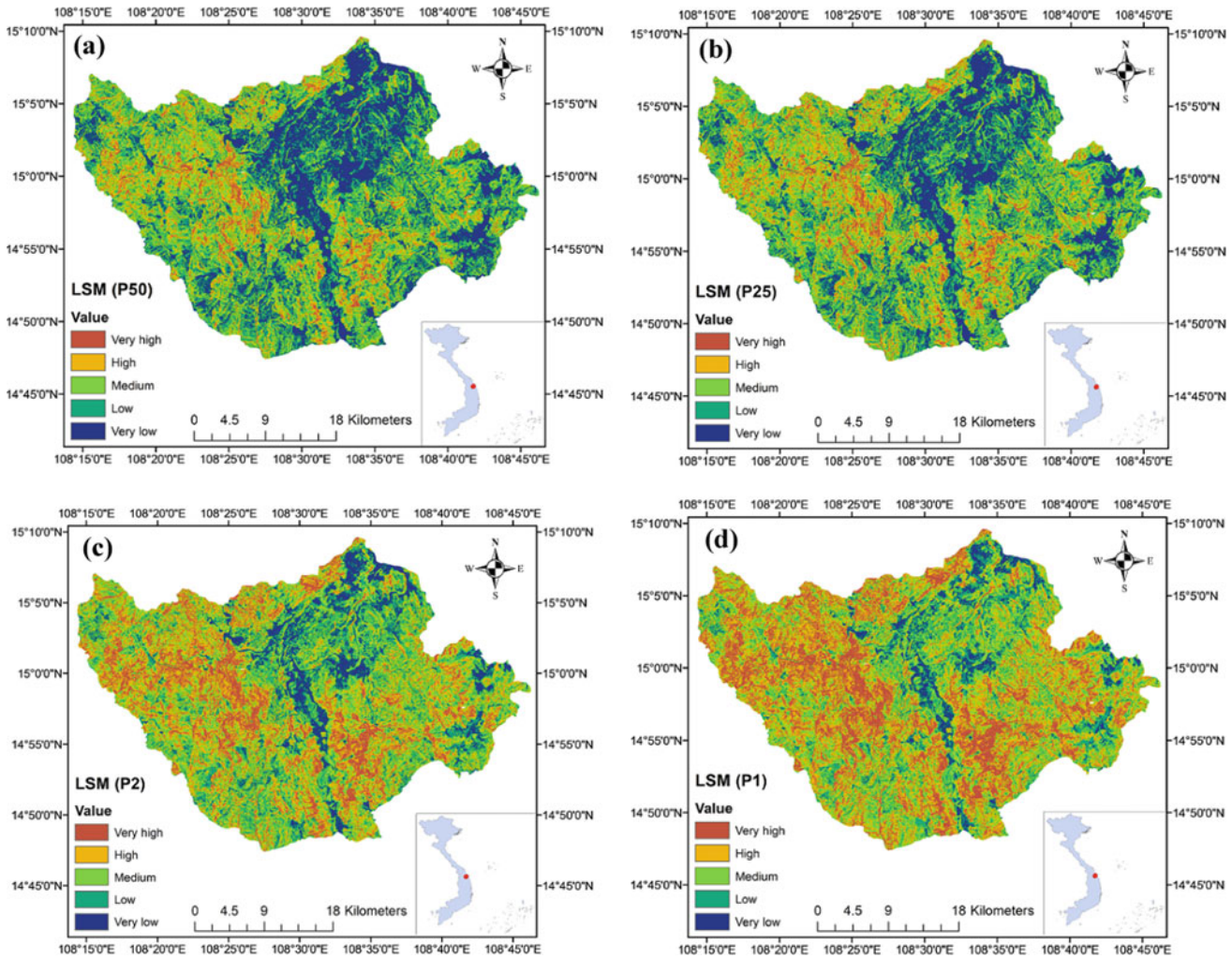

Fig. 5 Landside susceptibility maps for 4 rainfall frequencies scenarios **a** P50%, **b** P25%, **c** P2%, **d** P1%

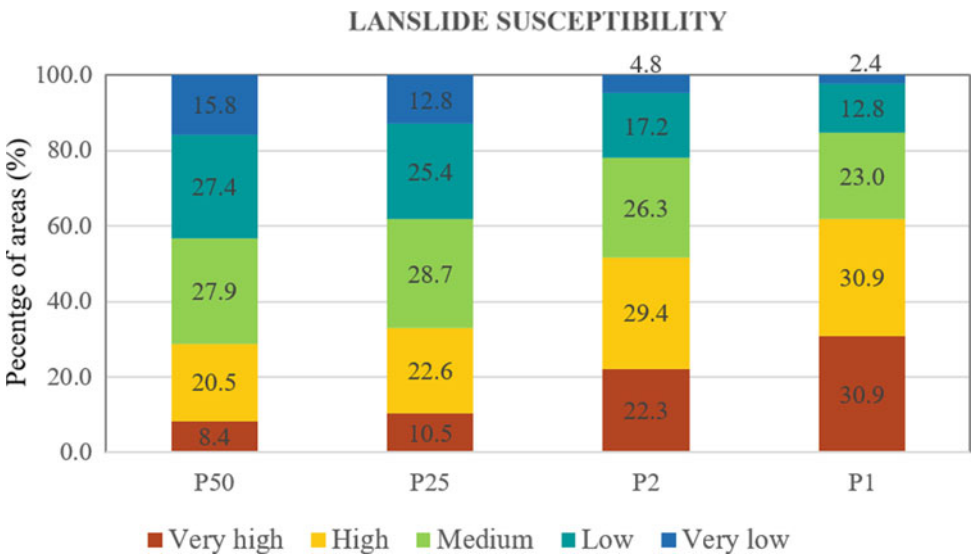

Fig. 6 Area percentage of five landslide susceptibility levels for 4 rainfall frequencies scenarios

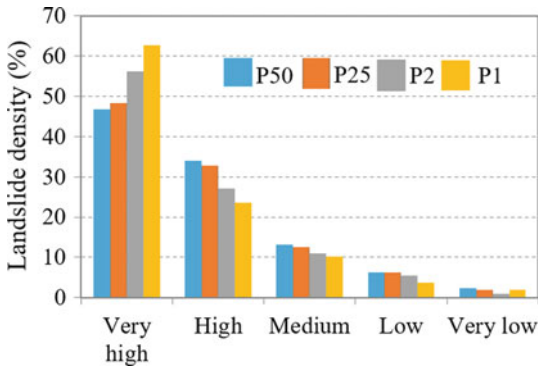

Fig. 7 Landslide density for five landslide susceptibility levels for 4 rainfall frequencies

Figure 7 indicates the agreement on project landslide susceptibility following the AHP process for this study area and recorded events. The obtained results represent that most landslide susceptibility falls into high and very high categories. In the maps of P50%, the proportion of high and very high classes is just over 20% while accounting for 80% of landslide density. The significant figure is very high with only 4% of the area but accounts for 48% of landslide density. Some landslides fall into low and very low classes. However, the proportion of these two levels is very low, with under 10% of a recorded landslide. The increase in landslide density is marked at the highest level. On the other hand, the percentage of landslides in the lower class has decreased following frequencies.

The AUC assessment has been highlighted appropriately of the AHP method in producing landslides susceptibility maps (see Fig. 8). The AUC index based on training landslide sites is slightly higher than the testing data. The AUC indexes of different rainfall return periods models are around 0.75. This assessment indicates that the application of AHP is suitable for landslide susceptibility predition in this region. So, applied parameters for this study can be utilise for other tropical monsoon climate areas where rainfall is the most significant trigger of landslides. The obtained results can also propose a fundamental reference for further studies that should approach more modern methods in landslide susceptibilities such as machine learning and deep learning to improve computing efficiency.

5 Conclusion

The research has represented a method to generate a landslides susceptibility map by application of the Analytic Hierarchy Process to produce an index for landslide projections. Eight major impact factors are analyzed to highlight the importance of causative factors. The slope is the highest contributing factor to landslides with a weight of 0.318, while land use is the second-highest factor. The smallest contribution weight to landslide susceptibility in the area is elevation, which accounts for only 0.018. With CI = 0.1005 and CR = 0.072 < 01, the matrix is adequate for further analysis in regional scale or event place have similar conditions.

Result also highlights the importance of selecting rainfall in landslide susceptibility prediction. Landslide susceptibility maps that result from different scenarios can be used to produce landslides warning according to rainfall forecasting. Application of Regional Frequency Analysis (RFA)s in the analysis provide an alternative approach for investigation the influence of rainfall on zonation of landslides susceptibility in the area where precipitation is the most dominatant trigger for landslide events.

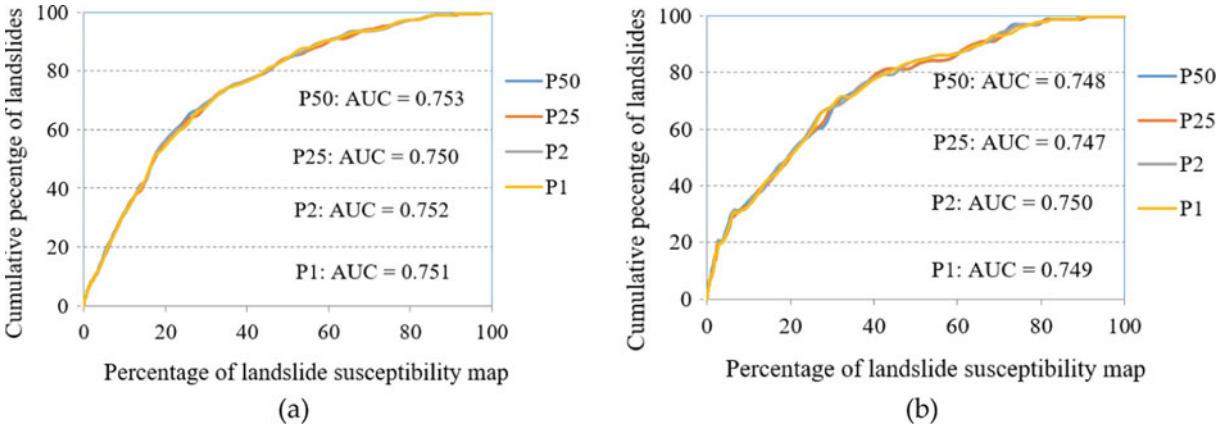

Fig. 8 **a** The success rate curves and **b** prediction rate curves corresponding to 4 rainfall frequencies scenarios

Acknowledgements **Doan Viet Long** was funded by Vingroup Joint Stock Company and supported by the Domestic Master/Ph.D. Scholarship Programme of Vingroup Innovation Foundation (VINIF), Vingroup Big Data Institute (VINBIGDATA), **VINIF.2021.TS.122**.The study is partly funded by Project NVTX. 2022.03.09 and TNMT.2019.03.01

References

Brabb EE (1985) Innovative approaches to landslide hazard and risk mapping. In: International landslide symposium proceedings, Toronto, Canada, pp 17–22

Chuang YC, Shiu YS (2018) Relationship between landslides and mountain development-Integrating geospatial statistics and a new long-term database. Sci Total Environ 622–623:1265–1276

Cruden DM, Varnes DJ (1996) Landslides: investigation and mitigation. Chapter 3-Landslide types and processes. Transportation research board special report

Dalrymple T (1960) Flood frequency analyses, volume 1543-A of Water Supply Paper. US Geological Survey, Reston, Va

Feizizadeh B, Roodposhti MS, Jankowski P, Blaschke T (2014) A GIS-based extended fuzzy multi-criteria evaluation for landslide susceptibility mapping. Comput Geosci 73:208–221

Gaume E, Gaál L, Viglione A, Szolgay J, Kohnová S, Blöschl G (2010) Bayesian MCMC approach to regional flood frequency analyses involving extraordinary flood events at ungauged sites. J Hydrol 394:101–117

Guzzetti F, Carrara A, Cardinali M, Reichenbach P (1999) Landslide hazard evaluation: a review of current techniques and their application in a multi-scale study, Central Italy. Geomorphology 31:181–216

Hansen A, Franks C, Kirk P, Brimicombe A, Tung F (1995) Application of GIS to hazard assessment, with particular reference to landslides in Hong Kong. Geographical Information Systems in Assessing Natural Hazards. Springer

Hansen MJ (1984) Strategies for classification of landslides. Slope Instability 1–25

Hosking J, Wallis J (1997) Regional frequencys analysis.[sl]. Cambridge University Press

Hosking JRM, Wallis JR (2005) Regional frequency analysis: an approach based on L-moments. Cambridge University Press

Hung PV (2011) Review of current status and landslide hazard zonation for the Quang Nam province. Vietnam J Earth Sci 33

Kanungo D, Arora M, Sarkar S, Gupta R (2012) Landslide susceptibility zonation (LSZ) mapping–a review

Khan H, Shafique M, Khan MA, Bacha MA, Shah SU, Calligaris C (2019) Landslide susceptibility assessment using frequency ratio, a case study of northern Pakistan. Egypt J Remote Sens Space Sci 22:11–24

Naidu S, Sajinkumar K, Oommen T, Anuja V, Samuel RA, Muraleedharan C (2018) Early warning system for shallow landslides using rainfall threshold and slope stability analysis. Geosci Front 9:1871–1882

Ngongondo CS, Xu C-Y, Tallaksen LM, Alemaw B, Chirwa T (2011) Regional frequency analysis of rainfall extremes in Southern Malawi using the index rainfall and L-moments approaches. Stoch Env Res Risk Assess 25:939–955

Nguyen CC, Gaume E, Payrastre O (2014) Regional flood frequency analyses involving extraordinary flood events at ungauged sites: further developments and validations. J Hydrol 508:385–396

Pham BT, Prakash I, Chen W, Ly H-B, Ho LS, Omidvar E, Tran VP, Bui DT (2019) A novel intelligence approach of a sequential minimal optimization-based support vector machine for landslide susceptibility mapping. Sustainability 11:6323

Pham BT, Tien Bui D, Prakash I, Dholakia MB (2017) Hybrid integration of Multilayer Perceptron Neural Networks and machine learning ensembles for landslide susceptibility assessment at Himalayan area (India) using GIS. Catena 149:52–63

Phuoc VND, Binh NQ, Hung PD, Long DV, Cong NC (2019) Studies on the causes of landslides for mountainous regions in central region of Vietnam. J Sci Technol Univ Danang 17:5

Pourghasemi HR, Pradhan B, Gokceoglu C (2012) Application of fuzzy logic and analytical hierarchy process (AHP) to landslide susceptibility mapping at Haraz watershed Iran. Nat Hazards 63:965–996

Pradhan AMS, Kang H-S, Lee J-S, Kim Y-T (2017) An ensemble landslide hazard model incorporating rainfall threshold for Mt. Umyeon, South Korea. Bull Eng Geol Env 78:131–146

Pradhan B, Althuwaynee O, Ensemble of data-driven EBF model with knowledge based AHP model for slope failure assessment in GIS using cluster pattern

Reichenbach P, Rossi M, Malamud BD, Mihir M, Guzzetti F (2018) A review of statistically-based landslide susceptibility models. Earth Sci Rev 180:60–91

Reis S, Yalcin A, Atasoy M, Nisanci R, Bayrak T, Erduran M, Sancar C, Ekercin S (2012) Remote sensing and GIS-based landslide susceptibility mapping using frequency ratio and analytical hierarchy methods in Rize province (NE Turkey). Environ Earth Sci 66:2063–2073

Saaty RW (1987) The analytic hierarchy process—what it is and how it is used. Math Model 9:161–176

Saaty TL, Vargas LG (1991) Prediction, projection, and forecasting: applications of the analytic hierarchy process in economics, finance, politics, games, and sports, Kluwer Academic Pub

Van NTH, van Son P, Khanh NH, Binh LT (2016) Landslide susceptibility mapping by combining the analytical hierarchy process and weighted linear combination methods: a case study in the upper Lo River catchment (Vietnam). Landslides 13:1285–1301

Varnes DJ (1984) Landslide hazard zonation: a review of principles and practice

Suffosion Landslides as a Specific Type of Slope Deformations in the European Part of Russia

Oleg V. Zerkal and Olga S. Barykina

Abstract

Landslide classification systems are based on the analysis of mechanisms of slope deformation and consideration of landslide-forming earth materials. The main types of landslide movement are fall, topple, slide, spread and flow. Within the European part of Russia, a specific type of slope deformation is often observed, where suffosion (the process of washout and mechanical removal of fine particles from saturated soils under the influence of infiltrating groundwater flow) plays an essential role. Suffosion landslides are defined as a type of complex landslide formed in regions characterized by alternating horizons of unsaturated and saturated sands, loams and clays. Such hydrogeological conditions occur in the European part of Russia, most of which is occupied by the East European Plain. In the East European Plain, suffosion landslides are confined to the valleys of large rivers and their tributaries (Volga, Oka, Don, etc.), where their volumes can reach several million m^3. In the Volgograd and Moscow regions, suffosion can result in soil decompaction at the base of slopes, or the formation of underground cavities in massifs, niches and grottoes on slopes, ultimately leading to the formation of suffosion landslides. Suffosion landslides are complex displacements of waterlogged soil masses formed as a result of suffosion and the subsequent associated collapse of the sides of suffosion cavities and niches. Indicators of suffosion landslides are: (1) the presence of a prograding fan of finely dispersed material at the base of slope and adjacent terrain, whose boundaries often exceed the landslide limits; and (2) a large number of ledges of different sizes on the surface of the landslide body created by uneven settling of blocks into the roof of suffosion cavities, and on the sides of suffosion niches. Suffosion landslides are often elongated, horseshoe-shaped, or ∞-shaped with a narrowing in the central part formed in saturated soils breaching from an underground suffosion cavity. Suffosion landslides do not have a marked sliding surface. Rather, soil displacement occurs over layers with strongly dispersed groundwater. The displacement rate of such landslides depends on the scale and speed of development of mechanical suffosion at the base of the slope.

Keywords

Suffosion • Suffosion landslides • Typology • Mechanisms • East European plain

1 Introduction

At present, landslide typology is based on analysis of the mechanism of slope deformation and consideration landslide-forming material types. The main types of landslide movement are considered as fall, topple, slide, spread and flow (Varnes 1978; Zolotarev and Janič 1980; WP/WLI 1993b; Cruden and Varnes 1996; Hungr et al. 2014). Of course, there are many intermediate, "complex" landslide types in nature, combining different displacement mechanism. Such "polyphase landslides" have been called "complex" (where at least two types of movement are involved) or "composite" (when two different types of movement occur in different areas of the displaced mass) (Varnes 1978; Cruden and Varnes 1996; WP/WLI 1993a). In the Varnes (1978) landslide classification system, rock, debris, and soil are distinguished among landslide-forming material types. In specialized classifications, one can additionally distinguish landslides in permafrost (or cryogenic landslides) (McRoberts and Morgenstern 1974; Zerkal and Strom 2021), slides

O. V. Zerkal (✉) · O. S. Barykina
Geological Department, Lomonosov Moscow State University, Moscow, 119991, Russia
e-mail: zerkalov@geol.msu.ru

O. S. Barykina
e-mail: barykina@geol.msu.ru

I. Alcántara-Ayala et al. (eds.), *Progress in Landslide Research and Technology, Volume 1 Issue 2, 2022*, Progress in Landslide Research and Technology,
https://doi.org/10.1007/978-3-031-18471-0_8

in periglacial clays (Hutchinson 1988), and slides in sensitive clays (or quick clays) (Mitchell and Markell 1977; Locat et al. 2011). Hungr et al. (2014) suggested using geotechnical material typing (rock, clay, mud, non-plastic (or very low plasticity) sorted soil, debris, peat and ice) when updating the Varnes classification system (Hungr et al. 2014). Recent studies of landslide activity in the plains and lowland areas of European Russia, recognize a specific type of mass wasting and slope deformation formed through suffosion. This paper outlines our current research into formation of suffosion landslides.

2 Suffosion

The widespread occurrence of suffosion throughout the territory of the East European Plain was first noticed by A. P. Pavlov, who introduced the term "suffosion" (Pavlov 1898), and is now recognized as the process of sediment washout—the mechanical removal of small particles from saturated earth material—under the influence of filtering groundwater flow. In contrast to karst, in which dissolution rock material takes place, the main process in suffosion is mechanical removal of poorly consolidated bedrock and unconsolidated surface deposits. In natural conditions, mixed (chemical–mechanical) removal of material from rock massifs is, of course, not uncommon. For example, when dissolution of cement in rocks occurs, followed by the mechanical removal of small particles from a deposit. Another difference between suffosion and karst is the speed of the process. While the rate of formation of karst cavities can be very slow (especially in carbonates due to their low solubility), the rate of formation of suffosion cavities is primarily controlled by the intensity of the filtering groundwater flow speed and head gradient.

The main conditions influencing suffosion activity are: (1) the presence of unstable earth materials susceptible to suffosion; and (2) the possibility of intensive groundwater flow, especially with large groundwater level fluctuations. The free movement of the smallest particles in soil pores, under the influence of the filtered groundwater flow, determines the suffosion stability of the slope. Suffosion failure begins when the velocity and head gradient of groundwater flow reaches critical values. At which time, fine particles smaller than the diameter of the pore channels can be transported and carried away by groundwater. The removal of large quantities of fine particles from the soil is accompanied by a gradual increase in the diameter of the pore channels.

Suffosion failure can result in an increase in soil porosity and permeability that can extend to a considerable depth and cause a reduction in slope strength. Under conditions of favorable transport (removal) of fracture products by the filtration flow beyond the zone of suffosion development, underground cavities in massifs, depressions, sinkholes and closed depressions develop on the surface, while niches and grottos form on the slopes.

Massifs, composed of fine-grained soils with mixed-grained sands or with internal structures characterized by interstratification of sand, silt and clay are most susceptible to suffosion. High suffosion activity is typical for slopes of riverbanks, lakeshores and coastlines as well as around water reservoirs. Such slopes are located in the zones affected by surface water level changes and accompanied by sharp changes—increasing to critical values—in groundwater level gradients.

3 Suffosion Landslides. General Concepts

3.1 Formation Mechanism and Delineation Signs of Suffosion Landslides

"Suffosion landslides" or "landslides of suffosion genesis" are triggered by a reduction of soil strength characteristics at the base of a slope due to suffosion decompaction of the soil, or by destruction of suffosion cavity roofs and flanks of suffosion niches on a slope, followed by landsliding of material.

As such, suffosion landslides are displacements of saturated soil masses caused by suffosion and subsequent collapse of suffosion cavity sides. Such landslides develop regressively through successive cycles of collapse in suffosion cavities or niches due to loss of sand, sandy loam or clay loam through groundwater flow in the aquifer. Collapsed, saturated and unstructured masses move in the direction of the slope in the form of a flow (Fig. 1). This process often masks the primary genesis of the slope deformation, making it difficult to identify suffosion landslides.

Suffosion landslides do not have a clearly defined sliding surface. Soil displacement occurs over a layer of heavily watered (i.e. saturated) sand. The landslide masses move impulsively by leaps, sometimes at a very high velocity, depending on the scale and speed of development of mechanical suffosion of sand particles at the base of the slope. Sub-vertical displacement often prevails over horizontal movement at the crown and head of suffosion landslides when underlying water-saturated sandy sediments have a significant thickness.

Several features indicate the leading role of suffosion in landslide formation. At the sites where suffosion landslides spread, removal fans composed of fine-grained sediment are often observed prograding at the base of the slope and over adjacent territory, whose contours often exceed the landslide boundaries. Another genetic characteristic of suffosion

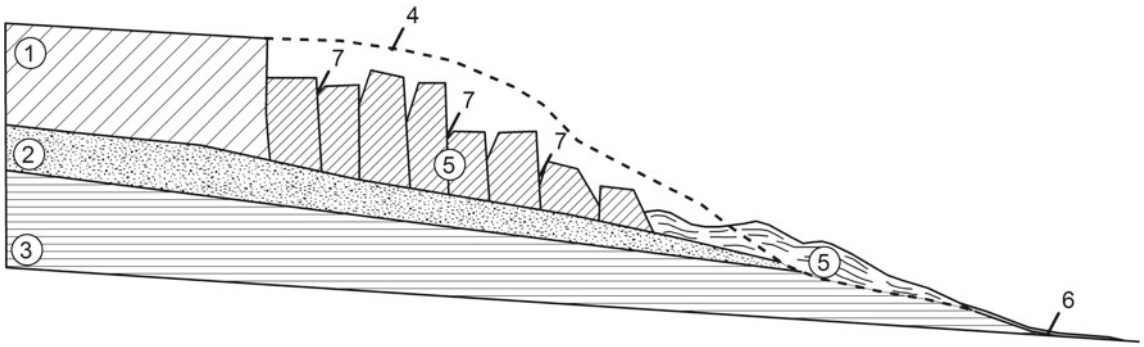

Fig. 1 A general scheme for the formation of a suffosion landslide. 1. Loam and sandy loam. 2. Saturated sands. 3. Clays. 4. Pre-slope relief. 5. Suffosion landslide. 6. A fan of fine material removal. 7. Landslide crack

landslides is a large number of scarps of different sizes across the landslide body. These scarps form as a result of irregular settling of soil blocks into the roof of underlying suffosion cavities, and along the sides of suffosion depressions. Suffosion landslides are often elongated, horseshoe-shaped, or ∞-shaped with a constriction in the central part formed in the area of a breach of saturated soils from an underground suffosion cavity. The direction of the long axis of the landslide basin inherits the direction of the underground suffosion channel formed in the slope massif.

Hutchinson (1981) described suffosion-induced landslides across England from Cromer to Overstrand (Norfolk), in the Christchurch Bay coastal cliff (Hampshire), and in Newhaven (East Sussex). In these landslides, suffosion in aquifer sand interlayers enclosed in beds of clay, silty clay and silt caused overlying sand layers to collapse. Collapsed soils were crushed, then clay and sand were mixed with flowing groundwater to form mudslides. Hutchinson (1981) did not present results of in-situ measurements of the rate of development of such landslides, but noted that in Newhaven, according to a comparison of the topographic maps of 1898 and 1926, the rate of coastal retreat was 0.2 m per year. This rate was assumed to be consistent with the rate at which the sand bed collapsed under the action of suffosion.

3.2 Suffosion Landslides in Landslide Classification Systems

Suffosion landslides are specific in the nature of their development, and characterized by their displacement patterns. Therefore, in many landslide classification systems, where "suffosion landslides" are recognized as a separate type of displacement, they are classified as a group/class of "complex" or "composite" landslides.

Pavlov (1903) was the first to describe suffosion landslides as a separate type of slope displacement observed in the Volga River valley. Rodionov (1937) presented a scheme for the classification of landslide phenomena on the Black Sea coast of the Caucasus and distinguished sixteen landslide types united in three groups according to the structure of landslide-forming earth material. He included suffosion landslides in third group (special cases of displacement), distinguishing as a separate type of displacement the slope deformations caused by suffosion-induced removal of soil particles. Among the main causes of suffosion landslides, Rodionov (1937) indicated high content of dust particles and significant groundwater gradients. Later Rodionov (1939) proposed a division of suffosion landslides into three sub-types (Table 1). Klevtsov (1964), who studied landslides in the foothill areas of the Caucasus, proposed different sub-types of suffosion landslides formed where fine-grained "dusty sands" lay at the base of loess strata (Table 2).

Hutchinson (1988) identified landslides caused by suffosion material removal at the base of a slope as "slides caused by seepage erosion" within complex slope movements, where as Tikhvinsky (1988) distinguished two sub-types caused by the removal of suffosion material at the base of a slope (Table 3). Most recently, Khomenko (2011) proposed three types of displacements to distinguish among suffosion landslides caused by suffosion removal of material (Table 4).

4 Suffosion Landslides in the European Part of Russia

Much of the European part of Russia is occupied by the East European Plain, framed to the south by the Caucasus Mountains and to the west by the Ural Mountains. The main areas of landslide activity in the Eastern European Plain are confined to the valleys of large rivers and their tributaries (Volga, Oka, Don, etc.) (Zerkal and Strom 2017). Suffosion landslides are most widespread in the middle and lower parts of the right (west, high) side of the Volga River valley. This is due to the peculiarities of the hydrogeological properties and structure of Quaternary deposits in the area, which are characterized by alternating horizons of unsaturated and saturated sands, loams and clays in the section (Fig. 2).

Table 1 Sub-types of suffosion landslides after Rodionov (1939)

Landslide sub-type	Landslide characteristics
Suffosion-consistent landslides	• Displacement of a slope or a portion as a result of suffosion processes • Presence of bedrock and unconsolidated sediments capable of changing consistency • Alternation of sandy (suffosion-unstable) and clayey deposits – Slope structure does not significantly affect development of landslide phenomena
Suffosion landslides	• Displacement is a consequence of suffosion processes developed in the slope • Slope structure is not predisposed to development of "classical" types of landslides
Suffosion-structural landslides	• Slope displacement caused by suffosion processes in layers dipping towards the slope

Table 2 Sub-types of suffosion landslides after Klevtsov (1964)

Landslide sub-type	Landslide characteristics
Suffosion-structural landslides	• Displacements caused by suffosion of sandy earth materials under conditions of: (a) Rapid lowering of river water levels during floods and inundations (b) During low tides in the seas (c) Intensive thawing of the winter frost zone in the near-slope parts of the massifs (d) Surface bursting of underlying pressurized water-bearing horizon (e) Rapid watering of sandy bedrock and unconsolidated deposits on slopes by atmospheric and technogenic waters (f) Formation of head waters
Suffosion-plastic landslides	• Displacement caused by suffosion of sandy material • Suffosion conditions require strong moistening of enclosing clay soils
Suffosion-subsidence landslides	• Displacement caused by the suffosion of sandy material • Base of loess strata experiencing subsidence • Accompanied by a change in bedding structure and compaction with watering

Table 3 Sub-types of suffosion landslides after Hutchinson (1988) and Tikhvinsky (1988)

Landslide sub-type	Landslide characteristics
Slide caused by seepage erosion	• Landslides caused by suffosion material removal at the base of a slope • Seepage erosion within complex slope movements
Suffosion landslides	• Displacements caused by the suffosion removal of sandy material at the base of a slope • Landslide activity due to the ongoing suffosion removal of sandy material • Subsequent landslide activity caused by other factors

In the area of Quaternary glaciations, the section is formed by alternating glacial loams and fluvioglacial sands of different glaciation stages. Outside the area of glaciations, the structure of the section includes subaerial deposits (loess, elastic silt), alternating alluvial (of different-age terraces) and marine (different stages of transgression) sands, loams and clays.

4.1 Suffosion Landslides in the Volga River Valley

The first detailed descriptions of landslides caused by "friable sediments from springs flowing out of the mountain" date back to 1724, when the buildings of the Uspensky Monastery in Simbirsk (now Ulyanovsk) were deformed as a result of landslide displacement.

Active study of landslides on the slopes of the right (west, high) side in the middle and lower parts of the Volga River valley started at the beginning of the 20th Century and was connected with construction of the railway network in this region (Martin 1911; Vasilevsky 1929). One of the largest landslides occurred on July 12, 1941 on the bank of the Volga in the southern part of Stalingrad (now Volgograd). The landslide formed on a slope composed of Upper Pleistocene Khvalyn clays (about 20 m thick), underlain by Middle Quaternary Khazar sands. The landslide covered the

Table 4 Sub-types of suffosion landslides after Khomenko (2011)

Landslide sub-type	Landslide characteristics
Type I	• Landslides on slopes composed of water permeable, non-water-saturated dispersed soils • Underlain by non-water permeable rocks outcropping at the base of the slope • Suffosion landslide formation is preceded by groundwater encroachment of the lower part of water permeable dispersed soils • One or more niches are formed as a result of suffosion withdrawal under the action of filtration flow, which emerge on the slope • Formation of a suffosion scarp in the lower part of the slope, as a result of which, a landslide is formed
Type II	• Suffosion landslide caused by the seepage failure of water-saturated sand beds • Groundwater horizon in the lower part of the sand bed experiences a very rapid rise in flow • Alternatively, a very rapid lowering of the discharge base (as in the case of a fall in the water level of a river or reservoir) is present • Landslide occurs as a structure less flowing mass of water-saturated sand
Type III	• Suffosion landslide formed by seepage failure of water-saturated sands, which are overlapped by water proof sediments (e.g. clays) • Groundwater experiences an increase in the head gradient • At critical values head gradient, overlying clay horizon will be destroyed • Landslide develops as a flow of unstructured mass of saturated sand transporting clay blocks after their collapse into a suffosion cavity

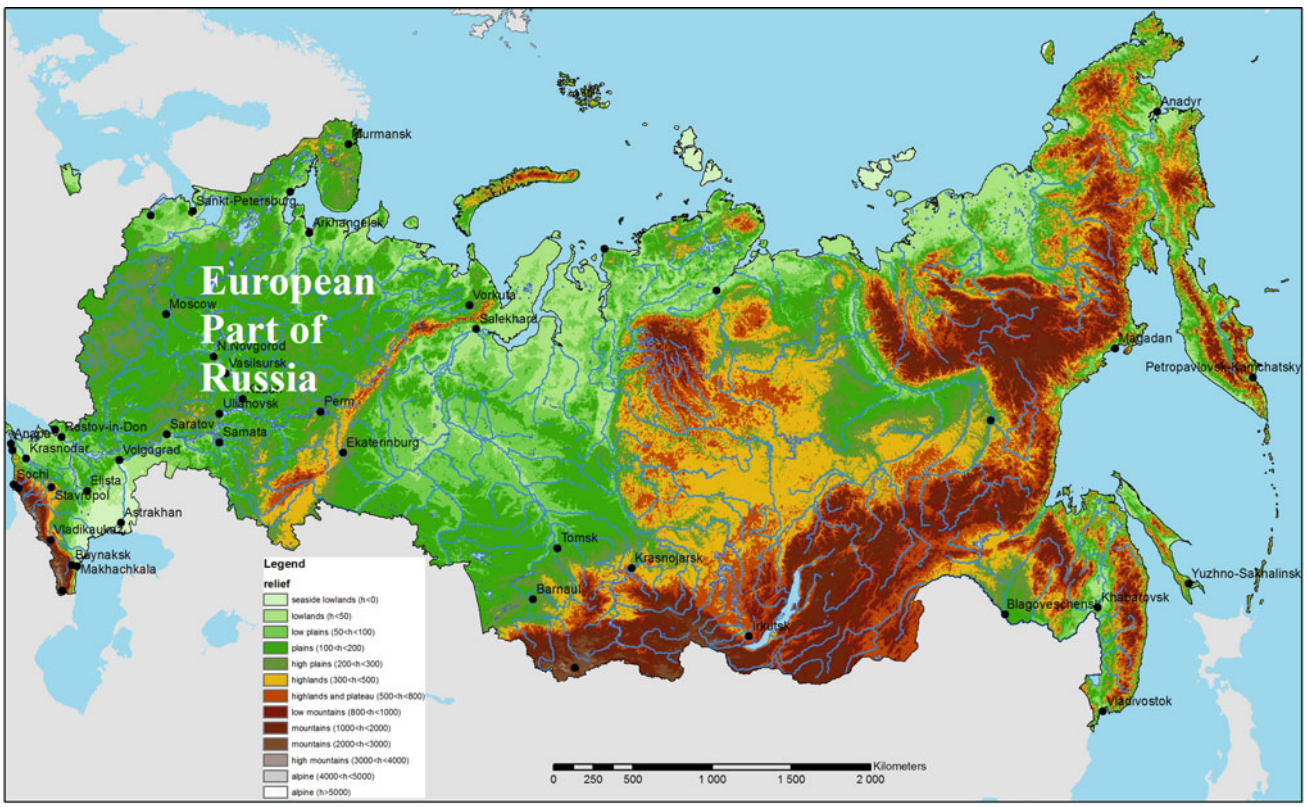

Fig. 2 The European part of Russia—the research territory of suffosion landslides

entire thickness of the Khvalyn clays up to their base. The landslide, which lasted about 40 min, formed a depression 10–12 m deep, 250 m along the axis, and up to 275 m along the front. The basin exited to the Volga River through a relatively narrow neck 110–140 m wide. In the part of the landslide that advanced into the Volga River and in the half

of the landslide basin adjacent to the bank, the displaced soil was a non-structural saturated mass (Cheprasov 1972; Tikhvinsky 1988). The upper part of the basin was filled with displaced blocks of Khvalyn clay. Researchers noted a decrease in the average thickness of 0.6 m in the Khazar sands beneath the landslide body, which is about one third less than the thickness of the Khazar sands outside the landslide. This reduced thickness can be seen as a consequence of their removal by suffosion during the preparation and development of the displacement.

In addition to the lower part of the Volga valley near Volgograd, suffosion landslides are widespread in the middle part of the Volga valley between Ulyanovsk (formerly Simbirsk) and Saratov (Cheprasov 1972; Rogozin and Dunaeva 1962; Rogozin and Kiseleva 1965; Tikhvinsky 1988) and in the piedmont areas of the Caucasus (Klevtsov 1964).

4.2 Suffosion Landslides in Moscow Region

A peculiarity of the geological structure of the Moscow region is the wide distribution of erosion-cut Quaternary fluvioglacial and alluvial-fluvioglacial silty sands interbedded with glacial clay loams (with a total thickness up to 35–40 m), overlying fine-grained silty sands with interlayers of loams and clays of Lower Cretaceous age (with a total thickness up to 50–55 m). As a rule, these strata contain groundwater horizons, including pressurized (artesian) groundwater. These hydrogeological condition are favorable for the development of suffosion and the formation of suffosion landslides (Fig. 3).

The "Vorobyovy Gory" landslide site, located on the right bank of the Moscow River valley, is one of the areas where landslide displacements are associated with active suffosion. In this section of the Moscow River valley, the right bank is up to 70 m high (Barykina et al. 2021). It is composed of Quaternary fluvioglacial sands interbedded with glacial clay loams that are underlain by Cretaceous sands with interlayers of loams and clay. Jurassic clay beds occur only at the base of the slope. In the middle and lower parts of the slope, numerous springs are observed as a consequence of groundwater discharge.

Landslide at "Vorobyovy Gory"site is a complex, multi-stage landslide. The volume of soil involved in the landslide deformation is estimated at 2 million m^3 (Barykina et al. 2019). The study of landslide structure showed that the upper tier of landslide blocks is composed of Quaternary sands and loams, as well as Cretaceous sands. Often the landslide is marked by the absence of some horizons of Cretaceous sands, which may be due to their destruction by suffosion.

The Cretaceous-age sands that make up the slope on the "Vorobyovy Gory" site were investigated to determine suffosion stability. According to stratigraphic data, sand strata susceptible to suffosion include: (1) the Volgushinskaya formation (K_1vlg), Vorokhobinskaya formation (K_1vr), and Ikshinskaya formation (K_1ik) (Aptian Stage, 113–121 Ma). (2) The Butovskaya formation (K_1bt) (Barremian Stage, 121–131 Ma). (3) The Kotelnikovo formation (K_1kt),

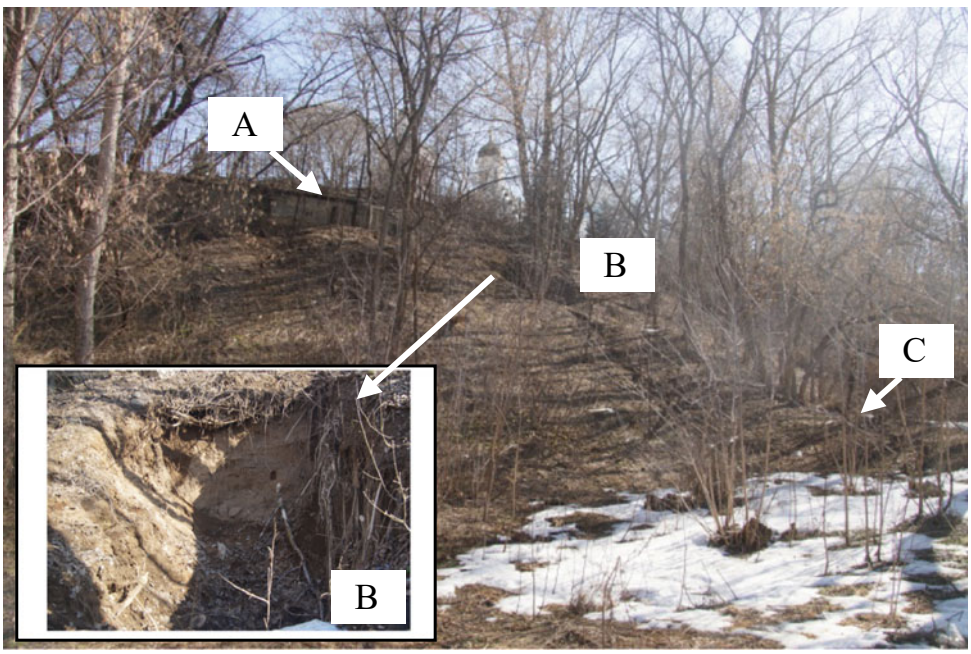

Fig. 3 The suffosion niches at the "Karamyshevo" landslide site, left bank of the Moscow River valley, Moscow. A—the landslide deformations; B—the suffosion niche; C—the suffosion fan

Gremyachevskaya formation (K_1gr), Savelievskaya formation (K_1sv), and Dyakovskaya formation (K_1dk) (Hauterivian Stage, 131–134 Ma). (4) The Kuntsev formation (K_1kn) and the upper part of the Lopatin formation (K_1lp_2) (the Berriasian Stage, 139–145 Ma).

Quartz with varying degrees of ferruginization dominated the mineral composition of all studied sands. Sands were diverse and dissimilar in their grain-size composition. The results of the grain-size analysis (Fig. 4) show that sands of the Volgushinskaya, Savelievskaya, and Dyakovskaya formations are unimodal, while those of the Ikshinskaya and Gremyachevskaya formations are bimodal, which is typical of sands of marine genesis. The dominant particle dimension in almost all the formations is 0.10–0.25 mm, except for the Volgushinskaya formation (0.25–0.50 mm).

Suffosion-stability of Cretaceous sands was evaluated in two ways: (1) by calculation; and (2) by using physical simulation. To determine the suffosion properties of sands, the computational method used the coefficient of heterogeneity of the grain size distribution of soils, calculated as the ratio of fractions containing 60% and 10% ($K_n = d_{60}/d_{10}$) (cf. Istomina, 1957). Suffosion-resistant soils include sands with $K_n < 10$. Suffosion-unstable are sands with $K_n > 20$. Soils in the transition region can be both suffosion-stable and suffosion-unstable.

The next step was to estimate the size of particles that can move through soil pore spaces under the influence of filtering groundwater flow. For the studied sands, values obtained for the maximum particle sizes that can be moved by the filtration flow as a result of suffosion—ranged from 0.019 mm for the Volgushinskaya formation, 0.131 mm for the Vorokhobinskaya formation, to 0.075 mm for the Ikshinskaya formation, and for the Gremyachevskaya formation, 0.057 mm. The homogeneous sands of the Butovskaya formation proved to be suffosion-resistant ($K_n > 10.8$).

The determination of suffosion stability of the sands in the physical model confirmed the results of the simulation. The least homogeneous Vorokhobinskii sand was the least resistant to suffosion: the intensity of sand particle removal was 0.000104 g/cm^3*s. The same values for suffosion particle removal were obtained for sands of the Ikshinskaya formation (0.000104 g/cm^3*s). A slightly lower intensity of particle removal was characteristic of the Volgushinskaya formation sands (0.000094 g/cm^3*s) and sands of the Gremyachevskaya formation (0.000083 g/cm^3*s). The sizes of grains removed by the filtration flow in the modeling of suffosion mostly coincided with the sizes obtained from calculations.

These results confirm the susceptibility of Cretaceous sands in the "Vorobyovy Gory" area to suffosion processes, which in turn, influences the development of landslide processes. Sands of the Butovskaya formation in the upper tier landslide blocks have a thickness close to that of undisturbed

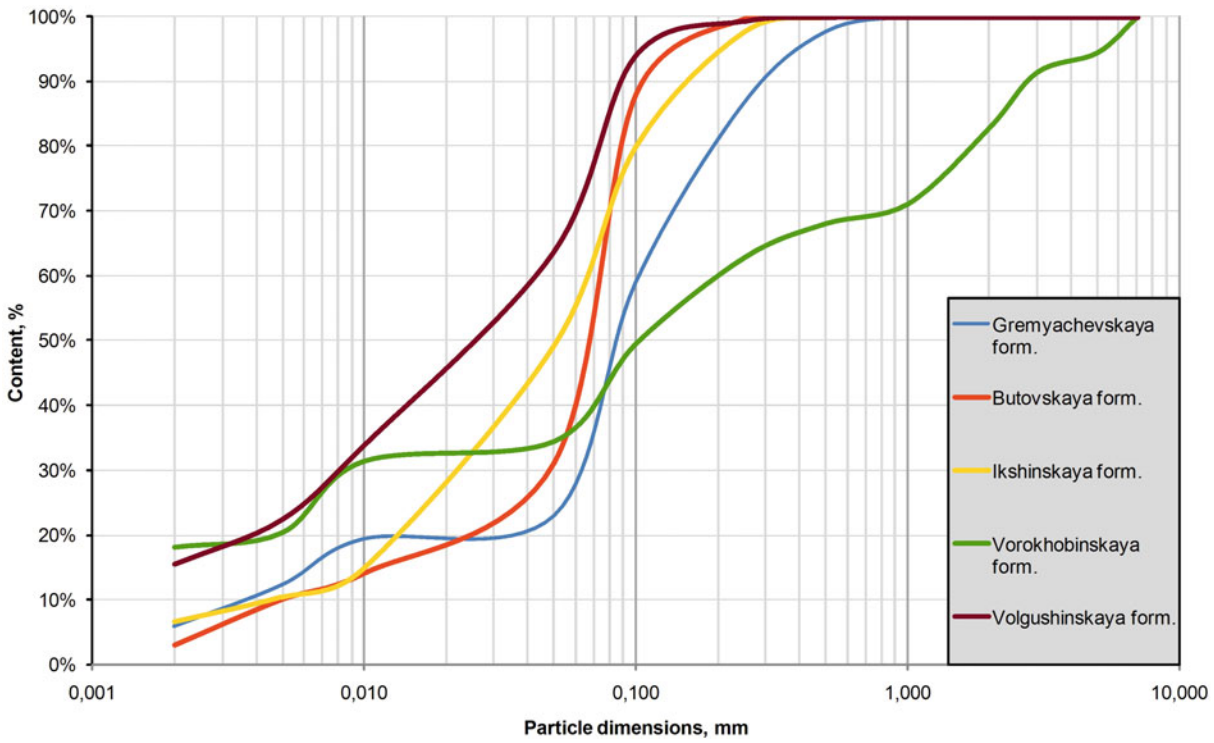

Fig. 4 Integral graphs of the granulometric composition of the studied soils

bedding. Sands of other formations in the blocks of the upper landslide tier are characterized by a decrease in thickness, completely disappearing in places.

Kotlov (1962) earlier suggested a suffosion genesis for some of the landslide deformations in the "Vorobyovy Gory" area: "Natural suffosion is most widely developed on the right (west) high bank of the Moscow River in places where the groundwater horizon, enclosed in Jurassic, Cretaceous and Quaternary fluvioglacial sands, outcrops at surface. On the "Leninskie Gory" (now the "Vorobyovy Gory") one can see hundreds of springs, most of which serve as foci of suffosion. Currently, there are several such sites on the slope of the "Vorobyovy Gory" (Fig. 5).

Suffosion outflow is promoted by significant hydrodynamic pressure during filtration flow. In the central part of the "Vorobyovy Gory" (Kotlov 1962), the drop in groundwater level across the landslide body is 20.7 m over 330 m, with the average values of i = 0.066. At a number of sites, the groundwater level slope increases up to an i = 0.08–0.1 and more. A localized suffosion fan of finely dispersed earth material is clearly seen in the middle and lower parts of the slope.

Fig. 5 Mid-slope suffosion niche at the "Vorobyovy Gory" site. A—the suffosion niche

Estimates of the amount of material eroded showed that the volume (of Cretaceous sand loss) was from 50 to 100 mg/l (Kotlov 1962). Considering groundwater discharge is confined to Lower Cretaceous and Quaternary fluvioglacial sands at the base of slope with the addition of more outlets (sources), removal of earth material by suffosion significant in scale. Over geological time, this has led to the formation of suffosion cavities and niches on the slope, that further contributed to active landslide deformations.

5 Conclusion

Suffosion is the process of washing out and mechanical removal of small particles from saturated soils under the influence of filtrating groundwater flow. Suffosion particle removal rate is controlled by the intensity of the filtering groundwater flow and head gradient. Destruction of soils by suffosion can result in their de-consolidation at the base of a slope, or in the formation of underground cavities in massifs, niches and grottos, which undoubtedly affect the stability of slopes.

Suffosion is only rarely considered in the analysis of landslide activity. Suffosion landslides are described in regions with alternating of horizons of unsaturated and saturated sands, loams and clays in section.

Displacement of saturated soil masses occurs as a result of sediment removal and the subsequent collapse of suffosion niche sides associated with it. Suffosion landslides develop regressively in the form of successive cycles of cavity or niche collapse. Resulting unstructured masses move (as flows) in the direction of the surface slope. At the landslide head, sub-vertical movements often prevail over horizontal movements when displacement occurs.

Signs of suffosion landslide genesis are: (1) the presence removal fans comprising fine material at the base of slope and extending into adjacent territory the contours of which often exceed the landslide boundaries. (2) The presence of a large number of ledges of different size on the surface of the landslide body, formed by irregular subsidence of soil blocks into the roof of suffosion cavities and on the sides of the suffosion niches. Often, when compared to the undisturbed part of the slope, a significant decrease the thickness of suffosion-unstable sandy soils in the landslide body is recorded.

Suffosion landslides are often elongated, horseshoe-shaped, or ∞-shaped with a narrowing in the central part formed in the area of breakthrough of saturated soils from an underground suffosion cavity. The long axis of the suffosion landslide is inherited from the direction of the underground suffosion channel formed in the slope massif.

Thus, suffosion landslides are specific in their development and are characterized by peculiarities of their

displacement. Therefore, in many landslide classification systems, where "suffosion landslides" are recognized as a separate type of displacement, they are referred to a group/class of "complex" or "composite" landslides. Suffosion landslides are divided into several sub-types according to the peculiarities of formation and displacement (Tables 1, 2, 3 and 4).

One of the regions where suffosion landslides are widespread is the East European Plain, which occupies the European part of Russia. The main areas of occurrence of suffosion landslides are confined to the valleys of large rivers and their tributaries (Volga, Oka, Don, etc.), where their volume can be up to several million m^3 (e.g., the landslide of July 12, 1941 on the bank of the Volga). Suffosion landslides are also widespread in the Moscow area. The study of the landslide at "Vorobyovy Gory" site (a complex, multi-storeyed landslide) has shown that suffosion plays a significant role in the formation of the upper tier of landslide blocks. Our simulation and physical modeling confirm the susceptibility of sandy earth materials to suffosion processes.

In conclusions, future development of landslide classification systems should pay attention to suffosion landslides as a separate type of displacement in regions underlain by unconsolidated fine-grained clastic bedrock and surface earth materials.

References

Barykina OS, Zerkal OV, Samarin EN, Gvozdeva IP (2019) The history of slope evolution—primary cause of its modern instability (by Example of the "Vorobyovy Gory" Landslide, Moscow). In: Svalova V (ed). Natural Hazards and risk research in Russia: Innovation and discovery in Russian science and engineering. Springer. pp 345–361 https://doi.org/10.1007/978-3-319-91833-4_24

Barykina O, Zerkal O, Averin I, Samarin E (2021) New data on geological conditions of landslide activity on vorobyovy gory (Moscow, Russia). In: Guzzetti F, Mihalic Arbanas S, Reichenbach P, Sassa K, Bobrowsky PT, Takara K (eds). Understanding and reducing landslide disaster risk. Proceedings of the 5th world landslide forum, vol 2. Springer. pp 143–148 https://doi.org/10.1007/978-3-030-60227-7_15

Cheprasov AF (1972) Landslides and experience of their control. Nizhne-Volzhskoe Book Publ., Volgograd. 88 p. (in Russian)

Cruden D, Varnes DJ (1996) Landslide types and processes. In: Turner AK, Schuster RLE (eds). Landslides: Investigation and Mitigation: Transportation Research Board. Special Report 247. National Academy Press, Washington. pp. 36–75

Hungr O, Leroueil S, Picarelli L (2014) The Varnes classification of landslide types, an update. Landslides 11(2):167–194. https://doi.org/10.1007/s10346-013-0436-y

Hutchinson JN (1981) Slope processes caused by suffosion in the sands. Landslides and debris flows. In: Proceedings of the Alma-Ata Intern Seminar. Center Intern Projects. Moscow. pp. 243–261. (in Russian)

Hutchinson JN (1988) General Report: Morphological and geotechnical parameters of landslides in relation to geology and hydrogeology. Bonnard C (ed). Proceedings of the 5th International Symposium on Landslides. vol 1. Balkema, Rotterdam. pp. 3–35

International Geotechnical Society's UNESCO Working Party on World Landslide Inventory (WP/WLI), 1993aInternational Geotechnical Society's UNESCO Working Party on World Landslide Inventory (WP/WLI) (1993b) A multi-lingual landslide glossary. Bitech Publishers, Vancouver. 59 p.

International Geotechnical Society's UNESCO Working Party on World Landslide Inventory (WP/WLI) (1993b) A multi-lingual landslide glossary. Bitech Publishers, Vancouver. 59 p.

Istomina VS (1957) Filtration stability of soils. Gosstroyizdat, Moscow. 295 p. (in Russian)

Khomenko VP (2011) Suffosion landslides and their danger to civil engineering. Ind Civil Eng 11:11–13 (in Russian)

Klevtsov IA (1964) Landslides of the North Caucasus, their types, conditions of formation, and mitigation measures. Landslides and their control. Proceedings of the North Caucasian Seminar on the study of landslides and experience of their control. Stavropol Books Press. pp 85–130. (in Russian)

Kotlov FV (1962) Changes of natural conditions of the territory of Moscow. AS USSR Press, Moscow.263 p. (in Russian)

Locat A, Leroueil S, Bernander S, Demers D, Jostad HP, Ouehb L (2011) Progressive failures in eastern Canadian and Scandinavian sensitive clays. Canadian Geotech J 48:1696–1712

MartinVF (1911) Landslides of the right bank of the Volga near Volsk town within the limits of Ryazansko-Uralskiy railway station. Bulletin Volsk of Ryazansko-Uralskiy railway (Vestnik Saratov branch of Russian Technical Society). 5:229–249 (in Russian)

McRoberts EC, Morgenstern NR (1974) The stability of thawing slopes. Canadian Geotech J 11:447–469

Mitchell RJ, Markell AR (1977) Flow slides in sensitive soils. Canadian Geotech J 9:11–31

Pavlov AP (1898) On the relief of the plains and its changes under the influence of groundwater and surface water. Earthscience V (in Russian)

Pavlov AP (1903) Landslides in the Simbirsk and Saratov Volga region. Moscow Univ. Press. Moscow. 124 p. (in Russian)

Rodionov NV (1939) On the issue of the classification of landslide phenomena. Trudy [Memory] of Moscow Geologo-Razvedochnogo Instituta. vol XV, pp 197–205. (in Russian)

Rodionov VE (1937) Scheme for the classification of landslide phenomena on the Black Sea coast of the Caucasus by morphological and genetic characteristics. Razvedka Nedr. 22:19–34 (in Russian)

Rogozin IS, Dunaeva GV (1962) Landslides in the Saratov Volga region. AS USSR Press, Moscow, 163 p. (in Russian)

Rogozin IS, Kiseleva ZT (1965) Landslides in the Ulyanovsk and Syzran Povolzhye. Nauka, Moscow, 159 p. (in Russian)

Tikhvinsky IO (1988) Assessment and forecast of the stability of landslide slopes. Nauka. Moscow, 144 p. (in Russian)

Varnes DJ (1978) Slope movement types and processes. In: Schuster RL, Krizek RJ (eds). Landslides, analysis and control: transportation research board. Special Report 176. National Academy of Sciences, Washington. pp 11–33

Vasilevsky MM (1929) On some landslides in Saratov Volga Region. Izv Geol Com. XLVIII(8):152–160. (in Russian)

Zerkal OV, Strom AL (2017) Overview of landslides distribution in Russian Federation and variation of their activity due to climatic change. In: Ho K, Lacasse S, Picarelli L (eds). Slope safety preparedness for impact of climatic change. Balkema, pp 253–288

Zerkal OV, Strom AL (2021) Classification of cryogenic landslides and related phenomena (by Example of the Territory of Russia). In:

Arbanas Z, Bobrowsky PT, Konagai K, Sassa K, Takara K (eds). Understanding and reducing landslide disaster risk. Proceedings of the 5th world landslide forum, vol 6. Springer. pp 377–383 https://doi.org/10.1007/978-3-030-60713-5_37

Zolotarev GS, Janič M (1980) A method of engineering-geological studies of the high rockfall and landslide slopes. Moscow University Press, Moscow. 184 p. (in Russian)

In Situ Triaxial Creep Test on Gravelly Slip Zone Soil of a Giant Landslide: Innovative Attempts and Findings

Qinwen Tan and Huiming Tang

Abstract

In recent years, numerous landslides catastrophes have occurred, generating considerable financial losses and other tolls. The deformational and mechanical properties of sliding zone soil would be of primary significance to landslide research, as the sliding zone basically controls the initiation and mobility of the landslide. An in situ triaxial test was carried out on a sample from the sliding zone of the Riverside Slump 1# landslide, a subdivision of the Huangtupo landslide in the Three Gorges area of China. The test results indicate that **a**. the sliding zone exhibits low compressibility due to the high rock content (54.3%) and long-time consolidation by the overlying soil mass; **b**. only decaying creep occurs without abrupt failure, and a constitutive equation with both linear and nonlinear viscoplastic terms is deduced to accurately fit the test data; **c**. the surface with an orientation of 35° presents anisotropic traits in terms of displacement, possibly due to cracks that formed at similar orientations within the sample cube; and **d**. the creep behavior of the landslide may be closely related to the properties of the sliding zone soil. When a similar stress magnitude to that of the in situ stress environment is applied to the sample, the sliding zone soil behavior matches the landslide behavior. The test results indicate that the Huangtupo 1# landslide will continue to creep, as interpreted from the deformation and properties of the sample. However, unavoidable limitations of the test and extreme external factors, namely, unexpected rainfall and water fluctuation, cannot be ignored.

Keywords

In situ triaxial creep test • Sliding zone soil • Constitutive law • Anisotropic deformation

1 Introduction

The sliding zone of a landslide has been recognized as a critical part that controls the initiation, motion, and even morphology of the landslide. Owning to its significance, studies on the properties of sliding zone soil were common throughout the past few decades, with the intention of gaining a better understanding and control of landslides. Traditional testing measures utilized on the sliding zone soil basically consist of shear tests (direct shear and ring shear) and triaxial tests, and most of these tests were conducted as indoor experiments. Indoor experiments have been long recognized due to superiorities such as convenient operation and accuracy control, but flaws inevitably exist, mainly due to the following aspects: **a**. the samples are structurally disturbed (loss of in situ stress); **b**. the sample constituents are usually changed by screening to achieve a finer mixture; and **c**. the sample size. These flaws have raised the concerns for researchers, who have tried various measures to address them. Boldini et al. (2009) conducted large-scale ring shear tests with a DPRI-6 ring shear apparatus developed at the Disaster Prevention Research Institute (DPRI), Kyoto University, to more accurately analyze tsunamigenic landslides. Jiang et al. (2016) emphasized the structure of the sliding zone soil by means of computed tomography (CT) scanning on undisturbed coarse-grained soil and mechanical testing on fine-grained soil. On the other hand, Pirone et al. (2015) and Tang et al. (2014) both intended to reduce experimental errors by combining indoor tests and in situ monitoring to more accurately predict landslides.

Soil deformation develops over time and ultimately ceases, depending on the applied stress magnitude, and this

Q. Tan · H. Tang (✉)
Badong National Observation and Research Station of Geohazards, China University of Geosciences, Wuhan, 430074, China
e-mail: tanghm@cug.edu.cn

Q. Tan
e-mail: tanqinwen@cug.edu.cn

I. Alcántara-Ayala et al. (eds.), *Progress in Landslide Research and Technology, Volume 1 Issue 2, 2022*, Progress in Landslide Research and Technology,
https://doi.org/10.1007/978-3-031-18471-0_9

process is time consuming. Consolidation theories of the early ages rarely consider the time factor; however, stress and strain always increase with time. Thus, stress–strain equations that do not consider time cannot accurately describe the soil deformation. In this sense, creep test has become increasingly necessary to investigate soil properties, including deformation traits and constitutive laws. Wahls (1962) conducted sets of soil compression tests under diverse loading rates, and the results showed that the primary consolidation was a time-dependent deformation, revealing that creeping also occurred during primary consolidation. Kabbaj et al. (1988) carried out in situ consolidation tests at various low strain rates and a series of indoor tests at normal strain rates, then discovered that the in situ tests exhibited larger deformations than those of the indoor tests. Notably, the above conclusions were drawn only through creep tests that were conducted with a sufficient time duration. Deformation occurs not only during an increase in stress but also during the consolidation and water drainage under constant stress; this trait of the creep test distinguishes creep from normal deformation. These fundamental discoveries have motivated numerous studies on creep tests in recent years, and deeper knowledge of the sliding zone soil properties and deformation has been achieved (Chang et al. 2021; Liao et al. 2021).

In recent years, studies on soil deformation traits and stress–strain relationships have become increasingly prevalent (Amiri et al. 2016; Miao et al. 2022), as soil behavior under external forces undoubtedly have a significant impact on engineering practices. However, most stress–strain relationships were determined in laboratories, where in most cases, the soil was disturbed, and the sample was remolded. The internal structure of the sliding zone soil mainly originates from the long-time consolidation that makes the soil matrix dense and cohesive; if the soil is remolded, loss of internal structure usually leads to a decrease on the strength. This is noteworthy for the sliding zone soil, which is usually buried deep beneath the slope surface, and therefore the consolidation degree is significant. This question has been discussed by Chen and Liu (2014) who carried out in situ tests and found that the in situ residual strength was less than the peak but greater than the residual strength measured in the laboratory. Similar results were reached by Wen et al. (2016) and Gao et al. (2010), who compared in situ test results with lab test results and reached the same conclusions. Therefore, neglecting the structure destruction would lead to overestimation of the deformation and, as a result, descriptions from the constitutive model may incorporate some errors.

In this paper, the deformation response of sliding zone soil was investigated by means of triaxial testing, in which the soil sample remains undisturbed. This is an innovative approach used to learn more about the soil behavior in its natural environment. To implement this testing scheme, a testing tunnel in the Three Gorges area, China, was utilized as the in situ testing site; at this site, the sliding zone of the Huangtupo 1# landslide is exposed.

2 Materials

2.1 The Huangtupo Landslide

The Huangtupo landslide is the largest reservoir landslide located on the south bank of the Yangtze River in the Three Gorges area of China (see Fig. 1a). The landslide is developed in the strata of the Middle Triassic Badong Formation (T_2b^2 and T_2b^3) and is mainly composed of mudstone, pelitic siltstone, and argillaceous limestone. The crown elevation of the landslide is approximately 600 m.a.s.l (meter above sea level), while its toe varies from 50 to 90 m but is submerged by the Yangzte River (Fig. 1c). The landslide has a volume of nearly 70 million m^3 and covers an area of 1.35 km^2, identified as the largest and most complex landslide in the TGR area of China. The Huangtupo landslide is a large composite deformation body composed of multiple landslides of different stages. It occurs under the influence of specific environmental geological conditions and external dynamic factors and evolves through long-term geological history. Based on previous studies, a landslide geotechnical model is established (Fig. 2), where the effects of rainfall, reservoir water, weak interlayer and cracks on landslide were briefly revealed.

Four sublandslides can be recognized based on geomorphic features and evolution history in the slope, namely, the Riverside Slump 1#, Riverside Slump 2#, Garden Spot Landslide and Substation Landslide, and the spatial relationships among the sliding surfaces of the four sliding masses were shown in Fig. 1b. Monitoring data (from GPS and borehole inclinometers) indicate that Riverside Slump 1# has deformed the most, meaning that it has the highest risk of failure. Therefore, a group of tunnels under the Riverside Slump 1# were constructed in 2010 (Tang et al. 2015; Hu et al. 2012a, b) to expose the landslide structures, carry out tests, and install monitoring instruments. The tunnel group is composed of a main tunnel and five branch tunnels (BR-1 to BR-5) (Fig. 1b). The test focused in this paper was carried out at the end of BR-3, where the sliding zone soil was exposed (presented in Fig. 1c); other four branch tunnels were not considered for the test mainly due to either not reaching the sliding zone or inconvenient testing environment.

According to the exposure by the main tunnel, the No. 1 landslide is a typical bedding landslide. The material

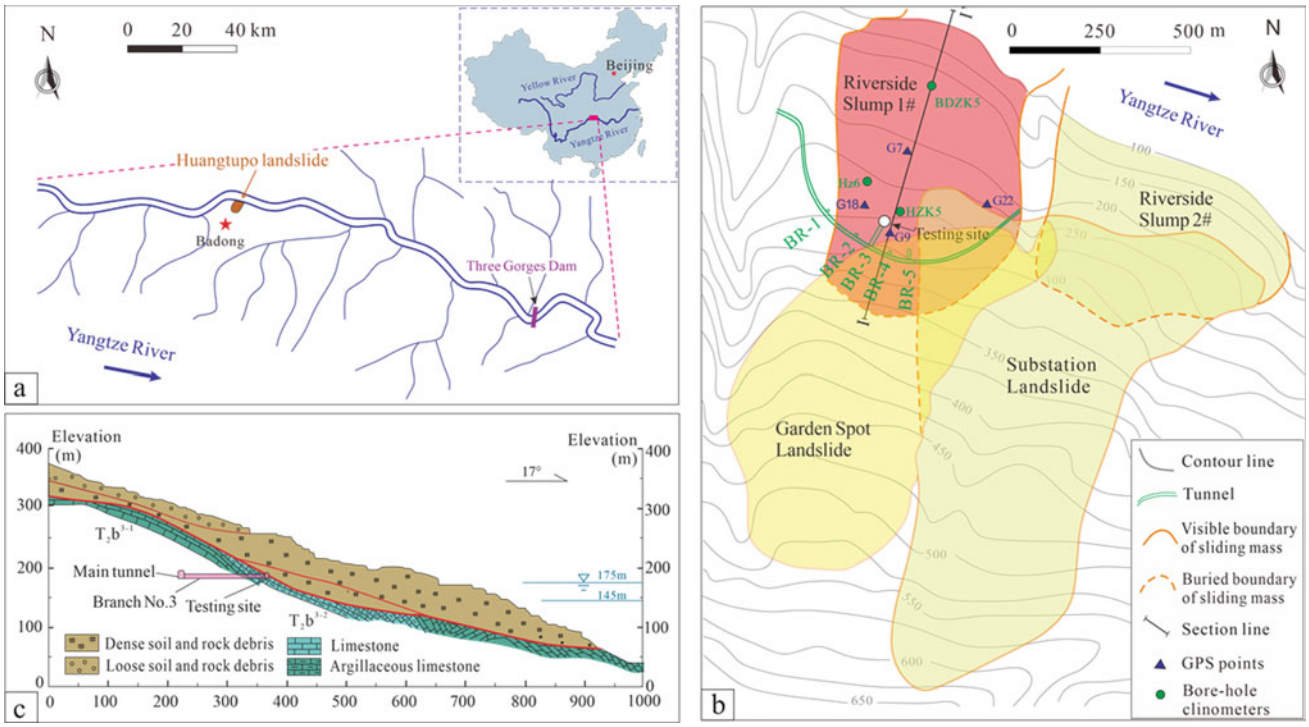

Fig. 1 **a** Location of the study area. **b** Plan of the Huangtupo landslide. **c** I-I' profile of the riverside slump 1#

composition of the landslide mass is mainly gravelly soil and block from the third segment of the Badong Formation (T_2b^3). Information of the main tunnel reveals that the gravelly soil of the No. 1 landslide mass is brown red and medium dense. The gravel is argillaceous limestone, light grey, gray yellow and strongly weathered. The particle size of gravel is 5–20 cm with the content about 30–60%. Rock blocks are locally visible, which are composed of argillaceous limestone and limestone of grey-green and blue-grey color. The soil is silty clay, brown red, plastic to hard plastic state, and the ratio of soil to rock is 2:8–3:7. As exposed by the test tunnel and boreholes, the contact between the sliding zone and bedrock is mostly in bedding mode, and the contact interface with underlying bedrock is obvious, where the interface is clear and the phenomenon of cutting layer is locally seen. The boundary between the sliding zone and the overlying landslide body is not clear, showing a gradual transition state. The sliding zone is composed of silty clay with gravel and debris. Its thickness varies from 50 to 100 cm, and the ratio of soil to rock is 6:4 to 8:2. The composition of gravel and fragment is argillaceous limestone with a diameter of 1–5 cm, mostly in the form of grinding circle-sub-angular. The bedrock of the No. 1 landslide belongs to the third segment of the Badong Formation (T_2b^3) in the middle Triassic. The rock mass integrity is good, it is medium-thick layer with a thickness of about 20–40 cm. And the landslide and material properties of soil and rocks is shown in Fig. 1c.

2.2 Evolution Mode of the Landslide

Figure 2 presents a schematic of evolution process of the Huangtupo landslide (Tang et al. 2015; Deng et al. 2017). Along the axes of the Guandukou Syncline (Fig. 3a), the dip-slope of the Huangtupo landslide emerges and evolves into a gravitationally unstable state. The slope will keep stability to avoid fully sliding until it is deformed by the precedent long-term gravitational deformation (PLTGD) of toppling and deep-seated creep (Fig. 3b). The PLTGD gradually reduces the integrity and strength of the rock mass, and this reduction process will continue and deteriorate under the role of the river cut. When the integrity and strength of the rock mass are reduced to a certain extent that insufficiently maintains the slope stability, large-scale landslides occur, which we call pre-landsides as shown in Fig. 3c. Subsequently, the Huangtupo landslide undergoes long-term dismantling under the influence of river erosion, rainfall, and river water fluctuation (Fig. 3d).

3 Methodology

3.1 Instrument Employed for the Test

The YXSW-12 instrument was used for the test, which was developed jointly by the Changjiang River Scientific Research Institute (China) and Zhaoyang Experimental

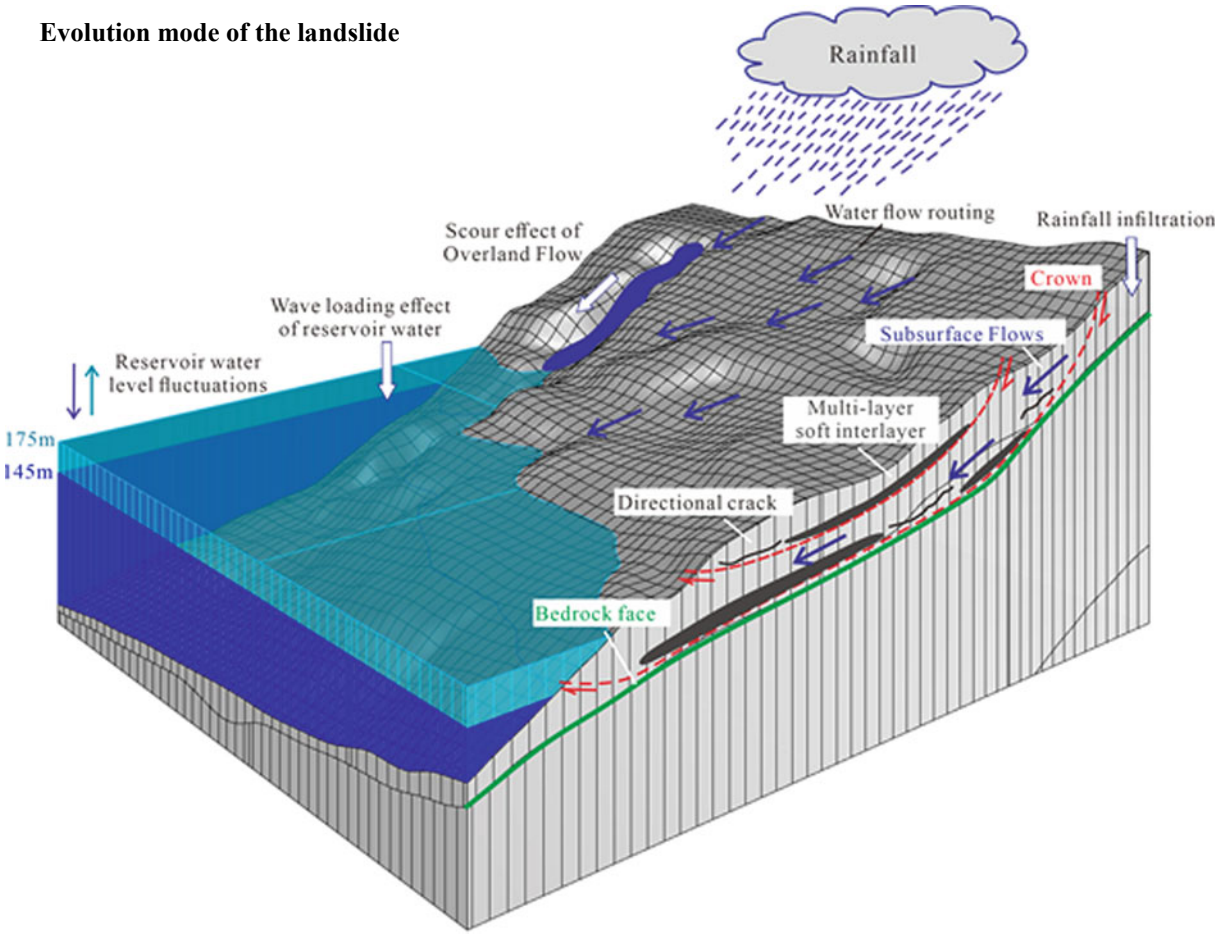

Fig. 2 Geotechnical model and triggering factors

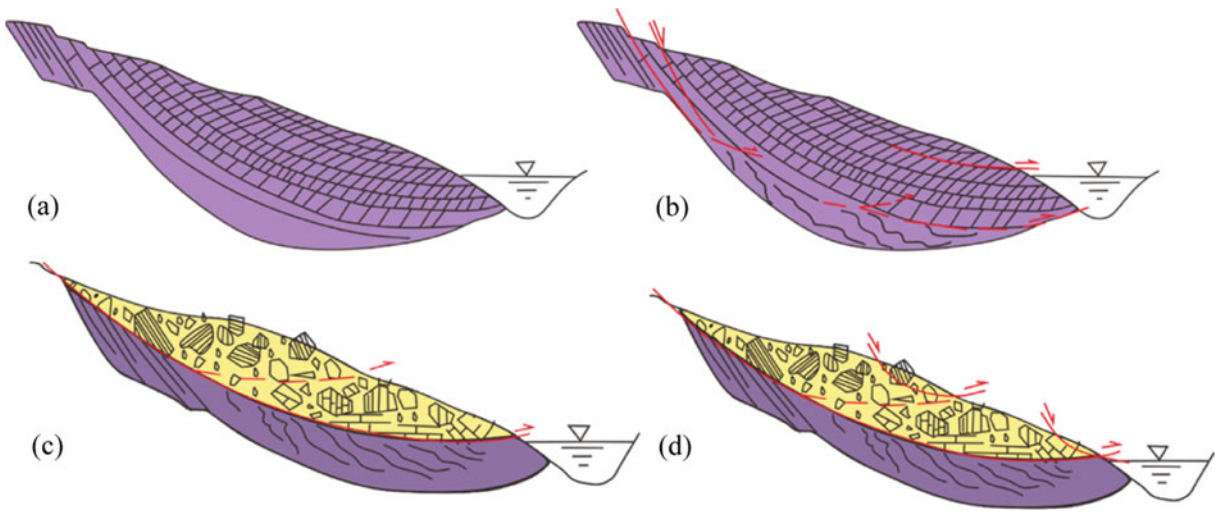

Fig. 3 Evolution mode of the Huangtupo landslide

Instruments Co., Ltd. (China). The testing system comprises. **a**. components such as a vertical loading unit (jack), horizontal loading unit (hydraulic pressure pillow), deformation gauge and counterforce frame, as plotted in Fig. 4, and **b**. a power and control unit, composed of a personal computer (PC) that acts as a command center and collects data, an

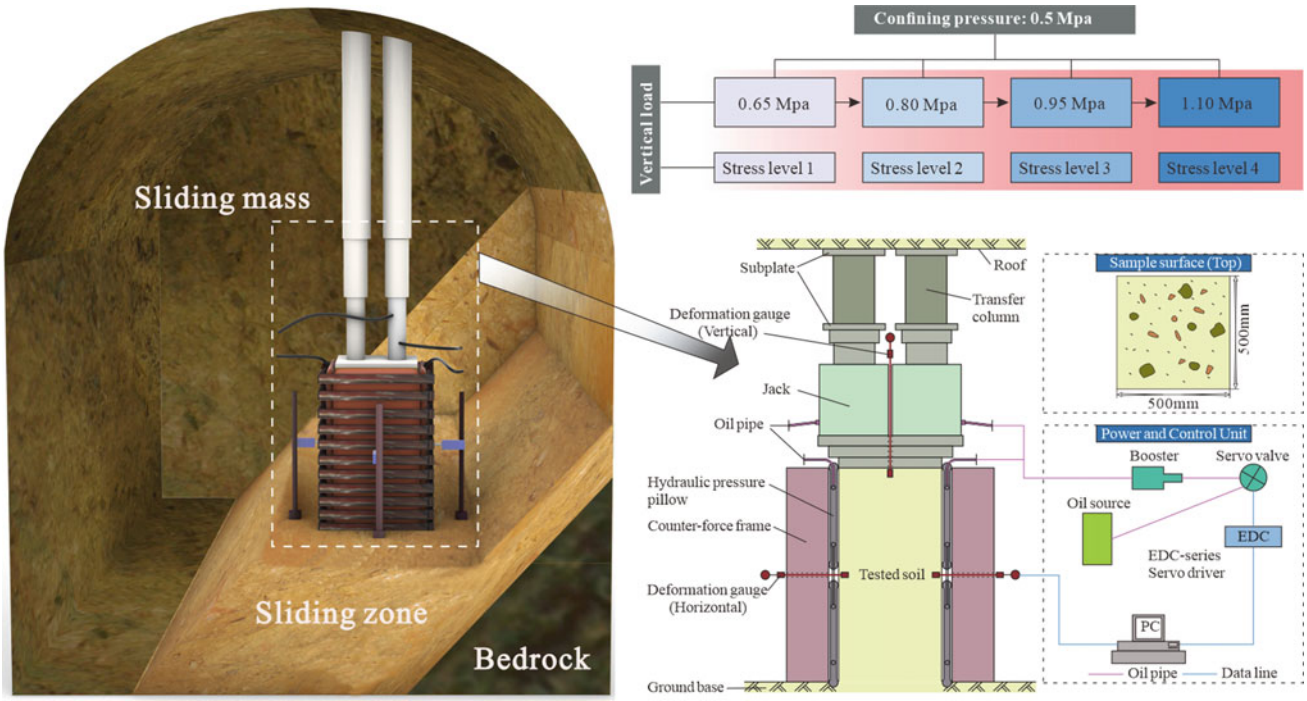

Fig. 4 Structural representation of the YXSW-12 instrument

EDC-series servo driver for converting and transmitting the signals, and a servo valve, booster and an oil source for supercharging the vertical and horizontal loading units.

Specifically, the hydraulic pressure pillow expands when charged with oil and exerts forces on the soil sample. Horizontal deformation could occur as the pillows would be compressed to deformation under the forces from the creeping soil; during this process, the horizontal pressure would be held constant by the computer-servo system. Specifically, the applied stress would be kept constant using a system that has a stress compensation system. The system runs with the connected line of PC, the EDC, the servo valve and the booster. When the actual stress changes because of external factors, e.g. soil compression and horizontal expansion, the compensation system will automatically detect and then compensate or discharge the pressure by adding or discharging the used oil. The system has also been successfully employed in previous tests by its creation team (Zhang et al. 2011).

The tested cuboid sample had a height of 1000 mm and a cross-sectional area of 500 mm × 500 mm, as presented in Fig. 3. The soil was cut out of the horizontally enveloping soil blocks using a procedure that reduced the disturbance to the soil, and the bottom surface of the cuboid remained connected to the base soil. The four vertical planes of the sample were oriented at 35°, 125°, 215° and 305°, wherein the 35° plane was approximately oriented parallel to the moving direction of the landslide (as plotted in Fig. 5).

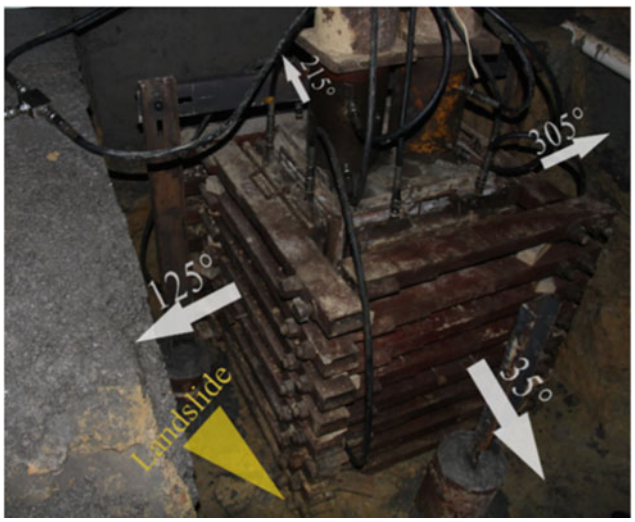

Fig. 5 Orientations of each testing surface and the landslide

3.2 Loading Scheme and Test Result

The loading scheme is described using a flow chart, presented Fig. 4. For the vertical stress series, it was set according to the overlying load of the sliding zone soil; for the lateral stress, it was determined by in situ measurement. The confining pressure was set according to the measured initial ground stress. Therefore, the confining pressure was kept at 0.5 MPa during the test, and the vertical pressures of

0.65 MPa, 0.80 MPa, 0.95 MPa and 1.10 MPa were sequentially applied. The loads, starting with stress level 1, were instantaneously applied on the top surface of the sample, and the subsequent level of stress would be applied when the increase in displacement approximately ceased.

4 Results

4.1 Deformation Results and Characters

Deformations of the five sample faces were simultaneously detected by deformation gauges (marked in Fig. 4), and the resultant curves are plotted in Figs. 6, 7 and 8. Figure 6 presents the displacement development under stress level 1, in which each face first undergoes an instantaneous elastic deformation and then undergoes an attenuating creep.

Specifically, the 35° face quickly deforms by 7 mm in approximately 15 h and then begins an attenuating phase until reaching a steady value at 17.3 mm. The 125°, 215° and 305° faces deform much like the 35° face, although the magnitudes vary; the total displacements are 1.2 mm, 5.9 mm and 6.3 mm, respectively. Reasons giving rise to the anisotropic deformation traits of the surfaces would be later discussed in the section "Anisotropic deformation".

The vertical deformation curve from this test also undergoes a linear increase followed by an attenuating creep phase, but the linear phase continues for a much larger time than that of the other faces, nearly 350 h. In total, the vertical displacement during stage 1 (under stress level 1) is 13.6 mm. This phenomenon is unique and can be explained by the following observations. The unsaturated soil undergoes water drainage and volume change under applied forces; therefore, the stress would be transferred to the soil matrix as the water drains out, and the deformation ultimately ceases. This represents a general consolidation process. In this test, the transient vertical loading on the sample induces a fast pore pressure increase, which concentrates near the loading surface.

As shown in Fig. 4, stress levels 2 and 3 were applied vertically and in succession when the displacement in the former stage had approximately ceased. Figure 7 presents the displacements of all the faces in stage 2 (stress level 2), and Fig. 8 shows the results from stages 3 and 4 (stress levels 3 and 4). These curves are plotted independently for clarity, as the change in displacement during stages 2–4 are very small. The greatest increases in the deformation curves for stages 2–4 are only approximately 1 mm. Notably, stress levels 3 and 4 respectively equals and exceeds the initial in-situ stress calculated at the embedment depth of the sliding zone. Therefore, the deformation curves generally exhibit attenuation (Wen and Jiang 2017), indicating that only creep happens, and soil failure will not occur no matter how long the creep continues.

4.2 Analysis on the Low Compressibility of the Sample

Two factors mainly account for the low compressibility: a high preexisting compression degree of the soil and a high rock content.

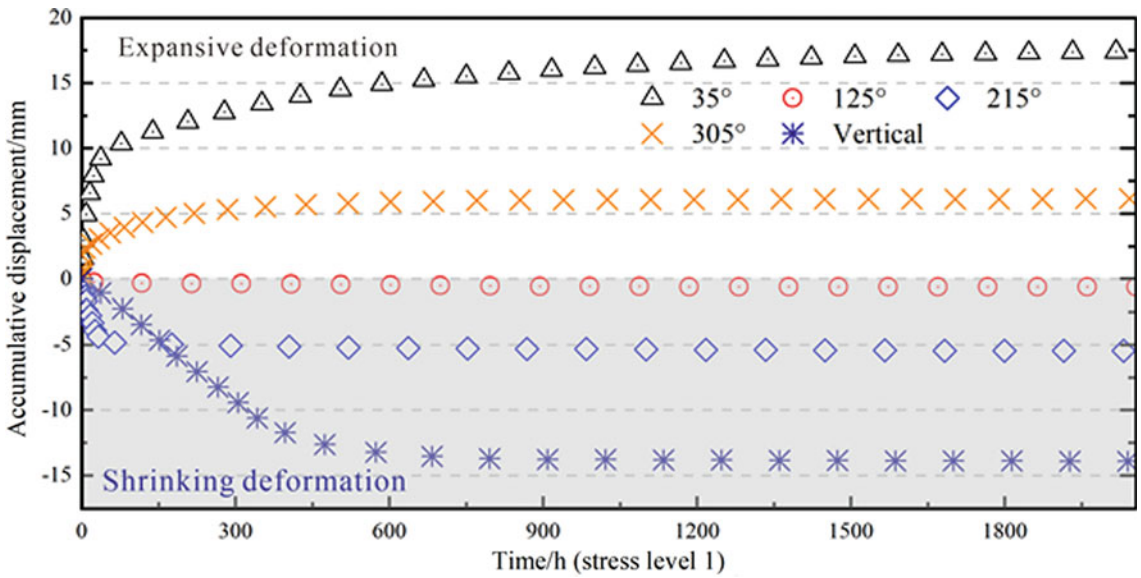

Fig. 6 Displacement–time curves of the 5 surfaces under stress level 1. Negative values indicate shrinking deformation, which is discussed in the section "Anisotropic deformation"

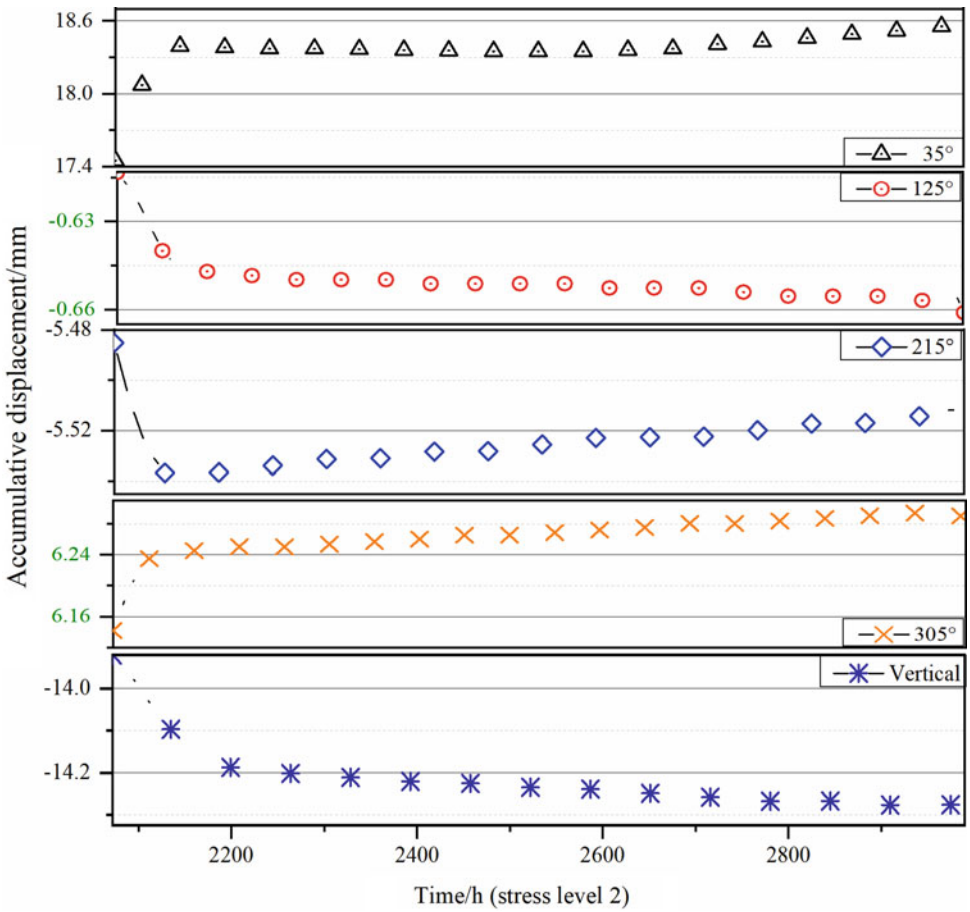

Fig. 7 Displacement–time curves of the 5 surfaces under stress level 2

(a) **High preexisting compression degree**

For clay samples, the primary consolidation that normally occurs due to external pressure would stop once the excess pore water pressure has dissipated. However, continuous forces on the soil would ultimately lead to secondary consolidation, enhancing interparticle forces and solidifying some cementing constituents. Clay that undergoes secondary consolidation usually exhibits a higher compression modulus and bears capacity in engineering applications, behaving like "old clay," which refers to clay that formed earlier than the late Pleistocene (Li 2004).

Figure 9 presents two void ratio (e) reduction curves (blue) developing with various geological times for the same clay. In Fig. 9, P0 is the applied force for normal consolidation, and e_0 is the final void ratio; P_{cq} is a greater stress applied on identical soil, and e_0' equals e_0. The results indicate that compression to T_0 under P_0 takes 10 thousand years; however, under the higher pressure Pcq, the time required to reach the same e value (T_{cq}) decreases to less than 0.1 year. Similarly, P_{cq} and P_0 curves can serve as a laboratory normally consolidated soil case and a historical consolidation case, respectively. A greater force is needed in the laboratory to reach the density equal to that in historically consolidated soil. We call such historically consolidated soil quasi-over consolidation (QOC) soil, with its quantitative parameter defined as:

$$QOCR = P_0/P_{cq} \tag{1}$$

where QOCR denotes the quasi-over consolidation ratio.

The Riverside Slump 1# has a deep-seated sliding zone; consequently, the compressibility of the sliding zone soil tends to be smaller than that of a normally consolidated soil from a laboratory experiment, as QOC can create a denser soil structure.

(b) **High rock content**

Rock content considerably affects soil compressibility. Xu et al. (2009) discovered, after testing samples with rock contents of 30%, 40%, 50% and 60%, that the uniaxial compressive strength (UCS) of soil samples increases with the rock content. Tests by Li and Wang (2004) showed that gravelly soil with low rock contents (<30%) behaved like a fine-grained soil; conversely, gravelly soil with high rock contents (>60%) behaved like a rock mass.

In this test, the rock blocks generally have a sparse to dense distribution from the sample top to the bottom, and the total

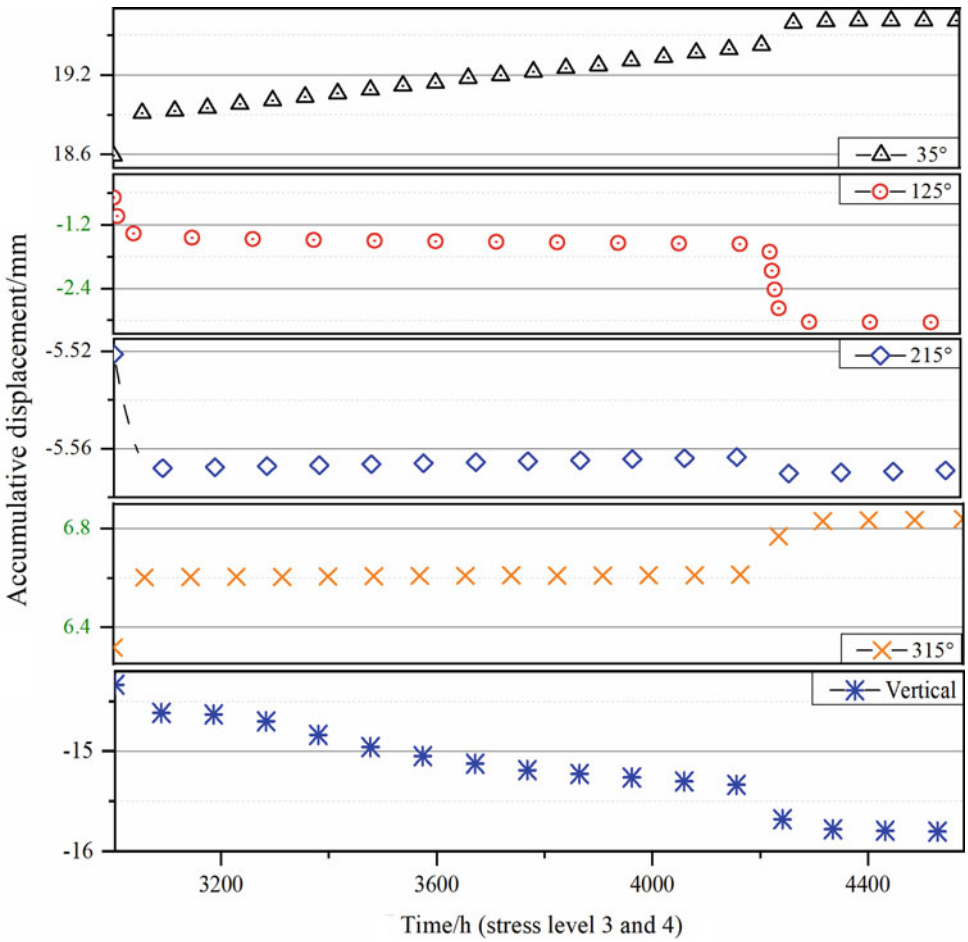

Fig. 8 Displacement–time curves of the 5 surfaces under stress levels 3 and 4

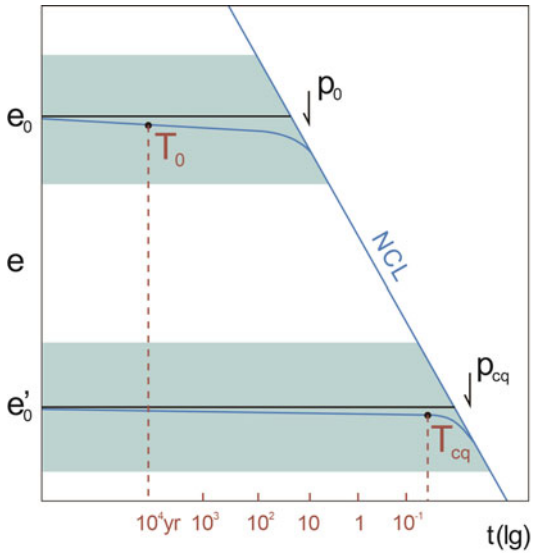

Fig. 9 Void ratio (e) reduction curves developing with various geological times, where NCL denotes the natural consolidation line (based on Li 2004)

rock content (particle diameter > 5 mm) reaches 54.3% in the sample cube. Therefore, the cube is characterized as gravelly soil with inhomogeneously embedded rock blocks. As demonstrated by previous studies, the compressibility of soils decreases with the increase in rock content in the soil mass, due to the following reasons: a. When neighboring rocks obstruct each other during shearing, the soil movement is locked. b. Peculiarly located rocks have the potential to block the development of shear zones and cracks. Some test results suggest that once the rock content exceeds 50%, the largest rocks in the soil generally determine the shear zone shape and location, and mechanical properties (Xu et al. 2009).

4.3 Constitutive Law

The semi-empirical and semi-theoretical model, which combines element model and empirical model, is established based on the analysis of the creep characteristics of sliding zone soil samples in the in situ test, and can describe the

nonlinear creep characteristics of sliding zone soil well. As indicated by Figs. 6, 7 and 8, the in-situ compression creep test exhibits typical attenuated creep characters, where total strain is normally separated into the linear viscoplastic element and the nonlinear viscoplastic element. Specifically, the linear viscoplastic element is reflected by the assembly of rheology bodies frequently used for studying soil behavior; empirical equations will be introduced to describe the nonlinear viscoplasticity, which cannot be described by the rheology bodies.

Viscoelastic deformation is not incorporated in the constitutive equation as an independent term because it is not clearly displayed in the deformation data, which usually exhibits apparent linearity. Reasons of lacking the viscoelastic deformation may well the due to the pre-existing vertical pressure on the sample from the overlying soil, which had lasted long during the historical period. Elastic deformation already occurred in the historical period, but no obvious rebound took place owning to the creep generated by the long-time vertical load acting on the soil. Thus, the long-time and high-intensity compression on the soil caused irreversible creep that may account for a considerable proportion of the deformation. Consequently, the configuration is shown in Fig. 10, where a term of linear viscoplasticity and a term of nonlinear viscoplasticity are connected in series (Wang 2007; Zheng 2016); notably, the linear viscoelasticity term (dashed) is excluded from the constitutive equation.

4.4 Expression of the Constitutive Model

The constitutive equation is deduced based on the element configuration given in Fig. 10. Based on previous studies, the linear viscoplasticity term can be written as:

$$\varepsilon_l = \frac{\sigma - \sigma_s}{E_l}\left(1 - \exp\left(-\frac{E_l}{\eta_l}t\right)\right) \tag{2}$$

where E_l and η_l denote the elasticity modulus and viscosity coefficient of the rheology bodies, respectively. σ_s denotes the yield stress of the soil.

On the other hand, the nonlinear viscoplasticity term can be expressed by an empirical model that reflects such deformation traits. Empirical models frequently adopted for describing the rheological behavior generally include the power function, exponential function and logarithmic function. Specifically, the power function is usually used for reflecting the decaying creep; the exponential function, for steady creep; and the logarithmic function, for accelerating creep. In this sense, the power function is selected to describe the decaying creep in this test, expressed as

$$\varepsilon_n = \left(\frac{\sigma - \sigma_s}{A}\right)^m \tag{3}$$

where $m = 1/m'$ and $m > 1$.

Nonlinear viscoplastic creep relaxes with time; thus, A and m in Eq. (3) should be time-related parameters, which can be written as:

$$A = A(t), \quad m = m(t) \tag{4}$$

$A(t)$ can also be represented by a power function (Sun 1999), which can be expressed as:

$$A(t) = A_0 t^{-\alpha} \tag{5}$$

Then, Eqs. (3) and (5) are combined so that the nonlinear viscoplasticity term can be finally obtained:

$$\varepsilon_n = \left(\frac{\sigma - \sigma_s}{A_0 t^{-\alpha}}\right)^m = \left(\frac{\sigma - \sigma_s}{A_0}\right)^m t^{\beta} \tag{6}$$

where β is the creep index, $\beta = m\alpha$, and A_0 is the nonlinear coefficient of the deformation.

Therefore, the final expression of constitutive law can be obtained through series connection of two terms (Wang 2007; Zheng 2016), with the final relationship obtained as

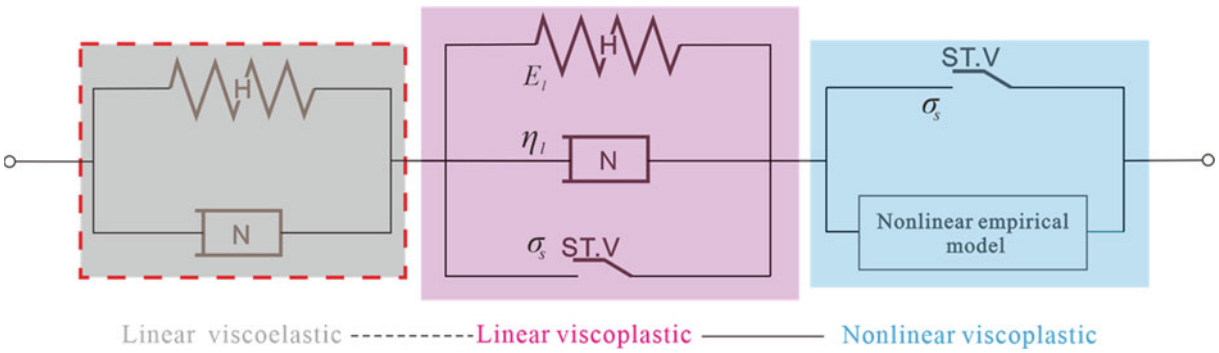

Fig. 10 Configuration of the constitutive equation. The term inside the dashed rectangle is eliminated

$$\varepsilon = \frac{\sigma - \sigma_s}{E_l}\left(1 - \exp\left(-\frac{E_l}{\eta_l}t\right)\right) + \left(\frac{\sigma - \sigma_s}{A_0}\right)^m t^\beta \quad (7)$$

As indicated by Eq. (7), all parameters σ, σ_s, E_l, η_l, A_0, m and β are included. The σ (deviatoric stress) was calculated to be 0.15 MPa by vertical pressure subtracting confining pressure. σ_s is evaluated by fitting the compression model with test results, as this parameter is decided by viscoelastic deformation of testing curve, which is considered nonexistent for the tested soil. E_l (elasticity modulus) and η_l (viscosity coefficient) were recognized from the initial linear segment of the vertical deformation curve. The remaining parameters, namely A_0, m and β, were obtained by fitting with the ***Origin*** and the result is shown in Fig. 11. The coefficient of determination (r^2) turns out 0.9768, indicating that the created model is convictive to match the test data. Therefore, Eq. (7) is ultimately determined to interpret the constitutive law of the tested sample.

It is noteworthy that Eq. (7) is verified employing only the data of the first stage (stress level 1), mainly because those data possess manifest linear and nonlinear courses of deformation, and thus the random errors can be shrunk to the minimum. Further, Eq. (7) is utilized to fit the data respectively of stages 2, 3 and 4, and the data prove to be ideally fitted as well (not displayed in the text).

5 Discussion

5.1 Anisotropic Deformation

The displacement–time curves presented in Figs. 6, 7 and 8 indicate that strain is directionally favoring the 35°, 215°, 305° and vertical surfaces, respectively. Specifically, the 35° surface expands the most among the horizontally oriented surfaces, expanding approximately 3 times the amount of displacement at the 215° and 305° surfaces.

When compressed by vertical stress, the high rock content in the soil would enable the sample to behave like a rock mass. That is, cracks may emerge at locations that have concentrated stress and at the soil-rock interfaces, where the cementation is weakest. For the tested sample, the areas of concentrated stress are generally oriented along the $45° + \phi/2$ direction (marked in Fig. 12), along which the generated shear strength is generally the greatest for a compressed cube. Additionally, as the rock content (particle diameter > 5 mm) reaches 54.3% of the soil-rock mixture, the numerous soil-rock interfaces in the sample induce cracks widely distributed throughout the sample.

The 35° surface is similar to the landslide orientation (see Fig. 5). As has been previously discussed, particles within the sliding zone would gradually align with the sliding direction after long-time creep and movement of the soils

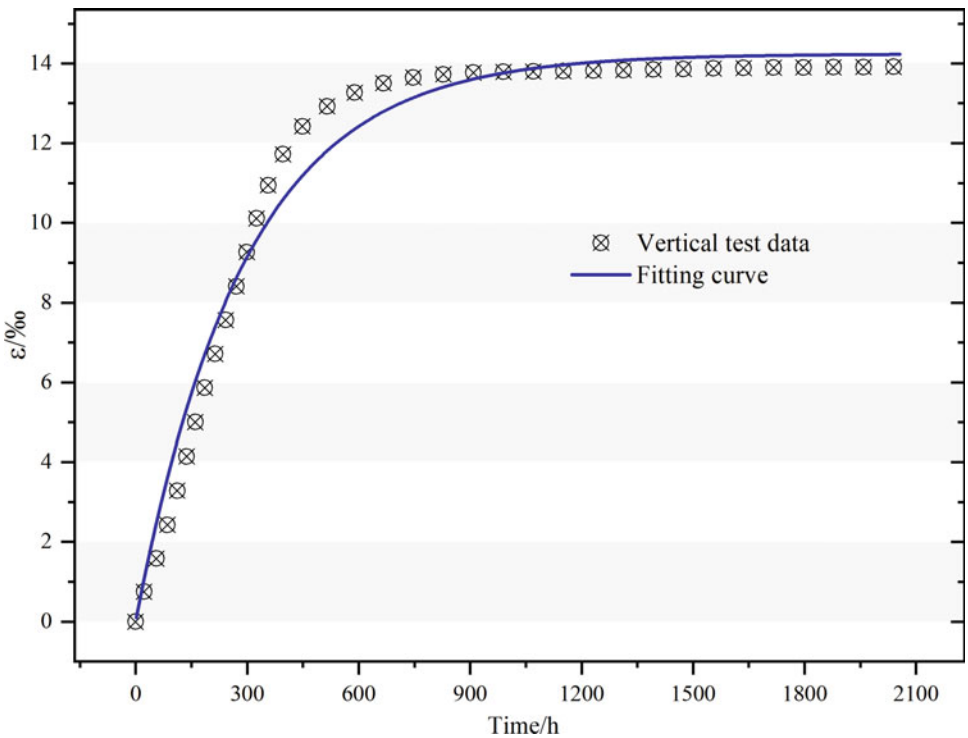

Fig. 11 Fitting result for the intact data during stress level 1

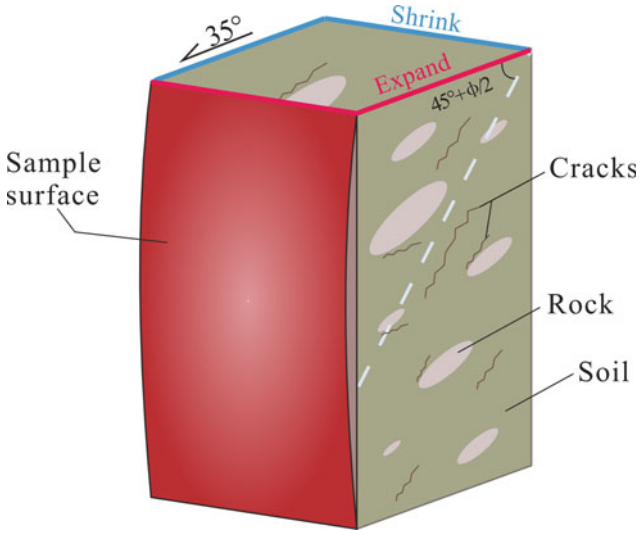

Fig. 12 Schematic diagram showing the deformed 35°-oriented surface of the cube and structures within the cube after testing

and rocks. Therefore, cracks that form at the soil-rock interfaces would also be oriented at 35°, possibly inducing deformation towards this orientation. This explains why the 35° surface deforms much more intensely than the other surfaces.

The 215° surface, however, presents a shrinkage trait (negative displacement in Figs. 6, 7 and 8) under the joint action of a vertical load and constant confining pressure of 0.5 MPa. With respect to the cracks mentioned above, because the soils and rocks generally move towards the orientation of 35°, a shrinkage in that orientation is expected. The 125° and 305° surfaces are also expected to be characterized with a distribution of cracks, which would result in an inhomogeneous shear strength under compression; specifically, orientations of the main cracks (35°) may have components to the orientation of 125°, which is estimated from the intersection angle between the sliding direction and the 35° orientation (plotted in Fig. 5). Therefore, the deformations of these surfaces would be very different.

5.2 Landslide Movement Related to the Sample

The Riverside Slump 1# has been monitored since 2003; various measures including the use of GPS, borehole drilling, and time-domain reflectometry (TDR) have been employed in this monitoring effort. Some monitoring sites on the Riverside Slump 1# are presented in Fig. 1b, c; these sites are distributed not far from tested sample. The monitoring measures shown in Fig. 1b consist of GPS sites and boreholes; specifically, the GPS sites are responsible for detecting deformation of the slope surface, and boreholes were drilled into the sliding zone and instrumented to detect the deformation of the sliding zone. Monitoring data are presented in Fig. 13.

G9 is located above the sample, and the average deformation velocity at this location is 22.97 mm/year, while the average deformation velocities for the data curves in Fig. 13

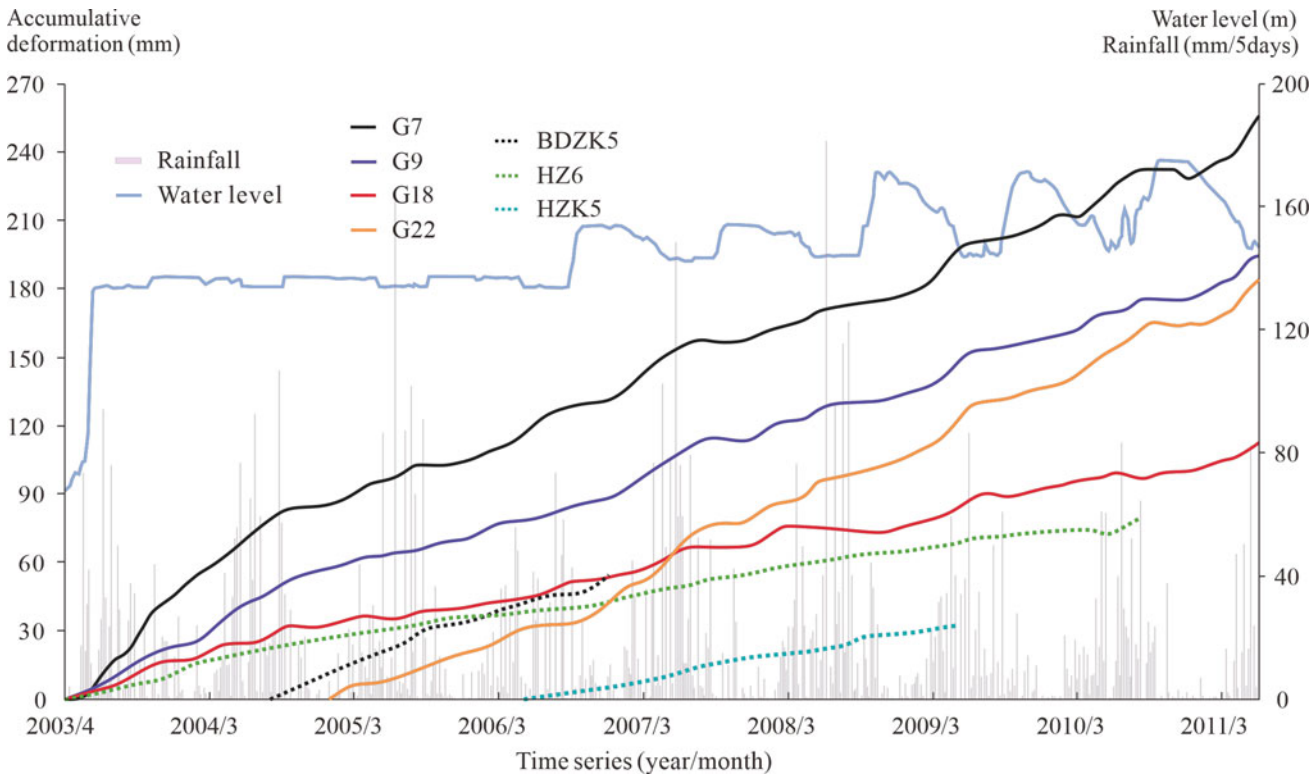

Fig. 13 Time series monitoring data from 2003 to 2011

range from 13.71 mm to 26.78 mm/year. HZK5 extends to the sliding zone soil positioned very close to the tested sample, as clearly marked in Fig. 13 with a dotted line. The calculated deformation velocity at HZK5 is 10.65 mm/year.

The displacement developed under stress level 3 (see Fig. 8) is selected to represent the deformation velocity of the soil cube because the stress applied in the third stage (0.95 MPa) equals the in situ overlying load, which can be estimated from the burial depth and the specific gravity of the tested sliding mass. At this time, the sample enters into a sustained nonlinear viscoplastic phase, consistent with the ordinary state for soil creeping. The calculated velocity is 5.84 mm/year for the 35°-oriented surface, whose normal direction is basically parallel to the landslide direction, as explained in the previous section.

The deformation laws of the soil cube and the sliding zone are compared, as a similar stress environment was considered for both the confining pressures and the vertical loads. Nonetheless, a distinction of approximately 5 mm appears between the detected velocity from HZK5 and the calculated velocity for the sample, even though they are located very close to one another. This phenomenon may be due to external factors, namely, rainfall and water level fluctuations. The impacts of these factors have been demonstrated to be significant for the Huangtupo 1# landslide. Wang et al. (2016) investigated the roles on the deformation of the Huangtupo 1# landslide played by rainfall and water level fluctuation, with the results indicating that approximately half of the total deformation was attributed to rainfall and water level decrease. Therefore, the final velocity to be evaluated must take rainfall and water fluctuation (presented in Fig. 13) into account.

The data indicates, to some extent, that deformation decreases from the landslide surface to the sliding zone. In addition, the landslide undergoes creeping without a high risk of abrupt failure, as determined by the attributes of the sliding zone soil. As previously analyzed, the sliding zone possesses very low compressibility due to its high rock content and high degree of historical consolidation. The applied vertical force, which is even higher than the original stress induced by the overlying soil, cannot cause the abrupt failure of the sliding zone soil. That is, the Huangtupo 1# landslide has been creeping for years, and this will not change under normal circumstances. Nonetheless, extreme conditions for rainfall and water fluctuation in the Three Gorges Reservoir area must be considered, as they may generate problems such as a considerable increase in the hydrodynamic pressure and water content, possibly leading to failure.

However, further discussion is still requested on the topic, that since the sample tested is situated near the mid location of the sliding surface, the corresponding traits may be not representative enough for the intact sliding zone. On this issue, some discussions would be further given in the followings:

(a) The intact sliding zone is embedded beneath the same material of the landslide mass, which can be clearly seen from Fig. 1c. In this sense, it is reasonable to consider that the whole sliding zone soil has no much difference in terms of the deforming traits and mechanism compared with the tested sample.
(b) The landslide has been creeping for years according to data from the monitoring sites, which are installed widely on the landslide surface (Wang et al. 2016). Therefore, creeping keeps occurring throughout the landslide, which is a general character for the whole sliding mass and zone. In this sense, behavior of other locations can be positively analyzed based on the results of this study.

6 Conclusions

An in situ triaxial creep test was carried out for exploring the properties of the sliding zone soil, which is characterized by a high rock content and high degree of compression. The tested sample was located in the tunnel that passes through Riverside Slump 1#, a subdivision of the Huangtupo landslide. The test was completed over 191 days, and the results were then analyzed. The conclusions are as follows:

(a) The tested sample exhibits very low compressibility due to the high rock content (54.3%) and long-term compression exerted from the overlying soil. The dense structure leads to a high strength and stability, resulting only the decaying creep of the creep test.
(b) The constitutive model of the vertical stress–strain-time relationship is discussed and deduced. Linear viscoplasticity and nonlinear viscoplasticity terms are used in series to establish the equation, with which an empirical model (power function) is combined to more accurately describe the nonlinear viscoplasticity. The results show a strong fitting relation between the testing data and the constitutive model.
(c) The anisotropic traits of the horizontal deformation of the sample are discussed. The surface at an orientation of 35° generates much larger displacement than those at the other surfaces, possibly attributable to the alignment of cracks within the sample cube.

The monitored data from HZK5 behave similarly to the measured data from the 35° surface in terms of the velocity of displacement. The data from the GPS sites and boreholes indicate that the Riverside Slump 1# has been creeping over the past years. This creep may be controlled by the properties of the sliding zone: decaying creep occurs and no abrupt failure occurs in the tested sample when stress magnitudes similar to those of the in situ stress environment are applied.

However, unavoidable limitations of the test and extreme external factors, such as unexpected rainfall and water fluctuation in the Three Gorges area, cannot be neglected when evaluating the long-time stability of the Huangtupo Riverside Slump 1# landslide.

Acknowledgements This study was financially supported by the National Key R&D Program of China (grant number 2017YFC1501305), Key National Natural Science Foundation of China (grant number 41230637) and National Natural Science Foundation of China (grant number 41502290 and 41702319).

References

Amiri SAG, Grimstad G, Kadivar M, Nodar S (2016) Constitutive model for rate-independent behavior of saturated frozen soils. Can Geotech J 53(10):1646–1657

Boldini D, Wang FW, Sassa K, Tommasi P (2009) Application of large-scale ring shear tests to the analysis of tsunamigenic landslides at the Stromboli volcano, Italy. Landslides 6(3):231–240

Chang WB, Wang P, Xing AG, Wang HJ, Yu YF, Li XD (2021) Failure mode and dynamic response of loess slopes with tectonic joints under seismic action. Environ Earth Sci 80:531

Chen XP, Liu D (2014) Residual strength of slip zone soils. Landslides 11(2):305–314

Deng QL, Fu M, Ren XW, Liu FZ, Tang HM (2017) Precedent long-term gravitational deformation of large scale landslides in the Three Gorges reservoir area, China. Eng Geol 221:170–183

Gao ZB, Gao YF, Tan HM (2010) Lab and in-situ tests on maximum dynamic shear modulus of saturated clay soils. Chin J Geotech Eng 32(5):731–735 (in Chinese with English abstract)

Hu XL, Tang HM, Li CD, Sun RX (2012a) Stability of Huangtupo I# Landslide under Three Gorges Reservoir Operation. Appl Mech Mater 170-173:1116–1123

Hu XL, Tang HM, Li CD, Sun RX (2012b) Stability of Huangtupo Riverside Slumping mass II# under water level fluctuation of Three Gorges Reservoir. J Earth Sci China 23(3):326–334

Jiang JW, Xiang W, Rohn J, Schleier M, Pan JJ, Zhang W (2016) Research on mechanical parameters of coarse-grained sliding soil based on CT scanning and numerical tests. Landslides 13(5):1216–1272

Kabbaj M, Tavenas F, Leroueil S (1988) In situ and laboratory stress–strain relationships. Géotechnique 38(1):83–100

Li GX (2004) Advanced soil mechanics. Tsinghua Press, Beijing (in Chinese)

Li SH, Wang YN (2004) Stochastic model and numerical simulation of uniaxial loading test for rock and soil blending by 3D-DEM. Chin J Geotech Eng 26(2):172–177 (in Chinese with English abstract)

Liao K, Wu YP, Miao FS, Li LW, Xue Y (2021) Effect of weakening of sliding zone soils in hydro-fluctuation belt on long-term reliability of reservoir landslides. Bull Eng Geol Env 80(6):3801–3815

Miao FS, Zhao FC, Wu YP, Li LW, Xve Y, Meng JJ (2022) A novel seepage device and ring-shear test on slip zone soils of landslide in the Three Gorges reservoir area. Eng Geol 307:106779

Pirone M, Papa R, Nicotera MV, Urciuoli G (2015) In situ monitoring of the groundwater field in an unsaturated pyroclastic slope for slope stability evaluation. Landslides 12(2):259–276

Sun J (1999) Rheology of rock and soil materials and its engineering application. China Architecture and Building Press, Beijing (in Chinese)

Tang HM, Li CD, Hu XL, Su AJ, Wang LQ, Wu YP, Criss R, Xiong CR, Li YA (2014) Evolution characteristics of the Huangtupo landslide based on in situ tunneling and monitoring. Landslides 12(3):511–521

Tang HM, Li CD, Xiong CR, Hu XL, Wang LQ, Criss R, Su AJ, Wu YP (2015) Deformation response of the Huangtupo landslide to rainfall and the changing levels of the three Gorges Reservoir. Bull Eng Geol Environ 74(3):933–942

Wahls HE (1962) Analysis of primary and secondary consolidation. ASCE 88(6):207–234

Wang B (2007) Research on the interaction of coupling seepage and stress and deformation of landslide the condition of water level fluctuation. Dissertation, China University of Geosciences, Wuhan, China

Wang JE, Su AJ, Xiang W, Yeh HF, Xiong CR, Zou ZX, Zhong C, Liu QB (2016) New data and interpretations of the shallow and deep deformation of Huangtupo no. 1 riverside sliding mass during seasonal rainfall and water level fluctuation. Landslides 13(4):795–804

Wen BP, Jiang XZ (2017) Effect of gravel content on creep behavior of clayey soil at residual state: implication for its role in slow-moving landslides. Landslides 14:559–576

Wen Y, Yang GH, Tang LS, Xu CB, Huang ZX, Huang ZM, Zhang YC (2016) Tests and parameters study of mechanical properties of granite residual soil in Guangzhou area. Rock Soil Mech 37(Supp. 2):209–215 (in Chinese with English abstract)

Xu WJ, Hu RL, Yue ZQ (2009) Development of random mesostructure generating system of soil-rock mixture and study of its mesostructural mechanics based on numerical test. Chin J Rock Mechan Eng 28(8):1652–1665

Zhang YH, Zhou HM, Zhong ZW, Xiong SH, Hao QZ (2011) In situ rock masses triaxial test system YXSW–12 and its application. Chin J Rock Mech Eng 30(11):2312–2320 (in Chinese with English abstract)

Zheng J (2016) Research on the consolidation properties of saturated remolded clay considering the timeliness. Dissertation, Chang'an University, Xi'an, China

Challenges and Lessons Learned from Heavy Rainfall-Induced Geo-disasters Over the Last Decade in Kyushu Island, Japan

Noriyuki Yasufuku and Adel Alowiasy

Abstract

Recently, heavy rainfall events have been inducing devastating geo-disasters, floods, sediments and debris flows in different regions around Japan, causing severe damage to lives and properties. According to the Intergovernmental Panel on Climate Change (IPCC), the frequency and intensity of localized torrential rainfall events are expected to increase. This study initially highlights the increasing geo-disaster-inducing forces in relation to the deterioration of the social infrastructure and the decline in the labor forces in Japan. Furthermore, several geo-disasters within Kyushu Island, Japan, which seem to occur repeatedly, were analyzed considering the prevailed conditions and the adopted mitigation and prevention protocols. Consequently, the necessity for developing innovative systems and techniques that integrate the academic disciplines in collaboration with the residents and the government was evidently asserted. Moreover, the recent progress in establishing comprehensive geo-hazard vulnerability assessment methods and techniques that consider the regional characteristics, mainly Kyushu and Hokkaido islands, was introduced.

Keywords

Geo-disasters prevention and mitigation • Torrential rainfall • Sediments and debris flow

1 Introduction

On the 5th and 6th of July 2017, a heavy rainfall storm struck Northern Kyushu Island, Japan. The storm affected mainly the Northern parts of Fukuoka prefecture (Asakura City) and Oita prefecture (Hita region). The storm, which the Japanese Meteorological Agency (JMA) named "Northern Kyushu heavy rainfall in July 2017", has caused severe damage to the mountainous area extending between Asakura city and Hita region, Fig. 1. 12-h cumulative precipitation of 511.5, 329.5, and 532 mm were recorded at Asakura meteorological agency observatory, Hita rainfall observation center, and Tsurukawauchi rainfall observatory, respectively. The latter was confirmed to significantly exceed the cumulative precipitation of Kyushu Island's heavy rainfall events in 2009 and 2012 (JGS 2010, 2013, 2018). Consequently, geo-disasters, including mud and debris flows and landslides occurred within the affected area.

Several large-scale slope failure cases were reported, including failure of the top parts of the slopes, scouring, and failure of the beds and shores in the middle basin. It must be noted that the ground is mainly comprised of severely weathered granodiorite and metamorphic rocks. Consequently, large amounts of sediments and driftwood have flooded and accumulated in the downstream region, spreading over private houses and farmlands, causing extensive sediments, driftwoods, and water-induced damage to lives and properties, as illustrated in Fig. 2. Immediately, an investigation team was formed to investigate the affected mountainous area. The team investigated the prevailing situation and conducted various geotechnical tests to define the affected area's soil mechanical and hydrological characteristics.

The ultimate priority in large-scale geo-disasters is to prevent injuries and fatalities. Several approaches to protect human lives were developed, such as constructing infrastructures like Sabo dams. However, considering the current rainfall patterns, the variations in the scale and type of the

N. Yasufuku (✉) · A. Alowiasy
Department of Civil and Structural Engineering, Kyushu University, Fukuoka, Japan
e-mail: yasufuku@civil.kyushu-u.ac.jp

A. Alowiasy
e-mail: a.adel@civil.kyushu-u.ac.jp

I. Alcántara-Ayala et al. (eds.), *Progress in Landslide Research and Technology, Volume 1 Issue 2, 2022*, Progress in Landslide Research and Technology,
https://doi.org/10.1007/978-3-031-18471-0_10

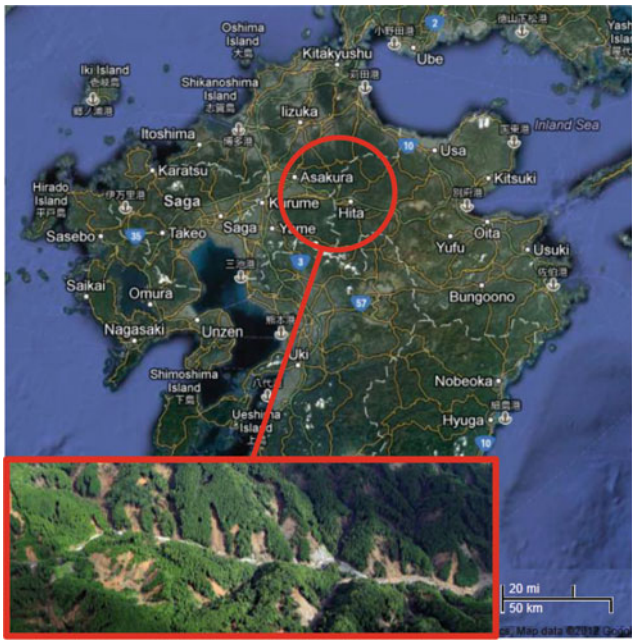

Fig. 1 Mountainous area location of the northern Kyushu heavy rainfall-induced geo-disasters, July 2017 (Chikugo river report 2017)

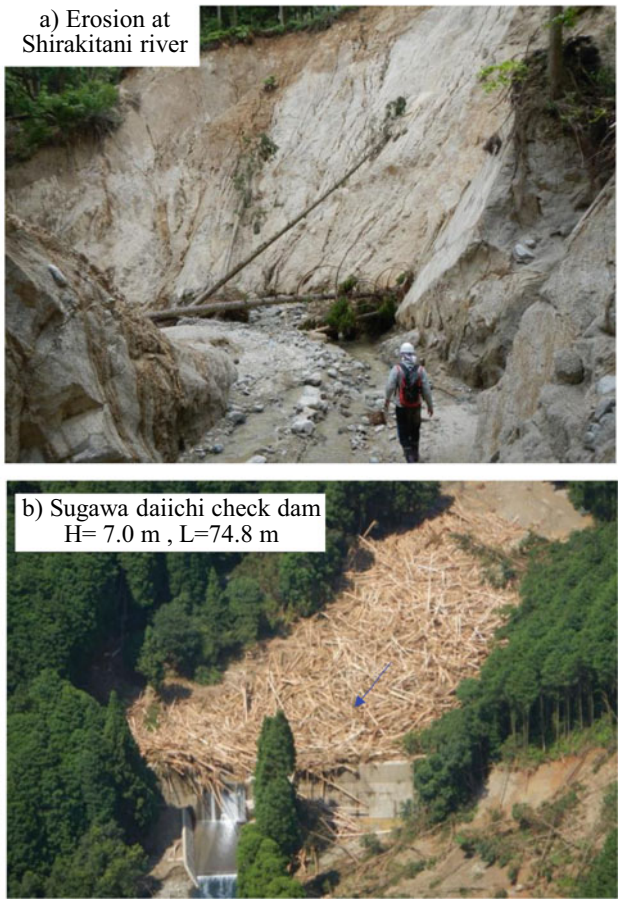

Fig. 2 **a** Typical erosion at Shirakitani river. **b** Catchment of driftwood by check dam (JGS 2018)

impacts that are felt, and the adopted countermeasures, novel and innovative approaches are needed. Those approaches are better based on soft measures such as "an evacuation warning system" and "restrictions on land use" to protect human life and define vulnerable zones.

This paper comprehensively summarizes the recent heavy rainfall-induced geo-disaster in Japan, especially in Kyushu Island. The cases are analyzed, and a group of learned lessons is delineated. It provides a fundamental database for effective preparations for future similar geo-disasters subjected to similar external forces. Furthermore, technical obstacles and new approaches to deal with such events are elaborated on from geotechnical and geological points of view. The term "geo-disaster" is used in this context to describe various slope disasters, including debris flows, driftwood, slope failures, landslides, and embankment damages.

2 Characteristics and Potential of the Geo-disasters During the Northern Kyushu Heavy Rainfall in July 2017

The historical maximum cumulative rainfall recorded at Asakura, Kita-Kouji Public hall, and the national AMeDAS and their historical rankings are illustrated in Fig. 3. The values corresponding to AMeDAS are based on the data recorded between January 1976 to July 2017. The Kita-koji Public hall, located 10 km east of Asakura, falls in the top 25 for all cumulative elapsed times. It is ranked 5th for 2-h cumulative precipitation, 4th for 3-h, 2nd for 6-h (close to the maximum record), and 1st for 12-h (exceeding the maximum record of Asakura in 2017 by 100 mm). The rainfall was unprecedented for 1–3 h and one of the largest for 6 and 12-h cumulative records. The intense rainfall lasted 9 h and is considered one of the most devastating records. Figure 4 shows the precipitation records for Fukuoka in 2017 compared to Hiroshima in 2014, where rainfall lasting more than 9 h (Fukuoka record) is considered an unusual extreme phenomenon in the region.

In general, northern Kyushu is experiencing frequent occurrences of high precipitation in a relatively short time, such as the recent 2009 and 2012 events. Statistical studies by the Japanese Geotechnical Society, including data over the past 4 decades in Japan, have revealed a distinct increasing tendency for more frequent heavy rainfall events with hourly precipitation exceeding 50 mm or even over 80 mm (JGS 2010, 2013, 2018).

On a global scale, according to the report released by the Intergovernmental Panel on Climate Change (IPCC 2013),

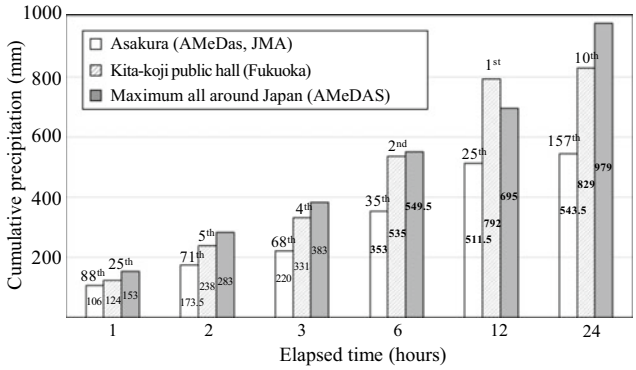

Fig. 3 Comparison and ranking of the recorded cumulative precipitation with time

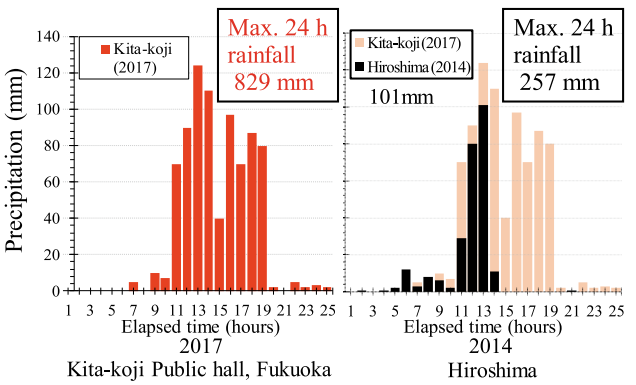

Fig. 4 Comparison of precipitation records (Fukuoka and Hiroshima prefectures in Japan)

global warming is expected to cause an increase in the heavy rainfall-induced geo-disasters and affect the rainfall concentration, frequency of typhoons and tornados, and wind speed. Coping with the associated significant increase in the potential of geo-disaster occurrence requires effective adaptations and implementations, which are expected to be in high demand in the near future. Under such circumstances, geotechnical engineering is expected to play a vital role. In Japan, a research initiative was launched to establish a geo-hazard vulnerability assessment framework for areas affected by climate change. It incorporates the regional differences between Kyushu and Hokkaido islands (JSPS, Grant-in-Aid for Scientific Research A 2020).

3 Types of Heavy Rainfall-Induced Slope Failures and Sediments Movement

3.1 Geotechnical and Geological Factors

The factors causing slopes to fail can be broadly categorized into predisposition and inducing force factors. Generally, the predisposition factor depends on the geological conditions, topographical conditions, and the presence of vegetation, while the inducing forces include rainfall and earthquakes. In the case of the Northern Kyushu heavy rainfall in July 2017, the inducing force of the slope failure was the heavy rainfall. A specific slope to collapse requires a weak predisposition and a trigger to induce the failure (Iseda et al. 1982). Such a phenomenon occurs only when those conditions coexist, but the thresholds are macroscopically regional and mechanically exclusive for a specific slope.

To be more specific, slope failures can be related to several points, including (1) the increase of the sliding force and decrease of the soil strength due to the saturation, (2) the decrease in the effective stress associated with the rise of the groundwater level which results in increasing the pore water pressure, (3) the collapse of a soil layer or a bedrock stratum, (4) the generation of an osmotic pressure acting as a slipping force due to seepage flow, (5) scouring, erosion, and transport of sediments due to the surface runoff, (6) the piping phenomenon caused by preferential water pathways, (7) the difference in the precipitation and infiltration rate, where the water flowing into the ground surface at a specific rate induces a hydraulic gradient leading to developing a shearing force that contributes to the sliding force (JGS 2018; AMeDAS 2018; IPCC 2013; Iseda et al. 1982). However, such typical relationships change over time for various reasons, including the progress of weathering of the comprising soil and rock layers.

Considering the unprecedented heavy rainfall that lasted for a relatively long time during the Northern Kyushu heavy rainfall in July 2017, the 7 factors mentioned above might have coexisted. Consequently, several slopes failed simultaneously within the affected area, specifically the zone located on the right bank of the Chikugo River in Asakura. However, the intercorrelation of the factors and the occurrence of the slope failure are not well understood yet. Therefore, developing a comprehensive slope stability analysis and collapsing potential evaluation techniques based on in-situ investigations and laboratory testing is crucial and urgent.

Several attempts are being approached from a geotechnical engineering perspective in response to the urgent need. For example, supported by the JSPS and in collaboration with researchers around Japan, the following research objectives are being challenged:

1. Evaluation of the ground resilience against failure. The study considers the changes in the natural and man-made slopes comprising soil profile characteristics with time, adopting statistical and mechanical approaches (Yasufuku et al. 2021; Alowaisy et al. 2020). Furthermore, the development of the rainfall patterns in Fukuoka prefecture

with time was analyzed using the AMeDAS rainfall data provided by the Japan Meteorological Agency starting from 1988. Consequently, it was found that the 2020 rainfall-induced road damages were located within high-risk zones, where a relatively long-lasting heavy downpour was probable (Murakami and Oda 2021).

2. Comprehensive analysis of the regional characteristics of the landslide hazard criterion lines (CLs). The CLs are established in each region, considering the ground, topography, geological characteristics, and rainfall information while expanding the existing database. A real-time slope failure evaluation was proposed by combining machine learning with a physically-based slope stability model that considers the strength parameters, water retention curve, topography, geological characteristics, and rainfall conditions (Sakamoto et al. 2022).
3. Update the existing CLs records to include undefined areas not covered by the Landslide Disaster Warning Information System or categorized as non-disaster rainfall. The attempt aims at enhancing the accuracy of the CLs estimation to evaluate the ground resilience reflecting the regional characteristics of rainfall and ground using Artificial Intelligence (AI). Furthermore, precise determination of the dangerous spots on slopes and releasing warning was investigated, focusing on the runoff, infiltration, and snowmelt simultaneously in a wide and narrow area (He and Ishikawa 2022). The post-rainfall earthquakes' loading on the stability of embankments was investigated by Nguyen and Kawamura (2022). Moreover, Kasama et al. (2021) investigated the effect of spatial variability on the stability of the 3D slope subjected to earthquakes. A stochastic response surface method (VRSRSM) combined with a variance reduction method that considers the spatial averaging of soil parameters in three-dimensional space was proposed to reduce the computational cost. The VRSRSM was applied to evaluate the deep-seated landslides caused by the 2016 Kumamoto earthquake together with the inverse determination of the strength parameters.
4. Propose a multi-scale slope stability analysis method that considers infiltration and runoff during heavy rainfall events. Furthermore, the results are then used for identifying slope hazard risk areas based on the surface water generation associated with rainfall probabilities, which generally cannot be handled using the standard rainfall design criteria (He and Ishikawa 2022).

Ultimately, these results are expected to be integrated into an engineering assessment of ground immunity, a modified definition of ground resilience to disasters that considers the changes with time. The study focuses on defining risk areas based on the changes in the rainfall and snowmelt patterns while upgrading the risk assessment methods for natural and man-made slopes in Kyushu and Hokkaido regions as disaster vulnerable areas affected by climate change. Furthermore, the project promotes prioritizing the order of the countermeasures for establishing disaster risk maps that consider the change over time.

3.2 Rainfall Patterns and Forms of Slope Failure

Figure 5 shows the collapsed slope and floods distribution during the 2017 rainfall. Figure 5a corresponds to 3-h cumulative rainfall contours, while Fig. 5b illustrates the 12-h contours. The highlighted blue regions represent the flooded areas, while the red highlights correspond to the failed slopes. It can be observed that for 3-h of cumulative rainfall, most of the collapses occurred in regions with rainfall exceeding 200 mm. While, in the Shirakidani River and the Sozu River, collapses associated with rainfall less than 150 and 200 mm were reported, Fig. 5a. On the other hand, for 12-h rainfall exceeding 300 mm, collapses extended over vast regions while exceeding 400 mm became more localized.

Figure 6 summarizes the recorded cumulative precipitation versus the collapsed area ratio of the slopes at the right

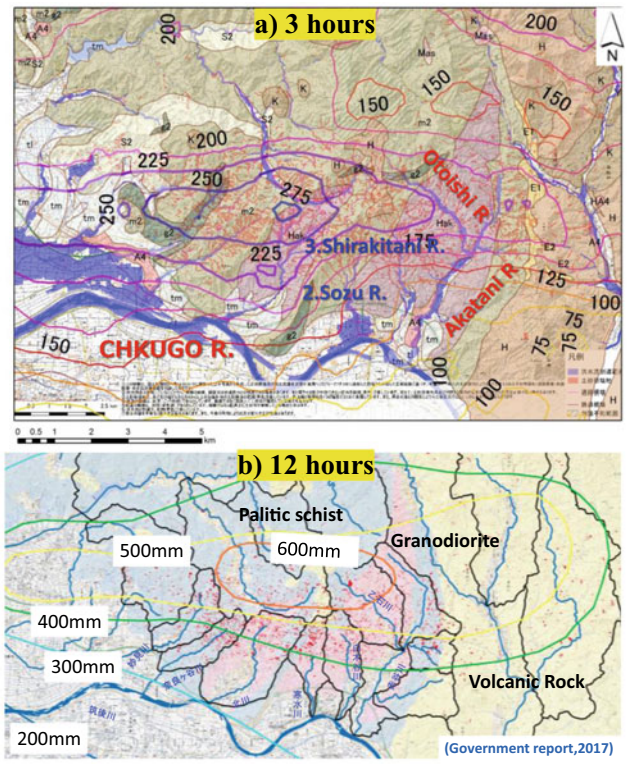

Fig. 5 Slope failure distribution (red highlights) and flood reach range. **a** 3 h rainfall contour. **b** 12 h rainfall contour

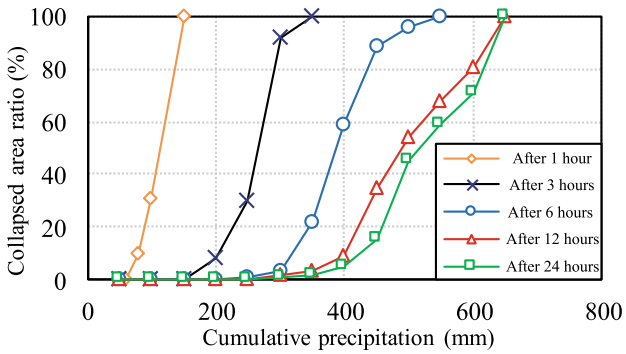

Fig. 6 Relationship between the cumulative precipitation and the collapsed area ratio (Committee of Chikogu river 2017)

bank of the Chikugo river basin for several durations (Jitozono 2017; Committee of Chikugo river 2017). The collapsed area ratio was determined based on field surveys and investigations for different rainfall durations at various slopes within the affected zone. It can be observed that when the precipitation exceeds 100 mm for 1 h, 250 mm for 3 h, 350 mm for 6 h, 400 mm for12 h, and 450 mm for 24 h, the collapsed area ratio increases rapidly. Establishing a robust statistical-based system that considers the regional characteristics for comprehensively analyzing the rainfall and investigation records is expected to serve as an effective tool for risk assessment, disaster prevention, and mitigation.

Estimating the amount of generated sediments and driftwoods due to extreme heavy rainfall-induced slope failures is essential when determining the type and scale of the preventive measure structure (such as Sabo dam) built around rivers' facilities. Therefore, it is crucial to properly evaluate the scale of the slope failure under a specific pattern of heavy rainfall. However, the scale and failure pattern vary significantly depending on many factors such as geological conditions, topographical conditions, vegetation cover, and rainfall intensity. An accurate method to estimate the amount of generated sediments does not exist for the time being. Therefore, a method utilizing a statistical approach based on measurable mechanical factors is needed.

In an attempt to establish such a system, the records of the sediment transport were analyzed, focusing on the heavy rainfall-induced slope failures for the Akatani river basin in Asakura. Figure 7 illustrates the relationship between the cumulative precipitation and the generated amount of sediments (Jitozono 2017). It can be observed that the larger amounts of generated sediments are generated for higher cumulative precipitation, which is expected to follow a power formula trend. Besides, a typical collapse mode is expected to occur once the cumulative precipitation reaches 200–500 mm. Although this figure does not include the actual measured amount of generated sediments, reflecting the history of such disasters might be efficient for predicting the type of failure and the amount of generated sediments under specific cumulative precipitation at the considered basin. When considering such heavy rainfall-induced geo-disasters in mountainous areas, enhancing the resiliency of the basin is inevitable. Therefore, a reliable

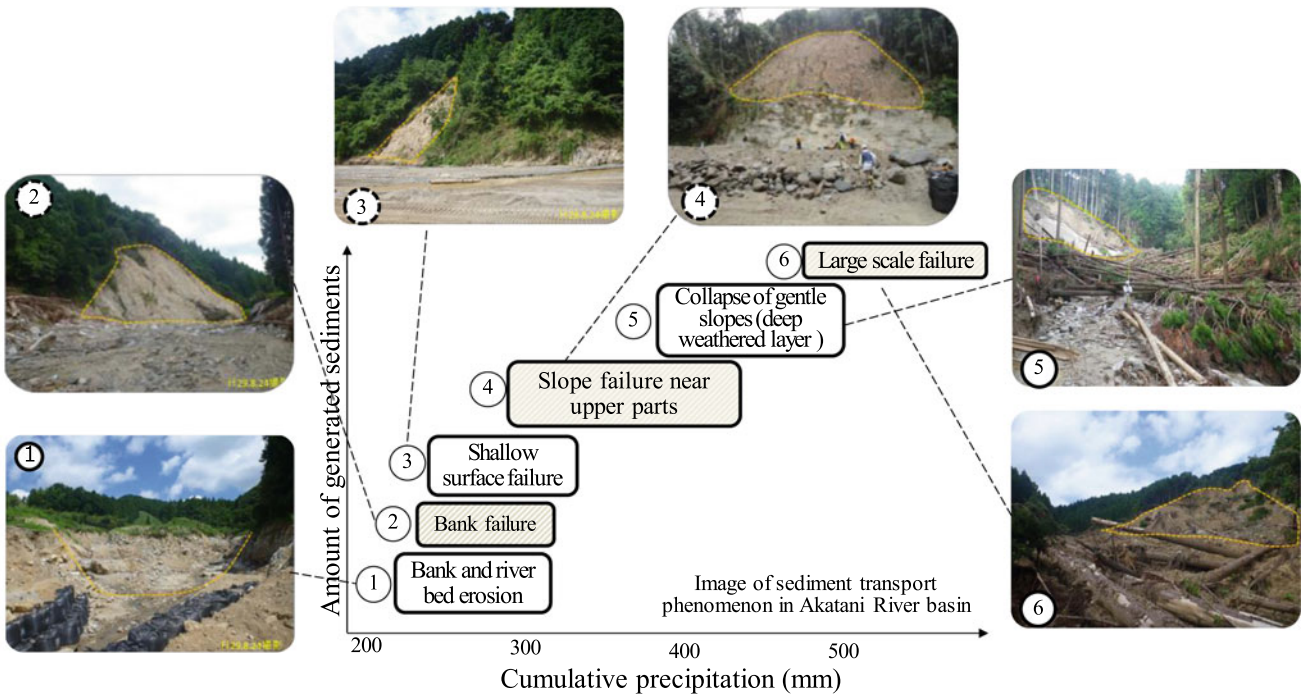

Fig. 7 Relationship between the cumulative precipitation and the amount of generated sediments (Jitozono 2017)

evaluation approach is needed to analyze the existing risks and factors for future mitigation and countermeasure plans. Such attempts are expected to contribute to various geotechnical engineering aspects, including improving the accuracy of flood inundation analyses that directly affects the generated volume of driftwood and sediment.

4 Shapes and Patterns of Slope Failure

The geometry and the pattern of failure, including the collapsed height and depth of the heavy rainfall-induced collapsed slopes in 2017, were analyzed by Kasama (2018). The studied area included the basin where slope failures were reported in Asakura city, Fukuoka prefecture (Akatani river, Otoishi river, Shirakidani river, Sozu river, Kita river, and Naragaya river). A comparison utilizing laser scanning results of the area profile before and after the collapse was carried out. A detailed description of the adopted methods and the geological formation can be found in Kasama (2018).

Figure 8 shows the slope inclination angle, for the studied basins in Asakura city, versus the collapse frequency and cumulative frequency distribution before and after the failure. Furthermore, Japan's average cumulative frequency of slope failures is also illustrated (Koyamauchi et al. 2009). It can be observed that the highest frequency in the Northern Kyushu rainfall disaster of 2017 corresponds to an inclination angle of around 40°, while Japan's average failure inclination angle is around 60°. Moreover, 80% of slope failures occurred at an inclination angle of 38° or less, which can be considered a unique feature of this region. This angle is 20° smaller than the average angle corresponding to the average in Japan. Similarly, Fig. 9 shows the slope collapsed height versus the collapse frequency and cumulative frequency distribution before and after the failure. By conducting cumulative frequency comparative analysis and correlating them to the geological and geotechnical characteristics of the comprising profiles, it is expected that the collapsed slopes can be categorized from a statistical perspective and accumulated as a record.

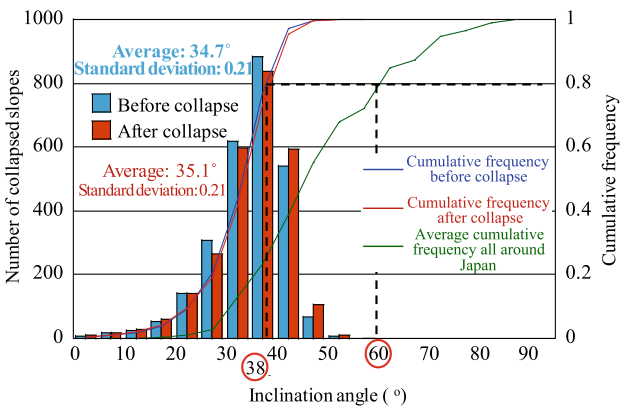

Fig. 8 Slope's angle distribution of collapsed slopes (Kasama 2018)

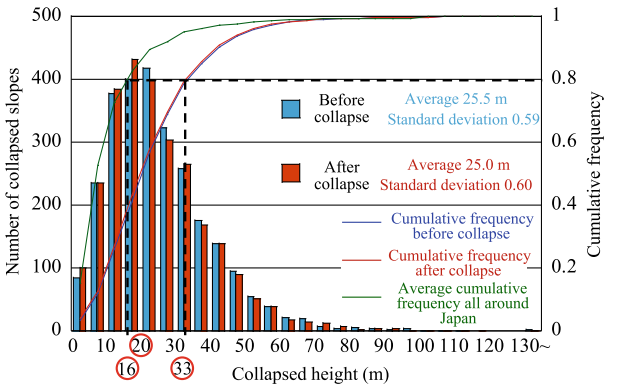

Fig. 9 Slope's height distribution of collapsed slopes (Kasama 2018)

Figure 10 summarizes the average collapsed depth for the studied slopes in Asakura city. Furthermore, the collapsed geological formation and area ratio for each catchment basin, defined as the ratio of the failed area to the catchment area, are illustrated in Fig. 11. It can be seen from Fig. 10 that the average landslide and slope failure depth in all basins ranges from 0.4 to 1.3 m. However, several large landslides from deep layers with an average depth exceeding 8 m have occurred. In addition, from Fig. 11, it can be seen that the collapse area ratio in each basin under the prevailed rainfall falls in the range of 3–8%. Integrating various indices reflecting the rainfall and the generated soil volume into a statistical record of the failed slopes is expected to serve as an efficient risk assessment tool for prevention, mitigation, and estimating the scale of impact on society under such events.

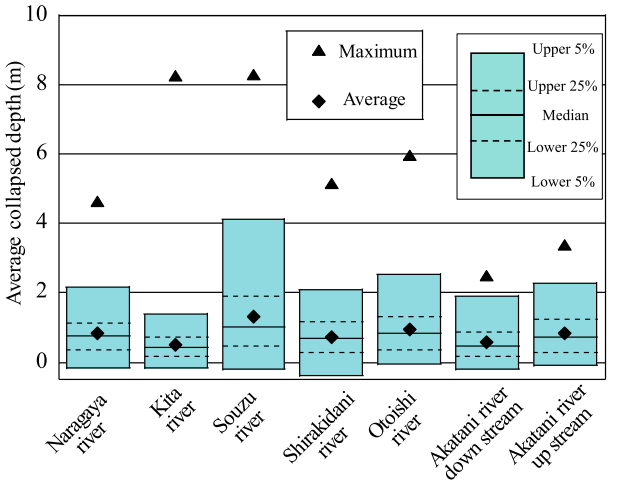

Fig. 10 Distribution of the average collapsed depth (Kasama 2018)

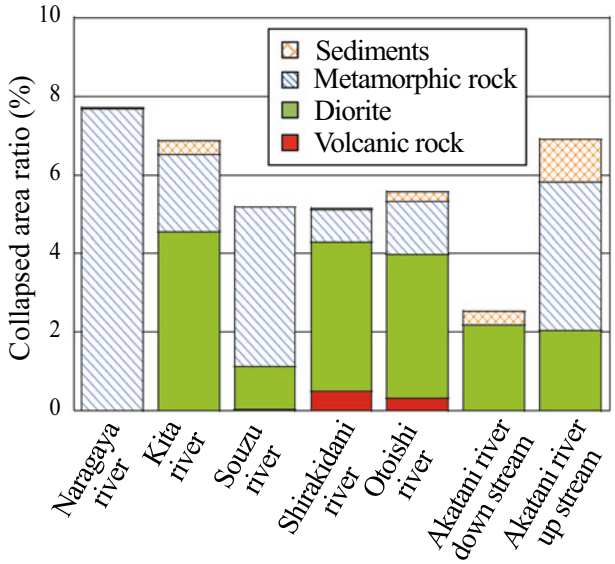

Fig. 11 Comparison of the collapsed area ratio (Kasama 2018)

5 Technical Issues Related to Geo-disasters Prevention and Mitigation

Based on the lessons learned from the geo-disasters history in Kyushu, geotechnical and geological-related issues and concerns are summarized in Fig. 12, considering enhancing the geo-disasters prevention and mitigation protocols.

5.1 Preparation of the Past Disaster Records as a Database for Effective Usage

The Northern parts of Kyushu island have experienced several heavy rainfall-induced geo-disasters that have occurred repeatedly with different scales over the past few decades. Although many valuable records exist for Northern Kyushu and all of Japan, they are not efficiently organized for risk management and mitigation usage. Those records are preserved separately in each department, such as the administrative office. The records are not effectively organized as an integrated geo-disasters database due to the lack of efficient, accessible, and easy-to-use digital storage format. Therefore, developing an organized system to collect the geo-disasters history records in cooperation with the national and local governments under the leadership of academic and professional engineers specializing in geo-disaster prevention and mitigation is essential. The efficient and accessible database and system are expected to be conveyed to the next generation as a reference for future geo-disasters.

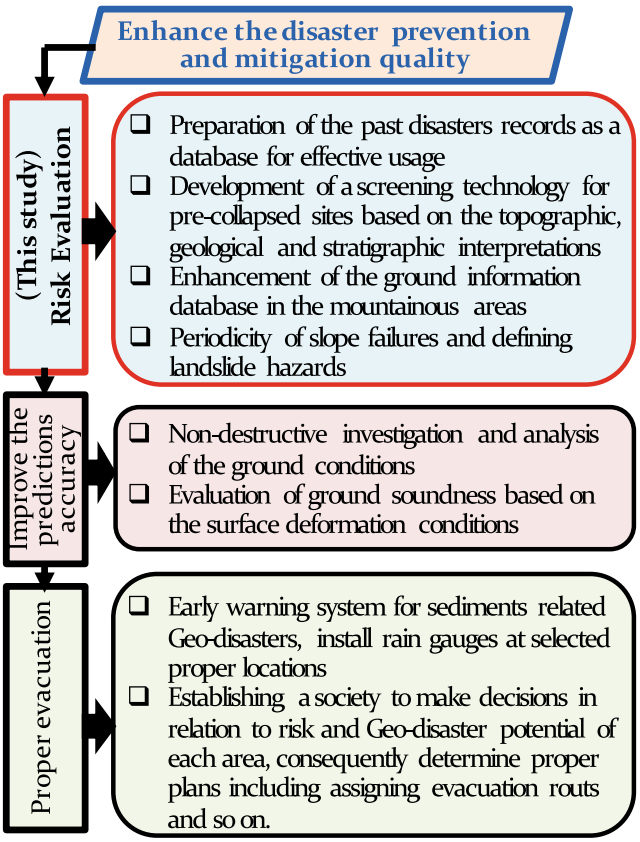

Fig. 12 Geotechnical and geological considerations for slope-related Geo-disasters mitigation and prevention system

5.2 Screening Technology Considering the Stratigraphy, Topographical, and Geological Interpretations

Recently, the accuracy of the laser profile scanning data and the C-X synthetic band radar has improved dramatically. Besides, image analysis technologies using drones have improved remarkably. During the last decade, many organizations have been utilizing the latest technologies in developing topological interpretations and screening techniques based on the analysis of the geological and stratigraphic conditions. Utilizing such technologies, if the vulnerable slopes can be defined using practical indices with high accuracy, it is expected to significantly improve the quality and efficiency of geo-disasters prevention and mitigation. Such academic and practical integrated approaches are highly needed.

5.3 Enhancement of the Ground Information Database in the Mountainous Areas

Kyushu branch of the Japanese Geotechnical Society has created and published a database including geotechnical and

geological information with more than 80,000 boring data in seven prefectures within Kyushu Island. The database is open for access to public users through the JGS society. These data are enormous in number and include both urban and coastal areas. However, it is essential to enrich the data of the mountainous regions to efficiently contribute to the recovery and restoration in the case of geo-disasters in such regions. There are various cases and ways where geotechnical engineers can efficiently enrich the database during their response to the requests of the state and the local governments. For example, when collecting data from ground surveys and field investigations in the case of a specific geo-disaster and its restoration, establishing a system for checking the collected data is of significant value. Especially for recent geo-disasters, it is necessary to develop a reliable database for disaster response that can be effectively used when deciding on a countermeasure while analyzing the characteristics of that specific region. The system should be easy-to-understand and consider the risk analysis from an academic perspective to objectively explain the reason for deciding on a specific group of actions in response to a geo-disaster.

5.4 Geo-disasters Periodicity

The periodicity of landslides or slope failures in areas comprised of granite was studied in the 1980s (Shimokawa et al. 1984). The elapsed time since the occurrence of the previous landslide, the changes in the soil surface layer thickness, and the rainfall catchment area were analyzed using surveys and field investigation records. The study aimed to define the average cycle time for a landslide. It was reported that for an average failure depth of about 0.7 m, the periodicity is approximately 200 years. Establishing a system to accurately estimate the risk of a slope failure based on its periodicity requires extensive research to investigate the surface soil weathering and restoration rates as functions of time, geotechnical and geological characteristics of the comprising profiles. In Kyushu, several high-risk zones are mainly comprised of granite. Thus when considering geo-disasters, the surface soil weathering and restoration due to sediment deposits over time are vital factors. Therefore, it is not sufficient to specify a landslide hazard based only on an ordinary topographical analysis. Instead, it is crucial to investigate the distribution of sediments on slopes and mountain streams, vegetation at the site, the degree of weathering of granite at the head and toe of slopes, and the periodicity of the past slope failures and debris flow at that relevant site, to efficiently reduce the risk of slopes related geo-disasters. Finally, based on such practical detailed knowledge, society is urged to accelerate the efforts to define landslide and slope failure hazard areas.

5.5 Assessment of Time-Dependent Geo-disaster Immunity

Road cut slopes are man-made and common infrastructures usually constructed with surface reinforcement to prevent erosion and weathering. However, it has been observed that decades after construction, the ground behind the cut-and-fill surface comprised of soil and rocks deteriorates due to the weathering, resulting in deformation and finally collapse.

Recently, a practical and simple method for assessing slopes' stability considering the degree of weathering and the aging factor is being developed (Yasufuku et al. 2021).

It is not economically feasible to implement preventive measures covering all the existing hazardous areas of the existing slopes. Therefore, it is necessary to incorporate a social impact index, for example, the traffic volume or the distance of diversion roads and detours, to prioritize the cut slope surfaces that need to be managed first. The method proposes a term called slope 'disaster immunity', defined as the product of the 'disaster resistance', which is an index of the physical stability of the slope, and the 'disaster resilience', which reflects the social impact. Supposing the geo-disaster immunity can be objectively and concretely evaluated, it is expected to be used as a system to support the administrative evaluation for prioritizing management and measures of slopes, taking into account the changes over time. Ultimately, it is expected to be utilized for both natural and man-made slopes.

$$I(t) = S(t) \times R(t) \tag{1}$$

where I(t): the expected value of time-dependent disaster immunity of the target slope; S(t): the probability of soundness of the target slope (disaster resilience), taking into account the time-dependent deterioration, R(t): the ability to mitigate social losses in the event of a geo-disaster.

6 Conclusions

Recently, heavy rainfall events have induced various geo-disasters, including floods, sediments, and debris flows in Kyushu Island and all around Japan, which have caused severe damage to lives and properties. Table 1 summarizes the geo-disasters that occurred in Kyushu island from 1969 to 2020, with the 2017 event analyzed through this paper in bold. Figure 13 illustrates the numbers and the corresponding percentages of the slope geo-disasters all around Japan in the period ranging from 1967 to 2012 (Ministry of Land, Infrastructure, Transport and Tourism 2013). The slope-related geo-disasters in the Kyushu-Okinawa region are remarkably higher than the other regions, accounting for approximately 31%, where on average, 390 slope-related geo-disasters occur annually.

Table 1 History of geo-disasters mainly in Kyushu from 1969 to 2020

Year	Month	Place	Triggering factor	Casualties
1969	June	Kagoshima-shi, Kagoshima	Localized downpour	52
1971	August	Kagoshima-shi, Kagoshima	Localized downpour	47
1972	July	Asakusa, Kumamoto	Localized downpour	115
1976	June	Kagoshima-shi, Kagoshima	Localized downpour	32
1982	July	All prefectures, mainly Nagasaki	Localized downpour	259
1984	June	Itsuki-machi, Kumamoto	Seasonal rain front	16
1986	July	Kagoshima-shi, Kagoshima	Localized downpour	18
1990	July	Ichinomiya-machi, Kumamoto	Seasonal rain front	11
1990	September	Setouchi-machi, Kagoshima	Typhoon No. 19	11
1993	August	Kagoshima-shi, Kagoshima	Localized downpour	47
1997	July	Izumi-shi, Kagoshima	Seasonal rain front	21
1999	June	All prefectures, mainly Hiroshima	Seasonal rain front	24
2003	July	Middle Kyushu	Seasonal rain front	24
2004	September	Western Japan	Typhoon No. 21	17
2005	September	Yamaguchi and Western Kyushu	Typhoon No. 14	25
2006	July	Kagoshima	Seasonal rain front	5
2007	July	Kumamoto and Kagoshima	Seasonal rain front	2
2008	June	Kumamoto	Seasonal rain front	1
2009	July	Northern Kyushu	Seasonal rain front	34
2010	October	Amami Ohshima, Kagoshima	Localized downpour	3
2012	July	Northern Kyushu	Seasonal rain front	34
2014	August	Hiroshima	Seasonal rain front	77
2017	**July**	**Northern Kyushu**	**Seasonal rain front**	**42**
2020	July	Middle southern Kyushu	Seasonal rain front	65

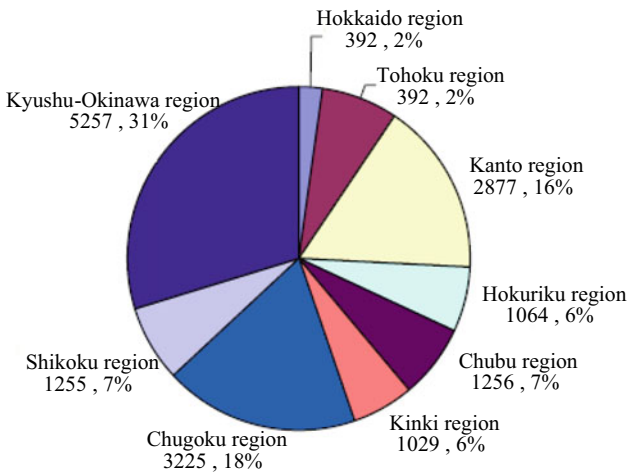

Fig. 13 Slopes related geo-disasters frequency since 1967 (Ministry of Land, Infrastructure, Transport and Tourism 2013)

According to the Intergovernmental Panel on Climate Change (IPCC 2013), the frequency and intensity of localized torrential rainfall events are expected to increase. Through this study, the anticipated increase in the geo-disasters inducing forces due to climate change (rainfall), deterioration of the infrastructure, and the decline in the labor forces, limiting the prevention and restoration capabilities due to the increasing difference in the death to birth ratio, were discussed and several lessons and recommendations for dealing with future similar events were introduced.

By carefully comparing and analyzing the situation of the repeated geo-disasters and reflecting the obtained results to the geo-disasters mitigation and prevention practice, developing innovative systems and techniques that integrate the academic disciplines in collaboration with the residents and government is now strongly needed more than ever, see Fig. 12.

Finally, A new concept called ‘disaster immunity’, which can reflect the past rainfall and earthquake histories and the characteristics of particular landforms that change over time was introduced. The concept is being tested and used in a comparative study of Kyushu and Hokkaido islands, where both regions include soil profiles comprised of volcanic ash and weathered residual soils that are vulnerable to climate change-related disasters. For the time being, the obtained results indicate that it can be used as a system to support the

administrative evaluation for prioritizing management and measures of slopes, taking into account the changes over time to save lives reliably.

Acknowledgements This research was supported in part by Grants-in-Aid for Scientific Research (A) (20H00266) from the Japan Society for the Promotion of Science (JSPS) KAKENHI. The authors express their gratitude and appreciation to the Ministry of Land, Infrastructure, Transport, and Tourism, Kyushu Regional Development Bureau, the Fukuoka prefecture local government, and Oita prefecture local government for their great support during the geo-disaster affected sites investigations.

References

Alowaisy A, Yasufuku N, Ishikura R, Hatakeyama M, Kyono S (2020) Continuous pressurization method for a rapid determination of the soil water characteristics curve for remolded and undisturbed cohesionless soils. Soils Found 60(3):634–647. https://doi.org/10.1016/j.sandf.2020.03.014

Committee of Chikugo river right bank basin and Sabo dam restoration technology (Chairman Komatsu T) (2017) Report on "Chikugo river right bank basin and Sabo dam restoration technology" (in Japanese)

Digital Typhoon, AMeDAS torrential rain-past heavy rainfall ranking (2018). http://agora.ex.nii.ac.jp/digitaltyphoon/heavy_rain/ [2018.3] (in Japanese)

Hayashizaki S, Kawajiri S, Koyama M, Hikichi S (2022) Influence of earthquake motion and tsunami on slope stability of highway embankment. Technical report of Hokkaido Branch of Geotechnical Engineering Society of Japan, vol 62, pp 313–320 (in Japanese)

He W, Ishikawa T (2022) Slope stability analysis of wide and narrow slopes considering infiltration and runoff. Technical report of Hokkaido Branch, Geotechnical Engineering Society of Japan, vol, 62, pp 265–174

Intergovernmental Panel on Climate Change [IPCC] (2013) Climate change 2013. Cambridge University Press, Cambridge

Iseda T, Ochiai H, Tanahashi Y (1982) Relationship between actual conditions of landslides and rainfall characteristics. Report on a disaster survey caused by heavy rainfall in Nagasaki in July 1982, Nagasaki University Academic Research Team, pp 59–71 (in Japanese)

Japan Geotechnical Society [JGS] (2010) Report on "Geodisasters in 2009 July Northern Kyushu and Chugoku region torrential rainfall (Representative member: Noriyuki Yasufuku)" (in Japanese)

Japan Geotechnical Society [JGS] (2013) Report on "Geodisasters in 2012 July Northern Kyushu torrential rainfall (Representative member: Noriyuki Yasufuku)" (in Japanese)

Japan Geotechnical Society [JGS] (2018) Report on "Geodisasters in 2017 July Northern Kyushu torrential rainfall (Representative member: Noriyuki Yasufuku)" (in Japanese)

Japan Society for Promotion of Science [JSPS] (2020) Development of a regional geo-disaster vulnerability assessment method based on a novel time-dependent immunity index reflecting the climate changes and its applications, Grant-in-Aid for Scientific Research A (No. 20H00266) (in Japanese)

Jitozono T (2017) Sediment-related disasters in the Ono district of Hita City, textbook of the Sabo Society of Japan seminar, pp 19–30 (in Japanese)

Kasama K (2018) Field study on slope failure analysis and the related deep weathering. Special Grants-in-Aid for Scientific Research of FY2017 (Representative member: Juichiro Akiyama), 17k20140, vol 3, no 3, pp 127–139 (in Japanese)

Kasama K, Furukawa Z, Hu L (2021) Practical reliability analysis for earthquake-induced 3D landslide using stochastic response surface method. Comput Geotech 137. http://doi.org/10.1016/j.compgeo.2021.104303

Koyamauchi N, Tomita Y, Akiyama K, Matsushita S (2009) The actual conditions of the landslide, no 530. National Institute of Land and Infrastructure Management, pp 1–210 (in Japanese)

Ministry of Land, Infrastructure, Transport and Tourism (2013) Annual report on disaster management 2012 (in Japanese)

Murakami S, Oda S (2021) Analysis of road damage caused by July 2020 torrential rainfall in Fukuoka Prefecture using rainfall characteristic values. Japan Society of Civil Engineers (JSCE) 75th annual meeting, III-67 (in Japanese)

Nguyen, T, Kawamura S (2022) Earthquake-induced failure of volcanic embankments subjected to previous rainfall. Int J GEOMATE 23 (97) (in Press)

Sakamoto T, Kasama K, Furukawa Z (2022) Evaluation of regional slope failure risk using machine learning. In: Proceedings of the Western branch meeting of JSCE (in Japanese)

Shimokawa E, Jitozono T, Hori Y (1984) History of landslides in granite area. Nichirin Kyushu branch annual paper, vol 37, pp 299–300 (in Japanese)

Tsukamoto D, Sako K, Ito S (2021) Parametric study on slope failure morphology by two-dimensional slope failure simulation using SPH method. In: The 56th annual meeting of the Japan national conference on geotechnical engineering, 12-10-2-07 (in Japanese)

Yasufuku N, Uda R, Ishikura R, Alowaisy A (2021) Application of a stability index for cut slopes reflecting stratigraphic and weathering characteristics. In: The 56th annual meeting of the Japan national conference on geotechnical engineering, 12-10-3-01 (in Japanese)

Effect of Landslide Deformation on the Stability of St. Andrew's Church (Kyiv, Ukraine): Applications of Remote Sensing and Mathematical Modeling

Oleksandr Trofymchuk, Iurii Kaliukh, Oleksiy Lebid, Viktoriia Klymenko, Viacheslav Vyshniakov, Dmytro Kreta, and Yasser Elshayeb

Abstract

This article presents the work conducted by the authors to analyze the stability of the St. Andrew's Church which contains architecture, painting and decorative arts of the XVIII century. The church is located on a landslide-hazardous hill in the historic part of Kyiv, the capital of Ukraine. The architectural monument was built in 1747–1762 upon the project of Francois Bartolomeo Rastrelli in the Baroque style. It is one of the most important architectural monuments in Ukraine, which has cultural and historical value. Fluctuations in the height of the soil of the upper and lower part of the hill, on which St. Andrew's Church is located, vary from 181.7 to 118.5 m. There are physical and geological hazards around the historic building, such as landslides, loose soil, soil inhomogeneities, and external erosion of the hill. To preserve this national heritage monument, a set of measures needed (monitoring the monument, identifying dangerous areas, carrying out fortification works, etc.). Monitoring of architectural monument in large areas could be carried out using optoelectronic and radar-location data and remote sensing of the Earth from space. Radar-location observations make it possible to determine reliable information about objects that are exposed to landslides and endure displacements (Casagli et al. in Landslides 7:291–301, 2010). Optoelectronic observations are effective for identifying areas and objects, identifying threats, operational assessment of the state of environmental objects, identifying areas that are affected, etc. After obtaining information on specific landslide-hazardous objects, with the help of geographic information systems (GIS) tools, areas of interest are identified for space survey of ultra-high spatial diversity to further assess the state of the architectural monument and the surrounding area. Subsequently, ground research and mathematical calculations of the object under study are carried out and measures are taken to eliminate landslide hazards and preserve the national heritage. With the results of this research, geotechnical works were already carried out to strengthen, restore and reinforce the damaged building structures.

Keywords

Landslide deformations • Remote sensing • Mathematical modeling • GIS

O. Trofymchuk · I. Kaliukh · O. Lebid · V. Klymenko · V. Vyshniakov · D. Kreta
Institute of Telecommunications and Global Information Space, National Academy of Science of Ukraine, Chokolovsky Boulevard, 13, Kyiv, 03186, Ukraine
e-mail: itgis@nas.gov.ua

I. Kaliukh
e-mail: kalyukh2002@gmail.com

O. Lebid
e-mail: o.g.lebid@gmail.com

V. Klymenko
e-mail: klimenko_vika@ukr.net

V. Vyshniakov
e-mail: wishnya_dzz@ukr.net

D. Kreta
e-mail: dim.leo@gmail.com

Y. Elshayeb (✉)
The American University in Cairo, AUC Avenue, New Cairo, 11835, Egypt
e-mail: yasser.elshayeb@aucegypt.edu

1 Introduction

The hill on which the unique historical and architectural church is located, is special for Ukraine, as the birth of Christianity in Ukraine began from this place. According to the chronicle "The Tale of Bygone Years". The first preacher of Christianity in the lands of Kievan Rus: called "Andrew the First", erected, in the first century AD, a Cross on this site and foretold the emergence of a great city. Wooden and

I. Alcántara-Ayala et al. (eds.), *Progress in Landslide Research and Technology, Volume 1 Issue 2, 2022*, Progress in Landslide Research and Technology,
https://doi.org/10.1007/978-3-031-18471-0_11

stone churches in the name of Andrew the First were built and destroyed as time passed on this site. In 1747, the construction of St. Andrew's Church started with the project of Bartolomeo Rastrelli (Fig. 1).

The historic building is constructed on a very complex geological landslide hill, which is washed by groundwater and spring waters.

At time of construction, complex engineering and geological studies of the area under construction were conducted and extensive work on the construction of strip stone foundation was carried out to create a massive foundation—church stylobate and its porch. During the construction works, the soil was removed, and groundwater and spring waters were drained. The foundations of the stylobate is made of natural stone and broken brick in lime-stone mortar, were laid at the depth of 3.5 m from the stylobate floor on the eastern side, 4.8 m on the western side. Given the problem area (such as the risk of landslides). Regular monitoring and fortification works are carried out. There are ravines on the slopes of the hill, where active displacements and erosion processes develop (Fig. 2). Around the development site there is a complex of unfavorable physical and

Fig. 1 Study area. Location of St. Andrew's Church in Ukraine

Fig. 2 An example of the active development of landslide processes with active developments and erosion processes on the slope of the Church

geological phenomena such as landslides, considerable thickness of fill-up ground, significant ground heterogeneity, mechanical suffixation of clay particles into an existing inactive gallery, and external erosion of the hill massif. The base of the foundations of the southern, western and northern Church facades is eolian-deluvial loess-like loamy sands, which have sagging properties. The base of the foundations at the eastern part is morainic loam. Hydrogeological conditions are characterized by the presence of two groundwater levels.

Due to high landslide risk of the hill and great cultural value of the building, the historical and architectural site needs constant monitoring, strengthening and preservation for posterity [https://andriyivska-tserkva.kiev.ua/].

The World Heritage Convention of 1972 aimed at promoting and supporting the conservation of the world's cultural and natural heritage. The basic principles of the convention states that the obligation of each participating state is to ensure the identification, protection, preservation, presentation and transmission of the cultural and natural heritage located in its territory to future generations (UNESCO 1972; The World Heritage Convention 1972).

The methodological issues and practical realization of these problems are analyzed in the in the publications of authors (Atzeni et al. 2015; Mainwaring and Olsen 2018; Miranda et al. 2020; Barla et al. 2014; Highland and Bobrowsky 2008; Carvalho et al. 2018; de Brito et al. 2018; Farenyuk et al. 2021; Kaliukh et al. 2018a, b; Lollino 2014; Mazzolani and Calado 2019; Zanakis et al. 2003; Papadopoulos and Vayas 2019 and others), building codes and documents EN 1992-1-1-2004, fib Bulletin 34, among others.

With respect to the usage of remote sensing of the earth from space, there are many works by scientists: Greben et al. (2020), Baum (2014), Trofymchuk (2020), Khyzhniak and Fedorovskyi (2020) and many others. A number of specialists worked on attracting information technologies to study landslide-hazardous areas, objects located on them, modeling and determining landslides, monitoring areas and to solve environmental and recreational and economic issues (Popov et al. 2020; Yue et al. 2021; Piestova et al. 2019).

GIS methods for creating landslide probability maps have been studied by several authors (Aleotti and Chowdhury 1999; Kanungo et al. 2009, Mersha and Meten 2020). The analysis in GIS can be numerical using actual data, or qualitative with a probability of occurrence of the event. Qualitative methods include geomorphological analysis and overlay and intersection inventory methods, with expert judgement, qualitative maps are created.

1.1 Surveyed Structural Damages and Previous Landslides

The visible superstructure of the church is based on a slightly wider underground two-story foundation. The base of the foundations of the eastern part is morainic loam.

During structural surveys, it was discovered that the superstructure had significant damages as follows:

- Vertical and inclined cracks with a width of up to 2.0 cm in the walls of the superstructure.
- Cracks width up to 2.0 cm (Fig. 3) in brick vaulted ceilings.
- Walls and ceilings soaking and fungosity;
- Deviation from the superstructure vertical wall.

Whereas for the runway walls, the following damages were detected:

- Diagonal cracks with a width of up to 3.0 cm;
- Frost destruction of the brickwork and deviation from vertical of the reinforced concrete retaining wall,
- Through cracks.
- Local destruction of the outer layer and brickwork mortar.

The main source of detected damages was the uneven foundation subsidence, caused by the presence of subsiding ground and sloping ground movements.

In the 1970s, a landslide occurred, after which, the slopes of the hill were fixed with semi-rings of Gambia piles up to 20 m deep, on which a reinforced concrete support pillow-block was mounted, and an observation deck was arranged on top of it. Another landslide was recorded in June 2012.

Fig. 3 Vertical crack with a width of up to 2.0 cm

2 Methods

This research included data collection and analysis, use and processing of remote sensing data, data from geographic information systems, analysis in the Earth Observation (EO) Browser service using the java script programming method, mathematical calculation of the stability of the structures, modeling of the stress-deformed state of the object and adjacent territory and recommendations for consolidation (Fig. 4).

2.1 Data Collection and Organization

Data necessary for this study were collected from various sources. The study of relevant literature from published articles and monographs, data collection on the object of the study and the surrounding area, topographic map of 1: 50000, geological maps, radar-location images Sentinel-1A, B (spatial resolution 10 m) and images from Google Earth (spatial resolution up to 1 m). Ground studies and analysis of geological conditions of the study area were also conducted.

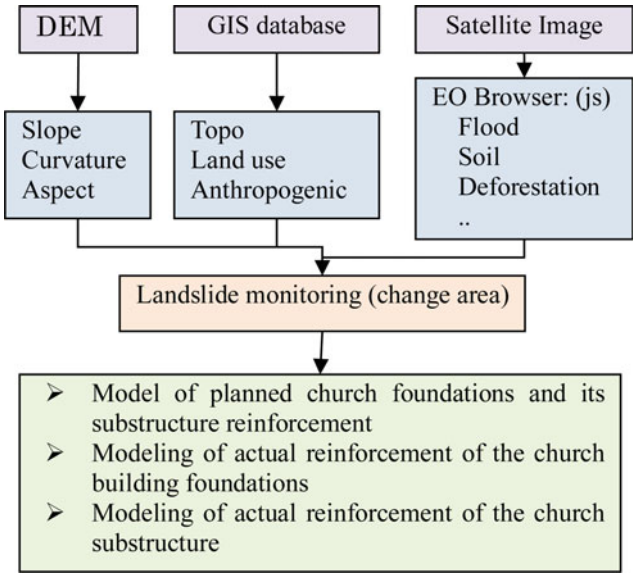

Fig. 4 Structure scheme of the research work

2.2 Use and Data Processing of Remote Sensing

Compared to traditional methods of studying the earth surface, remote sensing methods have significant advantages in terms of the scale of survey, obtaining global and local information about objects and their monitoring. The use of Persistent Scatterers (PS) of interferometric data allows the processing of a large number of different-time/radar-location images obtained by radar locators with synthesized aperture (PCA) from the satellite Sentinel-1 of European remote sensing system Copernicus, which enables the determination of vertical displacements with an accuracy of 4 mm/year, including the shear activity of research objects in large areas, while determining specific places of displacement.

The use of optoelectronic data from space surveys allows the detection landslide-hazardous areas, buildings located on them, active and temporarily stable landslides, and to monitor the dynamics of their movement, which enables a fast response to the findings, namely to collect material, select photos, maps, etc. on the object under study and take timely action to prevent emergencies.

Google Earth space images were used to further explore St. Andrew's Church and the surrounding area. On the slope of the object under study on June 28 2012, there was a landslide. Figure 8 shows a map of time changes before and after the landslide, indicating the movement and area of the landslide. Therefore, the analysis of space images made it possible to assess the scale of the landslide hazard, calculate the area of the affected areas of the slope, and provided recommendations for specifying the location of ground research to further avoid negative consequences that could lead to emergencies.

2.3 Involvement of Geographic Information Systems

The geographic information system ArcGIS, was used to determine the area of the monitored object and its specific features (terrain, the presence of plantations, roads, water, buildings, etc.).

The spatial distribution and density of landslides mainly depend on topography, weather conditions, geology, land use/soil cover, and anthropogenic factors. Topographic factors include slope, aspect, and curvature based on digital elevation model data (DEM) as shown in (Fig. 5).

Slope is a very important parameter for landslide studies because it has a direct relationship with landslide occurrence (Yalcin and Bulut 2007). Landslides are more likely to occur on higher slopes as a result of gravitational stress. The curvature map shows concave, convex, and flat surfaces (Fig. 3). After a rainfall event, a convex or concave slope contains more water and holds it for a longer period of time (Lee and Talib 2005). The more positive or negative it is, the more likely a landslide will occur. Aspect refers to the orientation of the slope, which is usually given in degrees from 0 to 360. It is widely viewed as an important factor in landslide studies because it controls slope exposure to sunlight, wind direction, precipitation (degree of saturation), and break conditions (Komac 2006).

Land use is the most important factor influencing the formation of landslides resulting from rainfall (Fig. 6). Changes in land use/cover due to anthropogenic activities such as deforestation, grazing, intensive farming and cultivation on a slope that is extremely steep can lead to slope instability. Vegetation contributes to resistance to slope movement. Vegetation reduces the effects of erosion and increases slope stability.

Sentinel hub is open-source data. The EO Browser service provides access to space images of both visible and radar range. For monitoring, space images in resolution of 10 m per pixel are available (Fig. 7).

The maps of water saturation of the soil were obtained using the EO Browser services. Combinations of images and selection by various criteria were used in the java scripts language. Soil moisture saturation maps were obtained.

2.4 Mathematical Calculation of Slope Stability, Modeling of Stress–strain State of the Object and the Surrounding Area and Recommendations for Strengthening

Calculations were performed taking into account the zones of weakness and gaps in the soil caused by the suffusion of soil into the drainage system of the building. This made it possible to obtain the values of the stress–strain state for the

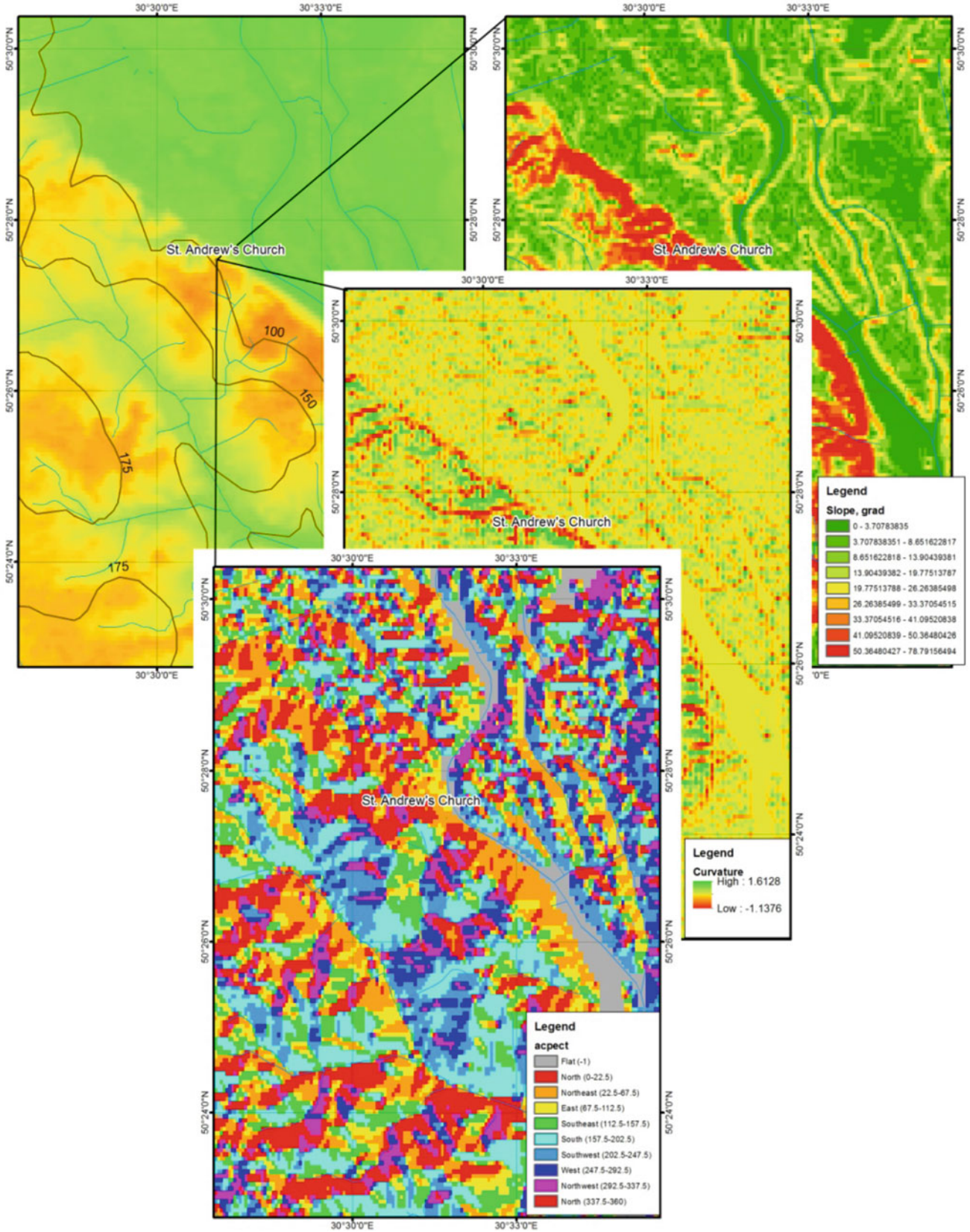

Fig. 5 Slope, aspect, and curvature based on digital elevation model data

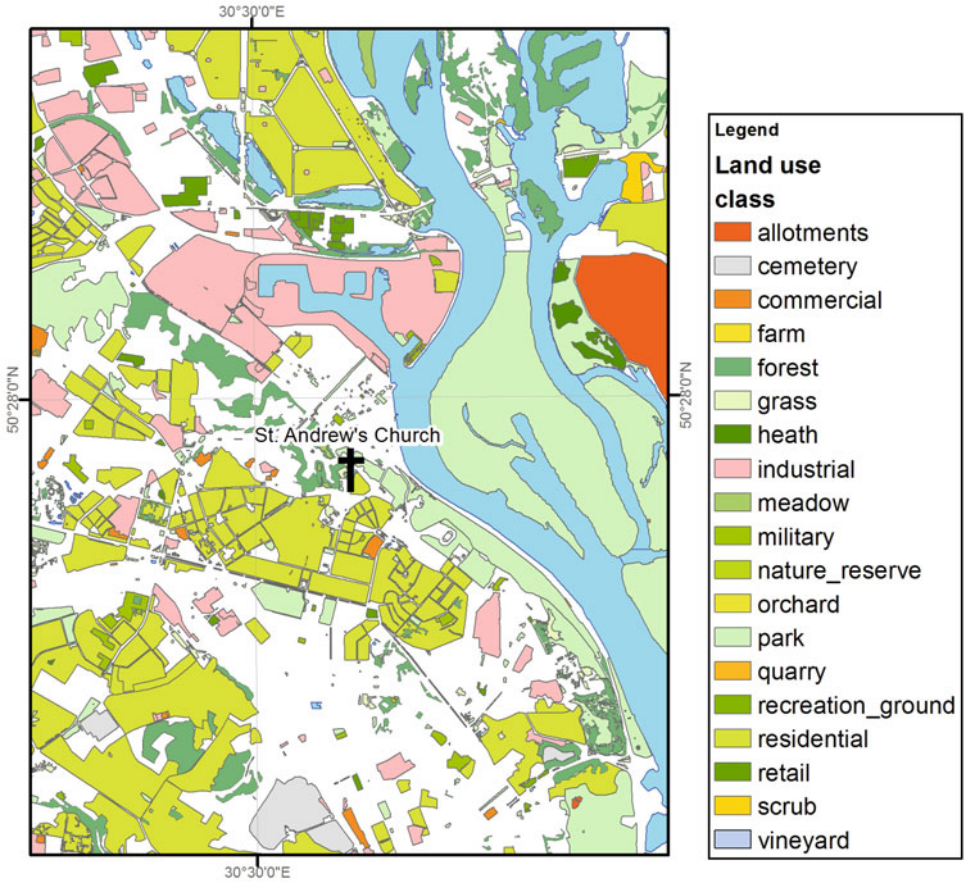

Fig. 6 Land use

load-bearing civil structures of St. Andrew's Church and to compare the numerical results and standard values of the strength of the main building structures. Software LIRA 9.6 (Ukraine) was used for the finite element method, the average size of the grid was 0.3 m. A model for the stabilization of the foundation using the method of "grounds jet grouting" was carried out on the basis of the calculation scheme, which took into account the detected cracks in the cross section of the masonry and the foundation in the wet state (Fig. 7).

The location of "jet"-columns under part of the object's foundations was taken into account in the simulation model by changing the soil deformation modulus from the natural state to the weighted average deformation modulus and jet grouting jet-columns "jet grout", which was determined by the formula (Farenyuk et al. 2021):

$$\overline{E} = \frac{(A_{bn} \cdot E_{bn}) + (A_{jt} \cdot E_{jt})}{A_{bn} + A_{jt}}$$

where

$\overline{E}$ is the weighted average module of stabilized ground deformation under foundations site.

A_{bn} is area of reinforced site under foundations without regard to "jet"-columns area.

E_{bn} module of ground deformation in natural state.

A_{jt} area of "jet"-columns on the site under foundations.

E_{jt} module of "jet"-columns material deformation.

A brief characteristic of the calculation options is given in the Table 1.

To determine the effectiveness of the actions to strengthen the building of St. Andrew's Church, several calculation were conducted, which also took into account the transverse existing cracks in the building. Different variants of water saturation of the base under the whole church building and its stylobate part were considered.

Modeling of soil water saturation in the calculations was performed by attributing values of soil properties corresponding to water saturation. The appearance of zones of weakening and voids in the soil due to suffusion into the drainage system located near the foundations was also taken into account. Modeling of base watering was carried out only on areas of foundations that were not stabilized by the "jet grouting" of the base.

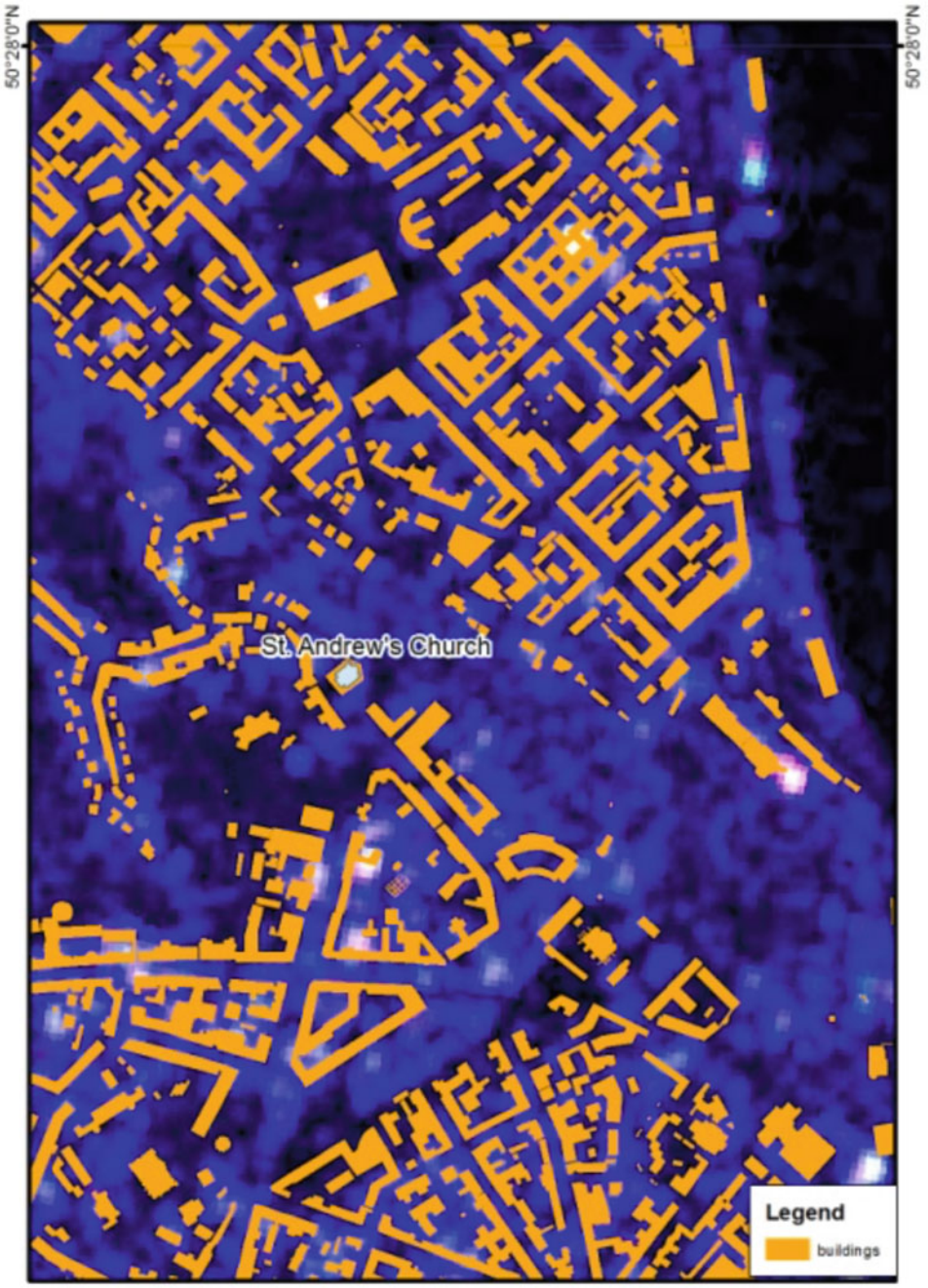

Fig. 7 The maps of water saturation of the soil

3 Result and Discussion

The ArcGIS geographic information system was used to determine the boundaries of the monitoring area with the studied object, its features (terrain, presence of forest plantations, roads, water reservoirs, buildings). The particularity of the location required the implementation of space photography of ultra-high spatial diversity on the eastern side of St. Andrew's Church. The selection of different-time space images for the period of 2012–2019 was carried out for a certain parts. All selected images underwent orthorectification procedure based on ground data, followed by determination of the landslide-prone area (Fig. 8).

In the first stage, a stability analysis was carried out regarding the landslide hazard slopes of the studied territory (Fig. 9). Based on the historical materials study, visual inspection of the slopes adjacent to the St. Andrew's Church building and performed calculations, it was established that a significant part of the St. Andrew's Church hill slopes were in a state close to ultimate equilibrium. At the second stage, the analysis of the stress–strain state of the building and

Table 1 "Building foundation" system calculations options

Option code	Brief description
1	Modeling of planned church foundations and its substructure reinforcement according to technical decisions developed using grounds jet grouting method by "jet"-columns
2	Modeling of actual reinforcement of the church building foundations and its substructure using basis jet grouting method by "jet"-columns
3	Modeling of actual reinforcement of the church substructure using basis jet grouting method and arrangement of over superstructure reinforced concrete slab by "jet"-columns

Fig. 8 Identification of landslide-hazardous areas according to Google Earth

foundation soil was carried out using the graphic model of the stylobate block (Fig. 10) and building constructions of the superstructure of the St. Andrew's Church (Fig. 11).

The calculations were carried out considering the results of visual inspections and foundation soil deformations calculations. In building numerical modelling, the following three groups of the "building—foundation" system stress–strain state calculations were performed:

1. Group 1—the stress–strain state calculation to determine the causes of the cracks' occurrence in the building and its stylobate block walls in cases of the values of soil properties in a natural state, the water saturated foundation soils under the entire of St. Andrew's Church building and its stylobate block, as well as in other unfavorable cases.
2. Group 2—the calculation to determine the actual stress–strain state of SAC structures considering the damage

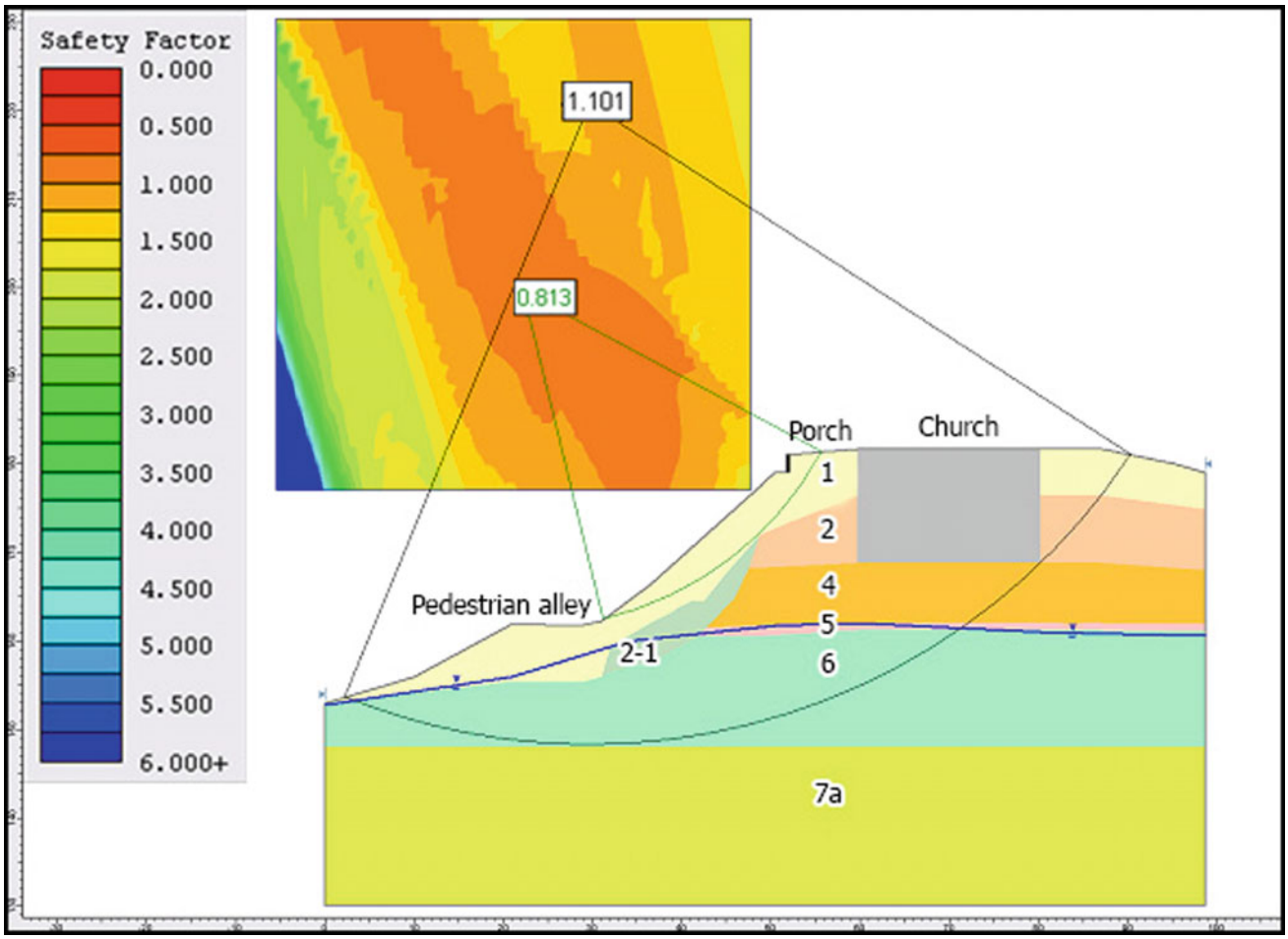

Fig. 9 Example of the results of calculation of SAC hill landslide hazard

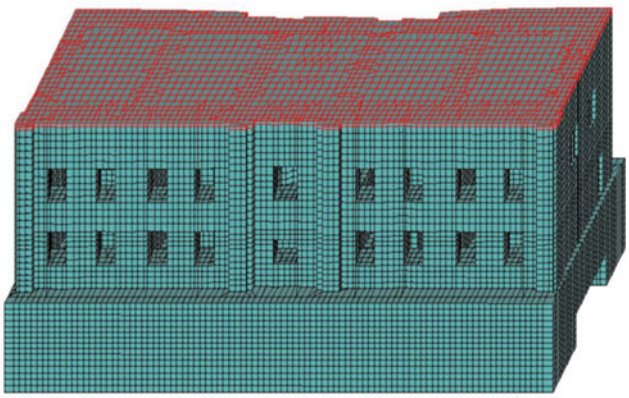

Fig. 10 General view of the computational model of the SAC stylobate block installed above-stylobate slab

recorded during their visual inspection. The modeling was performed during several stages:

First stage: the calculations were performed to determine the causes of cracks in the walls of the church building and its stylobate part with the characteristics of the base soil in their natural state; modeling of a base soaking under the entire church building and its stylobate part; modeling of a foundations base soaking at the north-eastern part of the church building; modeling of a soaking of the stylobate foundations base and the south-western and central parts of the church building.

Second stage: the calculations were performed to determine the actual stress–strain state of the building structures, considering damages detected during the visual inspection.

The third stage: the calculations were performed to forecast the stress–strain state of the building structures under the possible conditions of the base operation.

The design scheme of the building considered the through cracks detected during the visual inspection. The occurrence of loosening zones and voids in the soils due to suffusion from the adit systems located in the immediate vicinity of the church foundations was also considered. The first stage of calculations was designed to

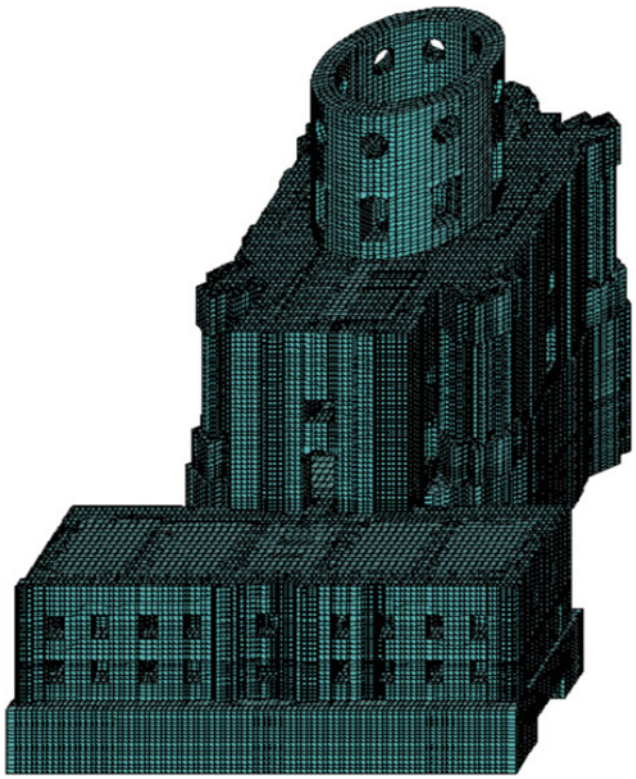

Fig. 11 General view of the computer model of the church building on the south-eastern side

model the stress–strain state of structures under various possible operating conditions of the base, and to determine the causes of cracks. For the second and third stages of calculations, the detected through cracks in the brickwork were considered in the building analytical scheme. In addition, cracks in the overstressed sections of the foundations obtained by the first stage of calculations were modeled. The results of the second stage of calculations allowed to estimate the actual stress–strain state of the structures. The results of the third stage calculations allowed to assess the changes in the structures stress–strain state if the base was soaked.

3. Group 3—mathematical modelling of the of St. Andrew's Church structures stress–strain state in case of possible degradation of the physical and mechanical characteristics of the foundation soils. In the calculations, the base soils soaking was modeled by assigning to the soils underlying the foundations, parameters that corresponded to water saturation state (based on the engineering geological survey data). Accordingly, to model most unfavorable conditions, reduced stiffness coefficients were assigned for some base areas or for the entire foundation.

Based on the results of calculations, we may conclude that the main cause of cracks in the masonry of the load-bearing elements of the church and stylobate are the excessive values of relative deformations in the foundation, along with the unstable loads resulting from the structural system of the building.

Modeling of the soaking of the base showed significant overstressed zones, which indicates a probable additional expansion of cracks and the possible emergence of new ones, with an exception of the soaking base of the foundations at the north-eastern part of the stylobate, where the building is somewhat leveled, relative deformations are reduced and, in turn, zones of overstressed areas are reduced (Farenyuk et al. 2021; Slyusarenko et al. 2022).

The actual stress–strain state of structures for the period of inspection is characterized by the presence of extremely tense zones in which the values of the effective tensile and compressive stresses are at the limit of the strength of the masonry as follows:

(a) Maximum tensile stresses:
- Foundation areas lying below the wall of the main facade of the stylobate at its intersection with the foundations under the transverse walls;
- Areas of masonry wall of the main facade of the stylobate below the window openings, and in places adjacent to the transverse walls of the stylobate;
- Sections of walls and ceilings on the second floor of the stylobate in the area of the main entrance to the church;
- Areas of the church ceiling at the places adjacent to the brick cylinder of the dome;

(b) Maximum compressive stresses:
- Local areas of destruction of masonry (crumpling) in places where the change of marks of the intersecting foundations' sole comes in contact with the stylobate walls (Fig. 12).

The values of the main stresses in the walls of the church building do not exceed the strength of the brickwork, except for local areas on the floor at the junction with the brick dome. At the same time, the brickwork of the church floor (ceiling of the 2nd floor of the stylobate) in the area of the main entrance and the iconostasis is within maximum allowable stresses. Overstressed areas are identified in the masonry of the stylobate foundations and in the wall of its main facade.

To predict the change in the stress–strain state of the load-bearing structures of the church building and stylobate

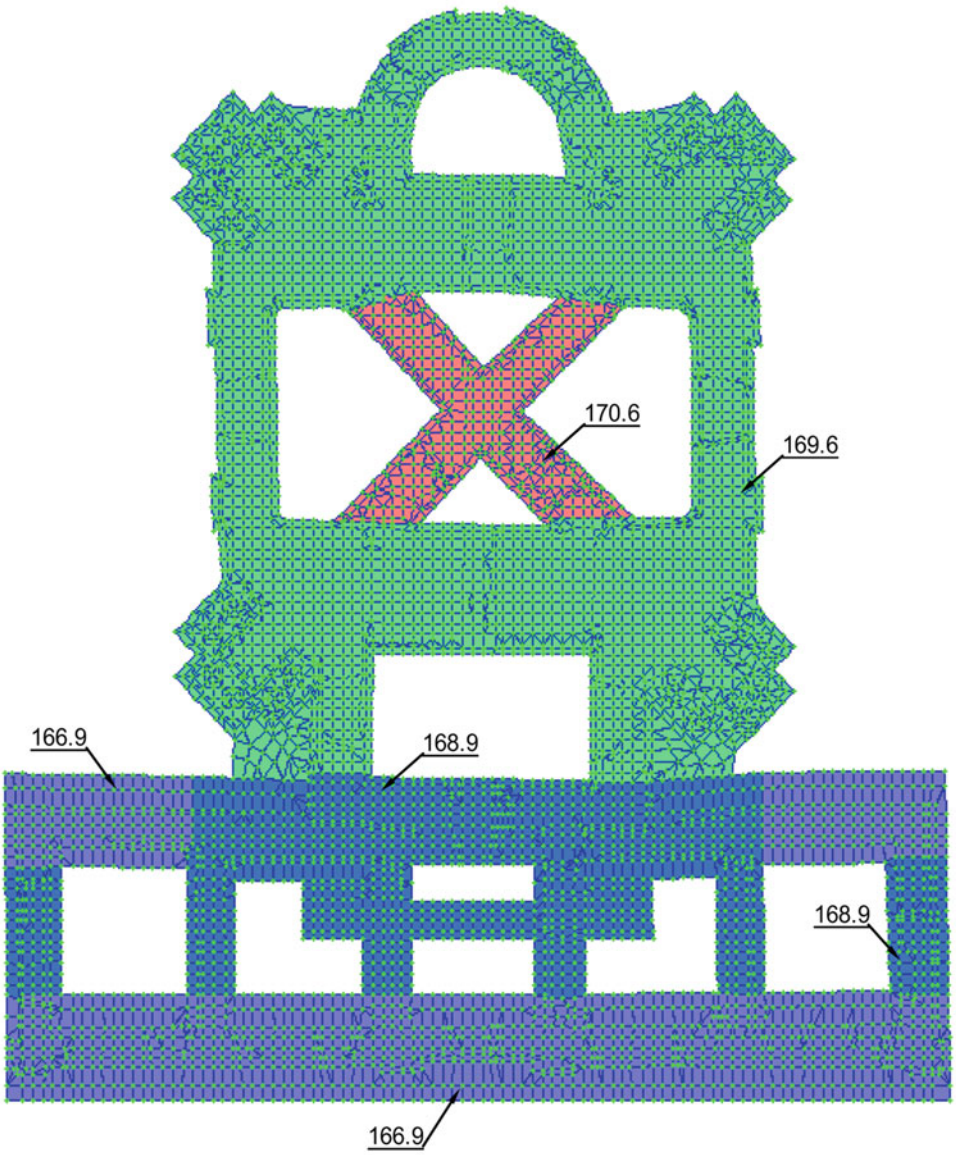

Fig. 12 Scheme of the foundations of the church building and the stylobate part with the indication of the marks of their pedestal

when changing the operating conditions of the foundation, another numerical simulation for stresses was made to simulate the soaking of the foundations of stylobate, including its cracks. The results of the calculation shows an establishment of the structural system of the church building and stylobate that is extremely sensitive to additional deformations at the base due to soaking. Such sensitivity is manifested in the appearance of additional areas of overstrained sections of brickwork, where the values of tensile stresses is increased by 50–200%. Such changes are also applicable to stylobate structures, where the calculation shows the largest changes in the stress–strain state. (The values of the main tensile stresses in the roof of the church building are increased by 50–60%). These tensions will inevitably provoke the appearance of new cracks in the load-bearing structures of the stylobate, the church building and the opening of existing ones.

Given the current technical condition of the building, the process of cracks opening may lead to the destruction of individual structural elements and might be critical to the stability of the building.

4 Conclusions

Effective methods of monitoring changes of archeological buildings should include the use of radar-location and optoelectronic data of remote sensing, as the use of such techniques provide opportunities to search for objects and areas that are prone to be destroyed by landslide processes,

to provide an opportunity to assess the scale of potential problem(s) and trends in future development of displacements. This allows to remotely identify a list of objects at risk of destruction, and provide a tool for making management decisions.

Based on the results of mathematical modeling of the actual stress–strain state of the building structure, recommendations for consolidation/restoration/strengthening were given, and geotechnical works of St. Andrew's Church and the surrounding area were performed:

- Restoration and strengthening of damaged building structure.
- Strengthening the church foundation by "jet"-columns, restoration of facades and interiors.
- Improvement of technical condition of the adjacent landslide and restoration of integrity of church buildings by reinforcing damaged areas were made.

Techniques of information technology, remote sensing of the earth from space and geotechnical protection are proved to provide historical monuments with reliable protection from adverse geological processes and ensure long-term reliable operation.

Acknowledgements We would like to express our very great appreciation to the Ukrainian SE RIBC scientists, who have been directly involved in visual and instrumental survey and mathematic simulation of the stress-strain state of the SAC and adjacent area. Our special thanks are extended to our colleague from the SRIBC, Yuriy Slyusarenko, Volodymyr Tytarenko, Anton Dvornyk, Valeriy Shuminskiy for his support in the site and office work. We would like to express our very great appreciation to the Ukrainian experts of "OSNOVA-SOLSIF" private Consultancy, who have performed not only the working design for SAC foundations reinforcement, but also all works on foundations reinforcement by jet-grouting columns.

References

Aleotti P, Chowdhury R (1999) Landslide hazard assessment: summary, review and new perspectives. Bull Eng Geol Environ 58:21–44. http://doi.org/10.1007/s100640050066

Atzeni C, Barla M, Pieraccini M, Antolini F (2015) Early warning monitoring of natural and engineered slopes with ground-based synthetic aperture radar. Rock Mech Rock Eng 48(1):235–246. ISSN 0723-2632. http://doi.org/10.1007/s00603-014-0554-4

Barla M, Antolini F, Dao S (2014) Il monitoraggio delle frane in tempo reale. Strade & Autostrade 107(5):154–157. ISSN 1723-2155

Baum R, Miyagi T, Lee S, Trofymchuk O (2014) Introduction: hazard mapping. In: Landslide science for a safer geoenvironment. Springer, Cham, pp 395–396. http://doi.org/10.1007/978-3-319-05050-8_61

Carvalho C, de Brito J, Flores-Colen I, Pereira C (2018) Inspection, diagnosis and rehabilitation system for vinyl and linoleum floorings in health infrastructures. J Perform Constructed Facil 32(6). ASCE: 0001229. http://doi.org/10.1061/(ASCE)CF.1943-5509.0001229

Casagli N, Catani F, Del Ventisette C, Luzi G (2010) Monitoring, prediction, and early warning using ground-based radar interferometry. Landslides 7(3):291–301. https://doi.org/10.1007/s10346-010-0215-y

de Brito J, Kurda R, Silva P (2018) Can we truly predict the compressive strength of concrete without knowing the properties of aggregates? Appl Sci 8(7). Paper 1095. http://doi.org/10.3390/app8071095

EN 1992-1-1-2004. Eurocode 2: design of concrete structures—part 1-1: general rules and rules for buildings

Farenyuk G, Slyusarenko Y, Tytarenko V, Melashenko Y, Dvornyk A, Ischenko Y, Shuminskiy V, Kosheleva N, Dombrovskyi Y, Kaliukh I (2021) Repairing and strengthening measures on the St. Andrew's Church. In: Proceedings of the fib symposium 2021 "Concrete structures: new trends for eco-efficiency and performance", Lisbon, Portugal, 14–16 June 2021, pp 1184–1193

fib Bulletin 34 (2006) Model code for service life design. Fédération Internationale du Béton (*fib*), Lausanne, Switzerland

Ghorbani S, Taji I, Tavkholizadeh M, Davodi A, de Brito J (2018) Improving corrosion resistance of steel rebars in concrete with marble and granite waste dust as partial cement replacement. Constr Build Mater 185:110–119. https://doi.org/10.1016/j.conbuildmat.2018.07.066

Greben A, Trofymchuk O, Trysnyuk V, Krasovskiy G (2020) Interpretation of remote sensing data for ecological tasks. In: 2020 IEEE Ukrainian microwave week (UkrMW). 10th international Kharkiv symposium on physics and engineering of microwaves, millimeter and submillimeter waves. https://doi.org/10.1109/UkrMW49653.2020.9252736

Highland L, Bobrowsky P (2008) The landslide handbook—a guide to understanding landslides: Reston, U.S. Geological Survey Circular, Virginia, 129 p

Kaliukh I, Dunin V, Berchun Y (2018a) Decreasing service life of buildings under regular explosion loads. Cybern Syst Anal 54:948–956. https://doi.org/10.1007/s10559-018-0098-9

Kaliukh I, Farenyuk G, Farenyuk I (2018b) Geotechnical issues of landslides in Ukraine: simulation, monitoring and protection. In: Wu W, Yu H-S (eds) Proceedings of China-Europe conference on geotechnical engineering. Springer series in geomechanics and geoengineering. Springer, Cham, pp 1466–1469. http://doi.org/10.1007/978-3-319-97115-5_124

Kanungo D, Arora M, Sarkar S, Gupta R (2009) Landslide susceptibility zonation (LSZ) mapping—a review. J South Asia Disaster Stud 2:81–105

Khyzhniak AV, Fedorovskyi OD (2020) Integration of remote sensing data and ground-based information to solve natural resources and environmental problems. Космічна наука і технологія 26(4) (125):31–37. https://doi.org/10.15407/knit2020.04.031

Komac M (2006) A landslide susceptibility model using the analytical hierarchy process method and multivariate statistics in perialpine Slovenia. Geomorphology 74(1–4):17–28. http://doi.org/10.1016/j.geomorph.2005.07.005

Lee S, Talib JA (2005) Probabilistic landslide susceptibility and factor effect analysis. Environ Geol 47:982–990. https://doi.org/10.1007/s00254-005-1228-z

Lollino G (ed) (2014) Engineering geology for society and territory IAEG XII congress, vol 8643, p 8

Mainwaring G, Olsen TO (2018) Long undersea tunnels: recognizing and overcoming the logistics of operation and construction. Engineering 4(02):249–253. https://doi.org/10.1016/j.eng.2018.03.004

Mazzolani FM, Calado L (2019) Selected papers from the 3rd international conference on protection of historical constructions (Prohitech'17). Int J Architectural Heritage 13(1):1. https://doi.org/10.1080/15583058.2018.1564591

Mersha T, Meten M (2020) GIS-based landslide susceptibility mapping and assessment using bivariate statistical methods in Simada area, northwestern Ethiopia. Geoenviron Disasters 7:20. https://doi.org/10.1186/s40677-020-00155-x

Miranda J, Valença J, Costa H, Júlio E (2020) Chromatic design and application of restoration mortars on smooth surfaces of white and GRAY concrete. Structural concrete, Technical paper. First published: 05.09.2020. https://doi.org/10.1002/suco.202000054

Papadopoulos K, Vayas I (2019) Restoration and strengthening techniques for ancient-Greek monuments. Int J Architectural Heritage 13(1):33–46. https://doi.org/10.1080/15583058.2018.1497233

Piestova IO, Lubskyi MS, Svideniuk MO, Golubov SI, Laptiev OA (2019) Urban thermal micro-mapping using satellite imagery and ground-truth measurements: Kyiv city area case study. Ukrainian J Remote Sens 21:40–48. http://doi.org/10.36023/ujrs.2019.21.149

Popov MO, Topolnytskyi MV, Titarenko OV, Stankevich SA, Andreiev AA (2020) Forecasting gas and oil potential of subsoil plots via co-analysis of satellite, geological, geophysical and geochemical information by means of subjective logic. WSEAS Trans Comput Res 8(11):90–101. https://doi.org/10.37394/232018.2020.8.11

Slyusarenko Y, Tytarenko V, Shuminskiy V, Dvornyk A, Dombrovskyi Y (2022) Protection of St. Andrew's Church located within landslide hazardous sites and ground constraints. In: Vayas I, Mazzolani FM (eds) Protection of historical constructions. PROHITECH 2021. Lecture notes in civil engineering, vol 209. Springer, Cham. http://doi.org/10.1007/978-3-030-90788-4_88

St. Andrew's Church. History of St. Andrew's Church (2021) https://andriyivska-tserkva.kiev.ua/andriyivska-cerkva/istoriya-andriyivskoyi-cerkvi/

The World Heritage Convention (1972) http://whc.unesco.org/en/convention/

Trofymchuk O, Klymenko V, Anpilova Y, Sheviakina N, Zahorodnya S (2020) The aspects of using GIS in monitoring of environmental components. In: International multidisciplinary scientific geoconference SGEM 2020, Albena, Bulgaria, 16–25 Aug 2020, pp 581–588. http://doi.org/10.5593/sgem2020/2.1/s08.075

UNESCO (1972) Convention concerning the protection of the world's cultural and natural heritage. http://whc.unesco.org/en/conventiontext/

Yalcin A, Bulut F (2007) Landslide susceptibility mapping using GIS and digital photogrammetric techniques: a case study from Ardesen (NE-Turkey). Nat Hazards 41:201–226. https://doi.org/10.1007/s11069-006-9030-0

Yue Z, Sheviakina N, Zagorodnia S, Kreta D, Radchuk I (2021) Geoinformation technologies for geoecological monitoring of urbanized water bodies. Environ Sci 4(37):18–27. http://doi.org/10.32846/2306-9716/2021.eco.4-37.2

Zanakis S, Theofanides S, Kontaratos A, Tassios T (2003) Ancient Greeks' practices and contributions in public and entrepreneurship decision making. Interfaces 33(6):72–88. Retrieved from http://www.jstor.org/stable/20141304

Application of Global Satellite Positioning and Automatic Monitoring in Slopeland Disaster Prevention

Thanh-Van Hoang, Tien-Yin Chou, Yao-Min Fang, Chun-Tse Wang, Ming Chang Tsai, Quoc Dinh Nguyen, Quoc Huy Nguyen, Quang Thanh Bui, and Quoc Tuan Nguyen

Abstract

The Global Positioning System (GPS) is satellite-based, with receiving equipment worldwide utilizing geographic positioning satellites in Earth orbit. The system is unaffected by the radio positioning system, so it provides highly accurate three-dimensional positioning, velocity, and time data to users. In this paper, Alishan Township, Chiayi County, central Taiwan, is selected to test an automatic real-time monitoring system comprising of one machine with multiple GPS antennas. To this end, the Alishan Public Works Section installed advanced measuring instruments and a landslide-monitoring system composed of a high-efficiency transmission system. A pre- and post-rainfall data survey was conducted on this slope section. Together with the rainfall records, real-time ground-slip monitoring data was collected, and subsequently analyzed to understand the disaster situation and ground slip characteristics of the Alishan Highway following an earthquake (1998). In the future, more effective management values will be set to reduce the loss of slope disasters to conserve land and public safety. For the first time in Taiwan, this paper presents displacement data indicating that after the typhoon rains, a maximum surface movement velocity of 2.5 cm every six days is attained, while the total displacement per month is as high as 10 cm. These data can be used as for the remediation of this section of the Alishan Highway.

Keywords

Multi-antenna global positioning system • Slope disaster • Monitoring system

T.-V. Hoang (✉) · T.-Y. Chou · Y.-M. Fang · M. C. Tsai
Geographic Information System Research Center, Feng Chia University, 100 Wenhwa Rd, Seatwen District, Taichung City, 40724, Taiwan
e-mail: van@gis.tw

T.-Y. Chou
e-mail: jimmy@gis.tw

Y.-M. Fang
e-mail: frankfang@gis.tw

M. C. Tsai
e-mail: akira@gis.tw

C.-T. Wang
Ph.D program of Infrastructure Planning and Engineering, College of Construction and Development, Feng Chia University, Taiwan, Taichung, Taiwan
e-mail: james@gis.tw

Q. D. Nguyen
Vietnam Institute of Geosciences and Mineral Resources, 67 Chien Thang Rd, Van Quan District, Ha Dong, Hanoi, Vietnam

Q. H. Nguyen · Q. T. Bui
Geography Department, Vietnam National University of Science, 334 Nguyen Trai Rd, Thanh Xuan Trung District, Thanh Xuan, Hanoi, Vietnam
e-mail: huyquoc2311@hus.edu.vn

Q. T. Bui
e-mail: thanhbq@vnu.edu.vn

Q. T. Nguyen
Department of Geography and Geology, Hue University of Sciences, 77 Nguyen Hue St., Hue City, Vietnam
e-mail: nguyenquangtuan@hueuni.edu.vn

1 Introduction

Taiwan is located in the place where the Banyan Tree is squeezed. Earthquakes are frequent, the geology is fragmented, the terrain is mountainous, the rivers are short and steep, and rainfall is unevenly distributed in time and space. Slope collapse disasters such as rockfalls, landslides, and debris flows seriously endanger the development of regional transportation and the industrial economy. Mountain roads are often the only external access in the region, and the stability of road slopes is critical to the safety of life and property of residents. It is therefore important to introduce automatic monitoring systems and emergency notification using various advanced technologies in steep-sloped areas with disaster potentials.

I. Alcántara-Ayala et al. (eds.), *Progress in Landslide Research and Technology, Volume 1 Issue 2, 2022*, Progress in Landslide Research and Technology,
https://doi.org/10.1007/978-3-031-18471-0_12

Disaster prevention and response systems have evolved from the traditional disaster prevention operations into disaster management, becoming an important direction for slope disaster prevention and control in recent years. The Global Positioning System (GPS) is a satellite-based radio positioning system. Utilizing positioning satellites in the earth's orbit, it can provide users, operating receiving equipment around the world, with highly accurate three-dimensional positioning, velocity, and time data without restrictions. The system is unaffected by weather, and can provide globally unified longitude and latitude reference data. It has an extensive range of applications and is already a mature technology. Due to the mass production of GPS modules, the low price further increases the accessibility of the technology and their intrinsic value to slope disaster monitoring applications.

In addition to accumulating sufficient historical monitoring data to provide follow-up scientific research and development, the automated monitoring system also hopes to capture the precursors of slope disasters and their dynamic behaviour when they occur, decreasing the response time of residents, and providing a reference for disaster prevention and responsible decision-making. Since these benefits significantly reduce the damage caused by disasters, real-time and effective communication transmission will be one of the critical links in the overall monitoring system.

This paper is an in-depth discussion on the application of a GPS and automatic monitoring system in road slope and landslide disaster reduction. It proposes, for the first time in Taiwan, that after a rainfall event, the maximum moving ground speed velocity of a section of the Alishan Highway section is 2.5 cm every six days, while the monthly total displacement is up to 10 cm. This information can be used as a reference for mitigation and basis for the regulation of this section of the Alishan Highway.

2 Literature Review

The landslide in Lishan area (Fig. 1) covers a vast area (Su et al. 2009), mainly including the Lishan Village at the intersection of Zhongheng Highway (Taiwan Line 8) and Yilan Branch Line (Taiwan Line 7A).

Large-scale stratigraphic sliding occurred in this area in April 1990. To prevent the continuous expansion of landslide disasters and maintain the safety of residents and smooth roads, the Bureau of Soil and Water Conservation of the Agriculture Committee of the Executive Yuan implemented the "Slope Disaster Remediation" plan in the Lishan area in 1995. Soil moisture detection (TDR) and GPS observation systems were established.

The Lishan Skid Warning Center was established to provide real-time notifications. A static GPS generated baseline

Fig. 1 Lishan area. *Source* Open street map

measurements of high accuracy within 3 h of receiving satellite data that is suitable for ground slip monitoring. The system uses GPS to measure the baseline length change for 3 h on different days, then compares the displacement and amount of displacement using a ground extensometer in the Lishan slip area. These displacement values, along with a wide range of environmental baseline measurements, are used to better understand the trend of large-area soil slides. To assess the feasibility of long-term GPS monitoring of landslides, Zeng (2003) and Shen (2004) undertook observations in the Lishan landslide area. Both researchers found that the most suitable measurement method for long-term landslide monitoring was static GPS baseline measurements, receiving satellite data at a rate of one measurement every second for a 3-h static baseline solution, averaging the movement over a 1-h interval. This method was most suitable for landslide monitoring with millimeter-level accuracy. A long-term GPS monitoring landslide reference value was determined using the GPS accuracy and displacement velocity. Preliminary monitoring results confirms the feasibility of this management reference value.

Jian (2002) studied the influence of various factors on the sliding mechanism of the slope using in situ measurement data. The study area was on the hillside along the highway near Wuwanzai, Gongtian Village, Fanlu Township, Chiayi County (Jian 2002). This area belongs to the old landslide area and has suffered from strata slip since the road was opened. Beginning in 2000, several monitoring instruments were set up in this area to observe the local strata, surface deformation, groundwater level, and rainfall for a continuous period of about two years, concurrently with theoretical analysis and laboratory test results. Observations show that this area is in a volatile state, with the sliding behavior closely related to the rainfall. According to the monitoring data in 2000, the accumulated rainfall required for accelerated sliding of the slope was about 80–270 mm, which is equivalent to the accumulated rainfall of 3–5 days.

Qiu (2004) and Jian (2002) used in situ measurement and theoretical analyses to explore the influence of related factors on the slope sliding mechanism. Long-term monitoring of surface and strata displacement, rainfall, groundwater level, groundwater flow, and other projects began in 2000, near Wuwanzai on the 18th line of Taiwan. On June 26, 2003, severe damage occurred, causing the loss of 150 m of road subgrade and interrupting traffic flow for about 1.5 months. The cause of edge damage was analyzed, discussed and compared with on-site monitoring results and theoretical analyses. The stability of the residual slope after the injury was evaluated, and a possible remediation plan was proposed.

The Linbeikeng area of Pingding Village, the upper reaches of Pingding River, Linnei Township, Yunlin County, known as the Little Yellow Mountain (Fig. 2), experienced a significant collapse after 921 earthquakes in 1988. Slope collapses continued to occur during Typhoon Lee and continuous heavy rain in 2006. The Bureau of Soil and Water Conservation conducted on-site slope hydrology and geology data collection to monitor collapse disasters in these areas. The ground collapse was monitored with surface extensometers and traditional GPS slope ground deformation-monitoring systems. Completing the real-time measurement of slope collapse during the typhoon established monitoring and management values, and strengthened the software and hardware of the local disaster prevention and response center in the Linbeikeng area of Pingding Village and the upper reaches of the Pingding River (Min 2020).

Lumb (1975), Brand (1982), and Slosson and Larson (1995) all show that slope failure often occurs after heavy rain. In addition to torrential rain, triggering slope damage also requires certain immediate hydrological conditions. Early on, rainfall must saturate the slope's surface, making it easier for water to flow downslope. Then subsequent heavy rain can start the mechanism of slope damage. The impact of previous rainfall on slope stability has been studied for many years. Lumb (1975) found that previous rainfall damaged slopes, especially if the current rainfall was high, and will be accompanied by more slope damage events. Four types of slope damage events were caused by rainfall:

1. The worst incident resulted in more than 50 slope damages in one day,
2. A severe incident caused 10–50 slope damages in a day,
3. Minor incidents caused less than ten slope damages in a day,
4. An independent incident caused only one slope damage in a day.

Based on the rainfall data obtained, Lumb (1975) defined the range of events of different magnitudes, illustrated by 15 days of precipitation and 24 h of heavy rain. The most severe event occurred with more than 100 mm of rain in 24 h and 15 days of upfront rainfall of more than 350 mm. Severe incidents occurred within 24 h of heavy rain of more than 100 mm when earlier rainfall reached 200 mm. With the correlation between rainfall and slope damage confirmed, it is possible to determine when slope damage has reached the threshold for research.

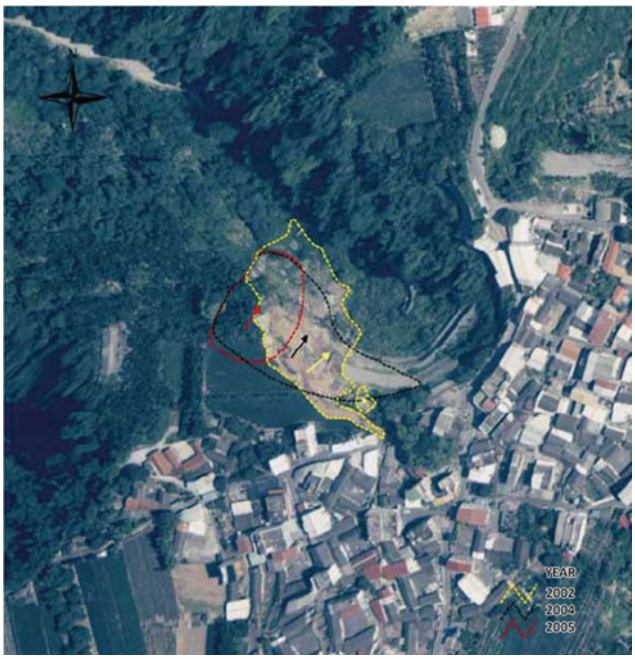

Fig. 2 Collapse areas of Pingding River upstream, Linbeiken area, and Pingding Village during different periods of time [24]. *Note* The yellow parts refer to the collapse condition on June 2002 (caused by Jiji Earthquake and Typhoon Toraji); the black parts are the collapses on 9 September 2004, while the parts in red are the collapses on 11 January 2005. The arrows indicate the sliding directions of each collapse

3 Research Methodology

3.1 Study Site

One of the limiting factors affecting the large-scale use of GPS in landslide monitoring is the high cost of hardware. For continuous monitoring of deformable bodies, each monitored point needs to be equipped with high-quality geodetic GPS receivers. This makes the equipment cost too expensive. To this end, we introduced the concept of using multiple GPS antennas connected to one receiver. This one-machine multi-antenna GPS is especially suitable for structural deformation and displacement monitoring, using an external off-the-shelf, standard commercial GPS receiver and a specially designed GPS multi-antenna switch (GMS: GPS multi-antenna switch). This allows multiple antennas to

be connected to one receiver, reducing the cost of hardware at each monitoring point exponentially, and making GPS more practical in many applications.

The one-machine multi-antenna GPS adopts the principle of time-sharing to allow each antenna to be connected to the receiver, and to collect GPS observation data according to the set time sequence. This principle is implemented under the control of an industrial personal computer (PC) using a specially designed GPS multi-antenna switch (GMS). Data collected by each antenna is used to calculate the position of the responding antenna, or the displacement of each corresponding antenna using the differential positioning mode. The architecture of a complete multi-antenna GPS is shown in Fig. 2. The system only needs two GPS receivers. The Reference Point refers to a fixed point and the Antenna Array is a moving point, while displacement is obtained through the Data Processing Center.

The Alishan Public Works Section commissioned the Feng Chia University team to complete the installation of various instruments, and share the project implementation results of the fourth bend of Taiwan 18 Line 44K and Xiaogongtian Village. Ground surface displacement measuring equipment included three CCD cameras with infrared projection, two lamps, a displacement meter, a surface extensometer, and image data-transmission equipment. The instrument deployment is shown in Fig. 3 (after Zheng et al. 2008).

3.2 Introduction to Global Satellite Positioning Monitoring System

In the past two decades, GPS has been widely used in many disciplines and fields, proving to be a potent tool for monitoring deformation and displacement of artificial and natural structures. GPS has many advantages over traditional measurement technology: it is more accurate and efficient, is high suited for automation, and installation requires low labor intensity. The dual-channel GPS satellite-positioning receiver has many advantages, including ultra-high precision, ultra-high sampling frequency, and all-weather observations. GPS is often used as a continuous tracking station for high-precision geodetic surveying and crustal change measurement. Since the On-The-Fly (OTF) method can solve in real-time, the undetermined value of the cycle, it is also often used for fast dynamic (kinematic) measurements (i.e. RTK), with aerial photogrammetry, or in fast-running vehicles. Since hardware is relatively expensive, single-channel satellite positioning receivers are used since they are relatively cheap to manufacture when compared with dual-channel GPS satellite positioning receivers. However, the number of receiving channels is small, so the ability to support dynamic measurement is inferior when compared to the dynamic capabilities of dual-channel GPS receivers. After years of changes in software and hardware, and with new technologies for solving undetermined cycles, single-channel GPS satellite positioning receivers are still inferior to dual-channel GPS receivers, but can be used for monitoring and measurement with smaller dynamic amplitudes. Performance is also excellent, with GPS successfully solving the undetermined value of the cycle and providing the accuracy of long-term monitoring. In addition, with wireless communication equipment and sophisticated analysis software, the single-channel GPS satellite-positioning receiver is sufficient to support the monitoring of displaced and deformed buildings and slopes (Fig. 4).

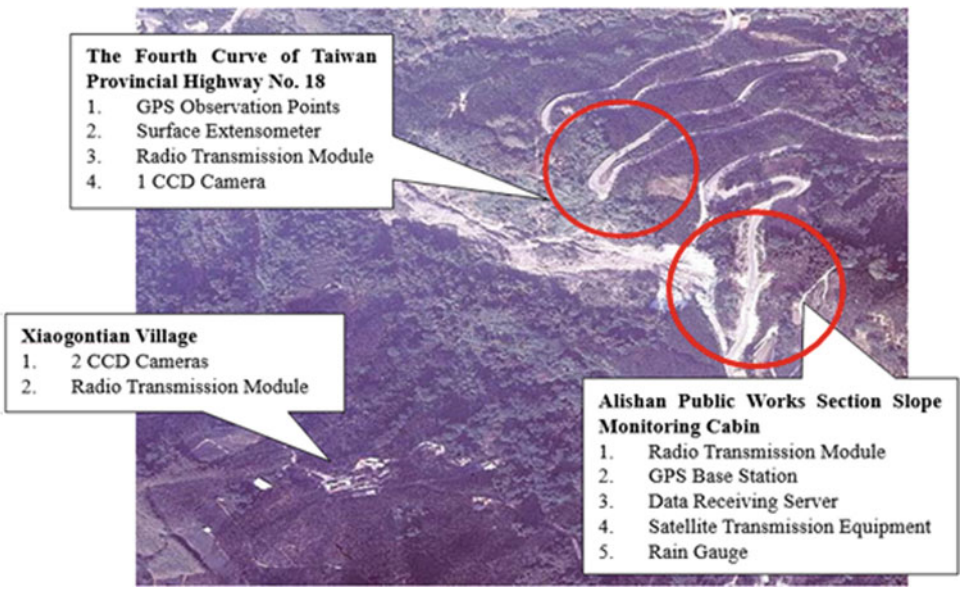

Fig. 3 Instrument installation location map

3.3 Global Satellite Positioning Monitoring System Test

To ensure the accuracy and stability of the one-machine multi-antenna monitoring system, laboratory tests were completed before onsite installation for real-time monitoring. This test was conducted at the Business School of Feng Chia University.

3.3.1 Introduction to the Experimental Site

The test was conducted on the top floor of the Business School of Feng Chia University to ensure a convenient place where the experiment had an unobstructed view of the horizon and sky. The storage room used as the instrument control room contained a multi-antenna GPS switch (Switch), two GPS receivers (Receiver), and a PC host. An existing GPS fixed station at the Ministry of the Interior was used as the multi-antenna GPS measurement base station. The layout and location of the entire one-machine multi-antenna GPS are shown in Fig. 5, comprising one base station and four mobile stations.

3.3.2 Static Initial Value Measurement

To confirm the accuracy of the GPS measurement, a laser theodolite was used to measure the level and elevation of the fixed and mobile stations (GPS0 to GPS7). Since the leveling measurement use a particular direction as fixed, other points were measured relative to this direction. With the connection direction between Base and GPS1 taken as fixed, the results obtained were compared with the multi-antenna GPS measurements (Fig. 6). Coordinates at the end of the test are shown in Table 1. Differences in the vertical direction are large, while a large error in the horizontal direction of the GPS8 is also noted. The poor accuracy of the multi-antenna GPS8 resulted from positioning the GPS antenna too low to the ground so that the signal was reflected. Antennas should be placed more than 100 cm from the ground to avoid signal interference. In addition, a multi-path effect was generated because the position of the roof (instrument house) on the top floor blocks about half of the line of sight to the air.

4 Field Test of Global Satellite Positioning Monitoring System

The fixed station with instruments installed by early October 2007, and included one set of GPS base stations and four sets of mobile monitoring GPS antennas, as shown in Fig. 7.

Static measurements and reception data were collected for two days (i.e. 48 h) from 2007/10/17 to 2007/10/19 to calculate the static coordinates (Table 2). Dynamic real-time monitoring began on 2007/10/19. Results for three days from 2007/10/19 to 2007/10/21 are shown in Table 3. Except for GMS3 and GMS4, which have a continuous displacement in the Y direction (about 2.4 cm), the rest oscillate back and forth, and are in a stable state. The dynamic real-time monitoring results for 20 days from 2007/10/19 to 2007/11/12 show that, except for the continuous displacement in the Y direction of GMS3 and GMS4

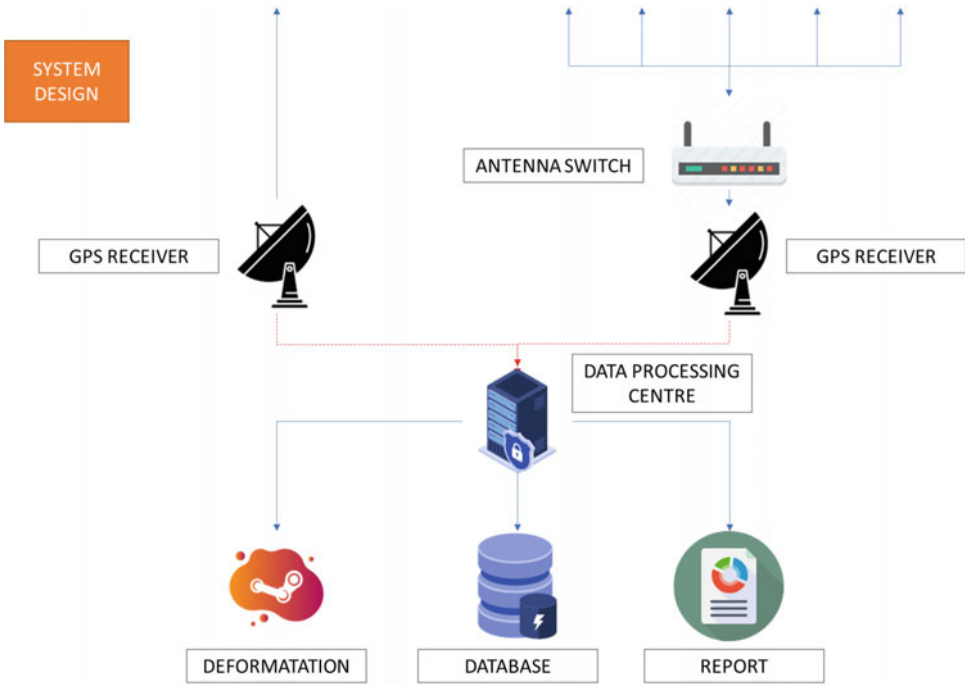

Fig. 4 Differential positioning structure of a new generation of multi-antenna systems

Fig. 5 Multi-antenna GPS test configuration diagram (4 mobile stations)

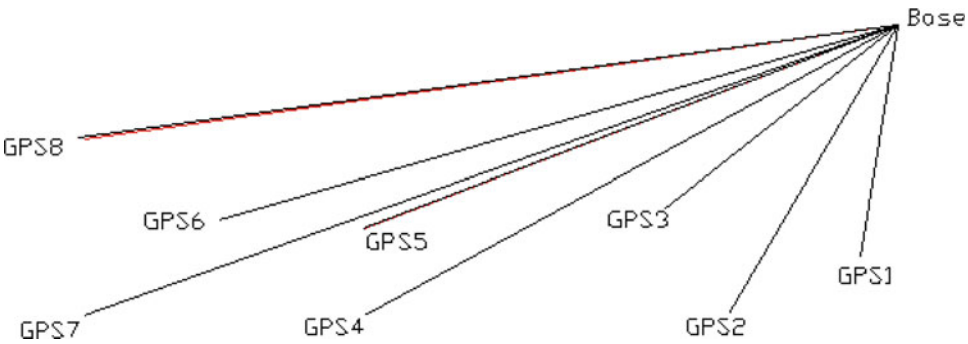

Fig. 6 Eight multi-antenna GPS test location diagram (Unit: cm)

(about 9.76 cm), the remaining antennas continued to oscillate back and forth in a stable state. On-site observations on 2007/10/25 confirmed that the behaviours recorded were the result of slope displacement and ground slip, and not caused by abnormal instruments or shaking of the fixed GPS rod. Monitoring results over 100 days from 2007/10/19 to 2008/1/25 show that there was a continuous displacement (about 17.19 cm) in the Y direction of GMS1 to GMS4. A site visit in March 2008 confirmed the displacement of the slope and landslide. Figures 8 and 9 show graphs of the dynamic coordinates of continuous time and displacement changes of GPS3 and GPS4, with displacement direction and displacement (X, Y, H) corresponding to (N, E, H) in Table 3.

Finally, the results measured by the above four sets of GPS were compared with the dynamic coordinates of the last stroke and the initial static coordinates and a spatial relationship diagram is drawn, as shown in Fig. 10. The direction of the arrow in the figure represents the direction of GPS displacement, and the length of the arrow represents the amount of displacement. It shows that GPS1–GPS4 move in the same direction and are the same moving the N2 block, as shown in Fig. 10.

GPS data received by the base station antennas were collected for seven days a month from October 2007 to February 2008 to confirm the GPS fixed station was not moving (Fig. 11). The Zhuzaki County e-GPS fixed station was used as the benchmark for baseline calculation (this station was about 13.4 km from the experimental area). The five-month data from the base station recorded a horizontal coordinate difference of about 1 cm and is regarded to be within the error range. The average value is calculated as the coordinates of the base station, and is shown in Table 4.

Table 1 Comparison of multi-antenna GPS measurement results

Station number	Equipment	N	E	H
GPS2	Theodolite (m)	109.3634	97.7714	11.6688
	GPS (m)	109.37	97.772	11.664
	Variance (cm)	−0.66	−0.06	0.48
GPS 3	Theodolite (m)	106.0288	103.147	11.3648
	GPS (m)	106.025	103.147	11.351
	Variance (m)	0.38	0	1.38
GPS 4	Theodolite (m)	90.6461	97.655	11.5724
	GPS (m)	90.66	97.652	11.391
	Variance (m)	−1.39	0.3	18.14
GPS 5	Theodolite (m)	90.5877	102.1316	11.3974
	GPS (m)	90.612	102.126	11.386
	Variance (m)	−2.43	0.56	1.14
GPS 6	Theodolite (m)	83.1861	102.5695	11.3486
	GPS (m)	83.208	102.57	11.336
	Variance (m)	−2.19	−0.05	1.26
GPS 7	Theodolite (m)	76.2541	97.6472	11.4703
	GPS (m)	76.277	97.636	11.458
	Variance (m)	−2.29	1.12	1.23
GPS 8	Theodolite (m)	76.0137	106.8461	11.5876
	GPS (m)	76.262	106.721	11.63
	Variance (m)	−24.83	12.51	−4.24

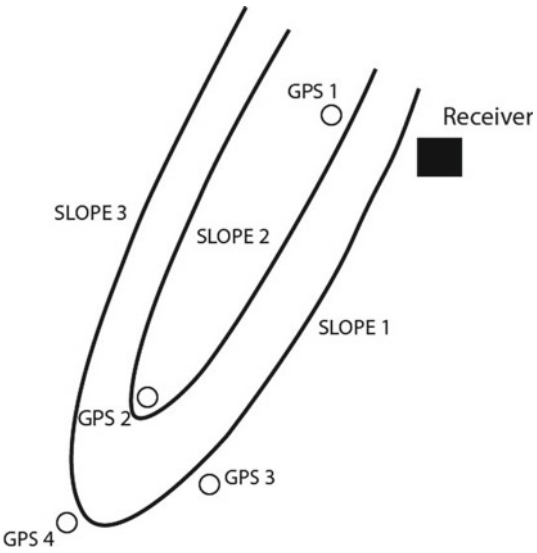

Fig. 7 Schematic diagram of local multi-antenna instrument configuration

Table 2 GPS static coordinates

Station	Static coordinates (m) 2007, 10, 17–18		
	N	E	H
GPS1	334.7169	−173.6945	−66.1253
GPS2	285.491	−218.9558	−75.3336
GPS3	269.0273	−207.2832	−77.9727
GPS4	270.1067	−232.2456	−82.5404

Slope landslides often occur after heavy or torrential rains, hinting at a specific relationship between slope damage and rainfall, in addition to certain hydrological conditions. Early rainfall can saturate surface soils with moisture, making it easier for water to flow over the slope and initiate slope failure. Rainfall data was collected in Alishan during the typhoon period from 2007 to 2008, as shown in Table 5. Figure 8 shows the relationship between the ground slip velocity and rainfall from October 2007 to February 2008. To represent the significance of ground slip, velocities are presented as displacement amounts over six days (cm/6 days). GPS1, GPS4 display severe displacement in the east–west direction, with the maximum westward sliding velocities equivalent to 10 cm per 30 days. Elevation changes and displacements in north–south direction were not large and values are not presented.

Figures 12 and 13 compare sliding velocity (cm/6 days) and accumulated rainfall for 6 days (1093 mm) from 2007/10/19 to 2008/02/14. Smaller rainfalls before the end of the year had a relatively insignificant impact. The figure shows that sliding velocity is obviously the fastest when the

Table 3 Multi-antenna GPS dynamic coordinates

N	E	H	dN	dE	dH
3 days dynamic coordinates (m) 2007/10/19–21			*3 days displacement (cm)*		
334.7145	−173.7077	−66.1578	−0.24	−1.32	−3.25
285.4819	−218.9744	−74.8855	−0.91	−1.86	−2.76
269.0205	−207.3074	−77.9852	−0.68	−2.42	−1.25
270.1033	−232.2671	−82.5615	−0.34	−2.15	−2.11
20 days dynamic coordinates (m) 2007/10/19–11/12			*20 days displacement (cm)*		
334.7129	−173.7236	−66.191	−0.4	−2.91	−6.57
285.4887	−218.0387	−74.9328	−0.23	−8.29	−7.49
269.0205	−207.3808	−77.0147	−0.68	−9.76	−4.2
270.0954	−232.3301	−82.605	−1.13	−8.45	−6.46
100-day dynamic coordinates (m) 2007/10/19–2008/1/25			*100 days displacement (cm)*		
334.709	−173.7408	−66.2009	−0.79	−4.63	−7.56
285.4801	−219.1143	−74.9693	−1.09	−15.85	−11.14
269.0101	−207.4551	−78.0555	−1.72	−17.19	−8.28
270.0846	−232.4142	−82.6526	−2.21	−16.86	−11.22

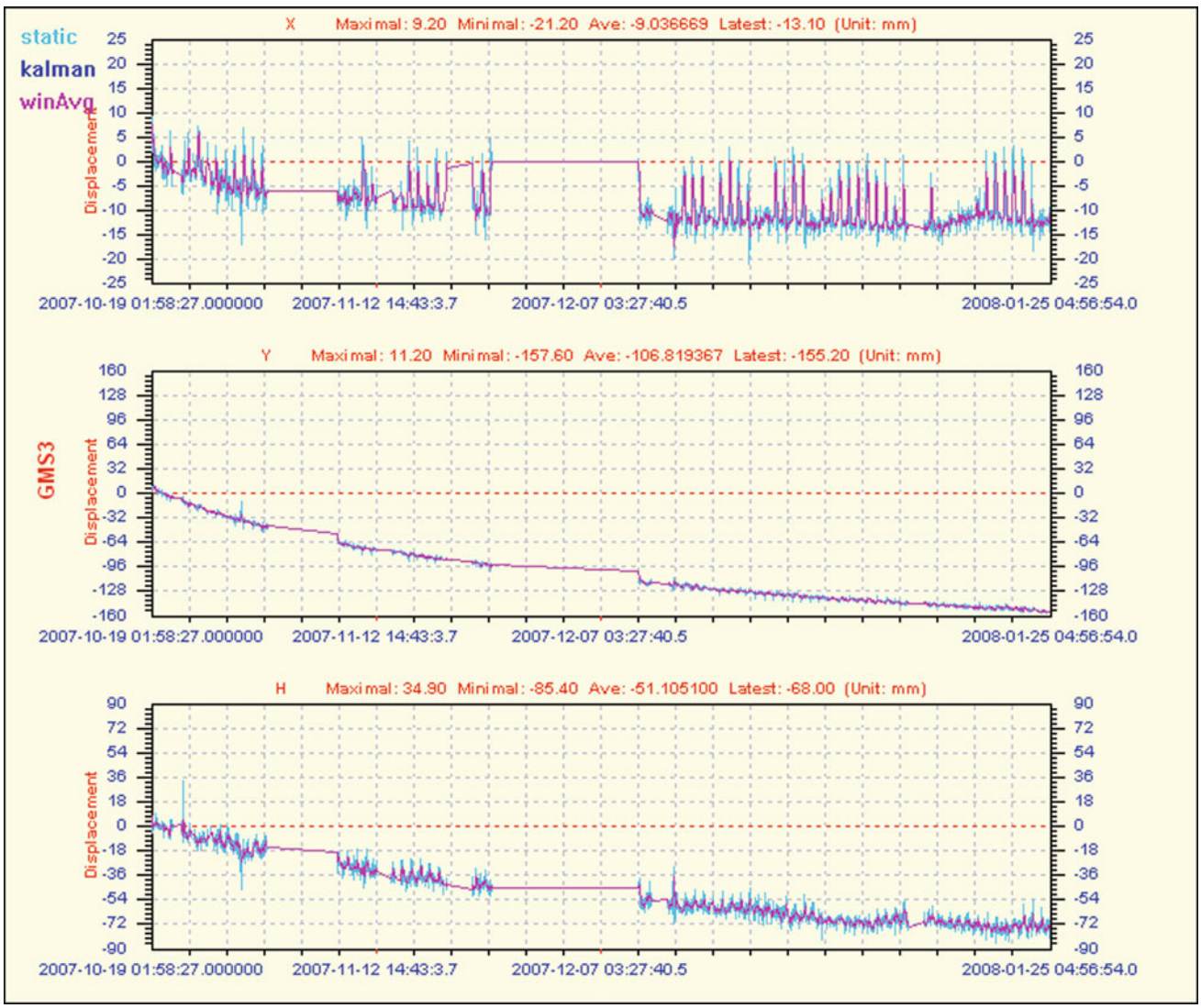

Fig. 8 Road slope automatic monitoring system (Antenna No. 3 2007/10/19–2008/1/25)

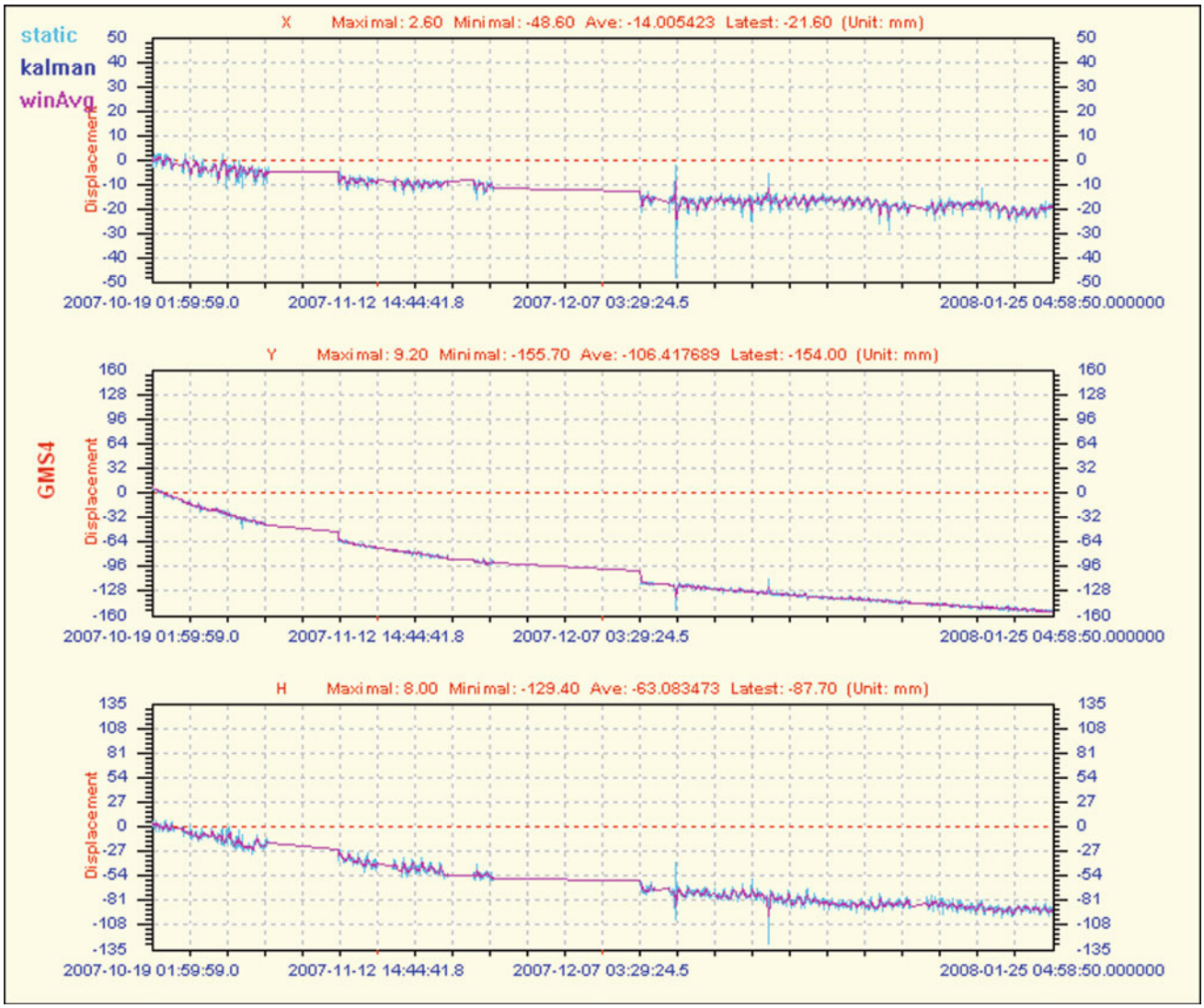

Fig. 9 Road slope automatic monitoring system (No. 4 Antenna 2007/10/19–2008/1/25)

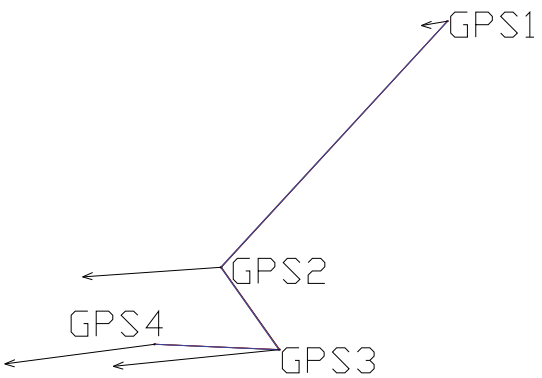

Fig. 10 Schematic diagram of GPS sliding displacement direction and relative displacement

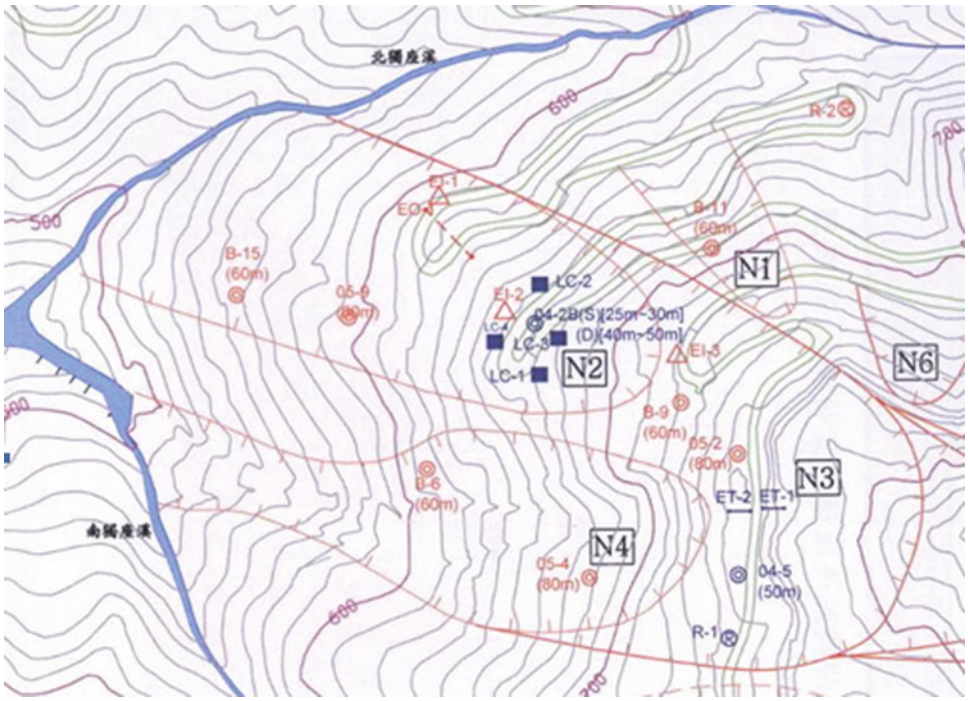

Fig. 11 GPS antenna position and moving block diagram

Table 4 Calculated average differences in horizontal coordinate

Date	N coordinate (m)	E coordinate (m)	H elevation (m)
2007/10	2,591,861.401	213,379.664	775.014
2007/11	2,591,861.407	213,379.658	775.014
2007/12	2,591,861.408	213,379.668	775.023
2008/01	2,591,861.434	213,379.645	775.018
2008/02	2,591,861.428	213,379.65	775.027
Average value	2,591,861.416	213,379.657	775.019
Standard deviation	0.013	0.009	0.005

Table 5 Statistical table of rainfall brought by typhoons in Alishan from 2007 to 2008

Typhoon name	Invasion time	Cumulative rainfall (mm)	Strength
Pabuk	2007/8/6–8/8	31	Light
Wutip	2007/8/8–8/9	21	Light
Sepat	2007/8/16–8/19	654.7	Strong
Wipha	2007/9/17–9/19	302	Medium
Krosa	2007/10/4–10/7	1093	Strong
Pabuk	2007/8/6–8/8	31	Light
Wutip	2007/8/8–8/9	21	Light

typhoon rainfall hits. When the rainfall stops, sliding gradually slows. The sliding velocity presents a parabolic trend when each point is fitted with a binary linear equation (Figs. 14 and 15). The R-square values of the fitting trend lines of Antenna 3 and Antenna 4 are both as high as 0.9, indicating a trend in sliding velocities during this period. The mathematical relationship of a slow descent of the quadratic equation of one variable, and the similar fitting equations of Antenna 3 and Antenna 4, indicate their sliding velocity and direction are the same. Following the rains of Typhoon Kerosa, the maximum displacement velocities of Antenna 3 and Antenna 4 were 2.4 cm/6 days and 2.5 cm/6 days, respectively. Displacement of GPS3 and GPS4 slowed at the same time, 74 days after the rainfall event.

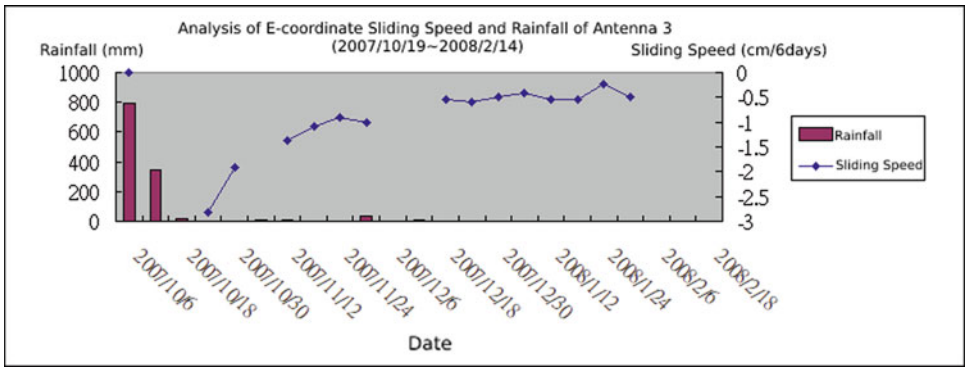

Fig. 12 Analysis of E-coordinate sliding speed and rainfall of Antenna 3

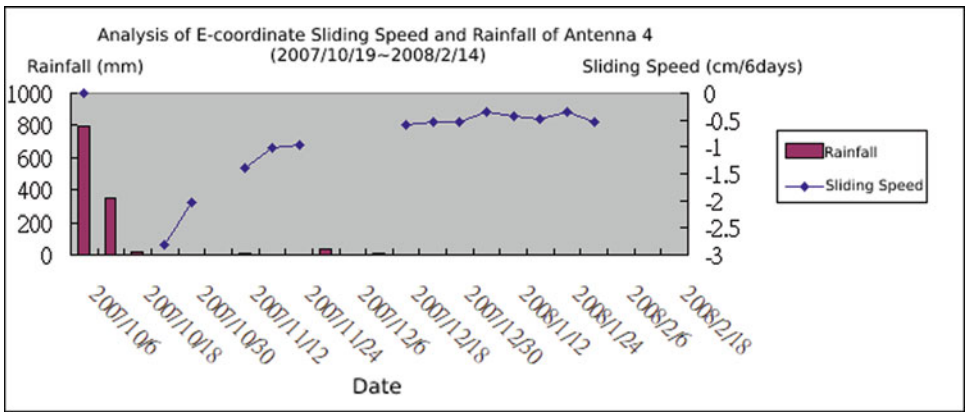

Fig. 13 Analysis of E-coordinate sliding speed and rainfall of Antenna 4

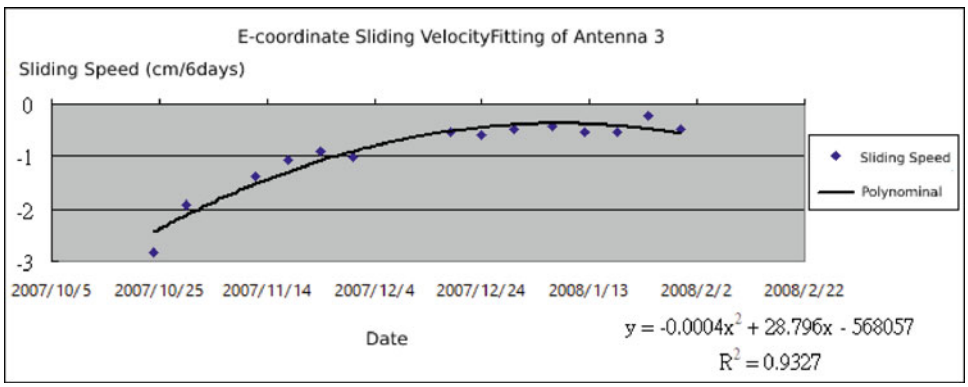

Fig. 14 E-coordinate sliding velocity fitting of Antenna 3

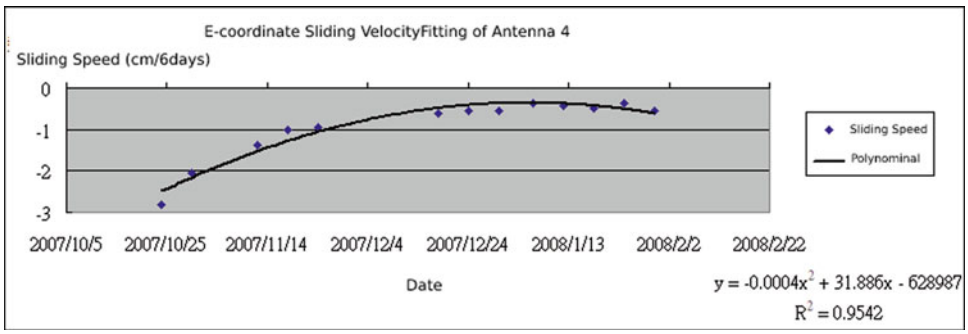

Fig. 15 E-coordinate sliding velocity fitting of Antenna 4

5 Conclusion

This study proposes a specific solution for disaster prevention with the application of a one-machine multi-antenna GPS. This innovative monitoring system is tested on a section of the Alishan highway traversing steep sloping land (the fourth bend area), and forms the basis for a disaster prevention and response approach and subsequent research.

The fourth bend area experienced severe weather with sustained, heavy rainfalls during typhoons Pabuk, Uti, Sanpa and Kelosa (Table 5). A site investigation of this area in early October 2007 found many surface sliding phenomena triggered by typhoon rainfall, including a large (20 cm) fissure. Such large-scale sliding conditions in the Wuwanzai area can be understood through continuous measurement of absolute coordinates with the satellite tracking station data at the Land Survey Bureau and the GPS base station.

After the installation of the one-machine multi-antenna GPS was completed, monitoring was undertaken. After 100 days of monitoring, there was a maximum displacement of 17.19 cm. It is speculated that due to the influence of Typhoon Kerosa upon Taiwan at the time, the accumulated rainfall in the area around the Alishan Highway was greater than 600 mm. It was due to this large rainfall amount and surface runoff, that the slope sliding phenomenon in the fourth bend area was aggravated.

The one-machine multi-antenna GPS proven to monitor ground slip of the colluvium along the Alishan Highway. After the torrential rain, there was obvious ground slip in the sensitive areas of this road section, with the displacement rate reaching 10 cm/month (30 days). During sunny conditions, ground slip velocity slows in the form of a mathematical quadratic equation with time as a variable. The results of measurements by four sets of GPS are compared with the dynamic coordinates of the last stroke and the initial static coordinates. A spatial relationship diagram is shown in Fig. 10, with the direction of arrows depicting the 100-day dynamic coordinates, while the length of arrows represent the amount of displacement. This relationship shows that GPS1 to GPS4 move in the same direction, and are part of the same NE moving block (Fig. 11).

References

Brand EW (1982) Analysis and design in residual soil. In: Proceedings of the ASCE geotechnical engineering division specialty conference-engineering and construction in tropical and residual soils, Honolulu, Hawaii, pp 89–141, January 11–15

Jian S (2002) Study on the sliding mechanism and stability of the Wuwanzai ground sliding area in Alishan. Master's thesis of the Department of Construction Engineering, National Yunlin University of Science and Technology (Chinese version)

Lumb P (1975) Slope failures in Hong Kong. Q J Eng Geol 8:31–65

Min FY, Chou TY, Hoang TV, Bui QT, Nguyen DB, Nguyen QH (2020) New landslide disaster monitoring system: case study of Pingding Village. Appl Sci 10(19):6718. http://doi.org/10.3390/app10196718

Qiu Y (2004) Discussion on the mechanism of slope 626 in Wuwanzai, Alishan. Master's thesis, Department of Construction Engineering, National Yunlin University of Science and Technology (Chinese version)

Rao Z, Lin Y, Hong B, Li S, Li B, Zhou T, Xiao T, Fang Y (2008) Application of global satellite positioning and automatic monitoring system in slope disaster prevention (2/4). Institute of Transportation, Ministry of Communications (Chinese version)

Shen J (2004) The feasibility study of using GPS for long-term monitoring of landslide surface displacement. Master's thesis, Institute of Civil Engineering, National Chung Hsing University (Chinese version)

Slosson JE, Larson RA (1995) Slope failures in southern California: rainfall threshold, prediction, and human causes. Environ Eng GeoSci I(4):393–401

Su M-B, Chen I-H, Liao C-H (2009) Using TDR cables and GPS for landslide monitoring in high mountain area. J Geotech Geoenviron Eng 135(8). http://doi.org/10.1061/(ASCE)GT.1943-5606.0000074

Zeng G (2003) Comprehensive evaluation of Lishan landslide management benchmark values. Master's thesis, Institute of Civil Engineering, National Chung Hsing University (Chinese version)

Landslide Warning Systems in Upper Middle-Income Countries: Current Insights and New Perspectives

Irasema Alcántara-Ayala and Ricardo J. Garnica-Peña

Abstract

Early Warning Systems (EWSs) are considered one of the main mechanisms for disaster risk reduction (DRR). In this sense, several efforts have been made by the international science and technology community to support the implementation of the Sendai Framework for Disaster Risk Reduction (SFDRR), giving special attention to the seventh global target focused on increasing the availability and access to multi-hazard early warning systems. Considering that landslides are one of the natural and socio-natural hazards that affect society in various parts of the world, the International Consortium on Landslides (ICL) has taken on the task of establishing regional and global network initiatives that promote the establishment of landslides early warnings systems (LEWSs). Although studies have recognised the significance of LEWSs, research has yet to systematically investigate the degree of implementation around the world. Therefore, and building on previous work, this chapter aims to provide an overview concerning enforcement of LEWSs in Upper Middle-Income Countries (UMIs). Based on a systematic literature review, the overall structure of the study takes the form of five sections. An introduction to the significance of LEWSs is provided in the first part. The second section provides an overview of the common architecture of LEWSs. The third part is concerned with the methodology employed for this study. Results of the study are presented in the fourth section and the final part brings together the key findings. Of the total publications that met the specified criteria and were analysed, only 19, that is, 5%, focused on different dimensions of the actual implementation of the LEWS.

Keywords

Landslide early warning systems • Upper middle-income countries • Implementation • Disaster risk reduction

1 Introduction

Early Warning Systems (EWSs) are considered a fundamental mechanism for disaster risk reduction (DRR). In supporting the implementation of the Sendai Framework for Disaster Risk Reduction (SFDRR) (UNISDR 2015), the scientific and technological community have made major efforts to build EWSs associated with different hazards. To this regard, the International Consortium for Landslides (ICL) have provided a sustained platform for international collaboration consisting of high-recognised experts and Centres of Excellence. Through research, capacity building, networking, and practice, ICL specialists have undertaken diverse projects around the world in benefit of society. Examples of this type of global strategies include the Sendai Landslide Partnerships 2015–2025 (Sassa 2015, 2016) and the Kyoto Landslide Commitment 2020 (KLC2020) (Alcántara-Ayala and Sassa 2021).

One of the main pillars of the KCL2020 is to promote greater awareness of the significance of people-centred early warning aiming at achieving high accuracy and reliable prediction technology for landslides in time and space, within a changing climate context (Sassa 2019, 2020). This endeavour goes hand in hand with the recognition of the need to implement the Sendai Framework for Disaster Risk Reduction (SFDRR) and particularly its seventh global target focused on "Substantially increase the availability of and

I. Alcántara-Ayala (✉) · R. J. Garnica-Peña
Institute of Geography, National Autonomous University of Mexico (UNAM), 04510 Mexico City, Mexico
e-mail: ialcantara@geografia.unam.mx

R. J. Garnica-Peña
e-mail: garnica@geografia.unam.mx

I. Alcántara-Ayala et al. (eds.), *Progress in Landslide Research and Technology, Volume 1 Issue 2, 2022*, Progress in Landslide Research and Technology,
https://doi.org/10.1007/978-3-031-18471-0_13

access to multi-hazard early warning systems and disaster risk information and assessments to people by 2030." (UNISDR 2015).

The design and implementation of landslide early warning systems (LEWSs) is central in all regions of the world. Building on previous research concerning the implementation of LEWSs in low- and lower-middle-income countries (LICs and MICs), the analysis presented here seeks to provide an overview concerning enforcement of LEWSs in Upper Middle-Income Countries (UMIs), from 1991 to 2021. In addition to the introduction, this chapter is composed of four sections: a brief account concerning the architecture of EWSs, the methodology, results, and a final reflection on the current insights and new perspectives.

2 Landslide Early Warning Systems (LEWSs): Common Architecture

Despite the definition of people-centred EWSs (ISDR-PPEW 2005), efforts have mostly been implemented from technical perspectives. EWSs are linked to a greater extent to the response to emergencies and humanitarian crises, while technological interventions are accepted as solutions to explicitly advance integrated analysis, instead of guiding practices in the formulation of policies that guarantee the reduction of disaster risk (Alcántara-Ayala and Oliver-Smith 2019).

Such experiences are neither articulated nor specifically oriented to the understanding of disaster risk (Alcántara-Ayala and Oliver-Smith 2017) and what is more, lack engagement of people into co-production of knowledge processes, and therefore in the appropriation of warnings.

Quite often the main architecture of LEWSs is made up of three basic ingredients: landslide instrumentation and monitoring, identification of thresholds and diverse data for the establishment of warnings and final alerts, and landslide communication and response (Fig. 1).

It would be understandable that many of the experts in charge of the technical aspects of the development of warning systems are not interested in preparedness strategies, risk communication processes and even less in disaster risk governance issues. However, because all such processes require the articulation of institutions, sectors, and actors, it should be a priority to focus on the participation of relevant stakeholders in disaster risk (Alcántara-Ayala 2021). Therefore, it also needs to be recognised that the organisation and functioning of transdisciplinary teams could lead to the implementation of LEWS in specific social contexts in a satisfactory and sustained manner.

Fig. 1 The three main components generally included in LEWSs

3 Methodology

The study was conducted in the form of a systematic review of literature, with data being gathered via ISI Web of Science database. It comprised definition of the review scope, literature search, literature analysis and synthesis, along with current insights and new perspectives of LEWSs.

The literature search was conducted between January and February 2022. Analogously to the study carried out for low- and lower-middle-income countries (LICs and MICs) (Alcántara-Ayala and Garnica-Peña 2022) the analysis involved search criteria and keywords by considering the words "landslide", "warning system", and "early warning" in the title and abstract of the articles.

A total of 1762 articles were included as search outputs, and the publication period of 1991–2021 was chosen to elude the inclusion of work in progress in 2022 (Fig. 2).

After filtering process to exclude papers which did not have the full abstract available, search results were limited to 1691 papers. Furthermore, following the filtering of publications issued in other language than English, number of papers decreased to 1669.

Due to additional filtering, the number of publications was reduced to 1129 by removing articles that were not suitable for the scope of the review, as well as data papers, retracted publications, editorial material, and letters.

The final step of filtering comprised the classification of the articles according to the countries of publication. Low, Lower middle, Upper middle- and High-income categories were considered. The final selection concentrated on upper-middle income countries. Thus, the number of documents examined for this study was 384 (Fig. 2).

Considering the previous experience in this topic, the analysis and synthesis of the literature included geographical analysis, time, institutions, research areas, methodological typology, and approaches (Fig. 2).

After the final selection of publications, differences were reviewed and further discussed by two researchers to ensure relevance to the specified objective.

Data management and analysis was carried out using Excel and HistCite.

Current insights and new perspectives of LEWS in upper-middle income countries (UMICs) were built on the basis of the relevant insights included in the set of articles analysed and the practical knowledge of the authors.

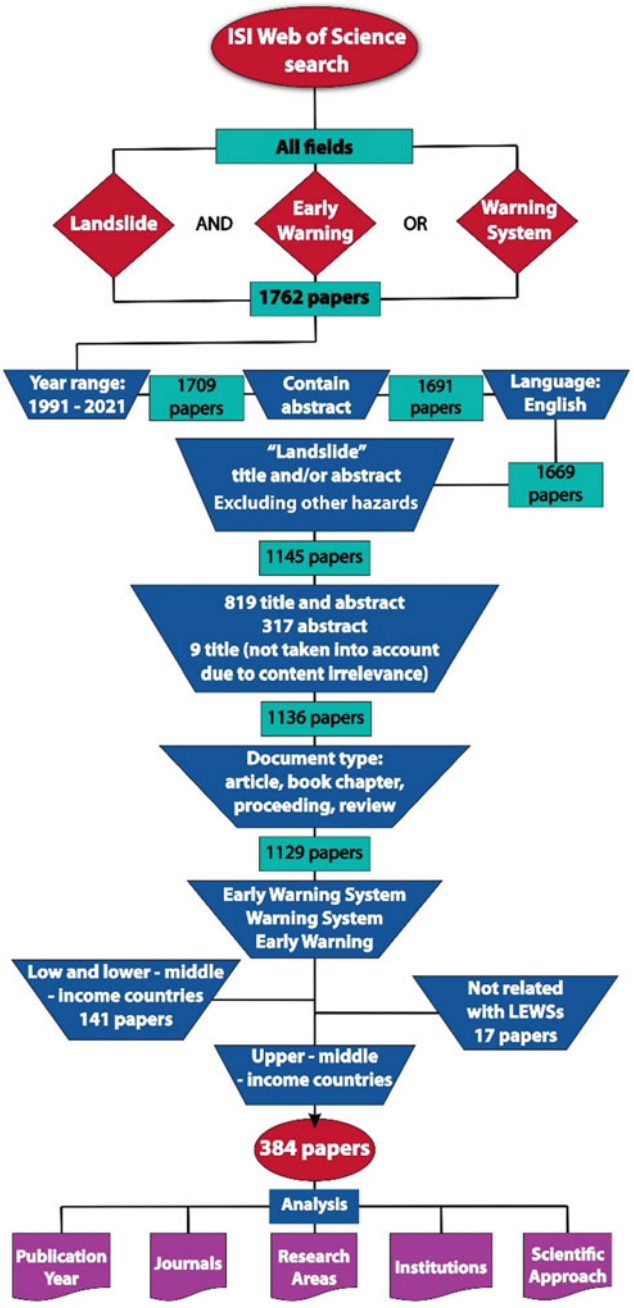

Fig. 2 Search strategy for systematic review

4 Results

Publications considered in this analysis were carried out by researchers working in institutions situated in UMICs including Argentina, Brazil, Bulgaria, Colombia, China, Cuba, Ecuador, Kazakhstan, Malaysia, Mexico, Thailand, Turkey, Romania, and Russia.

While the first publication concerning LEWS included in ISI Web of Science was available in 1991, it was until 1998 that the first publication in UMICSs appeared. As such, the period of analysis included here is 1998–2021 (Fig. 3).

After the first publication on LEWSs in UMICs in 1998, there was a period of time in which this type of publication was irregular, and it was until 2012 that the number increased to 21 publications.

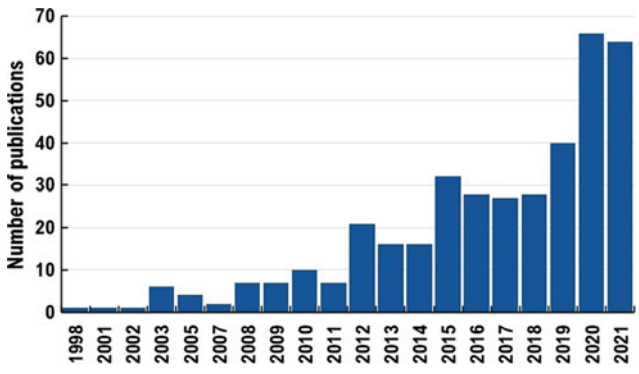

Fig. 3 Time analysis: number of publications analysed concerning LEWSs in UMICs

As of 2015, the number of publications increased to 32 and between this year and 2021, practically 75% of the total publications on this topic have been made.

Types of publications analysed included articles (N = 261), conference proceedings (N = 117), book chapters (N = 2) and reviews (N = 4). The publications focused on various fields of research in the diverse topic areas associated with landslides. Of the total publications, 40% was concentrated in the areas of geological engineering (N = 66), followed by engineering (N = 41), geology-water resources (N = 28) and geology (N = 20). Additional relevant areas included instrumentation (N = 12), computer science (N = 12), environmental science and ecology (N = 12), remote sensing (N = 12) and water resources (N = 11) (Fig. 4). The predominance of technical approaches associated with LEWS is clearly expressed in the scarcity of publications from the perspective of the social sciences. Not a single publication was issue from this field.

Most of the papers regarding these topics were published, in the Landslides Journal (N = 35), followed by Natural Hazards (N = 14), the Bulletin of Engineering Geology and the Environment (N = 13), Remote Sensing (N = 12) and Sensors (N = 12). Further publications were included in publications such as Environmental Earth Sciences (N = 11), Engineering Geology (N = 10), Applied Sciences-Basel (N = 9) and the Journal of Mountain Science (N = 9) (Fig. 5).

Experts from 528 institutions participated as contributors of more than one publication, whereas those of 384 contributed to one publication. Main institutions regarding participation in the largest number of publications involved China University Geosciences (N = 50), Chinese Academy of Sciences (N = 39), Chengdu University of Technology (N = 29) and Changan University (N = 16) (Fig. 6).

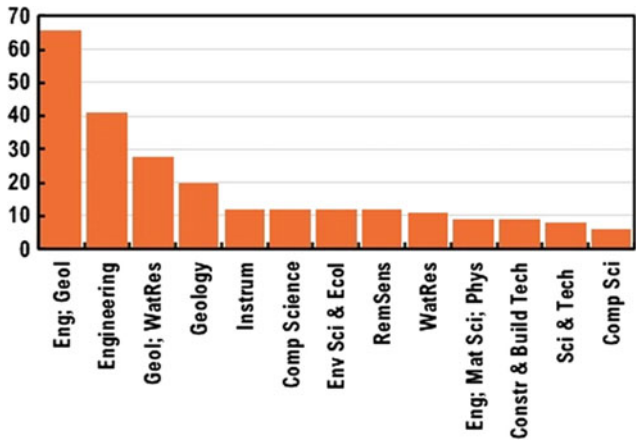

Fig. 4 Research areas concerning the publications analysed on LEWSs UMICs

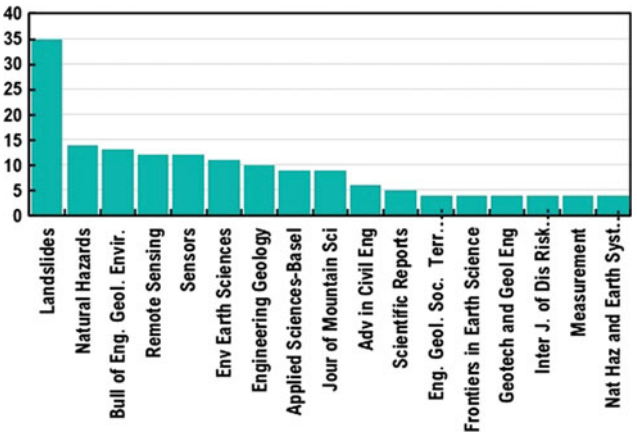

Fig. 5 Journals of publications regarding LEWSs in UMICs

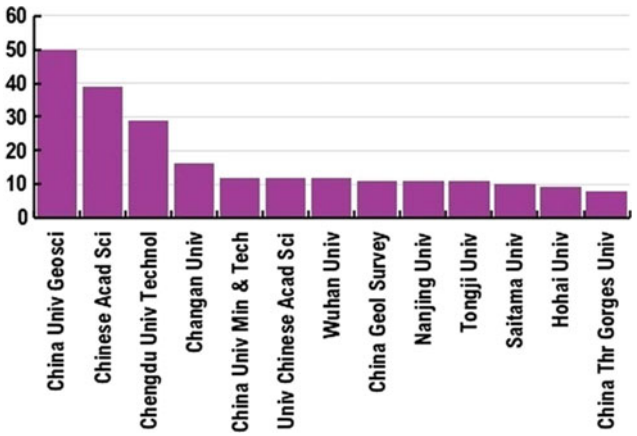

Fig. 6 Research and academic institutions to which the authors of the analysed publications are affiliated

Additional institutions included China University of Mining and Technology (N = 12), University Chinese Academy of Sci (N = 12), Wuhan University (N = 12), China Geological Survey (N = 11), Nanjing University (N = 11), Tongji University (N = 11), Saitama University (N = 10), Hohai University (N = 9), and China Three Gorges University (N = 8) (Fig. 6).

According to the results, the published investigations were focused on four main lines of work: hazard analysis for LEWSs, technical developments for potential LEWSs, models and prototypes for LEWSs, and actual implementation of LEWSs, including those concerning community-based approaches (Fig. 7).

Hazard analysis for LEWSs was the area for which the highest percentage of publications was identified (N = 215, 56%). The second area concerned technological developments for potential LEWSs (N = 73, 19%), while the third, involved the design, development, calibration and validation of models and prototypes for LEWSs (N = 55, 14%).

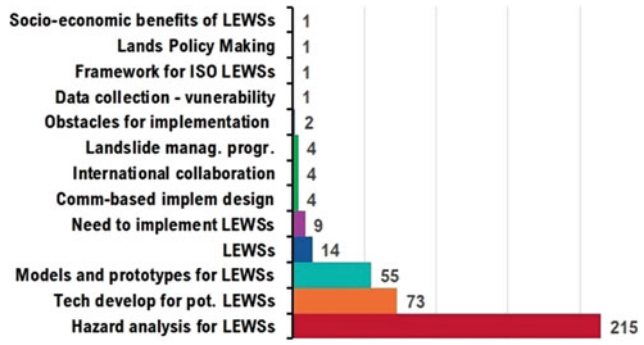

Fig. 7 Thematic lines of research associated with LEWSs in UMICs, based on the systematic literature review

Publications regarding the actual implementation of LEWSs and community-based approaches for LEWSs were regarded as the fourth area of concern (N = 18, 5%).

Additional themes derived from the results of the analysis included socio-economic benefits of LEWSs, data collection concerning vulnerability factors, framework for ISO LEWSs, necessity to implement LEWSs, obstacles for implementation, landslide management programs, landslide policy making and scientific international collaborations (Fig. 7).

While there is every indication that there is a growing interest in the development of LEWSs in UMICs, number of publications in different countries was uneven.

The largest number of publications per country was concentrated in China (N = 326, 86.5%), followed by Malaysia (N = 16, 4.1%) and Brazil (N = 14, 3.5%) (Fig. 8). The number of study cases per country showed a similar pattern with the largest concentration in China (N = 200, 74%), Malaysia (N = 11, 4%) and Brazil (N = 10, 3.7%) (Fig. 9). Yet, results of the literature review suggested that there are only a limited number of publications concerning the actual implementation of LEWS.

4.1 Hazard Analysis for LEWSs

Of the total publications, 56% focused on different aspects related to the production of information about the dynamics of landslide hazards. Publications included topics as diverse as susceptibility and hazard maps, the use of Geographic Information Systems, Digital Terrain Models and LiDAR-derived DEMs, GPS technology, in situ monitoring, geological and geomorphological research, identification of rainfall intensity-duration thresholds, laboratory experiments and simulations, displacement prediction models, physics-based landslide forecasting models, numerical simulations and modelling, machine learning algorithms, ground based synthetic aperture radar interferometry, among others.

4.2 Technical Developments for Potential LEWSs

Wide interest in developing LEWSs was identified in the publications. These comprised and innovative diverse approaches. Among these are model tests on loess, creep models of rock slides, alert velocity thresholds for pre-alert,

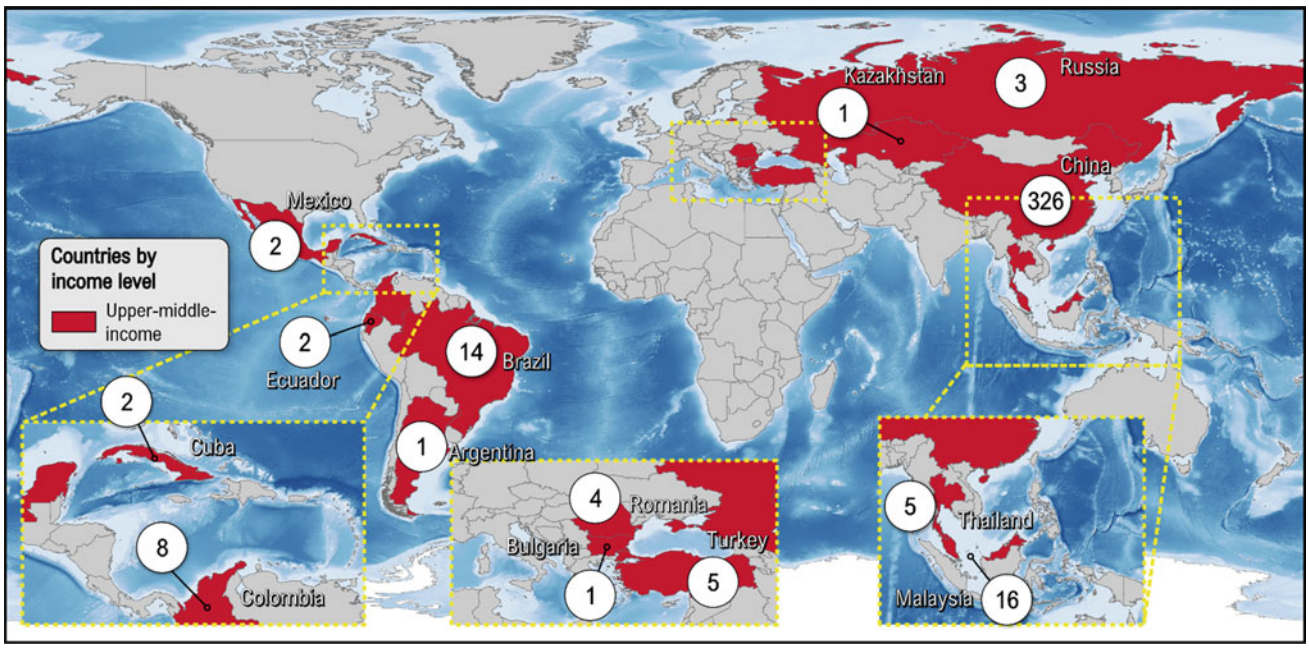

Fig. 8 Countries of the research and academic institutions to which the authors of the analysed publications are affiliated. The number inside the circle represents the number of publications per country

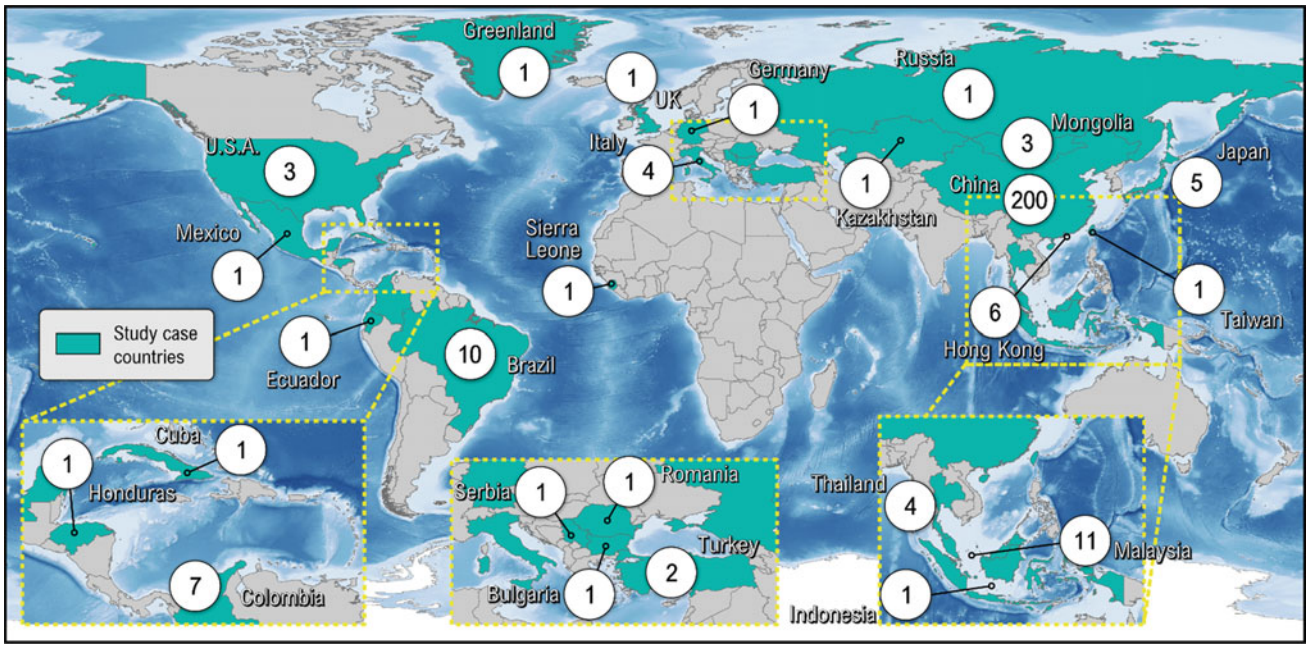

Fig. 9 Study case countries reported in the analysed publications. The number inside the circle represents the number of study cases per country, including those which are not categorised as UMICs

alert and emergency phases, wireless monitoring, 5G Internet of Things technology, WebGIS, black box models based on statistical analysis, sensor technologies, spatial information technologies, 3D visualization technologies, landslide-forecasting models, early warning indicator system of dump landslide in opencast mines, multi-parameter integrated monitoring systems, meteorological-geotechnical early warning systems, extreme learning machine, and artificial neural network methods.

4.3 Models and Prototypes for LEWSs

Numerous models and prototypes for the development of LEWSs have been documented in the analysed publications. These were the equivalent to 14.3% of the total publications.

Among the different technologies used for the creation and operation of LEWSs stand out 3D thresholds for alerting zones, micro electro mechanical systems, multivariate wireless monitoring sensor units, novel frameworks that employs Earth Observations technologies, coupling hydrological and geotechnical models, intelligent monitoring and early warning system based on microservice architecture, and transmission and display of key monitoring data by 5G communication and advanced data visualisation technologies.

In practice, this means that models and prototypes are developed according to the different technologies available particularly but not exclusively in countries such as China, which can be relevantly used in terms of the potential implementation of LEWSs.

4.4 Operational LEWSs from Publications in UMICs

In total, 14 publications referred to the implementation of LEWSs. Four of them concerned the enforcement of LEWSs in Brazil, and ten in China.

In Brazil, experiences derived from the implementation of a LEWS based on meteorological information, rainfall data and field observation to forecast the occurrence of landslides in Serra do Mar, State of São Paulo, were discussed by Macedo et al. (1998). Likewise, the Rio-Watch project, was set up to provide two hours in advance early warning for rainfall induced landslides in Rio de Janeiro (Ortigao et al. 2001), an area severely affected by landslides.

Kong et al. (2020) focused on a sustained effort around evaluating the performance over a 40-year period of the Landslip Warning System established by the Geotechnical Engineering Office of Hong Kong government, which has been considered the first territorial-wide early warning system for landslides of the world. Previous works have paid attention to improvements to this LEWS to provide guidance on slope design, landslide preparedness, and planning for rainfall-induced landslides (Chan et al. 2003; Pang 2003).

Other notable publications included the implementation of LEWSs in diverse regions of China. For example, Ju et al.

(2015) designed and applied a four-level LEWSs (zero, outlook, attention, and warning) in Guizhou Province. Hu (2005) provided an account of the background, configuration and major achievements of the Upper Yangtze Mudflow and Landslide Early Warning System (EWS) and shows how it has been operating through both a structural and non-structural approaches. Moreover, the reliability and efficiency of a LEWS in Sichuan Province, China has been intensively investigated based on the experience of the Panzhihua Airport landslide (Wang et al. 2013).

A well-known study that is often cited in LEWS research is that of Yin et al. (2010), who have been conducting real-time monitoring and early warning of landslides in the Three Gorges Reservoir since 1999. Additional efforts have been reinforced since 2003 in the relocated city of Wushan in the same region, in which four risk levels have been included as criteria for alerting critical situations.

To further examine the role of early warning and emergency response, Fan et al. (2019) documented the case of a successful early warning and timely evacuation well in advance of a large rockslide that occurred on 17 February 2019 in Guizhou Province, China.

Another recurring theme in the LEWS literature is the impact of landslides and debris flows on pipelines. In this sense, Jia (2010) carried out a spatial analysis with forecast rainfall data in a GIS platform to produce a hazard zoning as the basis for the implementation of a LEWS for the Lanzhou-Chengdu-Chongqing pipeline, and additionally measures of protection were also suggested.

4.4.1 Community-Based Approaches to LEWSs

A significant analysis and discussion on the implementation of LEWS for disaster risk reduction was presented by Yang et al. (2012). They recognized the importance of governance and risk management in the context of global climate change and the impact of rainfall-induced landslides in the Wenchuan earthquake region. Therefore, the participation of the government, a research centre and the local community for landslide prediction, monitoring and warning was encouraged. This trilateral cooperation, which included effective communication during the rainy season after the Wenchuan earthquake, led to successful hazard monitoring, forecasting, and warning.

In another important study, Liu et al. (2016) developed a government-led, community-based LEWS in the Wanzhou district of the Three Gorges Reservoir. They reported several strategies to improve community resilience to landslides. This included the establishment of a real-time landslide monitoring system in which community members carried out various monitoring activities, and the understanding of the early warning system and landslide response protocols were also considered in the strategy emergencies.

Building on the experience derived from the occurrence of the Boli landslide on the right bank of Taozi Gully, a branch of the Jiami River in Taozi town, Sichuan Province, China, Hu et al. (2019) proposed a community based LEWSs on the basis of real-time evacuation.

4.5 Additional Topics of Concern Related to LEWSs in UMICs

Further to the four main lines of work identified in the review, the publications focused on several notable contributions that represent new directions in the growing body of research on LEWS.

In order to identify priority areas related to vulnerable populations to be included in LEWS, de Assis Dias et al. (2020) developed an Operational Index for Vulnerability Analysis for 443 Brazilian municipalities. Obtained results indicated the feasibility of incorporating socioeconomic information in the context of the Brazilian Early Warning System.

Pun et al. (2020) provided an account of the development of the Geotechnical Engineering Office, which was originally established to manage Slope Safety System in Hong Kong, particularly from a technical perspective. Recent advances have given rise to multi-pronged risk management strategies aimed at improving emergency preparedness considering the occurrence of more frequent and intense events under the effect of climate change.

Yin et al. (2018) argued that, despite the importance of the direct effects of the occurrence of landslides along the shorelines of reservoirs, attention should be paid to the indirect consequences in terms of impacts on maritime transport or the coastal properties. In this sense, they also provided information on how to build alliances between geologists and administrative agencies within risk management frameworks.

Melo et al. (2017) used a survey to evaluate the various aspects related to the perception of community leaders about the LEWSs alert system in Rio de Janeiro, Brazil. They analysed data from 71 interviews and concluded that there is low public adherence to the LEWS due to local violence preventing people from evacuating by staying home to protect one's property. Additional problems with temporary shelters and routes also contributed to people's lack of participation in the implementation of the LEWS.

Using a questionnaire in the Longmen Shan region of Southwest China, public responses to landslide risks were assessed with respect to various types of countermeasures, including structural engineering measures and early warning systems. In this helpful survey, Huang et al. (2021) were able to show that the public has a good general understanding of landslide risks with a high level of belief in the positive impact of countermeasures. Also, it was found that people are more likely to trust a LEWS than an engineering

measure. Based on the various insights derived from the analysis, they also concluded that false alarm intolerance should be considered in LEWS.

From another angle, a free and open-source toolbox for landslide risk analysis and a disaster warning system was designed in accordance with international standards to support Turkey's Provincial Disaster Management Centres (Aydinoglu and Bilgin 2015).

To determine the economic benefit of geo-hazard monitoring and warning engineering in the Three Gorges Reservoir, Yu et al. (2015) analysed the case of the Zhangjiawan landslide in Guojiaba Town, Zigui County. This study suggested the effectiveness of these measures as land has the greatest benefit in direct reduction loss, while the largest indirect reduction losses are in agricultural production and the ecological environment.

4.6 Scientific International Collaborations

The successful implementation of the SFDRR relies on the significant role of scientific collaborations at different scales and across regions (UNISDR 2015). As recently stated in the Global Assessment Report 2022, mutual communication and cross-boundary and cross-disciplinary collaborations are needed to be able to share and apply in the best possible way expertise, multiple perspectives, strategic vision, and creativity (UNDRR 2022).

Although from the literature review presented here it is difficult to identify all collaborations on LEWSs between countries, results indicate more than hundred partnerships. Accordingly, China has built 86 reported collaborations with diverse countries, in particular Italy, United Kingdom, Canada, United States of America, Australia, Hungary, Qatar, New Zealand, France, Norway, Austria, Spain, Japan, Netherlands, Taiwan, Germany and Czechia (Fig. 10).

Likewise, Brazil strengthened scientific ties with Canada, China, Switzerland, Colombia and Italy, while Colombia set-up partnerships with Canada, Switzerland, Austria and Italy, and Russia with Germany, China, Italy and Japan (Fig. 10).

A fruitful collaboration worth to mention is that between Brazil and Italy led to the implementation of both Alerta-Rio LEWSs (Calvello et al. 2015a) and community-based alert and alarm system for rainfall induced landslides in Rio de Janeiro (Calvello et al. 2015b).

Other examples of collaboration have been mirrored in the interactions among ICL regional and thematic networks. For example, Guo et al. (2013) enhanced partnerships to study landslides in the permafrost regions and regions with extreme weather conditions.

5 Discussion

Despite the existence of a series of international, regional, and national initiatives to promote the establishment of EWSs associated with diverse type of hazards, efforts have not been encouraged from integrated perspectives yet.

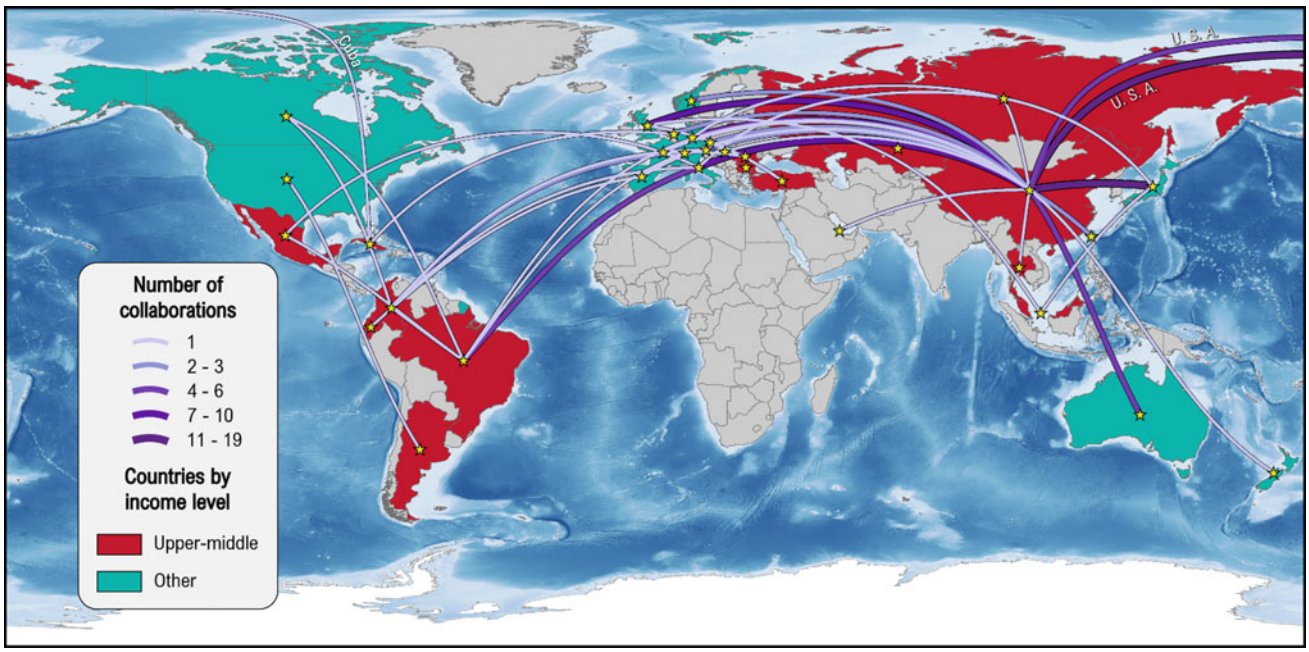

Fig. 10 Regional and international collaborations among UMICs and other countries

The significance of the development of LEWSs has been clearly recognised and this has promoted the design of diverse architectures on which the ingredients of landslide disaster risk assessments have been considered. Nonetheless, according to results presented here, the pace of implementation of such efforts is not as dynamic as reality requires.

Several topics concerning LEWSs were identified through the literature review. They were as diverse as operational LEWSs from publications in UMICs and community-based approaches to LEWSs, hazard analysis, technical developments for potential LEWSs, models and prototypes, socio-economic benefits of LEWSs, data collection concerning vulnerability factors, framework for ISO LEWSs, necessity to implement LEWSs, obstacles for implementation, landslide management programs, landslide policy making and scientific international collaborations. However, there is still a clear trend toward concentration of hazards and technical related issues.

Scientific networks and alliances developed in the recent years have provided strong support for the design of LEWS through research collaborations. Although the science behind LEWSs does not seem to be an obstacle for implementation, one of the arguments involved in explaining the poor implementation of LEWSs in different countries is the lack of integrated efforts and communication among the relevant stakeholders, particularly the communities at risk.

6 Concluding Remarks

This systematic literature review has provided additional evidence with respect to the implementation of actual LEWSs in UMICs.

More generally, research is also needed to determine whether, in addition to the analysis of scientific literature, it is possible to systematically identify the implementation of LEWSs derived from information associated with policy and practice.

New collaborations and partnerships to manage disaster risk demand solid partnerships between institutions responsible for disaster risk reduction and related topics such as environmental management, climate change action, planning and finance (UNDRR 2022). In this vein, it can be noted that future progress in landslide disaster research should consider advances in the largest possible number of countries, inclusive of UMICs.

The creation of a successful LEWS require a sustained effort and commitment from different stakeholders, from the authorities to the communities at risk, where scientists can play a significant role bringing together insights and diverse approaches.

Therefore, scientific collaborations are compelled to recognise that indigenous and traditional knowledge are equally valuable for shaping alliances and transdisciplinary efforts oriented to the co-production of knowledge.

Essential efforts must encompass the design and implementation of LEWS at different scales, but particularly in and with the sustained active engagement of local communities.

Acknowledgements Our sincere gratitude to DGAPA-UNAM, who kindly provided financial support to carry out landslide risk research through Project PAPIIT IN300823. Thanks, are also due to Prof. Veronica Tofani from the University of Florence for her valuable review of this manuscript.

References

Alcántara-Ayala I (2021) Integrated Landslide Disaster Risk Management (ILDRiM): the challenge to avoid the construction of new disaster risk. Environ Hazards 20(3):1–22. https://doi.org/10.1080/17477891.2020.1810609

Alcántara-Ayala I, Garnica-Peña RJ (2022) Landslide warning systems in low- and lower-middle-income countries: future challenges and societal impact. In: Progress in landslide research and technology, vol 1, no 1. Book series of the international consortium on landslides. Springer Nature, Switzerland

Alcántara-Ayala I, Oliver-Smith A (2017) The necessity of early warning articulated systems (EWASs): critical issues beyond response. In: Sudmeier-Rieux K, Fernández M, Penna IM, Jaboyedoff M, Gaillard JC (eds) Identifying emerging issues in disaster risk reduction, migration, climate change and sustainable development. Springer, Cham, Switzerland, pp 101−124. http://doi.org/10.1007/978-3-319-33880-4_7

Alcántara-Ayala I, Oliver-Smith A (2019) Early warning systems: lost in translation or late by definition? A FORIN approach. Int J Disaster Risk Sci 10:317–331. https://doi.org/10.1007/s13753-019-00231-3

Alcántara-Ayala I, Sassa K (2021) Contribution of the international consortium on landslides to the implementation of the Sendai framework for disaster risk reduction: engraining to the science and technology roadmap. Landslides 18:21–29. https://doi.org/10.1007/s10346-020-01539-8

Aydinoglu AC, Bilgin MS (2015) Developing an open geographic data model and analysis tools for disaster management: landslide case. Nat Hazard 15(2):335–347. https://doi.org/10.5194/nhess-15-335-2015

Calvello M, d'Orsi RN, Piciullo L, Paes N, Magalhaes M, Lacerda WA (2015a) The Rio de Janeiro early warning system for rainfall-induced landslides: analysis of performance for the years 2010–2013. Int J Disaster Risk Reduction 12:3–15. https://doi.org/10.1016/j.ijdrr.2014.10.005

Calvello M, D'Orsi RN, Piciullo L, Paes NM, Magalhaes MA, Coelho R, Lacerda WA (2015b) The community-based alert and alarm system for rainfall induced landslides in Rio de Janeiro, Brazil. In: Engineering geology for society and territory, vol 2. Springer, Cham, pp 653–657. http://doi.org/10.1007/978-3-319-09057-3_109

Chan RKS, Pang PLR, Pun WK (2003) Recent developments in the landslip warning system in Hong Kong. In: Proceedings of the 14th Southeast Asian geotechnical conference, Balkema, Lisse, The Netherlands, pp 137–151

de Assis Dias MC, Saito SM, dos Santos Alvalá RC, Seluchi ME, Bernardes T, Camarinha PIM, Nobre CA (2020) Vulnerability index related to populations at-risk for landslides in the Brazilian Early Warning System (BEWS). Int J Disaster Risk Reduction 49:101742. https://doi.org/10.1016/j.ijdrr.2020.101742

Fan X, Xu Q, Liu J, Subramanian SS, He C, Zhu X, Zhou L (2019) Successful early warning and emergency response of a disastrous rockslide in Guizhou province, China. Landslides 16(12):2445–2457. https://doi.org/10.1007/s10346-019-01269-6

Guo Y, Canuti P, Strom A, Hideaki M, Shan W (2013) The first meeting of ICL landslides in cold regions network, Harbin, 2012. Landslides 10(1):99–102. https://doi.org/10.1007/s10346-012-0369-x

Hu D (2005) The Upper Yangtze landslide and mudflow early-warning system (EWS). In: Shang H (ed) Proceedings of the 2nd international yellow river forum on keeping healthy life of the river, vol II, pp 445–454

Hu G, Liu M, Chen N, Zhang X, Wu K, Raj Khanal B, Han D (2019) Real-time evacuation and failure mechanism of a giant soil landslide on 19 July 2018 in Yanyuan County, Sichuan Province, China. Landslides 16(6):1177–1187. https://doi.org/10.1007/s10346-019-01175-x

Huang H, Huang J, Liu D, He Z (2021) Understanding the public responses to landslide countermeasures in southwest China. Int J Disaster Risk Reduction 64:102500. https://doi.org/10.1016/j.ijdrr.2021.102500

ISDR-PPEW (2005) International Early Warning Programme (IEWP). Brochure, 4 p. ISDR Platform for the Promotion of Early Warning (PPEW), Bonn

Jia S (2010) Pipeline geo-hazard prediction and early warning during summer monsoon based on GIS technology. In: International pipeline conference, vol 44205, pp 59–67

Ju NP, Huang J, Huang RQ, He CY, Li YR (2015) A real-time monitoring and early warning system for landslides in Southwest China. J Mt Sci 12(5):1219–1228. https://doi.org/10.1007/s11629-014-3307-7

Kong VWW, Kwan JSH, Pun WK (2020) Hong Kong's landslip warning system 40 years of progress. Landslides 17(6):1453–1463. https://doi.org/10.1007/s10346-020-01379-6

Liu Y, Yin K, Chen L, Wang W, Liu Y (2016) A community-based disaster risk reduction system in Wanzhou, China. Int J Disaster Risk Reduction 19:379–389. https://doi.org/10.1016/j.ijdrr.2016.09.009

Macedo ES, Ogura AT, Santoro J (1998) Landslide warning system in Serra do Mar slopes, São Paulo, Brazil. In: Engineering geology: a global view from the Pacific Rim, pp 1967–1971

Melo PDO, de Britto RM, Fontainha TC, Leiras A, Bandeira RADM (2017) Evaluation of community leaders' perception regarding Alerta Rio, the warning system for landslides caused by heavy rains in Rio de Janeiro. Nat Hazards 89(3):1343–1368. https://doi.org/10.1007/s11069-017-3023-z

Ortigao JAR, Justi MG, d'Orsi R, Brito H (2001) Rio-Watch 2001: the Rio de Janeiro landslide alarm system. In: Ho, Li (eds) Proceedings of 14th Southeast Asian geotechnical conference, Hong Kong, Balkema, vol 3, pp 237–241

Pang PLR (2003) Selected studies related to rain-induced landslides in Hong Kong. In: Proceedings of the twelfth Asian regional conference on soil mechanics and geotechnical engineering, vol 1 and 2, pp 1403–1412

Pun WK, Chung PWK, Wong TKC, Lam HWK, Wong LA (2020) Landslide risk management in Hong Kong—experience in the past and planning for the future. https://doi.org/10.1007/s10346-019-01291-8

Sassa K (2015) ISDR-ICL Sendai partnerships 2015–2025 for global promotion of understanding and reducing landslide. Landslides 12(4):631–640. https://doi.org/10.1007/s10346-015-0586-1

Sassa K (2016) Implementation of the ISDR-ICL Sendai partnerships 2015–2025 for global promotion of understanding and reducing landslide disaster risk. Landslides 13(2):211–214. https://doi.org/10.1007/s10346-016-0690-x

Sassa K (2019) The fifth world landslide forum and the final draft of the Kyoto 2020 commitment. Landslides 16(2):201–211. https://doi.org/10.1007/s10346-018-01133-z

Sassa K (2020) Launching session of the Kyoto landslide commitment 2020. Landslides 17(8):1743–1744. https://doi.org/10.1007/s10346-020-01467-7

UNDRR [United Nations Office for Disaster Risk Reduction] (2022) Global assessment report on disaster risk reduction. UNDRR, Geneva, Switzerland

UNISDR (United Nations International Strategy for Disaster Reduction) (2015) Sendai framework for disaster risk reduction 2015–2030. UNISDR, Geneva

Wang HH, Tuo XG, Zhang GY, Peng FL (2013) Panzhihua airport landslide (Oct. 3rd 2009) and an emergency monitoring and warning system based on the internet of things. J Mt Sci 10(5):873–884. http://doi.org/10.1007/s11629-013-2368-3

Yang ZJ, Qiao JP, Shi LL (2012) Application of stakeholder engagement based risk management system on geological hazards: a case study in Wenchuan earthquake hit region. In: Conference on information systems for crisis response and management Asia 2012, pp 8–12

Yin Y, Wang H, Gao Y, Li X (2010) Real-time monitoring and early warning of landslides at relocated Wushan Town, the Three Gorges Reservoir, China. Landslides 7(3):339–349. https://doi.org/10.1007/s10346-010-0220-1

Yin K, Chen L, Ma F, Cheng W (2018) Practice and thinking of landslide risk management considering their secondary consequences in the Three-Gorges Reservoir, China. In: Landslides and engineered slopes. Experience, theory and practice. CRC Press, Boca Raton, pp 2097–2105

Yu S, Hou J, Lv J, Ba G (2015) Economic benefit assessment of the geo-hazard monitoring and warning engineering system in the Three Gorges Reservoir area: a case study of the landslide in Zigui. Nat Hazards 75(2):219–231. https://doi.org/10.1007/s11069-014-1112-9

30 Years of Cultural Heritage Landslides and Block Movements Risk Assessment: Case Studies from Egypt

Yasser Elshayeb

Abstract

Throughout history, sites of high societal values, such as temples, tombs or palaces were mainly constructed through the digging/carving of rocks, built on hills or plateaus, or through the usage of carved/cut displaced rocks. Ancient designers/engineers/workers usually chose construction sites as to facilitate the building or the carving of stones, while, at the same time, serving the purpose of the building/constructions. In Egypt, throughout the ancient Egyptian Civilization, Egyptians have chosen to carve their temples and tombs in the soft limestone, shales and sandstones that are covering most of the modern Egypt, whereas in few temples and tombs, hard igneous and metamorphic rocks were used as ornament material for tombs and statutes. In this paper, we will present an account of the development of landslide risk assessment for various cultural heritage sites around Egypt, for different eras of Egyptian history and different sites. This paper aims at discussing different case studies and success stories of landslides and block movements hazards assessment around or inside Egyptian Cultural Heritage sites.

Keywords

Landslides • Ancient Egypt • Cultural heritage sites • Zone risk mapping

1 Introduction

Egypt is located on the Northeastern part of Africa. A layer of limestone covers most of the surface of modern Egypt. Beneath this lies a bed of sandstone, and this earlier sandstone is the surface rock in Nubia and southern Upper Egypt, as far north as the area between Edfu and Luxor. The oldest ground of modern Egypt comprises outcrops of metamorphic and igneous rocks (Hamimi et al. 2020; Rushdi, 1990). Figure 1 shows a general distribution of basement rock (Igneous and Metamorphic) outcrops in Egypt.

Ancient Egyptian civilizations are extended over a period of almost 4000 years, starting from the predynastic period around 4300 BC until its conquest by Alexander the Great in 332 BC. Historians divide Ancient Egypt dynastic period into 31 dynasties comprising three main kingdoms: Old Kingdom, Middle Kingdom, and Modern Kingdom, where intermediate periods separating each of those three kingdoms.

Throughout such rich history of civilization, Ancient Egyptian kings and queens had the habit to construct temples (to worship Goddesses and Gods) and dig tombs to commemorate their bodies and souls, in preparation for the afterlife.

Therefore, it was natural that most of the temples and tombs are in contact with the soft limestone, shale and sandstone layers that constitutes most of the surface of Egypt, and to master the carving of those rocks for their construction sites, with all inherited stability problems from those rocks (shale swelling, cliff stability, relative block movements, etc.).

We don't dispose of any account that ancient Egyptians were able to study slope stability or rock mechanics for their construction's sites, but their engineers and designers were aware of potential stability problem that they may face, especially in temples constructed at the toe of a cliff, or tombs designed with large roof spans.

Y. Elshayeb (✉)
Petroleum and Energy Engineering Department,
School of Sciences and Engineering, The American University in Cairo, Cairo, Egypt
e-mail: yasser.elshayeb@aucegypt.edu

I. Alcántara-Ayala et al. (eds.), *Progress in Landslide Research and Technology, Volume 1 Issue 2, 2022*, Progress in Landslide Research and Technology,
https://doi.org/10.1007/978-3-031-18471-0_14

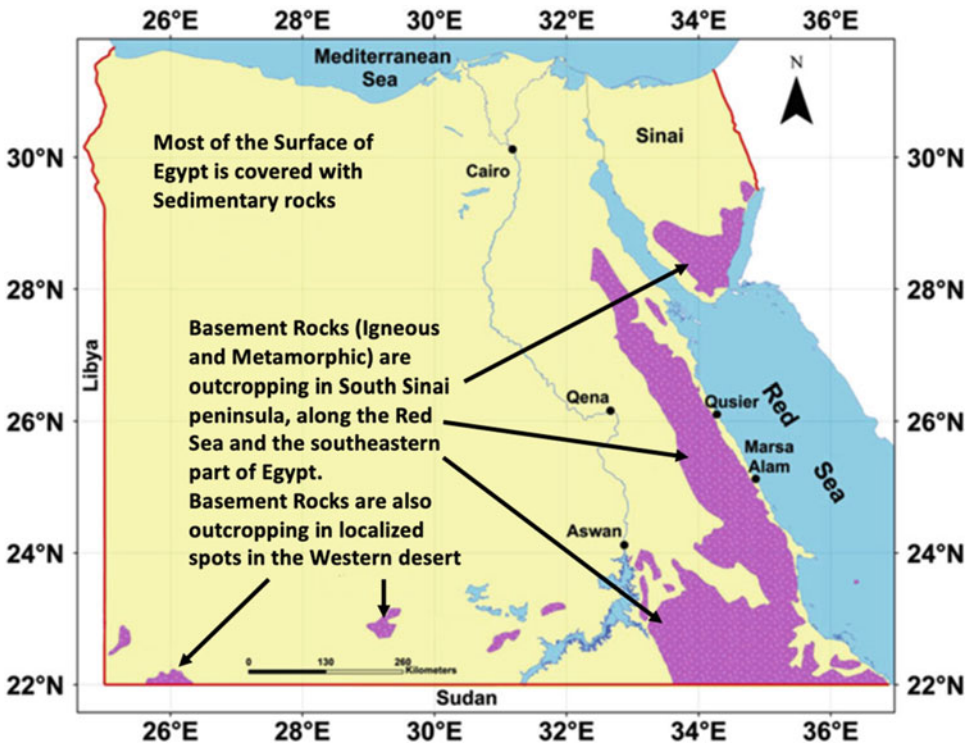

Fig. 1 Distribution of basement rocks (Igneous and Metamorphic) rocks in Egypt (Hamimi et al. 2020)

During the past 30 years and beyond, several studies were carried out on different cultural heritage sites in Egypt to investigate stability problems resulting from landslides and relative block movements.

In this paper, we will present three examples of dealing with cultural heritage sites in Egypt, where those sites are exposed to different types of risks of landslides and stability problems due to block movement: The Temple of Queen Hatshepsut at Eldeir Elbahary, Luxor, the tombs of Rasmses I at the Valley of the Kings, Luxor, and the tomb of the Serapeum in Saqqara, Giza.

2 Queen Hatshepsut Temple of Eldeir Elbahary

The Queen Hatshepsut Temple at E1dier E1bahary is located on the west bank of the Nile in Luxor Egypt at the toe of the Theban cliff (cf. Fig. 2) where the Theban Mountain is composed mainly of successions of shales and Limestones (cf. Fig. 3).

The temple was built in the fifteenth century BC and was dedicated to the cult of the Gods Amon, Hathor and to the memory of ruler Queen Hatshepsut of the 18th dynasty (1490–1468 BC).

The Temple is carved into the limestone cliff that is about 100 m high and composed mainly of Esna shale overlaid by highly fractured Thebes limestone.

Structural damage of the cliff and temple are attributed mainly to the swelling of the Esna shale, which includes buckling of casing walls, cracking of walls and ceilings and dislocation of stone blocks forming structural elements. In 1986, the casing wall of the upper court, reconstructed 80 years ago, was destroyed (Helal and Abdallah 1990).

Most rock slope failures occurs because of sliding and/or rotation of blocks or wedges defined by intersecting structural discontinuities. However, when the rock mass contains several discontinuities sets and the spacing of the discontinuities is small with respect to the size of the slope, as in the case of E1deir Elbahary, failure can occur because of sliding along a shear surface like that which occurs in soil slopes (Helal and Abdallah 1990).

Several modeling techniques were used to analyze the stability of the cliff under which the temple is constructed, coupled with rock discontinuities mapping and rock testing, to understand the mechanisms of failure of the cliff elements and suggest engineering solutions (Helal and Abdallah 1990; Dziedzic and Michiewicz 2018).

3 Tomb of Ramses I at the Valley of the Kings

The tomb of Ramses I is situated at the Valley of the kings in Luxor—Egypt, and is attributed to the king Ramses I, the founding king of Egypt's 19th dynasty. The dates for his

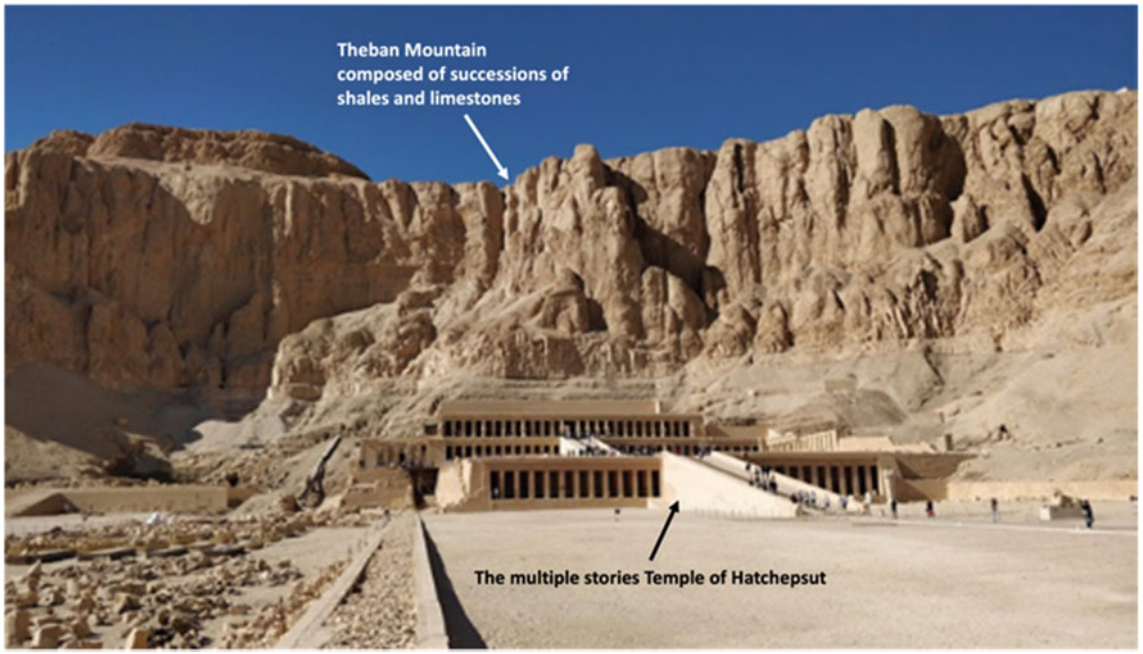

Fig. 2 General view of the temple of Queen Hatshepsut at Eldeir Elbahary, Luxor

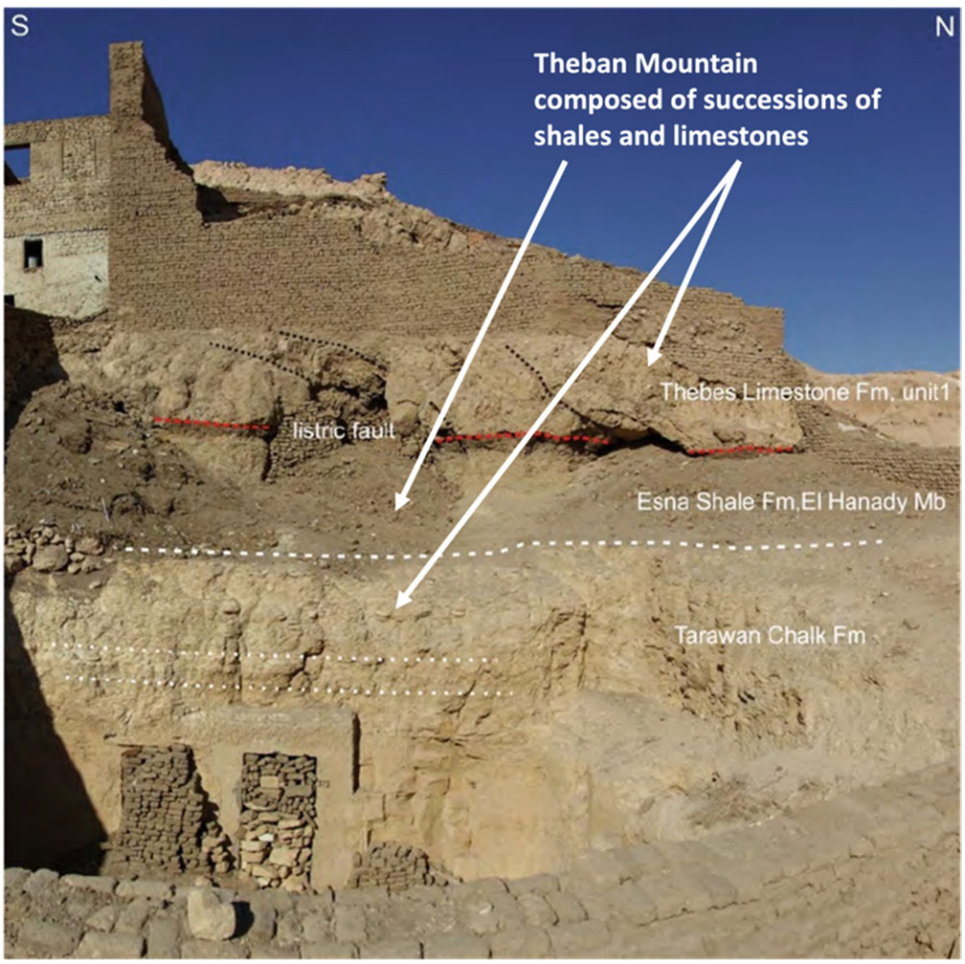

Fig. 3 Esna Shale overlaid by fractured limestone at the cliff of the Queen Hatshpsut cliff of Eldeir Elbahary

short reign are not completely known but the time-line of late 1292–1290 BC is frequently cited. Rameses I brief reign mainly serves to mark the transition between the reign of Horemheb, who stabilized Egypt in the late 18th dynasty, and the rule of the powerful pharaohs of his own dynasty, in particular his son Seti I, and grandson Rameses II.

The tomb is located in a succession of limestone layers interlayered with Esna shales, which is subject to swelling due to humidity, thus creating stresses on the walls of the tomb and the hanging layers of the roof, thus causing some instabilities in the tomb.

Nevertheless, due to the dry nature of the city of Luxor and the Valley of the Kings, effect of swelling of the shale is not severely affecting the stability of the tomb. On the other hand, a system of east–west discontinuities is observed all along the axis of the tomb (Fig. 4).

The tomb is facing typical problems of instability showing possible risks of block movements and requires a global risk analysis study.

To assess the possible instability of the tomb, a derived technique of Fuzzy Logic inference was used to account for Rock Mass Ratings inside various zones of the tomb, resulting is a complete zone risk map all along the three zones of the tomb illustrated in Fig. 4. The Fuzzy Logic inference technique included the definition of sensitivity and activity block falling phenomena (Elshayeb and Verdel 2005).

The application of Fuzzy Logic inference for zone risk mapping indicated high risk of block movements at zone III, thus leading to the installation of wooden structure at the burial chamber of the tomb, as shown in Fig. 5 (Elshayeb and Verdel 2005).

Fig. 5 View of the entrance to the tomb of Ramses I and its interiors galleries (upper photos), and a view of the wooden support installed at the burial chamber (lower photo)

Fig. 4 Plan and cross-section of the tomb of Ramses I

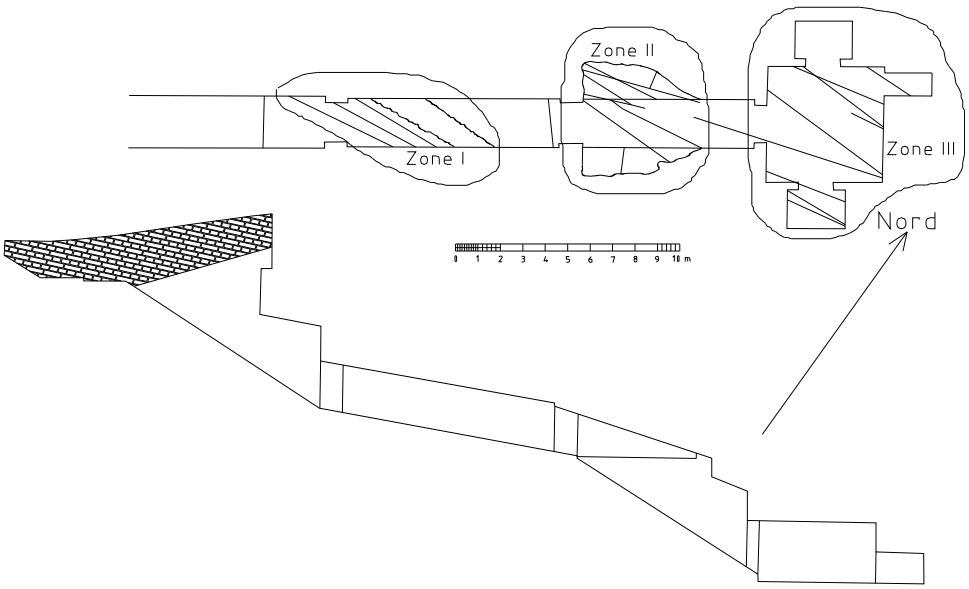

4 The Serapeum Tomb in Saqqara

The Serapeum is considered historically as the tomb of burial the arks of the sacred bulls of the "Apis" cult at Memphis. It was believed that the bulls were incarnations of the God Ptah, which would become immortal after death.

Over a timespan of circa 1400 years, from the New Kingdom to the Ptolemaic Period, at least sixty Apis are attested to have been interred at the Serapeum. The earliest burials are found in isolated tombs. As the cult gained importance, underground galleries were dug to connect subsequent burial chambers. One of the cult practices involved the dedication of commemorative stone tablets with dates relating to the life and death of the "Apis".

Saqqara Serapeum tomb is a valuable archaeological unit that has been subjected to serious structural damages and deterioration.

Figure 6 shows a plan of the tomb which is composed of two almost horizontal galleries: one known as main gallery of 211 m in length, 3 m wide and 4 m height. The second gallery is smaller in length (about 50 m), but similar in other dimensions. Along the sides of the main gallery, there exist 28 burial chambers in alternating manner, only 24 contained granitic and hard limestone coffins for burial arks of the sacred bull "Apis". They were excavated at levels lower than the excavated main gallery level.

The tomb of the Serapeum is located in a succession of limestones, marl and shale, where the shale is highly affected by humidity and causing several instability problems at the base and at the roof of the tomb (cf. Fig. 7).

Several geotechnical investigations and analysis of stresses were carried out at the Serapeum to identify stress distribution systems and scenarios of failure, which would lead to consolidation and support structures (Hamdy 2021; Imam et al. 2007, 1985).

Jointing systems, dynamic loading of adjacent limestone quarries, swelling of shale, and deterioration of limestones due to aging and inadequate drainage system in nearby urban area, were the main reasons for instability of the tomb. During the period of 2001–2010, an extensive analysis of the stability of the tomb, led to the conclusion of installation of a complete steel arches support system inside the tomb galleries and many of its burial chambers.

From an engineering point of view, such a solution would eliminate the risk of instability, block movements and landslides inside the tomb, whereas the adequacy of such supporting structure must be studied carefully as it risks leading to the loss of the archeological value of the site. Figures 8 and 9 show some photos of the installed supporting structure installed at the tomb as reported in the work of (Hamdy 2021).

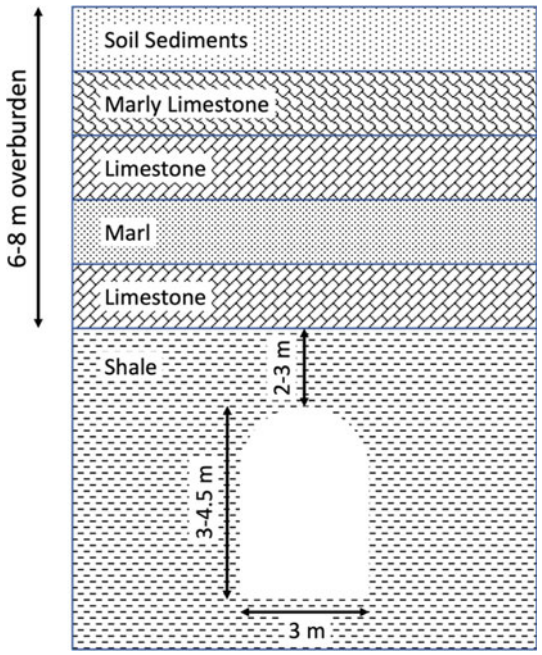

Fig. 7 Typical dimensions and succession of layers at the Serapeum of Saqqara (Hamdy 2021)

Fig. 6 Plan of the Serapeum in Saqqara

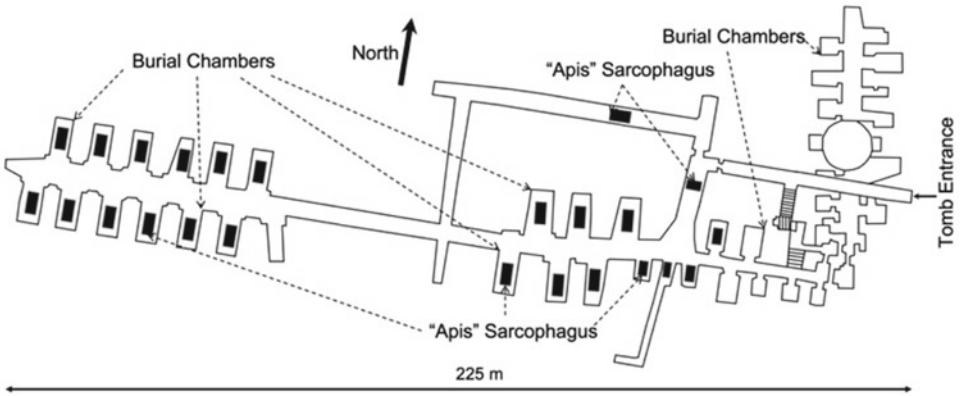

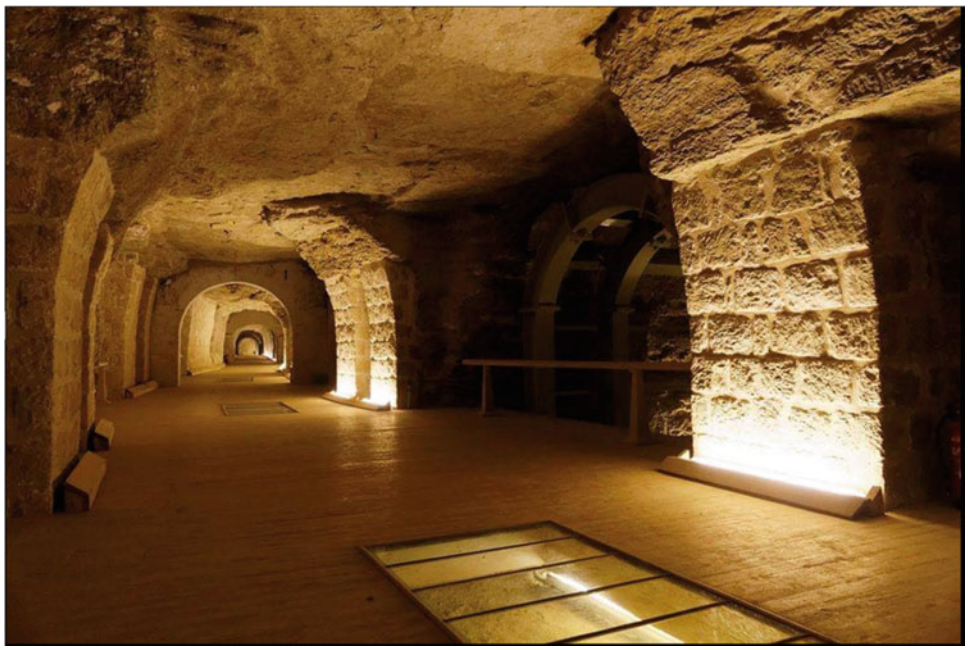

Fig. 8 General view of the main gallery of the Serapeum in Saqqara

Fig. 9 A typical view of the metallic support structures installed at the burial chambers of the Serapeum in Saqqara

5 Conclusions

Applications of Rock Mechanics, Geomechanics and Slope Stability to Egyptian Cultural Heritage were introduced in the late 1980s with analytical and later numerical analysis of stresses induced from rocks surrounding the abundant sites of cultural heritage in Egypt.

During the 1990s and early 2000s several studies and analysis has been carried out to analyze stresses and risks around various cultural heritage sites, but it was not until later in the 2010s and until now, that the Egyptian Supreme Council of Antiquities and currently the Ministry of Antiquities, have adopted the systematic approach to stability of cultural heritage structures, thus paving the way for a lot of stability studies, with subsequent consolidation/supporting

civil works carried out at various cultural heritage sites in Egypt.

In the paper, three different cases from Egypt were presented, each is a unique case with unique environment and unique risks of instability. Nevertheless, Engineering intervention in those sites allowed better understanding and better preservation of those world cultural heritage sites.

References

Dziedzic T, Michiewicz M (2018) Research of the Theban limestone: the case of Temple of Hatshepsut in Deir el-Bahari. In: E3S web of conferences. Solina

Elshayeb Y, Verdel T (2005) Geotechnical landslides risk analysis on historical monuments: methodological approach. In: Sassa K (ed) Landslides risk analysis and sustainable disaster management. Springer

Hamdy G (2021) Stabilization of the Ancient Serapeum at Saqqara—strengthening proposals using advanced composite materials. In: Mahgoub Y, Cavalagli N, Versaci A, Bougdah H, Serra-Permanyer M (eds) Cities identity through architecture and arts. Advances in science, technology & innovation. Springer, Cham, pp 15–24

Hamimi Z, El-Barkooky A, Frías JM (2020) In: El-Rahman YA (ed) The geology of Egypt. Springer

Helal H, Abdallah T (1990) Risk evaluation of rock mass sliding in El-Dier El-Bahary valley, Luxor, Egypt. Bull Int Assoc Eng Geol 42:3–9

Imam H, Helal H, Abdallah T (1985) Field investigation and measurements. Technical reports about Serapeum tomb. Supreme Council of Antiquities—Egypt

Imam H, Eltouny S, Abdelkader N (2007) Surveying and architectural documentation of all Serapeum units. Supreme Council of Archeology—Egypt

Rushdi S (1990) The geology of Egypt. A.A. Balmkema, Rotterdam

Review Articles

Review of the Founding Issue of P-LRT: Progress in Landslide Research and Technology

Shinji Sassa

Abstract

This article presents an overview and a concise review of the founding issue of Progress in Landslide Research and Technology (P-LRT). The Vol. 1, No. 1 issue of P-LRT was comprised of a total of twenty-four articles from twenty-five countries/regions worldwide. The inaugural issue embodies recent progress in landslide research and technology for practical applications and the benefit for the society contributing to the Kyoto Landslide Commitment 2020 for a global promotion of understanding and reducing landslide disaster risk.

Keywords

Early warning • Design • Climate change • UNESCO • Experimental/numerical analysis • ISO • Real-time prediction • Landslide-induced tsunami • Hazard mapping • Resilience • Sustainability • Advanced monitoring technology • Rainfall-induced landslide • Giant landslides on volcanic islands • Rockslide

1 Introduction

The founding issue of P-LRT: Progress in Landslide Research and Technology was composed of the contributions of twenty-four relevant articles from twenty-five countries/regions worldwide. The articles represented a total of eleven original articles, one review article, a total of ten articles on the projects of the International Programme on Landslides (IPL) and the World Centres of Excellence on Landslide Risk Reduction (WCoEs), and Kyoto Landslide Commitment, one teaching tool, and one technical note from a total of one-hundred and fifteen researchers/practitioners. The themes were diverse and ranged from landslide-induced tsunamis to natural-hazard-related web observatories, port-fire erosion rates mapping, mechanisms and early warning of rainfall-induced landslides, design of protection structures against flow-like landslides, landslide warning systems, translational landslides, spectral element method in slope instability analysis, climate change-induced landslide susceptibility and exposure assessment, using experimental models to calibrate numerical models for slope stability/deformation analysis, sustainability of geosynthetics-based landslide stabilization, establishment of the disaster risk reduction unit in UNESCO, real-time high-resolution prediction of orographic rainfall, landslide monitoring best practices and advanced technology, International Organization for Standardization (ISO), rockslide inventory, global database of giant landslides on volcanic islands, 2018 Easter Iburi landslide disasters, empirical-statistical modeling of landslide travel distances, landslide hazard resilience and geometry for restoration, teaching tool/manual of the integrated landslide simulation model LS-RAPID, and rainfall thresholds for landslide early warning systems.

2 Review of the Founding Issue of P-LRT

The founding issue of Progress in Landslide Research and Technology featured a total of 24 articles that represented original articles (11), review article (1), IPL/WCoEs/Kyoto Commitment activities articles (10), teaching tool (1) and technical note (1), which will be reviewed in order as below.

Sassa et al. presented the outcome of the panel discussion (Fig. 1) organized across America, Europe, and Asia and the review of the World Tsunami Awareness Day Special Event of the Fifth World Landslide Forum. The article presented some recent advances, the current state and challenges in understanding and reducing the disaster risk of landslide-induced tsunamis.

S. Sassa (✉)
Port and Airport Research Institute, National Institute of Maritime, Port and Aviation Technology, Yokosuka, Japan
e-mail: sassa@p.mpat.go.jp

I. Alcántara-Ayala et al. (eds.), *Progress in Landslide Research and Technology, Volume 1 Issue 2, 2022*, Progress in Landslide Research and Technology,
https://doi.org/10.1007/978-3-031-18471-0_15

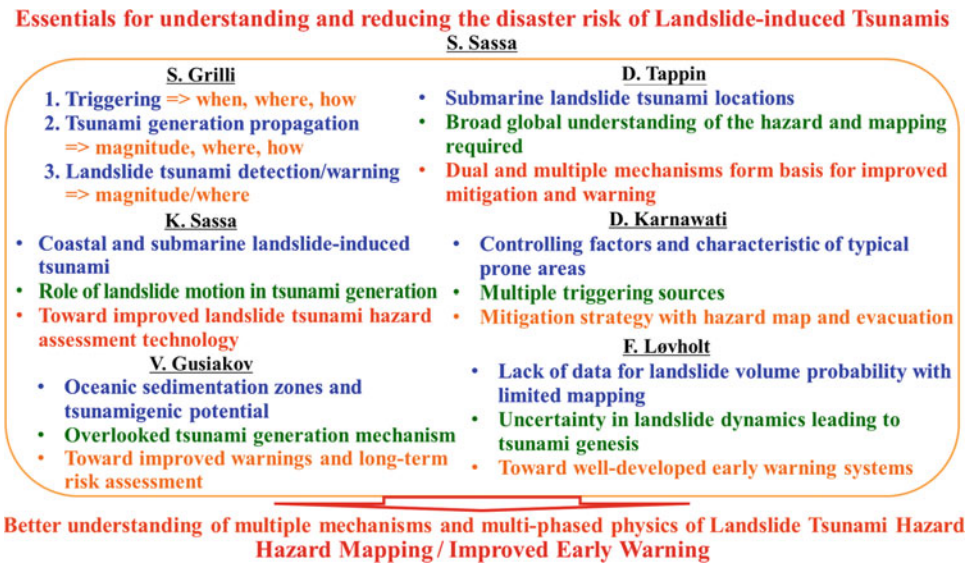

Fig. 1 The framework, essential content and a short summary of the panel discussion in the World Tsunami Awareness Day Special Event of the Fifth World Landslide Forum (Sassa et al. 2022a) (Fig. 22 in Sassa et al. 2022b)

Mikoš et al. presented a natural-hazard-related web observatory on landsides as a sustainable development tool. The information gathered on the internet (e.g. Fig. 2) is structured, and shown using geolocators for different regions and/or countries to be used by different stakeholders when implementing global climate adaptation policies and relevant European Union strategies.

Vacha et al. mapped post-fire monthly erosion rates at the catchment scale on GIS in the north-western Italian Alps. They highlighted the marked increase (more than 20 times) in erosion rates, quantified by expressing both the EI (erodibility index), the A (monthly soil loss) and the SL (monthly sediment loss) rise (Table 1) in the post-fire scenario than the pre-fire one.

Gratchev et al. presented the mechanisms of rainfall-induced shallow landslides in Australia (Fig. 3). The major factors causing the landslide mass such as geology, weathering, and rainfall patterns were discussed based on the field and laboratory investigations, showing the role of the formation of wetting (moisture) front, increases in water content, and the excess pore water pressure generation.

Cuomo et al. presented the analysis of LSI (Landslide-Structure-Interaction) for flow-like landslides against protection barriers for their design, on the basis of a general

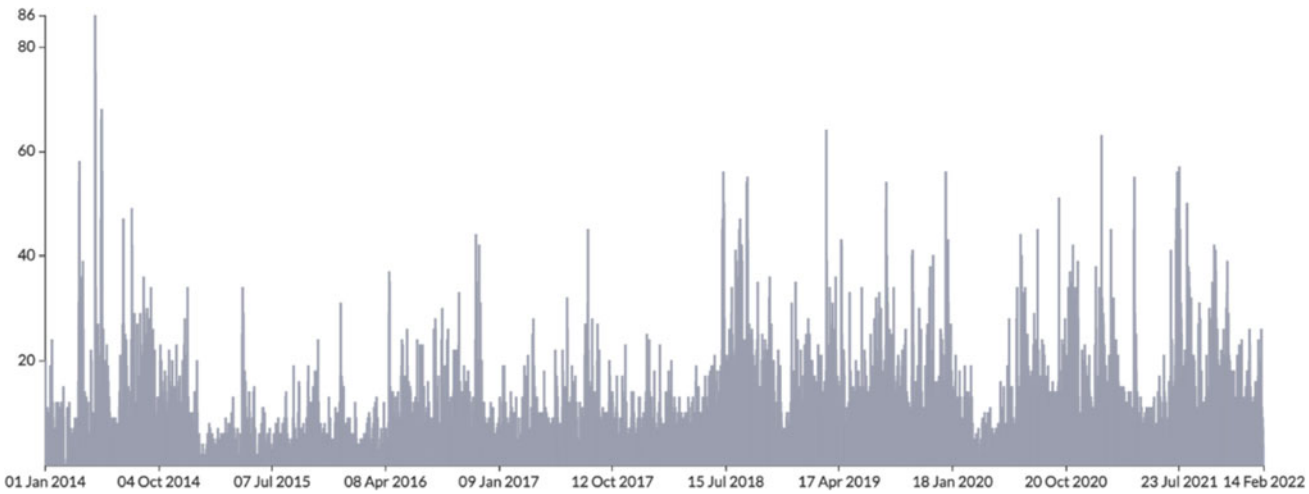

Fig. 2 Exploring a timeline of worldwide news on landslide events throughout 927,847 articles in eight years of collected data (Fig. 9 in Mikoš et al. 2022)

Table 1 Spatially averaged mean soil loss (A) and averaged monthly sediment loss (SL) comparison for the burned and unburned situation (Table 7 in Vacha et al. 2022)

Month	Burned		Unburned	
	A (Mg/ha*m)	SL (Mg/m)	A (Mg/ha*m)	SL (Mg/m)
9-17	0.000	0.00	0.000	0.00
10-17	0.000	0.00	0.000	0.00
11-17	0.133	17.32	0.005	0.66
12-17	0.208	27.07	0.008	1.03
1-18	3.342	434.36	0.127	16.48
2-18	0.014	1.82	0.001	0.07
3-18	0.310	40.28	0.012	1.53
4-18	4.223	548.87	0.160	20.83
5-18	8.081	1050.28	0.307	39.86
6-18	2.371	308.14	0.090	11.69
7-18	0.981	127.55	0.037	4.84
8-18	1.014	131.75	0.038	5.00
Total	20.677	2687.45	0.785	101.98

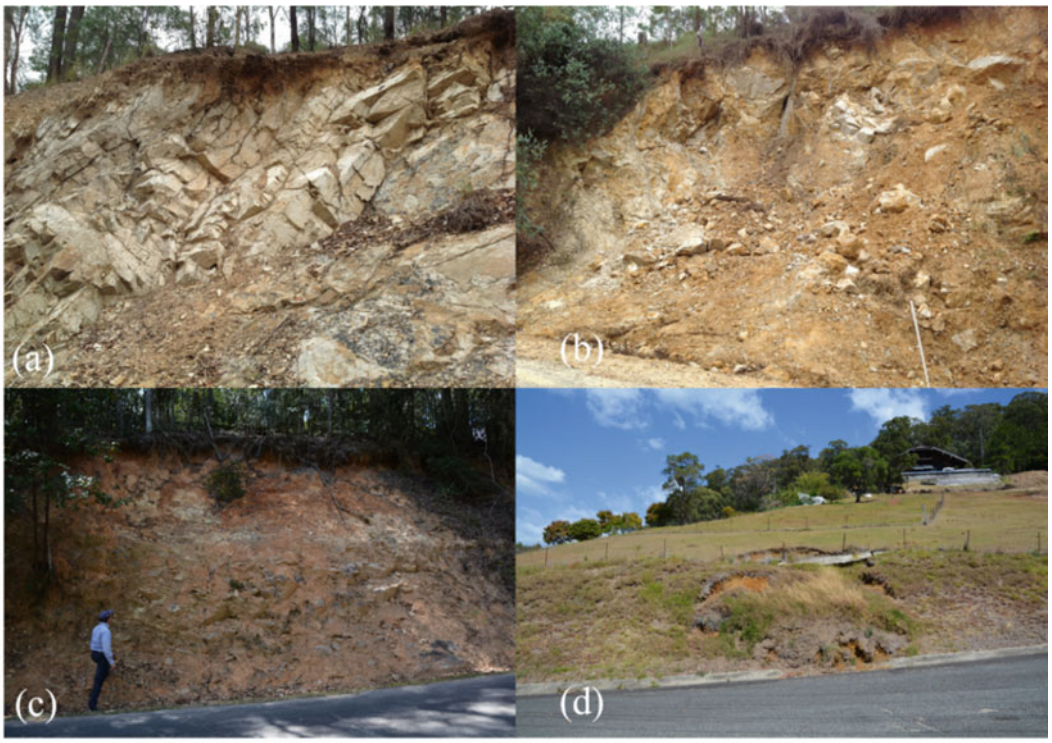

Fig. 3 Examples of rainfall-induced landslides from Australia: **a** failure in rock mass of the Neranleigh–Fernvale Beds formation. The bedding planes of sandstone and argillite are steeply inclined, producing an adverse effect on rock mass stability; **b** landslide in heavily weathered volcanic deposits; **c** shallow slide of heavily weathered material caused by the Cyclone Debbie in 2017; **d** shallow landslide in weathered material (Fig. 2 in Gratchev et al. 2022)

conceptual scheme (Fig. 4) and empirical, analytical and numerical approaches including the estimate of the amount of landslide volume overtopping the barrier. Different tools and options to design a protection barrier have been provided.

Alcántara-Ayala and Garnica-Peña presented the systematic literature analysis of Landslide Early Warning Systems (LEWS) in low- and lower-middle-income countries. The demand for effective regional and international

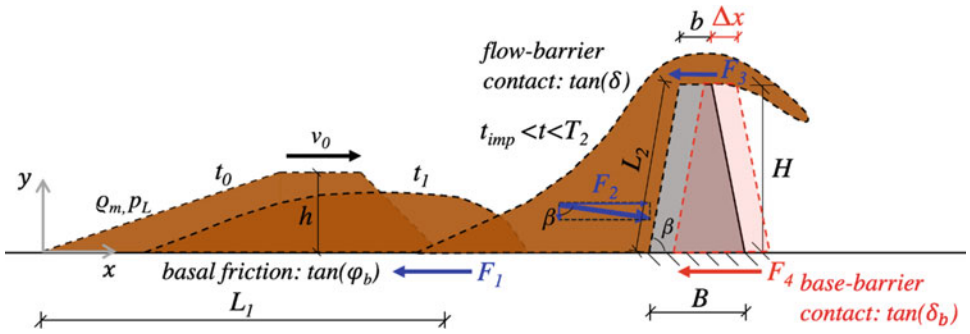

Fig. 4 General conceptual scheme for Landslide Structure Interaction (LSI) (Fig. 1 in Cuomo et al. 2022)

collaborations (Fig. 5) with the scientific community for the disaster risk reduction (DRR) in terms of LEWSs advancement was highlighted.

Abe et al. presented the role of translational landslides (Fig. 6) in the evolution of cuesta topography based on the field surveys in Japan, Taiwan, Switzerland, and Nepal. The results indicate that the translational bedrock landslides occurring on the cuesta's back slopes have repeatedly denuded intact sliding surfaces over the long term while maintaining the cuesta landscape.

Tiwari and Bhandary presented the application of spectral element method (SEM) in slope instability analysis (e.g. Fig. 7). The SEM procedure has three major benefits over the existing FEM procedures: (1) geometrical flexibility, (2) high computational efficiency, and (3) reliable spectral accuracy (i.e., exponential reduction of errors with increasing degree of polynomials).

Wijaya et al. presented the climate change-induced regional landslide hazard and exposure assessment (Fig. 8) in mountainous regions under extreme rainfalls in Nepal. They developed high-resolution landslide hazard models based on the Frequency Ratio (FR) and Analytical Hierarchical Process (AHP) methods, which may aid climate resilient road infrastructure planning.

Tiwari and Tran described the use of experimental models to calibrate numerical models (Fig. 9) for slope stability and deformation analysis. They showed how various soil and ground parameters influence the stability of slopes and how numerical models can be calibrated with the experimental modeling results to apply the calibrated numerical models for field slopes/landslides.

Damians et al. identified sustainability factors to consider when applying geosynthetics (Fig. 10) for mitigating landslide risks. They showed how a value integrated model for

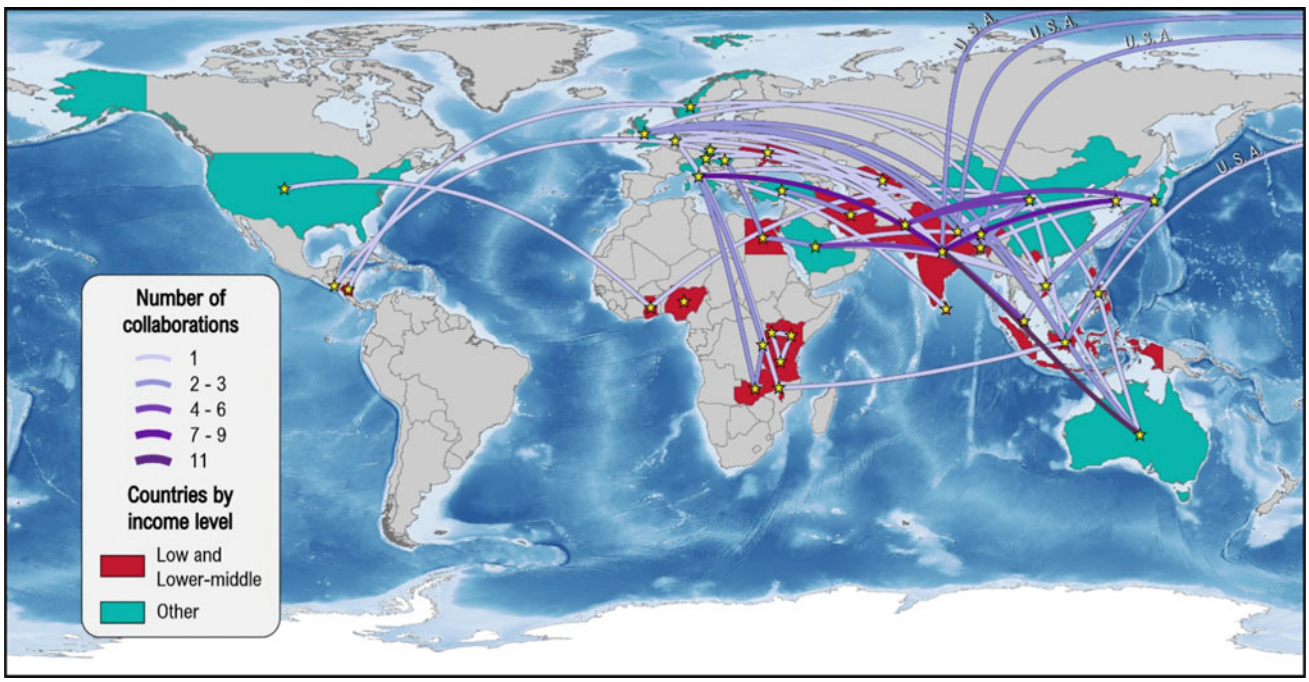

Fig. 5 Regional and international collaborations among LICs and MICs and other countries (Fig. 10 in Alcántara-Ayala and Garnica-Peña 2022)

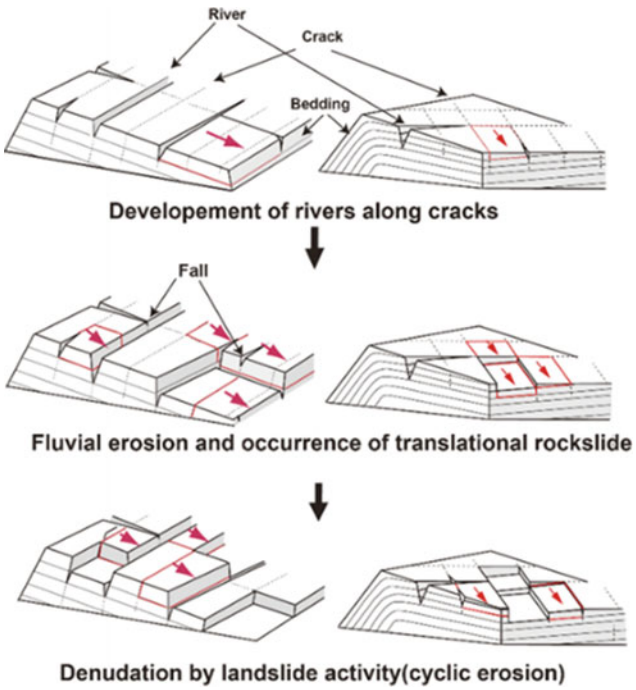

Fig. 6 Schematic models of the landslide history induced by the development of cracks and streams (Fig. 11 in Abe et al. 2022)

sustainable evaluations (MIVES) methodology can be applied to evaluate and compare alternative methods for remediation of landslides and recommended further studies using this tool.

Delgado et al. reported the establishment of the disaster risk reduction (DRR) unit in UNESCO and UNESCO's contribution to global resilience. UNESCO's DRR unit will continue to support the development of global, regional and national multi-hazard early warning systems, the improvement of the scientific basis for developing technologies and tools for landslide multi-risk identification and management (Delgado et al. 2022).

Konagai et al. reported an outline of the joint research project "Development of early warning technology of Rain-induced Rapid and Long-travelling Landslides (Project RRLL)" between the International Consortium on Landslides (ICL) and the National Building Research Organization, Sri Lanka (NBRO). It aims at developing critical technologies for the early warning system against rainfall-induced landslides (e.g. Fig. 11).

Onishi et al. described a recent development of reliable high-resolution prediction of orographic rainfall using a next-generation numerical weather prediction model, the Multi-Scale Simulator for the Geoenvironment (MSSG, Fig. 12). The model facilitates reliable predictions of orographic rainfall for realizing early warning of landslides.

Casagli et al. presented Advanced Technologies for LandSlides (ATLaS). They outlined research activities on landslide monitoring and early warning through innovative technologies, exploitation of earth observation data and technology (Fig. 13) to detect, map, monitor and forecast

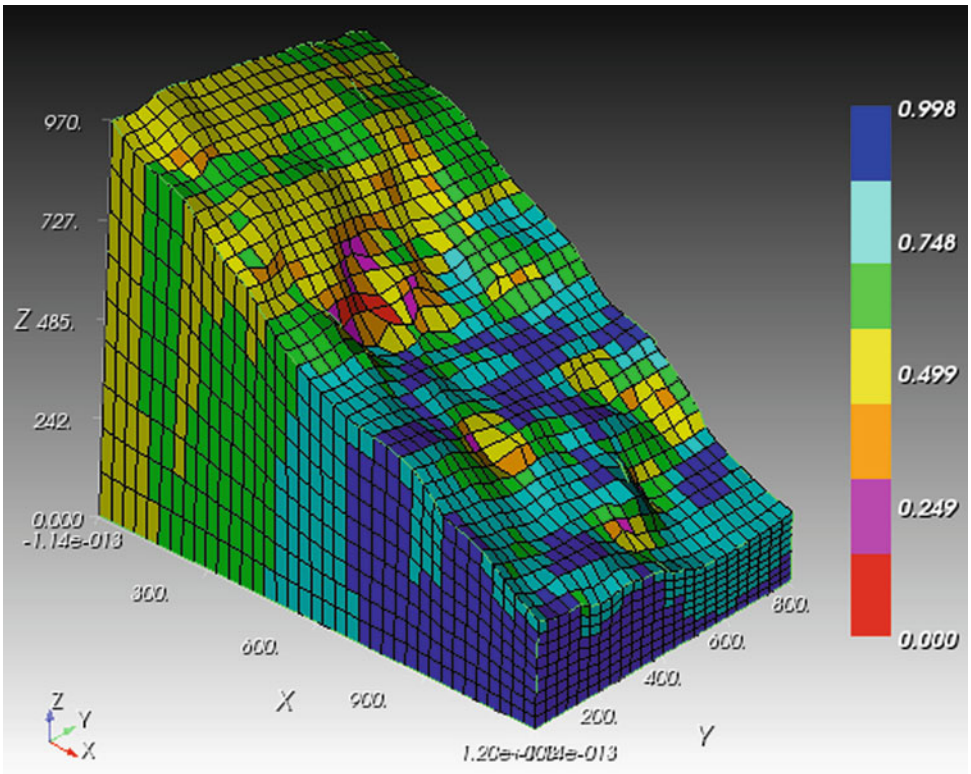

Fig. 7 3D model of Jure Sindhupalchowk landslide with Meshing (27°46′1.55″ N latitude and 85°52′17.10″ E longitude) (Fig. 14 in Tiwari and Bhandary 2022)

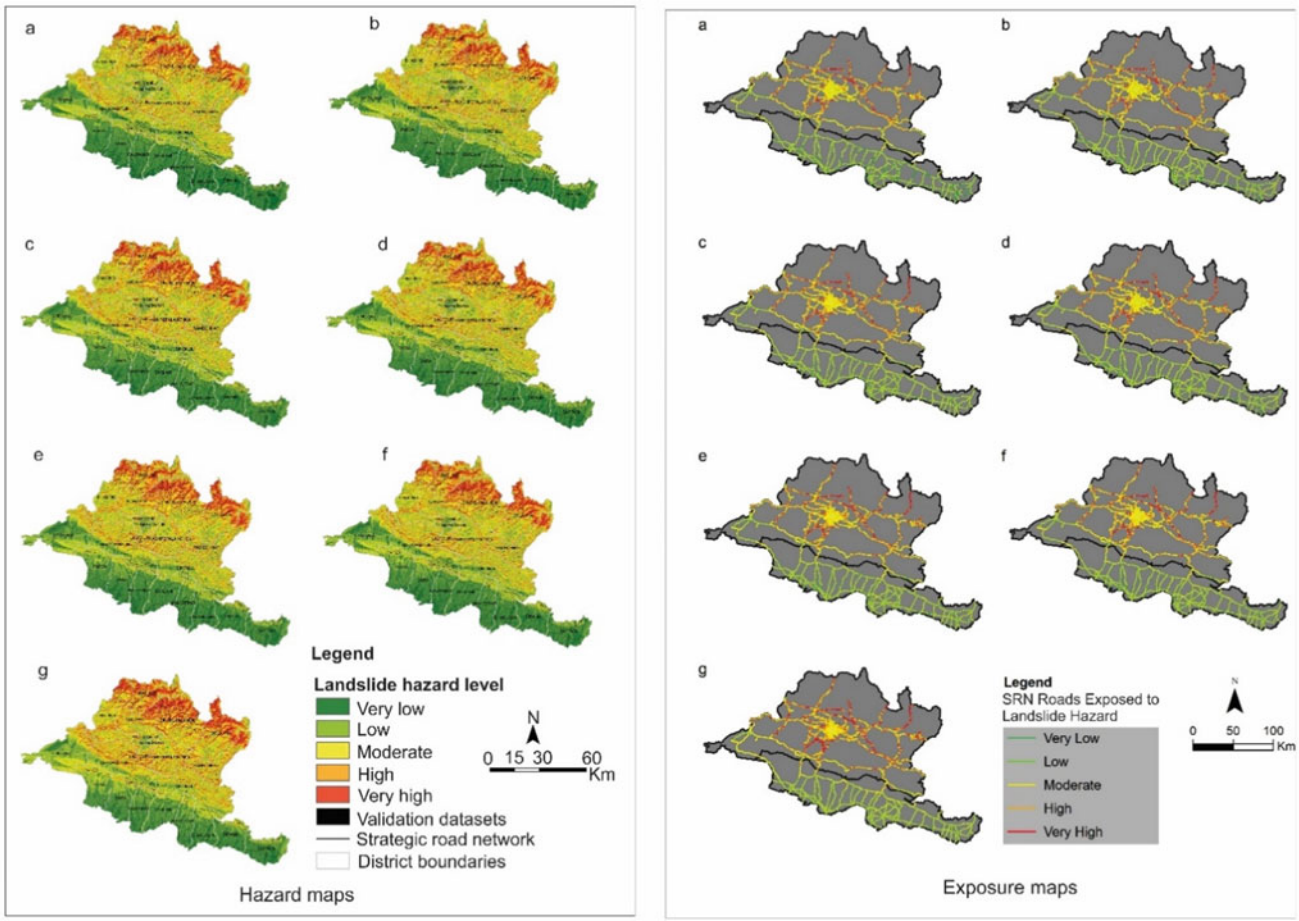

Fig. 8 Landslide hazard and exposure maps for **a** baseline period (1976–2005), **b** time horizon 2030s for RCP4.5, **c** time horizon 2030s with RCP8.5, **d** time horizon 2050s for RCP4.5, **e** time horizon 2050s for RCP8.5, **f** time horizon 2080s for RCP4.5 and **g** time horizon 2080s for RCP8.5. RCP denotes representative concentration pathways (Fig. 7 in Wijaya et al. 2022)

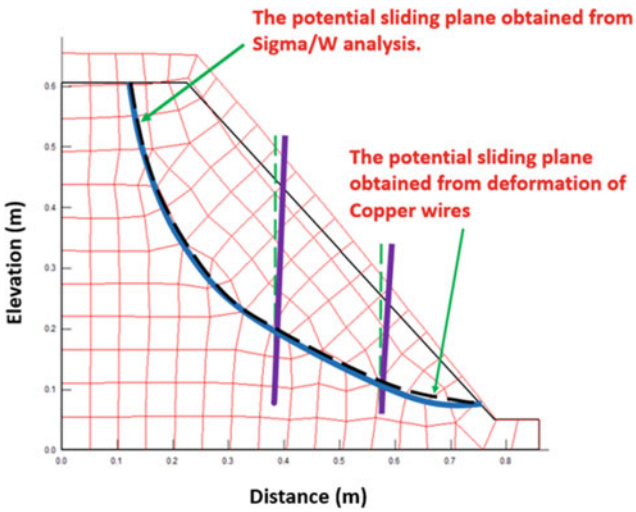

Fig. 9 Weakest plane obtained from numerical and experimental analyses—Sigma/W for model 6 (Fig. 19 in Tiwari and Tran 2022)

ground deformations, regional forecasting models for landslides risk reduction.

Huntley et al. reported the outcome of the IPL Project 202: Landslide monitoring best practices for climate-resilient railway transportation corridors in southwestern British Columbia, Canada. They proposed a best-practice solution involving three levels of investigation (Fig. 14) to describe the form and function of the wide range of rapid and slow-moving landslides.

Fathani et al. reported the implementation of a new standard for landslide early warning systems to the International Organization for Standardization (ISO). It empowers individuals and communities vulnerable to landslides (Fig. 15) to act in sufficient time and appropriate ways to reduce the possibility of injuries, loss of life, and damage to property and the environment.

Strom reported the activities of the World Centre of Excellence (WCoE) of JSC "Hydroproject Institute" and of

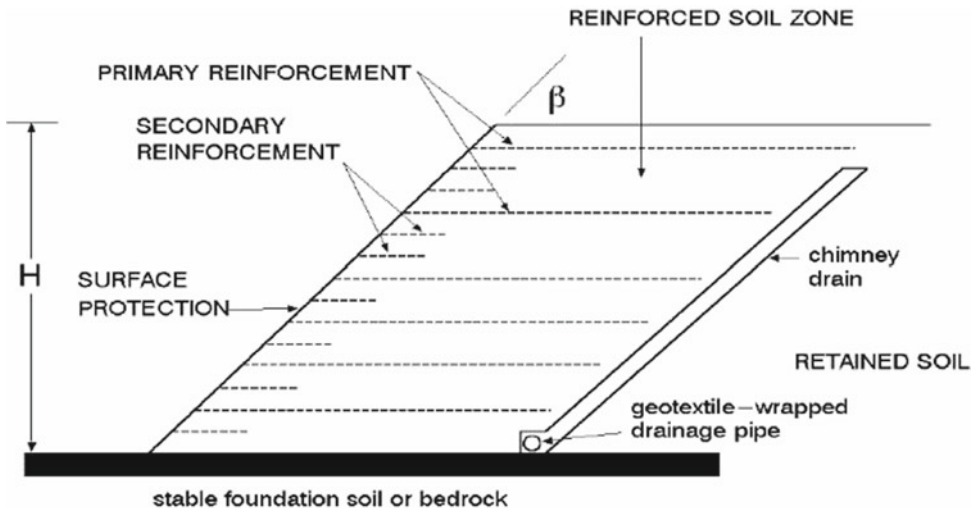

Fig. 10 Scheme of a geosynthetic reinforced soil slope (from IGS leaflet "Geosynthetics in Slopes over Stable Foundations") (Fig. 1 in Damians et al. 2022)

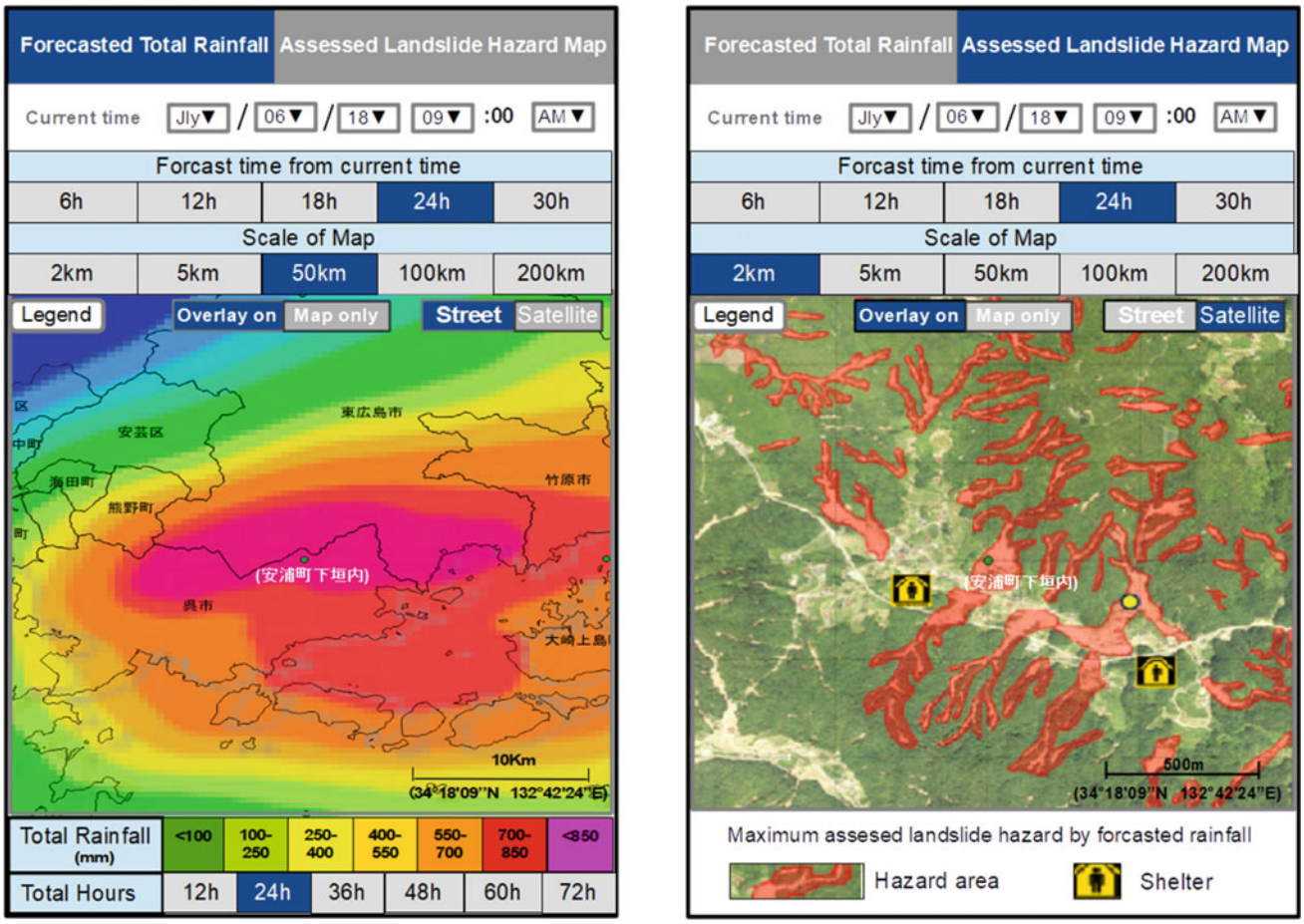

Fig. 11 Rendering image of augmented reality dioramas of the predicted rains and locations of rain-induced rapid long-traveling landslides (RRLLs) with a bird's-eye view of the area as their background on tablet's screen (Fig. 24 in Konagai et al. 2022)

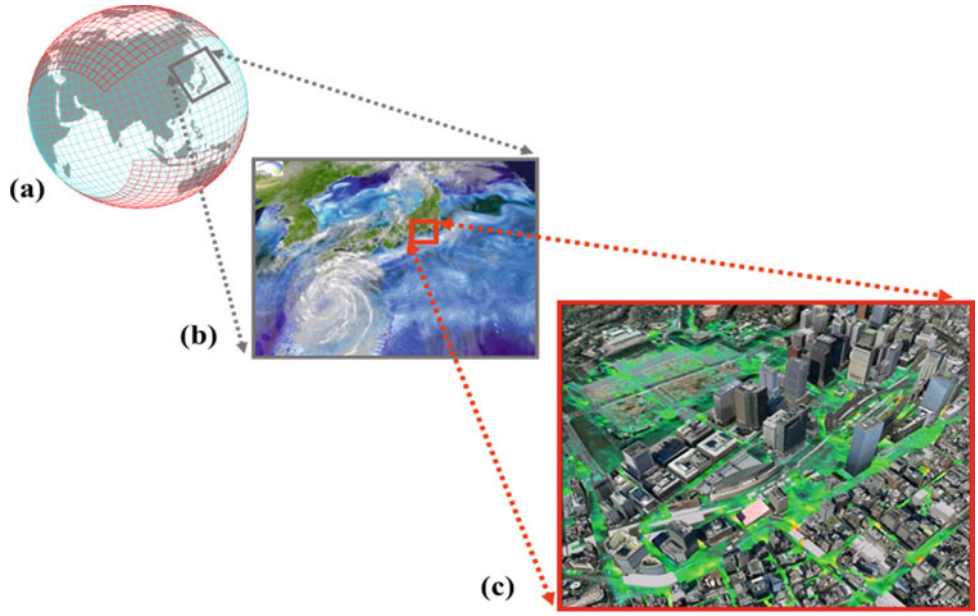

Fig. 12 MSSG is designed to be applicable to **a** global scale, **b** meso scales and up to **c** urban scales. The Yin-Yang grid system, which consists of two overlapping latitude–longitude grids indicated in blue and red, is adopted for global simulations (Fig. 1 in Onishi et al. 2022)

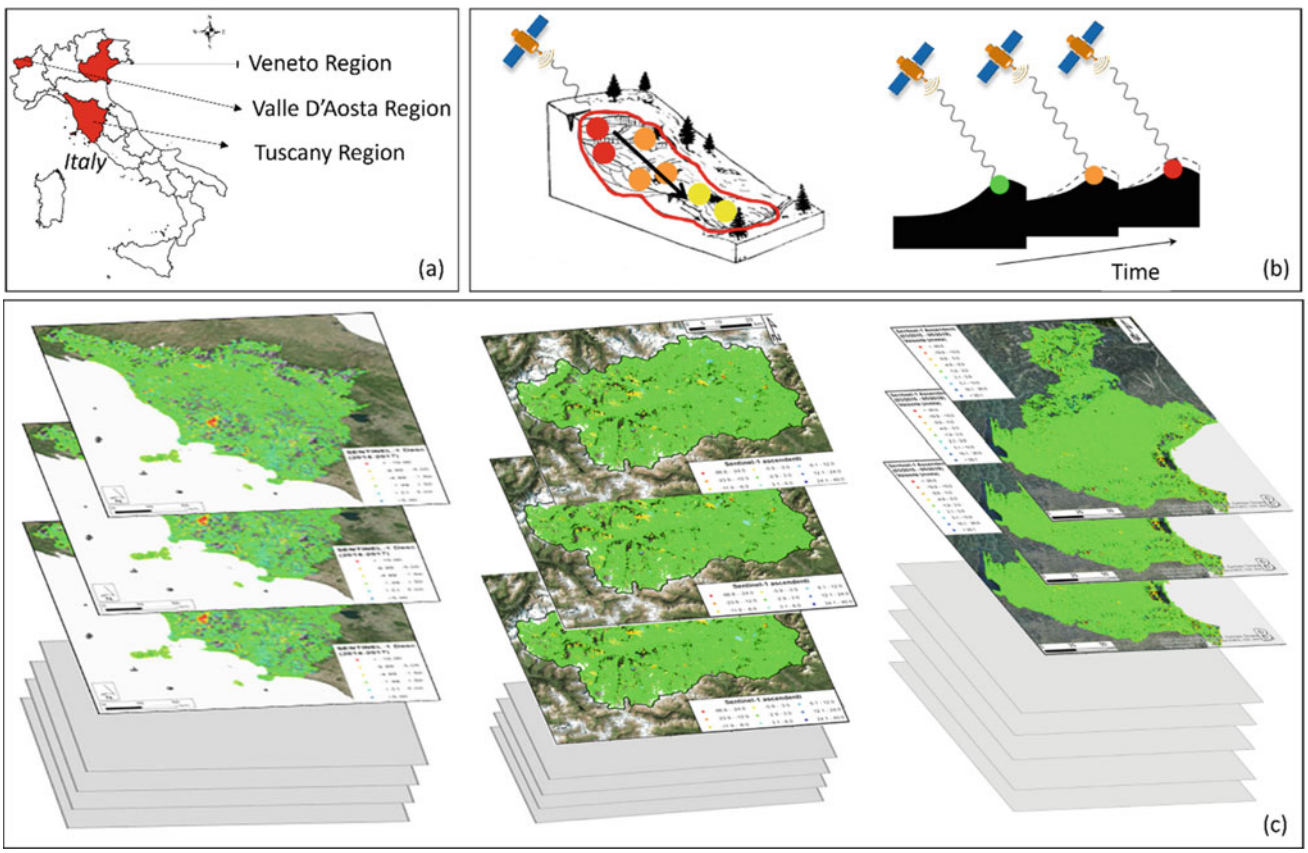

Fig. 13 Satellite-based services at regional scale in Italy: **a** location of Tuscany, Valle d'Aosta, Veneto Region in Italy; **b** example of "PS mapping" activity to highlight highest ground motion rates and of "PS monitoring" activity to periodically scan the territory across time; **c** sketch of systematically updated ground deformation maps based on Sentinel-1 PSI data of Tuscany, Valle d'Aosta, Veneto Region (Fig. 2 in Casagli et al. 2022)

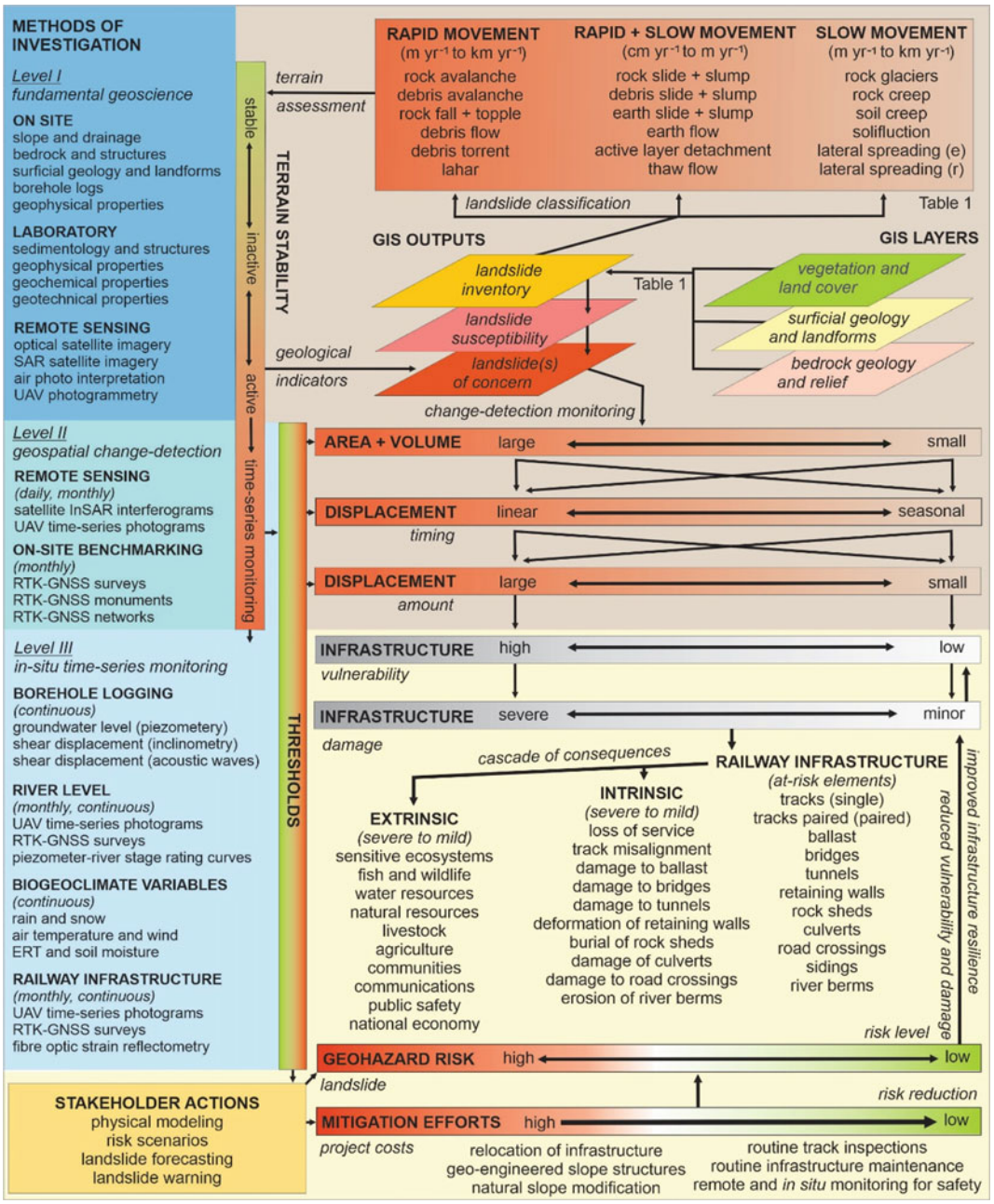

Fig. 14 Conceptual model outlining three levels of investigation to classify, determine susceptibility, and identify landslides of concern for monitoring. Inventory maps, geospatial change-detection, and in-situ time-series monitoring define the interactions between landslides of varying sizes, displacement amounts, and timing of activity; and contribute to estimates of infrastructure vulnerability, anticipated damage, and cascade of consequences contributing to landslide risk. Mitigation solutions reduce the risks to railway transportation corridors running through terrain susceptible to landslides (Fig. 7 in Huntley et al. 2022)

Institute of Seismology of National Academy of Sciences of Kyrgyz Republic. The study for the most disastrous types of landslides in mountainous regions—large-scale rockslides and rock avalanches (Fig. 16) led to the Central Asia Rockslides Inventory.

Rowberry et al. described a comprehensive online database of giant landslides on volcanic islands compiled by researchers from the Institute of Rock Structure and Mechanics, Czech Academy of Sciences, in the framework of IPL Project 212. The global distribution of giant

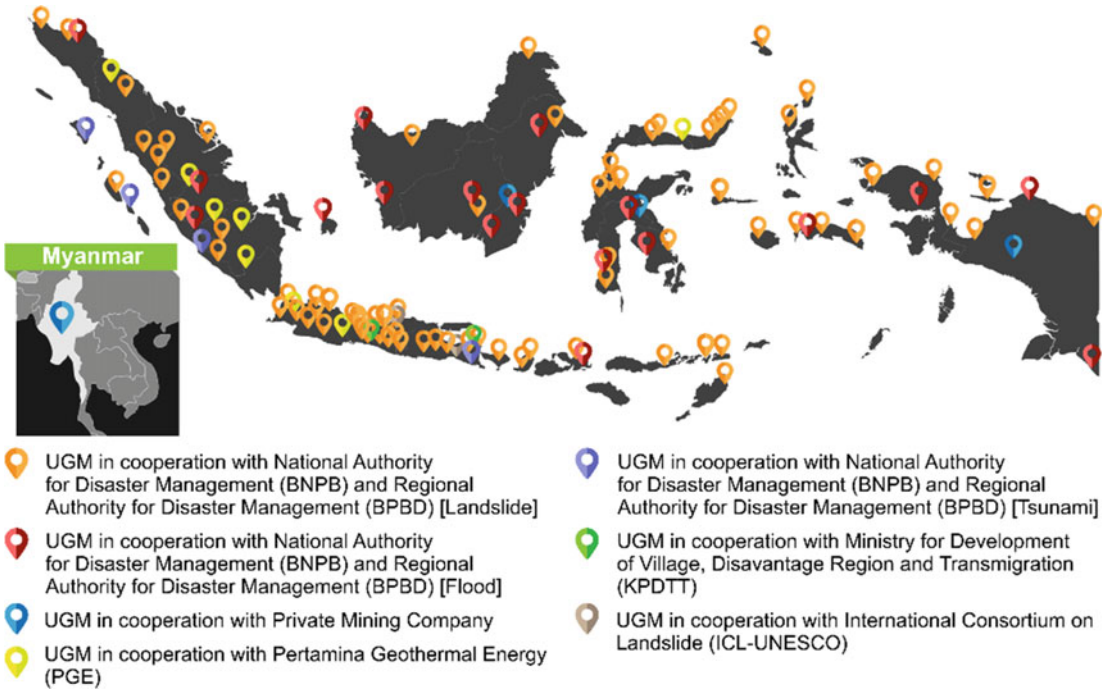

Fig. 15 Locations of landslides and floods early warning system implementation in Indonesia (2007–2021) (Fig. 6 in Fathani et al. 2022)

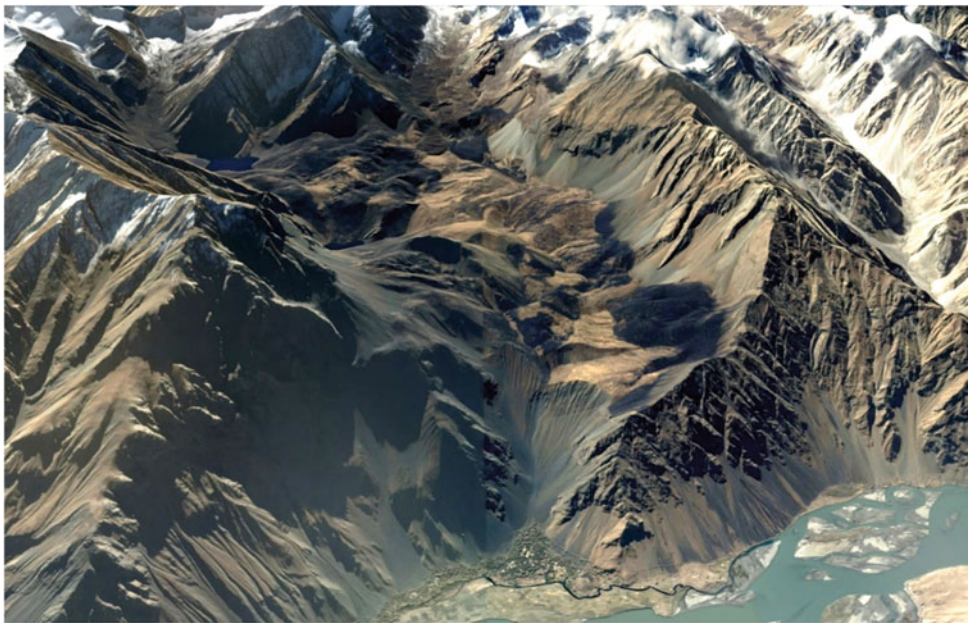

Fig. 16 Oblique view of the giant Padjvar rockslide in Afghan Badakhshan ca. 6 km^3 in volume. The entire ridge about 6 km long collapsed in the adjacent valley of the left tributary of the Pianj River and filled it almost completely with the deposits up to 650–700 m thick that cover 19.72 km^2, while the total affected area is about 27 km^2 (Fig. 12 in Strom 2022)

landslides on volcanic islands (Fig. 17) was described in depth.

Wang and Nam described landslide disasters caused by the 2018 Eastern Iburi Earthquake in Hokkaido Japan. They reported novel findings pertaining to distinctive properties of the widely distributed, weathered Plinian Ta-d tephra deposit (Fig. 18) from Tarumae volcano and their impact on the spatial clustering of the Iburi landslides.

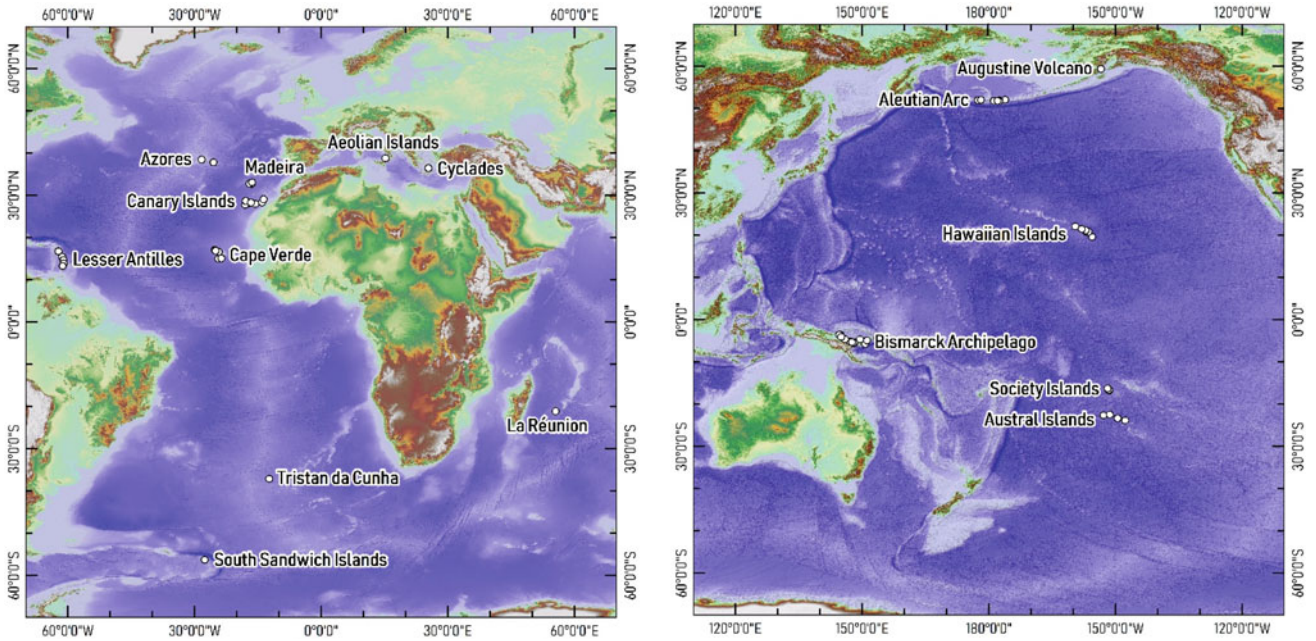

Fig. 17 Distribution of giant landslides on volcanic islands from the Atlantic and Indian Oceans (left) and the Pacific Ocean (right). *Source* Global relief model derived from Global Bathymetry and Topography at 15 Arc Sec: SRTM15 + V2.1 (Tozer et al. 2019) (Figs. 4 and 5 in Rowberry et al. 2022)

Moncayo and Ávila presented the analysis of the database of 123 landslides from the Andean region of Colombia. The empirical-statistical modelling showed that the volume of the displaced mass, the slope angle, the maximum landslide height, and geomorphological environment were the predominant factors controlling the landslides travel distances in the area (Fig. 19).

Dias et al. presented landform geometry pertaining to the restoration of mountain roads and landslide hazard resilience. They showed that the complexity of slope geometries, potential deformities, ground discontinuities, and soil-rock composite nature are compulsory elements to understand and dominant parameters to describe the on-site stability of earth cut slope (e.g. Fig. 20).

Ajmera et al. presented the teaching tool and manual of LS-RAPID, an integrated simulation model capable of capturing the entire landslide process starting from a state of stability to landslide initiation and movement to the mass deposition. Three tutorials were shown illustrating the applications to (1) a rainfall-induced failure, (2) an earthquake-induced failure, and (3) the case study of the Atami debris flow (Fig. 21), as supplemented by the video tutorials.

Gariano et al. described the LANDSLIP project aimed at developing a landslide early warning system (LEWS) to forecast the occurrence of rainfall-induced landslides in two Indian pilot areas: Darjeeling and Nilgiris (Fig. 22). The rainfall thresholds at different non-exceedance probabilities were determined by adopting a frequentist statistical method and an automatic tool.

3 Conclusion

This article has presented an overview and a concise review of the founding issue of P-LRT: Progress in Landslide Research and Technology. The themes for the Vol. 1, No. 1 of P-LRT were diverse as described above, with a total of one-hundred and fifteen researchers/practitioners from twenty-five countries/regions worldwide contributing to the inaugural issue of the ICL Open Access Book Series. It is hoped that P-LRT will serve as a common, long-standing platform for the publication of recent progress in landslide research and technology for practical applications and the benefit for the society contributing to the Kyoto Landslide

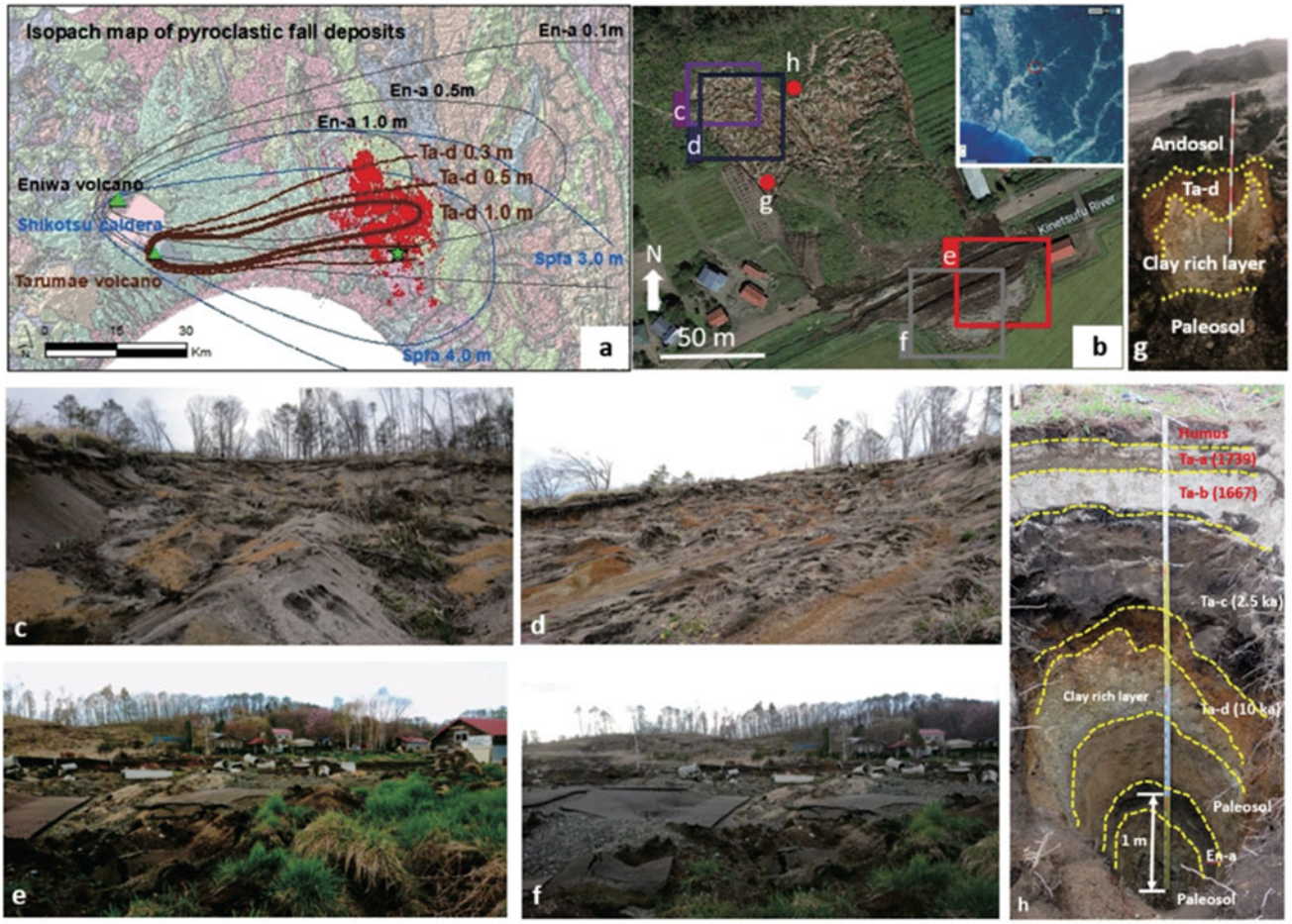

Fig. 18 Isopach map of pyroclastic fall deposits (Ta-a, Ta-b, Ta-c, Ta-d, En-a and Spfa-1) and field investigation on sliding surface (general view: a–d, and soil profiling: e and f) for the 2018 Iburi landslide disasters (Fig. 3 in Wang and Nam 2022)

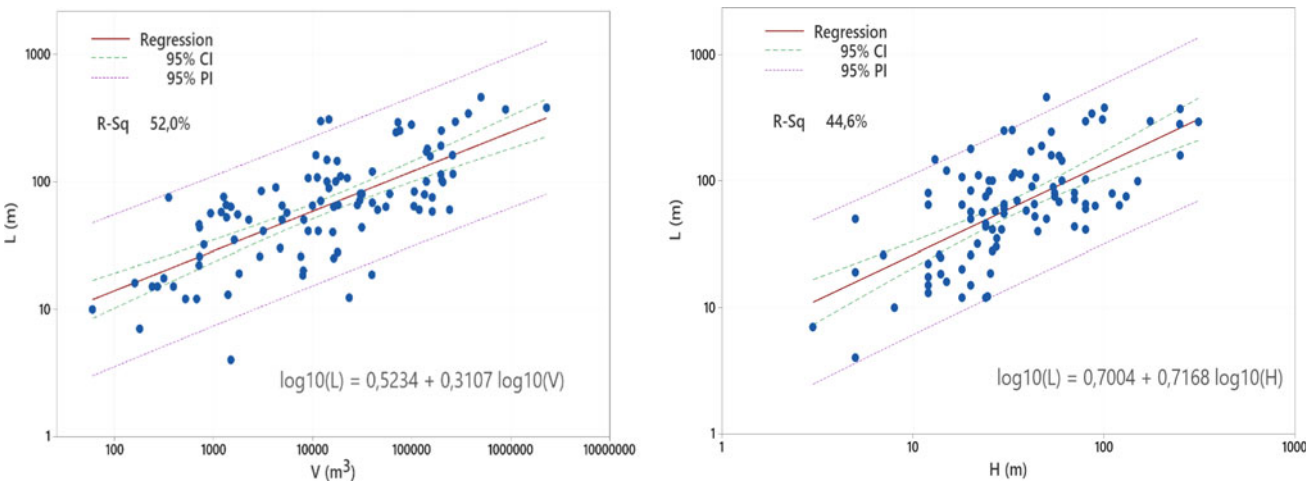

Fig. 19 Relationship between travel distance L and landslide volume V (left) and maximum landslide height H (right) (Figs. 3 and 4 in Moncayo and Ávila 2022)

Fig. 20 Example of rock formed failures along the road side slope. Wedge failure, translational slides and falling rocks are very much significant along the road sides. High hazard potential zone can be observed due to foliated and jointed rock formations (Fig. 13 in Dias et al. 2022)

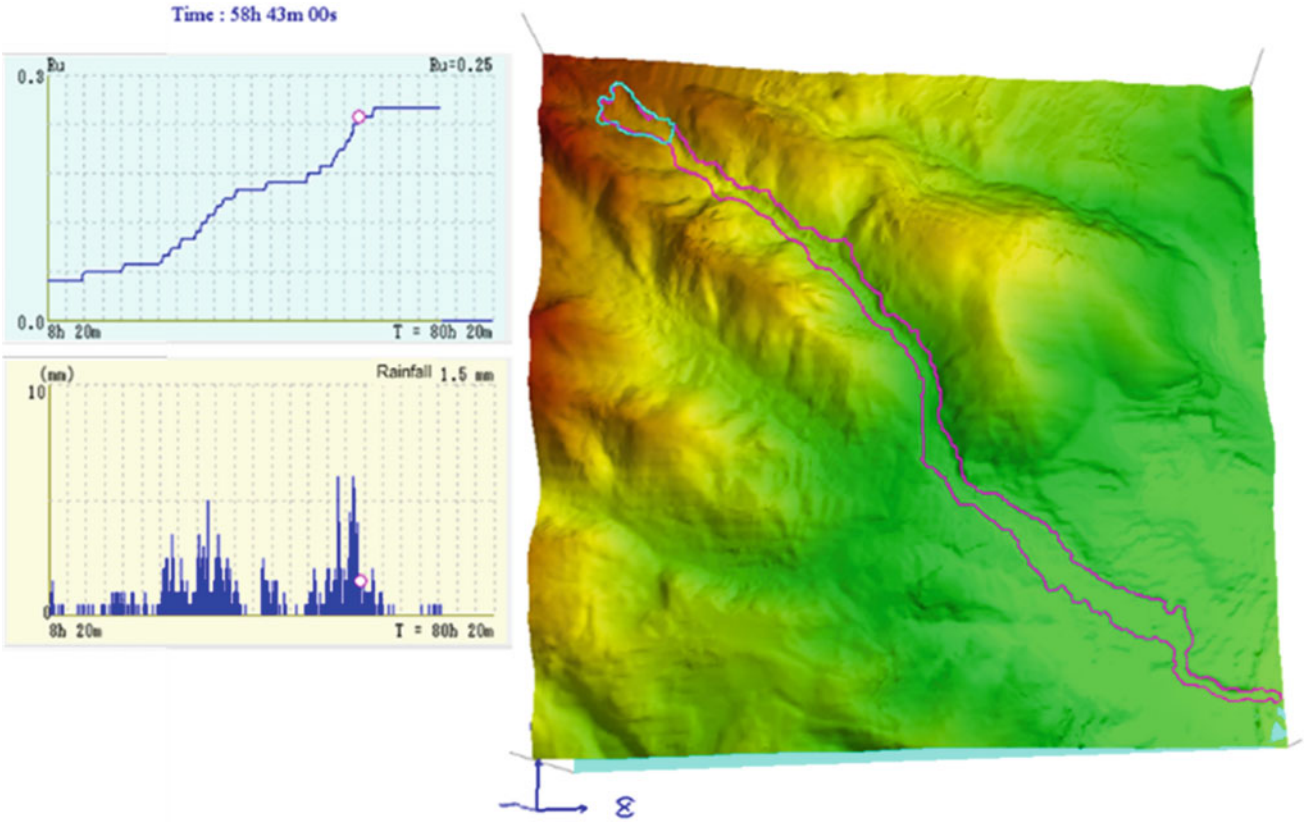

Fig. 21 Simulation Results of Atami Debris Flow at 58 h 43 m 00 s from the Start of Rainfall (Fig. 4.39(d) in Ajmera et al. 2022)

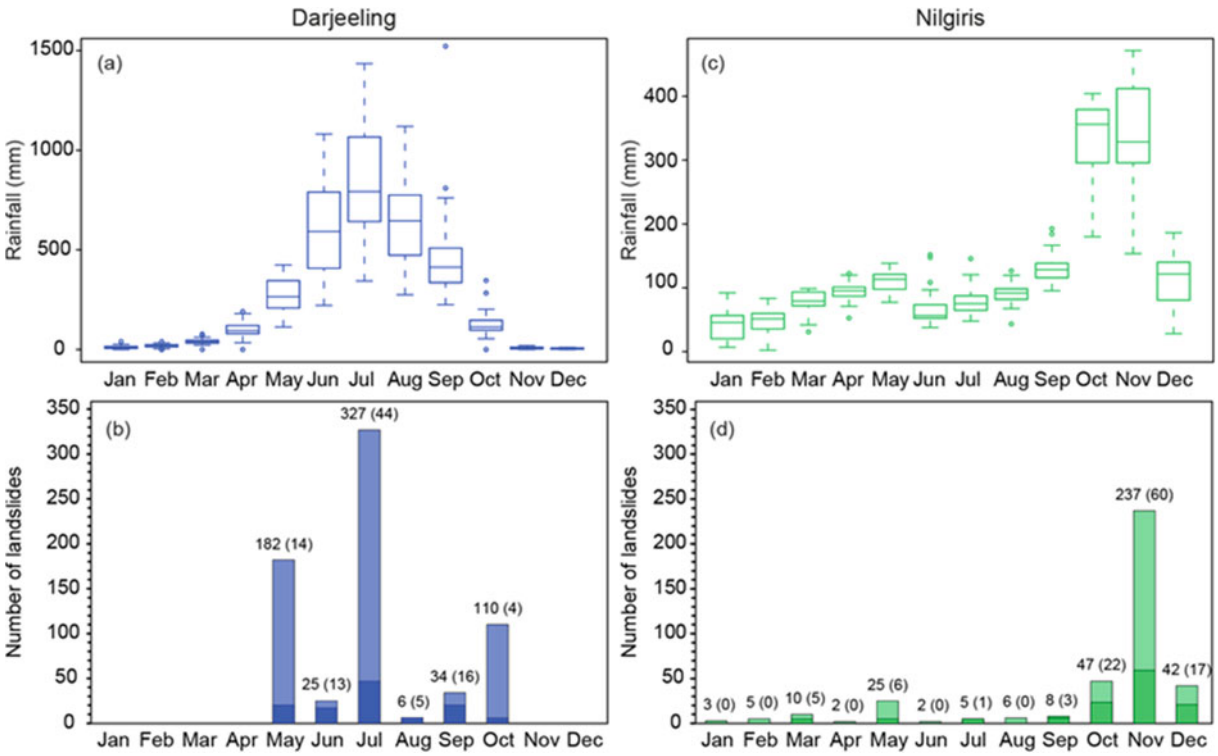

Fig. 22 Top: annual distribution of monthly rainfall in **a** Darjeeling (1959–2017) and **c** Nilgiris (1987–2017). Bottom: monthly distribution of landslides in **b** Darjeeling and **d** Nilgiris; lighter bars indicate the total numbers of catalogued landslides in each pilot area; darker bars indicate the landslides used to calculate the thresholds (values in brackets) (Fig. 3 in Gariano et al. 2022)

Commitment 2020 to globally promote understanding and reducing landslide disaster risk.

References

Abe S, Higaki D, Hayashi K (2022) The role of translational landslides in the evolution of cuesta topography. Prog Landslide Res Technol 1(1):2–7

Ajmera B, Ahari HE, Loi DH, Setiawan H, Dang K, Sassa K (2022) LS-RAPID manual with video tutorials. Prog Landslide Res Technol 1(1):5-1

Alcántara-Ayala I, Garnica-Peña RJ (2022) Landslide warning systems in low- and lower-middle-income countries: future challenges and societal impact. Prog Landslide Res Technol 1(1):2–6

Casagli N, Tofani V, Moretti S, Fanti R, Gigli G, Bianchini S, Segoni S, Frodella W, Carlà T (2022) Advanced technologies for landslides—ATLaS (WCoE 2020–2023). Prog Landslide Res Technol 1(1):4-4

Cuomo S, Perna AD, Martinelli M (2022) Design protection barriers against flow-like landslides. Prog Landslide Res Technol 1(1):2–5

Damians IP, Miyata Y, Rimoldi P, Touze N, Kraus J (2022) Sustainability of geosynthetics-based landslide stabilization solutions. Prog Landslide Res Technol 1(1):2–11

Delgado LMB, Pavlova I, Yasukawa S, Esperancinha S (2022) Establishment of the disaster risk reduction unit in UNESCO and UNESCO's contribution to global resilience. Prog Landslide Res Technol 1(1):3-1

Dias AAV, Herath HMJMK, Kulathilake LKNS (2022) Landform geometry for restoration of mountain roads and landslide hazard resilience. Prog Landslide Res Technol 1(1):4–10

Fathani TK, Karnawati D, Wilopo W, Setiawan H (2022) Strengthening the resilience by implementing a standard for landslide early warning system. Prog Landslide Res Technol 1(1):4–5

Gariano SL, Melillo M, Brunetti MT, Kumar S, Mathiyalagan R, Peruccacci S (2022) Challenges in defining frequentist rainfall thresholds to be implemented in a landslide early warning system in India. Prog Landslide Res Technol 1(1):6-1

Gratchev I, Ravindran S, Kim DH, Cui C, Tang O (2022) Mechanisms of shallow rainfall-induced landslides from Australia: insights into field and laboratory investigations. Prog Landslide Res Technol 1 (1):2–4

Huntley D, Bobrowsky P, MacLeod R, Rotheram-Clarke D, Cocking R, Joseph J, Holmes J, Sattler K, Chambers J, Meldrum P, Wilkinson P, Donohue S, Elwood D (2022) IPL Project 202: landslide monitoring best practices for climate-resilient railway transportation corridors in southwestern British Columbia, Canada. Prog Landslide Res Technol 1(1):4-3

Konagai K, Karunawardena A, Bandara KN, Sassa K, Onishi R, Uzuoka R, Asano R, Sasahara K, Jayakody S, Ariyarathna I (2022) Early warning system against rainfall-induced landslide in Sri Lanka. Prog Landslide Res Technol 1(1):4-1

Mikoš M, Bezak N, Costa JP, Massri MB, Novalija I, Jermol M, Grobelnik M (2022) Natural-hazard-related web observatory as a sustainable development tool. Prog Landslide Res Technol 1(1):2-2

Moncayo S, Ávila G (2022) Landslide travel distances in Colombia from national landslide database analysis. Prog Landslide Res Technol 1(1):4–9

Onishi R, Hirai J, Kolomenskiy D, Yasuda Y (2022) Real-time high-resolution prediction of orographic rainfall for early warning of landslides. Prog Landslide Res Technol 1(1):4-2

Rowberry M, Klimeš J, Blahůt J, Balek J, Kusák M (2022) A global database of giant landslides on volcanic islands. Prog Landslide Res Technol 1(1):4–7

Sassa S, Grilli ST, Tappin DR, Sassa K, Karnawati D, Gusiakov VK, Løvholt F (2022a) Understanding and reducing the disaster risk of landslide-induced tsunamis: a short summary of the panel discussion in the World Tsunami Awareness Day Special Event of the Fifth World Landslide Forum. Landslides 19(2):533–535

Sassa S, Grilli ST, Tappin DR, Sassa K, Karnawati D, Gusiakov VK, Løvholt F (2022b) Understanding and reducing the disaster risk of landslide-induced tsunamis: outcome of the panel discussion and the World Tsunami Awareness Day Special Event of the Fifth World Landslide Forum. Prog Landslide Res Technol 1(1):2-1

Strom A (2022) Central Asia rockslides inventory: compilation, analysis and training—progress of the IPL WCoE. Prog Landslide Res Technol 1(1):4–6

Tiwari B, Tran D (2022) Using experimental models to calibrate numerical models for slope stability and deformation analysis. Prog Landslide Res Technol 1(1):2–10

Tiwari RC, Bhandary NP (2022) Application of spectral element method (SEM) in slope instability analysis. Prog Landslide Res Technol 1(1):2–8

Tozer B, Sandwell D, Smith W, Olson C, Beale J, Wessel P (2019) Global bathymetry and topography at 15 arc sec: SRTM15+. Earth Space Sci 6:1847–1864. https://doi.org/10.1029/2019EA000658

Vacha D, Mandrone G, Morresi D, Garbarino M (2022) Mapping post-fire monthly erosion rates at the catchment scale using empirical models implemented in GIS. A case study in Northern Italy. Prog Landslide Res Technol 1(1):2–3

Wang F, Nam K (2022) Landslide disasters caused by the 2018 Eastern Iburi Earthquake in Hokkaido Japan and the countermeasures to completely prevent the similar disasters in the future. Prog Landslide Res Technol 1(1):4–8

Wijaya IPK, Towashiraporn P, Joshi A, Jayasinghe S, Dewi A, Alam MN (2022) Climate change-induced regional landslide hazard and exposure assessment for aiding climate resilient road infrastructure planning: a case study in Bagmati and Madhesh Provinces, Nepal. Prog Landslide Res Technol 1(1):2–9

Landslide Detection and Spatial Prediction: Application of Data and Information from Landslide Maps

Snježana Mihalić Arbanas, Sanja Bernat Gazibara, Martin Krkač, Marko Sinčić, Hrvoje Lukačić, Petra Jagodnik, and Željko Arbanas

Abstract

The need for landslide maps of wider areas has increased with the understanding that proper planning will considerably decrease the construction and maintenance cost of structures. The main objective of the paper is to present types of data and information on landslides that can be derived from landslide inventory and landslide susceptibility maps and their use for spatial and urban planning. Recent examples of landslide zonation maps from Croatia are given to show the possibility of the derivation of data about landslides by using LIDAR (Light Detection and Ranging) DTM (Digital Terrain Model) for the compilation of historical landslide inventory. The application of data about landslide phenomena is compared with the application of information from landslide susceptibility zonation maps. It is concluded that a multi-level and hierarchical approach is necessary to reach the cost-effectiveness of nationwide production of landside maps for land-use planning.

Keywords

Landslide detection • Landslide maps • Landslide susceptibility zonation • Land use planning

1 Introduction

The first review of landslide hazard zonation maps was compiled by Varnes and the IAEG Commission on Landslides and other Mass-Movements (Varnes 1984) as part of the landslide risk mitigation programme published by UNESCO. Given the content of these maps, there are two basic types that are fundamentally different: maps presenting records of landslide phenomena and maps showing a prediction of landslide processes in terms of spatial probability (i.e., landslide susceptibility) or temporal probability (i.e., landslide hazard). Landslide records in the form of landslide contours are collected by landslide detection and mapping. The results are displayed on the landslide inventory maps that are discussed in detail in the paper Guzzetti et al. (2012). Spatial prediction of landslides is the result of landslide susceptibility assessment and it is displayed on the landslide susceptibility zonation maps that present the distribution of resulting susceptibility in the form of a few zones. The most recent overview of the main methods to predict populations of landslides in space and time is given by Guzzetti et al. (2021).

During the period of more than 35 years, numerous attempts and unquestionable progress happened in landslide mapping and zonation. The most recent and revolutionary change in methods and techniques used to detect and map landslides is an application of high-resolution LiDAR (Light Detection and Ranging) bare earth DTM (Razak et al. 2011). The capability of the derivation of the detailed landslide inventory in highly vegetated areas with shallow landslides is enabling further development of landslide maps for application in spatial and urban planning. This will also have

S. Mihalić Arbanas (✉) · S. Bernat Gazibara · M. Krkač · M. Sinčić · H. Lukačić · P. Jagodnik
Faculty of Mining, Geology and Petroleum Engineering, University of Zagreb, 10000 Zagreb, Croatia
e-mail: smihalic@rgn.hr

S. Bernat Gazibara
e-mail: sbernat@rgn.hr

M. Krkač
e-mail: mkrkac@rgn.hr

M. Sinčić
e-mail: marko.sincic@rgn.hr

H. Lukačić
e-mail: hrvoje.lukacic@rgn.hr

P. Jagodnik
e-mail: petra.jagodnik@gradri.uniri.hr

P. Jagodnik · Ž. Arbanas
Faculty of Civil Engineering, University of Rijeka, Rijeka, Croatia
e-mail: zeljko.arbanas@gradri.uniri.hr

I. Alcántara-Ayala et al. (eds.), *Progress in Landslide Research and Technology, Volume 1 Issue 2, 2022*, Progress in Landslide Research and Technology,
https://doi.org/10.1007/978-3-031-18471-0_16

a positive impact on the enhancement of landslide zoning maps by offering new opportunities to prescribe provision of legislative action for the purpose of regulating the land use and the construction of buildings within the area under the jurisdiction of the legislative body concerned.

The main objective of the paper is to present types of data and information on landslides that can be derived from landslide inventory and landslide susceptibility maps and their use for spatial and urban planning. The paper is organized into three main chapters. Some methodological aspects of the preparation of landslide inventory maps are dealt with in the chapter "Landslide detection and mapping". Emphasis is on applying the LIDAR technology and ALS (Airborne Laser Scanning) to landslide inventory mapping. Examples of historical landslide inventories are given to illustrate the quality and quantity of data derived by visual identification of shallow landslides and by compilation of complete detailed landslide inventories. The chapter "Susceptibility modelling and zonation" introduces basic concepts related to landslide susceptibility assessment and resulting zonation maps. A multi-stage approach to landslide susceptibility mapping is noted, from small to large scale. Examples of landslide susceptibility maps derived from an assessment on the national, regional and local levels are given to illustrate the quality of map information. The chapter "Application of landslide data and information" summarises general considerations of applying data and information from landslide maps in land use planning. Scale-related objectives are given for a hierarchical approach to producing landslide zoning maps. We have used examples of spatial planning documents of different levels from Croatia and landslide maps of multiple study areas (Fig. 1).

2 Landslide Detection and Mapping

Detecting or identifying landslide features on the ground surface is part of the landslide mapping, which precedes the cartographic representation of slope movements. The task of the expert performing mapping is the recognition of changes in the surface topography left by the occurrence of a landslide (or landslide signature, Pike 1988). The choice of the type and scale of the resulting map depends on many factors, primarily on the end user's requirements and the ultimate purpose of the landslide mapping (Mihalić Arbanas and Arbanas 2015).

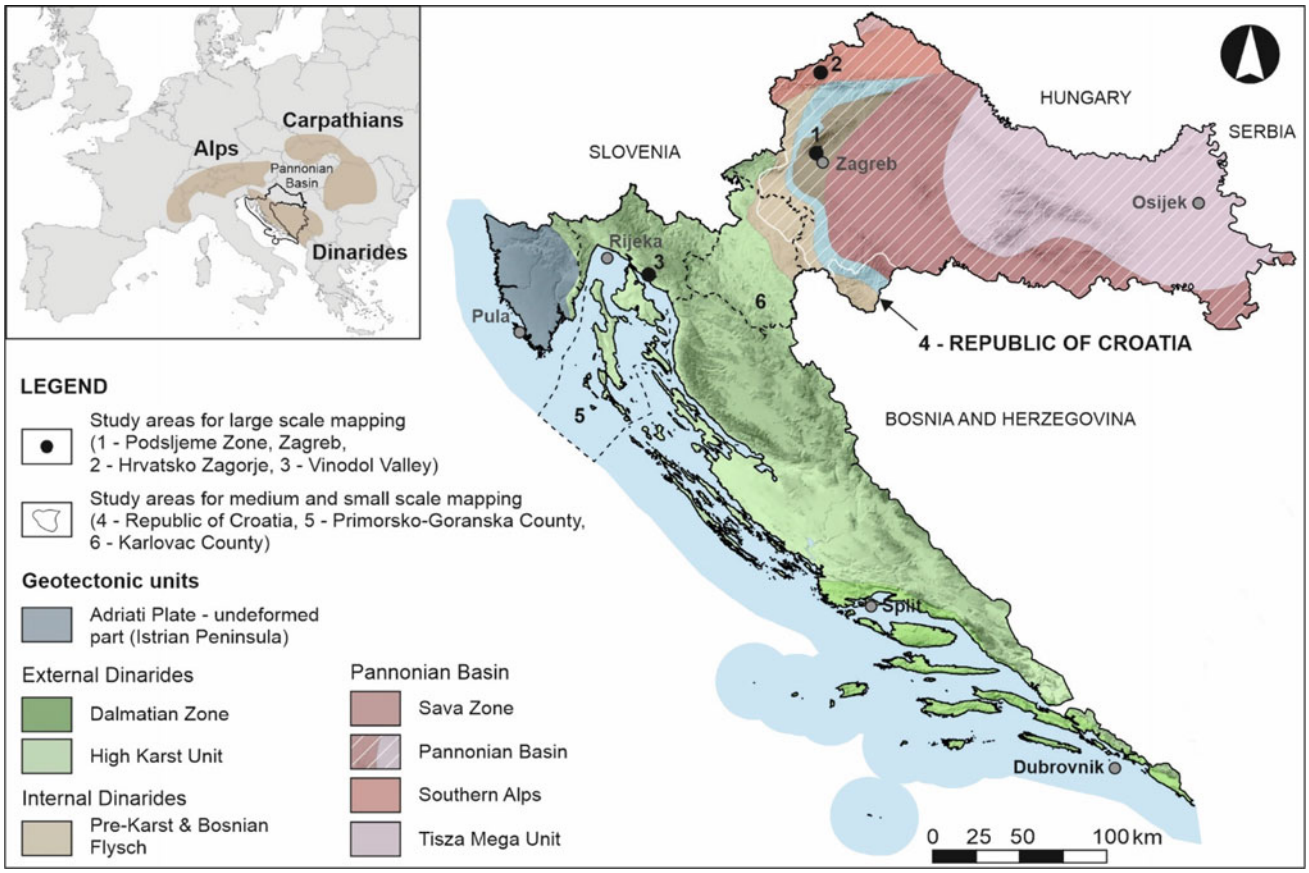

Fig. 1 Study areas used as pilot areas for landslide inventory mapping and landslide susceptibility mapping

Guzzetti et al. (2012) provide an overview of types of landslide inventory maps followed by a comprehensive description of methods and techniques for their preparation. There are two main types of inventory maps, archive and geomorphological maps. Methods of their preparation include some or all of the following: remote sensing, ground surveys and archive data from different sources (e.g., literature etc.). Generally, archive landslide inventories are of small scale (> 1:200,000), compiled based on literature or other archive sources (inquires to public organisations and private consultants, chronicles, journals, technical and scientific reports, interviews of landslide experts etc.) without involved procedures of landslide detection and mapping. Contrary, geomorphological landslide inventories contain landslide data derived through the process of interpretation of aerial photographs, very high-resolution satellite images or digital terrain models (DTM), followed by limited ground survey (i.e., field checks) to derive medium- (1:25,000–1:200,000) or large-scale (>1:25,000) landslide inventory maps. The types of geomorphological landslide inventories differ depending on the time-span of input data (photographs, images, DTM) that are used for landslide detection. Summarised overview of the main characteristics of historical, event, seasonal and multi-temporal landslide inventory maps, according to Guzzetti et al. (2012), is given in Table 1.

The objective of landslide detection aims to determine landslide boundaries at the ground surface. Regardless of the adopted technique, detecting and mapping landslides are complex, time-consuming, and error-prone task (Galli et al. 2008). Over the last decade, airborne laser scanning has been made available and has been used to identify and map landslide morphology in areas partially or completely covered by dense vegetation (Carter et al. 2001; Razak et al. 2011). Airborne laser scanning (ALS) is also known as airborne LiDAR or airborne laser swath mapping (ALSM). LiDAR elevation data prove particularly effective where the terrain is forested, a condition where old and very old, deep-seated landslides are difficult to identify using traditional aerial photography or satellite imagery (Eeckhaut et al. 2007; Razak et al. 2011), and perform well also in arid and sub-arid regions where the vegetation cover is sparse or inexistent. Recognition of small cracks and detailed geomorphological features might be the best surface landslide characteristics that can be interpreted from these images (Fig. 2), which provides additional information compared with other types of images or photos.

A relatively new remote-sensing tool uses airborne mounted lasers to obtain digital representations of the topographic surface for areas ranging from a few hectares to thousands of square kilometers (Shan and Toth 2017). Visual analysis and interpretation of the topographic surface remain the most common and most promising application of a very-high-resolution (metric to decametric) DEM captured by airborne LiDAR sensors for detecting and mapping landslides over large areas (Guzzetti et al. 2012). The required resolution of a bare-earth LiDAR DEM for identifying landslides primarily depends on the landslide size.

Table 1 Geomorphological landslide inventories classified by their scale and the type of mapping (Guzzetti et al. 2000, 2012, 2021; Malamud et al. 2004; Galli et al. 2008)

Type (Guzzetti et al. 2004, 2005; Galli et al. 2008; Fiorucci et al. 2011)	Landslide map data	Landslide age
Historical	Many landslide events throughout tens, hundreds or thousands of years	The age of the landslides is not differentiated or is given in relative terms, i.e., recent, old or very old
	Examples: Brabb and Pampeyan (1972), Antonini et al. (1993), Cardinali et al. (2001), and Galli et al. (2008)	
Event	Landslides caused by a single trigger, such as an earthquake, rainfall event or snowmelt event	The landslides' date corresponds to the triggering event's date (or period)
	Examples: Harp and Jibson (1996), Buckman and Jeffrey (2001), Lin et al. (2004), Guzzetti et al. (2004), Cardinali et al. (2006), Tsai et al. (2010), Dai et al. (2011), Parker et al. (2011), and Gorum et al. (2011)	
Seasonal	Landsides triggered by single or multiple events during a single season, or a few seasons identified by exploiting multiple sets of aerial or satellite images of different dates	The date (or periods) of the landslides is attributed based on the date (or periods) of the triggers and the date of the imagery or the field surveys carried out to compile the inventories
	Examples: Guzzetti et al. (2004, 2005), Galli et al. (2008), and Fiorucci et al. (2011)	
Multi-temporal	Landslides triggered by multiple events over more extended periods (e.g., years to decades) identified by exploiting multiple sets of aerial or satellite images of different dates	The date (or periods) of the landslides is attributed based on the date (or periods) of the triggers and the date of the imagery or the field surveys carried out to compile the inventories
	Examples: Guzzetti et al. (2004, 2005), Galli et al. (2008), and Fiorucci et al. (2011)	

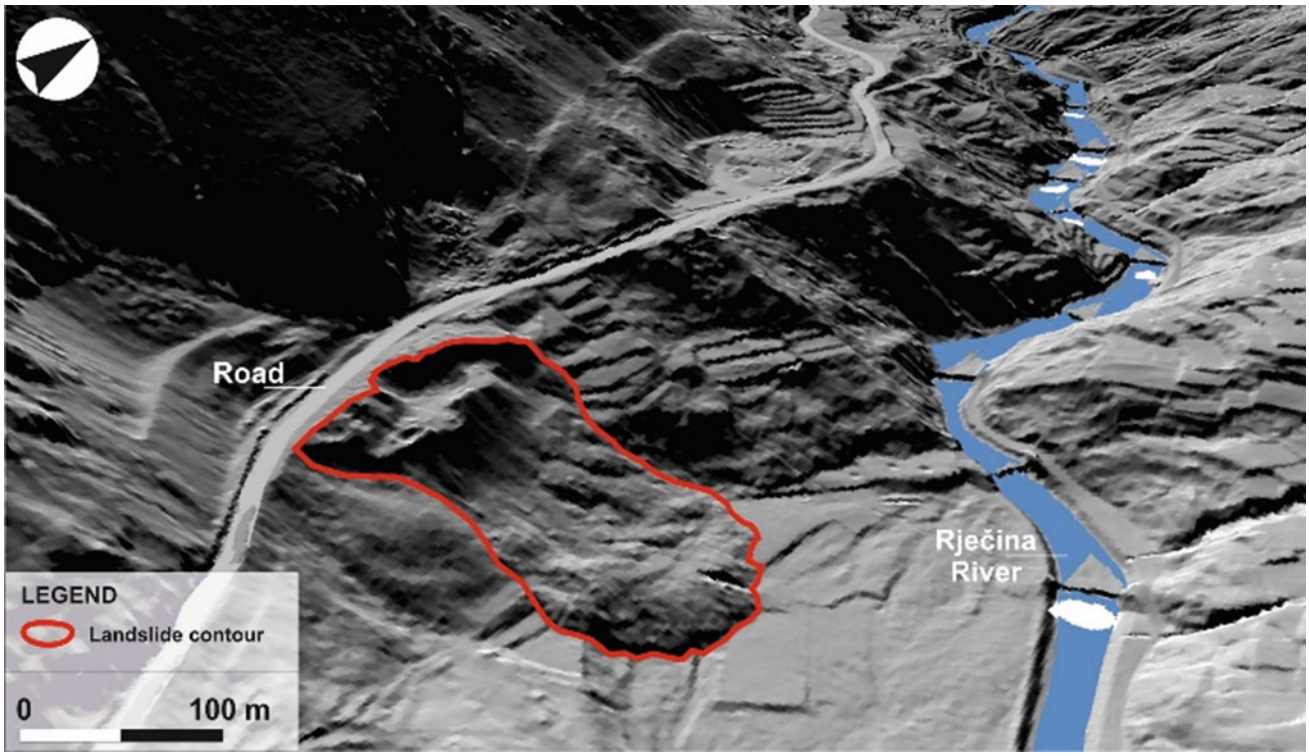

Fig. 2 Oblique aerial view prepared from the LIDAR-derived bare-earth DTM of the Rječina River Basin (Croatia) (Mihalić Arbanas and Arbanas 2015)

Examples from the literature reveal that investigators have used 5-m resolution DEM (Glenn et al. 2006; Eeckhaut et al. 2007), 2-m resolution DEM (Ardizzone et al. 2007), 1.8-m resolution DEM (Schulz 2007), 1-m resolution DEM (McKean and Roering 2004; Chen et al. 2006; Mihalić et al. 2013; Đomlija et al. 2014; Đomlija 2018) and 30-cm resolution DEM (Bernat Gazibara 2019; Sinčić et al. 2022).

2.1 Historical Inventories Derived from LiDAR Images

A geomorphological historical inventory shows the cumulative effects of many landslide events throughout tens, hundreds or thousands of years (Guzzetti et al. 2012). This chapter presents the experience gained in Croatia, collected through detecting and mapping landslides from high-resolution LiDAR images produced based on ALS in different landslide-prone geomorphological settings in Croatia. Recognition of landslides was performed through the visual analysis of a series of LiDAR derivatives by experienced and trained landslide scientists, using a systematic methodology and well-defined interpretation criteria (Bernat Gazibara et al. 2019a; Jagodnik et al. 2020a; Krkač et al. 2022).

The first study area, located in the hills of the Zagreb city (known as the Podsljeme area), belongs to the continental part of Croatia in the Pannonian Basin (Fig. 1). The study area (of 21 km^2), at the southeastern-facing slope of the Medvednica Mt., is urbanized and densely populated, with prevailing artificial surfaces (about 56%) and equally represented agricultural areas and forests (both about 22%). The area is composed of Quaternary soils (heterogeneous mixtures of unfoliated, mostly impermeable clayey-silty soils) and stratified upper Miocene soils and soft rocks (sands, silts and marls) (Šikić 1995). Gentle relief combined with geomechanical properties of the abovementioned soils is a preparatory causal factor for shallow soil slides, as it is confirmed by the landslide inventory presented in Fig. 3. Intense precipitation is the main triggering factor (Bernat Gazibara et al. 2019a). In total, the landslide inventory from the Zagreb city consists of 702 landslides with a non-uniform distribution across the pilot area (Bernat Gazibara et al. 2019a). The prevailing types are shallow soil slides; only ten landslides were classified as earth flows. Nearly 65% of all the identified landslides were evaluated as 'high confidence' due to the visible landslide features on the LiDAR derivatives, and almost 60% of all mapped landslides were evaluated as 'high precision' due to the fresh and clearly visible landslide boundaries on the LiDAR

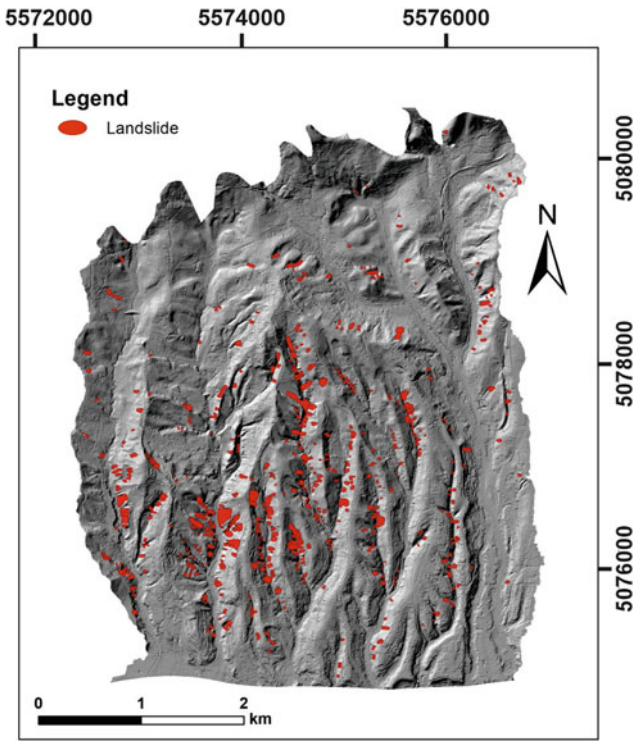

Fig. 3 Landslide inventory of the study area in the Zagreb city (area 21 km^2) derived by visual interpretation of LiDAR DTM morphometric maps (modified from Bernat Gazibara et al. 2019a, b)

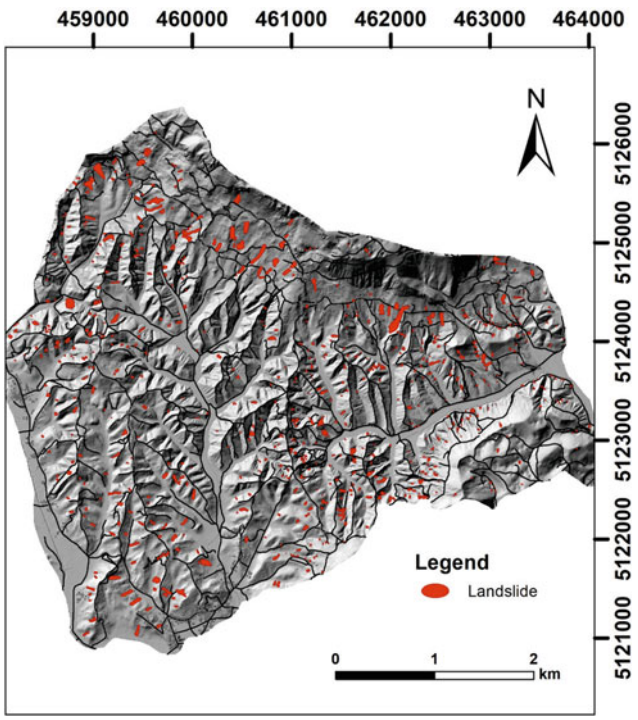

Fig. 4 Landslide inventory of the study area in the Hrvatsko Zagorje (area 20.22 km^2) derived by visual interpretation of LiDAR DTM morphometric maps (modified from Sinčić et al. 2022)

derivatives. Based on the landslide inventory, the total landslide area is 0.5 km^2 (about 2.43% of the pilot area). The mean landslide density is 33.4 slope failures per square kilometer.

The second study area is located in the hills of the Hrvatsko Zagorje region in the Pannonian Basin (Fig. 1). The study area (20.22 km^2) differs from the previous one based on geomorphological settings and land use. According to Krkač et al. (2022) this study area is covered with forests (52%), agricultural areas and pastures (40%) and sporadic artificial areas (8%). Slopes are composed chiefly of Miocene soils, soft- and hard rocks (sandstones, marls, sands, tuffs and biogenic, sandy and marly limestone, calcareous marls and sandstones) and Triassic hard rocks (sandstones, shales, dolomites, limestone and dolomitized breccias) (Šimunić et al. 1982; Aničić and Juriša 1984). The inclination of bedding in Miocene and Triassic rocks vary depending on structural geological settings. Quaternary soils cover only flat areas in valleys around superficial streams.

Non-uniform distribution across the pilot area is caused by changes in relief types (from steeper to more gentle slopes) and lithologies (soft rocks and hard rocks). In total, the landslide inventory from the Hrvatsko Zagorje region consists of 912 landslides (Fig. 4), mainly shallow soil slides and earth flows (Sinčić et al. 2022). Nearly 58% of all the identified landslides on the LiDAR DTM were evaluated as 'high confidence' due to the clearly visible landslide features on the LiDAR derivatives. Based on the landslide inventory, the total landslide area is 0.408 km^2 or 2.02% of the pilot area. The mean landslide density is 45.1 slope failures per square kilometer.

The third study area is in the Vinodol Valley (area of 64.57 km^2), situated in Dinarides (Fig. 1), in the NW coastal part of the Adriatic Sea (Jagodnik et al. 2020a, b, c). The geomorphological settings of the area is controlled by the valley's tectonic origin that resulted in an elongated shape stretched the in Dinaric NW–SE direction. The area is predominantly rural, with approximately 30 settlements connected by a network of county and local or unnamed roads. Comparing to the two abovementioned study areas, the valley is characterized by higher precipitation. The valley flanks are composed of Upper Cretaceous and Palaeogene hard rocks (carbonates), while the lower parts and the bottom of the valley are built of Palaeogene flyschoid rock (Šušnjar et al. 1970). Superficial deposits in the valley are formed by various geomorphological processes on slopes, such as rock falls, debris flows, debris slides, and gully erosion. Fluvial deposits cover flat areas around the Dubračina river and its tributes. Heterogenous geological settings of the valley resulted in numerous landslide types. Đomlija (2018)

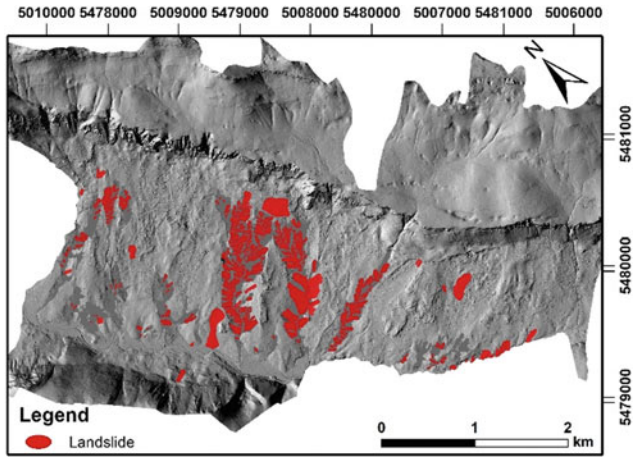

Fig. 5 Details from the historical landslide inventory of the Vinodol Valley (modified from Đomlija 2018) for the southeastern part of the Dubračina River Basin

identified 10 types of landslides using a modified Varnes classification (Hungr et al. 2014). The five landslide types were identified and mapped using LiDAR DTM morphological derivative maps: rotational rock and soil slide, debris slide and avalanche, and debris slide-debris flow. Figure 5 presents part of the landslide inventory. In total, the inventory consists of 631 landslides with a non-uniform distribution across the area (Đomlija 2018). The most abundant landslide phenomena are shallow debris slides (approx. 98%) of all activity styles (complex, composite, successive, single, multiple), typically activated along the contact between the flysch bedrock and superficial deposits. Regardless on the landslide type, about 80% are developed within the gully landforms (Jagodnik et al. 2020a). Because of that, 236 gullies are also mapped, with a total area of 1.89 km^2. The smallest gully channel has an area of 317 m^2, the largest 0.48 km^2, while the average has an area of 6700 m^2. The smallest mapped landslide is debris slide of 65 m^2 and the largest is rotational rock slide of 63,708.5 m^2. Nearly 24% of all the identified landslides (394 phenomena), which could be outlined in their entirety by visual interpretation of the LiDAR DTM, were evaluated as 'clearly expressed', and nearly 76% as 'poorly expressed'. Based on the landslide inventory, the total landslide area is 1.51 km^2 or 2.3% of the pilot area. The mean density of landslides is 9.77 slope failures per square kilometer. Besides abundant debris slides, there are only 11 phenomena determined and mapped as rock and soil slides and rock avalanche. The remaining six landslide types identified by Đomlija (2018) were impossible to map as separate phenomena. Most of them are phenomena of processes on steep rocky slopes.

2.2 Landslide Statistics and Completeness of the Inventory

This chapter presents the landslide statistics obtained from three inventory maps that represent hilly areas in Zagreb city, the Hrvatsko Zagorje region and Vinodol Valley. The quality, reliability and completeness of the landslide inventory affect (i.e., control) the quality of the resulting susceptibility assessment (Carrara et al. 1992; Ardizzone et al. 2002). The characteristics and the quality of the three inventories was evaluated using the methodology proposed by Malamud et al. (2004).

In the first study area in Zagreb city, with the mean landslide density of 33.3 slope failures per square kilometer, the smallest identified landslide has a planimetric area (A_L) of 43 m^2 (Bernat Gazibara et al. 2017). The mapped landslides extend in size to a maximum of 8064 m^2, while the mean landslide area is approx. 700 m^2 (mean = 704 m^2, median = 411 m^2, std. dev. = 921 m^2). The most frequent landslides in the inventory have an area of approx. 400 m^2, and 90% of the landslide bodies showed a size between 100 and 2000 m^2. The frequency–size distribution of all mapped landslides in the pilot area (Fig. 6a) shows two regimes: a positive power-law behavior for small landslides and a negative power-law behavior for medium and large landslides. The transition between the positive and the negative power-law relations can be used to distinguish between small and medium landslides. Based on the maximum value at approximately A_L = 400 m^2, 48% of the mapped landslides are small (A_L < 400 m^2) in size.

In the study area of the Hrvatsko Zagorje region, the mean landslide density is 45.1 slope failures per square kilometre. The size of the identified landslides ranges from a minimum value of 3.3 m^2 to a maximum of 13,779 m^2, whereas the average area is 448 m^2 (median = 173 m^2, std. dev. = 880 m^2). The most frequent landslides in the inventory have an area of approx. 200 m^2, and almost 85% of the landslide bodies showed a size between 40 and 2000 m^2. The frequency–size distribution of all mapped landslides in the pilot area (Fig. 6b) shows two regimes: a positive power-law behavior for small landslides and a negative power-law behavior for medium and large landslides. The transition between the positive and the negative power-law relations can be used to distinguish between small and medium landslides. Based on the maximum value at approximately A_L = 200 m^2, 48% of the mapped landslides are small (A_L < 200 m^2) and 52% are medium and large (A_L > 200 m^2) in size. The prevailing dominant types of landslides are shallow soil slides.

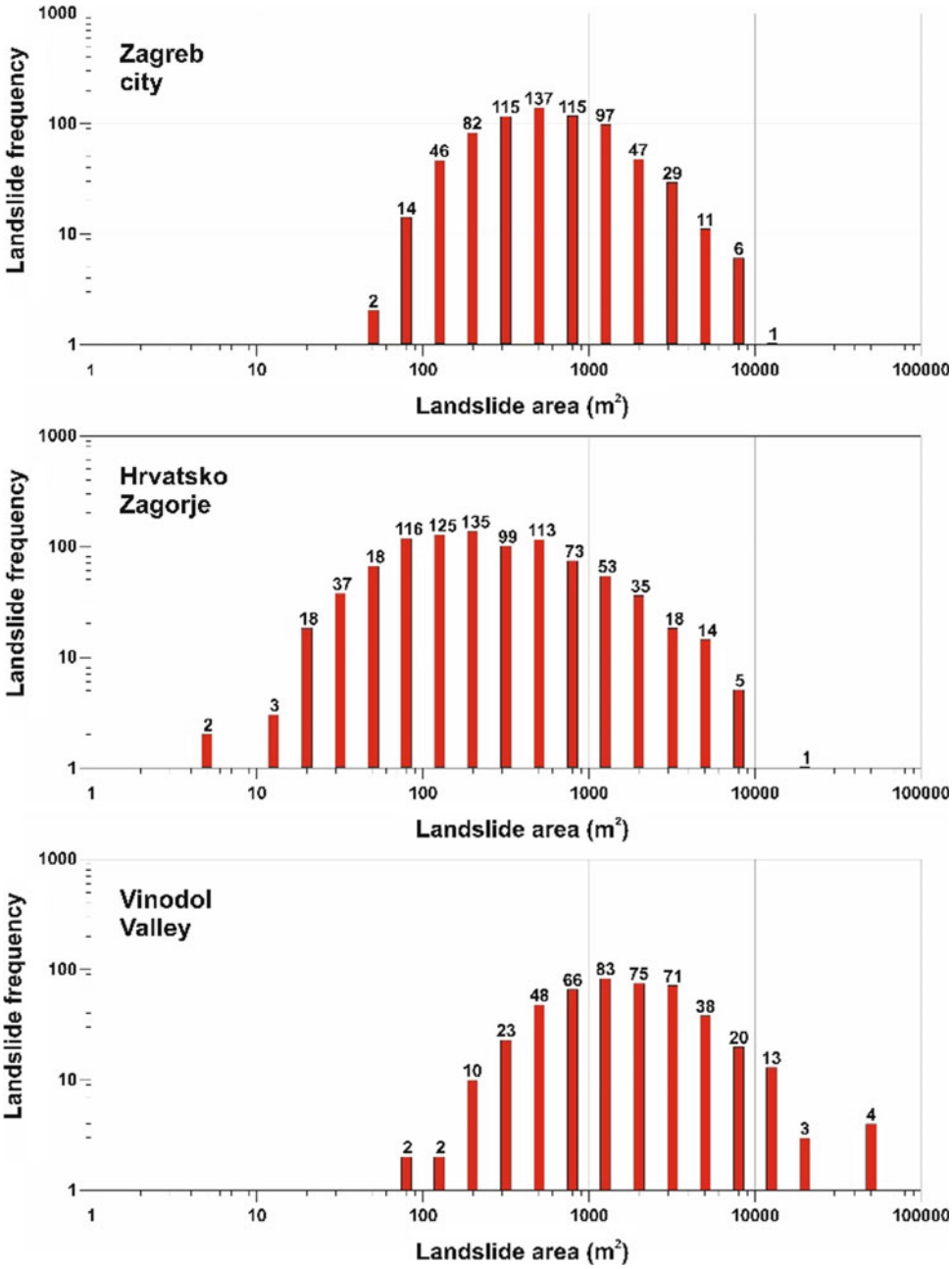

Fig. 6 Frequency–size distribution of all mapped landslides in: (1) the study area (21 km^2) of the Podsljeme area (Zagreb city in Pannonian Basin); (2) the study area (20 km^2) of the Hrvatsko Zagorje region in Pannonian Basin; (3) the study area (64.57 km^2) of the Vinodol Valley in the Dinarides

In the study area of Vinodol Valley, the mean landslide density is 9.77 slope failures per square kilometer. The size of the identified landslides ranges from a minimum value of 64.8 m^2 to a maximum of 49,461.62 m^2, whereas the average area is 2336.70 m^2 (median = 1218.17 m^2, std. dev. = 4,498.11 m^2). The most frequent landslides in the inventory have an area of approx. 1200 m^2, and almost 80% of the landslide bodies showed a size between 500 and 20,000 m^2. The frequency–size distribution of all mapped landslides in the pilot area (Fig. 6c) shows two regimes: a positive power-law behavior for small landslides and a negative power-law behavior for medium and large landslides. The transition between the positive and the negative power-law relations can be used to distinguish between small and medium landslides. Based on the maximum value at approximately A_L = 1500 m^2, 58% of the mapped landslides are small (A_L < 1500 m^2), and 52% are medium-large (A_L > 1500 m^2) in size. The dominant types of landslides are debris slide and debris slide-debris flow (Jagodnik et al. 2020a).

The distribution obtained for the mapped landslides in the two study areas in Pannonian Basin and in one in the Dinarides can be explained by the 'universal distribution' described by Malamud et al. (2004), which implies that the occurrence of a landslide in the pilot area is a result of either

natural triggering factors (e.g., rainfall or rapid snowmelt) or human actions with regional impacts (e.g., widespread deforestation and urbanisation). Frequency–size distribution of all mapped landslides in Zagreb city (Fig. 6a), the Hrvatsko Zagorje region (Fig. 6b) and the Vinodol Valey (Fig. 6c) are complete landslide inventory maps because they include a substantial fraction of all landslides at all scales.

3 Susceptibility Modelling and Zonation

The identification and map portrayal of areas highly susceptible to damaging landslides is the first and necessary steps toward loss reduction. This section uses several essential terms, such as 'hazard', 'susceptibility' and 'zonation'. The terminology used in this work is consistent with the landslide hazard and risk definitions proposed by such international committees as Varnes (1984), Fell et al. (2008), United Nations Human Settlements Programme (2012) and ISSMGE TC32 (2004). Predicting where, when, how many, and how large landslides are expected in an area and during a particular period is the main aim of landslide hazard assessment (Varnes 1984; Guzzetti et al. 2005, 2021). Landslide hazard zonation is commonly portrayed on maps. Landslide susceptibility assessment and modelling are limited to the spatial prediction of landslides. Landslide susceptibility maps present spatial, time-independent probability of landslides occurring in an area depending on local terrain conditions (Guzzetti et al. 1999, 2005). The most frequent input data about terrain conditions belong to the categories of geomorphological, geological, hydrological and anthropogenic landslide factors.

The first extensive papers on the use of digital spatial data for landslide susceptibility mapping date back to the late seventies and early eighties of the last century. Among the pioneers in this field were (Brabb et al. 1972) in California and Carrara et al. (1977) in Italy. All research on landslide susceptibility and hazard mapping uses Geographic Information System (GIS) as digital tools for handling spatial data. Van Westen's dissertation (Van Westen 1993) is the first comprehensive overview of the application of GIS technology to landslide susceptibility assessment followed by a classification of analysis methods. Thirteen years later, a dissertation by Guzzetti (2006) provided numerous examples of analysis, assessment, and zonation of landslide susceptibility, hazard, and risk in Italy, which have been subjects of numerous scientific studies. Soon after that, 'Guidelines for Landslide Susceptibility, Hazard and Risk Zoning for Land Use Planning' (Fell et al. 2008) was prepared by the Joint Technical Committee on Landslides and Engineered Slopes of three international societies. Simultaneously, an overview of the types of spatial data required for landslide susceptibility, hazard, and vulnerability assessment and the methods for obtaining these data was published in van Westen et al. (2008). The most recently published recommended methodologies for the quantitative analysis of landslide hazard, vulnerability, and risk at different scales (site-specific, local, regional, and national) are from Corominas et al. (2013). These methodologies primarily include quantitative approaches developed worldwide during the preceding decade. Reichenbach et al. (2018) performed critical review of statistical methods for landslide susceptibility modelling and associated terrain zonations based on compiled extensive database of 565 peer-review articles from 1983 to 2016. They also provide recommendations for the preparation, evaluation, and use of landslide susceptibility models and associated terrain zonations. Results can be exploited for different purposes that are spatial and urban planning, identification of the most suitable scenarios of risk mitigation measures, prioritization of the areas that require control works in tandem with their design, and the use of funds earmarked for mitigating the risk. Landslide susceptibility assessment can be considered the initial step towards a landslide hazard and risk assessment, but it can also be an end-product that can be used in land-use planning and environmental impact assessment.

Landslide susceptibility zonation involves a degree of interpretation aimed at the prediction of spatial distribution and rating of the terrain units according to their propensity to produce landslides. Moreover, landslide susceptibility is defined as the tendency of a specific area to be affected by a particular type of landslide in the future (Brabb 1984; Guzzetti et al. 2005). The value of susceptibility is usually a relative one and the quality of landslide susceptibility models is known to be highly dependent on the quality of input data (Sinčić et al. 2022), such as the landslide inventory (Guzzetti et al. 2012) and the terrain attributes (predictors) (van Westen et al. 2008). The possibility of obtaining the required input data strongly affects the type of assessment method that can be used and the scale of analysis. All the susceptibility assessment approaches and methods proposed in the literature can be grouped into five broad categories (Reichenbach et al. 2018), namely: (i) geomorphological mapping; (ii) analysis of landslide inventories; (iii) heuristic or index-based approaches; (iv) process-based, or physically based numerical modelling methods; and (v) statistically based modelling methods. Qualitative approaches are subjective, ascertain susceptibility heuristically, and portray susceptibility levels using descriptive (qualitative) terms. Quantitative methods produce numerical estimates for susceptibility zones, resulting in more precise probabilities of occurrence of landslide phenomena (Guzzetti et al. 1999).

Maps are a useful and convenient tool for presenting information on landslide susceptibility. They can present

many kinds and combinations of information at different levels of detail. Susceptibility maps used in conjunction with land-use maps are a valuable planning tool. The development of a clear hierarchical methodology in hazard zonation is necessary to obtain an acceptable cost–benefit ratio and to ensure the practical applicability of the zonation (Soeters and Van Westen 1996). The working scale for a susceptibility analysis is determined by the requirements of the user for whom the assessment or zonation is executed. Because planners and engineers form the most important user community, the following scales of analysis can be differentiated for landslide hazard zonation (IAEG 1976): Small scale maps (<1:100,000); Medium scale maps (1:10,000 to 1:100,000); Large scale maps (>1:10,000). The current practice in Europe (Corominas and Mavrouli 2010) shows that the scale of the landslide zoning maps required by state or local authorities varies significantly from country to country, depending on the coverage, input data and methods that are used as well as the information provided (qualitative or quantitative). Commonly, there is a multi-stage approach to landslide susceptibility and hazard mapping, from national maps on a small scale to local maps on a large scale. If resources are limited, it may be more prudent to bypass small-scale mapping and concentrate on a few known areas of concern (Highland and Bobrowsky 2008).

3.1 National and Regional Level Assessment

National landslide zoning maps at a small scale are created to give a general overview of critical areas for an entire country and can be used to inform national policymakers and the public (Soeters and Van Westen 1996). The next stage is regional mapping, which synthesizes available data and identifies general problem areas at the regional level to produce small- or medium-scale susceptibility maps. The third stage is the local-level mapping, a more detailed susceptibility mapping program on a large scale that includes areas of local administrative units (municipality or city) or complex critical areas. We present here two types of susceptibility mapping performed in Croatia that resulted from national and regional level landslide susceptibility modelling and zonation. This presented experience is gained through heuristic modelling of landslide susceptibility for the whole territory of Croatia and for two counties, Karlovac County and Primorsko-Goranska County (Fig. 1). Susceptibility zonation was performed by experienced landslide scientists, using knowledge to decide about the relative influence of factor maps (van Westen et al. 2008).

The Republic of Croatia covers an area of 56,594 km^2 and has about 4 million inhabitants. As it is depicted in Fig. 1, 49% of the Croatian area belongs to the Pannonian Basin, 51% to the Dinarides and Adriatic Plate (Istrian Peninsula) (Mihalić Arbanas et al. 2017). Mean annual rainfall ranges from 300 to 1000 mm/year in the Pannonian part of Croatia to more than 3000 mm/year in the Adriatic region. Multiple-Occurrence Regional Landslide Events (MORLE) have been triggered by intense precipitation events during very wet seasons in 2006, 2010, 2013, 2014, and 2018. There are no systematic landslide inventories at the country level, neither archival nor geomorphological. Risk assessment of the Republic of Croatia (Mihalić Arbanas et al. 2019) showed that the MORLE with the greatest consequences happened in 2013 (Bernat et al. 2014a, b), and the most likely MORLE is from 2018 (Bernat Gazibara et al. 2019b). In the winter period of 2012/2013, more than 900 (re)activated landslides were recorded in NW Croatia, and the largest number was in the Krapina-Zagorje County, with 521 landslides in total.

To develop a national landslide susceptibility map (Fig. 7), the fuzzy logic method has been applied to 15 different combinations of causal factors, because of lack of complete landslide inventory. The Area Under the Receiver Operating Characteristic Curve (AUROC) was used to validate all derived landslide susceptibility maps and the best was selected as the final one for further classification into three susceptibility zones (Table 2, Fig. 7) based on natural breaks classification method. With over 90% of mapped landslides falling in high and very high susceptibility zones, the results are considered satisfactory for national scale landslide modelling. The analysis showed that approximately 28% of the area of Croatia is potentially prone to sliding. Particularly landslide-prone areas in Croatia are

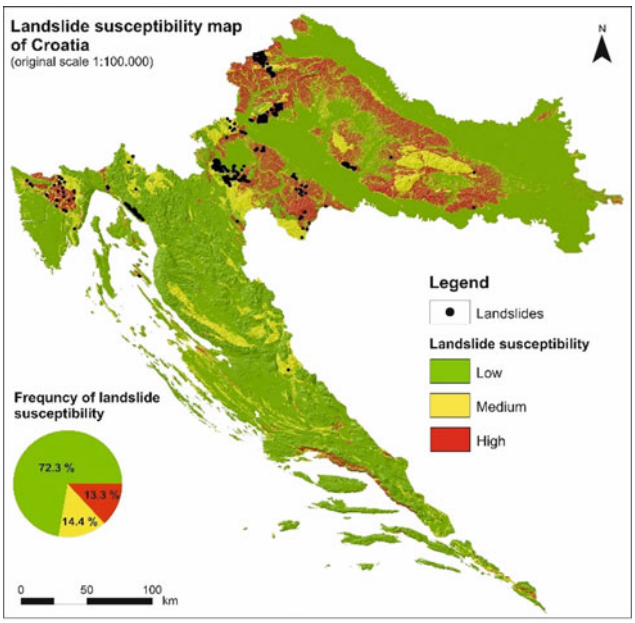

Fig. 7 Landslide susceptibility map of Croatia, original scale 1:100,000 (Bernat Gazibara et al. 2022)

Table 2 Spatial distribution of landslide susceptibility zones in the Republic of Croatia

Landslide susceptibility zone	Area (km^2)	Area (%)
Non-susceptible	40,922.37	72.33
Low susceptibility	8144.12	14.39
High susceptibility	7512.43	13.28

lowlands and hills in the Pannonian Basin, the hills of the Istrian Peninsula and isolated narrow valleys in the Dinarides, such as Rječina River Valley and Vinodol Valley in Primorje.

To develop a regional-scale landslide susceptibility map of the Karlovac County (Fig. 8a) and of the Primorsko-Goranska County (Fig. 8b) on a medium scale (1:25,000), the same Fuzzy heuristic approach was used. It was applied for both counties because of the lack of representative landslide inventory using the same factor maps were analyzed for geomorphological and anthropogenic factors. The main difference in the methodology assessment, compared to the abovementioned assessment on a national scale, is the use of a more detailed geological map, i.e., the Basic Geological Maps on the scale of 1:100,000. Results are more detailed susceptibility zonations on the county level. Based on AUROC, several derived landslide susceptibility maps were validated to select the final one for both counties, which were classified into three susceptibilities. With over 89% of mapped landslides falling in high and very high susceptibility zones, the results are considered satisfactory for regional scale landslide modelling. The analysis showed that approximately 27% of the area of Karlovac County and approx. 10% of the area of Primorsko-Goranska County is potentially prone to sliding (Table 3, Fig. 8a and b). The highest susceptible areas in Karlovac County are in the western and north-western part that belongs to the lowlands and hills of the Pannonian Basin. In Primorsko-Goranska County located in the Dinarides, several isolated zones throughout almost whole the county are highlighted, either in the form of narrow or otherwise relatively small, isolated zones. A comparison of both county maps with the national landslide susceptibility map shows that there is more detailed elaboration on the county map.

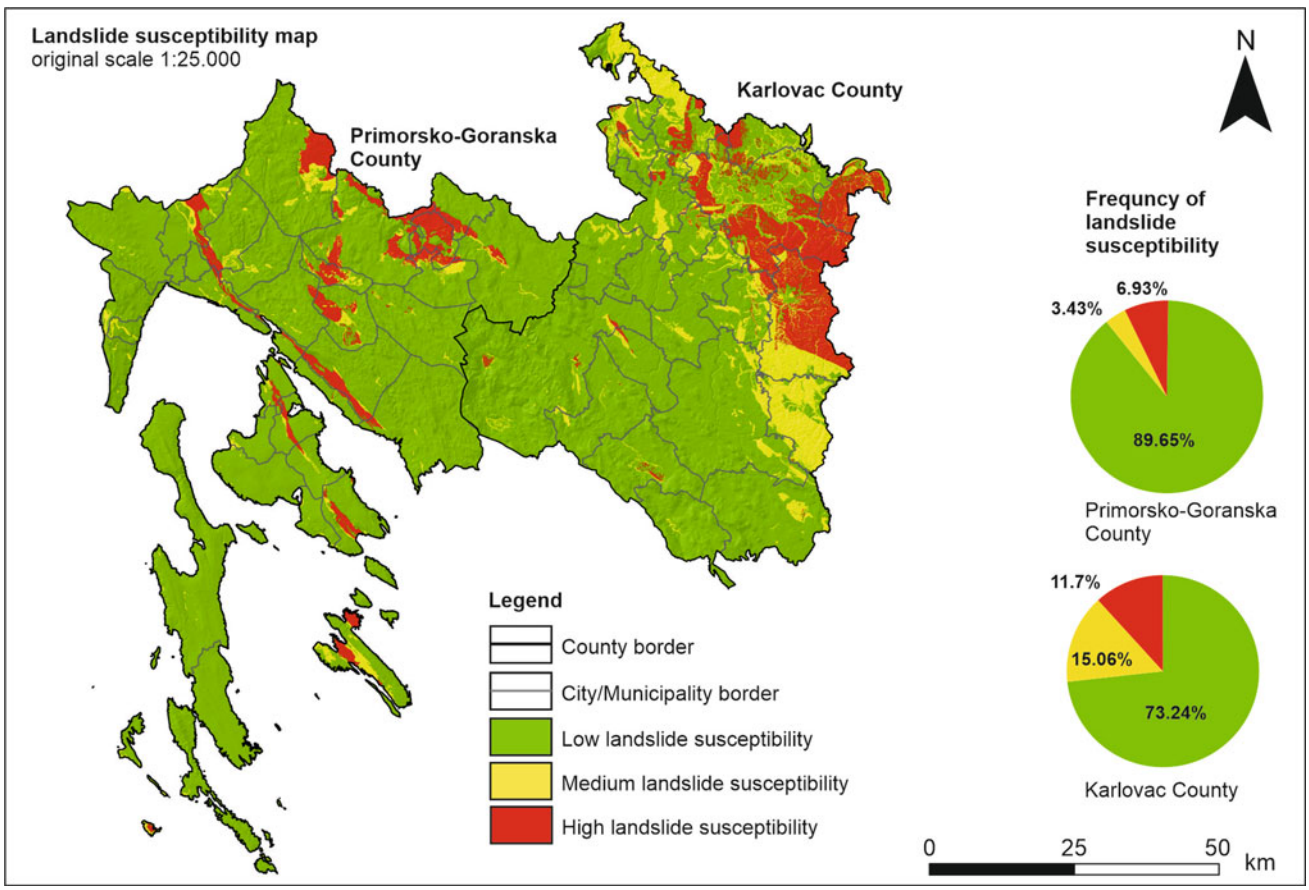

Fig. 8 Regional-level landslide susceptibility maps of the Primorsko-Goranska County and the Karlovac County, original scale 1:25,000

Table 3 Spatial distribution of landslide susceptibility zones in Primorsko-Goranska County and Karlovac County

Landslide susceptibility class	Karlovac County		Primorsko-Goranska County	
	Area (km^2)	Area (%)	Area (km^2)	Area (%)
Non-susceptible	2816.33	73.24	3216.04	89.65
Low	579.02	15.06	122.91	3.43
High	450.24	11.71	248.58	6.93

3.2 Local Level Assessment

Landslide zoning maps at a large scale can be used for the determination of hazard zones in areas affected by urbanization or large engineering structures and roads. The areas to be investigated may cover upward of a few hundreds of square kilometers, yet a considerably higher level of detail is required at this scale. The detail should be such that adjacent slopes in the same lithology are evaluated separately and may obtain different hazard scores depending on their characteristics, such as slope angle or form and type of land use. Within the same terrain unit, a distinction should be made between different slope segments. For example, a concave slope should receive a different rating, when appropriate, then an adjacent straight or convex slope. We present here one example of preliminary large-scale susceptibility mapping performed for the urbanized hilly area in the Zagreb city (Croatia) that resulted from local level landslide susceptibility modelling and zonation. The presented experience is obtained by Bernat Gazibara et al. (2019a) through statistical modelling of landslide susceptibility at the pilot area of 21 km^2 (Fig. 1) that is representative for the whole Podsljeme area (Bernat Gazibara et al. in press). Susceptibility zonation was performed by experienced landslide scientists, using high-resolution LiDAR morphometric derivative maps and univariate statistical analysis. Landslide susceptibility analysis on a large scale of 1:5000, conducted for the pilot area of the Podsljeme zone using bivariate statistics, is fully described in the doctoral thesis by Bernat Gazibara (2019) and here is shortly presented only necessary information to enable comparison of input data and resulting information with susceptibility assessment performed in medium and small scale for national and regional level zonation.

Podsljeme area of 180 km^2 is described in the previous chapter together with its geomorphological historical landslide inventory map. In the densely populated area with 56% settlement construction area, most of the terrain remained in a natural condition or has been slightly modified by urbanization. This enabled the derivation of a complete detailed inventory (Bernat Gazibara et al. 2019a) by visual interpretation of LiDAR DTM derivative maps.

The landslide susceptibility assessment on a large scale was performed based on the described landslide inventory and on a series of geofactors relevant to landslide occurrence divided into the following main groups: geomorphological (elevation, slope gradient, slope orientation), geological (lithology-rock type, proximity to geological contacts, proximity to faults), hydrological (proximity to drainage network) and anthropogenic (proximity to traffic infrastructure and buildings, land cover). The final preliminary landslide susceptibility model was derived using nine geofactors selected based on weights evaluated by the Weights-of-Evidence (WoE) model. The cut-off values of landslide susceptibility were defined based on classification of the ROC curve according to the criteria from Bernat Gazibara (2019), based on cumulative number of landslides: $\geq$ 85% —very high susceptibility; 15%—high susceptibility; 5%—medium susceptibility; 1% low susceptibility. The resulting susceptibility zonation (Table 4, Fig. 9) has a success and prediction rate of 88% making it a highly accurate source of preliminary information for the study area.

Table 4 Spatial distribution of landslide susceptibility zones in the Podsljeme area

Landslide susceptibility zone	Area (km^2)	Area (%)
Non-susceptible	9.03	42.75
Low susceptibility	4.36	20.63
Medium susceptibility	3.04	14.40
High susceptibility	4.69	22.22

4 Application of Landslide Data and Information

Due to the severe socioeconomic and environmental damage and losses that result from landslides, a considerable variety of techniques and practices have been employed to mitigate the potential losses arising from landslide occurrence. The approach of avoiding landslide-prone areas is rarely feasible, and it is neither possible nor desirable to proscribe development in all landslide-prone areas. The question then becomes one of identifying the most effective of the various mitigation approaches and obtaining funding to apply the best. The USGS proposal for a national landslide hazards mitigation strategy (Spiker and Gori 2000) clearly summarizes the major mitigation approaches, including: Restricting development in landslide-prone areas; Enforcing codes for

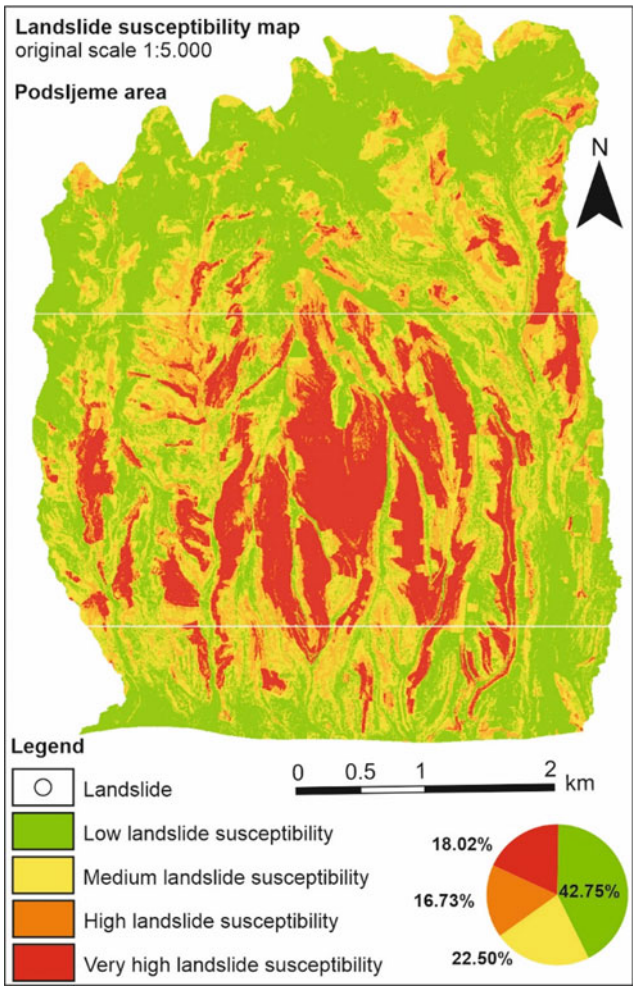

Fig. 9 Local-level landslide susceptibility map, original scale 1:5000, of the Podsljeme area (21 km^2) derived by statistical univariate analysis using landslides represented by points from a complete landslide inventory map depicting 702 phenomena (modified from Bernat Gazibara 2019)

excavation, construction, and grading; Engineering for slope stability; Deploying monitoring and warning systems; and Providing landslide insurance.

The USGS proposal for a national strategy aimed at mitigation of landslide hazard (Spiker and Gori 2000) also states that "landslide inventory and landslide susceptibility maps are critically needed in landslide-prone regions of the nation". These maps must be sufficiently detailed to support mitigation action at the local level. The identified three activities that will be required to provide the landslide maps, assessments, and other information needed by officials and planners to reduce landslide risk and losses are:

1. Develop and implement a plan for mapping and assessing landslide and other ground failure hazards nationwide;
2. Develop an inventory of known landslide and other ground failure hazards nationwide;
3. Develop and encourage the use of standards and guidelines for landslide hazard maps and assessments.

Members of users of landslide data and information differ widely in the kinds of information they need and, in their ability, to use that information (Wold et al. 1989). There are four general categories of these potential users:

1. Scientists and engineers who use the information directly;
2. Planners and decision-makers who consider landslide hazards among other land-use and development criteria;
3. Developers, builders, and financial and insuring organizations; and
4. Interested citizens, educators, and others with little or no technical experience.

4.1 General Considerations

The most comprehensive overview of the application of data and information from landslide maps in land use planning is given by the JTC-1 Joint Technical Committee on Landslides and Engineered Slopes in the form of Guidelines for Landslide Susceptibility, Hazard and Risk Zoning for Land Use Planning (Fell et al. 2008). They use the term "landslide zoning" for the creation of the multiple types of maps: landslide inventory; susceptibility; hazard and risk zoning maps. The practical value of the Guidelines is for those who are considering the introduction of land use management controls for landsliding. The Guidelines provide recommendations to decide the type of the zoning (inventory, susceptibility, hazard, risk) and level of detail (preliminary, intermediate, advanced) which they require based on the purpose of the zoning (information, advisory, statutory, design). They may choose to scale the zoning (regional, local, site-specific) and implementation of land use controls. Landslide zoning for land use planning is most commonly required at the local government level for planning urban development but may be required by state or federal governments for regional land use planning or disaster management planning. It may also be required by land developers, those developing major infrastructure such as highways and railways or managing recreational areas.

In some countries, landslide inventory, susceptibility, hazard and risk maps are introduced across the country. Fell et al. (2008) point out examples of the PPR (Plans de Prevention des Riques Naturels Previsibles) in France (Ministère de l'Aménagement du Territoire et de l'Environnement, 1999) and the Cartes de Dangers or

Gefahrenkarten in Switzerland which are carried out at the Canton level but with Federal funding support (Leroi et al. 2005). Lateltin et al. (2005) state that the Federal regulation introduced in 1991 in Switzerland required the 26 Cantons to establish hazard maps and landslide zoning for all types of mass movements to restrict development on hazard-prone land. The cantonal authorities have been participating actively in this hazard mapping to prevent and reduce the potential losses and the number of victims, through better land use planning. After 14 years, mapping works were still in progress to cover the Swiss territory by landslide hazard maps at different scales. Based on the nationwide experience, Lateltin et al. (2005) consider that the application of a strict management policy, carried out with the approval of the citizens, allows for a significant decrease in landslide risks.

In practice, those considering landslide zoning for land use management would be well advised to seek advice from an Engineering Geologist or a Geotechnical Professional who is familiar with landslide zoning and risk management to provide advice in planning the landslide zoning study and applying the outcomes to land use planning. Moreover, the scales for landslide susceptibility zoning maps must be harmonized with the scales and requirements of spatial plans.

4.2 Scale-Related Objectives

This chapter presents the experience gained in Croatia, collected through the production of detailed landslide inventory maps from high-resolution ALS LiDAR images (Figs. 3, 4 and 5) as well as landslide susceptibility maps on a small, medium and large scales (Figs. 7, 8 and 9). Proposed possibilities for application of the presented landslide maps are derived based on numerous discussions with Croatian planners and decision-makers who consider landslide data and information together with other land-use criteria. There are three levels of spatial plans in Croatia. Table 5 shows types of spatial and urban plans at the State, Regional and Local levels. The largest scale required will determine the level and scale of landslide zoning.

Generally, the small scale landslide susceptibility map of Croatia (1:100,000) is more likely to be used in the preliminary stages of development at the national level. In the case of a medium scale landslide susceptibility map of the county (1:25,000), the use of mapping which defines a planning control area may be sufficient to identify where a more detailed landslide risk assessment is needed. Detailed stages of development require a large scale landslide susceptibility map and a landslide inventory map of the city or municipality (1:5000).

Figures 10 and 11 present part of the previously described detailed landslide inventory maps on a large scale overlapped with land use in the urban area in Zagreb and in the rural area in Hrvatskoj Zagorje (NW Croatia). Both examples prove that they are large scale maps containing data at appropriate levels of input for proposing statutory land use planning constraints. These examples of zoning in terms of landslide inventory could be used to manage landslide hazard in urban areas by excluding development in areas endangered by registered landslides. This landslide inventory map in combination with a landslide susceptibility map on a large scale provides detailed boundaries of higher hazard areas to propose requirements for geotechnical engineering assessment of slope stability before development is approved in these areas.

In this regard, it should be noted that State and County governments have significantly different requirements from Local governments. The use of landslide zoning maps at the National and Regional levels in Croatia will provide information for areas where more detailed data and information about landslides are necessary. In addition to planners and developers, the information and data about landslides built into spatial and urban plans are intended for designers and other Engineering geologists or Geotechnical professionals involved in construction, as preliminary information about geohazards that is necessary to define site investigation requirements.

Table 5 Levels and scale of spatial plans in Croatia

Spatial plan level	Spatial plan type	Scale
National level	National spatial development plan	1:300,000
	UPU of state importance	1:100,000
	Spatial plans of areas of special features	1:100,000 or 1:25,000 or 1:10,000 or 1:5,000
Regional level	County spatial plans	1:100,000, 1:25,000 (PPGZ[a])
	UPU of county importance	1:25,000
Local level	Spatial plans of cities/municipalities	1:25,000 (1:5000 for determination of construction areas of settlements)
	General urban plan (GUP)	1:5000 or 1:10,000
	Urban development plan (UPU)	1:5000 or 1:1000 or 1:2000

[a] PPGZ—Spatial Plan of the City of Zagreb (county level)

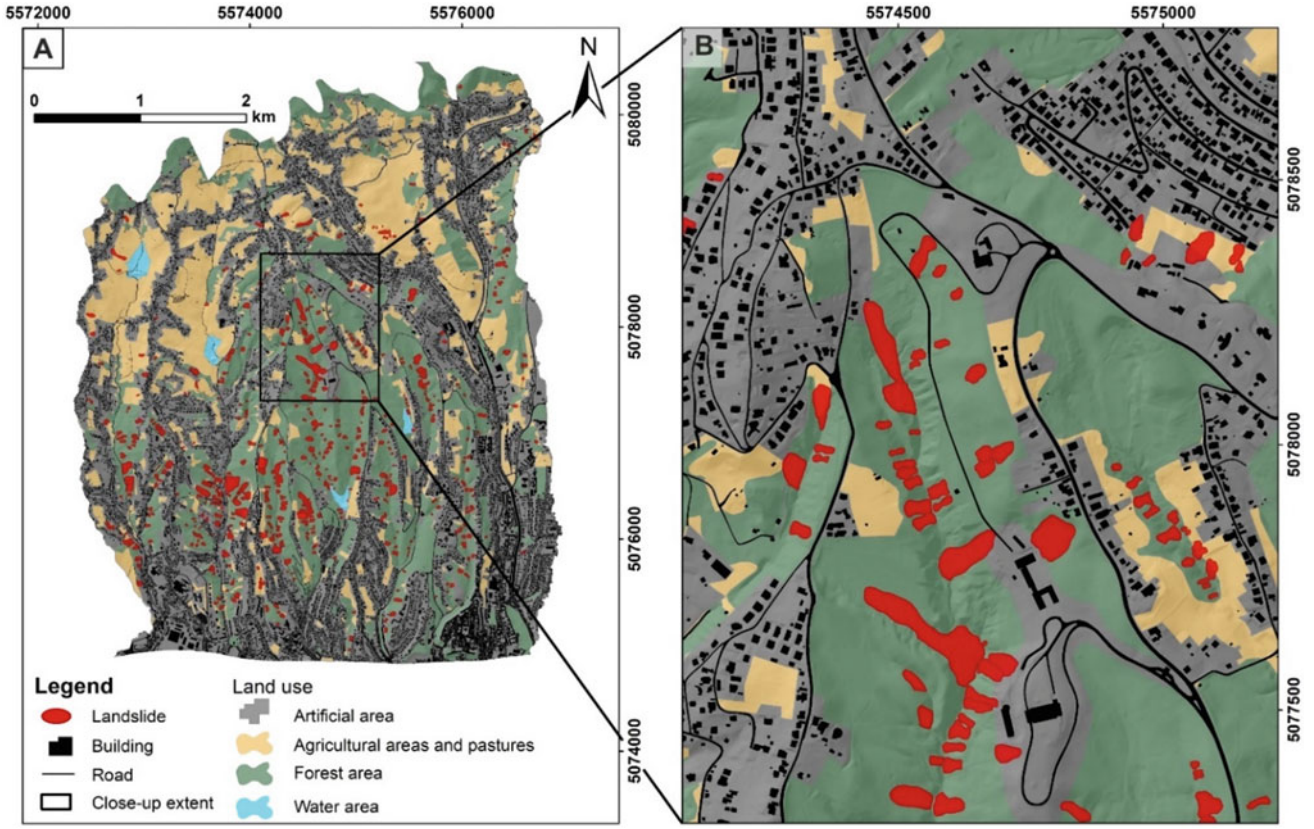

Fig. 10 Detailed landslide inventory map (21 km^2) overlapped with land use categories from the Spatial Plan of the City of Zagreb (modified from Bernat Gazibara et al. 2019a)

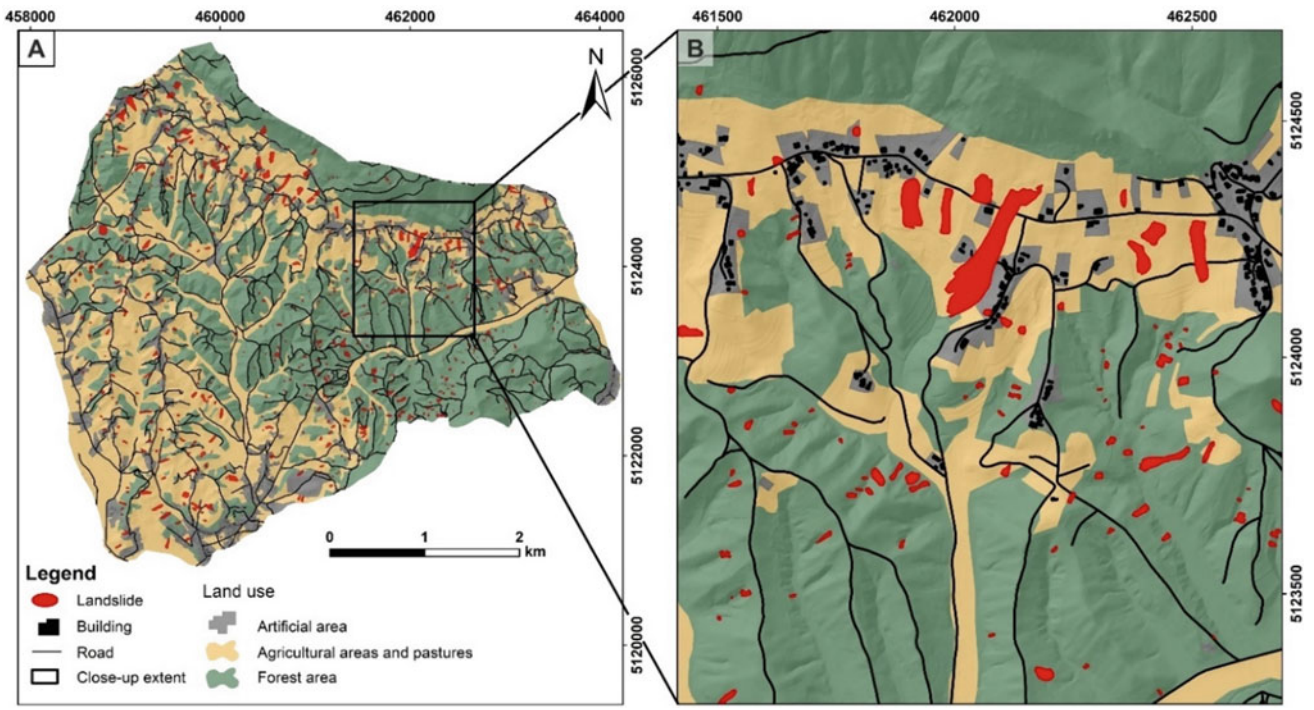

Fig. 11 Detailed landslide inventory map (20.22 km^2) overlapped with land use categories from the Spatial Plan of the Lepoglava City and Bednja Municipality (modified from Sinčić et al. 2022)

5 Final Remarks

Advances in aerial laser scanning technology (ALS LiDAR) have made possible to produce high-resolution bare-earth digital terrain models that are the best source of data for mapping landslide phenomena and for deriving a range of morphological causal factors for landslide susceptibility analysis. Since the primary purpose of landslide maps presenting landslide inventory and landslide susceptibility is often land use management and control measures for sliding, it can be concluded that new technological possibilities enable obtaining data and information on landslides that we have always needed.

New and emerging techniques based on airborne LiDAR remote sensing technology, facilitate the production of landslide maps, reducing the time and resources required for their compilation and systematic update. At the same time, they enable the detection and mapping of small and shallow landslides overgrown, and often hidden by vegetation. These maps are sufficiently detailed to support mitigation actions at the local level. Moreover, the quality and completeness of the landslide maps will enhance the reliability of the estimates obtained from the inventories. The question then becomes one of identifying the most effective of the various mitigation approaches and obtaining funding to apply the best mitigation measures. Examples of detailed and complete landslide inventories compiled for three pilot areas in Croatia proved that they can be used for all major mitigation approaches: restricting development in landslide-prone areas; enforcing codes for excavation, construction, and grading; engineering for slope stability; deploying monitoring and warning systems; and providing landslide insurance.

The levels of zonation define scales of susceptibility maps. It is recommended that the map scales should be in accordance with scales and types of spatial planning maps. Landslide susceptibility zonation at the large scale that needs to enable planning of urban development at the local level, is shown on the example map from the Zagreb City pilot area. Landslides from the complete inventory were used for the statistical susceptibility analysis method, as well as morphometric maps derived from LiDAR DTM, which contributed to the reliability of the map. For the needs of landslide susceptibility zonation required by state or federal governments, for regional land use planning or disaster management planning, medium or small scale maps obtained by assessment from lower quality but widely available data are sufficient. We have presented the susceptibility maps obtained by the heuristic assessment that are of satisfactory reliability for defining obligations where a more detailed susceptibility mapping is needed, whether the users are spatial planners developing low-level spatial/urban plans or land developers, those developing major infrastructure such as highways and railways or managing recreational areas.

It will be appropriate to carry out landslide susceptibility zonation in small scale as a first stage in the multi-stage development of landslide susceptibility zonation for planning purposes. Multiscale mapping will allow better control of the process and may reduce the costs of the zoning by limiting the more detailed zoning only to areas where it is necessary. Data and information needed by officials and planners to reduce landslide risk and losses provided from the landslide susceptibility maps and assessments require the development and implementation of a plan for mapping and assessing landslide and other ground failure hazards, from nationwide susceptibility maps to landslide inventories at the local level. The use of standards and guidelines for landslide hazard maps and assessments will provide advice in planning the landslide zonation study and applying the outcomes to land use planning. Moreover, improved documentation and more active communication among different stakeholders would, however, contribute to more effective landslide management.

Preventive actions and measures can and are frequently taken to reduce accidents and their consequences. Data and information from landslide inventory and susceptibility maps could be also used for some of generic measures, and these are most often non-physical such as legislation and education at the national, regional, or local level. International directives and agreements, such as the Sendai Framework for Disaster Risk Reduction 2015–2030 (UN 2015), exert an influence on the development of national strategies and legislation. Landslide maps are tools that are necessary for identification and visualization of disaster risk factors and scenarios, including emerging disaster risks, in the medium and long term. In this way they can also contribute to the following: to increase research for regional, national, and local application; support action by local communities and authorities; and support the interface between policy and science for decision-making.

Acknowledgements This work was supported by the Croatian Science Foundation under the Grants for the project "Methodology Development for Landslide Susceptibility Assessment for Land-use Planning Based on LiDAR Technology" (HRZZ IP-2019-04-9900 and HRZZ DOK-2020-01-2432), and by the European Union, European Structural and Investment Funds under Grant for the project "Applied Landslide Research for Development of Risk Mitigation and Prevention Measures" (KK.05.1.1.02.0020). The first support by research program SATREPS FY2008 under the auspices of the Japan Science and Technology Agency (JST) and the Japan International Cooperation Agency (JICA) under Grant for the Croatian-Japanese project "Risk Identification and Land-Use Planning for Disaster Mitigation of Landslides and Floods in Croatia".

References

Aničić B, Juriša M (1984) Basic geological map, scale 1:100,000, Rogatec, Sheet 33–68

Antonini G, Cardinali M, Guzzetti F, Reichenbach P, Sorrentino A (1993) Carta Inventario dei Fenomeni Franosi della Regione Marche ed aree limitrofe

Ardizzone F, Cardinali M, Carrara A, Guzzetti F, Reichenbach P (2002) Uncertainty and errors in landslide mapping and landslide hazard assessment. Nat Hazards Earth Syst Sci 2(1–2):3–14

Ardizzone F, Cardinali M, Galli M, Guzzetti F, Reichenbach P (2007) Identification and mapping of recent rainfall-induced landslides using elevation data collected by airborne Lidar. Nat Hazards Earth Syst Sci 7:637–650. https://doi.org/10.5194/nhess-7-637-2007

Bernat S, Mihalić Arbanas S, Krkač M (2014a) Inventory of precipitation triggered landslides in the winter of 2013 in Zagreb (Croatia, Europe). In: Sassa K, Canuti P, Yin Y (eds) Landslide science for a safer geoenvironment. Springer, Cham, pp 829–835

Bernat S, Mihalić Arbanas S, Krkač M (2014b) Landslides triggered in the continental part of Croatia by extreme precipitation in 2013. In: Lollino G, Giordan D, Crosta GB et al (eds) Engineering geology for society and territory, vol 2. Springer, Cham, pp 1599–1603

Bernat Gazibara S, Krkač M, Sečanj M, Mihalić Arbanas S (2017) Identification and mapping of shallow landslides in the City of Zagreb (Croatia) using the LiDAR–based terrain model. In: Mikos M, Tiwari B, Yin Y, Sassa K (eds) Advancing culture of living with landslides. Springer, Cham, pp 1093–1100

Bernat Gazibara S, Krkač M, Mihalić Arbanas S (2019a) Landslide inventory mapping using LiDAR data in the City of Zagreb (Croatia). J Maps 15:773–779. https://doi.org/10.1080/17445647.2019.1671906

Bernat Gazibara S, Krkač M, Mihalić Arbanas S (2019b) Verification of historical landslide inventory maps for the Podsljeme area in the City of Zagreb using LiDAR based landslide inventory. MGPB 34. https://doi.org/10.17794/rgn.2019.1.5

Bernat Gazibara S, Damjanović V, Krkač M, Sinčić M, Jagodnik P, Mihalić Arbanas S (2022) Landslide susceptibility map of Croatia based on limited data and fuzzy logic approach. In: Proceedings of the 5th regional symposium on landslides in the Adriatic-Balkan Region. Faculty of Civil Engineering, University of Rijeka and Faculty of Mining, Geology and Petroleum Engineering, University of Zagreb

Bernat Gazibara S, Sinčić M, Krkač M, Lukačić H, Mihalić Arbanas S (in press) Landslide susceptibility assessment on a large scale in the Podsljeme area, City of Zagreb (Croatia). J Maps

Bernat Gazibara S (2019) Methodology for landslide mapping using high resolution digital elevation model in the Podsljeme area (City of Zagreb). Doctoral Thesis, Faculty of Mining, Geology and Petroleum Engineering, University of Zagreb

Brabb EE, Pampeyan EH (1972) Preliminary map of landslide deposits in San Mateo County, California

Brabb EE, Pampeyan EH, Bonilla MG (1972) Landslide susceptibility in San Mateo County, California

Brabb EE (1984) Innovative approaches to landslide hazard and risk mapping, pp 307–232

Buckman RC, Jeffrey AC (2001) Landslides triggered by Hurricane Mitch in Guatemala—inventory and discussion

Cardinali M, Galli M, Guzzetti F, Ardizzone F, Reichenbach P, Bratoccini P (2006) Rainfall induced landslides in December 2004 in south-western Umbria, central Italy: types, extent, damage and risk assessment. Nat Hazards Earth Syst Sci 6:237–260. https://doi.org/10.5194/nhess-6-237-2006

Cardinali M, Antonini G, Reichenbach P, Guzzetti F (2001) Photo geological and landslide inventory map for the Upper Tiber River basin

Carrara A, Catalano E, Sorriso Valvo M, Reali C, Merenda L, Rizzo V (1977) Landslide morphometry and typology in two zones, Calabria, Italy. Bull Int Assoc Eng Geol 16:8–13. https://doi.org/10.1007/BF02591433

Carrara A, Cardinali M, Guzzetti F (1992) Uncertainty in assessing landslide hazard and risk. ITC J 2:172–183

Carter W, Shrestha R, Tuell G, Bloomquist D, Sartori M (2001) Airborne laser swath mapping shines new light on Earth's topography. Eos Trans AGU 82:549–549. https://doi.org/10.1029/01EO00321

Chen R-F, Chang K-J, Angelier J, Chan Y-C, Deffontaines B, Lee C-T, Lin M-L (2006) Topographical changes revealed by high-resolution airborne LiDAR data: the 1999 Tsaoling landslide induced by the Chi-Chi earthquake. Eng Geol 88:160–172. https://doi.org/10.1016/j.enggeo.2006.09.008

Corominas J, van Westen C, Frattini P, Cascini L, Malet J-P, Fotopoulou S, Catani F, Eeckhaut MVD, Mavrouli O, Agliardi F, Pitilakis K, Winter MG, Pastor M, Ferlisi S, Tofani V, Hervas J, Smith J-T (2013) Recommendations for the quantitative analysis of landslide risk. Bull Eng Geol Environ. https://doi.org/10.1007/s10064-013-0538-8

Corominas J, Mavrouli O (eds) (2010) SafeLand Deliverable D2.1: overview of landslide hazard and risk assessment practices, 138p. Available at: http://www.safeland-fp7.eu/

Dai FC, Xu C, Yao X, Xu L, Tu XB, Gong QM (2011) Spatial distribution of landslides triggered by the 2008 Ms 8.0 Wenchuan earthquake, China. J Asian Earth Sci 40:883–895. https://doi.org/10.1016/j.jseaes.2010.04.010

Đomlija P, Bernat S, Arbanas Mihalić S, Benac Č (2014) Landslide inventory in the area of Dubračina River Basin (Croatia). In: Sassa K, Canuti P, Yin Y (eds) Landslide science for a safer geoenvironment. Springer, Cham, pp 837–842

Đomlija P (2018) Identification and classification of landslides and erosion phenomena using the visual interpretation of the Vinodol Valley digital elevation model. Doctoral Thesis, Faculty of Mining, Geology and Petroleum Engineering, University of Zagreb

Eeckhaut MVD, Poesen J, Verstraeten G, Vanacker V, Nyssen J, Moeyersons J, Beek LPHV, Vandekerckhove L (2007) Use of LIDAR-derived images for mapping old landslides under forest. Earth Surf Process Landforms 32:754–769. https://doi.org/10.1002/esp.1417

Fell R, Corominas J, Bonnard C, Cascini L, Leroi E, Savage WZ (2008) Guidelines for landslide susceptibility, hazard and risk zoning for land use planning. Eng Geol 102:85–98. https://doi.org/10.1016/j.enggeo.2008.03.022

Fiorucci F, Cardinali M, Carlà R, Rossi M, Mondini AC, Santurri L, Ardizzone F, Guzzetti F (2011) Seasonal landslide mapping and estimation of landslide mobilization rates using aerial and satellite images. Geomorphology 129:59–70. https://doi.org/10.1016/j.geomorph.2011.01.013

Galli M, Ardizzone F, Cardinali M, Guzzetti F, Reichenbach P (2008) Comparing landslide inventory maps. Geomorphology 94:268–289. https://doi.org/10.1016/j.geomorph.2006.09.023

Glenn NF, Streutker DR, Chadwick DJ, Glenn DT, Dorsch SJ (2006) Analysis of LiDAR-derived topographic information for characterizing and differentiating landslide morphology and activity. Geomorphology 73:131–148. https://doi.org/10.1016/j.geomorph.2005.07.006

Gorum T, Fan X, van Westen CJ, Huang RQ, Xu Q, Tang C, Wang G (2011) Distribution pattern of earthquake-induced landslides triggered by the 12 May 2008 Wenchuan earthquake. Geomorphology 133:152–167. https://doi.org/10.1016/j.geomorph.2010.12.030

Guzzetti F (2006) Landslide hazard and risk assessment. Doctoral Thesis, Mathematisch- Naturwissenschaftlichen Fakultät der Rheinischen Friedrich-Wilhelms- Universität, University of Bonn

Guzzetti F (2021) On the prediction of landslides and their consequences. In: Sassa K, Mikoš M, Sassa S et al (eds) Understanding and reducing landslide disaster risk. Springer, Cham, pp 3–32

Guzzetti F, Carrara A, Cardinali M, Reichenbach P (1999) Landslide hazard evaluation: a review of current techniques and their application in a multi-scale study, Central Italy. Geomorphology 31:181–216. https://doi.org/10.1016/S0169-555X(99)00078-1

Guzzetti F, Cardinali M, Reichenbach P, Carrara A (2000) Comparing landslide maps: a case study in the Upper Tiber River Basin, Central Italy. Environ Manag 25:247–263. https://doi.org/10.1007/s002679910020

Guzzetti F, Cardinali M, Reichenbach P, Cipolla F, Sebastini C, Galli M, Salvati P (2004) Landslides triggered by the 23 November 2000 rainfall event in the Imperia Province, Western Liguria, Italy. Eng Geol 73:229–245. https://doi.org/10.1016/j.enggeo.2004.01.006

Guzzetti F, Reichenbach P, Cardinali M, Galli M, Ardizzone F (2005) Probabilistic landslide hazard assessment at the basin scale. Geomorphology 72:272–299. https://doi.org/10.1016/j.geomorph.2005.06.002

Guzzetti F, Mondini AC, Cardinali M, Fiorucci F, Santangelo M, Chang KT (2012) Landslide inventory maps: new tools for an old problem. Earth Sci Rev 112:42–66. https://doi.org/10.1016/j.earscirev.2012.02.001

Harp EL, Jibson RW (1996) Inventory of landslides triggered by the 1994 Northridge, California earthquake. U.S. Geological Survey

Highland L, Bobrowsky P (2008) The landslide handbook—a guide to understanding landslides

Hungr O, Leroueil S, Picarelli L (2014) The Varnes classification of landslide types, an update. Landslides 11:167–194. https://doi.org/10.1007/s10346-013-0436-y

IAEG Commission on Landslides (1990) Suggested nomenclature for landslides. Bull Int Assoc Eng Geol 41(1):13–16. https://doi.org/10.1007/BF02590202

ISSMGE TC32 (Technical Committee on Risk Assessment and Management) (2004) Glossary of risk assessment terms. Retrieved from: http://140.112.12.21/issmge/2004Glossary_Draft1.pdf

Jagodnik P, Bernat Gazibara S, Arbanas Ž, Mihalić Arbanas S (2020a) Engineering geological mapping using airborne LiDAR datasets—an example from the Vinodol Valley, Croatia. J Maps 16:855–866. https://doi.org/10.1080/17445647.2020.1831980

Jagodnik P, Bernat Gazibara S, Jagodnik V, Mihalić Arbanas S (2020b) Types and distribution of Quaternary deposits originating from carbonate rock slopes in the Vinodol Valley, Croatia—new insight using airborne LiDAR data. MGPB 35:57–77. https://doi.org/10.17794/rgn.2020.4.6

Jagodnik P, Jagodnik V, Arbanas Ž, Mihalić Arbanas S (2020c) Landslide types in the Slani Potok gully, Croatia. Geologia Croatica 73(1):13–28. https://doi.org/10.4154/gc.2020.04

Krkač M, Bernat Gazibara S, Sinčić M, Lukačić H, Mihalić Arbanas S (2022) Landslide inventory mapping based on LiDAR data: a case study from Hrvatsko Zagorje (Croatia). In: Proceedings of the 5th regional symposium on landslides in the Adriatic-Balkan Region. Faculty of Civil Engineering, University of Rijeka and Faculty of Mining, Geology and Petroleum Engineering, University of Zagreb, pp 81–86

Lateltin O, Haemmig C, Raetzo H, Bonnard C (2005) Landslide risk management in Switzerland. Landslides 2:313–320. https://doi.org/10.1007/s10346-005-0018-8

Leroi E, Bonnard C, McInnes R (2005) Risk assessment and management. In: Landslide risk management. CRC Press, p 40

Lin C-W, Shieh C-L, Yuan B-D, Hsieh Y-C, Liu S-H, Lee S-Y (2004) Impact of Chi-Chi earthquake on the occurrence of landslides and debris flows: example from the Chenyulan River watershed, Nantou, Taiwan. Eng Geol 71:49–61. https://doi.org/10.1016/S0013-7952(03)00125-X

Malamud BD, Turcotte DL, Guzzetti F, Reichenbach P (2004) Landslide inventories and their statistical properties. Earth Surf Process Landforms 29:687–711. https://doi.org/10.1002/esp.1064

McKean J, Roering J (2004) Objective landslide detection and surface morphology mapping using high-resolution airborne laser altimetry. Geomorphology 57:331–351. https://doi.org/10.1016/S0169-555X(03)00164-8

Mihalić S, Marui H, Nagai O, Yagi H, Miyagi T (2013) Landslide inventory in the area of Zagreb City: effectiveness of using LiDAR DEM. In: Margottini C, Canuti P, Sassa K (eds) Landslide science and practice. Springer, Berlin, Heidelberg, pp 155–161

Mihalić Arbanas S, Sečanj M, Bernat Gazibara S, Krkač M, Begić H, Džindo A, Zekan S, Arbanas Ž (2017) Landslides in the Dinarides and Pannonian Basin—from the largest historical and recent landslides in Croatia to catastrophic landslides caused by Cyclone Tamara (2014) in Bosnia and Herzegovina. Landslides 14:1861–1876. https://doi.org/10.1007/s10346-017-0880-1

Mihalić Arbanas S, Arbanas Ž (2015) Landslides: a guide to researching landslide phenomena and processes. In: Transportation systems and engineering: concepts, methodologies, tools, and applications. https://www.igi-global.com/chapter/landslides/www.igi-global.com/chapter/landslides/128730. Accessed 28 Jun 2022

Mihalić Arbanas S, Bernat Gazibara S, Sečanj M, Damjanović V, Oršanić D, Penović S, Krkač M, Cindić K, Jagodnik P, Jagodnik V, Arbanas Ž (2019) Landslide risk management in Croatia: current state. Proceedings of 4th regional symposium on landslides in the Adriatic-Balkan Region, 23–25 Oct 2019. Sarajevo, Bosnia and Herzegovina, pp 243–250. https://doi.org/10.35123/ReSyLAB_2019_40

Ministère de l'Aménagement du Territoire et de l'Environnement (1999) Guide méthodologique plans de prévention des risques de mouvements de terrain. La Documentation française, p 72

Parker RN, Densmore AL, Rosser NJ, de Michele M, Li Y, Huang R, Whadcoat S, Petley DN (2011) Mass wasting triggered by the 2008 Wenchuan earthquake is greater than orogenic growth. Nat Geosci 4:449–452. https://doi.org/10.1038/ngeo1154

Pike RJ (1988) The geometric signature: Quantifying landslide-terrain types from digital elevation models. Math Geol 20:491–511. https://doi.org/10.1007/BF00890333

Razak KA, Straatsma MW, van Westen CJ, Malet J-P, de Jong SM (2011) Airborne laser scanning of forested landslides characterization: terrain model quality and visualization. Geomorphology 126:186–200. https://doi.org/10.1016/j.geomorph.2010.11.003

Reichenbach P, Rossi M, Malamud BD, Mihir M, Guzzetti F (2018) A review of statistically-based landslide susceptibility models. Earth Sci Rev 180:60–91. https://doi.org/10.1016/j.earscirev.2018.03.001

Schulz WH (2007) Landslide susceptibility revealed by LIDAR imagery and historical records, Seattle, Washington. Eng Geol 89:67–87. https://doi.org/10.1016/j.enggeo.2006.09.019

Shan J, Toth CK (eds) (2017) topographic laser ranging and scanning: principles and processing, 1st edn. CRC Press

Šikić K (1995) Geological guide of Mt. Medvednica. Croatian Geological Institute-Croatian Geological Society, INA–Oil Industry, Zagreb, Croatia

Šimunić A, Pikija M, Hečimović I (1982) Basic geological map, scale 1:100,000, Varaždin, Sheet 33–69

Sinčić M, Bernat Gazibara S, Krkač M, Lukačić H, Mihalić Arbanas S (2022) The use of high-resolution remote sensing data in preparation 2 of input data for large-scale landslide hazard assessments. Land 11(8):1360. https://doi.org/10.3390/land11081360

Soeters R, Van Westen CJ (1996) Slope instability recognition analysis and zonation. In: Turner AK, Schuster RL (eds) Landslides:

investigation and mitigation. National Academy Press, Washington, DC, pp 129–177
Spiker EC, Gori PL (2000) National landslide hazards mitigation strategy: a framework for loss reduction. U.S. Dept. of the Interior, U.S. Geological Survey
Šušnjar M, Bukovac J, Nikler L, Crnolatac I, Milan A, Šikić D, Grimani I, Vulić Ž, Blašković I (1970) Basic Geological Map of Yugoslavia 1:100,000, Crikvenica Sheet L33–102
Tsai F, Hwang J-H, Chen L-C, Lin T-H (2010) Post-disaster assessment of landslides in southern Taiwan after 2009 Typhoon Morakot using remote sensing and spatial analysis. Nat Hazards Earth Syst Sci 10:2179–2190. https://doi.org/10.5194/nhess-10-2179-2010
UN (2015) Sendai Framework for Disaster Risk Reduction 2015–2030, 37p. https://www.undrr.org/publication/sendai-framework-disaster-risk-reduction-2015-2030
United Nations Human Settlements Programme (ed) (2012) Mid-term evaluation of the cities and climate change initiative. UN-HABITAT, Nairobi, Kenya
Van Westen CJ, Castellanos E, Kuriakose SL (2008) Spatial data for landslide susceptibility, hazard, and vulnerability assessment: an overview. Eng Geol 102:112–131. https://doi.org/10.1016/j.enggeo.2008.03.010
Van Westen CJ (1993) Application of geographic information systems to landslide hazard zonation. Doctoral Thesis, International Institute for Geo-Information Science and Earth Observation
Varnes DJ (1984) Landslide hazard zonation: a review of principles and practice. UNESCO, Paris
Wold RL, Jochim CL, Agency USFEM, Survey CG (1989) Landslide loss reduction: a guide for state and local government planning. Federal Emergency Management Agency

Long-lasting Post-quake Deformation Buildups in the Grounds that Spread Laterally in Recent Earthquakes

Kazuo Konagai, Takashi Kiyota, Ryoichi Furuta, Masataka Shiga, Rama Mohan Pokhrel, and Takaaki Ikeda

Abstract

In seismically active regions, loose saturated sandy soils are prone to liquefaction. A strong ground shake can create considerable excess pore water pressures in these soils and temporarily decreases the effective stress and shear strength, leading to strength loss, excessive ground settlements, and lateral spreading. Not to mention the immediate ground deformation, post-seismic settlement, and lateral ground spreading often build up slowly and steadily, causing problems for quick rehabilitations to lifeline facilities, etc. However, this long-lasting post-quake deformation buildup has caught less public attention, and quantitative pieces of evidence are less numerous than those about immediate impacts. This article reviews case histories, showing quantitatively that liquefied soils can remain soft for months.

Keywords

Lateral spreading • Soil liquefaction • Post-quake deformation • 2018 Sulawesi Earthquake • 2015 Gorkha earthquake

1 Introduction

Large seismic lateral ground movements that can cause severe damage to lifeline facilities, including roads, railways, waterworks, sewers, transmission lines, etc., are most often associated with soil liquefaction. However, there is more to liquefaction-induced impact than just the immediate damage. Liquefied soil can remain soft, thus causing some problems for post-quake rehabilitation works. The question of how long the liquefied soil can remain soft does not seem to have received as much attention as those on the direct impact of liquefaction. Aguirre and Irikura (1997) examined the main shock and after-shocks of the 1995 Kobe Earthquake, Japan. This earthquake caused severe liquefaction of Port Island, an artificial island of Kobe, the largest in the world at the time of construction, with various facilities including container ship berths, a convention center, universities, etc. Aguirre and Irikura (1997) conducted a back analysis to obtain the chronological change in the shear wave velocities of the island's fill before, during, and after the mainshock. Their study showed that the liquefied state remained at least three hours after the mainshock but no more than 24 h. The fill's stiffness decreased close to zero when liquefaction occurred and later increased gradually, following a trend that resembles a consolidation curve.

Konagai et al. (2003) reported that sand ejecta lined a dried river trace in a dry, barren valley about 100 km west of Tehran, Iran, after the Changureh Earthquake of June 22, 2002, that hit this semidesert area. A trench excavated across the sand ejecta revealed liquefaction escape structures, i.e., sand-filled vertical fissures through a silty surface layer.

K. Konagai (✉)
International Consortium on Landslides, Secretariat, Kyoto, 606-8226, Japan
e-mail: konagai@iclhq.org

T. Kiyota · M. Shiga
Institute of Industrial Science, University of Tokyo, Tokyo, 153-8505, Japan
e-mail: kiyota@iis.u-tokyo.ac.jp

M. Shiga
e-mail: shiga815@iis.u-tokyo.ac.jp

R. Furuta
R&D Department, Remote Sensing Technology Center of Japan, Tokyo, 105-0001, Japan
e-mail: furuta_ryoichi@restec.or.jp

R. M. Pokhrel
Earth Investigation and Solution, Nepal Pvt. Ltd., Kirtipur-2, Kathmandu, Nepal
e-mail: pokhrelrmohan@gmail.com

T. Ikeda
Department of Civil and Environmental Engineering, Nagaoka University of Technology, Niigata, 1603-1, Japan
e-mail: ikeda@vos.nagaokaut.ac.jp

I. Alcántara-Ayala et al. (eds.), *Progress in Landslide Research and Technology, Volume 1 Issue 2, 2022*, Progress in Landslide Research and Technology,
https://doi.org/10.1007/978-3-031-18471-0_17

When a loader, a heavy wheeled tractor used to excavate the trench, reached the wet and soft sandy layer 2 m below the ground surface, the loader had stuck in the liquefied sand. It took a while for the loader to get out of the liquefied sand layer. The trench was excavated on July 29, 2002, about a month after the earthquake. This fact suggested that liquefied sands can remain soft even a month after an earthquake, making rehabilitation works with heavy equipment extremely difficult.

This article reviews case histories showing that liquefied soils can remain soft for months.

2 Quantitative Evidence on How Long Liquefied Sand Remains Soft

The 2011 Tohoku Earthquake, also known as the Great East Japan Earthquake, has shown that a long stretch of landfills along the northern shorelines of Tokyo Bay had very high liquefaction susceptibility. These landfills are almost flat, and there was little to see regarding lateral spreading. However, some field surveys have shown quantitative evidence on how long liquefied sand remains soft. Before getting to the main point, we had better have an overall picture of the liquefied Tokyo Bay shore area. Konagai et al. (2013) attempted to detect soil subsidence from raster images converted from airborne LiDAR (Light Detection and Ranging) data before and after the earthquake. Konagai et al. (2013) used the template matching technique for clusters of pile-supported buildings and bridge piers chosen as templates in source images of the target areas to eliminate deep-seated tectonic displacements and thus extract ground subsidence caused solely by soil liquefaction. Figure 1a shows the obtained soil subsidence map of Urayasu. Since the LiDAR survey was conducted for Urayasu on April 20 after almost all sand ejecta were cleared up from streets, the amount of ground elevation loss is considered to be primarily due to the removal of sand ejecta. The aerial photograph of the same area (Fig. 1b) was taken in 1948 by the US Army [19]. This photo clearly shows that it was post-World War II when most of the land reclamation in Urayasu was undertaken and that today, most of the city spreads over the reclaimed land of sand dredged from Tokyo Bay.

At the location shown by a placemark in Fig. 1, where significant liquefaction occurred during the earthquake, Kiyota et al. (2016) conducted a series of routine Swedish Weight Sounding (SWS) tests once every one or a few months. A pre-quake SWS test was also conducted in 2002, 9 years before the earthquake. SWS is a simple manually operated penetration test under a dead-load of 100 kg in which the number of half-rotations (N_{SW}) required for a 25 cm penetration of a rod (screw point) is recorded (Japanese Industrial Standards (JIS) A1221). The obtained N_{SW} values for the fill layer were then converted to equivalent N values in the standard penetration test (SPT) (see Fig. 2). A significant reduction in the SPT-N value was seen about a week after the earthquake. Then, the SPT-N values increased with time later and returned to the original values about two months after the quake. Once the shaking is over, the excess pore water pressures that developed in water-saturated sand during the earthquake gradually dissipate. However, this figure suggests that pore water pressure dissipation can take a long time, and liquefied sand can remain soft for months. Even after this long period, the sand barely regains its original strength and hardly exceeds it. The sand is again loosely consolidated with high susceptibility to re-liquefaction.

To examine if the loosely deposited granular fabric of sand was reproduced, Yamamoto (2015) conducted a Multi-channel Analysis of Surface Waves (MASW) in the Shin-Kiba area, another reclaimed land immediately west of Urayasu. MASW measures the dispersive nature of surface waves (usually the fundamental-mode Rayleigh waves) using an array of geophones and thereby can be used to back-analyze the shallow underground shear-wave velocity distribution. Figure 3 shows a bird's-eye view of the Shin-Kiba area overlain by the liquefaction-induced soil-subsidence map (Kajihara et al. 2017; Konagai et al. 2013). The MASW survey was conducted along a street through two severely subsided blocks (depicted by two broken-line ellipses in Fig. 3). Figure 3 also shows the shear wave velocity (v_s) profile in 2D (surface distance and depth) format. The profile shows low v_s zones 2–5 m underground immediately beneath the two severely subsided blocks. This finding suggests that sands within the low v_s zones are as weak as before the earthquake and thus remain vulnerable to re-liquefaction.

3 Lateral Spreading and Post-liquefaction Movements

Lateral spreading is one of the most damaging forms of liquefaction. Typically, it occurs on sloping ground. When the underlying soils liquefy, then even a mild slope drives the liquefied soils towards open channels, waterways, etc. The lateral movement due to spreading can be significant depending on the geometries of the moving soil mass confined by the topographic surfaces and the underlying liquefied layer. The travel distance can vary from tens of centimeters to tens of meters or even more. Regardless of whether the movement is large or small, the liquefied sand can remain soft, causing post-liquefaction settlements, lateral deformations, etc. This chapter introduces two case histories of lateral spreading. Particularly, the former is extreme in terms of runout distance.

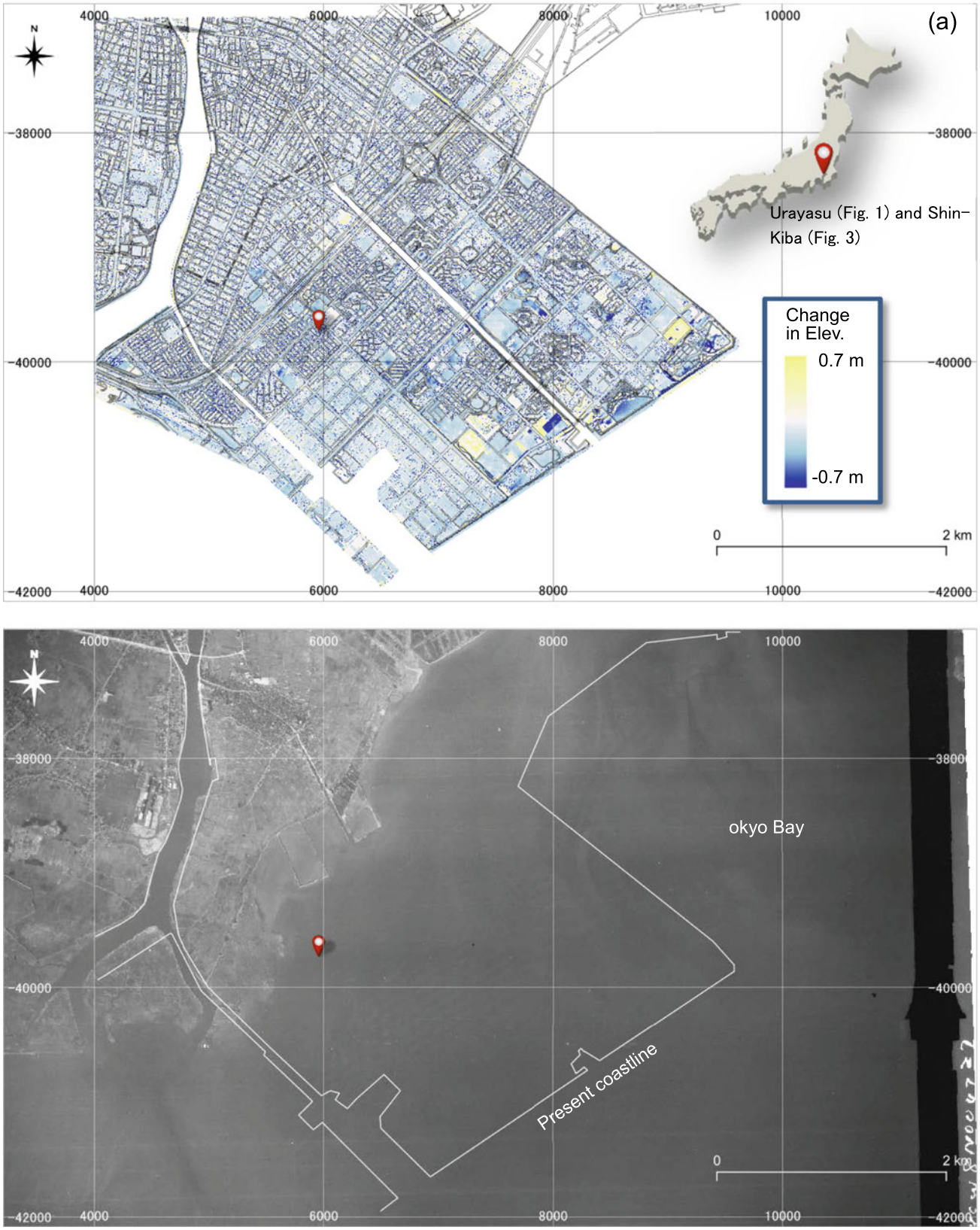

Fig. 1 **a** Soil subsidence map of Urayasu (based on Konagai et al. 2013), and **b** aerial photo of Urayasu on Nov. 8, 1947 [USA M636-A-No2, altitude: 6096 m, photo scale by flight: 39974, Geospatial Information Authority of Japan (2011)]

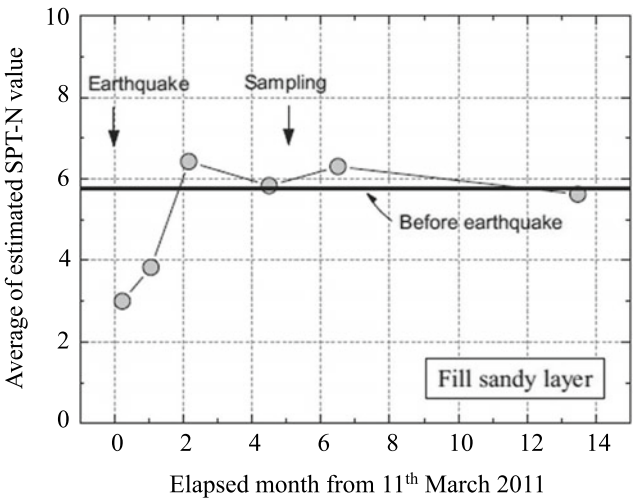

Fig. 2 Chronological change in estimated SPT-*N* values of fill layer in Urayasu City (Kiyota et al. 2016)

3.1 Widespread Ground Deformation Caused by the 2018 Sulawesi, Indonesia Earthquake

A devastating Mw 7.5 earthquake struck Central Sulawesi, Indonesia, on September 28, 2018, resulting in over 4000 fatalities and severe damage to several areas in and around Palu City. Sulawesi is a vast island of Indonesia with four spindly arms spinning outward. Palu city is the innermost part of Palu Bay that cuts into the northernmost arm joint. The south-north trending Palu Basin that extends straight to Palu Bay features the unique terrain of the epicentral area. The epicentral area is a typical pull-apart tectonic basin with a thick alluvial deposit filling the valley. This earthquake's most spectacular and devastating aspect was lateral slides of the almost flat alluvial soil deposit along the west and east bounds of the basin. Lateral spreads were the most serious in Balaroa, Petobo, Jono Oge, and Sibalaya (Rohit et al. 2021; Kiyota et al. 2020). The maximum flow distance at each site was reportedly several hundred meters or more. Thus, this is a case history of extremely large lateral spreading.

Various theories for lateral-spread initiations and motions are discussed by many researchers (Kiyota et al. 2020; Rohit et al. 2021). They have a common opinion that liquefiable deposits and multiple capping layers might have triggered the flow slides. Bradley et al. (2019) reported that aqueduct-supported cultivation, primarily for wet rice, raised the water table near ground level, saturating sandy alluvial soils. Thus, the devastating lateral spreading in the Palu Valley could have been a direct consequence of irrigation. However, the cause of the flow slide cannot be determined solely by the presence of the irrigation channel because there was no primary irrigation channel in Balaroa, the west side of Palu Valley (Kiyota et al. 2020).

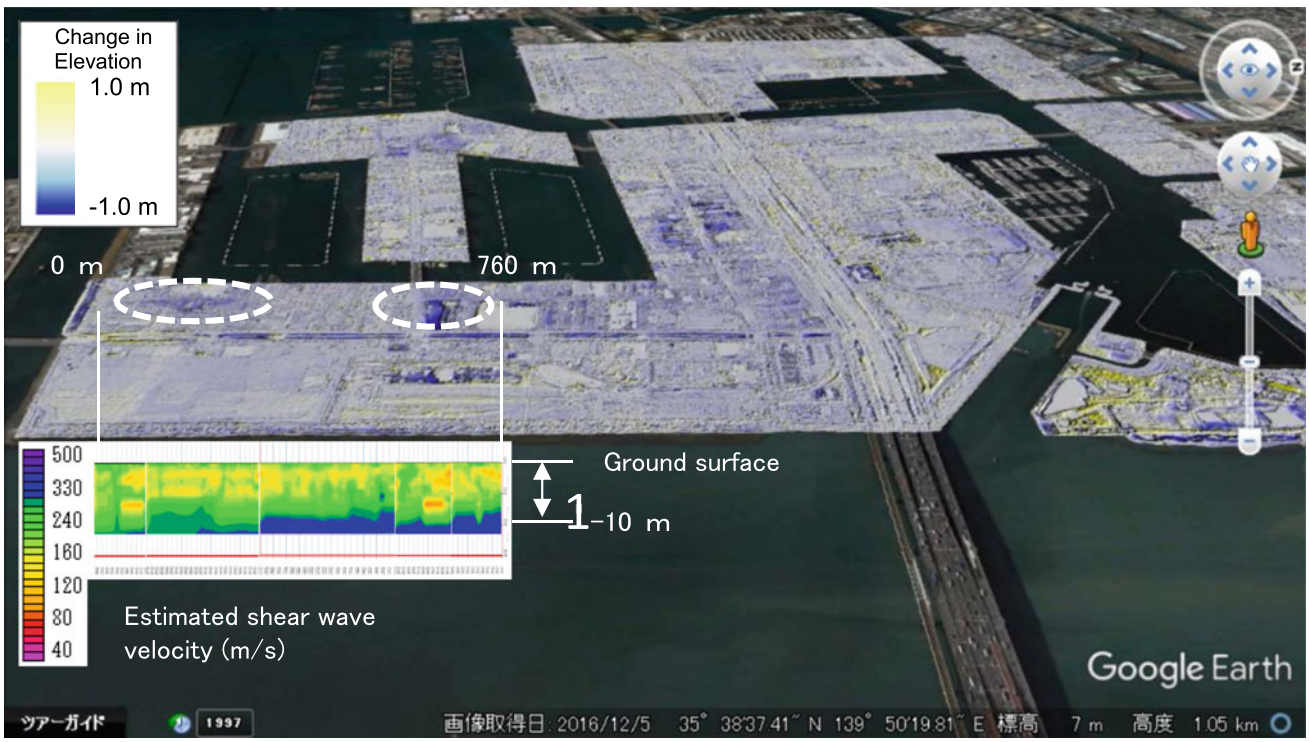

Fig. 3 Bird's-eye view of Shin-Kiba area (Google Earth) overlain by the liquefaction-induced soil-subsidence map. Subsided areas are shown in blue. Shear wave velocity (v_s) profile in 2D (surface distance and depth) format along a 760-m stretch of a road is also overlain

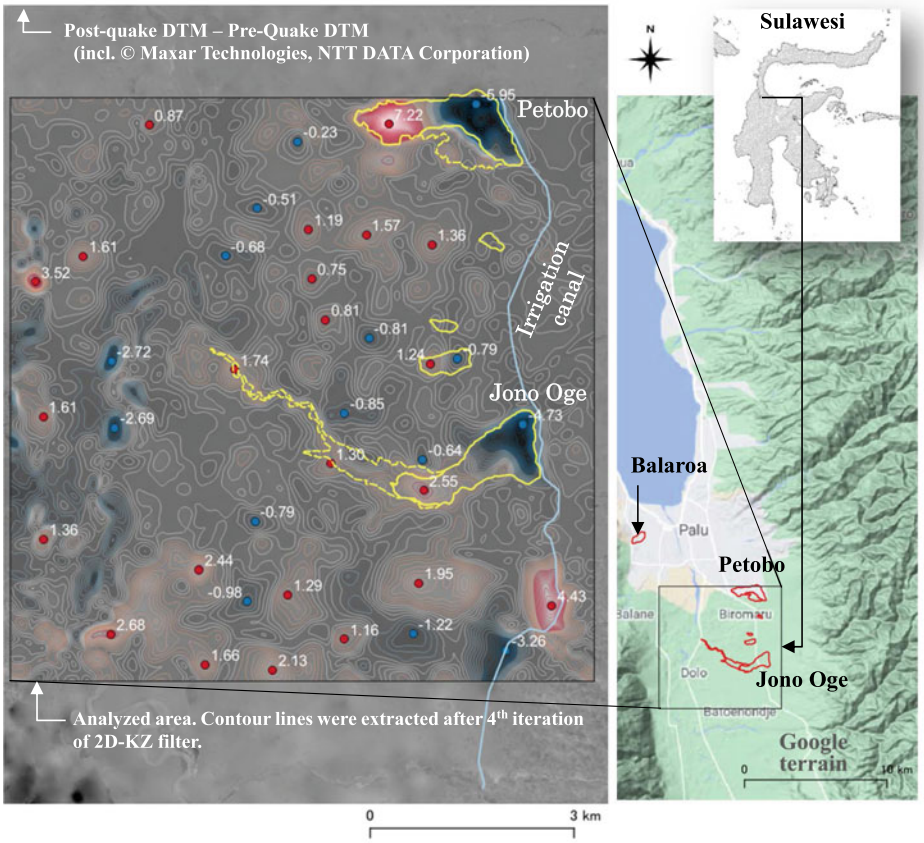

Fig. 4 Difference in the digital terrain models (incl. © Maxar Technologies, NTT DATA Corporation) before and after the earthquake: the two-dimensional (2D) Kolmogorov–Zurbenko (KZ) filter was applied to the image to smear the rapid intensity changes and draw smoother contour lines. The contour lines are drawn with the unit and the interval set at the "meter" and "0.2 m," respectively. Yellow polygons show locations of extensive flow slides (Konagai et al. 2022)

To discuss (1) immediate and (2) post-quake ground deformations, Konagai et al. (2022) used two sets of topographic data; (1) Pre-and Post-quake Digital Terrain Models of the Palu Basin and (2) Line-of-sight (LOS) deformations over the Palu Basin obtained from ALOS 2/PALSAR 2 on October 12, 2018, and January 4, 2019. The Digital Terrain Models [AW3D DTMs, 2 m resolution, NTT Data, RESTEC] before and after the earthquake are random gatherings of various source data sets at different times. The DTM before the earthquake covers the period from January 1, 2010, to September 27, 2018, while the post-quake DTM covers the period from September 28, 2018, to November 20, 2018. Konagai et al. (2022) subtracted the pre-quake DTM from the post-quake DTM to evaluate the vertical components of the quake-induced Eulerian ground displacement. The difference of the DTMs was first resampled for a blurred image of 10 m resolution to avoid rapid scatters in the image intensity. Then, the Two-Dimensional (2D) Kolmogorov–Zurbenko (KZ) filter (Zurbenko 1986, Yang and Zurbenko 2010) was applied to the image to smear the rapid intensity changes further. The 2D-KZ filter is a series of iterations of a moving average square filter $(2L+1) \times (2L+1)$, where L is a positive integer. It has thus two parameters, the half-length L of the square window and the number of iterations k of the moving average operation. Since the resampled DTM has a 10 m resolution and L was set at 5, the moving average window is 110-m square.

Figure 4 shows the 2D-KZ filtered image of the elevation change over the 8600 m × 8600 m flat-land area south of Palu City. Note that the 4th iteration of the moving average with the half-length of the window set at 50 m conservatively truncates the original target area of 9000 m × 9000 m by 400 m and 400 m in north–south and east–west directions. The area includes two extensive earth flows at Petobo and Jono Oge. The ground deformation was not exclusive to these large flow slide sites. Surprisingly, almost the entire analyzed area, particularly west of the irrigation canal, shows a checkerboard elevation change pattern. The pattern shows alternating positive and negative values of elevation change ranging from − 1.0 m or below to + 1.0 m or more prominent. Though the calibrations of the DTMs are needed, these peak values are substantially large enough to acknowledge the statistical significance of the 2D-KZ filtered image of the elevation change. The positive and negative peaks appear periodically at an average interval of about 1 km. This pattern can reflect the subsurface soil profile that can include liquefied layers.

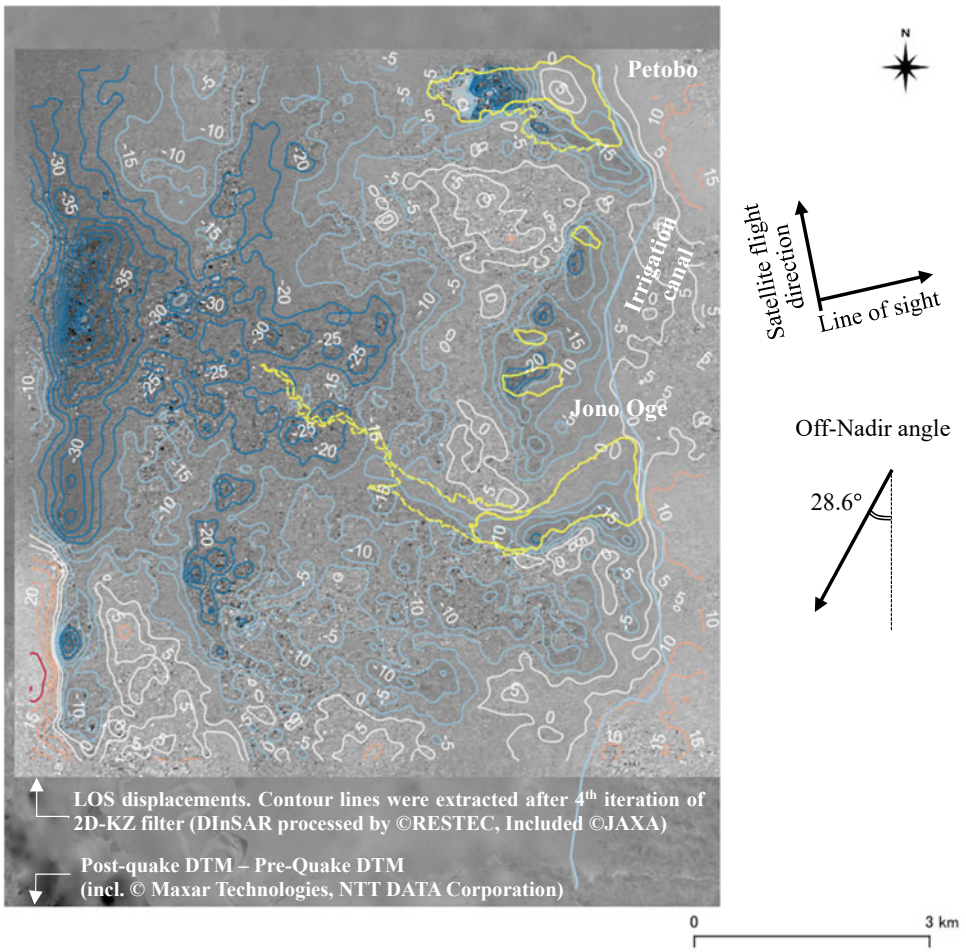

Fig. 5 Line-of-sight (LOS) deformations over the same area as Fig. 1 from ALOS 2/PALSAR 2 on two different days after the earthquake (October 12, 2018, and January 4, 2019): DInSAR processed by ©RESTEC, Included ©JAXA. The two-dimensional (2D) Kolmogorov–Zurbenko (KZ) filter was applied to the image to smear the rapid intensity changes and draw smoother contour lines. The contour lines are drawn with unit and interval set at the "millimeter" and "5 mm," respectively. Yellow polygons show locations of extensive flow slides (Konagai et al. 2022)

For confirmation of the post-liquefaction displacement buildup, Konagai et al. (2022) obtained Line-of-sight (LOS) deformations over the same area from ALOS 2/PALSAR 2 on two different days after the earthquake (October 12, 2018, and January 4, 2019). The 2D-KZ filter was applied to the image of LOS deformations to smear the rapid intensity changes and extract smooth contour lines. Figure 5 shows during the three months that the widespread area west of the irrigation canal had been deforming with ridges developing about 15 mm high and troughs sunken about 20–30 mm deep. The troughs drawn with blue contour lines seem to have developed on the depositional areas of the extensive flow slides and along the meandering trace of Palu River. This pattern of LOS displacements contains errors arising from the uncertainty of estimated orbit or topography and the delay caused by the disturbance of water vapor in the atmosphere. However, the LOS displacements are remarkable, mainly on the western side of the irrigation canal. Thus, this pattern triggers us to acknowledge the statistical significance of the 2D-KZ filtered image of the LOS displacements.

We have heard little about the severe problems confronting rehabilitation of the liquefied Palu Basin, probably because the liquefied flat land was primarily agricultural. However, the findings mentioned above teach us essential lessons to enter the immediate and following stages of rehabilitating liquefaction-devastated areas. We must take necessary measures considering the liquefied ground can remain soft for an extended period.

3.2 Ground Fissures that Diagonally Traversed a Highway at Kausaltar, Kathmandu, Nepal

The 2015 Nepal earthquake (Mw = 7.8), also known as the Gorkha earthquake, struck central Nepal on April 25, 2015, at 11:56 a.m. local time (6:11 a.m. UTC), one of the worst natural disasters to hit central Nepal since 1934 Nepal-Bihar Earthquake. An about 500 m embankment section of the Kathmandu-Bhaktapur Road, a part of Nepal's arterial Araniko Highway, diagonally crosses a small shallow swampy valley in Kathmandu Basin (Fig. 6). The location is

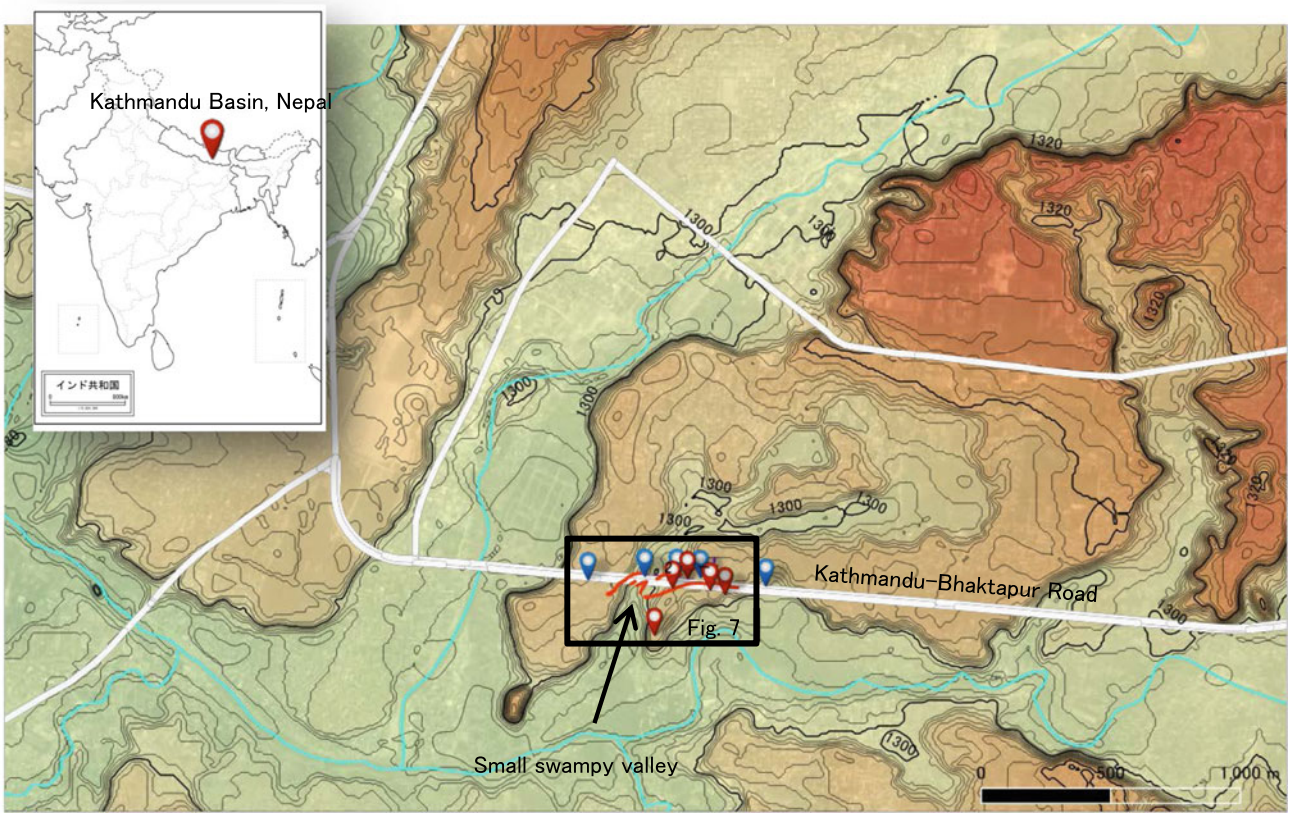

Fig. 6 Kathmandu-Bhaktapur road crossing a small swampy valley: red lines show ground fissures diagonally traversing the road. Blue and red place marks are boreholes drilled by JICA and the authors' team (Konagai et al. 2016; Shiga et al. 2022)

about 2 km southeast of the Tribhuvan International Airport, Kathmandu. Several lines of vertical ground offsets traversed diagonally across this road, making up a swath of ground offset lines (red lines in Fig. 6).

The Japan International Cooperation Agency (JICA 2022a) provided grant aid to widen the existing two-lane highway to an arterial, high-standard four-lane road with two service lanes (Construction period: November 2008 to March 2011). The government of Nepal later constructed service roads on both sides and other facilities like overhead pedestrian bridges to secure the efficient utilization of the road. Therefore, the damage to the highway and its quick rehabilitation was a matter of serious worry for concerned parties on both the Japanese and Nepali sides.

Geological and fossil evidence indicates that the Kathmandu Valley was covered by a large lake called Paleo Kathmandu Lake between approximately 2.8 million and 10,000 years ago (Sakai 2001). The small, shallow swampy valley traversed by the highway may have been one of the marks of disappearing lake water, which dried up almost 10,000 years ago.

The offset lines on the ground are about parallel, trending in ENE to WSW direction. These offset lines disappeared beyond their eastern and western ends and were about 300–400 m long at the most, indicating that the failure was just localized within this short extent of the swath. On the eastern end of the fissures, there was a two-span continuous pedestrian overpass. Konagai et al. (2015, 2016) measured elevations of the middle lane of the highway from the eastern pedestrian bridge using a laser rangefinder (Fig. 7). The maximum vertical offset of about 2 m reached near the boundaries between the terrace and the valley. On the other hand, the sagging part of the highway embankment has been slightly pushed up, as shown in Fig. 7.

There has been little visible evidence of soil liquefaction on the ground surface at Kausaltar. No clear sand ejecta was found. However, some reports indicated the lateral spreading was due to underground liquefaction. The reconnaissance team of the Geotechnical Extreme Event Reconnaissance (GEER) Association (Hashash et al. 2015) excavated a 2.5 m deep trench across the easternmost large fissure, and it revealed liquefaction escape structures that were capped by the clay/fill layers. There were five borehole logs available along the deformed section of the highway. The authors' team drilled four more boreholes to obtain the soil profiles and the groundwater levels in the target area. Shiga et al.

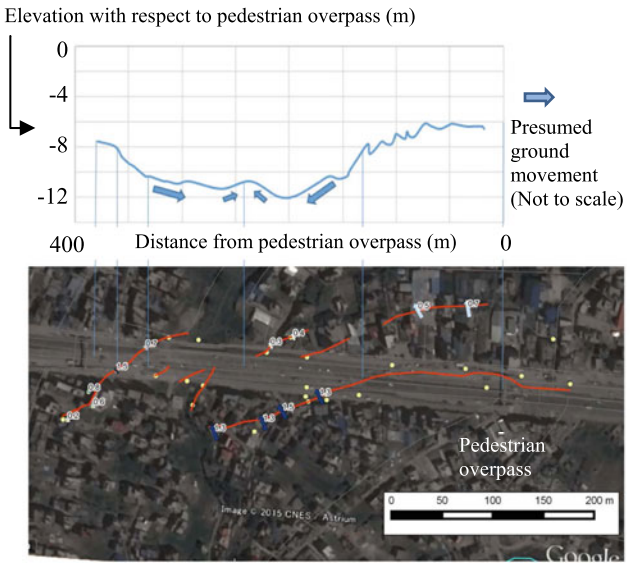

Fig. 7 Change in elevation along the deformed section of Kathmandu-Bhaktapur road (Konagai et al. 2015)

(2022) then obtained the height difference between the upper surface of the aquifer and the lower surface of the silty sand layer at each borehole. They deduced spatial variation of the height difference as shown in Fig. 8. It stands out that the red area where the silty sand lies beneath the groundwater level overlaps the area of fissures associated with vertical ground offsets (white lines). Though the groundwater level may occasionally fluctuate, this suggests that the deeper silty sand layer within the aquifer could have been the primary cause of the lateral spreading.

This ground deformation was responsible for the damage to the two-span continuous pedestrian overpass (Fig. 9), from which the authors measured the highway elevations (Konagai et al. 2015, 2016). Its north pier rested immediately on the northeastern-most line of ground offset, while the other two were on the relatively intact hill terrace. Consequently, the northern pier was on an outward tilt, causing the joint between the pier and the deck to open up. The opening expanded even more during the one month between the two authors' surveys (May 2 to May 31, 2015). There could have been a good chance for any single supported overpass deck to fall upon the highway with its spans expanded. Though it was a two-span continuous overpass, the northern half of the deck was demolished, given the authors' report. This sequence of events indicates that the ground had moved a little even after the earthquake.

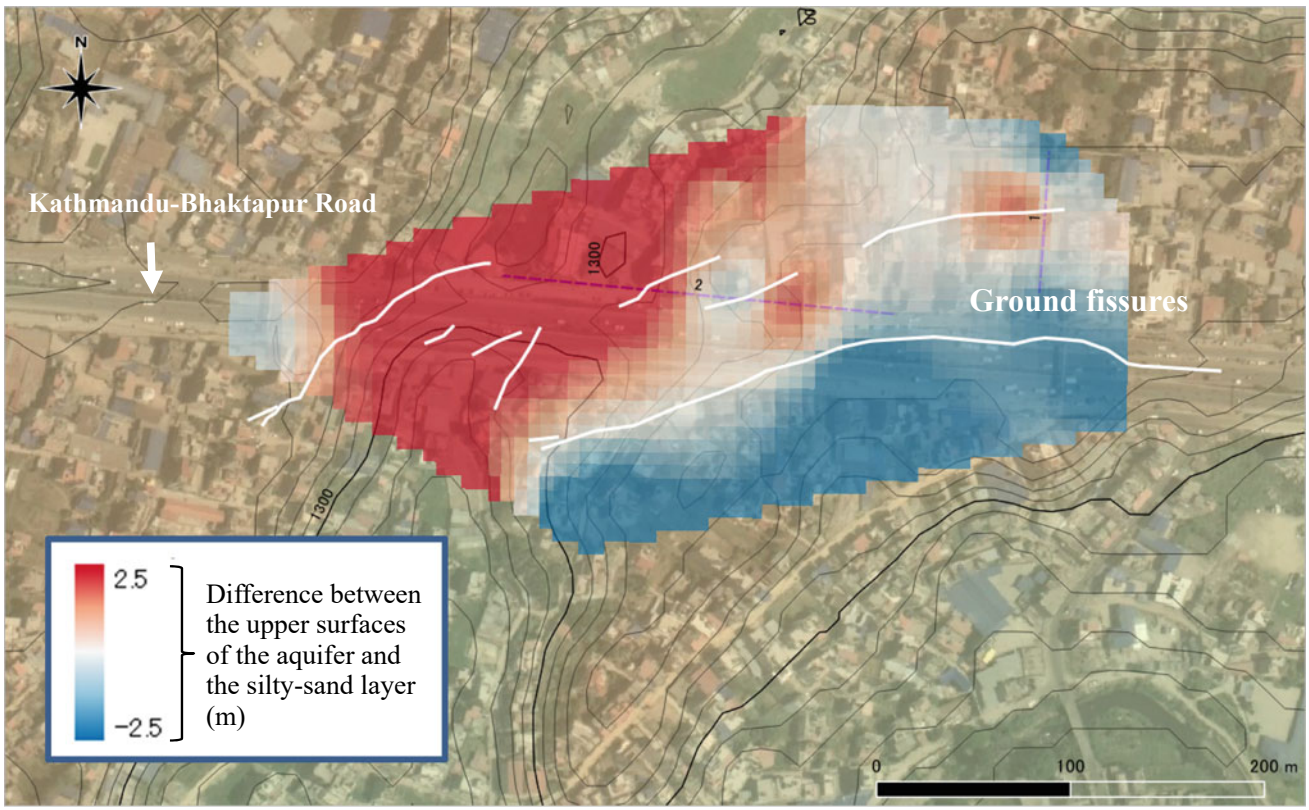

Fig. 8 Difference between the upper surfaces of the aquifer and the silty-sand layer in Kausaltar (based on Shiga et al. 2022)

Fig. 9 Pedestrian overpass over Kathmandu-Bhaktapur Road at Kausaltar (27°40.475′ N 85° 21.865′ E) (based on Konagai et al. 2015): the northern pier was on an outward tilt, causing the joint between the pier and the deck to open up

4 Summary

A strong earthquake motion can create excess pore water pressure in water-saturated sandy soils and temporarily decrease the effective stress and shear strength, leading to excessive ground settlements and lateral spreading. The excess pore water pressures often dissipate too slowly, leaving the soil soft even for months, thus causing some problems for post-quake rehabilitation works. The question of how long the liquefied soil can remain soft did not seem to have received due attention compared with those on the direct impact of liquefaction. Two case histories introduced in this article were:

(1) Widespread ground deformation of Palu Basin caused by the 2018 Sulawesi, Indonesia Earthquake, and
(2) Ground offsets traversed a highway diagonally at Kausaltar, Kathmandu, Nepal, in the 2015 Gorkha earthquake.

In Case history (1), the post-quake InSAR imageries from ALOS 2/PALSAR 2 showed that the widespread area west of the irrigation canal of Palu Basin had been deforming, with ridges developing about 15 mm high and troughs sunken about 20–30 mm deep over the three months (October 12, 2018, to January 4, 2019).

In Case history (2), several lines of vertical ground offsets reaching 2 m traversed diagonally across a 500 m embankment section of the Kathmandu-Bhaktapur Road, a part of Nepal's arterial Araniko Highway, thus slowing the traffic for rehabilitation. Though the lateral spreading was confined within a narrow and shallow swampy valley at the bottom of Kathmandu Basin, there were some pieces of evidence that the ground was deforming slowly and steadily. A pedestrian overpass span increased gradually over a month (May 2 to May 31, 2015). Given this observation, the deck of the overpass was demolished.

Those involved in post-quake rehabilitation works should remember that liquefied soils can remain soft for months. For this, more case histories like those shown in this article are essential and expected to be collected for further quantitative discussion about post-quake soil deformation buildups.

Acknowledgements The works reviewed in this article have been financially supported by the Japan Society for the Promotion of Science (Projects No. 26249069, and No. 19KK0108). The Digital Terrain Models of the Palu Basin before and after the earthquake were provided by the Project for Development of Regional Disaster Risk Resilience Plan in Central Sulawesi in the Republic of Indonesia, Japan International Cooperation Agency (JICA 2022b). The Line-of-sight (LOS) deformations over the Palu Basin obtained from ALOS 2/PALSAR 2 were analyzed at the Remote Sensing Technology Center of Japan (RESTEC).

References

Aguirre J, Irikura K (1997) Nonlinearity, liquefaction, and velocity variation of soft soil layers in Port Island, Kobe, during the Hyogo-ken Nanbu earthquake. Bull Seismol Soc Am 87(5):1244–1258. https://doi.org/10.1785/BSSA0870051244

Bradley K, Mallick R, Andikagumi H et al (2019) Earthquake-triggered 2018 Palu Valley landslides enabled by wet rice cultivation. Nat Geosci 12:935–939. https://doi.org/10.1038/s41561-019-0444-1

Geospatial Information Authority of Japan (2011) Archives of aerial photographs for tracing the history of land. http://www.gsi.go.jp/tizu-kutyu.html

Hashash Y, Tiwari B, Moss R, Asimaki D, Clahan K, Kieffer D, Dreger D, MacDonald A, Madugo CM, Mason B, Pehlivan M, Rajamajhi D, Acharya I, Adhikari B (2015) Gorkha (Nepal) Earthquake of April 25, 2015, and related shaking sequence. Geotechnical Extreme Event Reconnaissance GEER Association Report, No. GEER-040, Version 1.1. https://geerassociation.org/component/geer_reports/?view=geerreports&id=26&layout=default

Japanese Industrial Standards (JIS) A1221 (2020) Method for screw weight sounding test. http://kikakurui.com/a1/A1221-2020-01.html

Japan International Cooperation Agency (JICA) (2022a) The project for improvement of Kathmandu-Bhaktapur road in the Kingdom of Nepal. https://www.jica.go.jp/english/our_work/social_environmental/archive/grantaid/nepal_3.html

Japan International Cooperation Agency (JICA) (2022b) Project for development of regional disaster risk resilience plan in Central Sulawesi, updated on 13 Jan 2022b. https://www.jica.go.jp/project/english/indonesia/020/index.html. Accessed 1 March 2022

Kajihara K, Konagai K, Kiyota T (2017) Soil subsidence map for the west part of Tokyo Bay Area liquefied in the March 11th, Off the Pacific Coast of Tohoku Earthquake. J Jpn Soc Civ Eng Ser. A1 (Struct Eng Earthq Eng (SE/EE)), 73(4). https://doi.org/10.2208/jscejseee.73.I_243

Kiyota T, Ikeda T, Yokoyama Y, Kyokawa H (2016) Effect of in-situ sample quality on undrained cyclic strength and liquefaction assessment. Soils Found 56(4):691–703. https://doi.org/10.1016/j.sandf.2016.07.009

Kiyota T, Furuichi H, Hidayat RF, Tada N, Nawir H (2020) Overview of long-distance flow-slide caused by the 2018 Sulawesi earthquake, Indonesia. Soils Found 60(3):722–735. ISSN: 0038-0806. https://doi.org/10.1016/j.sandf.2020.03.015

Konagai K, Azuma T, Goto H, Noorzad A, Hooshiar SK, Sadr A (2003) Seismic fault and soil-related damage in the June 22, 2002, Changureh Earthquake, Iran. Bulletin of Earthquake Resistant Structure Research Center (ERS), No. 36. http://www.ers.iis.u-tokyo.ac.jp/ers-no36.html

Konagai K, Kiyota T, Suyama S, Asakura T, Shibuya K, Eto C (2013) Maps of soil subsidence for Tokyo bay shore areas liquefied in the March 11th, 2011 off the Pacific Coast of Tohoku Earthquake. Soil Dyn Earthq Eng 53:240–253. https://doi.org/10.1016/j.soildyn.2013.06.012

Konagai K, Pokhrel RM, Matsubara H, Shiga M (2015) Geotechnical aspect of the damage caused by the April 25th, 2015 Gorkha earthquake of Nepal. JSCE J Disaster Factsheets FS2015-E-0002. https://committees.jsce.or.jp/disaster/FS2015-E-0002

Konagai K, Rama Mohan Pokhrel RM, Ikeda T, Shiga M, Aftabur RM, Okuda H (2016) Follow-up report of damage caused by the Gorkha Earthquake, Nepal, of April 25th, 2015. JSCE J Disaster Factsheets FS2016-E-0002. https://committees.jsce.or.jp/disaster/FS2016-E-0002

Konagai K, Furuta R, Kiyota T (2022) Widespread ground deformation over the Palu Basin caused by the 2018 Sulawesi, Indonesia Earthquake. JSCE J Disaster Factsheets FS2022-E-0001. https://committees.jsce.or.jp/disaster/FS2022-E-0001

Sakai H (2001) Stratigraphic division and sedimentary facies of the Kathmandu Basin Group, central Nepal. J Nepal Geol Soc 25:19–32. https://doi.org/10.3126/jngs.v25i0.32043

Shiga M, Konagai K, Pokhrel RM et al (2022) Investigation of ground fissures at Kausaltar, Kathmandu by in-situ testing and spatial geographical mapping. Geoenviron Disasters 9:11. https://doi.org/10.1186/s40677-022-00213-6

Rohit D, Hazarika H, Maeda T et al (2021) Forensic investigation of flowslides triggered by the 2018 Sulawesi earthquake. Prog Earth Planet Sci 8:Article No. 60. https://doi.org/10.1186/s40645-021-00452-5

Yamamoto K (2015) Study on the ground subsidence of the liquefied Tokyo Bay shore area. Graduation Thesis, Department of Civil Engineering, Yokohama National University

Zurbenko I (1986) The spectral analysis of time series. North-Holland series in statistics and probability. Elsevier, Amsterdam

Yang W, Zurbenko I (2010) Kolmogorov-Zurbenko filters. Wiley Interdiscip Rev: Comput Stat 2(3):340–351. https://doi.org/10.1002/wics.71

10th Anniversary of ICL Adriatic-Balkan Network and 5th Regional Symposium on Landslides

Željko Arbanas and Snježana Mihalić Arbanas

Abstract

The Adriatic-Balkan Network (ABN) was established in January 2012 as one of regional networks in the framework of International Consortium on Landslides (ICL) and its 10th Anniversary was concluded with 5th Regional Symposium on Landslides in Adriatic-Balkan Region (ReSyLAB) in Rijeka, Croatia, in March 2022. The Adriatic-Balkan Network was formally established during the 14th Serbian Symposium on Engineering Geology and Geotechnics in Belgrade in September 2012 based on the Proposal of the ICL Adriatic-Balkan Network that was approved at the 10th Anniversary Meeting of ICL held in Kyoto, Japan, in January 2012. The main outcome of the Adriatic-Balkan Network activity is organization of biannual Regional Symposiums on Landslides, organized in Zagreb, Croatia, 2013; Belgrade, Serbia, 2015; Ljubljana, Slovenia, 2017; Sarajevo, Bosnia and Herzegovina, 2019; and the last one in Rijeka, Croatia in March 2022. In this paper, the establishment, objectives and activities of Adriatic-Balkan Network (ABN) within last ten years were presented as well as main outcomes of the 5th ReSyLAB held in Rijeka, Croatia, in March 2022.

Keywords

ICL • Adriatic-Balkan regional network • Regional symposium • ReSyLAB • Croatian Landslide Group

1 Introduction

International Consortium on Landslides (ICL) Adriatic-Balkan Network was established in January 2012 as one of eight regional and thematic ICL networks to promote activi-ties of the International Consortium on Landslides and the International Programme on Landslides based on the Proposal of the ICL Adriatic-Balkan Network that was approved at the 10th Anniversary Meeting of ICL held in Kyoto, Japan, in January 2012. The Adriatic-Balkan Network was formally established during the 14th Serbian Symposium on Engineering Geology and Geotechnics in Belgrade in September 2012 when seven organizations, current members of ICL, signed the Letter of intent and Declaration of the regionl cooperation and International Consortium on Landslides' Adriatic-Balkan Network constitution. These seven initial members of the Adriatic-Balkan Network were University of Zagreb, Faculty of Mining, Geology and Petroleum Engineering, Zagreb, Croatia; and University of Rijeka, Faculty Civil Engineering, Rijeka, Croatia; University of Belgrade, Faculty Mining and Geology, Belgrade, Serbia; University of Ljubljana, Faculty Civil Engineering and Geodesy, Ljubljana, Slovenia; Geological Survey of Slovenia, Ljubljana, Slovenia, Albanian Geological Survey, Tirana, Albania and City of Zagreb, City Office of Emergency Management, Zagreb, Croatia. In the Declaration was highlighted that ICL ABN is open to adopt new members those can be: inter-governmental organizations, non-governmental organizations, governmental organizations and public organizations or other organizations and entities, ICL members and non-members, those express the interest to join ICL Adriatic–Balkan Network' activities.

The general objective of the ICL Adriatic–Balkan Network is advancing landslide science and its practical application in the region for the benefit of society and the environment. Specific objectives are: (i) to set up scientific and legislative background for regional cooperation; (ii) regional unification of information about landslides and

Ž. Arbanas (✉)
Faculty of Civil Engineering, University of Rijeka,
51000 Rijeka, Croatia
e-mail: zeljko.arbanas@gradri.uniri.hr

S. Mihalić Arbanas
Faculty of Mining, Geology and Petroleum Engineering,
University of Zagreb, 10000 Zagreb, Croatia
e-mail: snjezana.mihalic@rgn.unizg.hr

I. Alcántara-Ayala et al. (eds.), *Progress in Landslide Research and Technology, Volume 1 Issue 2, 2022*, Progress in Landslide Research and Technology,
https://doi.org/10.1007/978-3-031-18471-0_18

landslide research at national levels; and (iii) development of landslide science by capacity building at regional level and practical applications of outcomes to societies in the region.

The first and the most important ICL ABN initiative was organization of the 1st Regional Symposiums on Landslides in Adriatic-Balkan Region, entitled Landslide and Flood Hazard Assessment, organized in Zagreb, Croatia, in March 2013, organized by Croatian Landslide Group, member of ICL, consisted of Scientists from University of Zagreb, Faculty of Mining, Geology and Petroleum Engineering, Croatia; and University of Rijeka, Faculty Civil Engineering, Croatia, together with the 3rd Workshop of the Croatian-Japanese Project Risk Identification and Land-Use Planning for Disaster Mitigation of Landslides and Floods in Croatia. More than 110 participants from 12 countries presented 77 scientific and professional papers about landslides and floods hazard assessment as well as other topics related to the landslide science and praxis (Arbanas et al. 2014). The importance of the 1st ReSyLAB for development of landslide science and regional cooperation was recognized by all ICL ABN members and it was adopted that organization of biannual Symposiums will be the most important chain in the maintaining ICL Adriatic–Balkan Network' activities. The 1st ReSyLAB was followed by next four Symposiums held in Belgrade, Serbia, 2015; Ljubljana, Slovenia, 2017; Sarajevo, Bosnia and Herzegovina, 2019; and the last one in Rijeka, Croatia in March 2022.

2 Establishment of ICL ABN and Regional Cooperation

Regional cooperation in Adriatic–Balkan Region was initiated during the First Workshop of the bilateral Japanese-Croatian Project 'Risk Identification and Land-Use Planning for Disaster Mitigation of Landslides and Floods in Croatia', which was held in Dubrovnik (Croatia) in November 2010 (Mihalić and Arbanas 2012). This workshop was an opportunity for scientists in the fields of geological and geotechnical engineering and risk management to share knowledge through presentations of work and research of regional institutions, scientists and professionals. The workshop addressed a range of topics in the fields of investigation of the project members and 25 regional guest experts from eight universities, two geological surveys and four institutes from Bosnia and Herzegovina, Bulgaria, Macedonia, Serbia and Slovenia (Mihalić et al. 2012).

The Ministry of Foreign Affairs of Japan (MOFA) enhanced the regional cooperation on landslides by organizing a workshop for South-Eastern European countries on disaster management in December 2010 in Tokyo. The main result of this workshop was an initiative of the invited participants from Albania, Bosnia and Herzegovina, Croatia, Montenegro, Serbia and Slovenia to establish a regional Adriatic-Balkan Network on Landslides to increase the capacity in landslide disaster risk reduction through regional collaborative work within the ICL. The International Programme on Landslides of ICL (IPL ICL) discussed the establishment of regional consortiums on landslides at the secretarial meeting in Kyoto in January 2011, at the IPL-ICL Session at the Global Platform for Disaster Risk Reduction 2011 in Geneva in May 2011 and at the secretarial meeting in Rome in October 2011 during the 2nd World Landslide Forum. The round table discussions in Geneva and Rome enabled sharing of ideas with other participants and considered an integrated action plan for building the resilience of nations and communities in landslide disaster risk reduction.

General concept of the organization of regional Adriatic-Balkan Network was discussed within the ICL members (Croatian Landslide Group from Faculty of Civil Engineering, University of Rijeka, Rijeka, Croatia and Faculty of Mining, Geology and Petroleum Engineering, University of Zagreb, Zagreb, Croatia; University of Belgrade, Faculty Mining and Geology, Belgrade, Serbia; University of Ljubljana, Faculty Civil Engineering and Geodesy, Ljubljana, Slovenia; Geological Survey of Slovenia, Ljubljana, Slovenia, Albanian Geological Survey, Tirana, Albania and City of Zagreb, City Office of Emergency Management, Zagreb, Croatia) during the Second Workshop of the Bilateral Japanese-Croatian Project in Rijeka (Croatia) in December 2011. Regional ICL meeting was also organized for non-members willing to contribute with advice: the City of Zagreb (local government authority), scientific institutions from Bosnia and Herzegovina and representatives from Kosovo.

According to the preliminary proposal, the common interests to establish this regional Adriatic-Balkan Network on Landslides were: (i) alignment of professional and scientific resources at the regional level by initiating and implementing joint bilateral or multilateral regional projects; (ii) sharing of information and knowledge (e.g., organization of regional workshops and conferences, establishing a newsletter of the regional research network; development of a multilingual landslide glossary using languages of the countries in the region); (iii) enhancing education and training by exchanging scientists and professionals between regional institutions, establishing courses and schools on landslides for young researchers, and educating the public and local administrations; and (iv) development of regionally harmonized strategies for landslide hazard/risk prevention and mitigation (Mihalić Arbanas et al. 2012).

At the 10th Anniversary Meeting held in Kyoto, Japan, in January 2012 ICL has encouraged the establishment of thematic and regional networks in the framework of its ten-year strategic Plan and one of eight proposed regional

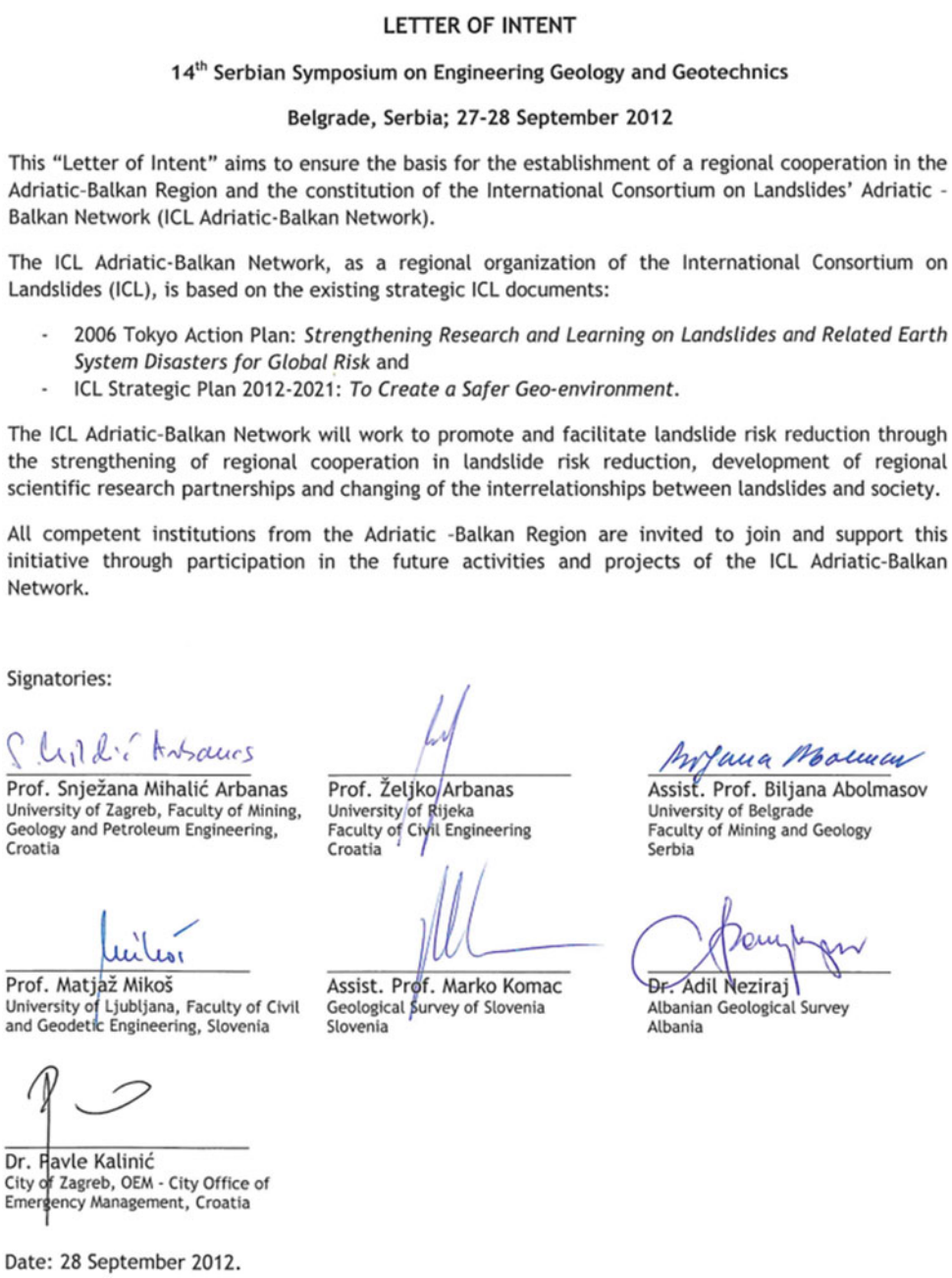

LETTER OF INTENT

14th Serbian Symposium on Engineering Geology and Geotechnics

Belgrade, Serbia; 27-28 September 2012

This "Letter of Intent" aims to ensure the basis for the establishment of a regional cooperation in the Adriatic-Balkan Region and the constitution of the International Consortium on Landslides' Adriatic - Balkan Network (ICL Adriatic-Balkan Network).

The ICL Adriatic-Balkan Network, as a regional organization of the International Consortium on Landslides (ICL), is based on the existing strategic ICL documents:

- 2006 Tokyo Action Plan: *Strengthening Research and Learning on Landslides and Related Earth System Disasters for Global Risk* and
- ICL Strategic Plan 2012-2021: *To Create a Safer Geo-environment*.

The ICL Adriatic-Balkan Network will work to promote and facilitate landslide risk reduction through the strengthening of regional cooperation in landslide risk reduction, development of regional scientific research partnerships and changing of the interrelationships between landslides and society.

All competent institutions from the Adriatic -Balkan Region are invited to join and support this initiative through participation in the future activities and projects of the ICL Adriatic-Balkan Network.

Signatories:

Prof. Snježana Mihalić Arbanas
University of Zagreb, Faculty of Mining, Geology and Petroleum Engineering, Croatia

Prof. Željko Arbanas
University of Rijeka
Faculty of Civil Engineering
Croatia

Assist. Prof. Biljana Abolmasov
University of Belgrade
Faculty of Mining and Geology
Serbia

Prof. Matjaž Mikoš
University of Ljubljana, Faculty of Civil and Geodetic Engineering, Slovenia

Assist. Prof. Marko Komac
Geological Survey of Slovenia
Slovenia

Dr. Adil Neziraj
Albanian Geological Survey
Albania

Dr. Pavle Kalinić
City of Zagreb, OEM - City Office of Emergency Management, Croatia

Date: 28 September 2012.

Fig. 1 Letter of Intent signed in Belgrade on 28 September 2012

and thematic ICL networks was Adriatic-Balkan Network. The Adriatic-Balkan Network was formally established during the 14th Serbian Symposium on Engineering Geology and Geotechnics in Belgrade in September 2012 when seven organizations, current members of ICL, signed the Letter of intent (Fig. 1) and Declaration of the regional cooperation and International Consortium on Landslides' Adriatic-Balkan Network constitution (Fig. 2). These seven initial members of the Adriatic-Balkan Network were University of Zagreb, Faculty of Mining, Geology and Petroleum Engineering, Croatia; University of Rijeka, Faculty Civil Engineering, Croatia; University of Belgrade, Faculty Mining and Geology, Serbia; University of Ljubljana, Faculty Civil Engineering and Geodesy, Slovenia; Geological Survey of Slovenia, Ljubljana, Slovenia, Albanian Geological Survey, Tirana, Albania and City of Zagreb, City Office of Emergency Management, Croatia.

ICL Adriatic–Balkan Network is constituted as a regional International Consortium on Landslides organization based on the existing strategic International Consortium on Landslides' documents: 2006 Tokyo Action Plan: Strengthening Research and Learning on Landslides and Related Earth System Disasters for Global Risk Preparedness (Sassa 2006a, b) and ICL Strategic Plan 2012–2021: To Create a

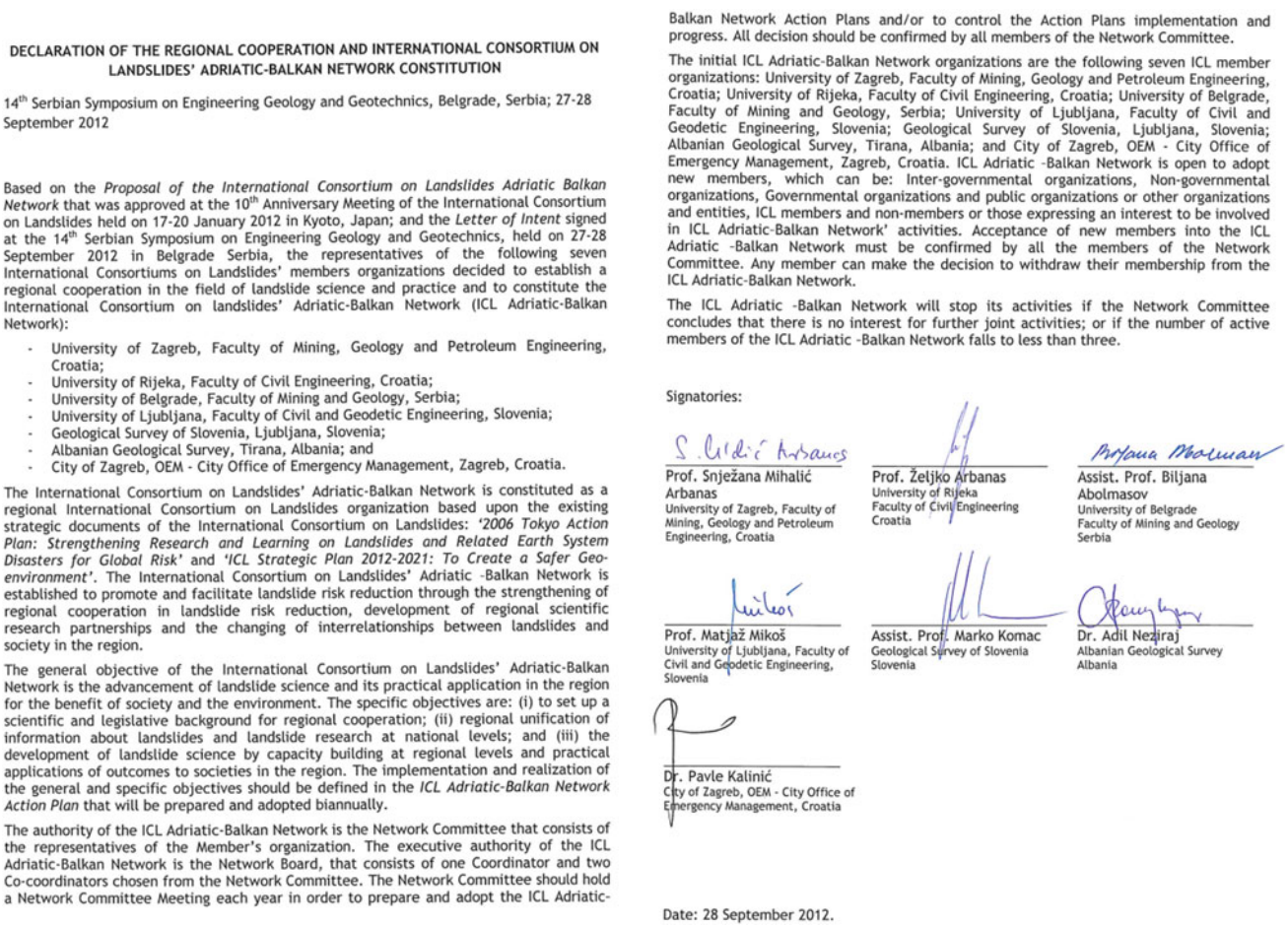

DECLARATION OF THE REGIONAL COOPERATION AND INTERNATIONAL CONSORTIUM ON LANDSLIDES' ADRIATIC-BALKAN NETWORK CONSTITUTION

14th Serbian Symposium on Engineering Geology and Geotechnics, Belgrade, Serbia; 27-28 September 2012

Based on the *Proposal of the International Consortium on Landslides Adriatic Balkan Network* that was approved at the 10th Anniversary Meeting of the International Consortium on Landslides held on 17-20 January 2012 in Kyoto, Japan; and the *Letter of Intent* signed at the 14th Serbian Symposium on Engineering Geology and Geotechnics, held on 27-28 September 2012 in Belgrade Serbia, the representatives of the following seven International Consortiums on Landslides' members organizations decided to establish a regional cooperation in the field of landslide science and practice and to constitute the International Consortium on landslides' Adriatic-Balkan Network (ICL Adriatic-Balkan Network):

- University of Zagreb, Faculty of Mining, Geology and Petroleum Engineering, Croatia;
- University of Rijeka, Faculty of Civil Engineering, Croatia;
- University of Belgrade, Faculty of Mining and Geology, Serbia;
- University of Ljubljana, Faculty of Civil and Geodetic Engineering, Slovenia;
- Geological Survey of Slovenia, Ljubljana, Slovenia;
- Albanian Geological Survey, Tirana, Albania; and
- City of Zagreb, OEM - City Office of Emergency Management, Zagreb, Croatia.

The International Consortium on Landslides' Adriatic-Balkan Network is constituted as a regional International Consortium on Landslides organization based upon the existing strategic documents of the International Consortium on Landslides: *'2006 Tokyo Action Plan: Strengthening Research and Learning on Landslides and Related Earth System Disasters for Global Risk'* and *'ICL Strategic Plan 2012-2021: To Create a Safer Geo-environment'*. The International Consortium on Landslides' Adriatic -Balkan Network is established to promote and facilitate landslide risk reduction through the strengthening of regional cooperation in landslide risk reduction, development of regional scientific research partnerships and the changing of interrelationships between landslides and society in the region.

The general objective of the International Consortium on Landslides' Adriatic-Balkan Network is the advancement of landslide science and its practical application in the region for the benefit of society and the environment. The specific objectives are: (i) to set up a scientific and legislative background for regional cooperation; (ii) regional unification of information about landslides and landslide research at national levels; and (iii) the development of landslide science by capacity building at regional levels and practical applications of outcomes to societies in the region. The implementation and realization of the general and specific objectives should be defined in the *ICL Adriatic-Balkan Network Action Plan* that will be prepared and adopted biannually.

The authority of the ICL Adriatic-Balkan Network is the Network Committee that consists of the representatives of the Member's organization. The executive authority of the ICL Adriatic-Balkan Network is the Network Board, that consists of one Coordinator and two Co-coordinators chosen from the Network Committee. The Network Committee should hold a Network Committee Meeting each year in order to prepare and adopt the ICL Adriatic-Balkan Network Action Plans and/or to control the Action Plans implementation and progress. All decision should be confirmed by all members of the Network Committee.

The initial ICL Adriatic-Balkan Network organizations are the following seven ICL member organizations: University of Zagreb, Faculty of Mining, Geology and Petroleum Engineering, Croatia; University of Rijeka, Faculty of Civil Engineering, Croatia; University of Belgrade, Faculty of Mining and Geology, Serbia; University of Ljubljana, Faculty of Civil and Geodetic Engineering, Slovenia; Geological Survey of Slovenia, Ljubljana, Slovenia; Albanian Geological Survey, Tirana, Albania; and City of Zagreb, OEM - City Office of Emergency Management, Zagreb, Croatia. ICL Adriatic -Balkan Network is open to adopt new members, which can be: Inter-governmental organizations, Non-governmental organizations, Governmental organizations and public organizations or other organizations and entities, ICL members and non-members or those expressing an interest to be involved in ICL Adriatic-Balkan Network' activities. Acceptance of new members into the ICL Adriatic -Balkan Network must be confirmed by all the members of the Network Committee. Any member can make the decision to withdraw their membership from the ICL Adriatic-Balkan Network.

The ICL Adriatic -Balkan Network will stop its activities if the Network Committee concludes that there is no interest for further joint activities; or if the number of active members of the ICL Adriatic -Balkan Network falls to less than three.

Signatories:

Prof. Snježana Mihalić Arbanas
University of Zagreb, Faculty of Mining, Geology and Petroleum Engineering, Croatia

Prof. Željko Arbanas
University of Rijeka
Faculty of Civil Engineering
Croatia

Assist. Prof. Biljana Abolmasov
University of Belgrade
Faculty of Mining and Geology
Serbia

Prof. Matjaž Mikoš
University of Ljubljana, Faculty of Civil and Geodetic Engineering, Slovenia

Assist. Prof. Marko Komac
Geological Survey of Slovenia
Slovenia

Dr. Adil Neziraj
Albanian Geological Survey
Albania

Dr. Pavle Kalinić
City of Zagreb, OEM - City Office of Emergency Management, Croatia

Date: 28 September 2012.

Fig. 2 Declaration of the regional cooperation and International Consortium on Landslides' Adriatic-Balkan Network constitution signed in Belgrade on 28 September 2012

Safer Geo-environment (Sassa 2012). ICL Adriatic–Balkan Network is established to promote and facilitate landslide risk reduction through strengthening of regional cooperation in landslide risk reduction, developing of regional scientific research partnership and changing of interrelationships between landslides and society in the region.

The general objective of the ICL Adriatic–Balkan Network is advancing landslide science and its practical application in the region for the benefit of society and the environment. Specific objectives are: (i) to set up scientific and legislative background for regional cooperation; (ii) regional unification of information about landslides and landslide research at national levels; and (iii) development of landslide science by capacity building at regional level and practical applications of outcomes to societies in the region.

The objectives and planned activities were defined based on analyses about basic information about landslides in the Region and evaluation and mitigation of landslide hazard in the Region (Mihalić Arbanas et al. 2013).

The authority of the ICL Adriatic-Balkan Network is Network Committee consisted of representatives of Member's organization. Executive authority of the ICL Adriatic-Balkan Network is Network Committee consisted of one Coordinator and two Co-coordinators chosen from the Network Committee. All decision should be confirmed by all the members of the Network Committee.

In the Declaration was highlighted that ICL ABN is open to adopt new members those can be: inter-governmental organizations, non-governmental organizations, governmental organizations and public organizations or other organizations and entities, ICL members and non-members, those express the interest to join ICL Adriatic–Balkan Network' activities. Over the time three additional institutions have joined to ICL Adriatic Balkan Network: The Geotechnical Society of Bosnia and Herzegovina, Sarajevo, Bosnia and Herzegovina (2014); University of Ljubljana, Faculty of Natural Sciences and Engineering, Ljubljana, Slovenia (2016); and Macedonian Association for Geotechnics, Skopje, North Macedonia (2021). Unfortunately, Albanian Geological Survey stopped to participating in the ICL Adriatic-Balkan Network in 2020, while in reorganization of the City of Zagreb, City Office of

Emergency Management was attached to other city offices (2021) and is not included in Network activities. Currently, ICL Adriatic-Balkan Network is consisted of five full ICL members and two ICL associates.

3 Regional Symposiums on Landslides in Adriatic-Balkan Region

The most important ICL ABN outcome, organization of biannual landslide Symposiums, started with organization of the 1st Regional Symposiums on Landslides in Adriatic-Balkan Region, held in Zagreb, Croatia, in March 2013, organized by Croatian Landslide Group. The 1st ReSyLAB was organized together with the 3rd Workshop of the Croatian-Japanese Project "Risk Identification and Land-Use Planning for Disaster Mitigation of Landslides and Floods in Croatia", and the title of Symposium was "Landslide and Flood Hazard Assessment". The Symposium attended 111 participants from 12 countries (Albania, Bosnia and Herzegovina, Bulgaria, Croatia, Japan, Kosovo, Macedonia, Romania, Russia, Serbia, Slovenia, Vietnam) and presented 77 scientific and professional papers about landslides and floods hazard assessment as well as other topics related to the landslide science and praxis (Arbanas et al. 2014). All reviewed papers were published in Symposium Proceedings (Fig. 3) (Mihalić Arbanas and Arbanas 2014). The Symposium technical sessions were accompanied by series of side events: round tables, photo exhibition, field trip and book promotion. Two round tables were organized entitled: "Application of Croatian-Japanese Project Results in the Systems of Land-Use Planning, Construction and Civil Protection in Croatia" and "Discussion and Endorsement in the Course of the ICL Adriatic-Balkan Network Activities". The photo exhibition "Living with Landslides" presented 35 photos of landslides and was exhibited ZgForum Gallery and Multimedia Center located in the downtown of the Zagreb city and it was published in the photo exhibition brochure. The field trip was organized to the Kostanjek Landslide Observatory for Landslide Monitoring, observatory of the biggest landslide in Republic of Croatia, equipped within the Croatian-Japanese Project "Risk Identification and Land-Use Planning for Disaster Mitigation of Landslides and Floods in Croatia".

The importance of the 1st ReSyLAB for development of landslide science and regional cooperation was recognized by all ICL ABN members at the round table in Zagreb "Discussion and Endorsement in the Course of the ICL Adriatic-Balkan Network Activities" and it was adopted that organization of biannual Symposiums will be the most important chain in the maintaining ICL Adriatic–Balkan Network' activities. The 1st ReSyLAB was followed by next four Symposiums held in Belgrade, Serbia, 2015; Ljubljana, Slovenia, 2017; Sarajevo, Bosnia and Herzegovina, 2019; and the last one in Rijeka, Croatia in March 2022.

The 2nd Regional Symposiums on Landslides in Adriatic-Balkan Region, was held in Belgrade, Serbia, in May 2015, organized by University of Belgrade, Faculty Mining and Geology, Serbia. The Symposium attended more than 80 participants from 13 countries (Albania, Bosnia and Herzegovina, Croatia, Germany, Greece, Italy, Japan, Macedonia, Montenegro, Romania, Russia, Serbia, Slovenia, Switzerland) and presented 49 scientific and professional papers in Symposium sessions related recent case histories, theoretical advances, laboratory and field-testing and design methods beneficial to practitioners, researchers and other professionals. All reviewed papers were published in Symposium Proceedings (Fig. 3) (Abolmasov et al. 2017). The Symposium also included five invited lectures presented by Leonardo Cascini (Italy), Michael Krautblatter

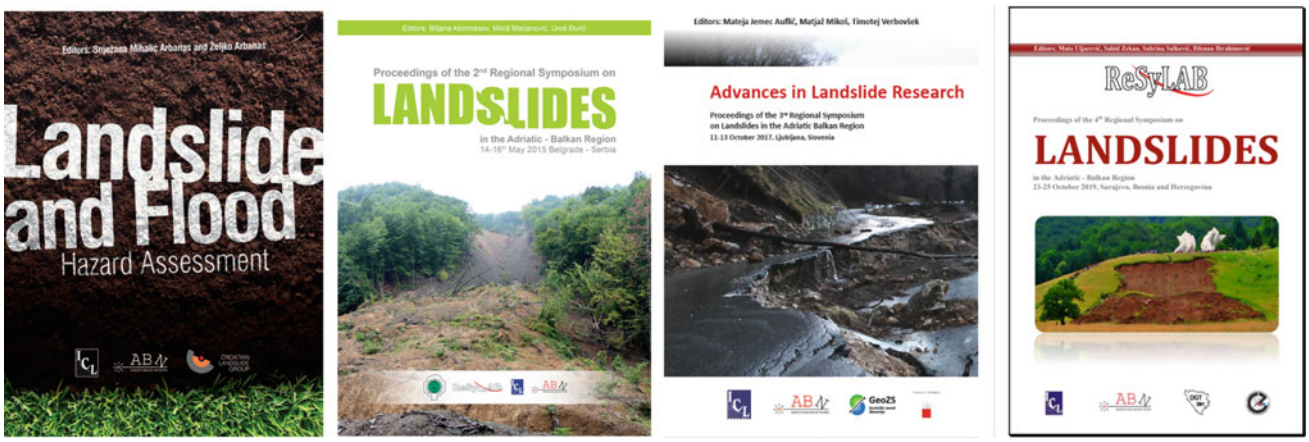

Fig. 3 Cover pages of the Proceedings of the Regional Symposiums on Landslides in Adriatic-Balkan Region: Zagreb (2013), Belgrade (2015), Ljubljana (2017) and Sarajevo (2019)

(Germany), Kyoji Sassa (Japan), Marinos Skempas (Greece) and Janusz Wasowski (Italy). The Symposium technical sessions were accompanied by field trip to the Umka Landslide near Belgrade.

The 3rd Regional Symposiums on Landslides in Adriatic-Balkan Region entitled "Advances in Landslide Research" was held in Ljubljana, Slovenia, in October 2017, organized by Geological Survey of Slovenia and University of Ljubljana, Faculty of Civil and Geodetic Engineering and Faculty of Natural Sciences and Engineering (Jemec Auflič et al. 2017a, b). The Symposium attended 70 participants from 9 countries (Austria, Bosnia and Herzegovina, Croatia, Czech Republic, Italy, Macedonia, Serbia, Slovenia, Spain) and presented 30 scientific and professional papers about landslides disaster risk factors and scenarios, including emerging disaster risks, in the medium and long term; enhance research for local, regional, national applications; support actions by local communities and authorities; and support decision-making with interaction between policy makers and the scientific community. (Jemec Auflič et al. 2018). All reviewed papers (25) were published in Symposium Proceedings (Fig. 3) (Jemec Auflič et al. 2017a, b). The Symposium also included three invited lectures presented by Veronica Tofani (Italy), Lisa Borgatti (Italy) and Miloš Bavec (Slovenia). The Symposium technical sessions were accompanied with round table, photo exhibition and field trips. The round table entitled: "Enhancing cooperation between the landslide science community and end users" moderated by Professor Matjaž Mikoš, Head of the UNESCO Chair on Water-related Disaster Risk Reduction, Faculty of Civil and Geodetic Engineering, University of Ljubljana, Slovenia, covers the topics related to: (1) Disaster risk factors and scenarios, including emerging disaster risks, in the medium and long term; (2) Enhance research for local, regional, national applications; (3) Support actions by local communities and authorities; and (4) Support decision-making with interaction between policy makers and the scientific community. The photo exhibition was organized as a selection of 24 photos from the WLF4 Landslide Photo Contest "Landslides and Mankind" and was exhibited at the Faculty of Civil and Geodetic Engineering of the University of Ljubljana. The field trips were organized to landslides in the Vipava Valley and Potoška planina landslide.

The 4th Regional Symposiums on Landslides in Adriatic-Balkan Region was held in Sarajevo, Bosnia and Herzegovina, in October 2019, organized by Geotechnical Society of Bosnia and Herzegovina, Federal Institute for Geology, Bosnia and Herzegovina and Republic Survey for Geological Researches of the Republic of Srpska (Uljarević et al. 2019a). The Symposium attended about 100 participants from 14 countries (Albania, Austria, Bosnia and Herzegovina, Bulgaria, Croatia, Czech Republic, Italy, Japan, Serbia, Slovenia, Spain, Switzerland, Turkey, Ukraine) and presented 41 scientific and professional papers about landslides mapping, investigation, monitoring and mitigation as well as impact to the environment and living. All reviewed papers (41) were published in Symposium Proceedings (Fig. 3) (Uljarević et al. 2019b). The Symposium included five invited lectures presented by Norikauzu Shimizu (Japan), Charles Wang Wang (Hong Kong), Alessandro Corsini (Italy), Željko Arbanas (Croatia) and Marina Vivoda Prodan (Croatia). The Symposium technical sessions were accompanied with round table discussion and field trips. The round table entitled: "Enhancing cooperation between the landslide scientist and stakeholders from public bodies dealing with policies or decision making" moderated by Professor Snježana Mihalić Arbanas, Faculty of Mining, Geology and Petroleum Engineering, University of Zagreb, Croatia, dealing with the existing experiences in cooperation of landslide scientists and stakeholders at local, regional and state levels in landslide risk reduction. The field trip was organized to landslide in the Memorial complex Tjentište inside the Sutjeska National Park, as well as landslides Bogatići and Čemerno located nearby to the route to the Sutjeska National Park.

4 5th Regional Symposium on Landslides in Adriatic-Balkan Region, Rijeka

The last 5th Regional Symposium in Adriatic-Balkan Region, was held in Rijeka, Croatia, in March 2022 (Fig. 4). Previously provided for October 2021, because of Covid-19 pandemic conditions, the Symposium was postponed to March 2022, but existing conditions forced the organizer to prepare Symposium as hybrid conference enabling participants to participate on site or online via Zoom platform. Current pandemic conditions surely affected the reduced interest to Symposium contribution, but, as one of the first landslide conferences that enable online presentation after relaxation of pandemic restrictions, significant number of landslide scientist from the region gathered the Symposium in Rijeka.

The 5th Regional Symposiums on Landslides in Adriatic-Balkan Region, held in Rijeka, Croatia, in March 2022, entitled "Landslide Modelling & Applications" was organized by Croatian Landslide Group at the Faculty of Civil Engineering University of Rijeka. The chairs of the Symposium were Željko Arbanas, University of Rijeka, Faculty of Civil Engineering and Snježana Mihalić Arbanas, University of Zagreb, Faculty of Mining, Geology and Petroleum Engineering. The Symposium attended about 85 participants on site and online from 13 countries (Albania, Austria, Bosnia and Herzegovina, Croatia, Greece, Italy, Mexico, Montenegro, North Macedonia, Russia, Serbia, Slovenia, Switzerland, USA) and presented 46 scientific and

Fig. 4 Poster of the 5th ReSyLAB held in Rijeka Croatia in March 2022

professional papers in oral (30) and poster (16) presentations. In total 41 reviewed papers were published in Symposium Proceedings (Peranić et al. 2022). The main Sessions of the Symposium where Landslide Monitoring (6 papers), Landslide Mapping (2 papers), Landslide Susceptibility (6 papers), Laboratory Testing, Physical and Numerical Modelling of Landslides (9 papers), Landslide Case Studies (3 papers) and Landslide Investigation (4 papers) (Peranić et al. 2022). The most of contributions came from Croatia (12 papers), Italy (11 papers) and Slovenia (9 papers).

Five invited lectures were presented within Symposium sessions: Nicola Casagli (Italy): The International Consortium on Landslides for disaster risk reduction and sustainable development; Michel Jaboyedoff (Switzerland): Failure hazard of rockfall sources: some aspects of the hazard quantification; Binod Tiwari (USA): Physical Modeling of Landslides and Slopes—Advancements and Challenges; Snježana Mihalić Arbanas (Croatia): Landslide evidence and spatial prediction: Application of data and information from landslide maps; Nejc Bezak (Slovenia): Rainfall-induced

Fig. 5 Cover pages of the 5th Regional Symposiums on Landslides in Adriatic-Balkan Region publications; from left to right: Book of Abstracts; Proceedings; Workshop on Landslide Physical and Numerical Modelling and Field Trip. All publications are available at the Symposium web page: https://5resylab.uniri.hr/

landslides and debris flows under the influence of climate change: review of recent Slovenian studies.

The Symposium technical sessions were accompanied by series of side events: workshop on landslide physical and numerical modelling, photo exhibition, round table discussion and post symposium field trip to the Grohovo Landslide and Brus Landslide. All Symposium activates were followed by adequate publications, Fig. 5. All publications are available at the Symposium web page: https://5resylab.uniri.hr/.

4.1 Workshop on Landslide Physical and Numerical Modelling

The aim of the Workshop on Landslide Physical and Numerical Modelling was to provide new insights in the behavior of landslides obtained through the research of small scale landslide models at 1g conditions. The more widespread view into available measuring methodologies and techniques leads to further development in the field of physical modelling, especially in the domain of 1g physical models. By sharing the scientific ideas and creative approaches, idea was to provide useful information and insights to the landslide community and facilitate the development of new technologies and methods. This Workshop is organized in the frame of the Project IP-2018-01-1503 "Physical modelling of landslide remediation constructions behavior under static and seismic actions (ModLandRemSS)" and supported by Croatian Science Foundation.

Within the Workshop four presentations were presented: Josip Peranić (Croatia): Small-scale physical landslide models under 1g infiltration conditions and the role of hydrological monitoring; Nina Čeh (Croatia): Digital image correlation and the use of high-speed cameras for 3D displacement monitoring in 1g small-scale physical models of landslides; Giovanna Capparelli (Italy): Physical modelling investigation and integrated analysis of landslides for defining risk scenarios; and Sabatino Cuomo (Italy): Numerical simulations of landslide physical model experimental results. The Workshop was held as a hybrid event with contribution of about 30 participants on site and online.

As a part of the Workshop, a laboratory test at small scale slope physical model was conducted presenting to the Workshop auditorium behavior of the sandy-clayey slope supported by gabion gravity wall exposed to impact of prolonged artificial rainfall, Fig. 6.

4.2 Photo Exhibition "Take a Look at the Landslide"

The photo exhibition "Take a look at the Landslide" presented 28 photos of landslides and was exhibited at The Faculty of Civil Engineering University of Rijeka and it was published in the photo exhibition brochure (Fig. 7). The exhibition presents 28 photos taken by 14 photographers from Croatia and Slovenia.

Every photo is accompanied by a short landslide story. Photo exhibition jury selected the best three photos as follows: 1st prize—Martin Krkač for the photo "Green Landslide" taken in Croatia (Fig. 8); 2nd prize—Martina Vivoda Prodan for the photo "Istrian Desert: Mučan Badland" taken in Istria, Croatia, 3rd prize—Martina Vivoda Prodan for photo "Supporting the landslide" taken in Italy, presenting the part of Corvara Landslide in Badia region, Italy.

Fig. 6 Photo of small-scale model of a slope supported by gabion gravity wall exposed to impact of prolonged artificial rainfall

4.3 Round Table "State of the Art of Landslide Susceptibility Modelling: Application in Adriatic-Balkan Region"

Following the World Landslide Forum 5 (WLF5), Paola Reichenbach and Snježana Mihalić Arbanas, coordinators of the WLF5 Theme 2 "From Mapping to Hazard and Risk Zonation" have organized Round Table with the objective to discuss, between participants of the 5th Regional Symposium on Landslides, good practice on landslide susceptibility modelling and zonation. The topic was applications of landslide susceptibility modelling in countries in the Adriatic-Balkan Region (Croatia, Serbia, Slovenia, North Macedonia, Bosnia and Herzegovina). The Round Table was organized as a hybrid event, starting with three introductory speeches that preceded the discussion of all participants.

Introductory speeches were given by: Mauro Rossi, CNR-IRPI, Italy, "A review of statistical landslide susceptibility modelling"; Sanja Bernat Gazibara, UNIZG-RGNF, Croatia, "Geo-environmental information for landslide susceptibility modelling—Availability of data in Croatia"; Igor Peshevski, SS. Cyril and Methodius University in Skopje, North Macedonia, "Preliminary regional landslide susceptibility assessment using limited data".

The Round Table participants were three world-leading landslide scientists from Italy (Paola Reichenbach and Mauro Rossi) and Switzerland (Professor Michel Jaboyedoff) and 14 landslide scientists from Adriatic-Balkan Countries (Bosnia and Herzegovina, Croatia, Serbia, Slovenia, N. Macedonia, Montenegro). The following institutions were represented at the Round Table: CNR/IRPI, Italy; Institute of Earth Sciences, University of Lausanne, Lausanne, Switzerland; Faculty of Mining, Geology and Petroleum Engineering, University of Zagreb, Croatia; Faculty of Mining and Geology, University of Belgrade, Belgrade; Geological Information Centre, Geological Survey of Slovenia, Ljubljana, Slovenia; Faculty of Natural Sciences and Engineering, University of Ljubljana, Ljubljana, Slovenia; Faculty of Civil Engineering, University SS Cyril and Methodius, Skopje, North Macedonia; Faculty of Mining, Geology and Civil Engineering, University of Tuzla, Tuzla. BIH. The discussion of the Round Table followed the following discussion themes:

Fig. 7 Cover page of the Photo Exhibition brochure "Take a look at the Landslide"

- Recommendations on landslide susceptibility zonation (landslide types, sources of landslide information, sources of geo-environmental information, mapping units and model types, model performance evaluation, use of landslide susceptibility);
- Data and modelling scale and possible applications;
- Future challenges in the Adriatic-Balkan Region;
- Possible contributions to World Landslide Forum 6, Florence, Italy.

5 Conclusions

In this paper the establishment and activities of the Adriatic-Balkan Network (ABN) are presented. The ICL Adriatic-Balkan Network was established as one of eight thematic and regional networks of ICKL at the 10th Anniversary Meeting held in Kyoto, Japan, in January 2012. The Adriatic-Balkan Network was formally established

Fig. 8 The 1st prize Photo Exhibition—Martin Krkač for the photo "Green Landslide" taken in Croatia

during the 14th Serbian Symposium on Engineering Geology and Geotechnics in Belgrade in September 2012 when seven organizations, current members of ICL, signed the Letter of intent and Declaration of the regional cooperation and International Consortium on Landslides' Adriatic-Balkan Network constitution. The general objective of the ICL Adriatic–Balkan Network is advancing landslide science and its practical application in the region for the benefit of society and the environment. Specific objectives are: (i) set up scientific and legislative background for regional cooperation; (ii) regional unification of information about landslides and landslide research at national levels; and (iii) development of landslide science by capacity building at regional level and practical applications of outcomes to societies in the region.

In realization of planned activities the main advances were reached in the field of information and knowledge sharing through the regional Symposium on Landslides, but in other set activities modest results were achieved, mostly through small bilateral scientific projects (Croatia-Slovenia, Slovenia-Serbia, Croatia-Serbia) and scientist exchange, but joint contribution in large European projects was absent. Cooperation was additionally reduced in the last three years, caused by Covid-19 pandemic conditions, and just the 5th ReSyLAB organization pointed out on to reviving existing relationships within the Adriatic-Balkan Network.

The 5th ReSyLAB pointed out on importance of regional cooperation in landslide risk reduction through sharing and exchange of knowledge and experience in the region with similar geohazards and risks as well as sharing information related to causes and consequences of landslide disasters caused by climate changes as those significantly impact on the rise of landslide occurrences in the region and over the world.

References

Abolmasov B, Marjanović M, Đurić U (2017) Proceedings of the 1st regional symposium on landslides in Adriatic-Balkan Region.

University of Belgrade, Faculty Mining and Geology, Belgrade, 255p. ISBN: 978-86-7352-296-8

Arbanas Ž, Mihalić Arbanas S, Vivoda M, Martinović K, Bernat S (2014) Landslide knowledge exchange through the regional cooperation in the Adriatic-Balkan Region. In: Sassa K, Canuti P, Yin Y (eds) Landslide science for a safer geoenvironment. Springer, Cham, pp 199–205

Jemec Auflič M, Verbovšek T, Mikoš M (2017a) 3rd Regional Symposium on Landslides in the Adriatic-Balkan Region-Ljubljana, Slovenia. Landslides 14:1855–1856. https://doi.org/10.1007/s10346-017-0863-2

Jemec Auflič M, Mikoš M, Verbovšek T (2017b) Advances in landslide research. Proceedings of the 3rd regional symposium on landslides in the Adriatic Balkan Region, 11–13 Oct 2017, Ljubljana, Slovenia. Geological Survey of Slovenia, Ljubljana, 156 p. ISBN: 978-961-6498-58-6

Jemec Auflič M, Mikoš M, Verbovšek T, Mihalić Arbanas S, Arbanas Ž (2018) 3rd Regional Symposium on Landslides in the Adriatic-Balkan Region (3rd ReSyLAB)—a final report. Landslides 15:381–384. https://doi.org/10.1007/s10346-017-0934-4

Mihalić Arbanas S, Arbanas Ž, Abolmasov B, Mikoš M, Komac M (2012a) Regional cooperation in the frame of the ICL Adriatic-Balkan network. In: Sunarić D, Jevremović D (eds) Proceedings of 14th symposium on engineering geology and geotechnics, 27–28 Sept 2012, Belgrade, Serbia. Društvo geoloških inženjera i tehničara Srbije, Belgrade, pp 43–56

Mihalić Arbanas S, Arbanas Ž, Abolmasov B et al (2013) The ICL Adriatic-Balkan Network: analysis of current state and planned activities. Landslides 10:103–109. https://doi.org/10.1007/s10346-012-0364-2

Mihalić Arbanas S, Arbanas Ž (2014) Landslide and flood hazard assessment. Proceedings of the 1st regional symposium on landslides in Adriatic-Balkan Region with the 3rd workshop of the Croatian–Japanese project risk identification and land-use planning for disaster mitigation of landslides and floods in Croatia. Croatian Landslide Group Zagreb, 268p. ISBN: 978-953-7479-28-2

Mihalić S, Arbanas Ž (2012) The Croatian–Japanese Joint Research Project on Landslides: activities and public benefits. In: Sassa K, Rouhban B, Briceno S, He B (eds) Landslides: global risk preparedness. Springer, Berlin, Heidelberg, pp 345–361. ISBN: 978-3642220869

Mihalić S, Arbanas Ž, Mikoš M, Abolmasov B (2012) The ICL Adriatic-Balkan Network: scientific background, opportunities and challenges for regional cooperation. In: Sassa K, Takara K, He B (eds) Proceedings of IPL symposium, 20 Jan 2012, Kyoto, Japan. ICL, Kyoto, pp 27–37

Peranić J, Vivoda Prodan M, Bernat Gazibara S, Krkač M, Mihalić Arbanas S, Arbanas Ž (2022) Landslide modelling and applications. Proceedings of the 5th regional symposium on landslides in Adriatic-Balkan Region. Croatian Landslide Group Zagreb, 257 p. ISBN: 978-953-6953-55-4

Sassa K (2006a) "2006 Tokyo Action Plan"—strengthening research and learning on landslides and related earth system disasters for global risk preparedness. Landslides 3:361–369. https://doi.org/10.1007/s10346-006-0065-9

Sassa K (2006b) ICL strategic plan 2012–2021—to create a safer geo-environment. Landslides 9:155–164. https://doi.org/10.1007/s10346-012-0334-8

Uljarević M, Zekan S, Salković S (2019a) 4th Regional Symposium on Landslides in the Adriatic-Balkan Region-Sarajevo, Bosnia and Herzegovina. Landslides 16:1821–1822. https://doi.org/10.1007/s10346-019-01227-2

Uljarević M, Zekan S, Salković S, Ibrahimović D (2019b) Proceedings of the 4th regional symposium on landslides in Adriatic-Balkan Region. Geotechnical Society of Bosnia and Herzegovina, Sarajevo, 255 p

Coseismic Stress Changes, Landslides in the 2004 Mid-Niigata Prefecture Earthquake, and Their Impact on Post-quake Rehabilitations

Kazuo Konagai

Abstract

The impact of a large inland earthquake is profound because of its intense shakes and the associated landslides and debris flows. The quake-induced landslides and debris flow are often the most devastating secondary effect of an earthquake in terms of all kinds of losses, causing long-lasting problems in post-quake rehabilitation activities. An earthquake-induced landslide is just one scene of ever-evolving mountain topography. Therefore, studying terrain dynamics is vital to comprehend the possibility of hazards and propose and apply rational rehabilitation tactics. Though serious, the damage caused by the Mid-Niigata Prefecture Earthquake of October 23, 2004, has given us a rare opportunity to study the landform changes caused by an earthquake that hit an active-folding mountainous terrain. To deal with rehabilitation problems in a scientific manner, a research program, "Earthquake damage in active-folding areas: the creation of a comprehensive data archive and suggestions for its application to remedial measures for civil-infrastructure systems," was set up getting the Special Coordination Funds for Promoting Science and Technology, Ministry of Education, Culture, Sports, Science and Technology (MEXT). This article reviews some significant findings obtained through this project and even beyond it. The results show that essential aspects of quake-caused problems were linked to deep-seated tectonic displacements, namely the internal driving stress field associated with earthquakes to evolve the active-folding terrain.

Keywords

Quake-induced landslides • Active folding • The 2004 mid-Niigata Prefecture Earthquake

1 Introduction

In many earthquakes, landslides have often been responsible for more damage to lifelines than other seismic hazards combined. In the 2016 Kumamoto Earthquake, Kyushu, Japan, about 750 locations along conventional railway lines reportedly suffered severe damage, of which 73% were caused by landslides, debris flows, rockfalls, etc. (Kyushu Railway Company, 2017). All are beyond the direct jurisdiction of lifeline management organizations. Kobayashi (1981) reported that more than half of deaths in earthquakes with magnitudes larger than 6.9 in Japan between 1964 and 1980 were caused by landslides.

An earthquake-induced landslide is just one scene of ever-evolving mountain topography. The fact indicates that there are always pros and cons to living in these areas. The cons are obviously landslide disasters, while the pros are geographical and hydrogeographic benefits the people have long been enjoying. Therefore, rehabilitation of lifelines and civil infrastructures in the landslide-devastated regions should not simply restore existing facilities but proceed with the build-back-better policy.

From this viewpoint, it pays to know rock fold dimensions associated with steadily evolving tectonic movements can often govern landslides' representative sizes and distributions in active folding zones.

To deal with rehabilitation problems in a scientific manner, a three-year research program (2005–2007), "Earthquake damage in active-folding areas: the creation of a comprehensive data archive and suggestions for its application to remedial measures for civil-infrastructure systems," was set up getting the Special Coordination Funds for

K. Konagai (✉)
International Consortium on Landslides, Secretariat, Kyoto, 606-8226, Japan
e-mail: konagai@iclhq.org

I. Alcántara-Ayala et al. (eds.), *Progress in Landslide Research and Technology, Volume 1 Issue 2, 2022*, Progress in Landslide Research and Technology,
https://doi.org/10.1007/978-3-031-18471-0_19

Promoting Science and Technology, Ministry of Education, Culture, Sports, Science and Technology, MEXT for short. This program was unique among various MEXT-funded research programs in that an advisory panel was set up under the Japan Society of Civil Engineers (JSCE Active folding Project, 2008). This framework allowed researchers and experts from authorities such as the Niigata prefectural government, Ministry of Land, Infrastructure, Transport and Tourism (MLIT), etc., to join. All members were concerned about rehabilitation affairs. The idea was to facilitate real-time research information sharing among relevant organizations for rational rehabilitations. This article reviews some notable findings obtained through this three-year research program and even beyond it.

2 The 2004 Mid-Niigata Prefecture Earthquake

The 2004 Mid-Niigata Prefecture Earthquake, also known as the "Chuetsu" Earthquake, occurred in Niigata Prefecture, Japan, at 17:56 local time (08:56 UTC) on Saturday, October 23, 2004 (Fig. 1). The hypocenter of the mainshock was located at 37.29° N, 138.87° E, in mid-Niigata Prefecture, at a depth of 13 km. The acceleration reached its maximum value of 1500 cm/s^2 at K-net Ojiya station, about 7 km west of the epicenter (Earthquake Research Institute (ERI), University of Tokyo, 2004). A series of strong aftershocks followed the mainshock in rapid succession. These strong earthquakes had focal mechanisms of reverse fault type with the compressional axes oriented in NW/SE direction. The orientation is consistent with the historical information of large earthquakes in this area.

This continual tectonic movement has formed NNE-SSW-trending geological folds of sedimentary rocks in the source region (Fig. 1). Up-folded rocks along anticlines expand and crack over a long geological time. Anticlines, thus, have often their crests deeply worn away. Consequently, many debris deposits rim the deeply eroded hollows called anticlinal valleys while down-folded synclines remain as ridges. Thus, the anticlinal valleys and the synclinal ridges often make up an inverted relief. However, the folding is still young, about 3 million years old or younger (Geological Survey of Japan (GSJ), 2007) in the quake-hit area, preserving remnants of the initial folding structure. Namely, a steep cliff or escarpment on one side and a gentle dip or back slope on the other feature the landform of this area; the landform is called "Cuesta." Thus, large-scale landslides occur even on gentle mountainsides dipping towards synclines. Therefore, the site is one of the most landslide-prone zones in Japan.

3 Tectonic Displacements

Interferometric Synthetic Aperture Radar (InSAR) is one of the most advanced technologies to measure elevation changes with high precision, and the RADARSAT-I satellite (C-band at 5.3 GHz) flew over the epicentral area at 20:45 (UTC). However, thick vegetation and thousands of landslides have severely blurred its InSAR fringe patterns in the epicentral area (Ozawa et al. 2005). Therefore, we have obtained precise digital terrain models (DTMs, hereafter) before (1975–1976) and after the earthquake (October 24, 2004) using stereoscopy and "Laser Imaging Detection and Ranging (LiDAR)" technology, respectively. The DTMs were then compared to detect elevation changes and translations of the topography. Lastly, all the changes in landforms due to landslides and artificial changes are removed to detect tectonic deformations of the ground surface, which can be useful in estimating the deformation of the whole mountains.

However, subtracting the pre-quake DTM from the post-quake DTM allows us to detect displacements only in the Eulerian description. Namely, the motion is described in terms of the spatial coordinates that do not follow the motion of soil particles. Discussions of earthquake-inflicted geotechnical issues require a more direct description of soil particle movements because soils are typically history-dependent materials. Konagai et al. (2009a) obtained three orthogonal components of tectonically induced surface displacement (tectonic displacement, hereafter) by assuming that the tectonic displacement varies gently in space. That is to say, three pixels of DTM arranged next to each other would undergo the same Lagrangian displacements because the DTM has a substantially high resolution of 2.0 × 2.0 m per pixel. Thus, the observed changes in elevation (Eulerian displacements) at three pixels arranged side by side could determine the three orthogonal components of the Lagrangian displacements common to these pixels. This calculation is repeatedly performed while moving over the target terrain to obtain all Lagrangian displacements. The method later underwent major upgrades by Zhao (2010) and Zhao and Konagai (2014) in a manner that detected tectonic displacements better conform to the measured displacements at triangulation points on the intact ground in the earthquake-hit area.

However, the obtained Lagrangian displacement components often show a remarkable scatter. The causes of the scatter are:

(1) Quake-induced landslides,
(2) Artificial terrain changes during the time between the two DTMs, and
(3) the presence of some non-surface objects on digital surface models.

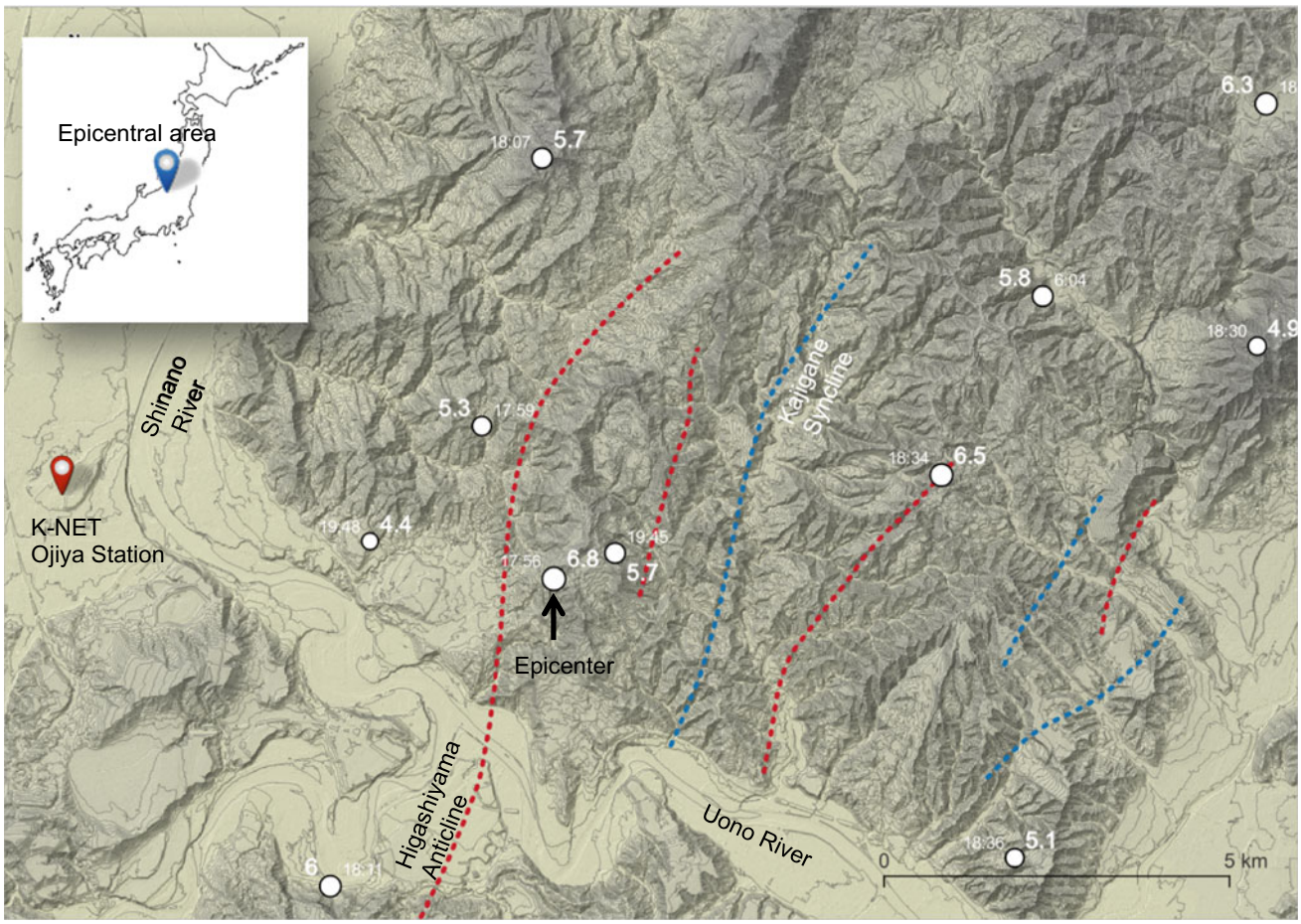

Fig. 1 Epicentral area of the Mid-Niigata Prefecture Earthquake of October 23, 2004: the earthquake of magnitude 6.8 was followed by many aftershocks (open circles in the figure), with four of magnitude 6 or greater in rapid succession (M6.3 at 18:03 JST, M6.0 at 18:11 JST, and M6.5 at 18:34 JST), resulting from complex multi-segment fault geometry (Hikima and Koketsu 2005). The earthquake hit the active-folding area with anticlines (red broken lines) and synclines (blue broken lines) trending in an NNE-SSW direction. Both Shinano and Uono Rivers flowing through the area meander remarkably, controlled by the folding structure

The spatial frequencies resulting from the causes mentioned above are remarkably higher than the tectonic displacement. Thus, the moving average method allows us to see the overall features of tectonic displacements. Assuming that the scattered values follow the Gaussian distribution within a square window, the most frequent value (mode) can represent the actual vector of the soil displacement in this area.

The size of the smoothing window has to be set based on its physical interpretation. The window size is desirable to be larger than the largest landslide in the target area to minimize the effect of the coherent landslide mass movements. At the same time, the size should not be too large to allow significant variation of the tectonic deformations within the smoothing window. The size of the square window was set at 1400 m by 1400 m for smoothing both vertical and lateral components of Lagrangian displacements in the quake-hit area.

Figure 2 shows the lateral components of surface tectonic displacements obtained through a 1400 m by 1400 m smoothing window. There are two clusters of large lateral displacements. Large displacement vectors reaching almost 0.5–1 m form a belt between the Kajigane syncline and the Higashiyama anticline in the southeastern cluster. The other cluster is northwest of the Higashiyama anticline. The former cluster along the Kajigane syncline is located around the surface extension of the hidden fault rupture planes for the mainshock and the largest aftershock of the Mid-Niigata Prefecture Earthquake (Hikima and Koketsu 2005).

Figure 3 shows the vertical components of surface tectonic displacements obtained through a 1400 m by 1400 m smoothing window. The vertical components show a hump in the southwestern part of the target zone. This hump is where the Uono River joins the Shinano River. Measurements of the benchmarks along the Uono River (Shinano River Office, Hokuriku Regional Bureau of the Ministry of

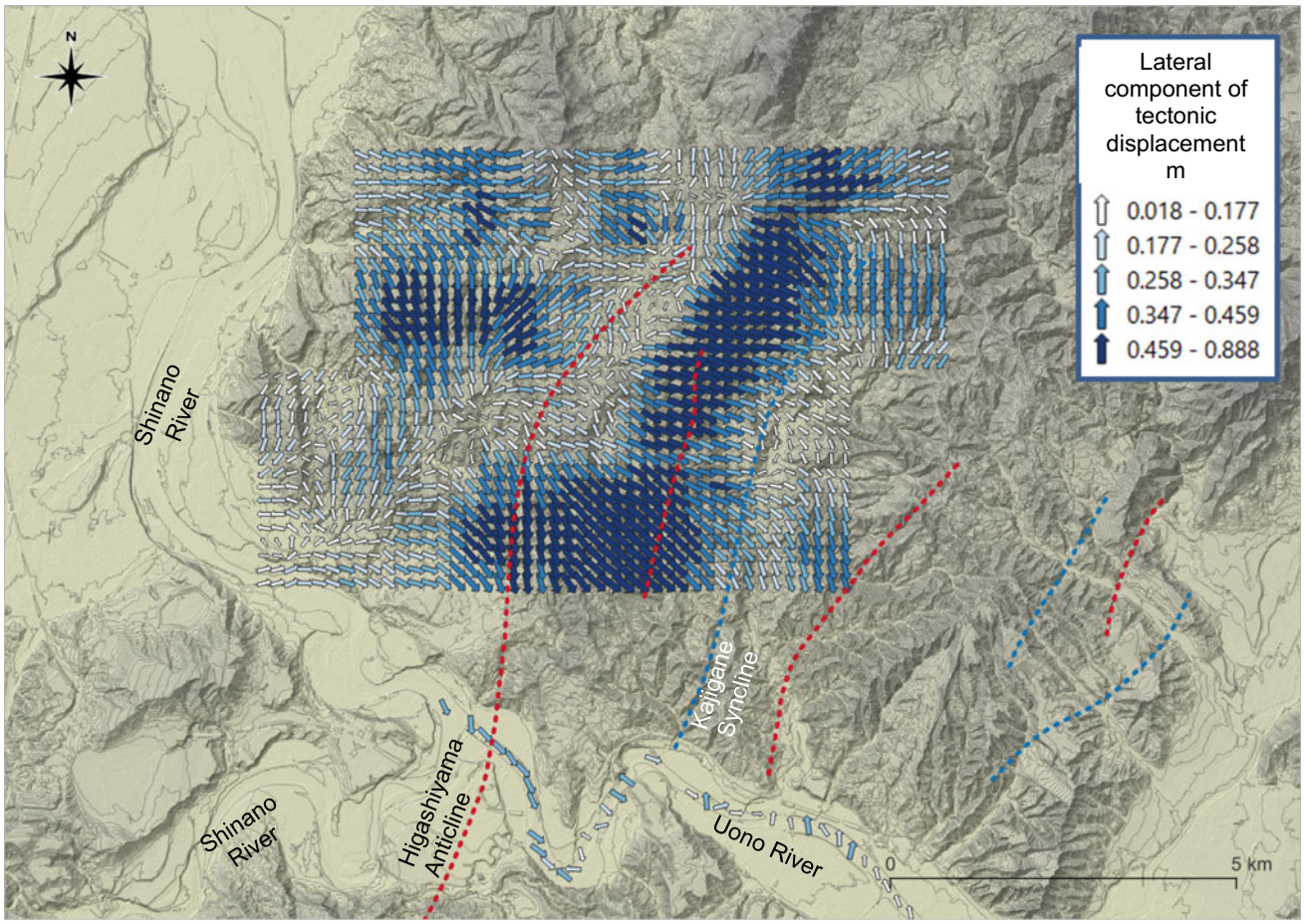

Fig. 2 Lateral components of surface tectonic displacement of the target zone on Zone VIII of the Japanese National Grid System. There are two clusters of large lateral displacements. Large displacement vectors reaching almost 0.5–1 m form a belt between the Kajigane syncline and the Higashiyama anticline in the southeastern cluster. The other cluster is northwest of the Higashiyama anticline

Land, Infrastructure, and Transport), marked in Fig. 3, have shown that the area downstream of the Kajigane syncline has moved up. There is a cause-and-effect relationship between these tectonic displacements and flooding along the Uono River during heavy rains of June 2005 and August 2011. Blue polygons in Fig. 3 are areas along the Uono River inundated in the flood of June 2005.

4 Underground Stress Field Associated with the Earthquake

Kazmi et al. (2013) further conducted an inversion analysis of the Lagrangian surface tectonic displacements to determine the spatial distribution of slips on fault rupture planes for known fault geometry, thus obtaining the co-seismic change in the stress field in the mountains (Kazmi et al. 2013). The fault geometry for this earthquake was complex such that three aftershocks with JMA magnitudes of 6.0 or greater occurred in rapid sequence. Hikima and Koketsu (2005) proposed a multi-segment fault model with five fault planes corresponding to the mainshock and the following four most significant aftershocks with magnitudes larger than 6 (Fig. 4). This fault model was adopted in this study. We need an appropriate kernel function for a half-space of stratified sedimentary rocks for the inversion analysis. Kazmi et al. (2013) used a robust and stable numerical scheme developed by Wang (Wang 1999; Wang et al. 2003). Material properties of each layer (material density, ρ, and two Lame's constants λ and μ) are determined from the representative velocity structure of the source region (shown in Fig. 5), obtained by combining borehole data logging, geological information, and seismic exploration (Honda et al. 2005).

Besides the earthquake-induced stress changes mentioned above, it is necessary to incorporate the initial rock stresses in the whole mountains before the earthquake, which is particularly important to discuss the impact of quake-induced ground deformation on underground facilities such as tunnels. With less probability of measuring directly complicated stress conditions before the earthquake,

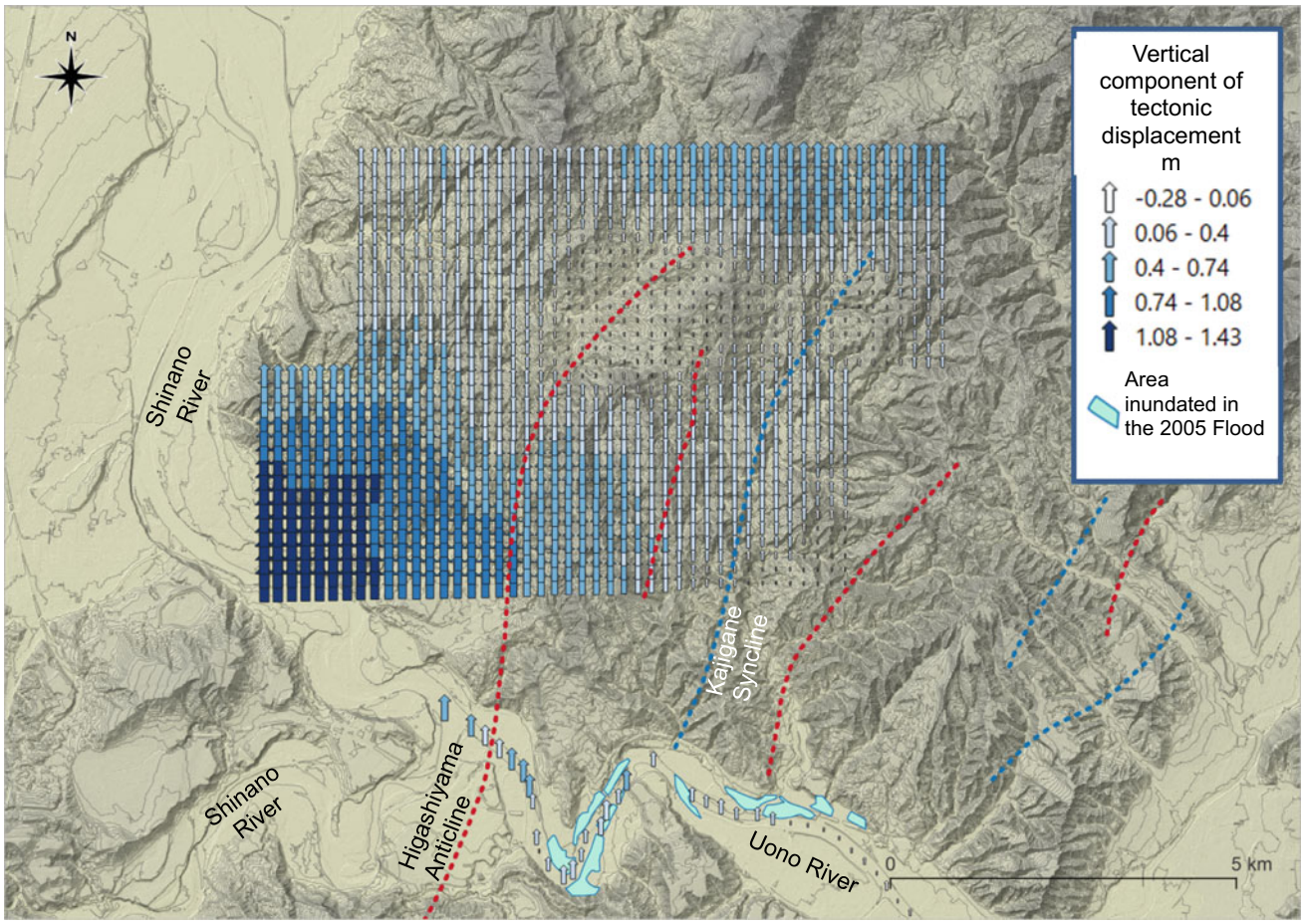

Fig. 3 Vertical components of surface tectonic displacement of the target zone on Zone VIII of the Japanese National Grid System. The vertical components show a hump exceeding 1 m in the southwestern part of the target zone. Since this hump is where the Uono River joins the Shinano River, the upper reach (blue polygons) of the Uono River was flooded in the torrential rain of June 28, 2005

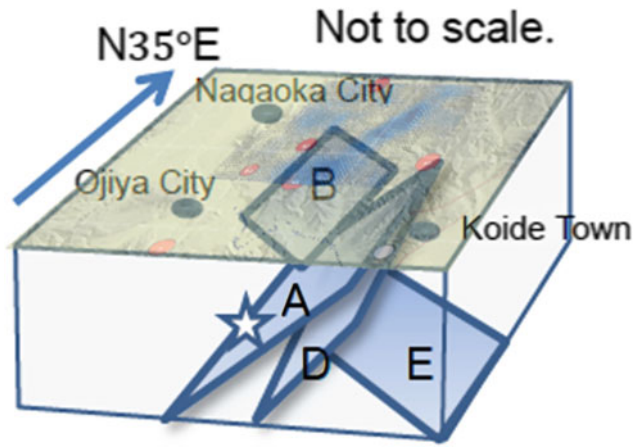

Fig. 4 Illustration of multi-segment fault model (not to scale) beneath the epicentral area of the 2004 Mid-Niigata Prefecture Earthquake (based on Hikima and Koketsu 2005). Segments A and D have caused the mainshock and the largest aftershock, respectively

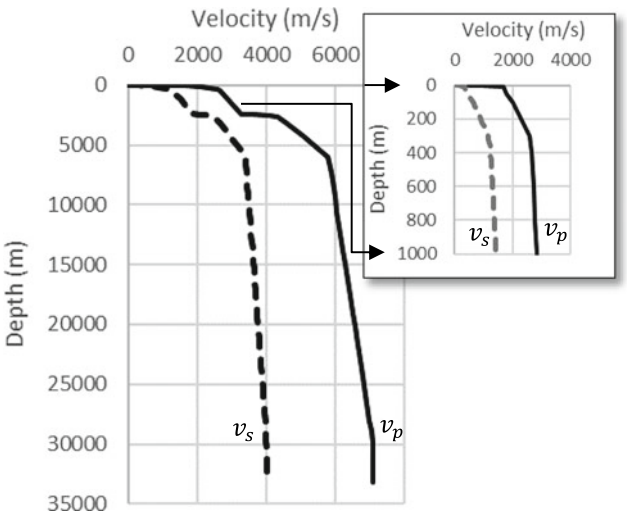

Fig. 5 Velocity structure model. v_p and v_s are the primary and secondary wave velocities, respectively (based on Honda et al. 2005)

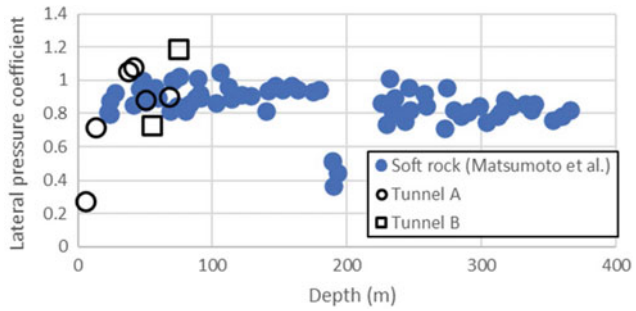

Fig. 6 Coefficient of lateral pressure calculated from ground displacement data. Tunnels A and B are two tunnels with available convergence data within the study area

coefficients of lateral rock pressure help estimate the stresses before the quake. We used some records of pre-quake tunneling through the epicentral area, and the records suggested that the coefficients are almost 1.0, excluding shallow locations near the tunnel mouses. This finding is consistent with what Matsumoto and Nishioka (1991) have shown for tunnels through sedimentary rocks excavated using the New Austrian Tunneling Method (NATM). The New Austrian Tunneling Method (NATM), which relies on the inherent strength of the surrounding rock mass, requires the installation of sophisticated measurement instrumentation. By virtue of this requirement, they could examine the measured convergence values of tunnel cross-sections in both the transverse and vertical directions. The coefficients of lateral rock pressure in soft rocks deeper than 50 m were about 0.9 to 1.0, with few exceptions (Fig. 6).

The square root of the second principal invariant of the deviatoric stress tensor, $\sqrt{J_2}$, can be considered as an index for rocks' and soils' deformability in the absence of reliable rock failure criterion and spatial coverage of soil/rock properties. The change in $\sqrt{J_2}$ values associated with the earthquake was calculated at 75 m below the ground surface; 75 m was the average depth of the tunnels of the Joetsu-Shinkansen, a high-speed railway line connecting Tokyo and Niigata. $\sqrt{J_2}$ values at this depth are also deemed to represent the internal driving stress field associated with earthquakes to evolve the active-folding terrain.

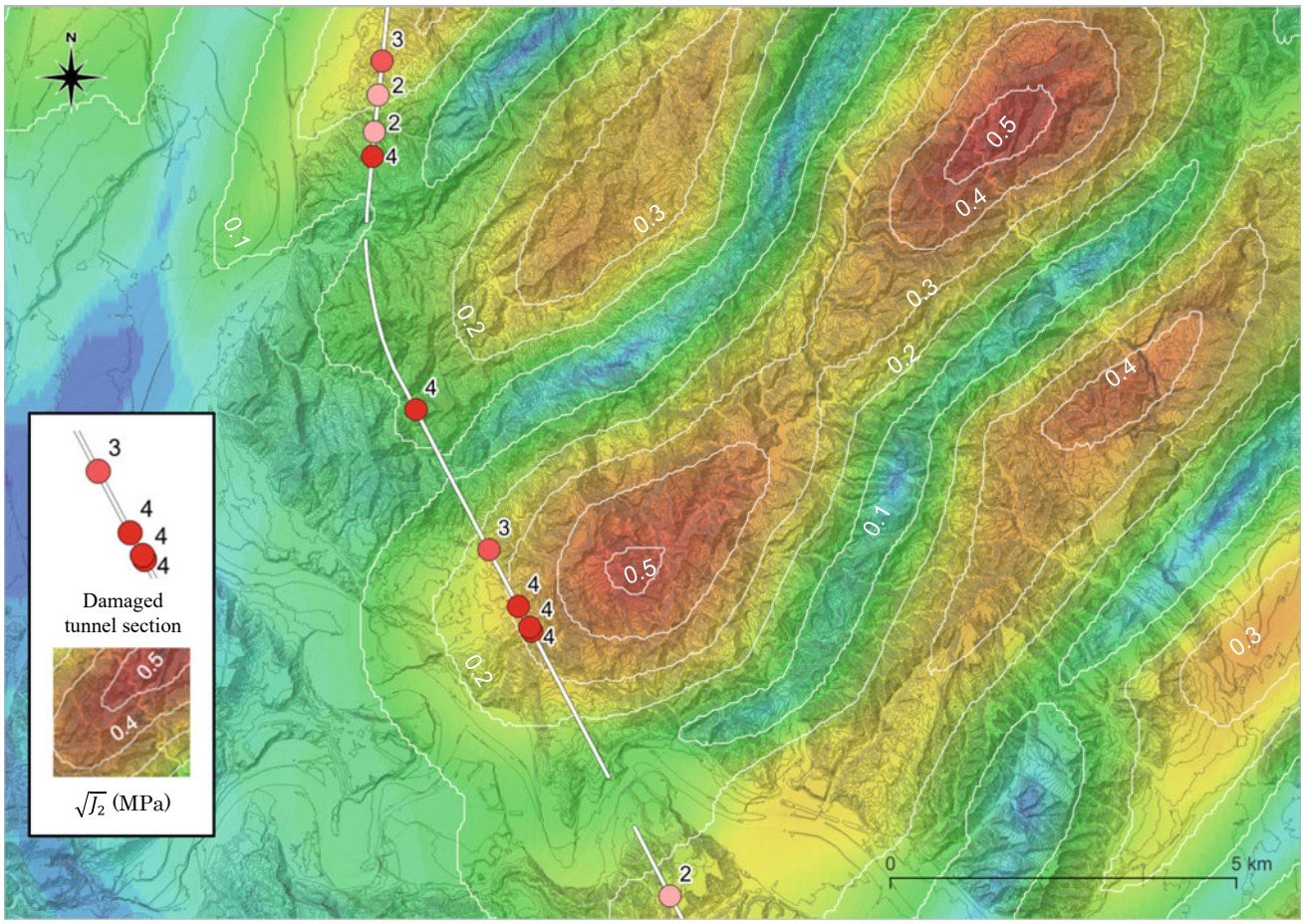

Fig. 7 Distribution of second principal invariant of the stress deviator tensor, $\sqrt{J_2}$, over the entire target zone at a depth of 75 m from the ground surface, with locations of damaged tunnel sections (based on Kazmi et al. 2013). East Japan Railway Company grouped the damaged sections into four categories based on their damage extents as shown in the legend, with a higher number indicating more severe damage

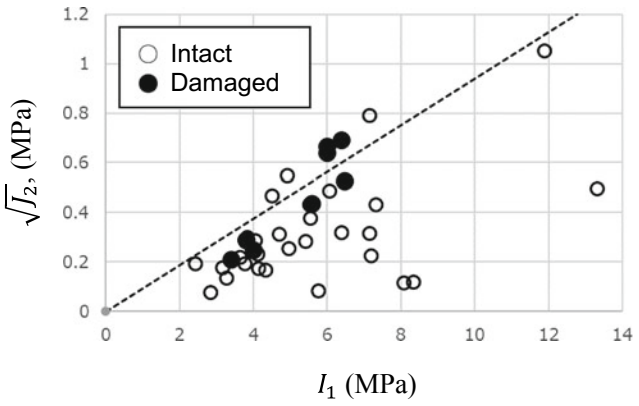

Fig. 8 Scatter diagram of I_1 and $\sqrt{J_2}$ along the tunnels (based on Kazmi et al. 2013)

Figure 7 shows the spatial distribution of $\sqrt{J_2}$. Remarkably, several stripes of large $\sqrt{J_2}$ values appear parallel at a regular interval of about 4 km, with each stripe trending in the NE–SW direction. This figure also shows the locations of damaged tunnel cross-sections. East Japan Railway Company grouped the damaged sections into four categories based on their damage extents, with a higher number indicating more severe damage (East Japan Railway Company 2006). Almost all damaged tunnel sections deeper than 40 m (colored circles in Fig. 7) are found within these stripes (Kazmi and Konagai 2018).

The first invariant of the Cauchy stress tensor I_1 and the square root of the second principal invariant of the stress deviator tensor $\sqrt{J_2}$ were calculated at a regular interval for each tunnel. The examined points included the damaged sections. Assuming that the lateral pressure coefficient before the earthquake was unity as suggested above in Fig. 6, the initial confining pressure was set at its overburden pressure at each point. When the values of I_1 and $\sqrt{J_2}$ are plotted on a scatter diagram (Fig. 8), points for the damaged sections (solid circles in Fig. 8) are found clustered along the upper bound of the entire cluster of points. This upper bound

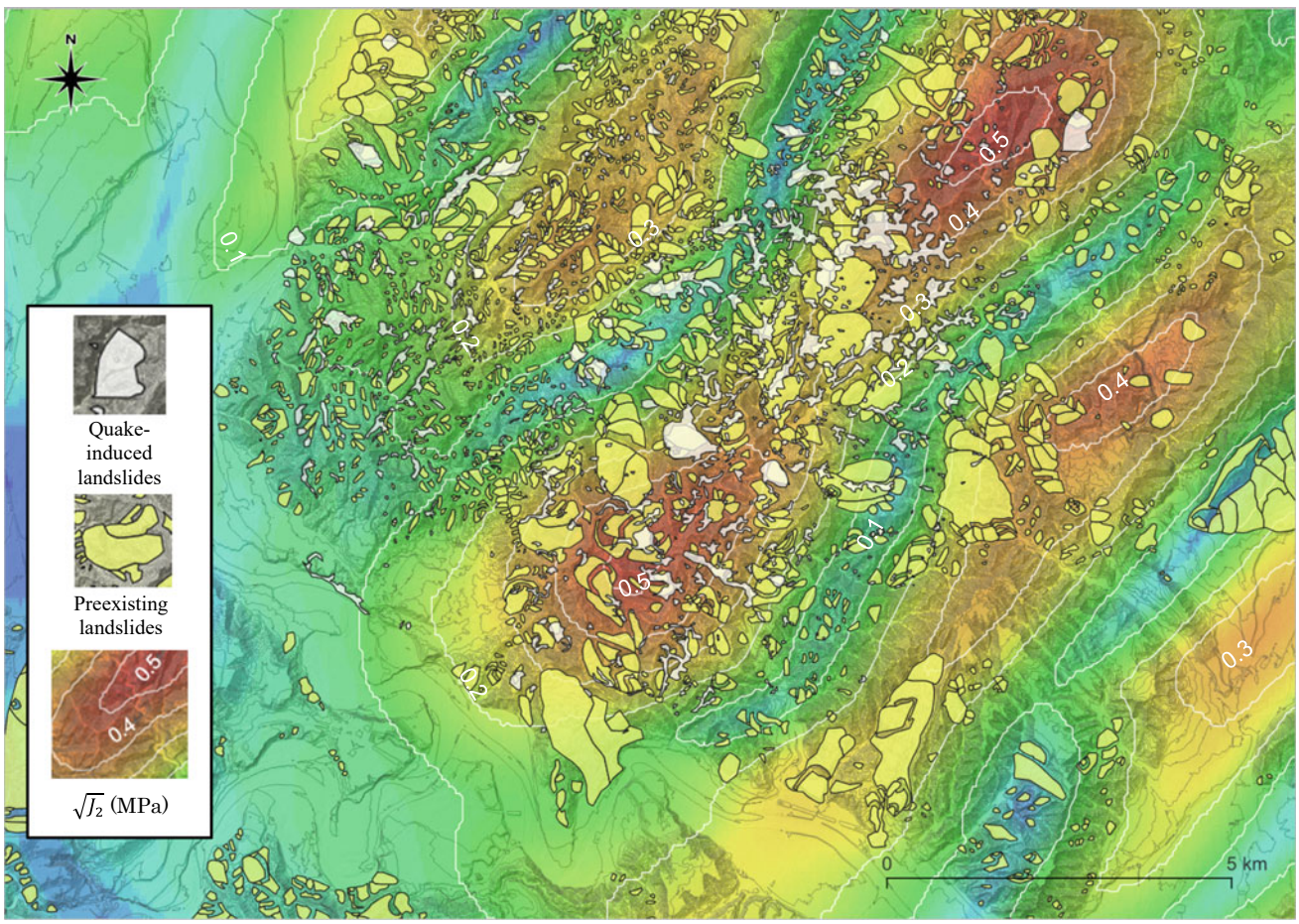

Fig. 9 Distribution of second principal invariant of the stress deviator tensor, $\sqrt{J_2}$, over the entire target zone at a depth of 75 m from the ground surface, with locations of quake-induced and preexisting landslides (based on National Research Institute for Earth Science and Disaster Prevention 2000; Kazmi and Konagai 2018)

line evokes the Drucker–Prager yield criterion. This line's gradient, 0.939, is relatively small for ordinary sedimentary rocks. Perhaps the value reflects the overall features of the sedimentary rocks with weak joints and cracks smeared over the whole domain (Kazmi and Konagai 2018).

Many landslides triggered by this earthquake appeared over these stripes of large $\sqrt{J_2}$ values (white polygons in Fig. 9). This stripes' pattern highlights the importance of the internal seismic stresses in causing and reactivating landslides. It is also noteworthy that all existing landslides identified as of 2000 (yellow polygons in Fig. 9, National Research Institute for Earth Science and Disaster Prevention 2000) form clearer clusters over the stripes of large $\sqrt{J_2}$ values. Figure 9 thus suggests that similar co-seismic events repeatedly occurred over a long geological time, causing the active folding terrain to evolve (Kazmi and Konagai 2018).

5 Landslide Masses Perching on the cuesta's Gentle Slopes

Many inhabitants in the quake-hit area depend upon rice and carp breeding for their livelihood, enjoying geographic and hydrogeographic benefits unique to this active-folding terrain. Figure 10 shows that ponds for irrigation and carp breeding are also found over the intense $\sqrt{J_2}$ stripes. Therefore, relocating inhabitants in the quake-hit area is not always the best course of action. As long as they continue living in this area, a map showing the spatial distribution of landslides that moved a little downslope in the earthquake and still perch on the cuesta's gentle slopes will help the inhabitants go along with these landslide masses.

As said above, the Lagrangian displacement components obtained from pre-and post-quake DTMs often show a

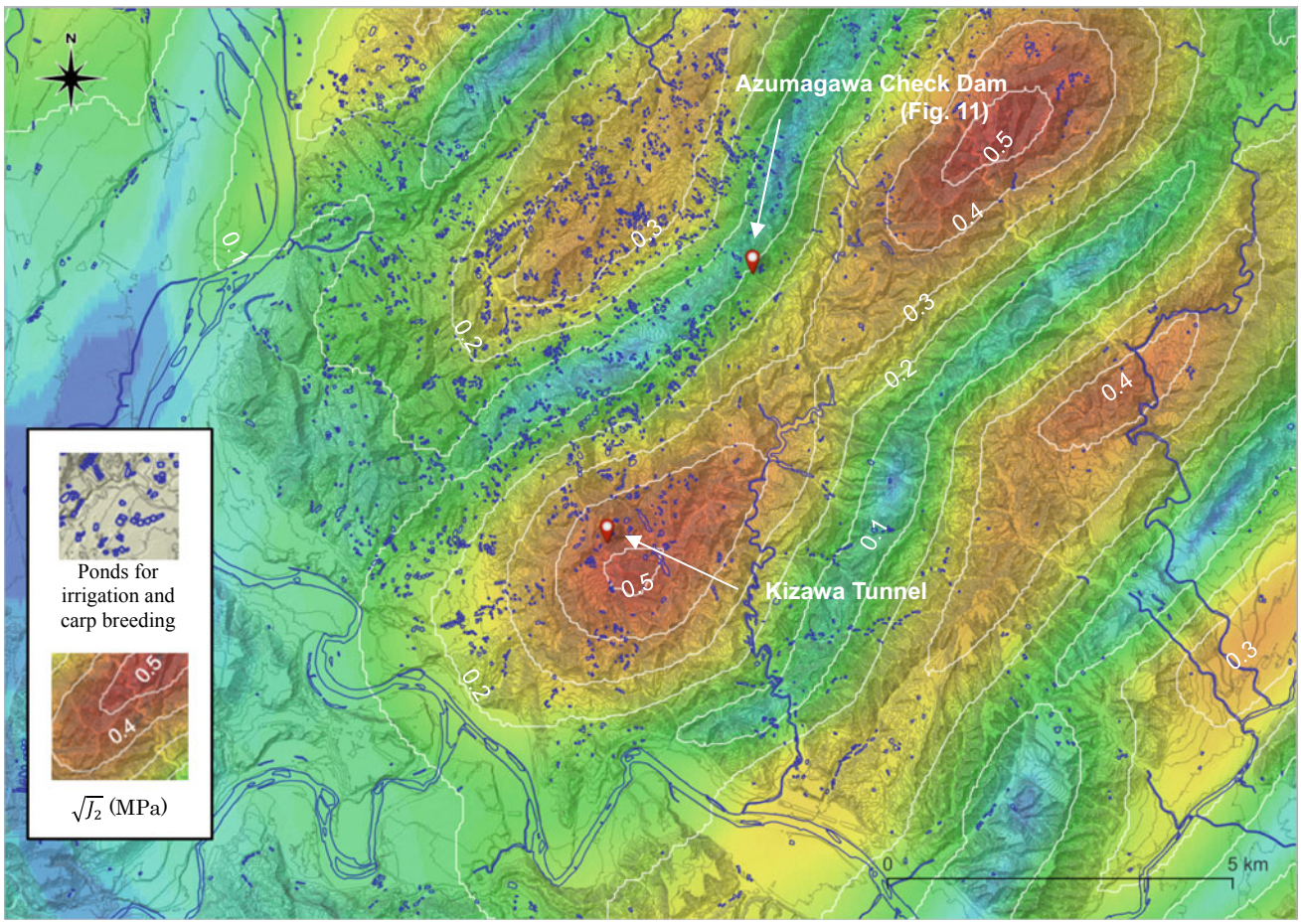

Fig. 10 Distribution of second principal invariant of the stress deviator tensor, $\sqrt{J_2}$, over the entire target zone at a depth of 75 m from the ground surface, with locations of ponds for irrigation and carp breeding. This figure also shows the locations of the north mouth of Kizawa Tunnel and Azumagawa Check Dam (see Fig. 11)

remarkable scatter, and a 1400 m by 1400 m smoothing window moved over the quake-hit area to filter out shallow disturbances such as landslides. We can filter out small-scale artificial terrain changes by reducing the smoothing window size as the next step. Then, by subtracting the once-obtained tectonic displacements from those extracted using the smaller window, we can detect shallower soil displacements caused by landslides. Sugawara et al. (2015) tuned the smaller window size so that the detected displacements better conform to the deformed alignment of the Kizawa Tunnel. Kizawa Tunnel is a shallow road tunnel going through a landslide mass that moved a little in the earthquake, causing the southern part of the tunnel embedded in the hidden landslide mass to move about a half meter in its transverse direction and expand by about 1.5 m (Konagai et al. 2009a, b; Zhao and Konagai 2014). Setting the window size at 200 m by 200 m, Sugawara et al. (2015) obtained displacements of hidden landslide masses, which moved a few meters downslope and are still perching on the quake-hit area's mountain slopes. Figure 11 shows detected downslope movement vectors around Azumagawa Check Dam. Many of these vectors are deemed to have appeared in the quake. But they can include those caused by the other causes because the pre-quake DTM was from aerial photos taken in 1975 and 1976. Some reports say that some mudflows covered paddy fields in Yamakoshi in the torrential rain in July 2004, about three months before the earthquake. In any case, Fig. 11 indicates that unstable soil masses are still perching on slopes in the quake-hit area, and they can move again anytime.

Azumagawa Check Dam was constructed to prevent Prefectural Route 24, one of the major arteries necessary to rehabilitate the quake-devastated area. The dam's construction started in March 2005, the following year of the earthquake, waiting for the thaw, and was completed in December 2006. Precast concrete blocks were stacked one after another to form the whole dam body. A dam photo taken on November 13, 2013 (Fig. 12) shows that the dam body turned slightly up. We first suspected that the downslope movement of the landslide mass on the western river wall may have pushed the dam against the eastern river wall. But comparing post-quake DTMs did not yield any

Fig. 11 Detected displacements of hidden landslide masses, which moved a few meters downslope and are still perching on the quake-hit area's mountain slopes (based on Sugawara et al. 2015)

Fig. 12 Azumagawa Check Dam at N 37.3300°, E 138.9021°. The center of the dam crest was 0.4–0.5 m higher than the abutments as of November 17, 2013

significant Lagrangian displacements of this landslide mass (Sugawara et al. 2015). According to the Yuzawa Sediment-Control Office, Ministry of Land, Infrastructure, Transport, and Tourism, the dam started to deform even during its construction period, probably because its abutments were immediately on the toe of the landslide mass. The toe was soft enough for heavy precast concrete blocks to sink. At any rate, it was wise to construct the check dam by stacking precast concrete blocks so that the whole dam body could conform to the ground deformation.

Given that there are still many landslide masses remaining on mountain slopes, the rehabilitation went forward following the steps shown below:

(1) Slipped major landslide masses were first stabilized, not allowing their toe parts to be eroded,
(2) Roads were then rerouted and reconstructed, avoiding remaining unstable soil masses, and finally,
(3) Houses, farmlands, and carp-breeding ponds were relocated to safer places or reconstructed at the same locations where stabilization works have been done.

6 Summary

Though serious, the damage caused by the Mid-Niigata Prefecture Earthquake of October 23, 2004, has given us a rare opportunity to study the landform changes caused by an earthquake that hit an active-folding mountainous terrain. This article reviewed some significant findings that have been obtained through a MEXT-funded research program, "Earthquake damage in active-folding areas: the creation of a comprehensive data archive and suggestions for its application to remedial measures for civil-infrastructure systems." The findings highlighted that the deep-seated tectonic displacements had something to do with unique features of damage caused by the earthquake.

The points to be highlighted are:

(1) The change in $\sqrt{J_2}$ values (square root of the second principal invariant of the deviatoric stress tensor) associated with the earthquake was calculated at 75 m below the ground surface (average depth of the Joetsu

Shinkansen Railway tunnels). $\sqrt{J_2}$ values deep in the ground can represent the internal driving stress field associated with earthquakes to evolve the active-folding terrain. Several stripes of large $\sqrt{J_2}$ values appear parallel at a regular interval of about 4 km, with each stripe trending in the NE–SW direction. Almost all damaged tunnel sections were found clustered within these parallel stripes.

(2) Many landslides triggered by this earthquake also appeared over these stripes of large $\sqrt{J_2}$ values.

(3) It is also noteworthy that all existing landslides identified as of 2000 (National Research Institute for Earth Science and Disaster Prevention 2000) form clearer clusters over the stripes of large $\sqrt{J_2}$ values. This finding suggests that similar co-seismic events repeatedly occurred over a long geological time, causing the active folding terrain to evolve.

(4) Displacements of landslides that moved a few meters downslope in the earthquake and are still perching on the cuesta's back slopes were extracted.

(5) Given the presence of these landslide masses, slipped major landslide masses were first stabilized, not allowing their toe parts to be eroded. Then rehabilitation works followed.

Acknowledgements This review article summarizes some of the outcomes of the Research and Development program for Resolving Critical Issues, "Earthquake damage in active-folding areas: the creation of a comprehensive data archive and suggestions for its application to remedial measures for civil-infrastructure systems," Special Coordination Funds for Promoting Science and Technology, Ministry of Education, Culture, Sports, Science, and Technology. The author would like to express his sincere thanks to all members of the project steering committee under the Japan Society for Civil Engineers as the project's core. Special thanks are firstly due to Dr. Takasuke Suzuki, not only for his general influence as a distinguished geologist and geo-morphologist but also for his willingness to support the program. Secondly, Mr. Keizan Murakami, Aero-Ahahi Co., has devoted much energy to preparing DTMs. The author is indebted to experts at the Nagaoka Regional Development Bureau, Niigata Prefectural Government, Kiso-Jiban Consultants Co. Ltd., Honma Corporation, and Hoshino Boring Co. They have kindly provided the authors with helpful information about the Kizawa locality and Kizawa Tunnel. The author is also grateful to Mr. Tomohiro Fujita, Public Works Research Institute, Dr. Yu Zhao, Professor, Zhejiang University, Ms. Yuriko Tomiyasu, Central Japan Railway Company, and Dr. Zaheer A. Kazmi, Assistant Professor, Imam Abdulrahman Bin Faisal University; they are all formerly students at the author's laboratory, and have devoted much of their energies to field surveys and analyzing DTMs.

References

Earthquake Research Institute (ERI), The University of Tokyo (2004) Special Event Page—the Mid Niigata prefecture earthquake in 2004. https://www.eri.u-tokyo.ac.jp/TOPICS_OLD/CHUETSU2004/index-e.html

East Japan Railway Company (2006) Commission report on the damaged railway tunnels in the 2004 Mid-Niigata-Prefecture earthquake. East Japan Railway Company

Geological Survey of Japan (2007) The geological background of the 2007 Chūetsu offshore earthquake. https://www.gsj.jp/hazards/earthquake/niigata2007/taisekibonchi.html

Hikima K, Koketsu K (2005) Rupture processes of the 2004 Chuetsu (mid-Niigata prefecture) earthquake, Japan: a series of events in a complex fault system. Geophys Res Lett 32L18303:5. https://doi.org/10.1029/2005GL023588

Honda R, Aoi S, Sekiguchi H, Kunugi T, Fujiwara H (2005) Ground motion and rupture process of the 2004 Mid Niigata Prefecture Earthquake obtained from strong motion data of K-net and KiK-net. Earth Planets Space 57:527–532. https://doi.org/10.1186/BF03352587

JSCE Active folding Project (2008) Earthquake damage in active-folding areas: creation of a comprehensive data archive and suggestions for its application to remedial measures for civil-infrastructure systems (2005–2007). Research and Development Program for Resolving Critical Issues, Special Coordination Funds for Promoting Science and Technology (Core research organization: JSCE, Leader: K. Konagai). https://www.jst.go.jp/shincho/database/pdf/20051260/2007/200512602007rr.pdf

Kazmi ZA, Konagai K, Sekiguchi K (2013) Extracting earthquake induced Lagrangian ground displacements and their implication for source inversion analysis. Soil Dyn Earthq Eng 48:98–208. https://doi.org/10.1016/j.soildyn.2013.01.022

Kazmi ZA, Konagai K (2018) Co-seismic stress changes and damage to tunnels in the 23 October 2004 Mid-Niigata Prefecture earthquake. Can Geotech J 55(5):736–748. https://doi.org/10.1139/cgj-2016-0658

Kobayashi Y (1981) Causes of fatalities in recent earthquakes in Japan. J Disaster Sci 3:15–22. https://www.jsnds.org/jnds/3_2_15.html

Konagai K, Fujita T, Ikeda T, Takatsu S (2009a) Tectonic deformation buildup in folded mountain terrains in the October 23, 2004, Mid-Niigata earthquake. Soil Dyn Earthq Eng 29(2):261–267. https://doi.org/10.1016/j.soildyn.2008.04.002

Konagai K, Takatsu S, Kanai T, Fujita T, Ikeda T, Johansson J (2009b) Kizawa tunnel cracked on 23 October 2004 Mid-Niigata earthquake: an example of earthquake-induced damage to tunnels in active-folding zones. Soil Dyn Earthq Eng 29(2):394–403. https://doi.org/10.1016/j.soildyn.2008.04.002

Kyushu Railway Company (2017) Damage to railways and the current progress of rehabilitation. First Anniversary Debriefing Session of the 2016 Kumamoto Earthquake, Japan Society of Civil Engineers. https://committees.jsce.or.jp/eec2/node/96

Matsumoto Y, Nishioka T (1991) Theoretical tunnel mechanics. University of Tokyo Press, Japan. ISBN: 4-13-068203-2, ISBN: 0-86008-482-5

National Research Institute for Earth Science and Disaster Prevention (2000) Landslide distribution maps (shapefiles). http://www.j-shis.bosai.go.jp/map/?lang=en

Ozawa T, Nishimura S, Wada Y et al (2005) Coseismic deformation of the Mid Niigata Prefecture Earthquake in 2004 detected by RADARSAT/InSAR. Earth Planet Space 57:423–428. https://doi.org/10.1186/BF03351828

Sugawara C, Fukuda K, Konagai K (2015) Detection of hidden landslides in the mountain terrain affected by the Mid-Niigata Earthquake of October 23rd, 2004. J Jpn Soc Civ Eng Ser. A1 (Struct Eng Earthq Eng (SE/EE)) 71(4):I_395–I_400. https://doi.org/10.2208/jscejseee.71.I_395

Wang R (1999) A simple orthonormalization method for the stable and efficient computation of Green's functions. Bull Seismol Soc Am 89:733–741. https://doi.org/10.1785/BSSA0890030733

Wang R, Martin FL, Roth F (2003) Computation of deformation induced by earthquakes in a multi-layered elastic crust—FORTRAN programs EDGRN/EDCMP. Comput Geosci 29:195–207. https://doi.org/10.1016/S0098-3004(02)00111-5

Zhao Y (2010) Tectonic deformations and shallow soil deformations induced in the active folding zone in the Oct. 23rd, 2004 Mid-Niigata Earthquake. Doctoral dissertation, Department of Civil Engineering, University of Tokyo. https://repository.dl.itc.u-tokyo.ac.jp/record/6321/files/A29820.pdf

Zhao Y, Konagai K (2014) Evidence of a hidden landslide slip surface beneath a mountain hamlet. Environ Earth Sci 71:4615–4624. https://doi.org/10.1007/s12665-014-3078-z

Deep Learning in Landslide Studies: A Review

Hemalatha Thirugnanam

Abstract

This study reviews deep learning architectures and techniques used in the landslide domain. This study aims to understand the state of the art, challenges, and opportunities of applying deep learning to landslide research. Every paper discussed in this article is reviewed for the deep learning approach employed, the study area where it is implemented, additional benchmark algorithms implemented, model assessment metrics, the best model that is selected, and the limitations mentioned by the authors. This review increases visibility into (1) various deep learning methodologies as implemented in real-world landslide mapping, detection, monitoring, and prediction case studies, (2) projects constraints of applying deep learning to landslide research (3) provides recommendations and breakthroughs that must be established in certain areas of landslide studies.

Keywords

Landslide • Deep learning

1 Introduction

Deep Learning (DL), is a subset of Artificial Intelligence (AI), and Machine Learning (ML) approaches are entirely based on Artificial Neural Networks (ANN). ANNs are designed to mimic the human brain; hence deep learning is likewise a human brain mimic. DL algorithms are in high demand due to the exponential growth of data in all domains and the need for analysis and inferences from huge data. DL algorithms have proven to be highly powerful among the different popular techniques employed in ML. Their success is credited to the availability of a vast amount of data and the power of the graphical processor units. Deep learning models are used in several applications such as health care, autonomous vehicles, e-commerce, personal assistance, computer vision, etc. Several frameworks are available for implementing DL algorithms, each tailored to a certain context; TensorFlow, Pytorch, and Keras are the most well-known frameworks. Likewise, there are several types of DL architectures available. The multilayer perceptron (MLP), the convolutional neural network (CNN), the recurrent neural network (RNN), the self-organizing map (SOM), the generative adversarial network (GAN), and the auto-encoders (AE) are some of the most popular DL architectures. Each of these architectures has its own advantages and they work well for certain applications compared to others. In this section, we briefly discuss MLP, CNN, and RNN architectures in light of their application to landslide studies.

The MLP, or multilayer feed-forward neural network, is the first and most basic DL architecture. It has one input layer that receives the signal, one output layer that predicts the input, and numerous hidden layers that act as the network's computational engine. Each layer has a different amount of neurons, and they are all fully linked. With a significant amount of training data, these networks are commonly utilized for regression and classification purposes. Backpropagation is used to train MLP architectures, which belong to the class of supervised learning techniques. Each perceptron in the network is connected to every other perceptron; therefore, the total number of parameters can quickly grow. Another drawback of MLP is that it does not take into account geographical information when making predictions. It uses flattened vectors as inputs, allowing it to make pixel-by-pixel predictions, which makes its usage limited in landslides studies that require spatio-temporal correlation.

CNN overcomes the inadequacies of MLP networks. CNNs are specifically designed for 2D data or structures

H. Thirugnanam (✉)
Center for Wireless Networks and Applications (WNA), Amrita Vishwa Vidyapeetham, Amritapuri, India
e-mail: hemalathat@am.amrita.edu

I. Alcántara-Ayala et al. (eds.), *Progress in Landslide Research and Technology, Volume 1 Issue 2, 2022*, Progress in Landslide Research and Technology,
https://doi.org/10.1007/978-3-031-18471-0_20

such as images, videos, or sequences. CNN basically performs successive convolution operations to the input data in order to identify features and minimize the data sizes automatically. The CNN network has four basic layers in addition to the input and output layers: a convolution layer, a pooling layer, a flattening layer, and a fully connected layer. The main advantage of CNN is that it gathers spatial contextual information without human interaction by detecting relevant features through its convolutional layer. In the realm of computer vision and image interpretation, semantic segmentation of images using CNNs has produced promising results. Researchers are now using the same methodology to study landslides using satellite and aerial images such as susceptibility mapping, hazard mapping, landslide identification, etc.

While CNNs work well for extracting spatial information, RNNs are designed for sequential data, such as in time series, sound, or natural language processing. RNN networks have a feedback loop that allows them to make predictions using information from prior layers. However, two significant difficulties might arise while using RNN architectures: vanishing and exploding gradients. Two RNN variations have been created to address these limitations: the long short-term memory (LSTM) and, more recently, the gated recurrent unit (GRU). LSTM and GRU have nearly identical core ideas, have gated systems, and can handle longer sequences of tasks. The input, output, and forget gates are used in the LSTM design, whereas the reset and update gates are used in the GRU. In landslide studies, RNN and its variants are used to analyze long time-series data such as rainfall, moisture, displacement, etc.

In this paper, we have examined deep learning approaches applied in real-world case studies. We have reviewed the case studies based on (i) landslide mapping, (ii) landslide detection, (iii) landslide monitoring, and (iv) landslide prediction applications. In each of these reviews, the deep learning methodology used, the study area where it is implemented, additional benchmark algorithms implemented, model assessment metrics, the best model selected, and the limitations mentioned in the study by the authors are mentioned. Finally, the generic limitations in adapting deep learning to landslide studies are explored, as well as new prospects and breakthroughs that must be developed are discussed.

2 Paper Selection Criteria

Most of the papers retrieved by Google Scholar while searching for "deep learning and landslides" were about landslide susceptibility mapping and detection. Deep learning is commonly used for mapping applications in the landslide domain. This technology is directly derived from deeper architectures that are built and developed for applications like computer vision and augmented reality that works with RGB images. Other landslide studies, such as prediction and monitoring applications, use deep learning less than the landslide mapping studies. One reason for this is that deep learning outperforms most of the other ML-based algorithms when the amount of data is large. The availability of such large data in natural hazard areas like landslide monitoring and prediction is a limitation, and data with actual landslide incidents is indeed limited. To identify other landslide research that uses deep learning, we used Google Scholar's advanced search option, excluding the words 'susceptibility', 'mapping', and 'detection' from the search. This paper considers the most relevant papers with the most citations from January 2017 to May 2022 for review.

3 Deep Learning in Landslide Susceptibility Mapping

The study Prakash et al. (2020) describes landslide mapping using CNN as a semantic segmentation problem. The study area is 1270 km^2 in size and is located in Douglas County, Oregon, USA. The mapping for this investigation was done with a high-resolution Lidar DEM and a cloud-free optical image from Sentinel-2. Pixel-based, object-based, and DL methods are implemented for generating landslide susceptibility maps. This paper introduces CNN-based U-Net and ResNet architectures for mapping landslides. U-Net was introduced in 2015 by Ronneberger et al. (2015) for segmentation in biomedical images and has been modified to be used for mapping from satellite images (Peng et al. 2019; Schuegraf and Bittner 2019). U-net architecture is used for semantic segmentation of landslide-affected regions, and ResNet is used for feature identification in this paper. This paper applies U-Net architecture with a ResNet34 architecture for feature extraction backbone for landslide mapping and compares it to existing pixel-based and object-based machine learning approaches. The authors have demonstrated that the U-Net with ResNet34 strategy outperforms pixel-based and object-based machine learning algorithms on a regional scale. In the study area mentioned in Prakash et al. (2020), all three approaches identified landslides greater than 0.21 km^2. However, all three methods were unsuccessful in detecting minor landslides. The pixel-based method performs best in detecting minor landslides; however, it has an extremely high probability of false detection. Authors also highlight that when landslides are close together, all approaches have trouble distinguishing individual landslides, and they prefer to predict them as one large landslide area. As a result, the predicted landslide profile does not resemble the actual landslide profile (Table 1).

Table 1 Deep learning case studies in landslide susceptibility mapping applications

Study area	Data used	Methodologies used in the study	Model assessment metrics	Best selected method	Limitations mentioned	References
Douglas County, Oregon, USA	Lidar DEM, optical image from Sentinel-2, landslide inventory	Modified U-net with a ResNet34 model, pixel-based and object-based machine learning algorithms	Matthews correlation coefficient, probability of detection, Probability of false detection	Modified U-net with ResNet34	Limited training examples, few landslide conditioning features	(Prakash et al. 2020)
Mt. Umyeon, Seoul, Korea	Aerial photographs and a landslide inventory	DNN, kernel-based DNN, and CNN	The average precision score and root mean square error	kernel-based DNN, and CNN	Related variable selection before developing the model	(Lee et al. 2020)
Muong Lay district of Vietnam	Geospatial database which includes 217 historic landslide events and conditioning factors	Deep learning model, quadratic discriminant analysis, Fisher's linear discriminant analysis, and a multi-layer perceptron neural network	Area under curve (AUC), accuracy, root mean square error (RMSE), Wilcoxon signed-rank test	Deep learning model	Computation time, related variable selection	(Van Dao et al. 2020)
Kon Tum Province of Vietnam	Geospatial database which includes 1657 landslide locations and nine landslide-related variables	Deep learning neural network model, multilayer perceptron neural network, a support vector machine, a C4.5-Decision Tree model, and a random forest model	Classification accuracy, sensitivity, specificity, and area under the success and predictive rate curves	Deep learning neural network model	Tuning structural parameters, optimal number of hidden layers and processing elements	(Bui et al. 2020a, b)
Iran national scale	Geospatial database which includes 4069 historical landslides and 11 conditioning factors	Recurrent neural network (RNN) and the convolutional neural network (CNN)	Receiver operating characteristic (ROC) curve and the area under the curve (AUC)	Convolutional neural network (CNN)	Author points out to the unidentified or unacknowledged error sources in CNN and RNN	(Ngo et al. 2021)
Maoxian County, China	Using historical records, field observations, and remote sensing techniques, a total of 1290 landslide records were created	Convolutional neural network (CNN), deep neural network (DNN), long short-term memory (LSTM) networks, and recurrent neural network (RNN)	Area under the curve (AUC)	DNN algorithm	Time, degree, or frequency of landslide occurrences could not be predicted using the created model	(Habumugisha et al. 2022)
Isfahan province, Iran	222 historical landslide occurrences, geomorphologic, geologic, environmental, and human activity-related covariates	Deep convolution neural network, support vector machine (SVM), logistic regression (LR), Gaussian naïve Bayes (GNB), multilayer perceptron (MLP), Bernoulli Naïve Bayes (BNB) and decision tree (DT)	AUC, MSE, RMSE	Deep convolution neural network	Limited number of reference landslides, quality of the input database, powerful processors to manage the inputs	(Azarafza et al. 2021)

The researchers looked into the possibility of a deep convolution neural network for spatially predicting landslide susceptibility (Azarafza et al. 2021). The technique was tested using data from Iran's Isfahan province (Azarafza et al. 2021). The landslide inventory dataset consisted of indices linked with 222 historical landslide occurrences, which were randomly separated into training (80%) and testing (20%) sets for the analysis. Based on field and remote sensing investigations, four key covariates were identified: geomorphologic, geologic, environmental, and human activity-related covariates. The deep convolution neural network model could accurately construct a susceptibility map for the research area. Compared to the benchmark models, the results reveal a considerable improvement in landslide susceptibility prediction accuracy. Despite the increased accuracy of the proposed deep convolution neural network, and predictive model for landslide susceptibility mapping, the authors highlight certain limitations to this work that should be taken into account in future research. (i) Fieldwork, historical landslide records, and remote-sensing data were used to create the primary database. Modeling was difficult due to the limited number of reference landslides in the recorded data (as is often the case); (ii) The quality of the input database was directly affected by the spatial resolutions of satellite imagery and DEM data quality, which influence the input data. (iii) During landslide susceptibility evaluations, the predictive model requires powerful processors to manage the inputs. The authors also addressed the question of whether landslides should be regarded as spatially continuous occurrences or spatial objects and another open research question.

To predict the susceptibility of future landslides in densely populated urban areas in Mt. Umyeon, Seoul, Korea, deep learning methodologies were used in Lee et al. (2020). Aerial photographs and a landslide inventory were used to create Deep Neural Network-DNN, kernel-based DNN, and convolutional neural network models. The average precision score and root mean square error for each of the three models were used to assess model performance. The average precision score curve revealed that the DNN, kernel-based DNN, and CNN models performed at 99.45%, 99.44%, and 99.41%, respectively. The accuracy of all three models was greater than 99%, indicating that each model is very good at predicting landslides. However, the kernel-based DNN and CNN models outperformed the DNN model slightly. This is evident that the models are based on the kernel approach. Lee et al. (2020) also mention one limitation in terms of choosing the appropriate hyperparameters. In order to understand the fundamental relationship between variables and landslides, it is necessary to apply a different methodology in advance when selecting variables, which requires experience.

The development and validation of a spatially explicit deep learning neural network model for predicting landslide susceptibility are described in Van Dao et al. (2020). Based on 217 landslide events from the Muong Lay district of Vietnam, a geospatial database was created, from which a set of nine landslide conditioning factors was derived with the help of the Relief-F feature selection method. Several performance metrics showed that the DL model performed well in terms of goodness-of-fit with the training dataset (AUC = 0.90; accuracy = 82%; RMSE = 0.36) and ability to predict future landslides (AUC = 0.89; accuracy = 82%; RMSE = 0.38). The model's efficiency was compared to quadratic discriminant analysis, Fisher's linear discriminant analysis, and a multilayer perceptron neural network. A Wilcoxon signed-rank test comparison revealed that the spatially explicit DL model outperformed the other models in terms of landslide prediction.

Landslide susceptibility assessments and comparison of its predictive performance to state-of-the-art machine learning models were implemented in Bui et al. (2020a, b). The efficiency of the Deep learning neural network model was estimated for the Kon Tum Province of Vietnam, which is characterized by the presence of landslide phenomena. 1657 landslide locations and nine landslide-related variables were used to generate the training and validation datasets for the landslide susceptibility assessment. The deep learning neural network model's learning ability was evaluated and compared to a Multilayer Perceptron Neural Network, a Support Vector Machine, a C4.5-Decision Tree model, and a Random Forest model. To assess each model's learning and predictive capacity, the classification accuracy, sensitivity, specificity, and area under the success and predictive rate curves (AUC) were calculated. According to the results, the proposed deep learning neural network model outperformed the four benchmark models. The study concludes that using a deep learning approach could be a viable alternative approach for landslide susceptibility mapping.

For a national-level landslide susceptibility mapping in Iran, two unique deep learning algorithms: the recurrent neural network (RNN) and the convolutional neural network (CNN), are used and compared in Ngo et al. (2021). A geospatial database was created with 4069 historical landslides and 11 conditioning factors. The data was split into two datasets: training and testing. RNN and CNN algorithms built landslide susceptibility maps for Iran using the training dataset. The receiver operating characteristic (ROC) curve and the area under the curve (AUC) are used to quantify the landslide susceptibility maps using the testing dataset. The RNN algorithm (AUC = 0.88) outperformed the CNN method (AUC = 0.85) in both the training and testing phases. Authors assessed regions of susceptibility for each province and discovered that 6 and 14% of Iran's land area are very

highly and highly vulnerable to future landslides. Approximately 31% of Iran's cities are prone to landslides. The findings of this research will aid in developing landslide risk mitigation strategies. Ngo et al. (2021) also highlight previous research, limitations, and future recommendations. The design of CNN and RNN algorithms, including the training technique, input window size, and layer depth, significantly impacts their performance. These algorithms yield consistent output sequences, yet they have unidentified or unacknowledged error sources; hence their results should be interpreted with caution. The authors also point out that, when compared to other models, RNN enhances landslide prediction accuracy, particularly in tropical locations.

Another study in Maoxian County, Sichuan, China, applied four deep learning algorithms; namely, (1) the convolutional neural network (CNN), (2) deep neural network (DNN), (3) long short-term memory (LSTM) networks, and (4) recurrent neural network (RNN), were used to assess the risk of landslides (Habumugisha et al. 2022). With historical records, field observations, and remote sensing techniques, a total of 1290 landslide records were created. According to this study, the DNN algorithm outperformed the LSTM, CNN, and RNN algorithms in detecting landslides in Maoxian County, with AUC values of 87.30%, 86.50%, 85.60%, and 82.90%, respectively.

Several other studies have also employed deep learning algorithms to map landslide susceptibility worldwide. However, most studies are primarily concerned with using deep learning approaches to achieve high accuracy in landslide mapping when compared to existing benchmark machine learning algorithms. There is little research focusing on making modifications and improvements to address the image segmentation problem for landslides, which is distinct from image segmentation in other disciplines such as biomedical images. On the other hand, landslide mapping is an unbalanced learning problem with more data belonging to the no landslide category and extremely limited data belonging to the landslide category. In particular, approaches to coping with unbalanced data and the segmentation process for landslides, must be specifically created. Few researchers have used deep learning to tackle landslide mapping as a semantic segmentation problem (Prakash et al. 2020). Conditional random fields have been successfully employed to post-process segmentation results in other disciplines (Christ et al. 2016). These methodologies specific to the context of landslide mapping should be examined more in the future.

4 Deep Learning in Landslide Detection

The study in Bui et al. (2020a, b) explores a system for detecting landslides from satellite images that combines deep learning and image transform algorithms. A convolution neural network is utilized in the deep learning section to classify satellite photos that contain landslides. This work presents a transformation technique, Hue–Bi-dimensional empirical mode decomposition, to calculate the landslide region and magnitude from landslide photographs categorized in order to reliably identify landslides under diverse illumination situations. After detecting the landslide's position, the authors determine the landslide's size changes over time. This paper presents the results of a simulation study using a limited set of satellite images, and it has not been tested or validated for identifying landslides in a real scenario using satellite images (Table 2).

In the study in Kamiyama et al. (2018), the ability of CNN algorithms to detect landslides from differential interferograms is tested. Changes in the interference fringes in DInSAR differential interferograms could be caused by things other than ground motions too. Local impacts that occur on slopes are difficult to separate from global influences on a wide spatial scale. However, separating local impacts that appear on slopes from global effects on a large spatial scale is difficult. Moreover, experts would need a lot of time and effort to evaluate all of the differential interferograms formed from observational data collected at high frequency over large areas. The work in Kamiyama et al. (2018) examined the effectiveness of adopting a CNN model to detect interference fringes that may indicate landslides from differential interferograms with the goal of efficiently detecting interference fringes that may represent landslides. CNN models were found to be capable of detecting interference fringes with the possibility of landslides with high reproducibility, with recall values of around 90% in the validation instance. On the other hand, Landslide interference fringes were discovered in greater numbers than in the training data, indicating that the precision is low. Expert-like procedures were used to create fringes that represented landslide motions.

For landslide detection from satellite photos, a preprocessing method based on Bi-dimensional empirical mode decomposition is used along with deep learning by Bui et al. (2019). The results are better with this combination than with an individual CNN training model or solely identifying using the Bi-dimensional empirical mode decomposition process. This paper also presents the results of a simulation study using a limited set of satellite images. It has not been tested or validated for identifying landslides in a real scenario using satellite images.

Orland et al. (2020) suggested a novel framework for detecting and classifying natural disasters. The system relies primarily on a hybrid of the convolutional neural network (CNN) for feature extraction. Due to the lack of a dataset concerning several disasters, a new dataset was created to evaluate the framework's capabilities. The model is made up of five separate CNNs that have been grouped together.

Table 2 Deep learning case studies in landslide detection applications

Study area	Data used	Methodologies used in the study	Model assessment metrics	Best selected method	Limitations mentioned	References
Simulation study	Landsat 8 satellite data	CNN and Hue–Bi-dimensional empirical mode decomposition	Accuracy and loss values	NA	Training dataset used as example for 'without landslide' category needs improvement	(Bui et al. 2020a, b)
Mt. Gassan, Mt. Hakusan, Northern Nagano, Kii Peninsula, Eastern Kochi	Differential interferograms of ALOS/PALSAR from 2006 to 2011	CNN algorithm	Precision and recall	NA	Limited data in landslide category	(Kamiyama et al. 2018)
Simulation study	Satellite image	CNN and bi-dimensional empirical mode decomposition, CNN, bi-dimensional empirical mode decomposition	Accuracy and loss values	CNN and bi-dimensional empirical mode decomposition	Error in bi-dimensional empirical mode decomposition when performing conversion calculation through the sine and cosine values	(Bui et al. 2019)
Nil	Dataset for natural calamities were created by the authors from various sources	CNN + SVM, KNN, RF	Accuracy	CNN + SVM	Unavailability of open-source dataset for natural calamities	(Orland et al. 2020)

Each CNN model makes use of a pre-trained AlexNet architecture on the ImageNet dataset that has been fine-tuned for the generated dataset. The proposed method employs CNN and SVM to identify and classify ten different types of natural disasters. The proposed framework was observed to outperform when compared with the state-of-the-art algorithms. According to the authors, this model can be used further by satellite and aerial real-time image processing systems to locate the geographical locations of places affected by these natural disasters (Table 3).

5 Discussion

Deep learning techniques are now applied in almost all real-world applications, and the landslide domain is no exception. However, research into the use of DL algorithms for landslides is still in its early stages and has some unique challenges. The major factors that limit the use of DL for landslide research are summarized in this section.

Techniques are not well utilized for real-time monitoring and forecasting.

(i) To acquire satisfactory results using DL algorithms, it is required to employ a large training dataset. Despite the fact that certain training datasets are available in the remote sensing community, there is, however, a major lack of data categorized as landslides, in contrast to the techniques such as computer vision, augmented reality etc., which uses large image datasets for creating deep learning models. Working with landslides, the issue of limited training samples is much more important. To get accurate predictions, it is essential to construct a large time series of data belonging to the landslide category.

(ii) The majority of landslide studies rely on satellite data, and unlike RGB images, these images are complex and varied, the preprocessing procedure takes a long time and requires the assistance of a remote sensing expert. Although optical images are utilized, the presence of clouds on the photographs is a serious concern. Even though several strategies are used to overcome this limitation, the quality of the data produced is altered and as a result, the accuracy of prediction also decreases.

Table 3 Deep learning case studies in landslide monitoring applications

Study area	Data used	Methodologies used in the study	Model assessment metrics	Best selected method	Limitations mentioned	References
Baishuihe landslide, Yangtze, China	Displacement time series, rainfall, reservoir water level	LSTM	Mean absolute error (MAE), mean absolute percentage error (MAPE), mean square error (MSE), and root mean square error (RMSE)	NA	Solving the problem of long term dependencies. LSTM is better approach to handle compared to standard RNN	(Meng et al. 2020)
Landslide prone hillslopes, Oregon, USA	Rainfall, soil moisture, pore pressure	LSTM	Root mean square error (RMSE)	NA	Quantity and quality of the training data, heterogeneity of the soil, issue of extrapolation beyond conditions within the period of record	(Orland et al. 2020)
Experimental study	Historical environment monitoring datasets (rainfall intensity and soil moisture) from the Soil & Water Conservation Bureau, Taiwan	LSTM	Root mean square error (RMSE)	NA	Not mentioned	(Utomo et al. 2020)
Baishuihe landslide and the Shuping landslide	Displacement time series	Graph convolutional network (GC) and gated recurrent unit (GRU), ARIMA, LSTM, SVR	Mean absolute error (MAE), mean absolute scaled error (MASE), and root mean square error (RMSE)	Graph convolution and gated recurrent unit (CG-GRU)	Availability of data in lesser frequency to model abrupt transition states in the study area. Limited dataset in geohazard domain	(Jiang et al. 2022)

(iii) Existing deeper architectures are mostly designed and developed for applications such as computer vision, and augmented reality that works with RGB images. Landslide studies, on the other hand, use (a) satellite and aerial images that are extremely large and may or may not be in RGB bands; (b) instrumental data such as geotechnical, geophysical and IoT data that are one dimensional or two dimensional time series unlike RGB data. When the size of images and sequence lengths rise, Moskolaï et al. (2020) state that using the ConvLSTM one among the deep learning architecture is not recommended. Therefore it is necessary to build deep learning models and architectures that are specific and suitable for natural hazard studies such as landslides.

(iv) Existing DL methods are majorly utilized for mapping applications when it comes to landslide research. Application of DL in prediction, monitoring and early warning are limited and this is another area worth investigating because this component of landslide study indeed requires more precise results and forecasts.

6 Conclusion

This article reviewed recent papers from 2017 to till date that used Deep learning algorithms and architectures to study landslides. Deep learning finds its major application in

susceptibility mapping of landslides. Promising results are obtained in all the studies that used deep learning approaches compared to the benchmark algorithms such as SVM, Naive Bayes, Decision trees, Neural networks, etc. Despite the positive results produced from deep learning approaches, limitations still exist, and these limitations are summarized in the discussion section. The major limitations are the lack of available training datasets, existing deep learning architectures and models are not fine-tuned to suit landslide data such as satellite images, the complexity of satellite images, the need of preprocessing, etc. Therefore, it is necessary to (i) design architectures and frameworks that are dedicated to natural disaster studies involving both satellite and ground data. (ii) Fine tune the existing deep learning architectures to be able to produce efficient outcomes for research of natural disaster studies such as landslides.

Acknowledgements I would like to express my heartfelt gratitude to the Chancellor of our institution Sadguru Sri Mata Amritanandamayi Devi, for providing me a platform and opportunity to work in landslide domain. I also would like to express my thanks and gratitude to Dr. Maneesha Vinodini Ramesh, Director, Amrita Center for Wireless Networks and Applications who is guiding and leading the landslide research. Sincere thanks to my family, colleagues and all the landslide team members.

References

Azarafza M, Azarafza M, Akgün H, Atkinson PM, Derakhshani R (2021) Deep learning-based landslide susceptibility mapping. Sci Rep 11(1):1–16

Bui DT, Tsangaratos P, Nguyen VT, Van Liem N, Trinh PT (2020a) Comparing the prediction performance of a Deep Learning Neural Network model with conventional machine learning models in landslide susceptibility assessment. CATENA 188:104426

Bui TA, Lee PJ, Lum KY, Chen CR, Shiu SH (2019) Using BEMD in CNN to identify landslide in satellite image. In: 2019 international conference on system science and engineering (ICSSE). IEEE, pp 94–97

Bui TA, Lee PJ, Lum KY, Loh C, Tan K (2020b) Deep learning for landslide recognition in satellite architecture. IEEE Access 8:143665–143678

Christ PF, Elshaer MEA, Ettlinger F, Tatavarty S, Bickel M, Bilic P, Rempfler M, Armbruster M, Hofmann F, D'Anastasi M, Sommer WH (2016) Automatic liver and lesion segmentation in CT using cascaded fully convolutional neural networks and 3D conditional random fields. In: International conference on medical image computing and computer-assisted intervention. Springer, Cham, pp 415–423

Habumugisha JM, Chen N, Rahman M, Islam MM, Ahmad H, Elbeltagi A, Sharma G, Liza SN, Dewan A (2022) Landslide susceptibility mapping with deep learning algorithms. Sustainability 14(3):1734

Jiang Y, Luo H, Xu Q, Lu Z, Liao L, Li H, Hao L (2022) A graph convolutional incorporating GRU network for landslide displacement forecasting based on spatiotemporal analysis of GNSS observations. Remote Sens 14(4):1016

Kamiyama J, Noro T, Sakagami M, Suzuki Y, Yoshikawa K, Hikosaka S, Hirata I (2018) Detection of landslide candidate interference fringes in DInSAR imagery using deep learning. Recall 90(94.5):94–95

Lee S, Baek WK, Jung HS, Lee S (2020) Susceptibility mapping on urban landslides using deep learning approaches in Mt. Umyeon. Appl Sci 10(22):8189

Meng Q, Wang H, He M, Gu J, Qi J, Yang L (2020) Displacement prediction of water-induced landslides using a recurrent deep learning model. Eur J Environ Civ Eng 1–15

Moskolaï W, Abdou W, Dipanda A, Kolyang DT (2020) Application of LSTM architectures for next frame forecasting in Sentinel-1 images time series. arXiv preprint arXiv:2009.00841

Ngo PTT, Panahi M, Khosravi K, Ghorbanzadeh O, Kariminejad N, Cerda A, Lee S (2021) Evaluation of deep learning algorithms for national scale landslide susceptibility mapping of Iran. Geosci Front 12(2):505–519

Orland E, Roering JJ, Thomas MA, Mirus BB (2020) Deep learning as a tool to forecast hydrologic response for landslide-prone hillslopes. Geophys Res Lett 47(16):e2020GL088731

Peng D, Zhang Y, Guan H (2019) End-to-end change detection for high resolution satellite images using improved UNet++. Remote Sens 11(11):1382

Prakash N, Manconi A, Loew S (2020) Mapping landslides on EO data: performance of deep learning models vs. traditional machine learning models. Remote Sens 12(3):346

Ronneberger O, Fischer P, Brox T (2015) U-net: convolutional networks for biomedical image segmentation. In: International conference on medical image computing and computer-assisted intervention. Springer, Cham, pp 234–241

Schuegraf P, Bittner K (2019) Automatic building footprint extraction from multi-resolution remote sensing images using a hybrid FCN. ISPRS Int J Geo Inf 8(4):191

Utomo D, Hu LC, Hsiung PA (2020) Deep neural network-based data reconstruction for landslide detection. In: IGARSS 2020–2020 IEEE international geoscience and remote sensing symposium. IEEE, pp 3119–3122

Van Dao D, Jaafari A, Bayat M, Mafi-Gholami D, Qi C, Moayedi H, Van Phong T, Ly HB, Le TT, Trinh PT, Luu C (2020) A spatially explicit deep learning neural network model for the prediction of landslide susceptibility. CATENA 188:104451

IPL Projects, World Centres of Excellence on Landslide Risk Reduction, and Kyoto Landslide Coommitment 2020

Landslide Early Warning Systems: Requirements and Solutions for Disaster Risk Reduction—India

Maneesha Vinodini Ramesh, Hemalatha Thirugnanam, Balmukund Singh, M. Nitin Kumar, and Divya Pullarkatt

Abstract

Globally the prevalence of landslides has increased, impacting more than 4.8 million people between 1998 and 2017 and reported more than 18,000 casualties [UNDP]. The scenario has worsened dramatically, and it has become imperative to develop early warning systems to save human life. This demands the need for systems that could identify the potential of imminent landslides and disseminate the information related to landslide initiation in real-time. This would provide the opportunity to save lives. However, globally the research on reliable end-to-end systems for early warning of landslides is still in its nascent stage. Therefore, this paper explores in detail the requirements for developing systems for real-time monitoring, detection, and early warning of landslides. An integrated solution for building the real-time landslide monitoring and early warning system to provide community-scale disaster resilience is also proposed. This solution integrates multiple modules such as a heterogeneous sensor system, data storage and management, event detection framework, alert dissemination, and emergency communication system to address issues such as capturing dynamic variability, managing multi-scale voluminous datasets, extracting key triggering information regarding the onset of possible landslide, multilevel alert dissemination, and robust emergency communication among the stakeholders respectively. The paper also presents two case studies of real-time landslide early warning systems deployed in North-eastern Himalayas and Western Ghats of India. These case studies demonstrate the approaches utilized for risk assessment, risk analysis, risk evaluation, risk visualization, risk control, risk communication, and risk governance. The results from the deployed system in the case study areas demonstrate the capability of the IoT system to gather Spatio-temporal triggers for multiple types of landslides, detection and decision of specific scenarios, and the impact of real-time data on mitigating the imminent disaster.

Keywords

Landslide early warning systems (LEWS) • Disaster risk reduction (DRR) • Internet of things (IoT)

1 Introduction

Extreme and dynamic variability in weather patterns is leading to an unprecedented increase in natural hazards. Globally, from 2004 to 2016, there were 4862 distinct landslide events resulting in 55,997 reported deaths (Froude and Petley 2018). A recent study reported that more than 42% of the municipalities in Italy had been affected by landslides. (Franceschini et al. 2022). Asian Countries like China, India, Nepal, and Japan have experienced significant losses every year due to several catastrophic landslides. India also has a history of landslides combined with multiple hazards, leading to massive loss of human life (UNDP 2018). During the 2013 monsoon in Uttarakhand, 6000 people lost their lives during numerous landslides and extreme rainfall that led to flash flooding (Martha et al.

M. V. Ramesh (✉) · B. Singh · M. Nitin Kumar · D. Pullarkatt
Amrita School of Sustainable Development, Amrita Center for Wireless Networks and Applications (Amrita WNA), Amrita Vishwa Vidyapeetham, Amritapuri, India
e-mail: maneesha@amrita.edu

B. Singh
e-mail: balmukundsingh@am.amrita.edu

M. Nitin Kumar
e-mail: nitinkm@am.amrita.edu

D. Pullarkatt
e-mail: divyap@am.amrita.edu

H. Thirugnanam
Amrita Center for Wireless Networks and Applications (Amrita WNA), Amrita Vishwa Vidyapeetham, Amritapuri, India
e-mail: hemalathat@am.amrita.edu

I. Alcántara-Ayala et al. (eds.), *Progress in Landslide Research and Technology, Volume 1 Issue 2, 2022*, Progress in Landslide Research and Technology,
https://doi.org/10.1007/978-3-031-18471-0_21

2015). The North Indian states of Jammu and Kashmir, Himachal Pradesh, Sikkim, Assam of Himalayas ranges, and Peninsular states of Maharashtra, Karnataka, Tamil Nadu, and Kerala also suffer the loss of life and property every year, predominantly in the monsoon season (Geological Survey of India, https://www.gsi.gov.in). This clearly shows there is an increasing trend in landslides globally.

Furthermore, in the past four years, 2018–2021, India has experienced extreme rainfall in unpredicted pockets leading to multi-hazards such as floods, landslides, etc. (Ramesh et al. 2022). Most of the landslides in India are reported during the monsoon season. Furthermore, in recent years due to unprecedented extreme heavy rainfall events within a short duration, numerous catastrophic landslides have been experienced. The unpredictability of landslide events in space and time is leading to an increase in loss of life and its impact on the established infrastructure. This situation demands solutions that are capable of reducing landslide risk and increasing the community's resilience to landslides.

The state of Kerala, India, has reported more than 200 landslides in 2018. There were tragedies and incidents of catastrophic scale caused by the more than 65 landslides reported in 2019 (Manorama Online 2019); the events over Puthumala and Kavalappara also caused 81 deaths (Wadhawan et al. 2020). In 2021, the Pettimudi landslide event took place, claiming 66 lives (Achu et al. 2021). During the field visits and semi-structured interviews, it was observed that the time difference between landslide initiation and occurrence was about 8–10 h (Wadhawan et al. 2020). However, the community members did not receive any warnings and were not prepared enough to handle this disaster situation. This led to massive loss of lives, which could have been avoided. These incidents clearly demonstrate that landslides are becoming more and more life-threatening worldwide, and their impact could be reduced by developing integrated solutions that will provide landslide risk reduction and landslide resilience.

This research work details the challenges and requirements for building landslide early warning systems and their sub-systems. These events and their sequence of sub-events differ for different types of landslide classifications. This work also focuses on enhancing community-scale landslide resilience. Additionally, two case study scenarios from (i) tectonically active North Eastern Himalayas, and (ii) the structurally moderate dissected hills of Western Ghats are elaborated to unveil the complexity of building a landslide early warning system.

Section 2 details the review of the existing literature. Section 3 details the landslide dynamics related to different landslide types and their importance in early warning systems. It also discusses the requirements of the landslide risk management framework. Further, in Sect. 4, experiences from decade-long operational early warning systems in India are elaborated. The focus will be on the real-world deployments of such systems in India. Section 5 covers the (Internet of Things-Landslide Early Warning Systems) IoT LEWS Discussions based landslide early warning system in case study areas and the last Sect. 6, concludes by summarizing the early warning systems, which is an effective solution for Disaster Risk Reduction.

2 Literature Review

For Disaster Risk Reduction (DRR), several solutions have been proposed in the literature. However, there exists a trade-off among the costs of systems, range of coverage, time of forewarning, and reliability of systems. (Izumi and Shaw 2022). Moreover, the design and development of solutions for Disaster Risk Reduction vary according to the concept utilized, i.e., through community champions or technology. In technology-based solutions, the systems perform either based on remote sensing data (Orimoloye et al. 2021) or by utilizing the geophysical sensors for in-situ measurements (Abraham et al. 2020). Further, in-situ measurements are classified into hydrological and movement-based measurements. The community champions-based solution is explained in detail later. Both these systems have both advantages and disadvantages. In general, the community champions-based system lacks the accurate detection of the event, whilst the technology-based solutions lack effective communication of detected risk.

According to a recently published review on landslide early warning systems, there is a lack of information on past landslide incidents, inhibiting the refinement of models used in early warnings (Guzzetti et al. 2020). There is also a lack of literature on the systematic instrumentation of LEWS. However, there has been an increasing global interest in designing, developing, and deploying landslide early warning systems as a solution to disaster risk reduction (Guzzetti et al. 2020; Pecoraro et al. 2019). New geographical areas are being explored for the deployment of landslide early warning systems utilizing the application of geospatial technology and Web-GIS in order to save human lives by utilizing precipitation measurement as a key indicator for a regional level warning (Ahmed et al. 2020; Hidayat et al. 2019).

Site-specific monitoring using heterogeneous sensors such as rain gauges, moisture sensors, pore pressure sensors, inclinometers, and tiltmeters are detailed in the publications (Ramesh and Rangan 2014; Michoud et al. 2013; Gian et al. 2017; Thirugnanam et al. 2022). However, landslide detection and early warning demand long-term monitoring using these sensor systems. Most of the time, the spatial scale of monitoring required for landslide detection covers a very large area. This will lead to incurring a very high cost of

deployment, operation, and maintenance. This makes it an impractical solution for some landslide-prone areas. The lifetime extension of these systems is highly challenging. Context-aware algorithms are applicable in extending the lifetime of such systems (Prabha et al. 2017; Tao 2020). Dixon et al. (2018) have proposed and prototyped a low-cost sensing using acoustic emission (AE) monitoring system. This system needs to be scaled and experimented with multiple sites having different types of landslide classifications. This solution needs to be further explored to understand its capability for early warning of landslides since the AE system lacks in deriving and mapping the multiple heterogeneous causative factors.

The recent literature covers the details of some of the relevant decision models for deriving rainfall thresholds, (Segoni et al. 2018; Harilal et al. 2019; Canavesi et al. 2020), pore pressure thresholds (Conrad et al. 2021; Thirugnanam et al. 2020), moisture thresholds (Orland et al. 2020) utilizing deep learning methods for forecasting the hydrologic response of hillslopes prone to landslides. Additionally, new attempts at utilizing soil moisture have given promising results with their own limitation after reaching the moisture saturation limit (Segoni et al. 2018; Wicki et al. 2020). However, none of these existing works have detailed a comprehensive decision model for early warning of landslides.

The review of selected recently published articles focused on the effectiveness and limitations of the landslide early warning systems. It briefly differentiates the research based on the landslide type, study area, types of sensors used, method for modeling, mode of data communication, and information dissemination capability. All these detailed analyses clearly show that existing landslide early warning systems need enhancements to incorporate the comprehensive needs for capturing the heterogeneous sensing to derive integrated decision models for forecasting imminent disasters and adaptively disseminate landslide early warnings to relevant stakeholders.

3 Landslide Dynamics and Requirements of LEWS

The most common categories of landslides detailed by Varnes (1978) include slides, flows, falls, topples, and spreads. However, each of these landslide types differs with respect to their causative factors or triggers and also with respect to the geological, morphological, hydrological, and meteorological conditions that lead to them. Therefore, one of the critical challenges in developing a LEWS is to identify and understand the distinct signals generated for different types of landslides. This would require in-depth knowledge of the different types of pre-events, failure mechanisms, and post-event spatial impacts for each type of landslide.

The proposed LEWS would require accurate capturing in real-time, the distinct signals generated due to pre-events, initiation of failure mechanism, and post-event scenario to provide an effective early warning to the at-risk, vulnerable community. This demands the identification of the sub-events involved in each type of landslide as well as the methodologies to timely collect those distinct signals accurately. Existing landslide-prone areas experience either single or multiple types of landslides at the same time. This demands the LEWS to capture the sub-events of multiple types of landslides for effectively delivering the location-specific landslide warnings. The key complexities lie in capturing location-specific causative or triggering signals based on the landslide type and developing context-aware decision models based on the interrelationship between the sub-events specific to each type of landslide.

Sensing and communication technologies, algorithms, and heterogeneous data analysis have to be designed and developed for deriving these decision models. The existing spatio-temporal relationship between these sub-events for specific landslide types needs to be uniquely knitted together for monitoring different types of landslides prevalent in specific landslide-prone areas. Table 1 details the landslide dynamics for major types of landslides prevalent in India. These landslide types include rock-topple, slide and fall, debris flow, debris slide, mudflow and slide, creep, and complex landslides. These have been analyzed for their precursor scenarios, failure mechanism, post-landslide scenario, sequence of sub-events, measurement techniques, and monitoring period.

For landslide detection, it is enough to identify the failure at its initiation point. However, when early warning of landslides is considered, it is necessary to detect the failure as well as to identify and monitor all the sub-events associated with the phenomena, including final deposition of the debris and sediments post landslide. Depending on the landslide type, debris rheology, and rate of movement, the location of sediment deposition will differ, thereby resulting in varying spatial impacts. Therefore, an efficient LEWS should be able to integrate multiple types of decision models for monitoring different types of landslides and deduce their final deposition areas as well. Based on the above factors, the risk levels will vary temporally as well as spatially and this demands the development of a metric of evaluation to map and assess these risk levels and identify the regions that can be impacted by these events in the future. Therefore the understanding of the real-time variability of landslide dynamics based on heterogeneous triggering factors, its spatial prevalence, and spatial impact on forecasted hazard zones need to be utilized to derive the lead time for effective landslide warning. Table 2 details the detection mechanism, decision model, expected temporal scale, and expected spatial scale for the key landslide types. These details need

Table 1 Landslide dynamics (part I) for major types of landslides prevalent in India

Landslide type	Precursor scenario	Failure mechanism	Post landslide scenario	Sequence of sub-events	Measurement techniques	Monitoring period
Rock:topple /slide/fall	Crack initiation, tree roots expansion, hanging rocks from clif, slanting electric poles etc. Increase in acoustic emissions (AEs) and micro-seismic activity	Crack initiation, crack propagation leading to rock failure, followed by rock–toppling, rock–sliding, rock-falling	Runout leading to road damages, infrastructure damages	(a) Crack initiation ⇒crack propagation⇒rock toppling (b) Crack initiation ⇒ crack propagation⇒ rock toppling⇒ rock sliding (c) Crack initiation⇒ rock rupture and collapse⇒ rock sliding (d) Crack initiation⇒ rock rupture and collapse⇒ rock fall	Geophone, crack meters, tiltmeters, extensometers, acoustic emission sensor, LiDAR scanning, time lapsed ground survey using drones cameras	Long term monitoring —multiple years
Debris flow	Tension cracks, flow of debris, seismic activity	Shearing sliding along the weak surface, rapid loss of strength	Depositing the mixed material at the mouth of debris flow gullies⇒often damming the main river ⇒formation of barrier lakes	(a) Shearing in the subsurface ⇒creation of tension cracks at the crown⇒rapid loss of strength⇒flow along the weak surfaces⇒formation of slurry⇒ moving very fast with relative movement between adjacent layers (b) Saturation⇒ loss of strength⇒ movement along the weak surface⇒ flow along the weak surfaces ⇒formation of slurry⇒ moving very fast with relative movement between adjacent layers (c) Seismic activity⇒ loss of strength⇒ movement along the weak surface⇒formation of slurry⇒ moving very fast with relative movement between adjacent layers	Rain gauge, moisture sensor, strain gauges, tiltmeters, geophone, accelerometers	Medium term monitoring — especially during monsoon period
Debris slide	Heavy rainfall, initiation of cracks followed by creation of slip zone, oversaturation of ground, rise in pore pressure	Unconsolidated soil deposits overlying highly fractured bedrock fails along the slip surface	Long runout	(a)Saturation⇒ loss of strength in the surficial deposits ⇒ movement along plane either bedrock/overburden interface or a surface ⇒ Rapid downward sliding and forward rolling of rock fragments	Rain Gauge, Moisture Sensor, Pore Pressure Transducer, Strain Gauges, Tiltmeters, Inclinometers, Geophone, Accelerometers	Medium to long term monitoring - especially during monsoon period

(continued)

Table 1 (continued)

Landslide type	Precursor scenario	Failure mechanism	Post landslide scenario	Sequence of sub-events	Measurement techniques	Monitoring period
Mud: flow/slide	Heavy rainfall leading to super saturation of ground	After oversaturation the topsoil flows	Mud movement in the downstream, often arrested by road, break in slopes	(a) Saturation ⇒ oversaturation ⇒ cracks and ruptures at the soil layer⇒formation of mud slurry ⇒ moving very fast with relative movement between adjacent layers ⇒ traveling long distance along the drainage channel / gullies eroding the channel	Rain Gauge, Moisture Sensor, Accelerometers, Pore Pressure	Medium to long term monitoring - especially during monsoon period
Creep	Cracks on roads, buildings, Tilting of trees, oversaturation of ground, water seepage at new location, formation of new springs, water logging, rise in pore pressure, deformation	Weathered fragile rock overlaid by thick soil cover fails under influence of gravity, washing away fine particles leading with/without soil piping Creep movement can be continuous, seasonal or progressive	Slow movement of slide from deep weathering leading to surface signatures like cracks on roads, buildings, surface slides. After few years slides can also happen	(a) Slow surface movements⇒ gravitational deformation ⇒creates large disturbances in landscape morphology, such as scarps, counter-slope scarps⇒ Outflow of mudstones due to the lithostatic pressure⇒ progressive toppling of a rock mass leading to the catastrophic rock collapse along bedding planes	Measuring morpho-structures and tectonic features using Geomorphological mapping and time lapsed electrical resistivity tomography (ERT) Monitoring real-time pore pressure, ground vibration and ground inclination, for observing the changes in the subsurface	Long term monitoring
Complex landslides	Crack initiation, internal shear oversaturation, ground vibrations, tree roots expansion and slanting electric poles etc	Multiple factors including weathered regolith, excess rainfall leading to oversaturations, earthquake tremors	Debris movement in the downslope	(a) Oversaturation⇒ Slip zone formation⇒ failure along the slip zone (b) Rock fracturing⇒ debris slide (c) Creep⇒ subsidence⇒ debris slide, etc	Rain gauge, moisture sensor, pore pressure transducer, strain gauges, tiltmeters, inclinometers, geophone, accelerometers, ERT, Drone imaging	Medium to long term monitoring

Table 2 Landslide dynamics (part II) for major types of landslides prevalent in India

Landslide type	Detection mechanism	Decision models	Expected temporal scale	Expected spatial scale
Rock: topple/slide/fall	(a) GEOPHONE: multiple sensors capturing low-frequency ground vibration (5–10 Hz) signals for a specific duration, (b) CRACK METER: multiple sensors capture the increase in crack length (c) TILTMETERS: sensors capture the change in orientation of the unstable rock body (d) EXTENSOMETERS: multiple sensor captures the increase in movement of the unstable rock with reference to stable rock body (e) LiDAR: periodic point cloud data points for change detection (f) DRONE CAMERAS: periodic change detection	In all four scenarios of sub-events, the same decision model could be used for identifying crack initiation and propagation. However, the threshold for detecting rock toppling, rock sliding, and rock fall using various detection mechanisms will be different. The threshold values can be determined from the strength of the material, size of the unstable mass, structural properties of the rock,	Immediate to short duration	Site specific
Debris flow	(a) RAIN GAUGE: crossing rainfall thresholds, (b) STRAIN GAUGES: change in strain measurements beyond the threshold levels, (c) GEOPHONES: low frequency microseismic signal detection (d) ACCELEROMETERS: variations in ground acceleration	Rainfall thresholds, thresholds from various sensors can be used to derive the integrated decisions to early warn the scenario	Immediate to maximum of 15 days of antecedent condition	Regional/catchment scale, site specific
Debris slide	(a) RAIN GAUGE: crossing rainfall thresholds, (b) PORE PRESSURE: crossing pore pressure threshold, (c) STRAIN GAUGES: change in strain measurements beyond the threshold levels, (d) INCLINOMETERS: change in inclination beyond threshold levels. monitoring at slip zones (e) SLOPE STABILITY: factor of safety value moves below one, (f) GEOPHONES: low-frequency microseismic signal detection (g) ACCELEROMETER: detection of change in acceleration	Meteorological models: rainfalls thresholds, Hydrological models: pore pressure thresholds geological models: slope stability (Factor of Safety) can be used, signal processing models, forecast models	Short term to a maximum of 15 days of antecedent condition	Regional/catchment scale, site-specific
Mud: flow/slide	(a) RAIN GAUGE: crossing of rainfall threshold (b) SOIL MOISTURE: initial moisture conditions (c) PORE PRESSURE: saturation condition (d) ACOUSTIC: capturing variability in acoustic emission (e) VIBRATION/ACCELERATION: detection of ground acceleration	Rainfall threshold based models, movement, acoustic and signal processing based models. Derive integrated decision models based on the sub-events	Very short term to a few days of antecedent rainfall condition	Regional/catchment scale, site specific

(continued)

Table 2 (continued)

Landslide type	Detection mechanism	Decision models	Expected temporal scale	Expected spatial scale
Creep	(a) CRACKMETERS: increase in crack length (b) RAIN GAUGE: crossing rainfall thresholds, (c) PORE PRESSURE: crossing pore pressure threshold, (d) STRAIN GAUGES: change in strain measurements beyond the threshold levels, (e) INCLINOMETERS: change in inclination beyond threshold levels. monitoring at slip zones (f) ERT: periodic resistivity profiles for moisture changes (g) GEOMORPHIC CHANGES: ground survey to mark the cracks, subsidence etc (h) SAR interferometry: deformation monitoring	Rainfall threshold-based models, multiple thresholds for monitoring the rate of change of movement, after few years it crosses factor of safety and can fail	Multiple months to years	Site specific
Complex landslides	(a) Landslide hydrology plays important role in a complex landslide (b) Three-dimensional groundwater regime in both the short and long term needs to be captured	Meteorological models: rainfalls thresholds, hydrological models: pore pressure thresholds geological models: slope stability model can be used	Immediate to long-term	Site specific

to be integrated with the decision model of the LEWS for large-scale spatial monitoring of landslides since each of these events has a different time scale and diverse spatial scale of prevalence. This is essential for effective early warning of imminent landslides to save lives. However, this comprehensive approach is lacking in existing landslide monitoring and detection systems. This demands our existing traditional systems to be enhanced to derive landslide early warning. Therefore, this study is devised to explore and detail a few case studies of LEWS deployed in India for capturing multidimensional and multilevel landslide dynamics to effectively issue early warnings to the vulnerable population at risk.

4 Landslide Risk Management Framework

To achieve a real-time understanding and forecasting of the complex and unpredictable landslide phenomena, the key functionalities that need to be performed are compiled into an integrated landslide risk management framework, as illustrated in Fig. 3. The framework consists of three sections as follows.

(a) Risk Assessment
   1. Measure
   2. Monitor
   3. Knowledge Discovery, Event detection: Risk analysis
   4. Forecast Model, Artificial Intelligence Model: Risk evaluation

(b) Cost-Benefit Analysis
   1. Risk Visualization
   2. Early warning: Risk control
   3. Dynamic Model
   4. Artificial intelligence model
   5. Multiphase Decision model
   6. Multiscale Early Warning Model

(c) Risk Communication and Risk Governance
   1. Risk policy/protocol development
   2. Operations management
   3. Community engagement
   4. Capacity development
   5. Real-time communication
   6. Multiscale communication model
   7. Services and Alerts

To implement the above framework, we require a system with requirements as shown in Fig. 1. Such a system can bring community-level disaster resilience. These requirements can only be achieved through a multi-domain approach since a single domain is not capable of providing solutions to the challenges encountered in each and every area. Experts from the domains of climate science,

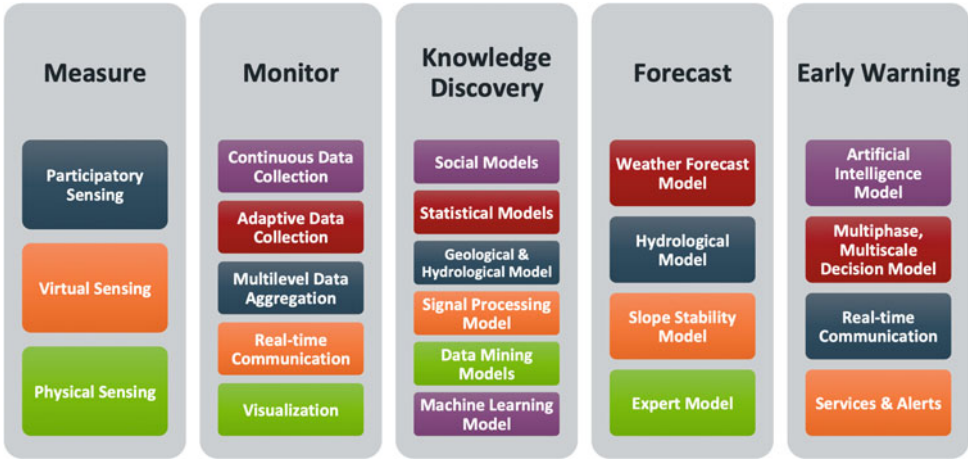

Fig. 1 Requirements for community level disaster resilience

geoscience, hydrology, engineering, data science, and social science, as well as community leaders, administrators, and community members, need to be involved to jointly design, develop, and deploy the solutions.

The complexity of landslide phenomena demands heterogeneous types of sensing to capture sub-events, unveiled through dynamic changes in multiple earth systems. Therefore it would require physical sensing of several events using sensors, where each sensor interacts with its surroundings to measure various environmental parameters. Participatory sensing by the community members is also very effective in capturing any anomaly, which could be a precursor. This is a community champions-based solution, where groups of individuals trained in physical landslide monitoring like measuring rainfall, new crack formation, old crack width tracking, open well water level tracking, etc., work as a group using social networking tools to detect the possibility of landslides and help the community to evacuate during disaster prone months of the year. Virtual sensing in landslide detection is another effective measurement tool to derive a few events based on the physical sensing of some other related parameters. This reduces the cost incurred for developing a direct sensing system and enhances the spatial and temporal coverage of sensing. The real-time measurement of causative factors and triggering mechanisms using physical sensors, participatory sensing approaches, and virtual sensing, need to be monitored either continuously or adaptively for each of the sub-events based on its domain characteristics. These data need to be aggregated in multiple levels based on the order of the sub-events and perform data visualization to extract inherent and useful knowledge for event detection.

Multilevel data aggregation, knowledge discovery, and event detection need to be utilized for risk analysis. However, the key challenge is that the different landslide classes differ in the temporal and spatial scale of prevalence. This demands the knowledge of landslide causative parameters, triggers, and causal relationship between the parameters, and dynamic thresholds. This knowledge will dynamically vary based on the context. Hence the sensing system needs to be

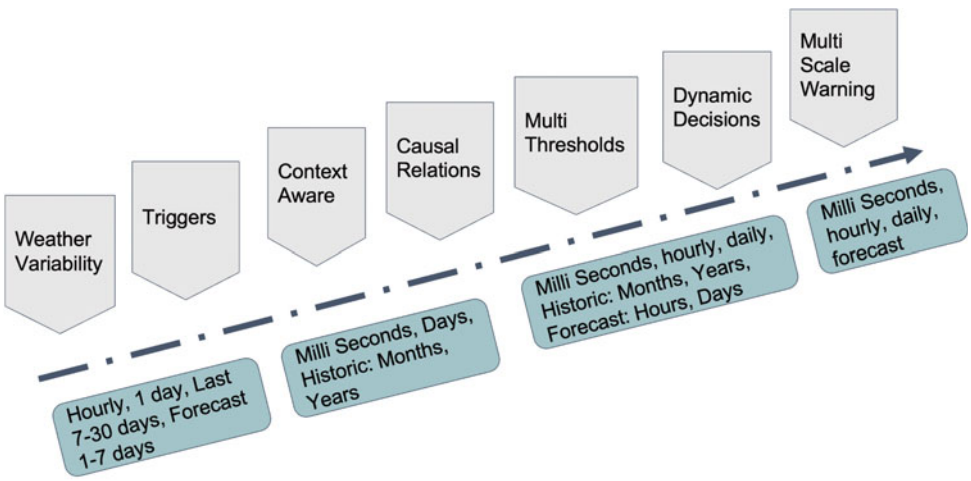

Fig. 2 Temporal variability in the landslide monitoring process

unique in capturing and processing the data on multiple scales to derive efficient landslide warnings. As Fig. 2 showcases, the temporal scale of monitoring and mapping of weather parameters, triggers, contexts, casual relationships, thresholds, decisions, and warnings differ. Therefore the sensing, processing, communication, and visualization system need to accommodate data collection, storage, and visualization in multiple time and spatial scales.

Specific to each of the landslide types and the characteristics of each of its sub-events, knowledge discovery and event detection need to be performed for real-time risk analysis. The knowledge discovery and event detection could be achieved using different models such as statistical, geological, hydrological, metrological, machine learning, and data analysis models. This derived knowledge will be utilized for risk evaluation by forecasting the events using existing and new models such as weather forecast models, hydrological models, slope instability models, and expert models. The output from these forecasting models will be utilized to provide early warning about the probable imminent landslides using artificial intelligence techniques, and multi-phase, multi-level decision models. The early warnings will be adaptively communicated in real-time using the different web and mobile app-based services.

The underlying dynamics resulting in landslides can be derived utilizing theoretical as well as data-driven models incorporating the real-time observations, historical data, and antecedent conditions of the triggering factors. This further leads to reliable forecasts of landslide initiation, incorporating meteorological, hydrological, and slope stability modeling systems along with advanced machine learning and artificial intelligence techniques. These forecasts will be utilized in a multi-phase, multi-level decision system in order to provide robust early warnings. Efficient web-based, as well as mobile app-based services, will enable the effective communication of these warnings in real-time. This process aids in providing warnings at regional, catchment, and site-specific scales. The visualization system further aids in the demonstration of the interrelations between the various heterogeneous parameters as well as their individual impact on landslide initiation.

Periodic cost-benefit analysis needs to be performed on such a system. This would require the deployment of continuous real-time visualization and risk control models. The visualization system should be equipped to deliver interrelationships between the spatio-temporal heterogeneous data collected from various sensing systems.

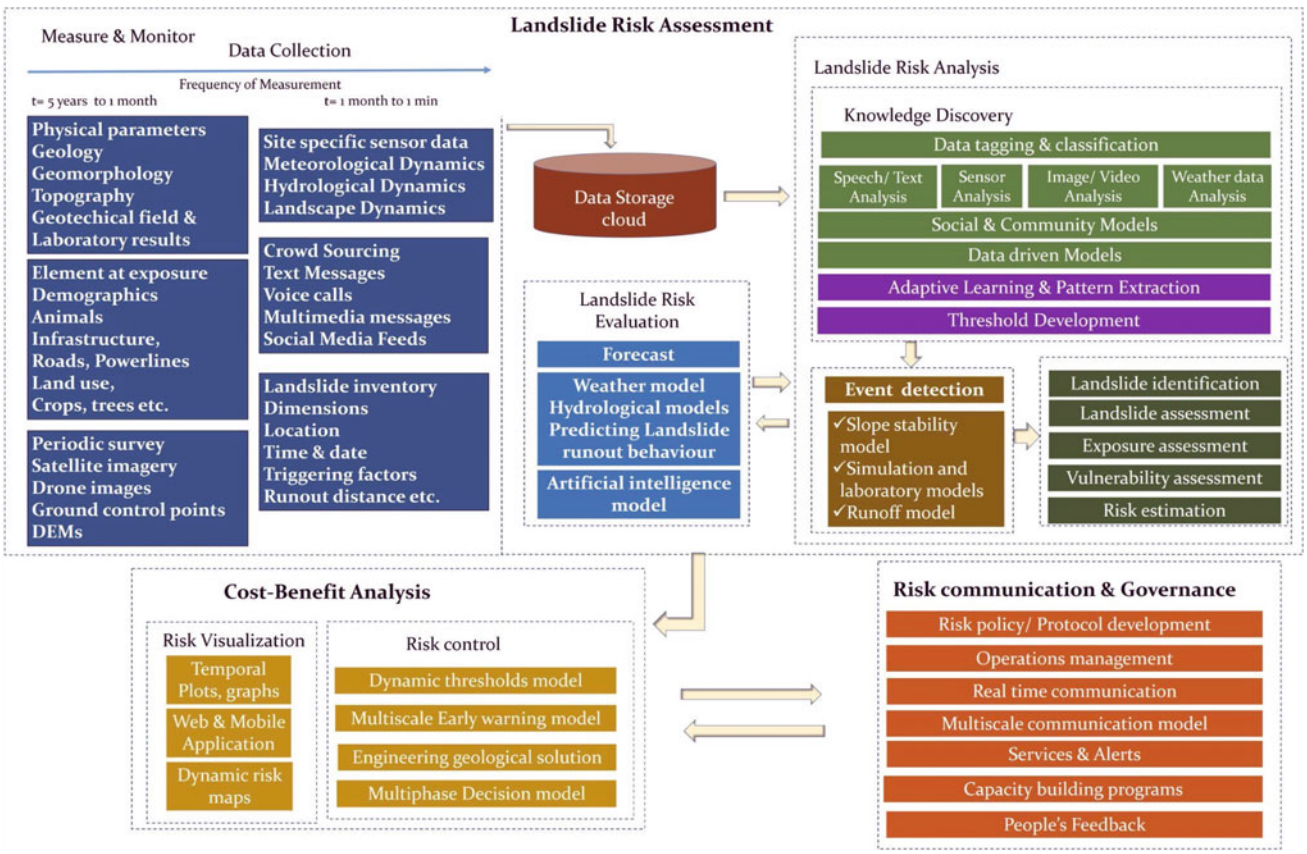

Fig. 3 Integrated landslide risk management framework

This will be utilized to elucidate the impacts due to individual parameters and their interrelationships on landslide initiation. Risk control demands the development of early warning models. This would require gathering an understanding of the dynamic variability of heterogeneous parameters, interrelationships, antecedent conditions, and their impact on landslide initiation. This knowledge could be utilized for developing machine learning-based models and artificial intelligence-based models to derive the thresholds and forecasts for single and multiple parameters. These models would be integrated based on the type of landslides prevalent in the deployment area, and the sequence of sub-events to derive the multiphase decision models. The output of the multiphase decision model will be utilized to derive the multiscale early warning model to produce warnings at regional, catchment, and site-specific scales.

In order to translate the outcomes of risk assessment and cost-benefit analysis, active risk communication, and an efficient risk governance mechanism are mandatory. Effective risk governance requires multi-level risk communication among the stakeholders such as scientists, research institutes, government bodies, local administration, non-profit organizations, and the community. To achieve this, specific risk policies or protocols need to be developed with the involvement of the stakeholders so that early warnings can be disseminated to the relevant stakeholders and local governance institutions in the expected region of landslide impact. The risk governance and risk communication are also dependent on end-to-end operations management, active community engagement, and integration of capacity development programs to equip the multi-stakeholders for operating and managing the LEWS.

The effectiveness of LEWS functionality is dependent on timely communication of real-time risk information and early warnings to relevant stakeholders. Multiscale communication models need to be developed to disseminate the risk levels to relevant stakeholders in specific landslide-prone areas. Additionally, this system needs to be adaptive to manage communication services during the dynamic scenarios of network and power outages. The real-time services and alerts need to be generated in local languages and disseminated using web services or mobile applications to reach a large number of stakeholders in the shortest time period.

Envisioning the need for a system integrated with the above requirements to provide an end-to-end solution for real-time landslide monitoring and early warning, a landslide risk management framework has been designed, as shown in Fig. 3. Multi-domain solutions such as IoT-based landslide early warning systems, social media analytics, community engagement, etc., are integrated to develop comprehensive solutions for landslide risk reduction and resilience building. Figure 3 depicts the landslide risk management framework and its sub-modules that could be utilized for developing landslide early warning systems for multiple landslide classifications.

5 Case Study: Real-World Deployment in India

The Himalayan region in North India and the Western Ghats in South India are major hotspots of landslides because of their ongoing tectonics and mass wasting processes, which are also accelerated due to anthropogenic activity (Martha et al. 2021). Therefore to observe and investigate these landslides with widely varying dynamics, one case study area has been chosen from each of the regions. These two case study areas are (i) Western Ghats region: Munnar, Idukki District, Kerala, (10° 5′ 26.56″ N; 77° 3′ 22.93″ E) (Ramesh and Vasudevan 2012) and (ii) North Eastern Himalayas region: Chandmari, Gangtok (Dist), Sikkim (27° 20′ 17.54″ N; 88° 37′ 22.78″ E) (Harilal et al. 2019) (see Fig. 4).

The first case study area, Munnar, being named after the confluence of three perennial rivers, lies in the Western Ghats. These are Precambrian mountains with Granitic bedrocks overlaid by a weathered regolith of aluminum-rich saprolites with variable thickness (GSI 2016). The mountain belts of Munnar are covered by tea estates, montane grasslands, shola forests, and urban areas which receive about 2470 mm of average rainfall annually (IMD, https://mausam.imd.gov.in/). These denudational hills see several landslides during the monsoon season resulting in the loss of lives and property (Ramesh and Vasudevan 2012). Rainfall is the major trigger for the landslides in this area and in the past 10 years, there have been more than 50, small and big landslides in less than 10 km^2 around Munnar (*Source* GSI 2018, 2020).

The second case study area, Chandmari comes under the main central thrust zone (MCT) of the Himalayas. Here the underlying lithology is weathered gneisses interbedded with mica-schists. This region receives more than 2500 mm of annual rainfall which makes it highly prone to landslides. The landslides here, and in the Himalayas in general, are induced by both rainfall and/or earthquakes. Therefore Chandmari is chosen as a representative case study area to learn about the dynamics of complex Himalayan landslides. Chandmari is an active landslide since the 1960s. It has been reactivated several times in the past with a huge landslide in 1968 and has experienced movements subsequently in 1984, 1997, 2007, and 2011. Recently during the monsoon periods of 2018–2022, several types of small and medium size landslides in the study area, Chandmari, have been observed as listed in Table 3. This mostly includes debris flow, shallow surface road-side slumps, rockfalls, mudslides, complex landslides, and deep-seated subsidences.

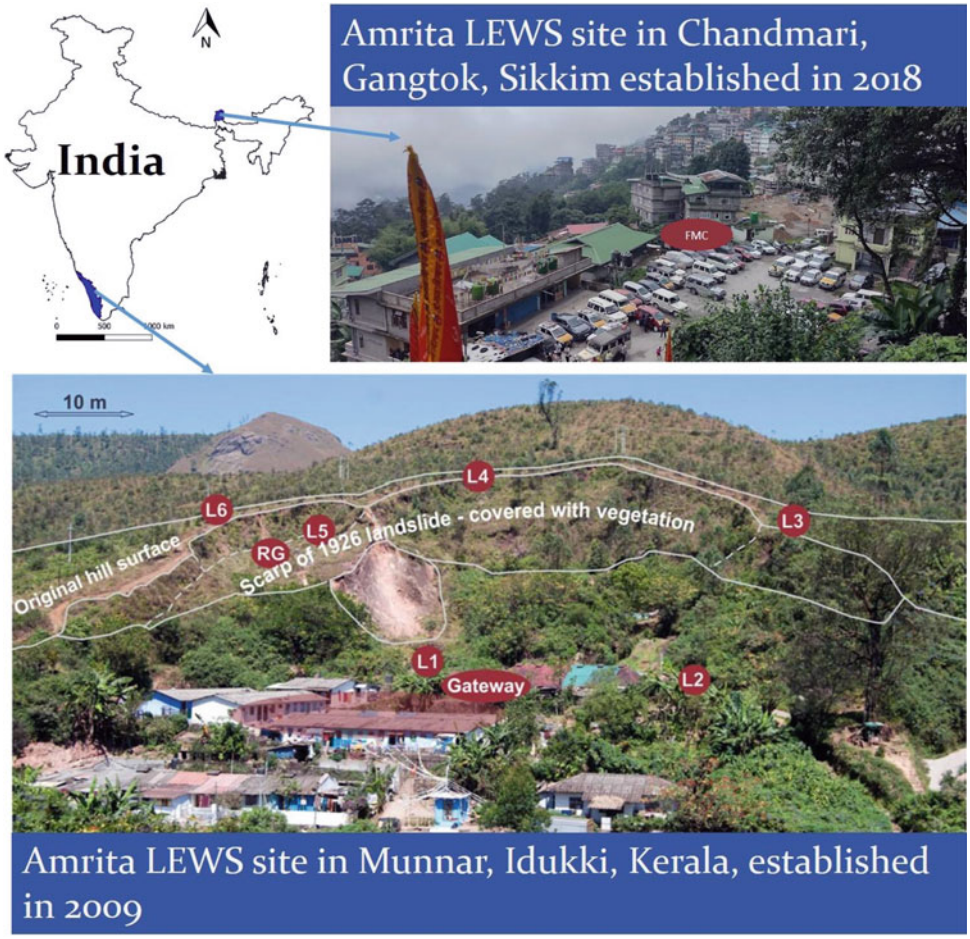

Fig. 4 Case study areas: the two Amrita-LEWS deployment sites

Additionally, anthropogenic activities such as unplanned construction, road widening, unscientific changes to land-use land cover, mining activities, heavy vehicular movement, seepage from sewages drains, etc., have accelerated the landslide activity in both the study areas (Kanungo et al. 2020). The architecture of buildings is also unique to both sites. In Munnar, there are buildings with mostly one to two stories whereas in Chandmari the buildings have three to six stories. These building practices are also influenced by the population density of both the sites; the population density of Chandmari is 1858 people per km^2 whereas at Munnar it is 170 people per km^2. In terms of seismic activity, Munnar lies in Zone III of Seismic maps whereas Sikkim comes under Zone IV, often experiencing micro tremors. Topsoil composition in Munnar is weathered granitic gneiss overlaid by red weathered saprolite (red colored soil where feldspars weathers to clay) whereas Chandmari has interbedded mica-schists in gneissic rock (sandy soil layers where mica minerals weathers to partially expansible clays such as illite and vermiculite).

In Chandmari the landslides are both rainfall-induced and earthquake-induced; whereas in Munnar the landslides are majorly rainfall-induced. The prominent types of landslides that occurred in Chandmari are rock falls, debris slides, and creep movement whereas debris-cum-earth slides, complex landslides with retrogrative movement, are active in Munnar. The design, development, and deployment of IoT-based LEWS at both the case study areas are unique due to the distinctive landslide dynamics present at each of the case study sites, as explained above. Moreover, this affects each of the LEWS subsystem's design in different ways. For example, the selection of sensor/detection mechanism has to be performed in accordance with the landslide triggers of the area and the decision models deployed in servers also have to be tweaked, for detection of these triggers and for tracking the evolution of the sub-events associated with the landslide type for generating warnings.

6 IoT Based Landslide Early Warning System in Case Study Areas

The Amrita's IoT-based LEWSs have been deployed and operational 24/7 in the two sites namely Munnar, Western Ghats and Chandmari, North Eastern Himalayas as depicted in Fig. 4. The LEWSs at both the sites consist of several

Table 3 Details the different types of landslide occurred in the study areas

Study area	Types of landslides	Location of landslide	Date of slide	Activity
Chandmari	Rockslide	Near Dep 1, 2 mile JN road	16 June 2022	Active
	Rockfall	Near Dep 5	Aug 2019	Suspended
	Debris flow	Below Dep 5	1997, 2005, 2018	Reactivated
	Debris slide	Above Dep 8	Aug 2019	Active
	MudSlide	Below Enchey Monastery	26 June 2022	Suspended
	Deep seated Subsidence/ creep	Near petrol pump near Dep 7, on the JN road above Dep 3, above Dep 1 (crown region)	Aug 2018, July 2019, Aug 2020, July 2021, June 2022	Active
	Complex landslides	Chandamri Hill	Recorded since 1984–2022	Active
	Channel wash	JN road along the drainges between Dep 1 and Dep 3	Aug 2019, 16th June 2022, 28th June 2022	Suspended
	Anthropogenic landslides	Below Enchey Monastery	28th June 2022	Active
Munnar and Devikulam villages	Debris cum earth slides	Nalathani road	2018	Suspended
	Deep seated complex landslide	Govt college Munnar	2018, 2019	Active
	Channel wash	Near Devikulam Hospital	Aug 2018	Inactive
	Rock falls	Gap road	Every monsoon 2018–2022	Active
	Mudslide	Behind Sarvana Bhavan, Munnar town	2018	Inactive
	Creep slide	Near Dep 4, Anthonior colony	2013–2022	Active
	Debris cum earth Slides	Behind SBI, Devikulam	Aug 2018	Active
	Debris cum earth Slides	Behind Brothers house, Devikulam	Aug 2018	Active
	Debris flow with long runout	Pettimudi landslide, Munnar	Aug 2020	Suspended

Deep Earth Probes (DEPs) installed below ground that can sense the various geophysical parameters and their dynamics. These DEPs are connected to above-ground, state-of-the-art embedded systems, heterogeneous communication systems, and smart algorithms to make them Intelligent Wireless Probes (IWPs). These IWPs constitute the edge nodes and are integrated within an IoT framework across the case study site and into the decision models in the cloud servers.

The pilot system of Munnar was deployed from January to March 2008, and the full-scale system from January to June 2009. Currently, the whole area consists of 20 Deep Earth Probes integrated with approximately 150 geophysical sensors connected to 20 wireless sensor nodes. At Chandmari in Sikkim, 11 potential locations for deployment of DEP were identified after detailed investigations. The pilot deployment was completed in 2015 and included three pore pressure sensors, two inclinometers, three 3-axis geophones, and one weather station to monitor the area. The full deployment was completed in 2018, with the area consisting of 11 IWPs with around 200 geophysical sensors.

Indeed for effective early warning of landslides, the IoT-based LEWS should integrate features such as multi-parameter sensing, adaptive scalability with respect to the dynamic contexts, heterogeneous coverage in sensing and networking, remote configuration, dynamically acquiring the sensing data based on the context, a scalable resilient communication network for handling heterogeneous upstream and downstream data transfer in harsh environments, spatial knowledge absorption, multiple level decisions based on both real-time and historic heterogeneous sensor data, and information dissemination to different stakeholders such as students, researchers, citizens, administrators, policymakers etc. Therefore, the subsystems need to be integrated with

features such as heterogeneity, flexibility, adaptability, and scalability for autonomous information generation. Considering all the above parameters Amrita LEWS has been developed and is designed for continuous monitoring and warning of landslides.

The unique features of the Amrita LEWS are summarized below:

1. Real-time risk assessment is performed by measuring and monitoring of multi-domain parameters using a dynamic IoT platform, crowd sourced- landslide tracker (Hariharan et al. 2021) and Amritakripa app (Guntha et al. 2020; Guntha and Vinodini Ramesh 2021) and Social media data collection (Phengsuwan et al. 2019) as opposed to traditional static maps. The dynamic platform of Amrita LEWS captures:
   (a) Meteorological dynamics: Rainfall, Temperature, Humidity, Wind speed and direction. Both Chandmari and Munnar have different climatic regimes. One is Himalayan tropical, temperate, and alpine climatic conditions with several snow-capped mountains and glaciers but the other is Western Ghats climate where heavy rainfall varies from 935 ± 185.33 to 1794 ± 247 mm. Rainfall patterns of both regions differ and thus rainfall threshold also varies both at regional and site-specific scales.
   (b) Hydrogeological dynamics: Volumetric water content from moisture sensor, hydraulic pressure, groundwater level, and soil temperature from piezometers.
   (c) Geophysical dynamics: Three components of ground velocity data from three axis geophones, Time-varying three-dimensional resistivity profiles from electrical resistivity tomography (ERT), (Ramesh 2017; Vinodini Ramesh et al. 2017).
   (d) Landscape dynamics: Movements along two axes from inclinometers, strain gauges, and tilt meters
   (e) Social dynamics: Response of community data from Twitter feeds and participatory sensing approaches such as mobile apps which include text, audio, video, maps, and lat-long information.
2. Risk analysis is performed by knowledge discovery by initiating continuous learning of dynamic behaviors and interrelationships between multiple heterogeneous parameters for identifying Precursor scenarios, understanding Failure Mechanisms, forecasting Post Landslide scenarios, and identifying Reinitiating mechanisms (Ramesh 2014).
3. Risk analysis is enhanced by integrating event detection modules through heterogeneous Models such as rainfall threshold (Prabha et al. 2017) Hydrological models, slope stability and IoT edge analytics (Kumar et al. 2020).
4. Risk evaluation is performed by forecasting and early warning through machine learning and artificial intelligence-based models (Hemalatha et al. 2019) to predict the pore pressure variability and factor of safety of the hill.
5. Cost-benefit analysis is performed by utilizing "Amrita Drishti", a web-based visualization software integrated with decision models for spatio-temporal data analysis, deriving interrelationships, and multi-level thresholds for causative and triggering parameters
6. Enhancing the reliability of detection and early warning using heterogeneous detection models (Harilal et al. 2019; Thirugnanam et al. 2020) and integration of multi-domain parameters, for reducing false alarms.
7. Multi-phase decision models developed based on the expected sub-events for each type of landslides
8. Multi-scale early warnings utilizing the knowledge discovered from real-time heterogeneous data and historic data have been developed
9. Real-time risk communication and risk governance through participatory DRR approach and mobile applications (Amritanand et al. 2020) to adaptively disseminate context and location-aware information to relevant stakeholders
10. In-person multi-level multi-phase community engagements performed during pre-monsoon time period
11. Training provided for empowering the community Monitoring social dynamics related to rain, flood, members to map the triggers, causative factors, and real-time sub-events using the landslide tracker mobile application for achieving enhanced risk governance and risk communication to relevant stakeholders and landslides from automated tweet collection, event detection, and providing situational awareness of the real-world conditions from tweets and online news.

7 Uniqueness of LEWS: Munnar and Chandmari

Case Study Area 1: Munnar, Western Ghats

The key landslide types prevalent in Munnar are debris-cum-earth slides, complex landslides with retrogrative movement, creep landslides, and debris flow. Most of them are triggered by long-duration medium/heavy rainfall, changes in LULC, and anthropogenic activities. The material

type and heavy rainfall cause increased pore pressure leading to landslide initiation as shown in Fig. 5.

Based on the triggering mechanisms, the material type, and the major geological, hydrological, and meteorological features the key parameters that need to be measured by LEWS are selected. The key sub-event group is rainfall leading to water infiltration, and saturation of the material, which results in increased pore pressure leading to failure of the slope. This failure mechanism could initiate landslide types such as flow or slide or creep, based on the localized geomorphology. Therefore the risk assessment demands measurement and monitoring of Deep Earth Probe (DEP) integrated with sensors such as rain gauges, moisture sensors, pore pressure transducers, strain gauges, tiltmeters, etc. The slip surface activity of landslides in the Western Ghats is much lower in comparison to the Himalayas and hence strain gauges are good at detection of activity in comparison to inclinometers. The frequency of monitoring by each type of sensor will depend on the characteristics of (a) weather pattern to decide on rain gauge sampling rate, (b) water infiltration rate to decide on moisture sensor sampling rate, (c) water flow lines and soil layer properties to decide the pore pressure sampling rate, (d) strength of soil or rock materials in the deployment field and its geological structure to decide the rate for sampling strain gauge, tiltmeter, etc. This knowledge will provide the opportunity to finalize the dynamic temporal scale monitoring for the heterogeneous parameters. The monitoring of spatial variability of sensing parameters will be dependent on the sensing systems coverage and variability of parameters with respect to its domain, rainfall rate, and soil or rock properties. Based on these variabilities, the risk analysis is performed either in the edge node or in the cloud. The DEP integrated with the IoT system for edge analytics, real-time communication, and powering the whole system is known as the intelligent wireless probe (IWP), as shown in Fig. 6.

Risk analysis is performed through spatiotemporal analysis of single parameters for a long duration, deriving interrelationship among the parameters using data analysis or machine learning, and integrated multistage analysis for the heterogeneous parameters to derive the progression of sub-events using data analysis, machine learning and artificial intelligence approaches. This provides the opportunity for knowledge discovery and acts as the impetus for forecasting selected parameters and thus deriving the early warning models.

Over the years the rainfall patterns in the region have been drastically varying. The key rainfall data for more than ten years and the landslide event details are utilized in developing the Amrita Regional Rainfall Threshold Model and Amrita Site Specific Rainfall Threshold Model for Munnar. An integrated decision model using both real-time data and historic data is utilized to compare multiple models such as Caine, Amrita Model, and Innes Model (Harilal et al. 2019) for both real-time and antecedent rainfall scenarios. Based on this integrated model, both regional and site-specific warnings are provided for multi-stakeholders in Munnar. This will contribute to risk evaluation and risk control.

The unique soil properties in the Munnar region can lead to high pore pressure during extended periods of rainfall leading to landslides, hence pore pressure data collection by the detection mechanism in LEWS is very important. It is highly beneficial for risk evaluation and risk control if the

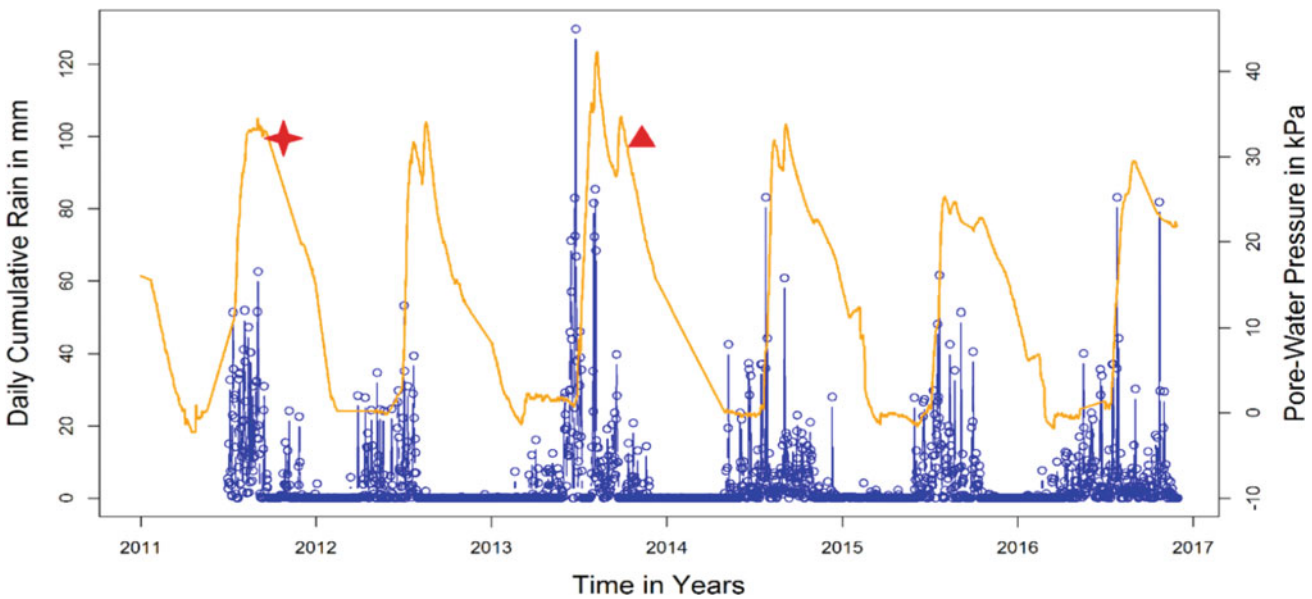

Fig. 5 Interrelationships of triggering factors and temporal variability

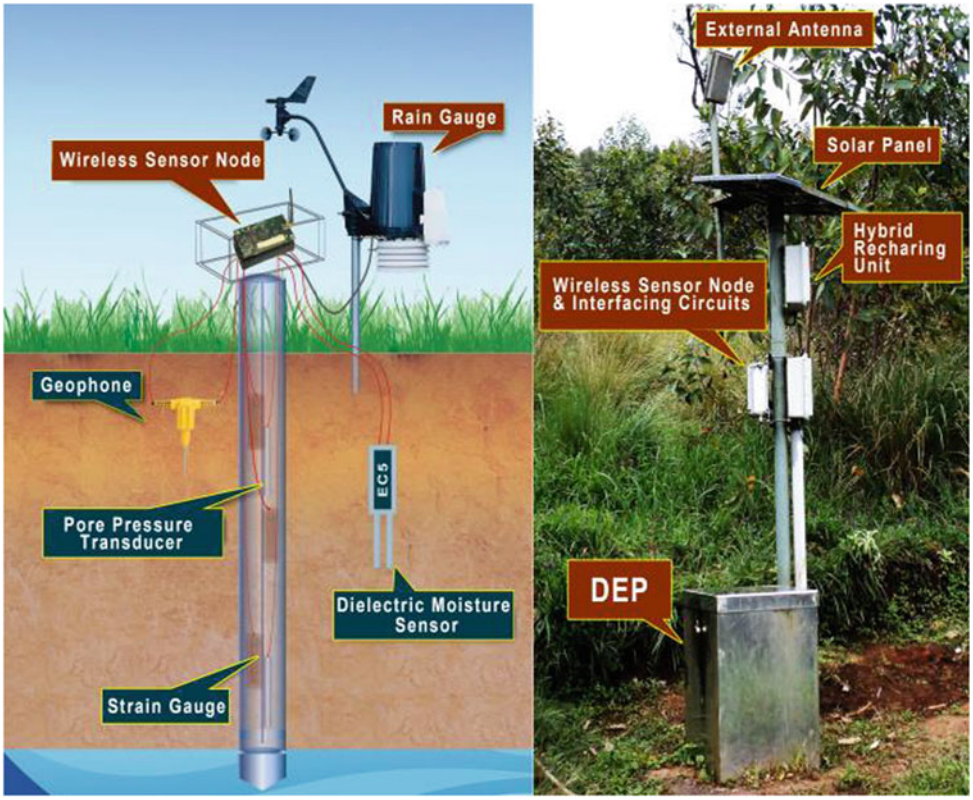

Fig. 6 Intelligent Wireless Probe with Edge Computation (Ramesh et al. 2014)

LEWS can forecast the pore pressure based on the real-time and antecedent rainfall conditions and soil properties of the specific location. The work detailed in Hemalatha et al. 2019, showcases the approaches used for nowcasting and forecasting the pore pressure and factor of safety values for the Munnar region using support vector regression methodology, as shown in Fig. 7. Support vector regression methodology is an adaptive learning methodology that takes into account the historic data and real-time data for learning and forecasts the futuristic condition of the slope 24 h ahead of time. The algorithm is designed in such a manner that even when real-time data from the field is not available due to any unforeseen reasons, the algorithm takes into account the rainfall forecast information from the Indian Meteorological Department to forecast the futuristic condition of the slope, thereby ensuring the reliability of the system. The forecasted futuristic conditions of the slope are utilized for risk evaluation and risk control. This approach is intended for enhancing the reliability of LEWS and provides extra lead-time for early warning.

The risk communication is integrated to perform automatically through the "Amrita Drishti" web platform to all stakeholders. However, based on the suggestion provided by Kerala State Disaster Management Authority (KSDMA), the initial communication will be sent to the secretary of KSDMA, the District collector, and Sub-district collector of the LEWS deployment location. KSDMA and District Government officials work with the local administration to implement the risk governance. In addition, has created a vast network of youngsters, women, and community members to inclusively work with Amrita and disseminate timely information. The team has also created a WhatsApp group named "Munnar community 4 DRR" for effective exchange of relevant information from multiple groups to enhance community-level disaster resilience.

Case Study Area 2: Chandmari, Eastern Himalayas

The key landslide types prevalent in Chandmari are triggered by short-duration heavy rainfall, seismic activity, high surface runoff, erosion, change in LULC, etc. Therefore in LEWS, the key parameters for observation are selected accordingly to detect these events and their subevents. In the Himalayas, geophones are key components of the detection mechanism, as seismic activity is very high and can lead to landslides with unique sub-events. Creep movement and subsidence along the slip surface of the slide is also commonly seen leading to landslide sub-events that require inclinometers and geophones to measure the slip surface activity and ground velocity. The pore pressure build-up and excessive pore pressure triggered landslides are much less in the selected case study area, possibly due to the presence of internal cracks leading to high drain out rates. Moreover, the design and maintenance of the subsystem are also complex due to the harsh operational conditions. For example, the

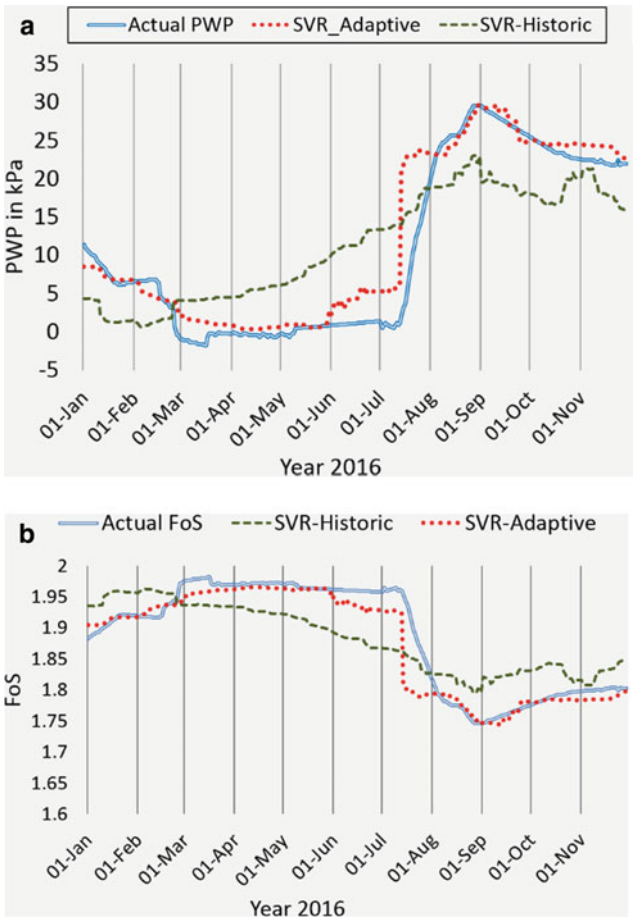

Fig. 7 Forecasting pore pressure. Forecasting factor of safety

thick vegetative cover introduces challenges for the operation of wireless communication and solar power systems. The wireless signal attenuation is very high in these conditions, requiring us to use heterogeneous communication architecture for better reliability. The challenges introduced by vegetation cover over solar panels have also led us to use a heterogeneous power system drawing power from multiple power sources.

Chandmari study area (32 ha) demonstrates the real-time risk analysis, risk evaluation, and risk control for multiple types of landslides (Fig. 8). The deployment area contains 11 Deep Earth Probes (DEP) integrated with heterogeneous sensors such as rain gauges, weather stations, moisture sensors, pore pressure sensors, strain gauges, inclinometers, and geophones.

The location of DEP 1 is more prominent for rock falls and rock slides, DEP 2 is more prominent for deep-seated landslides, DEP 3 is prominent for creep movements, DEP 4 creep movement, DEP 5 is prominent for debris flow and debris slide, DEP 6 is prominent for creep movements, DEP 7 is more prominent for subsidence cum complex movement, DEP 8 has shown debris slide, DEP 9 is relativity stable DEP 10 is more prominent for creep movements and debris flow or debris slide. Additionally, mudslides are also experienced within 1 km of the deployment area. The integrated IoT system deployed in each of these locations is fine-tuned to capture the causative factors, triggers, and the context using heterogeneous sensors. The thresholds of the decision models

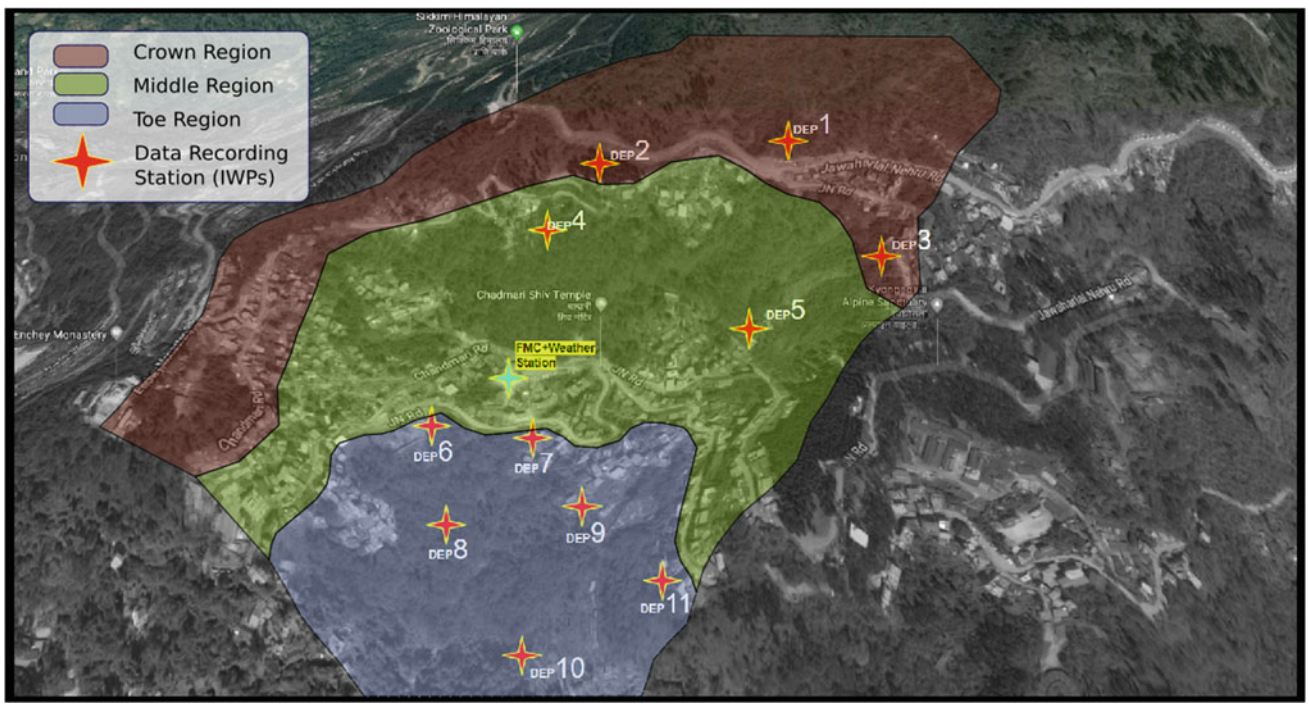

Fig. 8 Satellite view of Chandmari site, Sikkim (courtesy Google Maps)

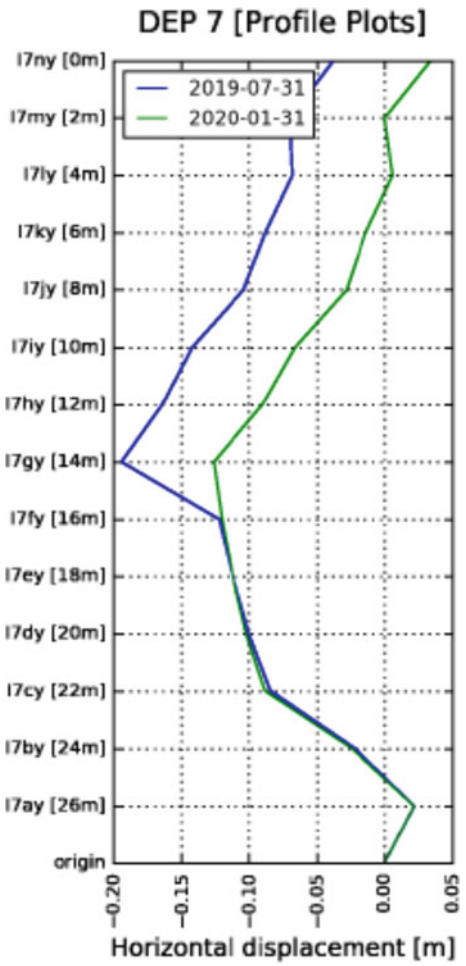

Fig. 9 Inclinometer data from Chandmari: detection of movements from 14 m beneath the earth

also differ due to the way the slopes react to the hydro-meteorological inputs. The integrated decision model for the whole deployment area had to integrate the models required for detecting the subevents of each landslide type. The decision model for Munnar is different from that of Chandmari as the sub-event types are different in both regions.

The risk assessment for the Chandmari case study area demands measurement and monitoring of Deep Earth Probe (DEP) integrated with sensors such as rain gauge, moisture sensor, pore pressure transducer, strain gauges, inclinometers, geophones, etc. The data analysis, knowledge discovery and event detection using these multiple parameters provide the opportunity to derive real-time risk assessment. Figure 9 displays the inclinometer data from DEP 7 Sikkim showing considerable movements, indicating displacement along slip zones.

Figure 10 displays the microseismic activity in DEP 1 captured by the geophones. These microseismic activities indicate the cracks' initiation and propagation leading to rock fall at about 7:30 am on 17th June 2020 about 100 m from DEP 1. These indications are further analyzed for undertaking propagation of movement within the subsurface and dynamically varying risks in the crown, middle and bottom part of the hill slope.

Knowledge discovery and event detection are very key modules for risk analysis and risk evaluation. For Chandmari, the impact of rainfall intensity on landslide triggering is studied in detail. Daily rainfall observations from the India Meteorological Department (IMD), from six stations of Sikkim, namely Gangtok, Mangan, Namathang, Maziar, Dentam, and Damthang, during the period 1990–2017 and the rainfall observations from our R-LEWS in Chandmari from 2015 onwards were utilized to derive regional rainfall threshold and site-specific rainfall Threshold. For this work, an intensity–duration (I–D)-based regional rainfall threshold for Sikkim state (Fig. 11) is derived as $I = 43.26\ D^{-0.78}$ (I = rainfall intensity in mm/day and D = duration in days) for the rainfall-triggered landslides, and a site-specific rainfall threshold for Gangtok area is derived as $I = 100\ D^{-0.92}$ (Fig. 12) (Harilal et al. 2019). Along with this, the influence of antecedent rainfall in landslide initiation is explored by considering the daily, 3-day, 5-day, 7-day, and 20-day cumulative rainfall values associated with landslides. The proposed threshold equations will aid in enhancing the real-time landslide early warning system (R-LEWS) being developed for Sikkim and will act as the first level regional and site-specific warning for the Chandmari region. Figures 11 and 12 showcases the implementation of the Amrita Regional Rainfall Threshold Model and Amrita Site Specific Rainfall Threshold Model in "Amrita Drishti"—a web-based platform respectively. Figure 13 shows a 7 days threshold crossed during 2021 in Chandmari and a comparison of three different types of thresholds. It compares and indicates how different models are utilized for generating early warnings for different types of landslides.

The LEWS at both the case study sites have been enhanced by the integration of an event-specific detection mechanism and corresponding response protocols. Each landslide event is thus sub-divided into a sequence of sub-events inside the LEWS as mentioned in Table 1. This knowledge of sub-events is generated based on learnings from the past landslide activity in the study area. The whole landslide process is therefore modeled as an evolution from one sub-event to another sub-event, from initiation to slope failure.

The detection mechanism as mentioned in Table 1 helps in capturing the dynamics of the signal from the geophysical sensors. The detection mechanism consists of heterogeneous sensors such as Meteorological, Hydrological, and other Geophysical sensors. Thresholds exist for each of the measured parameters such as rainfall or movement rate and for derived parameters such as slope factor of safety.

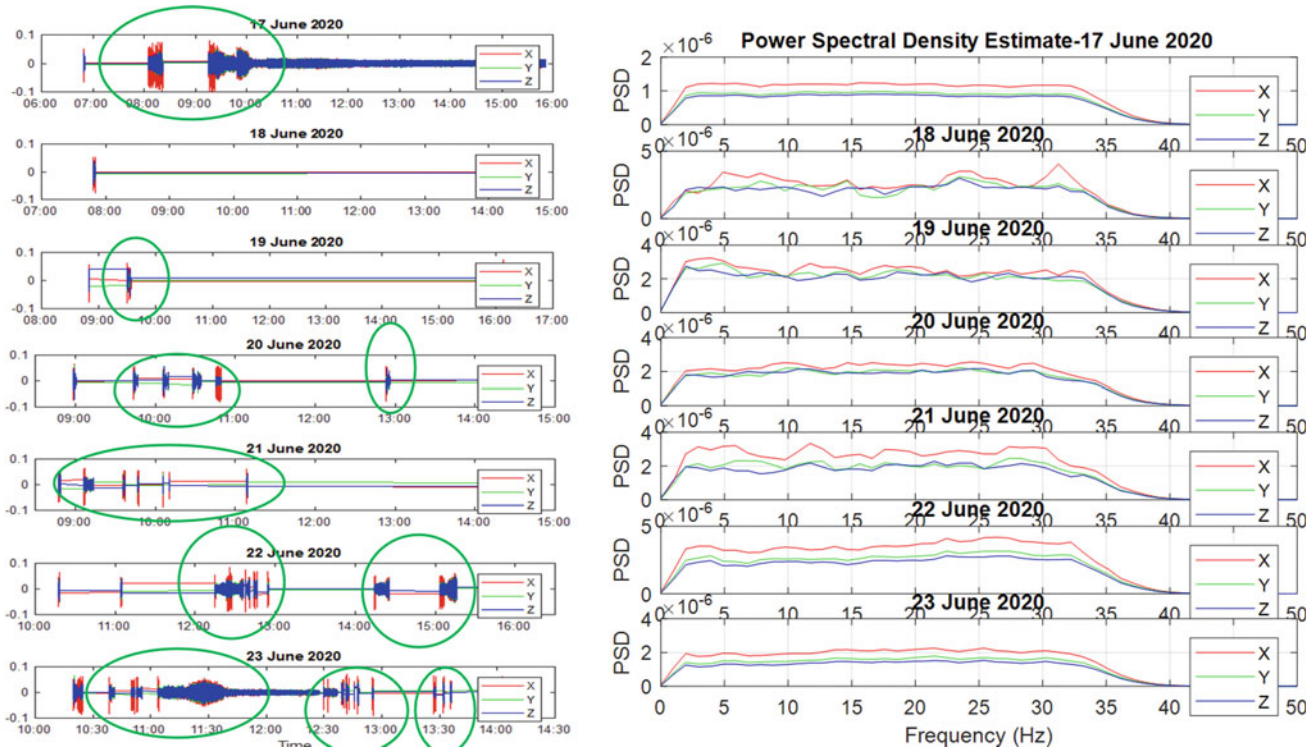

Fig. 10 Geophone data from Chandmari—micro seismic activity detection

The real-time data is collected from all the DEPS and stored into data servers for further processing. In order to increase the reliability of the LEWS and increase the available lead time for warning, edge processing based algorithms are also deployed on the IWPs and these also increase the reliability of the system.

In comparison to other LEWS globally, the LEWS deployed in both the case study sites monitor the sub-events of a landslide and pinpoint the evolution of the subevents. For example, Munnar has more prominently debris cum earth slides with head ward retreat movement owing to large soil thickness and extremely heavy rainfall. The sequence of events for such slides is saturation leading to loss of strength in the surficial deposits. After prolonged rainfall the movement along the plane either bedrock/overburden interface or a surface gets initiated which turns to rapid downward sliding and forward rolling of rock fragments within a few minutes. Whereas in Sikkim the terrain is more rocky with both rainfall and seismic tremors resulting to rock-cum debis falls. The sequence of events for such slides as detailed in Table 1, starts with crack initiation which over time progresses to crack propagation finally leading to rock toppling, rock sliding and rock fall. Although both in Munnar and Sikkim, several other types of landslides are prevalent at different locations as detailed in Table 3 and for each of them a combination of sequence of events needs to be captured.

The decision model is selected based on the sub-event type being encountered by the LEWS, this increases the reliability of the overall early warning system, as the detection algorithms are dealing with individual sub-events. In addition to this, the decision model outputs four levels of warnings based on the current status in the evolution of the landslide process. The four level warning generated by the system is shown in Fig. 14.

Based on the above shown four-level early warning system, the LEWS has generated warnings for Munnar sites in the year 2009, 2011, 2013, 2018, 2019, 2020, 2021 and 2022 and for Chandmari site in the year 2022. And these warnings have been relayed to various stakeholders for the purpose of evacuation (Fig. 16).

Risk control and mitigation could be initiated from the continuous measurement data. For example in Chandmari, the output from the inclinometer sensors has been selected by Sikkim State Disaster Management Authority to initiate mitigation activities near DEP6, DEP7 and DEP8. The output of the movement sensor (inclinometer) (Fig. 8) in the Chandmari site is used to map the downslope vulnerable areas associated with the landslide. The total volume of the unstable sliding mass was calculated as roughly 7×105 m^3. This entire unstable mass is also measured to be moving in the north 195° East [S15E] direction as per the sensor data. For calculating the mass of the unstable material, mean density for underlying material, biotite granite

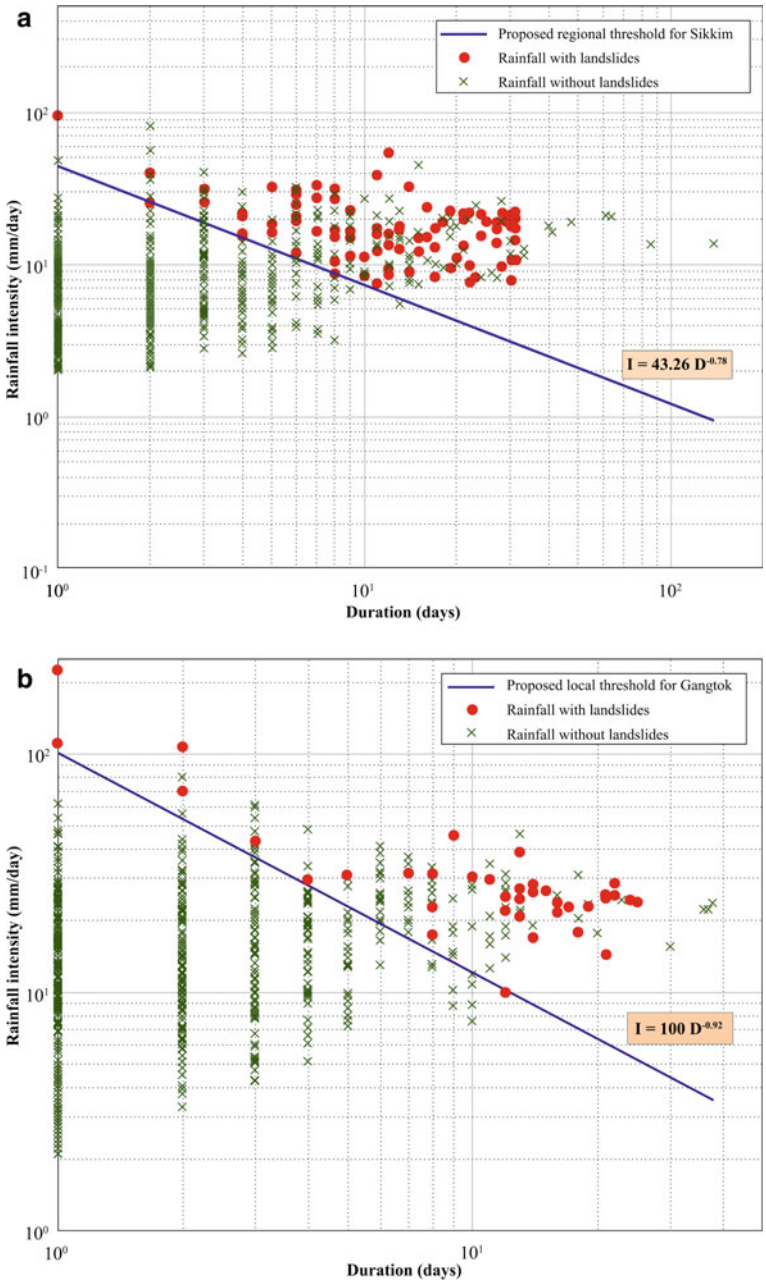

Fig. 11 Sikkim—Amrita regional rainfall threshold model. Implementation of Amrita regional rainfall threshold model in "Amrita Drishti"—web based platform

gneiss (1.65 gm/cm3) is used for rough estimates. The mass of the material is approximately 1.155 million tons. This indicates if a landslide is initiated 1.155 million tons of material will fall on individuals living on the downslope. The various elements at risk as a result of this movement are fuel stations, roads connecting the Gangtok Town to Nathula Pass, Numerous Human settlements, Schools and a Tourist Parking lot. With the calculated affected/ destabilized soil mass, the stability of the slope/vertical cut could be estimated and retaining structures could be built suiting the needs.

The risk control, communication and governance at Chandmari site is explained below. Figure 15 shows the rainfall thresholds were crossed on 28th July 2022 followed by initiation of six small landslides in the Chandmari.

For incorporating the comprehensive needs of end-to-end community disaster resilience, an adaptive and integrated approach is proposed. This approach has been developed and enhanced through the decade-long involvement in disaster management in the Munnar region and is also being implemented in Sikkim since 2018 in collaboration with state disaster management and Indian Meteorological

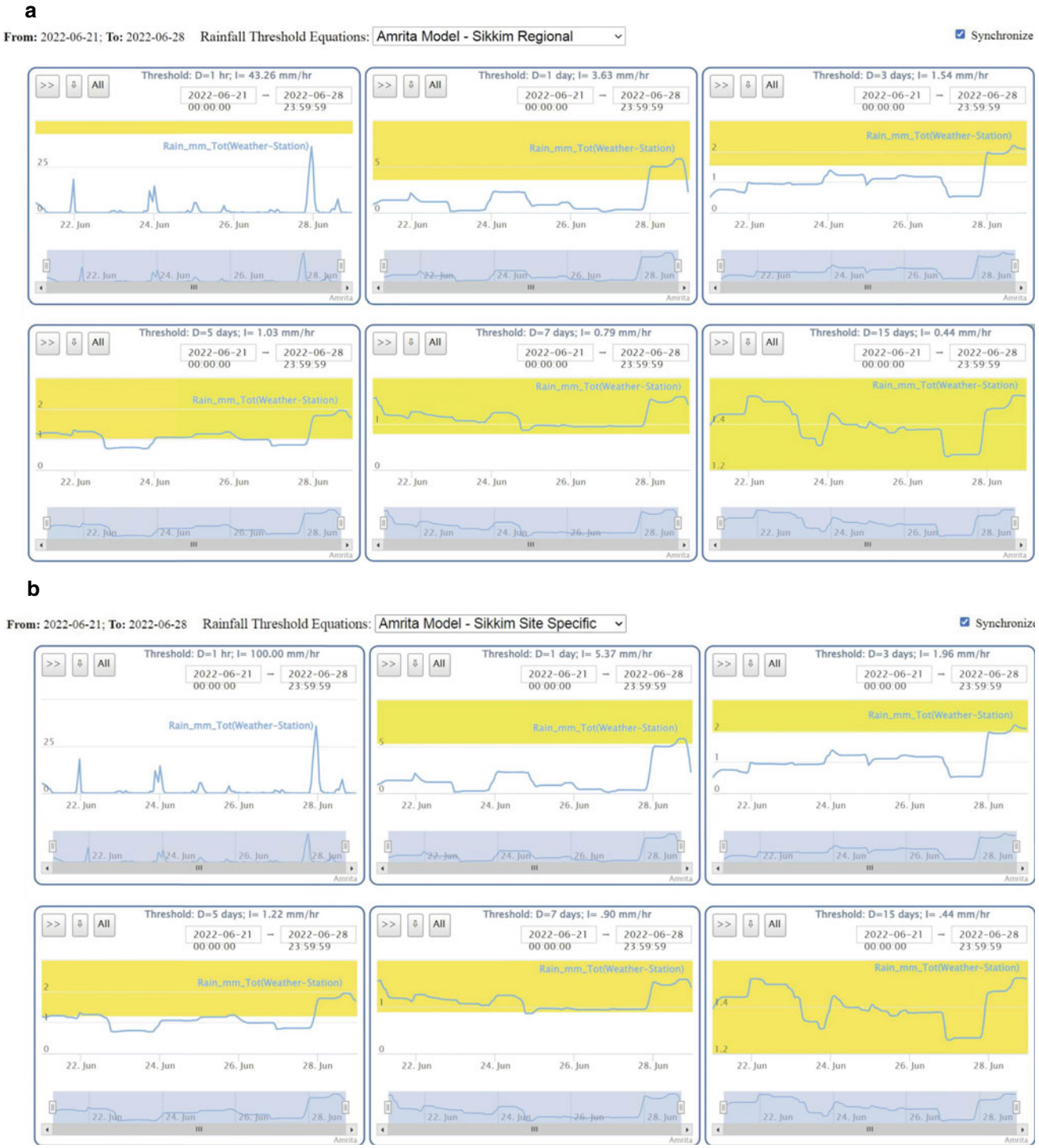

Fig. 12 Sikkim—Amrita site specific rainfall. Implementation of Amrita site specific rainfall threshold model in "Amrita Drishti"—web-based platform

Department (IMD). The adaptive integrated community disaster resilience solutions implemented in the case study area are detailed as follows (Fig. 17). For enhancing the preparedness development of crowdsourced applications, social media based awareness programs, IoT systems for monitoring have been implemented. In order to equip the rescue and response team, we developed Amrita Kripa Mobile app, 24/7 call centers, prepared and trained field volunteers during the 2018–2019 Kerala Multihazards. To optimize the response based on early warnings from the

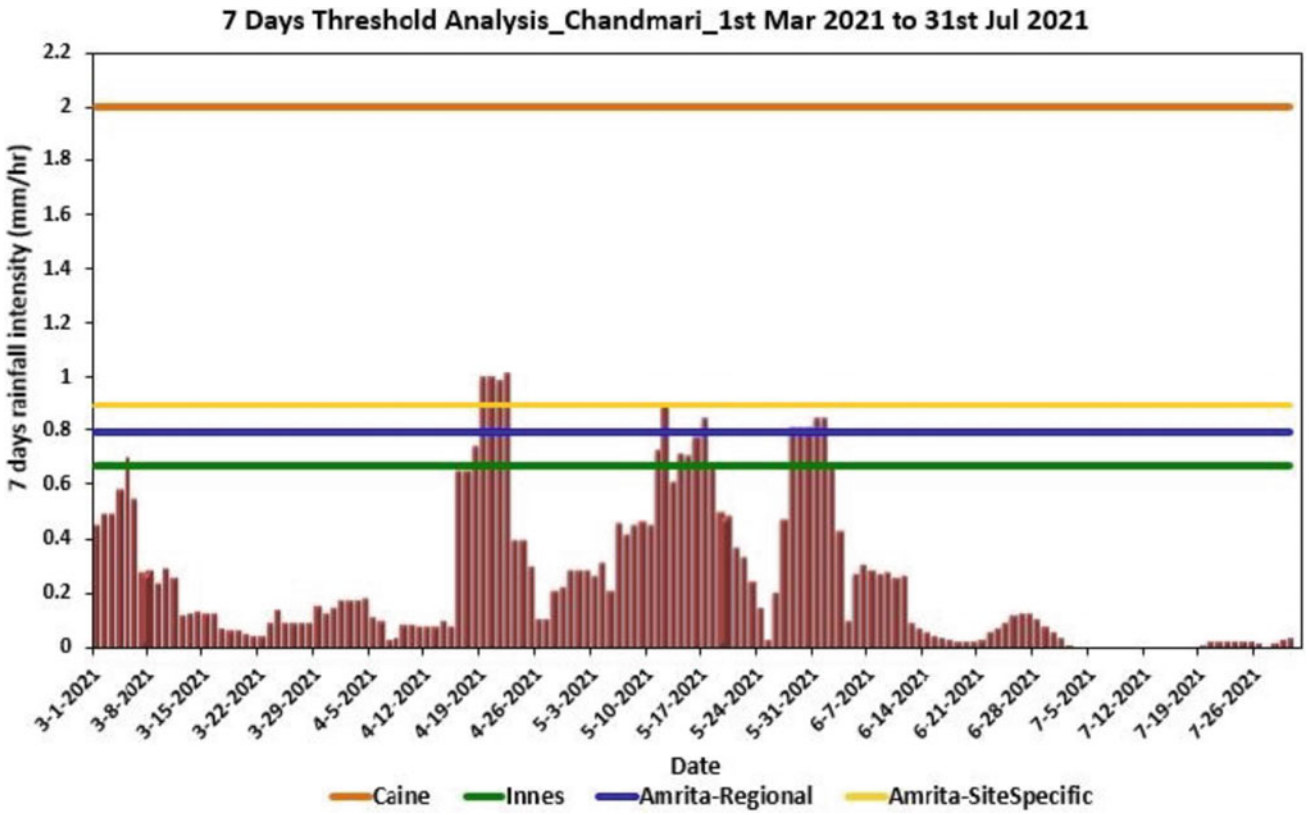

Fig. 13 Rainfall threshold and comparison of models: 7 days threshold crossed during 2021 in Chandmari

Fig. 14 Multi level warning: integration of heterogeneous spatio temporal data and intelligent knowledge management

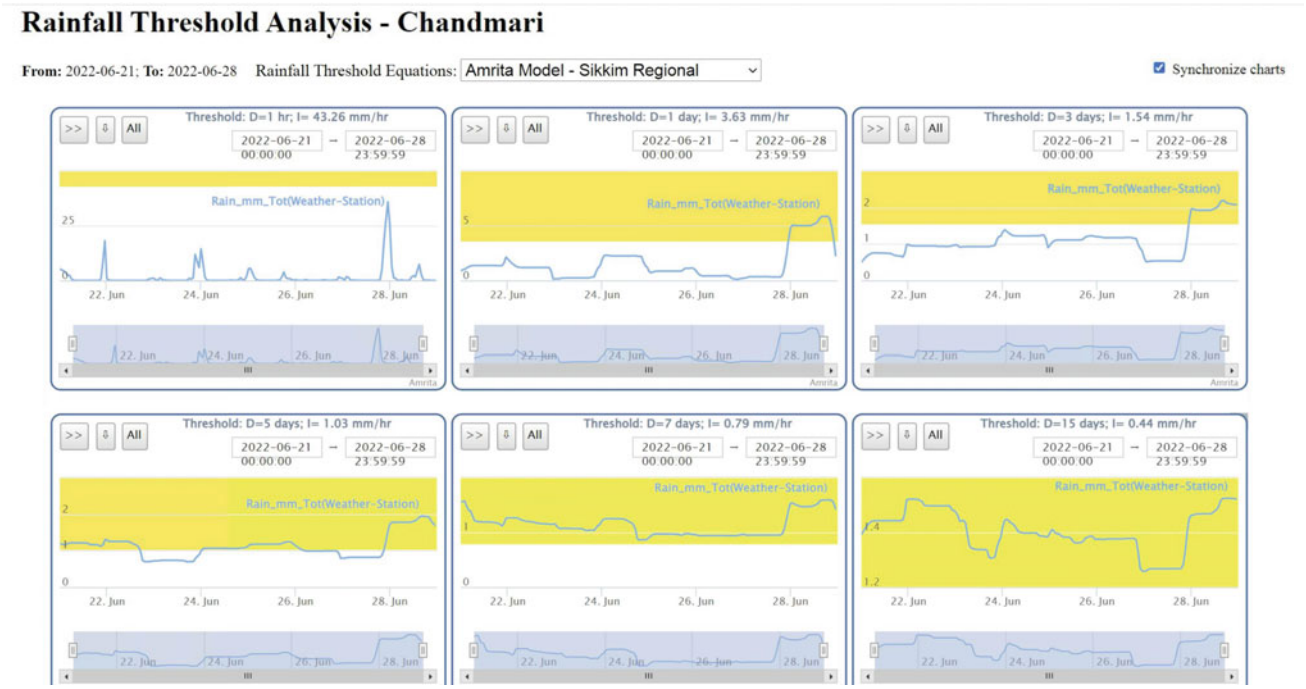

Fig. 15 Regional and site specific rainfall threshold crossed on 28th July 2022. Six landslides got initiated within 24 h of the issuing of warning in Chandmari area

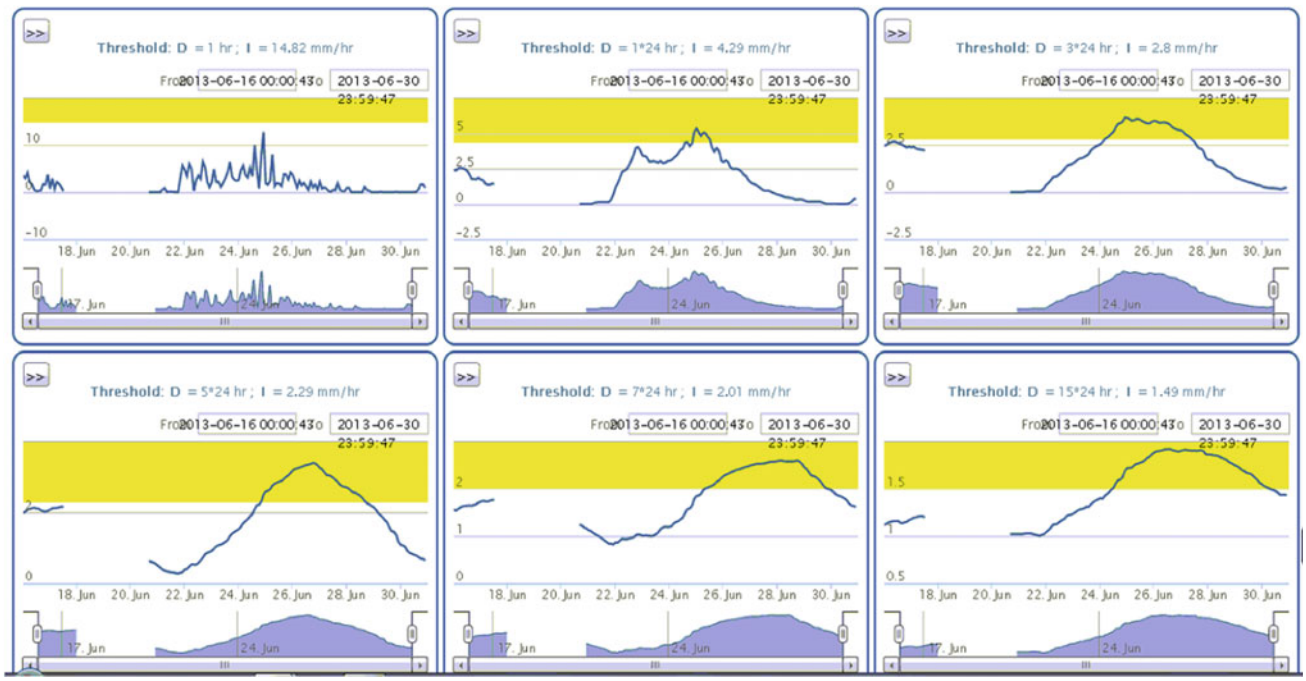

Fig. 16 Sample screenshot of a first level warning based on rainfall thresholds

Fig. 17 Snapshot of Kerala flood 2018 efforts to facilitate the rescue and relief operations: Amrita Kripa rescue app

LEWS, multi-level risk communication using mobile applications and early warning using social media were developed.

Furthermore, in LEWS design, we explored enhancing reliability, reducing false alarms through multi domain integration, reducing the cost of deployment and maintenance through bringing in the participatory approaches. In the year 2018 in Munnar, the automatic integrated decision model was used by LEWS and three effective warnings were issued on 12 July 2018, 15 July 2018, 9 Aug 2018. Based on these warnings the district administration and tahsildar evacuated the community members to safe places. During the initial phase of these monsoon periods, the Amrita IoT system was able to clearly convey that regional thresholds have crossed however site-specific thresholds have not. Based on these instructions from the LEWS, the community in the case study area stayed back in their home, trusting Amrita's warning. As these warnings were later validated by the absence of landslides in study site, the reliability of the warnings and the communities trust on these warnings from the LEWS has increased. The Amrita IoT systems capability to predict the regional landslides and denied the possibility of initiation of site specific landslides is highly appreciated by the community as this provides site specific warnings with higher reliability avoiding the need for unnecessary preparedness/evacuation based on regional warnings alone. The heavy downpour on 6 Aug 2020, initiated a regional warning and second level warning. These are communicated to KSDMA and its screenshot is shown in Fig. 18.

Further to increase the reliability of warnings, risk governance through capacity building and community participation has been initiated. As a first step, the community has been trained in measuring rainfall and updating these measurements via crowdsourcing platforms such as mobile apps and WhatsApp to derive better rainfall thresholds, which act as the first level community-wise warning for that region and enhances the risk perception of the community.

Therefore, by integrating all the components the early warning system has a comprehensive set of submodules to ensure the reliability of the landslide early warning as shown in Fig. 20. The key submodules include such as site characteristics, inputs from landslide laboratory, modeling and simulation, sensor system, algorithms, communication system, software system, dynamic learning and multilevel warning system. This clearly demonstrates that landslide risk reduction would be required to solve multi scale needs through a multipronged approach by utilizing transdisciplinary capabilities and community empowerment as shown in Fig. 21.

Extending landslide risk reduction to multihazard disaster risk reduction, the key solutions that has been developed and utilized are: (a) vulnerability mapping, (b) geotechnical analysis, (c) real-time monitoring of multihazards, (d) Multiscale decision models and early warning, (e) community resilience programs using social media. These integrated comprehensive solutions will enhance the capability to provide multihazard disaster risk reduction (Fig. 19).

Requirements and solutions discussed in this paper are summarized below.

(i) Real-time risk assessment through physical sensing using IoT platform
(ii) Threshold models for decision making from sub-events leading to a landslide
(iii) Machine learning and Artificial Intelligence based models to forecast the futuristic conditions of the slope.
(iv) Factor of Safety models to understand the dynamic variations in slope stability conditions
(v) Multi-level early warning models to provide site-specific and regional warnings.
(vi) Community awareness program to create awareness about landslides in the community and encourage the community to participate in collecting data related to landslides and multi-hazards
(vii) Participatory sensing approaches involving the community through Landslide Tracker mobile app to report landslides and other precursor events.
(viii) Amrita Kripa app to provide rescue and relief during a disaster

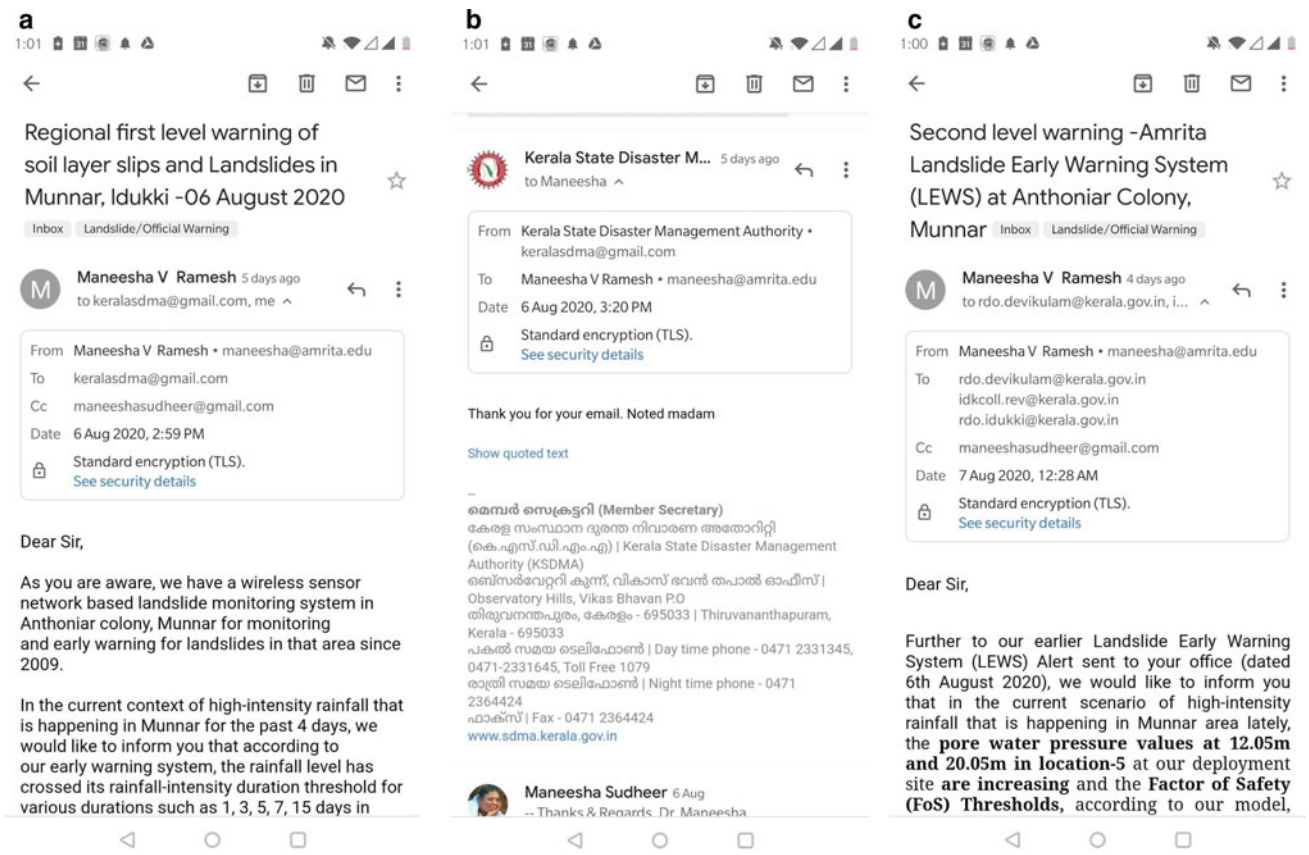

Fig. 18 Regional first level warning. Reply from the KSDMA. Second level warning

(ix) Social models for understanding the ground reality and people's reaction to disaster through social media data analytics.
(x) Twitter data-based automatic event detection, tracking and providing situational awareness models.

To facilitate disaster preparedness and response, specific solutions for the following areas to enhance the existing system are given below:

1. Strengthening activity in the existing volunteer group in Munnar, extending to other landslide-prone areas and facilitating them through community engagements and awareness programs for preparing the community to face future disasters
2. Conducting pre and post monsoon medical camps and providing ICU Ambulance facility during the time of monsoon
3. Providing a copy of LEWS alerts issued to the State government to the community through WhatsApp and facilitating relief and rescue operations through volunteer groups.
4. Facilitating Communication during the rough climate by providing radio-based communication devices
5. Further development of Amrita Kripa App to coordinate and facilitate the relief and rescue operations
6. Suggesting suitable mitigation measures for wherever possible
7. Providing alternative places for their stay after a landslide has destroyed their homes

There is still a long way to go. Also since the areas prone to landslides are quite large and it is challenging to cover the entire area with limited resources. However, the proposed integrated approach detailed in the present paper provides a feasible workflow to achieve this (Fig. 22).

8 Conclusion

The current study is intended to unveil the requirements for landslide risk reduction and design a comprehensive landslide risk management framework. Using this framework, IoT solutions have been proposed. The IoT system for

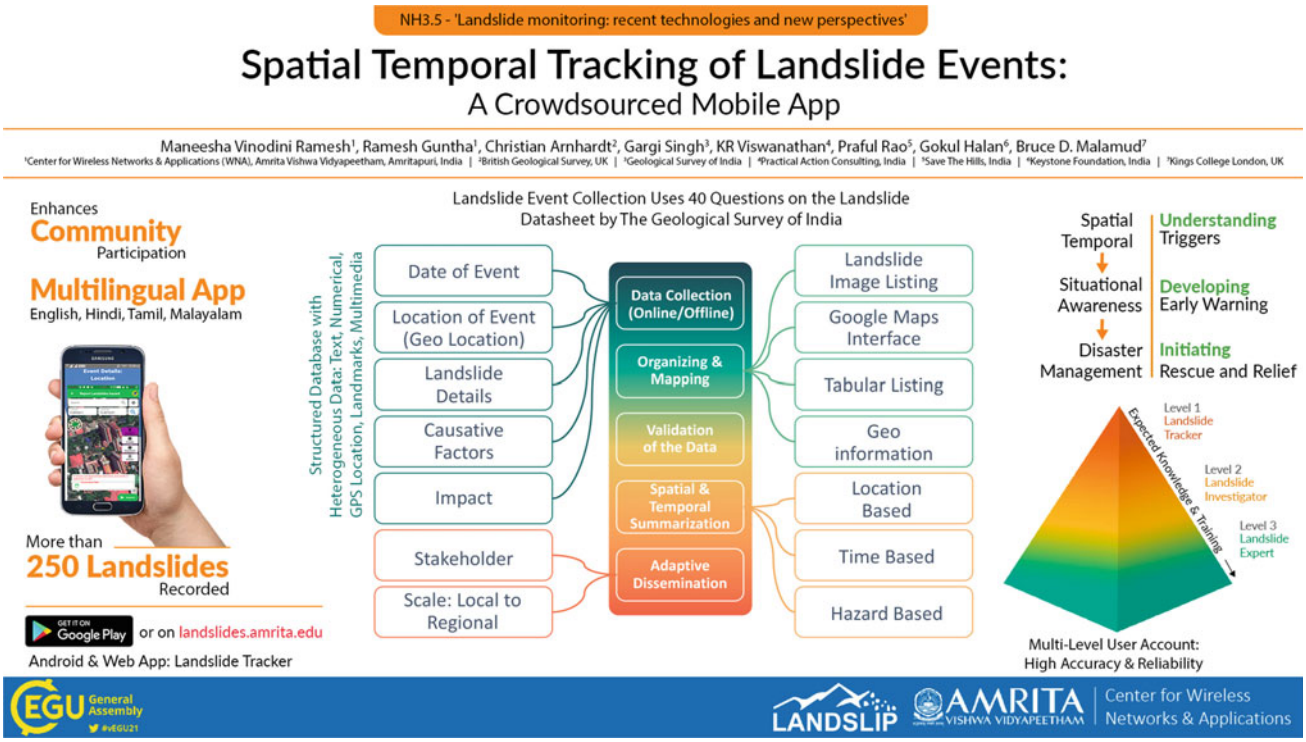

Fig. 19 Landslide tracker: a crowdsourced mobile application

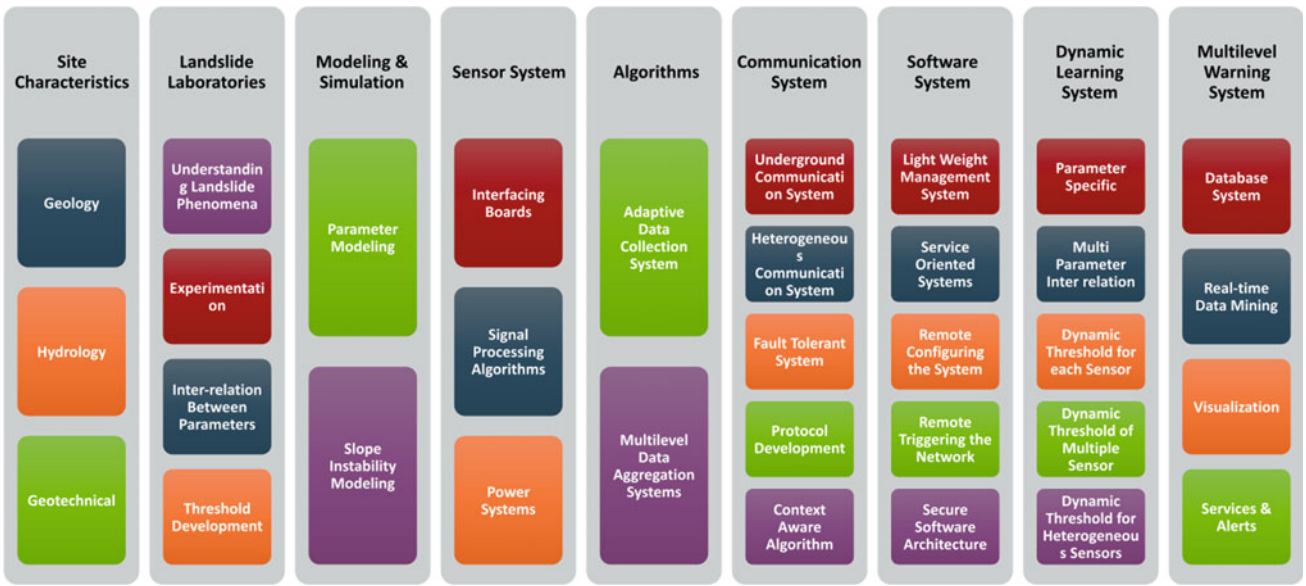

Fig. 20 Comprehensive landslide early warning system

landslide early warning systems deployed at North Eastern Himalayas and Western Ghats has been elaborated. It elaborated the decade-long experience of establishing an end-to-end system for landslide disaster risk reduction. An adaptable and integrated method is suggested for combining the entire requirements of end-to-end community disaster resilience in Amrita-LEWS. Landslide disaster risk reduction is continuously enhanced over a decade-long involvement in Munnar through various means such as threshold models, machine learning models, social models, community

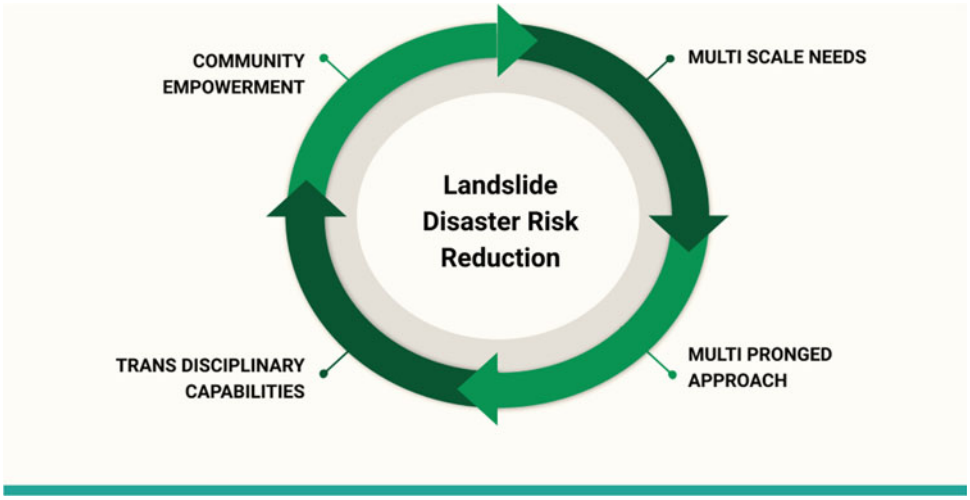

Fig. 21 Landslide risk reduction

Fig. 22 Multihazard disaster risk reduction: approaches and solutions

engagement, Landslide Tracker app and Amrita Kripa app. Amrita-LEWS is replicated in Sikkim region with customization for the terrain conditions there.

Acknowledgements The authors would like to express gratitude for the immense amount of motivation and guidance provided by Dr. Sri. Mata Amritanandamayi Devi, the Chancellor, Amrita Vishwa Vidyapeetham. The authors are thankful to all the involved faculty and students of Amrita Vishwa Vidyapeetham for their valuable support and hard work during the EWS deployment and community engagement activities in Munnar and Sikkim which includes but not limited to Dr. Venkat Rangan, Vice Chancellor, Amrita Vishwa Vidyapeetam, Prof. Balaji Hariharan, Prof. Sudesh Kumar Wadawan, Mr. Sudarshan V, Ms. Indukala P, Mr. Aravind H, Mr. Arun Kumar J, Mr. Deepak B, Dr. Rekha P, Mr. Tinu, Dr. Nirmala V, Kaushik R, Mr. Selvakumar G, and Mr. Dawa Lepcha We also thank Dr. Dhanya M, Assistant Professor (Sr. Grd.), Amrita Vishwa Vidyapeetham for proofreading and her valuable suggestions that improved the manuscript. Special Thanks to the community champions, the stakeholders and government administrations for on ground support. This work is a part of IPL/WCoE/Kyoto Commitment activities of the World Center of Excellence on Landslide Risk Reduction (WCoE 2017–2020; 2020–2023) "Enhancement of the existing Real-time Landslide Monitoring and Early warning System in Western Ghats and Himalayas, India" conducted by Amrita Vishwa Vidyapeetham (Leader: Maneesha Vinodini Ramesh). Amrita Vishwa Vidyapeetham, Kollam, Kerala, funded for this work under the project "Community Based Disaster Resilience through Landslide Early Warning System."

References

Abraham MT, Satyam N, Pradhan B, Alamri AM (2020) IoT-based geotechnical monitoring of unstable slopes for landslide early warning in the Darjeeling Himalayas. Sensors 20(9):2611

Achu AL, Joseph S, Aju CD, Mathai J (2021) Preliminary analysis of a catastrophic landslide event on 6 August 2020 at Pettimudi, Kerala State, India. Landslides 18(4):1459–1463

Ahmed B, Rahman MS, Sammonds P, Islam R, Uddin K (2020) Application of geospatial technologies in developing a dynamic landslide early warning system in a humanitarian context: the Rohingya refugee crisis in Cox's Bazar, Bangladesh. Geomatics Nat Hazards Risk 11(1):446–468

Amritanand S, Anand S, Amritesh AR (2020) Dynamic and time critical emergency management for level three disaster: a case study analysis of Kerala floods 2018. In: Proceedings of the 21st international conference on distributed computing and networking, pp 1–6

Canavesi V, Segoni S, Rosi A, Ting X, Nery T, Catani F, Casagli N (2020) Different approaches to use morphometric attributes in landslide susceptibility mapping based on meso-scale spatial units: a case study in Rio de Janeiro (Brazil). Remote Sens 12(11):1826

Conrad JL, Morphew MD, Baum RL, Mirus BB (2021) HydroMet: a new code for automated objective optimization of hydrometeorological thresholds for landslide initiation. Water 13(13):1752

Dixon N, Smith A, Flint JA, Khanna R, Clark B, Andjelkovic M (2018) An acoustic emission landslide early warning system for communities in low-income and middle-income countries. Landslides 15 (8):1631–1644

Franceschini R, Rosi A, Catani F, Casagli N (2022) Exploring a landslide inventory created by automated web data mining: the case of Italy. Landslides 19(4):841–853

Froude MJ, Petley DN (2018) Global fatal landslide occurrence from 2004 to 2016. Nat Hazards Earth Syst Sci 18(8):2161–2181
Geological Survey of India (2016) Landslide compendium of southern parts of Western Ghats. GSI, Kolkata
Geological Survey of India (2018) (http://bhukosh.gsi.gov.in)
Geological Survey of India (2020) (http://bhukosh.gsi.gov.in)
Gian QA, Tran DT, Nguyen DC, Nhu VH, Tien Bui D (2017) Design and implementation of site-specific rainfall-induced landslide early warning and monitoring system: a case study at Nam Dan landslide (Vietnam). Geomat Nat Haz Risk 8(2):1978–1996
Guntha R, Vinodini Ramesh M (2021) Technical considerations for building a landslide tracker mobile app. In: EGU general assembly conference abstracts, pp EGU21-6019
Guntha R, Rao SN, Ramesh MV (2020) Deployment experiences with Amrita Kripa: a user-friendly feature rich crowdsourced humanitarian application. Procedia Comput Sci 171:302–311
Guzzetti F, Gariano SL, Peruccacci S, Brunetti MT, Marchesini I, Rossi M, Melillo M (2020) Geographical landslide early warning systems. Earth Sci Rev 200:102973
Harilal GT, Madhu D, Ramesh MV, Pullarkatt D (2019) Towards establishing rainfall thresholds for a real-time landslide early warning system in Sikkim, India. Landslides 16(12):2395–2408
Hariharan B, Guntha R (2021) Crowdsourced landslide tracking-lessons from field experiences of landslide tracker mobile app. In: EGU general assembly conference abstracts, pp EGU21-12711
Hidayat S, Pachri H, Alimuddin I (2019) Analysis of landslide susceptibility zone using frequency ratio and logistic regression method in Hambalang, Citeureup District, Bogor Regency, West Java Province. In IOP conference series: earth and environmental science, vol 280, No 1, p 012005, IOP Publishing
Hemalatha T, Ramesh MV, Rangan VP (2019) Effective and accelerated forewarning of landslides using wireless sensor networks and machine learning. IEEE Sens J 19(21):9964–9975
https://www.manoramaonline.com/news/latest-news/2019/08/16/kerala-wayanad-puthumala-landsliderescue-video-story.html
Izumi T, Shaw R (2022) A multi-country comparative analysis of the impact of COVID-19 and natural hazards in India, Japan, the Philippines, and USA. Int J Disaster Risk Reduction 73:102899
Kanungo DP, Singh R, Dash RK (2020) Field observations and lessons learnt from the 2018 landslide disasters in Idukki District, Kerala, India. Curr Sci 119(11):1797
Kumar S, Duttagupta S, Rangan VP, Ramesh MV (2020) Reliable network connectivity in wireless sensor networks for remote monitoring of landslides. Wireless Netw 26(3):2137–2152
Martha TR, Roy P, Govindharaj KB, Vinod Kumar K, Diwakar PG, Dadhwal VK (2015) Landslide triggered by the June 2013 extreme rainfall event in parts of Uttarakhand state, India. Landslides 12 (1):135–146
Martha T, Roy P, Jain N, Kumar KV, Reddy P, Nalini J, Sharma S, Shukla A, Durga Rao K, Narender B, Rao P, Muralikrishnan S (2021) Rock avalanche induced flash flood on 07 February 2021 in Uttarakhand, India—a photogeological reconstruction of the event. Landslides 18(8):2881–2893. https://doi.org/10.1007/s10346-021-01691-9
Michoud C, Bazin S, Blikra LH, Derron MH, Jaboyedoff M (2013) Experiences from site-specific landslide early warning systems. Nat Hazard 13(10):2659–2673
Orland E, Roering JJ, Thomas MA, Mirus BB (2020) Deep learning as a tool to forecast hydrologic response for landslide-prone hillslopes. Geophys Res Lett 47(16):e2020GL088731
Orimoloye IR, Belle JA, Ololade OO (2021) Exploring the emerging evolution trends of disaster risk reduction research: a global scenario. Int J Environ Sci Technol 18(3):673–690
Pecoraro G, Calvello M, Piciullo L (2019) Monitoring strategies for local landslide early warning systems. Landslides 16(2):213–231
Phengsuwan J, Thekkummal NB, Shah T, James P, Thakker D, Sun R, Pullarkatt D, Hemalatha T, Ramesh MV, Ranjan R (2019) Context-based knowledge discovery and querying for social media data. In: 2019 IEEE 20th international conference on information reuse and integration for data science (IRI). IEEE, pp 307–314
Prabha R, Ramesh MV, Rangan VP, Ushakumari PV, Hemalatha T (2017) Energy efficient data acquisition techniques using context aware sensing for landslide monitoring systems. IEEE Sens J 17 (18):6006–6018
Ramesh MV (2014) Design, development, and deployment of a wireless sensor network for detection of landslides. Ad Hoc Netw 13:2–18
Ramesh MV (2017) Slope stability investigation of Chandmari in Sikkim, northeastern India. In: Workshop on world landslide forum. Springer, Cham, pp 363–369
Ramesh MV, Rangan VP (2014) Data reduction and energy sustenance in multisensor networks for landslide monitoring. IEEE Sens J 14 (5):1555–1563
Ramesh MV, Sudarshan VC, Harilal GT, Singh B, Sudheer A, Ekkirala HC (2022) Kerala floods 2018: causative factors that transformed single event to multi-hazard disaster. In: Civil engineering for disaster risk reduction. Springer, Singapore, pp 61–82
Ramesh MV, Vasudevan N (2012) The deployment of deep-earth sensor probes for landslide detection. Landslides 9(4):457–474
Segoni S, Rosi A, Lagomarsino D, Fanti R, Casagli N (2018) Brief communication: using averaged soil moisture estimates to improve the performances of a regional-scale landslide early warning system. Nat Hazard 18(3):807–812
Tao Z (2020) Advanced wavelet sampling algorithm for IoT based environmental monitoring and management. Comput Commun 150:547–555
Thirugnanam H, Ramesh MV, Rangan VP (2020) Enhancing the reliability of landslide early warning systems by machine learning. Landslides 17(9):2231–2246
Thirugnanam H, Uhlemann S, Reghunadh R, Ramesh MV, Rangan VP (2022) Review of landslide monitoring techniques with IoT integration opportunities. IEEE J Sel Top Appl Earth Observations Remote Sens
UNDP (2018) Economic losses, poverty and disasters 1998–2017. https://www.preventionweb.net/files/61119_credeconomiclosses.pdf
Varnes DJ (1978) Slope movement types and processes. Special report. 176:11–33
Vinodini Ramesh M, Pullarkatt D, Geethu TH, Venkat Rangan P (2017) Wireless sensor networks for early warning of landslides: experiences from a decade long deployment. In: Workshop on world landslide forum. Springer, Cham, pp 41–50
Wadhawan SK, Singh B, Ramesh MV (2020) Causative factors of landslides 2019: case study in Malappuram and Wayanad districts of Kerala, India. Landslides 17(11):2689–2697
Wicki A, Lehmann P, Hauck C, Seneviratne SI, Waldner P, Stähli M (2020) Assessing the potential of soil moisture measurements for regional landslide early warning. Landslides 17(8):1881–1896

Landslides and Countermeasures in Western Japan: Historical Largest Landslide in Unzen and Earthquake-Induced Landslides in Aso, and Rain-Induced Landslides in Hiroshima

Daisuke Higaki, Kiyoharu Hirota, Khang Dang, Shinji Nakai, Masahiro Kaibori, Satoshi Matsumoto, Masataka Yamada, Satoshi Tsuchiya, and Kyoji Sassa

Abstract

This paper introduces three catastrophic landslide disasters on the tectonic orogenic belt in Western Japan caused by rainfalls or earthquakes and the countermeasures against them. The first case story is the mega slide of Unzen-Mayuyama of Quaternary volcanic rock due to the 1792 earthquake. The landslide and subsequent tsunami caused the worst Japanese landslide-induced disaster in Shimabara and Ariake Bay. The stone pillars installed after the disaster, indicating the arrival points of the tsunami will generate awareness of the tsunami caused by landslides for future generations. Secondly, the Kumamoto earthquake of 2016 has induced many shallow landslides on tephra-covered slopes and massive slope failures that disrupted highway and rail traffic. Unmanned construction to secure workers has been introduced to stabilize the slope failure early. There is an urgent need for research on the identification of hazardous slopes for landslides on tephra-covered slopes. Thirdly, the Hiroshima disaster in 2018 was characterized by landslides, mainly in the suburban residential areas in Hiroshima City, where heavy rains have caused landslides from the weathered soil, so-called "Masa," of granitic rocks. Similar disasters occurred in 1999 and 2014 in Hiroshima. The restoration project has been carried out by adopting necessary structural measures such as Sabo dams and non-structural measures such as land use regulations and/or early warning systems based on the Sediment Disaster Prevention Act.

Keywords

Landslides • Earthquakes • Rainfall • Tephra • Tsunami • Countermeasure

D. Higaki (✉) · M. Yamada
Nippon Koei Co., Ltd., Tokyo, Japan
e-mail: a9024@n-koei.co.jp

M. Yamada
e-mail: a9396@n-koei.co.jp

K. Hirota · K. Dang · K. Sassa
International Consortium on Landslides (ICL), Kyoto, Japan
e-mail: kiyoharu_hirota@kk-grp.jp

K. Dang
e-mail: khangdq@gmail.com

K. Sassa
e-mail: kyoji.sassa@gmail.com

K. Hirota
Kokusai Kogyo Co., Ltd., Tokyo, Japan

K. Dang
University of Science, Vietnam National University (VNU), Hanoi, Vietnam

S. Nakai
Fukken Co., Ltd., Hiroshima, Japan
e-mail: nakai@fukken.co.jp

M. Kaibori
Resilience Research Center, Hiroshima Univ., Hiroshima, Japan
e-mail: kaibori@hiroshima-u.ac.jp

S. Matsumoto
Nippon Koei Co., Ltd., Fukuoka, Japan
e-mail: a3892@n-koei.co.jp

S. Tsuchiya
Japan Conservation Engineers & Co. Ltd., Tokyo, Japan
e-mail: tsuchiya@jce.co.jp

1 Introduction

Erosion and sedimentation by various geomorphic processes have caused many disasters in Japan, which is characterized by a large population of 125 million in an area of 380,000 km^2. Both structural and non-structural measures have managed such geomorphic hazards for over a few hundred years (e.g., Kanbara and Imamori 2020). Western Japan is affected by warm currents such as the Kuroshio Current and the Tsushima Current. Especially in summer, the seawater becomes warmer, and the updrafts supply energy to typhoons and often form cumulonimbus clouds

I. Alcántara-Ayala et al. (eds.), *Progress in Landslide Research and Technology, Volume 1 Issue 2, 2022*, Progress in Landslide Research and Technology,
https://doi.org/10.1007/978-3-031-18471-0_22

continuously. They lead to heavy rainfall in Western Japan. The Japanese archipelago is situated parallel to and near the plate boundaries, so earthquakes have also been a significant threat. This paper introduces several cases of catastrophic sediment disasters caused by landslides and the countermeasures adopted in Western Japan. The word "sediment disaster" (Toki 1993) in this paper describes the disaster caused by the movement of rock, debris, soil or their combination under the influence of gravity and/or water due to erosion, transportation, and sedimentation processes.

2 Geological background of Western Japan

Geological Features in Japan

As mentioned above, the Japanese archipelago, with 111 active volcanoes (Japan Meteorological Agency 2017), lies in the tectonic orogenic belt. The Japanese Islands belong, based on tectonic regionalization, to four plates, namely: North American Plate, Pacific Plate, Eurasia Plate, and Philippine Sea Plate. It can also be divided into Northeastern Japan and Southwestern Japan by the geological structure. Their geological boundary is the Fossa Magna, which is part of the western boundary of the North American Plate.

Southwestern Japan is on the Eurasia Plate, on the subduction zone of the Philippine Sea Plate. Furthermore, the Median Tectonic Line (MTL) is divided into the inner zone of Southwest Japan (on the Sea of Japan side) and the outer zone of Southwest Japan (on the Pacific side) (The Japan landslide Society 2012). The outer zone of Southwestern (SW) Japan consists of the accretionary complex (AC) as sediments carried by the Philippine Sea Plate.

Figure 1 shows the geological structure of Western Japan and the locations and geology of the three sites, namely: Unzen, Aso, and Hiroshima introduced in this paper.

Local Geology Around Three Sites of Unzen, Aso, and Hiroshima

Figure 1 shows the geological structure classification of SW Japan. The three target sites are shown in Fig. 1a (Unzen site), Fig. 1b (Aso site), and Fig. 1c (Hiroshima site), which are partially quoted from "Seamless Digital Geological Map of Japan (1:200,000) V21" (Geological Survey of Japan 2022).

All three survey sites are located in the inner zone of SW Japan and belong to the Mino-Tamba belt of the Hiroshima site, the Ryoke belt of the Aso site, and the Suo metamorphic belt of the Unzen site (Fig. 1). The distribution area of granite is widespread near the Hiroshima site, and the granite (K21_pam_a) near the site is markedly weathered/decomposed, and erosion due to rainfall and outflow of decomposed granite soil are likely to occur. In the vicinity of the Aso site, tephra from the eruption of Aso Volcano covers a wide area and is susceptible to rainfall erosion. At the Unzen site, pyroclastic flows caused by the eruption of Mt. Unzen and rain-induced debris flows/mud flows occurred. The area is easily eroded/denudated in its present state.

3 Disaster of the Unzen-Mayuyama Mega Slide and Subsequent Tsunami in 1792

Outline of the 1792 Unzen-Mayuyama Landslide

The most famous and worst landslide and its resulting landslide-induced tsunami disaster in Japan is the 1792 Unzen-Mayuyama mega slide. This disaster in the history of volcanic hazards in Japan is called "the Shimabara Catastrophe." Mayuyama is one of the Unzen compound volcanoes in the eastern part of Shimabara Peninsula, Nagasaki Prefecture, Kyushu (Fig. 2).

At about 8 PM on 21 May 1792, the landslide was induced by the Shimabara-Shigatusaku earthquake that occurred under Shimabara in the last stage of eruptive activities of Mt. Fugen (Unzen Restoration Office 2002). After travelling around 5 km from the top of Mt. Mayuyama, a tremendous amount of debris and rocks rushed into the Ariake Sea and generated a giant tsunami that hit both sides of the inland sea. The landslide and tsunami reportedly killed a total of 15,153 persons. Out of 15,153 persons, 10,139 persons died in the Shimabara area, 5014 persons were killed on the opposite banks by the tsunami wave.

Documents and Research about the 1792 Unzen-Mayuyama Landslide and Tsunami

Many people well reported the Unzen-Mayuyama landslide and its subsequent tsunami. Many old documents and pictures were presented in pamphlets of the Unzen Restoration Office of Japan's Ministry of Land, Infrastructure, and Transport (MLIT) (2002, 2003). By comparing old figures and photos showing almost the same landscape of the Mayuyama, Inoue (1999) and the MLIT Unzen Restoration Office (2002) reconstructed the original ground surface before the landslide and the first sliding surface. Topographic changes before and after the 1792 Mayuyama landslide are presented in Fig. 3. There were several volcanic and seismic activities in the area of Unzen Volcano before the 1792 landslide (Unzen Restoration Office 2002). Frequent earthquakes occurred since Nov. 1791. Volcanic eruptions and lava flow with a length of 2 km occurred at Mt. Fugen, 2 km west of Mt. Mayuyama in Feb. 1792. Then the frequent earthquakes and a large landslide (scale: 1080 m in west–east, 720 m in north–south) at the southeast flank of Mt. Mayuyama occurred one month before the mega-slide on 21 May 1792.

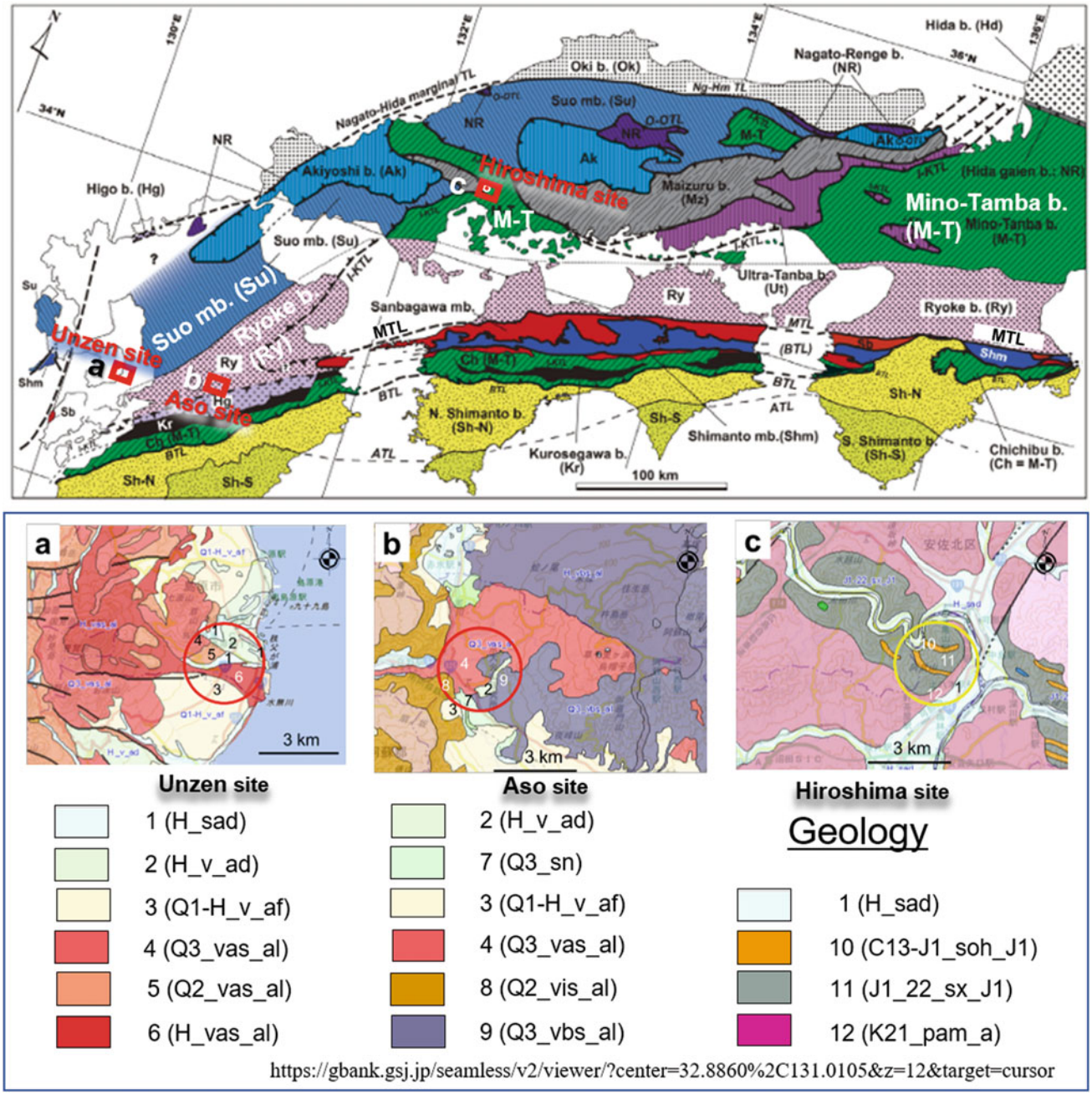

Fig. 1 Geotectonic subdivision of SW Japan (added three local geological sites to Isozaki et al. 2010: map view modified from Isozaki and Itaya (1991). Symbols for geotectonic units (belts) and major boundaries (tectonic lines) are from Isozaki et al. 2010. See text for details of Izozaki et al. 2010. The coordinates of the latitude and longitude of the center of the circle with a diameter of 3 km in Fig. 1a–c are as follows: Fig. 1a Unzen site: 32° 45′ 32.99″ N, 130° 21′ 26.61″ E, Fig. 1b Aso site: 34° 52′ 59.78″ N, 130° 59′ 23.18″ E, Fig. 1c Hiroshima site: 34° 28′ 53.32″ N, 132° 29′ 18.40″ E. [**Geology**] 1 (H_sad): valley floor, intermountain basin, river and coastal plain deposits, Cenozoic Quaternary Holocene, 2 (H_v_ad): volcanic rocks debris avalanche deposits, Cenozoic Quaternary Holocene, 3 (Q1-H_v_af): volcanic rocks volcanic fan deposits, Cenozoic Quaternary Pleistocene Gelasian - Holocene, 4 (Q3_vas_al): dacite and rhyolite lava and pyroclastic rocks, Cenozoic Quaternary Late Pleistocene, 5 (Q2_vas_al): dacite and rhyolite lava and pyroclastic rocks, Cenozoic Quaternary Middle Pleistocene, 6 (H_vas_al): dacite and rhyolite lava and pyroclastic rocks, Cenozoic Quaternary Holocene, 7 (Q3_sn): non-marine sediments, Cenozoic Quaternary Late Pleistocene, 8 (Q2_vis_al): andesite and basaltic andesite lava and pyroclastic rocks, Cenozoic Quaternary Middle Pleistocene, 9 (Q3_vbs_al): basalt lava and pyroclastic rocks, Cenozoic Quaternary Late Pleistocene, 10 (C13-J1_soh_J1): chert Early to Middle Jurassic accretionary complex, 11 (J1_22_sx_J1): mixed rock Early to Middle Jurassic accretionary complex, 12 (K21_pam_a): Igneous rocks/ massive granite island arc and continental, Late Cretaceous Cenomanian–Santonian, (see Geological Survey of Japan 2022).

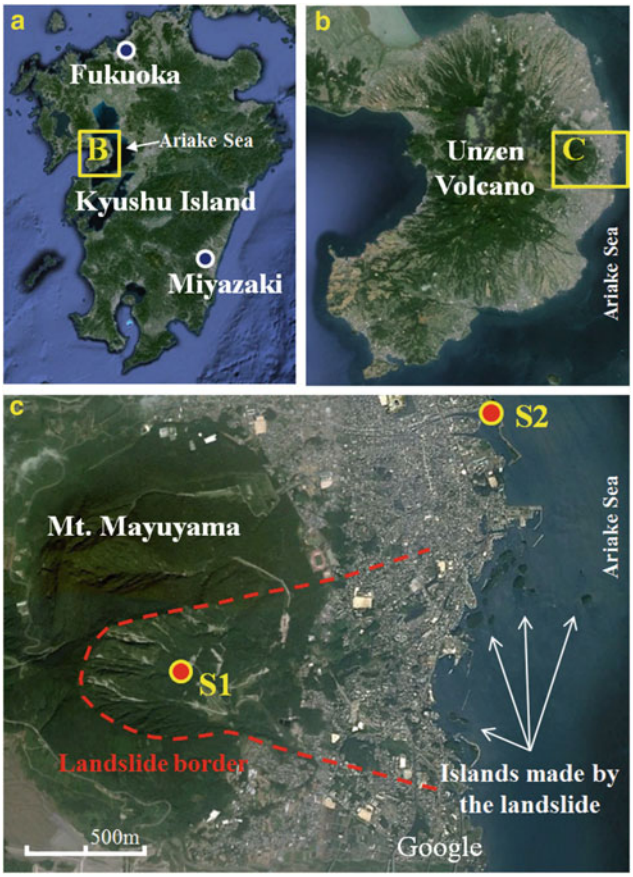

Fig. 2 Overview of the 1792 Unzen-Mayuyama landslide and sampling locations (Modified from source: Sassa et al. 2016)

The tsunami hit both sides of Ariake Bay, including Shimabara Peninsula, a coastal area of Kumamoto and the Amakusa Islands. From the present elevation of the stones, it is estimated that the maximum elevation of the tsunami was 57 m. The disaster investigated by the Unzen Restoration Office is shown in Fig. 4. The figure was created based on the previous investigation by Tsuji and Hino (1993) and Tsuji and Murakami (1997). The original image is written in Japanese including the historical data and the location of stone pillars (Tsunami-dome-ishi) which were installed to mark the places where the Tsunami reached. The Tsunami-dome-ishi aimed to share the experience with the future generation.

The total number of deaths is 15,153 persons. In Fig. 4, B to I indicate the followings.

B: The numbers of deaths are shown in the circles (See the legend: the largest is 500 persons), the size of which is proportional to the number of human fatalities in the area.

C: The most significant number of deaths was in Shimabara town around the castle (5251 persons).

D: The second largest deaths was in the southern part of the Shimabara Peninsula (around 3500 persons).

E, F, and G: Tsunami-Dome-Ishi (A stone showing the tsunami reaching that point) was set to record the tsunami by the communities in Kyodomari (E), Umedo (F) and Otao (G) of the Higo (Kumamoto) Han area. The Tsunami-Dome-Ishi in Kyodomari was moved to construct a road, but its former location is marked on the road retaining wall (by the regional education committee). The Tsunami-Dome-Ishi

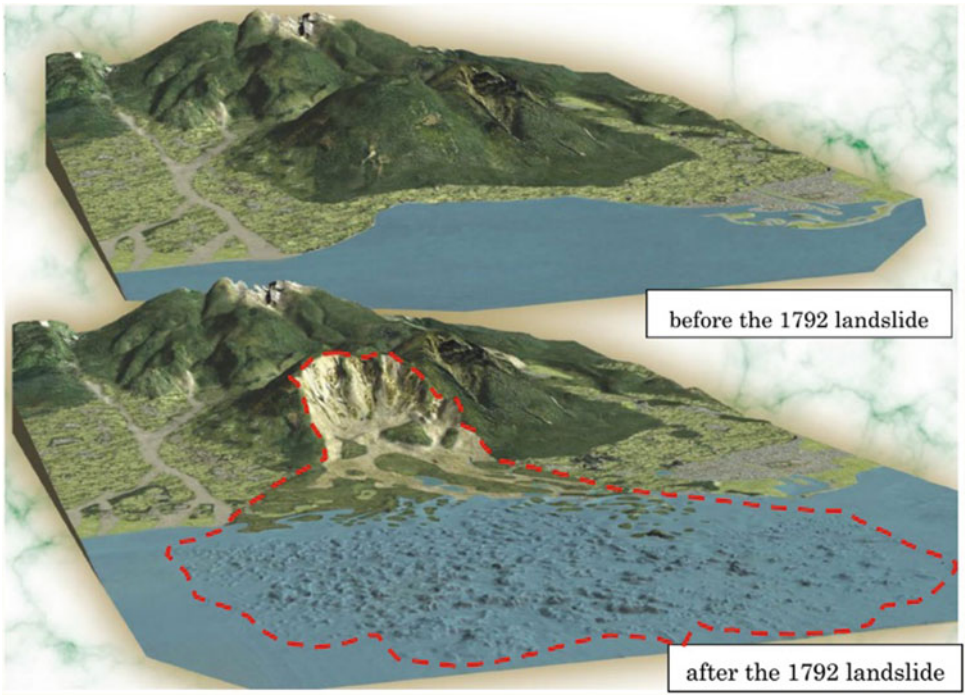

Fig. 3 The 1792 Mayuyama landslide before and after the event (Modified from source: leaflet by the Unzen Restoration office, MLIT 2003)

Fig. 4 Records of disaster by the Unzen landslide-and-tsunami disaster (Modified from source: Unzen Restoration Office 2002)

is limited in Higo (Kumamoto) Han area. These tsunami records are reliable.

H, I: Stone pillars for memorial services for deaths by tsunami in Futsu (H) and Mie (I) in Shimabara Han.

Sassa et al. (2016) interpreted the main sliding block and the secondary sliding block, which were pushed forward by the motion of the initial landslide mass. The combined profile of the landslide is presented in Fig. 5 including the initial main landslide block (red dotted mass) and the secondary sliding block (black dotted layer). The landslide's maximum depth and total volume were estimated to be 400 m and 3.4×10^8 m^3, respectively, based on previous research (Furuya 1974). The lines of slope angles for the initial landslide mass and the secondary landslide mass were estimated as 28.1 degrees and 6.5 degrees, respectively. They were used for the undrained dynamic loading ring-shear testing to simulate the initiation of the main landslide and the movement of the secondary sliding block due to the undrained loading from the displaced first landslide mass.

The sampling location is shown in Fig. 2, in which, sample S1 was taken from a sand layer exposed along a torrent gully in the source area of the landslide, and sample S2 was taken from the coastal area outside the landslide area.

Triggering Factor of the 1792 Unzen-Mayuyama Landslide

Tests on the sample S1 were preformed using the undrained dynamic loading ring shear apparatus (ICL-2) to investigate

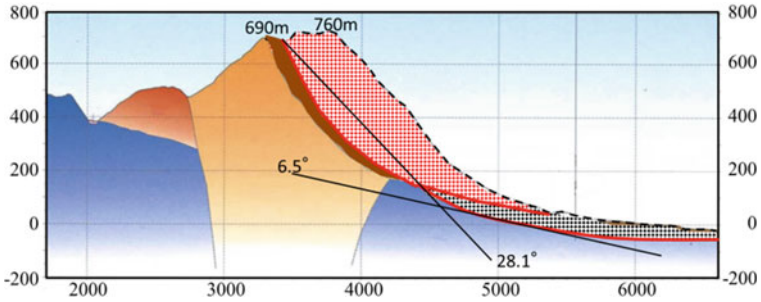

Fig. 5 Cross section of Mayuyama including 1792 landslide (Modified from Sassa et al. 2016)

the initiation and motion of the Unzen Mayuyama landslide. They consist of basic tests (monotonic undrained increasing shear stress tests, pore pressure control tests, undrained cyclic loading test) and landslide simulation tests (seismic-loading tests). Results of those tests were presented in detail in Sassa and Dang (2018).

The monotonic shear stress control tests are the tests of undrained capability, the stress control capability, the precision of stress, and pore pressure monitoring. A large excess pore pressure generation during shearing was observed in all tests suggesting the possibility of rapid landslide motion. The pore pressure control tests were performed to check which level of pore water pressure could initiate the landslide. The undrained cyclic loading test was performed to examine the shear behavior during seismic loading.

The seismic-loading ring-shear test is the most advanced and complicated test to simulate the landslide initiation by the combined effect of pore water pressure and earthquake shaking. The seismic record of the 1792 earthquake could not be obtained, so the authors decided to use a recent earthquake case. The 2008 Iwate-Miyagi Nairiku earthquake which had a similar scale and triggered a mega slide (Aratozawa landslide with a volume of 67×10^6 m^3) was selected. And the Iwate-Miyagi earthquake waveform recorded in Miyagi Prefecture (MYG004) was employed for the ring-shear simulation test and the computer simulation for 1792 Unzen Mayuyama landslide. It was suggested that around 1/3 smaller earthquake shaking than the Iwate-Miyagi earthquake should have caused failure under a slope condition with a pore pressure ratio of 0.21.

Reproduction of the 1792 Earthquake-induced Unzen-Mayuyama Landslide

Based on the landslide dynamics parameters measured by ring-shear testing, a computer simulation of the Unzen-Mayuyama was conducted using LS-RAPID software. Values used in the LS-RAPID are well presented in Sassa et al. (2016). The topography before the landslide and the possible sliding surface estimated by previous researchers (Unzen Restoration Office 2002 and 2003) were used in the software. Figure 6 presents the simulation result of the

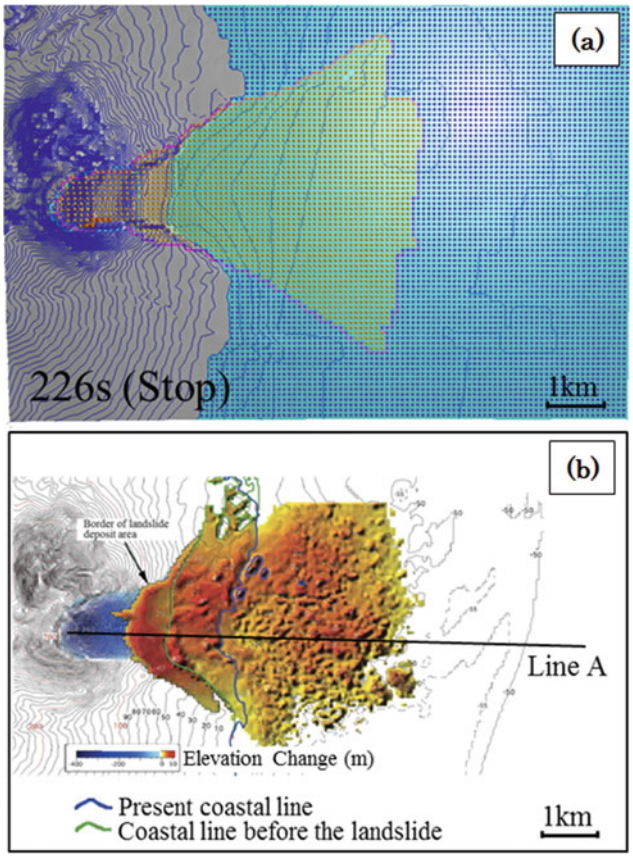

Fig. 6 Simulation result of the 1792 Unzen-Mayuyama landslide (**a**) and data investigated by the Unzen Restoration Office (2003) (**b**)

1792 earthquake-induced Unzen-Mayuyama landslide (Fig. 6a) and the investigated data (Fig. 6b) made by the Unzen Restoration Office (2002). It shows a similarity in the travel distance and the moving area between the simulated landslide and the actual case.

Reproduction of the 1792 Unzen-Mayuyama Landslide-induced Tsunami

The Tsunami triggered by the Unzen-Mayuyama landslide was also reproduced by LS-Tsunami software (Sassa et al. 2016) (Fig. 7). After the landslide occurred and entered into

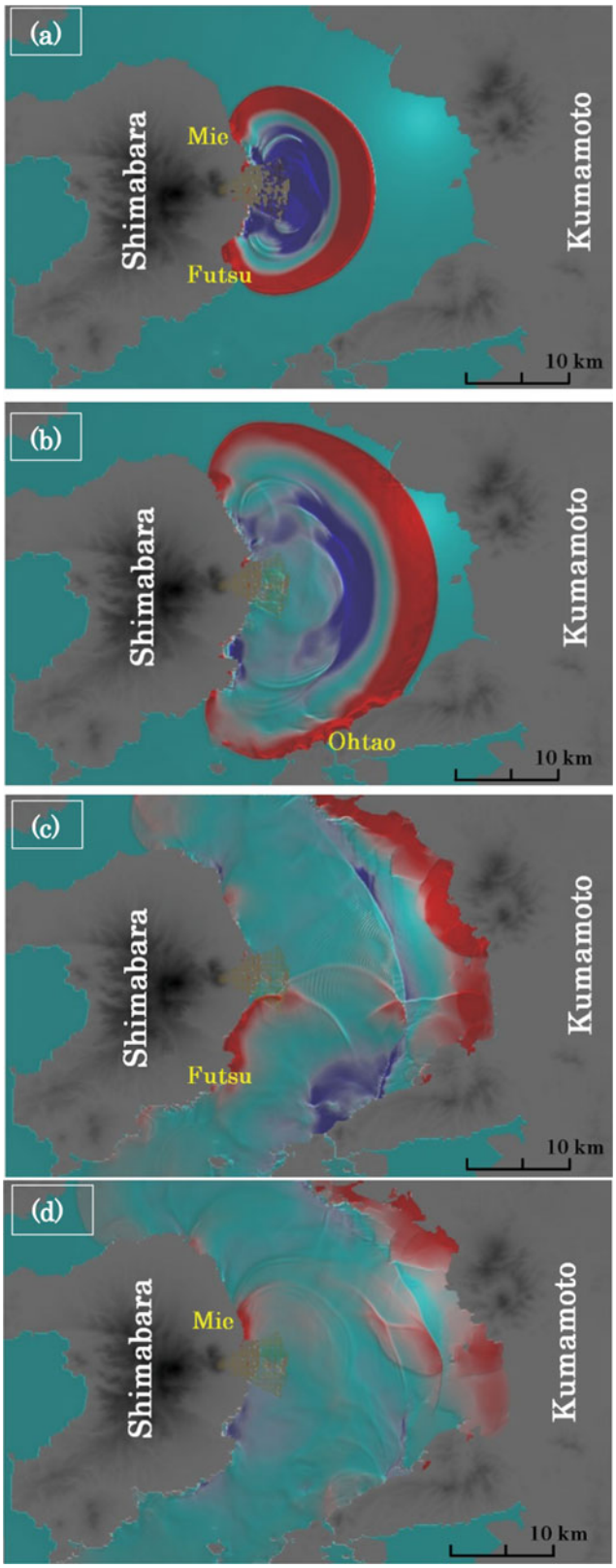

Fig. 7 Simulation result for the 1792 Unzen-Mayuyama landslide-induced tsunami (Modified from Sassa et al. 2016)

the Ariake Sea, the tsunami wave was triggered. In this figure, the bright red color presents the wave more than 5 m above sea level, and the dark blue color presents the wave less than 5 m below sea level. The top parts of the moving landslide blocks are seen above sea level as dark brown color dots. The first waves struck Mie and Futsu towns (Fig. 7a). Then, the wave expanded and reached Ohtao town, Kumamoto Prefecture, on the opposite bank (Fig. 7b). The tsunami wave was reflected from the opposite bank to strike the southern part of Shimabara Peninsula (around Futsu town) again (Fig. 7c). Another reflected wave hit the northern side of the Mayuyama landslide area (around Mie town) (Fig. 7d).

4 Landslides by the 2016 Kumamoto Earthquake

Outline of the Kumamoto Earthquake and Associated Landslide Disasters

An earthquake (Mj = 6.5) occurred at 9:26 PM on April 14, 2016, in the central part of Kumamoto Prefecture (epicenter: N32° 44.5′, E:130° 48.5′, focal depth: ca. 11 km) in Central Kyushu. The second earthquake (Mj = 7.3) occurred at 1:25 AM on April 16, 2016 (epicenter: N32° 45.2′, E:130° 45.7′, focal depth: ca. 12 km) (Fig. 8). The total fatality by these earthquakes was 120 people (Japan Meteorological Agency (JMA) 2016). Both epicenters are located near the junction of the Futagawa and the Hinagu active fault zones, extending NE–SW. The seismic faults, i.e., right lateral strike-slip faults, were traced along these fault zones where aftershocks have occurred. The earthquakes were named the 2016 Kumamoto Earthquake by the JMA. Figure 9 shows the three orthogonal components of the acceleration time history of the Kumamoto Earthquake at the K-net KMM005 station (NIED 2016a), about 10 km away from the Aso-Ohashi and Takanodai landslide sites. Aso-Ohashi and Takanaodai landslides will be described below.

The earthquake fault has been traced toward the east up to the western part of the Aso Caldera (Geospatial Information Authority of Japan 2017) with the diameters of 18 km and 25 km in E–W and N–S directions respectively. The maximum PGA was recorded at 1316 cm/s^2 at Kawayo in Minami-Aso Village (JMA 2016), which is located nearer than the KM005 site.

A Large-scale Slope Failure Near the Aso-Ohashi Bridge and Its Countermeasures

A large-scale slope failure near the Aso-Ohashi Bridge occurred from a slightly convex slope around a ridge of the

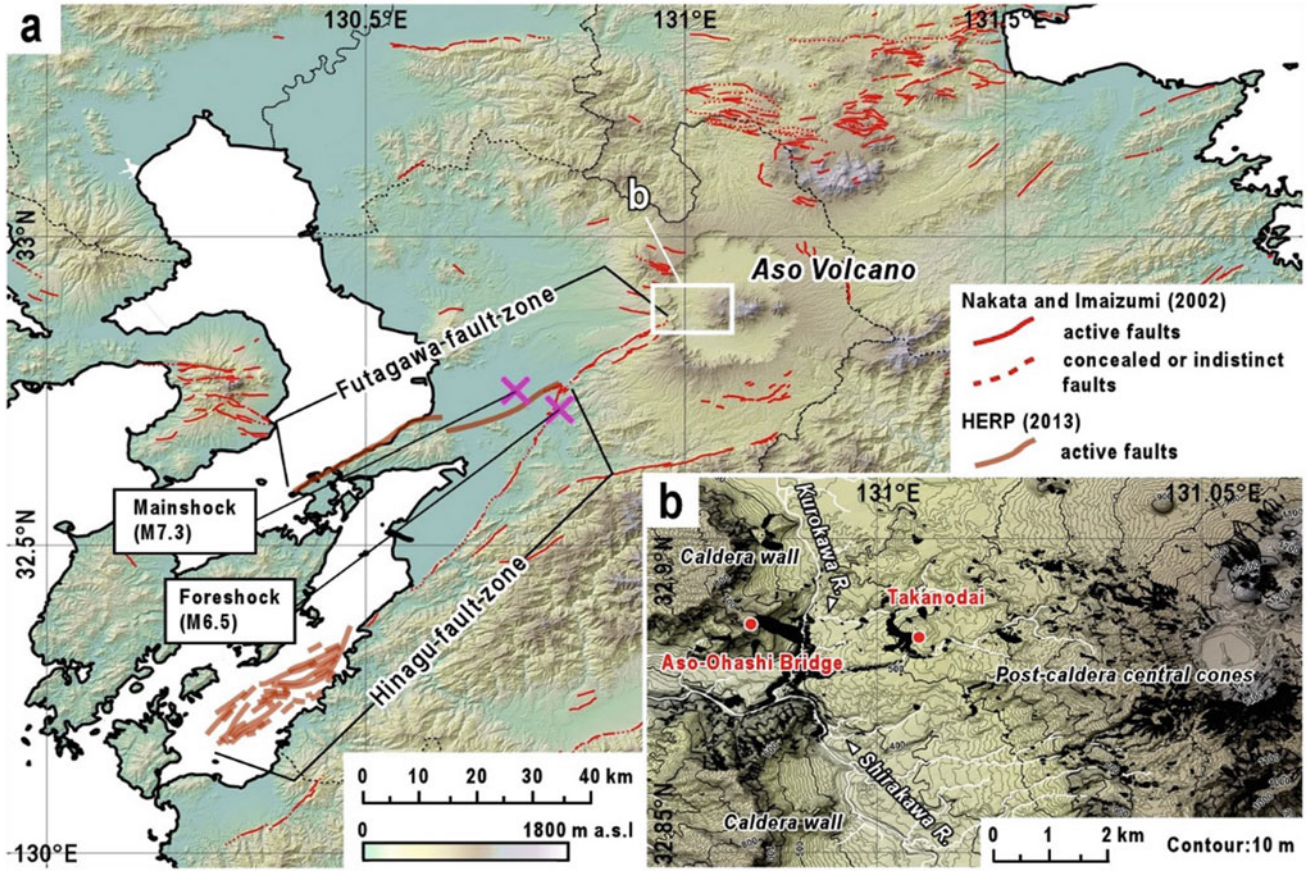

Fig. 8 Locations of the epicenters of the 2016 Kumamoto Earthquake and the Futagawa and Hinagu fault zones. **a** Distribution of active faults (red line after Nakata and Imaizumi 2002; brown line after HERP 2013) and epicenters of the M6.5 foreshock and the M7.3 mainshock of the series of earthquakes that occurred in April 2016 (pink cross after JMA 2016). Solid and dashed lines indicate shorelines and prefectural boundaries, respectively. **b** Distribution of landslides (black polygons) induced by the 2016 Kumamoto Earthquake and river channels (white lines) around the western rim of the Aso Caldera (after NIED 2016b)

Aso Caldera rim on April 16, 2016, with a width of 200 m, a length of 700 m, a relative height of 325 m, and a depth of 5–10 m (Fig. 10). The slope failure destroyed National Route 57, the JR Hohi Line, and collapsed the Aso-Ohashi Bridge on Route 325 over the Kurokawa River (Fig. 10). The Kyushu Development Bureau, MLIT, had carried out investigations and countermeasures since 2016 as national projects for the emergency and permanent remedial measures. They were to prevent secondary disasters caused by unstable sediment remaining at the upper slopes where many cracks have been formed and to perform permanent slope stabilization, respectively (Yamagami 2018; Matsumoto 2020; Aso Sabo Office, Kyushu Regional Development Bureau, MLIT 2021) (Fig. 11).

The geology around the slope failure is composed of andesite, auto-brecciated lava, and tuff breccia alternately deposited horizontally with some open fractures. The topsoil of the ridge behind the slope failure consists of debris deposits, including surficial Kuroboku soil (3 m in depth) and the underlying loosened rocks (Fig. 12). The geological structure shows a slightly reverse-dipping slope composed of volcanic deposits (Fig. 12).

Based on the topography before the earthquake and the distribution of elastic wave velocity, slope materials with Vp = 1.0 km/s or less in the shoulder part of the slopes were considered to have collapsed during the earthquake (Fig. 13) (Kyushu Regional Development Bureau 2016-2020).

Based on the slope micro-topography formed by the earthquake, and geological survey results, the slope failure and surrounding unstable slopes were divided into six areas (blocks), considering the assumed mass movement types, and the basic concepts for countermeasures were then determined (Fig. 13). The remedial measures for the slope

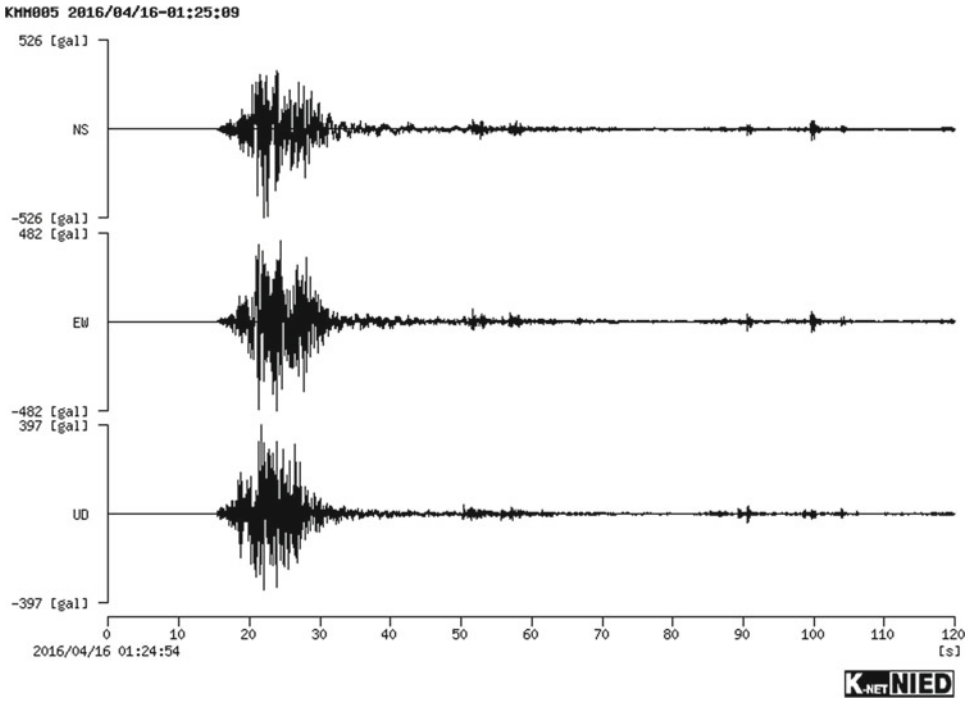

Fig. 9 Time history of acceleration in three directions for the mainshock of the Kumamoto Earthquake at KMM005 (NIED 2016a)

Fig. 10 A slope failure induced by the mainshock near the Aso-Ohashi Bridge (Modified from the Kyushu Regional Development Bureau, MLIT 2016)

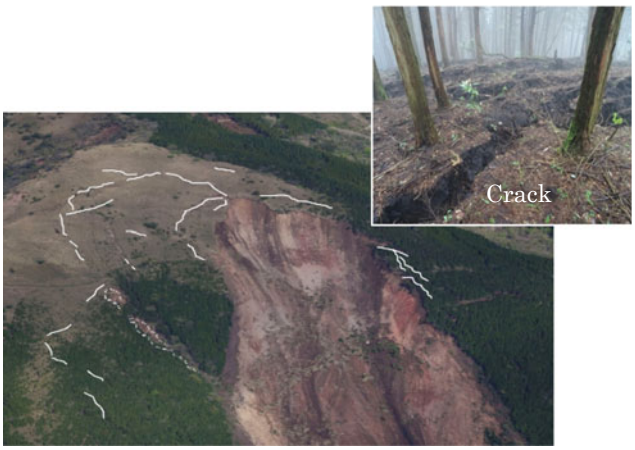

Fig. 11 The head part of the slope failure and the distribution of cracks around the failure (upper) and the cracks around the failure (white line: lower) (Photo: Kyushu Regional Development Bureau, MLIT 2016)

failure were: (1) to prevent rockfalls, surface failure, erosion, and weathering in the head part of the slope failure; and (2) to protect the lower part from erosion and surficial failures of debris deposits of the slope failure.

As emergency measures, the unstable slopes in and around the slope failure were firstly rounded to remove the unstable materials at the head. These works were carried out using an elevated slope excavator with a movable camera and network-enabled unmanned construction method to avoid accidents (Fig. 14). The construction method enabled up to 14 unmanned construction machines to operate on the

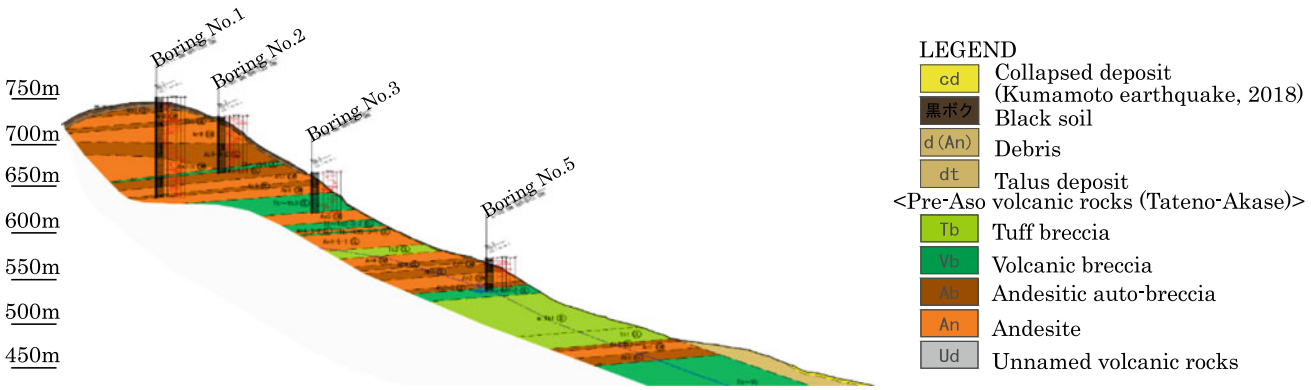

Fig. 12 Geological section of the slope failure near the Aso-Ohashi bridge (Modified from source: Kyushu Regional Development Bureau, MLIT 2016) (The location of the section is shown in Fig. 13)

slope failure site (Kitazawa and Motomura 2021). As a result, rocks and soils in the volume of 17,000 m^3 were removed in 70 days.

Then, using manned construction of slope stabilization as the permanent measures in the middle and lower parts of the slope failure, eight rows of steel-reinforced retaining walls 200 m long each had been constructed with re-vegetation since June 2017 (Fig. 15). A strong wire net has protected at the upper part of the slope failure with the support of steel bars installed into the ground. Anchor works were adopted to stabilize the loosened rock slopes at the side of the slope failure.

Given many cracks around the exposed bare earth, extensometers, GNSS, and ground inclinometers were installed to monitor the ground surface movement. In contrast, borehole inclinometers and pipe strain gauge were used to observe the underground movement. The in-site observation of cracks was also carried out.

These countermeasure works enabled National Highway No. 57 to be open to traffic in the summer of 2020. The management of the protected slopes has been handed over to the Kumamoto Prefectural Government.

Landslides in Takanodai

Over 1000 individual landslides occurred in the Aso Volcano area by the mainshock of the 2016 Kumamoto Earthquake (NIED 2016b). The slopes were widely covered with fallout tephra layers (Higaki et al. 2019). The Takanodai landslide in the Minami-Aso Village is an example of landslides which occurred in such tephra layers (Figs. 8 and 16). Several landslides were induced by the mainshock on the hill slopes of the area where the Kyoto University Institute of Volcanology stands atop (blocks A to E in Figs. 16, and 17). This hill originated from the Takano-Obane lava dome formed in 51 ka (Matsumoto et al. 1991), and it has been covered with tephra layers.

The source area of the largest landslide (block A) at the shoulder part of the hill had a width of 100 m and a depth of 5–10 m with a slope gradient of ca. 15° (Fig. 17a). Exposure at the head cliff show tephra and humic soil layers cover the gentle hill slopes cumulatively (Fig. 17b). The displaced mass of block A moved more than twice as long as the length of its source area (Fig. 16). The other landslides moved far toward the southwest, west-northwest, and then north. Since a telephone pole standing at an in-situ position has been buried by moving materials at the toe of block B (Fig. 17c), and parallel striation remains on the head scarp remain at the block E (Fig. 17d), both disruptive slide and translational slide occurred in the Takanodai landslide. The fact that the landslide of the block E moved 65 m with a house on it without the windows broken (Higaki et al. 2016) indicates the translational slide.

After forming the present Aso Caldera with the outflow of the Aso-4 pyroclastic flow (90 ka), the fallen tephra, mostly from the post-caldera central cones, reached a thickness of 100 m (Miyabuchi et al. 2003). The Kusasenrigahama Pumice (Kpfa), which has formed the slip surface of some of the Takanodai landslides, is a pumice layer fallen in 31 ka and is interbedded at a depth of 3–8 m on the slope (Fig. 18).

Kasama et al. (2018) pointed out that the Kpfa deposited in the loose condition indicated by the high void ratio was compacted quickly by repeated seismic shearing so that the shear strength was decreased and the landslides with large run-out displacement occurred.

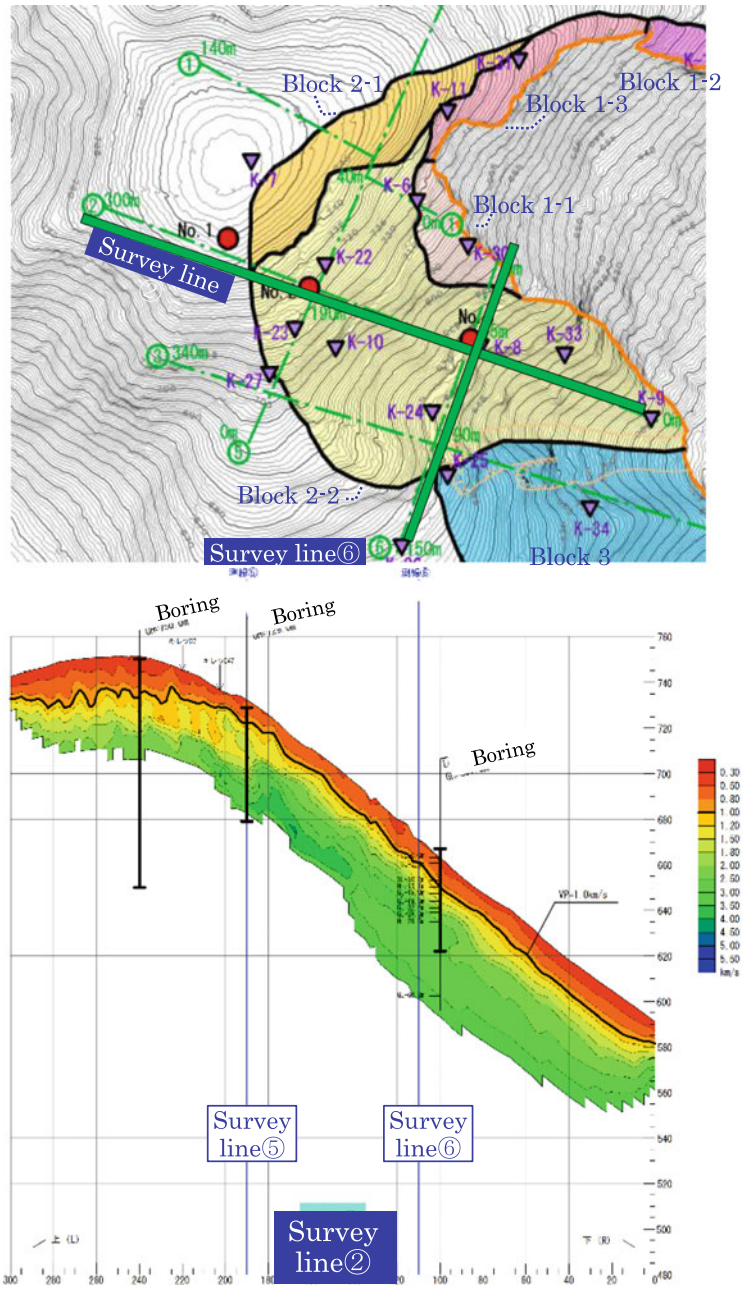

Fig. 13 Results of geological investigation around the slope failure near the Aso-Ohashi Bridge by seismic survey (Modified from source: Kyushu Regional Development Bureau, MLIT 2016) (The location of the section is shown in Fig. 13)

5 Landslides Induced by the 2018 Heavy Rain in Hiroshima

Encroachment of Urban Areas Toward Sloping Terrain

In Hiroshima City, with a population of 1.2 million, slope failures and debris flow often occur even with less rainfall than in areas such as Shikoku and Central and Southern Kyushu. One of the reasons for this is geology and rock types (Kaibori et al. 2018). Granitic rocks are widely distributed in and around Hiroshima City (Fig. 19) and are often highly weathered. In addition, many houses are located near the outlet of mountain streams and steep foot slopes, which are prone to sediment disasters. In the outskirts of Hiroshima City, catastrophic sediment disasters were also caused by heavy rain in 1999, 2014 (Tsuchida

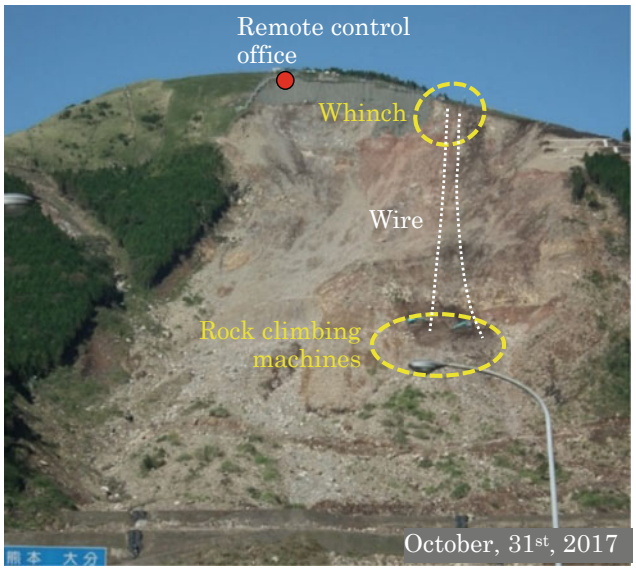

Fig. 14 Removal of unstable sediment by unmanned construction (Modified from source: Kyushu Regional Development Bureau, MLIT 2020)

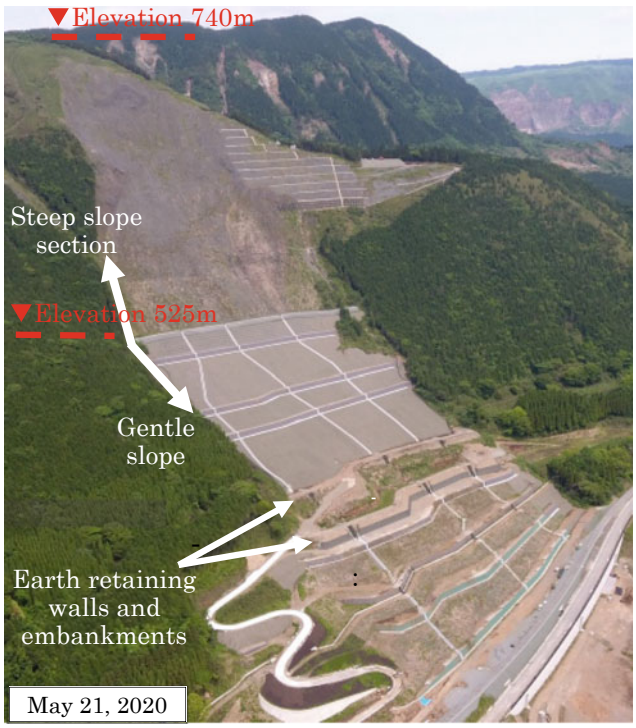

Fig. 15 Countermeasures adopted for the stabilization of each block (Embarkment and steel-reinforced soil at the lower slope and earth removal and soil shaping at the head slope) (Aso Sabo Office, Kushu Regional Development Bureau, MLIT 2020)

et al. 2019), and 2018 (Kaibori et al. 2018). Figure 20 shows a debris flow disaster in Hiroshima City that occurred in 2018. The geographical conditions of mountainous terrain encroaching on the plains where large city areas develop, and the spread of residential areas into the mountain sides cause an increase in the number of areas at risk of sediment disasters.

In 2000, the Government of Japan enacted the Sediment Disaster Prevention Act to prevent people from living in hazardous areas of sediment disasters, often without knowing the dangers. Under the Act, "sediment disaster hazard areas" are to be designated into two categories based on the investigation of the topography, geology, and land use in the sediment disaster-prone areas (Sabo Department, MLIT 2016). An area of exceptionally high risk is designated as Sediment Disaster Special Hazard Area, where housing and building developments are controlled. In contrast, an area prone topographically to sediment disaster is designated as Sediment Disaster Hazard Area.

In addition, non-structural measures are being developed to provide warning and evacuation from the hazard zones in conjunction with sediment disaster warning information issued by the local government based on local rainfall conditions. Hazard areas are set for debris flow, slope failure, and landslide, each likely to cause sediment disaster in Japan.

The 2018 Heavy Rainfall Disaster in Hiroshima City

During the July 2018 heavy rains, after Typhoon No. 7 passed between Kyushu and the Korean Peninsula on July 3–4, a front stalled between the cold Okhotsk High in the north and the subtropical Pacific High in the southwest of the Japanese archipelago, causing a remarkable inflow of water vapor from the southwest to continue, resulting in heavy rainfall over a wide area in Western Japan (Hiroshima West Mountain Range Sabo Office 2019). The total amount of rain from July 5 to 7 reached 430 mm, 1.7 times larger than the monthly rainfall in July, at Nukushima, Higashi-ku, Hiroshima City (Fig. 21). The precipitation of accumulated rainfall was 1.6–2.6 times larger than previous sediment disasters in 1999 and 2014, and continuous rain was 3.4–20.5 times longer in 2018 (Kaibori et al. 2018). Figure 21 shows the occurrence of slope failures and debris flows that are particularly concentrated in the southern part of Hiroshima Prefecture during the July heavy rains (Sediment Control Division, Public Works and Construction Bureau, Hiroshima Prefecture 2019). The number of

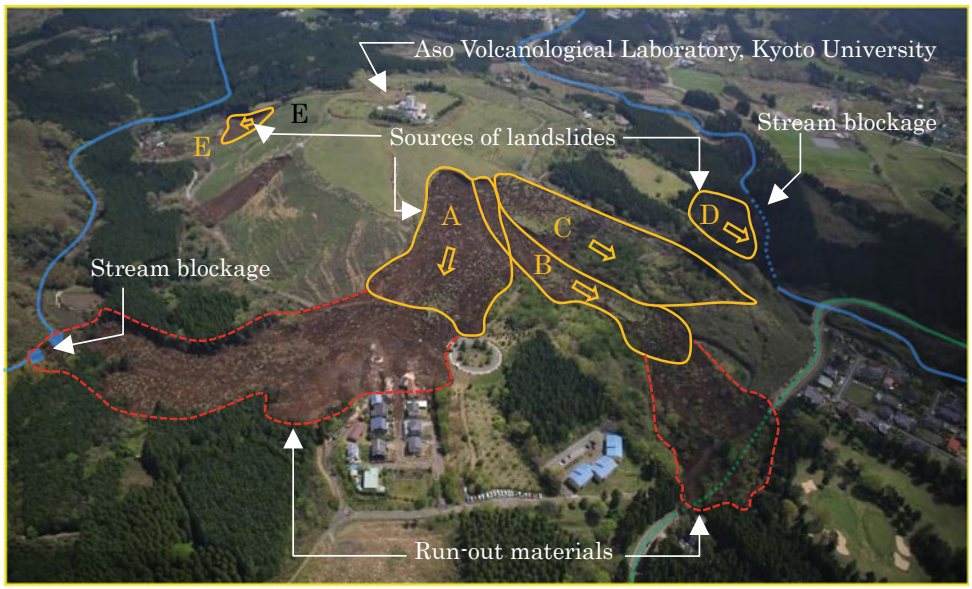

Fig. 16 Landslides at Takanodai caused by the earthquake. A-E: Landslide block (area) (Area of landslide block: Higaki et al. 2016)

debris flows was particularly high. The locations of the slope failures were widely distributed along the Seto Inland Sea in a zonal pattern from southwest to northeast, with a total sediment discharge of 8.1 million m^3 (Kaibori et al. 2018) and densities of debris flows and slope failures of 3.01 and 0.30 locations/km^2, respectively (Fig. 22: Hiroshima University 2018).

This extremely heavy rain caused 1242 sediment disaster locations in Hiroshima Prefecture, and the number of sediment disasters is larger than the recent national annual average of about 1100 sediment disasters (2008-2017) (Sabo Planning Division, MLIT 2018). The sediment disasters mainly occurred as steep slope failures and debris flows. Out of the 120 people killed or missing in Hiroshima Prefecture due to this calamity, 87 fatalities were caused by the sediment disasters (Hiroshima West Mountain Range Sabo Office 2019).

As an emergency response to this disaster, the Chugoku Regional Development Bureau of MLIT implemented emergency measures to prevent secondary disasters in the nine districts severely damaged by debris flows (Hiroshima West Mountain Range Sabo Office 2018). The adopted countermeasures included: (1) channel stabilization works using large sandbags to channel water downstream safely; (2) installation of warning devices such as wire sensors to detect the occurrence of debris flows (Fig. 23); and (3) installation of strong wire net barriers to supplement small debris flows as emergency measures (Fig. 24).

On the other hand, MLIT constructed Sabo dams and other structures as permanent countermeasures in 28 streams that urgently need to be addressed since 2014 (Fig. 25, Hiroshima West Mountain Range Sabo Office, MLIT 2020).

The Sabo dam constructed in Catchment No.19-299 (Fig. 24) trapped the sediments during the heavy rain in August 2021, protecting the downstream area (Fig. 26). In addition, 20 Sabo dams have been completed after the 2018 disaster for the debris flow-affected areas shown in Fig. 24).

6 Discussions

Western Japan has high precipitation in Japan because the region is susceptible to typhoons and rainy season fronts and is surrounded by waters where warm currents enter. In the 2018 Hiroshima heavy rain disaster, the East China Sea supplied water vapor, resulting in high precipitation. In addition, its proximity to a large plate border causes frequent earthquakes and creates many Quaternary volcanoes. Furthermore, geologically and topographically, the region has a wide distribution of mountains with medium to low relief terrain, where erosion proceeds slowly and weathered granitic rocks are easily formed. Sedimentary and metamorphic rocks that have undergone deformation and fracturing of the accretionary complex are distributed in the Shikoku and southern half of the Kyushu regions. There are many slopes covered with fallen tephra layers in and around the volcanic areas.

Compared to Eastern Japan, excluding the Tokyo metropolitan area, Western Japan is densely populated, with residential lands concentrated in the foothills. Because of

Fig. 17 **a** Long run-out landslide (A block), **b** Head scarp with the exposure of fallen tephra layers indicated as a red arrow (B block), **c** Run-out materials (Toe of B block), **d** Main scarp (back) and slide body (front) (E block)

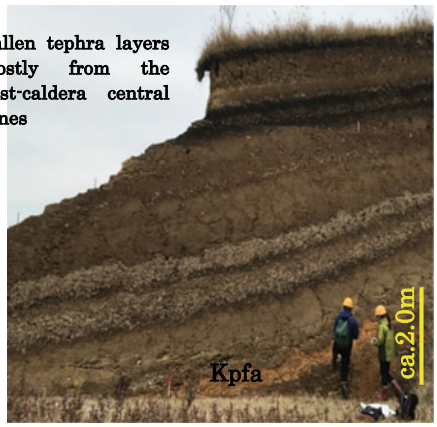

Fig. 18 Slip surface formed in the Kusasenrigahama Pumice fall layer

these natural and social conditions, sediment disasters, such as steep slope failures, landslides, and debris flows, frequently occur in Western Japan. Historically, a tsunami generated by the mega-slide at Unzen-Mayuyama due to an earthquake in 1792 killed ca. 15,000 people.

In Japan, various non-structural and structural measures have been taken to reduce the risk of sediment disasters (Kanbara and Imamori 2020). Stone pillars at various locations in the Ariake Sea, which mark the arrival points of the tsunami caused by the Mayuyama mega-slide, are still in place to remind the future occurrence of landslide tsunami risk. Previous documents, including drawings, are also helpful for recognizing the phenomena that induced catastrophic disasters in the ancient times (Inoue 1999). In addition, simulations of the dynamic motion of the earthquake-induced mega-slide and subsequent tsunamis are helpful for hazard mapping from a multi-hazard perspective. Hazard mapping and the resulting warnings and evacuations are necessary non-structural measures.

In Japan, the Sediment Disaster Prevention Act legally designates areas susceptible to rain-induced sediment disasters as hazardous areas of different types of sediment disasters, such as slope failures, debris flows, and landslides that can affect important protection objects. In the designated areas, warning and evacuation systems are under development (MLIT 2016).

On the other hand, as structural measures, check dams similar to the Sabo dams (see Fig. 26) have been constructed for a long time to control sediment discharge from mountain streams and to stop debris flows. The oldest masonry check dams, constructed by the Fukuyama-*han* (Edo era domain)

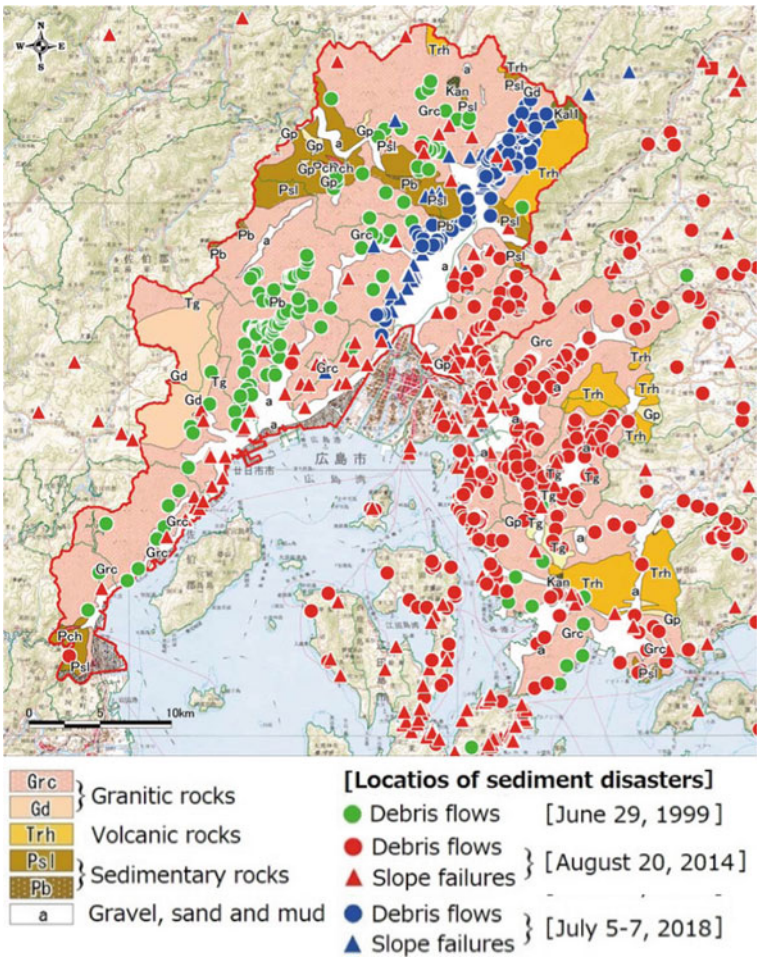

Fig. 19 Locations of recent sediment disasters and geological distribution around Hiroshima City (Modified from source: Hiroshima West Mountain Range Sabo Office, Chugoku Regional Development Bureau, MILT 2019)

320 years ago, still remain (Takanashi et al. 1997). After World War II, concrete dams became mainstream. The Sabo dams constructed in the wake of the 2018 Hiroshima heavy rain disaster captured a large amount of sediment and prevented damage to the downstream residential areas.

Recent developments in information technology have significantly advanced the prevention of secondary disasters, such as the search for missing persons and workers for disaster prevention work, and construction in watersheds and slopes where unstable sediments still remain after sediment disasters. Here, we introduced sensors for detecting debris flows and unmanned construction on slopes with unstable sediments.

However, temporal and spatial prediction of earthquake-induced sediment disasters is still difficult. The large-scale slope failure near the Aso-Ohashi Bridge due to the Kumamoto Earthquake occurred on a slope of the gentle convex ridge, covered with a thick weathered layer mainly of volcanic rocks. Because the restoration of roads, railways, and bridges connecting the prefectural capital was urgently required, the potential slope failure was stabilized by removing unstable sediment with Vp = 1.0 km/s or less on the upper slope, and by filling and earth retaining at the foot of the slope failure.

Concentrated co-seismic landslides in tephra mantled slopes, especially in hilly areas, have been reported for many earthquakes in Japan (Higaki and Abe 2012; Osanai et al. 2019). Long run-out distances in comparison with the length of source areas are also reported. Wang et al. (2021) pointed out that hydrated halloysite formation due to weathering in the pumice layer liquefied in the fallen tephra deposits during the 2018 Eastern Iburi Earthquake in Hokkaido. In the hills or slopes of dissected terraces around or on the eastern side of Quaternary volcanoes, such weak layers in fallen tephra tend to remain on gentle rather than steep slopes. This also inferred

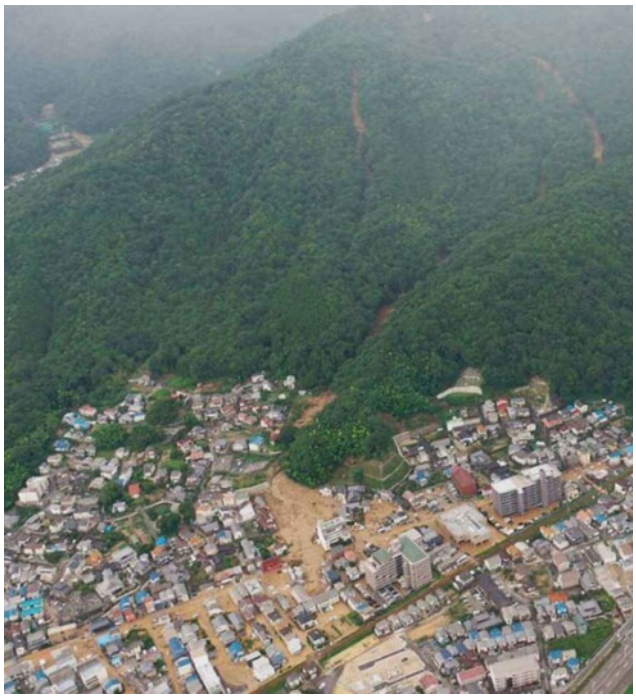

Fig. 20 Debris flow at Kuchita-minami 3 Chome in the Asa-kita Ward, Hiroshima City (Sediment Control Division, Public Works and Construction Bureau, Hiroshima Prefecture 2019)

geomorphologically landslide-favorable conditions. A further mechanism of slip surface formation and long run-out movement of earthquake-induced landslide in tephra layers is required to make susceptibility mapping of seismic landslide hazard zonation.

7 Conclusions

Western Japan is climatically prone to heavy rainfall and frequent earthquakes due to its proximity to a plate boundary. In Hiroshima Prefecture, debris flows are frequent due to the distribution of weathered granitic rocks. On the other hand, due to the dense population, many residential lands are located at the foot of mountains, and this tendency has become more pronounced with the recent development of residential lands. Many areas in Western Japan are at high risk of sediment disasters due to these natural and social conditions.

Here, in Western Japan, where sediment disasters occur frequently, we introduced some case histories. They were: (1) The large-scale landslide at Unzen-Mayuyama caused by the 1792 earthquake that generated a tsunami,

(2) The large-scale slope failure in weathered volcanic rocks, (3) Landslides in tephra layers, and

(4) The debris flows in residential areas close to mountainous areas in Hiroshima City. In addition, disaster prevention measures were described mainly for the 2018 Hiroshima City disasters and the slope failure near the Aso-Ohashi Bridge.

The 1792 Unzen-Mayuyama mega-slide alerts the tsunami risk caused by a mega-slide of over 10^8 m^3. Dynamic numerical simulation can be an effective tool for its hazard zoning. Stone pillars indicating the landslide-induced tsunami-affected areas are indigenous awareness creation means to the future generation.

In the 2016 Kumamoto Earthquake disaster, slope stabilization works were constructed by removing unstable

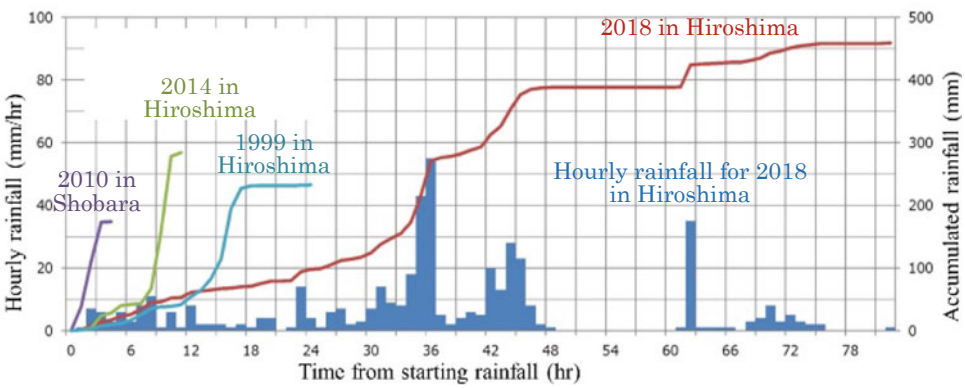

Fig. 21 Comparison of rainfalls between the past disasters in Hiroshima Prefecture and the 2018 Hiroshima disaster (Modified from source: Kaibori et al. 2018)

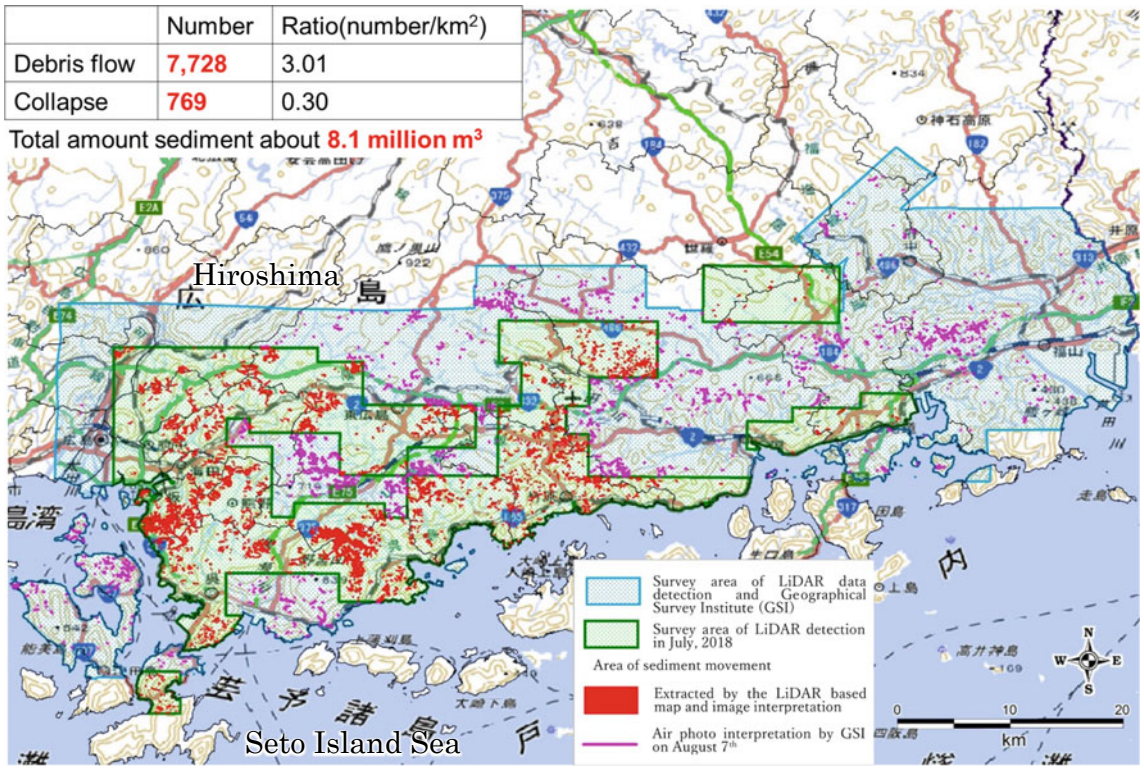

Fig. 22 Locations of slope failures and debris flows in the southern part of the Hiroshima Prefecture, the total number, and the total amount of sediment discharge volume Sediment Control Division, Public Works and Construction Bureau, Hiroshima Prefecture and Hiroshima University 2019 (Modified from; Base map: http://www.gsi.go.jp/BOUSAI/H30.taifuu7gou.html#6)

Fig. 23 Wire sensor for early detection of a debris flow occurrence **a** wire sensor, **b** warning device with a speaker and a pilot lump (Modified from source: Hiroshima West Mountain Range Sabo Office, MLIT 2019)

sediment at the head part and by filling and earth-retaining the areas at the foot of the slope for the early restoration of important traffic routes. Since the Hiroshima heavy rain disasters in 1999, 2014, and 2018, debris flows prevention projects such as the construction of Sabo dams have been promoted, and their effectiveness has been monitored.

Fig. 24 Wire net barrier to capture sediment (Hiroshima West Mountain Range Sabo Office, MLIT 2019)

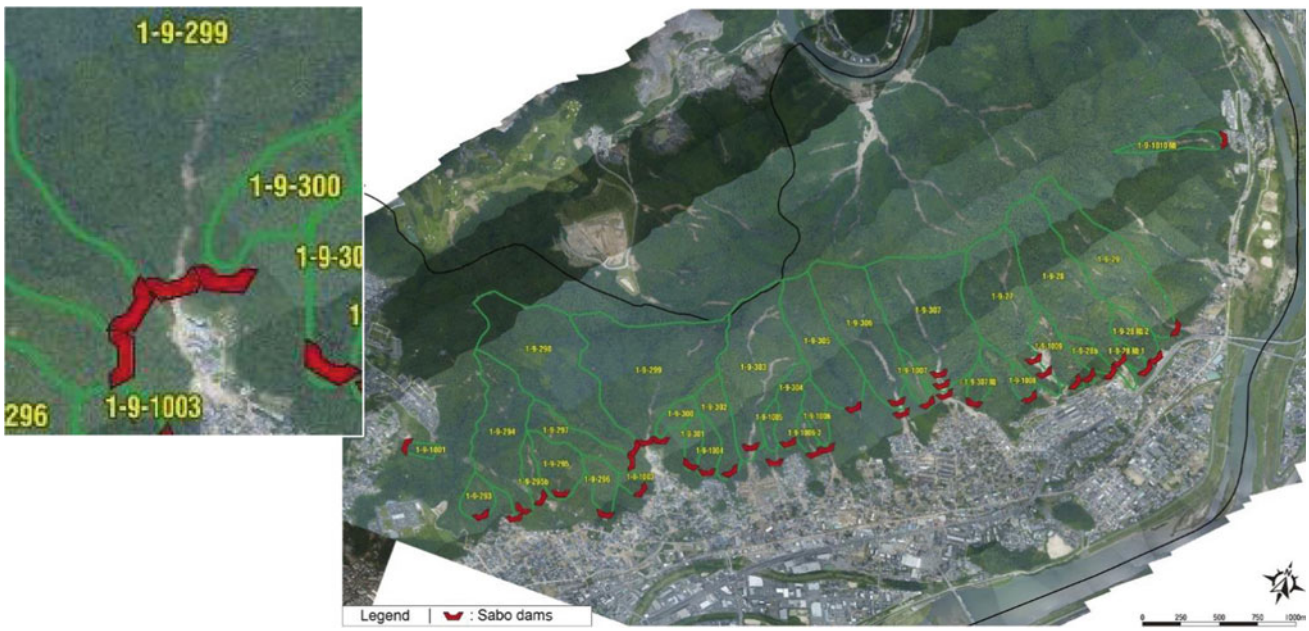

Fig. 25 Installation plan of Sabo dams for disaster recovery in the catchment of debris-flow affected streams (Modified from source: Hiroshima West Mountain Range Sabo Office, Chugoku Regional Development Bureau, MLIT 2020)

In these cases, recent advances in information and construction technologies and structure materials have made unmanned construction possible; early warning system installations are also progressing based on the designation of hazardous areas by the Sediment Disaster Prevention Act. On the other hand, earthquake-induced landslide damage in volcanic tephra-covered hills has occurred frequently. Identifying slopes where such landslides may occur is to be resolved as soon as possible.

Fig. 26 Sediment capture behind a Sabo dam in the catchment 1-9-299 in Fig. 25 (Modified from source: Hiroshima West Mountain Range Sabo Office, MLIT 2019)

Acknowledgements The authors gratefully acknowledge the enthusiasm and help from many colleagues and institutions as follows: Dr. T. Mukunoki of Kumamoto University, Dr. T. Tsuchida of Hiroshima University at the time, Dr. Y. Hasegawa of Hiroshima University, Unzen Restoration Office, MLIT, Dr. Takashi Kimura of Ehime University, Kumamoto Restoration Office, MLIT, Hiroshima West Mountain Range Sabo Office, MLIT, Hiroshima Prefectural Government, Shimabara Forest Management Office, Ministry of Agriculture, Forestry and Fisheries, and Sabo Frontier Foundation.Thanks are due to providing valuable materials on the Mayuyama mega slide, sediment disasters in Hiroshima 2018, and the 2016 Kumamoto Earthquake, which were very useful when writing the paper.

References

Aso Sabo Office, Kyushu Reginal Development Bureau, Ministry of Land, Infrastructure, Transport and Tourism (MLIT) (2021) The project summary of the protection of slope failure at the Aso-Ohashi area (in Japanese)

Furuya T (1974) A geomorphologic study of collapse of Mayu-Yama in 1792. Disaster Prev Res Inst Annal 17B:259–264 (in Japanese with English abstract)

Geological Survey of Japan, National Institute of Advanced Industrial Science and Technology (AIST) (2022) https://gbank.gsj.jp/seamless/v2/viewer/?center=32.7801%2C130.3533. (ref. Mar 11 2022)

Geospatial Information Authority of Japan (2017) 1/25000 Map of active faults "Aso". https://maps.gsi.go.jp/#14/32.836634/130.924244/&base=std&ls=std%7Cafm

Headquarters for Earthquake Research Promotion (HERP) (2013) Evaluation of the Futagawa and Hinagu fault zones (revised version). Long-term evaluation of major active faults 810, p 66. http://www.jishin.go.jp/main/chousa/katsudansou_pdf/93_futagawa_hinagu_2.pdf (in Japanese)

Higaki D, Abe S (2012) Classification of the geomorphology, geology and movement types of earthquake landslides. In: Ukai K, Yagi H, Wakai A (eds) Earthquake induced landslides: proceedings of the international symposium on earthquake-induced landslides. Springer, pp 37–44

Higaki D, Tsunaki R, Terada H, Sakaguchi T, Ueno Y (2016) Report of a joint investigation team of the Japan landslide society and Japan association for slope disaster management for Kumamoto earthquake. Slope Disaster Manage 43(3):52–66 (in Japanese)

Higaki D, Li X, Hayashi K, Tsou C-Y, Kimura T, Hayashi S, Sato G, Goto S (2019) Geomorphological setting of shallow landslides by heavy rainfall on tephra-covered slopes of Aso Volcano, southwest Japan. J Jpn Landslide Soc 56(Special issue):218–226 (in Japanese with English abstract)

Hiroshima University Research Team for the July 2018 Heavy Rain Disaster (Geography Group) (2018) Map of slope failure distribution in Hiroshima Prefecture caused by the July 2018 heavy rainfall (Report no 4). https://www.hiroshima-u.ac.jp/system/files/105540/201807_report004.pdf. (ref. Apr 21 2020)

Hiroshima West Mountain Range Sabo Office, Chugoku Regional Development Bureau, Ministry of Land, Infrastructure, Transport and Tourism (MLIT) (2019) The 2018 heavy rain in July, 2018—sediment disasters, p 50 (in Japanese)

Hiroshima West Mountain Range Sabo Office, Chugoku Regional Development Bureau, MLIT (2020) The heavy rainfall on 20 August 2014—Hiroshima sediment disaster, p 26

Inoue K (1999) Shimabara-Shigatusaku earthquake and topographic changes by Shimabara catastrophe. J Jpn Soc Erosion Control Eng 52(4):45–54 (in Japanese with English abstract)

Ishikawa Y, Kubota T, Aoto K, Iijima Y, Ikawa T, Ikegami T, Ikeda M, Ue H, Uehara Y, Uhimura Y, Egawa K, Osihi H, Okano K, Kaibori M, Katsura S, Kato M, Kawahara S, Koga S, Sakashima T, Sagara W, Jitouzono T, Shinohara Y, Shimizu O, Shimoda Y, Suzuki S, Suzuki M, Seto K, Tagata S, Terada H, Teramoto Y, Dounowaki M, Tobioka S, Torita E, Nakano K, Nishikawa T, Hanada R, Hirakawa Y, Fukuzuka K, Fujisawa Y, Fujita M, Maksaki K, Miyata N, Yamaguchi K, Yamashita S, Yamane M, Yokoo K (2016) Sediment-related disasters induced by the Kumamoto earthquake in April 2016. J Jpn Soc Erosion Control Eng 69(3):55–66 (in Japanese with English abstract)

Isozaki Y, Itaya T (1991) Pre-Jurassic Klippe in northern Chichibu Belt in west-central Shikoku, Southwest Japan-Kurosegawa Terrane as a tectonic outlier of the pre-Jurassic rocks of the Inner Zone. J Geol Soc Japan 97(6):431–450 (in Japanese with English abstract)

Isozaki Y, Maruyama S, Aoki K, Nakama T, Miyashita A, Otoh S (2010) Geotectonic subdivision of the Japanese Islands revisited: categorization and definition of elements and boundaries of Pacific-type (Miyashiro-type) Orogen. J Geogr (Chigaku Zasshi) 119(6):999–1053 (in Japanese with English abstract)

Japan Meteorological Agency (JMA) (2016) Earthquake disaster report: 2016 Kumamoto earthquake. Japan meteorological agency report on natural disaster phenomena, 2016, no 1. https://www.jma.go.jp/jma/kishou/books/saigaiji/saigaiji_2016/saigaiji_201601.pdf. (ref. Apr 30 2022) (in Japanese)

Japan Meteorological Agency (2016) The 2016 Kumamoto earthquake. https://www.data.jma.go.jp/svd/eqev/data/2016_04_14_kumamoto/index.html#kumamoto_data. (ref. Apr 30 2022) (in Japanese)

Japan Meteorological Agency (2017) Number of active volcanoes in Japan (as of June 2017). https://www.data.jma.go.jp/vois/data/tokyo/STOCK/kaisetsu/katsukazan_toha/katsukazan_toha.html#katsukazan (in Japanese)

Kaibori M, Hasegawa Y, Yamashita Y, Sakida H, Nakai S, Kuwada S, Hiramatsu S, Jitousono T, Irasawa M, Shimizu O, Imaizumi F, Nakatani K, Kashiwabara Y, Kato N, Torita E, Hirakawa Y, Yoshinaga S, Tanaka K, Hayashi S (2018) Sediment related disaster due to heavy rainfall in Hiroshima Prefecture in July 2018. J Jpn Soc Erosion Control Eng 71(4):49–60 (in Japanese)

Kaibori M, Ishikawa Y, Satofuka Y, Matsumura K, Nakatani K, Hasegawa Y, Matsumoto N, Takahara T, Fukutsuka K, Yoshino K, Nagano E, Fukuda M, Nakano Y, Shimada T, Hori D, Nishikawa T (2015) Sediment-related disasters induced by a heavy rainfall in Hiroshima-city on 20th August, 2014. Japan Meteorological Agency 2018. J Jpn Soc Erosion Control Eng 67(4):49–59 (in Japanese with English abstract)

Kanbara J, Imamori N (2020) Outline of measures for sediment disaster by the Sabo department of MLIT, Japan. Landslides 17:2503–2513

Kasama K, Yamagata S, Tanaka H, Furukawa Z, Yasufuku N (2018) Seismic stability evaluation of volcanic soil at Takanodai, Minami-aso village, Kumamoto. Jpn Geotech J 13(1):171–181 (in Japanese with English abstract)

Kitazawa T, Motomura T (2021) Project for the restoration of slope failure in the Aso-Ohashi Bridge area (Part 3)—approaches to construction. Bull Jpn Assoc Slope Disaster Manage 141:10–19 (in Japanese)

Kyushu Regional Development Bureau, Ministry of Land, Infrastructure, Transport and Tourism, 2016-2020 (2021) Materials for technical study meetings on the restoration of slope failure in the Aso-Ohashi Bridge area (1st to 10th meetings). http://www.qsr.mlit.go.jp/bousai_joho/tecforce/sabo/index.html. (ref. Aug 7 2021) (in Japanese)

Matsumoto S (2020) Project for the restoration of slope failure in the Aso-Ohashi Bridge area (Part 2)—permanent countermeasure works for the slope failure. Bull Jpn Assoc Slope Disaster Manage 47(3):12–19 (in Japanese)

Matsumoto A, Uto K, Ono K, Watanabe K (1991) K-Ar age determinations for Aso 6 volcanic rocks-concordance with volcanostratigraphy and application to 7 pyroclastic flows. Programme Abs Volcanological Soc Jpn 2:73 (in Japanese)

Miyabuchi Y, Hoshizumi H, Takada H, Watanabe K, Xu S (2003) Pumice fall deposits from Aso Volcano during the past 90,000 years, Southwestern Japan. Kazan 48(2):195–214 (in Japanese with English abstract)

Mukunoki T, Kasama K, Murakami S, Ikemi H, Ishikawa R, Fujikawa T, Yasufuku N, Kitazono Y (2014) Reconnaissance report on geotechnical damage caused by an earthquake with JMA seismic intensity 7 twice in 28 h, Kumamoto, Japan. Soils Found 56:947–964

Nakata T, Imaizumi T (eds) (2002) Digital active fault map of Japan. University of Tokyo Press, Tokyo (in Japanese)

National Research Institute for Earth Science and Disaster Resilience (NIED) (2016a) Strong ground motion of Kumamoto earthquake 2016. https://www.kyoshin.bosai.go.jp/kyoshin/topics/html20160416012405/main_20160416012405.html. (ref. May 30 2022) (in Japanese)

National Research Institute for Earth Science and Disaster Resilience (NIED) (2016b) Distribution map of landslides induced by the 2016 Kumamoto earthquake (final update on 27 June 2016). Storm, Flood and Landslide Research Division, NIED. http://www.bosai.go.jp/main/mizu/dosha.html (in Japanese)

Osanai N, Yamada T, Hayashi S, Katsura S, Furuichi T, Yanai S, Murakami Y, Miyazaki T, Tanioka Y, Takiguchi S, Miyazaki M (2019) Characteristics of landslides caused by the 2018 Hokkaido Eastern Iburi earthquake. Landslides 16:1517–1528

Sabo Department, MLIT (2016) Outline of non-structural measures against sediment disasters in Japan. Sabo Frontier Foundation, p 31

Sabo Planning Division, Water and Disaster Management Bureau, Ministry of Land, Infrastructure, Transport and Tourism (2018) Sediment disasters in Japan. http://www.mlit.go.jp/river/sabo/jirei/h29dosha/H29dosyasaigai.pdf. (ref. Apr 20 2021)

Sassa K, Dang K (2018) TXT-tool 0.081-1.1: landslide dynamics for risk assessment. Landslide dynamics: ISDR-ICL landslide interactive teaching tools. In: Sassa K, Guzzetti F, Yamagishi H, Arbanas Z, Casagli N, McSaveney M, Dang K (eds) Fundamental, mapping and monitoring, vol 1. Springer, pp 1–79

Sassa K, Dang K, Yanagisawa H et al (2016) A new landslide-induced tsunami simulation model and its application to the 1792 Unzen-Mayuyama landslide-and-tsunami disaster. Landslides 13(6):1405–1419

Takanashi K, Hanabusa H, Matsuda K (1997) The structure of the erosion-control masonry dam (Sunadome) in Fukuyama Han (Fukuyama District). J Jpn Soc Erosion Control Eng 50(1):45–51 (in Japanese)

The Japan Landslide Society (2012) Landslides in Japan, p 68

Toki K (ed) (1993) Multi-language glossary on natural disasters-English version. Japan National Committee of IDNDR, Tokyo, p 250

Tsuchida T, Moriwaki T, Nakai S, Athapaththu AMRG (2019) Investigation and consideration on landslide zoning of multiple slope failures and debris flows of 2014 disaster in Hiroshima Japan. Soils Found 59:1085–1102

Tsuji Y, Murakami Y (1997) Inundation height of the 1792 Mayuyama landslide tsunami in the Shimabara Peninsula side. Historical Earthquake 13, Soc Hist Earthq Stud 135–197

Tsuji Y, Hino T (1993) Damage and inundation height of the 1792 Shimabara landslide tsunami along the coast of Kumamoto Prefecture. Bull Earthquake Res Inst University of Tokyo 68:91–176 (in Japanese)

Unzen Restoration Office of the Ministry of Land, Infrastructure and Transport of Japan (2002) The catastrophe in Shimabara: 1791–1792 eruption of Unzen-Fugendake and the sector collapse of Mayu-Yama. An English leaflet p 21

Unzen Restoration Office of the Ministry of Land, Infrastructure and Transport of Japan (2003) The catastrophe in Shimabara—1791–1792 eruption of Unzen–Fugendake and the sector collapse of Mayu-Yama. A Japanese leaflet p 44 (in Japanese)

Wang F, Zhang S, Li R, Zhou R, Auer A, Ohira H, Dal Z, Inul T (2021) Hydrated halloysite: the pesky stuff responsible for a cascade of landslides triggered by the 2018 Iburi earthquake, Japan. Landslides 18:2869–2880. https://doi.org/10.1007/s10346-021-01656-y

Yamagami N (2018) Project for the restoration of slope failures in the Aso-Ohashi Bridge area (part 1)—overall project overview. Bull Jpn Assoc Slope Disaster Manage 45(3):13–20

Lessons Learned from Landslides of Socio-economic and Environmental Significance in India

Surya Parkash

Abstract

The World Centre of Excellence on Landslides Disaster Reduction at the National Institute of Disaster Management, Delhi, India carried out a brief study on documentation of landslides to prepare archival records of the socio-economically and environmentally significant landslides in India and bring out the lessons learned from these events. The relevant literature and reports on landslides have been studied along with the news archives of the landslide events from the media. The data, thus obtained, has been analyzed, compared and categorized based on certain parameters to classify them on the basis of socio-economic and environmental damages or losses by each event. The paper provides an insight into the approach adopted, criteria devised for defining and classifying the socio-economically and environmentally significant landslides while using the available information from thee archival records of these landslide events. Though there have been more than 70,000 landslides recorded by various organizations in different parts of the country yet the author could identify only 412 landslides that can be taken up as socio-economically and environmentally significant landslides from the year 1868 to 2022. Further, these landslides have been classified as low, moderate and high socio-economic significance to differentiate the degree of damages and losses from these events, including both direct and indirect costs. The study also attempted to focus on actions taken (right or wrong, good and the bad practices) as well as the lessons learned for key takeaways in future strategies and practices. The National Disaster Management Authority, Government of India, has already brought out National Guidelines on Management of Landslides during the year 2009 and National Landslides Risk Mitigation Strategy during the year 2019. Such guidelines, policies, plans, procedures and practices may be made more effective by considering the lessons drawn from the past landslides events.

Keywords

Socio-economic • Landslides • Lessons learned • Archives

1 Introduction

India has been adversely affected by frequent, sudden, swift and widespread landslides in the hilly terrains of the country. Landslides occur as primary hazards due to high intensity or prolonged low intensity rainfall, toe erosion by the rivers, anthropogenic interventions like construction, explosion, mining and so on. The landslides have also been witnessed as secondary hazards due to earthquakes, flash floods, forest fires, glacial lake outburst floods, dam burst/breaching and so on. Geological Survey of India (GSI), Ministry of Mines, Government of India, is the nodal agency for landslides studies and management in the country. It has carried out landslides mapping in 1:50,000 scale as part of its initiatives under National Landslides Susceptibility Mapping in the affected areas. According to Geological Survey of India (please refer to Fig. 1), about 12.6% (0.42 million km^2) of the country's land territory is affected by landslides to varying extents (National Disaster Management Guidelines 2009). The landslides data collected during the mapping has an inventory of approximately 70,000 landslide events at present, spread across more than 65,000 villages of about 19 states and union territories. However, this data is still not complete and need more efforts to incorporate all existing and past landslides.

The landslide susceptibility maps are also indicative of the potential landslide zones as well. The areas have been divided into different zones according to the propensity of the landslide disaster. Efforts are also being made to create maps that offer even greater accuracy in high hazard areas.

S. Parkash (✉)
National Institute of Disaster Management, Delhi, 110042, India
e-mail: surya.nidm@nic.in

I. Alcántara-Ayala et al. (eds.), *Progress in Landslide Research and Technology, Volume 1 Issue 2, 2022*, Progress in Landslide Research and Technology,
https://doi.org/10.1007/978-3-031-18471-0_23

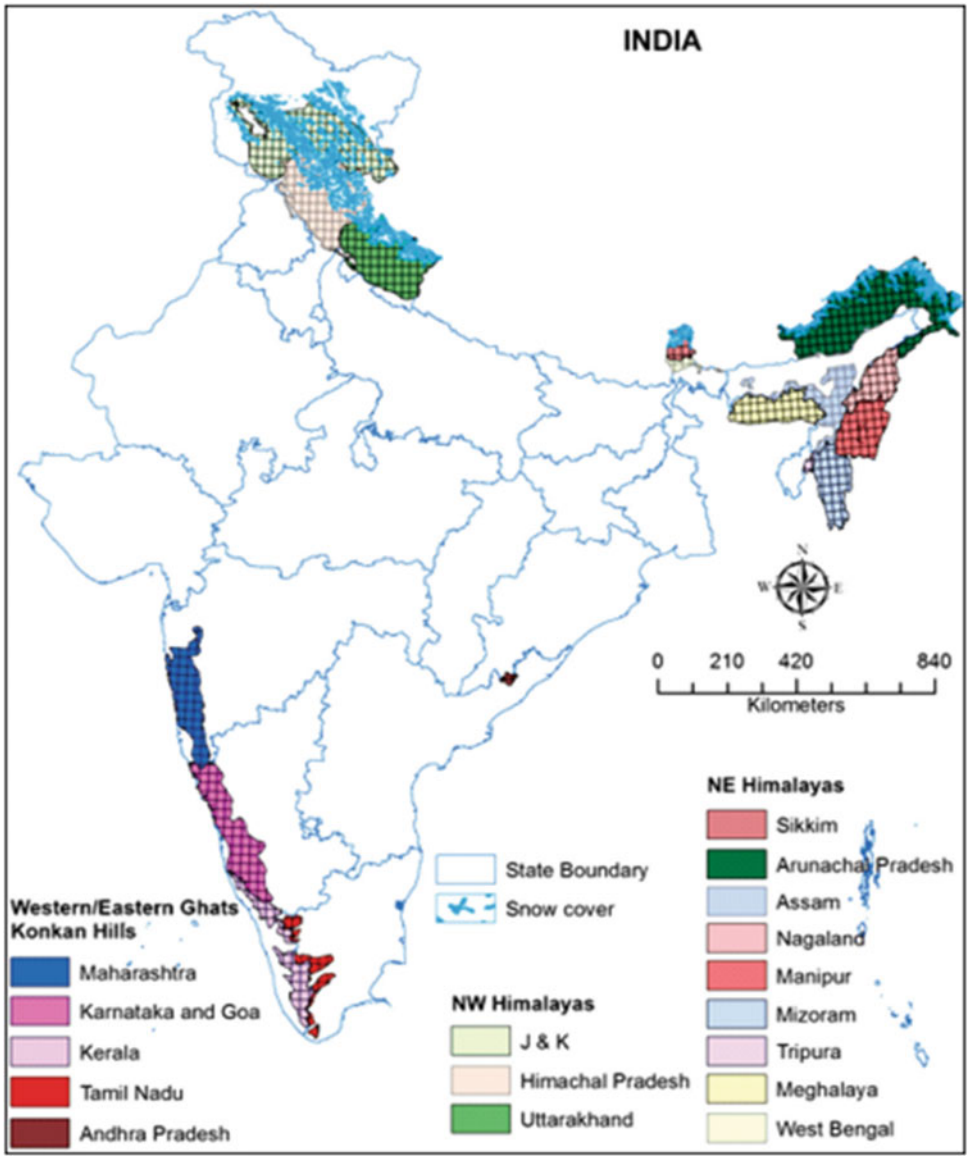

Fig. 1 National landslide susceptibility mapping (*Source* Geological Survey of India)

The maps, however, need to be localized to give a more magnified view of the locality to be more useful. This would help building plans and local construction activities. "These maps at 1:50,000 scale can be used to regulate land use in hilly/mountainous areas. For instance, areas with higher landslide probability can be spared big infrastructure".

In the present study, the author has made an attempt to segregate the data and information related to socio-economically and environmentally significant landslides within the country from the year 1867 to 2021. But there is a limitation in the study as such data is not well recorded and lacks any systematic formatted structured information due to ad-hoc casual piece-meal approach in the past, except in few events where detailed studies have been carried out by relevant scientific or academic organizations.

2 Terminology for Defining Socio-economically and Environmentally Significant Landslides

The term socio-economic comprises the two words "socio" and "economics". The consequences of any landslide event which either causes death/injury of human life, homeless people, the population affected, livestock, disrupts/changes in the pattern of livelihood like a way of people living, working, and spending their time, cultural ethics and social networks of the affected families can be classified as a "Social Impact".

The majority of incidents of serious injuries and deaths occur during the event (disaster) only, while disease

outbreaks and food shortages often occur much later, depending on the nature and duration of the disaster.

Other than killing the people and animals (both livestock and wildlife), landslides destroy or damage residential and industrial development as well as agriculture and negatively affect water quality in forest land and rivers and streams.

In addition, the "Economic Effects" of the occurrence of a landslide disaster can be described as direct and indirect losses.

According to the United Nations Office for Disaster Risk Reduction (UNISDR): "Direct losses refer to damage to human lives, buildings, infrastructure, and natural resources. Indirect disaster losses are declines in output or revenue, as a consequence of direct losses or owing to impacts on a supply chain".

Direct Losses are the most visible consequences of landslides. They may be comparatively easy to measure but they are not always the most significant outcome. They are caused by the immediate damage done to humans, resources, and the environment. On the other hand, the indirect losses rise mainly through the second-order consequences of landslides, such as disruption of economic and social activities in a community or onset of ill-health amongst disaster victims. These effects often outlast those of direct losses by months or even years and can be highly intangible. Generally, indirect costs can exceed direct costs, unfortunately, the former is difficult to assess, and thus are often overlooked or, when estimated, are too conservative.

Although most of the physical, environmental and economic impacts are noticeable, damages caused through physical destruction can be assessed in monetary terms. But the assessment of social impact is a comparatively difficult task because some of the losses are invisible. Thus, despite the absence of serious injuries and fatalities, landslides can also be recognized in terms of the significant landslides concerning their impact on the socio-economic elements.

The determination of the cost of individual and small landslides is often possible but the total cost of landslides of large geographic bodies is usually very difficult to obtain. There seems to be a clear lack of a landslide catalog database in terms of socio-economic importance in India. In this context, evaluation methodology needs to be defined.

The environmental impact of landslides are often evaluated in terms of damage and loss to biodiversity and ecosystem. Damage and loss of land is one of the most commonly affected natural element affected in every landslide and is often measures in terms of the area affected. However, in the present approach, the environmental impacts have been considered primarily in terms of loss of trees that have been damaged or uprooted by the landslide.

The author has attempted to define and classify socio-economic and environmental criteria as shown in Table 1 on significant landslides in India. The Socio-economic and environmentally significant landslides are classified broadly into three categories i.e., Low, Moderate, and High based on the range of the socio-economic and environmental damages incurred. The color codes normally used for low, moderate and high socio-economic and environmental significance are green, orange and red colors.

As the landslide data from different sources did not have any proper or pre-formatted structure, the author devised a new structured format for gathering the relevant data and information for the purpose of the present study.

3 Data Analysis and Criteria for Categorization

Extreme landslide events are frequent and sudden which directly or indirectly cause huge loss of human life, livestock, destruction of property, financial resources in a cumulative manner. However, landslide events can have significant socio-economic and environmental impacts even in the absence of fatalities and serious injuries. This paper discusses landslides in the context of the perspectives on socio-economic and environmentally significant landslides. It presents the criteria for defining socio-economic significant landslides in India, and finally summarizes 412 significant landslide incidences with respect to the above-said point of view. The present work will not be exhaustive, but will provide a criteria for classifying landslides on the basis of information on their socio-economic and environmental impacts. The said data has been gathered from the various sources including Geological Survey of India reports and Geology and Mines Department from the States, State Emergency Operations Centres, records of Revenue and Disaster Management Departments in hill states, Border Roads Organization, Public Works Department, Soil and Water Conservation Department, Irrigation and Flood Control Department, Disaster Management Authority, Planning Department, Statistics, Space Application Centre, Media Reports and News Archives, Research Publications of Universities and Research Organizations etc. The author has tried to compile relevant data on landslide disasters from the year 1868 to 2022 from all the above information/data sources.

Landslides can be caused by either natural processes or anthropogenic activity, but their socioeconomic significance is usually the result of the human-landslide interface. Landslides are usually not isolated from other natural hazards, such as excessive rainfall, earthquakes, floods and avalanches, leading to underestimation of the socio-economic and environmental impact of landslides. This underestimation is one factor in reducing the awareness and concern of both the authorities and the general public about landslide risk.

The socio-economic significance of landslides in India is a function of the country's unique geographical landscape in

Table 1 Criteria for classifying socio-economically and environmentally significant landslides in India

Low socio-economic and environmental significance	Moderate socio-economic and environmental significance	High socio-economic and environmental significance
Number of human casualties: 1–5 Number of injured people: 1–10 Number of homeless people: 1–15 Population affected: 1–100 *Economic damage and loss: 1–5 Million (INR) [67,837.10 United States Dollar (USD)] (As per 20 Sep, 2021; 1 USD = 73.71 INR) **Gross domestic product loss: 0.5–1% Impacts on bio-diversity/number of trees affected or uprooted: 1–10	Number of human casualties: 6–10 Number of injured people: 11–20 Number of homeless people: 16–25 Population affected: 101–199 *Economic damage and loss: 5–10 Million (INR) [67,837.10 United States Dollar (USD)] (As per 20 Sep, 2021; 1 USD = 73.71 INR) **Gross domestic product loss: 1–2% Impacts on bio-diversity/number of trees affected or uprooted: 11–20	Number of human casualties: > 10 Number of injured people: > 20 Number of homeless people: > = 25 Population affected: > 200 *Economic damage and loss: > 10 Million (INR) [135,689.80 (USD)] (As per 20 Sep, 2021; 1 USD = 73.71 INR) **Gross domestic product loss: > 2% Impacts on bio-diversity/number of trees affected or uprooted: > 20

* Includes any direct physical damage or a direct net loss. ** The rate of the day needs to be considered i.e., the day when the disaster happened. ***If the landslide event qualifies even any one of the criteria as given above in Table 1, then it can be categorized in either low, moderate, or high class of socio-economically and environmentally significant landslide event***

terms of geology, lithology, rainfall distribution, land use/land cover, soil properties, and road and stream networks.

It's impossible to achieve a complete accounting of the significance of landslides. Direct costs are often imprecisely recorded. However, there is ample notable research's that attempts to study and characterize the landslide but none of the literature discusses the criteria for classifying the socio-economic impact of landslide hazard. Landslides are one of the most widespread hazards on Earth and cause thousands of deaths and injuries and billions of dollars in damage worldwide each year. Statistics from The Centre for Research on the Epidemiology of Disasters (CRED, http://www.cred.be/) show that landslides contribute to about 17% of the fatalities due to natural hazards.

During the 2004–16 period, one of the most affected countries by human-triggered fatal landslides was India. After analysis of approximately 5041 fatal landslides worldwide, from 829 landslides, India registered around 10,900 deaths, which made up 18% of the total global casualties. 28% of construction-triggered landslide events were reported for India, followed by China (9%), and Pakistan (6%), whereas rainfall accounted for 16% of the total landslides and mining for 12% in India, followed by Indonesia (11.7%) and China (10%).

The subsequent sections highlight the perspectives and criteria for defining socio-economic and environmentally significant landslides in India along with a brief discussion on the history of past landslides and their impact. However, in the present study the information related to socio-economic significant landslides have been confined to those events where either human life is lost or affected either in terms of injury, homelessness, evacuation, damage to their habitant and many more. This also includes some cases of landslides on highways where traffic connectivity was affected. The metadata of 412 significant landslides has been collected from various sources (Surya et al. 2022).

4 Discussions and Conclusions

Out of 412 landslides, 179 landslides have been classified as of low socio-economic impact, 91 as moderate and 141 as high impact landslides (please refer to Table 2).

In order to understand the nature of socio-economically and environmentally significant events along with their impacts, the data listed above (Table 1) are spatially and temporally analyzed.

Apart from the fatalities as mentioned above, many incidences either resulted in economic loss or a combination of both socio and economic loss. As per the published report by National Crime Records Bureau on accidental deaths and suicides in 2019, 264 persons died in landslides. Over 65% of these fatalities happened in the Himalayas and the Western Ghats.

To the end, it can be said that the Western Himalaya, which includes the regions of Kumaun, Garhwal, Himachal, Jammu and Kashmir and the Northwest Himalaya is more prone to fatal landslides and higher human casualties followed by East and Northeast India which is followed by the South India including Maharashtra. The significant socio-economic and environmental effects of landslides in India will continue, as they do elsewhere in the world. In India, landslides disrupt lives, injure people, livelihoods, roads, natural resources, power, energy and communication infrastructure. This paper documented a few significant landslides from the year 1868 to 2022, which are estimated to have resulted in direct and indirect costs, killed many

Table 2 Number of landslides in different categories of socio-economically and environmentally significant landslides

Class	Low	Moderate	High
Number of landslides	179	91	141

individuals, and destroyed or buried homes, roads and highways, bridges, rivers, pipelines and other infrastructure vital to the well-being of the affected population. But it should be kept in mind that the landslide data presented and discussed in this paper is neither complete nor fully authentic.

Damaging landslides occur where the natural landscape intersects a socio-economic landscape, and most historical landslides of significance have occurred at the human-landslide interface. However, as people continue to expand settlement into less stable areas, one need to be ever more cognizant of the landscape in which one live, and carefully manage our exposure to unnecessary risks that threaten the livelihood, lives, and the infrastructure.

5 Key Lessons Learned

The following key lessons have been learned from the brief study of 412 socio-economically and environmentally significant landslides in India.

- Traditional investigation and remediation works may not be able to control complex chronic landslides.
- The threshold of movements, movement rates, piezometric pressures, ground subsidence and heaves etc., need to be fixed in relation to the mode of failure and elements at risk.
- It is not enough to predict potential landslide susceptibility spatially but also assess the run-out distance, spread and damage potential of the expected landslides.
- Landslides hotspots must be identified and inventions prioritized.
- Drastic changes in the river water levels must be timely informed to concerned authorities and communities.
- Thunderous sound of rolling boulders along with dust storm have often been observed during falls and slides.
- Landslides can lead to blockade of river or its tributary, thereby forming temporary lakes/dams. Bursting of such lakes and transitory dams may cause flash floods and debris flows in the downstream areas and result in destruction and devastation.
- Population pressure has perhaps compelled masses to undertake cultivation on slopes that are otherwise considered unfit for such an activity. There may be a need to devise alternate or new agricultural practices to reduce slope stability risks.
- Selection of proper grazing sites, particularly in eco-fragile and sensitive zones, to reduce soil erosion, water seepages and landsides.
- Disaster Impact Assessment besides the Environmental Impact Assessment, should be made mandatory for all projects in ecologically sensitive unstable slope areas.
- In the Himalayan region, most of the landslide prone areas fall in seismic zone V and IV, that also receive heavy precipitation and high intensity rainfalls.
- Stability evaluation of debris/waste dumps and provisions for adequate drainage measures. Suitable precautionary, preventive and protection measures should be taken up to stabilize the unstable slope mass.
- Development activities should be executed only after the detailed investigation by specialists.
- Mushrooming of shops and buildings close to roadsides near river or tributaries, could be threatening.
- A dense network of rain measuring stations should be installed, particularly in areas with known history of cloudbursts and landslides. Dissemination of rain data along with landslide warning, may be disseminated to people living in high risk prone areas.
- Better weather forecasts are the need of the hour. Prepared for climate change.
- Risk informed building codes are imperative. Information related to landslides should be disseminated to every person in the households and made available to the public in a form that is accessible to all and understood by everyone. Anyone, who is planning to buy plot or building house or hotel, should consult large scale hazard zonation maps.
- Every stratum of society should have basic understanding and should undergo a basic curriculum for civil defence, first aid and response to landslide.
- Power supply gets disrupted, following continuous torrential rains along with thunder storms and lightning.
- Process of exhuming bodies from the landslide debris is mostly manual.
- Unscientific and unplanned Quarrying, mining, use of explosives, deforestation, desiltation in landslide prone areas, can lead to landslides.
- Wire created retaining walls or concrete slabs to prevent toe erosion or cutting by the river.

- Educational buildings must be carefully located to avoid landslide impacts.
- Encroachment over river channels and steep unstable slopes may be removed through a legal framework.
- Curriculum on DRR, mock drills for safety, network schools to share experiences and resolve challenges for landslides RR&R. Remnant risks must be mapped and monitored at the community/school levels.
- Appropriate legislative interventions desired.
- UAVs (Unmanned Aerial Vehicles) may be deployed for observation, mapping and monitoring, particularly in the inaccessible areas.
- A mechanism to alert and evacuate local communities at short notice through early warning systems. Sometimes, the instruments are vandalized by the local people.
- The existing emergency communication system must be reviewed regularly to ensure last mile connectivity during disasters.
- Recommend development of landuse zoning regulations in the landslide prone areas. Tourism related development should not be allowed along the vulnerable river banks.
- Community based disaster risk management at the local levels must be given utmost importance and strengthened through capacity enhancement programmes.
- Incident Response System may be established and dovetailed into the disaster management plans.
- The aspects of psycho-social support should be integrated into medical plans for disaster affected population.
- Waste water from hotels and local inhabitants being released into the slopes, should be diverted through lined drainage channels. Temporary phreatic surfaces within the debris, overburden and unsupported slopes, causing slope instability and eventually landslides, should be regulated and controlled.
- Drainage in the uphill area of the landslide should be channelized and diverted away from the slide to prevent water infiltration and rise in pore water pressure of slope mass. All drainage courses need to be kept clear of the runoff debris to enable smooth channelized flow of water.
- Precarious boulders above the crest and on the body of the slide, should be carefully removed. Immediate filling of tension cracks with suitable impervious materials on the top and permeable materials underground using appropriate techniques must be carried out to avoid infiltration of water and building up of pore water pressure within the slope mass.
- Incorporate lessons learned from the past events into future planning, policies, strategies and actions. Analyse past experiences to know what went well and what went wrong and what could have been done better for risk reduction and emergency response. Document these lessons annually after every disaster.
- Develop a minimum inventory list of instruments, sensors and field observation checklists required to understand the efficacy of remedial works in order to achieve the desired performance standards and develop an appropriate plan to monitor it regularly or periodically.
- Create a mechanism for regular inspection and maintenance of equipment and acquisition of new equipment for DRR & R.
- The failure of law enforcing agencies and local authorities to enforce building codes and standards/norms to reduce landslide risks, seems to be very apparent in these studies. Illegally raised additional floors and the owners' practices of using the basements for residential purposes (which are meant to be non-habitable) are some of the observations supporting the above argument. Some hotel owners even dug up basements while others have put the closed basement to inappropriate use. It also includes the constructions on drains to pave the way for multi-storey structures, which cause seepage and make the foundations weak. Illegal domestic water and electric connections in such buildings indicate lackadaisical attitude of the local officials in dealing with such violations.
- Forest serves not only as property markers but also as ecological barriers. Forest should be kept thick in places where it is "too steep to plant:"
- Continuous rainfall and decades of weathering of the slope mass deteriorates the slope stability through a gradual process that may take several years to culminate in a landslides
- Hefty use of pesticides, chemicals and herbicides, may also degrade the soil mass quality and stability
- Relocate settlements and infrastructure that fall in landslide prone zones. Microlevel mapping of geotechnical parameters should be done for extensive landuse planning. Construction in dormant or passive landslide areas should be discouraged for human settlements
- Construction of buildings in areas with critical slope stability conditions should be prohibited or permitted with adequate prevention and mitigation measures. Constructions in very high and high landslide hazard zones should be preferably avoided. Shift settlements away from hazardous slopes and rebuild at safe sites in less hazardous zone.
- Launch a landslide campaign in the villages/habitats located in fragile landslide prone environment. Conduct regular contact programmes for public awareness on landslides and related hazards, particularly during the pre-monsoon season. Implement safe and scientific methods of slope modification and stabilization.
- Identify stable ground for safe construction and urbanization with proper drainage measures and protection structures.

- Rock/Debris Deflectors to protect important infrastructures like bridges
- During rainy season, the traffic movements should be managed under strict onsite and offsite slope monitoring. Sign boards/banners at appropriately identified vulnerable locations for cautioning the commuters.
- Altering the geometry of unstable slopes by flattening and benching along with drainage to prevent ingress of water into the slopes
- Widespread advance communication/warning to dwellers/visitors regarding potential landslides should be done during expected landslide periods.
- Mainstream disaster risk reduction (DRR) into new development programmes and regularly monitor DRR actions to minimize future risks
- The stability of dams near the crash zones, should be properly monitored. Any evidence of piping erosion from the debris dams also need to be closely monitored. Monitoring of rivers for floods in the area should also be considered in view of secondary landslides.
- The roots play an important role in the stability of slopes through penetration and holding of soil particles together
- Though the local authority was prompt in response to landslides yet they are not well aware about mitigation funds and schemes that can be used to mitigate landslide risks.
- All terraced slopes should have weeping holes along the terrace walls that would partly prevent the occurrence and persistence of high perched water levels
- Overhanging regolith material should be terraced, covered with coir geotextiles and planted with deep rooting native grass and shrubs like Vetiver grass (Chrysopogon Zizanioides), lemon grass (Cymbopogon Citrates) that may be used to offer significant root reinforcement to ensure stability
- Establish demonstrative best practices of landslides management. Environment friendly human settlements with least potential landslide hazards, must be encouraged. Rethink policies from an environmental perspectives to preserve nature and protect lives and livelihoods. Afforestation should be taken up to restore the ecological balance.
- Better regulations and enforcement for landuse, construction and development, including policy, advocacy, implementation, monitoring and management. Stringent laws must be enacted for construction, development, maintenance and management of infrastructure in the landslide affected areas.
- Training and Capacity Enhancement in the field of landslides risk reduction and resilience at local levels is very much required. There is a dire need for coordination, networking and linkage among different stakeholders (National Landslide Risk Management Strategy 2019) working on landslides management including public works department, irrigation and flood control, department of geology and mines, Geological Survey of India, Disaster Management Authorities at district, state and national levels etc.

Acknowledgements The author would like to express sincere thanks to the Executive Director, National Institute of Disaster Management (NIDM), Ministry of Home Affairs, Government of India, Delhi, India. Thanks are also due to the colleagues and support staff in the Geo-meteorological Risks Management Division of NIDM, for kind support and cooperation in this work.

References

National disaster management guidelines on management of landslides and avalanches, released by National Disaster Management Authority, Government of India during June 2009. https://ndma.gov.in/sites/default/files/PDF/Guidelines/landslidessnowavalanches.pdf

National landslide risk management strategy, released by National Disaster Management Authority, Government of India on 27 Sept 2019. https://ndma.gov.in/sites/default/files/PDF/Guidelines/NLRMS.pdf

Surya P, Dipali J, Kumar BM, Anil K, Roy TKS (2022) Archival records of socio-economically significant landslides in India. Published by National Institute of Disaster Management, Delhi, India, p 270p

Application of Ichi-Nichi-Mae (The Day Before the Disaster) Project for Landslide Awareness and Risk Communication

Satoru Nishikawa

Abstract

Landslide disasters are common in most habitable areas and claim numerous lives, and cause havoc to livelihoods. However, most landslide survivors state that they never thought of being hit by landslides in their area. This indicates the need to effectively raise public awareness about landslides. Ichi-Nichi-Mae (The Day before the Disaster) Project started in 2005 and has been used to raise awareness against various types of disasters. Since landslides are common in many communities, the episodes by the survivors of landslides are found to be effective means for risk communication. This project has developed to be linked with community disaster management plans which started in 2014 in Japan.

Keywords

Public awareness • Risk communication • Storytelling • Educational material • Community disaster management

1 The Birth of 'Ichi-Nichi-Mae Project'

Raising public awareness of disasters is one of the main pillars of disaster reduction policy in Japan. Various educational materials, primarily targeting children, have been developed in Japan. Not many were targeted for adults. Those existing materials were mainly "Do's and Don'ts Preaching Style" and were not fully appreciated by adults, were not accepted as their own affair, and therefore were said to be not effective in making the adults to take action. Therefore, for the sake of inducing spontaneous preventive action by adults, the author, and his colleagues developed a new program (Sashida et al. 2012), the 'Ichi-Nichi-Mae (the Day before the Disaster) Project.' The 'Ichi-Nichi-Mae Project' interviews people who have been seriously affected by a major disaster, by posing the question 'What would you do if you were back the day before the disaster?', and edits the most impressive personal short stories which give clues for future preventive action. The interviews cover a wide variety of adults who experienced disasters, from housewives to small business owners and large enterprise employees. A wide variety of disasters are covered. These stories are compiled and have been used for disaster awareness seminars and have proven effective, since the real stories make participants feel that it may happen to them. The methodology of this project is published on the Cabinet Office Disaster Management website (2022) and is voluntarily applied by various communities.

As of April 2022, 872 episodes are collected and made available through the Cabinet Office Ichi-Nichi-Mae website.

2 Procedures for Collecting 'Ichi-Nichi-Mae Project' Stories

The following section describes the standard procedures for the 'Ichi-Nichi-Mae Project'. The main aim of this project is to make as many people as possible have empathy for the people affected by disasters, make them feel that they may experience a similar disaster, and urge them to take spontaneous preventive action. Therefore, extracting various personal stories arising from different standpoints in facing the disaster is important. Accordingly, we have designed a methodology to meet this purpose and have tried many tips to edit the impressive stories.

S. Nishikawa (✉)
Disaster Mitigation Research Center, Nagoya University, Nagoya, 464-8601, Japan
e-mail: nishikawas@nagoya-u.jp

I. Alcántara-Ayala et al. (eds.), *Progress in Landslide Research and Technology, Volume 1 Issue 2, 2022*, Progress in Landslide Research and Technology,
https://doi.org/10.1007/978-3-031-18471-0_24

Editing Personal Stories

Seven steps are required to extract personal stories. 1. Identifying suitable interviewers. 2. Identifying storytellers among the affected people. 3. Group Interview. 4. Extract impressive personal stories. 5. Edit the personal stories. 6. Add a headline to each story. 7. Selection by disaster reduction expert.

Identifying Interviewers

Anyone who is serious about promoting the 'Ichi-Nichi-Mae Project' is qualified to be an interviewer. The number of interviewers for a disaster case should be more than one. This is to have plural standpoints in the later editing process and to avoid delusion in understanding the story. Volunteers from the mass media, governmental services, civil societies, and the general public were briefed on the 'Ichi-Nichi-Mae Project' methodology and have served as successful interviewers.

Identifying Storytellers

Identify a few to several (5 to 6) storytellers per one disaster. Find a contact person in the disaster-affected area and ask him/her to bring his/her neighbors or friends who have experienced the same disaster. Asking the local school PTA or community center to assist in gathering several may be a good way. The storytellers can be varied; company employees, small business owners, local construction engineers, and community center participants may be asked to join. If the storytellers are acquaintances with each other, it will help to activate lively discussions. However, this is not mandatory since it is often the case that the survivors of the same disaster are eager to discuss their stories even at their first meeting. One important tip to make the storytelling meaningful is to include some who were responders, firefighters, or relief volunteers, so that they may add a responder's point of view.

There are so many survivors who wish to share their experiences and lessons from the disaster they faced. Many of them sincerely wish that their fellows do not suffer as they did. However, there are few opportunities for them, who are usually regarded as laymen, to tell their stories. On the other hand, many citizens seldom have a chance to listen to live experiences of a disaster, which can be eye-openers for them. The 'Ichi-Nichi-Mae Project' makes an ideal opportunity to link the two.

Group Interview

Ask 2 to 6 storytellers in the locality who experienced the same or similar disaster to come and tell their disaster experience for about 2 h. The interviewers will ask them to tell their experiences in chronological order and ask them how they felt. Interviews should be conducted in a relaxed manner, in places like community centers, cafes or local schools. The interviewers are recommended to bring news photographs and articles of the disaster as a hint to bring back the live memories of the storytellers. Serve tea and cookies to make people relax, and don't forget a voice recorder. The storytellers would not be previously notified of the questions that they are going to be asked to avoid burdening them and to let them speak freely out of their memories at the interview. This is to avoid their stories to be didactic. The interviewer should provide a relaxing atmosphere and should never wear uniforms.

The interviewers will ask, how was their everyday life, how the disaster changed their life, how do they feel after the disaster, and 'What would you do if you were back the day before the disaster?' By taking advantage of group interviews, let the remarks of one storyteller provoke another's recollection and bring a lively discussion on their experience. Be careful not to interrupt when a storyteller is speaking.

Extract Impressive Personal Stories

When the storytelling session is over, the interviewers shall bring together their memos taken during the session, and pick up keywords and the essence of stories that will attract people's ears. Interviewers should try to understand the wishes of the storytellers so that others do not make the same mistakes and pick up failure stories that will generate sympathy and also messages that the storytellers wish to convey. Interviewers should carefully remember the tone of the storytellers in identifying these essences of stories. The interviewers may pick up the points which they themselves felt sympathy for. However, it should be noted that stories, which do not fit with disaster risk reduction should be avoided. The interviewers may think of the headlines to be added to each story at this stage. This will ease the workload at a later stage.

Edit the Personal Stories

By supplementing the notes taken by the voice recorders, the keywords and essence identified above shall be edited as short stories. The short stories should be edited to 200–600 words long, leaving the flavor of the speaker's tone and dialects. The storytellers are not professional speakers. Therefore, their talks might be fragmented and may not be in chronological order. By editing their talks into short stories, their message becomes alive.

Add a Headline and Small Illustration to Each Short Story

Add a suitable headline to each short story. This headline serves the purpose of attracting the readers to be interested in the short story; therefore, it should not be too descriptive but rather should aim at drawing curiosity. The heart of the 'Ichi-Nichi-Mae Project' is how to attract people to read others' experiences. Therefore, attention should be paid to making the headline of each short story attractive while using plain words so that even children can also easily pick up what the story wants to convey. Add a small illustration or a photo that represents the essence of the story as an eye-catcher.

Selection by Disaster Reduction Expert

The significance of the 'Ichi-Nichi-Mae Project' comes from the fact that it opened the door to all citizens to contribute to disaster risk reduction. Anyone who has experienced a disaster can become a resource person. Anyone who is willing to listen to disaster experiences can be the interviewer. However, this requires some careful editing and selection process to maintain the quality of the collected material, which are posted and made public through the Japanese Government Cabinet Office Disaster Management Website.

Important Points for Quality Control

The following are important points to be noted for quality control in the interview, editing, and selection process.

Do not interview with prejudgments. Do not guide the storytelling by the interest of the interviewer. Do not add stories in the editing process, even if it may make the story attractive. Do not add moralistic or didactic stories. Make clear that erroneous action taken by the storyteller can be clearly recognized as such. Even if the erroneous action led to good results by luck, make sure that it is clearly understood that such cases are very rare. When the edited stories are finalized, they are sent to the storytellers for their approval and then posted on the Cabinet Office Disaster Management Website. Through these cautious procedures, the numerous experiences and lessons learnt by various citizens are widely shared.

3 Workshops Using the 'Ichi-Nichi-Mae Project' Stories

The 'Ichi-Nichi-Mae Project' stories can be used as materials for disaster reduction seminars and also as food for thought to induce discussions at workshops. Table 1 shows a model for conducting a workshop.

4 Tips to Enlarge Participation

The 'Ichi-Nichi-Mae Project' can be applied to a wide variety of disaster risk reduction activities. The aforementioned workshop is just one example. Stories can be used as short articles in community papers and township circulars. They can be used as texts for schools and adult education centers. The 'Ichi-Nichi-Mae Project' has flexibility, and users may innovate good ways for an application to their disaster reduction activities.

The 'Ichi-Nichi-Mae Project' started in 2005. In the initial years, the interviewing and editing were borne only by the author group. Starting from 2009, in order to enlarge this project, advocates in local governments and mass media were welcomed to join the interviewing and editing. Hence, we have transformed the 'Ichi-Nichi-Mae Project' into a universal methodology where any advocate can join.

Since Ichi-Nichi-Mae Project does not require any special equipment nor sophisticated engineering technique, the author is introducing this methodology in numerous JICA training courses in disaster risk reduction and encouraging

Table 1 Model of workshop using 'Ichi-Nichi-Mae Project'

Step 1 Read	Divide the participants into small groups of 4–7. Let the participants do self-introduction, chat and small games for ice-breaking. Read carefully the disaster experience story. It would be effective to watch a video footage of the disaster, prior to reading
Step 2 Write	Underline the points in the story where it was a surprise, a sorrow and a joy. Write memos on adhesive paper tags and put them on where the participant found important
Step 3 Discuss	Group members tack tags on a large piece of paper in turn. If there are same content tags, place them together. Classify the tags by, things to be done by individuals, things to be done in the community, things to be done as the society, and discuss among the group what should be done to reduce disaster risks
Step 4 Present	Discuss among the group and select several action points which the group thinks important for disaster reduction, and present
Step 5 Act	Execute the action points identified by your group and the attractive action points which were identified by other groups. Action points which can be easily executed by oneself, for example affixture of furniture for earthquake safety, should be done on return to home

Fig. 1 Example of negative experience of landslide disaster

Landslides, It is too dangerous to flee after the event

It was like messenger from hell; woods, rocks & debris smashed into my house

(Torrential Rains in July 2009) (Story by a man in the 50s, Hofu City, Yamaguchi)

A horrific noise like the theme music of messenger from hell blasted from the ground. The noise was approaching and when I looked out of my window, brown avalanche was pressing towards me. Fallen woods, numerous rocks and voluminous debris rushed to me.

Oh! My house will be crushed! The moment I fell back, something smashed my house, breaking noise, I was immersed up to my waist. The shattered window glass attacked me, my leg was cut, mud water turned red with my blood.

How can I escape out? "Oh I need shoes !", came to my mind. I snatched one of my shoes adrifting on mud water, hardly put them on, waded through fallen sofa and chairs, found another shoe, put it on and tried to escape out of the patio door, but the door sill was crooked and couldn't open.

I barely escaped out of the main door, where the debris broke in. Just outside of my doorsteps, torrents of mud water dug the ground for 4 to 5 meters like a river, roared noisily.

My house was new, but to my grief, I could never come back and live in my house again.

Fig. 2 Example of positive reaction experience against landslide

～Previously Decided Evacuation Way Out saved their Life～

～Ran for Safety without Hesitation～ July 2009 Torrential rains in Chugoku & N Kyushu（Story by local gov't official in 40s）

This is an impressive story I heard from a couple in my area.

The husband and wife was about to have lunch together in their house. They set their main & side dishes on the table and was about to eat lunch. Big sound from the hill, Rumble ! Rumble ! Rumble ! What is it ? They looked out. The hillside was collapsing, and the debris flow was running straight at them.

Oh! Danger! The husband was in his underwear, immediately grabbed his shirt. Hand in hand with his wife, fled into the bushes of the small hill in the back of their house.

I asked him. Why did you run to that direction? "When we built our house, we discussed where to run for safety in case of a disaster. We agreed that one option was the bushes of the small hill in the back." was his answer. "Our car was parked in the front street. But that was the direction of the debris flow. If we ran to that street, we would have perished."

If we are aware of the characteristics of our residence, the risks of that location, what were the past disasters, we can be prepared and think of specific safe way out. The important point is to think specifically and the conscious attitude to save oneself.

other countries to try this for public awareness and inheritance of disaster lessons in respective countries.

5 Application to Landslide Awareness at Communities

Starting in 2014, the "community disaster management plan" was newly introduced as a voluntary plan in Japan to encourage citizens' positive participation in disaster reduction activities. It is based on the revision of the Disaster Countermeasures Basic Act in 2013. The "community" referred to in this plan is flexible. It may be a condominium with residents of 100 households, it may be a suburban neighborhood with 30 families. If the members of that "community" agree on their voluntary disaster reduction action plan for themselves, they can ask the municipality they belong, to reflect their plan in the municipal disaster management plan. Then the community's voluntary action is authorized. The aim of this revision of the Act is to encourage as many "communities" to identify and recognize the risks they face, discuss possible action points and agree on their plan. Therefore, how to let the members of the community notice the potential hazard they face is the key. The 'Ichi-Nichi-Mae Project' episodes of their municipality or nearby were found to be good materials to make the community members imagine the possibility of disasters.

Landslides are common in most communities in Japan. The effect of the reading experience of negative (Fig. 1) and positive (Fig. 2) episodes of landslides was compared, and a significant difference was found (Kitagawa et al. 2021). Hence, the Cabinet Office is encouraging the use of Ichi-Nichi-Mae in various locations.

References

Cabinet Office Disaster Management Website 'Ichi-Nichi-Mae Project' [Online]. URL: https://www.bousai.go.jp/kyoiku/keigen/ichinitimae/index.html. Last Accessed 1 June 2022

Kitagawa N, Hirukawa R, Nishikawa S (2021) The consideration about changes of disaster prevention awareness, which occur in people have read "Ichi-Nichi-Mae Project" experiences. In: Proceedings of the institute of social safety science, no 48, pp 69–72

Sashida T, Ikegami M, Kagiya H, Suzuki N, Nakagawa K, Nishikawa S (2012) Report on the development and application of 'Ichi-Nichi-Mae Project' for disaster awareness; 'If we were back the day before the disaster, how can we better prepare?' J Soc Saf Sci 18:421–443

ICL Landsldie Teaching Tools

Teaching Tool "Undrained Dynamic Loading Ring Shear Testing with Video"

Doan Huy Loi, S. H. S. Jayakody, and Kyoji Sassa

Abstract

Undrained dynamic-loading ring-shear apparatus (UDRA) is most appropriate to study landslide dynamics by simulating the entire process from the initial stage of stress before landslide occurrence and stress changes due to static, dynamic loading or pore pressure changes or other types of stress loading to the formation of a sliding surface and the steady-state shear resistance. This paper describes the mechanical structure of the apparatus of UDRA and provides a manual for readers to begin using the UDRA. Specific steps for testing procedures with video tutorials and data analysis are also provided in this paper. The paper concludes with a manual from start to finish for common ring shear tests: undrained monotonic shear stress control test, undrained cyclic loading test, undrained seismic loading test, and pore pressure control test.

Keywords

Ring-shear apparatus • Video tutorials • Undrained monotonic shear stress control test • Undrained cyclic loading test • Undrained seismic loading test • And pore pressure control test

1 Introduction

The measurement of shear resistance mobilized from failure to the motion of landslides traveling onto the lower slope or an alluvial deposit plays an important role in studying landslide dynamics.

The ring shear test was introduced and improved by Bishop et al. (1971), Bromhead (1979), Savage and Sayed (1984), Sassa (1984), Hungr and Morgenstern (1984), Tika (1989), and Garga and Infante Sedano (2002). Sassa and his colleagues in the Disaster Prevention Research Institute (DPRI), Kyoto University, and International Consortium on Landslide (ICL) have developed nine designs of dynamic-loading ring shear apparatus since 1984 (DPRI-1, DPRI-2, DPRI-3, DPRI-4, DPRI-5, DPRI-6, DPRI-7, ICL-1, and ICL-2). Features of the previous ring shear apparatus, compared with the undrained dynamic loading ring shear apparatus in DPRI and ICL, are shown in Table 1. DPRI-3 is the trial version of an undrained dynamic-loading ring shear apparatus (UDRA). It could maintain some pore pressure within the shear box, and pore pressure was monitored to some extent. But it did not reach a practical undrained test level. DPRI-4, DPRI-5, DPRI-6, DPRI-7, ICL-1, and ICL-2 were improved for testing under the undrained condition.

With the support of SATREPS (Science and Technology Research Partnerships for Sustainable Development) projects funded by the Japan Science and Technology Agency (JST) and the Japan International Cooperation Agency (JICA), the UDRA was modified and upgraded to be used outside of Japan without the assistance of the manufacturers. The first was ICL-1 (a transportable UDRA), which was donated to the University of Rijeka in Croatia in 2012. The manual for this apparatus was published by Setiawan et al. (2018). ICL-2 is a high-stress UDRA, with a maximum loading capacity and undrained capacity of 3000 kPa, which was donated to the Institute of Transport Science and Technology (ITST) of the Ministry of Transport, Vietnam, in 2015). During the Vietnam-Japan project, the most sensitive

Supplementary Information
The online version contains supplementary material available at https://doi.org/10.1007/978-3-031-18471-0_25.

D. H. Loi (✉) · S. H. S. Jayakody
Department of Civil and Earth Resources Engineering, Kyoto University, Gokasho, Uji, Kyoto, 611-0011, Japan
e-mail: doanhuyloidkt@gmail.com

D. H. Loi · K. Sassa
International Consortium on Landslides, Kyoto, Japan

I. Alcántara-Ayala et al. (eds.), *Progress in Landslide Research and Technology, Volume 1 Issue 2, 2022*, Progress in Landslide Research and Technology,
https://doi.org/10.1007/978-3-031-18471-0_25

Table 1 Feature of previous ring shear apparatus and undrained dynamic loading ring shear apparatus in DPRI and ICL

Features and parameters	Bishop et al. (1971)	Hungr and Morgenstern (1984)	Tika (1989)	Garga and Infante Sedano (2002)	DPRI-3 (Sassa 1992)	DPRI-5 (Sassa 1997)	DPRI-6 (Sassa 1997)	DPRI-7 (Sassa et al. 2004)	ICL-1 (Sassa et al. 2012)	ICL-2 (Sassa et al. 2014)
Inner diameter (mm)	101.6	220	101.6	92	210	120	250	270	100	100
Outer diameter (mm)	152.4	300	152.4	133	310	180	350	350	140	142
Max. height of sample (mm)	19	20	19	20	90	115	150	115	52	52
Shear area (cm^2)	101.34	326.73	101.34	72.45	408.41	141.37	471.24	389.56	75.36	79.79
Max. normal stress (kPa)	980	200	980	660	500	2000	3000	500	1000	3000
Max. pore pressure (kPa)	N/A	N/A	N/A	N/A	N/A	400–600	400–600	400–600	1000	3000
Max. shear speed (cm/s)	N/A	100	9.33	N/A	30.0	10.0	224	300	5.4	50
Cyclic torque control testing	No	No	No	No	Yes	Yes	Yes	Yes	Yes	Yes
Possibility of undrained test	No	No	No	No		Yes	Yes	Yes	Yes	Yes
Possibility of pore water pressure control	No	No	No	No		Yes	Yes	Yes	Yes	Yes

undrained rubber edge and the loading system were designed for easy and low-cost maintenance. Based on the issues encountered by many Vietnamese trainees, several safety procedures have been devised to minimize possible damage to the device due to misuse. After completion of this project, ICL-2 was purchased by Shanghai University and the Chengdu University of Technology in China.

In 2022, the current version ICL-2, with a maximum loading capacity of 1000 kPa and the transparence box, was donated to the National Building Research Organization, Sri Lanka under the support of the SATREPS project titled "Development of early warning technology of Rain-induced Rapid and Long-traveling Landslides joint program from 2019–2025." This paper describes mainly the manual for the ICL-2 version in Kyoto with video tutorials.

2 Concept of Ring Shear Apparatus

The basic concept of the undrained dynamic-loading ring-shear apparatus (UDRA) is shown in Fig. 1. An examination of the shear behavior and pore pressure generation in the process of failure and the development of the sliding surface is conducted by taking a sample from the soil layer (left-top figure) where the sliding surface of the initial landslide originated within the slope. Another specimen (central figure) is obtained from the lower slope or stream deposits or alluvial deposits where a sliding surface will occur during the landslide's motion. These samples are fed into the ring shear box (left-bottom) with monotonic shear stress, seismic shear stress, or pore pressure control. The rotation will begin after the failure. The generated pore pressure, mobilized shear resistance, and shear displacement are all measured. The fundamental concept of UDRA is the replication of landslide processes within the testing equipment and the monitoring of shear behavior, i.e., a physical simulation of landslides with a focus on the sliding surface.

The ring shear apparatus accurately represents the slope's stress conditions as in Fig. 2. Taking into account a soil column per unit width along the slope, the vertical stress acting on the slope is calculated by multiplying the soil mass (m) and the force of gravity (g). The normal stress is $\sigma_0 = m \cdot g \cdot \cos\theta$, and the shear stress is $\tau_0 = m \cdot g \cdot \sin\theta$, where, $m = \gamma \cdot Z \cdot \cos\theta$ (γ: density of the soil layer, Z is vertical depth, θ is the slope angle). I (0, 0) is the original stress point in the slope before rain or earthquake (Fig. 2).

Due to rainfall infiltration, the groundwater table/pore-water pressure rises in the rainy season. Figure 2 depicts the scenario when initial stress plus pore water pressure exceeds the failure line (red line). As the beginning point (I) approaches the failure line, shear failure will occur at the failure stress (shown as a red circle along the failure line).

The seismic force of $k \cdot mg$ is applied when the earthquake with acceleration (a) happens (Fig. 3). The seismic

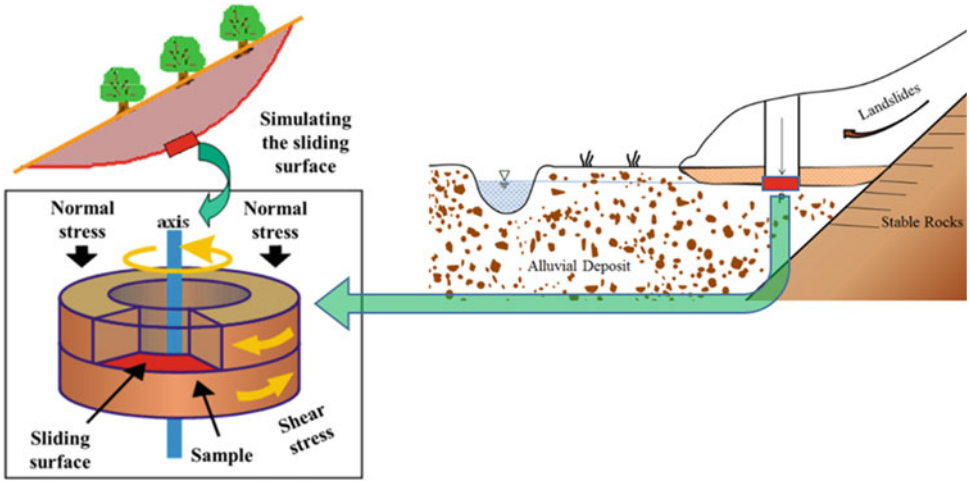

Fig. 1 Schematic figure of the concept of an undrained dynamic-loading ring-shear apparatus (UDRA) (Sassa and Dang 2018)

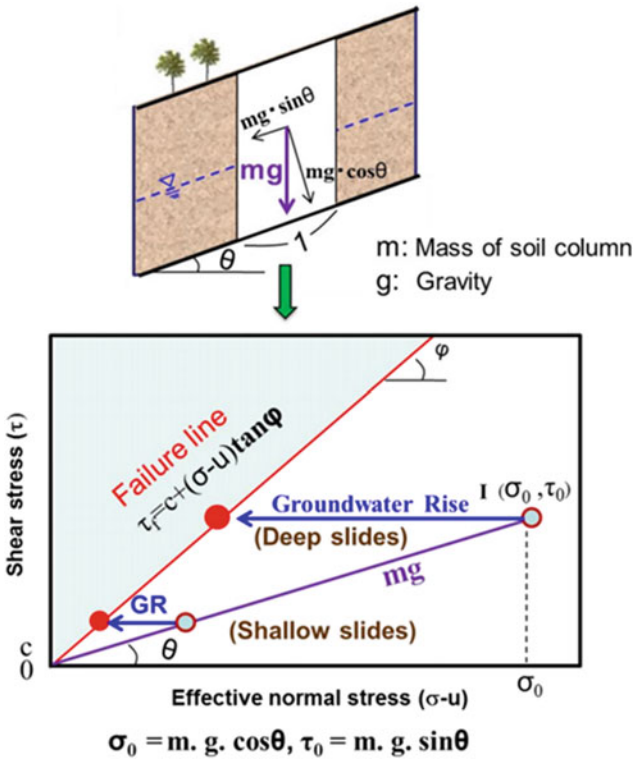

Fig. 2 Landslide-initiation mechanisms due to groundwater rise/pore-water pressure rise (Sassa and Dang 2018)

coefficient k is defined as the ratio of seismic acceleration (a) to gravity (g), or k = a/g. During seismic loading, the stress path is either represented as the total stress path (TSP) when no pore pressure is formed or the effective stress path (ESP) when pore pressure creation is taken into account. If shear stress is applied perpendicular to the slope inclination, TSP is vertical. Due to the formation of pore pressure, the effective stress path will move to the failure line. This route marks the beginning of a landslide in the field. A shear surface is created when samples fail in the ring shear apparatus owing to loading.

3 Structure and Control System of the UDRA (ICL-2)

3.1 Outline and Mechanical Structure

Figure 4 depicts the installation of the high-stress undrained dynamic-loading ring-shear apparatus (ICL-2) at the SATREPS office, Kyoto, Japan. The system consists of the seven units as follows:

(1) Computer network with two screens (the left screen is to set the testing and record conditions. Then the right screen monitors the stress path and the time series data of pore pressure, mobilized shear resistance, loaded normal stress, shear displacement, etc.). The current ICL-2 uses software version 6.06178.24990 to acquire data and control.
(2) Main control unit for control and monitoring is composed of a servo amplifier that provides feedback signal loading from the main ring shear apparatus's servo motor to the control box and vice versa.
(3) The main ring shear apparatus consists of the shear box, normal stress loading system and shear stress loading system, gap sensor, and vertical displacement.
(4) Power supply box for shear loads, gap control, pore water control.
(5) Power supply box for normal stress.
(6) Pore pressure supply system.
(7) De-aired water and De-aired sample system.

Figure 5 shows a close-up of the shear box, normal stress piston, and shear stress sensors. The pipe (I) is disconnected

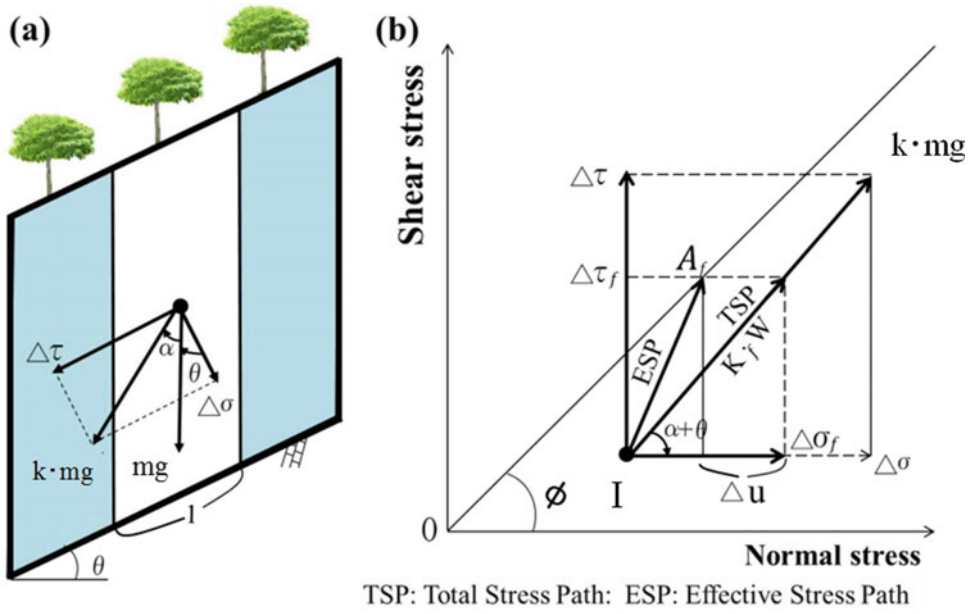

Fig. 3 Landslide-initiation mechanisms due to earthquake (Sassa and Dang 2018)

during the test because the lower shear box is rotating. Although it is not required to detach the drainage pipe (C) during testing, it is frequently removed in the undrained test.

A: Hanging frame to lifting the loading cap.
B: Normal stress loading piston.
C: One-touch plug for the water drainage from the shear box.
D: A pair of two shear stress sensors.
E: Shear box.
F: Pore pressure sensor.
G: Connection to the pore pressure control system.
I: One-touch plug for the De-aired water supply from the bottom of the shear box.

The mechanical structure of ICL-2 is shown in Fig. 6. The pieces of equipment in the diagram are coded in different colors as follows;

Part 1 (Gray) is the stable part.
Part 2 (Orange) is the lower shear box and will be rotated horizontally during testing.
Part 3 (Dark green) may move vertically and rotate horizontally and includes the upper shear box, loading cap, and central axis. Two load cells (S1 and S2) are used to measure shear stress. At the same time, a load cell detects normal stress (N) and retains this part vertically. To quantify forces, each load cell is gently expanded or compressed. The section below the rotary join (RJ) is not rotatable, but a servo-motor moves it vertically to adjust the gap. The gap control servo-motor moves the entire dark green section to alter the gap between the top and lower shear boxes.

Part 4 (light green) is the loading piston that supplies normal stress to the sample and the loading rods. When the oil pressure in the bottom chamber (blue) of the loading piston is raised, the central axis is dragged upward. As a result, the housing of the loading piston and the loading rods are pressed down on the sample, loading normal stress. Because tensile stress acts along the central axis throughout the process of oil pressure rise in the lower chamber of the piston, the load cell (N) measures the normal stress change.

3.2 Control System of the UDRA (ICL-2)

Figure 7 indicates the control system for the undrained dynamic-loading ring-shear apparatus (ICL-2). There are four servo-control systems for normal stress, shear stress/speed/shear displacement, pore pressure, and gap.

Normal-Stress Servo-control System

The static or seismic normal stress is generated by two oil pistons (LP-1 and LP-2) controlled by a servo-motor (SM; gray color) (Fig. 7). Normal tension is transmitted to the soil sample through three upright loading rods attached to the loading piston (LP-2). When the computer sends a control signal (red line) to the normal stress servo-amplifier, the servo-motor turns and results in the loading piston 1 (LP-1 and LP-2) moving. Therefore, normal stress to the sample will be increased or decreased correspondingly to the control signal. The normal stress is measured by the normal load cell

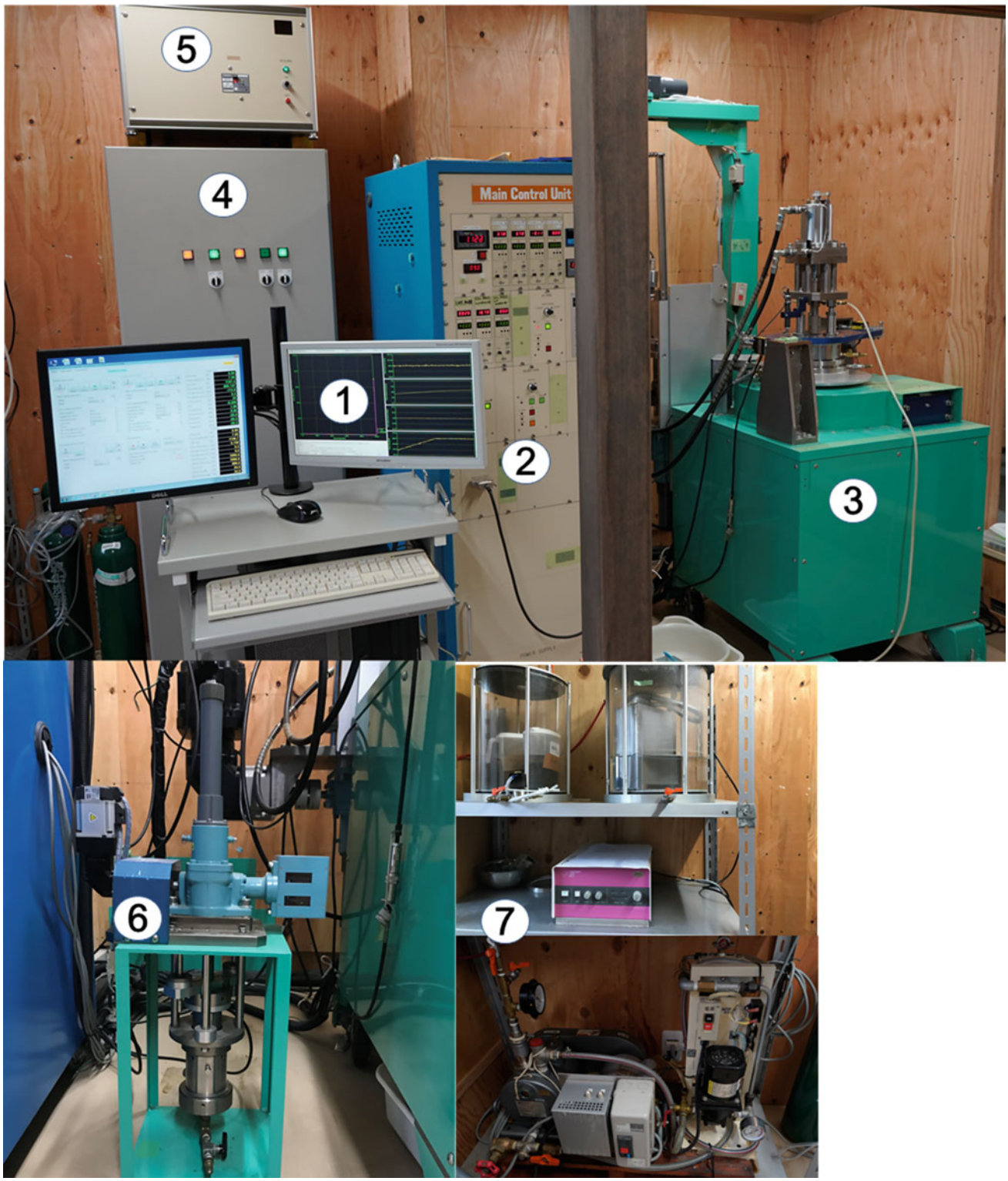

Fig. 4 Main units of the ICL-2 apparatus

(N: red color). The feedback signal (FS, black line) of the measured normal stress is supplied to the servo-amplifier (SA). By delivering a control signal to the servo-control motor (SM), the servo-amplifier (SA, red color) automatically regulates the value of loaded normal stress to the specified value.

Fig. 5 Photo of shear box and normal stress loading piston and shear stress sensor

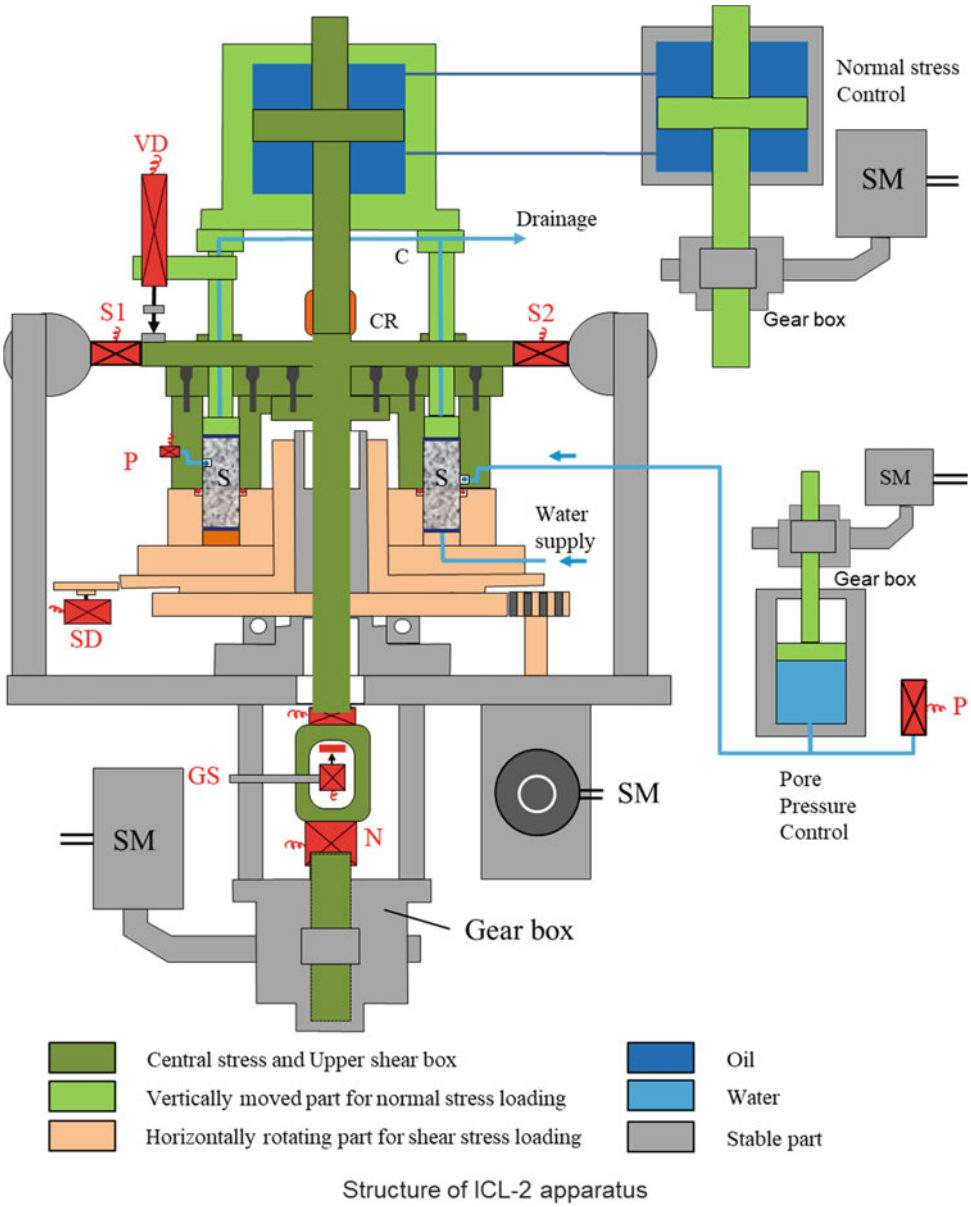

Fig. 6 Mechanical structure of ICL-2 (central section of the main body) (Sassa and Dang 2018)

Structure of ICL-2 apparatus

S- Sample; CR- Connection Ring; C- Connection; N- Load cell for Normal Stress; S1, S2- Load cell for shear resistance; GS- Gap sensor; FC- Feedback signal; CS- Control signal; PC- Computer; SG- Signal Generator; SM- Servo-motor; OP- Oil Piston; SA- Servo-amplifier

Figure 9 illustrates the dimensions of the shear box, with remarks below.

Inner ring radius, r_1 = 50 mm = 0.05 m.

Outer-ring radius, r_2 = 71 mm = 0.071 m.

Shear surface area, $A = \left(r_2^2 - r_1^2\right)\pi = (0.071^2 - 0.05^2)\pi = 0.007979\,\text{m}^2$.

The measured normal stress on the shear surface is equal to the measured vertical load divided by shear surface area:

$$\sigma_m = F_v/A = F_v/0.007979 = F_v \times 125.33$$

where,

σ_m is measured normal stress (kPa),

F_v is measured vertical load (kN),

A is shear surface area (m^2).

The ICL-2 uses the load cell of 30 kN, so the maximum normal stress that can be measured by the Ring shear apparatus ICL-2 as follows;

$$\sigma_{m,\max} = F_{v,\max} \times 125.33 = 30 \times 125.33 = 3759.90\,\text{kPa} = 3.76\,\text{MPa}.$$

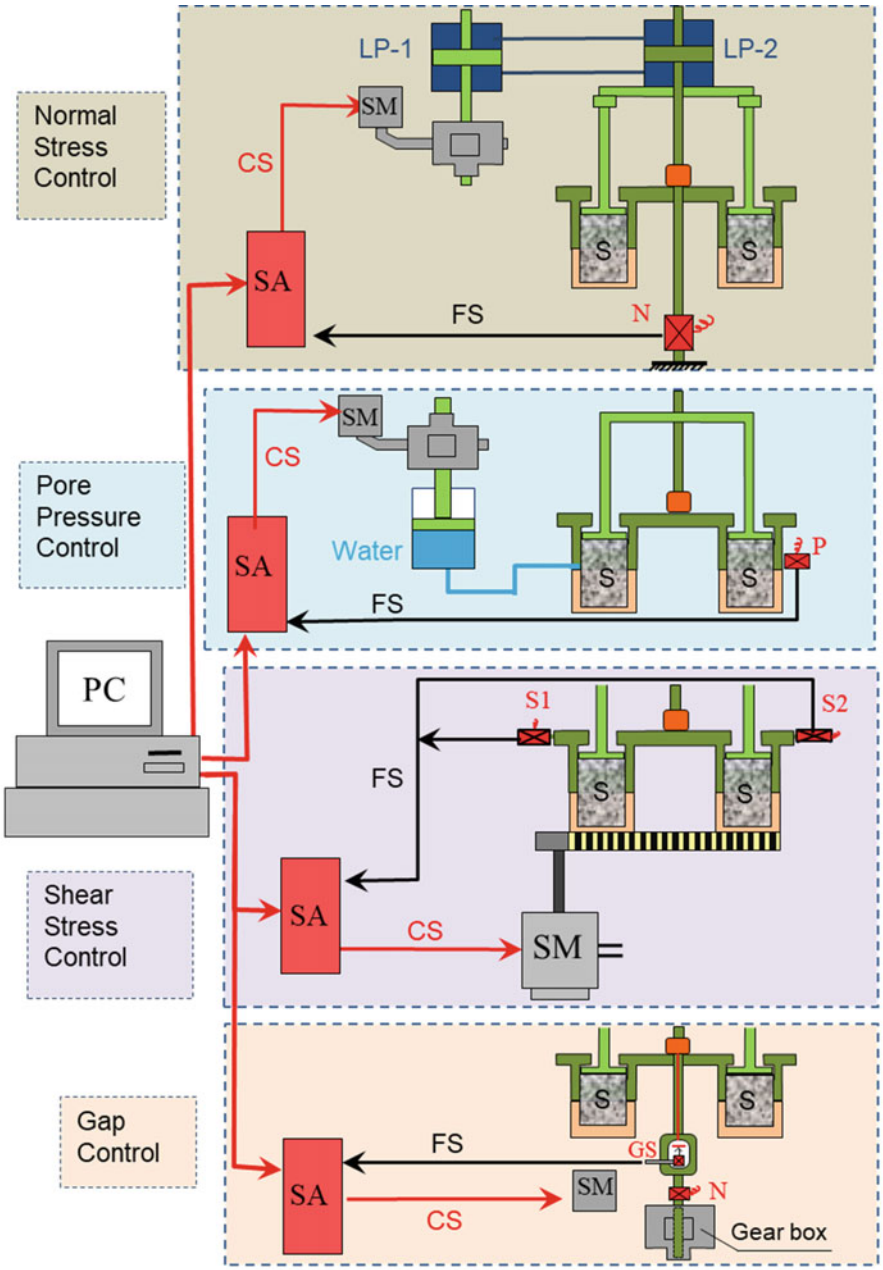

Fig. 7 Control system of the UDRA (ICL-2) (Sassa and Dang 2018)

The normal stress on the sliding surface is different from the sensor value and depends on a correction factor (α). A detailed investigation of the correction factor is presented in the "Effects of the rubber edge" section.

Shear (Stress/Speed/Displacement) Servo-control System

Similar to normal stress, the computer sends an electric control signal to the servo motor (SM) through the servo amplifier (SA), as shown in Fig. 7 (in the third column). The servo-control shear motor rotates the lower shear box (orange section) via a gear, while the upper shear box (dark green part) is held in place by the shear stress measuring sensors S1 and S2. S1 + S2 is utilized to monitor the shear stress produced on the sliding surface because the torque caused by the shear stress on the shear surface and the rubber edge shear resistance is balanced by the torque delivered by the two shear load cells. A servo-control motor may use

shear stress for a variety of purposes, including shear-stress control, speed control, and displacement control testing.

The shear stress (τ_t) is calculated from the shear load (Fs) by the equation below:

$$F_S \times R = \int_{r1}^{r2} 2\,\pi\,\tau_t\,r^2\,dr = 2\,\pi\,\tau_t\,\frac{1}{3}\left(r_2^3 - r_1^3\right) = \frac{2}{3}\pi\left(r_2^3 - r_1^3\right) \times \tau_t$$

$$\tau = \frac{3R \times F_s}{2\pi\left(r_2^3 - r_1^3\right)} = \frac{3 \times 0.3}{2\pi\left(0.071^3 - 0.05^3\right)} \times F_s = 615 \times F_s$$

where,

F_S is the shear load (kN),

τ_t is the shear stress total test value (kPa),

r_1 is the inner ring radius (m),

r_2 is the outer ring radius (m),

R is the distance between the shear load cells (S1, S2) and the axis of the shear box, R = 0.3 m.

The maximum shear stress that ICL-2 can measure is calculated from the total capacity of two shear load cells (S1 + S2) of 2 kN.

$$\tau_{\max} = 615 \times (2+2) = 2460\,(\text{kPa}) = 2.46\,(\text{MPa})$$

Pore-Water Pressure Control System

Pore pressure control tests are carried out to reproduce rain-induced landslides. The pore-water pressure servo-control system is present in the second column of Fig. 7. The pore pressure growth rate or program is first saved on the computer. Then the servo-amplifier receives the control signal (SA). It turns the servo-motor (SM), which subsequently supplies water pressure to the shear box. The pore-pressure sensor (P: red color) returns the feedback signal, which controls the pore pressure automatically. This system can only generate positive pore water pressure and use it for saturated samples.

Gap Servo-control System

The bottom column of Fig. 7 describes the gap control system (containing gearbox, servo-control motor, and gap sensor, GS). The gap between the lower and upper shear boxes must be maintained throughout testing to keep contact stress at the rubber edge larger than the pore water pressure acting on the shear box. The gap control servo-amplifier (SA: red) automatically maintains the gap value. The SA receives a feedback signal from the gap sensor and delivers a control signal to the servo-control motor (SM) for gap control (GS). After that, it maintains the gap at a constant value. The gap value precision of the ICL-2 instrument is 1/1000 mm. Even when the samples dilate during shearing or under cyclic or seismic stress, the gap between the upper and lower shear boxes is precisely controlled. When the sample dilates and the gap widens, the servo-motor responds quickly to maintain pressure and keep the gap constant.

Data Acquisition and Control Software for ICL-2

Figure 10 shows the screenshot of the software for the ring shear apparatus. It includes normal stress control, shear stress control, pore water pressure control, data acquisition, sensor value, and test value. Sensor Values are the actual values measured directly using the instrument box's sensors or load cells. The output file consists of both sensor and test values. When using the "Measure" button to set the initial value, the test value becomes 0, which is different from the sensor value.

Normal stress and shear stress control consist of static, cyclic, and wave functions. The wave function simulates an earthquake-induced landslide from recorded earthquake waves.

To set the parameters for ICL-2, click Setting (S) and select Apparatus (A). The apparatus box will appear, and the user can set the correction factor and the friction force of the rubber edge for each test. The other parameters must keep the default value, as shown in Fig. 11. Hereafter, Fig. 12 shows the protection setting. When the sensor value exceeds the sensor limitation, the software automatically stops the apparatus from protecting the sensors. We normally set 1001 cm in the limit shear displacement box. When the shear displacement reaches 1001 cm, the shear process is stopped.

4 Effects of the Rubber Edge

Preventing water leakage is the most difficult task of the undrained dynamic-loading ring-shear apparatus. In the ICL-2 version, the rubber edges are placed between the upper and the lower shear boxes. The Teflon ring holder was not used in the rubber edge system of the new ICL-2 apparatus, which was slightly modified compared with the ICL-2 in Sassa et al. (2014). A close-up of the rubber edge is shown in Fig. 8. A black color rubber edge is held by the stainless steel ring holder. It is simple to replace with a new rubber edge. A metal holder is to support the rubber edge in a vertical position against lateral pressure. The Teflon O-ring is to prevent damage caused by direct contact between the two shear boxes when the rubber edge thickness has been decreased after long shearing.

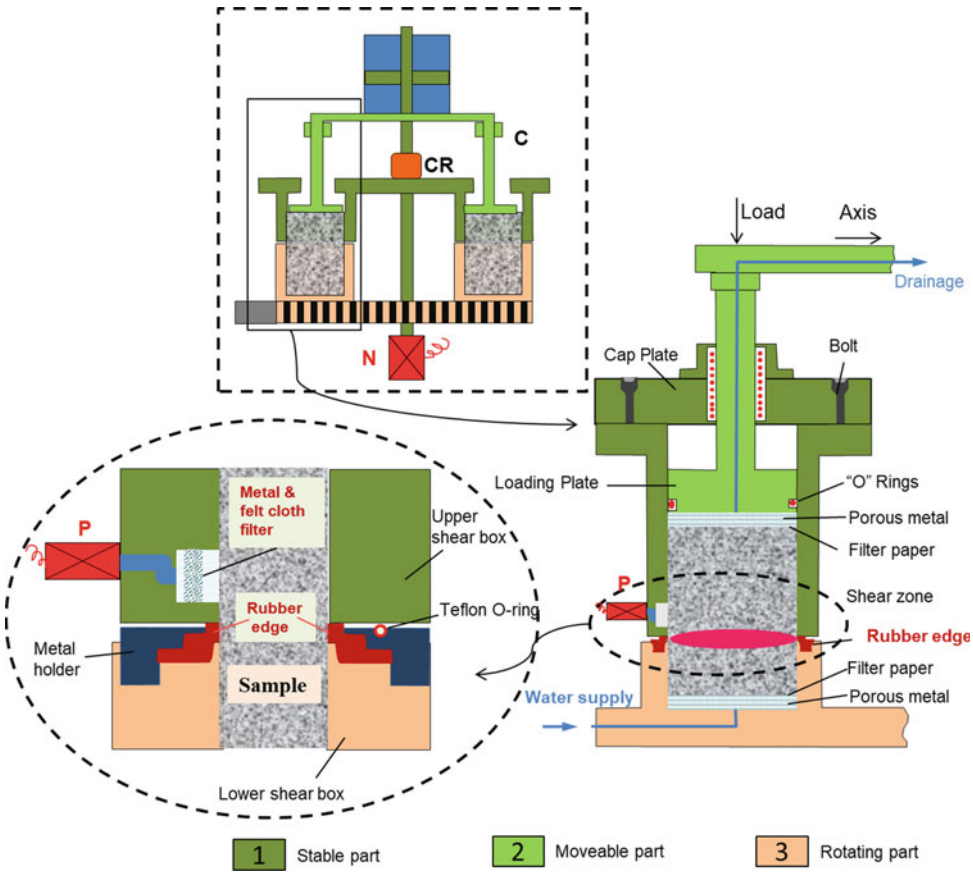

Fig. 8 Shear box and rubber edge. Modified from Sassa et al. (2014)

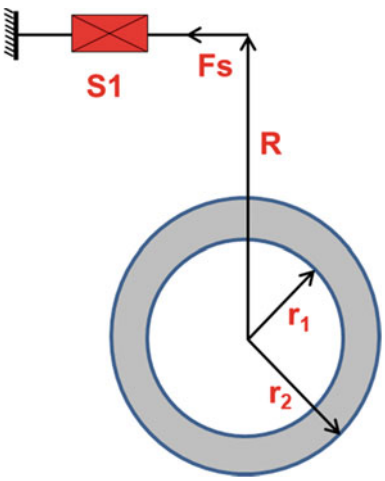

Fig. 9 Dimensions of the shear box

Figure 13 indicates a more detailed schematic drawing of the rubber edge and the parts around it. A horizontal tension (blue arrow) from the saturated sample pushes the black rubber edge to the left. The supporting force (yellow arrow) to the right comes from the Teflon ring holder being pushed down by the steel ring holder. So, the rubber edge is pushed horizontally from both sides. Since the space between the two shear boxes stays the same, it tends to push the upper shear box up. So, the vertical force (F-rubber) comes from the rubber edge to the upper shear box, which is vertical.

An initial contact force is applied to create a contact pressure between the upper ring shear box and the rubber edges on the lower shear box. A gap control system ensured that the contact force remained constant throughout the testing. The contact force can vary between 0 and 1.5 kN. The O-rings on the upper loading plate and the rubber edge system can prevent water leakage during the shearing process of the undrained condition test.

Figure 14a shows that three vertical forces are acting on the shear zone (Fsample), the rubber edge (F-rubber), and the central axis (F-axis). A vertical load cell is used to measure the F-axis (N). The vertical load cell (N) measures the sum of the normal stress on the surface and the rubber edge contact force. The following equation is found when the upper shear box's self-weight and the loading piston's dead weight are subtracted from the stress measured by the vertical load cell (N).

$$\text{F-sample} = \text{F-axis} - \text{F-rubber}$$

F-rubber depends on the horizontal stress acting at the rubber edge, which should be proportional to the vertical

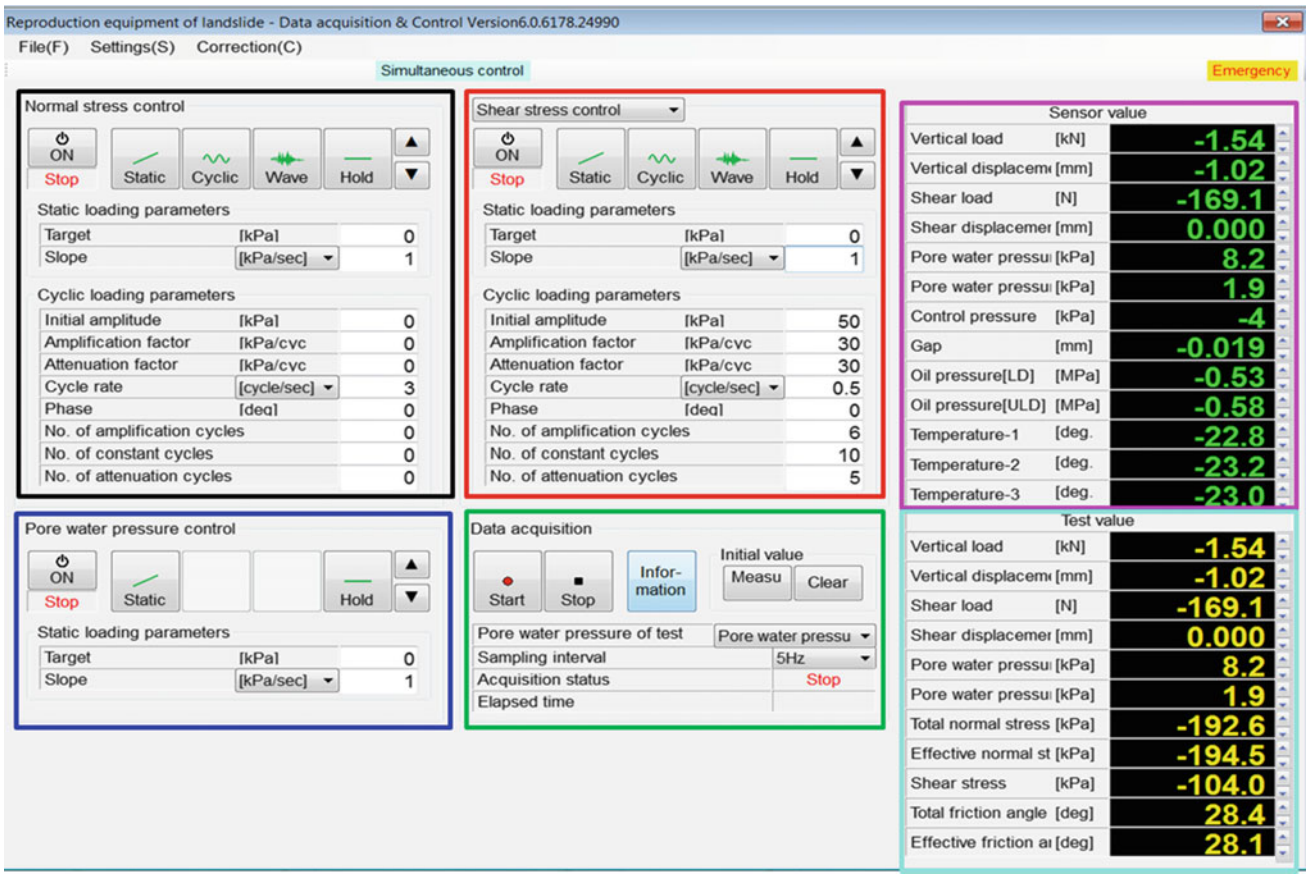

Fig. 10 Screenshot of the software for ring shear apparatus displaying normal stress control (in black frame), shear stress control (red frame), pore water pressure control (blue frame), data acquisition (green frame), sensor value (purple frame) and test value (aqua frame)

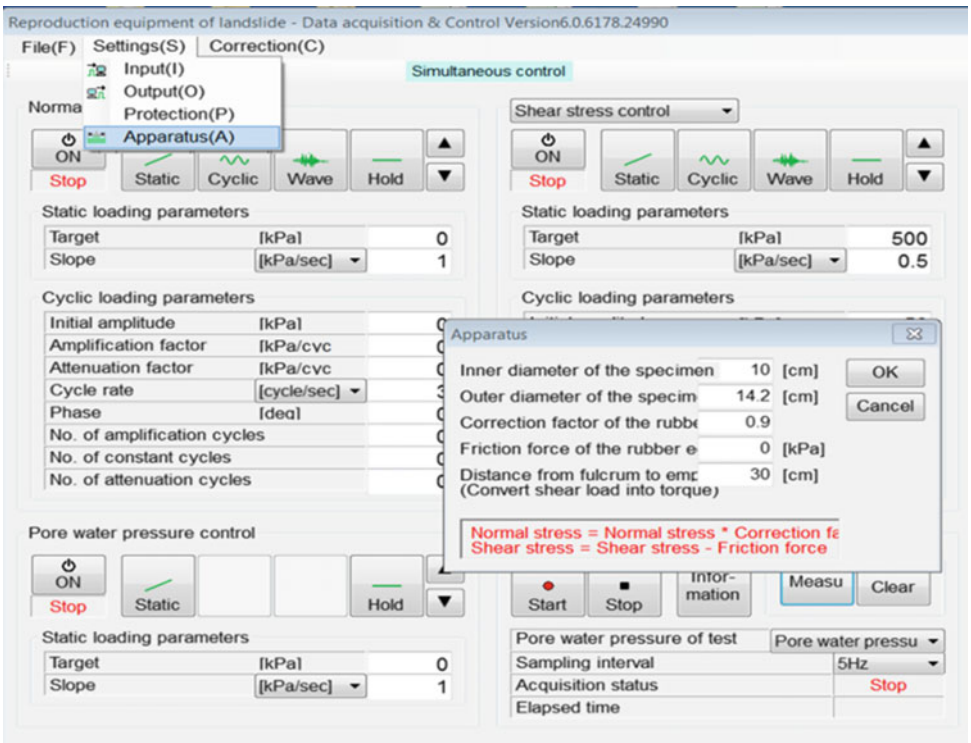

Fig. 11 Setting the correction factor of the rubber edge

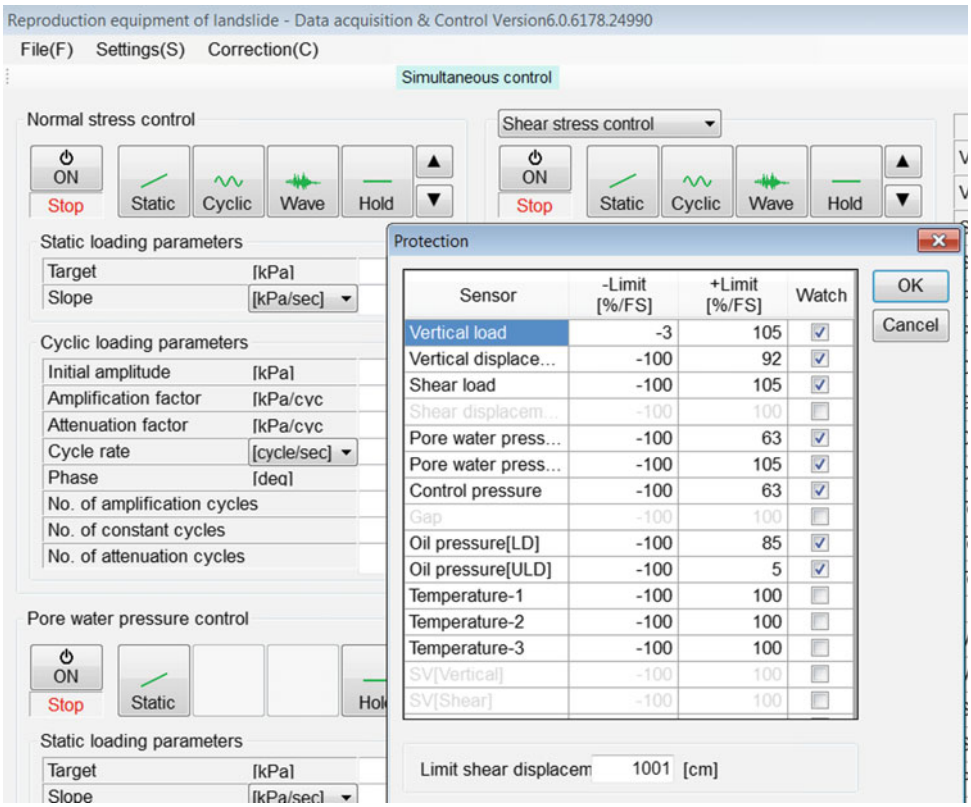

Fig. 12 Setting the protection for sensors

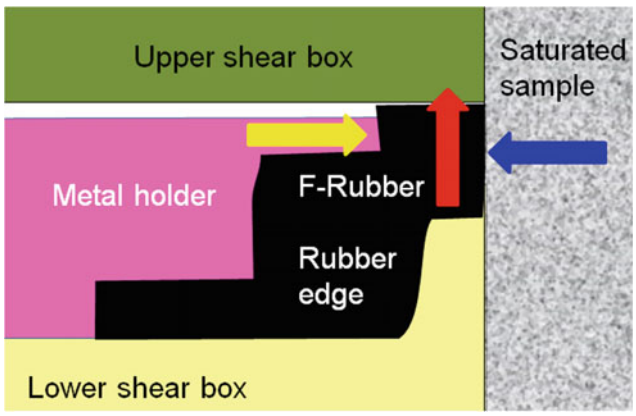

Fig. 13 Close-up diagram of the rubber edge

stress. F-rubber can be calculated from F-axis by the following equation: F-rubber = β × F-axis

$$\text{F-sample} = (1 - \beta) \times \text{F-axis} = a \times \text{F-axis}$$

Dividing by the shear area of the ring shear box, the following relation will be obtained.

$$\sigma = \alpha \times \sigma_m$$

where

σ_m: Measured normal stress calculated by F-axis/shear area, kPa,

σ: Normal stress working on the shear surface, kPa,

α: Normal stress correction factor.

5 Examine the Normal Stress Correction Factor A

The steps to calculate the normal stress correction factor α are as follows.

- Consolidate the saturated sample at specified normal stress, such as 100, 200, 300, 400, 500, 600, 700, 800, 900, and 1000 kPa.
- Using the pore pressure control system, raise the pore water pressure until the loading plate lifts and the hold button appears, as shown in Fig. 15. A water layer forms between the plate and the sample (Fig. 14b).
- Plot the time series data of pore water pressure and vertical displacement to get the maximum pore water pressure. Figure 16 shows the result with the normal stress of 1000 kPa. The maximum pore water pressure is 850 kPa.
- Figure 17 and Table 2 present the relationship between correction factor α and measured normal stress. The value of α changes from 0.85 to 0.96.

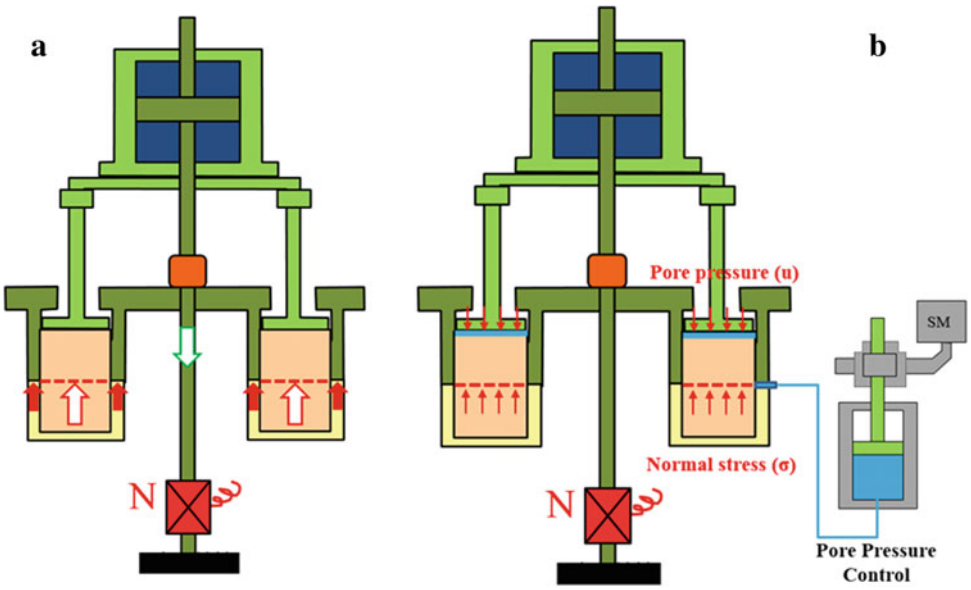

Fig. 14 Investigation of the normal stress that acts on the shear surface (Sassa and Dang 2018)

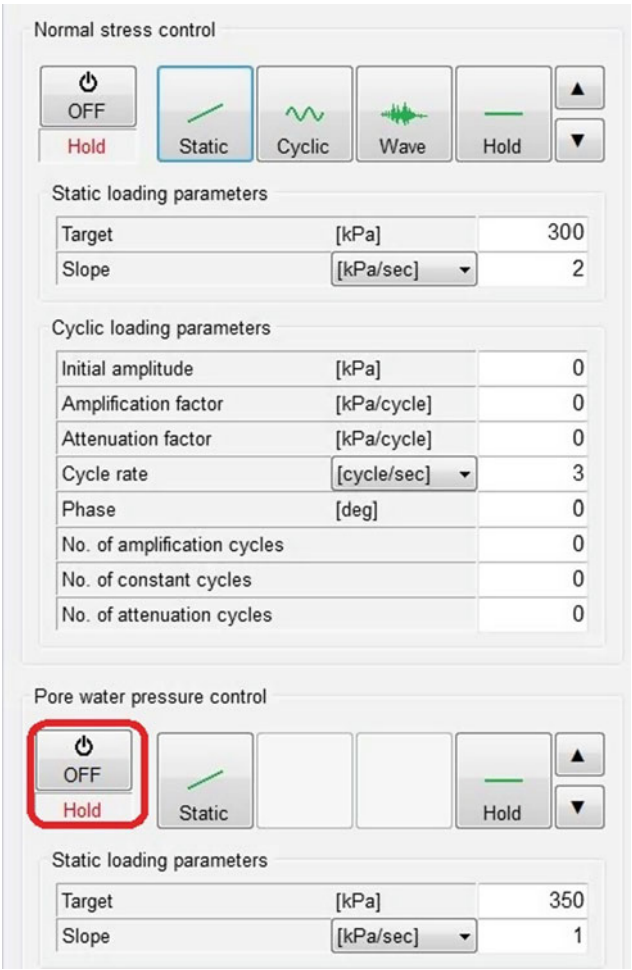

Fig. 15 Screenshot of ring shear program

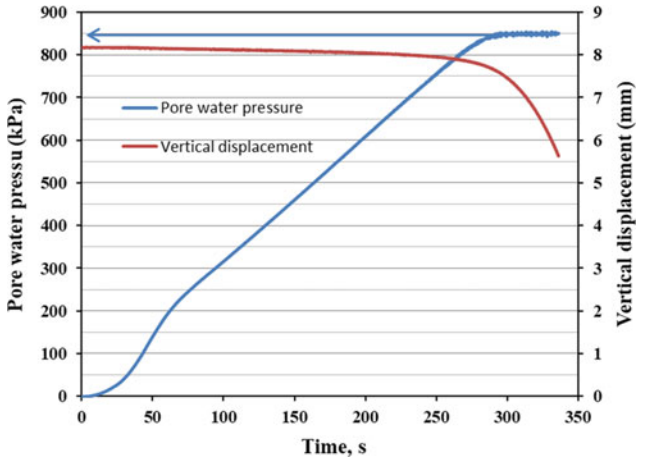

Fig. 16 Time series data of pore water pressure and vertical displacement with the normal stress of 1000 kPa

(A) Balance of vertical forces.

F-sample (normal stress on the shear surface : white arrow)
+ F-rubber (the rubber edge contact force : red arrow)
+ F-Axis (tensile force on the central axis : green arrow) = 0

(B) Measurement of the total normal stress acting on the shear surface of saturated soil samples after consolidation under a given normal stress.

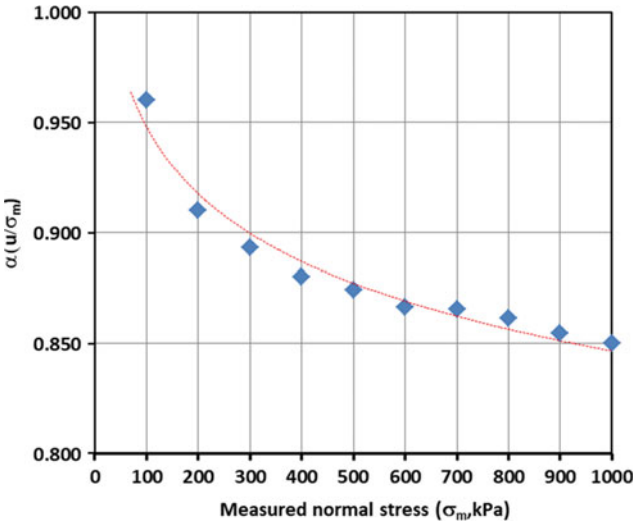

Fig. 17 Normal-stress correction factor (α) at different normal stress

Table 2 Values of measured normal stress (σ), pore pressure (u), and normal-stress correction factor (α)

Measured normal stress (kPa)	Pore water pressure (kPa)	α (u/σ_m)
100	96	0.960
200	182	0.910
300	268	0.893
400	352	0.880
500	437	0.874
600	520	0.867
700	606	0.866
800	689	0.861
900	769	0.854
1000	850	0.850

5.1 Examine the Rubber Edge Friction

Figure 18 shows the rubber edge friction at various water pressures ranging from 100 to 500 kPa. Since water has no resistance to shear, the shear stress is determined by the friction between the rubber edges. From what the graph shows, rubber edge friction is from 5 to 16 kPa.

The shear stress system monitors the shear stress on the shear surface and the rubber edge friction. To calculate the shear stress on the shear surface, the rubber edge friction must be subtracted from the measured shear resistance.

To look at this friction, water is sheared up to a shear displacement of 3000 mm in the shear box at different water pressures. After a large shear displacement, the steady-state shear resistance is the most important property of a landslide. A shear displacement of 2000–3000 mm is done to get this value.

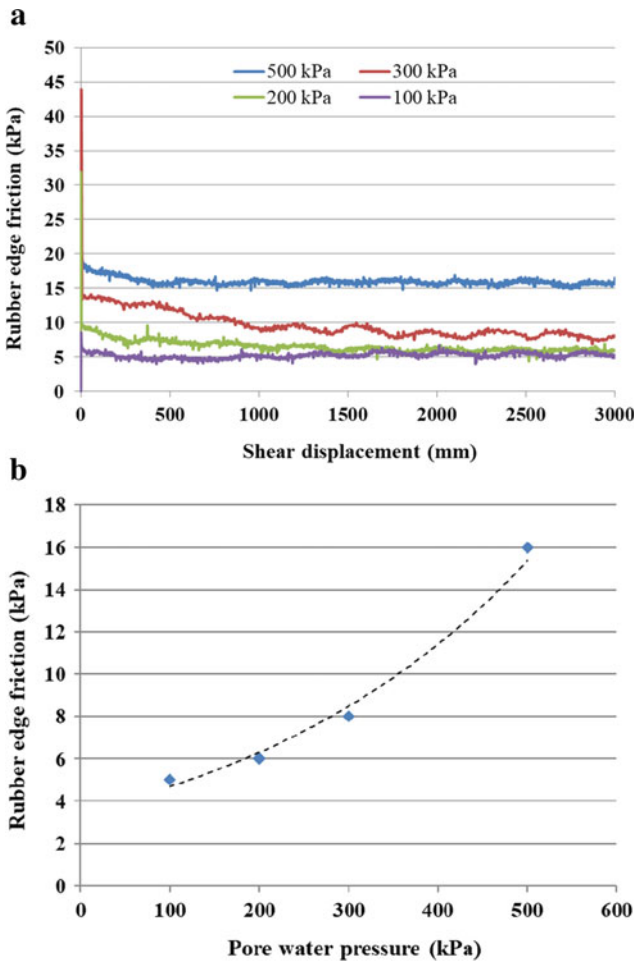

Fig. 18 Rubber edge frictions at various water pressures. **a** Shear stress due to rubber edge friction at four water pressures ranging from 100 to 500 kPa. **b** Shear stress is caused by rubber edge friction at a shear displacement of around 3000 mm

6 Manual for Basic Tests of UDRA

For ring shear experiments, soil samples might be dry or completely saturated. Different processes are utilized for samples that are completely saturated. The procedures are detailed in the following sections.

I. **De-aired water and sample preparation**
The methods for preparing the De-aired water are detailed in the video instruction titled "1. Sample saturation and water preparation." Following is a summary of the steps:

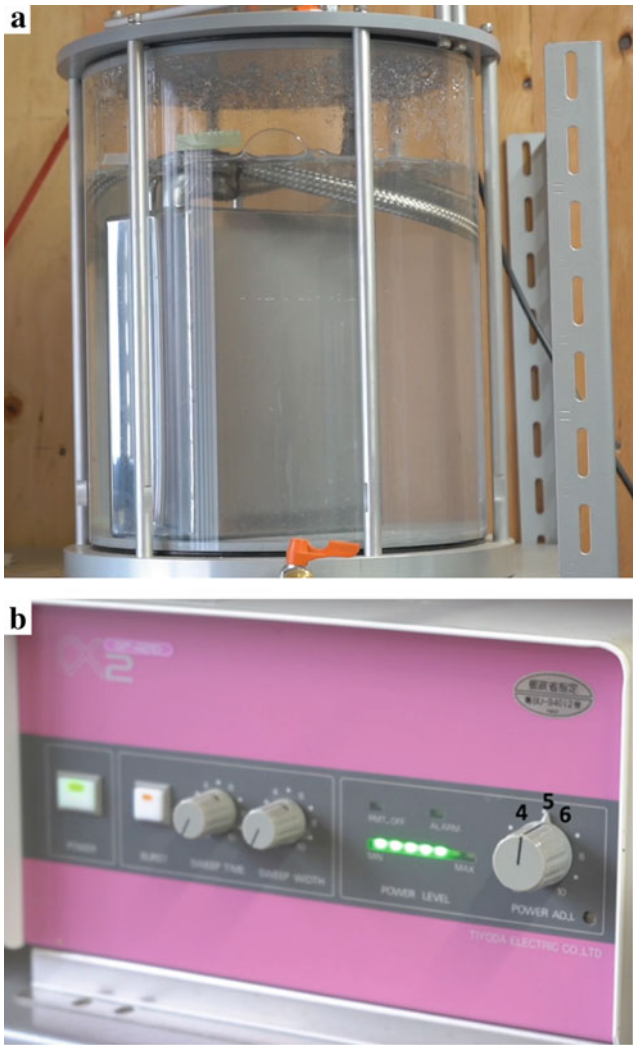

Fig. 19 Normal water in the tank (**a**) and vibrator (**b**)

- Normal water is placed in a water tank until the marker uses vacuum equipment (Fig. 19a). Turn on the vibrator and set it to level 5 (Fig. 19b).
- When the air bubbles are no longer visible, the preparation is complete. This procedure often takes several hours.
- Turn off the vibrator and close the connection valve between the water tank and vacuum. Then, turn the vacuum off.

Soil samples must be meticulously prepared to achieve a fully saturated state. The sample preparation methods are detailed in the video tutorial titled "1. Sample saturation and water preparation." The steps are as follows:

- The dry soil samples are sieved using a 2 mm sieve (Fig. 20a).

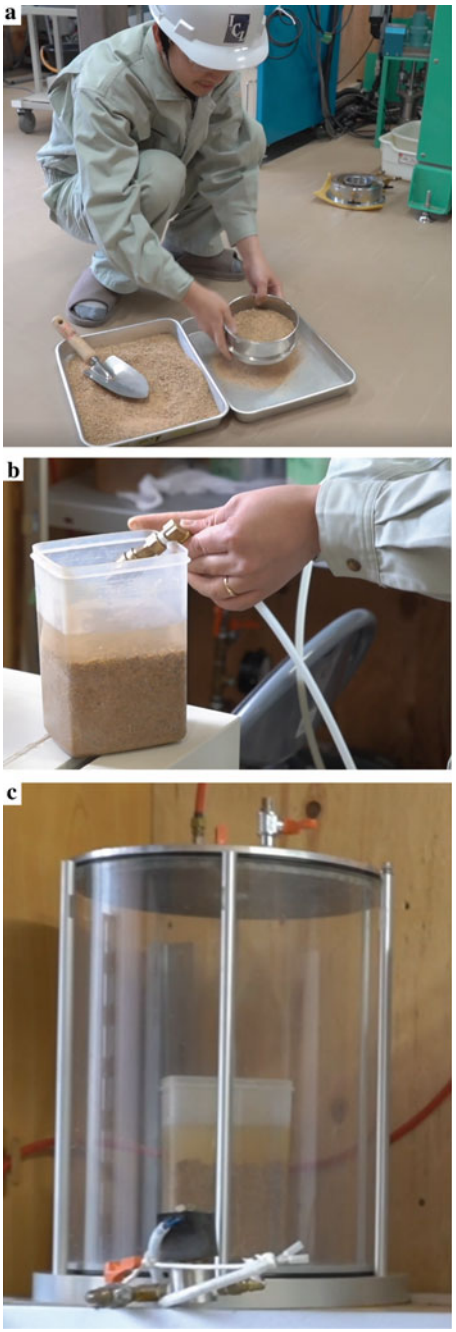

Fig. 20 Sample preparation

- Put about 0.8 kg of dry soil in a box with a volume of 1.5–2.0 l.
- Provide de-aired water to the box containing soil. Typically, the water level is above the soil surface by about 3 mm (Fig. 20b).
- The box containing samples and de-aerated water is placed into the vacuum tank (Fig. 20c). Turn on the vacuum equipment to saturate the sample. During this procedure, air will escape from the samples. The sample

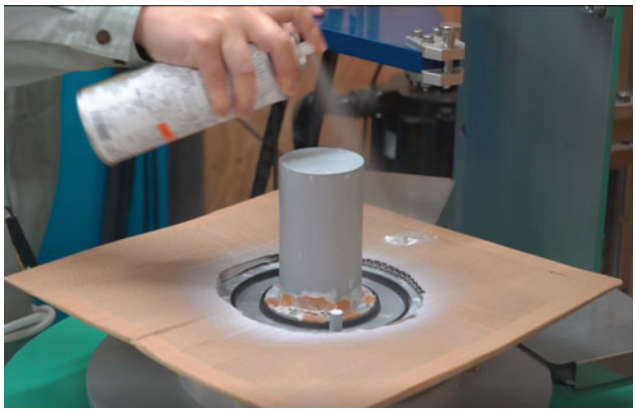

Fig. 21 Spray Teflon on rubber edge

is then kept in the vacuum until the air bubbles cease escaping and the material settles (it takes about one to two days).

II. **Preparing the sample mold**
Preparing the sample mold is important to maintain the undrained condition during the test and avoid damage to the rubber edge after long shearing. The steps to prepare the sample mold are provided below. A video tutorial titled "2. Preparing the sample mold" also shows the steps.
- Clean the rubber edge carefully by using Acetone.
- Spray Teflon on Rubber Edge (Inner and Outer) (Fig. 21): The Teflon is sprayed three times, approximately 10 min between, to allow it to dry.
- Grease the Inner and Outer Ring (Fig. 22): vacuum silicon grease (high-vacuum sealing compound) is used to coat the inner and outer rings.

III. **Switching on the Ring shear apparatus**
The steps of switching on the Ring Shear apparatus are summarized as follows. The reader can also find these steps in the video tutorial titled "3. Switching on the Ring shear apparatus."
- Start the computer.
- Turn on the main unit.
- Turn on breakers for shear loads, gap control, and pore water pressure control (Fig. 23a). Turn on the power supply for shear loads, gap control, and pore water pressure control (Fig. 23b). We only turn on the pore water control when conducting the pore water pressure test.
- Turn on the breaker and the power supply box for normal stress.

IV. **Gap adjustment**
The gap control system establishes the initial contact pressure (0.5–1.5 kN) between the upper pair of ring

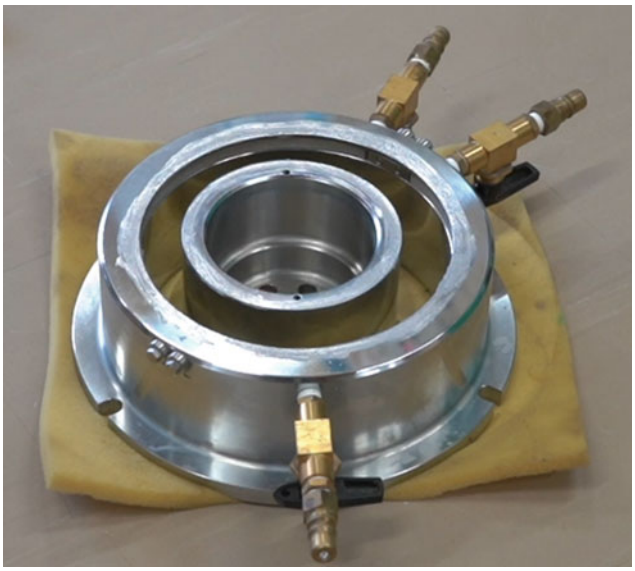

Fig. 22 Inner ring and outer ring after greasing

shear boxes and the rubber edges. A consistent gap value is required to maintain an undrained state during the test to avoid sample and water leaks during rapid shearing. The steps are shown in the video tutorial

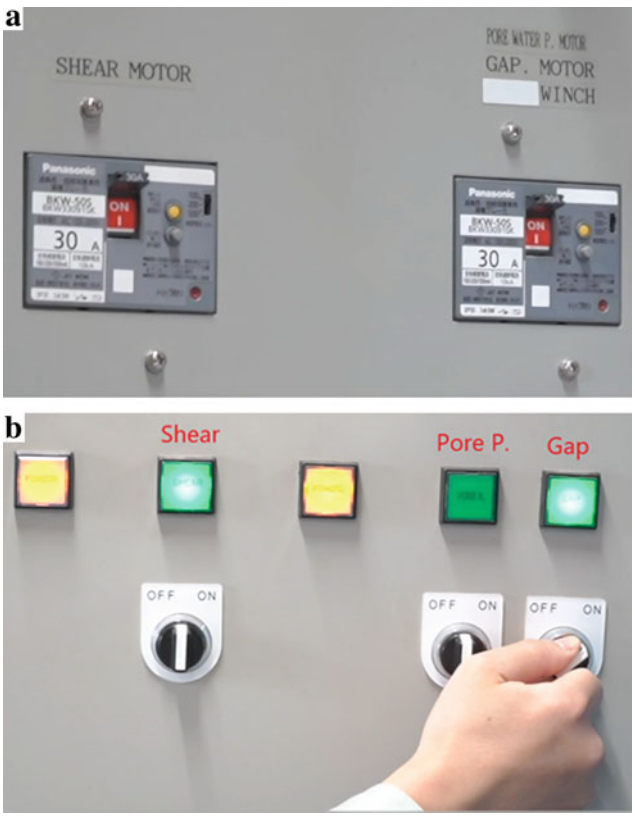

Fig. 23 Turn on the breaker (**a**) and the power supply box for shear loads, gap control, and pore water pressure control (**b**)

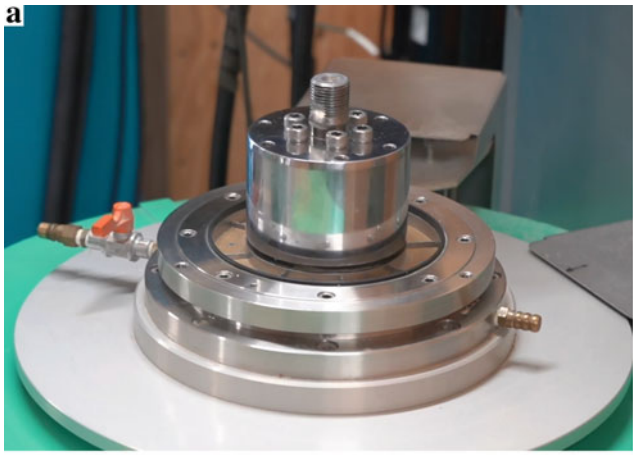

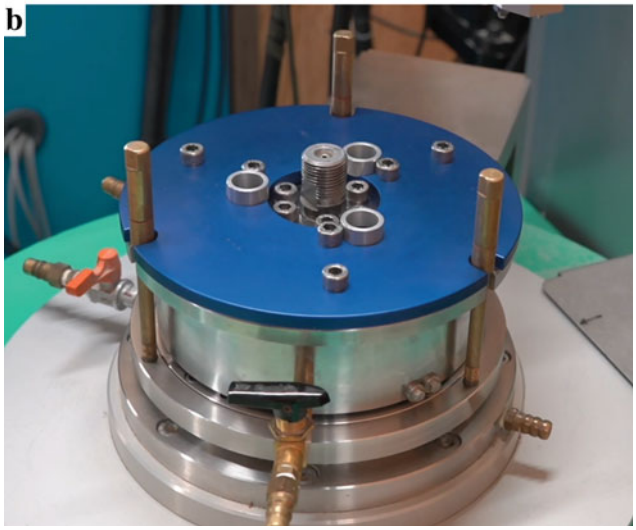

Fig. 24 Setting the inner ring (**a**) and the outer ring (**b**)

Fig. 25 Incensement of the contact force

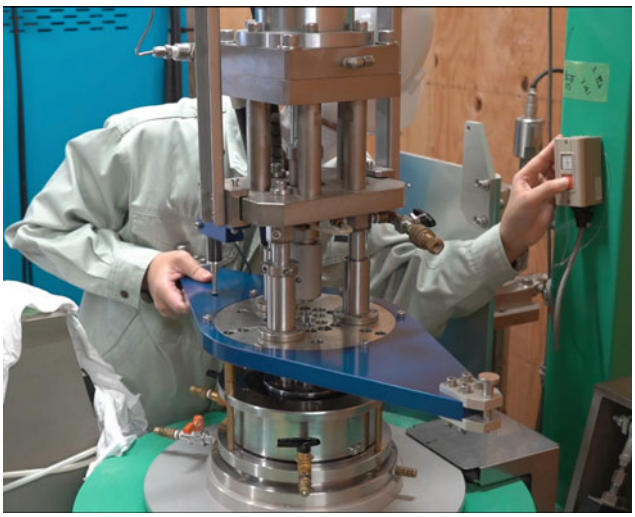

Fig. 26 Install loading plate

called "4. Gap adjustment." Here is a short summary of the steps:

- Screw Inner Ring with six screws (Fig. 24a) and check if the gap value is not 0. Adjust it manually to 0.
- Start Gap control.
- Put Outer Ring and Helping Screws (3 golden ones) to adjust position, leave them loose—unscrewed.
- Put Helping Ring and screw it with six screws (inner and outer ones) (Fig. 24b).
- Screw 3 Helping Screws and remove Helping Ring.
- Install Loading Plate (Fig. 26).
- Rotate Gap Control Button until F_v = 1.0 kN (or other value depending on specific circumstances) (Fig. 25). We often use F_v = 1.0 kN when normal stress is less than 1000 kPa.

V. **Shear Box Saturation**

Following the completion of the gap adjustment, the empty shear box is filled with CO_2 and de-aerated water. This procedure is required to prevent air from getting trapped in the shear box, particularly in the gutter. The following steps will describe how to saturate the shear box. Users may also refer to the video tutorial, titled "5. Shear box saturation."

- The CO_2 supply comes from the CO_2 tank, which is connected to Valve 05. It is necessary to open a valve at the CO_2 tank up to around 5 and 0.1 MPa (Fig. 27) and then check if CO_2 is going out to every shear box Valve, starting and finishing at Valve 02.
- The de-aired water supply comes from the vacuum tank connected to Shear box Valve 05. It is necessary to open the air valve at vacuum tank to enable gravity flow and then circulate De-aired water at every shear box Valve, starting and finishing at Valve 02 (Fig. 28).

Fig. 27 Open CO_2 tank

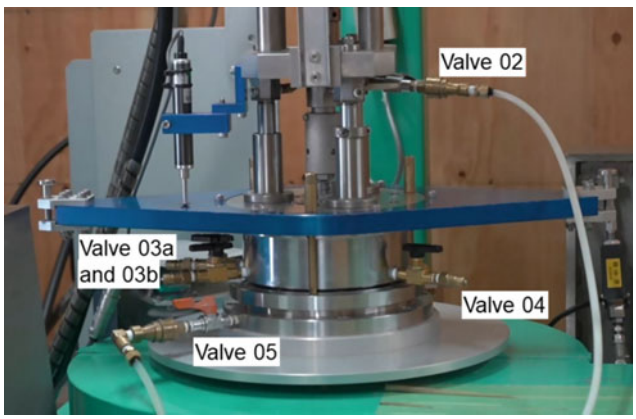

Fig. 28 Shear box with the location of the valve

- When the shear box is filled with de-aired water, close the water supply valve (05) and don't remove it. Water circulation is needed when the B_d (degree of saturation) value is not high enough. If the water supply is disconnected in this step, air may infiltrate inside the Shear box while reconnecting the water supply. To avoid this, we have to remove the water supply pipe after B_d value check.
- Install Pore pressure transducers (PPTs) (one to valve 03a, or another one to valve 03b, or both). When PPTs are connected to valves, open PPTs' drainage valves till a few drops of water come out, then reset u = 0.
- Remove Loading Plate (valve 02 should be opened during removal of LP from SB).

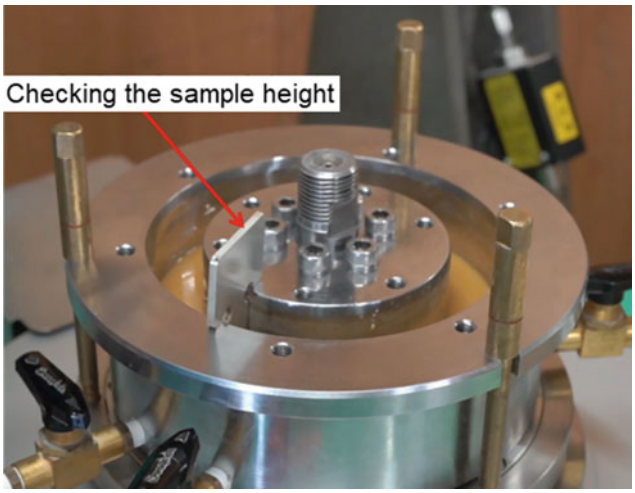

Fig. 29 Smooth the sample surface

VI. **Sample setting**

The steps of sample setting are summarized as follows. The reader can also find these steps in the video tutorial titled "6. Sample setting."

- Put a filter paper on the bottom of shear box.
- Slowly built in a sample, and smooth the sample surface. The sample height should be app. 30 mm from the top of the Shear Box (Fig. 29).
- Put a filter paper on the top of the sample, and tissues if fine-grained material is built in.
- Before setting of Loading Plate, grease it.
- Install Loading Plate, with valve (02) opened to enable water drainage. When the position is adjusted (Fixing screws are fitted on holes of LP) push down the system by button. Check Loading Plate position—red marks on FS should be on the LP surface (Fig. 30).
- Put 12 screws on LP but leave them loose.
- Unscrew and take out Helping screws (3 golden ones).
- Install Shear Load Cells, and rotate to adjust position (Fig. 31).
- Install Vertical Load Cylinder (VLC) by controlling on Vertical Control part of MCU (Main Control Unit) (Fig. 32) and check the speed set location. If not 0, turn it to 0 to ensure the central axis does not suddenly move → Click the Down button → Turn the speed set button to 2–4. The VLC goes down and when VLC contacts the central shaft, click the Stop button. Turn the speed set button to 0 and Lock the button.
- When VLC contact LP, screw the ring and additionally screw by the screw driver.
- After LP is fixed, unlock the protection screw on LP.

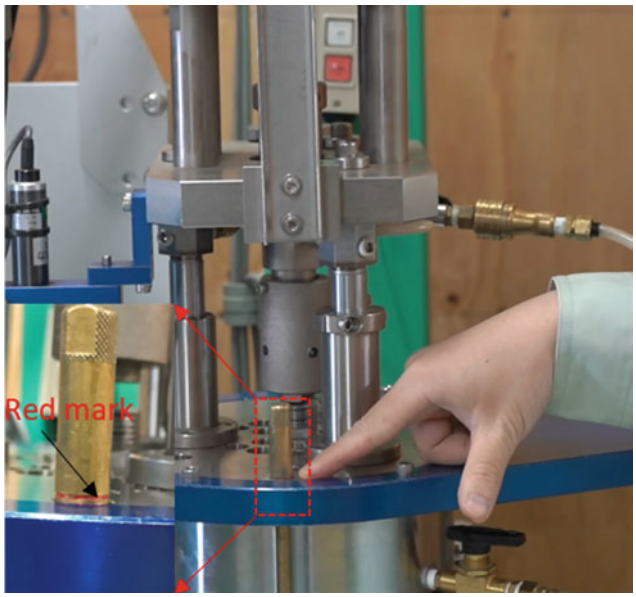

Fig. 30 Checking red mark after installation loading plate

Fig. 31 Adjust the position of loading plate to install shear load cells

VII. **Water circulation (gravity flow)**
The de-aired water supply comes from the vacuum tank from which is connected to Shear box Valve 05. It is necessary to open the air valve at vacuum tank to enable gravity flow and then circulate de-aired water though Valve 02. Users may also refer to the video tutorial, titled "7. Water circulation."

VIII. **B_d value measurement**
B_d is stressed by applying a load in increments of 50 kPa and measuring the generated-pore pressure at two-pore pressure transducers. It must be done in undrained conditions to generate pore water pressure. The B_d value depends on the Rubber Edge Correction Factor (α). The B_d value is calculated based on the following equation.

Fig. 32 Using vertical control to install vertical load cylinder

$$B_d = \Delta u / \Delta s$$

where
Δu is an increment of pore pressure,
$\Delta\sigma$ is an increment of normal stress.
The loading rate (slope value in kPa/s) depends on soil properties. Slow speeds are recommended for fine-grained materials with low permeability (e.g., for flysch, the slope of 0.1 or 0.25 kPa/s).
The steps are provided in the video tutorial titled, "8. Bd value". Here is a summary of the steps:

- Close the Valve 02.
- Turn ON the vertical control to manage normal stress.
- Fill the data form panel for Data acquisition with data appropriate for this specific test and start data acquisition.
- First, apply 50 kPa, then write u1 or/and u2 values and calculate the Bd value for this loading. Do the same for σ = 100, 150, 200 kPa. Continue to higher stresses if necessary.
- Calculate the Bd. Bd value should be large 0.95.
- Stop data acquisition after Bd value measurement is finished.
- After B_d measurement is finished, we can release normal stress to 0 and then open valve 02 for starting a consolidation process.

IX. **Consolidation**

For each test, sample consolidation is performed to simulate the initial stress condition. In drained conditions, the normal stress and shear stress was raised to a certain value (dependent on sample depth and slope angle). The steps are explained in the instructional videos "9. Consolidations 1" for simulating only normal stress and "10. Consolidations 2" for simulating both shear stress and normal stress, respectively. Here is a brief overview of the steps:

- Open the Valve 02 (Fig. 33).
- Enter the data appropriate for this specific test in the data form panel for data acquisition, then start the data acquisition.
- Calculate and set initial Normal and Shear stresses (σ_0, τ_0) and for the Speed Control test $\tau_0 = 0$. Stress loading speed (kPa/s) depends on material properties".
- Consolidation is finished when pore pressure dissipates (u = 0). Close the drainage valve 02 at that time and then stop the data acquisition.

X. **Shearing**

Shearing was performed following sample consolidation. It is shareable in both drained and undrained situations. In a condition of drainage, valve 2 is open, but in a state of undrained, it is closed.

A servo-controlled motor provides shear stress via shear stress control, speed control, or displacement control. The choice between a speed control test and a stress control test depends on the test's objective. Typically, a stress-control test is performed to simulate a landslide, while a speed-control test is utilized to acquire soil characteristics.

1. ***Monotonic shear-stress test (a basic shear stress control test)***

The monotonic shear-stress test is the most fundamental undrained dynamic-loading ring-shear test for measuring the undrained steady-state shear resistance as a key parameter for landslide dynamics. When stress exceeds the failure line, the decrease in shear resistance after peak strength accelerates shear displacement. Increased pore pressure will generate a fast motion during the subsequent post-failure motion. It will continue until it reaches a steady-state shear resistance in an undrained condition. Normally, we set the limit for shear displacement at 10 m. The shearing stops automatically when the shear displacement reaches 10 m.

The procedures for the monotonic shear-stress test are outlined here, but they are also available in the video instruction titled "11. Shear stress control."

- Remove the water supply pipe from Valve 05 and remove all obstacles to the rotation of lower plate (LP).
- Check again if Helping Rings are unscrewed and removed.
- Close valve 2 (for the undrained test).
- Push the remote button in the shear control box (Fig. 34).
- Click the "Information" button and fill information for Data acquisition (Fig. 35). Select the sampling interval. For the fast speed testing, we often select 5 Hz or 10 Hz for the sampling interval. For slow testing, the users can change the sampling interval to 1 s or higher.
- In the shear stress control of the software (Fig. 36), select the shear stress control and click "On" button.
- Input the parameters: target and slope for the static loading. The slope should be small, such as 0.5 kPa/s, or smaller for fine-grained material with low permeability.
- Click the "Start" button in the Data acquisition.
- Click the "Static" button (Fig. 36) to increase shear stress.
- Click the "Stop" button in the Data acquisition when shearing is finished.
- Chose the "Measure" button in the Data acquisition to reset the shear displacement to 0. This step is needed because when shear displacement reaches 10 m, the program stops controlling the system.

2. ***Shear-displacement control test or shear speed control test***

Shear stresses at the steady-state, the mobilized and peak friction angles may be determined by conducting an undrained shear displacement control or speed control test. For ICL-2, the maximum speed of the sheared servo-motor is 50 cm/s. A speed test can be conducted in cm/s, whereas a displacement test can be performed in mm/s, mm/min, and mm/h. Fine-grained materials with

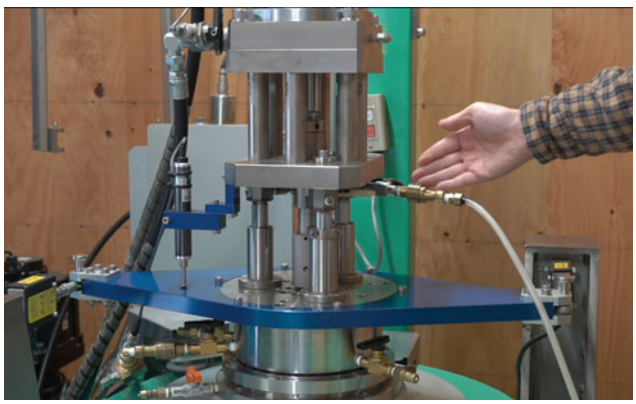

Fig. 33 Open the valve 2 for drainage

Fig. 34 Pushing the "Remote" button in the Shear control box

low permeability should be sheared at a slow speed to see pore pressure build up slowly. A shear-displacement control test is used for very slow shearing tests to test clayey soils for reactivated landslides.

The steps for the shear-displacement control test are presented here, but they are also available in the video instruction titled "12. Shear displacement control".

- Disconnect the water supply pipe from Valve 05 and remove all obstacles to the rotation of lower plate (LP).
- Verify that the Helping Rings have been unscrewed and removed.
- Close valve 2 (for the undrained test).
- Press the "remote" button in the shear control box.
- Fill out the details for data acquisition by clicking the "Information" button. Select the sampling interval that ranges from 600 s to 200 Hz. Sample intervals of 5 Hz or 10 Hz are frequently chosen for testing at high speeds. Users can adjust the sample interval to 1 s or higher for slow speed.
- Select the shear displacement control and click "On" in the program (Fig. 37).
- Enter the target and slope parameters for the static loading. Figure 37 shows an example with a target of

Fig. 35 Screenshot of setting data acquisition

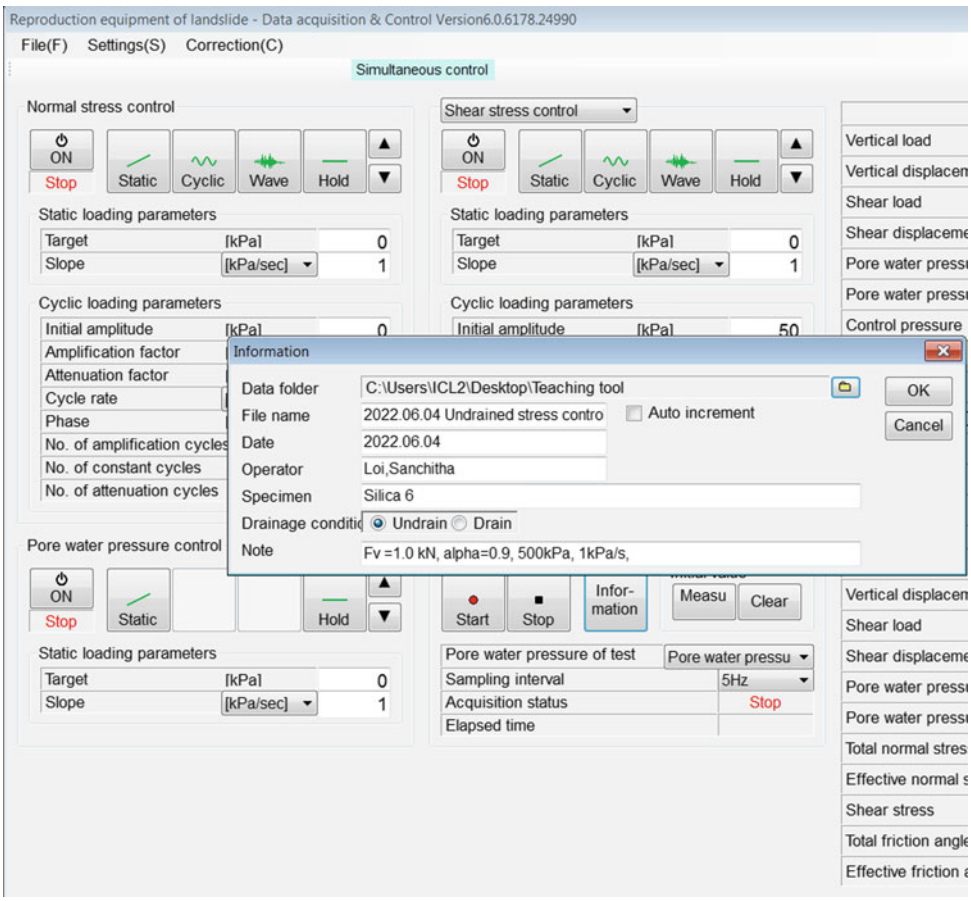

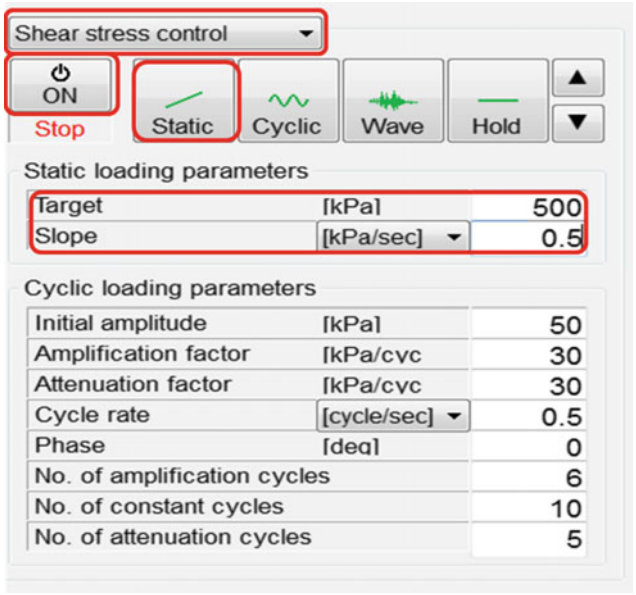

Fig. 36 Screenshot of setting stress control test

1000 mm and a slope of 0.05 mm. The test takes about 5.6 h.

- Click the "start" button in the data acquisition.
- Click the "static" (Fig. 37) to start shearing.
- Click the "Stop" button in the Data acquisition when shearing is finished.

The steps for the speed control test are similar to the shear-displacement control test. The difference is the setting of the loading parameters. Figure 38 presents an example of a speed control test. The "target" is the shear speed in cm/s and constant during the test. The "slope" is the time required to get constant shear velocity.

3. ***Cyclic-loading shear-stress control test***

The cyclic shear stress is the fundamental preliminary investigation of the behavior of earthquake-induced landslides. Before performing cyclic loading, the initial stress conditions (σ_0 and τ_0) must be calculated based on the depth of the sample and slope angle. In this example test, we selected normal stress of 1000 kPa and shear stress of 700 kPa. Normal and shear loads are applied in static mode and under drained conditions. The consolidation step is following the instructions in the video titled, "10. Consolidation 2".

The video tutorial titled, "13. Cyclic shear control," explains the procedure, which is also summarized below:

- Disconnect water supply pipe from Valve 05 and remove all obstacles to rotation of lower plate (LP).
- Verify that the Helping Rings have been unscrewed and removed.

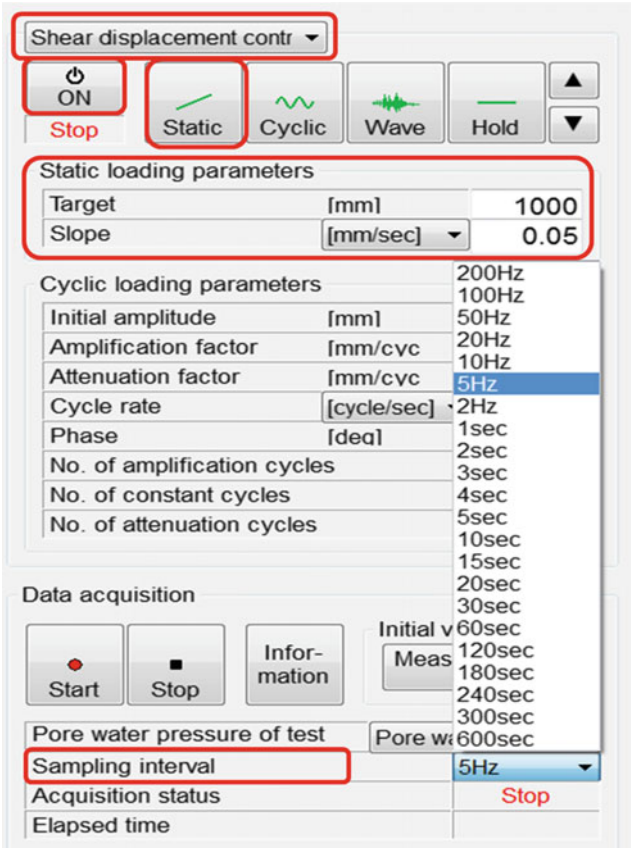

Fig. 37 Screenshot of setting shear displacement control test

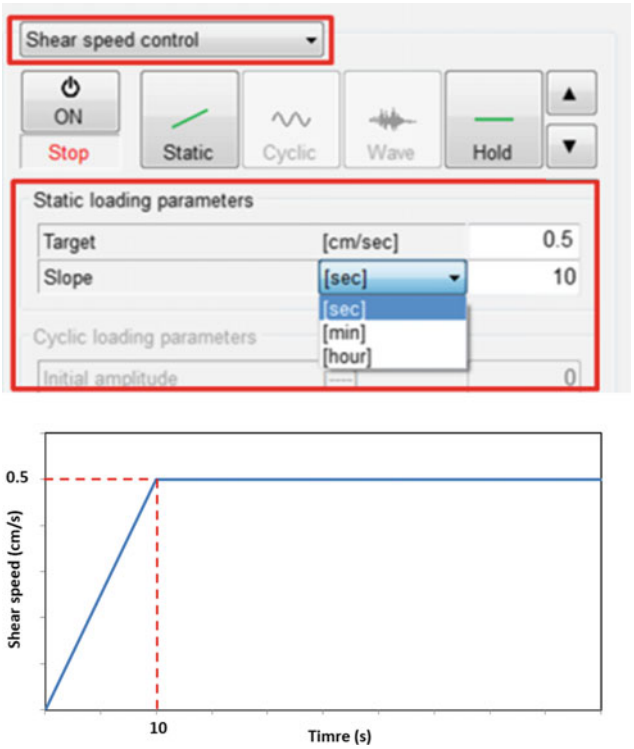

Fig. 38 Screenshot of setting speed control test and graph illustrating the slope required to achieve constant shear speed

- Close valve 2 (for the undrained test).
- Press the "remote" button in the shear control box.
- Click the "Information" button and fill in the information for Data acquisition. Select the sampling interval. For cyclic testing, we often select the sampling interval of 5 Hz or 10 Hz.
- Select the shear stress control and click "On" in the program (Fig. 39).
- Enter the cyclic loading parameters: Initial amplitude, amplification factor, attenuation factor, cycle rate, and phase, number of amplification cycles, number of constant cycles and number of attenuation cycles, period and number of cycles. The cycle rate chosen will depend on the soil's characteristics. For fine-grained materials, loading at a slow speed (cycle/hour) is preferred, but for coarse-grained materials, a higher rate (cycle/min or cycle/s) can be used. The maximum cyclic shear load is computed using the formula:

$$\tau_{\max} = \tau_0 + \Delta\tau_{im} + (N_{ac} - 1) \cdot \Delta\tau_{af}$$

where,
$\tau_{\max}$ is the maximum applied shear stress,
τ_0 is the initial shear stress,
N_{ac} is the number of amplification cycles,
$\Delta\tau_{af}$ is the amplification factor
$\Delta\tau_{im}$ is the initial amplitude
From the setting in Fig. 39, cyclic loading parameters are below:

- τ_0 = 700 kPa,
- N_{ac} = 6,
- $\Delta\tau_{af}$ = 30 kPa/cycle,
- $\Delta\tau_{im}$ = 50 kPa.
  Then, the maximum applied shear stress is as follows:
  $\tau_{\max} = 700 + 50 + (6 - 1).30 = 900$ kPa.
- Click the "start" button in the data acquisition.
- Click the "cyclic" (Fig. 39) to start shearing.
- Click the "Stop" button in the Data acquisition when shearing is finished.
- Chose the "Measure" button in the Data acquisition to reset the shear displacement to 0.

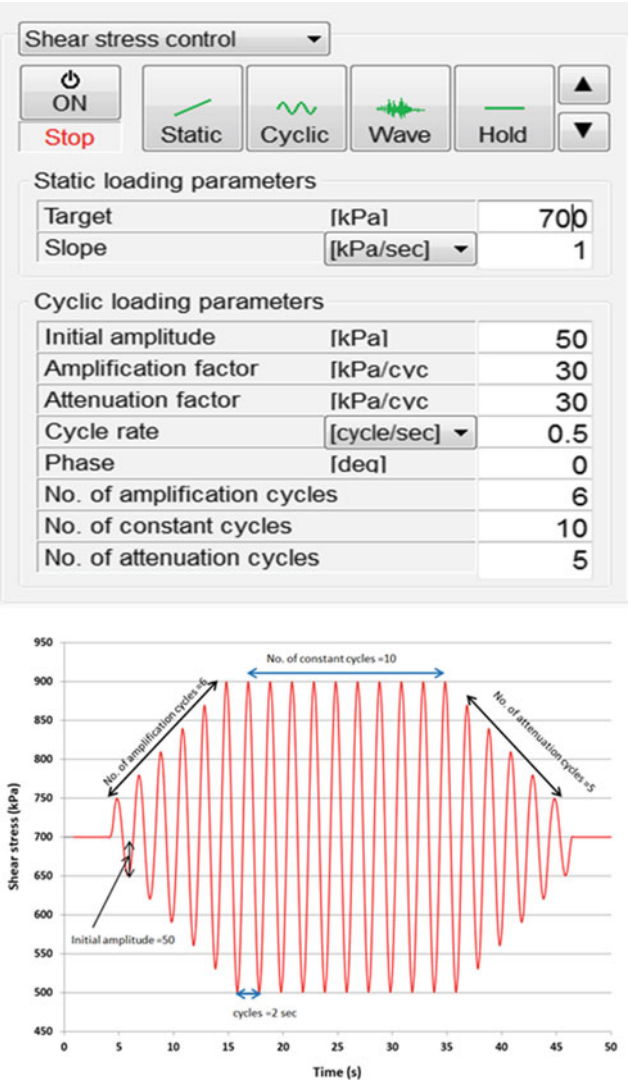

Fig. 39 Screenshot of setting and graph illustrating time and shear stress applied for cyclic loading of shear stress

4. ***Pore-water pressure control test—Rain-induced landslide simulation test***
   Numerous landslides are triggered by rainfall that can be simulated using ring shear apparatus. The sample was saturated, and then consolidated to initial stresses (σ_0 and τ_0) in a drained condition. This preparatory stage was to reproduce the initial stress on the slope. The pore pressure is gradually increased to simulate the rise in groundwater level during rainfall. The groundwater level rise on natural slopes may not be quick; hence the pore-water pressure loading in a drained condition. When shearing start, we can test under drained or undrained condition. The steps are detailed in the video instruction titled "14. Pore-water pressure control," with a summary of the steps below.
   - Disconnect water supply pipe from Valve 05 and remove all obstacles to rotation of lower plate (LP).
   - Verify that the Helping Rings have been unscrewed and removed.
   - Close the valve 2.
   - Connect the water pipe to the servo pore water pressure (Fig. 40).
   - Open the valve in the servo pore water pressure. Push the "loading" button and rotate the "speed set" in the pore water pressure to check the water coming out

Fig. 40 Connecting the water pipe to the servo pore water pressure

from the piston of the servo pore water pressure through the water pipe (Fig. 41).

- Connect the water pipe to the valve 4.
- Push the "stop" and then "remote" buttons to change manual to remote control
- Fill out the details for data acquisition by clicking the "Information" button. A sample interval of 5 Hz is frequently chosen for the pore water pressure control test.
- Enter the target and slope parameters for the static loading of pore water pressure.
- Click the "start" button in the data acquisition.
- Click the "static" (Fig. 42) to start increasing the pore water pressure.
- If we want to test in the undrained shearing, we need to close valve 4 when the lower shear box is rotating.
- Click the "Stop" button in the Data acquisition when shearing is finished.

Fig. 41 Checking water coming out from the piston of servo pore water pressure

- Chose the "Measure" button in the Data acquisition to reset the shear displacement to 0.
- Connect the water pipe to the water tank. Then, push the "Return" button to fill out the water to the piston of the servo pore water pressure, until the water comes out from the hole at the center of the piston (Fig. 43).
- Push the "stop" button in Fig. 42 and disconnect the water pipe.

5. ***Seismic Test—Earthquake-induced landslide simulation test***

To simulate an earthquake-induced landslide, we will input a shear-stress curve calculated from the real earthquake record or a past earthquake record in the computer.

When an earthquake occurs and a seismic acceleration is applied, the loaded stress is given as $k \cdot m \cdot g$; k is referred to as the seismic coefficient, which is the ratio of the seismic acceleration (a) and gravity (g), namely $k = a/g$. It can be used as the control signal for both normal stress and shear stress servo-motors. However, we often examine soils when they are completely saturated. In this instance, the change in normal stress will be negated by the creation of extra pore pressure, and the

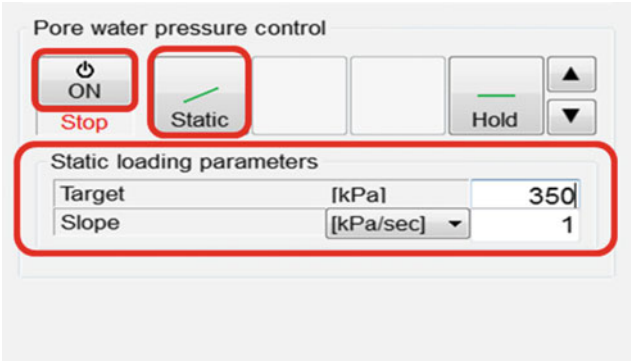

Fig. 42 Screenshot of setting pore water pressure control test

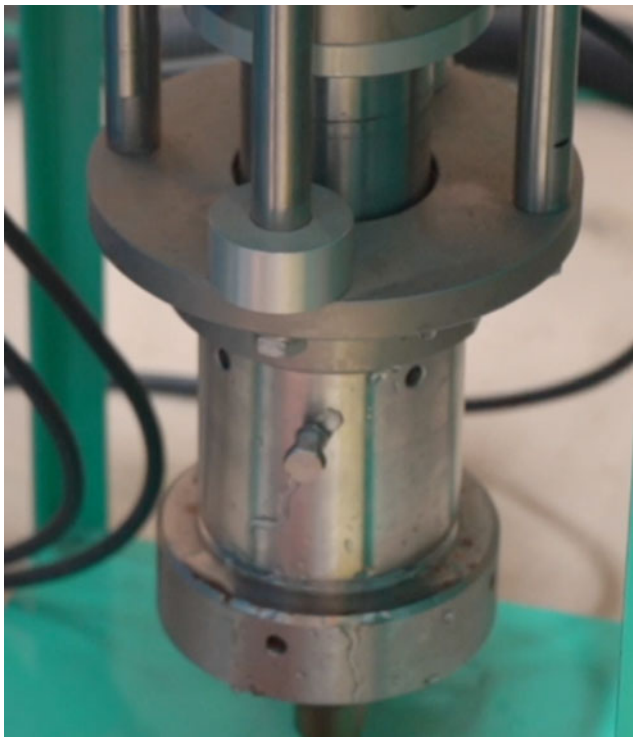

Fig. 43 Fill back the water into the piston

effective normal stress will be minimal. Then, during the earthquake-induced landslide simulation test, the seismic shear-stress variation is typically inputted while the total normal stress remains constant.

The additional shear load is simplified and computed using the following formula:

$$\Delta\tau_s = k \cdot m \cdot g = k \cdot \frac{\tau_0}{\sin\theta} = \frac{a \cdot \tau_0}{g \cdot \sin\theta}$$

where,

$\Delta\tau_s$ is the additional shear stress due to seismic waves,

τ_0 is the initial shear stress, $\tau_0 = m \cdot g \cdot \sin\theta$,

a is the seismic acceleration,

g: gravity.

In this manual, the test was consolidated to the normal stress of 400 kPa and shear stress of 300 kPa to create the initial state. The additional shear load was calculated based on the EW component of the 2016 Kumamoto earthquake wave, which caused many of the landslides in the Kumamoto area. The test was conducted at a five-times slower rate to monitor pore water pressure accurately.

The steps to conduct the seismic test are provided below and in the video titled, "15. Seismic test."

- Disconnect the water supply pipe from Valve 05 and remove all obstacles to the rotation of lower plate (LP).
- Verify that the Helping Rings have been unscrewed and removed.
- Close the valve 2 (for the undrained test).
- Fill out the details for data acquisition by clicking the "Information" button. A sample interval of 5 Hz or higher is frequently selected for the seismic tests.
- Read the wave data by clicking the "File" menu in the Toolbar, and selecting the "Read wave data (R)" option. Next, click on the "opening file icon" to select the text file in the testing computer that contains the wave data. It is noted that the text file containing the wave data should be in a CSV or excel format.
- Input the parameters for wave data (Fig. 44). The recorded seismic waves contain waves with high frequencies and, at times, great accelerations. The shearing servo motor cannot repeat the high acceleration and loading frequency. Due to constraints, the scale factor and output intervals are used to adjust the actual seismic data. To protect the shear motor and precisely monitor the pore water pressure, we selected an "output interval" of 0.05 s, which is five times lower than the sampling rate of the seismic waves, 0.01 s, that were recorded. In the "Shear stress or Shear displacement data," select Colum 1, which contains the shear stress or shear displacement, then choose "stress" for the data type and "kPa" for the unit of data.
- Click the "start" button in the data acquisition.
- Click the "wave" in the shear stress control (Fig. 44) to start seismic stress acting on the sample.
- Click the "Stop" button in the Data acquisition when shearing is finished.
- Chose the "Measure" button in the Data acquisition to reset the shear displacement to 0.

XI. De-installation

After completing the ring shear test, it is essential to remove and clean all apparatus components

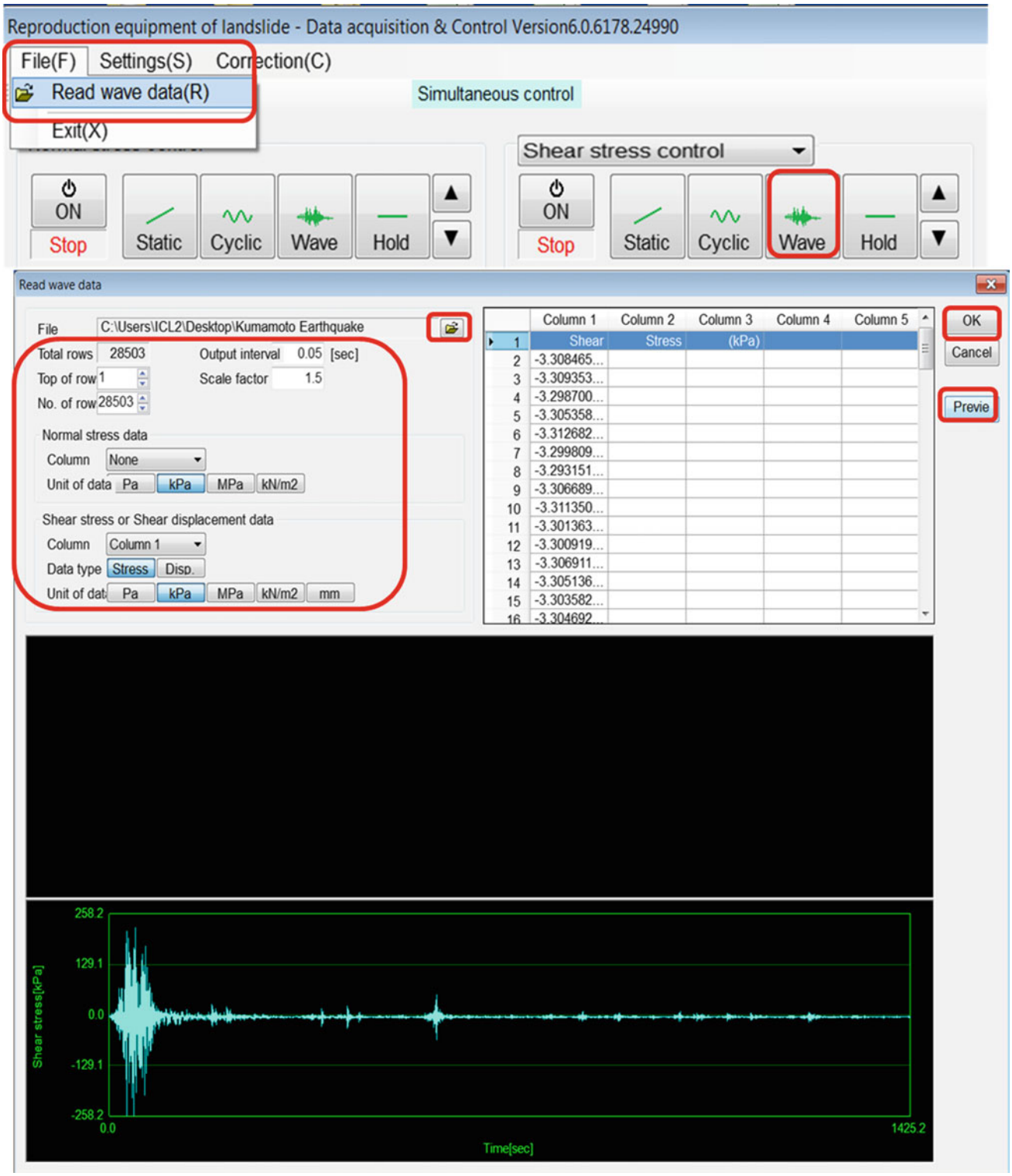

Fig. 44 Screenshot of setting the parameters for the input of wave data and preview of imported seismic shear stress in the software

meticulously to prevent damage. The steps of de-installation and cleaning are provided below and in the video titled, "16. De-installation."

- Release normal and shear stresses to 0 by computer control. Enter "0" in the target and 3–5 in the slope for the static loading parameters of both normal stress and shear stress. Click the "static" buttons in both normal stress and shear stress control. When stresses equal to 0, click the "off" buttons to stop controlling the stresses.
- Push the "remote" buttons in the main control unit to stop the remote control.
- Put Helping Screws (3 × golden ones) before removing Loading Plate
- Disconnect pore water pressure sensors and Shear Load Cells.
- Uninstall Vertical Load Cylinder (VLC) by Vertical Control part of MCU (Main Control Unit): Unscrew the ring connecting VLC and the loading plate. Check the speed set location. If not 0, turn it to 0 to ensure the central axis does not suddenly move → Click the Down button → Turn the speed set button to 2–4. The vertical displacement decrease and when it is around 0 → Stop → Lock the protection button → Click Up button → the speed set also 2–4, the central axis goes up until around marker → Stop → Turn the speed set button to 0.
- Unlock the Lifter and connect with VLC.
- Pull up the loading plate and put it back in to the neutral position.
- Remove sample, filter paper, and tissues.
- Remove and clean the inner and outer rings.
- Clean the rubber edge carefully using acetone to remove Teflon and silicone grease.
- Decrease Gap to 0 and then Push Gap Off.
- Turn off shear, gap, vertical, and pore water motors.
- Turn off the main control unit and computer (Fig. 45).

XII. **Data analysis**

The ring shear program records all measurable data from experiments. The output file (DAT file) contains sensor and test values. The data analysis utilizes only the test value using Excel or other software. To obtain accurate shear stress values, it is necessary to correct two effects of the rubber edge on shear stress and normal stress.

Granular materials, such as sand cannot sustain cohesiveness after a considerable shear displacement. This assumption holds for sands and other typical soils. This assumption is utilized for normal stress adjustment.

Fig. 45 Disconnecting the central axis and loading plate

The ICL-2 has a feature for inputting the normal stress correction factor into the normal stress control system. Figure 46a shows the original stress path result from an undrained cyclic shear stress control test. In the test, we selected a rubber edge correction factor of 0.9. At zero normal stress, the extension of the stress path passes the negative shear stress. When we apply the rubber edge correction factor of 0.86, normal stress equals 1000 * 0.86/0.9 = 955.6 kPa. The shape of the stress path is not changed but moved horizontally to the left. Based on the result in Fig. 18, the correction of rubber edge friction was lowered by 15 kPa from the graph in Fig. 46a. After the corrections of the rubber edge effects, the final stress path result is presented in Fig. 46b.

After data correction, the test result is displayed in the three relationships below.

- **A time series of data** (normal stress, pore water pressure, shear stress, and shear displacement) to examine the process of shearing.

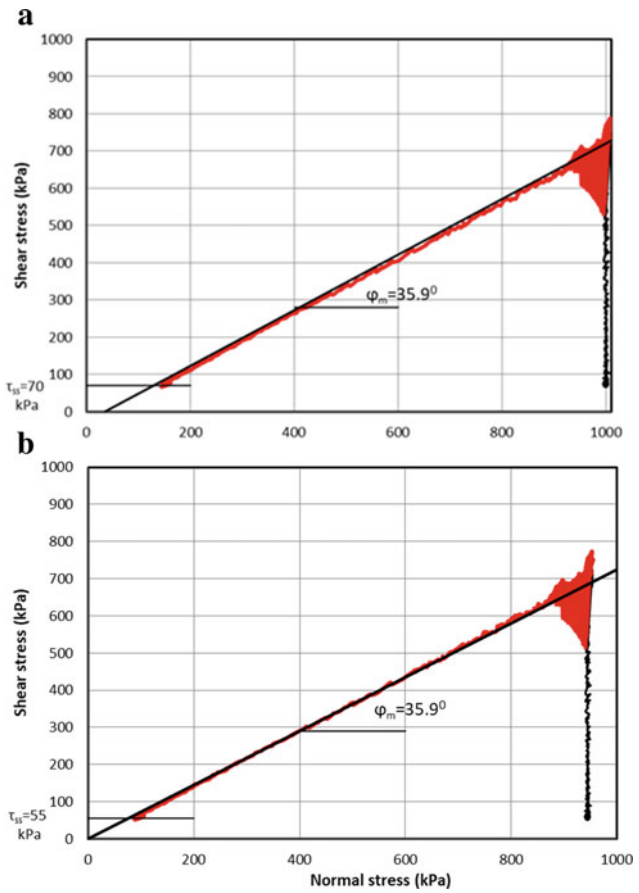

Fig. 46 Test result of the undrained cyclic shear-stress control test. Original test data (**a**) and the correction of rubber edge effects (**b**)

- **A stress path** (relationship between the total normal stress and effective stress and shear stress) to understand the dynamic behavior of the sample.
- **A relationship between shear stress and shear displacement**. Evaluating the drop in shear stress following a failure to steady-state is essential. When the shear displacement from the failure to the steady-state is short, and the loss in strength from the peak to the steady-state is significant, progressive failure development is quick.

1. ***Monotonic shear-stress test results***
   Figure 47 is a monotonic shear stress test result. This test was conducted under normal stress of 500 kPa. From this result, we can obtain friction angle at peak (φ_p = 43.1°), mobilized friction angle at failure (φ_m = 36.4°), steady state shear resistance (τ_{ss} = 50 kPa), shear displacement at the start of strength reduction (DL = 6 mm) and shear displacement at the start of steady state (DU = 700 mm).
2. ***Shear-displacement control test or shear speed control test***
   Figure 48 is a shear-displacement control test result. The

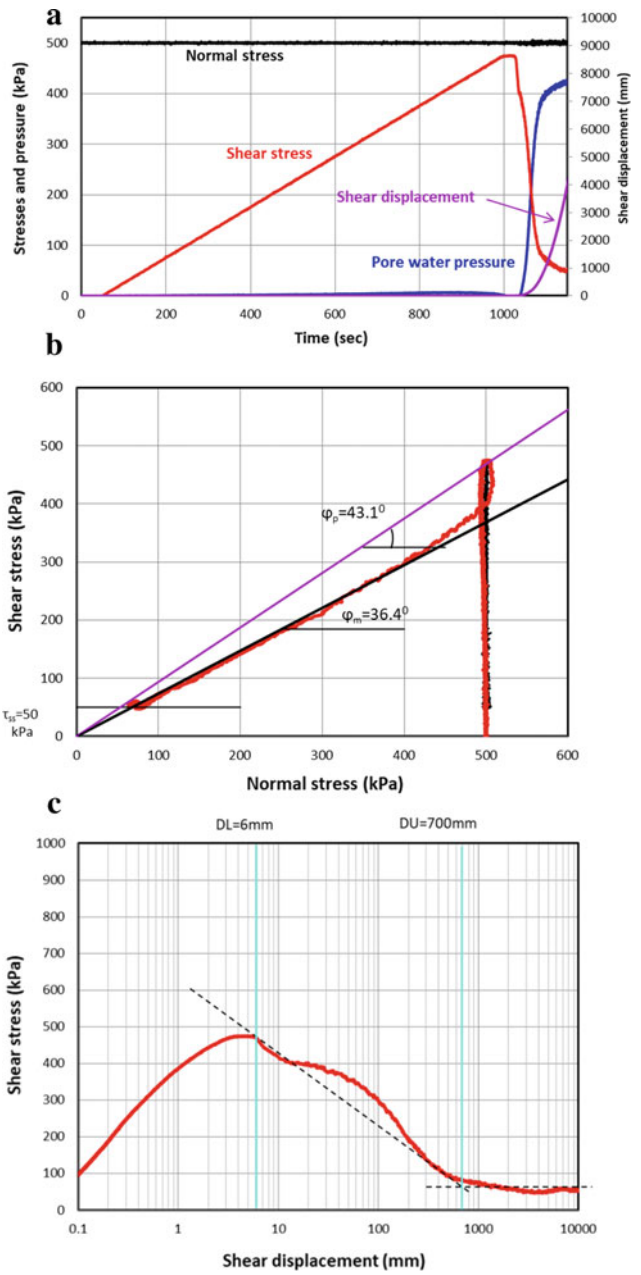

Fig. 47 Example data of a monotonic increasing shear-stress test. **a** Time series of data, **b** stress path, **c** shear stress and shear displacement relationships. Test conditions: sample: weathered granite soil, BD = 0.95, normal stress = 500 kPa, shear stress increment rate: 0.5 kPa/s

silica sand no. 4 was tested under normal stress of 1000 kPa and shear displacement increment rate of 0.05 mm/s. From this result, we can obtain friction angle at peak (φ_p = 37.2°), mobilized friction angle at failure (φ_m = 37.2°), steady state shear resistance (τ_{ss} = 215 kPa), shear displacement at the start of strength reduction (DL = 6 mm) and shear displacement at the start of steady state (DU = 102 mm).

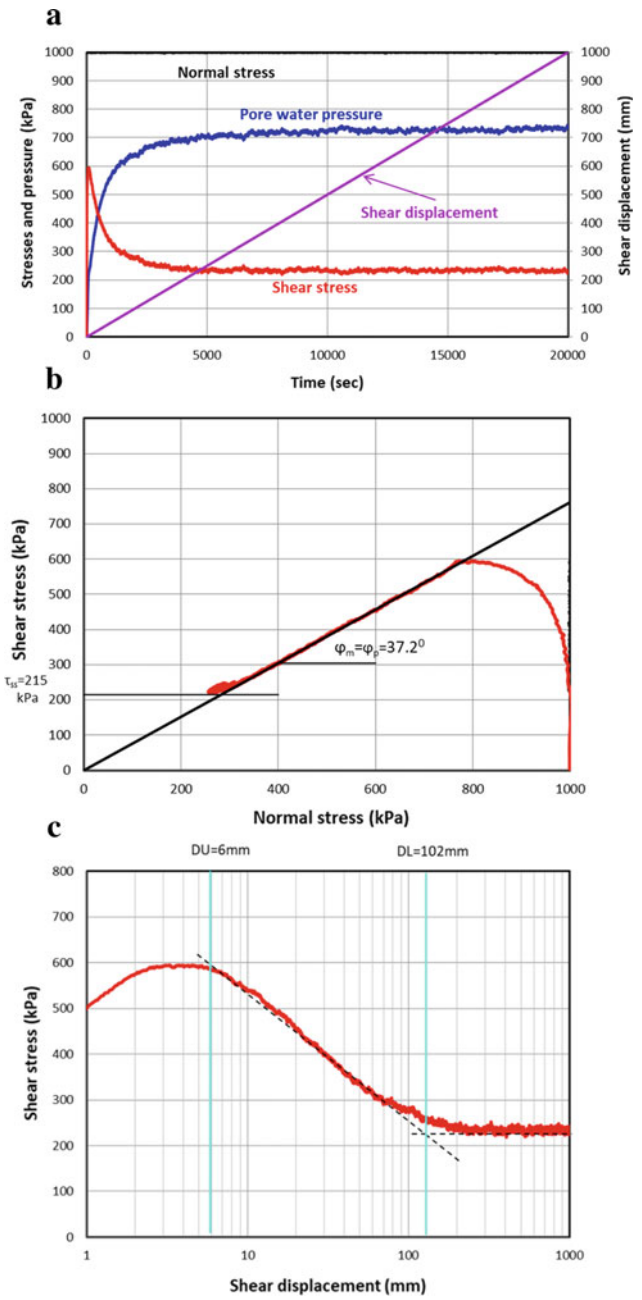

Fig. 48 Example data of a shear-displacement control test. **a** Time series of data, **b** stress path, **c** shear stress and shear displacement relationships. Test conditions: sample: silica sand no. 4, BD = 0.97, normal stress = 1000 kPa, shear displacement increment rate: 0.05 mm/s

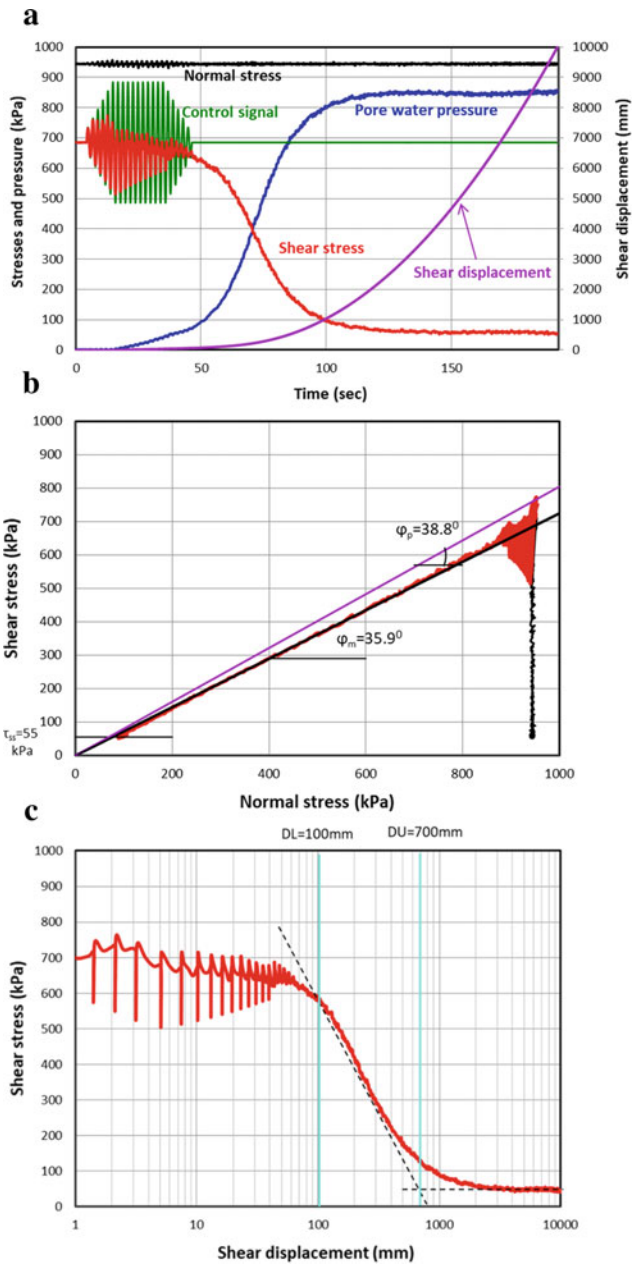

Fig. 49 Example data of a cyclic-loading shear-stress control test. **a** Time series of data, **b** stress path, **c** shear stress and shear displacement relationships. Test conditions: sample: silica sand no. 4, BD = 0.97, normal stress = 945 kPa, shear stress = 670 kPa, cyclic rate: 0.5 cycle/s, shear stress step = 30 kPa

3. ***Cyclic-loading shear-stress control test***

Figure 49 displays the results of the undrained cyclic test. The green line represents the shear-stress control signal applied to the stress-control servo-motor, while the red line represents the mobilized shear resistance. The control signal for shear stress and the mobilized shear resistance are at the same level in the beginning state. When soil collapse takes place, these two lines diverge. In line with the prescribed cyclic loading, the control signal rises as the shear resistance falls until a steady-state shear resistance that is less than the starting stress equivalent to the stress due to gravity. We can determine friction angle at peak (φ_p = 38.8°), mobilized friction angle at failure (φ_m = 35.9°), steady state shear resistance (τ_{ss} = 55 kPa), shear displacement at the start

of strength reduction (DL = 100 mm) and shear displacement at the start of steady state (DU = 700 mm).

4. ***Pore-water pressure control test—Rain-induced landslide simulation test***

   The undrained loading condition was not applied because, on natural slopes, the increase in groundwater level may not occur quickly. The pore water pressure is supplied to the shear box from the piston of the pore water pressure control through valve 4 and then the natural drained condition is applied to the sample. After failure, the test condition can change from drained to undrained by closing valve 4. As shown in Fig. 50, failure occurred at pore-water pressure of 50 kPa, that is pore-water pressure ratio r_u = 50/400 = 0.125.

5. ***Seismic Test—Earthquake-induced landslide simulation test***

   Figure 51 presents the test results of the undrained dynamic-loading ring-shear test on the silica sand no.6 using seismic shear stress of the 2016 Kumamoto earthquake wave. Pore pressure was generated during the seismic loading and the stress path reached the failure line. We can determine friction angle at peak (φ_p = 39.1°), mobilized friction angle at failure (φ_m = 36.4°), steady state shear resistance (τ_{ss} = 40 kPa), shear displacement at the start of strength reduction (DL = 20 mm) and shear displacement at the start of steady state (DU = 700 mm).

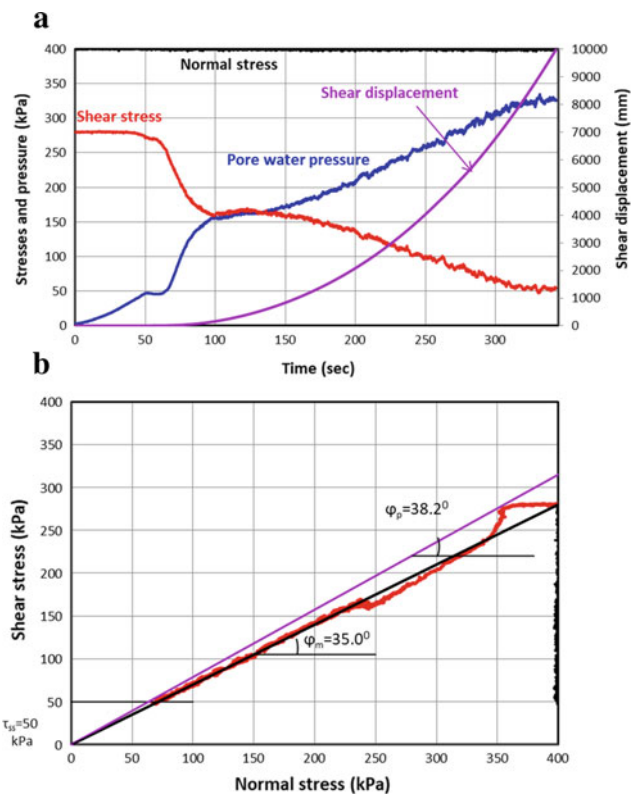

Fig. 50 Example data of a pore-water pressure control test-test. **a** Time series of data, **b** stress path. Test conditions: sample: silica sand no. 4, BD = 0.96, normal stress = 400 kPa, shear stress = 280 kPa, pore-water pressure rate = 1 kPa/s

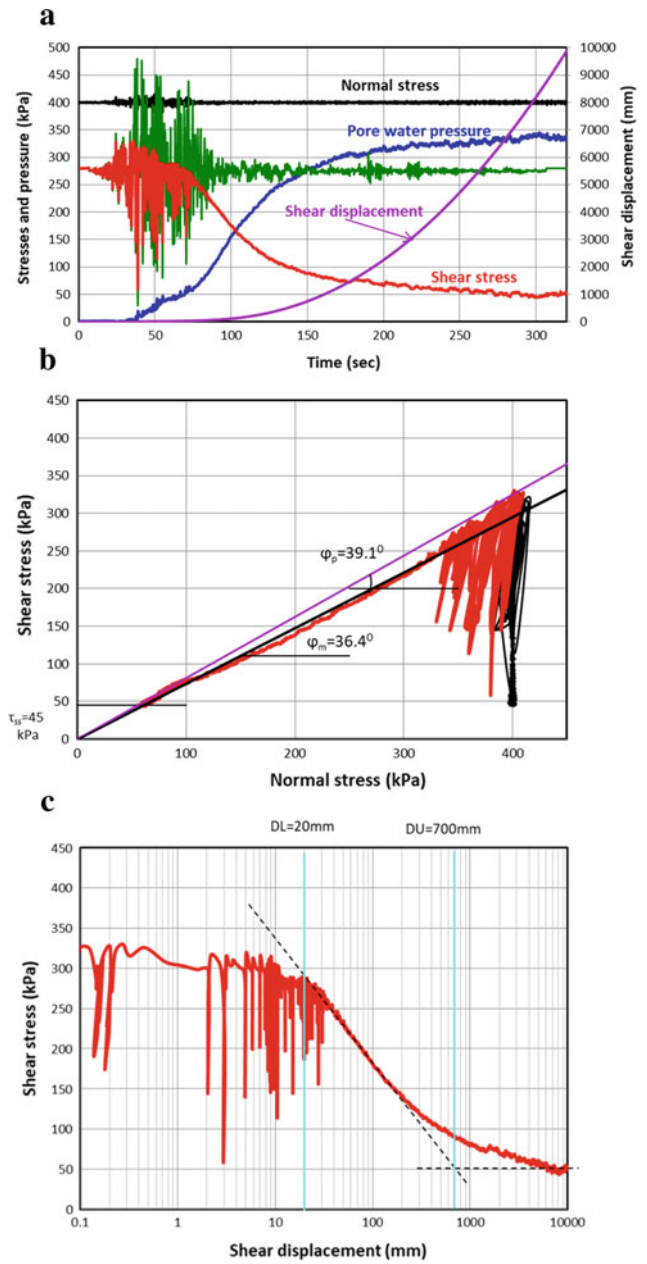

Fig. 51 Example data of a cyclic-loading shear-stress control test. **a** Time series of data, **b** stress path, **c** shear stress and shear displacement relationships. Test conditions: sample: silica sand no. 4, BD = 0.95, normal stress = 400 kPa, shear stress = 280 kPa, seismic wave: 2016 Kumamoto earthquake, five-time lower speed

7 Chapter 5: Conclusions

Sassa and his colleagues at ICL have invented and developed the ICL-1 and ICL-2 ring-shear apparatus series. Several safety protocols have been designed for ICL-2 to reduce any misuse-related harm to the equipment. The concept, design, and construction of the latest ring-shear apparatus, ICL-2, were introduced in this paper.

This article provided a comprehensive guide for interested people to rapidly and effectively operate the ring shear equipment. The user manual supplied in this article was complemented with video demonstrations visually representing each testing phase. In addition to presenting data analysis, the paper provides five basic test cases. Specifically, conventional silica sand no. 4 was tested using the 2016 Kumamoto earthquake wave, which caused many landslides.

Acknowledgements The authors gratefully acknowledge funding from a Japan-Sri Lanka bilateral SATREPS (Science and Technology Research Partnership for Sustainable Development) project titled "Development of early warning technology of Rain-induced Rapid and Long-traveling Landslides joint program from 2019–2025." The International Consortium on Landslides (ICL) and the National Building Research Organization of Sri Lanka (NBRO) are implementing this project.

Appendix: Test Check List

TEST CHECK LIST - ICL-2							EXTENDED CHECK LIST (with explanations)
0. GENERAL INFORMATION							0. GENERAL INFORMATION
1	Date						Current date (of testing)
2	Specimen						Type of soil specimen
3	Type of test						Type of test - Speed control/Stress control (monotonic, cyclic)
4	Drainage condition						Drainage conditions - drained/undrained
5	Specimen preparation						Specimen preparation method; dry or saturated
1. PREPARATION							1. PREPARATION
Check	Task	-					
	Teflon						Spray Teflon on Rubber Edge (Inner and Outer)
	Filter paper						Put filter paper
	Grease						Grease Inner & Outer Ring
2. GAP ADJUSTMENT							2. GAP ADJUSTMENT
Check	Task	Remarks					
	Screw inner ring						Screw Inner Ring with 3 screws (if gap value is not 0, adjust it manually)
	Adjust gap value manually to 0						
	Outer ring & HS loose						Put Outer Ring and Helping Screws (3 golden ones) to adjust position, leave them loose - unscrewed.
	HR screw 6x						Put Helping Ring and screw it with 6 screws (inner and outer ones)
	Start Gap	F_v=	[kN]	s =		Vol. position=	START Gap Control, Rotate Gap Control Button until F_v=1.5 kN (or 2,0 kN depending on specific circumstances). When F_v is reached - STOP Gap Control.
	Stop Gap	Gap=	[mm]				
	Screw 3x HS						Screw 3x Helping Screw and remove Helping Ring
	Remove HR						
	Install LP						Install Loading Plate by screwing all 9 screws
3. CO_2 and H_2O (de-aired water) saturation							3. CO_2 and H_2O (de-aired water) saturation **GENERAL REMARK: Use 05 supply for in-direction, and 02 & 03, 04 a&b for out-direction**
Check	Task	Remarks					
	CO_2 from valve 05 -> to valves 02, 03, 04a &b and to 02 again, out.						CO_2 supply comes from CO_2 tank from which is connected to Valve 05. It is necessary to open valve at CO_2 tank up to 5 l/min and then check if CO_2 is going out t every shear box Valve, starting and finishing at Valve 02.
	Deaired H_2O from valve 05 in -> to valves 02, 03, 04a&b and 02 again, out.						De-aired water supply comes from vacuum tank from which is connected to Shear box Valve 05. It is necessary to open air valve at vaccum tank to enable gravity flow and then circulate deaired water at every shear box Valve, starting and finishing at Valve 02.
	Close water supply valve (05) and leave it connected						When Shear Box is filled with de-aired water, close water supply valve (05) but don't remove it. *In case when Bd value is not high enough, water circulation is needed, and if water supply is disconnected in this step, it is possible that air infiltrates inside SB while reconnecting water supply. In order to avoid that, we have to remove water supply pipe after Bd value check (step 7).*
	Install PPT1&2 and drain them						Install Pore pressure transducers (small one to valve 03, and big one to valve 04a). When PPTs are connected to valves, open PPTs' drainage valves till few drops of water come out, then reset u=o.
	Reset u=0 kPa						
	Remove LP						Remove Loading Plate (valve 02 should be opened during removal of LP from SB, but when LP is removed, close valve).
4. SAMPLE SETTING (GAP is OFF during sample setting)							4. SAMPLE SETTING (GAP is OFF during sample setting)
Check	Task	Remarks					
	Built in a Sample	H_0=	[mm]				Slowly built in a sample, and smooth the sample surface. Sample height should be app. 30 mm from the top of the Shear Box.
	Filter paper & tissues						Put a filter paper on the top of the sample, and tissues if fine grained material is built in.
	Grease LP						Before setting of Loading Plate, grease it.
	Put LP with 02 open						Install Loading Plate, with valve (02) opened to enable water drainage. When position is adjusted (Fixing screws are fitted on holes of LP) push down the system by button. Check Loading Plate position – red marks on FS should be on LP surface
	12 screws (loose)						Put 12 screws on LP but leave them loose
	VDS + protect it's cable						Install Vertical Displacement Sensor (VDS) with longer screw and protect it by placing the wire on SLC (this will protect possible damage when Lower Plate start rotating)
	Unscrew and take out 3 x HS						Unscrew and take out Helping screws (3 golden ones)
	Install SLC						Install Shear Load Cells, rotate to adjust position
	Screw 12 screws on LP						
	VLC	On Vertical Control part of MCU (Main Control Unit): Manual -> Stop -> turn the button to Zero -> Start -> Turn the button to left side (down) until VLC contact with central shaft -> Stop -> Lock the button					Install Vertical Load Cylinder (VLC) by controling on Vertical Control part of MCU (Main Control Unit): Manual -> Stop -> turn the button to Zero -> Start -> Turn the button to left side (down) until VLC contact with central shaft -> Stop -> Lock the button
	Screw the ring						When VLC contact LP, screw the ring and additionally screw by screw driver
	Unlock protection screw						After LP is fixed, unlock the protection screw on LP
5. MAKING CONTACT OF FILTER PAPER AND SAMPLE - **drained**							5. MAKING CONTACT OF FILTER PAPER AND SAMPLE - **drained**
Check	Task	Remarks					
	Open Valve 02						In this process, valve 02 is open
	s=Fv= 0 reset						Normal stress should be reset on a monitoring box in order to apply load of exact value to make contact of filter paper and sample and loading plate.
	s -> xx kPa	s=	[kPa]	D_v=	[mm]		Apply load manually up to 25 kPa for fine grained soil material or to 30 kPa for sandy materials.
	Close Valve 02						Close Valve 02 after pore pressure dissipates to zero.
6. WATER CIRCULATION **(gravity flow)**							6. WATER CIRCULATION **(gravity flow)**
Check	Task	Remarks					
	Deaired H_2O from valve 05 into the SB.						De-aired water supply comes from vacuum tank from which is connected to Shear box Valve 05. It is necessary to open air valve at vaccum tank to enable gravity flow and then circulate deaired water trough Valve 02.
	Drain water from SB at valve 02						
	H_{BC} measure	H_{BC}=	[mm]	h_{BC}=H_{BC}-63,85	[mm]	h_{bc}= [mm]	Measure sample height h_{bc} before B_d value measurement.
	D_v	D_v=	[mm]				Measure vertical deformation height before B_d value measurement.

7. B_d VALUE MEASUREMENT - **undrained**											
Check	Task	Remarks									
	Valve 02 has to be closed										
	Remote ON										
	Data acquisition form	a=		Info.				Normal		[sec]	
	Initial test values (s, u1, u2)										
	START Data acquisition										
	Fill a table for Bd value calculation	s given	s	u_1	u_2	Ds	Du_1	Du_2	B_{d1}	B_{d2}
		0								
		50								
		100								
		150								
		200								
		250								
		300								
		350								
		400								
		450								
		500								
		550								
		600								
		650								
		700								
		750								
		800								
		850								
		900								
		950								
		1000								
		Slope=		[kPa/sec]				Average B_d =			
	STOP Data acquisition										

7. Bd VALUE MEASUREMENT - **undrained**
Valve 02 has to be closed
Remote ON (both Normal and Shear Stress)
Fill data form pannel for Data acquisition with data apropriate for this specific test and start data acquisition.
Bd is stressed by applying a load in increments of 50 kPa and measuring generated pore pressure at 2 Pore Pressure Transducers. It has to be done in undrained conditions in order to generate pore pressure. B_d value is Rubber Edge Correction Factor (a) dependant. **Bd= Δu/ Δs** Rate of loading (slope value in kPa/ sec) depends on soil properties. For fine grained materials with low permeability, slower rates are better (e.g. for flysch, slope of 0.1 or 0.25 kPa per sec.). First apply 50 kPa, then write u1 and u2 values and calculate Bd value for this loading. Do the same for s=100, 150, 200 kPa. Continue to higher stresses if necessary. Bd value should be 0.91-0,95 for sandy materials, and 0,95 to 1 for fine grained materials. After Bd measurement is finished, we can release pore pressure by draining trough valve 02 and additionally trough valve 05 (for fine grained materials), starting a consolidation process that way.
Stop data acquisition after B_d value measurement is finished.

8. CONSOLIDATION - **drained**									
Check	Task	Remarks							
	Data acquisition form	Information					Normal	[sec]	
	START Data acquisition								
	Open Valve 02 (+ 05 additional)								
	Consolidate to calculated s_0	s stress control		s=	kPa	slope=		kPa/sec	
	Consolidate to calculated t_o	t stress control		t=	kPa	slope=		kPa/sec	
	Close valve 02 and 05 after pore pressure dissipates.								
	STOP Data acquisition								
	H_{BC} measure	H_{BC}=	[mm]	$h_{BC}=H_{BC}-63,85$	[mm]	h_{bcs}=		[mm]	
	D_v	D_{vs}=	[mm]		D_{vi}=	[mm]			

8. CONSOLIDATION - **drained**
Fill data form pannel for Data acquisition with data apropriate for this specific test and start data acquisition.
Valve 02 has to be opened. If we have fine grained material, it is apropriate to drain also trough valve 05
Calculate and set initial Normal and Shear stresses (s_0,t_0). For Speed Control test t_0 =0. Stress loading speed [kPa/sec] depends of material properties
Consolidation process is finished when pore pressure dissipates (u=0). In that moment close drainage valves (02 and 05).
Stop data acquisition when consolidation process is finished.
Measure sample height h_{bc} before shearing.
Measure vertical deformation height before shearing.

9. SHEARING		
Check	Task	Remarks
	Remove 05 water supply	
	HS 3x taken out	
	VDS protected	
	Close valve 04a (PPT2)	
	Waiting for input	**Waiting for input**
	Valve 02 has to be closed	
	Data acquisition form	Information / High speed [Hz]
	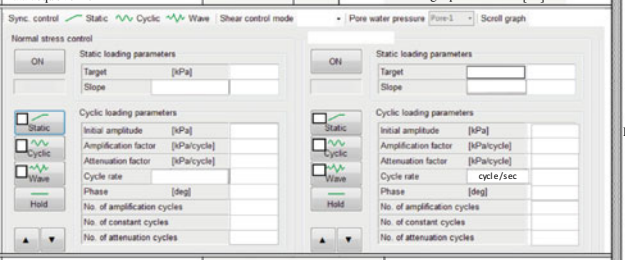	
	START Data acquisition	Protection: cm
	START stress control	
	STOP Data acquisition	
	H_{BC} measure	H_{BC}= [mm] $h_{BC}=H_{BC}-63{,}85$ [mm] h_{bc}= [mm]
	D_v	D_v= [mm]

9. SHEARING	
Remove water supply pipe from Valve 05 due to removing all obstacles to rotation of lower plate (LP). Check again if Helping Rings are unscrewed and removed and Vertical Displacement Sensor is protected.	
Valve 04 has to be closed during test, so pore pressures could be measured only by PPT1.	
Waiting for input	**Waiting for input**
Valve 02 has to be closed during test	
Fill data form pannels for Data acquisition and Stress control with data apropriate for this specific test and start data acquisition.	
Start stress control after everything is checked and prepared in earlier steps.	
Stop data aquisition after s_{ss} and t_{ss} is reached	
Measure sample height h_{bc} before deinstalation.	
Measure vertical deformation height before deinstalation.	

10. DEINSTALATION		
Check	Task	Remarks
	Release s & t to zero	
	HS 3x	
	Uninstall VDS, VLC, disconnect SLC	VLC by Normal stress control on MCU: Manual -> Start -> Unlock button and turn down (right side) until maximum -> Lock protection screw -> Unscrew central ring -> Lift up VLC to original position -> press stop button
	Unlock Lifter and connect with VLC	
	Take out 12 screws	
	Pull up LP and put back to the neutral position	
	Remove sample, filter paper and tissues	
	Remove OR and IR	
	Gap to 0	
	Gap OFF	

10. DEINSTALATION	
Release stresses by computer control and manually to 0 [kPa]	
Put Helping Screws (3x golden ones) before removing Loading Plate	
Uninstall Vertical Displacement Sensor, Vertical Load Cylinder and disconnect Shear Load Cells	
Pull up LP with remote control buttons and put back lifter to neutral position (lock when in neutral position)	
Remove sample with vacuum cleaner, or manually (if sample measurements are necessary to be done) and put it in a paret.	
Remove Outer and Inner Ring and clean them.	
Decrease Gap to 0 by Gap Control button	
Gap OFF	

References

Bishop AW, Green GE, Garga VK, Andersen A, Brown JD (1971) A new ring shear apparatus and its application to the measurement of residual strength. Géotechnique 21(1):273–328

Bromhead EN (1979) A simple ring shear apparatus. Ground Eng 12 (5):40–44

Garga V, Infante Sedano JA (2002) Steady state strength of sands in a constant volume ring shear apparatus. Geotech Test J 25(4):414–421

Hungr O, Morgenstern NR (1984) High velocity ring shear tests on sand. Géotechnique 34(3):415–421

Savage SB, Sayed M (1984) Stresses developed in dry cohesionless granular materials sheared in an annular shear cell. J Fluid Mech 142:391–430

Sassa K (1984) The mechanism starting liquefied landslides and debris flows. In: Proceedings of 4th international symposium on landslides, Toronto, June, pp 349–354

Sassa K (1992) Access to the dynamics of landslides during earthquakes by a new cyclic loading high-speed ring-shear apparatus (keynote paper). In: 6th international symposium on landslides, "Landslides", A.A. Balkema, Christchurch, 10–14 Feb, vol 3, pp 1919–1937

Sassa K (1997) A new intelligent-type dynamic-loading ring-shear apparatus. Landslide News 10:33

Sassa K, Fukuoka H, Wang G, Ishikawa N (2004) Undrained dynamic-loading ring-shear apparatus and its application to landslide dynamics. Landslides 1(1):7–19

Sassa K, He B, Miyagi T, Strasser M, Konagai K, Ostric M, Setiawan H, Takara K, Nagai O, Yamashiki Y, Tutumi Y (2012) A hypothesis of the Senoumi submarine megaslide in Suruga Bay in Japan—based on the undrained dynamic-loading ring shear tests and computer simulation. Landslides 9(4):439–455

Sassa K, Dang K, He B et al (2014) A new high-stress undrained ring-shear apparatus and its application to the 1792 Unzen–Mayuyama megaslide in Japan. Landslides 11:827–842. https://doi.org/10.1007/s10346-014-0501-1

Sassa, K., Dang, K. (2018) Text tool 0.081-1.1 landslide dynamics for risk assessment. In: Sassa K, Tiwari B, Liu K, McSaveney M, Strom A, Setiawan H (eds) Landslide dynamics-ISDR-ICL landslide interactive teaching tools. Springer, pp 1–79

Setiawan H, Sassa K, He B (2018) TXT-tool 3.081-1.6: manual for undrained dynamic-loading ring shear apparatus. In: Sassa K et al (eds) Landslide dynamics: ISDR-ICL landslide interactive teaching tools, vol. 2: testing, risk management and country practices. Springer, Cham, pp 321–350. https://doi.org/10.1007/978-3-319-57777-7_18

Tika TM (1989) The effect of rate of shear on the residual strength of soil. PhD Thesis, University of London (Imperial College of Science and Technology), 494p

How to Teach Remotely the Vegetation Works to Protect Slopes Against Mass Wasting: A Case of Using Video Materials in Bhutan

Kiyoharu Hirota, Yasuhisa Suganuma, Tomoharu Iwasaki, and Takeshi Kuwano

Abstract

This paper describes the outline of the video tutorial prepared for vegetation workers and relevant officers in Bhutan to learn how vegetation works are to be done in remote areas. The Japan International Cooperation Agency (JICA for short) took a project on cutting unstable slopes in Gangthangkha, Wangdue, Bhutan, so that they should be gentler than 45° to improve slope stability with vegetation works. Particularly stabilizing slopes along Prime National Highway No. 1 (PNH-1 for short) was the overriding priority because slope failures along this highway have reportedly occurred in rainy seasons. Before vegetation works were carried out on the studied slope of the project, the authors conducted germination tests to choose seeds and methods suitable for the vegetation works. They chose Paspalum Atratum, Ruzi grass, and GM mixed (Grass Mixture seed formulating of Cock's foot 70% and Italian Ryegrass 30% of 100 kg) based on their test results. The soil thickness associated with sowing was set at 5 cm. The authors tried the following types of vegetation methods on the studied site. Type A is arranging on the slope stripes of soil mixed with seeds and fertilizer, Type B is spreading out a five cm-thick seeds-mixed soil layer over the slope, and Type C is transplanting germination beds. In conclusion, Type C is the best in terms of its performance because the whole slope is quickly covered with already grown plants. In Type B, it is not until grass covers the entire slope that the slope is finally stabilized. Type A is good for seeds-mixed soil stripes, but it takes time for the grass to spread gradually over the whole slope.

Keywords

Vegetation works • Cut slope • Video materials

1 Introduction

This teaching tool is a video medium that can help workers to learn how to perform vegetation works on cut slopes. The video has been prepared as a part of the JICA's Project "The Project for Capacity Development on Countermeasures of Slope Disaster on Roads in Bhutan." Behind this video production was the impact of the COVID-19 pandemic, which forced the JICA expert team including the authors to return to Japan in February 2020, during the project. The video was successful in enabling on-site vegetation works management remotely. This article introduces the outline of the vegetation works.

2 Outline of the Vegetation Works

The site of the vegetation works is in Gangthangkha, Wangdue where Lobeysa Regional Office (Lobeysa RO) of the Department of Road in Bhutan (Fig. 1).

Supplementary Information
The online version contains supplementary material available at https://doi.org/10.1007/978-3-031-18471-0_26.

K. Hirota (✉) · T. Iwasaki · T. Kuwano
International Consulting Department, Kokusai Kogyo Co., Ltd., Tokyo, 169-0074, Japan
e-mail: kiyoharu_hirota@kk-grp.jp

T. Iwasaki
e-mail: tomoharu_iwasaki@kk-grp.jp

T. Kuwano
e-mail: takeshi_kuwano@kk-grp.jp

Y. Suganuma
Kosai Consultants Co., Ltd., 5114 Washizu, Kosai City, Shizuoka, 431-0431, Japan
e-mail: suganuma@kosai-c.com

I. Alcántara-Ayala et al. (eds.), *Progress in Landslide Research and Technology, Volume 1 Issue 2, 2022*, Progress in Landslide Research and Technology,
https://doi.org/10.1007/978-3-031-18471-0_26

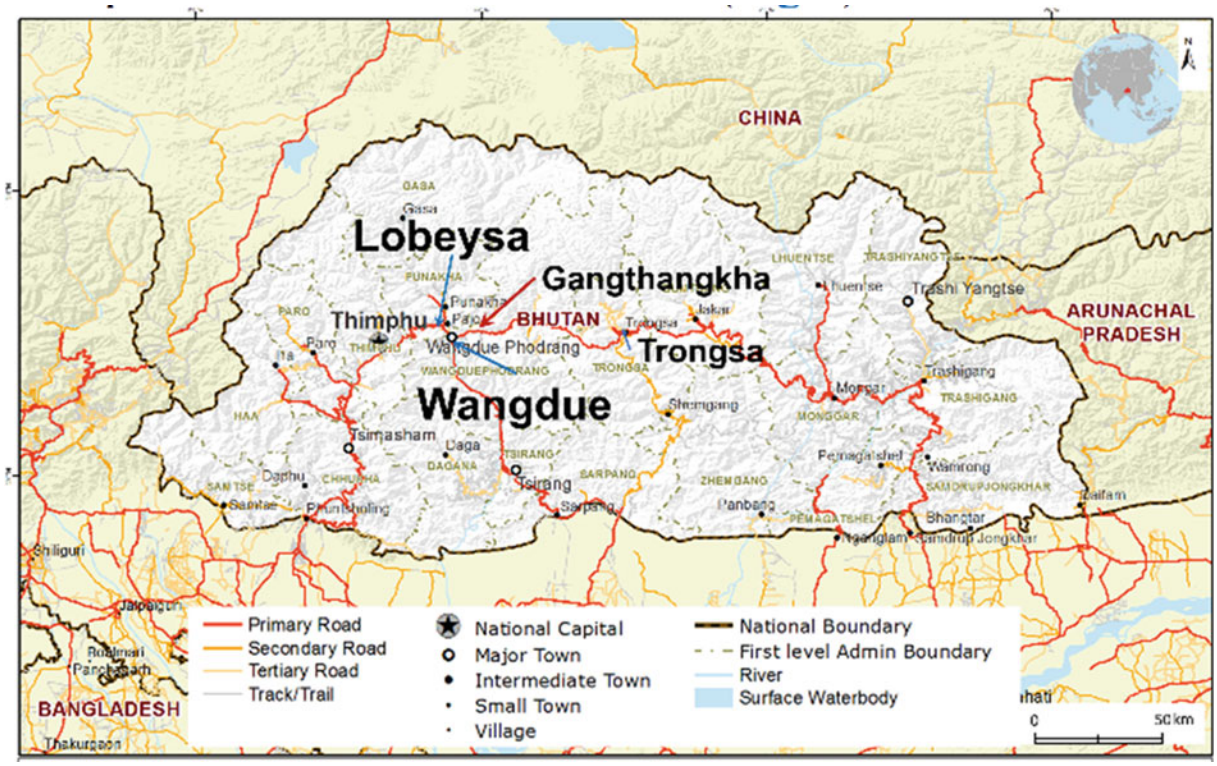

Fig. 1 Map of Bhutan with locations relevant to the JICA project (based on Bhutan Road Network Map (World Food Programme 2017))

The vegetation works were part of the output of the JICA's bioengineering project, which began with cutting a slope at a stable angle for it and then installing drainage works as shown in Fig. 2.

Three planting methods were examined: Type A is linearly planting, Type B is overall planting, and Type C is the transplantation of a germination bed. For all, jute nets were stuck over the germination beds with wooden stakes to stabilize them (Fig. 3).

The Department of Livestock of the Ministry of Agriculture and Forests, Bhutan, provides a list of perennial grass seeds suitable for vegetation works (Table 1). The authors have chosen (1) Paspalum Atratum Var.CIAT 26986 (*Paspalum atratum*), and (2) Ruzi Grass (*Brachiaria ruziziensis*) (Fig. 4). Also used were (3) GM mixed seeds composed of 30% Italian ryegrass (*Lolium multiflorum*) and 70% Cock's-foot, var. Amba (*Dactylis glomerate*) (Fig. 5).

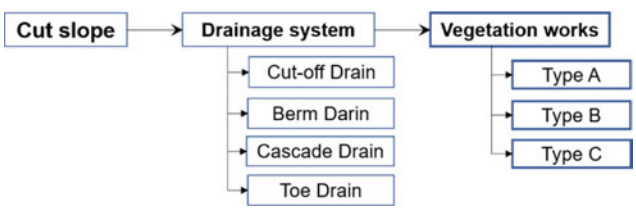

Fig. 2 Vegetation workflow chart (Type A: linearly planting, B: planner planting, and C: transplanting of germination bed)

The table says the altitude appropriate for planting GM mixed seeds would be 2000–3000 m above sea level (MaSL for short) from an agroecological viewpoint. This altitude is higher than the study site. However, the seeds are widely used in Bhutan's farmlands.

Methods for Germination Test

Before starting the vegetation works, the authors conducted 8 different germination trials, using three seed types to determine the suitable seed and soil thickness for the vegetation works (Fig. 6).

Beginning the germination test, all three seed types were well germinated for a little two weeks (Fig. 7). In particular, 5 cm thick seedbed shows a good sprouting condition (left side of Fig. 7b).

After cutting the slope, the vegetation works, Types A, B, and C, were carried out. Figure 10 (in Video Narration) illustrates these three types of planting. As said, Type A places stripes of seedbeds on the slope, Type B covers the slope with a wide seedbed, and Type C transplants germination beds. In each type, two kinds of seeds, i.e., *Paspalum atratum* and Ruzi grass were planted on the upper and lower parts of the slope, respectively.

In Type C, the grass to transplant was first removed in stripes from the plant bed (Fig. 8).

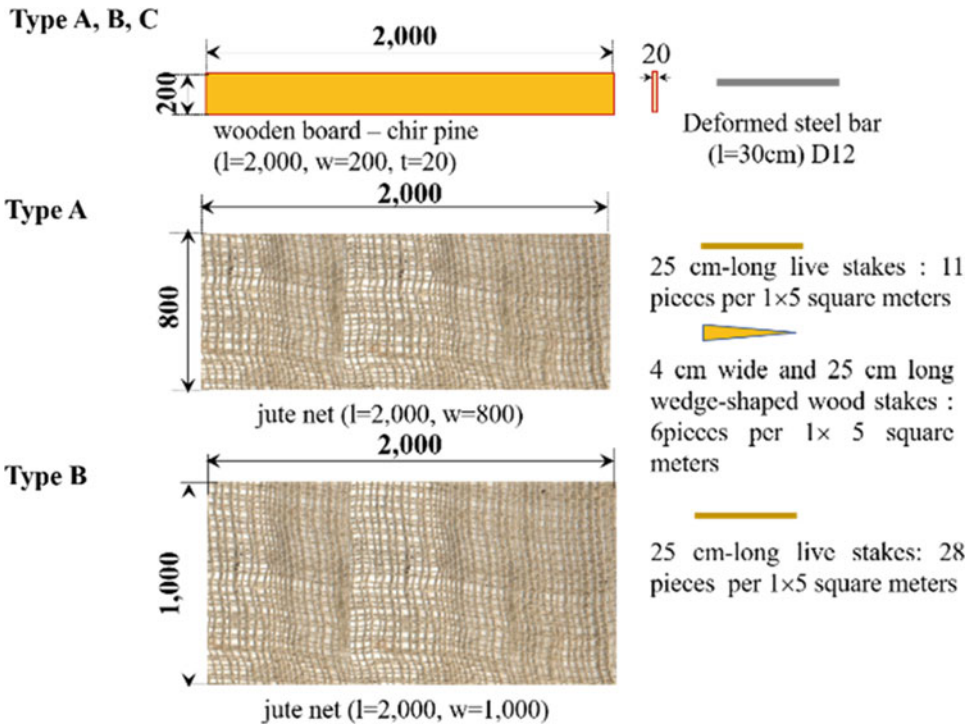

Fig. 3 Materials to stabilize soil beds containing seeds and fertilizer

Table 1 List of seeds for vegetation works (Data provided by DoL)

Seeds (Scientific name)	Yield potential (Dry matter)	Maturity for grazing	Recommended agro-ecology (MaSL)
Paspalum Atratum Var.CIAT 26986 (*Paspalum atratum*)	2.9–3	1 yr (Perennial)	< 1500
Ruzi grass (*Brachiaria ruziziensis*)	2.8–3.2	1 yr (Perennial)	500–2000
Italian Rye grass Var.Lipo (*Lolium multiflorum*)	1.2–2.2	1 yr (Perennial)	2000–3000
Cocks foot Var.Amba (*Dactylis glomerate*)	0.8–1.2	1 yr (Perennial)	2000–3000

DoL: Department of Livestock, yr: year, MaSL: meter above sea level

Fig. 4 Photos of seeds (left: Paspalum Atratum, right: Ruzi grass)

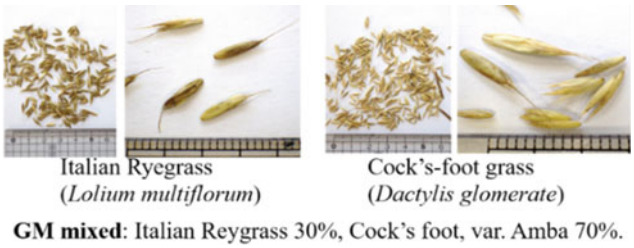

Fig. 5 Photos of seeds for GM mixed (left: Italian Ryegrass, right: Cock's foot grass)

In Type C, scraping grass is done before transplanting (Fig. 9).

3 Video Narration

Narration 1 (see Fig. 10)

There are three types of planting method (Fig. 10).

Type A is linearly planting, Type B is overall planting, and Type C is the transplantation of a germination bed.

Type A is a method that wraps all containing seeds and fertilizer with a Jute net.

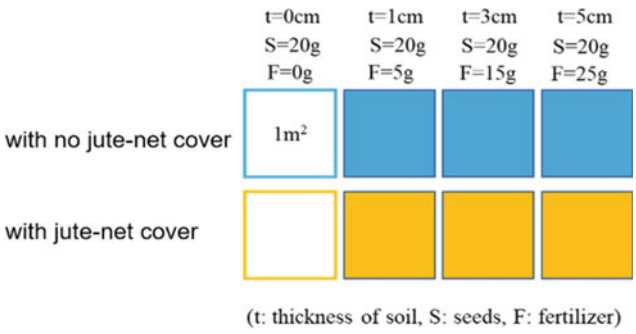

Fig. 6 Germination test cases

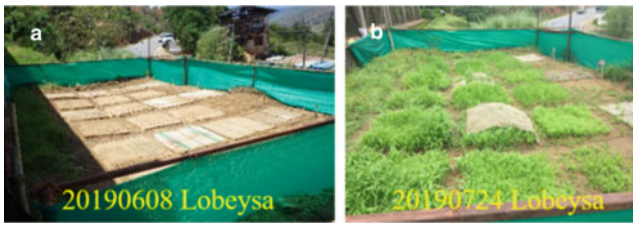

Fig. 7 Germination test at the yard of Lobeysa R.O. (**a**: Photo taken on June 8, 2019, **b**: Photo taken on July 24, 2019)

Type B is a method that lays soil containing seeds and fertilizer on a slope with a thickness of 5 cm and covers it with a Jute net.

Type C is a method that transplants germination beds grown on the site of the Lobeysa Regional Office and pastes it on the slope.

Preparation Work for Type A and B

Narration 2 (see Fig. 11)

As preparatory work, please place level strings in both Type A and Type B areas (Fig. 11a).

The level strings are installed at the position where the wooden boards are installed. Since wooden boards are installed at 1 m intervals, level strings will be installed at the position of the red line in the figure (Fig. 11b).

Narration 3 (see Fig. 12)

The length of the level strings should be a little longer than the length of 10 m for both Type A and Type B. The lowest

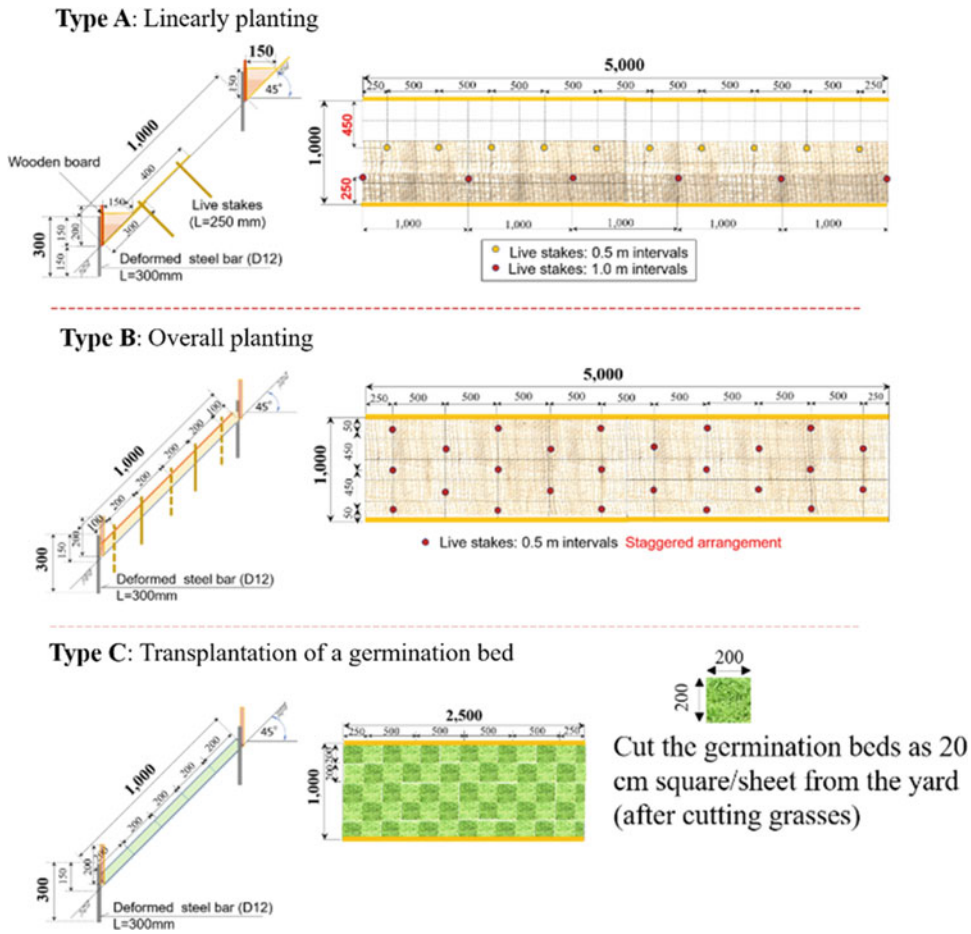

Fig. 8 Details of three vegetation works (left: cross-sections, right: front views)

Fig. 9 Plant bed for Type C vegetation works. The grass to transplant is first removed in stripes from the plant bed

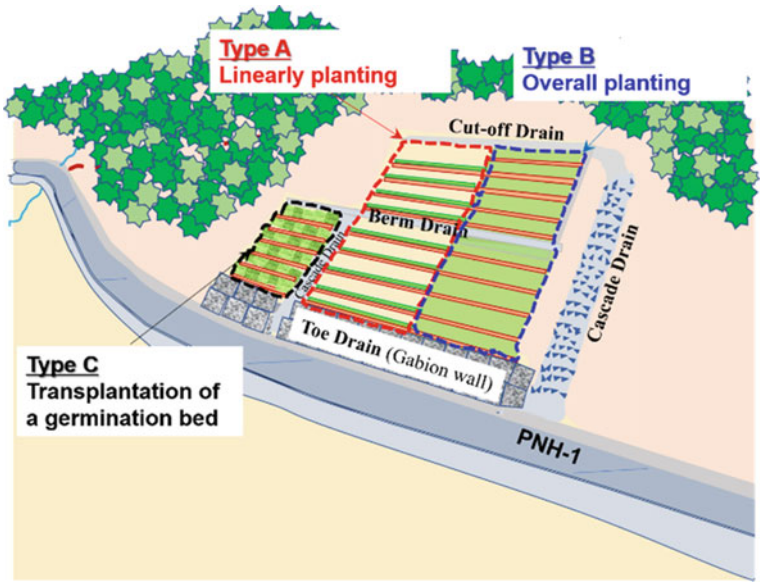

Fig. 10 Bird's-eye view of Types A, B, and C

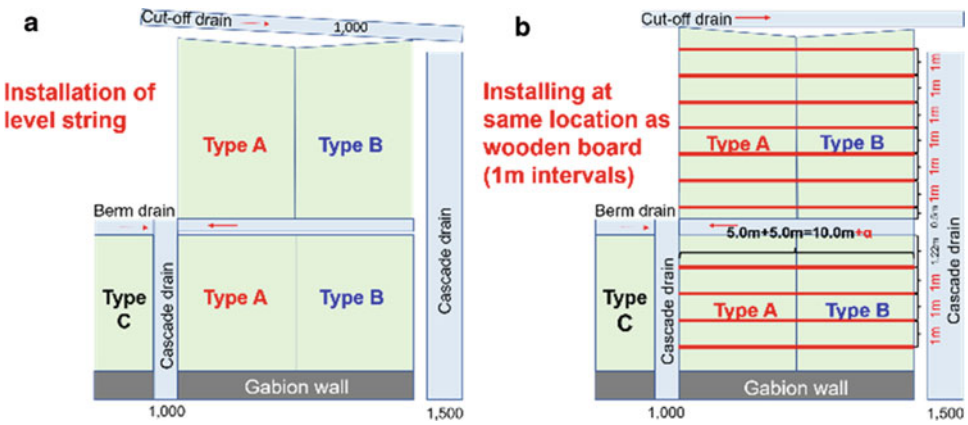

Fig. 11 Layout of Types A, B, and C preparatory works

level string of the lower slope is installed at the same elevation as the top of the gabion wall.

The lowermost level strings of the upper slope are installed 50 cm higher than the elevation of the berm drain (Fig. 12a). Next, please install deformed steel bars. The purpose of installing the deformed steel bar is to fix the wooden board on the slope, so please install it below the wooden board. All deformed steel bars are D12 and the length is 30 cm. Please set half of the bar 15 cm inside the ground (Fig. 12b). The deformed steel bar is installed every 1 m. The total length of type A and type B is 10 m, so if you install four 2.5 m long wooden boards, please use three deformed steel bars for each wooden board. Therefore, there will be a space of 25 cm at both ends of the wooden board

Fig. 12 Details of Type A

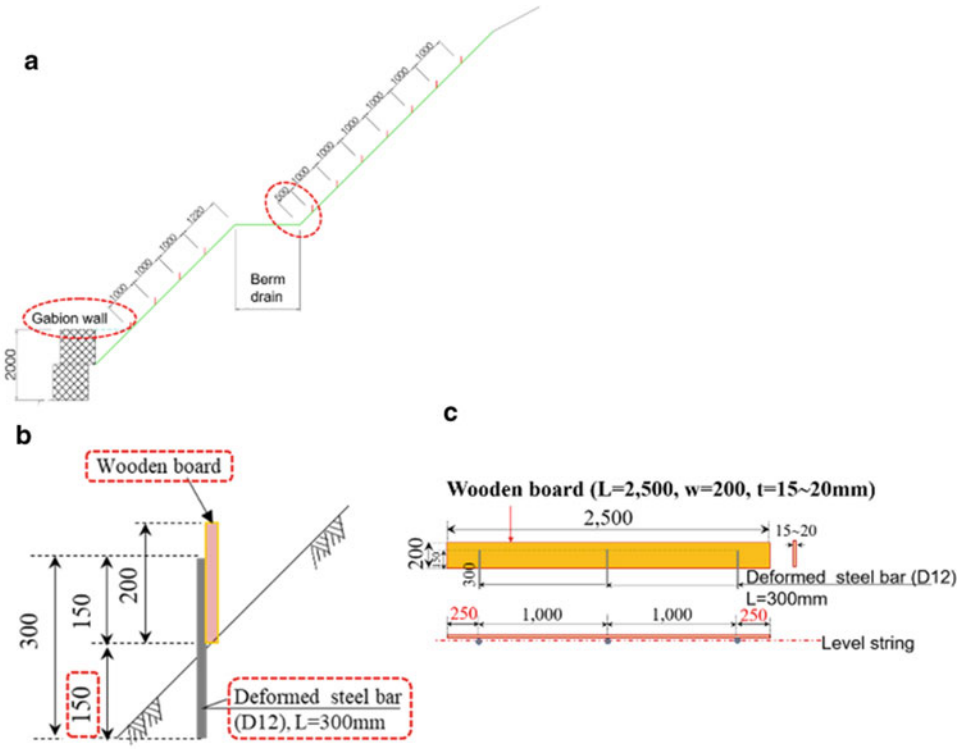

(Fig. 12c). Please prepare the soil for Type-A by mixing soil, seeds and fertilizer in advance. The mix proportion is 400 g of seeds, and 500 g of fertilizer per cubic meter of soil.

Narration 4 (see Fig. 13)

Two types of seeds are used for both Type A and Type B: *Paspalum atratum* and Ruzi grass. As shown in the figure, *Paspalum atratum* is planted on the upper slope and Ruzi grass is planted on the lower slope (Fig. 13).

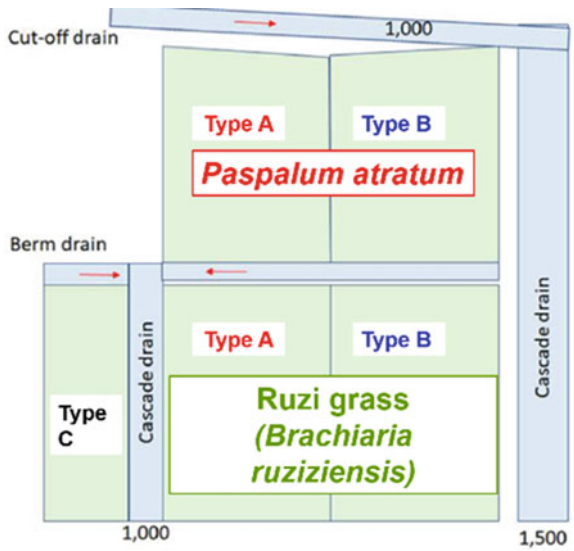

Fig. 13 Vegetation pattern with three different plants

Instruction-1 How to Install "Type-A"

Narration 5 (see Fig. 14)

Type A is a method of wrapping a triangular soil containing seeds and fertilizer with a Jute net, as shown in Fig. 14. Procedure of Type A is as shown here.

Firstly, installing a deformed steel bar, installing wooden board, placing a jute net, premixing seeds, soil, and fertilizer, placing soil portion, placing soil with seeds and fertilizer, folding and covering with jute net, and finally fixing jute net with live stakes.

Narration 6 (see Fig. 15)

Since the width of the jute net is 1 m, the dimensions when wrapping the soil are as shown in Fig. 15.

Narration 7 (see Fig. 16)

First, please place it 30 cm on the slope (Fig. 16a).

Next, please put the soil on the Jute net. The total depth of the soil is 15 cm. Please place only soil in the lower 10 cm part and then place mixed soil with seeds and fertilizer in the upper 5 cm part (Fig. 16b).

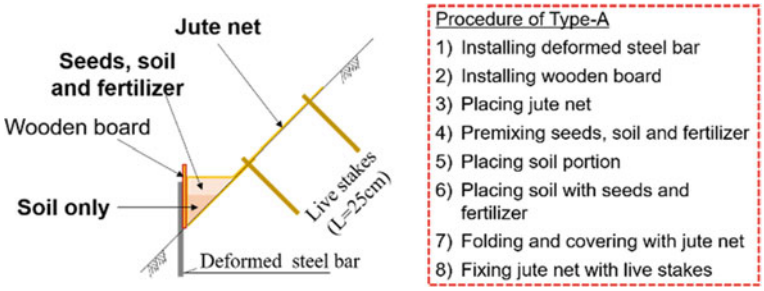

Fig. 14 Details of Type A. Contents of Type A-procedure are as follows: (1) Installing deformed steel bar, (2) Installing wooden board, (3) Placing jute net, (4) Premixing seeds, soil and fertilizer, (5) Placing soil portion, (6) Placing soil with seeds and fertilizer, (7) Folding and covering with jute net, and (8) Fixing jute net with live stakes

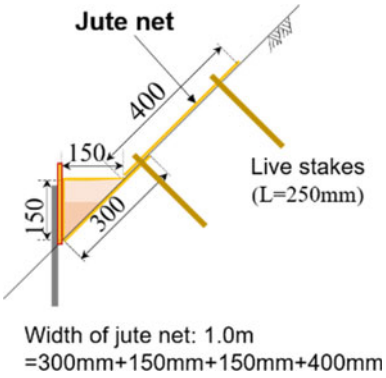

Fig. 15 Section view of Type A

Next, please fold the Jute net toward upper side and cover the soil on the slope (Fig. 16c).

Narration 8 (see Fig. 17)

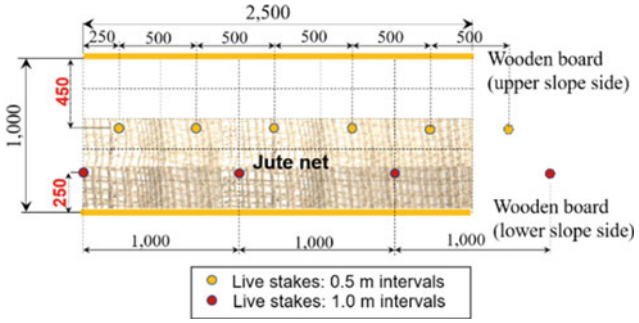

Fig. 17 Front view of Type A

Live stakes are installed to fix the Jute net on the slope. As shown in this figure, please install them at 50 cm intervals at 45 cm below the wooden board of the upper slope side. On the other hand, please install them at 1 m intervals at 25 cm above the wooden board of the lower slope side. You can also use wood stakes instead of live stakes (Fig. 17).

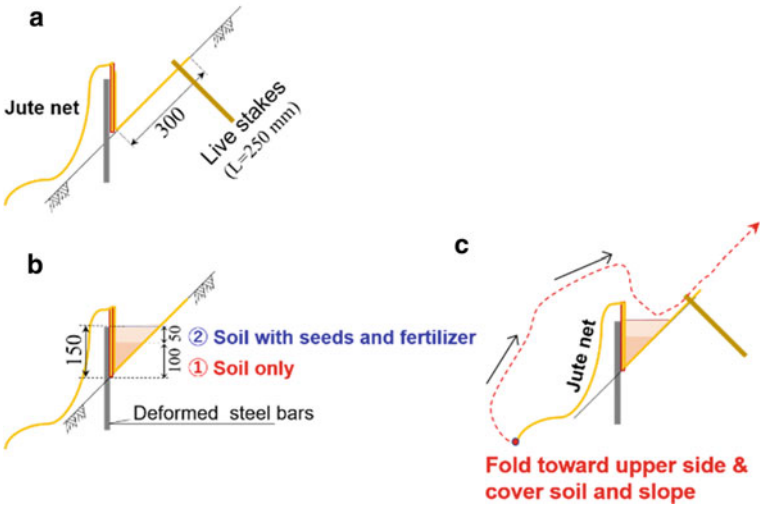

Fig. 16 Section view of Type B (**a**: setting a jute net, **b**: placing soil with seeds and fertilizer, **c**: folding a jute net)

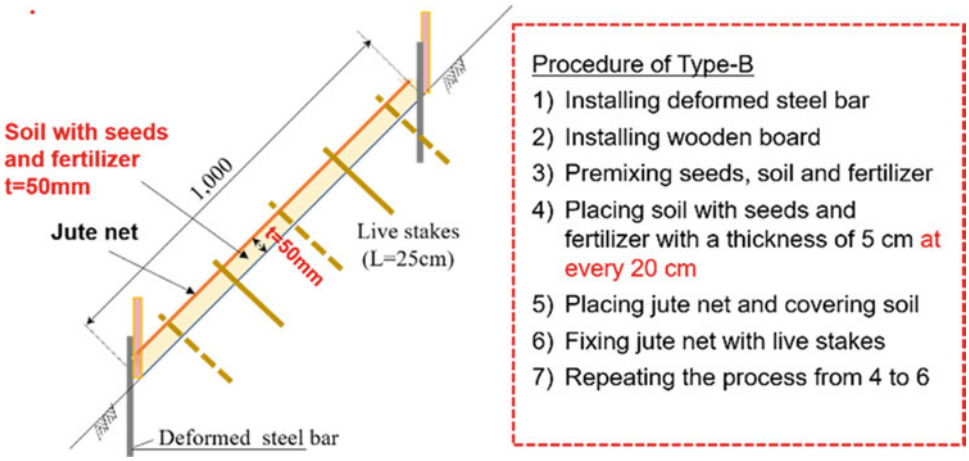

Fig. 18 Section of Type B. Contents of Type B-procedure are as follows: (1) Installing deformed steel bar, (2) Installing wooden board, (3) Premixing seeds, soil and fertilizer, (4) Placing soil with seeds and fertilizer with a thickness of 5 cm at every 20 cm, (5) Placing jute net and covering soil, (6) Fixing jute net with live stakes, and (7) Repeating the process from 4 to 6

Video Performance 1: Demonstration-1 How to install "Type A"

Instruction-2 How to Install "Type-B" (title)

This part of the video is only subtitled with no voice.

Narration 9 (see Fig. 18)

In Type B, we use a jute net to cover and stabilize a 5 cm thick soil bed containing seeds and fertilizer, as shown in Fig. 18. The work can be done following the steps shown below:

(1) makeup frames for a soil bed with deformed steel bars and wooden plates, (2) place a 5 cm-thick 20 cm-wide seeds/fertilizer-mixed soil stripe one after another at every 20 cm interval, (3) cover and stabilize the whole soil bed with a jute net.

Narration 10 (see Fig. 19)

Please spread the soil with seeds and fertilizer with a thickness of 5 cm evenly on the slope, and cover it with a jute net. Please conduct this procedure at every 20 cm interval (Fig. 19a). After installing the Jute net, please put live stakes to fix the Jute net on the slope (Fig. 19b).

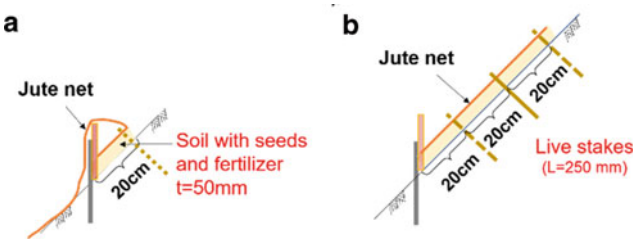

Fig. 19 Outline of Type B in section (Image **a** is the first stage of work and Image **b** shows a continuous work process)

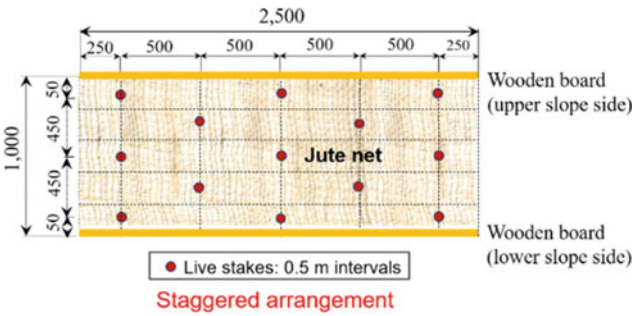

Fig. 20 Front view of Type B

Live stakes should be installed at 50 cm intervals in a staggered arrangement, as shown in Fig. 20.

Video Performance 2: Demonstration-2 How to install "Type B"

Instruction-3 How to Install "Type-C" (title)

This part of the video is only subtitled with no voice.

Narration 11 (see Fig. 21)

Type C is a method that transplants germination beds grown in the yard of the Lobeysa Regional Office and pastes them on the slope. Procedure of Type C is as shown here. Before transporting the grass materials, please cut the long grass at the yard on Lobeysa Regional Office. And then, please cut the grass into 20 cm^2 with at least 5 cm thickness of soil and transport it to the construction site. As preparation work,

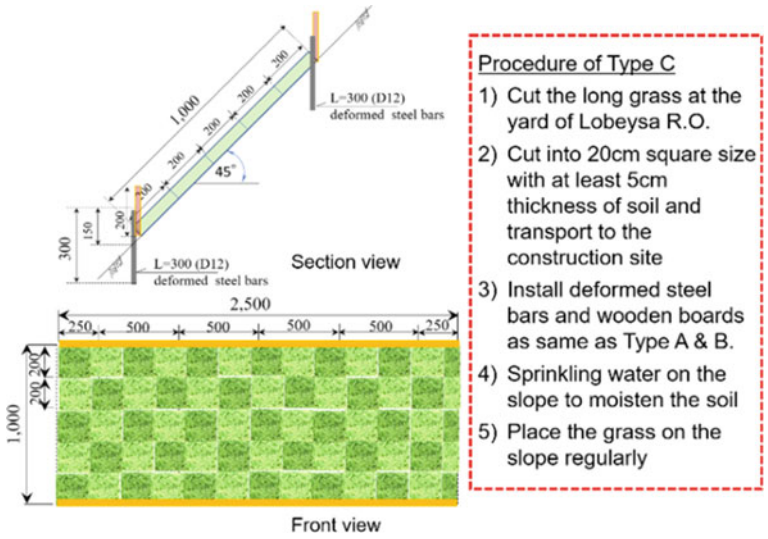

Fig. 21 Section and front views of Type C vegetation works. Contents of Type C-procedure are as follows: (1) Cut the long grass at the yard of Lobeysa R.O., (2) Cut into 20 cm^2 size with at least 5 cm thickness of soil and transport to the construction site, (3) Install deformed steel bars and wooden boards as same as Type-A and B, (4) Sprinkling water on the slope to moisten the soil, and 6) Place the grass on the slope regularly

Fig. 22 Sequence of events at the site of vegetation works, Gangthangkha, Wangdue (lat 27° 29′ 4.87″ N, long 89° 54′ 17.24″ E, alt 1309 m, **a** slope before vegetation works on May 29, 2019, **b** finished vegetation works on May 30, 2020, **c**, and **d** photos on June 26, 2020, about a month after the vegetation works, and on October 31, 2020, respectively)

please install deformed steel bars and wooden boards like Type-A and B. And please sprinkle water on the slope to moisten the soil, and finally, please the grass on the slope regularly (Fig. 21).

Video Performance 3: Demonstration-3 How to install "Type C"

This part of the video is only subtitled with no voice.

4 Sequence of Works

The target slope at Gangthangkha had occasionally been collapsing little by little due to mass wasting over time (Fig. 22a). The slope had an average angle of about 40° with its upper part much steeper. The slope could have been cut at a gentle angle of less than 40°, but it could have yielded a huge amount of soil to cut, making the work unrealistic. Therefore, the slope was cut to stay below the upper limit of 45° for vegetation works, and gabions retained the toe part of the cut slope. This work was then followed by vegetation works (Fig. 22b). Almost one month after the vegetation works were completed, germinations were observed at all the vegetation work sites for Types A, B, and C (Fig. 22c). Glasses have grown remarkably over three months since the vegetation works completed (Fig. 22d).

5 Summary

The video medium that was prepared during JICA's project successfully helped workers to learn how to perform vegetation works on cut slopes in Bhutan. In this project, three types of vegetation methods, Type A, Type B, and Type C, were examined. Out of these three methods, Type C was proven to be the most efficient in terms of its performance, transplanting germination beds directly on the target slope, though it requires a suitable nearby grass plant bed. In both Types B and C, it takes time for the target slope to be covered with grass. However, Type B would be preferable, because bare earth can remain exposed for a long time in Type A where only seed-and-fertilizer-mixed soil stripes are placed on the slope. Further studies will be necessary to broaden the variation of the planting methods.

Acknowledgements In this project, we would like to thank the following engineers for everything from seed selection to construction. Thanks to Mr. Yuji Nakano (Nakano Research Institute of Greening Technology), who taught us many things such as how to select seeds, cut slopes, install drainage channels, and types of fertilizers. Thanks to Mr. Gyeltshen Wangdi as a chief engineer of the Lobeysa Regional Office for providing us with a germination test yard and supporting site management. Thanks to Mr. Tshering as a Project Manager of Floriculture and Amenity Landscaping Center (FALC), for giving us information about suitable seeds and fertilizer on the site in Lobeysa. Thanks to Dr. Atsuko SATO of Civil Engineering Research Institute for Cold Region, for teaching how to transplant grass-growing areas. Thanks to Mr. Chimi Rinzin of the Department of Livestock, Animal Nutrition Division for giving us various seeds for vegetation works in Lobeysa, so we could try germination tests with pots and in the yard of Lobeysa R.O. and selected suitable seeds in Lobeysa smoothly. We would also like to thank the staff involved in the JICA Bhutan Office and Headquarters for their tremendous support for the project.

Reference

World Food Programme (2017) Bhutan road network. https://dlca.logcluster.org/display/public/DLCA/2.3+Bhutan+Road+Network. (browsed on 31 May 2019). Available maps can be obtained from logistics capacity assessments (LCAs)

Technical Notes and Case Studies

Landslide Inventory Map of the Valemount Area, British Columbia, Canada. A Detailed Methodological Description

Txomin Bornaetxea, Andrée Blais-Stevens, and Brendan Miller

Abstract

Landslides are a recurring geomorphological process in high mountainous areas like Valemount in the Canadian Rocky Mountains, British Columbia. The compilation of detailed information about the spatial distribution and characteristics of past landslides is essential for assessing future potential hazards. To provide baseline geoscience information to stakeholders and decision-makers, we carried out a landslide inventory that covers roughly 1200 km^2. Using visual interpretation of aerial orthophotos, a digital elevation model of 5 × 5 m resolution and satellite imagery, we compiled up to 1286 landslides and classified them into 11 categories and three levels of certainty. The current paper describes the mapping methodology and summarizes our results.

Keywords

Landslide inventory • Air photo-interpretation • LiDAR • Valemount • British Columbia

1 Introduction

Natural Resources Canada's Public Safety Geoscience Program (PSG) at the Geological Survey of Canada undertakes research on geohazards such as landslides, earthquakes, tsunamis, volcanoes, and space weather. PSG knowledge products provide baseline geoscience information to stakeholders and decision-makers to reduce the risk to the population and critical infrastructure.

In accordance with the PSG mandate, a landslide inventory was created along the transportation corridor between Moose Lake and Tête Jaune Cache village and continuing north along the Fraser River to Dunster, in east central British Columbia (Fig. 1). The study area covers roughly 1200 km^2 and includes both sides of Robson Valley extending eastward and upstream toward Jasper National Park, Alberta. The study area covers a key transportation corridor in which highways 16 and 5, Canadian National Railway, and an oil pipeline are located. The permanent population density in the study area is low, but the population can increase during summer months by tourists visiting the area.

The elevation within the study area ranges between 720 and 2800 m above sea level. Slope gradient varies from <2° on the alluvial plains at lower elevations to >80° in the high mountainous areas, with the average slope being 22.5°. Upper Proterozoic rocks of the Miette Group underlie the study area (Mountjoy 1980; Massey et al. 2005), with coarse clastic sedimentary rocks including sandstone, conglomerate, argillite, phyllite, diamictite and minor limestone exposed at lower elevations; while mudstone, siltstone and shale are exposed at higher elevations. In the northwest boundary of the study area, the McNaughton Formation is observed, consisting of massive quartz sandstone, siltstone, and minor pebble conglomerate.

The surficial materials on the valley's floor are composed mainly of a mixture of gravelly silts to clayey sands with various quantities of cobbles and boulders, while in the upper zones, colluvium (including debris, talus and scree) and morainal deposits predominate (Ministry of Transportation and Highways (MOTI 1999). The study area is located in a region of low to moderate seismic hazard (NRCan 2015).

T. Bornaetxea (✉)
Department of Geology, University of the Basque Country (UPV/EHU), Leioa, Spain
e-mail: txomin.bornaetxea@ehu.eus

A. Blais-Stevens
Natural Resources Canada, Ottawa, ON, Canada
e-mail: andree.blais-stevens@nrcan-rncan.gc.ca

B. Miller
Ministry of Forests, Prince George, BC, Canada
e-mail: Brendan.Miller@gov.bc.ca

I. Alcántara-Ayala et al. (eds.), *Progress in Landslide Research and Technology, Volume 1 Issue 2, 2022*, Progress in Landslide Research and Technology,
https://doi.org/10.1007/978-3-031-18471-0_27

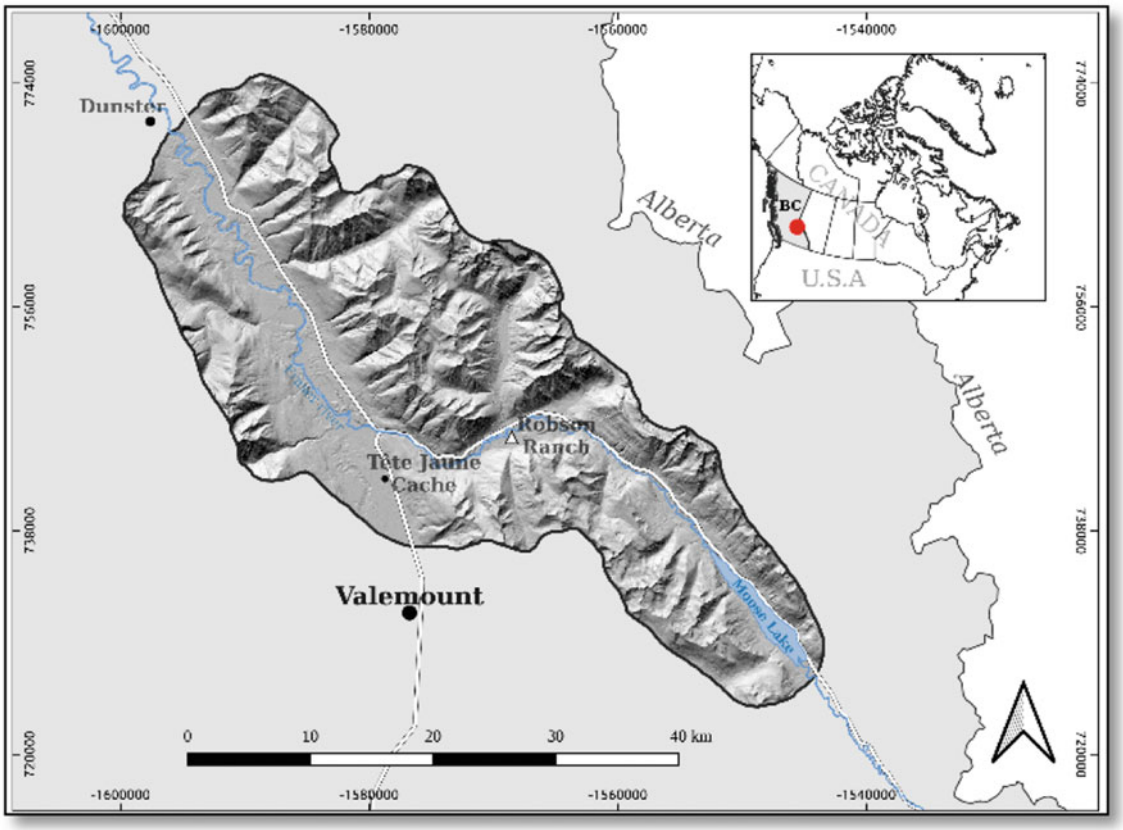

Fig. 1 Location map of the study area

The average annual precipitation at the Robson Ranch weather station is 594 mm (372.3 mm rain and 221.7 mm snow-water equivalent; Environment Canada 2022). Robson Ranch weather station is located at the bottom of the valley and may not accurately reflect the precipitation accumulation at higher elevations (Fig. 1).

Historically, the study area has witnessed several landslide events that have blocked Highway 16 and have caused damage to infrastructure. According to a report commissioned by the BC Ministry of Transportation and Highways (1999) "*several debris flows have occurred in Goslin Creek over the past 50 years*" including a May 1993 debris flow that reached Highway 16 leaving a deposit of up to 300,000 m^3. Later studies also documented the occurrence of several large deep-seated bedrock landslides in the upper basins of both Spittal and Leona creeks, with estimated return intervals of 100–500 years (MOTI 1999). Furthermore, at least six debris flow events took place between 1986 and 1997 within those two steep channels. In 2015, the BC Ministry of Transportation and Infrastructure commissioned a landslide hazard assessment for the Leona Creek landslide (BGC Engineering Inc. 2015). To provide context for their assessment, BGC Engineering Inc. (2015) conducted an inventory of nearby large ($\geq$ 1,000,000 m^3) rock landslides and documented 53 events.

These local studies indicate frequent occurrences of landslides in the study area, attesting to the need for a regional hazard assessment approach. However, there is no published regional landslide inventory available. Therefore, the objective of this study is to fill this gap by compiling a landslide inventory map that encompasses a portion of the Upper Fraser River valley.

Within, we provide a description of the data used and methodology followed to create the landslide inventory map. Our landslide inventory map (see Appendix 1, Fig. 8) is publicly available in PDF format (Bornaetxea et al. 2022) or as digital shapefiles (.shp).

2 Data

Data used for the interpretation include a digital elevation model (DEM) derived from LiDAR data, orthophotos, and geological maps. Additionally, Google Earth satellite

imagery provided support data. Analysis of the data was undertaken using QGIS software (QGIS Development Team 2022).

LiDAR Based DEMs

Since there is no publicly accessible high-resolution DEM in the study area, LiDAR data were obtained from three different sources, and combined to generate a 5 × 5 m resolution DEM (Fig. 2). This was achieved using the pdal library for laz file management and gdal library for the raster layers transformation (PDAL Contributors 2020; GDAL/OGR Contributors 2022). Details about the specific procedure followed to obtain the DEM are available in Appendix 2.

The DEM was then used to derive additional layers for use in our analysis, including contour maps with elevation intervals of 10 and 50 m, and shaded relief layers with variable azimuth light angles (commonly 45, 180, and 315°) to optimize the light orientation for terrain interpretation of different locations in the study area.

Orthophotos

Two orthophotos covered the study area (Fig. 2), 83D and 83E (1:250,000; NTS map area, 1 × 1 m resolution). These allowed for high-quality visualization of the terrain at 1:3000 scale. These color images were taken in 2005 and 2006, respectively.

Geology

As reference material, we used the Mount Robson and Canoe River geological maps published in 1980 (NTS 83E; Mountjoy 1980) and 2007 (NTS 83D; Murphy 2007) respectively, at 1:250,000 scale.

3 Methods

We prepared the landslides inventory following visual photo interpretation conventions (Guzzetti et al. 2012). Above all, the quality of the orthophotos, together with the shaded relief images allowed us to detect landslide features based on a set of characteristics such as shape, size, color, mottling, texture, pattern, site topography, and setting.

The high-resolution shaded relief images facilitate the recognition of the type of movement even in forested areas, as is evidenced from observable inactive rotational and translational landslides (Appendix 1), which would otherwise be difficult to detect using only photos (c.f. Ardizzone et al. 2007; van den Eeckhaut 2007). Debris flow and fan deposits were best observed by overlaying elevation contour lines on the hill shade images. On the other hand, the high-resolution orthophotos improved the detection of small and recent debris slides, colluvium deposits, and the delineation of debris flow initiation zones (Fell et al. 2008).

Nonetheless, we acknowledge that visual photo interpretation is considered as "*an empirical and uncertain technique that requires experience, training, a systematic methodology, and well-defined interpretation criteria*" (Guzzetti et al. 2012). For this reason, after the first landslide compilation, a verification process was completed to correct the preliminary results where needed. Furthermore, at the latter stage of the mapping process a limited field verification effort was done to confirm the accuracy of some of the mapped landslide polygons.

Landslide Type Definitions

Here, we provide a brief description of the landslide types and slope processes in the study area.

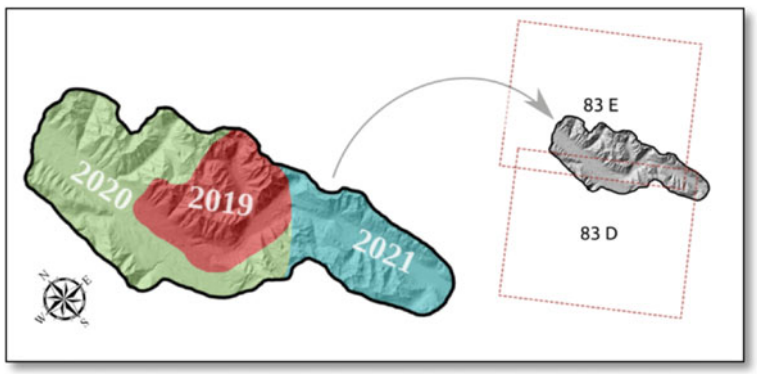

Fig. 2 Input data summary. Colored areas in the image on the left represent the different years in which LiDAR data were acquired. Dotted red lines in the image on the right represent the footprints of BC orthophotos, National Topographic System (NTS) 83D and E

Debris slide: A debris slide is a shallow movement of soil. The mobilized material usually begins moving with moderate cohesion but rapidly thereafter, cohesion diminishes and the slide mass lengthens. Usually, these landslides initiate near the crests of steep valleys. Their size typically ranges between 10^2 and 10^5 m^2.

Debris flow: A debris flow is a very rapid to extremely rapid surging flow of saturated debris in a steep channel (Hungr et al. 2014). Recognizable characteristics of debris flows include steeply sloping fans, and narrow and visibly eroded channels upstream of the fans with typically, boulder levees or train deposits on both sides of the channel. Usually, debris flows occur after periods of intense or prolonged precipitation, possibly coupled with rapid snow melt. They begin in steep sections of streams, often near the slope crests. They can be initiated by instability in the adjacent slopes, or by the instream mobilization of alluvium and debris. In a typical debris flow, the initial moving mass forms only a small portion of the final volume, with the remainder of the volume being entrained along the length of the channel (Hungr and Locat 2015).

Earthflow: Earthflows are defined as slow to rapid, flow-like movement of plastic clayey soils (Hungr et al. 2014). Thick accumulations of weathered clayey colluvium are the potential sites where earthflows can occur. Semicircular lobes at the toe of the deposits are a typical characteristic of these features.

Rock avalanche: A rock avalanche occurs when a large rock landslide on a mountain slope evolves into highly mobile mass of fragmented rock. It involves large volumes of failed material, in which the mobilized clasts collide with each other and share their momentum (Cruden and Varnes 1996).

Rockfall: A rockfall usually occurs on natural cliffs and excavation faces above transportation routes (Hungr and Locat 2015). They have rapid to extremely rapid rates of movement with the descent of material involving some freefall (Cruden and Varnes 1996). In mountainous areas, repeated detachment of rocks from steep slopes leaves exposed rock outcrops upslope and talus consisting of angular boulders and gravel at the base of the slope.

Rock slide: A slide involves displacement along a relatively thin surface of rupture (Cruden and Varnes 1996). Slides are subdivided into rotational, translational and compound types (Cruden and Varnes 1996).

Rotational slide: Rotational slides have concave upward rupture surfaces (spoon-shaped), with movement that rotates about an axis parallel to the contour of the slope (Sassa et al. 2017). The displaced mass usually moves in a relatively coherent fashion with little internal deformation. This type of slide often has an almost vertical head scarp.

Translational slides: Translational slides involve downslope movement along a relatively planar rupture surface with little or no rotation of the slide mass (Sassa et al. 2017). Translational slides commonly move along geological discontinuities such as faults, joints, bedding surfaces, or the contact between soil and rock or frozen soil. This type of slide may progress over considerable distances if the rupture surface is sufficiently inclined (Cruden and Varnes 1996).

Compound slides: Compound slides have attributes of both rotational and translational slide types (Cruden and Varnes 1996). Currently none of the mapped slides were classified as compound, but some Level 3 features may potentially be reclassified as such following field verification.

Deposit Type Definitions

To provide additional justification for our landslide mapping classifications, surficial deposits and associated landforms were also mapped. In the following paragraphs, we briefly describe their characteristics.

Coalescent debris deposit: Coalescent debris deposits are sites where multiple debris flow and debris slide deposits are superimposed upon one another, and perhaps on other sediments, forming a continuous deposit along the base of a slope.

Colluvium: Non-vegetated landslide deposits located at the base of slopes where there is no obvious source area. Colluvial deposits are generally composed of non-sorted, angular fragments of various sizes.

Talus: Rockfall deposits, comprising angular boulders, cobbles, and gravels that accumulate at the base of cliffs.

Landslide Zones

We delineated landslide paths by deposition, transportation and source, or potential source zones. Here, we provide descriptions of these zones.

Deposition: The deposition zone is where landslide sedimentation occurs. Here, the displaced material has lost kinetic energy due to a decrease in slope inclination. Deposition zones often display convex transverse profiles when compared to the adjacent, planar foot-slope area. A good example is a debris flow fan.

Transportation: The transportation zone is where colluvium transportation occurs. It connects the source and deposition zones. Additional material can be entrained from this zone during the passage of an event, leaving bare and elongated paths.

Source: The source zone is the area where displacement is initiated. Evidence for recent displacement at a source zone includes disrupted vegetation and exposed bedrock, or sediment outcrops. Depressions in the topography in steep areas are also a typical indicator of a source zone.

Potential source area: For debris flows in the study area, a source area might be the entire contributing drainage basin upstream of extensive debris flow fans. In such cases, we delineated the contributing basin as a "potential source area".

Ranking the Level of Certainty

With limited field verification, we qualitatively ranked each mapped polygon into three levels of certainty. These rankings are described below.

Level 1: This level is assigned when there is a high degree of certainty for our interpretation of the defined landslide type and delineated boundary.

Level 2: This level is assigned when either the landslide type is not certain, or its boundaries are not completely accurate due to resolution limitations of the DEM, orthophotos and satellite imagery.

Level 3: This level is assigned when there is a need for field verification. These circumstances might be the result of other possible mass-wasting processes forming the feature (e.g., rock glaciers, snow avalanche tracks, or anthropogenic slope modifications).

4 Results and Discussion

Figure 3 depicts the number of each type of mapped feature in the study area and provides the assigned ranking of the certainty level. A total of 1286 landslides and associated landforms were mapped. We found that debris flows are the most abundant feature (40%) followed by debris slides (14%) and rockfalls (11%). Furthermore, about 87% of features are assigned a certainty ranking of Level 1, 8.3% have certainty ranking of Level 2, and 4.7% have certainty ranking of Level 3.

Some specific features are entirely assigned certainty rankings of Level 2 or 3. For instance, all the coalescent debris deposits were ranked as Level 3, due to the difficulty in defining single deposits. A similar situation occurred for rock avalanches, where we classified them all as Level 2, due to difficulties in determining the nature of the mobilized material using air photo and satellite image interpretation. Differentiating between rock avalanches and rock slides was also challenging as the overall size of the displaced mass and the length of its deposits provided the only means of distinguishing the two features using our remote classification method. As a result, many rock slide—rock avalanche features area assigned certainty rankings of Level 2 or Level 3. Possible future field verification may allow us to upgrade the certainty rankings of some features.

Examples of Mapped Features

The following paragraphs provide descriptions of some of landslide types found in our study area.

Figure 4 shows an oblique perspective of an area affected by debris flows. The left image (Fig. 4a) shows several sub-basins with characteristic fan-shaped deposits at the base of a slope. Portions of the upper slope are either bare rock or sparsely vegetated suggesting recent erosion, possibly by debris flow activity. Figure 4b shows Fig. 4a, with a debris flow (certainty ranking of Level 1) source and transportation zone, and depositional zone fan at the bottom of the slope depicted by purple shading.

Figure 5 shows an oblique perspective of an area affected by debris slides. These features are found on steep slopes. The shape and size of these landslides are quite variable. Their extensive source areas suggest initial partial cohesion of the mobilized material. The debris slides stall on the slope a short distance below the initiation zone.

Debris slides are very similar to debris flows, with perhaps the principal difference being their rheology. As a result, many debris slides have been classified with certainty ranking of Level 2 due to the difficulty of clearly differentiating them from non-channelized debris flows.

Figure 6a and b show an inactive translational landslide. Thick vegetation cover obscured the landslide from view using orthophotos, suggesting that this feature has not been active for an extended period.

Although the extent of the landslide was defined with a high level of certainty (Fig. 6b), without field verification to distinguish between translational or rotational slide types, we are compelled to assign a certainty ranking of Level 2 to the classification.

Figure 7 shows coalescent debris flow deposits (green shading) and debris flows (from source area to deposition zone; purple shading). Although the coalescent fan-shaped debris flow deposits likely consist of debris flow colluvium, confirmation of this requires field-based investigations, and as such, it was assigned certainty ranking of Level 2.

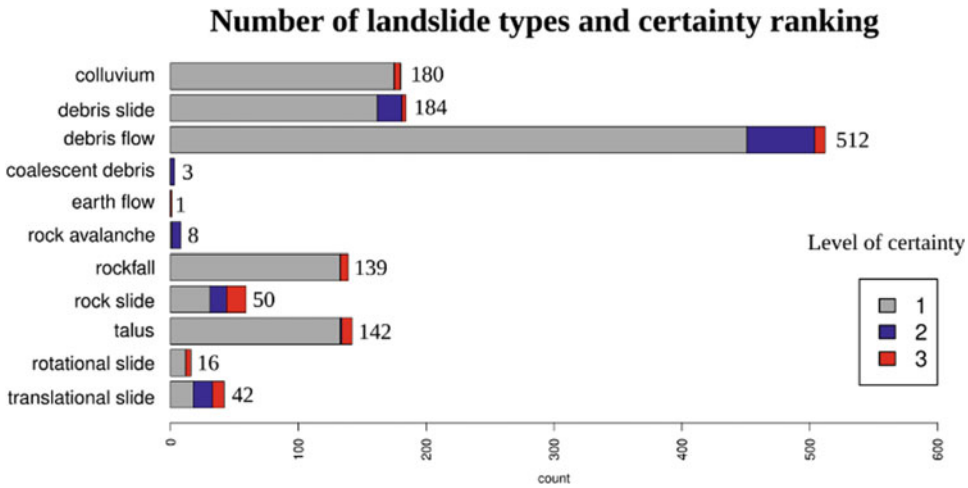

Fig. 3 Distribution of landslide types and deposits in the inventory. Horizontal bars represent the total number of features mapped for each feature type. Colors represent the proportion (%) of each feature type by level of certainty

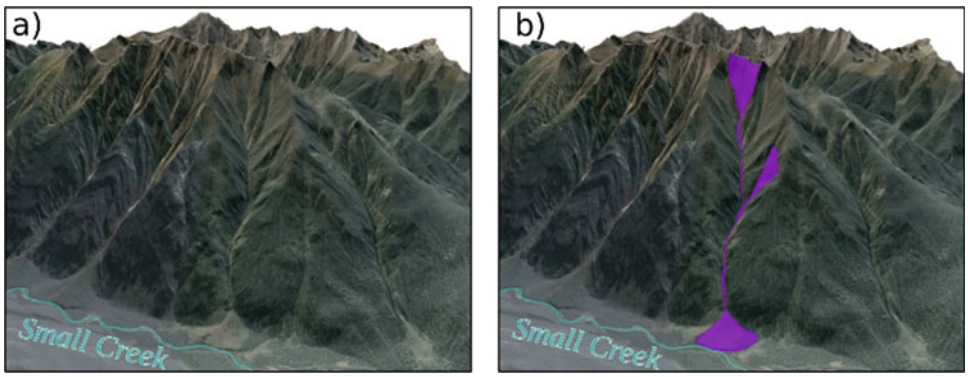

Fig. 4 **a** Oblique perspective showing a portion the study area with debris flows. **b** A debris flows source, transportation and deposition zone is shown in purple shading

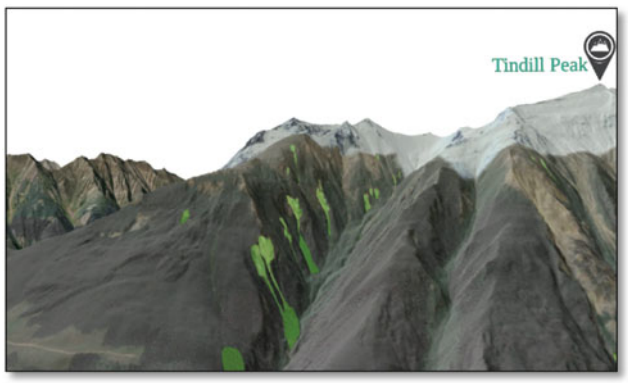

Fig. 5 Oblique perspective showing examples of debris slides (green shading)

5 Conclusions

We describe our methods for mapping landslides in the Canadian Rocky Mountains, near the town of Valemount, British Columbia, Canada.

We mapped 1286 landslides and associated landforms in a 1200 km^2 study area. The most frequent landslide types are debris flows (40%) and debris slides (14%). Eighty seven percent of features we observed were assigned the highest certainty ranking (Level 1).

This mapping project fills an information gap by providing baseline data on landslide processes and distribution for a critical infrastructure corridor in east central British Columbia. The data generated by this research will facilitate

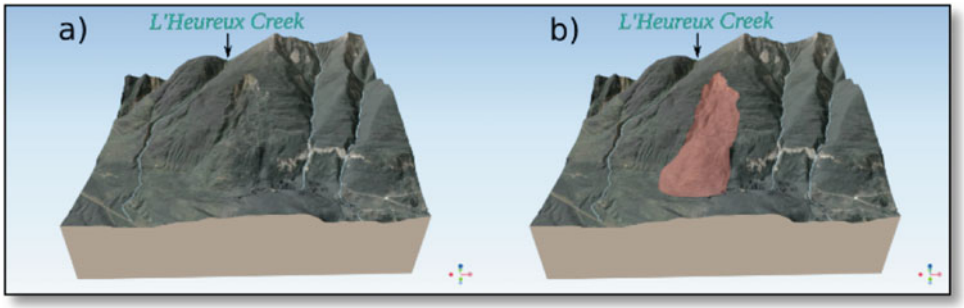

Fig. 6 **a** Oblique perspective showing a translational slide. **b** The mapped extent of the landslide is shown in salmon-colored shading

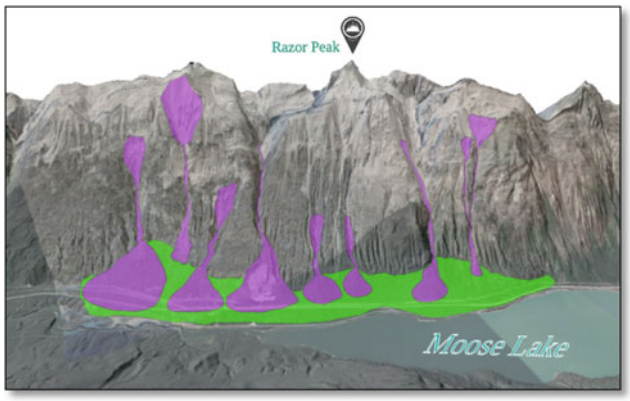

Fig. 7 Oblique perspective showing a coalescent fan-shaped debris flow deposits (green shading) and debris flows (purple shading)

future research on this and adjacent areas, and provide a reference for operational purposes.

Acknowledgements The authors want to acknowledge NRCan's Office of Energy Research and Development Project GSC-19-103 within Public Safety Geoscience Program at the Geological Survey of Canada (GSC) for providing LiDAR and field assistance. T.B. conducted much of the mapping with funding through a post-doctoral fellowship, granted by the Basque Government and the University of the Basque Country (UPV/EHU, group IT1678-22). In addition, the British Columbia Ministry of Forests provided access to LiDAR data and assistance in the field. J. Clague (Simon Fraser University) is thanked for assistance in the field. G. Hunter (British Columbia Ministry of Transportation and Infrastructure) provided assistance in the field and historic geotechnical reports. D. Huntley (GSC Pacific) peer-reviewed the paper in manuscript form. This is Geological Survey of Canada contribution number 20220201.

Appendix 1

In Fig. 8, we provide a low-resolution copy of our inventory map. The high-resolution landslide inventory map is publicly available in PDF format (Bornaetxea et al. 2022) or as digital shapefiles (.shp).

Appendix 2

Here, we provide a description of the methods used for processing our LiDAR data.

For the 2019 and 2020 data, only.laz files were available. The following data processing was undertaken to generate our final raster file in GeoTiff format:

(1) A new.laz file was created for each original file, which contained only points defined as Class 2 (ground).
(2) The files were then merged into one large file.
(3) Data were re-projected to UTM zone 11 N with WGS84 datum.
(4) A raster file of 2.5 × 2.5 m resolution was created from the LiDAR point cloud (.laz file), with the elevation value (z) being established as the lowest elevation point in the point cloud. If there were no points, then the pixel was set as NULL.
(5) For pixels that did not include an elevation value, an inverse distance weighted approach was used. For large empty areas such as lakes, a maximum number of four

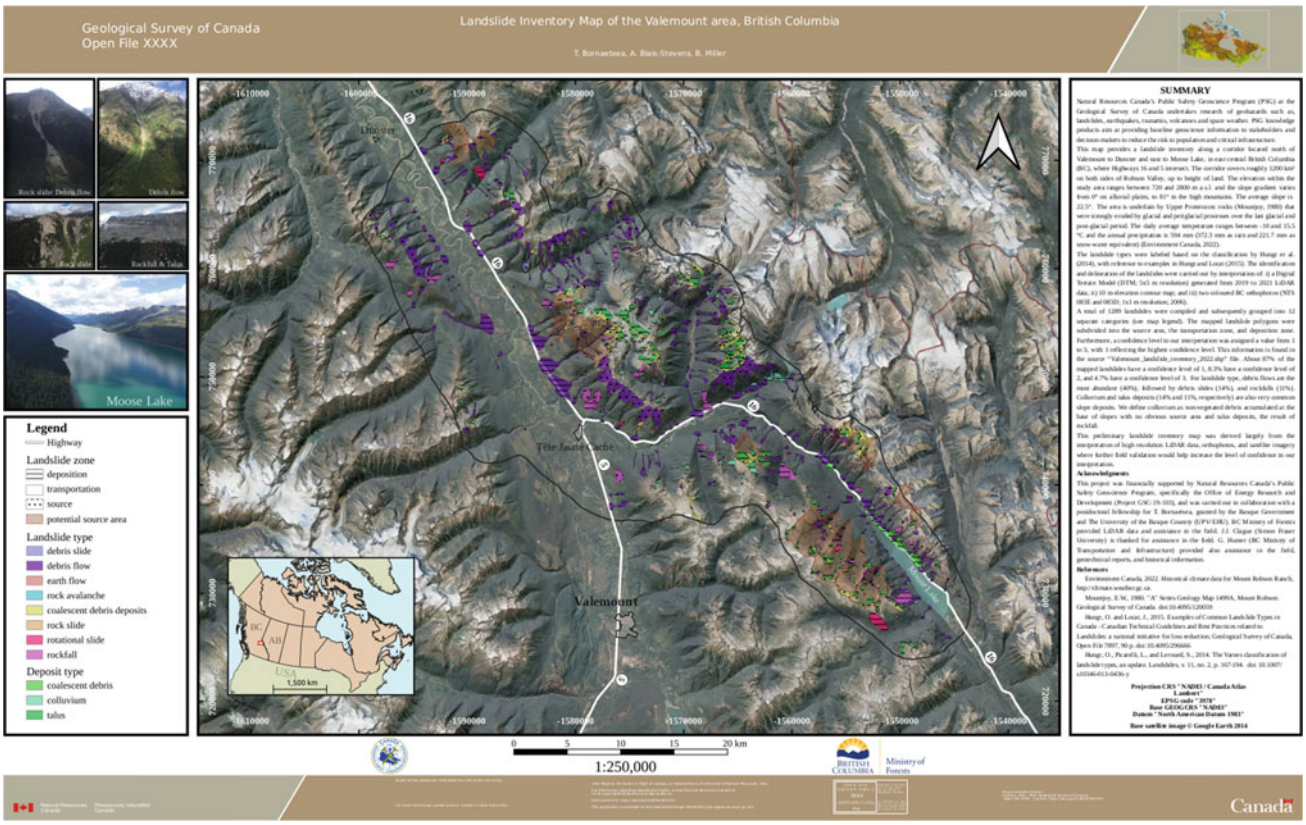

Fig. 8 Low-resolution image of our landslide inventory map for the Valemount area

consecutive pixels were used to avoid unrealistic elevation data assignments.

(6) Finally, the DEM was resampled to 5 × 5 m resolution, from 2.5 × 2.5 m resolution to satisfy the balance between resolution and file size, and to provide a smoother terrain surface for interpretation.

For the 2021 data surrounding Moose Lake, ESRI binary raster files with 1 × 1 m resolution were available. Therefore, the raster files were first transformed into generic GeoTiff format, and then resampled to 5 × 5 m resolution by means of the bilinear approach. These files were then merged with the 2019 and 2020 LiDAR files.

References

Ardizzone F, Cardinali M, Galli M, Guzzetti F, Reichenbach P (2007) Identification and mapping of recent rainfall-induced landslides using elevation data collected by airborne Lidar. Nat Hazard 7 (6):637–650. https://doi.org/10.5194/nhess-7-637-2007

BGC Engineering Inc. (2015) Leona Creek. Rock slope hazard assessment. Ministry of Transportation and Infrastructure, Vancouver, BC. p 63

Bornaetxea T, Blais-Stevens A, Miller B (2022) Landslide inventory map of the Valemount area, British Columbia. Geological Survey of Canada. Open File 8926. https://doi.org/10.4095/330911

Cruden DM, Varnes DJ (1996) Landslides: investigation and mitigation. Chapter 3-landslide types and processes. Transportation research board special report (247)

Environment Canada (2022) Historical climate data for Mount Robson Ranch weather station. http://climate.weather.gc.ca

Fell R, Corominas J, Bonnard C, Cascini L, Leroi E, Savage WZ (2008) Guidelines for landslide susceptibility, hazard and risk zoning for land-use planning. Eng Geol 102(3–4):99–111. https://doi.org/10.1016/j.enggeo.2008.03.014

GDAL/OGR Contributors (2022) GDAL/OGR geospatial data abstraction software library. Open-Source Geospatial Foundation. https://gdal.org

Guzzetti F, Mondini AC, Cardinali M, Fiorucci F, Santangelo M, Chang KT (2012) Landslide inventory maps: new tools for an old problem. Earth Sci Rev 112(1–2):42–66. https://doi.org/10.1016/j.earscirev.2012.02.001

Hungr O, Locat J (2015) Examples of common landslide types in Canada—Canadian technical guidelines and best practices related to landslides: a national initiative for loss reduction. Geological Survey of Canada, Open file 7897, p 90. https://doi.org/10.4095/296666

Hungr O, Picarelli L, Leroueil S (2014) The Varnes classification of landslide types, an update. Landslides 11(2):167–194

Massey NWD, MacIntyre DG, Desjardins PJ, Cooney RT (2005) Digital geology map of British Columbia. B.C. Ministry of Energy and Mines, Geofile 2005-1

Ministry of Transportation and Highways (1999) Hazard assessment, highway 16—Spittal and Leona Creeks, Robson District. Report submitted to the Robson District Highways Manager

Mountjoy EW (1980) "A" series geology map 1499A, Mount Robson. Geological Survey of Canada. https://doi.org/10.4095/120059

Murphy DC (2007) "A" series geology map 2110A, Canoe River, Geological Survey of Canada. https://doi.org/10.4095/223752

Natural Resources Canada (NRCAN) (2015) Seismic hazard map of Canada and local seismic hazard parameters. www.earthquakescanada.nrcan.gc.ca

PDAL Contributors (2020) PDAL point data abstraction library. https://doi.org/10.5281/zenodo.2556737

QGIS Development Team (2022) QGIS geographic information system. Open-Source geospatial foundation project. http://qgis.osgeo.org

Sassa K, Guzzetti F, Yamagishi H, Arbanas Ž, Casagli N, McSaveney M, Dang K (eds) (2017) Landslide dynamics: ISDR-ICL landslide interactive teaching tools. Volume 1: Fundamentals, mapping and monitoring. Springer

van den Eeckhaut M, Verstraeten G, Poesen J (2007) Morphology and internal structure of a dormant landslide in a hilly area: the Collinabos landslide (Belgium). Geomorphology 89(3–4):258–273. https://doi.org/10.1016/j.geomorph.2006.12.005

World Landslide Reports

The Anthropogenic Aggravation of Landslide Disasters in Bangladesh: Key Informants' Perspectives

Bayes Ahmed, S. M. R. Arfanul Alam, Imtiaz Ahmed, and Peter Sammonds

Abstract

Landslide disasters in Bangladesh's Chittagong hill districts (CHD) put lives, livelihood, and the ecosystem at risk. Therefore, understanding the causes of landslide events in CHD is crucial to preparing and implementing disaster risk reduction (DRR) strategies. The causes of landslides are generally seen through the lenses of physical science. However, to better understand the landslide disaster mechanism, it is essential to explore the human activities that trigger and aggravate the events. This article uses qualitative social science tools and techniques to investigate CHD's anthropogenic-induced landslide disasters. Forty key informants from diverse professions, ethnicities, communities, and backgrounds were interviewed between 9 June and 3 November 2020. The recorded interviews were translated, transcribed, and thematically analysed in NVivo software. The results show that human-induced landslides in CHD evolve around three broader areas: demography, climate change, and lack of coordination and regulation. First, increased population, hill cutting, deforestation, manipulated agricultural practices, and sand and stone extraction is the leading anthropogenic activities of landslides in CHD. Second, the influx of Rohingya refugees into Bangladesh significantly increased landslide vulnerability. Third, climate change-induced erratic rainfall is leading to more rainfall-induced landslides. Finally, a lack of coordination and regulations among various institutions hinders the DRR process. The short, medium- and long-term recommendations include stopping illegal hill cutting and deforestation, regulating heavy vehicles, increasing coordination, institutionalising early warning systems, conducting massive awareness campaigns, conducting further research, addressing challenges such as lightning, climate migration and conflict, and creating a master plan exclusive for the entire region and coming up with a political consensus for better implementation of the plan.

Keywords

Landslide • Indigenous knowledge • Chittagong hill tracts • Key informant interviews • Rohingya • Bangladesh

1 Introduction

Landslide is one of the deadly disasters in Bangladesh. The disaster sometimes costs life, livelihood, ecosystem, and the local economy. Bangladesh has significantly improved in disaster risk management over the years due to the country's comprehensive disaster prevention programmes and the inclusion of local and international organisations in the process. Common disasters in Bangladesh like cyclones and floods have come under an early warning system and broader disaster risk reduction (DRR) policies and programmes. As a result, the death rate from tropical cyclones —the historical deadliest disaster in Bangladesh—decreased significantly (Alam and Ray-Bennett 2021). However, in comparison to them, landslide disaster is often less discussed. The devastating 2017 landslide events in Chittagong hill districts (CHD) in Bangladesh that killed at least 170 people (Anas 2019) was a wake-up call for researchers and policymakers.

B. Ahmed (✉) · P. Sammonds
Institute for Risk and Disaster Reduction (IRDR), University College London (UCL), Gower Street, London, WC1E 6BT, UK
e-mail: bayes.ahmed@ucl.ac.uk

P. Sammonds
e-mail: p.sammonds@ucl.ac.uk

S. M. R. Arfanul Alam
Youth Conservation Corps—US Forest Service International Programs, Cox's Bazar, Bangladesh

I. Ahmed
Department of International Relations, Centre for Genocide Studies, University of Dhaka, Dhaka, 1000, Bangladesh

I. Alcántara-Ayala et al. (eds.), *Progress in Landslide Research and Technology, Volume 1 Issue 2, 2022*, Progress in Landslide Research and Technology,
https://doi.org/10.1007/978-3-031-18471-0_28

For effective DRR strategies, it is vital to understand the disaster risk first, which has also been prioritised in the Sendai Framework for Disaster Risk Reduction 2015–2030 (UNDRR 2015). In the case of landslides, looking at both the natural and human-induced factors is vital for formulating and evaluating policies and existing frameworks. Including multidisciplinary research to investigate disaster risks makes it more reliable and accurate. While the physical science domain still dominates landslide studies, there is an acute need for integrating qualitative social science research.

Anthropogenic or human-induced landslides are more common in economically less developed regions (Jaboyedoff et al. 2018). Various discussions on the root causes of landslides in CHD are found in the existing literature. Alam (2020) found hill cutting, deforestation, the settlement at risky slopes, population growth, and development works as the main anthropogenic activities of landslide events. Ahammad and Stacey (2016) discussed the manipulation of agricultural practices in the region responsible for landslides. One of the reasons why it is difficult for the government to implement effective DRR measures is that the hilly locations are hard-to-reach. Similar cases are found in rural China (Peng et al. 2017). Along with these challenges, various communities in CHD, urbanised hilly, indigenous, and Rohingyas, perceive and contribute to landslide disasters differently (Ahmed 2021).

The strategies need to be diverse as the risks originate from various sources. Thus, focusing on anthropogenic activities of landslide disasters is an essential aspect of developing a comprehensive and inclusive DRR strategy. Existing literature primarily focuses on the geomorphology, lithology, rainfall pattern and slope engineering perspectives (Kamal et al. 2022). Still, there is a severe lack of exploring the anthropogenic aggravation of landslide disasters in CHD, especially from an expert's point of view.

This article aims to collect in-depth micro-narratives from local experts/key informants to explore the anthropogenic-induced landslides in Bangladesh and formulate landslide DRR policies based on their opinions. By expert, here we mean a person having extensive experience working in the context of CHD and contributing to national policy formulation. The experts were selected from the various profession, backgrounds and ethnicity covering all the five hill districts of CHD and experts based in Dhaka, the capital of Bangladesh.

The collection of experts' in-depth narratives is unique in applying the qualitative method in landslide studies in Bangladesh. Sultana and Tan (2021) interviewed forty-five officials to examine how local-level institutions mitigate regional landslides. However, no survey of key informant interview (KII) based study on understanding the anthropogenic activities involved in landslides in CHD of this aptitude was conducted in Bangladesh. Thus, this article helps to minimise the literature gap. This article is highly focused on exploring human-induced landslides by applying social science tools that put the voices of the local people and experts at the centre.

2 Study Area Profile

Chittagong hill districts (CHD) consist of five districts of the Chittagong division in Bangladesh viz: Chittagong, Rangamati, Khagrachari, Bandarban, and Cox's Bazar (Fig. 1). Three districts—Rangamati, Khagrachari, and Bandarban—are named Chittagong hill tracts (CHT). The five CHD districts are situated in Southeast Bangladesh, and the population of CHD is nearly 12 million (Ahmed 2021).

While Chittagong and Cox's Bazar have similar topography and urban demography, the other three CHT districts are unique in terms of hills, demography and culture. CHT hosts 13 tribes (Banglapedia 2021), collectively known as Jumma people (here termed indigenous hilly people). The land of CHT had been a conflict zone for more than 20 years until a peace accord was signed between the insurgents—PCJSS—and the government of Bangladesh in 1997 (Ahmmed et al. 2013). CHT has an estimated population of 1.6 million (UNICEF 2019). Despite covering one-tenth of the country's area, CHT cannot be populated as it is in plainland due to the hilly topography, the hill's structure, and complex communication system. The primary professions in CHT are agriculture, fishing, and forest resource extraction.

Chittagong (recently renamed Chattogram) is well known as the country's business hub for its port facility. It has a population of about 8 million (BBS 2015). Cox's Bazar is well known for its iconic world's longest unbroken sea beach and associated tourism activities. It has a population of about 2.5 million (BBS 2014). Cox's Bazar also currently hosts over 1 million Rohingya refugees (UNHCR 2022). The urban hill dwellers in both districts are highly vulnerable to landslide disasters, mainly low-income jobholders, daily wage earners and small business owners. A good number of them are internally displaced persons (IDPs) and climate migrants (Sammonds et al. 2021).

The hills can be broadly categorised into low hills in Cox's Bazar and Chittagong districts and high hills in CHT (in some places, elevation can go above 1000 m from the mean sea level). The CHD region gets around 4000 mm of rainfall during the monsoon season (June–September), with the highest incidents reported in June and July (Ahmed 2017). Other essential factors triggering landslides in the region are rock types or lithology, age of the rocks, degree of weathering, and presence of weak zones and fissile shales. The rock types of the hills in CHD are primarily composed of sandstone, siltstone, and shale (Kamal et al. 2022). Among them,

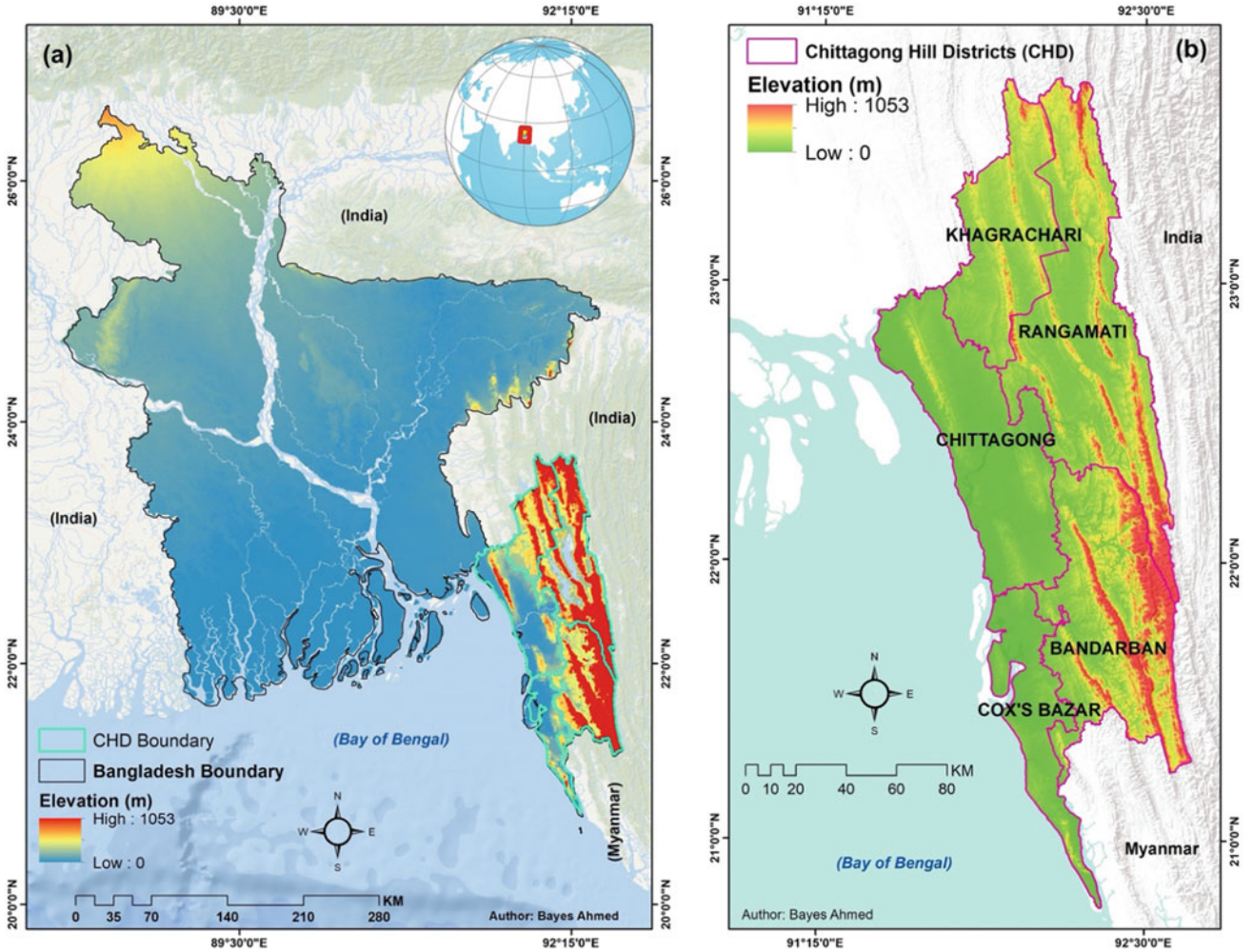

Fig. 1 The location of the Chittagong Hill Districts (CHD) in Bangladesh

sandstone grains are explicitly susceptible to coarse landslides and have more porosity and permeability. Such physical characteristics allow rainwater easily to penetrate the rocks, increasing pore water pressure, exceeding the rock strain, and initiating landslides. Due to its unique geological formations, intense precipitation, and socio-economic context, CHD is considered a hot spot for landslides.

3 Methodology

The study was conducted using multiple qualitative tools to collect and validate the data. The key informants were the experts/academics, local political representatives, journalists, local development/non-governmental organisation (NGO) workers, leaders of the ethnic communities, various government stakeholders including scientific officers, DRR specialists, forest officers, researchers and notable members of the civil society.

Later, to validate (where necessary) the data accumulated from the KIIs and understand the ground-level reality, a total of 82 micronarratives were collected from five tribes and the Bengali communities living in both urban and rural areas in Rangamati and Cox's Bazar districts from 8 to 15 December 2020 and 4 to 16 January 2021, respectively. Most of the participants of micronarratives had either been directly affected by the landslide disasters or were vulnerable to them. The field observation technique was also used, along with analysing the micronarratives.

3.1 Sampling

The study used purposive and snowball sampling methods (Bryman 2016). Since landslide is a less-discussed issue than other disasters in Bangladesh, several experts were selected through the purposive sampling method. An extensive review of journal articles, news and intellectual discussion

Table 1 KII distribution

Districts	KII distribution	Remarks
Chittagong	03	
Rangamati	11	
Bandarban	06	
Khagrachari	04	
Cox's Bazar	05	
Dhaka	11	Experts based in Dhaka
Total	40	

on landslides was done before choosing the key informants. After the purposive sample of the experts, the snowball technique was applied to select people from various fields who have in-depth knowledge of landslides either for their professional exposure or experiencing the impact of the disaster. In total, 40 key informant interviews were conducted in five hill districts and Dhaka from 9 June to 3 November 2020 (Table 1 and Appendix 1).

3.2 Data Collection

Since the data collection commenced during the early stage of the global pandemic of COVID-19, all the interviews were conducted virtually via Skype, Zoom, and phone calls to ensure the safety of the participants and the researchers. The interviews were recorded (audio) with the participants' permission and later transcribed and translated from the Bengali language into English by the researchers.

3.3 Questionnaire

An open-ended questionnaire was developed by the research team (Appendix 2) after several rounds of iteration. The objectives of the questionnaire were to explore the causes of landslides from the key informants' perspective, their impact, the historical change in landslide pattern, policy aspects and the recommendations to reduce the vulnerability to the disaster.

3.4 Data Analysis

The collected data were thematically analysed using qualitative data analysis software, NVivo. First, the data were coded in a deductive approach. Since this article is focused on the anthropogenic exacerbation of landslide disasters in five hill districts in Bangladesh, the data were coded deductively to exclude the other more prominent themes resulting from the KIIs. Second, the codes were systematically turned into broader themes according to the research objective, and finally, the results were written following the themes (Fig. 2).

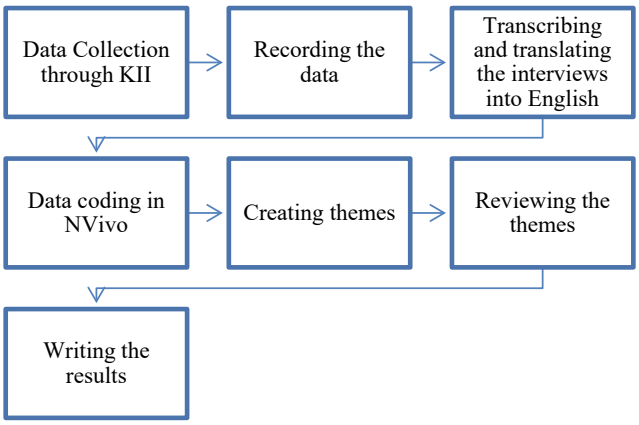

Fig. 2 The cycle of data collection and writing the results

3.5 Ethical Consideration

Data collection ethics were strictly maintained during the fieldwork and interviews. No security, safety and ethical issues were reported during or after the data collection. We obtained institutional ethical approval from UCL (ID: 12991/002). Before conducting the KII interviews, all other local and individual level permissions and consent were taken.

4 Results

In this section, the data gathered from the KII have been critically analysed. Since the contexts for all five CHD districts are different, CHT is mentioned where the situations are exclusive for CHT districts—Bandarban, Khagrachari, and Rangamati only. At the same time, CHD covers all five districts—Bandarban, Chittagong, Cox's Bazar, Khagrachari, and Rangamati. The landslides in the region mainly occur during the monsoon (June–September). However, the results section intentionally excludes physical factors of landslides such as precipitation, soil type, lithology, and earthquakes. A total of eight anthropogenic activities causing landslides in CHD were found through the thematic analysis.

4.1 Demography

The key informants put demography at the heart of the anthropogenic-induced landslide disasters. The data show that demography is the top-level influencer for landslide-inducing activities. While the context in CHT is different from that of Chittagong and Cox's Bazar, all five

districts experienced more people living on risky hill slopes and conducting landslide-triggering activities.

The CHT region observed a significant population growth compared to the other areas of Bangladesh. There are a few reasons for this sharp population increment besides Bangladesh's steady rapid population growth. The urban underprivileged non-indigenous communities are mostly internally displaced persons from various parts of the country. Most key informants blamed the policy of Bengali settlement in the CHT in the 1970s for the demographic impacts.

4.1.1 Increased Population in Urban Areas

Observing the previous events, it is seen that in CHT, deadly landslides mainly occur in township areas. One of the reasons for population growth in the townships is that people from rural hill villages are moving to the townships in CHT for better civic facilities. The hill districts have uneven topography, which makes communication very difficult. Consequently, people from different rural areas accumulate in the towns for a better life, education, jobs, and other community facilities. This can be described as the 'pull factor' of internal migration. The flow of people from the plains is also adding to it.

In the case of Cox's Bazar and Chittagong, the people living on risky hill slopes are predominantly daily wage earners, small business owners and very low to low income-generating jobholders. Many of these people are IDPs and climate migrants from extreme climatic-hotspot rural areas. They come to the city for a better livelihood and to live; they choose the cheapest places/houses, and the hills in the urban areas are the ideal places for that. Thus, it can be said that this kind of floating poverty contributes to landslide disasters.

4.1.2 Overpopulation Leading to More Agricultural Activities

Overall population growth necessitates more agricultural activities. The topography in CHT is unsuitable for all kinds of farming activities. However, due to the increased need, non-native agrarian practices such as horticulture, monoculture and planting/growing non-native species are taking place. In addition, the frequency of crop cultivation has amplified, which is unsuitable for the hills. The pressure from overpopulation also forced the traditional agricultural practice to mutilate its century-old form. As a result, the topsoil gets washed during the monsoon leading to various stages of erosion to landslides. This issue has been further discussed in the 'agricultural practices' section.

4.1.3 Increased Housing Needs

The population and land ratio are not compatible in CHT. Due to the high density of the population, more housing facilities are required. Most often, this kind of housing remains non-administered. The people build houses at random places- sometimes on risky slopes. Unplanned housing facilitates deforestation and hill cutting. In some cases, people living on risky slopes do not want to leave their houses during the evacuation process mainly because they are not sure whether they will be able to return to the same place again since the land is either illegally acquired or rented (Fig. 3).

In all five hill districts, the existing non-indigenous hill dwellers (i.e., predominantly Bengali ethnic population) help their relatives or close ones to settle in the hills, increasing the number of houses in that area. The non-indigenous hill communities do not know the traditional house-making practices in the hills. They treat the hills like plainland which increases their vulnerability to landslide disasters.

4.1.4 Rohingya Influx from Myanmar

The military crackdown, continual human rights violations and genocide in the Rakhine state of Myanmar in 2017 forced nearly a million Rohingya minority people to flee their homes (Martuscelli et al. 2022). The influx of forcibly displaced Myanmar nationals (FDMN), commonly known as Rohingyas, into Bangladesh has contributed significantly to the landslide vulnerability. Although more than a million FDMNs have been residing in Cox's Bazar district, their presence and the demographic impact have altered the hills. Since they did not have land, the Rohingyas settled at various places and made houses cutting the hills.

4.1.5 Alteration in the Habitat Style

Three CHT districts are unique in terms of landscape, demography and culture. The indigenous hilly communities have their unique style of constructing houses. Being in the hills for centuries, they created a strong cultural bond with the hill's environment. Consequently, their house construction method does not require hill cutting, cementation or large-scale forest destruction. Usually, they build houses on stilts at comparatively stable places in the hills. This way, the houses do not create any barrier to the natural water drainage, the topsoil does not erode since only some poles are earthed, and the residents remain safe from various wild animals.

Nowadays, many people from both the indigenous and non-indigenous hill communities are building houses following the methods used in the plains. It requires making the land plain by cutting the topsoil of the hills. Big, cemented pillars are also used, weakening the hill's load-bearing capacity. This type of housing hampers the proper rainwater drainage during the monsoon.

Besides the data gathered from the key informant interviews, it was also observed at the field level that most landslide-hit areas were generally densely populated with modern infrastructures. Some key informants mentioned that this transition from traditional house construction to the

Fig. 3 **a–d** Urban population inhabiting unstable hill slopes and the congested housing put more lives at risk. **e** Some residents are trying to protect their homes from mudflow using plastic sheets, corrugated-iron/tin sheets, and tarpaulin. **f** A family belonging to the non-indigenous hill community—originally migrated from the plains—made their house at a highly vulnerable location and denied leaving it even after falling victim to a landslide. *Source* Fieldwork, the authors

plainland building method is because of the influence of the non-indigenous/Bengali communities—they introduced the technique used in the plainland, and the indigenous communities started to follow them. But a counternarrative of this statement was found during the community-level fieldwork, which will be discussed in the 'discussion' section.

4.2 Hill Cutting

The most responded cause of landslide disasters is cutting the hills in all five districts. Hill cutting has the most tangible, direct and immediate impact on landslides. Cutting hills at inappropriate angles and not maintaining proper slope stability weakens the hills leading to landslides during monsoon. This non-scientific method of hill cutting is used by people at a small scale for personal needs like constructing a house and by larger groups at a medium to a larger scale for business and land grabbing purposes. This often happens under the auspices of influential local people. Many large-scale hill-cutting events occurred for numerous government-funded projects (Fig. 4).

It is important to understand why the hills are cut and how the causes of hill cutting differ in different areas of CHD. Although the consequences of hill cutting are similar, the reasons for hill cutting are multidimensional.

Fig. 4 Roads are being constructed, cutting the hills in **a** rural and **b** hilly urban areas. **c** A low hill is cut to sell the soil as construction material in a rural area in CHD. **d** Houses are made at risky slopes cutting the hill in the urban area of Chittagong. *Source* Fieldwork, the authors

First, hills are cut to extract the soil in brickyards and construction sites in rural and reasonably distant places from the townships. This hill cutting is done mainly by a larger group of people. Hill cutting without permission from the relevant authorities is illegal. This large-scale hill cutting is often done at night and during the monsoon when the soil is found to be relatively weaker in bonding strength. Hill cutting is done in daylight in remote areas where forest and administrative officers cannot reach faster.

Second, some hills are cut for government-funded projects like constructing roads and infrastructures for tourism and communication purposes. Generally, this hill cutting takes place at a large scale in CHT but is not rare in the other two districts. For example, in Chittagong, 18 hills were cut to construct a link road from Dhaka Trunk Road to Bayezid Bostami road, where the hills were cut at a 90° angle. The Chittagong development authority (CDA) was fined considerably by the Department of Environment in 2020 for destroying the hills (TBS 2020).

Third, the objective of hill cutting is not limited to extracting sand and soil or turning the high land into plains; it is a means of grabbing the land as well. Notably, in Chittagong and Cox's Bazar urban areas, some hills are cut so that the upper portion will slide during the monsoon. After the hill gets slid and the mud is cleared, the landowner uses the land for housing and other purposes. Besides this, the alleged local powerful groups facilitate the underprivileged people to live in the government-owned hills so that they can grab the land without any hassle. They make tiny temporary houses (stronger than makeshift houses) and rent them out.

Lastly, the causes of hill cutting by the Rohingyas in Cox's Bazar district are linked to constructing houses, making walking paths and selling the topsoil. During the early months of the influx in late 2017, some hilltops were cut to make it plain to construct roads and drainage systems and spread the water networking (supply) facilities.

It is essential to mention that the Rohingyas are involved in hill cutting in camp-adjacent areas. Often, they are being used as labourers for this job. Government officials book the on-spot workers when they raid the hill cutting sites. But the workers cannot be fined because, according to their living status in Bangladesh as the FDMNs, they should not have the Bangladeshi currency, and for the same reason, they cannot be brought under the local law. Their commands-influential local host community members- do not show up during the hill cutting or raid. This way, the main perpetrators remain out of the clutch.

4.3 Destruction of the Natural Setting

The KIIs described several components of destructing the natural setting in the hills as landslide triggering factors.

When the natural environment of the hills is destroyed, the entire ecosystem in that area gets disturbed. This contributes to waterlogging, soil erosion and ultimately landslides.

4.3.1 Deforestation

Deforestation has been going on for decades in CHD. Rapid urbanisation, tourism industry expansion, and legal and illegal timber businesses are responsible for deforestation. Illegal logging usually occurs in natural and reserved forests (Fig. 5). Although tree cutting from private property is legal, it largely contributes to deforestation because of the untimely logging of immature trees.

Large-scale sawmills and brickyards are seen in CHT, and the number of adjacent areas has risen at an alarming scale. The collected forest timbers are processed at those sawmills and sent to various parts of the country. The wood collected from CHD is coveted even in Dhaka and Chittagong. This increases the demand for more logging, both in legal and illegal ways. In addition, many trees are cut to fuel the brick kilns.

The recent most considerable deforestation occurred in Cox's Bazar district due to the influx of about a million FDMNs from the Rakhine state of Myanmar. The 6500 acres of reserved forest under the Social Forestry Programme—local communities took care of the trees under a mutually beneficial agreement with the government—were turned into the campsite. The Rohingyas cut the trees and cleared the forests for two reasons: they needed to make tents immediately after arriving in Bangladesh and cut many trees for fuelwood. The administration aided this deforestation to create living space for the Rohingyas while increasing the camp size. Tree cutting for fuelwood decreased after they had been provided with the Liquefied Petroleum Gas (LPG) cylinder for cooking at the end of 2018.

Uncontrolled tree cutting leaves the topsoil exposed to rain and overheat. The sandy topsoil absorbs water more than usual during monsoon due to its exposure. This helps open cracks and leads to various types of erosion. The cracks and erosion lead to landslides. The key informants observed that hills covered with naturally grown trees and shrubs are less susceptible to landslides.

Besides harming the environment and topsoil, deforestation generates another threat of landslides. Transporting the logs is usually tricky in hilly topography, and therefore powerful vehicles are used there. The overweight trucks carrying some extra tonnes of logs are unsuitable for hilly roads. The weight and vibration from the bizarrely heavy trucks form cracks and destroy the roads in CHT (Fig. 6a).

Fig. 5 Illegal logging activities inside the reserved forests in Ruma Upazila, Bandarban. *Source* The authors, fieldwork, January 2022

Fig. 6 **a** Heavy trucks carrying logs left a deep trail in the forest in a CHT district. **b** A brickyard close to the hills is in operation in a CHT district. **c** The monoculture of the teak tree is seen in a CHT district. The previous mature trees are already cut; the new ones are growing now. **d** Traditional houses made with lightweight materials (right) are now being replaced with built-construction materials (left) in an indigenous community in CHT. *Source* Fieldwork, the authors

4.3.2 Sand and Stone Extraction

Overexploitation of sand and stone occurs in all four districts—Rangamati, Khagrachari, Bandarban, and Cox's Bazar. The urban areas in Chittagong are not mentioned in this case. The intensity of sand and stone extraction is incredibly high in CHT.

The extraction of sand and stone from the streams and foothills is directly linked to landslides. This illegal exploitation is carried out for various construction works in the hilly region. The construction is supposed to take place using materials from legal sources. Still, the available materials from the surrounding areas illegally make it easy for the contractors to profit more. The people involved often dodge the administration and the conservation/climate activists.

4.3.3 Brickyards

Although the policies require brickyards to maintain some strict rules to safeguard the environment, they are not followed by the brickyard owners most of the time. The brickyards nearby the CHT outnumber the actual need. These brickyards adjacent to various hills require fuelwood; the primary sources are the forests. The soil from the foothills is used as the brick's raw material evading the administration's eyes (Fig. 6b).

4.4 Agricultural Practices

Various types of agricultural practices exist in CHT. Among them, the traditional swidden is the oldest one. It is named '*Jhum*' (slash and burn), and the people involved in Jhum cultivation for time immemorial are known as '*Jumma*'. The customary agricultural practices have been through many changes and manipulations. Some of the farming practices are contributing to landslides in CHT.

4.4.1 Root Crop Cultivation

The hill's soil and topography require zero-tillage system cultivation. This means the less the soil will be dug, the better it is for the topsoil. But due to the introduction of the modern cultivation system in the hills, various root crops are planted. Root crops like ginger, turmeric and taro are cultivated at a large scale in CHT. This needs to plough the soil twice—once during the plantation of the seed/rhizomes and again at the time of harvest. Due to this practice of root crop cultivation, a significant amount of soil is eroded yearly.

Besides increasing the landslide risks, the eroded soil deposits as sediment in the stream lead to water overflow during monsoon. According to the agricultural scientists

working in CHT, if the zero-tillage method is used for cultivation, there will be only 10–15 tonnes of soil erosion. In contrast, tillage erodes 70–80 tonnes of soil per year.

4.4.2 Monoculture

Large scale commercial plantation is taking place in the hills of CHT. This sort of plantation introduced monoculture in CHT, replacing the natural forests with native species of trees. For example, it is seen that the non-native teak tree is planted across the CHT. Non-native species like teak and rubber trees are responsible for topsoil deterioration and purging shrubberies that would otherwise safeguard the topsoil from rain and heat (Fig. 6c).

Rubber and tobacco cultivation are also turning the jungle into gardens' Due to the increasing practice of monoculture, native species like bamboo are being replaced with foreign species. Traditionally, bamboo is considered a natural land stabiliser. The existing teak and rubber gardens were once naturally grown forests. For example, the union (smallest administrative unit in Bangladesh) of Baishari in Bandarban district was covered with naturally grown forest but now is replaced by nearly 200 rubber gardens. Although these gardens are creating more jobs for the local people, they significantly contribute to destroying the hills' natural setting.

4.4.3 Jhum Cultivation

Jhum cultivation—slash and burn—is a century-old traditional agricultural method used by the indigenous hill communities in CHT. Jhum's contribution to the landslide disaster is a debated issue. The data show that the key informants from indigenous hill communities resist the idea that Jhum has a link with landslide disasters. In contrast, others hold it responsible for large-scale vegetation destruction and landslides.

The indigenous hill key informants argue that Jhum has been cultivated for centuries, and there were no landslides in CHT. Secondly, the Jhum cultivators leave the land for nearly three years once the Jhum is harvested, so they do not repeat the process every year. Thirdly, they do not cut the giant trees, and the fire to burn the soil and vegetation is controlled. Finally, they do not plough the ground as people do on plains. Subsequently, Jhum erodes some amount of topsoil but does not cause landslides.

The ground-level reality is that the frequency of Jhum cultivation has increased due to population growth. Most non-indigenous hill communities do not follow the century-old timeline for cultivation. The loss of vegetation and small trees is detrimental to the topsoil, leading to land degradation and landslides. Besides, the cultivation method, if not done correctly, can block the natural water drainage systems or stream networks in the hills.

4.5 Development Work

The globalisation of the economies has made the term development a catchphrase. It is generally perceived that more development equals more progress. While it is true in most cases, a few other matters must be considered. While undertaking infrastructural development works, keeping the local environment and geological factors in mind is necessary. This principle applies in the case of CHT. The following development activities are contributing to landslides in CHT.

4.5.1 Road Construction

Previous records of landslide events show that the deadliest ones occurred near a road. To ease communication for the growing population, road connection is vital. But unplanned road construction by hill cutting with no slope stabilisation measures increases the vulnerability to landslide disasters. Not maintaining proper slope, not constructing suitable retention walls, and hill cutting for the construction are the main reasons for the vulnerability. One of the geologists interviewed said that the roads on the back slope are stable, but the ones on the dip slope are unstable. These kinds of geological features are often ignored while constructing a road. Building roads in CHT is costlier than in any other region of Bangladesh because of its remote location and hilly communication system. Yet, the heavy log carrying trucks are destroying the roads—which require repair and maintenance within a short time.

4.5.2 Unplanned Tourism

The scenic beauty of CHT attracts many tourists every year. The tourism industry in Bangladesh has been growing faster in recent years. To meet the demand, unplanned infrastructures for tourism have been developed. The tourism industry is one of the reasons for land-related conflict between the indigenous hill communities and the non-hilly Bengali communities. Since CHT has different geological features than other parts of the country, so it needs specialised policies for construction. But no detailed plan for the tourism industry and specific construction policies for the brutal landscape have been found in action. The rapidly growing tourism infrastructures might threaten the environment and put the people involved at the risk of landslide hazards if they are not compatible with the area's natural setting.

4.6 Lack of Coordination

In CHD, various government and non-government agencies are working on DRR, climate change adaptation and safeguarding the environment. The government institutions are

responsible for planning and implementing multiple projects. The institutions run their activities without proper coordination with the others. For example, the Department of Agricultural Extension promoted the zero-tillage method for agricultural practices in the hills. However, a government bank was encouraging the farmers to plant turmeric and ginger by providing them loans with a minimum interest rate. Although landslide DRR is a task of the Ministry of Disaster Management and Relief, the local administration does the core activities- evacuation, relocation, and rehabilitation-. A severe lack of coordination is seen among the ministries in CHT. Some field-level irregularities were also found.

The previously discussed event of fining the Chittagong Development Authority (CDA) by the Department of Environment (DoE) for inappropriately cutting 18 hills to construct a road is another example of the lack of proper coordination among the institutions. Both the CDA and DoE are public institutions. This lack of coordination is generated by the absence of a holistic policy for the hill districts in Bangladesh.

4.7 Lack of Awareness

The lack of awareness among the low-income families living on the risky hill slopes was high. Lack of awareness increases the vulnerability to landslides at three stages: (a) during settlement—they do not avoid risky slopes; (b) they cut hills, making it even riskier to live; and (c) they do not leave their houses even during extreme rainfall events. The evacuation process during an emergency by the administration and the Bangladesh Fire Service and Civil Defence is greatly hampered by this.

4.8 Human-Induced Climate Change

The most visible cause of CHD's landslides is extreme rainfall events. The hill communities opined that the rainfall has become erratic. In recent years, the amount of rain in a short amount of time increased at an alarming rate. The 2017 landslide events in CHD were rainfall-induced; there was a rainfall event for several days at a stretch. Human-caused climate change is erratic: sometimes there is no rain, and sometimes there is excessive rainfall. The extreme precipitation in a short amount of time triggers landslides.

Figure 7 summarises findings linked to the anthropogenic causes of landslides as obtained from the KII interviews in eight major categories (orange rectangles) and their interlinkages with other sub-categories (blue rectangles).

5 Discussion

Landslide events in Bangladesh and other parts of South Asia and Latin America are closely associated with human factors (Ahmed 2021). The anthropogenic activities found in this study can be classified into three broader categories: demography, human-induced climate change, and lack of regulation and coordination.

5.1 Social Factors

The demographic impact is mainly responsible for landslides in CHD (Ahmed 2021). The demographic effects on landslide risk in CHD are intricate because it is difficult to classify whether all the results are equally generated from actual human need-based activities or a less regulated and less aware population. The spill-over effect of the demographic implications is actively influencing hill cutting, tree cutting, destruction of nature, and the manipulation of traditional agricultural and housing practices.

The population in CHT increased manifold. Although the three CHT districts cover about one-tenth of the total area of Bangladesh (Banglapedia 2021), they cannot be populated like the flatland due to the hilly geological and geomorphological conditions. The non-indigenous communities from flatland (Bengali) share tremendous responsibility for population growth in the hills; the Bengali population in CHT increased five times between 1961 and 1981 (Ahammad and Stacey 2016). In contrast, the cultural differences between the indigenous hill communities and the migrated Bengali hill communities often implement the agricultural and house-building methods used in the plains (Ahmed 2017).

The key informants from the indigenous hill communities blamed the Bengali hill community for introducing a non-traditional housing method that is replacing the stilts-made traditional lifted houses. It is to be mentioned that the traditional stilt houses are made with lightweight materials, contrary to the non-traditional ones that require comparatively heavier materials and flat space. However, some of the indigenous community members during the fieldwork explained why they prefer non-traditional housing methods used in flatlands. First, the stilts-made traditional housing needs regular maintenance, and the price of the material used is rising along with the labour cost. Second, the houses with clay/brick walls give better protection in winter and monsoon. Although the traditional stilts house is more comfortable in summer, it is impracticable for them to build both types of houses.

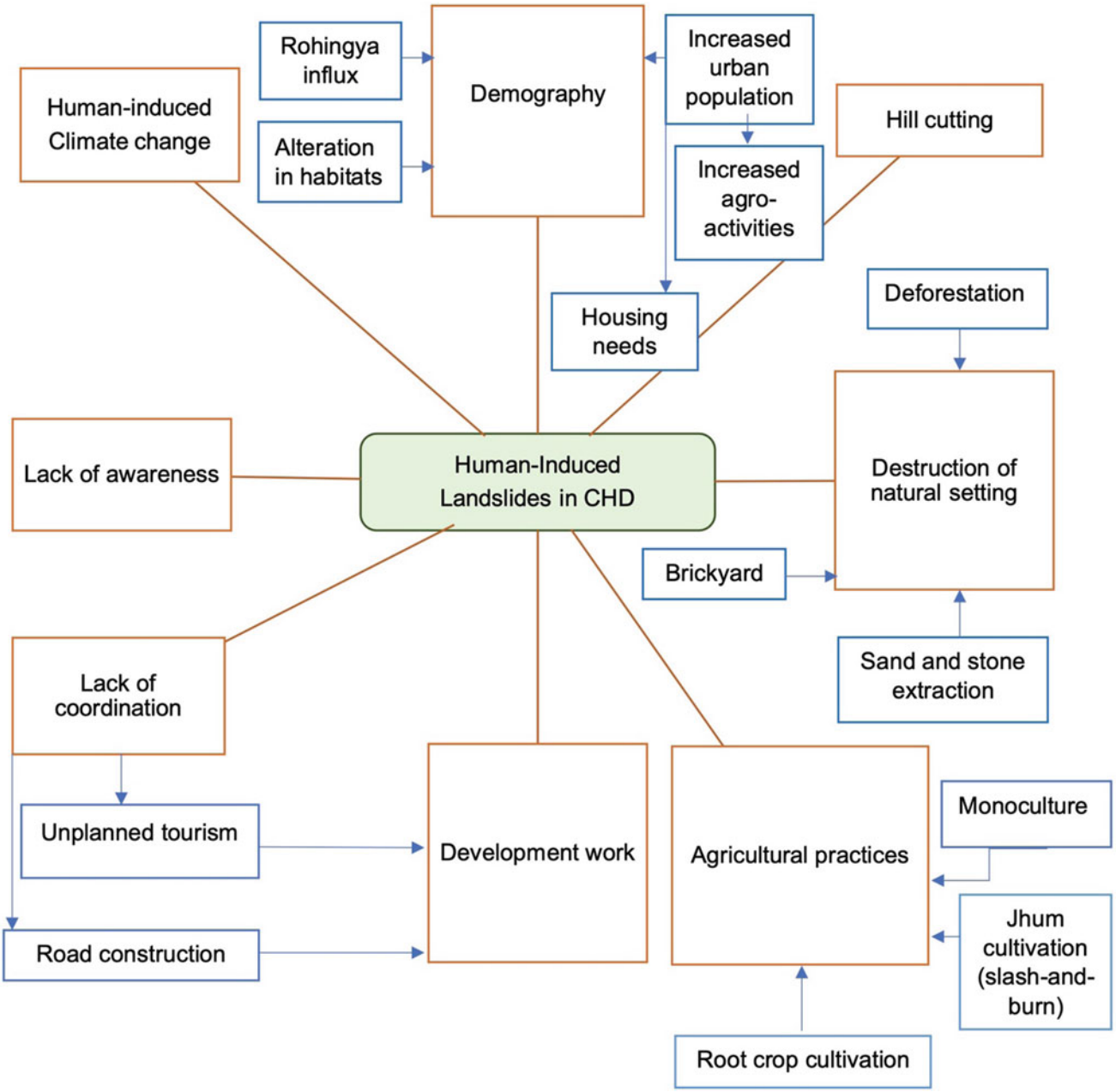

Fig. 7 The anthropogenic activities causing landslide disasters in CHD. *Source* The authors

The increased population needs more space for housing and agricultural activities, so they need to cut trees and hills. It is very challenging for the government to relocate the landslide-vulnerable communities living on dangerous hills to somewhere in a safer place/shelter, given that Bangladesh is already a densely populated country. Most people living on the risky hill slopes are economically insolvent, so they cannot choose an alternative, safer habitat either (Fig. 8). On top of all these complexities, the lack of awareness among the non-indigenous hill dwellers is high. It is a vicious cycle; if not broken, it will keep increasing the risk.

The manipulation of century-old agricultural practice works as an aggravating factor, while hill and tree cutting are triggering factors. The type of landscape and soil must be considered in agriculture. The agricultural activities needed to be done with a zero-tillage method to avoid soil erosion. But the increased practice of deep-rooted crop cultivation is seen. Ginger, turmeric, pineapple, and taro cultivation were encouraged, but this agricultural practice erodes the topsoil and leaves the pores open for the rainwater to infiltrate during the monsoon. Besides this, mono and horticulture are increasing due to the commercialisation of the hills

Fig. 8 Landslide disasters occurred on 18 June 2022, killing two people in an urbanised hilly area in Chittagong metropolitan area. *Source* Fieldwork, the authors

agro-industry. This practice threatens the existence of native species like jungle bamboo that would resist landslide triggers.

Hill cutting is a unique way of harming the environment compared to other mechanisms. Hill cutting does destroy not only biodiversity but also creates a non-replenishable loss for the future generation. The use of heavy machines to cut hills augments the process and helps the illegal soil smugglers to quickly cut and transport the hill soil, sand and stone. Road construction is a well-discussed anthropogenic-induced landslide. Road constructions without enough slope stabilisation mitigations measures and hill cutting are triggering factors. Besides this, road blockage after the landslide halts the communication that impacts the entire economy and community activities of the vicinity. For example, the vegetables, fruits and fish produced in the CHT get spoiled if they are not transported to the market on time. The overweight trucks carrying logs create vibration, which can intensify the process of the slide. This kind of vibration-instigated landslide event is also reported in Argentina (Jaboyedoff et al. 2018).

5.2 Weather and Climatic Factors

Climate change has connections in several ways with the landslide disaster. One of the causes of rainfall-induced landslide events is the unpredictable rainfall pattern. Extreme rainfall events within a short time are observed to be the main reason for landslides in CHD. Climate change influences this uneven precipitation pattern (IPCC 2021). The International Centre for Integrated Mountain Development (ICIMOD) reported that the wider eastern Himalayan region is experiencing fewer rainy days. However, the total amount of precipitation has not changed in the past five decades. It is causing a higher amount of rainfall in a short period and thus, triggering flash floods and landslides in the hilly regions (Wester et al. 2019, p. 73).

Poverty is connected to landslide disasters in hilly urban areas (Ahmed 2017). It is crucial to identify and acknowledge how the climate migrants- in this case, the people from southern coastal or northern flood-affected zones who lost their livelihood, homes, and land due to cyclones, salinity, land degradation, sea level rise and river erosion and the

disadvantaged section of the society rush to the city/township for a better living (Sammonds et al. 2021). While struggling with their daily basic needs, affording to live in a safer place becomes next to impossible for them. They look for cheap housing when the illegal landgrabbers/hilly landowners step in. They rent out small makeshift houses/the hilly land to these people cheaply, or the displaced people settle in the hills alone. The newly settled people came from plains and were unaware of the hill's nature and importance. They start cutting the trees and hills and building houses on risky slopes.

Consequently, climate-induced extreme disasters are forcing vulnerable people to their tipping points and creating a new migration flow of IDPs and climate migrants. Thus, they contribute to the vulnerability to landslide disasters directly and indirectly. In contrast, the CHT region is already facing severe land-tenure and indigenous rights-related conflicts with the Bengali ethnic population (Mohsin 2022). The influx of non-indigenous settlers would cause more armed insurgencies and destabilise the existing peace deals in the region.

Lightning has emerged as another significant disaster for Bangladesh in recent years. Since 1990 over 6000 casualties have been reported, with an annual average of about 115 fatalities in Bangladesh (Dewan et al. 2017). The south-eastern region is experiencing high lighting activity, especially during the pre-monsoon and monsoon seasons (Dewan et al. 2018). Correspondingly, the local people and KIIs frequently mentioned that lighting is another causative factor for landslides which needs to be addressed in future research.

5.3 Governance Factors

Lack of regulation and coordination among various actors and agencies contributes to regional landslides. Although hill cutting is associated with population density and poverty, large-scale hill cutting occurs due to the corrupt system, lack of proper monitoring, lack of enough government intervention, availability of technology and lack of awareness of the people in the specific areas. The people behind large-scale hill cutting are not insolvent; most often, they are the affluent and influential people in society. For example, in Chittagong and Cox's Bazar districts, the hill dwellers are mainly daily wage earners, and they cut hills mostly with the support and guidance of a powerful group of people.

People who experience the disaster are more aware of it (Damm et al. 2013). In this case, poverty and the high population density are contributing as push factors for the people to live in the hilly zones even after many experienced landslides. The construction works in the hills actively contribute to the overexploitation of forest resources. The extraction and use of sand and stone from the surrounding area of the construction sites are more accessible and cheaper than transporting the materials from outside. The lack of a robust monitoring system over the sources of construction materials in the hills is one of the reasons the illegal exploitation of these forest resources continues.

6 Conclusion

The article unveils the less explored sides of landslide disasters in Bangladesh's Chittagong Hill Districts (CHD). The anthropogenic-induced landslide disasters have been identified through the interviews of key informants from various sectors. This article reflects the ideas and critical thinking of participants from multidisciplinary professions and experiences. The results were validated with the field-level data and observation. This article contributes to the study of disaster management from a more people-centric approach.

The results show that anthropogenic activities like hill cutting, deforestation, sand and stone extraction, various construction works, and manipulation of agricultural practices generate by the demographic impact like dense population, internal migration, lack of awareness and cultural differences among the communities. The lack of regulation and coordination among the institutions works as an aggravating factor. The population–poverty–destruction of hills' natural setting nexus is fuelling the process.

Human-induced climate change plays direct and indirect roles in triggering landslides in CHD. Climate change is causing extreme precipitation within a short time, leading to rainfall-induced CHD landslides. In addition, climate migrants are moving to large cities for a better livelihood. They are forced to reside in the hilly areas without the orientation to adaptation strategies and local knowledge. In contrast, the indigenous hill communities were well adapted to the hills. This means they, by culture, do not cut the hills or mature trees and do not engage in excessive forest resource exploitation. But with the population growth, there has been a paradigm shift in their lifestyle, agricultural practices, and housing methods. This pattern of modernisation is more evident in urban indigenous communities.

It is highly recommended to stop illegal hill and tree cutting immediately and conduct massive awareness-building campaigns among the hilly communities. It would be beneficial to introduce anticipatory action-based activities such as regional landslide early warning systems, promoting nature-based solutions for tackling disasters, and establishing a forecast-based financing mechanism for protecting the hilly ecosystem, indigenous culture, and people. Finally, it is critical to producing a holistic master plan to manage CHD's population density and overall development and tourism activities. These need to come up with a political decision to

work on resolving conflict, bringing hill-friendly agricultural practices, and regulating the activities relating to natural resource extraction.

Acknowledgements This research was funded by the Royal Society as part of the project, 'Resilient Futures for the Rohingya Refugees' (Award Reference: CHL\R1\180288), supported under the UK Government's Global Challenges Research Fund (GCRF). We are indebted to the key informants for their valuable time and counsel.

Appendix 1: List of the Key Informant Interviewees

ID	Designation of the participants	District	Interview date
01	NGO Worker, Project Name: Community Empowerment and Action Against Illegal Stone Extraction to Preserve the Natural Environment in Bangladesh	Bandarban	09/06/2020
02	Chairman, Parbatta Chattagram Bon o Poribash Andolon-Bandarban Chapter [Chittagong Hill Tracks Forest and Environment (protection) Movement]	Bandarban	13/06/2020
03	Chief Scientific Officer, Soil Development Institute, Bandarban	Bandarban	17/06/2020
04	Ex-Chairman, Babuchara Union, Dighinala Upazila (i.e., sub-district)	Khagrachari	23/06/2020
05	NGO Worker; Organisation: Green Hill	Rangamati	25/06/2020
06	General Secretary, CHT Headman Network	Rangamati	25/06/2020
07	General Secretary, Parbatta Chattagram Bon o Poribash Andolon-Rangamati Chapter [Chittagong Hill Tracks Forest and Environment (protection) Movement]	Rangamati	27/06/2020
08	Range Officer, Forest Department, Bandarban	Bandarban	27/06/2020
09	Journalist, Ekushey Television, Khagrachari	Khagrachari	15/07/2020
10	Executive Director, Shining Hill, Rangamati	Rangamati	15/07/2020
11	Associate Professor, Geography and Environmental Studies, University of Chittagong	Chittagong	16/07/2020
12	Assistant Commissioner and Executive Magistrate, (In-Charge, Rohingya Refugee Camp), Office of the Refugee Relief and Repatriation Commissioner (RRRC)	Cox's Bazar	18/07/2020
13	President, Parbattya Chattagram Nagarik Committee; First Chairman of the Local Government in CHT	Rangamati	11/08/2020
14	Senior Journalist, *Prothom Alo* (national daily newspaper)	Dhaka	13/08/2020
15	Former Chairman, Thanchi Upazila	Bandarban	13/08/2020
16	Executive Director, Society for Environment and Human Development	Dhaka	17/08/2020
17	Former President, Rangamati Press Club	Rangamati	25/08/2020
18	Senior Journalist, Prothom Alo (national daily newspaper)	Bandarban	25/08/2020
19	Former Member, Bangladesh Human Rights Commission and Activist	Rangamati	26/08/2020
20	Range Officer, Bagkhali, Ramu, Cox's Bazar	Cox's Bazar	30/08/2020
21	Professor of Geology, University of Dhaka	Dhaka	01/09/2020
22	Professor of International Relations, University of Dhaka	Dhaka	08/09/2020
23	Senior Researcher, Bangladesh Centre for Advanced Studies (BCAS)	Dhaka	12/09/2020
24	Economics editor and journalist covering international development, migration, poverty, and the environment	Dhaka	13/09/2020
25	Associate Professor, Department of Peace and Conflict Studies, University of Dhaka	Dhaka	16/09/2020
26	Executive Director, Research Initiatives Bangladesh	Dhaka	17/09/2020
27	Range Officer, Department of Forestry (Positioned in Bashkhali, Chittagong)	Chittagong	20/09/2020
28	Member- SONAK, Transparency International Bangladesh (TIB)	Rangamati	22/09/2020
29	Activist, Committee on Hill Protection Movement	Chittagong	22/09/2020
30	President, Bangalee Odhikar Songrokkhon Andolon (Bengali Rights Movement)	Rangamati	22/09/2020
31	Social Worker/Local Businessman	Khagrachari	23/09/2020
32	Associate Professor, Environmental Economics, Dhaka School of Economics	Dhaka	25/09/2020
33	Former Chairman, Rangamati Pourashava (City Corporation)	Rangamati	25/09/2020

ID	Designation of the participants	District	Interview date
34	Chief of Policy and Deputy Director, Chittagong Hill Tracts Development Facility (CHTDF), United Nations Development Programme (UNDP)	Rangamati	27/09/2020
35	Chairman, Upazila Parishad, Khagrachari	Khagrachari	30/09/2020
36	Professor, Urban and Regional Planning, Jahangirnagar University	Dhaka	16/10/2020
37	Disaster risk reduction (DRR) specialist, American Red Cross	Cox's Bazar	20/10/2020
38	Professor, Department of Geography and Environment, University of Dhaka	Dhaka	28/10/2020
39	Project Manager, DRR Project, Nobolok (NGO)	Cox's Bazar	02/11/2020
40	Camp Manager, ACTED (NGO)	Cox's Bazar	03/11/2020

Appendix 2: Guiding Questions for the Key Informant Interviewers

[1] What causes landslide disasters in Chittagong Hill Districts (CHD)?
[2] Do you find any historical changes in landslide patterns in CHD?
[3] What are the social vulnerabilities linked to landslide disasters in CHD?
[4] What are the impacts of landslides on livelihood and vice-versa in CHD?
[5] What are the external forces that contribute to the vulnerabilities of the disaster?
[6] What are the internal forces that contribute to the vulnerabilities of the disaster?
[7] Could you please share your idea on different CHD communities' perceptions of the landslide disaster?
[8] What are the various psychological and gender aspects of landslide disasters in CHD?
[9] How would you evaluate the existing policies to address the landslide disasters in CHD?
[10] What are your recommendations at the local and national levels to prevent landslide disasters in CHD?

References

Ahammad R, Stacey N (2016) Forest and agrarian change in the Chittagong Hill Tracts region of Bangladesh. In: Agrarian change in tropical landscapes, p 190

Ahmed B (2017) Community vulnerability to landslides in Bangladesh. Ph.D. thesis, University College London (UCL). https://discovery.ucl.ac.uk/id/eprint/1572567/. Accessed on 7 June 2022

Ahmed B (2021) The root causes of landslide vulnerability in Bangladesh. Landslides 18(5):1707–1720

Ahmmed HU, Masud MMH, Faisal M, Morshed MN (2013) The Chittagong Hill Tracts PEACE ACCOrd in Bangladesh: an overview. Mediterr J Soc Sci 4(4):123

Alam E (2020) Landslide hazard knowledge, risk perception and preparedness in Southeast Bangladesh. Sustainability 12(16):6305

Alam E, Ray-Bennett NS (2021) Disaster risk governance for district-level landslide risk management in Bangladesh. Int J Disaster Risk Reduction 59:102220

Anas A (2019) Why landslides in Bangladesh's former conflict zone are becoming deadlier? The New Humanitarian. https://www.thenewhumanitarian.org/analysis/2019/06/25/Bangladesh-landslides-climate-change-Indigenous. Accessed on 29 Aug 2021

Banglapedia (2021) Chittagong Hill Tracts. The National Encyclopaedia of Bangladesh. https://en.banglapedia.org/index.php/Chittagong_Hill_Tracts. Accessed on 18 June 2022

BBS (2014) Community report, Zila: Cox's Bazar. Bangladesh population and housing census 2011. Bangladesh Bureau of Statistics (BBS), Statistics and Informatics Division (SID), Ministry of Planning, Dhaka, Bangladesh. http://203.112.218.65:8008/WebTestApplication/userfiles/Image/PopCen2011/Com_Cox%27s%20Bazar.pdf. Accessed on 26 Aug 2021

BBS (2015) Zila report: Chittagong. Bangladesh Bureau of Statistics (BBS). http://203.112.218.65:8008/WebTestApplication/userfiles/Image/PopCenZilz2011/Zila_Chittagong.pdf. Accessed on 25 Aug 2021

Bryman A (2016) Social research methods. University Press, Oxford, UK

Damm A, Eberhard K, Sendzimir J, Patt A (2013) Perception of landslides risk and responsibility: a case study in eastern Styria, Austria. Nat Hazards 69(1):165–183

Dewan A, Hossain MF, Rahman MM, Yamane Y, Holle RL (2017) Recent lightning-related fatalities and injuries in Bangladesh. Weather Clim Soc 9(3):575–589

Dewan A, Ongee ET, Rahman M, Mahmood R, Yamane Y (2018) Spatial and temporal analysis of a 17-year lightning climatology over Bangladesh with LIS data. Theoret Appl Climatol 134(1):347–362

IPCC (2021) Summary for policymakers. In: Masson-Delmotte V, Zhai P, Pirani A, Connors SL, Péan C, Berger S, Caud N, Chen Y, Goldfarb L, Gomis MI, Huang M, Leitzell K, Lonnoy E, Matthews JBR, Maycock TK, Waterfield T, Yelekçi O, Yu R, Zhou B (eds) Climate change 2021: the physical science basis. Contribution of Working Group I to the sixth assessment report of the Intergovernmental Panel on Climate Change (IPCC). Cambridge University Press, Cambridge

Jaboyedoff M, Michoud C, Derron MH, Voumard J, Leibundgut G, Sudmeier-Rieux K et al (2018) Human-induced landslides: toward the analysis of anthropogenic changes of the slope environment. In: Landslides and engineered slopes. Experience, theory and practice. CRC Press, Boca Raton, pp 217–232

Kamal ASMM, Hossain F, Rahman MZ, Ahmed B, Sammonds P (2022) Geological and soil engineering properties of shallow landslides occurring in the Kutupalong Rohingya Camp in Cox's Bazar, Bangladesh. Landslides 19:465–478

Martuscelli PN, Ahmed B, Sammonds P (2022) Defying genocide in Myanmar: everyday resistance narratives of Rohingyas. J Genocide Res. https://doi.org/10.1080/14623528.2022.2078074

Mohsin A (2022) The Chittagong Hill Tracts, Bangladesh. In: The emergence of Bangladesh. Palgrave Macmillan, Singapore, pp 251–258

Peng L, Lin L, Liu S, Xu D (2017) Interaction between risk perception and sense of place in disaster-prone mountain areas: a case study in China's Three Gorges Reservoir area. Nat Hazards 85(2):777–792

Sammonds P, Shamsudduha M, Ahmed B (2021) Climate change-driven disaster risks in Bangladesh and its journey towards resilience. J Br Acad 9(s8):55–77

Sultana N, Tan S (2021) Landslide mitigation strategies in southeast Bangladesh: lessons learned from the institutional responses. Int J Disaster Risk Reduction 102402

TBS (2020) Chittagong Development Authority fined Tk10cr for cutting hills. The Business Standard (TBS). https://www.tbsnews.net/bangladesh/cda-fined-tk1038cr-cutting-hills-build-road-40195. Accessed on 21 June 2022

UNDRR (2015) Sendai framework for disaster risk reduction 2015–2030. United Nations Office for Disaster Risk Reduction (UNDRR). https://www.preventionweb.net/files/resolutions/N1516716.pdf. Accessed on 18 June 2022

UNHCR (2022) Rohingya refugee response in Bangladesh. The United Nations High Commissioner for Refugees (UNHCR). https://data.unhcr.org/en/situations/myanmar_refugees. Accessed on 7 June 2022

UNICEF (2019) Many tracts one community. United Nations Children's Fund (UNICEF), Bangladesh. https://www.unicef.org/bangladesh/sites/unicef.org.bangladesh/files/2019-09/CHT-report-LR-August20-website.pdf. Accessed on 18 June 2022

Wester AM, Mukherji A, Shrestha AB (eds) (2019) The Hindu Kush Himalaya assessment—mountains, climate change, sustainability and people. Springer Nature Switzerland AG, Cham

Characteristics and Remedy Solutions for a New Mong Sen Deep-Seated Landslide, Sapa Town, Vietnam

Lan Chau Nguyen, Tuan-Nghia Do, and Quoc Dinh Nguyen

Abstract

Landslides govern the evolution of landforms and pose a serious threat across the globe, especially in mountainous areas. In the northwestern area of Vietnam, a deep-seated landslide occurred near the new Mong Sen bridge in Trung Chai commune, Sapa town, Laocai province. In October 2020, some serious cracks were observed above a natural slope near a road, which was under construction to connect the Noi Bai-Laocai highway to Sapa town. The crack area was divided into two zones. Since this phenomenon could not only cause loss of life but also damage to the properties located downhill, the construction was stopped until the slope was rehabilitated. In this study, geological investigations, laboratory tests, and stability analysis were conducted to understand the failure mechanism. The analysis results showed that cutting activities during the construction of the road contributed to the sliding of the sloping soil mass. The following rehabilitation works at the failed area were conducted: (1) removing the soil above the natural slope; and (2) constructing the retaining system, including ground anchors and soil nails to retain the remaining slope. Results of stability analysis demonstrated that the retained slope would be stable after treatment.

Keywords

Landslides • Cutting slopes • Ground anchor • Back analysis

1 Introduction

Landslides are one of the most prominent geo-hazards experienced by many countries around the world. They are more predominant in coastal and mountainous regions. Landslides can be caused due to various geological and environmental factors, and endanger the safety of human beings, properties, and infrastructure. Besides the effects of heavy and/or long rainfall events, landslides may occur due to human activities, such as cutting and filling the slope during the course of construction projects on slopes. These activities have not only affected the living environment but also increased the number of landslides. In Vietnam, many landslides have been reported in previous studies (Nguyen et al. 2020; Luong et al. 2017; Tien et al. 2016; Duc 2013).

Laocai is a mountainous province, located between the Northeast and Northwest regions of Vietnam. Previously, the old Mong Sen bridge landslide occurred many times in 1990, 1994, 1996, 1998, 2000, 2001, and 6/2002 due to heavy rainfall and geological complex condition in this area. With the increasing demand for transportation on National Highway 4D from Laocai City to Sapa Town, the Laocai-Sapa expressway was constructed in 2018. However, the section from Km12+720 to Km12+860 of the new expressway is located in an area with complex topography, geomorphology, and geological conditions. In 2020, two deep-seated landslides happened during the construction of excavated slope in this section. The landslides mass needs to be handled to ensure the safety of the area.

In this study, the failure mechanism of a new Mong Sen landslide was examined based on comprehensive laboratory testing and back analysis data. The effectiveness of

L. C. Nguyen
Civil Engineering Faculty, University of Transport and Communications, Hanoi, Vietnam
e-mail: nguyenchaulan@utc.edu.vn

T.-N. Do (✉)
Civil Engineering Faculty, Thuyloi University, Hanoi, Vietnam
e-mail: dotuannghia@tlu.edu.vn

Q. D. Nguyen
Economic Geology and Geomatics Department, Vietnam Institute of Geosciences and Mineral Resources (VIGMR), Chien-Thang-Str, Thanh Xuan, Hanoi, Vietnam

I. Alcántara-Ayala et al. (eds.), *Progress in Landslide Research and Technology, Volume 1 Issue 2, 2022*, Progress in Landslide Research and Technology,
https://doi.org/10.1007/978-3-031-18471-0_29

countermeasures was then evaluated through stability analysis using the finite element method with shear strength reduction. This paper presents these findings along with recommended practices for field implementation to mitigate landslides.

2 Topography and Geologic Setting

The new Mong Sen landslide occurred in the Trung Chai commune, Sapa town, Laocai province, Vietnam. It is located at 22° 25′ 1.68″ N and 103° 54′ 18.03″ E, approximately 0.6 km far from the new Mong Sen bridge (Fig. 1). Different formations and features located in the region can be observed in Fig. 1. The slope related to the landslide is a part of the Lo Suay Tong Mountain in the Hoang Lien Son range. This region is generally aligned in the northwest-southeast direction and covered by lush green vegetation. Its altitude varies from 1300 to 1700 m above sea level with many slopes having a horizontal angle greater than 25°. This area is based on Posen formation (dgPZ1ps) with intrusive rocks including diorite, granodiorite, and granite. The Posen formation was observed in many landslide events in Laocai province (Chu and Nguyen 2008; Nguyen et al. 2021). The angle of slope in this area was about 25° and the soil/rock layer was weathered crust.

3 Climate and Rainfall

During the winter season, the weather is foggy and cold with occasional snowfall (Leisz 2017). The rainy season begins from May to October and accounts for 80% of the total annual rainfall. The average annual rainfall is about 1500 mm per year with a maximum rainfall of more than 3500 mm. The least rainfall months have an average rainfall from 50 to 100 mm/month. Hail sometimes occurs in February, March, and April. The monthly rainfall during 2018–2020 can be seen in Fig. 2, according to the recorded data from the Sapa Meteorological station (http://dulieu.phongchongthientai.vn/vi/RealTime2/Data#). The cumulative rainfall in 2020 was 3000 mm.

4 Landslide Characteristics

The new Mong Sen landslide occurred in Trung Chai commune, Sapa town, Laocai province. In this area, a new road is under construction, connecting the Noi Bai-Laocai highway to Sapa town. If the road was finished, it would enhance the tourism of Sapa town. However, since the construction included cutting slopes, many landslides have occurred. Among them, the landslide near the new Mong Sen bridge on October 27th, 2020 was the biggest one. Figure 3 shows the morphological changes of the slope during the course of construction from October 30th, 2019 to October 27th, 2020. The landslide area included 2 zones, of which zone 1 was about 2.5 ha and zone 2 was about 0.5 ha. As shown in Fig. 3a, the slope was originally covered by lush green vegetation. Its appearance changed significantly during the road construction with lack of vegetation. Zones 1 and 2 were differentiated by the range of cracks, as marked in Fig. 3b. Particularly, in zone 1, the local road was broken with a 0.4 m-wide crack (Fig. 3c). There were many cracks along the head scarf with an average subsidence of 0.5 m (Fig. 3d, e). On the other hand, in zone 2, different head scarfs were observed, which indicated that the landslide took place in many stages (Fig. 3f).

After the site investigation on October 27th, 2020, observation stations were installed to monitor the ground surface displacement. As shown in Fig. 4, 30 stations from QT1 to QT30 were distributed in the main sliding zone only (zone 1). During the construction of a retaining system, ground surface displacement developed much along the head scarf with a maximum value of 0.4 m. This increase in ground surface displacement was partially attributed to the dynamic load of the drilling machine when installing ground anchors and soil nails. The layout of the cracks occurring in zones 1 and 2 was sketched in Fig. 5, in which the overall failure of the slope could be seen more clearly.

5 Geological Drilling and Soil Properties

Figure 5 shows the layout of boreholes and cross-sections performed in the geological investigation. There were 9 boreholes, among which 6 boreholes were distributed in zone 1 and 3 boreholes were in zone 2. Based on them, the cross-sections 1-1 and 2-2 of the slope were created for zone 1 while cross-section 3-3 was built for zone 2. Standard penetration tests (SPTs) were carried out at each of the boreholes and soil samples were taken to perform laboratory tests.

Figure 6 shows three cross-sections in the landslide area. As shown in the figure, there are ten layers within the stratigraphy. The 1st layer is yellow/brown medium sandy clay mixed with 40% boulder (ML). Its thickness changes from 5.0 to 15 m with uncorrected Nspt = 15–50. The 2nd layer is yellow/brown medium to hard sandy clay mixed with 40% boulder. This layer is located only at the cross-section 1-1 with the boreholes LKBS1, LKBS2, and LKBS3. Its thickness varies from 1 to 3 m with uncorrected Nspt = 21–30. The 3rd layer is medium sandy clay mixed with 40% boulders (ML). This layer is distributed only at the cross-section 1-1, which is the same as the 2nd layer. Its average thickness is 5 m with uncorrected Nspt = 5–14. The

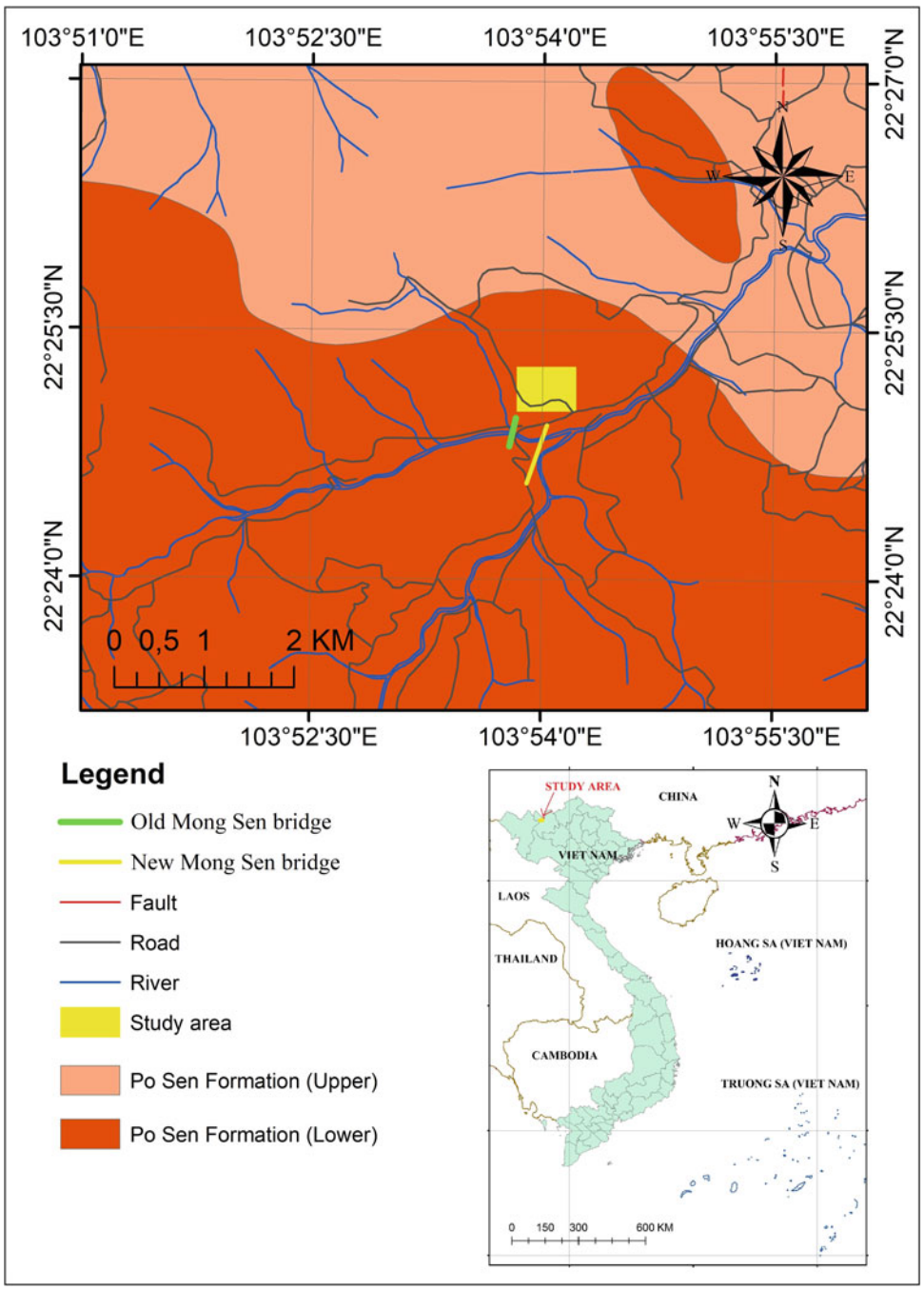

Fig. 1 Geological map and location of a new Mong Sen landslide

4th layer is yellow/brown medium sandy clay mixed with gravel (ML). This layer is found at the cross-section 3-3 with the boreholes LKBS7, LKBS8, and LKBS9. Its thickness varies from 4 to 10 m with uncorrected Nspt = 12–20. The 5th layer is yellow/dark medium to hard sandy clay mixed with gravel (ML). This layer is distributed across the site with the thickness from 5 to 15 m and uncorrected SPT value, Nspt = 20–50. The 6th layer is gray very hard gravel. Its thickness changes from 2 to 7 m with uncorrected Nspt = 50. The 7th layer is gray hard sandy clay mixed with gravel (ML). This layer is about 15 m thick with uncorrected Nspt = 30–50. The 8th layer is gray very hard sandy clay mixed with gravel (ML). Its thickness is approximately 10 m with uncorrected Nspt = 50. The 6th, 7th, and 8th layers can be found only in the cross-section 2-2. The 9th layer is gray strongly weathered rock. This layer has a total core recovery (TCR) = 40–50% and rock mass quality (RQD) = 30–40%. Its thickness varies from 3 to 10 m. The 10th layer is gray weathered rock. This layer has TCR = 60–70% and RQD = 50–60%. Its thickness is very large. The rock layers

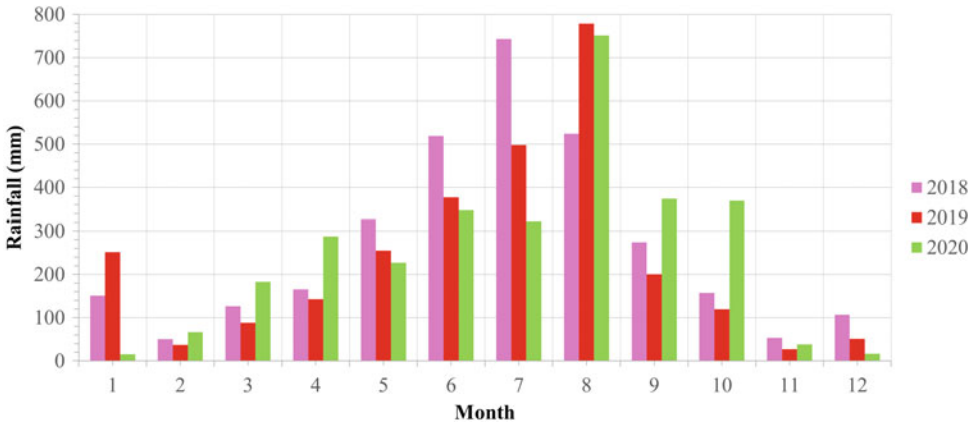

Fig. 2 Monthly rainfall by year from 2019 to 2021

are found at the depth of 10 m, 30 m, and 15 m corresponding to the cross-sections 1-1, 2-2, and 3-3, respectively. Due to the existence of thick topsoil, the slope in this area is prone to instability during road construction.

The grain-size curves of the 1st, 3rd, 4th, 5th, 7th, and 8th layers are plotted in Fig. 7. Their data were collected from both sieving and hydrometer tests. It can be observed that at each of the soil layers, the curves are consistent among the boreholes. Soil properties determined from laboratory tests are summarized in Table 1. The friction angle and cohesion of soil were determined from direct shear tests for both natural and saturated conditions. For the 9th and 10th layers, testing of compressive strength of weathered rock samples was conducted. The result showed that the average compressive strengths of saturated rock samples for the layer 9th and 10th layers were 26.27 MPa and 53.33 MPa, respectively.

6 Countermeasures and Stability Analysis

Based on the results of the site investigation and tests, countermeasures have been proposed to retain the sliding slope. Firstly, the very thick topsoil of the slope was partially removed, from 5 to 10 m, in order to reduce the soil weight and widen the new road to the designed width. Secondly, the ground anchor system was installed with length from 15 to 30 m. Each of the anchors had a 10 m bond length, which was located mostly in the rock layers. Also, it was composed of 4 prestressed strands of 12.7 mm type. The average anchor spacing was 3 m. A reinforced concrete beam network was employed to evenly distribute the anchor load to the ground surface. The beam cross-section was 0.3 m 0.3 m. Thirdly, the soil nail system was mobilized to retain the topsoil against shallow failure. Each of the soil nails consisted of a 32 mm steel bar, which was installed in 91 mm drilling holes and fixed by cement grout. The soil nail length was 11.7 m and the spacing was 3 m. Fourthly, the piping system was applied to lower the groundwater table. Each pipe was 75 mm in diameter and from 10 to 30 m in length. Finally, runoff water was collected using the shotcrete on the ground surface and the ditch system.

Stability analysis was performed using Plaxis 2D. This software is capable of modeling complicated stratigraphy and soil behaviors. Stability analysis will be performed using the finite element method with reduced shear strength. In principle, both input parameters, c, and tanϕ of soil were reduced from the original ones by dividing the M_{sf} coefficient (Nie et al. 2019; Tschuchnigg et al. 2015; Plaxis 2020). During stability analysis, the M_{sf} coefficient is gradually increased, which leads to the continuous reduction of the input c and tanϕ values. The analyzed slope will be weakened until the numerical solution cannot converge. This time is defined as the failure of the slope and the corresponding M_{sf} coefficient is treated as the factor of safety of the slope. The input parameters of soil and rock layers used in the analysis are summarized in Table 2. In this analysis, behaviors of both soil and weathered rock were assumed to be elastic perfectly plastic based on the Mohr–Coulomb model. This soil model purely requires five parameters. They are Young's modulus (E), Poisson's ratio (ν), friction angle (ϕ), cohesion (c), and dilatancy angle (ψ).

Figure 8a is the incremental displacement plot at the failure of the slope in zone 2 (the cross-section 3-3) before the application of the retaining system. The influence of the road construction is considered by removing a part of the soil at the slope toe. In essence, the incremental displacement exhibits the development of the nodal displacements during stability analysis when the M_{sf} coefficient is increased or the soil is weakened. Therefore, the failure surface of the slope can be determined based on the change of shadings in this plot. As marked in Fig. 8a, the predicted failure surface is consistent with the observed range of cracks at the site so that the result is reasonable. In addition, the maximum M_{sf} coefficient or the factor of safety in the analysis is 0.93, which is in good agreement with the instability of the slope.

Fig. 3 Morphological changes of the slope by time and landslide views: **a** before road construction on October 30th, 2019; **b** during road construction on October 27th, 2020; **c** crack on local road 155; **d** crack on head scarf at zone 1; **e** crack along slide body at zone 1, and **f** head scarfs at different stages at zone 2

After the application of the retaining system, as shown in Fig. 8b, the predicted failure surface goes through the anchor system. The corresponding safety factor is 1.27, which is greater than the required value of 1.25 in the Vietnamese standard (22TCN 171-87) and demonstrates the stability of the slope after treatment. Note that the influence of the anchor system is modeled through the structural elements and prestressed forces. Since the results of cross-sections 1-1 and 2-2 are similar to those of cross-section 3-3 as described above, they are not mentioned in this section.

7 Discussion

Based on the distribution of cracks throughout zones 1 and 2 (Figs. 3 and 5), the deep-seated failure mechanism has been identified in both zones. It is characterized by the curved cracks on the ground surface observed in Fig. 3b and the subsidence of the ground surface near the head scarf in Fig. 3d, f. Particularly, in the zone 2, many head scarfs could be seen in Fig. 3f, which demonstrates the occurrence of

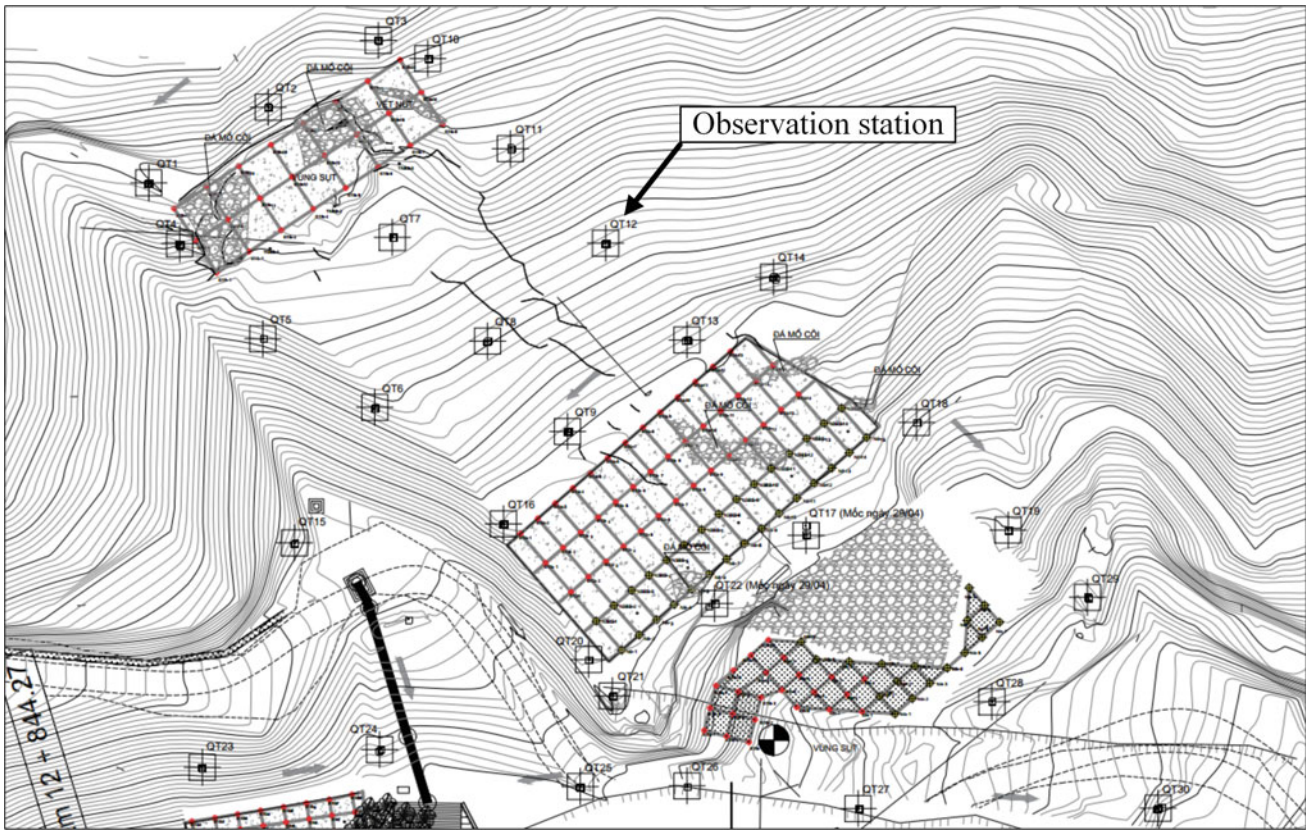

Fig. 4 Layout of observation stations in zone 1

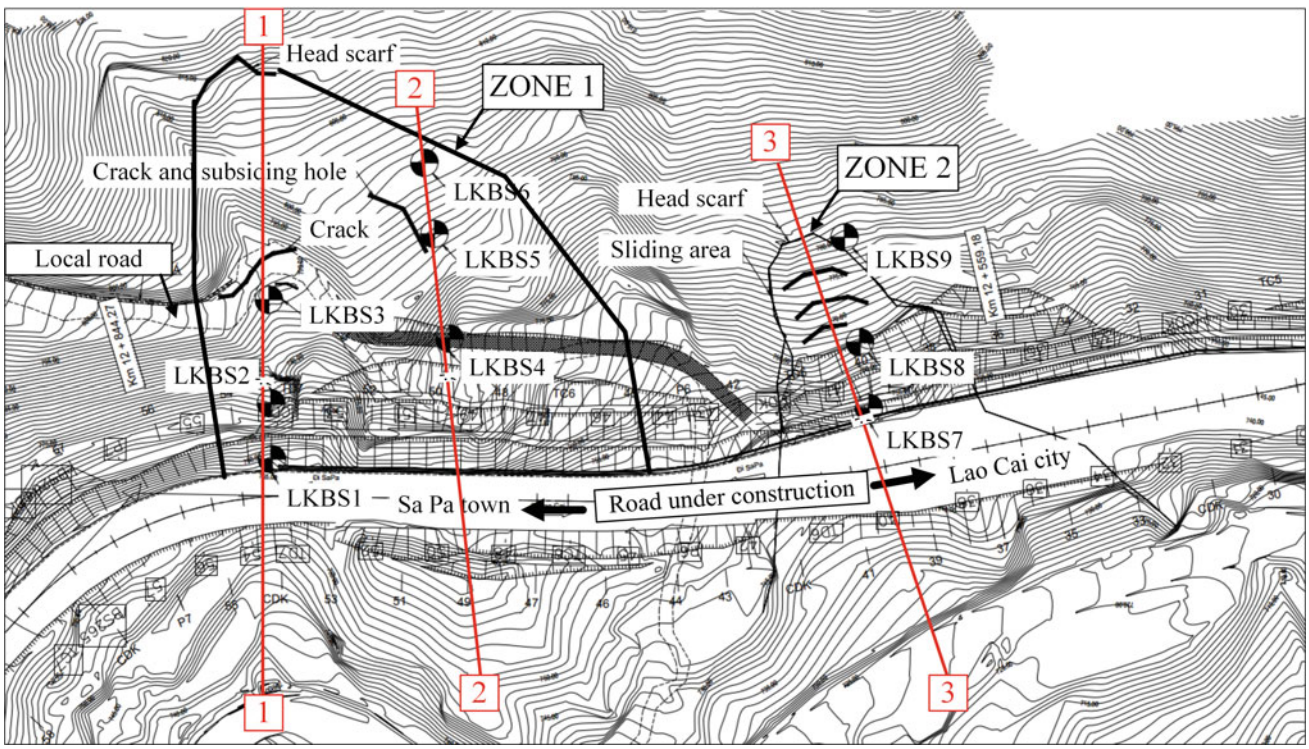

Fig. 5 Layout of cracks, boreholes, and cross-sections

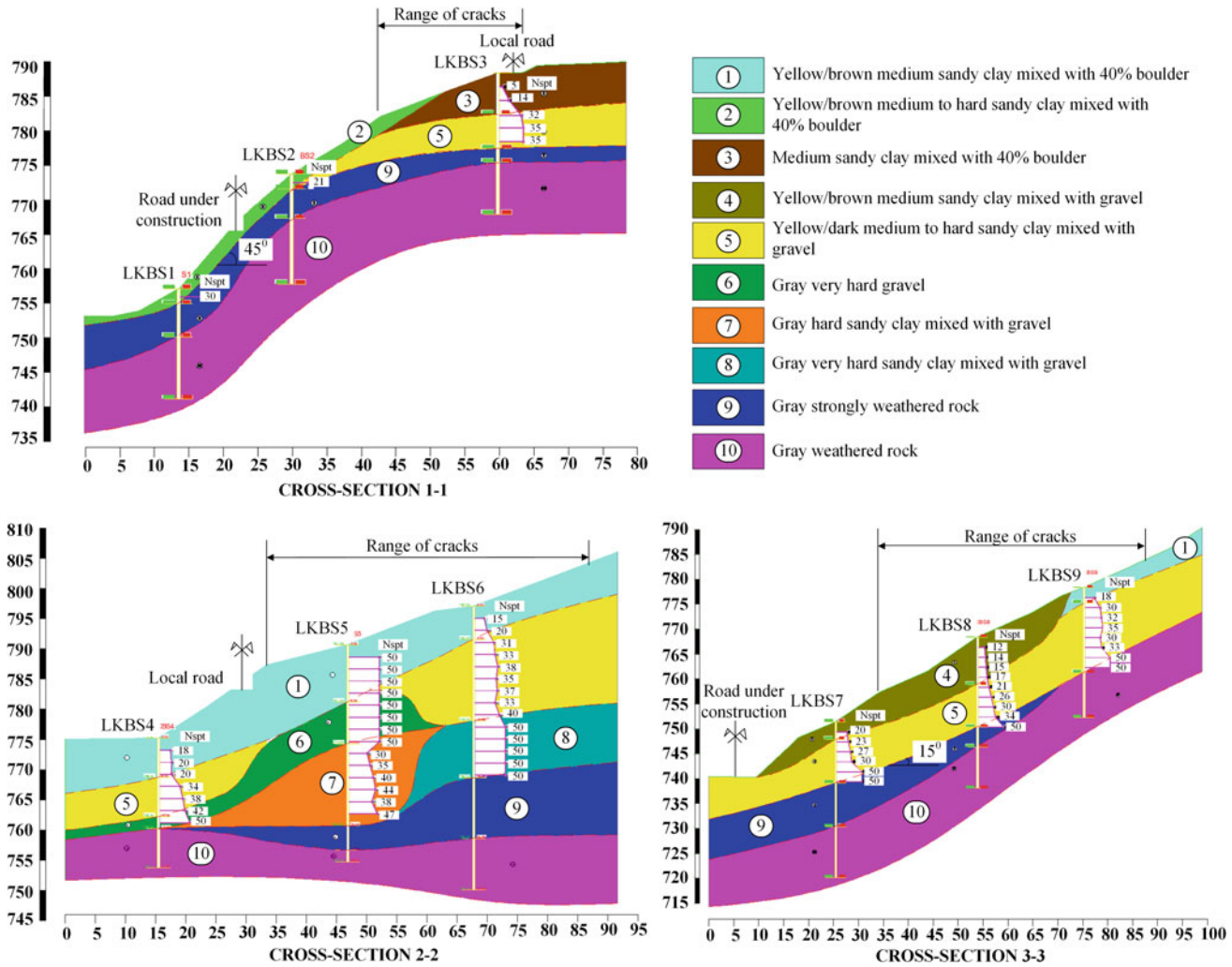

Fig. 6 Geological distribution within the landslide area

many failures at different stages during the course of road construction. Also, the deep-seated failure of the slope in the zone 2 might be inferred from the shape of the failure surface predicted by the stability analysis in Fig. 8a, which is deep and extends throughout the slope.

The results of the site investigation and back analysis show that the construction of the new road was a major triggering factor of the landslide. During the road construction, part of the soil located at the slope toe at both of the zones 1 and 2 was removed, which led to the instability of the slopes. Besides, the construction site locates at near the new Mong Sen bridge, at which many landslides have been recorded (Nguyen and Dao 2006). The site has a very thick topsoil, which is composed of clay, sand, gravel, and small rock. This topsoil is easily eroded and reduces shear strength during rainfall. In addition, since the inclination angle of the rocks layers (the 9th and 10th layers) is rather high (from 15° to 45° in Fig. 6), the geological and morphological features also play a role in the occurrence of the slope failure in the area.

8 Conclusions

This paper presented a study on a landslide that occurred near the new Mong Sen bridge in Trung Chai commune, Sapa town, Laocai province. The sliding area could be divided into zones 1 and 2. Based on the results of the study, some conclusions can be obtained as follows:

(i) The landslide mechanism belongs to a deep-seated type, which is characterized by the curved cracks along the failure surface on the ground and the

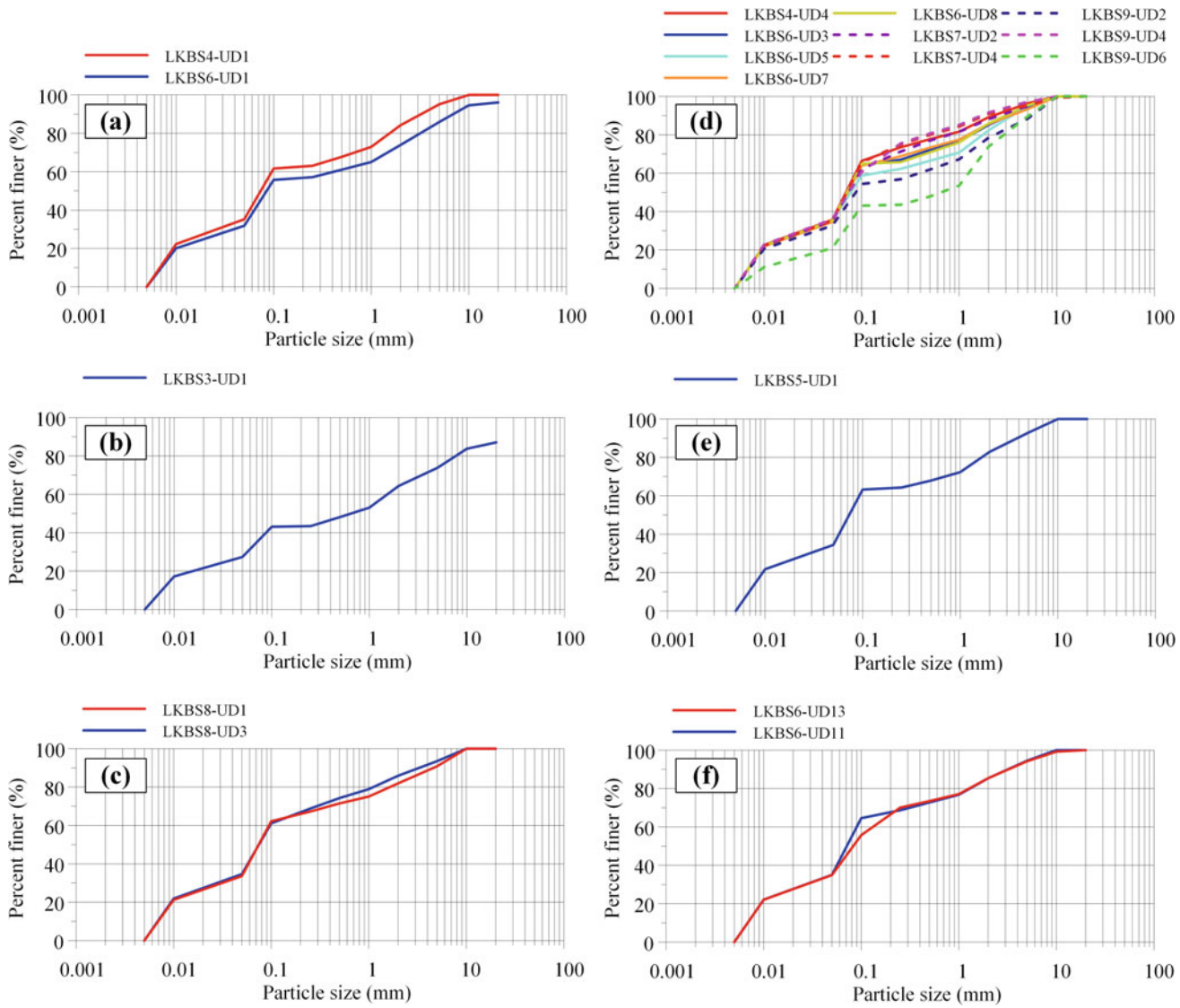

Fig. 7 Grain-size distribution of soils: **a** 1st, **b** 3rd, **c** 4th, **d** 5th, **e** 7th, and **f** 8th layers

Table 1 Soil properties from laboratory tests

Properties	1st layer	3rd layer	4th layer	5th layer	7th layer	8th layer
USCS	ML	ML	ML	ML	ML	ML
Water content (%), w	27.3	31.7	27.6	23.5	25.5	21.3
Natural unit weight (kN/m^3), γ	19.3	18.3	18.9	19.2	19.5	19.6
Dry unit weight (kN/m^3), γd	15.1	13.9	14.9	15.6	15.6	16.1
Specific gravity, Gs	2.69	2.67	2.69	2.68	2.68	2.68
Porosity (%), n	43.7	48.0	44.8	41.9	41.9	39.8
Void ratio, e	0.780	0.920	0.810	0.720	0.720	0.660
Degree of saturation (%), Sr	94.7	91.8	91.7	86.8	94.6	86.6
Liquid limit (%), LL	36.0	36.6	36.1	35.1	36.2	34.7
Plastic limit (%), PL	25.6	25.6	24.6	24.6	26.0	23.8
Plasticity index (%), PI	10.4	11.0	11.5	10.5	10.2	10.8

(continued)

Table 1 (continued)

Properties	1st layer	3rd layer	4th layer	5th layer	7th layer	8th layer
Coefficient of compressibility (av, 1-2, 1/kPa)	0.00036	0.00070	0.00042	0.00033	0.00031	0.00032
Cohesion at natural state (kPa), c′	21.80	20.50	22.00	22.90	23.10	22.20
Friction angle at natural state (°), ϕ′	20.0	10.7	16.2	22.5	23.5	22.4
Cohesion at saturated state (kPa), c′	20.2		19.8	19.2	18.7	21.8
Friction angle at saturated state (°), ϕ′	16.2		14.2	17.9	17.9	17.8

Table 2 Input parameters for Plaxis 2D model

Parameter	Symbol	Unit	Soil ID									
			1st layer	2nd layer	3rd layer	4th layer	5th layer	6th layer	7th layer	8th layer	9th layer	10th layer
Type of model			Mohr–Coulomb									
			Undrained					Drained	Undrained			
Unsaturated unit weight	γ_{unsat}	kN/m^3	19.5	19.0	18.3	19.0	19.0	19.0	19.1	20.0	26.9	26.9
Saturated unit weight	γ_{sat}	kN/m^3	19.6	19.5	18.7	19.2	19.5	19.5	19.7	20.1	27.0	27.0
Cohesion (saturated)	c′	kPa	20.20	0.0	19.4	19.8	19.2	0.0	18.70	20.9	50.0	100.0
Internal frictional angle (saturated)	ϕ′	°	16.3	30.0	10.2	14.3	17.9	32.0	16.1	18.2	30.0	30.0
Poisson's ratio	ν	–	0.30	0.30	0.33	0.30	0.31	0.30	0.30	0.30	0.30	0.30
Elastic modulus	Eref	kPa	10,710	31,000	4650	10,480	15,770	60,000	17,970	20,800	100,000	150,000

subsidence of the ground surface near the head scarf. In particular, in zone 2, many head scarfs corresponding to the different failures were observed during the road construction. The failure surface predicted by the stability analysis also agrees with the observed data.

(ii) The construction of the new road was the main trigger of the landslide, which removed part of the soil at the slope toe. Besides, the complicated geological conditions, including the thick topsoil and the high inclination angle of bedrock (from 15° to 45°), were also triggering factors for the landslide.

(iii) The countermeasures, which were applied to retain the landslide mass, were performed with the following steps: (1) removed part of the soil on the slope to reduce soil weight; (2) installed ground anchors and soil nails to retain the remaining slope; (3) lowered groundwater table using long pipes; and (4) gathered runoff water using the shotcrete and ditch system on the ground surface. The effectiveness of the countermeasures has been validated through the results of stability analysis, in which the factor of safety of the slope was greater than the required value.

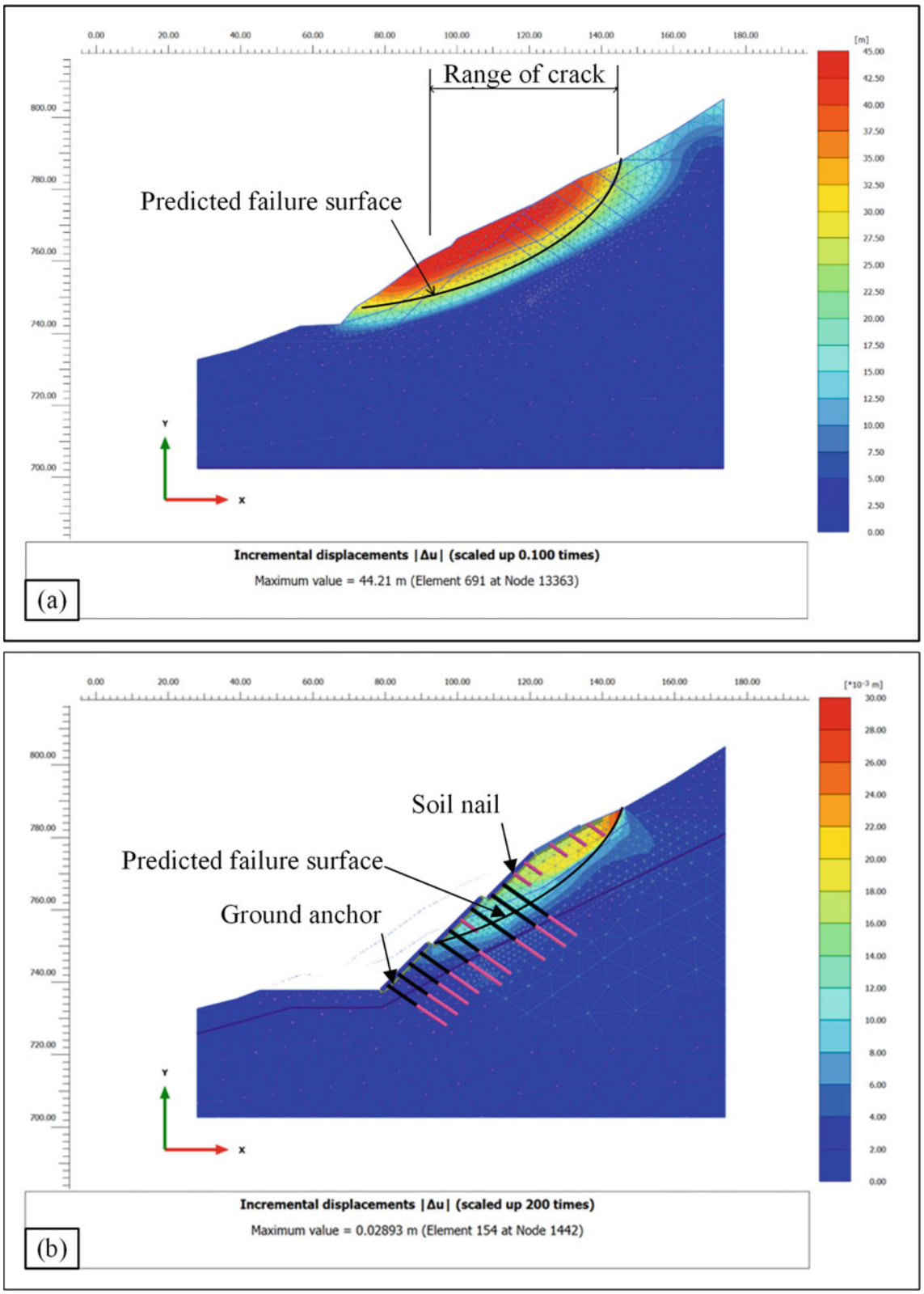

Fig. 8 Stability analysis of cross-section 3-3: **a** without and **b** with reinforcement system

References

22TCN 171-87 Soil investigation procedure and design of stabilizing method for road embankment in area vulnerable to landslide (in Vietnamese)

Chu VN, Nguyen TTH (2008) Assess the risk of landslides along the 4D route based on studying the relationship between geological structure and topography (in Vietnamese). http://idm.gov.vn/nguon_luc/Xuat_ban/2008/A305/a1.htm

Duc DM (2013) Rainfall-triggered large landslides on 15 December 2005 in Van Canh District, Binh Dinh province, Vietnam. Landslides 10:219–230. https://doi.org/10.1007/s10346-012-0362-4

Leisz SJ (2017) Land-cover and land-use transitions in northern Vietnam from the early 1990s to 2012 BT. Redefining diversity and dynamics of natural resources management in Asia, chap 6, vol 2, pp 77–86. http://doi.org/10.1016/B978-0-12-805453-6.00006-1

Luong LH, Miyagi T, Tien PV, Loi DH, Hamasaki E, Abe S (2017) Landslide risk evaluation in central provinces of Vietnam. In: Advancing culture of living with landslides, pp 1145–1153. https://doi.org/10.1007/978-3-319-53498-5

Nguyen VC, Dao VT (2006) Investigation and research of landslide geohazard in north-western part of Vietnam for the sustainable development of the territory. The Core University Program between Japan Society for the Promotion of Science (JSPS) and Vietnamese Academy of Science and Technology (VAST). Annual report of FY 2006, pp 269–280. http://hdl.handle.net/11094/13027

Nguyen LC, Tien PV, Do TN (2020) Deep-seated rainfall-induced landslides on a new expressway: a case study in Vietnam. Landslides 17:395–407. https://doi.org/10.1007/s10346-019-01293-6

Nguyen KT, Miyagi T, Isurugi S, Dinh VT (2021) Developing recognition and simple mapping by UAV/SfM for local resident in mountainous area in Vietnam—a case study in Po Xi Ngai community, Laocai province. In: Understanding and reducing landslide disaster risk, pp 103–109. https://doi.org/%2010.1007/978-3-030-60227-7_10

Nie Z, Zhang Z, Zheng H (2019) Slope stability analysis using convergent strength reduction method. Eng Anal Boundary Elem 108:402–410. https://doi.org/10.1016/j.enganabound.2019.09.003

Plaxis connect V20 (2020) Material models manual

Tien PV, Sassa K, Takara K, Tam DM, Quang LH, Khang DQ, Luong LH, Loi DH (2016) The influence of rainfalls on the potential of landslide occurrence on Hai Van Mountain in Vietnam. In: Proceeding of the final SATREPS workshop on landslides, 13 October, Hanoi, Vietnam, pp 112–121. ISBN: 978-4-9903382-3-7

Tschuchnigg F, Schweiger HF, Sloan SW, Lyamin AV, Raissakis I (2015) Comparison of finite-element limit analysis and strength reduction techniques. Geotechnique 65(4):249–257. https://doi.org/10.1680/geot.14.P.022

March 2019 Flood Impact on the Stability of Ambal Salt Ridge in the Gotvand Dam Reservoir, Southern Iran

Arash Barjasteh

Abstract

Ambal salt ridge is a unique exposure of salt piercement in the reservoir of Gotvand dam in the southwest of Iran. It is composed of evaporitic Gachsaran Formation of Oilgo-Miocene Age. This structurally controlled piercement is accompanied by subsidence and sliding of highly soluble layers into the dam reservoir. The region is affected by neotectonic activity due to proximity to two known active faults namely, Lahbari and Pir-Ahmad thrust faults. Based on a four year field observation and monitoring, a gradual and continuous sliding is occurring that is intensified by ground water circulation through evaporite karstic sinkholes and fracture systems. The subsidence and sliding of the Gachsaran evaporitic layers increased significantly after a severe flash flooding in March 2019. The water level rising due to flood event caused filling and saturation of the existing sinkholes in the salt ridge that facilitated and prompted development of land sliding. The situation is expected to be more critical if a moderate to high earthquake would happen since the dam lies in an active tectonic zone of the Zagros Fold Belt. Land subsidence and sliding was facilitated by high fracturing due to neotectonic activity. Finally, based on the Newmark method, slide potential of the largest landslide body of the Ambal ridge was calculated considering geotechnical parameters obtained from core drilling and partial saturation of the salt body during March, 2019 flooding of Karun River.

Keywords

Gotvand dam • Landslide • Ambal salt • Slope stability

1 Introduction

Floods and landslides can have severe and even disastrous consequences with fatalities, diseases, construction and infrastructure failures. The risks related to a flood or landslide can be described as the potential for loss, damage, or destruction of an asset as the result of a hazard exposing a vulnerability related to the event (Werner et al. 2010).

Floods cause damage by inundation, erosion, and by the impact of detritus against man's structures or by its deposition on valuable property. Each of these kinds of damage is influenced by the geology of the watershed contributing to the flooded region. Some dams are built solely to create a flood control reservoir. However, most reservoirs, called multi-purpose reservoirs, serve many objectives. When flood control is required, some of the storage space of the reservoir reserved for other purposes may also serve flood control, but not on a planned basis. Landslides occur on slopes in a variety of geological materials and develop through a variety of mechanisms and causes including river flooding (Bolt et al. 1977). Hazards arising from the earth's surface processes in terms of flooding and short-term climatic effects and as well as slope instability are widely recognized as ever-present dangers (Bromhead 1999; Andersson-Skold and Nyberg 2016). In addition to flooding, moderate to large earthquakes can also trigger landslides that could be dangerous for dam body (Keefer 1984). Reservoirs are one of the most important water resources in arid regions and play an important role in managing the limited surface runoff for different uses and controlling flash flooding (Jalali et al. 2019). However, the environmental impacts related to reservoirs and dams (e.g., hydrological, geomorphic, ecological) are a serious and growing concern in river basin management and environmental protection programs (Casale and Margottini 1999).

Scientific advances lead to periodical revisions of the influence of neotectonic activity on engineering structures (Marín-Córdova et al. 2004). The activity of faults and

A. Barjasteh (✉)
Dam and Power Plant Division, Khuzestan Water and Power Authority (KWPA), 61335-137 Ahvaz, Iran
e-mail: barjasteh@hotmail.com

I. Alcántara-Ayala et al. (eds.), *Progress in Landslide Research and Technology, Volume 1 Issue 2, 2022*, Progress in Landslide Research and Technology,
https://doi.org/10.1007/978-3-031-18471-0_30

related salt tectonics have affected engineering structures in the Zagros fold belt including the Gotvand Dam (Fig. 1) in Khuzestan Province of southwest Iran (Barjasteh 2012, 2013). The dam is a rockfill dam with a height of 182 m mainly built to generate hydroelectric power and provide flood control. The average annual runoff volume at the dam section is about 13.3 billion m^3 and the reservoir capacity with a length of 90 km is about 5.1 billion m^3 at the maximum normal operation elevation (234 masl). The stability of the dam reservoir becomes an important question as the existence of Ambal salt piercement could unfavourably damage highly fertile downstream farms and agricultural land (Hassanvand et al. 2011). The Karun River is the most important stream in the country originating and recharging from high Zagros mountain range. The River provides water for many cities, villages, agricultural projects and industrial factories along its nearly 380 km length downstream the reservoir of the Gotvand Dam.

This study was based on a four-year field observation and monitoring of land subsidence and sliding of the Ambal Salt Ridge. The study was accompanied by periodic site visits of the area especially after heavy rainfalls and fluctuations of the reservoir water level. During each site visit, the trends of newly formed fissures were recorded and subsequently compared to the last recorded ones. The number of the newly developed sinkholes and their extent were also evaluated and recorded and finally compared to the previous ones. Additionally, the situation and extent of the observed fissures and sinkholes and location of subsided lands were assessed and checked on the available Google Earth images. The subsidence and sliding of the Gachsaran evaporitic layers on the Ambal Salt Ridge were significantly increased after a severe flash flooding in March 2019 according to the last field trip on May 2019.

2 The Reservoir Hydrology and Geology

The dam and its reservoir are located in a semi-arid environment that experiences high summer temperatures up to 50 °C and many months without rain. The dry season generally starts in middle to late April and lasts for 6 months. The rains return in October, but most precipitations are from December onwards. (Fig. 2), mostly occurring during the early spring. Rising river levels, sometimes up to about 3 m can result in significant salt dissolution and slope failure along the Ambal ridge section, mostly in the form of slides and block toppling. Mean annual rainfall is 420 mm based on meteorological data from the Gotvand site, but totals have varied widely from one year to the next. The rainfall events tend to be sporadic, short and intense and such storm events result in appreciable water level rises in the Karun River.

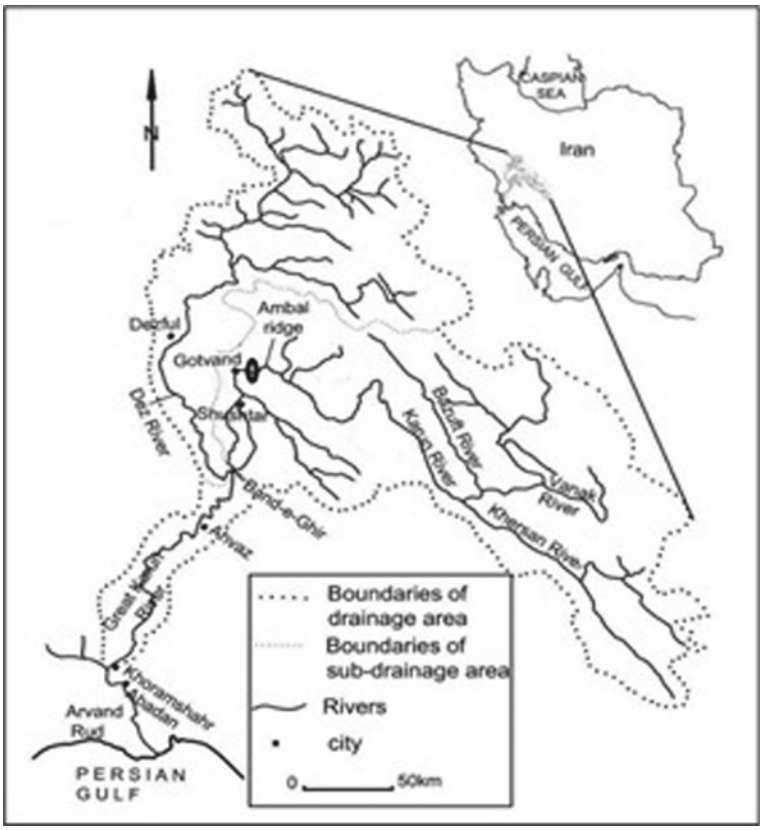

Fig. 1 Geographical location of the Gotvand Dam (oval) and Ambal Ridge in Karun River basin (after Aghdam et al. 2012)

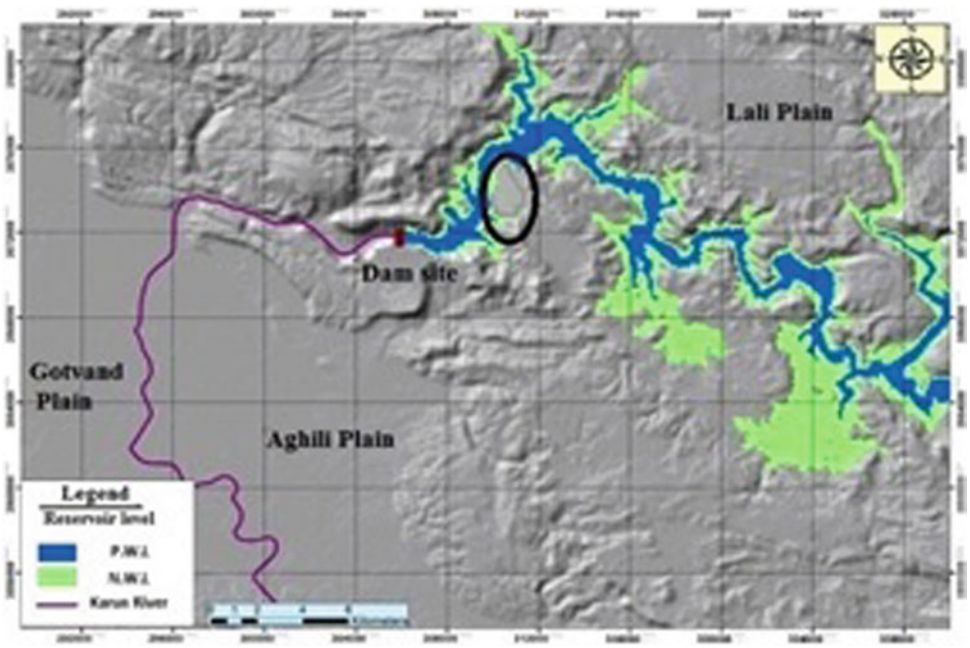

Fig. 2 Digital elevation model (DEM) of the Gotvand dam and reservoir region and location of Ambal ridge (black ellipse)

The Gotvand dam and reservoir are located in the Zagros Active Fold Belt from the seismotectonic point of view (Berberian 1995) in the northern part of Dezful Embayment structural unit. Fault plane solutions of the earthquakes in the region consistently show high-angle (40–50°) reverse faulting (Tatar 2012) with an estimated depth range from 8 to 13 km and 4–6 magnitudes. As part of Zagros Simply Folded Zone, the study area is comprised of parallel, long anticlines and Karun River syncline (Stocklin and Setudehnia 1977; Barjasteh 2018). The most important faults in the region are: Pir- Ahmad, Lahbari, Andeka, Lali and Shushtar thrust faults (Fig. 3) among which the first two are known as active faults (Barjasteh et al. 2017). The reservoir area is dominated by Lali Anticline which strikes NW–SE.

The reservoir area is dominated by Lali Anticline which strikes NW–SE. The Ambal salt ridge is located on the Lali Anticline and is occupied by Gachsaran Formation outcrop (Fig. 4). This Formation was named after the Gachsaran Oilfield in Khuzestan Province, where it is best developed (James and Wynd 1965). It was divided into seven members based on a type section composed of intervals from the well logs in the mentioned oil field (Stocklin and Setudehnia 1977). Members two, three, four and six have extensive salt units. The non-salt part of Gachsaran Formation is divided

Fig. 3 Google earth view of the main morphotectonic lineaments in the area including Lahbari active fault (thick red) and Lali-Ahvaz (thick yellow) lineament

into three members that are seen in the west and the south central part of Iran.

The tectonically incompetent units of the formation are highly subjected to dissolution effects, being characterized by extreme mobility and being responsive to differential stresses (Barjasteh 2016). Accordingly, one seldom finds a complete sequence of the formation as described at the type locality (Stocklin and Setudehnia 1977) due to high weathering and erosion. Agha Jari and Bakhtyari Formations are the main clastic deposits in the study area (Fig. 4). The principal lithology of Agha Jari Formation (Aj) including its Lahbari Member (Lb) consists of gypsum veins, calcareous sandstone, red marl and siltstone. Its age is Mio-Pliocene. A small outcrop of Mishan Formation (Mn) of Miocene Age is seen on the eastern side of the Ambal section. Its lithology is mainly consisted of marlstones. Bakhtiari Formation (Bk) is a terrigenous, clastic unit ranging in grain size from a silt grade to boulder conglomerate (Stocklin and Setudehnia 1977) of Pleistocene.

Ambal Salt Ridge

The Ambal salt ridge is a unique exposure of salt piercement in the reservoir of Gotvand dam in the southwest of Iran (Barjasteh 2016, 2018). It is composed of Gachsaran Formation of Oilgo-Miocene Age with dominant salt, gypsum and marly layers. This structurally controlled landscape (Bull 2009) is accompanied by subsidence and sliding of highly soluble layers into the reservoir (Milanović 2018; Milanović et al. 2019). The region is affected by neotectonic activity (Barjasteh 2018) in such a way that the Ambal ridge is aligned with an N–S basement lineament (Figs. 3 and 5). The ridge structure has a high density of sinkholes and landslides (Gutiérrez and Lizaga 2016). The Ambal ridge that is composed of the soluble Gachsaran layers has a local relief of 245 m, and comprises two adjoined dome-shaped hills in the northern and southern sectors, suggesting that there are two areas with higher differential uplift. A general direction of ground water flow from east and southeast (Fig. 6) is considered through the ridge (Aghdam et al. 2012; Gutiérrez and Lizaga 2016).

The trend of fractures bounding the landslides is mainly N–S. However, a second E–W trending fracture system was also observed in the field (Barjasteh 2016). These are the slopes with higher local relief and gradient, over steepened by fluvial down cutting and undermining, as well as halokinetic rise. Apparently, collapse sinkholes that are initially steep-walled hollows with sharp edges evolve to centers of large land subsidence and sliding. The highly elongated N–S-oriented landslide Ls3 (Fig. 5) is related to the collapse of the over steepened western flank of the Ambal ridge associated with the Karun River, where the strata have a dominant strike parallel to the valley (Gutiérrez and Lizaga 2016). Periodic site visits support the idea. (Barjasteh et al. 2017). The subsidence and rupturing of the land surface is continuously happening from 2014 to 2019 (Fig. 7). The phenomenon was amplified during and after the March 2019 flooding.

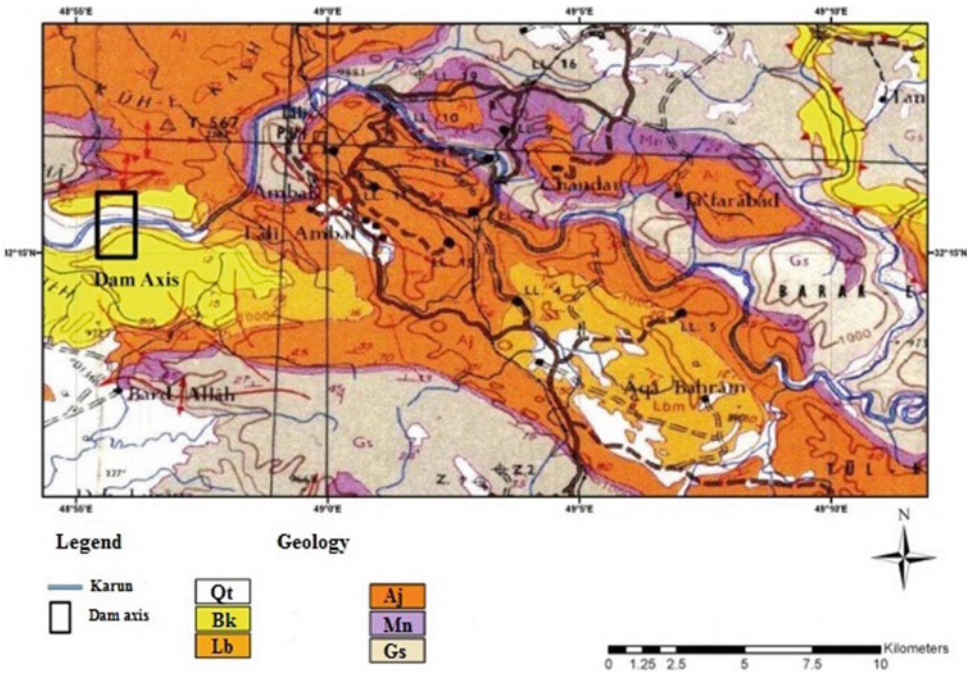

Fig. 4 Simplified geological map of the study area (after N.I.O.C 1977 and Hassanvand et al. 2011). See the text for outcrop lithologies

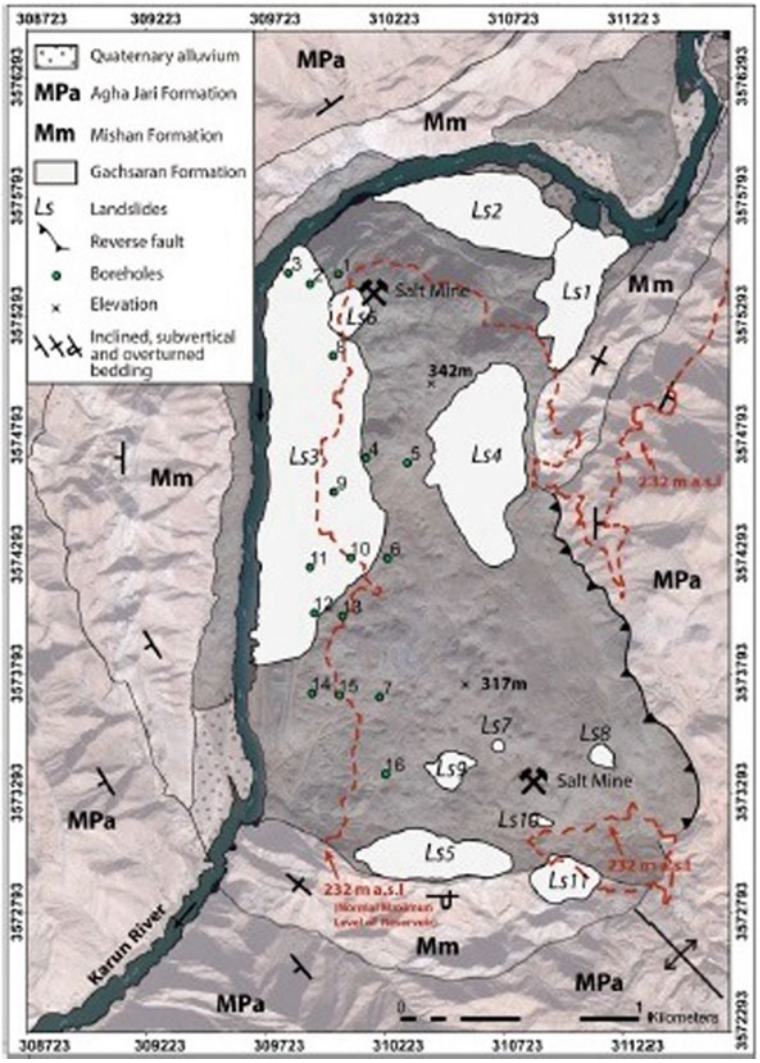

Fig. 5 Geomorphological map of the Ambal ridge (after Gutiérrez and Lizaga 2016) showing the distribution of the mapped landslides

3 Slope Stability

Based on the Newmark method (1965) as noted by Eq. 1, slide potential of the largest (Ls3) landslide body (Gutiérrez and Lizaga 2016) on the western flank of the Ambal piercement within the reservoir region was calculated (Eq. 1) applying geotechnical parameters obtained from the drilled bore holes besides partial saturation of the considered slope during March 2019 flooding (Fig. 8). In the Newmark method, the dynamic stability is related to static stability and the static factor of safety (FS) can be obtained by simple relationship (Jibson 2009). The Newmark (1965), the paper should start with the title section which has a showed that the critical acceleration of a potential landslide block is a simple function of the static factor of safety and the landslide geometry (Eq. 2).

$$ac = (FS-1)g \sin \alpha, \tag{1}$$

where ac is the critical (yield) acceleration in terms of g, the acceleration due to earth's gravity; FS is the static factor of safety; and a is the angle from the horizontal that the center of mass of the potential landslide block first moves.

$$FS = \frac{C'}{\gamma t \sin \alpha} + \frac{\tan \varphi'}{\tan \alpha} - \frac{m\gamma_w \tan \varphi'}{\gamma \tan \alpha}, \tag{2}$$

With regard to the available values for the geotechnical parameters of the Gachsaran Formation at Ambal ridge (Baghadashtaki et al. 2010) that is cohesion (zero) and internal friction angle (32°) and considering relevant saturated values for rock, FS was conservatively estimated to be equal to 1.086. After computing the static factor of safety regarding to the seismicity of the region (Fig. 9), the critical acceleration which can trigger initial sliding was estimated as 0.042 g that is much lower than the DBL value (0.27 g) of the dam site (Maleki and Behnam 2005). Accordingly, Ls3 landslide body shows highly critical condition during

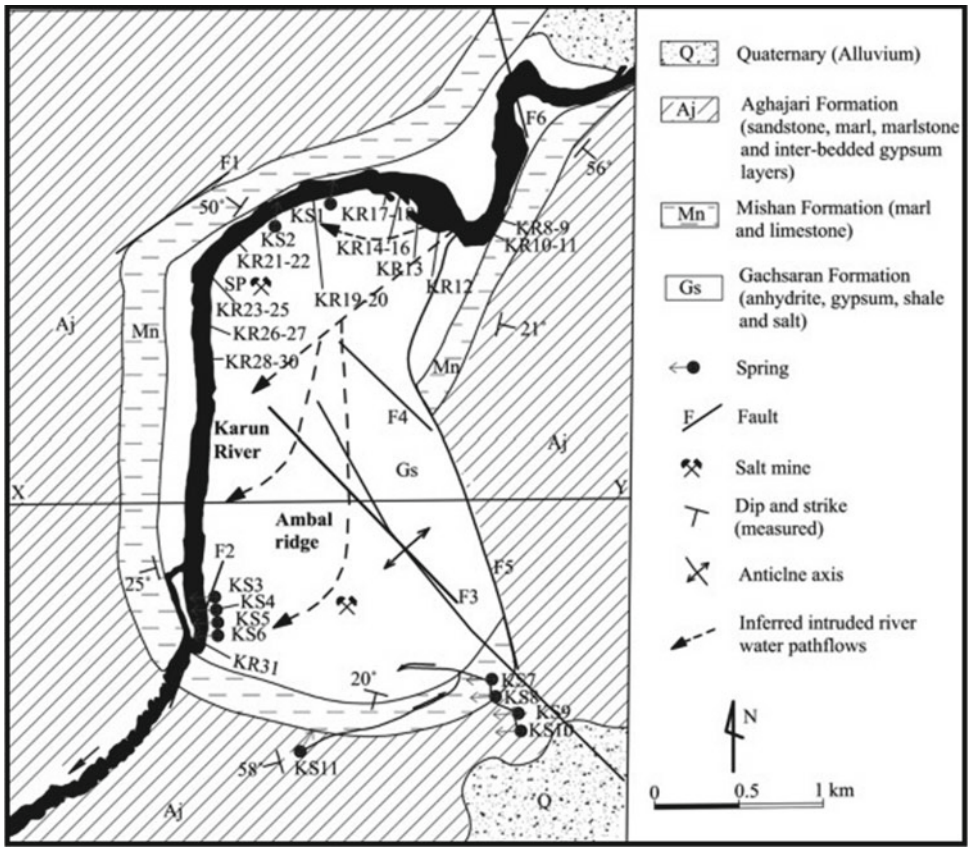

Fig. 6 Geological map of the Ambal ridge showing its groundwater regime (Aghdam et al. 2012)

Fig. 7 Progressive sliding and subsidence of the reservoir margin before (top) and after (bottom) the March 2019

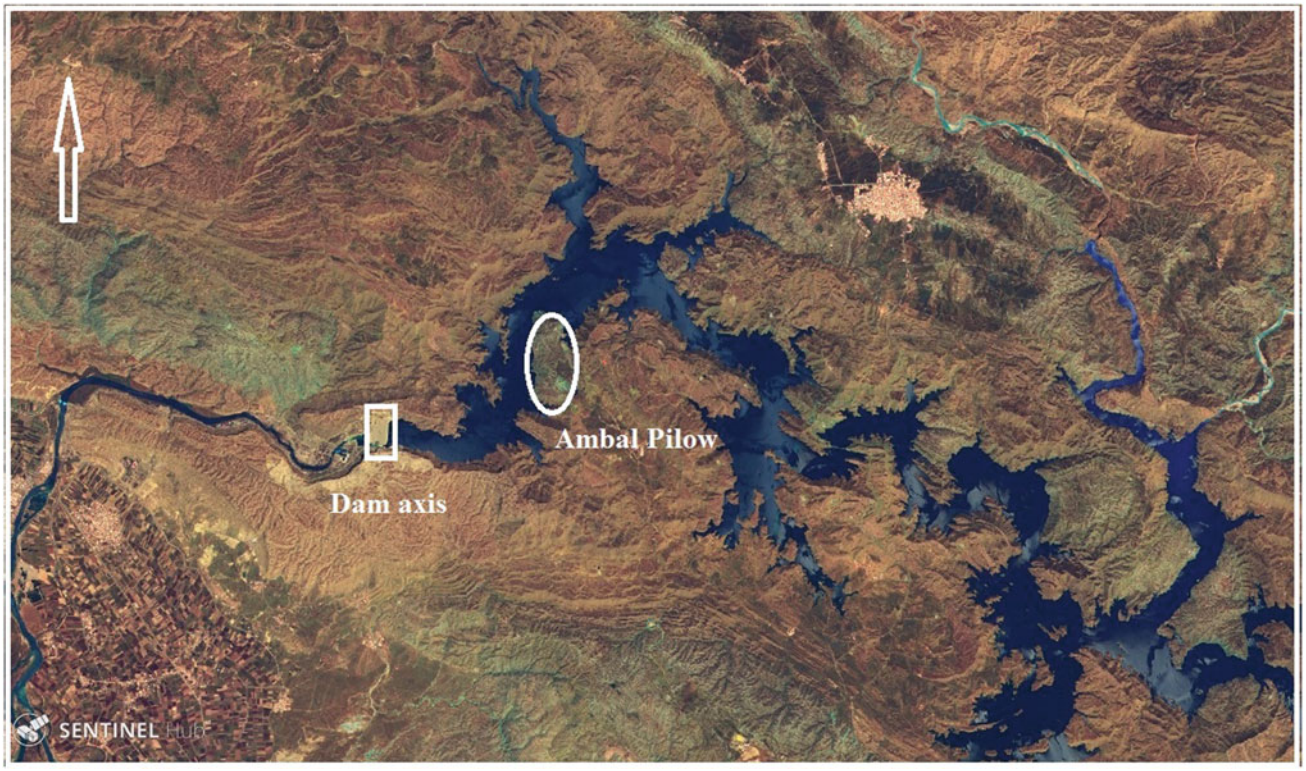

Fig. 8 Sentinel-2 image of the dam and reservoir region after the 2019 Karun River flooding (26.4.2019)

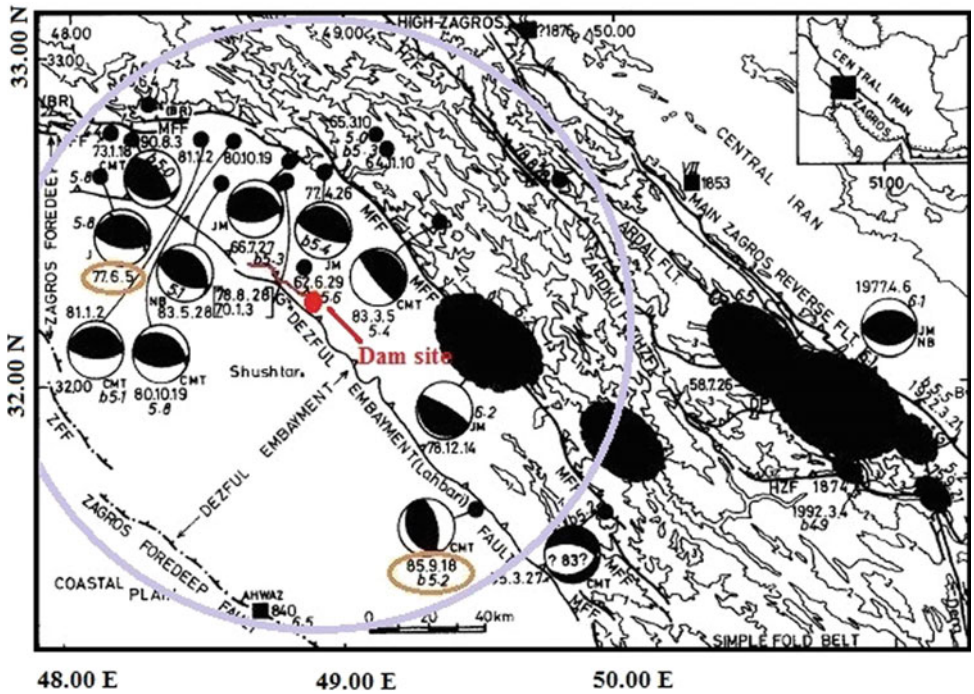

Fig. 9 Regional seismotectonic map in 100 km radius around the dam site (after Berberian 1995)

earthquake loading taking into account its partial saturation due to the March 2019 flooding. Such a condition could also be harmful for the dam body. Previous slope stability analyses (Water Institute 2005; Baghadashtaki et al. 2010) indicated a little larger safety factors but with lower ground water levels (Fig. 10) or smaller DBL values.

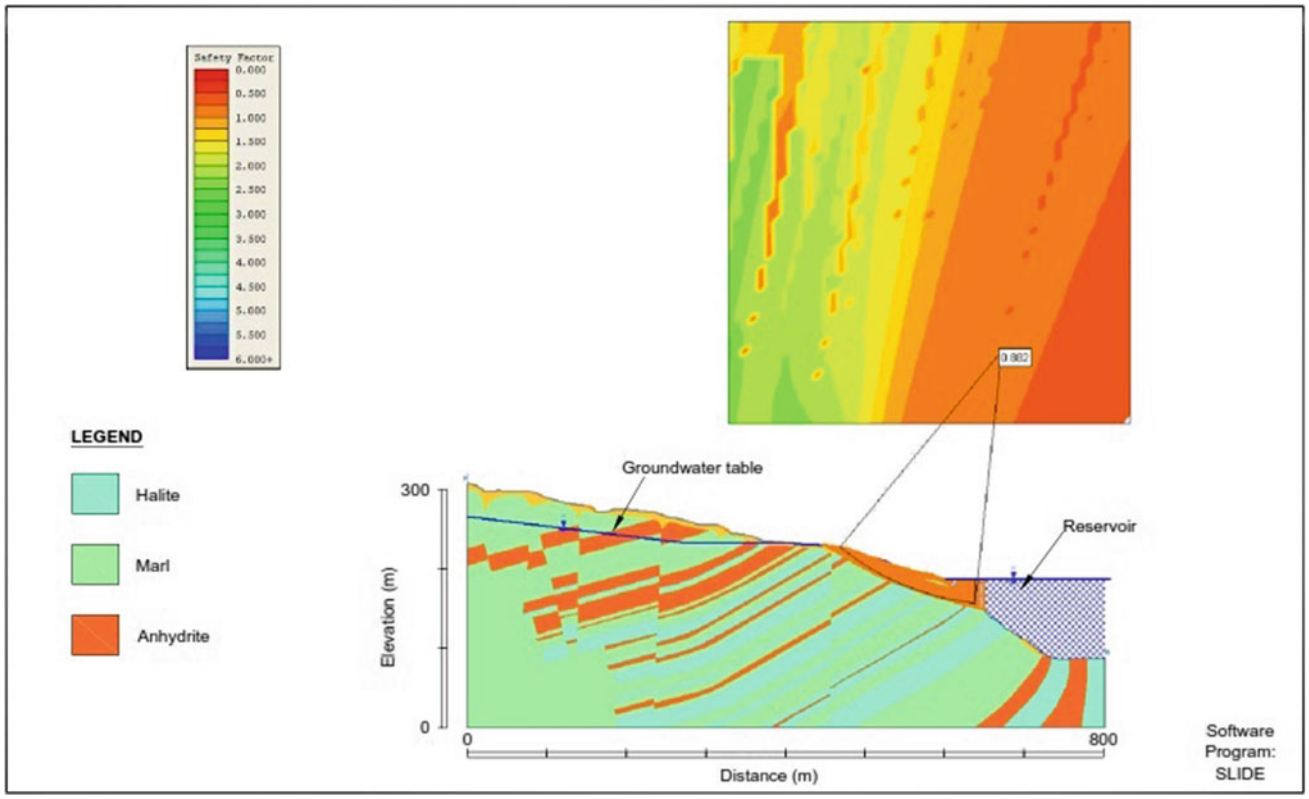

Fig. 10 Stability analysis of the upper section of the Ambal ridge (after Water Institute 2005)

4 Conclusions

The occurrence of Ambal salt ridge as an active halokinetic structure in the Gotvand Dam Reservoir imposed some problems to the project including subsidence and land sliding of highly soluble layers into the dam reservoir. The ridge is accompanied by several landslides and sinkholes. Periodic field investigations accompanied by satellite image observation show that Ambal salt pillow in the left bank of the reservoir is continuously sliding into the reservoir since its impounding. The gradual development of landslides is partly due to the halokinetic rise of the Ambal ridge and partly to the tectonic uplift of the region resulting from the regional tectonic compressive regime. The event of a severe flash flooding in March 2019 increased the reservoir water level to exceed the maximum normal operation elevation up to an elevation of about 236 masl, so that the subsidence and sliding of the Gachsaran evaporitic layers were significantly increased. As a result, the increase of ground water level saturated the existing sinkholes at different elevations that facilitated sliding of soluble layers. Considering tectonic activity of the region and regarding to the effect of moderate to large earthquakes to trigger landslides, based on the Newmark method, slide potential of the largest (Ls3) landslide body (Ls3) on the western flank of the Ambal piercement was calculated. It was shown that the landslide body has a low safety factor nearly 1.086 and could be critical during earthquake loading.

Acknowledgements The author wishes to thank his colleagues N.A. Damough, M.R. Hataf and M. Badiefar in Geology Group, Khuzestan Water and Power Authority (KWPA) for accompanying in field surveys. He also expresses his thanks to Mrs. R. Ghilav of the Technical Office for helping in review the manuscript. KWPA Managing Director, Dr. F. Izadjoo is especially acknowledged for his enthusiasm.

References

Aghdam JA, Zare M, Capaccioni B, Raeisi E, Forti P (2012) The Karun river waters in the Anbal ridge region (Zagros mountain Range, southwestern Iran): mixing calculation and hydrogeological implications. Carbonates Evaporites 27:251–267. https://doi.org/10.1007/s13146-012-0083-8

Andersson-Skold Y, Nyberg L (2016) Effective and sustainable flood and landslide risk reduction measures: an investigation of two assessment frameworks. Int J Disaster Risk Sci 7:374–392. https://doi.org/10.1007/s13753-016-0106-5

Baghadashtaki B, Khamehchiyan M, Nazari SM (2010) Stability study of Gachsaran formation slopes in reservoir of Gotvand dam with effect of reservoir recharge and dissolution of salty materials (in Persian). Iran J Eng Geol Spring-Summer 4(1):809–826

Barjasteh A (2012) Salt Tectonics Impact on Dam Construction in Khuzestan Province of Iran. In: 24th ICOLD congress. Kyoto, Japan, p 6

Barjasteh A (2013) Geologic structure control on seepage potential of the Upper Gotvand Dam, Iran. In: 81st ICOLD annual meeting. Seattle, USA, p 9

Barjasteh A (2016) Halotectonics and evaporite karst of the Upper Gotvand Dam Reservoir, SW Iran. In: 34th National and 2nd international geosciences congress, 15–17 Feb 2016, Tehran, Iran. GSI

Barjasteh A (2018) Neotectonic features of Gotvand-Lali region, southwest Iran. In: 1st International and 3rd national quaternary congress, 13–14 Feb 2018, Tehran, Iran

Barjasteh A, Damough NA, Hataf MR, Badiefar M (2017) Neotectonics related landslide of Ambal salt piercement within the Upper Gotvand dam reservoir, Iran. In: 19th ICSMGE, 17–22 Sep, Seoul, Korea, p 4

Berberian M (1995) Master "blind" thrust faults hidden under the Zagros folds: active basement tectonics and surface morphotectonics. Tectonophysics 241:193–224. https://doi.org/10.1016/0040-1951(94)00185-C

Bolt BA, Horn WL, Macdonald GA, Scott RF (1977) Geological hazards: earthquakes—tsunamis—volcanoes, avalanches—landslides—floods, 2nd edn. Springer, p 330. https://doi.org/10.1007/978-1-4615-7101-8

Bromhead EN (1999) The stability of slopes, 2nd edn. Spon Press, p 406

Bull WB (2009) Tectonically active landscapes. Wiley-Blackwell, p 326

Casale R, Margottini C (eds) (1999) Floods and landslides, integrated risk assessment. Springer, p 373

Gutiérrez F, Lizaga I (2016) Sinkholes, collapse structures and large landslides in an active salt dome submerged by a reservoir: the unique case of the Ambal ridge in the Karun River, Zagros Mountains, Iran. Geomorphology 254:88–103. https://doi.org/10.1016/j.geomorph.2015.11.020

Hassanvand M, Dahrazma B, Hafezi Moghadas N (2011) Assessment of formations surface area in the reservoir of Gotvand Dam and quality variations of water in different levels after impounding (in Persian). In: Proceedings of the 7th conference on NIAEG. Shahrood University of Technology, Shahrood, Iran, p 7

Jalali L, Zarei M, Gutierrez F (2019) Salinization of reservoirs in regions with exposed evaporites. The unique case of Upper Gotvand Dam, Iran. Water Res 157:587–599. https://doi.org/10.1016/j.watres.2019.04.015

James GA, Wynd JG (1965) Stratigraphic nomenclature of Iranian oil consortium agreement area. AAPG Bull 49(12):2182–2245

Jibson RW (2009) Methods to model co-seismic landslide movement. The next generation of research on earthquake-induced landslides. In: An international conference in commemoration of 10th anniversary of the Chi-Chi earthquake, p 13, 21–26 Sep 2009. National Central University, Taipei, Taiwan, pp 128–140

Keefer DK (1984) Landslides caused by earthquakes. Geol Soc Am Bull 95:406–421. https://doi.org/10.1130/0016-7606(1984)95

Maleki E, Behnam M (2005) Seismic aspects of cascading dams constructed on Karun River. In: 73rd ICOLD annual meeting, Tehran, Iran, p 10

Marín-Córdova S, Campos-Enríquez O, Herrera-Moro-Castillo M (2004) Neotectonic related geological risk at dams in the Mexico Basin: Guadalupe dam. Geofísica Internacional 43(3):435–443

Milanović P (2018) Engineering karstology of dams and reservoirs. Taylor & Francis Group, p 354

Milanović P, Maksimovich N, Meshcheriakova O (2019) Dams and reservoirs in evaporites. Springer Nature Switzerland, p 157

Newmark NM (1965) Effects of earthquakes on dams and embankments. Geotechnique 15(2):139–160

Stocklin J, Setudehnia A (1977) Stratigraphic lexicon of Iran, 2nd edn. Geological Survey of Iran, Report no 18, p 376

Tatar M (2012) Seismicity and seismotectonics in the Upper Gotvand dam region, (in Persian). In: Proceedings of the 1st international and 3rd national conference on dam and hydropower plants, IWPCO, Tehran, Iran, p 10

Water Institute (2005) Study and assessment of desalinization approaches for Gotvand dam reservoir. Reconnaissance Report, Tehran University, p 492

Werner ED, Friedman GP (eds) (2010) Landslides: causes, types and effects. Nova Science Publishers, Inc., p 404

KLC2020 Official Promoters

The Kyoto Landslide Commitment 2020 (KLC2020)

Kyoto 2020 Commitment for Global Promotion of Understanding and Reducing Landslide Disaster Risk

A Commitment to the Sendai Landslide Partnerships 2015–2025, the Sendai Framework for Disaster Risk Reduction 2015–2030, the 2030 Agenda Sustainable Development Goals, the New Urban Agenda and the Paris Climate Agreement

KLC2020 Official promoters are public and private organizations who promote the Kyoto Landslide Commitment 2020 and provide financial support for the implementation of the KLC2020 activities including the Open Access Book Series "Progress in Landslide Research and Technology."

Host organization

International Consortium on Landslides (ICL)/Nicola Casagli

Public sectors: KLC2020 Official Promoters-public

International Unions/Associations, Governmental organizations, Universities and Research institutes

- The International Union of Geological Sciences (IUGS)/John Ludden
- The International Union of Geodesy and Geophysics (IUGG)/Kathy Whaler
- The International Association for the Engineering Geology and the Environment/Rafig Azzam
- International Geosynthetics Society (IGS)/John Kraus
- Geological Survey of Canada, Natural Resources Canada, Canada/Daniel Lebel
- Faculty of Civil and Geodetic Engineering, University of Ljubljana, Slovenia/Matjaž Mikoš
- China University of Geosciences, Wuhan, China/Huiming Tang
- Department of Civil Engineering, National Taiwan University, Chinese Taipei/Shang-Hsien Hsien
- Institute of Rock Structure and Mechanics, the Czech Academy of Sciences/Josef Stemberk
- Institute of Cold Regions Science and Engineering, Northeast Forestry University/Wei shan.

Private sectors: **KLC2020 Official Promoters-private**

Companies and corporation

- Marui & Co. Ltd., Japan
- Nippon Koei Co., Ltd., Japan
- Ellegi srl, Italy
- IDS GeoRadar s.r.l., Italy
- Chuo Kaihatsu Corporation, Japan
- Godai Corporation, Japan
- Kiso-Jiban Consultants Co., Ltd., Japan
- Kokusai Kogyo Co., Ltd., Japan
- OSASI Technos, Inc., Japan.

I. Alcántara-Ayala et al. (eds.), *Progress in Landslide Research and Technology, Volume 1 Issue 2, 2022*, Progress in Landslide Research and Technology,
https://doi.org/10.1007/978-3-031-18471-0

The International Geosynthetics Society

International Geosynthetics Society

Introduction

The International Geosynthetics Society (IGS) is a non-profit learned society founded in Paris in 1983.

We are a member of the Federation of International Geo-Engineering Societies and also hold Liaison Organization status with International Organization for Standardization (ISO) Technical Committee 221 (TC 221) on Geosynthetics. The IGS is proud to be part of a multi-agency commitment with Kyoto Landslide Commitment 2020 (KLC2020).

The IGS is dedicated to the scientific and engineering development of geotextiles, geomembranes, related products, and associated technologies. Our membership forms a global community of over 3,000 including corporate, individual and student members, with a shared passion for what geosynthetics can achieve.

Geosynthetics are durable, high-performing polymeric materials used make infrastructure more sustainable in a variety of ways, for example:

Reduced energy consumption and emissions through:

- less on-site excavation;
- reduced transport of bulky construction materials;
- extended infrastructure lifetimes and reduced maintenance.

Protection of surface and groundwater through:

- landfill lining and containment of hazardous waste
- sludge dewatering and purification
- construction of sludge and tailings lagoon capping
- grey water storage for re-use
- preservation of potable and irrigation water supplies by lining canals, dams and reservoirs.

Replacement of other construction materials:

- sand and aggregate
- concrete, lime and cement
- steel.

Environmental protection:

- nuclear waste disposal
- sustainable urban drainage systems
- green and blue roof construction
- cost effective and resilient flood defences
- coastal defence.

Geosynthetics help prevent landslides in a number of ways, for example:

- performing a barrier and/or a filter function, mitigating the effects of water seepage;
- reinforcing soil and stabilising slopes;
- holding topsoil in place, preventing slippage;
- draining excess rainwater without washing soil away;
- encouraging growth of new vegetation, stabilizing slopes through natural means (Figs. B.1 and B.2).

International Geosynthetics Society
9225 Bee Caves Rd, Building B, Suite 206,
Austin, TX, 78733, USA
e-mail: igssec@geosyntheticssociety.org
URL: https://www.geosyntheticssociety.org/

I. Alcántara-Ayala et al. (eds.), *Progress in Landslide Research and Technology, Volume 1 Issue 2, 2022*, Progress in Landslide Research and Technology,
https://doi.org/10.1007/978-3-031-18471-0

Fig. B.1 Geosynthetics used to stabilize a slope using soil in-fill and seeding for plants

Fig. B.2 Geosynthetics used to stabilize a slope by interacting with vegetation root structures

Geological Survey of Canada, Natural Resources Canada

GSC-Pacific Division

Geological Survey of Canada—Who We Are

The Geological Survey of Canada (GSC) is part of the Earth Sciences Sector of Natural Resources Canada. The GSC is Canada's oldest scientific agency and one of its first government organizations. It was founded in 1842 to help develop a viable Canadian mineral industry by establishing the general geological base on which the industry could plan detailed investigations. Throughout its long and colourful history, the GSC has played a leading role in exploring the nation.

Today, the GSC is Canada's national organization for geoscientific information and research. Its world-class expertise focuses on the sustainable development of Canada's mineral, energy and water resources; stewardship of Canada's environment; management of natural geological and related hazards; and technology innovation (Fig. C.1).

The GSC celebrated its 175th anniversary in 2017 which coincided with Canada's 150th anniversary of Confederation.

The GSC co-leads the Canada-Nunavut Geoscience Office and works with dozens of universities and research institutes, industry organizations, other federal departments, provinces, territories and municipalities in Canada and across the world. In particular, we work closely with other geological survey organizations in Canada through the unique Intergovernmental Geoscience Accord.

Every year, we publish hundreds of maps, Open Files, peer-reviewed papers and other reports. Our scientists are recognized worldwide and sought after for their expert advice on locating mineral, energy and groundwater resources, reducing risk from natural hazards and reviewing environmental assessments.

Fig. C.1 Paleotsunami investigations in order to understand regional earthquake cycles and submarine landslide hazards

Strategic Priorities

The GSC has attempted to plot a course through this changing, uncertain world.

First, we identify three core areas of persistent scientific endeavour, which reflect stable, long-term needs of society:

- **Geological knowledge for Canada's onshore and offshore lands**
- **Geoscience for sustainable development**
- **Geoscience for keeping Canada safe**

Next, we outline a new, fourth area of endeavour, Geoscience for society, which is the need to address the uncertainties of the changing world by expanding the reach and impact of geoscience knowledge in land-use decision making and in efforts to reduce the risk of disasters.

GSC-Pacific Division
1500-605 Robson St, Vancouver, BC, V6B 5J3, Canada
e-mail: David.Huntley@nrcan-rncan.gc.ca

I. Alcántara-Ayala et al. (eds.), *Progress in Landslide Research and Technology, Volume 1 Issue 2, 2022*, Progress in Landslide Research and Technology,
https://doi.org/10.1007/978-3-031-18471-0

Finally, we recognize that our strength lies in a fifth area of endeavour, Our people, Our science, which we need to nurture to maintain a high-performing workforce capable of world-leading innovative geoscience for the benefit of Canada.

(a) Geological knowledge for Canada's onshore and offshore lands

Geoscientific knowledge is fundamental to managing our onshore and offshore lands and their abundant resources. With its 10 million km^2 of onshore land and an additional 7 million km^2 of ocean estate, Canada is a vast country and a core mission of the GSC is to map and understand the land and its resources. Our Geo-mapping for Energy and Minerals (GEM) program continues to advance our knowledge of the North and by 2020 will complete a first mapping of surface geology at a coarse scale.

In the offshore lands, our geoscience knowledge also serves to confirm the farthest extents of the Canadian territory. Our joint program with Global Affairs Canada and Fisheries and Oceans Canada to delineate the outer limits of the continental shelf in the Atlantic and Arctic Oceans will reach a critical milestone in 2019. The program will file its Arctic submission under the United Nations Convention on the Law of the Sea (UNCLOS) (Fig. C.2).

(b) Geoscience for sustainable development

Finding new resources remains a major challenge. Many near-surface deposits have been discovered in Canada, but significant mineral resources remain to be found in less accessible regions and at depths below the surface. Finding new resources requires systematic, intensive and innovative methods to assess the mineral potential in remote locations. It requires searching beneath overburden cover, imaging the 3-D structure of the earth and understanding the geological processes that lead to concentration of minerals in certain locations (Fig. C.3).

Fig. C.2 The GSC studies the sea floor of the Arctic to understand its geology and geohazards. Here a small craft surveys the bottom of Southwind Fjord (Baffin Island, N Nunavut)

Fig. C.3 GSC geologists near the Heiberg Formation in northern Ellesmere Island (NU) as part of the Geo-mapping for Energy and Minerals program. This formation is the primary host of major gas accumulations in the Canadian High Arctic

For the Energy sector, the greatest challenge is in the transition to a low-carbon economy. Although global fossil fuel use is likely to continue to grow over the foreseeable future, the trend will likely be at a decreasing rate. Canada has an abundant supply of conventional and unconventional (oil sands and shale) oil and gas, so development in frontier areas is likely to be slow. In addition, the government has placed a moratorium on exploration activity in the Arctic offshore lands.

(c) Geoscience for keeping Canada safe

The GSC will continue to work on understanding how landscapes will change, how infrastructure will be affected and how resilience to climate change can be built into new infrastructure. Climate change will likely have a significant impact on the water cycle. GSC research will shed light on the risk to potable water supplies, hydroelectric power generation, and hazards from floods and drought (Fig. C.4).

(d) Geoscience for society

The scientific knowledge required to assess cumulative effects is broad. The complex interactions between land use, water management and waste management require an integrated approach at a landscape scale. The GSC is a national provider of information on both land (surficial and solid geology) and water, including the integration of surface water and groundwater into the complete water cycle (Fig. C.5).

Fig. C.4 The GSC conducts climate change studies, here documenting the effects of fast melting permafrost leading to extreme coastal erosion on Pelly Island, NT

Fig. C.5 The GSC conducts geohazard studies to reduce risks to people and infrastructure, here installing equipment to monitor landslide activity above a critical railway corridor in central BC

The GSC recognizes that this area of endeavour involves inherent complexities and that our goals in this area will be to some degree aspirational. However, we will investigate new ways of planning our programs, undertaking our fieldwork, interacting with key stakeholders, and communicating our expert knowledge in ways that contribute positively to decision making about resource development.

(e) **Our people, Our science**

As a science organization within the federal government, the GSC's mandate is to conduct world-class science to inform public decision making. The Canadian government has articulated and adopted the principle of evidence-based decision making and reaffirmed the need for government science to be objective and non-partisan.

To remain at the leading edge, our scientists need to work with a variety of partners. We need to reinforce the central role that the GSC plays in the Canadian geoscience community by building networks of collaboration, fully participating in national geoscience initiatives, and advocating for Canadian geoscience at the international level (Fig. C.6).

Fig. C.6 Among many celebratory activities for the GSC's 175th anniversary in 2017, the GSC held a Rock and Fossil Exhibit, at its site at the Bedford Institute of Oceanography (Dartmouth, NS), as part of a two-day open-house event, where more than 20,000 visitors participated

Moving Forward

Some of the objectives and goals that the GSC has set represent familiar territory for a national geoscience organization, but many others will pull us out of our comfort zone. We will take the time to better understand the challenges of delivering objective, nonpartisan science to support evidence-based decision making in Canada at a time of great technological and social change.

We will not be able to do this alone, so we look forward to strengthening our ties to other federal departments, provinces and territories, universities, Indigenous organizations, the private sector and civil society as a whole.

We ask all our stakeholders to contact us, to challenge us and, most importantly, to join with us to assure the future of Canada through thoughtful, respectful dialogue about the land we live on, its resources and its future (Fig. C.7).

Exploring Canada

Through its history, the GSC has been responsible for mapping the land mass of Canada, which supported the integration of the western provinces and northern territories into the country that we have today. The limit of Canada's offshore territory is still being extended today though surveys conducted by the GSC and the Canadian Hydrographic Service.

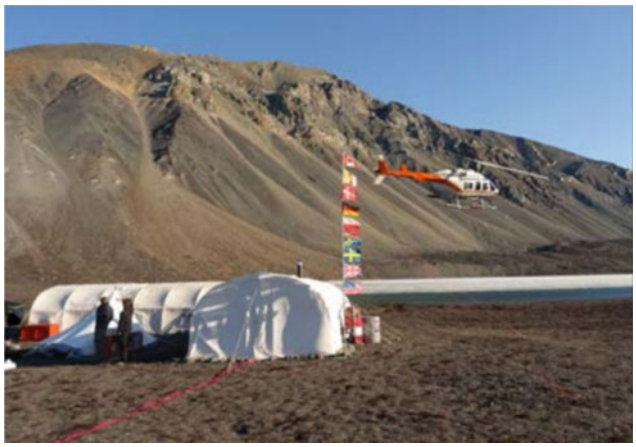

Fig. C.7 Joint Canadian/German (GSC/BGR) field mapping camp on northern Ellesmere Island, looking west as the fog covered sea ice of Yelverton Inlet, 2017

In more recent years, the GSC helped find the first economic diamond deposit in the Northwest Territories, leading to the expansion of diamond mining in Canada. These are only a few of the key GSC achievements that have built our knowledge of Canada's lands and provided the building blocks of its natural resource economy.

Today, exploration of this vast land is still reaping its natural resource rewards. The search for natural resources is difficult, akin to looking for a needle in a haystack.

The GSC's GEM program is exploring vast tracts of Canada's North, a land mass roughly equivalent to the combined areas of Quebec, Ontario and Manitoba, to find the "haystacks" with resource potential. This information is shared with the provinces and territories, as well as the private sector, so that the search for the "needles" can continue. The information is also critical to inform land-use planning.

In November 2016, the Royal Canadian Geographical Society (RCGS) awarded its prestigious Gold Medal to the GSC in recognition of the Survey's outstanding contribution to the development of Canada on the occasion of it's 175th anniversary.

Faculty of Civil and Geodetic Engineering, University of Ljubljana

Matjaž Mikoš

Summary

In 2019, the Faculty of Civil and Geodetic Engineering of the University of Ljubljana (ULFGG) celebrated its centennial: The precursor of the faculty was the Technical Faculty established in 1919 as one of five founding faculties of UL.

ULFGG, covering technical disciplines of civil and geodetic engineering, as well as water science and technology, has been involved in landslide risk reduction activities at the national level in Slovenia (former Yugoslavia, until 1991) for decades (Fig. D.1). In 2008, ULFGG became an ICL Full Member and has gradually developed its ICL engagement. ULFGG has been awarded the title of the World Centre of Excellence (WCoE) in Landslide Risk Reduction for 5 consecutive periods (2008–2011, 2011–2014, 2014–2017, 2017–2020, 2020–2023). Together with the Geological Survey of Slovenia, another ICL member in Slovenia, ULFGG hosted the 4th World Landslide Forum in Ljubljana, Slovenia, from May 29 to June 2, 2017. ULFGG strongly supports diverse activities of the International Consortium on Landslides, Kyoto, Japan, and thus contributes to the 2030 Agenda for Sustainable Development, as well as to the Sendai Framework for Disaster Risk Reduction 2015–2030 (SF DDR). ULFGG was a signatory of the Sendai Landslide Partnerships 2015–2030, and is a strong promoter of the Kyoto Landslide Commitment 2020, a SF DRR voluntary commitment by ICL.

In 2019, ULFGG hosted, together with the Slovenian Chamber of Engineers, the World Construction Forum 2019 (WCF 2019; www.wcf2019.org) in Ljubljana under the forum motto "Buildings and Infrastructure Resilience." The Forum with one of the themes on Disaster Risk Management and Governance for Resilient Communities was co-organized by the World Federation of Engineering Organizations (WFEO) in support to the implementation of the 2030 Agenda for Sustainable Development. All lectures given at the WCF2019 are available for free on the forum web page, as a contribution to Open Science efforts.

In the field of capacity building, ULFGG offers several courses for graduate and postgraduate students in landslide mechanics and dynamics, landslide stabilization and landslide risk mitigation. In this paper, a short overview of the past activities of ULFGG as ICL Full Member is shown.

World Centre of Excellence on Landslide Risk Reduction and IPL Projects

WCoE Activities

The title of World Centre of Excellence (WCoE) on Landslide Risk Reduction is given to a governmental or non-governmental entity, which contributes to the landslide disaster risk reduction at a regional and/or global level in a specific unique field of expertise, as well as helps promoting International Programme on Landslides (IPL) and landslide research intellectually, practically and financially (https://www.landslides.org/ipl-info/world-centre-of-excellence/). ULFGG was granted the title of WCoE five consecutive times:

- WCoE 2008–2011 and 2011–2014: Mechanisms of landslides in over-consolidated clays and flysch.
- WCoE 2014–2017: Mechanisms of landslides and creep in over-consolidated clays and flysch.
- WCoE 2017–2020: Landslides in Weathered Flysch: from activation to deposition.

M. Mikoš
Faculty of Civil and Geodetic Engineering, University of Ljubljana, Jamova cesta 2, 1000 Ljubljana, Slovenia
e-mail: matjaz.mikos@fgg.uni-lj.si

I. Alcántara-Ayala et al. (eds.), *Progress in Landslide Research and Technology, Volume 1 Issue 2, 2022*, Progress in Landslide Research and Technology,
https://doi.org/10.1007/978-3-031-18471-0

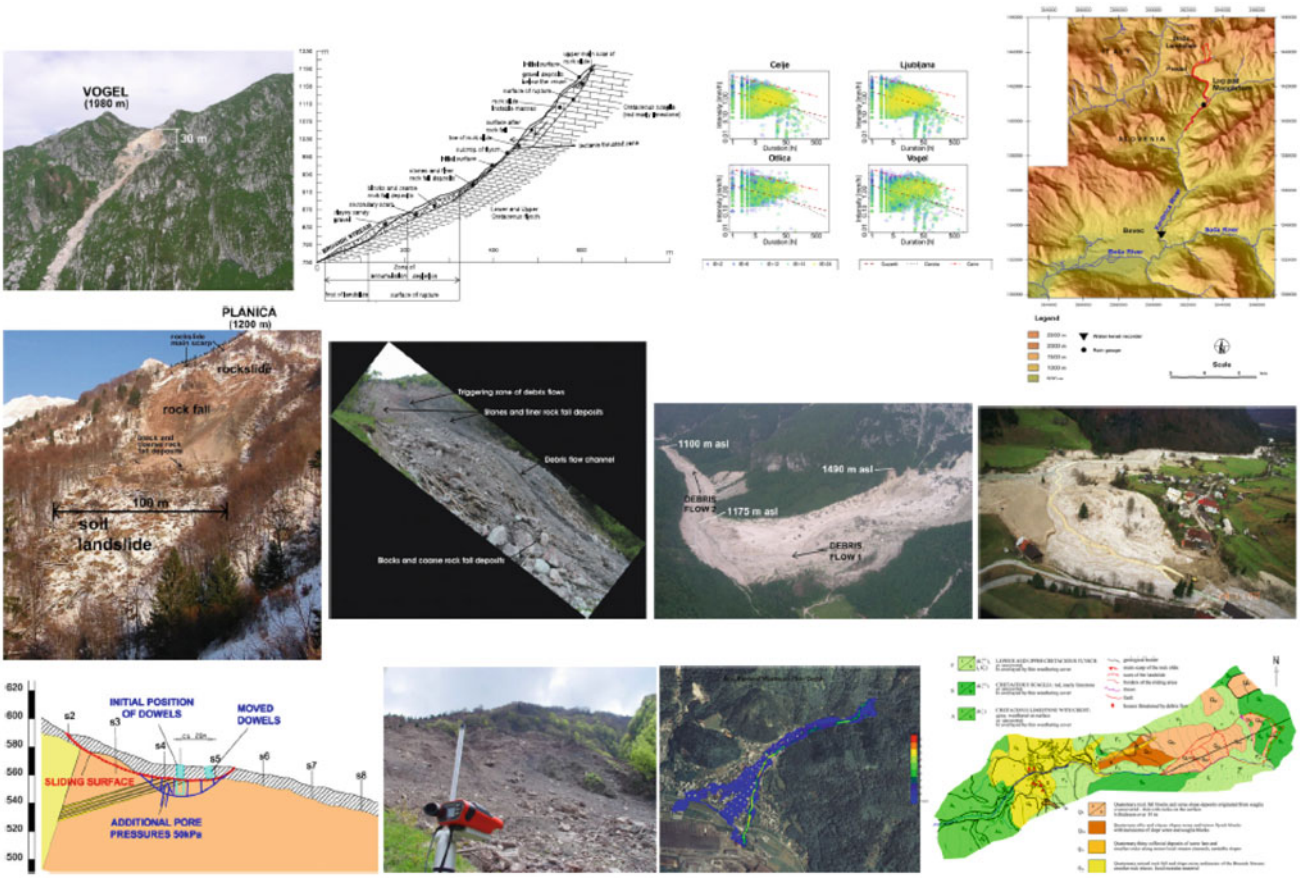

Fig. D.1 A collage of landslides in Slovenia and their investigation performed by UL FGG

- WCoE 2020–2023: Landslides in Weathered Heterogenous Sedimentary Rock Masses such as Flysch.

The research efforts at ULFGG were focused on:

- Mechanisms of triggering such landslides (mud flows), estimation of debris-flow magnitudes triggered as shallow or deep-seated landslides (debris slides), and triggering of shallow rainfall-induced landslides using advanced statistical methods.
- Field and laboratory investigations of suction in over-consolidated clays and flysch, such as to improve the understanding of softening in stiff over-consolidated clays and marls, using soil matrix suction as an indicator for mudflow occurrence, and executing suction long-term monitoring of the Slano Blato landslide.
- Laboratory investigations of coarse debris-flow rheological parameters and soil-water characteristic curve of residual soil from a flysch rock mass.
- Mathematical modelling of debris flows (hazard assessment in deposition areas), using different numerical models and different digital terrain models.

The WCoE activities were financially supported by the Slovenian Research Agency through the Research Programme P2-0180 "Water Science and Technology, and Geotechnical Engineering: Tools and Methods for Process Analyses and Simulations, and Development of Technologies," as well as by several national and international (bilateral) research projects.

ULFGG and the Geological Survey of Slovenia jointly organized 4th World Landslide Forum (WLF4), in Ljubljana between May 29 and June 2, 2017, followed by a three-day field study tour to see the variety of landslide forms in Slovenia and in its immediate NW surroundings. With over 600 participants from 49 countries and 5 international organizations, WLF4 was promoting the culture of living with natural hazards.

IPL Projects

An important ICL activity is IPL projects (https://www.landslides.org/projects/icl-world-report-on-landslides/).

The IPL Evaluation Committee examines the submitted proposals of ICL members by carefully reading the written proposals and by listening to their presentations at annual ICL conferences. The initially accepted proposals by the IPL Evaluation Committee are discussed and then approved at the annual Board of Representatives meeting of ICL members (Annual Assembly). Finally, the IPL projects are approved annually by the IPL Global Promotion Committee. ULFGG has successfully submitted several proposals for IPL projects and has been so far actively involved in the following ones:

- IPL-151 Soil matrix suction in active landslides in flysch—the Slano Blato landslide case (2010–2012).
- IPL-225 Recognition of potentially hazardous torrential fans using geomorphometric methods and simulating fan formation (2017–2020).
- IPL-226 Studying landslide movements from source areas to the zone of deposition using a deterministic approach (2017–2020)—coordinated by the Geological Survey of Slovenia.

ICL Thematic and Regional Networks

Following the ICL Strategic Plan 2012–2021, several thematic networks and regional networks have been established (for an overview, see https://www.landslides.org/projects/icl-networks/).

Landslide Monitoring and Warning Thematic Network

In 2012, ULFGG proposed the ICL landslide monitoring and warning thematic network (abbr. LaMaWaTheN), and almost 10 ICL members joined the initiative. The general objective of the proposed network was to compare experiences in the field of landslide monitoring and installed early warning systems for active landslides in various regions of the world. A proposal for landslide monitoring techniques database was. The network was later coordinated by the Croatian Landslide Group from the Faculty of Civil Engineering, University of Rijeka, Croatia, and the Faculty of Mining, Geology and Petroleum, University of Zagreb, Croatia. Lately, we contributed to the network activities by preparing practice guidelines on monitoring and warning technology for debris flows.

The idea of the network was partially taken over by the web database ICL World Report on Landslides (http://iplhq.org/ls-world-report-on-landslide/), created to be a platform to share landslide case studies among the global landslide community, with monitoring and warning systems being a part of the story.

ICL Adriatic-Balkan Network

Jointly with other ICL members from Croatia and Serbia, in 2013, ULFGG proposed to establish an ICL Adriatic-Balkan Regional Network (ICL ABN; https://www.klizista-hr.com/en/organization/about-us/icl-abn/). Various network activities were proposed, the most active being the organization of biennial regional symposia on landslide risk reduction in the Adriatic-Balkan Region (called ReSyLAB). ULFGG supported the 1st Symposium in Zagreb (Croatia) in 2013 (March 6–9), and the 2nd in Belgrade (Serbia) in 2015 (May 14–16), and jointly organized the 3rd in Ljubljana (Slovenia) in 2017 (October 11–13) together with the Geological Survey of Slovenia (also an ICL member).

In the last decade, ULFGG has signed bilateral research projects with the ICL members in the region: "Adriatic-Balkan Regional Network: Landslide Risk Mitigation for Society and Environment" (2012–13 with University of Belgrade, Serbia), "Study of landslides in flysch deposits: sliding mechanisms and geotechnical properties for landslide modelling and landslide mitigation SoLiFlyD" (2014–15 with University of Rijeka, Croatia), and "Laboratory investigations and numerical modelling of landslides in flysch deposits in Croatia and Slovenia" (2016–17 with the University of Rijeka, Croatia). This joint research has helped strengthen regional cooperation within the ICL ABN regional network.

Other ICL-Related International Activities

ULFGG served the ICL by taking different leading roles in the Consortium, i.e. ULFGG member served as Chair of IPL Evaluation Committee, twice as ICL Vice President, and was elected to Co-Chair and in 2021 to Chair of the IPL-KLC (https://www.landslides.org/ipl-info/ipl-klc-global-promotion-committee/).

ULFGG has been strongly supporting the journal Landslides: Journal of the International Consortium on Landslides, published by Springer Nature (https://link.springer.com/journal/10346) since its launch in 2004. ULFGG works for the journal in the roles of reviewers and an associate editor, and regularly publishes its top research results in the journal, as well as disseminates information important for capacity building in landslide risk reduction in the journal.

ULFGG followed the development of the journal from its bibliometric perspective, and compared scientometric impacts of the journal with the other ICL publications (monographs, volumes from World Landslide Forums) in the field of landslide research.

ULFGG also contributed to the two-volume set of Landslide Dynamics: ISDR-ICL Landslide Interactive Teaching Tools (LITT), namely to Volume 1: Fundamentals, Mapping and Monitoring by practice guidelines on monitoring and warning technology for debris flows (https://www.springer.com/gp/book/9783319577739), and to Volume 2: Testing, Risk Management and Country Practices (https://www.springer.com/gp/book/9783319577760) by a state-of-the-art overview on landslide disaster risk reduction in Slovenia, a study on two-dimensional debris-flow modelling and topographic data, and by study on intensity-duration frequency curves for rainfall-induced shallow landslides and debris flows using copula functions.

UNESCO Chair on Water-Related Disaster Risk Reduction

Experiences and knowledge accumulated in the past decades at the Chair on Hydrology and Hydraulic Engineering at ULFGG in the field of (applied) hydrology in experimental basins, landslide research, landslide risk reduction, and flood risk management, culminated in 2016 in the establishment of the UNESCO Chair on Water-related Disaster Risk Reduction (WRDRR Chair; www.unesco-floods.eu) at the University of Ljubljana. The UNESCO WRDRR Chair was positively evaluated in 2020 and prolonged for another 4 years (2020–2024). The Chair is associated to the university twinning and networking UNITWIN UNESCO—Kyoto University—ICL on "Landslide and Water-Related Disaster Risk Management".

ULFGG supports activities of the Slovenian National Committee for UNESCO Intergovernmental Hydrological Programme (www.ncihp.si)—focus of the activities is the development of the IHP-IX Programme (2022–2029).

Conclusions

ULFGG as one of World Centres of Excellence in Landslide Risk Reduction, hosts the UNESCO Chair on Water-related Disaster Risk Reduction. ULFGG strongly supports ISDR-ICL Sendai Partnerships 2015–2025 for global promotion of understanding and reducing landslide disaster risk, and its extension to 2030 and beyond: the Kyoto 2020 Commitment for Global Promotion of Understanding and Reducing Landslide Disaster Risk that that was signed in November 2020. ULFGG is proud to be its Official Promoter, and will specifically work for its Actions 2, 5, 6, 9 and 10.

This review contribution is intentionally written without giving references to described activities. For this purpose, listed websites and web search engines may be used.

The author wants to thank numerous colleagues from ULFGG and from the wide ICL community for a long-lasting excellent cooperation with a joint vision to reduce landslide disaster risk.

China University of Geosciences, Wuhan

Huiming Tang, Changdong Li, and Qinwen Tan

Introduction

China University of Geosciences, Wuhan (CUG), founded in 1952, is a national key university affiliated with the Ministry of Education. It is also listed in the National "211 Project", the "985 Innovation Platform for Advantageous Disciplines" and the "Double First-class Plan". CUG, featuring geosciences, is a comprehensive university that also offers a variety of degree programs in science, engineering, literature, management, economics, law, education and arts. Its Geology and Geological Resources and Engineering have both been ranked as national number one disciplines.

CUG has two campuses in Wuhan. The main campus is the Nanwang Mountain Campus, located in the heart of the Wuhan East Lake National Innovation Demonstration Zone, which is popularly known as China Optics Valley. The Future City Campus is located in the east of Wuhan and is 27 km from the main campus. These two picturesque campuses cover a combined area of 1,474,353 m^2. They are ideal places to study, work, and enjoy life. CUG owns a 4A-Level tourist attraction—the Yifu Museum. CUG also boasts four field training centers: Zhoukoudian in Beijing, Beidaihe in Hebei Province, Zigui in Hubei Province, and Badong in Hubei Province.

CUG has established a complete education system. As of December 2020, 30,239 full-time students, including 18,080 undergraduate students, 9302 master's students, 1916 doctoral students, and 941 international students have enrolled in its subsidiary 23 schools and 86 research institutes. CUG currently has a faculty of 1858 full-time teachers, among which there are 539 professors (11 of which are members of the Chinese Academy of Sciences) and 984 associate professors.

CUG is focused on fostering high-quality talent. Among its over 300,000 graduates, many have gone on to become scientific and technological elites, statesmen, business leaders and athletes. And they have made great contributions to the nation and society, represented by former Premier WEN Jiabao and 39 members of the Chinese Academy of Sciences and Chinese Academy of Engineering.

CUG has strengthened exchanges and cooperation with international universities. It has signed friendly cooperation agreements with more than 100 universities from the United States, France, Australia, Russia and other countries. CUG has actively carried out academic, scientific and cultural exchanges with universities around the world. There are about 1,000 international students from more than 100 countries studying at CUG. It also sponsors more than 900 teachers and students to study abroad or conduct international exchanges, and invites more than 400 international experts to visit, lecture, and teach at CUG every year. In 2012, CUG initiated and co-established the International University Consortium in Earth Science (IUCES) with 11 other world-renowned universities. IUCES is committed to promoting the common development of geosciences education and scientific research through resource sharing, exchange and cooperation among its member institutions. In addition, CUG has partnered with Bryant University from USA, Alfred University from USA, and Veliko Turnovo University from Bulgaria in establishing three Confucius institutes on their campuses.

Strategic Plan of Building a World-Renowned Research University in Earth Sciences—A Beautiful China and a Habitable Earth: Towards 2030

CUG reviewed and approved Strategic Plan of Building a World-Renowned Research University in Earth Sciences on December 25 of 2019 (Fig. E.1).

H. Tang
China University of Geosciences, No. 388 Lumo Road, Wuhan, P.R. China
e-mail: tanghm@cug.edu.cn

I. Alcántara-Ayala et al. (eds.), *Progress in Landslide Research and Technology, Volume 1 Issue 2, 2022*, Progress in Landslide Research and Technology,
https://doi.org/10.1007/978-3-031-18471-0

Fig. E.1 Strategic plan of building a world-renowned research university in earth science

Themed on "A Beautiful China and A Habitable Earth", the Plan depicts the blueprint of the second goal of the "three-steps strategic goals", which is to build a world-renowned research university in Earth Sciences by 2030 based on the attained goal of developing CUG into a "high-level university with first-class Earth Sciences and coordinated development of multi-disciplines".

According to the Plan, our education missions are: Remaining true to CUG's core value of "seeking harmonious development between man and nature", we are committed to cultivating innovative talents who have lofty morality, solid foundation, and profound expertise, and who pursue the unity of knowing and doing. We should provide personnel support, and endeavor to innovate, apply and spread knowledge in order to provide theories, technologies and approaches for the construction of a Beautiful China and a Habitable Earth. We should strive to optimize governance, reform culture, and fully invigorate the vitality of running a university. We should provide our service to the construction of an innovative country and to the promotion of a harmonious co-existence between man and nature. We should provide our service to the people and the governance of China. We should provide our service to the consolidation and development of the system of socialism with Chinese characteristics. We should provide our service to the reform and opening up and to the construction of the socialist modernization.

According to the Plan, our endeavoring goals are: By 2030, we will have built a world-renowned research university in Earth Sciences, whose main indexes will have reached or nearly reached the level of other world-class universities. To upgrade CUG into a world-class university, we will endeavor to make the discipline of Earth Sciences rank top in the world and forge boldly ahead in competition to improve the quality of other disciplines of CUG. We will assemble a contingent of teachers and researchers with international competitiveness and influences to build a university with Chinese characteristics and superiority. We will build a world-class university that will be fully engaged in international exchange and cooperation and that will achieve educational, academic, cultural, and administrative excellence.

Outstanding Recent Achievements

In recent years, CUG has achieved significant progress in the research fields of geohazards, water resource, geochemistry, paleontology, geodetic surveying and lunar exploration program, etc. To keep to the theme of KLC2020, recent achievements on geohazards researches of CUG are focused and introduced.

(a) **Approval of National Observation and Research Station for Geohazards in the Three Gorges Reservoir Area, Hubei**

CUG was newly approved **National Observation and Research Station for Geohazards in the Three Gorges Reservoir Area**, **Hubei**. This station, founded and administrated by Prof. Huiming Tang, is responsible to carry out field observations and scientific research on geohazards in condition of reservoir operation.

The central site of the station is located in Badong County of the Three Gorges Reservoir area (hereinafter abbreviated as the TGR area), and a larger monitoring network of multiple sites has been established, including the geohazard field test site for the Majiagou landslide, Zigui County, and systematic geophysical monitoring station for the whole TGR area, etc.

The Badong field site (also named Badong in-situ large-scale experimental station) is located in the Huangtupo landslide area, which has been recognized the largest reservoir landslide by volume in the TGR area. The field site consists of a tunnel complex and a series of monitoring systems (Fig. E.2). The tunnel complex, built in the Huangtupo riverside sliding mass #1, consists of a main tunnel with a length of 908 m and a width of 5 m, five branch tunnels (5–145 m long, 3.5 m wide), two test tunnels, and 35 observation windows. The test tunnels exposed the sliding zones of the landslide, facilitating their direct observation and the execution of scientific experiments, such as large-scale in-situ mechanical tests and deep deformation monitoring. The monitoring systems measure deformation as well as hydrologic, meteorological and hydro-chemical variables. The deformation system is composed of a slope

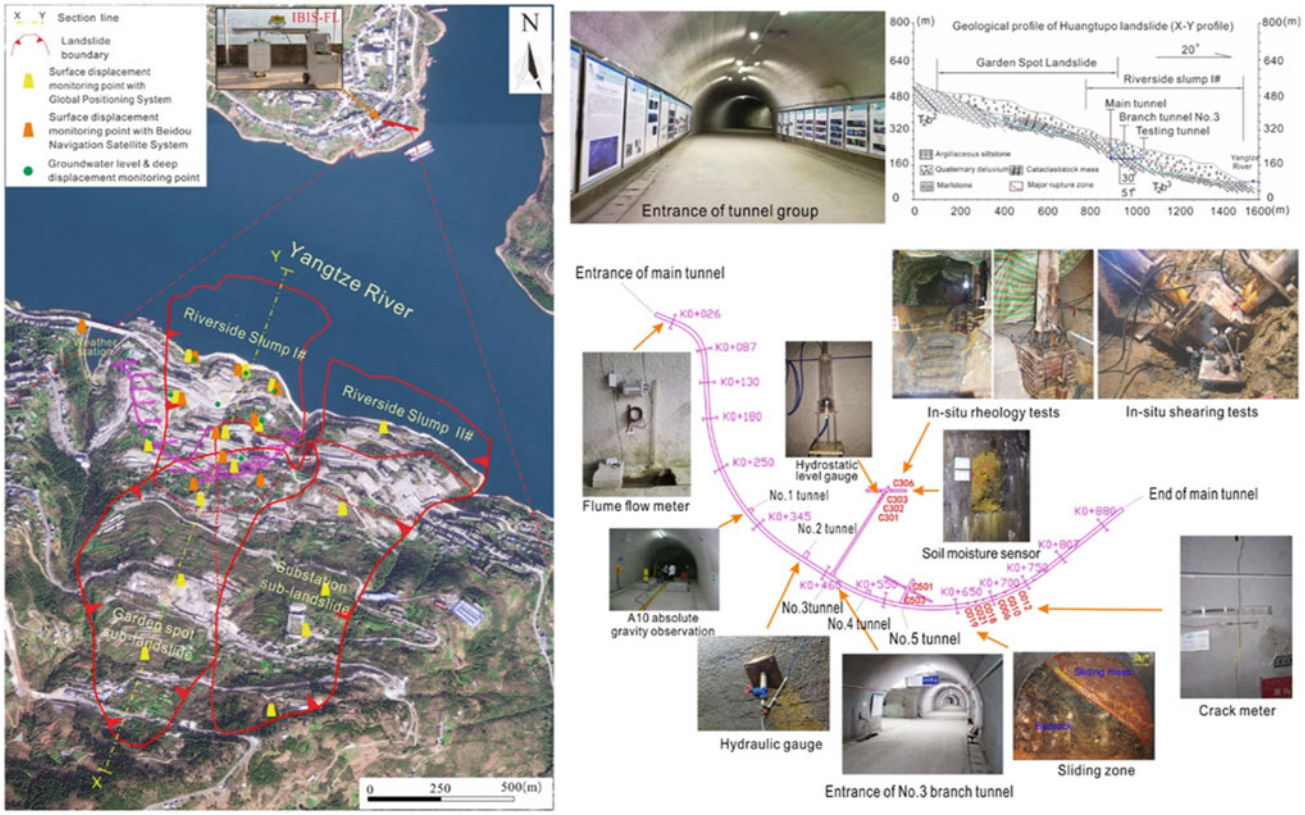

Fig. E.2 Badong in-situ large-scale experimental station of the National Observation and Research Station for Geohazards in the Three Gorges Reservoir Area, Hubei

surface displacement measurement unit and an underground displacement measurement unit. The slope surface displacement unit includes a number of GPS (Global Positioning System) and BDS (BeiDou Navigation Satellite System) measurement points, as well as an IBIS-FL (Interferometric Radar) monitoring system (Fig. E.2). The underground displacement unit includes nine deep inclinometer boreholes, a number of crack meters installed on the ground and the walls of tunnels, and many hydrostatic level gauges that measure the settlement of the tunnels in the sliding mass. The hydrologic system includes a number of devices that allow for observation of the water level of the Yangtze River, the ground water level and water discharge of the tunnels (Fig. E.2). A small meteorological station is located on the landslide and provides rainfall data. So far, multiple and massive data have been collected for the landslide area since the year 2012, when the field site was constructed; over 10,000 people with a variety of geology-related backgrounds from > 20 countries have visited this experimental station.

(b) **Approval of the Basic research on the prediction and forecasting of major landslides program supported by the Major Program of NSFC**

CUG was approved the **Basic research on the prediction and forecasting of major landslides** program (2021–2025), supported by the Major Program of the National Natural Science Foundation of China. The program was designed for the prediction and forecasting of major landslides, with the concentration on the core scientific problems of landslide evolution process and physical-mechanical mechanism. Three key scientific problems, including correlation mechanism for landslide initiation, physical-mechanical mechanism for landslide initiation, and prediction and forecasting theory based on landslide evolution were proposed.

Five topics were set up to achieving those objectives. Topic 1 was proposing the initiation classification of major landslides based on large field test platform, with the adoption of field prototype test and other technical means. Topics 2–4 aimed to reveal the physical and mechanical

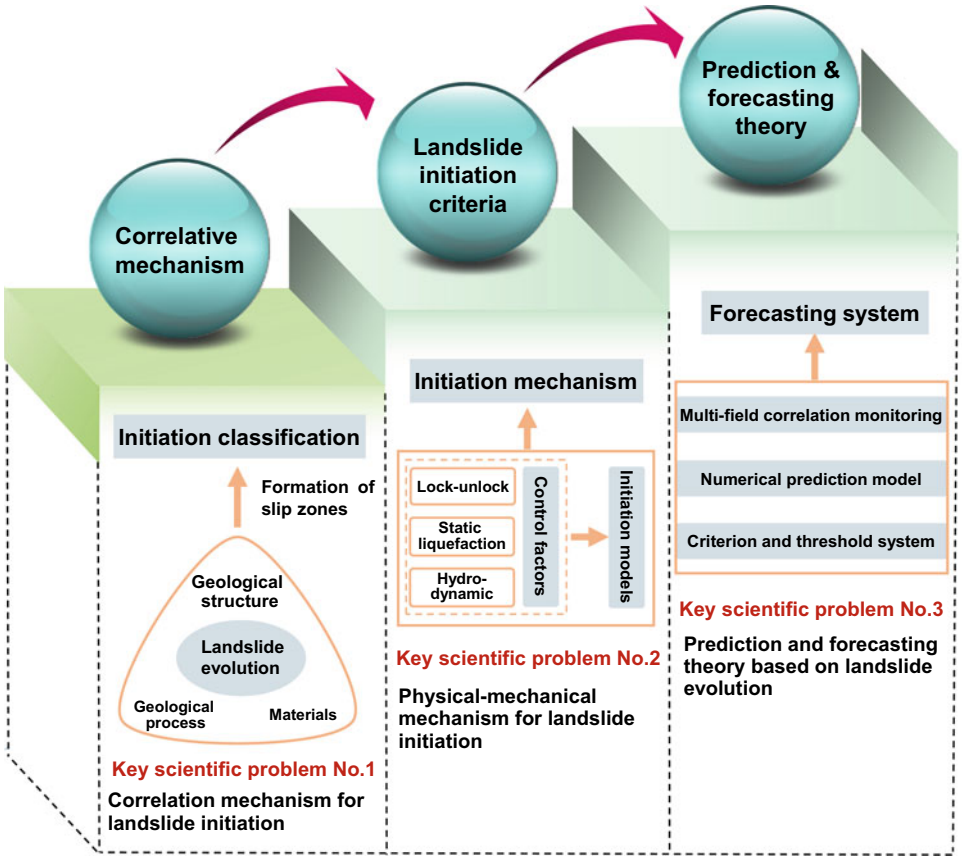

Fig. E.3 Scientific thought for the implement of research

mechanism of locked-segment dominated landslide, static liquefaction loess landslide and hydrodynamic pressure-driven landslide, and to establish the corresponding landslide initiation criteria, respectively. Topic 5 was responsible to established the prediction mode and real-time forecasting system. Ultimately, the landslide prediction and forecasting theory based on the evolution process and physical-mechanical mechanism would be put forward. The scientific thought for the implement of research is exhibited in Fig. E.3.

The implementation of the research is respected to lay the geological, mechanical and physical foundation for the above three types of landslide prediction, and to substantially promote the research on landslide prediction.

Department of Civil Engineering, National Taiwan University

Department of Civil Engineering, National Taiwan University

Introduction

National Taiwan University (NTU) was originallybestablished in 1928, when Taiwan was under Japanese rule, as Taihoku Imperial University. The current name dates back to 1945. As Taiwan's oldest and most prestigious university, we are also the largest comprehensive higher education institution (HEI) in the country. The academic freedom that we cherish and our excellent faculties attract both domestic and international students. Throughout our 90-year history, we have nurtured many talents, including leading academics and leaders in the public and private sectors. Our campus is vast, and spans across multiple locations, including Taipei, Yilan, Hsinchu, Yunlin, and mountainous areas in central Taiwan—accounting for nearly 1% of Taiwan's total land area. This provides teachers and students with an environment rich in biological and ecological diversity.

As the leading university in Taiwan, we are strongly committed to social responsibility as we strive to drive sustainable development and influence positive change in society. This was also reflected in the first University Impact Rankings launched in 2019 by Times Higher Education (THE), which measure the contributions of HEIs to the United Nations' Sustainable Development Goals (SDGs). We were ranked 70th in the world overall, and 1st in the world for SDG16: Peace, Justice, and Strong Institutions. Starting from creating a sustainable culture on campus, we aim awareness about sustainability throughout the university, through innovative teaching and research, environmental protection and recycling efforts, and a school administration that supports equality and wellbeing. Our sustainability efforts extend beyond our campus through industry-academia collaborations and service teams deployed to remote areas. In the near future, we will continue to reinforce the spirit of innovation and sustainability thinking among all faculty members and students. We will also continue our efforts to address economic, environmental, and social challenges through interdisciplinary collaboration, as we create connections between the local and the international community (Fig. F.1).

The Department of Civil Engineering can be regarded as the root of The College of Engineering. The early civil engineering education covers a wide range of professions. With the development and differentiation of various social industries, some fields have gradually separated and established specialized departments. We have also moved on, combining different fields and top-notch technology to remain as the leader of the tide.

Civil engineering is inseparable from the development of human civilization. From the beginning of civilization, all man-made structures have enchased and highlighted the value of civil engineering. NTU Civil Engineering is no exception. From the Department of Civil Engineering of the Imperial College of Taipei to the National Taiwan University Department of Civil Engineering today, the majority of Taiwan's significant constructions is and will always be our finest gallery.

In National Taiwan University, you will obtain high-quality guidance in and out of the classroom. Academic resources in the classroom and sports culture clubs, various student activities throughout the year, will bind you together with peers of the same dream. These friends may also be partners that can help you in future careers. If you are willing to take civil engineering as a career and take on the challenges and step forward as a team, then listen to your inner call, join us, and let us stride ahead hand in hand (Fig. F.2).

Department of Civil Engineering, National Taiwan University,
No. 1, Sec. 4, Roosevelt Road, Taipei, 10617, Taiwan

I. Alcántara-Ayala et al. (eds.), *Progress in Landslide Research and Technology, Volume 1 Issue 2, 2022*, Progress in Landslide Research and Technology,
https://doi.org/10.1007/978-3-031-18471-0

Fig. F.1 Quick facts of the Department of Civil Engineering

Fig. F.2 Life beyond classroom

Outstanding Recent Achievements

Mitigating the Impacts of Natural Disasters Via Cutting Edge Technology

Taiwan is located in the Circum-Pacific seismic belt, with many active faults and frequent typhoons. Due to the effects of climate change, extreme rainfall events that used to occur once in a century are now becoming more frequent, exacerbating the threat of landslides and debris flows. The prevention and mitigation of natural disasters such as earthquakes and flooding have therefore become a priority for the twenty-first century.

(a) **Earthquake Early Warning Systems: gain valuable response time**

For most natural disasters, potential losses to life and property can be mitigated through early warning and prevention. After the earthquake disaster of September 21st, 1999, building safety inspections needed to be conducted all across Taiwan. Our faculty and students with expertise in civil engineering and geology were quick to respond to this urgency, working closely with the National Center for Research on Earthquake Engineering to help the government improve the earthquake resistance standards and test specifications. Moreover, they proposed a more elaborate system for earthquake damage and liquefaction assessment, and conducted a complete review and classification of the earthquake risk tolerance for all areas in Taiwan. The team also developed new disaster prevention technologies. One of the most significant contributions was to assist the public high (vocational) schools around Taiwan with assessments of the earthquake resistance and reinforcement needs of old buildings. In the numerous earthquakes that have since occurred, the effect of these reinforcements has become apparent. The stronger earthquake resistance of these buildings has improved safety for 2.65 million teachers and students around Taiwan (Fig. F.3).

Our school has also developed technology to monitor the status of bridges with high traffic volumes. This optical fiber monitoring system will emit a warning whenever poor conditions are recorded, prompting an early response from management that can prevent a disaster from happening. When bridges in remote areas are damaged, a lightweight bridge developed by NTU out of composite materials can be assembled by residents in short time. In this way, access to affected areas can be quickly restored, and disaster relief provided more efficiently. In the event of an earthquake, Taiwan's citizens will immediately receive an emergency alert by text message. This warning system, which was developed by Professor Wu, Yih-Min at our Department of Geosciences, analyzes the properties of a P-wave within three seconds after detecting the wave so that it can issue an alert to citizens more than 10 s before the S-wave, which is most likely to cause damage arrives. This early warning system is accurate and fast, giving people valuable seconds

Fig. F.3 Taiwan Earthquake Loss Estimation System (TELES)

to escape to safety. Because it is also much cheaper to manufacture network of multiple sites has been established, including the geohazard field test site for the Majiagou landslide, Zigui County, and systematic geophysical monitoring station for the whole TGR area, etc. than previous seismographs, it could be rapidly rolled out to several hundred elementary and junior high schools, ensuring better protection of our country's younger generation. Moreover, this system has been successfully introduced in other earthquake-threatened countries, such as Indonesia, India, Vietnam, Nepal, and Mexico.

(b) **After the Flood: Rapid Mobilization and Improved Ability to Provide Relief**

Another critical area is flood disaster prevention. Also here, our faculty and students are actively involved in key activities ranging from early warning and response during the disaster, to raising the awareness of, and capability for, disaster prevention among citizens more generally. Our Center for Weather Climate and Disaster Research comprises experts in meteorology, hydrology, bioenvironmental engineering, and geology etc. This center helped New Taipei City and Keelung City establish an extreme weather and flood monitoring and warning system. Other projects include combining advanced deep learning with the analysis of radar data, which allows for closer monitoring of rainfall data in hydrologically sensitive areas. The improvement of flood models increases the accuracy of flood warnings and provides disaster prevention units with valuable information for them to rapidly formulate response strategies. From past experiences outside of Taiwan, we know that self-help and mutual support account for the largest share of the relief effort (90%) in the event of a disaster. In other words, even if flood warnings are effective, people in the affected area still need to be able to take own measures to protect themselves. At NTU, we actively participate in the community-level disaster relief preparations around the country, as well as in the training of disaster relief officers. Our experts provide citizens with the most up-to-date knowledge in disaster prevention, operate independent disaster relief systems, and evaluate the safety of shelters. These efforts contribute to the resilience and ability of local communities to mitigate impact, helping them recover more quickly. A plan for how to improve the disaster relief ability in the country proposed by our experts is another example of how we help make sure that the best disaster response capacity is in place. After improving the ability to respond to disasters, NTU's team also contributed to disaster prevention infrastructure around Taiwan, such as seismic isolation technology for buildings and equipment, or detention ponds in communities at risk. Our work and efforts in these areas help protect lives and property. As climate change continues to impact the world, we hope to leverage our technologies and expertise in these domains even further, and help strengthen the capacity to prevent and withstand natural disasters throughout the world.

Institute of Rock Structure and Mechanics, The Czech Academy of Sciences

Josef Stemberk

Introduction

The Institute of Rock Structure and Mechanics of the Czech Academy of Sciences is specializing in the study of the structure and properties of rocks and the rock environment. It is also involved in research into glass, ceramic materials for technical use, composite materials and biomaterials, their properties and application potential, and technological topics relating to the processing of inorganic as well as organic waste. Its research activities are spread across six scientific departments:

- Department of Geochemistry
- Department of Composites and Carbon Materials
- Department of Materials Structure and Properties
- Department of Neotectonics and Thermochronology
- Department of Engineering Geology
- Department of Seismotectonics.

The Department of Engineering Geology analyze and interpret the dangerous geodynamical phenomena and processes, which affect the behavior, development and stability of the rock environment in their natural deposition in the Earth's crust. These phenomena are linked with exogenous processes, such as slope deformations and weathering, as well as endogenous processes, such as tectonics, fault movements and gas emanations. Special attention is paid to the development of reliable and accurate methods of monitoring of slope and tectonic processes and predicting their development and occurrence in space and time.

Global and Regional Inventories

The Global Database of Giant Landslides on Volcanic Islands summarizes statistics and knowledge about giant landslides (mainly debris avalanches) on volcanic islands that are up to hundreds of cubic kilometers in size. They are among the largest geological features on Earth and are fully comparable in size to the extra-terrestrial landslides observed on Mars. (Landslides 16, 2045–2052, 2019).

The regional landslide database for the territory of Czechia is built by analyzing media news and reports from the "Landslide Tracker" mobile phone app. It provides a timely overview of events and related losses while it is shared with a worldwide audience through the NASA Landslide Reporter website: https://www.nasa.gov/solve/landslide_reporter (Figs. G.1 and G.2).

Landslide Monitoring

Čeřeniště site natural laboratory is a complex landslide in Tertiary neovolcanites of České středohoří. It is equipped with state-of-art monitoring systems including DMS multi-parametric column able to measure landslide movements in 2D, groundwater level and acceleration. The lower part of the landslide is equipped with continuous time-lapse ERT geophysical measurement, climatic station and streamflow measurement. Complementary measurements include geodetic (tachymetry and precise levelling) and geotechnical (extensometer) monitoring (Fig. G.3).

Crack meter monitoring on unstable rock slopes takes place in several parts of Czechia. It is coupled with observation of climatic variables and thermal properties inside the rock mass. As a consequence, the thermoelastic wave within the rock mass can be observed (Geosci. Instrum. Method. Data Syst., 10, 203–218) (Figs. G.4 and G.5).

J. Stemberk
Institute of Rock Structure and Mechanics, The Czech Academy of Sciences, V Holešovičkách 41, 18209 Prague, Czech Republic
e-mail: stemberk@irsm.cas.cz

I. Alcántara-Ayala et al. (eds.), *Progress in Landslide Research and Technology, Volume 1 Issue 2, 2022*, Progress in Landslide Research and Technology,
https://doi.org/10.1007/978-3-031-18471-0

Fig. G.1 Scarp of a giant landslide—volcano collapse named El Golfo. El Hierro, Canary Islands, Spain

Landslide Research for a Safer Society

Long-term activities aiming at landslide risk reduction are part of our voluntary commitment to the Sendai Partnerships 2015–2025 for "Global Promotion of Understanding and Reducing Landslide Disaster Risk".

The long-term collaboration with the Czech National Highway Authority resulted in several landslide hazard studies and the implementation of improved construction technical norms.

The Czech public is being involved in collaborative citizen science projects to improve their awareness about landslide risk. Similarly, the ongoing participative research in Peru involves inhabitants of mountain villages or local experts contributing to their sustainable economic development (e.g. infrastructure safety) or improving institutional resilience by implementing new monitoring approaches (e.g. rock monitoring at the National Archeological Park of Machupicchu) (Fig. G.6).

Research Cooperation

The Institute's research cooperation includes universities (e.g. Université de Liège, Wrocław University of Environmental and Life Sciences, University of Zurich), research institutes (e.g. Geophysical Institute of the Polish Academy of Sciences, Instituto Nacional de Investigación en Glaciares y Ecosistemas de Montaña) or private companies (e.g. Strix Engineering, RockNet, Gamma Remote Sensing).

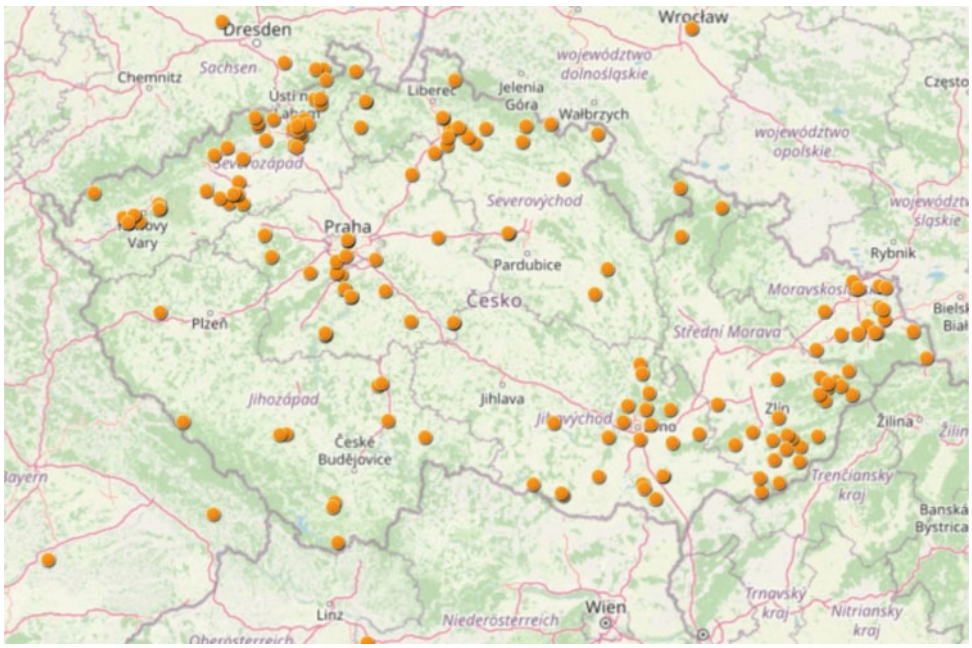

Fig. G.2 National landslide database based on media reports in Czechia as can be viewed on the NASA Landslide Viewer web page (yellow dots are reported landslides)

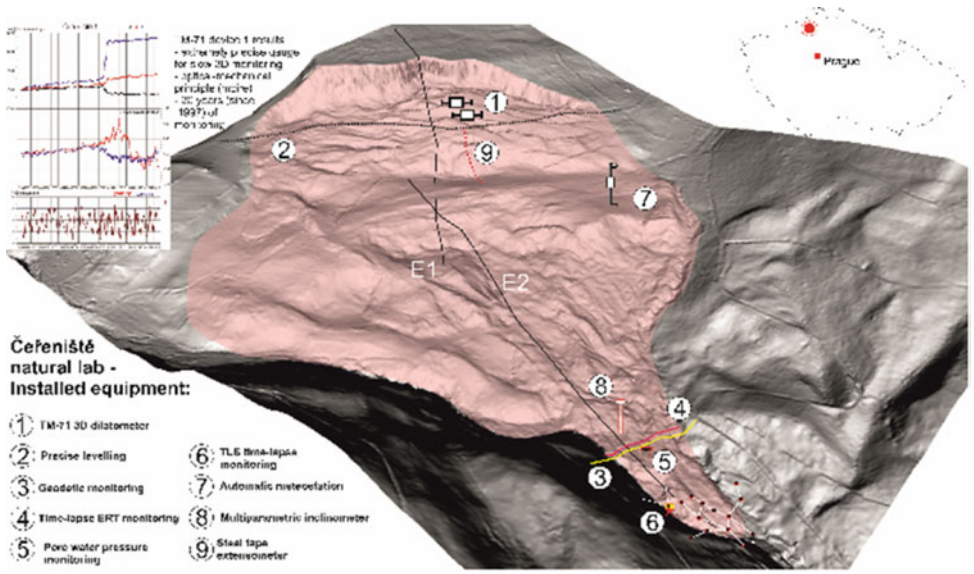

Fig. G.3 Monitoring equipment at the Čeřeniště natural laboratory. Inset: results of movement monitoring

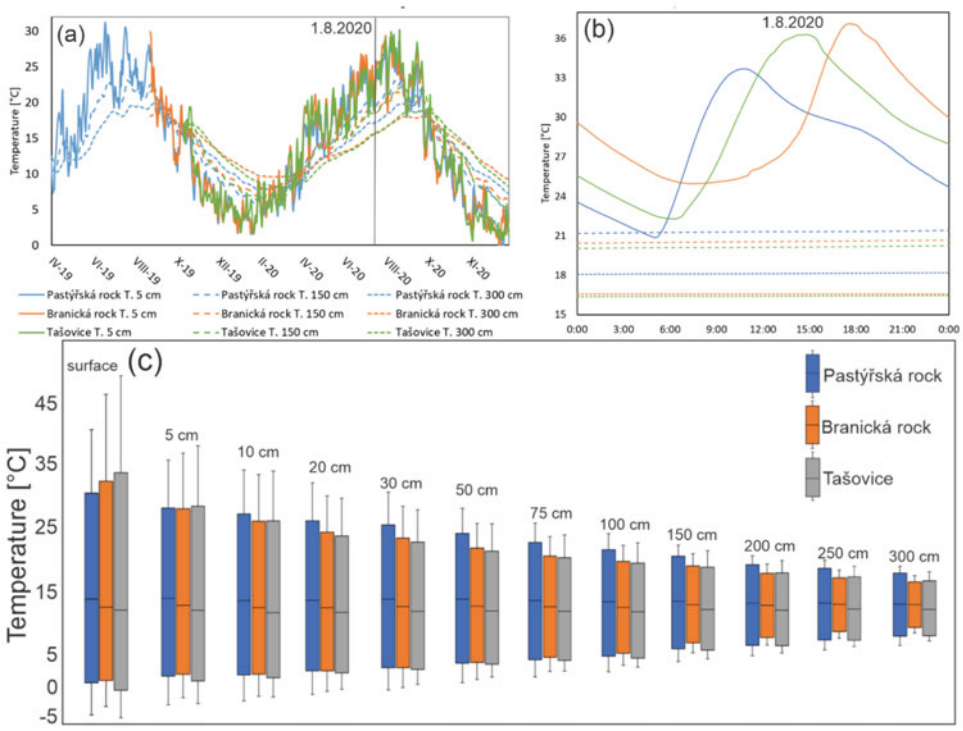

Fig. G.4 Comparison of temperatures at different rock slope depths at three different sites

Fig. G.5 Landslide (in red) in the way of the planned motorway D35 in eastern Czechia

Fig. G.6 Sharing and discussing results of landslide risk reduction project with its "recipients" empowers the community to modify the project according to their needs and allows them to become part of it. The photo shows the joint meeting of the community leaders and schoolchildren (Rampac Grande, Cordillera Negra, Peru)

Institute of Cold Regions Science and Engineering, Northeast Forestry University

Wei Shan and Ying Guo

Introduction

Institute of Cold Regions Science and Engineering of Northeast Forestry University (ICRSE-NEFU) is committed to the environmental geology and engineering geology of high latitude permafrost region and deep seasonal frozen area under the background of climate change, and attaches importance to the combination of basic research and applied research. With undergraduate, master, doctor, postdoctoral professional training system and standards, ICRSE-NEFU initiated "Geological environment risk research plan for permafrost degraded areas in Northeast China (GERRP)". With the support of the Chinese government, "Field scientific observation and research station of the Ministry of Education—Geological environment system of permafrost area in Northeast China (FSSE-PFNEC)" was established. Its observation stations cover all kinds of permafrost areas in Northeast China. At the same time, in order to develop and transfer technologies related to environmental governance and infrastructure construction in permafrost regions, "Provincial Collaborative Innovation Centre, Environment and road construction and maintenance in permafrost area of Northeast China (PCIC-PFER)" was established. Over the years, ICRSE-NEFU have continuously established cooperation with academic institutions and organizations at home and abroad, held various academic exchanges and regularly held "Academic Seminar on Engineering Geology and Environmental Geology in the Permafrost Along the Sino-Russian-Mongolian Economic Corridor", edited and published research cases of geoenvironmental disasters in permafrost regions in Northeast China, and shared the research results of GERRP. At present, the research results of GERRP are gradually enriched, some of them have highly academic value, and have been put into engineering practice.

ICRSE-NEFU has gradually shown its unique research charm since it became an ICL member in 20032002. In 2012, ICRSE-NEFU established a landslide research network in cold regions (ICL-CRLN), and then Research Center of Cold Regions Landslide was built.

Permafrost as one of the elements of the cryosphere, the change of thermodynamic stability of permafrost will directly affect the changes of hydrosphere, biosphere and lithosphere. Under the trend of global warming, the frequency and intensity of environmental and engineering geological disasters caused by permafrost degradation are getting higher and higher (Figs. H.1 and H.2). Taking the cold area in the southern boundary of the permafrost zone in Northeast China as study area, disasters such as ground subsidence, slope icing, landslides and other disasters caused by permafrost melting were studied. At the same time, we found melting permafrost also leads to seasonally high concentrations of greenhouse gases, triggering wildfires that may further accelerate permafrost degradation and environmental changes of terrestrial ecosystems and roads.

W. Shan · Y. Guo
Institute of Cold Regions Science and Engineering, Northeast Forestry University, Harbin, China
e-mail: shanwei456@163.com

I. Alcántara-Ayala et al. (eds.), *Progress in Landslide Research and Technology, Volume 1 Issue 2, 2022*, Progress in Landslide Research and Technology,
https://doi.org/10.1007/978-3-031-18471-0

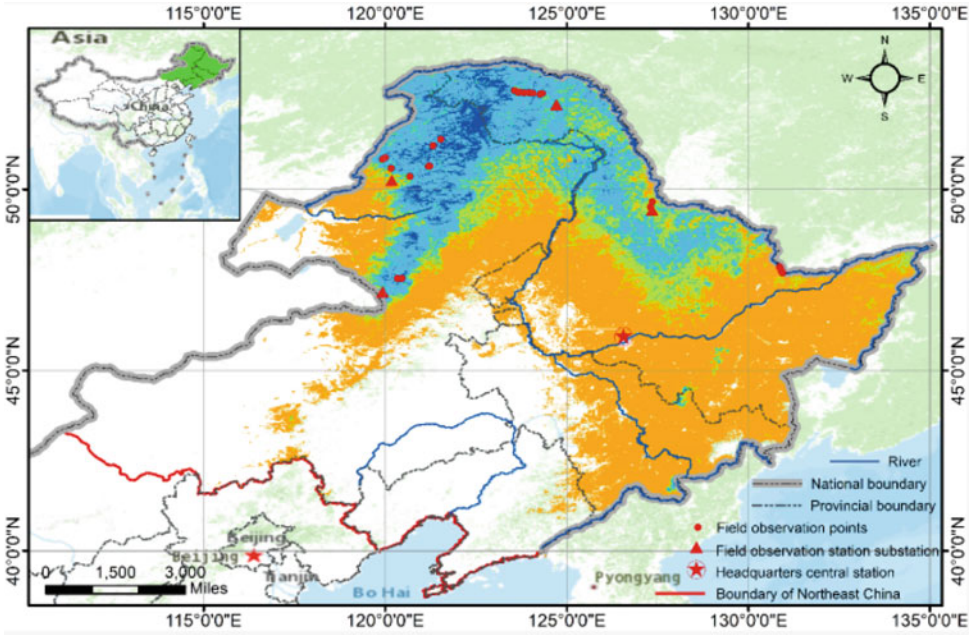

Fig. H.1 Permafrost distribution in NE of China (2014–2019)

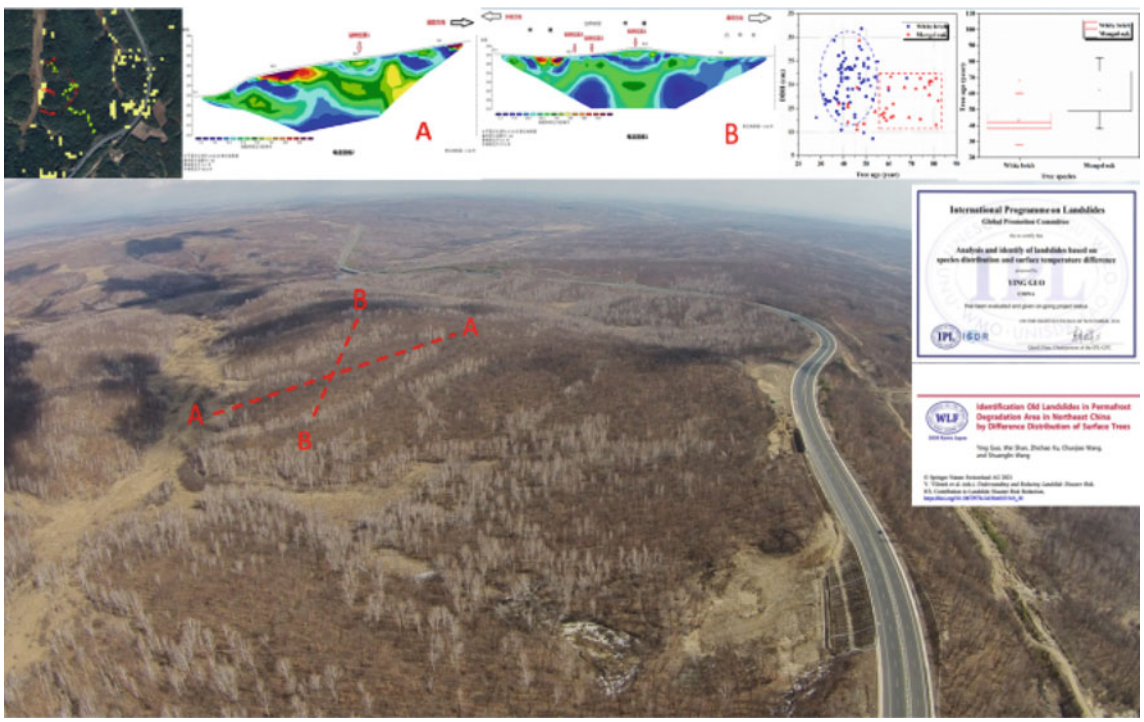

Fig. H.2 Different tree species and ages in the landslide area caused by permafrost degradation

Marui & Co. Ltd.

Taketoshi Marui and Yuji Ikari

Introduction

Marui & Co. Ltd. celebrates its 100th anniversary in 2020. Marui, as one of the leading manufacturers of testing apparatuses in Japan, has been constantly striving to further improve its service since its foundation in 1920, thus contributing to the sustainable development of our nation and society. Our main products cover a wide variety of destructive and non-destructive testing apparatuses in the fields of geotechnical engineering, concrete engineering (mortar, aggregates, etc.), and ceramic engineering (Fig. I.1). Of special note is that Marui has been helping to manufacture ring-shear apparatuses (Fig. I.2) for the past half-century based on the leading-edge ideas of Dr. Kyoji Sassa, Professor Emeritus at the Kyoto University. Marui has delivered a total of seven ring-shear apparatuses to the Disaster Prevention Research Institute, Kyoto University, and two to the International Consortium on Landslides. Also, the apparatuses have been exported to the United States of America, China, Croatia and Vietnam.

Since 2002, Marui has been a supporter of the International Consortium on Landslides (ICL) and has gradually been intensifying its contribution to the ICL worldwide efforts for landslide risk reduction and international promotion of landslide research. According to NASA, more frequent and intense rainfall events due to climate change have been causing frequent landslides particularly in mountains of Asian regions including Japan where waters can be stored in various ways. Summer monsoon rains as well as snow and glacier melt waters can destabilize steep mountainsides, triggering landslides, which are down-slope movements of rocks, soils, water, trees, etc. Marui, as an engineering

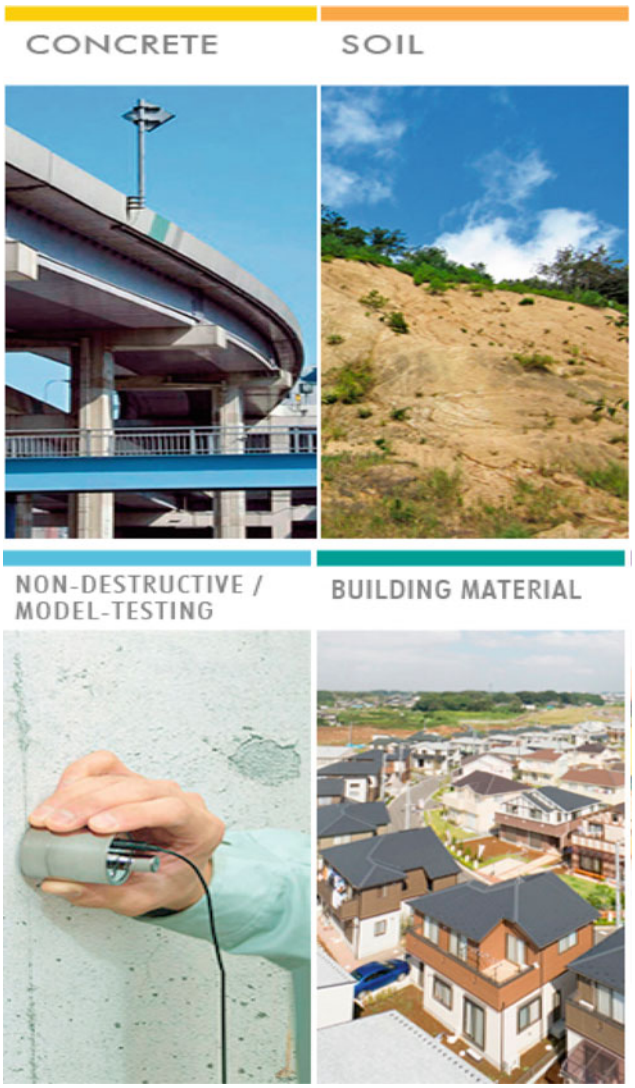

Fig. I.1 Products of testing apparatus such as non-destructive/model-testing for mesuring intensity, physical property, durability, etc. for concrete, soil, building material, etc.

T. Marui · Y. Ikari
1-9-17 Goryo, Daito City, Osaka 574-0064, Japan
e-mail: hp-mail@marui-group.co.jp
URL: http://marui-group.co.jp/en/index.html

I. Alcántara-Ayala et al. (eds.), *Progress in Landslide Research and Technology, Volume 1 Issue 2, 2022*, Progress in Landslide Research and Technology,
https://doi.org/10.1007/978-3-031-18471-0

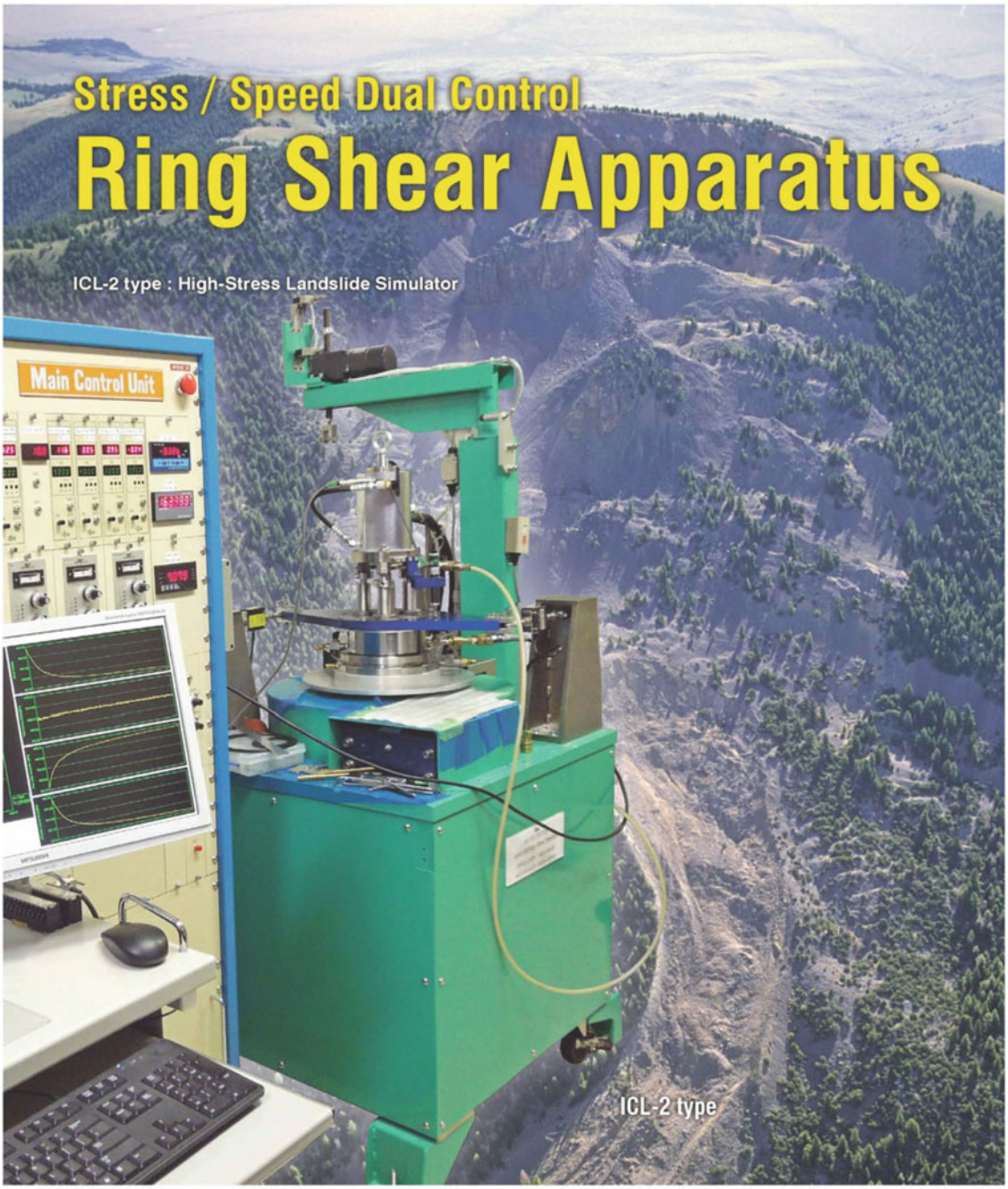

Fig. I.2 High-stress landslide simulator

supporter, commits deeply to various activities of research particularly on triggering mechanisms of landslides.

Marui & Co. Ltd. takes great pleasure in developing, manufacturing, and providing new products of high value sharing the delight of achievement with our customers, and thus contributing to the social development. The entire staff of Marui & Co. Ltd. is determined to devote ceaseless efforts to keep its organization optimized for its speedy and high-quality services, by the motto “Creativity and Revolution”, and strive hard to take a step further, as a leading manufacturer of testing apparatuses, to answer our customer's expectations for the 22nd century to come.

Marui continuously contributes to the 2030 Agenda for Sustainable Development, as well as to the Sendai Framework for Disaster Risk Reduction 2015–2030. In line with this, Marui signed KLC 2020 in 2019 and will strongly support its actions, especially KCL2020 actions 3, 4, 5, and 9.

NIPPON KOEI Nippon Koei Co., Ltd., Geohazard Management Division

Hiroaki Tauchi

For the supplemental information, please scan the QR code or visit this link: Nippon Koei Co., Ltd.—7th Asia–Pacific Climate Change Adaptation Forum (asiapacificadapt.net).

Introduction

The Nippon Koei Group (NK) has been a leading international consultant in providing engineering consulting services to over 5500 multi-disciplinary infrastructure and development projects in 160 countries all over the world. The landslide prevention specialist team (at present called Geohazard Management Division) was established in 1966 to specifically provide countermeasures against sediment disasters. Over the last 50 years, we have significantly improved the capacity of countries to respond and reduce risk from debris flows, slope instabilities, landslides, avalanches and rock falls due to torrential rains, large-scale earthquakes, and volcanic eruptions that threaten a country's vital economic infrastructure lifelines, especially the road networks. At present, approximately 160 engineers provide engineering consulting services to protect communities from a variety of disasters (Figs. J.1 and J.2). During disasters, we provide experienced professional engineers to quickly make a risk assessment and promptly respond with a series of engineering design analyses, emergency and permanent measures based on our extensive experience and know-how. To maximize the effectiveness of infrastructures, we address efficient countermeasure plans, design and research in terms of cost reduction and cost-effectiveness using various numerical analyses such as finite element method (FEM) and discrete element method (DEM), etc.

In Japan, we have worked hard to restore and recover from sediment-related disasters caused by earthquakes and heavy rainfalls that have frequently occurred in recent years (the 2011 Great East Japan Earthquake, the Northern Kyushu Flood in 2017, etc.). We have received letters of appreciation for our efforts from the national and local governments.

Our major international projects include "The Project for Countermeasure Construction Against the Landslides on Sindhuli Road Section II, Nepal," "The project for the rehabilitation of Sindhuli road affected by the 2015 Gorkha Earthquake, Nepal," and "The project for landslide prevention for National Road 6 in Honduras"; all funded by the Japan International Cooperation Agency (JICA) grants-in-aid. Through these projects, we are contributing to the socioeconomic development of each country by improving vulnerable locations in road networks against sediment disasters, promoting traffic safety, and providing logistics assistance for road users. In particular, the 1st of the three NK's projects mentioned above won the "3rd JAPAN Construction International Award" from the Ministry of Land, Infrastructure, Transport and Tourism as the project that has realized "high-quality infrastructures" through its excellent know-how, technical capabilities, and project management capabilities.

NK is an ICL member and has been using its technology to reduce geohazard risk. Through various projects, NK is continuously contributing to the 2030 Agenda for Sustainable Development and the Sendai Framework for Disaster Reduction 2015–2030. Using our full capability with

H. Tauchi
Geohazard Management Division, Nippon Koei Co., Ltd.,
5-4 Kojimachi, Chiyoda-ku, Tokyo 102-8539, Japan
e-mail: tauchi-hr@n-koei.jp
URL: https://www.n-koei.co.jp/english/

I. Alcántara-Ayala et al. (eds.), *Progress in Landslide Research and Technology, Volume 1 Issue 2, 2022*, Progress in Landslide Research and Technology,
https://doi.org/10.1007/978-3-031-18471-0

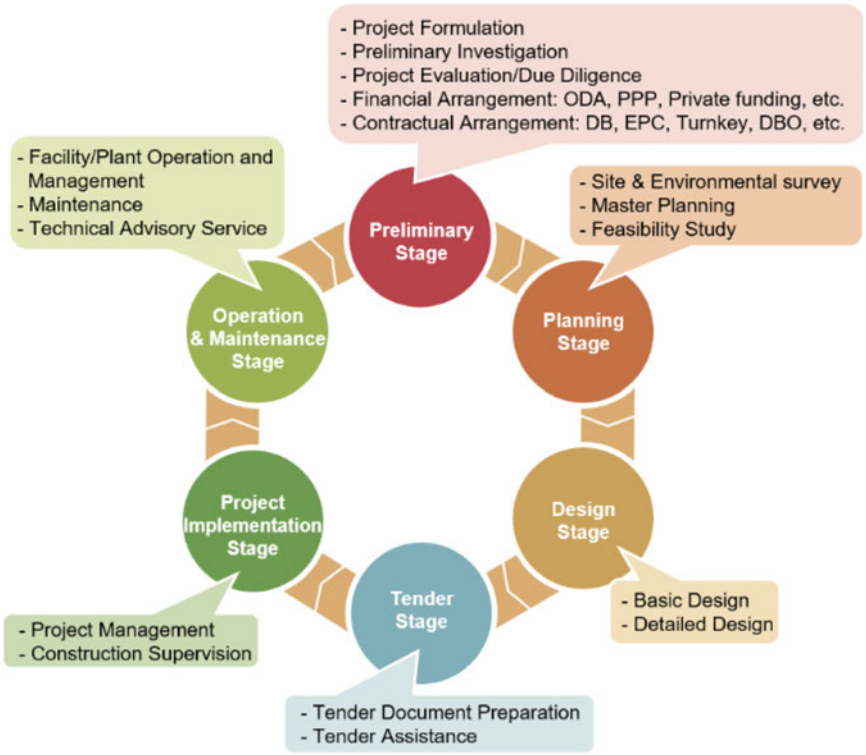

Fig. J.1 Our service for geohazard management

abundant experiences in Japan and Asia prone to natural disasters, we hope to contribute much more to a reduction of global sediment disasters including landslides. In line with this, NK has signed the KLC 2020, and will strongly support its actions, especially KCL2020 actions 1, 2, 3, 5, 6, and 8.

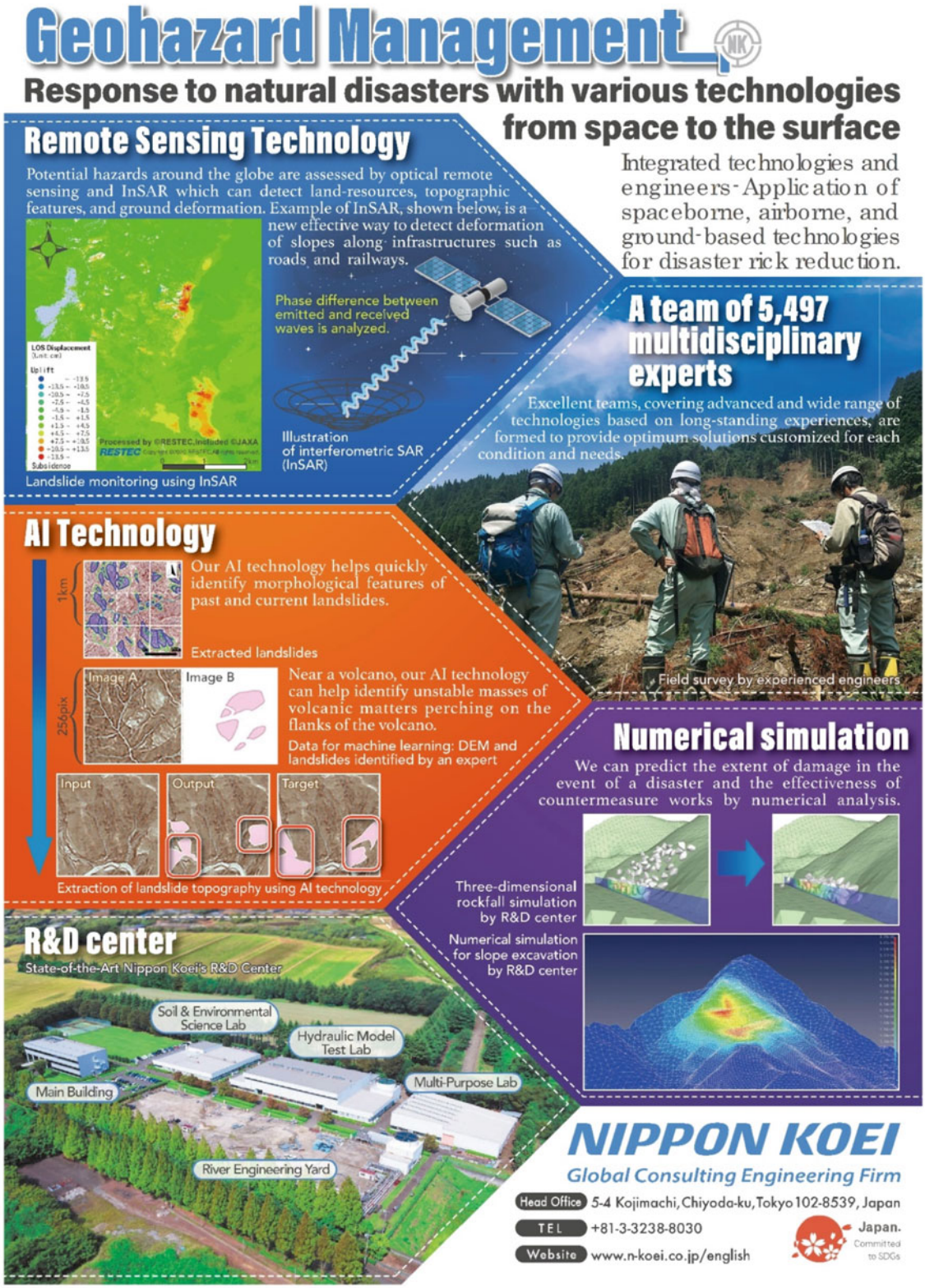

Fig. J.2 Introduction of our survey analysis technology for geohazard

Ellegi Srl

Ellegi Srl

Introduction

Ellegi srl provides worldwide monitoring services and produces Ground Based synthetic aperture radar (GBInsAR) for remote measurement of displacements and deformations on natural hazards and manmade buildings using its own designed and patented LiSALab system.

Its activities started in 2003 as a spin off project to exploit commercially the Ground Based Linear Synthetic Aperture Radars technology developed by European Commission's Ispra Joint Research Centre and based on the results of more than 10 years of research. Since then, Ellegi has industrialized and developed the core technology of the LiSALab system and latest LiSAmobile system represents the 5th generation of development.

In 2003 it was the first commercial company in the world to provide GBInSAR measurements of natural hazards and structure.

Ellegi srl offers:

- Displacement fields measurement, control and monitoring of the deformation caused by natural hazards, like landslides, rockslides, sinkhole, volcanic deformation in every operative condition, including emergencies,
- Structural strain fields measurement, control, monitoring and diagnosis of the deformation affecting buildings, bridges, viaducts, dams.
- GBInSAR monitoring systems, installation, management and maintenance in order to provide information about natural hazards or anthropic activity, that can generate or cause slopes failures or buildings instabilities (Figs. K.1 and K.2).

In all the above-mentioned activities Ellegi srl uses the GBInSAR LiSALab technology that represents a real "break-through".

Ellegi Srl
Via Petrarca, 55, 22070 Rovello Porro, Como, Italy

I. Alcántara-Ayala et al. (eds.), *Progress in Landslide Research and Technology, Volume 1 Issue 2, 2022*, Progress in Landslide Research and Technology,
https://doi.org/10.1007/978-3-031-18471-0

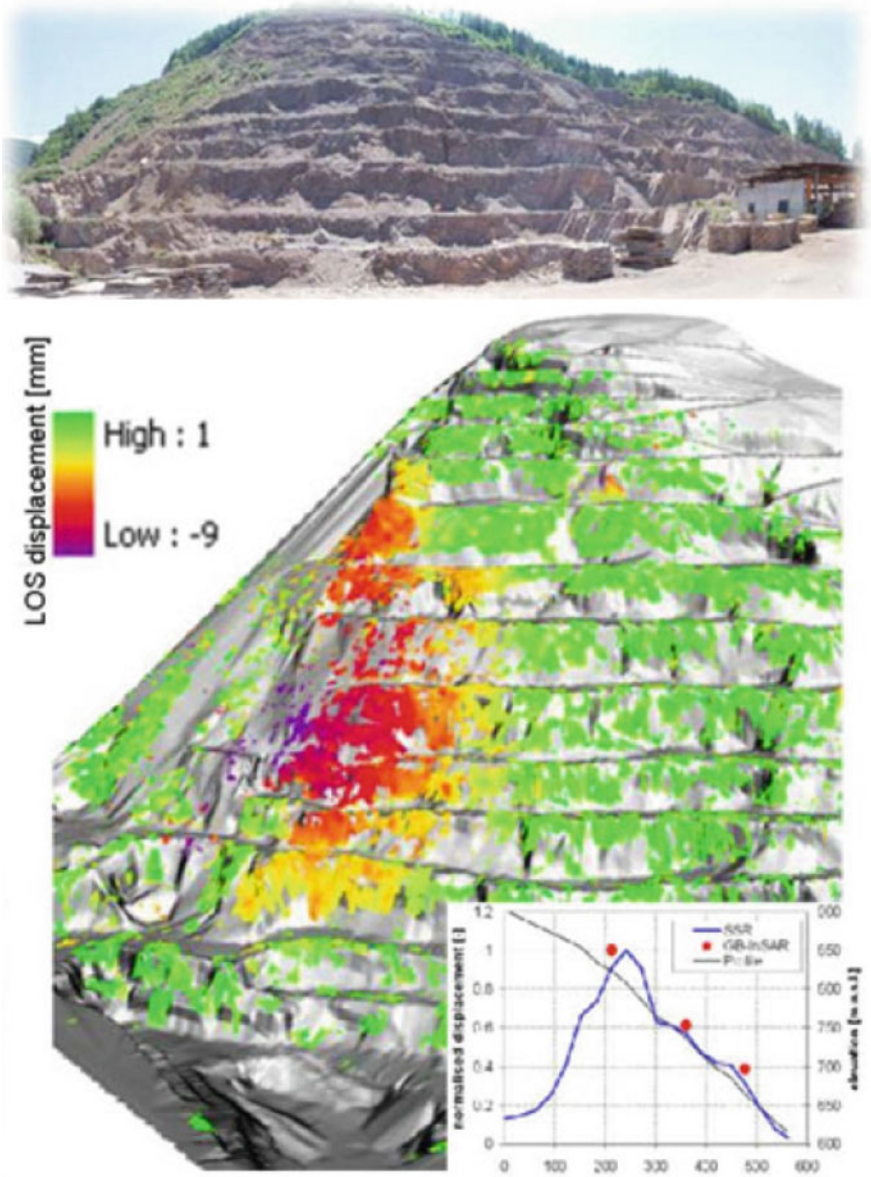

Fig. K.1 GBInSAR LiSALab technology quarry monitoring example and displacements' field comparison between the GBInSAR measurement and FEM model results

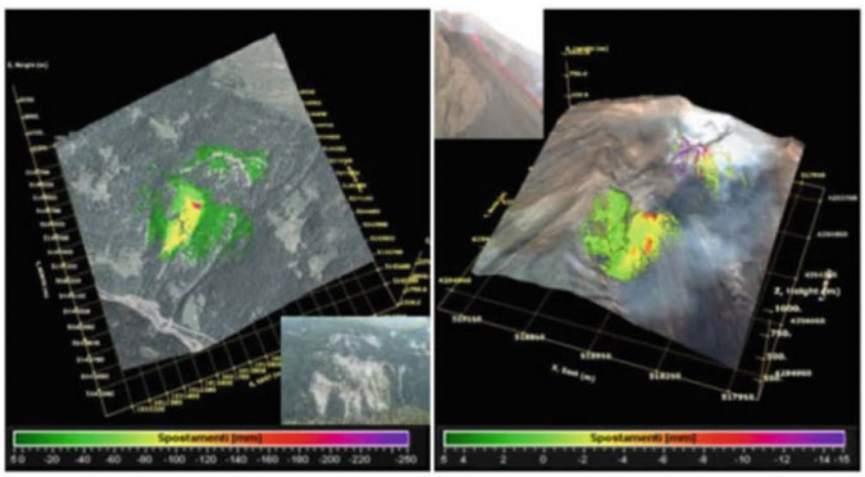

Fig. K.2 GBInSAR LiSALab technology result in monitoring a slope affected by a landslide (left) and a volcanic slope affected by deformation (right). Landslide or moving area mapping and boundaries identification is made easy by GBInSAR LiSALab technology

IDS GeoRadar s.r.l.

IDS GeoRadar s.r.l.

Introduction

IDS GeoRadar, part of Hexagon, provides products and solutions, based on radar technology, for monitoring applications including landslides, rockfalls, complex structures, mining and civil engineering. The company is a leading provider of Ground Penetrating Radar (GPR) and Interferometric Radar solutions worldwide.

IDS GeoRadar is committed to delivering best-in-class performance solutions and to the pursuit of product excellence, through the creation of application-specific, innovative and cost-efficient systems for a wide range of applications:

- Utility mapping and detection
- Civil engineering
- Railway and road engineering
- Geology and environment management
- Archaelogy
- Forensics
- Landslide monitoring
- Mining safety.

Natural Hazard Monitoring Solution

The use of slope monitoring radar is now the standard practice for the active monitoring of slope in open pit mines and for safety critical landslide monitoring with the aim of providing alerts in the event of progressive movements which could potentially lead to slope failure and assessing worker safety. The unique IBIS-FM EVO radar system accurately monitors multiple scales of displacements in real time, from early detection of slow movements to fast accelerations associated with slope collapse. The great operative range, up to 5000 m, allows to safely deploying the system in comfortably accessible areas, without exposing people and equipment to hazardous zones.

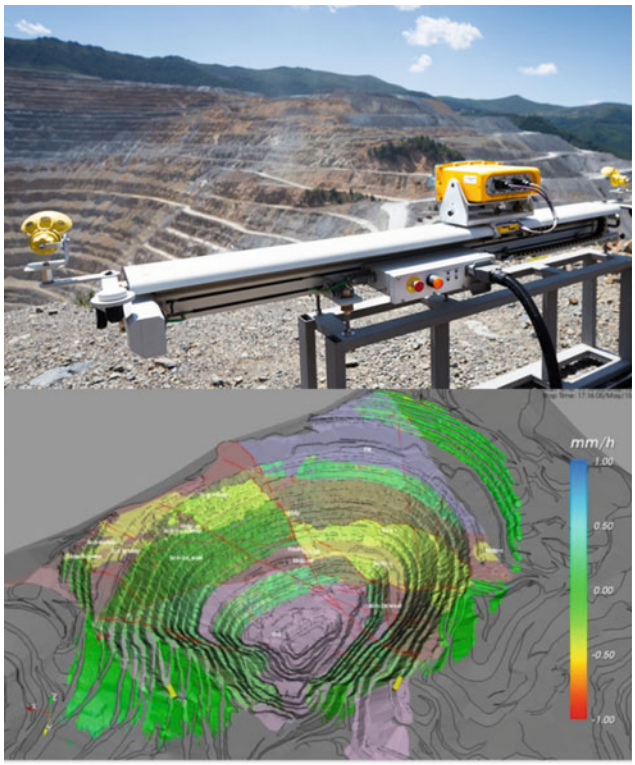

Fig. L.1 IDS GeoRadar: innovative interferometric radar for mining, environmental and civil engineering

IDS GeoRadar s.r.l.
Via Augusto Righi, 6, 6A, 8, Loc. Ospedaletto, 56121 Pisa, Italy

I. Alcántara-Ayala et al. (eds.), *Progress in Landslide Research and Technology, Volume 1 Issue 2, 2022*, Progress in Landslide Research and Technology,
https://doi.org/10.1007/978-3-031-18471-0

IDS GeoRadar cooperate with TRE ALTAMIRA, the worldwide leader in ground monitoring services using satellite InSAR offer a comprehensive solution—InSAR Service—to fulfill all mine stability needs, ranging from monitoring large-scale mining operations over hundreds of square kilometers, to specific movements at the pit scale. With the large spatial coverage of satellite data, mining engineers can identify unstable areas over wide areas, also with the ability to extend the analysis of deformation back in time. All mining assets can be monitored regularly and precisely for deformation (Figs. L.1 and L.2).

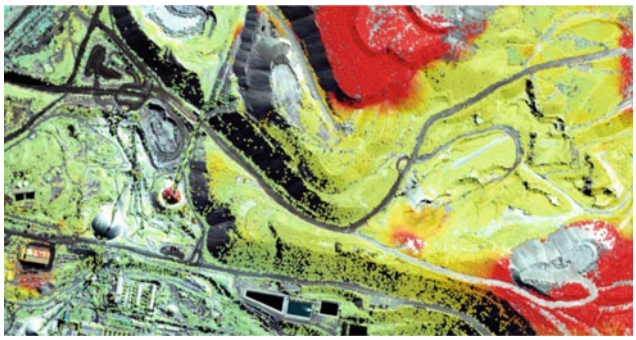

Fig. L.2 InSAR service—ground motion monitoring for mining operations

Chuo Kaihatsu Corporation

Lin Wanghttps://www.ckcnet.co.jp/contactus/

Introduction

Chuo Kaihatsu Corporation (CKC) was founded in 1946, and has been aiming to become the "Only One" consultant for our customers. We engage in the hands-on work that will "Remain with the earth, Remain in people's hearts, and Lead to a prosperous future". We focus on road, river and dam engineering to flesh out industrial infrastructures specifically by means of geophysical/geotechnical/geological investigations, civil engineering surveys and project implementations. In recent years, we make significant efforts on earthquake disaster mitigation, sediment disaster prevention/mitigation and ICT information services. Many achievements of ours have already contributed to the mitigation of natural disasters such as landslides, earthquakes and slope failures in Japan, Asia and the Pacific Region. We aim to provide technological contributions so that a sustainable society will continue to develop in the future (Figs. M.1, M.2, M.3 and M.4).

Fig. M.1 Design for various structures

L. Wang
Chuo Kaihatsu Corporation, 3-13-5 Nishi-waseda, Shinjuku-ku, Tokyo, 169-8612, Japan
e-mail: wang@ckcnet.co.jp
URL: https://www.ckcnet.co.jp/global/https://www.ckcnet.co.jp/contactus/

I. Alcántara-Ayala et al. (eds.), *Progress in Landslide Research and Technology, Volume 1 Issue 2, 2022*, Progress in Landslide Research and Technology,
https://doi.org/10.1007/978-3-031-18471-0

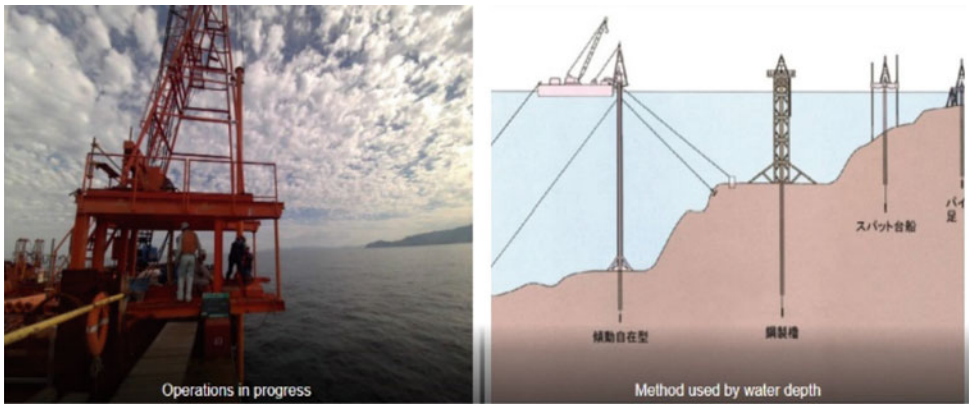

Fig. M.2 Deepwater drilling surveys

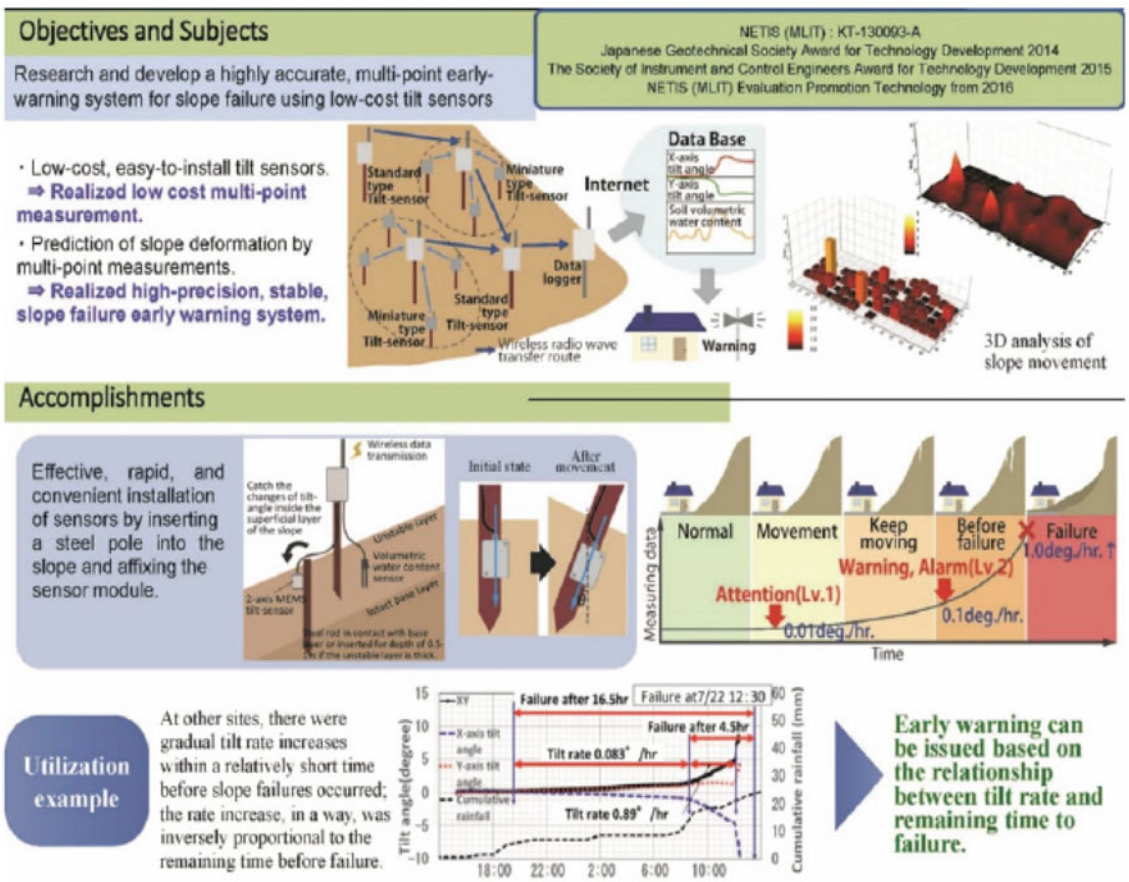

Fig. M.3 The early warning monitoring system of slope failure using multi-point tilt change and volumetric water content

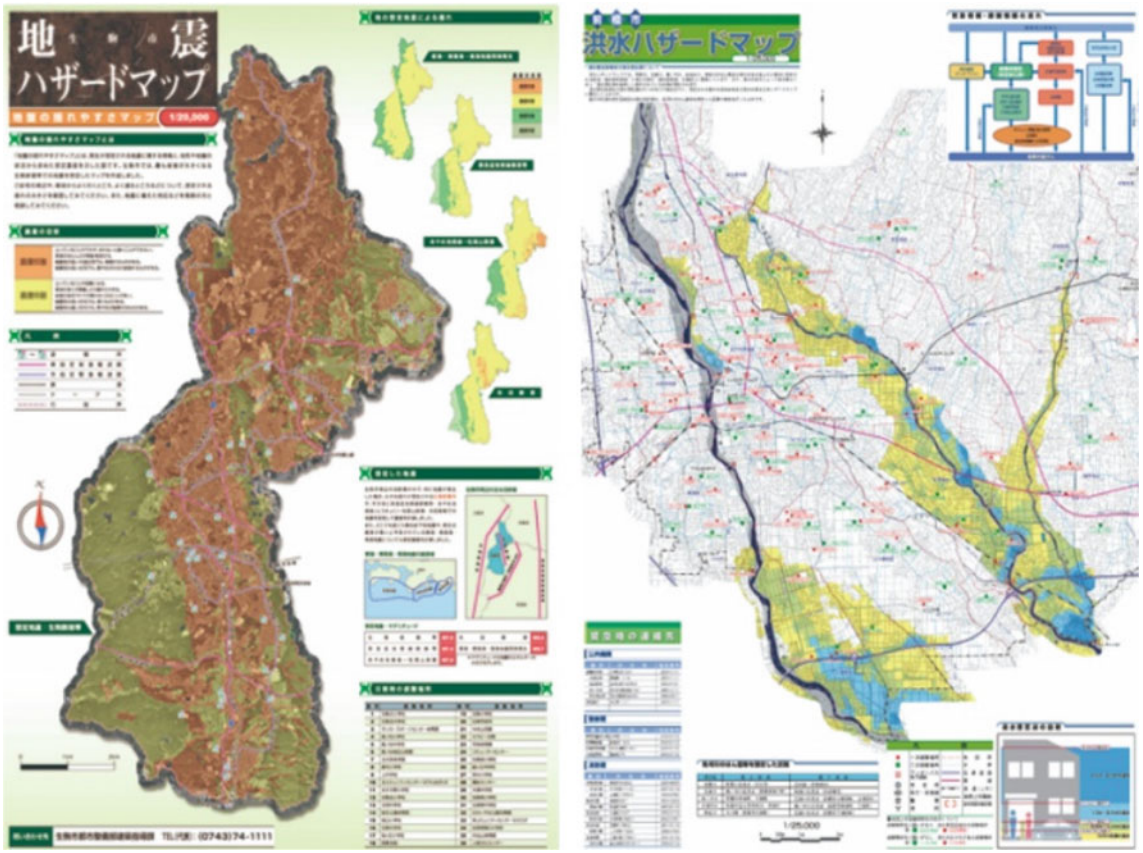

Fig. M.4 Making hazard map for sediment disaster, tsunami, flood, earthquake, liquefaction, etc…

Godai Corporation

Godai Corporation

Introduction

Ever since its foundation in 1965, Godai Kaihatsu Co. Ltd. a civil engineering consulting firm, has long been providing a variety of software and measures particularly for natural disaster mitigation. With its rich expertise in both civil engineering and information technology (IT), the company has its primary goal to address real-world needs of disaster mitigation. All the staff of Godai Kaihatsu Co. Ltd. feels it more than happy that their cutting-edge technologies help mitigate natural disasters (Figs. N.1, N.2, N.3 and N.4).

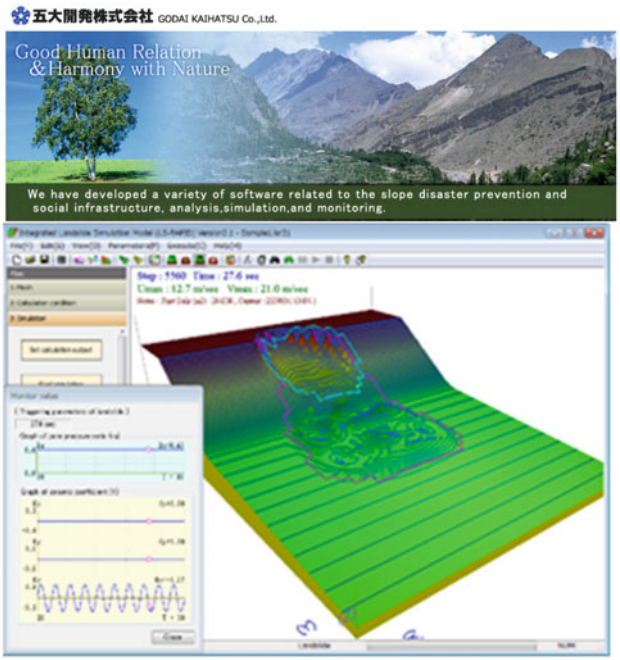

Fig. N.1 Integrated model simulating of earthquake and rain induced rapid landslides (LS-RAPID)

Godai Corporation
1-35 Kuroda, Kanazawa City, Ishikawa, Japan
e-mail: pp-sales@godai.co.jp
URL: https://soft.godai.co.jp/soft/

I. Alcántara-Ayala et al. (eds.), *Progress in Landslide Research and Technology, Volume 1 Issue 2, 2022*, Progress in Landslide Research and Technology,
https://doi.org/10.1007/978-3-031-18471-0

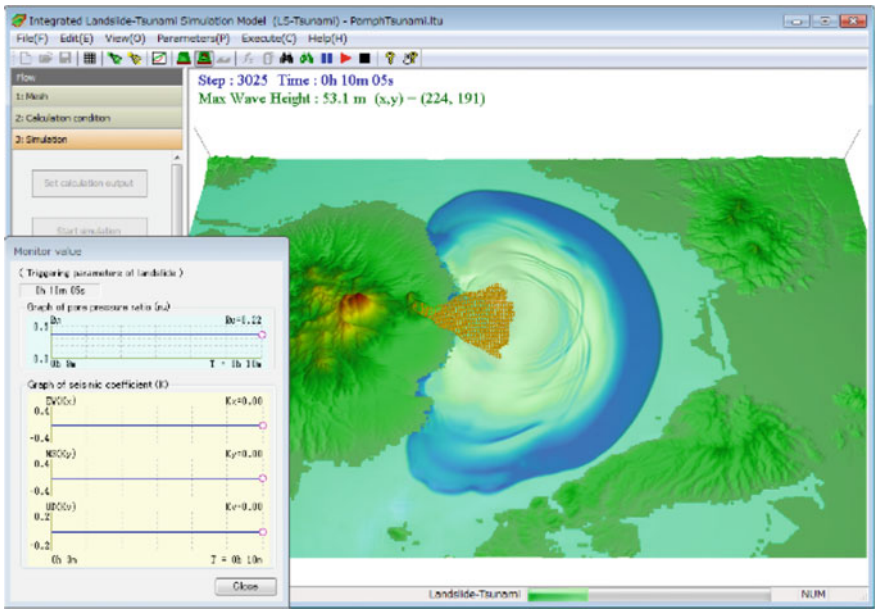

Fig. N.2 Tsunami model (LS-Tsunami)

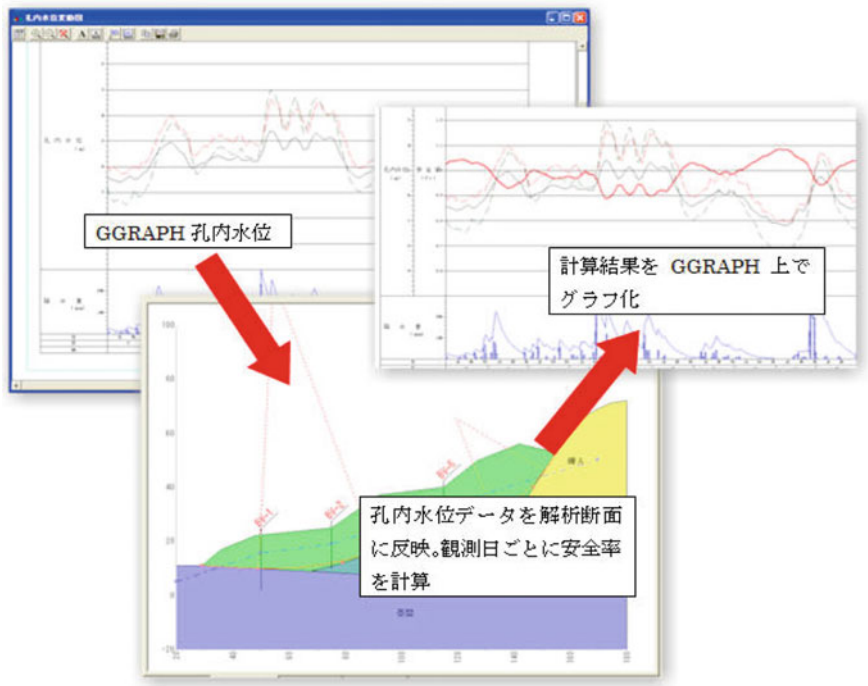

Fig. N.3 Power SSA PRO-two-dimensional slope stability calculation of earthquake and rain induced landslide

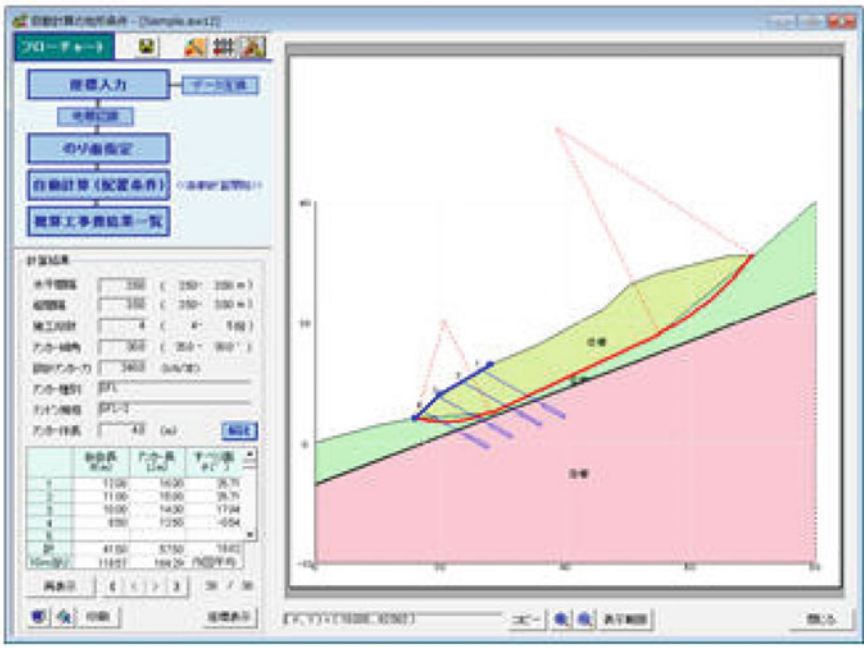

Fig. N.4 Anchor software- Slope stability analysis for ground ancho

Kisojiban Kiso-Jiban Consultants Co. Ltd.

Kaoru Hanai and Junichiro Odaka

Introduction

Since its establishment in 1953, Kiso-Jiban has been contributing on the development of social infrastructure as a "comprehensive construction consultant with strong geotechnical capabilities" in various situations, such as ground investigation, laboratory testing, analysis, civil structure design, etc. Kiso-Jiban has been working on the technological development for disaster prevention and mitigation against the recent exacerbation of natural disasters.

InSAR (Interferometric Synthetic Aperture Radar)

SAR is a technique that utilizes interference of radio waves for precise determination of distance. Kiso-Jiban has succeeded in estimation of both extent and rate of landslide movements by combining the topography interpretation and InSAR analysis.

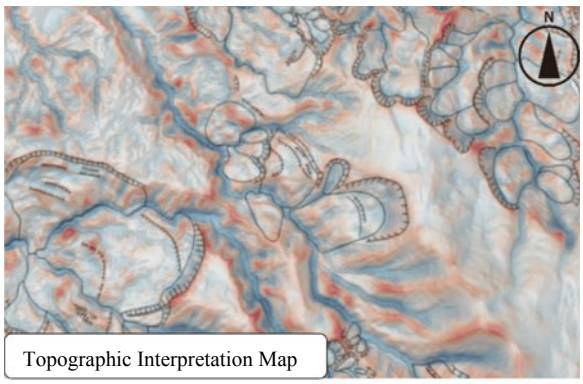

Topographic Interpretation Map

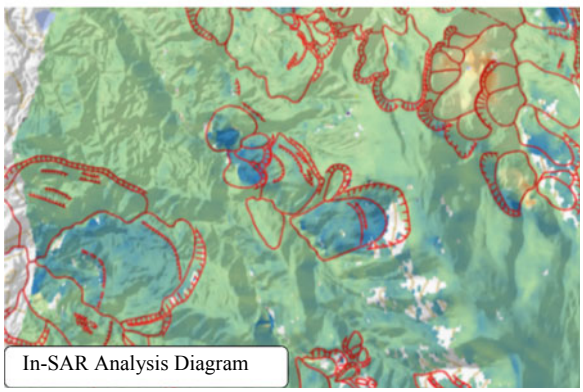

In-SAR Analysis Diagram

GP (Gel-Push) Sampling

GP Sampling can collect gravelly soil, etc., which is difficult to be collected by conventional samplers, by using a highly-concentrated water-soluble polymeric gel. GP Sampling was introduced in ISO 22475-1: 2021 revised in October 2021 as Category A, which provides the highest quality soil samples.

K. Hanai · J. Odaka
Kiso-Jiban Consultants Co. Ltd., Kinshicho Prime Tower 12 Floor, 1-5-7 Kameido, Koto-ku, Tokyo, 136-8577, Japan
e-mail: kisojiban-contactus@kiso.co.jp
URL: https://www.kisojiban.com/

I. Alcántara-Ayala et al. (eds.), *Progress in Landslide Research and Technology, Volume 1 Issue 2, 2022*, Progress in Landslide Research and Technology,
https://doi.org/10.1007/978-3-031-18471-0

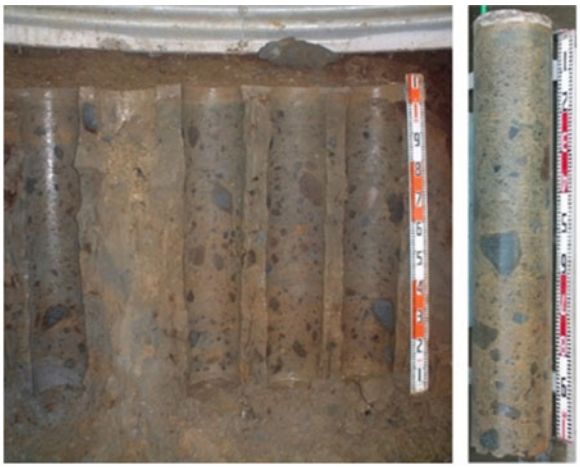

GP Sampling was performed in the disturbed soil mass right above the landslide surface (left) and the soil sample collected (right)

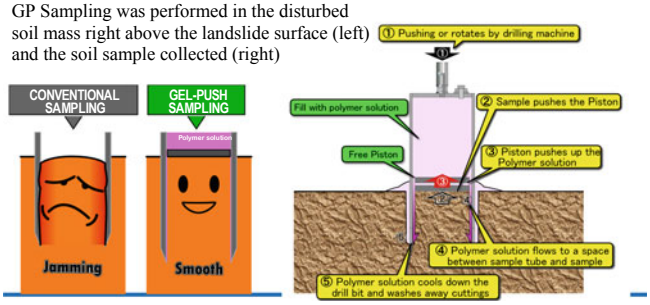

Slope Stability Analysis and Evaluation

Kiso-Jiban provides a wide range of numerical analyses related to slope stability evaluation. We have a wide range of analysis methods, from general two-dimensional limit equilibrium analysis to finite element analysis and analysis of rock masses with discontinuities, and we are challenging on the analysis that considers variability of ground and modelling uncertainty.

3D Rockfall Simulation

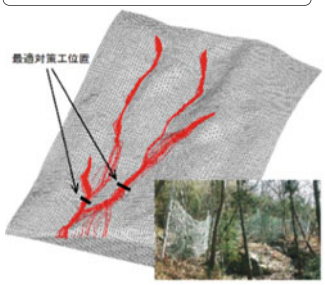

3D Finite Element Analysis

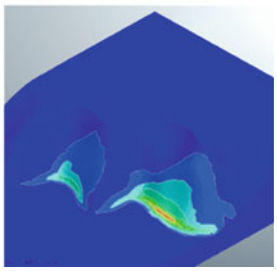

Kokusai Kogyo Co. Ltd

Kokusai Kogyo Co. Ltd.

Introduction

Kokusai Kogyo Co. Ltd. as a leading company of geospatial information technologies has long been providing public services with its comprehensive expertise to address real-world needs and cutting-edge measurement technologies. Kokusai Kogyo Co. Ltd. helps rebuild "Green Communities," which has been of our great concern in terms of "environment and energy," "disaster risk reduction" and "asset management". Kokusai Kogyo Co. Ltd. offers advanced and comprehensive analyses of geospatial information for developing new government policies, maintaining and operating social infrastructures safe and secure, and implementing low-carbon measures in cities. Influenced by the recent global climate change, extreme rainfall events have become more frequent worldwide and resultant hydro-meteorological hazards are creating more deaths and devastations particularly in many developing countries where effective advanced countermeasures are not readily available. Kokusai Kogyo Co. Ltd. is proud of its achievements in establishing resilient infrastructure systems and implementing effective monitoring/early warning systems in developing countries, which have long been helping reduce the risks from natural hazards (Figs. P.1, P.2, P.3 and P.4).

Fig. P.1 Our realtime hazard map reflects up-to-date information of soil natures and precipitations at landslide hazard sites, etc. that can constantly be changing, and evaluates area-wide hazard risk in real-time

Kokusai Kogyo Co. Ltd.
2 Rokubancho, Chiyoda-ku, Tokyo, 102-0085, Japan

I. Alcántara-Ayala et al. (eds.), *Progress in Landslide Research and Technology, Volume 1 Issue 2, 2022*, Progress in Landslide Research and Technology,
https://doi.org/10.1007/978-3-031-18471-0

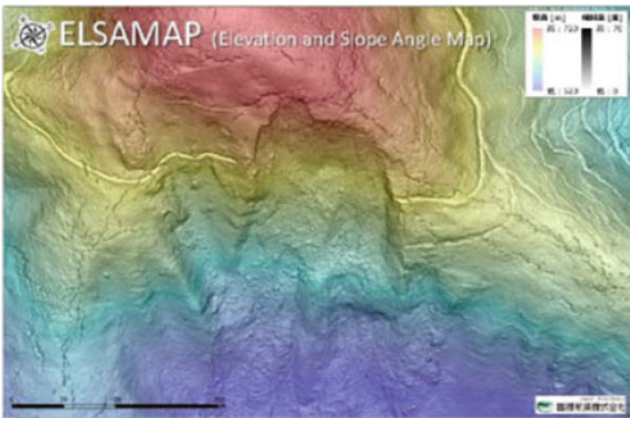

Fig. P.2 ELSAMAP is our cutting-edge 3D terrain visualization method allowing great geomorphological details to be visualized in one glance with gray-scaled slope inclinations and colored altitudes. ELSAMAP has been used to interpret micro-topographies, landslides and some other things

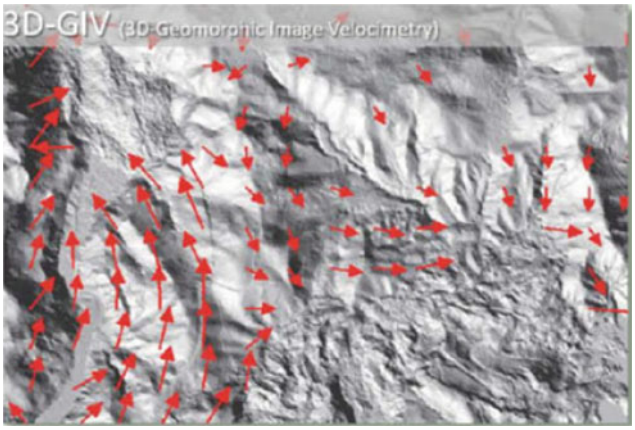

Fig. P.3 3D-GIV can help grasp the ground surface displacement caused by natural phenomena such as landslide by analyzing differences between digital geomorphic images obtained through ad hoc Airborne Laser Surveys

Fig. P.4 "Shamen-net" is a total monitoring system integrating GNSS and other monitoring device (Measurement precision: ± mm, on a real time basis)

OSASI Technos, Inc.

OSASI Technos, Inc.

Introduction

OSASI Technos, Inc. has been making its best efforts to develop its cutting-edge technologies for landslide early warning. Its unique compact and lightweight sensors making up the Landslide Early Warning System enable long-term monitoring of unstable landslide mass movements, precipitations, porewater pressure buildups, etc. in a remote mountainous area where commercial power is often unavailable. OSASI Technos, Inc. is also proud of its advanced technology to transfer observed data even in areas with poor telecom environments as proven in the successful implementations in South Asia. All staff members of OSASI Technos work together for mitigation of landslide disasters worldwide (Figs. Q.1, Q.2 and Q.3).

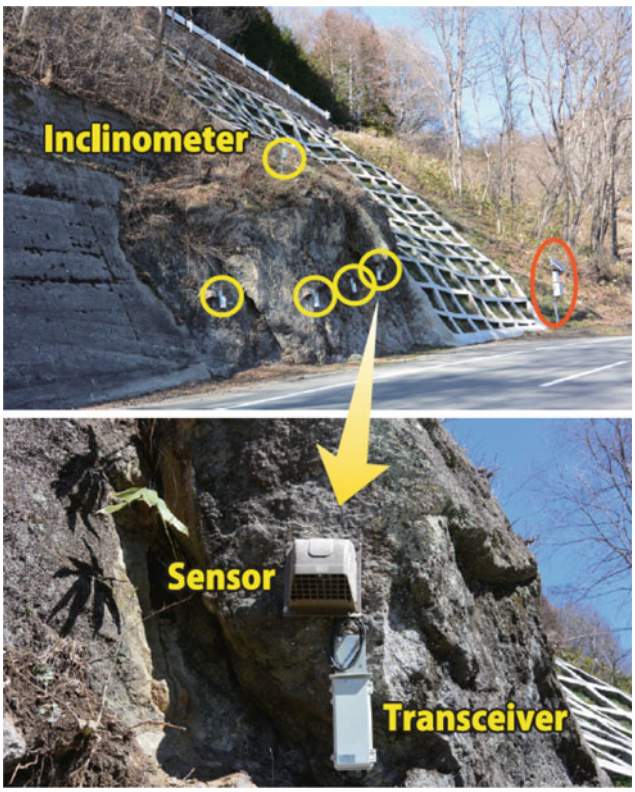

Fig. Q.1 Bedrock slope monitoring (maintenance control)

OSASI Technos, Inc.
65-3 Hongu-cho, Kochi City, Kochi, 780-0945, Japan

I. Alcántara-Ayala et al. (eds.), *Progress in Landslide Research and Technology, Volume 1 Issue 2, 2022*, Progress in Landslide Research and Technology,
https://doi.org/10.1007/978-3-031-18471-0

Fig. Q.2 Measurement of the dynamic state of landslide using inclinometers with a wireless function

Fig. Q.3 Cut slope monitoring

List of ICL Members

International Consortium on Landslides
An international non-government and non-profit scientific organization promoting landslide research and capacity building for the benefit of society and the environment
President: Nicola Casagi (University Florence, Italy)
Vice Presidents: Peter Bobrowsky (Geological Survey of Canada. Canada), Zeljko Arbanas (University of Rijeka, Croatia), Binod Tiwari (California State University, USA), Faisal Fathani (University of Gadjah Mada, Indonesia), Veronica Tofani (University of Florence, Italy), Vit Vilimek (Charles University, Czech Republic) Executive Director: Kaoru Takara (Kyoto University, Japan), Treasurer: Kyoji Sassa (Prof. Emeritus, Kyoto University, Japan)

Country/Region	ICL full member
Bosnia and Herzegovina	The Geotechnical Society of Bosnia and Herzegovina
Brazil	Center for Scientific Support in Disasters—Federal University of Parana
Canada	Geological Survey of Canada
Canada	University of Alberta
China	Northeast Forestry University, Institute of Cold Regions Science and Engineering
	China University of Geosciences
	Chinese Academy of Sciences, Institute of Mountain Hazards and Environment
	Tongji University, College of Surveying and Geo-Informatics
	Shanghai Jiao Tong University
	Tsinghua University
	Civil Engineering and Development Department, Geotechnical Engineering Office, Hong Kong
	The Hong Kong University of Science and Technology
	The University of Hong Kong
Colombia	Universidad Nacional de Colombia
Croatia	Croatian Landslide Group from Faculty of Civil Engineering University of Rijeka and Faculty of Mining, Geology and Petroleum Engineering University of Zagreb
Czech Republic	Charles University, Faculty of Science
	Institute of Rock Structure and Mechanics, Department of Engineering Geology
	Brown Coal Research Institute
Egypt	The American University in Cairo
Germany	Technische Universitat Darmstadt, Institute and Laboratory of Geotechnics
Georgia	Department of Geology of National Environmental Agency of Georgia
Honduras	Universidad Nacional Autónoma de Honduras (UNAH)
India	Amrita Vishwa Vidyapeetham, Amrita University
	National Institute of Disaster Management, New Delhi
Indonesia	Gadjah Mada University, Center for Disaster Mitigation and Technological Innovation (GAMA-InaTEK)
	Parahyangan Catholic University
	Agency for Meteorology, Climatology, and Geophysics of the Republic of Indonesia (BMKG Indonesia)

(continued)

I. Alcántara-Ayala et al. (eds.), *Progress in Landslide Research and Technology, Volume 1 Issue 2, 2022*, Progress in Landslide Research and Technology,
https://doi.org/10.1007/978-3-031-18471-0

Italy	UNESCO Chair for the prevention and the sustainable management of geo-hydrological hazards—University of Florence
	ISPRA-Italian Institute form Environmental Protection and Research
	University of Calabria, DIMES, CAMILAB
	Istituto di Ricerca per la Protezione Idrogeologica (IRPI), of the Italian National Research Council (CNR)
	Universita di Torino, Department of Earth science
	Centro di Ricerca CERI—Sapienza Università di Roma
	National Institute of Oceanography and Applied Geophysics—OGS, Italy
Japan	Kyoto University, Disaster Prevention Research Institute
	Japan Landslide Society
	International Consortium on Geo-disaster Reduction
Korea	Korea Institute of Geoscience and Mineral Resources (KIGAM)
	Korean Society of Forest Engineering
	National Institute of Forest Science
	Korea Authority of Land and Infrastructure Safety
	Korea Institute of Civil Engineering and Building Technology
Malaysia	Slope Engineering Branch, Public Works Department of Malaysia
Mexico	Institute of Geography, National Autonomous University of Mexico (UNAM)
Russia	Moscow State University, Department of Engineering and Ecological Geology
	JSC "Hydroproject Institute"
Serbia	University of Belgrade, Faculty of Mining and Geology
Slovakia	Comenius University, Faculty of Natural Sciences, Department of Engineering Geology
Slovenia	University of Ljubljana, Faculty of Civil and Geodetic Engineering (ULFGG)
	Geological Survey of Slovenia
Sri Lanka	Central Engineering Consultancy Bureau (CECB)
	National Building Research Organization
Chinese Taipei	Landslide group in National Central University from Graduate Institute of Applied Geology, Department of Civil Engineering, Center for Environmental Studies
	National Taiwan University, Department of Civil Engineering
Thailand	Ministry of Agriculture and Cooperatives, Land Development Department
	Asian Disaster Preparedness Center (ADPC)
Ukraine	Institute of Telecommunication and Global Information Space
United Kingdom	British Geological Survey
USA and Nepal	California State University, Fullerton & Tribhuvan University, Institute of Engineering
Viet Nam	Institute of Transport Science and Technology
	Vietnam Institute of Geosciences and Mineral Resources (VIGMR)
Country/Region	**ICL associate member**
Belgium	Liege University, Georisk and Environment (G&E) group
China	State Key Laboratory of Geohazard Prevention and Geoenvironment Protection (Chengdu University of Technology)
	State Key Laboratory of Plateau Ecology and Agriculture (Qinghai University)
Czech Republic	Czech Geological Survey
Italy	Department of Earth and Environmental Sciences, University Aldo Moro, Bari
	University of Sannio, Department of Sciences and Technologies
	Geotechnical Engineering Group (GEG), University of Salerno
	Department of Earth and Environmental Sciences—University of Pavia
	University of Chieti-Pescara, Department of Engineering and Geology
	Federico II University of Naples, Department of Earth, Environmental and Resource Sciences
	DIA—Università degli Studi di Parma
	University of Urbino "Carlo Bo", Department of Pure and Applied Sciences

(continued)

Japan	Ehime University, Center for Disaster Management Informatics Research	
Macedonia	Macedonian Association for Geotechnics	
Russia	Russian State Geological Prospecting University n.a. Sergo Ordzhonikidze (MGRI-RSGPU)	
Slovenia	University of Ljubljana, Faculty of Natural Sciences and Engineering (UL NTF)	
Switzerland	Institute of Earth Sciences, Faculty of Geoscience and Environment/University of Lausanne	
USA	Iowa State University	
Country/Region	**ICL supporter**	
Italy	IDS GeoRadar s.r.l.	
Japan	Marui & Co., Ltd., Osaka	Okuyama Boring Co., Ltd., Yokote
	Ohta Geo-Research Co., Ltd., Nishinomiya	Japan Conservation Engineers Co., Ltd., Tokyo
	Sabo Technical Center, Tokyo	GODAI Development Corp., Kanazawa
	OYO Corporation, Tokyo	Kokusai Kogyo Co., Ltd., Tokyo
	OSASI Technos Inc., Kochi	NIPPON KOEI CO., LTD
Chinese Taipei	Sinotech Engineering Consultants, Inc	

ICL Secretariat
Secretary General: Kyoji Sassa
International Consortium on Landslides, 138-1 Tanaka Asukai-cho, Sakyo-ku, Kyoto, 606-8226, Japan
Web: http://icl.iplhq.org/, http://www.iplhq.org/, E-mail: secretariat@iclhq.org
Tel: +81 (75) 723 0640, Fax: +81(75) 950 0910

Author Index

I. Alcántara-Ayala et al. (eds.), *Progress in Landslide Research and Technology, Volume 1 Issue 2, 2022*, Progress in Landslide Research and Technology,
https://doi.org/10.1007/978-3-031-18471-0